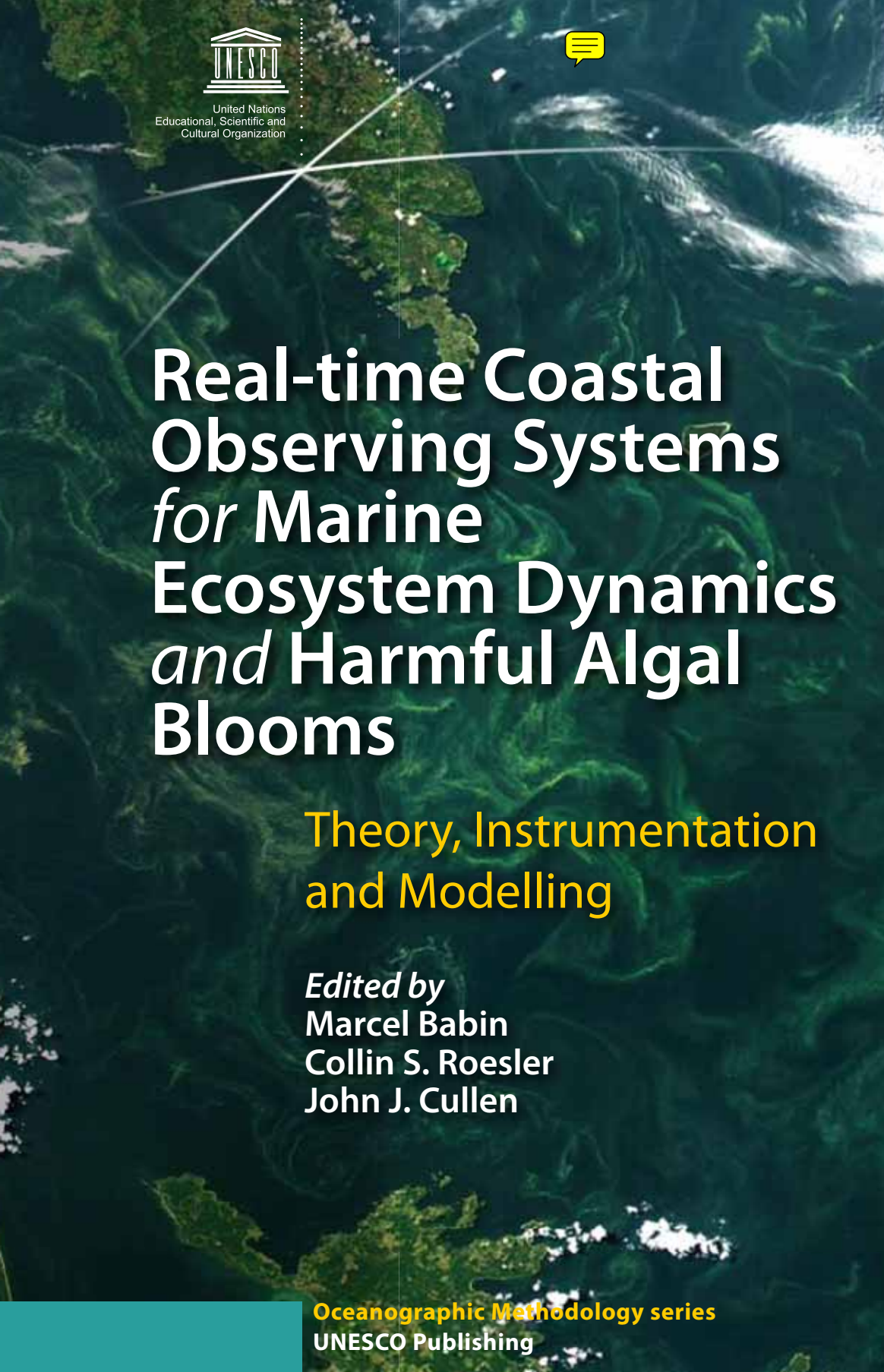

Real-time Coastal Observing Systems *for* Marine Ecosystem Dynamics *and* Harmful Algal Blooms

Theory, Instrumentation and Modelling

Edited by
Marcel Babin
Collin S. Roesler
John J. Cullen

Oceanographic Methodology series
UNESCO Publishing

Real-time Coastal Observing Systems for Marine Ecosystem Dynamics and Harmful Algal Blooms: Theory, Instrumentation and Modelling

Edited by Marcel Babin, Collin S. Roesler and John J. Cullen

Published in 2008 by the United Nations Educational,
Scientific and Cultural Organization
7, place de Fontenoy, 75352 Paris 07 SP, France

ISBN 978-92-3-104042-9

Cover photos:
Background:
Surface bloom of toxic cyanobacterium of the *Nodularia* genus in the Baltic Sea as discerned through a 250-m resolution quasi-true colour MODIS-Aqua image (M. Kahru).
Insets (from top to bottom):
Observation system using meteorological, hydrographic and optical sensors deployed by the Marine Environmental Prediction System in Nova Scotia, Canada (P. Kuhn).
Light micrograph of two cells of toxic dinoflagellate *Alexandrium tamarense* (A. Cembella).
Plan view of destabilized linear front accompanied by along-front jet (J. M. Pringle and P. J. S. Franks).
Bio-optical glider of the Laboratoire d'Océanographie de Villefranche-sur-mer (D. Luquet and H. Claustre).

Cover design: Catherine Brown

Typeset by Thomson Digital (Mauritius) LTD
Printed by Graphic3, Valencia

Printed in Spain

Preface

The Intergovernmental Oceanographic Commission of UNESCO has for more than a decade given attention to activities aimed at developing capacity in research, sustained observations and management of harmful microalgae through its Harmful Algal Bloom Programme and the Global Ocean Observing System.

The term 'harmful algae' is not a scientific but a societal one. It calls attention to the increasing detrimental effects caused by these organisms on national economies. The aim of supporting improved observation systems for harmful algae is to help mitigate their negative effects on fisheries, aquaculture, human health and recreation areas. Understanding the causes of harmful algal events and developing contingency plans links directly with other important areas of societal concern such as eutrophication, integrated coastal area management, fisheries management, and transfer and introduction of non-indigenous marine species. These linkages are important for addressing the problem of harmful algae adequately so that society can understand and better appreciate the results of science in this field.

The first comprehensive guidance on research and management methodologies for harmful algae was the *Manual on Harmful Marine Microalgae* first published in the IOC Manual and Guides series in 1995 and subsequently in revised editions in 2000 and 2003 in the UNESCO series on Oceanographic Methodology. Rapid developments in technology and a strong focus in the international community on operational marine observation systems have now made it relevant to complement the *Manual* with this new volume on real-time coastal observing systems for marine ecosystem dynamics and harmful algal blooms.

The IOC expresses its profound appreciation to the 58 scientists who prepared the manuscripts for this *Manual*, and wishes to give its particular thanks to the editors Drs Marcel Babin, Collin Roesler and John Cullen for their devoted involvement in this project[1].

The publication of this monograph has been made possible through support from the European Commission, the Danish Natural Research Council, and the Danish Ministry of Foreign Affairs (DANIDA), contributions that we are most happy to acknowledge.

Patricio Bernal
Assistant Director General of UNESCO
Executive Secretary
Intergovernmental Oceanographic Commission

[1]The scientific opinions expressed in this work are those of the authors and are not necessarily those of UNESCO and its IOC. Equipment and materials have been cited as examples of those most currently used by the authors, and their inclusion does not imply that they should be considered as preferable to others available at that time or developed since.

Contents

Contributors

Mario Adani
Istituto Nazionale di Geofisica e Vulcanologia, Sezione di Bologna, Via A. Moro 44, 40127 Bologna, Italy

E-mail: adani@bo.ingv.it

Don M. Anderson
Woods Hole Oceanographic Institution, Woods Hole, MA 02543, USA

E-mail: danderson@whoi.edu

Feleke Arega
South Carolina Department of Natural Resource, Columbia, SC 29201, USA

E-mail: aregaf@dnr.sc.gov

Robert Arnone
Code 7330, Naval Research Laboratory, Stennis Space Center, MS39529, USA

E-mail: arnone@nrlssc.navy.mil

Marcel Babin
Laboratoire d'Océanographie de Villefranche, BP 8, 06238 Villefranche-sur-Mer Cedex, France

E-mail: marcel@obs-vlfr.fr

Stewart Bernard
Department of Oceanography, University of Cape Town, Cape Town 7701, South Africa

E-mail: bstewart@ocean.uct.ac.za

Paul Bissett
Florida Environmental Research Institute, 10500 University Center Drive, Suite 140, Tampa, FL 33612, USA

E-mail: pbissett@feriweb. org

Jennifer Bosch
Coastal Ocean Observation Laboratory, Institute of Marine and Coastal Sciences, Rutgers University, New Brunswick, NJ 08901, USA

E-mail: bosch@marine.rutgers.edu

Emmanuel Boss
School of Marine Sciences, University of Maine, Orono, Maine 04469, USA

E-mail: emmanuel.boss@maine.edu

Allan D. Cembella
Alfred Wegener Institute, Am Handelschafen 12, Bremerhaven, Germany
E-mail: Allan.Cembella@awi.de

Grace Chang
Ocean Physics Laboratory, University of California Santa Barbara, 6487 Calle Real Unit A, Santa Barbara, CA 93117, USA
E-mail: grace.chang@opl.ucsb.edu

David K. W. Choi
Department of Civil Engineering, University of Hong Kong, Pokfulam, Hong Kong, China
E-mail: choidkw@hkucc.hku.hk

Chantal Compère
Ifremer ERT/IC, BP70, 29280 Plouzané, France
E-mail: chantal.compere@ifremer.fr

John J. Cullen
Department of Oceanography, Dalhousie University, Halifax, Nova Scotia B3H 4J1, Canada
E-mail: john.cullen@dal.ca

Sharon DeBra
Florida Environmental Research Institute, 10500 University Center Drive, Suite 140, Tampa, FL 33612, USA
E-mail:sdebra@feriweb.org

Vera De Cauwer
Management Unit of the North Sea Mathematical Models (MUMM), Royal Belgian Institute of Natural Sciences (RBINS), 100 Gulledelle, B-1200 Brussels, Belgium (now at Department of Land Management, Polytechnic of Namibia), P/Bag 13388, Windhoek, Namibia
E-mail: vdecauwer@polytechnic.edu.na

Laurent Delauney
Ifremer ERT/IC, BP70, 29280 Plouzané, France
E-mail: laurent.delauney@ifremer.fr

Tommy D. Dickey
Ocean Physics Laboratory, University of California Santa Barbara, 6487 Calle Real Unit A, Santa Barbara, CA 93117, USA
E-mail: tommy.dickey@opl.ucsb.edu

Greg J. Doucette
NOAA/National Ocean Service, Marine Biotoxins Program, 219 Fort Johnson Rd, Charleston, SC 29412, USA
E-mail: Greg.Doucette@noaa.gov

D. Dye
Florida Environmental Research Institute, 10500 University Center Drive, Suite 140, Tampa, FL 33612, USA
E-mail: ddye@feriweb.org

Alexandra Fawcett
Department of Oceanography, University of Cape Town, Cape Town 7701, South Africa
E-mail: afawcett@ocean.uct.ac.za

Wolfgang Fennel
Section of Physical Oceanography and Instrumentation, Baltic Sea Research Institute, 18119 Rostock, Germany
E-mail: wolfgang.fennel@io-warnemuende.de

Peter J. S. Franks
Integrative Oceanography Division, Scripps Institution of Oceanography, University of California, La Jolla, CA 92093-0218, USA
E-mail: pfranks@ucsd.edu

Claudia Fratianni
Istituto Nazionale di Geofisica e Vulcanologia, Sezione di Bologna, Via A. Moro 44, 40127 Bologna, Italy
E-mail: fratianni@bo.ingv.it

Scott Glenn
Coastal Ocean Observation Laboratory, Institute of Marine and Coastal Sciences, Rutgers University, New Brunswick, NJ 08901, USA
E-mail: glenn@marine.rutgers.edu

Gwyn Griffiths
National Oceanography Centre, Empress Dock, Southampton SO14 3ZH, UK
E-mail: gxg@soc.soton.ac.uk

Jules S. Jaffe
Marine Physical Laboratory, Scripps Institution of Oceanography, University of California, San Diego, La Jolla, CA 92093-0238, USA
E-mail: jules@mpl.ucsd.edu

John Kerfoot
Coastal Ocean Observation Laboratory, Institute of Marine and Coastal Sciences, Rutgers University, New Brunswick, NJ 08901, USA
E-mail: kerfoot@marine.rutgers.edu

Gary Kirkpatrick
Mote Marine Laboratory, 1600 Thompson Parkway, Sarasota, FL 34236, USA
E-mail: gkirkpat@mote.org

Geneviève Lacroix
Management Unit of the North Sea Mathematical Models (MUMM), Royal Belgian Institute of Natural Sciences (RBINS), 100 Gulledelle, B-1200 Brussels, Belgium

E-mail: G.Lacroix@mumm.ac.be

Joseph Hun-wei Lee
Department of Civil Engineering, University of Hong Kong, Pokfulam, Hong Kong, China

E-mail: hreclhw@hkucc.hku.hk

Michel Lehaitre
Laboratoire ERT/IC, IFREMER Centre de Brest, BP 70 29280 Plouzane, France

E-mail: michel.lehaitre@ifremer.fr

Marlon R. Lewis
Department of Oceanography, Dalhousie University, Halifax, Nova Scotia, Canada B3H4J1

E-mail: marlon.lewis@dal.ca

Steve Lohrenz
Department of Marine Science, 1020 Balch Blvd, Stennis Space Center, MS 39529-9904, USA

E-mail: steven.lohrenz@usm.edu

Daniel R. Lynch
Thayer School of Engineering, Dartmouth College, Hanover, NH 03755, USA

E-mail: daniel.r.lynch@darmouth.edu

Thomas C. Malone
Horn Point Laboratory, University of Maryland Center for Environmental Science, Cambridge, MD 21613, USA

E-mail: malone@hpl.umces.edu

Dennis J. McGillicuddy Jr
Woods Hole Oceanographic Institution, Woods Hole, MA 02543, USA

E-mail: dmcgillicuddy@whoi.edu

Curtis Mobley
Sequoia Scientific, Inc., 2700 Richards Road, Suite 107, Bellevue, WA 98005, USA

E-mail: curtis.mobley@sequoiasci.com

Mark Moline
Biological Sciences Department, California Polytechnic State University, San Luis Obispo, CA 93407, USA

E-mail: mmoline@marine.calpoly.edu

André Morel
Laboratoire d'Océanographie de Villefranche, CNRS & Univ. P. et M. Curie (Paris VI), 06238 Villefranche-sur-Mer CEDEX, France

E-mail: morel@obs-vlfr.fr

Thomas Neumann
Section of Physical Oceanography and Instrumentation, Baltic Sea Research Institute, 18119 Rostock, Germany

E-mail: thomas.neumann@io-warnemuende.de

Matthew Oliver
Coastal Ocean Observation Laboratory, Institute of Marine and Coastal Sciences, Rutgers University, New Brunswick, NJ 08901, USA

E-mail: oliver@marine.rutgers.edu

Youngje Park
Management Unit of the North Sea Mathematical Models (MUMM), Royal Belgian Institute of Natural Sciences (RBINS), 100 Gulledelle, B-1200 Brussels, Belgium

E-mail: Y.Park@mumm.ac.be

Nadia Pinardi
Corso di Scienze Ambientali, Via S. Alberto 163, University of Bologna, 48100 Ravenna, Italy

E-mail: pinardi@sincem.unibo.it

Grant C. Pitcher
Marine & Coastal Management, Cape Town 8012, South Africa

E-mail: gpitcher@deat.gov.za

Bo Qu
C/O Department of Civil Engineering, University of Hong Kong, Pokfulam Road, Hong Kong, China

E-mail: qubo62@gmail.com

Collin S. Roesler
Bigelow Laboratory for Ocean Sciences, West Boothbay Harbor, Maine, 04575, USA

E-mail: croesler@bigelow.org

Véronique Rousseau
Écologie des Systèmes Aquatiques (ESA), Université Libre de Bruxelles (ULB), Campus de la Plaine CP221, B-1050 Brussels, Belgium

E-mail: vrousso@ulb.ac.be

Kevin Ruddick
Management Unit of the North Sea Mathematical Models (MUMM), Royal Belgian Institute of Natural Sciences (RBINS), 100 Gulledelle, B-1200 Brussels, Belgium

E-mail: k.ruddick@mumm.ac.be

Oscar M. Schofield
Coastal Ocean Observation Laboratory, Institute of Marine and Coastal Sciences, Rutgers University, New Brunswick, NJ 08901, USA

E-mail: oscar@marine.rutgers.edu

Christopher A. Scholin
Monterey Bay Aquarium Research Institute, 7700 Sandholdt Rd, Moss Landing, CA 95039, USA

E-mail: scholin@mbari.org

Heidi M. Sosik
Woods Hole Oceanic Institution, Woods Hole, MA 02543, USA

E-mail: hsosik@whoi.edu

Sindy Sterckx
Flemish Institute for Technological Research (VITO), Boeretang 200, B-2400 Mol, Belgium

E-mail: sindy.sterckx@vito.be

C. A. Stock
Woods Hole Oceanographic Institution, Woods Hole, MA 02543, USA
E-mail: cstock@whoi.edu

David W. Townsend
School of Marine Sciences, University of Maine, Orono, ME 04469, USA

E-mail: davidt@maine.edu

Ken T. M. Wong
Strategic Research and Development, WL/Delft Hydraulics, The Netherlands

E-mail: ktmwong@graduate.hku.hk

Acknowledgements

Chapter 1 was supported by the Natural Sciences and Engineering Research Council and the National Research Council of Canada, the US Office of Naval Research, National Oceanic & Atmospheric Administration, the Canadian Foundation for Climate and Atmospheric Sciences and the US National Oceanographic Partnership Program. The author thanks reviewers for their comments and Don Anderson for many helpful interactions over the past decade.

Much of the work described in Chapter 2 was supported by the US Office of Naval Research, National Oceanographic Partnership Program and National Science Foundation. The authors thank John Kerfoot, Josh Kohut, Richard Gould and Robert Arnone for the vertical migration data, HF-radar image, MODIS satellite image and associated satellite-derived products. They express their appreciation to Frank Spada, who provided illustrations for several figures, and Derek Manov, who supplied photographs. Marcel Babin, John Cullen, Christy Herren, Cristina Orrico and Oscar Schofield provided valuable insights.

Much of the data and many of the ideas in Chapter 3 represent the collective effort of a large number of COOL collaborators. The authors especially thank Robert Arnone, Barbara Berg, Trisha Bergman, Shelly Blackwell, Robert Chant, Elizabeth Creed, Michael Crowley, Gary Fahnenstiel, Katja Fennel, Barbara Kirkpatrick, Alex Kahl, Josh Kohut, Kevin Mahoney, Chaya Mugdal, David Millie, Brad Pederson, Hugh Roharty, Emmilene Romana, Karen Steindinger, Patricia Tester and Alan Weidemann. Finally, ONR-optics, the ONR-NOAA-EPA ECOHAB Program and the US National Science Foundation are acknowledged for their generous support.

The authors wish to thank John Cullen and two anonymous reviewers for their constructive comments on early versions of Chapter 5. This chapter is the result of many years of work with many colleagues and students but the authors would like to specifically acknowledge Mary Jane Perry, Ron Zaneveld, Scott Pegau, Andrew Barnard, Stacey Etheridge, Wayne Slade and Grant Pitcher. None of this work would have been possible without the generous support of the ONR Code 32 Environmental Optics Program and NASA's Ocean Biology and Biogeochemistry Program.

The work in Chapter 6 has benefited from the support by the Natural Sciences and Engineering Research Council (Canada), the U.S. Office of Naval Research, and the U.S. National Aeronautics and Space Administration. It reflects insight from John Cullen, tommy Dickey, Andre Morel, Marcel Babin, Scott McLean, and in particular, Colin Roessler, who provided much appreciated editorial guidance as well.

The author thanks Yannick Huot, Heidi Sosik and Collin Roesler for their constructive comments on a previous version of Chapter 7, and Edouard Leymarie and Bernard Gentili for their help in preparing some of the figures. Finally, he is grateful

to the sponsors of the Habwatch workshop and to the programmes and organizations endorsing that event.

The author thanks Emmanuel Boss, Norm Nelson and Collin Roesler, who provided graphics for Chapter 8. She benefited greatly from Collin Roesler's perceptive thoughts about HABs and optical properties. Rob Olson, Michele DuRand and Rebecca Green offered constructive comments on a draft. She is also indebted to Ron Zaneveld for generously providing reference materials compiled over many years of dedication to biogeochemical interpretation of optical properties. The NSF Biocomplexity Program, ONR Environmental Optics Program, NASA Ocean Biology and Biogeochemistry Program, and a fellowship from the Woods Hole Oceanographic Institution (WHOI) Coastal Ocean and Ocean Life Institutes provided support during the work. This is WHOI contribution #11146.

The study reported in Chapter 9 was funded by the Belgian Science Policy Office within the framework of the STEREO BELCOLOUR project (SR/00/03) and the PADD-II AMORE-II project (EV/36/19B). The authors thank Bouchra Nechad, Christiane Lancelot, Arnold Dekker, Herman Gons, Walter Debruyn and the REVAMP project scientists for various discussions on optical remote sensing and phytoplankton optics. Mati Kahru and Robert Arnone are acknowledged as reviewers for many constructive comments and Collin Roesler, Marcel Babin and John Cullen are thanked as editors for many suggestions and for their efforts to strengthen the relevance of this review for HAB applications.

The author would like to thank the Seaver Foundation, the US National Science Foundation and the Office of Naval Research for supporting the research outlined in Chapter 10. Several colleagues, T. Stanton, M. Benfield, D. Van Holliday and M. Ohman, provided helpful discussions and information. He is also grateful to A. De Robertis for providing a critical review of the draft.

The following colleagues are gratefully acknowledged for sharing photographic material and unpublished results used in Chapter 11: D. Anderson, D. Caron, C. Elliott, D. Fries, Y. Fukuyo, A. Haywood, J. Jellett, M. Laycock, N. Lundholm, L. Medlin, P. Miller, J. Pancrazio, M. Quilliam and K. Steidinger. The National Ocean Service (NOS) does not approve, recommend, or endorse any product or material mentioned in this publication. No reference shall be made to NOS, or to this publication furnished by NOS, in any advertising or sales promotion which would indicate or imply that NOS approves, recommends, or endorses any product or material mentioned herein or which has as its purpose any intent to cause directly or indirectly the advertised product to be used or purchased because of NOS publication. This chapter was produced with technical assistance and support from the Institute for Marine Biosciences, NRC, Canada. Certain chapter elements are a contribution from the MARCOPOLI programme COAST research topics on Chemical Interactions: Function and Effects and Observation and Information for Coastal Management, conducted jointly between the Alfred Wegener Institute for Polar and Marine Research and GKSS within the Helmholz Society in Germany.

The BROS programme was sponsored by the European Community. The authors gratefully acknowledge T. Dickey for information and John Cullen for his very pertinent comments. They also thank Pierre Arzel and Michel Segonzac and acknowledge the assistance of Max Conte in preparing Chapter 12.

The author is very grateful to the following individuals and companies for permission to refer to their results and use their illustrations in Chapter 13: Andrew Brierley, Tommy Dickey, Larry Langebrake, Alain Norro, Oscar Schofield, Glen

Tarran, George Voulgaris, Hafmynd, University of South Florida (Centre for Ocean Technology), McLean Research, Autonomous Surface Vehicles Ltd and Webb Research Corporation. Thanks are also due to John Cullen for his helpful comments on the draft.

Chapter 14 is based on and has been enriched by discussions with Keith Thompson, John Cullen, Bob Bowen, Julie Hall, Worth Nowlin Jr and the entire Coastal Ocean Observing Panel, including Dagoberto Arcos, Bodo von Bodungen, Alfonso Botello, Lauro Calliari, Mike Depledge, Eric Dewailly, Juliusz Gajewski, Johannes Guddal, Hiroshi Kawamura, Coleen Moloney, Nadia Pinardi, Hillel Shuval, Vladimir Smirnov and Mohideen Wafar. The panel's work was supported by the Intergovernmental Oceanographic Commission of UNESCO and its Member States.

Emmanuele Di Lorenzo gave some very constructive criticism of an early draft of Chapter 15. This work would not have been synthesized without the prompting and encouragement of Colin Roesler and Marcel Babin, and their oversight of this endeavour was much appreciated. Chapter 15 was prepared while Peter Franks was supported by the NOAA ECOHAB program.

The authors of Chapter 16 gratefully acknowledge the support of the US ECOHAB programme, sponsored by NOAA, NSF, EPA, NASA and ONR. Data from the Gulf of Maine Regional Marine Research Program were also used. They thank Valery Kosnyrev for executing the climatological simulations described in Section 16.5. Olga Kosnyreva, Anita Norton and Sue Stasiowski all provided expert technical assistance in preparing the figures. They thank Bruce Keafer for his valuable insights and outstanding contributions to the observational efforts that made this study possible. They are also grateful for constructive reviews by two anonymous referees. This is WHOI contribution 11280 and US ECOHAB contribution 120. Correspondence and requests for materials to D. J. McGillicuddy Jr.

The authors of Chapter 17 are grateful to Marcel Babin and two anonymous referees for critical and helpful comments, and they thank Herbert Siegel for providing pictures of cyanobacteria.

The work reported in Chapter 18 was supported by the Croucher Foundation in the early stages and more recently by a Hong Kong Research Grants Council (RGC) group research project (HKU 2/98C and 1/02C), and in part by the Hong Kong Environment and Conservation Fund.

Chapter 19 was supported by the Office of Naval Research. Water quality data were provided by Florida International University's Southeast Environmental Research Center (SERC-FIU) Water Quality Monitoring Network, which is supported by SFWMD/SERC Cooperative Agreements #C-10244 and #C-13178 as well as EPA Agreement #X994621-94-0. Water quality data were also provided by the following agencies: Florida Environmental Protection Agency's Office of Water Quality STORET (Storage and Retrieval) Database, US Geological Survey Water Quality for the Nation, US Army Corps of Engineers, Southwest Florida Water Management District, South Florida Water Management District's DBHYDRO Database and the University of South Florida's ECOHAB Cruises. The nutrient data from the ECOHAB cruises were processed by Dr K. Fanning's laboratory at the University of South Florida.

Chapter 20 was partially supported by EU Project MFSTEP (Contract EVK3-CT-2002-00075).

The authors of Chapter 21 thank the organizers of the workshop on Real-time Coastal Observing Systems for Ecosystem Dynamics and Harmful Algal Blooms for their invitation to participate.

A special thanks regarding the HABWatch Workshop 2003 to: Lewis Conference International for the logistical organization, and more specifically Mrs Trudy Lewis. We also wish to thank ACRI ST for the support in website development and tutorial preparation (specifically Vincent Fournier Sicre and Grigor Obolensky).

Introduction

Harmful algal blooms are environmentally forced ecological phenomena that must be described and predicted as dynamic processes. Consequently, the ICES-IOC Working Group on Harmful Algal Bloom Dynamics [WGHABD] was established in 1994 with a mandate to outline the various physical, chemical and biological interactions important to HABs and to identify the main gaps in research. Recognizing that technologies for real-time observation and modelling of coastal ecosystem dynamics were rapidly being developed, the WGHABD, chaired by Kaisa Kononen, met in Dublin, Ireland, from 12–16 March 2001 to prepare a resolution for a workshop on "Real Time Observation Systems Applied to Harmful Algal Bloom Dynamics Studies and Global Ecosystem Functioning." Discussions during the meeting focused on many aspects of the observation and prediction of HABs; it was concluded that the time was right for a broad-based workshop. A resolution was prepared, outlining the scientific justification, content and format of the proposed workshop.

The resolution published by the ICES-IOC WGHABD was strongly endorsed by the international programs GEOHAB (Global Ecology and Oceanography of Harmful Algal Blooms) and GOOS (Global Ocean Observing System). Marcel Babin, member of the GEOHAB Scientific Steering Committee, and John Cullen, member of the Coastal Ocean Observations Panel of GOOS, partnered to implement the resolution by convening the "Workshop on Real-Time Coastal Observing Systems for Ecosystem Dynamics and Harmful Algal Blooms", also known as the "Habwatch" workshop. They assembled an Organizing Committee comprising James Aiken, Allan Cembella, Vincent Fournier-Sicre, Hervé Claustre, Tommy Dickey, Patrick Gentien, Joseph Hun-Wei Lee, Bengt Karlson, and Collin Roesler. The major sponsor of the event, the European Commission, was joined by the U.S. National Science Foundation, the Office of Naval Research (ONR and ONR-International Foreign Office), the European Space Agency, the Centre National d'Etudes Spatiales, the National Oceanic and Atmospheric Administration, the Centre National de la Recherche Scientifique, the Institut Français de Recherche pour l'Exploitation de la Mer, the Intergovermental Oceanographic Commission, and the Scientific Committee on Oceanic Research.

The workshop was held in Villefranche-sur-Mer (France) at the Observatoire Océanologique de Villefranche from 11 to 21 June, 2003. Eighty-nine participants attended the workshop (51 "students" and 38 lecturers and tutors). The students were selected among 130 candidates based on their profile (graduate student, postdoc, scientist, or manager), scientific interest and country of origin. Lectures and contributed talks were presented during morning plenary sessions to provide the underlying theory and example applications of different techniques used for autonomous observation of the sea. Tutorials in the afternoon introduced the participants to the techniques and instruments in a laboratory, field or computer-class setting. Lectures and contributed talks were recorded with voice and made available, together with most of the posters presented during a dedicated session, on the workshop website (http://www.obs-vlfr.fr/habwatch). A short synthesis of the workshop was published by Babin et al. (2005) in the magazine *Oceanography* of The Oceanography Society.

(http://www.tos.org/oceanography/issues/issue_archive/issue_pdfs/18_2/18.2_babin_et_al.pdf). This book presents the extended content of the lectures of the Habwatch workshop.

Introductory chapters (Chapters 1 to 3)

In the introductory chapter of this volume, John Cullen reviews the rationale for focusing on real-time observation and prediction of HABs and introduces a classification of harmful algal blooms that highlights the strengths of different strategies for detecting, characterizing, and ultimately forecasting HABs, depending on environmental context. A discussion of modelling approaches and technologies for observations leads to a prospectus for the transition from detection and prediction of HABs for research to a capability for operational monitoring and forecasting using real-time observing systems. Chapter 2, by Grace Chang and Tommy Dickey, provides an example-filled overview of the sensor systems, platforms and deployment strategies that have been and should be used for characterizing the dynamics of HABs. Their review clearly illustrated the need to consider the spatial and temporal scales of physical, chemical and biological variability, relevant to HABs, in the design of observing systems. The third and final overview chapter, by Oscar Schofield and colleagues, explains the utility of optical measurements in the detection and prediction of HABs, describing recent technological advances to support an optimistic assessment of optics-supported ecosystem research.

Optical tools (Chapters 4 to 10)

The last decade has been characterized by an explosion in the development of in situ optical instrumentation for use on satellites, aircraft, moorings, floats, gliders and powered autonomous vehicles. We now have the capability to measure optical properties that were only a dream less than a decade ago (absorption, volume scattering functions, diffuse attenuation coefficients, average cosines); sensors have miniaturized from hefty meter-long barrels to hockey-puck-sized disposable radiometers and fluorometers; single channel transmissometers and spectrally integrated PAR radiometers have evolved into hyperspectral absorption, attenuation and backscattering sensors and hyperspectral radiance and irradiance sensors. Bio-optical modelling has been leading the technological advances, resulting in the capability for describing enumerable optical proxies for biogeochemical parameters. What have these highly technical advances done for oceanographic research? The composition of seawater can now be optically discerned into its constituents: colored dissolved matter, phytoplankton, other organic particles including detrital matter, and inorganic minerals, so we can use autonomous sensors to distinguish terrestrial versus marine sources of dissolved matter, ecosystem size structure and even phytoplankton functional types. Optically-determined photophysiological parameters provide us with indicators of light and nutrient stress, photoacclimation and ultimately better estimates of primary productivity. And all of these on time and space scales ranging from microseconds to decades and millimeters to thousands of kilometers, depending upon the platform. While no platform/sensor suite has the capability for all time and space scales, operational observing programs are being designed so as to merge observations from one or two dimensions into fully resolved horizontal and vertical time series

(four dimensions) by combining observations from the array of possible platforms. This is particularly suited to the study of algal blooms in general and harmful blooms specifically, which are generally patchy in space and time, even when large in scale, and can dominate the optical properties or be only a minor constituent.

We begin the optics and remote sensing section of this book with a chapter by André Morel on optical theory (Chapter 4), which outlines the absorption and scattering processes and delineates the relationship between the optical properties of seawater and its constituents, including phytoplankton, the penetration of solar radiation into the ocean, and the resulting ocean color properties. The practical applications to this theoretical chapter are presented in three subsequent chapters. First, the applications and practical approaches to measuring the optical properties of seawater and its constituents are presented in Chapter 5 by Collin Roesler and Emmanuel Boss, with specific recommendations for optimizing observations and instrumentation for HAB detection. Second, the applications and practical approaches to measuring the optical properties of the light field within the water and leaving the water surface are presented in Chapter 6 by Marlon Lewis. Finally, the theory and application of remote sensing of ocean color to ecosystem dynamics and HABs is presented in Chapter 9 by Kevin Ruddick and co-authors. Optical measurements provide more than just estimates of constituents concentrations and compositions, they additionally can provide information on physiological rates. This is demonstrated particularly by the use of in vivo chlorophyll fluorescence, the basis for Chapter 7 by Marcel Babin. Bio-optical modeling provides the links between observations and descriptions of the dynamics of coastal ecosystems and HABs. The foundations of this approach are described by Heidi Sosik in Chapter 8. Finally, observational programs for ecosystem dynamics cannot hope to solve the HAB problems without information on the higher trophic levels. Chapter 10 by Jules Jaffe deals with imaging and acoustic approaches to in situ zooplankton sensing. Thus optical sensors and approaches, in combination with bio-optical modelling, may provide a key to observing and understanding critical HAB and ecosystem dynamics. The chapters in this volume provide a basis for the theory, observation and interpretation of those signals; the key to these approaches is understanding the limitations of the observations and the models that might exist, especially under the extreme ecological conditions induced by HABs.

Other autonomous observation techniques and platforms, and integration into observing systems (Chapters 11 to 14)

Exciting developments in the autonomous sensing of plankton dynamics are by no means confined to optical and acoustical techniques. In Chapter 11, Chris Scholin and colleagues describe sensitive and promising molecular methods that are being used for detecting harmful algae and their toxins, with appropriate treatment of the challenges that must be overcome to use these new techniques in automated observing systems. Their chapter ends with a description of a prototype system for automated detection of HABs and their toxins, a holy grail in HAB research.

Our consideration of the great potential for ocean sensing systems must be tempered by harsh realities, including biofouling, the inevitable consequence of deploying instruments in seawater. Michel LeHaître and colleagues (Chapter 12) review the process of biofouling and its influence on sensing systems, providing clear guidance

for making rational decisions about anti-fouling strategies and setting expectations for instrument systems deployed at sea.

Moving from innovative sensor systems to equally impressive advances in platforms that convey them, Gwyn Griffiths provides a thorough review of autonomous underwater vehicles (Chapter 13), a rapidly advancing technology that promises to provide unprecedented capabilities for interdisciplinary observations of the ocean interior. His presentation of strengths and limitations of each class of platform provides useful guidance for the development of ocean observation strategies, which will ultimately be implemented in operational ocean observing systems, discussed by Tom Malone in Chapter 14. This chapter, a transition between presentations on observations and modelling, provides a rationale for operational observation and prediction of HABs, strongly linked with plans for a coastal component of the Global Ocean Observing System. Ultimately, ocean observing systems must provide useful forecasts of ocean conditions, based on measurements and models.

Modelling and the user point of view (Chapters 15 to 21)

Measurements using new autonomous sensing technologies mounted on various platforms will improve the spatial and temporal description of coastal ecosystems. Nevertheless, observation will always be incomplete; space and time will never be fully covered and several crucial variables will not be measurable *in situ*. Many of these gaps, however, can be filled using coupled physical-biological ecosystem models. Besides being the most powerful and rigorous interpolation tools, models provide information about important variables and processes that cannot be measured directly. In addition to describing the present state of an ecosystem, modelling allows predictions to be made. These predictions, broadly defined as hindcasts, nowcasts and forecasts, are essential for understanding the biotic interactions within an ecosystem, testing scenarios, and releasing warnings in case of HABs. Six chapters are dedicated to modelling of HABs with special relevance to real-time autonomous observation. First, Chapter 15 by Peter Franks provides an introduction to the hydrodynamical processes accounted for by coupled physical-biological ecosystem modelling, and, more specifically, those affecting algal blooms. Chapters 16 to 19 present different modelling approaches. Chapter 16 by Dennis McGillicuddy and collaborators presents a physical-biological model expressed as a three-dimensional (3-D) advection-diffusion-reaction equation to represent the population dynamics of the toxic dinoflagellate *Alexandrium fundyense*. This model is applied in three different ways: (1) idealized settings to investigate fundamental processes, (2) climatological conditions to examine controls on the large-scale seasonal development of blooms in the Gulf of Maine, and (3) data-assimilative frameworks for hindcasting, nowcasting, and forecasting.

Chapter 17 by Wolfgang Fennel and Thomas Neumann presents a model consisting of a biogeochemical module embedded in a 3-D hydrodynamical module. To simulate species succession, it describes explicitly three functional groups: diatoms, flagellates and blue greens (cyanobacteria). Simulating the seasonal succession is important, because some cyanobacteria can fix atmospheric nitrogen if the nitrate in the water is depleted, providing a competitive advantage that can lead to blooms. The biogeochemical module is embedded in a full 3-D circulation model, forced with

historical data on meteorological conditions, river run-off and nutrient loading. As illustrated in the chapter, it can be used for Baltic Sea scenario experiments, where cyanobacterial blooms commonly occur. Chapter 18 by Joseph Lee and co-authors is a review of deterministic water quality and hydrodynamic models for the study of ecosystem dynamics and fisheries management. The major features of the detailed water quality model (incorporating key carbon and nutrient cycles) are (1) to predict short term trends in dissolved oxygen dynamics in response to nutrient loading and hydro-meteorological conditions, (2) to effectively integrate 3-D hydrodynamic models and water quality models to give quantitative determination of carrying capacity of fish farms, and (3) to use hydrodynamic models to unravel the cause of major HAB outbreaks. The EcoSim model presented in Chapter 19 by Paul Bissett and collaborators is an attempt to model the interaction between phytoplankton ecophysiology and inherent optical properties in a way that allows feedback between light absorption and growth, including nutrient limitation. It focuses on both phytoplankton specific absorption changes and non-stoichiometric nutrient uptake and assimilation in order to drive changes in species-specific mass and optical properties, as well as bulk mass and optical properties. This allows validation of ecological simulations using physical measurements of absorption and scattering and radiance. This focus on directly simulating the inherent optical properties may eventually provide a critical link between HAB nowcast/forecast efforts and data assimilation models that seek to use optical observations from satellite measurements and in-water autonomous sensors. Chapter 20 by Nadia Pinardi and collaborators goes one step further and shows how data assimilation techniques are used to combine real-time observations with a model to produce the best predictions of the state of ocean and associated biochemical fields. The basic concepts of data assimilation are exposed. Basin-scale multivariate data assimilation is illustrated with the Mediterranean Forecasting System which includes remote sensing and *in situ* real-time observations. The final Chapter of this book, 21, prepared by Grant Pitcher and co-authors, reviews all the technologies and approaches explored in the previous chapters, providing a real world context for observations and modelling and examines how they meet the needs and expectations of users, including biologists, managers, fish farmers, and many other members of coastal communities.

1

Observation and prediction of harmful algal blooms

J. J. Cullen

1.1 Introduction

Phytoplankton are the principal source of food for life in the sea, and the dynamics of phytoplankton communities are centrally important to the structure and function of pelagic ecosystems. Life forms of phytoplankton have evolved to exploit different regimes of turbulence and hence nutrients (Margalef, 1978) but by their nature, planktonic food webs are structured by grazing and other biological interactions (Kiørboe, 1993; Smetacek, 1998). Consequently, physical processes determine the structure of pelagic ecosystems, directly by their influence on the growth of phytoplankton and indirectly by affecting food-web interactions (Cullen et al., 2002). Phytoplankton dynamics are particularly variable in coastal ecosystems because physical, chemical and biological influences are forced in complex ways: flows of water are constrained by coastlines and shallow, highly variable bathymetry; nutrients are supplied from terrestrial and benthic sources as well as from deeper water offshore; and benthic and intertidal communities actively interact with those in the water column. The increasing concentration of human activities in the coastal region (Nicholls and Small, 2002) and the multifaceted importance of coastal ecosystems to the sustainability of the planet (Costanza et al., 1997) ensure the prominence of biological variability in coastal ecosystems as an environmental concern.

Transient proliferations of phytoplankton, referred to as blooms, are common and natural in coastal environments. In pelagic systems, such outbreaks are the principal means by which flows of matter and energy escape the tightly coupled microbial loop to feed higher trophic levels and export organic matter to deeper waters and the bottom as sinking particles (Michaels and Silver, 1988; Legendre and Le Fèvre, 1989; Kiørboe, 1993). Algal blooms are thus integral to planktonic ecosystem dynamics and biogeochemical cycles. However, some phytoplankton blooms in coastal or brackish waters are perceived as harmful. They can cause massive fish kills, contaminate seafood with toxins, and alter ecosystems in ways that humans do not like. These are harmful algal blooms (HABs), a generic term that glosses over that facts that not all HAB species are classified as algae and some species cause harmful effects when present in low cell densities, nothing like a bloom (Smayda, 1997*b*). A thorough review of the HAB problem was recently prepared as part of the Science Plan for an international research programme on HABs (GEOHAB, 2001). As this chapter shares many objectives with the GEOHAB Science Plan, some material from that document is repeated here, with added emphasis on observation and prediction of HABs in the context of real-time observation systems.

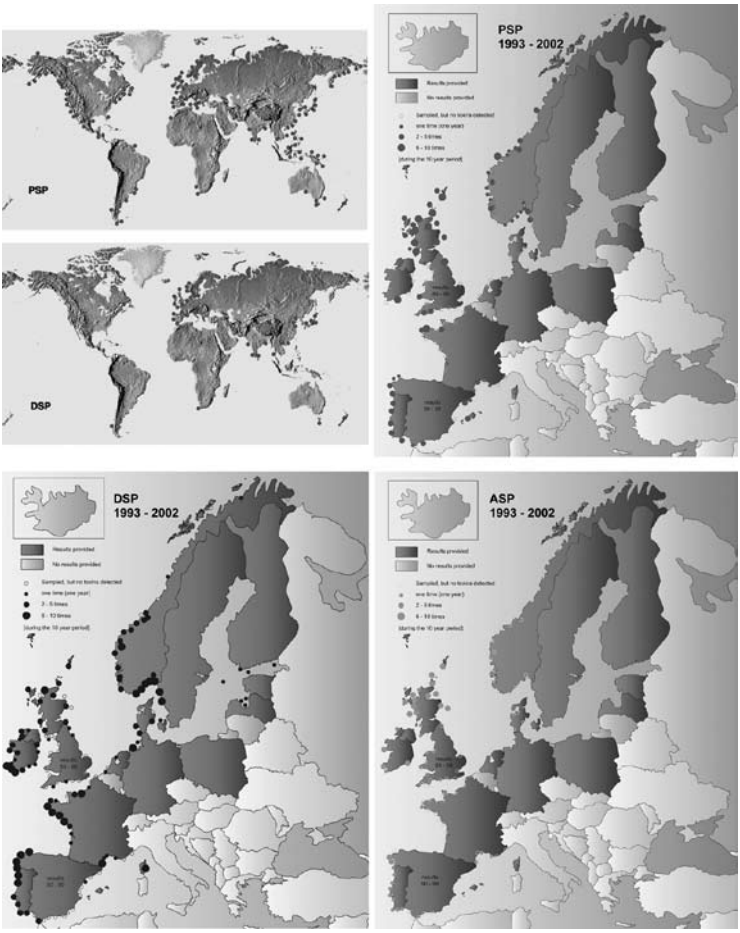

Figure 1.1
Maps of reported occurrences of HAB toxicity demonstrate many aspects of the HAB problem. Top left: global distributions of reported paralytic shellfish poisoning (PSP) and diarrhetic shellfish poisoning (DSP) events show that harmful effects are widespread. Regional patterns are to some extent related to the presence of systems for monitoring and reporting; absence of reports does not necessarily mean that HABs have not occurred (US National Office for Marine Biotoxins and Harmful Algal Blooms). Other panels: Occurrences of PSP, DSP and amnesic shellfish poisoning (ASP) in ICES countries[2] from 1993–2002 show that some locations are affected by several types of HAB, whereas certain types of toxicity are more restricted. None of these maps can show the diversity of species that generate these effects (Table 1.1). The Coastal Module of the Global Ocean Observing System (IOC, 2003) is being established to facilitate more effective monitoring of HABs and other phenomena in coastal environments worldwide, so temporal and spatial patterns can be resolved and explained.[3]
Source: Harmful Algae Event Data Base (HAEDAT), © IFREMER.

[2]ICES (International Council for the Exploration of the Sea) member countries are Belgium, Canada, Denmark, Estonia, Finland, France, Germany, Iceland, Ireland, Latvia, Netherlands, Norway, Poland, Portugal, Russian Federation, Spain, Sweden, United Kingdom and United States.
[3]http://www.ifremer.fr/envlit/documentation/dossiers/ciem/aciem-c1.htm

1.1.1 Diversity of HABs

The great diversity of HAB species and effects (Table 1.1, Figure 1.1) precludes effective generalization. Still, harmful algae are commonly classified in two groups:

- toxin producers, which can contaminate seafood, kill fish, or cause health problems in humans through direct exposure to the toxins;
- high-biomass producers, which can kill or damage marine life after reaching dense concentrations, for example by causing anoxia after collapse of a bloom or by chronically shading benthic vegetation.

Blooms of high-biomass producers also affect tourism and recreation by discolouring coastal waters and generating noxious foams, slimes or odours. Even this broad classification of harmful algae is not exclusive: several HAB species that are toxic also form dense blooms. To compromise generalization further, closely related species can occur in high concentrations in some regions but not others. For example, *Alexandrium* discolours water in the Gulf of St Lawrence but generally forms only low-density blooms in the Gulf of Maine, although it contaminates shellfish in each environment (Anderson, 1997; Weise et al., 2002). Other species exhibit variable toxicity, for reasons that are as yet unresolved (e.g. Granéli et al., 1993; Scholin et al., 2007 – Chapter 11 this volume). Formal definitions of algal blooms are thus neither practical nor particularly helpful (Smayda, 1997*b*); in this chapter, bloom is synonymous with an increase in the abundance of a phytoplankton species above a background concentration, in either space or time.

Considered broadly, HABs are a grab-bag of phenomena with little in common except for effects that humans perceive as being harmful. Due to their diversity, no

Table 1.1 Some deleterious effects caused by harmful algae in coastal and brackish waters

Effect	**Examples of causative organisms**	
Human health		
Paralytic shellfish poisoning (PSP)	Dinoflagellates	*Alexandrium* spp., *Pyrodinium bahamense* var. *compressum, Gymnodinium catenatum*
	Cyanobacteria	*Anabaena circinalis*
Diarrhetic shellfish poisoning (DSP)	Dinoflagellates	*Dinophysis* spp., *Prorocentrum* spp.
Neurotoxic shellfish poisoning (NSP)	Dinoflagellates	*Karenia brevis*
Amnesic shellfish poisoning (ASP)	Diatoms	*Pseudo-nitzschia* spp.
Azaspiracid shellfish poisoning (AZP)	Dinoflagellate	*Protoperidinium crassipes**
Ciguatera fish poisoning (CFP)	Dinoflagellates	*Gambierdiscus toxicus*
Respiratory problems and skin irritation, neurological effects	Dinoflagellates	*Karenia brevis, Pfiesteria piscicida*
	Cyanobacteria	*Nodularia spumigena*
Hepatotoxicity	Cyanobacteria	*Microcystis aeruginosa, Nodularia spumigena*

(Continued)

Table 1.1 *(continued)*

Effect	Examples of causative organisms	
Natural and cultured marine resources		
Hemolytic, hepatotoxic, osmoregulatory effects and other unspecified toxicity	Dinoflagellates	*Gymnodinium* spp., *Cochlodinium polykrikoides, Heterocapsa circularisquama, Pfiesteria piscicida, Gonyaulax* spp.
	Raphidophytes	*Heterosigma akashiwo, Chattonella* spp., *Fibrocapsa japonica*
	Prymnesiophytes	*Chrysochromulina* spp., *Phaeocystis pouchetii, Prymnesium* spp.
	Cyanobacteria	*Microcystis aeruginosa, Nodularia* spp.
Negative effects on feeding behaviour	Pelagophytes	*Aureococcus anophagefferens*
Hypoxia, anoxia	Dinoflagellates	*Prorocentrum micans, Ceratium furca*
Mechanical damage	Diatoms	*Chaetoceros* spp.
Gill clogging and necrosis	Prymnesiophytes	*Phaeocystis* spp.
Tourism and recreational activities		
Production of foam, mucilage, discoloration, repellent odour	Dinoflagellates	*Noctiluca scintillans, Prorocentrum* spp.
	Prymnesiophytes	*Phaeocystis* spp.
	Diatoms	*Cylindrotheca closterium*
	Cyanobacteria	*Nodularia spumigena, Aphanizomenon flos-aquae, Microcystis aeruginosa, Lyngbya* spp.
Marine ecosystem impacts		
Hypoxia, anoxia	Dinoflagellates	*Noctiluca scintillans, Heterocapsa triquetra*
	Diatoms	*Skeletonema costatum*
	Prymnesiophytes	*Phaeocystis* spp.
Negative effects on feeding behaviour and reduction of water clarity	Pelagophytes	*Aureococcus anophagefferens, Aureoumbra lagunensis*
	Dinoflagellates	*Prorocentrum minimum*
Toxicity to marine organisms, including invertebrates, fish, mammals and birds	Dinoflagellates Diatoms	*Karenia brevis, Alexandrium* spp. *Pseudo-nitzschia australis*

Sources: Zingone and Enevoldsen (2000) as modified by GEOHAB (2001), with further modifications.

*Recently described by James et al. (2003).

one cause for HABs can be found, and no single strategy for detection or prediction will suffice. The major challenge for understanding HABs to support management and mitigation is to describe, for each species, what conditions promote its development instead of (or in concert with) other phytoplankton (GEOHAB, 2001).

1.1.2 Harmful algae and environmental variability

It is axiomatic that HAB species have adapted to many niches (suites of ecological factors that determine their distributions and activities), and that the matches between the adaptations of harmful species and oceanographic variability are good enough to ensure their survival from year to year, and their proliferation when conditions are conducive. The great diversity of HABs – with respect to taxonomy, region, hydrographic regime and harmful effects – reflects in a fundamental way that environmental forcing has selected for a wide variety of harmful algae, on timescales from evolutionary to days and spatial scales from ocean basins to bays. For each harmful species, the challenge is to unlock its secrets: why does it bloom or exert its harmful effects in one situation and not in another? The answers lie in detailed information about the distributions and activities of phytoplankton species in relation to the oceanographic and ecological processes that influence them. This should be complemented with experimental results describing how each species responds to these environmental factors, and with models – either conceptual or mechanistic – that describe the principal controls on population dynamics of the target species in relation to the phytoplankton community.

Even though it is an enormously daunting task to resolve the complex interactions that determine the population dynamics of a phytoplankton species in coastal or estuarine waters, significant progress has been made through the careful work of insightful researchers. The contributions of Ramón Margalef (e.g. Margalef, 1978; Margalef et al., 1979) are widely regarded as a seminal influence. Considering life forms of phytoplankton, that is their gross morphological and physiological traits, Margalef and colleagues described how functional groups of phytoplankton (with representative species identified) could be plotted against axes representing nutrient availability and the intensity of turbulence (Margalef, 1978). The typical seasonal succession of phytoplankton, from fast-growing diatoms to motile dinoflagellates, corresponds to the temporal transition from a well-mixed, nutrient-rich water column during winter to a nutrient-poor, stratified environment later in the year. This model was later modified to include a 'red-tide sequence', a trajectory parallel to the typical succession, but in environments with higher levels of nutrients (Figure 1.2). Using a similar approach, Colin Reynolds and colleagues (reviewed briefly by Reynolds and Smayda, 1998; revisited by Smayda, 2002) developed 'habitat matrices' that relate variability of phytoplankton species composition in lakes to several axes of variation, still dominated by nutrients and turbulence.

Summarizing efforts to describe variability in phytoplankton communities, Reynolds (2002) concluded that the dynamics of individual species are unpredictable, except on the scale of days, and only then if based on full knowledge of initial distributions. However, he felt that at a higher lever of generality (i.e. for functional groups or trait-based associations of phytoplankton), responses of phytoplankton communities to environmental conditions would be increasingly predictable. A key link to predictability is that variability in community composition is 'explicable in retrospect' (Reynolds, 2002). That is, the confidence we can have in predictions of phytoplankton communities under future scenarios depends largely on how well the same conceptual models explain historical variability of phytoplankton.

As the ecological implications of morphological (Karp-Boss et al., 1996), physiological and behavioural (Cullen and MacIntyre, 1998) adaptations of harmful algae become better understood, new and more powerful definitions of functional groups will emerge, guiding how phytoplankton species should be classified, and which

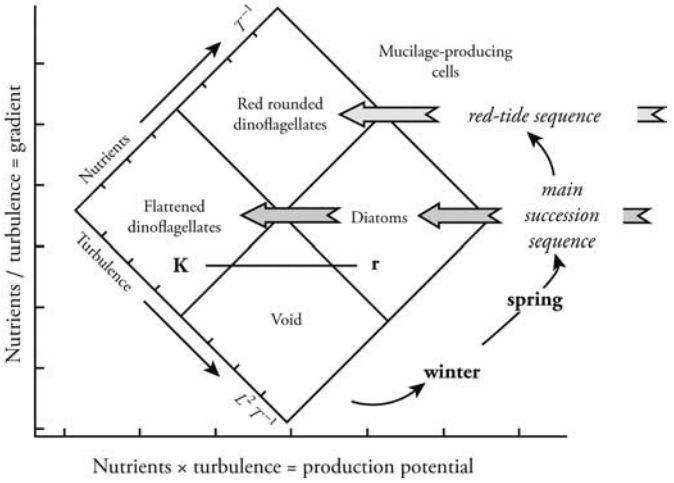

Figure 1.2
The 'Mandala' redrawn from Margalef et al. (1979). This diagram, rich with information on phytoplankton succession, is extremely useful for developing generalizations about relationships between life forms of phytoplankton and hydrographic conditions, particularly during seasonal succession. The 'red-tide sequence' (development of a high-biomass HAB) can be viewed as related to elevated nutrients, independent of changes in turbulence regime. This conceptual model it is not directly applicable to real-time observation and prediction of HABs. Nonetheless, Margalef's framework is a cornerstone of phytoplankton ecology and it should support the roots of any model of seasonal phytoplankton community dynamics as influenced by local conditions.

environmental factors must be considered, when trying to predict their dynamics. These more detailed classifications should lead to improvements in predicting the probability of HAB occurrence for a particular location and time, given measured or modelled scenarios of physical and chemical conditions. Moving beyond probabilities of occurrence, the dynamics of HABs may be predictable over the course of days, given initial data on species distributions from coastal observation systems (Johnsen et al., 1997; Stumpf et al., 2003). Development and testing of any predictive model will thus require effective systems for observing the distributions of phytoplankton, including HABs, in the context of coastal ecosystem dynamics.

1.1.3 Observation and modelling in the 'old days'

Observations of HAB dynamics have seldom been adequate to describe the three stages of an event: development, maintenance and decline (Tester and Steidinger, 1997). So, much of what is known about HABs comes from careful analysis of limited data, with much reliance on inference. Comprehensive observations of events preceding a bloom are particularly rare, because the unpredictability that justifies research on harmful algae also precludes the scheduling of cruises to coincide with HABs. The unpredictable nature of HABs has led to facetious acceptance of the maxim that the best way to prevent them is to schedule a major research programme to study them.

Some of the most effective studies of HABs and other phytoplankton blooms in coastal and estuarine waters come from regions where conditions are similar year to year, and sustained observations have shown relationships between the population dynamics of phytoplankton species and hydrographic conditions. Several are described in this volume. A study by Tyler and Seliger (1978, 1981) is an excellent example of observation and modelling in the days before autonomous observation systems and three-dimensional coupled models. The approach they used is just as appropriate today as it was 25 years ago. The best available sampling techniques were used to characterize the distributions of the target species (*Prorocentrum minimum*, formerly *Prorocentrum mariae-lebouriae*) in relation to light and hydrographic conditions. In turn, the physiological and behavioural responses of these motile algae to the same environmental factors were characterized experimentally. By considering the interaction of physiology and behaviour of the phytoplankton with the vertical structure of the water column and seasonal transport by estuarine circulation, selection for the target species was explained and the general features of population dynamics predicted. All this was done with limited information. Still, it took 128 ship days during 40 cruises over two years (plus hundreds of hours counting cells under a microscope) to acquire the data for describing the dynamics of *Prorocentrum* in Chesapeake Bay (Tyler and Seliger, 1978). Subsequently, much more has been learned about the dynamics of *Prorocentrum minimum* in Chesapeake Bay and elsewhere (Heil et al., 2005), but the validity of Tyler and Seliger's multifaceted approach (observations, experimentation, modelling, validation) has not diminished.

Many of the old limitations on coastal ecological research are vanishing. As described in this volume, advances in observation technology and modelling, supported by greatly enhanced capabilities for communications and computing, are transforming the nature of ecological investigation from a labour-intensive effort to collect precious data, interpreted largely through inference, to a process in which unprecedented quantities of data and model output must be managed effectively to yield useful information. Still, it is essential to remember that the fundamental principles of the research will not change. Species must be identified and their physiological, behavioural and ecological interactions must be considered in the context of oceanographic processes to understand and describe the population dynamics of harmful species as members of phytoplankton communities. Insights from the 'old days' of the twentieth century will certainly help to guide HAB research when the widespread availability of observations threatens to mask the fundamental need for focused questions about controls on the population dynamics of the causative species.

1.2 Detection and prediction for monitoring and management of HABs

The HAB problem is rich with unanswered questions that will occupy scientists for decades. More immediately, it represents threats to coastal ecosystems and activities, and these must be dealt with now (Malone, 2007 – Chapter 14 this volume). Authorities responsible for environmental protection, economic development and public health must develop and implement plans for the monitoring and management of HABs (Anderson et al., 2001; Andersen et al., 2003). These plans may include:

- Strategies for monitoring coastal waters for detection of HABs, including their effects, with an aim to develop early warning systems.
- Development of a modelling system for short-term forecasts of HAB movements.

- Integration of observations, forecasts and communications into an action plan for rapid response to HAB events, including criteria for initiating strategic sampling, beach closures, shellfish bans and communication to the public.
- Mitigation strategies, from direct actions to neutralize blooms or minimize their effects (e.g. application of clay or movement of fish cages) to long-term nutrient management plans or bans on ballast water discharges.
- A programme of research to predict the likelihood of HABs, i.e. changes in their frequency or impacts, in response to human activities or climate change.
- Integration of monitoring, predictions and communications in support of policy decisions.

All aspects of monitoring and management require the means to detect, and broadly to predict, the occurrences and impacts of HABs on scales from days to decades. These challenges can only be met through fundamental scientific research, but there is no benefit in conducting this research independently from ongoing monitoring programmes.

In some jurisdictions, and in the minds of many scientists, basic research has been considered to be distinct from routine activities such as monitoring. As a consequence, monitoring activities may be specifically excluded from funding programmes for research and, in turn, sustained sampling programmes established for research are regularly threatened with cuts or termination, even though they have proved invaluable for describing long-term trends in ecosystems (e.g. Tont, 1976; Roemmich and McGowan, 1995; Fromentin and Planque, 1996; Karl et al., 2001). With the advent of real-time coastal observation systems with capabilities for environmental forecasts, the goals of scientists and coastal managers are aligning, as are the means for attaining these goals: real-time detection of HABs is essential for early warning; prediction of dynamics with forecast models supports rapid response and mitigation; and sustained observations (equivalent to monitoring) are required to develop and validate the long-range models of HAB probabilities needed to develop coastal management strategies.

The conclusion is that the research topics of real-time detection, sustained observations and quantitative prediction of HABs must be integrated with the operational requirements for monitoring and management. To justify the large investment in research and infrastructure, results from real-time coastal observation systems must be accessible, understandable and useful to a broad range of user groups. Research must be more closely coordinated with operational oceanography (Chapter 14), which will have to change with time to serve a wide range of users. This will require restructuring, not only in the way coastal research is organized, but also in the way scientists communicate their results – a healthy challenge.

1.3 Classification of HABs for observation systems

No observing system can provide the oceanographic ideal of continuous and synoptic measurements of physical, chemical and biological properties and processes, so efforts must be made to match observations and their scales to the HAB phenomena of interest (Franks and Keafer, 2003; Smayda, 2003; Chang and Dickey, 2007 – Chapter 2 this volume). This is no easy task, however. The range of scales for HABs is immense (Hallegraeff, 2003). Some may be confined to inlets (Seliger et al., 1970), others are

observed over large expanses (Kahru et al., 1994). Blooms may come and go over days to weeks, often terminated by wind events which may transport the algae offshore or cause direct mortality from turbulence (but see Smayda, 2002). Other blooms can persist for months, for example *Karenia brevis* blooms off Florida (Tester and Steidinger, 1997), or even years (*Aureoumbra lagunensis* in Laguna Madre, Texas; DeYoe and Suttle, 1994). Many are found close to the surface, not surprisingly as discoloration of the water draws attention. Some of these can be traced to subsurface layers, brought near the surface by physical transport, including frontal processes (McMahon et al., 1998) and vertical mixing (see Section 1.5.1). Other surface blooms develop through vertical migration of phytoplankton (Oliver, 1994; Kamykowski, 1995). A coarse classification of HABs can be useful as an initial guide to identify relevant scales and appropriate observation strategies for local or regional observation programmes. The classification is summarized here, with suggestions for observation strategies.

1.3.1 Widespread HABs

Generally, a harmful algal bloom must have widespread effects to attract the attention of the scientific community and the general public. Discoloured water, dead fish and noxious foam, scums or aerosols over hundreds of kilometres of coastline make the news, and with good reason. The blooms are extensive and the algae are easily identified as the cause of harm. The features that make such blooms noteworthy are also useful for classification and the design of strategies for early warning, monitoring and prediction: relatively large extent; persistence; and, often but not always, dominance of the phytoplankton by one species. Three somewhat idealized categories within this loose classification can be proposed.

1.3.1.1 Extensive, progressive coastal blooms

Some of the most challenging oceanographic and ecological questions are raised by extensive blooms, nearly monospecific and often toxic, that appear in a coastal waters and progress along the shoreline, leaving a trail of shellfish closures, ravaged fish farms or spoiled beaches. Some examples include blooms of *Karenia brevis* in the Gulf of Mexico (Tester and Steidinger, 1997; Stumpf et al., 2003), *Karenia mikimotoi* (formerly *Gyrodinium aureolum* or *Gymnodinium mikimotoi*) in northern European shelf waters (e.g. Holligan, 1979; Dahl and Tangen, 1993; Gentien, 1998), the toxic bloom of *Chrysochromulina polylepis* in Scandinavian waters in 1988 (Granéli et al., 1993; Gjøsæter et al., 2000), blooms of *Heterosigma* in the Strait of Georgia and adjacent waters in Canada (Taylor and Haigh, 1993), and the dramatic bloom of *Karenia digitata* in Hong Kong waters in April 1998 (Lee et al., 2007 – Chapter 18 this volume).

Hypotheses about bloom dynamics focus on the processes of initiation, transport and interactions of populations with surface circulation (Tester and Steidinger, 1997). Assessment of impacts requires information on transmission of harm (e.g. decay leading to anoxia, direct contact, toxin transfer through ingestion, production of aerosols), how these processes relate to the distributions of harmful algae, and environmental influences on the production of noxious effects.

Many environmental properties must be measured for effective early warning, monitoring and prediction. When conditions permit, remote sensing of ocean colour and sometimes sea surface temperature from satellites and aircraft can provide key information on distributions and transport (Stumpf et al., 2003; Ruddick et al., 2007 – Chapter 9 this volume), especially when supplemented by observation

networks that include direct sampling (Johnsen et al., 1997; Tangen, 1997). Even if surface distributions of developed blooms are resolved with remote sensing, early stages and subsurface distributions must be described by other means. In particular, vertical distributions of phytoplankton should be well resolved because the interaction of swimming, sinking or floating with frontal features (Franks, 1997), aggregation of seed populations in subsurface layers near the pycnocline (McMahon et al., 1998), and changes of behaviour in mixed waters landward of a front (Dahl and Tangen, 1993; Gentien, 1998), possibly associated with nutrition (Cullen and MacIntyre, 1998), all may be important in initiation, maintenance and transport of extensive, progressive, coastal blooms. Consequently, for early warning and monitoring, observation systems must resolve vertical distributions of phytoplankton in relation to temperature, salinity and currents, and they must have the means to identify target species *in situ*. Nutrient availability can influence toxicity (Bates, 1998; Cembella, 1998) and depletion of nutrients can terminate a bloom. So, for effective monitoring and modelling, the nutrient regime should also be assessed.

Progressive coastal blooms move with coastal currents and can appear or disappear on the timescale of days. Effective monitoring thus requires nearly continuous measurements, and mitigation responses (such as the movement of aquaculture cages) require communications in near real time (Tangen, 1997). Strategies for management, such as controls on coastal nutrient loading or site selection for aquaculture, depend on long time series of observations to determine the relationships between environmental variability, human influences, bloom occurrences and their impacts. Sustained deployment of real-time observation systems is thus ideally suited for observation and prediction of extensive, progressive coastal blooms.

1.3.1.2 Extensive blooms in open waters

It has long been recognized that phytoplankton blooms in open waters are part of the natural ecology of the oceans. The phenomenology of some, such as the vernal diatom bloom in temperate waters (Sverdrup, 1953), surface aggregation of *Trichodesmium* during calm periods (Capone et al., 1998), *Phaeocystis* and diatom blooms associated with receding ice edges (Lancelot et al., 1998) and the green waters of upwelling systems (Barber and Smith, 1981) are fairly well understood. The root causes of dramatic expanses of milky water from coccolithophores are open to informed speculation (e.g. Olson and Strom, 2002) and examination through numerical modelling (Merico et al., 2004). Satellite imagery[4] reveals many other blooms in open waters that will remain curiosities until they are studied further. In the context of this chapter, interest is focused on harmful or potentially harmful blooms that occur in open waters in semi-enclosed seas or near coasts, where they can influence coastal ecosystems and be affected by terrestrial inputs of fresh water and nutrients. The Baltic, North Sea and Bohai (China) are exemplary. It serves little purpose to apply this classification strictly; extensive blooms in open waters are grouped so the potential forcing functions – climate change and nutrient sources – can be discussed along with strategies for observing and predicting ecological responses to these influences.

Open water HABs can cause problems when they impinge on the coast, delivering scums, foams or toxicity. For example, summer blooms of nitrogen-fixing cyanobacteria in the Baltic Sea are common (Sellner, 1997). The hepatotoxic *Nodularia spumigena* is conspicuous; during the latter stages of a bloom, filaments form highly visible aggregates at the surface that can be detected from space (Kahru et al., 1994). Nitrogen

[4]For example: http://visibleearthnasa.gov/

enrichment as well as toxicity on landfall are concerns. Blooms of *Phaeocystis* in the North Sea can deliver prodigious quantities of noxious foams to beaches. Hallegraeff (2003) reviews the relation between eutrophication and occurrences of *Phaeocystis* and other HABs.

Although there is a need to predict the trajectories of open water blooms that may impinge on coastlines, observation and prediction of extensive HABs in open waters tends to focus on their importance as ecological indicators and modifiers of the marine or brackish water environment. Particular emphasis is placed on the interactions of climate, circulation, nutrient inputs and algal physiology. Proposed scenarios include:

- Springtime blooms of *Phaeocystis* in the North Sea can be related to discharges from seven major west European rivers, which introduce new and unbalanced sources of nutrients, including excesses of nitrate and phosphate compared with silicate (Lancelot, 1995; Riegman, 1998).
- Relatively cool and windy conditions favoured the vertically migrating, depth-seeking *Heterocapsa triquetra* over cyanobacteria in the entrance to the Gulf of Finland during summer 1998 (Kononen et al., 2003).
- Eutrophication of the Baltic leads to deep water hypoxia, liberation of phosphorus from sediments, and hence decreased nitrogen:phosphorus ratio in the nutrients supplied to the surface layer; N-fixing cyanobacteria, including toxic bloom-formers, are favoured (discussed and critically evaluated by Bianchi et al., 2000).
- The flow of saline, oxygen depleted water into the Baltic in 1993 triggered the eastward expansion of *Nodularia spumigena* blooms into the Gulf of Finland. *Nodularia* was previously absent due to relatively high N:P ratios, and thus reduced competitive advantage for N-fixers. Salty water increased stratification in the bottom layers; oxygen concentrations decreased, P was liberated from sediments, water-column N:P decreased, and the N-fixing cyanobacteria bloomed (Kahru et al., 2000).

Year-to-year comparisons of bloom dynamics were central to the development and testing of these scenarios. Observation systems, including monitoring programmes, have thus contributed very significantly to these and other studies of algal blooms in open waters. Remote sensing figures prominently, particularly because cyanobacterial blooms can be detected with satellites (AVHRR) that have been deployed for decades (Kahru, 1997). Under-way measurements from ferries[5] have been incorporated into a system that now can describe in some detail the variability, in space and time, of blooms in Scandinavian waters.

For extensive blooms in open waters, the needs for observation and prediction include long records that can characterize fundamental changes in both the physico-chemical environment and the ecological system, including the frequency, duration and extent of blooms. Predictions could include long-term trends in bloom frequency and yearly projections of probabilities. Except for properties like N:P ratios and deep-water salinity and oxygen, periodic surveys are inadequate to develop and test predictive models, because transient and patchy events cannot be resolved. The strategy of routine continuous transects from ferries and remote sensing, supplemented with cruises to monitor physical, chemical and biological conditions, appears to be on the right track. Although the ideal of continuous and synoptic observations cannot be attained, the data can be used to describe the variability of phytoplankton with unprecedented temporal and spatial resolution.

[5]Alg@line: www.itameriportaali.fi

Smaller than the Baltic Sea, but also subject to HABs and strong anthropogenic influences, the Seto Inland Sea in Japan has been studied intensively to resolve environmental influences on the frequency, species composition and impacts of HABs (Okaichi, 1997). Although near-shore processes figure prominently in many studies, the influences of eutrophication and nutrient controls on long-term trends of bloom frequency and composition are central questions (Yamamoto, 2003), as they are in the Baltic. Research has been backed by a broad range of monitoring, including records of water clarity (Secchi depth) dating back more than 60 years (Yanagi and Okaichi, 1997). These records are an especially useful resource, a prime example of long-term optical monitoring of environmental variability in coastal waters (Cullen et al., 1997). During the 1990s, a programme for high-resolution marine biogeochemical sampling from ferries was used in East Asian marginal seas (Harashima et al., 1997). Ferry tracks included a transect along the Seto Inland Sea.

Examples from Japan and the Baltic illustrate the great value of sustained observations, and the potential uses of continuous measurements, such as those from ferries. The capability for viewing observations in real time is perhaps less important than in near-shore environments, but timely knowledge of offshore events can guide sampling and provide information for early warning systems.

1.3.1.3 Blooms in upwelling systems

Phytoplankton proliferate when hydrographic conditions deliver nutrients to a well-lighted surface layer in the absence of deep vertical mixing, so upwelling systems generate blooms by their nature, forming the bases of the most productive ecosystems in the ocean (Ryther, 1969; Barber and Smith, 1981). Because the wind-driven delivery of nutrients to the surface layer and the coupled transport of developing blooms offshore are dominant influences on phytoplankton population dynamics in coastal upwelling systems, blooms in upwelling regimes are prime examples of phytoplankton dynamics under oceanographic control. Of course, not all blooms in upwelling systems are the same: complex interactions among large-scale circulation, the chemical composition of upwelled water and local circulation (e.g. Tont, 1976; Grantham et al., 2004), plus varying timescales of change of wind-driven circulation (Moloney et al., 1991; Carr, 1998), and frontal dynamics (Franks, 2006 – Chapter 15 this volume) all influence the development of phytoplankton populations and thus the species composition of blooms and their effects on coastal ecosystems.

Upwelling systems, such as those off the coast of Portugal and Spain, Peru, the west coast of the United States and Mexico, West Africa, Southern Africa, Japan and Australia, are affected by HABs (GEOHAB, 2001). Effects include anoxia associated with accumulation and degradation of organic material from blooms, and toxicity associated with blooms of toxic algae brought into contact with shellfish, for example. Wind-driven transport is a major theme; it can have a direct influence by bringing populations in contact (or not) with shellfish (Fraga et al., 1988; Franks and Anderson, 1992*a*), or in setting up circulation patterns that encourage the development of migrating populations (Weise et al., 2002) or the concentration of organic matter leading to anoxia (Pitcher et al., 1998). The turbulence regime is important, because HABs are often associated with the relaxation of upwelling (Anderson, 1995). This relationship might reflect direct influences of turbulence on the growth of dinoflagellates (Pollingher and Zemel, 1981; Juhl and Latz, 2002), or indirect effects related more to upwelling circulation and transport (Smayda, 2002).

Because of their oceanographic significance and commercial importance, upwelling regions are among the best studied of coastal environments, providing opportunities to integrate targeted observation of HAB phenomena with broader-based research and monitoring programmes (Pitcher, 2007 – Chapter 21 this volume). The new tools and approaches for real-time observations described elsewhere in this volume are almost all well suited for observation and prediction of HABs in upwelling systems.

1.3.2 Localized blooms

When they occur, HABs cause local problems, regardless of regional extent. Within regions (defined as the next larger scale that must be observed to understand the local scale of interest, IOC, 2003) some locations experience recurrent, though not necessarily predictable, HABs; other nearby locations are spared. Even though the phenomena are likely to be related to larger-scale forcings, for many types of HAB, local conditions have a strong influence on occurrence and impacts and thus merit direct focus in the development of observation and prediction systems for monitoring and management.

Almost any recurrent HAB could be studied as a local phenomenon, at least partially explainable by local conditions. A few of many examples include:

- Blooms of *Heterosigma akashiwo* (Honjo, 1993) or *Alexandrium tamarense* (Yamamoto et al., 2002) in Hiroshima Bay, which can be related to patterns of eutrophication and local hydrography, invoking cyst dynamics, growth and behaviour of the algae.
- Paralytic shellfish poisoning (PSP) toxicity in oceanic bays (*rias*) of north-west Spain, where *Gymnodinium catenatum* is transported from elsewhere but exerts its effects on local mussel farms due to interactions between longshore transport, estuarine circulation under the influence of winds, and swimming behaviour of the dinoflagellates (Figueiras et al., 1996; Hallegraeff and Fraga, 1998).
- Brown tides of the pelagophyte *Aureococcus anophagefferens* (Bricelj and Lonsdale, 1997) in US mid-Atlantic coastal waters. Blooms are recurrent and persistent, but not predictable. Explanatory hypotheses invoke preferences for organic nitrogen and other nutrients that could be advantageous when estuarine flushing is reduced, and also top-down control as influenced by suppressed grazing (Gobler et al., 2002).

Description and prediction of localized blooms requires assessment of their extent and duration in relation to local conditions, quantification of exchanges with adjacent waters, and enough observations of nearby systems to explain why the HABs occur in one location and not another. The design of an appropriate observation system and the development of hypotheses and predictive models requires careful consideration of the life history of the alga (including cyst dynamics, when relevant), its buoyancy or swimming behaviour, important effects on growth, and local oceanographic conditions and ecological interactions. Clearly, these can be developed only through an iterative procedure of observation, analysis and improved observations. The example of *Prorocentrum* in Chesapeake Bay (Section 1.1.3; Tyler and Seliger, 1981) illustrates the kinds of processes and interactions that should be observed and modelled. The emphasis should be different for each localized bloom phenomenon, guided by targeted research.

1.3.3 Blooms strongly influenced by buoyancy or swimming behaviour

Some of the most dramatic pictures of blooms depict strong discoloration of water near frontal features in coastal waters (Figure 1.3). These phenomena can have significant impacts, for example when they impinge on aquaculture sites or decay in restricted

Figure 1.3
Dense blooms associated with physical discontinuities in the water demonstrate the interaction of swimming, sinking or floating of phytoplankton with small-scale circulation and interfaces (Franks, 1997). A, *Noctiluca* (from GEOHAB, 2001)
Source: after Malone (2001).

inlets, causing anoxia. Regardless, the patterns are spectacular, clearly illustrating the importance of biological-physical interactions in determining the patterns of algal blooms. A hallmark of these aggregations is a concentration of nutrient in phytoplankton cells (e.g. mmol particulate N m^{-3} of seawater) greater than what could have been available as dissolved nutrient in the water (Holmes et al., 1967); this explicitly demonstrates movement of cells relative to the water, in a sense scavenging nutrients from the water column.

Dense aggregations of phytoplankton, such as those at fronts, surface scums, concentrated subsurface layers, and transient surface accumulations due to diel vertical migration (DVM), are all associated with interactions between vertical movements of phytoplankton and discontinuities in the water column (Franks, 1997). Buoyancy and swimming behaviour are thus integral to the determination of population growth and transport (Kamykowski, 1995; Donaghay and Osborn, 1997). In turn, algal adaptations for vertical movements are important determinants of ecological selection (Levandowsky and Kaneta, 1987; Oliver, 1994; Cullen and MacIntyre, 1998). Consequently, detection and description of these blooms requires effective sampling of phytoplankton and physical-chemical properties on the scales of the biological-physical interaction, and modelling to describe the consequences of these interactions in three dimensions.

Subsurface layers illustrate the challenges of observation and modelling. Many species of phytoplankton, including dinoflagellates (Margalef et al., 1979; Eppley et al., 1984; Gentien et al., 1995), the prymnesiophyte *Chrysochromulina polylepis* (Granéli et al., 1993) and diatoms of the genus *Pseudo-nitzschia* (Rines et al., 2002) can form subsurface thin layers, thereby evading detection with conventional sampling. Considering that thin layers are commonly found when appropriate sampling is conducted, and that specialized sampling and analysis has not been widely employed, it is reasonable to guess that many toxic species (and other phytoplankton species) will be found in thin layers of stratified coastal waters (Dekshenieks et al., 2001). Highly resolved vertical profiles, for example with special samplers (Dekshenieks et al., 2001; Cowles, 2003; Kononen et al., 2003) and moored, towed, or autonomous under-way

profiling systems (Griffiths, 2007 – Chapter 13 this volume), are required to describe the distributions of subsurface blooms. Because buoyancy and swimming behaviour of phytoplankton are strongly influenced by nutrition (Oliver, 1994; Kamykowski, 1995; Cullen and MacIntyre, 1998), the association of subsurface layers with nutrient gradients is quite likely, though only rarely explored on this scale of thin layers (e.g. Kononen et al., 2003). Well-resolved determination of nutrient concentrations (Hanson and Donaghay, 1998; Johnson and Coletti, 2002), as well as temperature, salinity and currents, is thus needed to resolve causes and dynamics of subsurface blooms in thin layers (Cowles, 2003).

1.3.3.1 Modelling phytoplankton behaviour in coastal waters

Models of biological-physical interactions in behaviourally influenced blooms have described important processes that generate patterns observed in nature (Kamykowski, 1974; Donaghay and Osborn, 1997; Franks, 1997; Franks, 2007 – Chapter 15 this volume). Models designed to simulate local dynamics, including behaviour (Levandowsky and Kaneta, 1987; Kamykowski, 1995), describe the conditions conducive to bloom development (Tyler and Seliger, 1981; Amano et al., 1998; Yamamoto et al., 2002). Detailed prognostic modelling of behaviourally influenced bloom dynamics is quite difficult because not only must the three-dimensional evolution of physical discontinuities be described realistically, but also the physiological control on depth regulation, be it buoyancy regulation or swimming (Cullen and MacIntyre, 1998; Kamykowski et al., 1999). Fortunately, general features of transport and dynamics can be described without specifying the details of swimming and buoyancy by making simplifying assumptions, such as prescribed scavenging of nutrients in the surface layer by a population implicitly capable of migration (e.g. McGillicuddy et al., 2007 – Chapter 16 this volume), or confinement of a population to the pycnocline.

1.3.4 Toxic HABs

Blooms of toxic algae can be studied in the framework described in the previous sections, but toxic HABs merit special consideration for several reasons:

- They can have harmful effects even if the species is not dominant (e.g. Anderson, 1997), so effective detection at species level against a background of more abundant phytoplankton may be required.
- However, some HAB species cannot be distinguished on the basis of gross morphology or pigmentation, for example the toxic species of the diatom genus *Pseudo-nitzschia*.
- The production of toxin can vary among strains within a species (Anderson, 1990), and because it is under physiological control (Bates, 1998; Cembella, 1998) will vary with environmental conditions during the course of a bloom. Toxicity must therefore be detected in concert with distributions of the toxic species and, if possible, assessment of their physiological state (Scholin et al., 2007 – Chapter 11 this volume).
- The effects of toxic HABs depend on the toxin, the targets, and how the toxin gets to the target. Pathways of transfer must be understood and assessed (GEOHAB, 2001).
- Effective prediction of toxic HABs (especially as a phenomenon that occurs instead of a non-toxic bloom) requires an understanding of how toxicity influences ecological interactions, particularly loss processes such as grazing by zooplankton (Turner

and Tester, 1997) and shellfish (e.g. Tracey, 1988), and competition through allelopathy (Pratt, 1966; Gentien and Arzul, 1990; Schmidt and Hansen, 2001).

Consequently, studies of toxic HABs should include several components in addition to characterization of phytoplankton biomass in relationship to oceanographic processes: detection and physiological characterization at the species level; measurement of toxin; assessment of toxic effects; and description of how toxins reach the target species. Toxic effects on competitors, grazers or predators that feed back on population dynamics should also be explored.

Observation and prediction of algal blooms is a challenge that requires a multidisciplinary approach to detect phytoplankton (Cullen et al., 1997; Schofield et al., 1999) and to describe physical-biological interactions (Donaghay and Osborn, 1997). With the inclusion of toxic effects as a factor, the problem becomes even more multidisciplinary, complicated and challenging. Fortunately, the tools (Chapter 11) and the willingness to collaborate in multidisciplinary research and monitoring are developing rapidly.

1.4 Prediction of HABs

In the context of ocean observation systems, prediction can be defined as the estimation of properties that are not observed directly with known certainty (IOC, 2003). This broad and etymologically incorrect, but practical, definition includes hindcasts, nowcasts and forecasts of conditions:

- Hindcasts can be used to test if events are 'explicable in retrospect' (Reynolds, 2002), critical for the development and testing of models. For example, Franks and Anderson (1992*b*) compared historical records of PSP toxicity with hindcasts based on a model of wind-induced transport of *Alexandrium* to test hypotheses about physical control of toxicity in the Gulf of Maine.
- Nowcasts (comparable to weather maps) are essentially interpolations and extrapolations of observations, including those obtained in real time. They might include maps of the distributions of blooms in relation to currents. A time series of nowcasts (which become hindcasts as time passes and can be supplemented with more data) can serve as a record of environmental change that is richer than a compilation of direct observations alone; this is the future of coastal monitoring.
- Forecasts are the ultimate goal of marine prediction. The timescale could be hours to days, for predicting the course of events such as HABs; months, for prediction of seasonal bloom probabilities; or years to decades or longer, in simulations of eutrophication and climate change to support integrated coastal management.

A prediction with no bounds on its certainty has little practical value, so predictions should include estimation of associated errors (assessment of skill). Estimation of error is integral to some types of predictive model (Walstad and McGillicuddy, 2000; Pinardi et al., 2007 – Chapter 20 this volume), but hardly a feature of others. It may be some time before a requirement for error estimation in the prediction of ecological processes is universally embraced, but the need for error estimation is immediate.

There are many ways to model coastal ecosystems and HABs, and predictions span a large range of spatial and temporal scales and levels of biological detail. Some analytical models and a broad range of numerical predictive models are reviewed in this volume, so only the one class of prediction not explicitly addressed, empirical models, is discussed in the following section.

1.4.1 Empirical models

Many existing models of HABs are based on empirical relationships between the dynamics of HAB species and environmental variables measured concurrently over an extended period of observations. Generally backed up by a large amount of supplementary observations and research, empirical models may be formulated as statements, such as that of Taylor and Haigh (1993), based on figures reproduced here (Figure 1.4): 'The appearance of substantial numbers of *Heterosigma* at Jericho coincides with both a rise in temperature of about 15°C and a decrease in salinity below 15 ppt.' This straightforward prediction is both interpretable in ecological terms and suitable for forecasting the likelihood of blooms in the region, given information on temperature and salinity. With the availability of suitable data, such predictions can be evaluated statistically and refined. The same general approach can apply for empirical models relating HABs to eutrophication (Lam and Ho, 1989; Zhang, 1994).

By definition, empirical models must be based on observations. And, as predictions must have bounds, statistical validation and estimation of error is necessary at some point. Unbiased and unaliased data on the distributions of HAB species in relation to relevant environmental factors are thus centrally important. This is where multi-platform real-time coastal observation systems assume prominence (Chang and Dickey, 2007 – Chapter 2 this volume). As described in Section 1.2, and discussed in some detail below (Section 1.5.1), the observation strategy must be appropriate for the phenomena being observed, in discrimination (bulk phytoplankton biomass in some

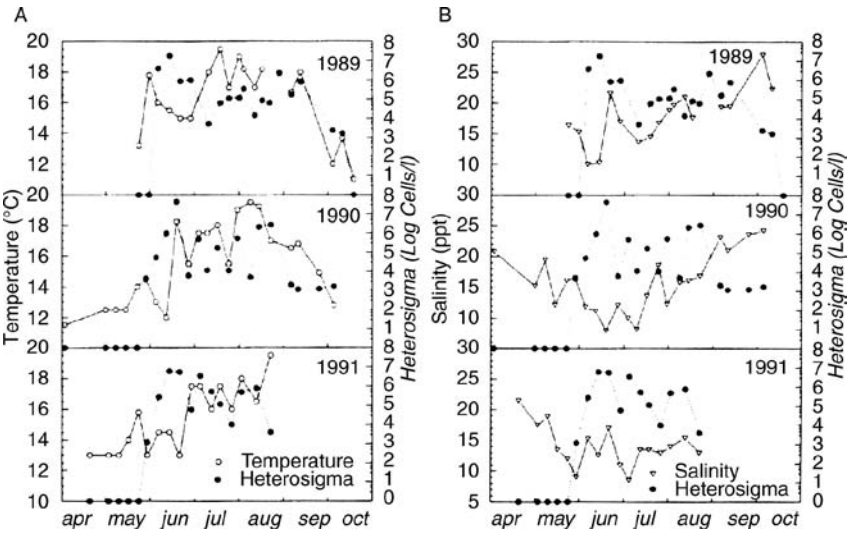

Figure 1.4
A, temperature, B, salinity, and concentrations of *Heterosigma* at Jericho Pier, in English Bay, Vancouver, Canada.
Source: Taylor and Haigh (1993). Copyright 1993, reprinted with permission from Elsevier.

cases, species and toxicity in others), environmental properties measured (temperature, salinity, currents, nutrients), vertical and temporal resolution, and spatial scale.

As reviewed in this volume, sophisticated and powerful modelling techniques, mostly numerical, are being developed for prediction of HABs. Empirical models will nonetheless retain an important role in predicting probabilities of HABs. As for all approaches, the quality of the predictions will depend on the data, and coastal observation systems will have to be designed with these applications in mind.

1.5 Observation technologies

For any HAB phenomenon and scale of interest, development and evaluation of early warning and prediction systems requires observations to characterize algal distributions in relation to environmental factors, and models that relate algal population dynamics to the observed properties of the environment (Anderson et al., 2001; GEOHAB, 2001; IOC, 2003). Algal blooms are episodic and patchy, so observations of algal distributions in relation to physical and chemical properties should be both continuous and synoptic. This ideal is unachievable, but a new generation of oceanographic instruments can provide continuous measurements of many physical, chemical and biological properties from autonomous moorings and underwater vehicles, in vertical profile and along ship-tracks. Also, remote sensing from aircraft and satellites can provide synoptic views of coastal processes when conditions allow. Many of these relatively new technologies and approaches are reviewed in this volume. The following discussion highlights a few approaches and raises some issues that have general relevance to observation and prediction of HABs.

1.5.1 Need for observations on relevant scales

As discussed in Section 1.2, HABs encompass a very broad range of scales, and detecting them involves many different challenges, depending on the species, its proclivities and the associated properties that should be measured. Considering that coastal observation systems should serve many purposes (IOC, 2003), technological approaches and scales of measurement must be very carefully chosen to provide data of maximum usefulness. This requires explicit consideration of the important phenomena to be detected and predicted, the scales of variability to be addressed, and the environmental forcings that should be characterized (Chang and Dickey, 2007 – Chapter 2 this volume).

The implications of sampling strategies are illustrated by an example from Bedford Basin, Nova Scotia, a well-studied coastal embayment (Li and Dickie, 2001). A dense subsurface bloom of *Gonyaulax digitale* persisted in a thin subsurface layer during summertime in the Basin, exposing itself to observers in the afternoons when winds eroded the pycnocline and the water turned reddish-brown (Cullen et al., 1994). Shortly after detailed observations were made (Figure 1.5), the bloom collapsed, leading to anoxia, a fish kill and considerable public concern. Key aspects of bloom dynamics were easy to document with frequent, highly resolved vertical profiles of optical and physical properties. Critical observations included weekly vertical profiles of temperature, salinity and chlorophyll fluorescence over the course of the summer (Bedford Institute, 2003), repeated profiles over the course of a day (Figure 1.5), targeted sampling of the thin layer to determine species composition, and measurement of meteorological conditions.

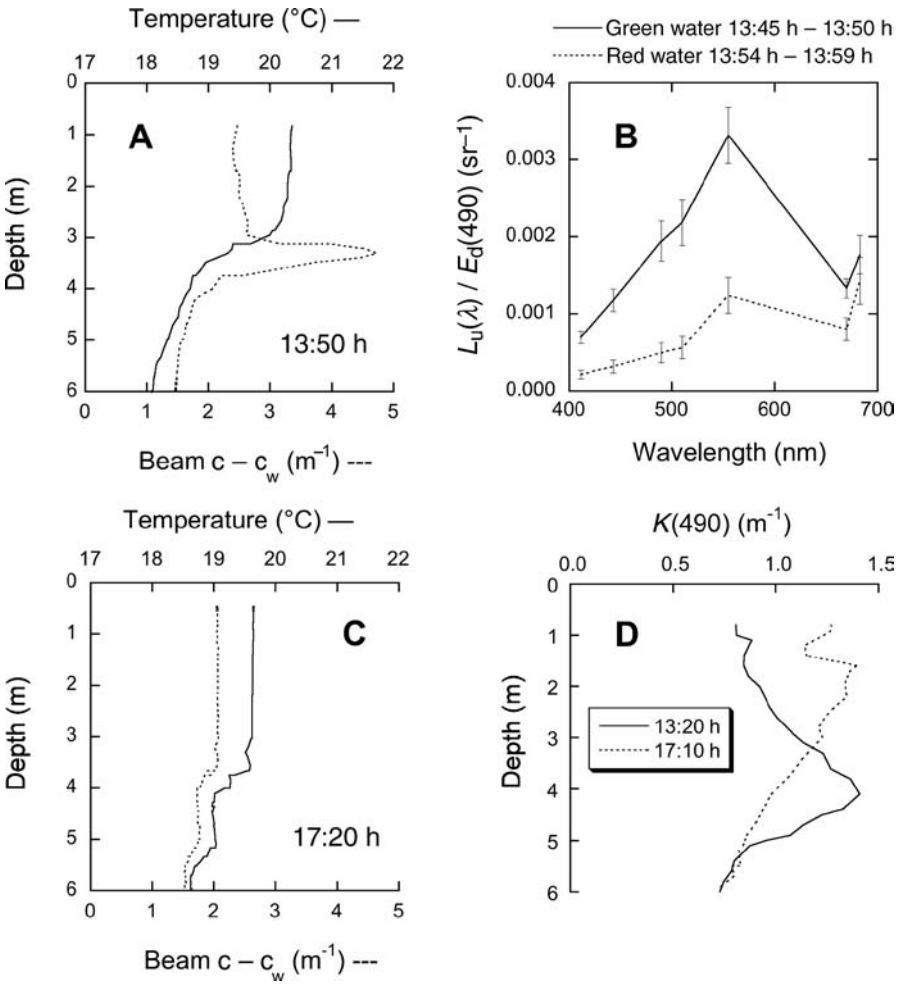

Figure 1.5
Changes in the vertical distribution of a *Gonyaulax digitale* bloom in Bedford Basin on 18 August 1993.
A, profiles of temperature (solid line) and beam attenuation, corrected for the contribution of pure water ($c - c_w$, m^{-1}; dotted line) show dinoflagellates predominantly confined to a thin subsurface layer at 13:50 h. This was the typical distribution during the morning and early afternoon.
B, measurements from a tethered spectral radiometer buoy show green water (solid line) changing rapidly to reddish-brown water (dotted line) as wind-mixing eroded the mixed layer and entrained the dinoflagellates into the surface layer.
C, mixing is demonstrated in profiles taken at 17:20 h.
D, the subsurface layer, and its entrainment into the surface layer, could also be resolved with measurements of light attenuation ($k_d(490)$, m^{-1}), which was profiled here, but could be measured with a chain of irradiance sensors. Measurements of ocean colour or samples from fixed depths could not describe the temporal changes of this population.
Source: Cullen et al. (1994).

Dynamics of the *Gonyaulax digitale* HAB would have been impossible to describe if observations were available only from the surface (ocean colour) or from conventional sampling at fixed depths. It is thus not surprising that an earlier study of *G. digitale* dynamics in Bedford Basin (Amadi et al., 1992), conducted with conventional periodic sampling, did not reveal clear patterns, and that a time series of chlorophyll concentration at 5 m detected the bloom on only one weekly sampling (Li and Dickie, 2001) when the layer happened to be at the nominal depth. The records from 5 m, especially when sustained for many years, are nonetheless extremely useful for describing annual and interannual trends of phytoplankton and nutrients, for example as influenced by increased nutrient loading and changes in climate (Li et al., 2003).

The message is that the same sampling programme can be used in different ways, depending on the questions, but that if the spatial or temporal resolution of sampling is inadequate, some phenomena cannot be described. In turn, measurements must be repeated for years to reveal trends and to test predictive models. Therefore, to address the range of scales that influence HABs and coastal ecosystems, observations must be highly resolved and sustained. With the advent of autonomous systems with sensors for physical, chemical, optical and biological properties, this is possible.

1.5.2 Fundamental strengths and limitations of bio-optical observations

The following chapters describe a stunning array of approaches for observing and describing the distributions of phytoplankton in relation to the oceanography and ecology of coastal systems. Bio-optical measurements are among the most promising, especially when integrated with systems to measure physical, chemical and biological properties on similar scales from a variety of platforms, in support of modelling. Using a few examples and without going into much detail, it is possible to illustrate some fundamental strengths and limitations that are generic to bio-optical observations.

1.5.2.1 Apparent optical properties

The absorption and scattering of light by algae, other micro-organisms, detrital and inorganic particles, dissolved substances and water modify both the underwater and upwelling (emergent) light fields. The influences of algae, which are generally distinct from those of other components (Morel and Bricaud, 1986; Morel, 2006 – Chapter 4 this volume), can be detected and quantified by determining the fate of sunlight in the ocean from measurements of apparent optical properties (AOPs) such as spectral reflectance or attenuation coefficients (Sosik, 2007 – Chapter 8 this volume). Consequently, where algal blooms occur in sufficient biomass, they may be detected by passive optical instruments (radiometers), including ocean-colour sensors on moorings, aircraft, or satellites (Lewis, 2007; Ruddick et al., 2007 – Chapters 6 and 9 this volume). Passive optical sensors cannot detect toxic algae that occur as minor components of the phytoplankton, but estimates of total pigment and information such as spectral attenuation from these sensors can provide important data for biological-chemical-physical models of algal dynamics.

One great strength of AOP measurements is that they are derived from radiometric quantities that retain their validity for long-term and wide-ranging comparisons over time or between sites (e.g. for resolving influences of eutrophication or climate variability). Interpretations of the measurements may change for the better, but if proper calibration is ensured, comparability and continuity of records should be guaranteed (Cullen et al., 1997). This contrasts with techniques for other observations, such as determination of chlorophyll concentration, measurement of turbidity, and enumeration

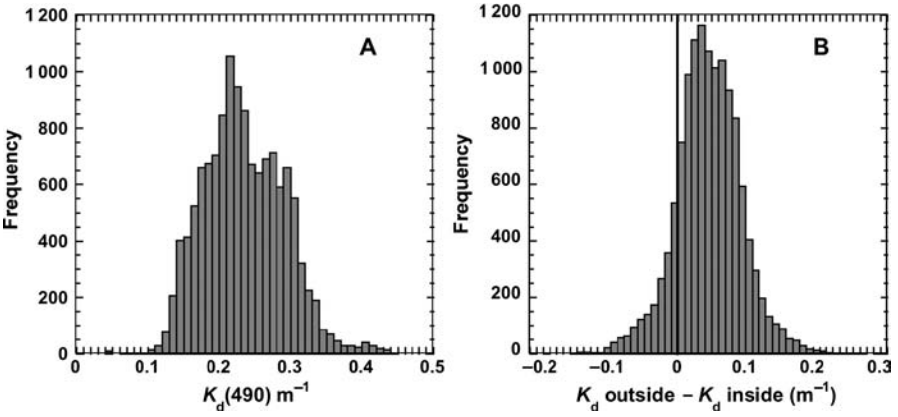

Figure 1.6
Diffuse attenuation coefficient at 490 nm (k_d(490), m^{-1}) for the depth range 4–8 m, measured with moored irradiance sensors (Tethered Attenuation Coefficient Chain Sensor, TACCS, Satlantic, Inc.) in Ship Harbour, Nova Scotia, during summer 2002.
A, these observations from a mooring near a mussel farm provide a permanent record of water clarity, with statistical moments. Although they do not reveal the sources of variability, simple, direct and robust measurements like this could be compared over decades to reveal secular trends in water clarity and changes in seasonal patterns.
B, comparison with concurrent measurements at a second mooring within the mussel farm show depletion of absorbing substances (seston) within the farm. The average change is significantly different from zero, and it could be related directly to feeding by mussels. But variability was such that direct sampling from boats on a regular schedule (hourly, daily, weekly) would be unlikely to distinguish the pattern. Measurements of attenuation have the added advantage of integrating the influence of all substances in the depth range between sensors (corresponding to the suspended mussels), so the scale is correct and thin layers should not be missed.
Source: D. A. Ibarra, Dalhousie University.

of picoplankton, which have changed over the years and still vary today, complicating the interpretation of long time series and regional comparisons, despite the availability of some overlap of newer and older measurements (Karl et al., 2001).

Measurements of diffuse attenuation in a coastal inlet (Figure 1.6) illustrate the simple power of radiometric measurements for quantifying conditions in coastal waters: the nearly continuous records are valid for direct comparison with the near-by measurements made concurrently (Figure 1.6B). Comparisons could also be made over decades at the same site, or among sites in regional or global networks (IOC, 2003).

Attenuation at one wavelength (Figure 1.6) is an excellent comparative measure of water clarity, much better than the attenuation coefficient for photosynthetically available radiation (PAR), which will vary with depth even in optically uniform waters due to the spectral filtering effect (Kirk, 1994). However, measurements at one

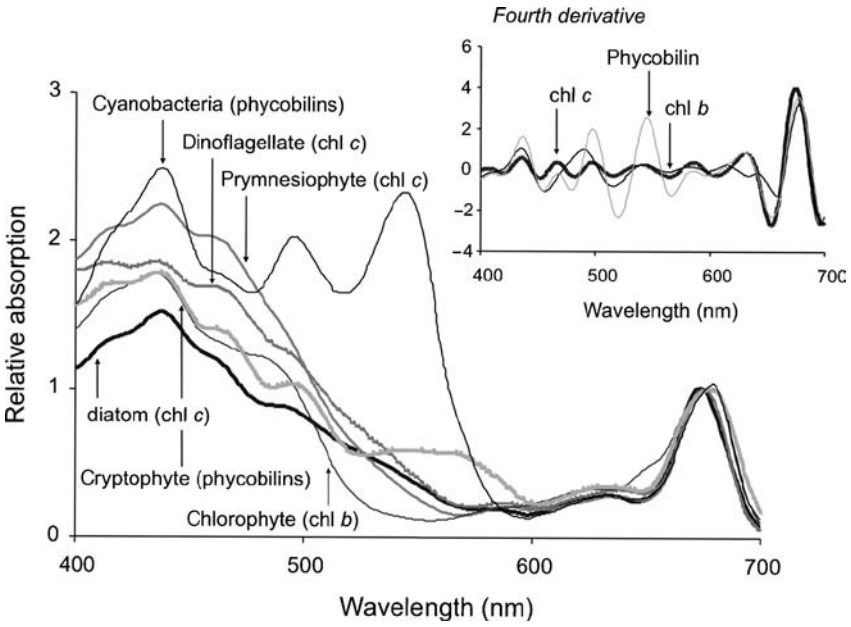

Figure 1.7
The absorption characteristics of photosynthetic pigments, and differences in pigment composition among phytoplankton taxa, are used to discriminate taxonomic status of phytoplankton from optical measurements. Absorption for representatives of the major phytoplankton taxa are presented here, normalized at 675 nm. Measurements, including these, are made using samples collected on glass-fibre filters, but new systems, including a flow-through spectrometer (Schofield et al., 2007 – Chapter 3 this volume), measure absorption characteristics in real time. Variability in spectral shapes reflects the presence of different accessory chlorophyll and carotenoid pigments, with a major contributor identified for each group.
Sources: after Johnsen et al. (1994); Schofield et al. (1996).
Inset: fourth-derivative spectra for the major spectral classes of algae are used to resolve the positions of absorption features attributable to specific pigments (Bidigare et al., 1989; Millie et al., 1995; Schofield et al., 2007 – Chapter 3 this volume).
Source: Bissett et al., 2001.

wavelength reveal nothing about the attenuating substances in the water. Spectrally resolved measurements are required to retrieve information about the constituents of the water, including phytoplankton (Figure 1.7). For example, highly resolved spectra of reflectance (ratio of upwelling radiance to downwelling irradiance, an AOP) from the Bering Sea (Figures 1.8B, 1.8C) show several distinguishing features that were repeatable over the course of a research cruise and surely related to pigmentation and fluorescence characteristics of assemblages dominated by diatoms and *Phaeocystis*, in fairly close proximity (lighter- and darker-green regions in Figure 1.8A as deduced from shipboard sampling). We have not yet perfected an analytical procedure to

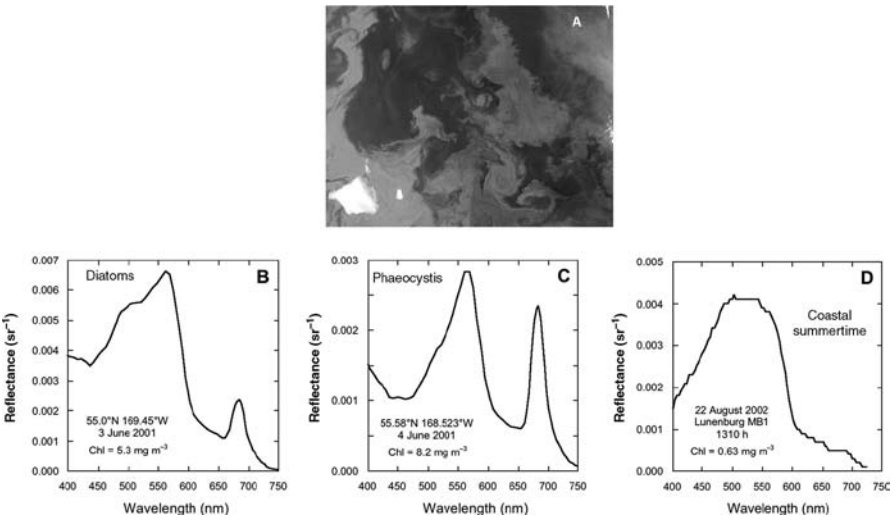

Figure 1.8
A, satellite image of a phytoplankton bloom in the Bering Sea on 7 June 2001 (292 km by 200 km centred near 58.7°N, 177°W). During this period, shipboard sampling and measurements of reflectance indicated blooms dominated by diatoms and *Phaeocystis*, in close proximity, probably corresponding to the lighter and darker green features in the image. Coccolithophore blooms are highly reflective and may be responsible for the brighter features in the SW corner of the image. *Sources*: SeaWiFS Project, NASA Goddard Space Flight Center and ORBIMAGE.
B, C, in-water measurements of hyperspectral reflectance at the surface in the Bering Sea during early June reveal irregularities between 400 nm and 550 nm that are associated with pigment absorption, which reduces reflectance (Sosik, 2006 – Chapter 8 this volume), and large peaks near 680 nm from sun-induced chlorophyll fluorescence (Babin, 2007 – Chapter 7 this volume). Here, reflectance is upwelling radiance at 65 cm divided by downwelling irradiance above the surface, measured with a Hyperspectral TSRB Tethered Spectral Radiometer Buoy (Satlantic, Inc.)
D, similar measurements from a mooring in Lunenburg Bay, Nova Scotia, show much less interpretable structure because pigment concentrations are about 10-fold lower, and much of the absorption in blue wavelengths is due to chromophoric dissolved organic matter (CDOM).

distinguish these groups and perhaps their physiological status from such measurements, but we are working on it. The spectra show that we have much information with which to work, but analyses (Brown, Huot and Cullen, unpublished) indicate that the influences of chromophoric dissolved organic matter (CDOM) represent a chronic problem that is not easily addressed.

Measurements representing non-bloom conditions illustrate some limitations of using AOPs such as reflectance for discerning species composition, or even for obtaining accurate

estimates of chlorophyll concentration, in coastal waters. In a coastal bay of Nova Scotia (Figure 1.8D), the absorption by pigments in the 400–550 nm range is overwhelmed by CDOM so the reflectance spectrum shows little structure associated with phytoplankton pigments, clearly evident as depressed reflectance in Figures 1.8B and 1.8C. Sustained observations backed up by careful analysis will show, for different regions, what can be discerned about phytoplankton dynamics from measurements of AOPs in coastal waters.

This discussion of AOPs hardly scratches the surface. The important message of this overview is that the fate of light in the ocean is strongly determined by its constituents, so when effectively analysed, variability in AOPs reflects variability of what is in the water. When measured with properly constructed and calibrated instruments, AOPs represent a permanent and robust record of environmental variability that is certainly relevant to HABs and ecosystem dynamics. Apparent optical properties can be measured on many scales (Lewis, 2007; Ruddick et al., 2007 – Chapters 6 and 9 this volume) and will be centrally important to developing coastal observation systems (Malone, 2007 – Chapter 14 this volume). Enthusiasm for bio-optical interpretation of AOPs is warranted, but it should be tempered with a healthy appreciation of the difficulties encountered when working in optically complex coastal waters (IOCCG, 2000). Research on the interpretation of AOPs in coastal waters will continue for years; it is important that the technology becomes recognized more widely, so that it can be incorporated into coastal monitoring programmes.

1.5.2.2 Inherent optical properties

In the context of coastal observing systems and ecosystem dynamics, optical properties of the water are measured primarily to infer the distributions of phytoplankton and other constituents in the water. Inherent optical properties (IOPs) are the bio-optical connection between what is in the water and the AOPs that can be observed with passive optical instruments. The IOPs – coefficients for absorption and scattering, and the volume scattering function – do not depend on the geometry of the ambient light field; they are inherent to water, particles and dissolved substances, and can generally be assumed to act additively (Roesler and Boss, 2007 – Chapter 5 this volume). The bio-optical chain of evidence therefore can go:

- from AOPs to IOPs, using some quantitative guesswork to find the combination of IOPs that best explains observations, with consideration of the ambient light field and generalizations about the optical properties of phytoplankton, other particles and CDOM; and
- from IOPs to the concentration of constituents, using those same generalizations about their optical properties.

Approaches for inferring the constituents of water from optical properties are reviewed in Chapter 8 (Sosik, 2007). Progress has been rapid in recent years, bolstered by enhanced appreciation of optics by biologists and greater incorporation of biological and ecological processes into the growing field of bio-optical oceanography.

For coastal observing systems, it makes theoretical and practical sense to measure IOPs directly and make inferences about the constituents of the water directly from the measurements. Why try to infer optical properties from AOPs when the optical properties can be measured directly? Instruments are now available to characterize spectral absorption and scattering well enough to contribute significantly to the description of phytoplankton communities in coastal waters (Roesler and Boss, 2007; Schofield et al., 2007 – Chapters 5 and 3 this volume). The instruments have their own light sources

and therefore operate day and night. Some, such as absorption-attenuation meters with and without prefiltration units (Chapter 5) and a capillary flow-through spectrometer system (Chapter 3), can use physical separation to discriminate contributions of particles versus dissolved constituents. When designed, constructed, calibrated and operated correctly (Chapter 5), their measurements are robust and comparable, just as are measurements of AOPs. And, just as with other optical measurement systems, fouling and instrument drift can be major problems during prolonged deployment. Fouling can be assessed and addressed (Chang and Dickey, 2007; Lehaitre et al., 2007 – Chapters 2 and 12 this volume). However, instrument drift, for example in the blank, can be a particular problem during long deployments (Davis et al., 2000) and when appropriate blanks are not or cannot be measured (Cullen and Davis, 2003).

The measurement and interpretation of IOPs should have a central role in coastal observing systems. As with any analytical approach, the value of the measurements will largely depend on careful design and operation of instruments and informed interpretation of the measurements (Chapter 5). Continued research, and a commitment to training those who will use the instruments operationally, should ensure that IOPs are used effectively in early warning, prediction and monitoring of HABs.

1.5.2.3 Fluorescence

Of all the optical properties observable in the ocean, chlorophyll fluorescence is the only one directly attributable to phytoplankton. Also, the method for estimating chlorophyll concentration from the measurement of *in vivo* fluorescence has been with us for nearly 40 years (Lorenzen, 1966) and small, relatively inexpensive *in situ* fluorometers are widely available. Consequently, stimulated fluorescence (i.e. as detected with a fluorometer) is the most commonly used measure of phytoplankton distributions in vertical profile and on moorings and under-way systems. It is also well established that sun-induced chlorophyll fluorescence can be detected with passive radiometers, including airborne imagers and satellite sensors, and related to both the biomass and photosynthetic properties of phytoplankton (reviewed by Babin, 2007 – Chapter 7 this volume).

Early on (reviewed by Cullen, 1982), it was well established that fluorescence was an imprecise measure of chlorophyll, strongly influenced by irradiance *in situ*, dark adaptation of samples (if any), species composition, physiological state and light history of the phytoplankton. Beyond that, excitation light sources in fluorometers differ significantly in spectral quality, duration and magnitude of exposure (Cullen et al., 1988; Chapter 7), making comparisons between instruments difficult (see also Neale et al., 1989). To compound the uncertainty, chlorophyll *a* constitutes a variable proportion of phytoplankton biomass, varying more than a factor of 10 with species group and environmental conditions (Geider, 1987; Cullen et al., 1993). The ease of measuring fluorescence to assess the distributions of phytoplankton thus invites trouble, as illustrated in Figure 1.9, in which one of the simpler environmental influences on fluorescence yield, sunlight, is shown to affect the measurement in a way that is seldom accounted for in calibrations (but see Marra, 1992).

As reviewed by Babin in Chapter 7, fluorometers that are now commercially available provide much more than a simple index of chlorophyll concentration. Some (for example the bbe Moldenke Fluoroprobe 2 and the SAFire by WET Labs) are capable of discriminating phytoplankton groups on the basis of their different photosynthetic absorption characteristics (see Figure 1.7) detected on the basis

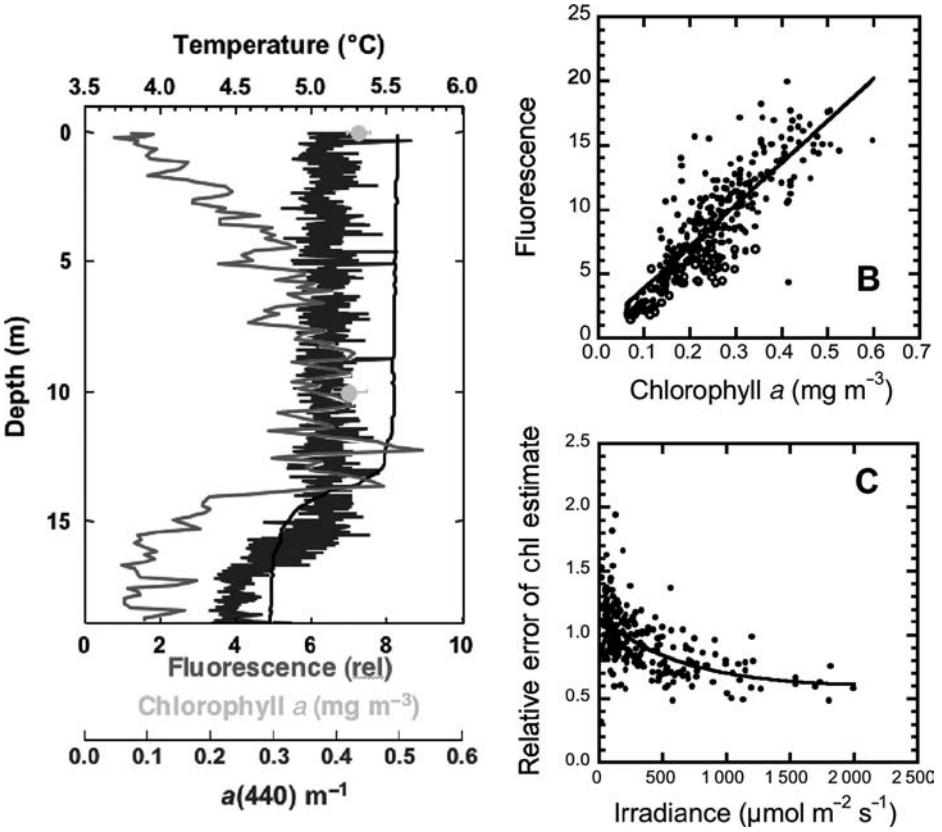

Figure 1.9
Effects of irradiance on fluorescence yield.
A, this profile from the Bering Sea shows an optically uniform mixed layer of about 12 m in which chlorophyll concentration (filled grey circles: ± s.e., n = 3) is the same at top and bottom, and the absorption coefficient at 440 nm (WET Labs ac-9; middle line), an IOP strongly influenced by phytoplankton pigment, is vertically uniform. It may be concluded that the concentration of phytoplankton is uniform in the upper 10 m. Fluorescence (WET Labs WETStar; left-hand line), however, is suppressed near the surface by nonphotochemical quenching (Babin, 2007 – Chapter 7 this volume). This distribution of fluorescence could be incorrectly interpreted as surface avoidance by phytoplankton.
Source: J.J. Cullen, unpublished.
B, when fluorometers are calibrated with concurrent measurements of chlorophyll concentration, the observations near the surface (open symbols) may not have a particularly strong influence on the regression, so the effect of bright light can be ignored while maintaining a fairly good regression coefficient.
C, the effect of bright light is real, though, and readily accounted for with a simple model that quantifies the underestimate of chlorophyll due to fluorescence quenching as a function of ambient irradiance.
Source: Cullen and Lewis (1995).

of relative fluorescence yield under multispectral excitation (Beutler et al., 2002). The physiology of phytoplankton can also be explored: by measuring fluorescence yield while manipulating flash intensity or background irradiance, it is possible to determine parameters that describe the photosynthetic apparatus – maximum quantum yield for charge separation, photosynthetic cross-section, and turnover time of photosystem II (e.g. Schreiber et al., 1986; Kolber and Falkowski, 1993; Falkowski and Kolber, 1995). In principle, these parameters can be used to calculate the rate of photosynthesis (Kolber and Falkowski, 1993; Suggett et al., 2003). More importantly, perhaps, they are very sensitive to physiological state and environmental conditions and thus may be excellent diagnostics of environmental stresses such as nutrient limitation (e.g. Kolber et al., 1988; Geider et al., 1993; Parkhill et al., 2001). The development of robust diagnostics and their measurement in the field is anything but straightforward, however: differences in culture conditions can have a strong influence on the relationship between nutrient stress and maximum quantum yield (Cullen et al., 1992; Parkhill et al., 2001); little experimental work has been done on phytoplankton grown under high irradiance characteristic of the sea surface (Cullen and Lewis, 1995); and critical evaluation of the new generation of fluorometers under a range of conditions at sea is difficult and not yet widely demonstrated (Cullen and Davis, 2003; Chapter 7).

A fundamental strength and an unfortunate limitation of fluorescence as an optical measurement is that it is very strongly tied to photosynthesis and physiology of phytoplankton. This is a strength, because the measurement has such great potential (which has already been demonstrated) – it is also a limitation, because interpretation of the measurements requires a working knowledge of algal physiology, including the fundamentals of fluorescence and photosynthesis (Chapter 7). Experience has shown that the fluorescence literature seems nearly impenetrable to many aquatic scientists, though perseverance pays off. Even if the process is understood, the measurement needs further attention: the design of instruments and evaluation of their performance requires a good appreciation of the principles of measuring fluorescence and, for fluorometers such as the fast repetition rate fluorometer (Kolber and Falkowski, 1993), the statistical determination of parameters from kinetic curves (Laney, 2003). The rewards from measuring fluorescence are potentially great, and the pitfalls are many.

1.6 Towards real-time observation and prediction of HABs

As amply demonstrated in this volume (see also Glasgow et al., 2004), advances in observation technology and modelling, along with greatly enhanced capabilities for communications and computing, make a revolution in coastal oceanography, monitoring and management inevitable. Much as remote sensing from space has fundamentally changed our view of the oceans and allowed questions to be addressed that could hardly be posed before (e.g. mesoscale variability, discussed by Lewis, 2002), automated, real-time observing systems will transform the way the ocean is sampled and understood. With advancing technology, the potential for describing biological and physical variability on a very broad range of scales is almost limitless, and many applications will be directly relevant to the coastal ocean (IOC, 2003). Science will deliver the capability to detect ecosystem processes and the dynamics of some harmful algae in real time, and predictive models will improve. Continued progress will require

large investments of time and resources, and this can be justified only with the promise of operational monitoring and prediction systems for HABs and other ecological phenomena. Consequently, scientific research and operational oceanography must work together as never before (Malone, 2007 – Chapter 14 this volume). An assessment of the present capabilities and limitations of real-time observation and prediction systems, and their links to monitoring and management, can be helpful in preparing for the challenges and opportunities that lie ahead.

1.6.1 Enabling research

1.6.1.1 Observation technologies

Progress in the observation of ecosystem processes in coastal waters has been rapid and significant. Optical and acoustical instruments, mounted on a variety of platforms, can already provide unprecedented views of coastal processes on scales from those relevant to cellular interactions all the way to climate change (Chang and Dickey, 2007; Griffiths, 2007; Jaffe, 2007; Schofield et al., 2007 – Chapters 2, 13, 10 and 3 this volume). The measurements are not direct assessments of species distributions and activities – they are proxies that must be interpreted through careful analysis (e.g. Sosik, 2007 – Chapter 8 this volume); quantitative evaluation of analytical approaches and widespread acceptance for use in monitoring are major challenges (Figure 1.10). To foster effective development of coastal observation systems, the users of measurements from optical or acoustical instruments should have a good appreciation of their theoretical foundations and limitations. In turn, designers of the instruments can do their jobs better if the biological reasons for variations in instrument response (e.g. environmental influences on fluorescence yield; effects of plankton community structure on scattering) are more fully understood. Enhanced collaboration among scientists from different disciplines and the designers of instruments is the key to rapid advancement, and in many research communities this is being pursued actively with good results.

Detection of HABs cannot rely completely on indirect measurements of phytoplankton abundance. In many situations there is a need for identification of species or assessment of toxicity, sometimes at cellular level. As with other fields of ocean observation, progress has been rapid (Scholin et al., 2007 – Chapter 11 this volume) and collaborations have been effective. As methods for autonomous assessment of HABs become more developed, approaches for quantifying the abundance of zooplankton and other consumers will become increasingly important (Jaffe, 2007 – Chapter 10 this volume).

Judging by the leading edge, research on coastal observation technologies is a major success story, on a good track and gaining momentum. Sustained progress of widespread significance depends on expanding the base of scientists who use these tools for coastal research, so observation of HABs and ecosystem dynamics can be addressed under a broad range of conditions worldwide. This can be accomplished through education, for example inclusion of bio-optics in curricula, and enhanced accessibility of instruments or data. The latter is a challenge well beyond the scope of a scientific review; nonetheless, many observation systems provide free access to data over the internet and several provide opportunities for collaborative deployment of new instruments. This, along with development, testing, acceptance and commercialization of robust and more affordable instruments, should help to sustain the ongoing revolution in coastal observation.

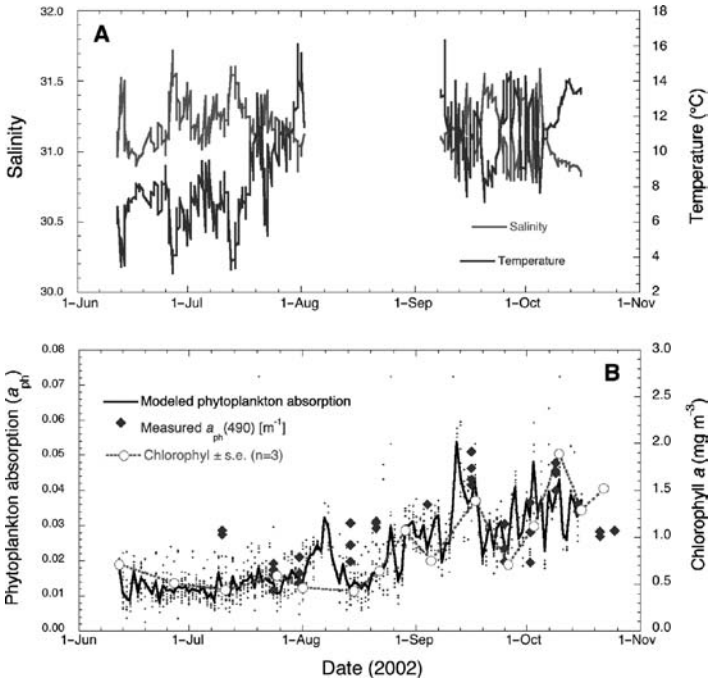

Figure 1.10
Early results from a coastal observatory illustrate some of the promise of coastal observing systems and many of the challenges that must be overcome before systems for research and development become operational and comparable between sites (Glenn et al., 2000; IOC, 2003; Malone, 2007 – Chapter 14 this volume). The MEPS-Bay system[6] has three moorings with temperature-salinity chains, current meters, meteorology and optics; a data assimilation model is being developed to incorporate these data and other local observations into a real-time, coupled, atmosphere-ocean simulation of the bay (Sheng and Wang, 2004).
A, the records of temperature and salinity from the 11 m conductivity-temperature (CT) sensor on a mooring (Lunenburg Bay, MB1) show the seasonal development of temperature, and many event-scale changes of water in the bay that could not be resolved with conventional monitoring. It also shows a gap corresponding to a technical failure; operational systems must be robust and provision must be made to correct such problems quickly.
B, nearly continuous measurements of hyperspectral ocean colour (as in Figure 1.8D) were analysed by Brown and Huot (unpublished) with an inverse model, generating relative estimates of phytoplankton absorption (Roesler and Perry, 1995; Sosik, 2007 – Chapter 8 this volume) corrected for the substantial contribution of CDOM and other constituents of the water (black dots; the black line is a locally weighted least-squares regression to indicate trends). Blue symbols show direct measurements of phytoplankton absorption (filter pad method, corrected for detritus) and open red symbols are determinations of extracted chlorophyll.
Development, quantitative evaluation and widespread acceptance of robust optical measures of phytoplankton is required for routine monitoring. This is a major challenge.

[6]Marine Environmental Prediction System-Bay; Lunenburg, Nova, Scotia; www.cmep.ca/bay

1.6.1.2 Prediction systems

For a long time, the development and evaluation of marine models was fundamentally limited by availability of data. A prediction was untestable if the process could not be resolved with real measurements. This has not stopped the development of models, but it has certainly limited their rigorous evaluation in the context of predicting the occurrence of HABs. Until recently, most models of HABs have been either conceptual descriptions, somewhat general predictions based on empirical data or theoretical models, or idealized simulations of responses to forcing factors. Such models are valuable – to a large extent, they represent the foundations of our understanding of HABs. However, data-limited models are not suitable for real-time forecasts of HABs. With the advent of coastal observation systems, this is changing. It is now possible to construct numerical simulations of ecosystem dynamics and HABs in local flow fields (Bissett et al., 2007; Fennel and Neumann, 2007; Lee et al., 2007; McGillicuddy et al., 2007 – Chapters 17, 18 and 16 this volume), and data assimilation procedures for integrating observations into models (Pinardi et al., 2007 – Chapter 20 this volume) are being extended to include biological processes (Walstad and McGillicuddy, 2000). Also, blooms have been detected by remote sensing and tracked, with forecasts of trajectories (Stumpf et al., 2003). Prediction of ecosystem dynamics in the coastal zone is in its infancy, so expectations for immediate successes should not be too high. Still, results to date and the confluence of observation and modelling systems suggest that research will provide the means to predict the dynamics of HABs for some, but certainly not all, scales and locations.

Many of the limitations of predictive models have to do with scales of prediction and the limits of predictability. As with all ecological models, a tradeoff will always exist between generality and realistic simulation. No deterministic model will ever simulate the time-dependent evolution of a natural algal bloom in three dimensions at the scale of a cell's interaction with the environment. Predictive models will adopt different approaches, relying on carefully chosen schemes for generalization. Success will depend to a large extent on the suitability of the approach for the coastal system being modelled, and the accuracy of the ecological information on which the model is constructed. Close ties between biological and modelling research will be essential.

Many aspects of phytoplankton dynamics can be modelled using functions based on experimental results (e.g. growth rate as a function of temperature and irradiance, grazing rate as a function of cell concentration). However, important ecological properties and processes must be better resolved to improve the prediction of HABs. For example:

- There is a need for information on what ecophysiological factors distinguish a HAB species from a closely related species that does not cause the harmful effects (Smayda, 1997*a*; GEOHAB, 2001).
- Descriptions of food-web interactions should be better constrained with observations and experimental results, including more assessments of grazing and grazers in coastal observation systems, and descriptions of chemical and other defences against grazing (Smetacek, 1998).
- Research is needed to improve the predictability of algal growth and behaviour in a complex environment, including variable light and nutrients (and vertical migration when warranted). Currently, most experimental results are obtained for one isolate of a species grown in well-defined conditions (Cullen and MacIntyre, 1998).

These examples from biology are only a few of the many gaps in knowledge that should be filled as predictive models are developed. Other requirements for ecological information, observations, physical models and numerical techniques are identified in this volume (see also GEOHAB, 2001).

Even if the research is done, there is a great need for effective transfer of information between experimentalists, oceanographers and modellers (by no means mutually exclusive categories). This could be accelerated through the development of interactive modelling and visualization systems. Working together, biologists and modellers could 'tinker' with a model while discussing the merits of different biological parameterizations and their consequences for output from the model. Turnaround time for feedback would be reduced by orders of magnitude from the old model of scientific publication or annual meetings. Implementation of these interactive systems could transform coastal ecosystem modelling and, with modifications, serve an important role in coastal management and education of the public.

1.6.2 Transition to routine operations

An ultimate goal of research on observation and prediction of HABs is the establishment of real-time systems for routine monitoring, early warning and prediction. This is operational oceanography. Malone (2007 – Chapter 14 this volume) explains why the requirements for operational oceanography are much different than for research, and suggests that fundamental changes in the relationships between scientists, managers and society in general are needed not only to meet societal goals, but also to maintain the integrity of the scientific process as it serves the many stakeholders who invest in it and depend on it for their livelihoods, enjoyment, safety or survival. This grand challenge must be met if the revolution in coastal observation technology is to spread. Here, the discussion is confined to some practical issues that are nearly universal and must be addressed.

Early results from a nascent coastal observing system, under development as a research project, demonstrate the great value of autonomous systems for monitoring and prediction (Figure 1.10). They also illustrate many of the scientific, logistical and structural problems that must be confronted as observation systems for research contribute to and eventually merge with operational oceanography. The record of temperature and salinity from one of many sensors in the observation system (Figure 1.10A) shows the temporal resolution of moored observatories (Chang and Dickey, 2007 – Chapter 2 this volume). Nothing less would serve to describe hydrographic variability in the bay. A record with a gap is shown to highlight the importance of continuous observations in operational systems. Researchers are familiar with such technical problems, and fix them as quickly as is feasible under a broad range of constraints; as coastal observation systems become established and more useful for sustained monitoring and detection, it will be important to develop support systems for the operational components. That is, as the systems become operational, responsibility for running them should migrate from scientists to agencies. The necessary coordination is not well developed in many jurisdictions.

Novel optical observations from the coastal observatory reveal difficulties that will arise during the integration of results from research systems into coastal monitoring for operational oceanography (Figure 1.10B):

- Measurements of ocean colour from a mooring provide nearly continuous records of phytoplankton absorption, an optical estimate of phytoplankton abundance. It could be argued that the measure is as good as chlorophyll *a*, the widely used

indicator of phytoplankton, and better than *in vivo* fluorescence. The estimate is generated using a fairly complicated inverse model, however, and many other bio-optical models exist (Sosik, 2007 – Chapter 8 this volume). Is it reasonable to expect that regional or global observing systems will adopt highly derived data products as operational measures of phytoplankton or other constituents of the water? Who will decide, and how?

- Evaluation of the model for phytoplankton absorption must include direct comparison with sea-truth samples. Although collection and analysis of water samples is straightforward, comprehensive evaluation is difficult and expensive: regular sampling at our site (about three times per month; discrete samples in Figure 1.10B) required a substantial commitment of time and resources, yet obviously it missed interesting and possibly important events. Statistical analysis of results will not be as powerful as we would like. Adaptive sampling based on cues from real-time sensors, and participation of community volunteers who can easily visit the sites for sampling, will help us to acquire more and better data.
- More broadly, the measurements that form the foundations of operational systems for monitoring and prediction of HABs and ecosystem dynamics will have to be reliable and affordable, and they should be simple to operate, with measurements that are easy to interpret. Currently, the triumvirate of optical measurements for environmental monitoring are *in vivo* fluorescence, turbidity and PAR. Bio-optical research, reviewed in this volume, has shown that much more discriminating measurements are now available. Greater efforts should be made to develop and test robust sensors so that emerging observation systems can start out with newer measurements that are likely to be the standards in coming decades.

The gap between the state of the art in bio-optical oceanography and well established practices in coastal monitoring has parallels in almost every other aspect of observation and prediction of HABs. Given the promise of the science and the immediacy of its practical application, there is excellent justification for pursuing new ways to coordinate research with operational oceanography, using observation and prediction for monitoring and management. This will come through education, training, communication and genuine interest in cooperation.

1.7 Conclusions

Excitement about real-time coastal observing systems is developing rapidly, and systems are being deployed worldwide (Glasgow et al., 2004). Scientific and technical advances are building a capability for observing and describing dynamics of the coastal ocean in real time on the scales that really matter, rather than poring over sparse, hard-fought data to infer what occurred months or years before. Ironically, achievements in specialized fields (e.g. optics, acoustics, algal physiology, molecular biology, ocean engineering, numerical modelling techniques) have led to the development of a truly interdisciplinary approach for describing ecosystem dynamics. Interactions among biologists, physicists, engineers and modellers are stronger than ever before, and better links with managers and policy-makers are sure to develop. Classic research of the data-starved but thinking-rich 'old days' is highly relevant as efforts to describe HABs progress. This is a dynamic time, with much to do. As technology and research march forward, we should remember to maintain our roots in ecology and oceanography and to pay special attention to making our work accessible to those who will use it.

References

Amadi, I., Subba Rao, D. V. and Pan, Y. 1992. A *Gonyaulax digitale* red water bloom in the Bedford Basin, Nova Scotia, Canada. *Bot. Marina*, 35, pp. 451–55.

Amano, K., Watanabe, M., Kohata, K. and Harada, S. 1998. Conditions necessary for *Chattonella antiqua* red tide outbreaks. *Limnol. Oceanogr.*, 43, pp. 117–28.

Andersen, P., Enevoldsen, H. and Anderson, D. 2003. Harmful algal monitoring programme and action plan design. In: Hallegraeff et al. (eds), op. cit., pp. 627–47.

Anderson, D. M. 1990. Toxin variability in *Alexandrium* species. In: E. Granéli, B. Sundström, L. Edler and D. M. Anderson (eds), *Toxic Marine Phytoplankton*. Elsevier, New York, pp. 41–51.

Anderson, D. M. 1995. Toxic red tides and harmful algal blooms: a practical challenge in coastal oceanography. *Rev. Geophys.*, 33, Suppl., pp. 1189–200. (US National Report to IUGG 1991–1994.)

Anderson, D. M. 1997. Bloom dynamics of toxic *Alexandrium* species in the northeastern US. *Limnol. Oceanogr.*, 42, pp 1009–22.

Anderson, D. M., Andersen, P., Bricelj, V. M., Cullen, J. J. and Rensel, J. E. 2001. *Monitoring and Management Strategies for Harmful Algal Blooms in Coastal Waters*. Paris, Intergovernmental Oceanographic Commission of UNESCO. (IOC Technical Series 59.)

Anderson, D. M., Cembella, A. D. and Hallegraeff, G. M. (eds). 1998. *Physiological Ecology of Harmful Algal Blooms*. Heidelburg, Springer-Verlag.

Babin, M. 2007. Phytoplankton fluorescence: theory, current literature and in situ measurement. In: Babin et al. (eds), op. cit., this volume.

Barber, R. T. and Smith, R. L. 1981. Coastal upwelling ecosystems. In: A. R. Longhurst (ed.), *Analysis of Marine Ecosystems*. San Diego, Calif., Academic Press, pp. 31–68.

Bates, S. S. 1998. Ecophysiology and metabolism of ASP toxin production. In: Anderson et al. (eds), op. cit., pp. 405–26.

Bedford Institute. 2003. www.mar.dfo-mpo.gc.ca/science/ocean/BedfordBasin/CTD/

Beutler, M., Wiltshire, K. H., Meyer, B., Moldaenke, C., Lüring, C., Meyerhöfer, M., Hansen, U.P. and Dau, H. 2002. A fluorometric method for the differentiation of algal populations *in vivo* and *in situ*. *Photosyn. Res.*, 72, pp. 39–53.

Bianchi, T. S., Engelhaupt, E., Westman, P., Andrén, T., Rolff, C. and Elmgren, R. 2000. Cyanobacterial blooms in the Baltic Sea: natural or human-induced? *Limnol. Oceanogr.*, 45, pp. 716–26.

Bidigare, R. R., Morrow, J. H. and Kiefer, D. A. 1989. Derivative analysis of spectral absorption by photosynthetic pigments in the western Sargasso Sea. *J. Mar. Res.*, 47, pp. 323–41.

Bissett, W. P., Schofield, O., Glenn, S., Cullen, J. J., Miller, W. L., Plueddemann, A. J. and Mobley, C. D. 2001. Resolving the impacts and feedback of ocean optics on upper ocean ecology. *Oceanogr. Mag.*, 14, pp. 30–53.

Bissett, W. P., Arnone R., Debra S., Dye D., Kirkpatrick G., Mobley C. and Schofield O. M. 2007. Integration of ocean-colour remote sensing with coastal nowcast/forecast simulations of harmful algal blooms. In Babin et al (eds) op. cit., this volume.

Bricelj, V. M. and Lonsdale, D. J. 1997. *Aureococcus anophagefferens*: causes and ecological consequences of brown tides in US mid-Atlantic coastal waters. *Limnol. Oceanogr.*, 42, pp. 1023–38.

Capone, D. G., Subramaniam, A., Montoya, J. P., Voss, M., Humborg, C., Johansen, A. M., Siefert, R. L. and Carpenter, E. J. 1998. An extensive bloom of the N_2-fixing cyanobacterium *Trichodesmium erythraeum* in the central Arabian Sea. *Mar. Ecol. Progr. Ser.*, 172, pp. 281–92.

Carr, M. E. 1998. A numerical study of the effect of periodic nutrient supply on pathways of carbon in a coastal upwelling regime. *J. Plankton Res.*, 20, pp. 491–516.

Cembella, A. D. 1998. Ecophysiology and metabolism of paralytic shellfish toxins in marine microalgae. In: Anderson et al. (eds), op. cit., pp. 381–403.

Chang, G. C. and Dickey, T. D. 2007. Interdisciplinary sampling strategies for detection and characterization of harmful algal blooms. In: Babin et al. (eds), op. cit., this volume.

Costanza, R., d'Arge, R., deGroot, R., Farber, S., Grasso, M., Hannon, B., Limburg, K., Naeem, S., O'Neill, R., Paruelo, J., Raskin, R., Sutton, P. and Vandenbelt, M. 1997. The value of the world's ecosystem services and natural capital. *Nature*, 387, pp. 253–60.

Cowles, T. J. 2003. Planktonic layers: physical and biological interactions on the small scale. In: *Handbook of Scaling Methods in Aquatic Ecology: Measurements, Analysis, Simulation*. Boca Raton, Fl., CRC Press, pp. 31–49.

Cullen, J. J. 1982. The deep chlorophyll maximum: comparing vertical profiles of chlorophyll *a. Can. J. Fish. Aquat. Sci.,* 39, pp. 791–803.

Cullen, J. J., Ciotti, A. M., Davis, R. F. and Lewis, M. R. 1997. Optical detection and assessment of algal blooms. *Limnol. Oceanogr.*, 42, pp. 1223–39.

Cullen, J. J., Ciotti, A. M. and Lewis, M. R. 1994. Observing biologically induced optical variability in coastal waters. *Ocean Optics XII, Proc. SPIE*, 2258, pp. 105–15.

Cullen, J. J. and Davis, R. F. 2003. The blank can make a big difference in oceanographic measurements. *Limnol. Oceanogr. Bull.*, 12, pp. 29–35.

Cullen, J. J., Franks, P. J. S., Karl, D. M. and Longhurst, A. 2002. Physical influences on marine ecosystem dynamics. In: A. R. Robinson, J. J. McCarthy and B. J. Rothschild (eds), *The Sea.* Vol. 12: *Biological-Physical Interactions in the Ocean.* New York, John Wiley & Sons, pp. 297–335.

Cullen, J. J., Geider, R. J., Ishizaka, J., Kiefer, D. A., Marra, J., Sakshaug, E. and Raven, J. A. 1993. Toward a general description of phytoplankton growth for biogeochemical models. In: G. T. Evans and M. J. R. Fasham (eds), *Towards a Model of Ocean Biogeochemical Processes*. Berlin, Springer-Verlag, pp. 153–76.

Cullen, J. J. and Lewis, M. R. 1995. Biological processes and optical measurements near the sea-surface: some issues relevant to remote sensing. *J. Geophys. Res.*, 100, pp. 13255–66.

Cullen, J. J. and MacIntyre, J. G. 1998. Behavior, physiology and the niche of depth-regulating phytoplankton. In: Anderson et al. (eds), op. cit., pp. 559–80.

Cullen, J. J., Yang, X. and MacIntyre, H. L. 1992. Nutrient limitation of marine photosynthesis. In: P. G. Falkowski and A. Woodhead (eds), *Primary Productivity and Biogeochemical Cycles in the Sea*. New York, Plenum Press, pp. 69–88.

Cullen, J. J., Yentsch, C. S., Cucci, T. L. and MacIntyre, H. L. 1988. Autofluorescence and other optical properties as tools in biological oceanography. *Proc. SPIE*, 925, pp. 149–56.

Dahl, E. and Tangen, K. 1993. 25 years experience with *Gyrodinium aureolum* in Norwegian waters. In: Smayda and Shimizu (eds), op. cit., pp. 15–21.

Davis, R. F., Stabeno, P. J. and Cullen, J. J. 2000. Use of optical measurements from moorings to detect coccolithophore blooms in the Bering Sea. *Ocean Optics XV, Proc. SPIE*, (CD-ROM)

Dekshenieks, M. M., Donaghay, P. L., Sullivan, J. M., Rines, J. E. B., Osborn, T. R. and Twardowski, M. S. 2001. Temporal and spatial occurrence of thin phytoplankton layers in relation to physical processes. *Mar. Ecol. Progr. Ser.*, 223, pp. 61–71.

Deyoe, H. R. and Suttle, C. A. 1994. The inability of the Texas 'brown tide' alga to use nitrate and the role of nitrogen in the initiation of a persistent bloom of this organism. *J. Phycol.*, 30, pp. 800–06.

Donaghay, P. L. and Osborn, T. R. 1997. Toward a theory of biological-physical control of harmful algal bloom dynamics and impacts. *Limnol. Oceanogr.*, 42, pp. 1283–96.

Eppley, R. W., Reid, F. M. H., Cullen, J. J., Winant, C. D. and Stewart, E. 1984. Subsurface patch of a dinoflagellate (*Ceratium tripos*) off Southern California: patch length, growth rate, associated vertically migrating species. *Mar. Biol.*, 80, pp. 207–14.

Falkowski, P. G. and Kolber, Z. 1995. Variations in chlorophyll fluorescence yields in phytoplankton in the world oceans. *Aust. J. Plant Physiol.*, 22, pp. 341–55.

Fennel, W. and Neumann, T. 2007. Modelling coastal dynamics and harmful algal blooms in the Baltic Sea. In: Babin et al. (eds), op. cit., this volume.

Figueiras, F. G., Gomez, E., Nogueira, E. and Villarino, M. L. 1996. Selection of *Gymnodinium catenatum* under downwelling conditions in the Ria del Vigo. In: T. Yasumoto, Y. Oshima and Y. Fukuyo (eds), *Harmful and Toxic Algal Blooms*. Paris, Intergovernmental Oceanographic Commission of UNESCO, pp. 215–18.

Fraga, S., Anderson, D. M., Bravo, I., Reguera, B., Steidinger, K. A. and Yentsch, C. M. 1988. Influence of upwelling relaxation on dinoflagellates and shellfish toxicity in Ria de Vigo, Spain. *Estuar. Coast. Mar. Sci*., 27, pp. 349–61.

Franks, P. J. S. 1997. Spatial patterns in dense algal blooms. *Limnol. Oceanogr*., 42, pp. 1297–305.

Franks, P. J. S. 2007. Physics and physical modelling of harmful algal blooms. In: Babin et al. (eds), op. cit., this volume.

Franks, P. J. S. and Anderson, D. M. 1992*a*. Alongshore transport of a toxic phytoplankton bloom in a buoyancy current: *Alexandrium tamarense* in the Gulf of Maine. *Mar. Biol*., 112, pp. 153–64.

Franks, P. J. S. and Anderson, D. M. 1992*b*. Toxic phytoplankton blooms in the southwestern Gulf of Maine: testing hypotheses of physical control using historical data. *Mar. Biol*., 112, pp. 165–74.

Franks, P. J. S. and Keafer, B. A. 2003. Sampling techniques and strategies for coastal phytoplankton blooms. In: Hallegraeff et al. (eds), op. cit., pp. 51–76.

Fromentin, J. M. and Planque, B. 1996. *Calanus* and environment in the eastern North Atlantic. II. Influence of the North Atlantic Oscillation on *C. finmarchicus* and *C. helgolandicus*. *Mar. Ecol. Progr. Ser*., 134, pp. 111–18.

Geider, R. J. 1987. Light and temperature dependence of the carbon to chlorophyll *a* ratio in microalgae and cyanobacteria: implications for physiology and growth of phytoplankton. *New Phytol*., 106, pp. 1–34.

Geider, R. J., Greene, R. M., Kolber, Z., MacIntyre, H. L. and Falkowski, P. G. 1993. Fluorescence assessment of the maximum quantum efficiency of photosynthesis in the western North Atlantic. *Deep Sea Res*., 40, pp. 1204–24.

Gentien, P. 1998. Bloom dynamics and ecophysiology of the *Gymnodinium mikimotoi* species complex. In: Anderson et al. (eds), op. cit., pp. 155–73.

Gentien, P. and Arzul, G. 1990. Exotoxin production by *Gyrodinium* cf. *aureolum* (Dinophyceae). *J. Mar. Biol. Assoc. UK*, 70, pp. 571–81.

Gentien, P., Lunven, M., Lehaitre, M. and Duvent, J. L. 1995. *In situ* depth profiling of particles sizes. *Deep Sea Res*., 42, pp. 1297–312.

GEOHAB. 2001. *Global Ecology and Oceanography of Harmful Algal Blooms, Science Plan*. Baltimore/Paris, Scientific Committee on Oceanic Research/Intergovernmental Oceanographic Commission of UNESCO.

Gjøsæter, J., Lekve, K., Stenseth, N. C., Leinaas, H. P., Christie, H., Dahl, E., Danielssen, D. S., Edvardsen, B., Olsgard, F., Oug, E. and Paasche, E. 2000. A long-term perspective on the *Chrysochromulina bloom* on the Norwegian Skagerrak coast 1988: a catastrophe or an innocent incident? *Mar. Ecol. Progr. Ser*., 207, pp. 201–18.

Glasgow, H. B., Burkholder, J. M., Reed, R. E., Lewitus, A. J. and Kleinman, J. E. 2004. Real-time remote monitoring of water quality: a review of current applications, and advancements in sensor, telemetry, and computing technologies. *J. Exp. Mar. Biol. Ecol*., 300, pp. 409–48.

Glenn, S. M., Dickey, T. D., Parker, B. and Boicourt, W. 2000. Long-term real-time coastal ocean observation networks. *Oceanogr. Mag*., 13, pp. 24–34.

Gobler, C. J., Renaghan, M. J. and Buck, N. J. 2002. Impacts of nutrients and grazing mortality on the abundance of *Aureococcus anophagefferens* during a New York brown tide bloom. *Limnol. Oceanogr*., 47, pp. 129–41.

Granéli, E., Paasche, E. and Maestrini, S. Y. 1993. Three years after the *Chrysochromulina polylepis* bloom in Scandinavian waters in 1988: some conclusions of recent research and monitoring. In: Smayda and Shimizu (eds), op. cit., pp. 23–32.

Grantham, B. A., Chan, F., Nielsen, K. J., Fox, D. S., Barth, J. A., Huyer, A., Lubchenco, J. and Menge, B. A. 2004. Upwelling-driven nearshore hypoxia signals ecosystem and oceanographic changes in the northeast Pacific. *Nature*, 249, pp. 749–54.

Griffiths, G. 2007. Glider and autonomous underwater vehicle observing systems. In: Babin et al. (eds), op. cit., this volume.

Hallegraeff, G. M. 2003. Harmful algal blooms: a global overview. In: Hallegraeff et al. (eds), op. cit., pp. 25–49.

Hallegraeff, G. M., Anderson, D. M. and Cembella, A. D. (eds). 2003. *Manual on Harmful Marine Microalgae*. Paris, Intergovernmental Oceanographic Commission of UNESCO. (Monographs on Oceanographic Methodology 11.)

Hallegraeff, G. M. and Fraga, S. 1998. Bloom dynamics of the toxic dinoflagellate *Gymnodinium catenatum*, with emphasis on Tasmanian and Spanish coastal waters. In: Anderson et al. (eds), op. cit., pp. 59–80.

Hanson, A. K. Jr and Donaghay, P. L. 1998. Micro- to fine-scale chemical gradients and layers in stratified coastal waters. *Oceanogr. Mag.*, 11, pp. 10–17.

Harashima, A., Tsuda, R., Tanaka, Y., Kimoto, T., Tatsuta, H. and Furusawa, K. 1997. Monitoring algal blooms and related biogeochemical changes with a flow-through system deployed on ferries in the adjacent seas of Japan. In: Kahru and Brown (eds), op. cit., pp. 85–112.

Heil, C. A., Glibert, P. M. and Fan, C. 2005. *Prorocentrum minimum* (Pavillard) Schiller: a review of a harmful algal bloom species of growing worldwide importance. *Harmful Algae*, 4, pp. 449–70.

Holligan, P. M. 1979. Dinoflagellate blooms associated with tidal fronts around the British Isles. In: Taylor and Seliger (eds), op. cit., pp. 249–56.

Holmes, R. W., Williams, P. M. and Eppley, R. W. 1967. Red water in La Jolla Bay, 1964–1966. *Limnol. Oceanogr.*, 12, pp. 503–12.

Honjo, T. 1993. Overview on bloom dynamics and physiological ecology of *Heterosigma akashiwo*. In: Smayda and Shimizu (eds), op. cit., pp. 33–42.

IOC. 2003. *The Integrated, Strategic Design Plan for the Coastal Ocean Observations Module of the Global Ocean Observing System*. Paris, Intergovernmental Oceanographic Commission of UNESCO.

IOCCG. 2000. *Remote Sensing of Ocean Colour in Coastal, and Other Optically-Complex, Waters*. Dartmouth, Nova Scotia, International Ocean-Colour Coordinating Group.

Jaffe, J. S. 2007. Sensing plankton: acoustics and optical imaging. In: Babin et al. (eds), op. cit., this volume.

James, K., Moroney, C., Roden, C., Satake, M., Yasumoto, T., Lehane, M. and Furey, A. 2003. Ubiquitous 'benign' alga emerges as the cause of shellfish contamination responsible for the human toxic syndrome, azaspiracid poisoning. *Toxicon*, 41, pp. 145–51.

Johnsen, G., Samset, O., Granskog, L. and Sakshaug, E. 1994. *In vivo* absorption characteristics in 10 classes of bloom-forming phytoplankton: taxonomic characteristics and responses to photoadaptation by means of discriminant and HPLC analysis. *Mar. Ecol. Progr. Ser.*, 105, pp. 149–57.

Johnsen, G., Volent, Z., Tangen, K. and Sakshaug, E. 1997. Time series of harmful and benign phytoplankton blooms in northwest European waters using the Seawatch buoy system. In: Kahru and Brown (eds), op. cit., pp. 115–43.

Johnson, K. S. and Coletti, L. J. 2002. *In situ* ultraviolet spectrophotometry for high resolution and long-term monitoring of nitrate, bromide and bisulfide in the ocean. *Deep Sea Res. I.*, 49, pp. 1291–305.

Juhl, A. R. and Latz, M. I. 2002. Mechanisms of fluid shear-induced inhibition of population growth in a red-tide dinoflagellate. *J. Phycol.*, 38, pp. 683–94.

Kahru, M. 1997. Using satellites to monitor large-scale environmental change: case study of cyanobacterial blooms in the Baltic Sea. In: Kahru and Brown (eds), op. cit., pp. 43–61.

Kahru, M. and Brown, W. (eds). 1997. *Monitoring Algal Blooms: New Technologies for Detecting Large-Scale Environmental Change*. Austin, Tex., Landes Bioscience.

Kahru, M., Horstmann, U. and Rud, O. 1994. Satellite detection of increased cyanobacterial blooms in the Baltic Sea: natural fluctuation or ecosystem change? Ambio, 23, pp. 469–72.

Kahru, M., Leppänen, J.-M., Rud, O. and Savchuk, O. P. 2000. Cyanobacteria blooms in the Gulf of Finland triggered by saltwater inflow into the Baltic Sea. *Mar. Ecol. Progr. Ser.*, 207, pp. 13–18.

Kamykowski, D. 1974. Possible interactions between phytoplankton and semidiurnal internal tides. *J. Mar. Res.*, 32, pp. 67–89.

Kamykowski, D. 1995. Trajectories of autotrophic marine dinoflagellates. *J. Phycol.*, 31, pp. 200–08.

Kamykowski, D., Milligan, E. J., Reed, R. E. and Liu, W. 1999. Geotaxis/phototaxis and biochemical patterns in *Heterocapsa illdefina* (Dinophyceae) during vertical migrations. *J. Phycol.*, 35, pp. 1397–1403.

Karl, D. M., Bidigare, R. R. and Letelier, R. M. 2001. Long-term changes in plankton community structure and productivity in the North Pacific Subtropical Gyre: the domain shift hypothesis. *Deep Sea Res.* II, 48, pp. 1449–70.

Karp-Boss, L., Boss, E. and Jumars, P. A. 1996. Nutrient fluxes to planktonic osmotrophs in the presence of fluid motion. *Oceanogr. Mar. Biol. Ann. Rev.*, 34, pp. 71–107.

Kiørboe, T. 1993. Turbulence, phytoplankton cell size, and the structure of pelagic food webs. *Adv. Mar. Biol.*, 29, pp. 1–72.

Kirk, J. T. O. 1994. *Light and Photosynthesis in Aquatic Ecosystems*. Cambridge, UK, Cambridge University Press, 509 pp.

Kolber, Z. and Falkowski, P. G. 1993. Use of active fluorescence to estimate phytoplankton photosynthesis *in situ. Limnol. Oceanogr.*, 38, pp. 1646–65.

Kolber, Z., Zehr, J. R. and Falkowski, P. G. 1988. Effects of growth irradiance and nitrogen limitation on photosynthetic energy conversion in photosystem II. *Plant Physiol.*, 88, pp. 923–29.

Kononen, K., Huttunen, M., Hällfors, S., Gentien, P., Lunven, M., Huttula, T., Laanemets, J., Lilover, M. and Pavelson, J. 2003. Development of a deep chlorophyll maximum of *Heterocapsa triquetra* Ehrenb. at the entrance to the Gulf of Finland. *Limnol. Oceanogr.*, 48, pp. 594–607.

Lam, C. W. Y. and Ho, K. C. 1989. Red tides in Tolo Harbour, Hong Kong. In: T. Okaichi, D. M. Anderson and T. Nemoto (eds), *Red Tides: Biology, Environmental Science, and Toxicology*. New York, Elsevier, pp. 49–52.

Lancelot, C. 1995. The mucilage phenomenon in the continental coastal water of the North Sea. *Sci. Total Environ.*, 165, pp. 83–102.

Lancelot, C., Keller, M. D., Rousseau, V., Smith, W. O. Jr and Mathot, S. 1998. Autecology of the marine haptophyte *Phaeocystis* sp. In: Anderson et al. (eds), op. cit., pp. 209–24.

Laney, S. R. 2003. Assessing the error in photosynthetic properties determined by fast repetition rate fluorometry. *Limnol. Oceanogr.*, 48, pp. 2234–42.

Lee, J. H. W., Choi, D. K. W., Wong, K. T. M., Qu, B. and Arega, F. 2007. Modelling algal dynamics in eutrophic coastal waters. In: Babin et al. (eds), op. cit., this volume.

Legendre, L. and Le Fevre, J. 1989. Hydrodynamic singularities as controls of recycled versus export production in oceans. In: W. H. Berger, V. S. Smetacek and G. Wefer (eds), *Productivity of the Ocean: Present and Past*. New York, John Wiley & Sons, pp. 49–63.

Lehaitre, M., Delauney, L. and Compère, C. 2007. Biofouling and underwater measurements. In: Babin et al. (eds), op. cit., this volume.

Levandowsky, M. and Kaneta, P. J. 1987. Behaviour in dinoflagellates. In: F. J. R. Taylor (ed.), *The Biology of Dinoflagellates*. Oxford, Blackwell Scientific Publications, pp. 360–97.

Lewis, M. R. 2002. Variability of plankton and plankton processes on the mesoscale. In: P. J. L. Williams, D. N. Thomas and C. S. Reynolds (eds), *Phytoplankton Productivity: Carbon Assimilation in Marine and Freshwater Ecosystems*. Oxford, Blackwell Science, pp. 141–55.

Lewis, M. R. 2007. Measurement of apparent optical properties for diagnosis of harmful algal blooms. In: Babin et al. (eds), op. cit., this volume.

Li, W. K. W. and Dickie, P. M. 2001. Monitoring phytoplankton, bacterioplankton, and virioplankton in a coastal inlet (Bedford Basin) by flow cytometry. *Cytometry*, 44, pp. 236–46.

Li, W. K. W., Dickie, P. M., Spry, J. A., Perry, T. and Head, E. J. H. 2003. Bedford Basin Plankton Monitoring Program: 1992–2002. Department of Fisheries and Oceans Canada. www.mar.dfompo.gc.ca/science/ocean/BedfordBasin/Publications/BBPMP_Poster.pdf

Lorenzen, C. J. 1966. A method for the continuous measurement of *in vivo* chlorophyll concentration. *Deep Sea Res.*, 13, pp. 223–27.

Malone, T. C. 2001. Harmful Algal Events. In: *GOOS Data Products and Services Bulletin*. http://ioc.unesco.org/gpsbulletin/GPS1&2/issue2.htm

Malone, T. C. 2006. Ecosystem dynamics, harmful algal blooms and operational oceanography. In: Babin et al. (eds), op. cit., pp. 237–280 this volume.

Margalef, R. 1978. Life forms of phytoplankton as survival alternatives in an unstable environment. *Oceanol. Acta*, 1, pp. 493–509.

Margalef, R., Estrada, M. and Blasco, D. 1979. Functional morphology of organisms involved in red tides, as adapted to decaying turbulence. In: Taylor and Seliger (eds), op. cit., pp. 89–94.

Marra, J. 1992. Diurnal variability in chlorophyll fluorescence: observations and modelling. *Ocean Optics XI, Proc. SPIE*, 1750, pp. 233–44.

McGillicuddy, D. J. Jr, Anderson, D. M., Stock, C. A., Lynch, D. R. and Townsend, D. W. 2007. Modelling blooms of *Alexandrium fundyense* in the Gulf of Maine. In: Babin et al. (eds), op. cit., this volume.

McMahon, T., Raine, R. and Silke, J. 1998. Oceanographic control of harmful phytoplankton blooms in and around southwestern Ireland. In: Reguera et al. (eds), op. cit., pp. 128–30.

Merico, A., Tyrrell, T., Lessard, E. J., Oguz, T., Stabeno, P. J., Zeeman, S. I. and Whitledge, T. E. 2004. Modelling phytoplankton succession on the Bering Sea shelf: role of climate influences and trophic interactions in generating *Emiliania huxleyi* blooms 1997–2000. *Deep Sea Res*. I, 51, pp. 1803–26.

Michaels, A. F. and Silver, M. W. 1988. Primary production, sinking fluxes and the microbial food web. *Deep Sea Res.*, 35, pp. 473–90.

Millie, D. F., Kirkpatrick, G. J. and Vinyard, B. T. 1995. Relating photosynthetic pigments and *in vivo* optical density spectra to irradiance for the Florida red-tide dinoflagellate *Gymnodinium breve. Mar. Ecol. Progr. Ser*., 120, pp. 65–75.

Moloney, C. L., Field, J. G. and Lucas, M. I. 1991. The size-based dynamics of plankton food webs. II: Simulations of three contrasting southern Benguela food webs. *J. Plankton Res*., 13, pp. 1039–92.

Morel, A. 2007. Introduction to optical properties in the sea: theoretical aspects. In: Babin et al. (eds), op. cit., this volume.

Morel, A. and Bricaud, A. 1986. Inherent properties of algal cells including picoplankton: theoretical and experimental results. In: T. Platt and W. K. W. Li (eds), *Photosynthetic Picoplankton*. Toronto, *Can. Bull. Fish. Aquat. Sci*., 214, pp. 521–59.

Neale, P. J., Cullen, J. J. and Yentsch, C. M. 1989. Bio-optical inferences from chlorophyll *a* fluorescence: what kind of fluorescence is measured in flow cytometry? *Limnol. Oceanogr.*, 34, pp. 1739–48.

Nicholls, R. J. and Small, C. 2002. Improved estimates of coastal population and exposure to hazards. *EOS: Trans. Am. Geophys. Union*, 83, p. 301.

Okaichi, T. 1997. Red tides in the Seto Inland Sea. In: T. Okaichi and T. Yanagi (eds), *Sustainable Development in the Seto Inland Sea, Japan – From the Viewpoint of Fisheries*. Tokyo, Terra Scientific Publishing Company, pp. 251–304.

Oliver, R. L. 1994. Floating and sinking in gas-vacuolate cyanobacteria. *J. Phycol*., 30, pp. 161–73.

Olson, M. B. and Strom, S. L. 2002. Phytoplankton growth, microzooplankton herbivory and community structure in the southeast Bering Sea: insight into the formation and temporal persistence of an *Emiliania huxleyi* bloom. *Deep Sea Res. II*, 49, pp. 5969–90.

Parkhill, J.-P., Maillet, G. and Cullen, J. J. 2001. Fluorescence-based maximal quantum yield for photosystem II as a diagnostic of nutrient limitation. *J. Phycol.*, 37, pp. 517–29.

Pinardi, N., Fratianni, C. and Adani, M. 2007. Use of real-time observations in an operational data assimilation system: the Mediterranean case. In: Babin et al. (eds), op. cit., this volume.

Pitcher, G. C., Bernard, S. and Fawcett, A. 2007. Real-time coastal observing systems for ecosystem dynamics and harmful algal blooms: needs and expectations of users. In: Babin et al. (eds), op. cit., this volume.

Pitcher, G. C., Boyd, A. J., Horstman, D. A. and Mitchell-Innes, B. A. 1998. Subsurface dinoflagellate populations, frontal blooms and the formation of red tide in the southern Benguela upwelling system. *Mar. Ecol. Progr. Ser.*, 172, pp. 253–64.

Pollingher, U. and Zemel, E. 1981. *In situ* and experimental evidence of the influence of turbulence on cell division processes of *Peridinium cinctum* forma *westii* (Lemm.) Lefevre. *Br. Phycol. J.*, 16, pp. 281–87.

Pratt, D. M. 1966. Competition between *Skeletonema costatum* and *Olisthodiscus luteus* in Narragansett Bay and in culture. *Limnol. Oceanogr.*, 11, pp. 447–55.

Reguera, B., Blanco, J., Fernández, M. L. and Wyatt, T. (eds), 1998. *Harmful Algae*. Proc. VIII International Conference on Harmful Algae (June 1997, Vigo, Spain). Santiago de Compostela/Paris, Xunta de Galicia/Intergovernmental Oceanographic Commission of UNESCO.

Reynolds, C. S. 2002. On the interannual variability in phytoplankton production in freshwaters. In: P. J. L. Williams, D. N. Thomas and C. S. Reynolds, (eds), *Phytoplankton Productivity: Carbon Assimilation in Marine and Freshwater Ecosystems*. Oxford, UK, Blackwell Science, pp. 187–221.

Reynolds, C. S. and Smayda, T. J. 1998. Principles of species selection and community assembly in phytoplankton; Further explorations of the mandala. In: Reguera et al. (eds), op. cit., pp. 8–10.

Riegman, R. 1998. Species composition of harmful algal blooms in relation to macronutrient dynamics. In: Anderson et al. (eds), op. cit., pp. 475–86.

Rines, J. E. B., Donaghay, P. L., Dekshenieks, M. M., Sullivan, J. M. and Twardowski, M. S. 2002. Thin layers and camouflage: hidden *Pseudo-nitzschia* spp. (Bacillariophyceae) populations in a fjord in the San Juan Islands, Washington, USA. *Mar. Ecol. Progr. Ser.*, 225, pp. 123–37.

Roemmich, D. and Mcgowan, J. 1995. Climatic warming and the decline of zooplankton in the California Current. *Science*, 267, pp. 1324–26.

Roesler, C. and Perry, M. J. 1995. *In situ* phytoplankton absorption, fluorescence emission, and particulate backscattering spectra determined from reflectance. *J. Geophys. Res.*, 100, pp. 13279–94.

Roesler, C. S. and Boss, E. 2007. *In situ* measurement of inherent optical properties and potential for harmful algal bloom detection and coastal ecosystem observations. In: Babin et al. (eds), op. cit., this volume.

Ruddick, K., Lacroix, G., Park, Y., Rousseau, V., De Cauwer, V. and Sterckx, S. 2007. Overview of ocean colour: theoretical background, sensors and applicability to detection and monitoring of harmful algal blooms (capabilities and limitations). In: Babin et al. (eds), op. cit., this volume.

Ryther, J. H. 1969. Photosynthesis and fish production in the sea. *Science*, 166, pp. 72–76.

Schmidt, L. E. and Hansen, P. J. 2001. Allelopathy in the prymnesiophyte *Chrysochromulina polylepis*: effect of cell concentration, growth phase and pH. *Mar. Ecol. Progr. Ser.*, 216, pp. 67–81.

Schofield, O., Bosch, J., Glenn, S., Kirkpatrick, G., Kerfoot, J., Lohrenz, S., Moline, M., Oliver, M. and Bissett, P. 2007. Bio-optics in integrated ocean observing networks: potential for studying harmful algal blooms. In: Babin et al. (eds), op. cit., this volume.

Schofield, O., Grzymski, J., Bissett, W. P., Kirkpatrick, G. J., Millie, D. F., Moline, M. and Roesler, C. S. 1999. Optical monitoring and forecasting systems for harmful algal blooms: possibility or pipe dream? *J. Phycol.*, 35, pp. 1476–96.

Schofield, O., Prézelin, B. B. and Johnsen, G. 1996. Wavelength dependency in the photosynthetic parameters for two dinoflagellate species *Heterocapsa pygmaea* and *Prorocentrum minimum*, implications for the bio-optical modeling of photosynthetic rates. *J. Phycol.*, 32, pp. 574–83.

Scholin, C. A., Doucette, G. J. and Cembella, A. D. 2007. Prospects for developing automated systems for *in situ* detection of harmful algae and their toxins. In: Babin et al. (eds), op. cit., this volume.

Schreiber, U., Schliwa, U. and Bilger, B. 1986. Continuous recording of photochemical and nonphotochemical chlorophyll fluorescence quenching with a new type of modulation fluorometer. *Photosyn. Res.*, 10, pp. 51–62.

Seliger, H. H., Carpenter, J. H., Loftus, M. and McElroy, W. D. 1970. Mechanism for the accumulations of high concentrations of dinoflagellates in a bioluminescent bay. *Limnol. Oceanogr.*, 15, pp. 234–45.

Sellner, K. G. 1997. Physiology, ecology, and toxic properties of marine cyanobacteria blooms. *Limnol. Oceanogr.*, 42, pp. 1089–1104.

Sheng, J. and Wang, L. 2004. A high-resolution coastal circulation model for Lunenburg Bay, Nova Scotia. *Proc. 8th International Conference on Estuarine and Coastal Modeling*, pp. 372–87.

Smayda, T. J. 1997*a*. Harmful algal blooms: their ecophysiology and general relevance to phytoplankton blooms in the sea. *Limnol. Oceanogr.*, 42, pp. 1137–53.

Smayda, T. J. 1997*b*. What is a bloom? A commentary. *Limnol. Oceanogr.*, 42, pp. 1132–36.

Smayda, T. J. 2002. Turbulence, watermass stratification and harmful algal blooms: an alternative view and frontal zones as 'pelagic seed banks'. *Harmful Algae*, 1, pp. 95–112.

Smayda, T. J. 2003. Environmental monitoring, with examples from Narragansett Bay. In: Hallegraeff et al., op. cit., pp. 595–625.

Smayda, T. J. and Shimizu, Y. (eds). 1993. *Toxic Phytoplankton Blooms in the Sea*. Amsterdam, Elsevier.

Smetacek, V. 1998. How mainstream biological oceanography can profit from harmful-algal-bloom studies and vice versa. In: Reguera et al. (eds), op. cit., pp. 109–13.

Sosik, H. M. 2007. Characterizing seawater constituents from optical properties. In: Babin et al. (eds), op. cit., this volume.

Stumpf, R. P., Culver, M. E., Tester, P. A., Tomlinson, M., Kirkpatrick, G. J., Pederson, B. A., Truby, E., Ransibrahmanakul, V. and Soracco, M. 2003. Monitoring *Karenia brevis* blooms in the Gulf of Mexico using satellite ocean color imagery and other data. *Harmful Algae*, 2, pp. 147–60.

Suggett, D. J., Oxborough, K., Baker, N. R., Macintyre, H. L., Kana, T. M. and Geider, R. J. 2003. Fast repetition rate and pulse amplitude modulation chlorophyll *a* fluorescence measurements for assessment of photosynthetic electron transport in marine phytoplankton. *Eur. J. Phycol.*, 38, pp. 371–84.

Sverdrup, H. U. 1953. On conditions for the vernal blooming of phytoplankton. *J. Cons. Int. Explor. Mer.*, 18, pp. 287–95.

Tangen, K. 1997. Monitoring phytoplankton blooms continuously with SEAWATCH technology. In: J. H. Stel, H. W. A. Behrens, J. C. Borst, L. J. Droppert and J. V. D. Meulen (eds), *Operational Oceanography: The Challenge for European Cooperation*. Amsterdam, Elsevier Science, p. 539.

Taylor, D. L. and Seliger, H. H. (eds). 1979. *Toxic Dinoflagellate Blooms*. New York, Elsevier-North Holland.

Taylor, F. J. R. and Haigh, R. 1993. The ecology of fish-killing blooms of the chloromonad flagellate *Heterosigma* in the Strait of Georgia and adjacent waters. In: Smayda and Shimizu (eds), op. cit., pp. 705–10.

Tester, P. A. and Steidinger, K. A. 1997. *Gymnodinium breve* red tide blooms: initiation, transport, and consequences of surface circulation. *Limnol. Oceanogr.*, 42, pp. 1039–51.

Tont, S. A. 1976. Short-period climatic fluctuations: effects on diatom biomass. *Science*,194, pp. 942–44.

Tracey, G. A. 1988. Feeding reduction, reproductive failure, and mortality in *Mytilus edulis* during the 1985 'brown tide' in Narragansett Bay, Rhode Island. *Mar. Ecol. Progr. Ser.*, 50, pp. 73–81.

Turner, J. T. and Tester, P. A. 1997. Toxic marine phytoplankton, zooplankton grazers, and pelagic food webs. *Limnol. Oceanogr.*, 42, pp. 1203–14.

Tyler, M. A. and Seliger, H. H. 1978. Annual subsurface transport of a red tide dinoflagellate to its bloom area: water circulation patterns and organism distributions in the Chesapeake bay. *Limnol. Oceanogr.*, 23, pp. 227–46.

Tyler, M. A. and Seliger, H. H. 1981. Selection for a red tide organism: physiological responses to the physical environment. *Limnol. Oceanogr.*, 26, pp. 310–24.

Walstad, L. J. and McGillicuddy, D. J. 2000. Data assimilation for coastal observation systems. *Oceanography Mag.*, 13, pp. 47–53.

Weise, A. M., Levasseur, M., Saucier, F. J., Senneville, S., Bonneau, E., Roy, S., Sauve, G., Michaud, S. and Fauchot, J. 2002. The link between precipitation, river runoff, and blooms of the toxic dinoflagellate *Alexandrium tamarense* in the St. Lawrence. *Can. J. Fish. Aquat. Sci.*, 59, pp. 464–73.

Yamamoto, T. 2003. The Seto Inland Sea – eutrophic or oligotrophic? *Mar. Poll. Bull.*, 47, pp. 37–42.

Yamamoto, T., Seike, T., Hashimoto, T. and Tarutani, K. 2002. Modelling the population dynamics of the toxic dinoflagellate *Alexandrium tamarense* in Hiroshima Bay, Japan. *J. Plankton Res.*, 24, pp. 33–47.

Yanagi, T. and Okaichi, T. 1997. Seto Inland Sea — historical background. In: T. Okaichi and T. Yanagi (eds), *Sustainable Development in the Seto Inland Sea, Japan — From the Viewpoint of Fisheries*. Tokyo, Terra Scientific Publishing Company, pp. 9–14.

Zhang, J. 1994. Atmospheric wet depositions of nutrient elements: Correlations with harmful biological blooms in the northwest Pacific coastal zones. *Ambio.*, 23, pp. 464–68.

Zingone, A. and Enevoldsen, H. O. 2000. The diversity of harmful algal blooms: a challenge for science and management. *Ocean Coast. Manag.*, 43, pp. 725–48.

2

Interdisciplinary sampling strategies for detection and characterization of harmful algal blooms

G. Chang and T. D. Dickey

2.1 Introduction

Many harmful algal blooms (HABs) are marked by the presence of toxic or noxious algae that result in a negative impact on human activities. Mass mortalities of fish and shellfish (farmed and natural), decreases in fecundity in fish, and death of marine mammals and birds have been reported as a result of the consumption of toxic algae. Transfer of toxins through the food web may also lead to human illnesses (Anderson et al., 2001, Table 1.1; Cullen, 2007, Table 1.1). Harmful algal species can also have deleterious effects on ecology without producing toxins, e.g. mucilage-producing or spine-bearing species that clog or damage gills of fish and other invertebrates (Zingone and Enevoldsen, 2000) and large blooms that cause hypoxia or anoxia – as HABs decline and biomass decays – leading to fish kills (Horner et al., 1997). These problems often result in extreme economic losses in coastal regions, affecting the fish and shellfish industries, aquaculture and tourism.

It was once thought that HABs were small, localized problems but recent evidence suggests that these phenomena occur in nearly every coastal region throughout the world (Anderson, 1995). Despite the increasing occurrences of HABs and the escalating number of affected resources, existing detection and prediction techniques are limited and many present-day monitoring efforts are time intensive and/or costly. Most current HAB monitoring programmes are not designed to focus on understanding the environmental or anthropogenic conditions that contribute to the formation and cessation of HABs. Consequently, they have limited potential for prediction. This is changing through the establishment of HAB research programmes.

2.1.1 Examples of HAB programmes

Since 1992, the California Department of Health Services (CDHS) has enlisted the help of more than 20 research institutions to collect water samples along the California coast on a weekly basis. These water samples are then shipped to the CDHS in northern California for laboratory analyses (species identification, cell concentration, chemical analyses, etc.). The CDHS then compiles the data and releases Monthly Biotoxin Reports (e.g. CDHS, 2001) that describe the health of California's coastal waters. Several other coastal regions worldwide have implemented HAB sampling programmes similar to that of the CDHS (e.g. Harmful Algal Bloom Initiation and Prediction in

Large European Marine Ecosystems (HABILE) in the North Sea, Fisheries & Oceans Canada, South Carolina Task Group on Harmful Algae; see Anderson et al., 2001).

Some other monitoring programmes enlist volunteer fishermen, beachgoers and/or trained citizens to report any signs of HAB formation to responsible authorities (e.g. University of Maine Red Tide Monitoring Network; the 'fish farm observation network' in Norway; Johnson and Sakshaug, 2000; Kawaga fish culture monitoring in Japan; and Chilean Salmon Farmer's Association; Anderson et al., 2001). This method has reduced human consumption of toxic organisms and provides educational outreach to the local community, but does not advance research on the scientific problem of HAB formation. HAB monitoring efforts such as the CDHS or the fish farm observation network, although detail-oriented, accurate and relatively low-cost, may ignore shorter-lived or small-scale, patchy HABs. HABs can persist for as short as a few days to as long as several months and can exist in spatial domains of a few metres to coast-wide. Spatio-temporal irregularity in observations can lead to aliases in sampling and misinterpretation of results, that is overlooked HABs. Importantly, these programmes are not intended to predict, characterize, or mitigate HABs.

Recent coastal ecology research efforts have been aimed at characterizing HABs and the causes of their formation, persistence and termination. The US Ecology and Oceanography of Harmful Algal Blooms (ECOHAB) programme has generally been directed towards studies of specific harmful algal species in an oceanographic context. The US Monitoring and Event Response for Harmful Algal Blooms (MERHAB) programme is designed for research and regional intensive monitoring of HABs. Its current projects, in the Pacific Northwest (Olympic Region HAB, ORHAB), Maryland and Florida, show promise for the development of state-of-the-art HAB monitoring networks, prediction and early warning of events to the local community. Johnsen and Sakshaug (2000) describe a HAB monitoring programme along the Norwegian coast that uses a network of observers in addition to moored buoys (SEAWATCH) that provide continuous time series of bio-optical, biological, chemical and physical parameters. When a potential bloom is detected by the buoy system, that is when certain properties exceed pre-specified threshold values, the Norwegian Food Hygiene Control Authorities are informed and complementary ship-based sampling is conducted. This monitoring and research programme has proved useful for advance public warning of HABs and provided information regarding the environmental conditions leading to HABs along the Norwegian coast. In Japan, government-sponsored monitoring and research programmes resulted in greatly increased understanding of the causes of formation of HABs in the Seto Inland Sea (see Section 2.2.3; Murakawa, 1987; Okaichi, 1989).

On-going HAB monitoring programmes can benefit from augmentation with real-time autonomous sampling systems on a wide variety of spatial and temporal scales. In this chapter we argue that it is necessary to develop, verify, and implement long-term interdisciplinary HAB monitoring programmes that collect physical, bio-optical, biological and chemical data on timescales as short as a few hours and on spatial scales from metres to coast-wide. These data should be accessible in (near) real-time and alert researchers and responsible authorities to the possibility of HAB formation, specifically when key HAB parameters exceed specified threshold values. The programme should also allow for adaptive sampling (see review by Robinson and Glenn, 1999), specifically changing sampling locations and changing sampling rates using two-way data communication during periods of HAB formation, persistence and cessation. This is especially important because scales of interdisciplinary sampling are dependent on the

HAB species as well as regional ecology (Cullen, 2007 – Chapter 1 this volume). These new techniques would complement existing detail-oriented HAB monitoring efforts such as those conducted by the CDHS, providing shorter temporal scale measurements on a wide range of spatial domains and more timely and adaptive sampling strategies.

The purpose of this chapter is to motivate the use of interdisciplinary, autonomous sampling strategies for HAB studies. We first briefly review some of the physical, chemical and biological oceanographic processes that can affect the formation, persistence and cessation of HABs and include some examples of HAB studies relating to these disciplines. We then summarize sensor and system technologies relevant to HAB detection and characterization. Lastly, we suggest new sampling strategies for future HAB research and monitoring programmes.

2.2 Processes in the coastal ocean

2.2.1 Physical processes

Time-series data and extensive spatial observations of physical oceanographic parameters enable the identification of some of the major forcing factors affecting the formation, persistence and cessation of HABs in the coastal ocean (Figure 2.1; also see Franks, Chapter 15). The timescales of variability for these forcing factors can vary from minutes (e.g. turbulence and internal solitary waves) to hours (e.g. tidal and inertial processes) to days and months (e.g. upwelling and fronts) and longer (e.g. El Niño and the North Atlantic Oscillation). Spatial scales are equally wide-ranging, from metre-scale processes or smaller (bioturbation) to basin-wide (El Niño) to global scales (air/sea interaction and the hydrologic cycle; Figure 2.1).

Small-scale physical phenomena are generally dominated by turbulence, which affects molecular and cellular-scale processes. Diel cycles of solar insolation and tidal frequencies (diurnal and semi-diurnal) often control variability of various physical, bio-optical and chemical parameters (Figure 2.2; Stramska and Dickey, 1992; Abbott et al., 1995; Chang and Dickey, 2001; Chang et al., 2002). Solar insolation influences radiant heating rates of the upper ocean (e.g. Lewis et al., 1983, 1990; Ohlmann et al., 2000; Ohlmann and Siegel, 2000; Chang and Dickey, 2004), and thus affects stratification and the vertical movement of nutrients, phytoplankton and their grazers. Tidal processes, in addition to surface and internal gravity and solitary waves (e.g. Bogucki et al., 1997), can vertically redistribute phytoplankton with respect to the light field, nutrients and grazers (Kamykowski, 1974).

Many important processes are quasi-periodic and episodic, occurring at scales of days to months and tens of metres to thousands of kilometres. Inertial and other periodic oscillations are often caused by wind events, for example storms and hurricanes (Figure 2.3; Dickey et al., 1998a; Chang et al., 2001). These oscillations act similarly to tidal processes and have been reported to pump nutrients from below the mixed layer into the euphotic zone where they can be used by phytoplankton (McNeil et al., 1999). Persistent winds influence upwelling and downwelling and hence nutrient availability, which is often seasonally important to coast-wide and regional ecology and HABs (see Section 2.2.4). Mesoscale features (scales of days to months and tens of kilometres) include, but are not limited to, fronts (Barth et al., 1998, Figure 2.4), jets (Chang et al., 2002) and eddies (e.g. McNeil et al., 1999). These physical processes can enhance or inhibit nutrient

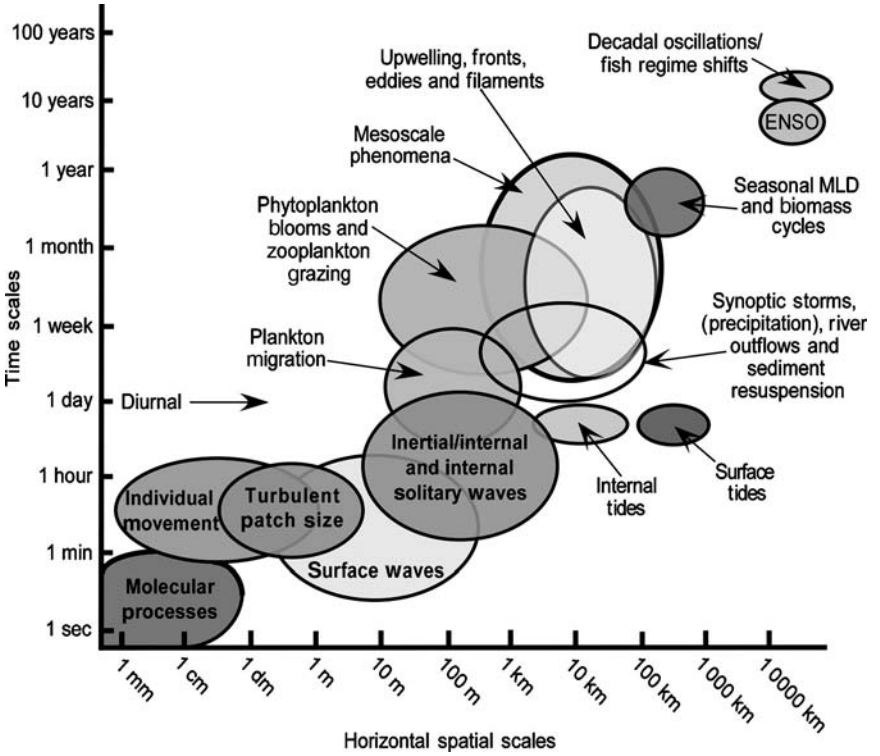

Figure 2.1
Time-space diagram illustrating some of the processes that are important for harmful algal blooms.
Source: modified from Dickey (1991).

and particulate movement and hence phytoplankton bloom formation and termination (Franks, 2007 – Chapter 15 this volume). Longer-term and larger-scale physical forcing associated with equatorial processes (El Niño-Southern Oscillation – ENSO; e.g. Chavez et al., 2002) and other decadal-scale processes around the earth (North Atlantic Oscillation, NAO; Pacific Decadal Oscillation, PDO; and others) can also have impacts on the coastal ocean through alterations of ocean-atmosphere interactions and nutrient and light availability.

Some examples of studies that have investigated physical processes and their roles in HABs follow. Tester and Steidinger (1997) found that blooms of the toxic dinoflagellate, *Karenia brevis* (formerly *Gymnodinium breve*; neurotoxic shellfish poisoning; e.g. Anderson, 1995), on the West Florida Shelf (WFS) are closely coupled with physical processes. Shoreward movements of the Gulf of Mexico Loop Current or spin-offs of eddies from the Loop Current often trigger *K. brevis* blooms on timescales of days to weeks, covering much of the eastern Gulf of Mexico. Stumpf et al. (2003) use ocean-colour imagery to monitor the occurrence and presence of these blooms. These HABs tend to accumulate and grow at a persistent mid-shelf convergence front that is maintained by seasonal winds along the west Florida coast. Gulf of Mexico eddy

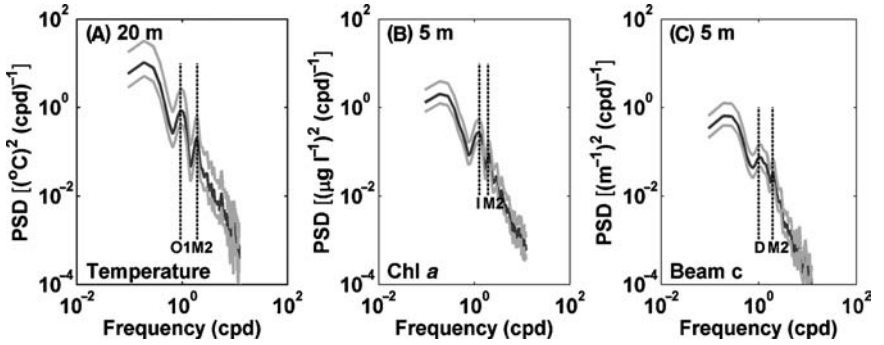

Figure 2.2
Frequency power spectral density functions (PSDs) of A, 20 m temperature; B, 5 m chlorophyll *a* concentration, an indicator of phytoplankton; C, 5 m beam attenuation data, a proxy for particles, collected off the coast of New Jersey in 24 m water depth.
O1, diurnal tidal; M2, semidiurnal tidal; I, inertial; D, diel frequencies.
The grey lines represent the 95% confidence intervals.
This figure shows that diel and tidal oscillations can dominate both physical and particulate processes.

circulation affects bloom retention and distribution, and the Florida Current and Gulf Stream act to transport the *K. brevis* blooms out of the WFS region. It is thought that decreasing water temperatures may also contribute to cessation of blooms of the warm-water species, *K. brevis*.

Coastal buoyant plumes have been found to be responsible for the transport of *Alexandrium tamarense* in the south-western Gulf of Maine (Keafer and Anderson, 1991). *A. tamarense* is a toxic dinoflagellate, found to produce biotoxins and result in paralytic shellfish poisoning syndrome (e.g. Anderson, 1995). Keafer and Anderson (1991) used sea surface temperature (SST), estimated from remotely sensed imagery, to track a warm coastal plume that formed from spring runoff. This buoyant plume was found to be responsible for the southerly transport of *A. tamarense* along the east coast of the US springtime coastal upwelling then shifted the plume of warmer water containing *A. tamarense* offshore. This study by Keafer and Anderson (1991) demonstrates the utility of large-scale, remotely sensed SST data for HAB characterization and monitoring (see Section 2.3.2).

Lindahl (1986) found a correlation between high-salinity plumes of Skagerrak (northern European) waters and blooms of the toxic dinoflagellate *Gymnodinium mikimotoi* (formerly *Gyrodinium aureolum*) on the west coast of Scandinavia. Lindahl (1986) hypothesized that *G. mikimotoi* blooms offshore and is transported towards the coast by wind-induced currents and convergent flows. These examples illustrate the need for high temporal and spatial resolution and judiciously placed physical instrumentation for understanding HAB dynamics in a coastal region.

2.2.2 Biological processes

The growth of harmful algae generally has two principal requirements: nutrients and light. Nutrient uptake and light adaptation in phytoplankton take place on timescales

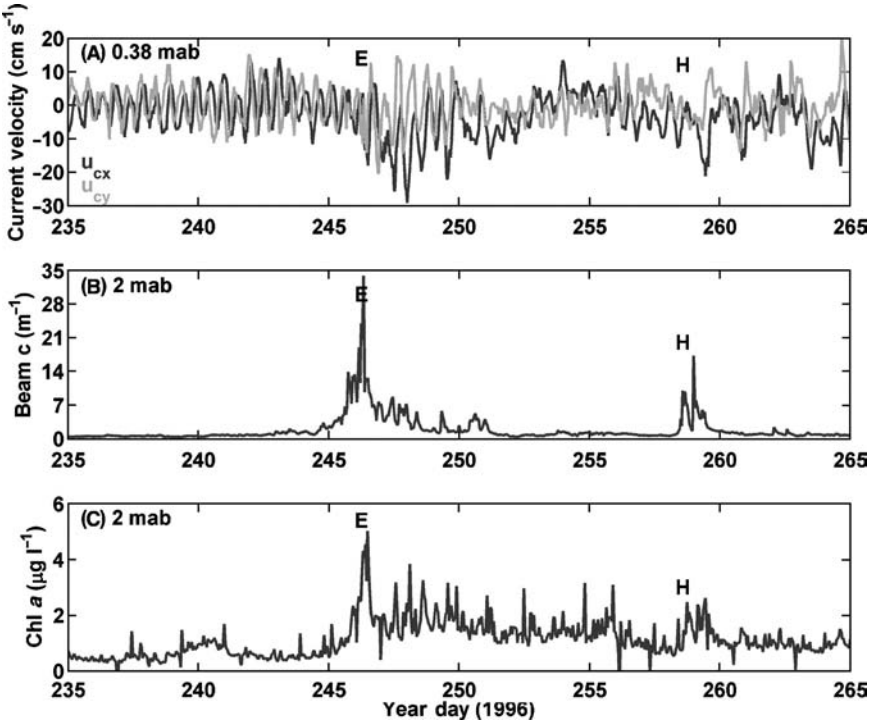

Figure 2.3
Time series of A, current velocity at 0.38 mab above the ocean bottom (u_{cx} = east-west currents, u_{cy} = north-south currents); B, beam attenuation coefficient at 2 mab (660 nm); C, chlorophyll *a* concentration at 2 mab during the passages of Hurricanes Edouard (2 September) and Hortense (14 September; E and H respectively) during autumn 1996. These data show (A) storm-induced oscillations and intense mixing followed by (B and C) resuspension of sediments and relict pigments. All data were collected on a mooring off the coast of Cape Cod, Massachusetts, in 70 m water depth.

of hours to days and are generally more spatially important in the vertical direction, that is with depth of the water column. The observations and sampling of biological parameters are focused on phytoplankton behaviour (e.g. motility), physiology (nutrient uptake) and grazing pressures.

Many harmful algae are dinoflagellates, which have been observed to be adapted to decaying turbulence and thus tend to bloom during well-stratified, quiescent waters. However, dinoflagellates are biophysically adapted for swimming, allowing this particular phytoplankton group to perhaps avoid or dampen turbulence and vertically migrate (Smayda, 1997; 2002). Also, some toxic dinoflagellates species form from a resting state (a cyst) that falls to the ocean floor (Anderson et al., 1984; Marasovic, 1989; Nagai et al., 2003). This allows the dinoflagellates to lay dormant when chemical conditions are not optimal for their growth. When nutrients are in abundance or when triggered by internal biorhythms, the algae return to the water column as

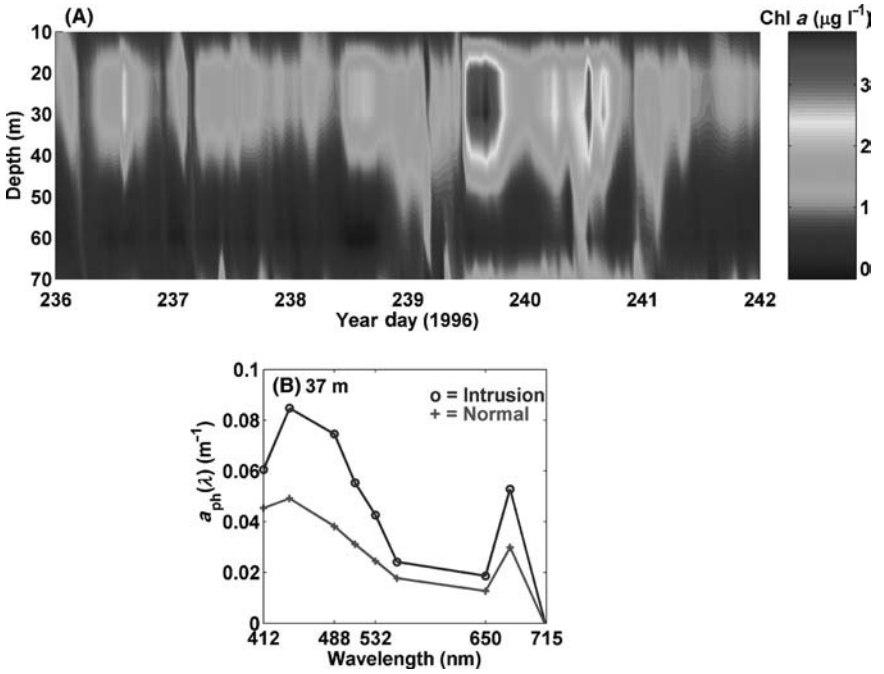

Figure 2.4
A, time-series contour plot of chlorophyll *a* concentration. The increase on Year Day 239 (26 August 1996) was due to convergence of phytoplankton at a shelf-slope front just south of Martha's Vineyard, Cape Cod, Mass.
B, phytoplankton absorption spectra deconvolved from *in situ* optical measurements of the total absorption coefficient (following Roesler et al., 1989) during 'normal' conditions (pluses) and during an intrusion of a shelf-slope front (circles), indicating an increase of diatoms. Diatoms can be discerned from other phytoplankton species by their marker pigment, fucoxanthin, which has a peak in phytoplankton absorption at about 450–470 nm (Jeffrey et al., 1997). Data were obtained on a mooring in 70 m water depth.

phytoplankton (Burkholder and Glasgow, 1997; Donaghay and Osborn, 1997). Cysts can also be resuspended off of the ocean floor through physical forcing (high currents and/or waves; Figure 2.3). The vertical movement of phytoplankton, e.g. diel vertical migration, can be observed using stationary, high temporal and vertical resolution measurement platforms (see Section 2.3.1; Kerfoot et al., 2002; Figure 2.5).

Harmful algal species may out-compete other phytoplankton with their ability to adapt and compete for nutrients other than the macronutrients: nitrate, ammonium or phosphate. Dzurica et al. (1989) found that *Aureococcus anophagefferens* is capable of using glutamic acid and glucose for carbon and energy sources. Maldonado et al. (2002) examined the influence of micronutrient (iron and copper) uptake on the toxicity of cultured diatoms, *Pseudo-nitzschia multiseries* and *Pseudo-nitzschia australis*

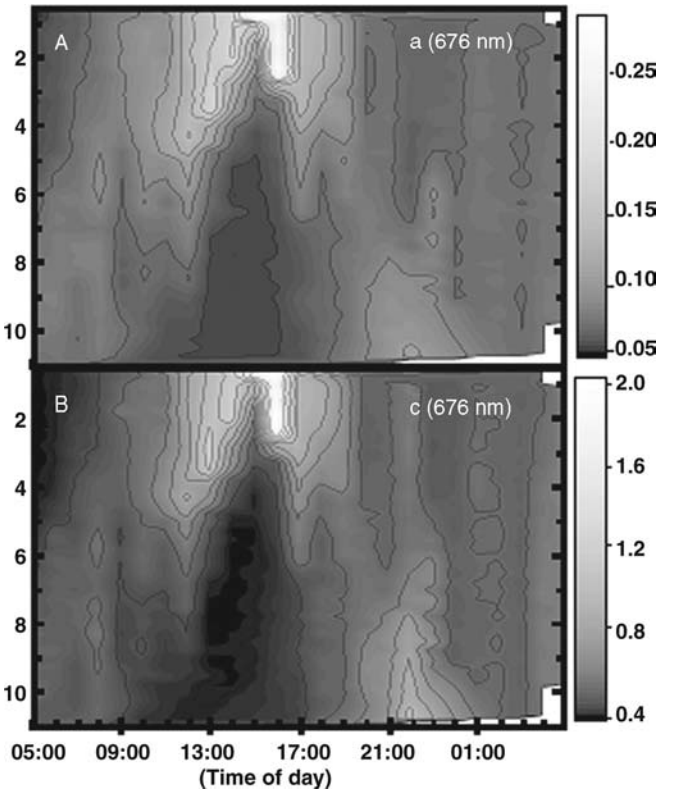

Figure 2.5
Time-series contour plot of A, absorption coefficient; B, attenuation coefficient at 676 nm, measured by an absorption-attenuation meter (ac-9) deployed on a moored vertical profiler. Vertical migration (positive phototaxis) of phytoplankton is well illustrated in these figures; phytoplankton swim towards the sunlight during the daylight hours and migrate towards the ocean bottom during the night. Water samples indicate that dinoflagellates were present.
Source: courtesy of John Kerfoot and Oscar Schofield, Rutgers University.

(for further details see Section 2.2.3). *In situ* observations of *P. australis* blooms in Monterey Bay, California, showed that this toxic species bloomed in waters low in iron, suggesting that *P. australis* may sequester iron from other species.[7] These measurements were obtained using high spatial resolution platforms carrying interdisciplinary sampling devices (see Section 2.3).

Interactions between phytoplankton species (toxic with non-toxic) and harmful algae with grazers (e.g. zooplankton) are situation-specific (e.g. Turner and Tester, 1997; Cullen et al., 2002). Attempts have been made to generalize phytoplankton species succession prior to and following HABs (the 'Mandala' from Margalef et al.,

[7] Data not yet published: see http://www.mbari.org/MUSE/intro.htm

1979; see Cullen, 2007 – Chapter 1 this volume) and grazing stresses on HABs. This type of broad overview, although by and large informative, is not applicable to all phytoplankton blooms or all HABs. Quantification of phytoplankton community composition variability must be accomplished using long-term, continuous monitoring efforts.

2.2.3 Chemical processes

Both physical and biological processes influence variability in ocean chemistry. Coastal ocean chemistry is primarily driven by input of 'new' nutrients rather than recycling, as in the open ocean (e.g. Mann and Lazier, 1991). New nutrients are introduced to the system through physical forcing (upwelling, advection, resuspension, river outflows, etc.) that occurs on spatio-temporal scales of tens of metres to coast-wide and days to months. Recycled nutrients are generally contributed through biological means (exudation, 'sloppy feeding', benthic regeneration, etc.), which occur on timescales of hours to months. For example, HABs of *Karenia brevis* may be triggered by nitrogen-fixing cyanophytes, which bloom during natural iron enrichment through Saharan dust deposition (Walsh and Steidinger, 2001).

Many attribute the occurrences of HABs to nutrient loading and coastal eutrophication (e.g. Parsons et al., 2002). The nutrient loading has been blamed on human population growth and increased pollution to coastal waters. Some commonly cited examples are Tolo Harbour in Hong Kong and the Seto Inland Sea of Japan. In Tolo Harbour, red-tide events had grown almost 8-fold while human population had increased almost 6-fold over a 10-year period in the 1970s and 1980s (Lam and Ho, 1989). A similar discovery was made in the Seto Inland Sea, Japan, where observed red tides increased from 44 per year in 1965 to over 300 in the 1970s, parallel with human population growth in the region. These HABs in the Seto Inland Sea of Japan were attributed to nutrient loading from pollution (Murakawa, 1987). The Japanese Government has since issued controls on effluents in the area and red-tide events have decreased by 50% over two decades (Anderson, 1995). Population growth can also increase atmospheric deposition and groundwater discharge to coastal areas. These are potential sources of new nitrogen and micronutrients, e.g. trace metals, for the development of HABs (Paerl, 1997). It is essential for coastal ecological studies to incorporate judiciously placed chemical measurements for the quantification of nutrients important to HAB species (see Section 2.3.1).

During low nitrogen or extremely elevated phosphorus conditions, blooms of nitrogen-fixing cyanobacteria may dominate a coastal region (Sellner, 1997). In the Baltic Sea and along the coast of Finland, low nitrogen concentrations in the summer followed by phosphorus enrichment through upwelling, intrusions or eddy-induced mixing often leads to the development of *Nodularia* blooms (Sellner, 1997). Lukatelich and McComb (1986) have observed similar blooms in Australian estuaries that are directly related to enhanced phosphorous through river flows. Again, blooms of *Karenia brevis* may be associated with nitrogen-fixing cyanophytes (Walsh and Steidinger, 2001). Although marine cyanobacteria blooms are rarely toxic, they produce extremely high amounts of biomass (nuisance blooms) and have been linked with salmon pen liver diseases (Codd, 2001). Also, toxic *Nodularia* and *Aphanizomenon* species may reduce planktonic herbivory and bacterial community development (Sellner, 1997). See Bianchi et al. (2000) for the history and characteristics of the formation

of blooms of nitrogen-fixing cyanobacteria in the Baltic Sea (also discussed in Cullen, 2007 – Chapter 1 this volume).

Maldonado et al. (2002) studied the effects of trace metals iron (Fe) and copper (Cu) on the growth and toxin production in diatoms, *Pseudo-nitzschia multiseries* and *Pseudo-nitzschia australis*. They found that iron limitation and copper toxicity directly inhibited the growth rates of these species. Domoic acid production increased by about 8-fold from optimal to Fe-limited conditions and by about 20-fold from optimal to Cu-stressed conditions. Iron uptake rates increased 3-fold when iron was added to an optimal growth system. Importantly, 95% of produced domoic acid was released into the surrounding aquatic medium, which suggests that trace metals and other micronutrients can have a strong influence on the toxicity of HABs (Maldonado et al., 2002).

2.2.4 Interactions between physical, biological and chemical processes

Physical, chemical and biological processes operate in concert and result in cascades of energy (variability) to both smaller and larger time and space scales (Dickey, 1991, 2003; Figure 2.1). For example, Pacific Ocean-wide El Niño events impact continental shelf nutrient dynamics on the west coasts of North and South America, particularly during boreal springtime upwelling. Internal solitary waves, which occur on timescales of minutes, can influence the vertical movement of particles (Figure 2.6) and nutrients and hence, phytoplankton blooms on temporal scales of days to months (Bogucki et al., 1997; Chang and Dickey, 1998). Coastal phenomena such as upwelling and freshwater plumes and their influences on HABs are highly dynamic in nature, emphasizing the need for careful design of interdisciplinary coastal monitoring efforts in terms of sensors, platforms and spatio-temporal scales (see Section 2.4.1). Some examples of interdisciplinary HAB-related processes follow.

Coastal upwelling regions are highly productive areas of the world's oceans, often supporting HAB species. Meteorological, physical, chemical and biological processes at variable scales all play crucial roles in HAB formation caused by upwelling. For example, along the west coast of the US, northerly winds typically prevail in the spring and early summer. The increase in nutrients to well-lit surface waters from upwelling stimulates primary production. In California waters, blooms directly following upwelling generally consist of non-toxic diatoms, followed by non-toxic dinoflagellates (Horner et al., 1997). Blooms of toxic species along the US west coast generally form when upwelling ceases or becomes sporadic, between May and October. It is hypothesized that HABs, nutrients or both build up at offshore frontal waters (e.g. Figure 2.4). During upwelling, a front can form to separate freshly upwelled waters from inshore waters. When upwelling relaxes, the cross-shelf flow can reverse direction and advect great concentrations of harmful algae onshore and into bays and inlets, resulting in a nearshore HAB or red tide (Donaghay and Osborn, 1997; Horner et al., 1997). Biophysically, many species of toxic or red-tide-forming dinoflagellates are intolerant to turbulence (Section 2.2.2; Smayda, 2000, 2002). Therefore, when upwelling ceases, nearshore waters can become stratified and conducive to HAB persistence.

HAB formation as the result of relaxation of upwelling has been observed not only along the US west coast, but also off Peru, Spain and the west coast of Africa (Anderson, 1995). Pitcher et al. (1993) investigated the relationship between physical processes and the characteristics of red tides in the upwelling region of the Benguela Current, South Africa. Nuisance red tides in this region were coincident with seasonal upwelling, occurring from January to May when upwelling diminishes and stratification

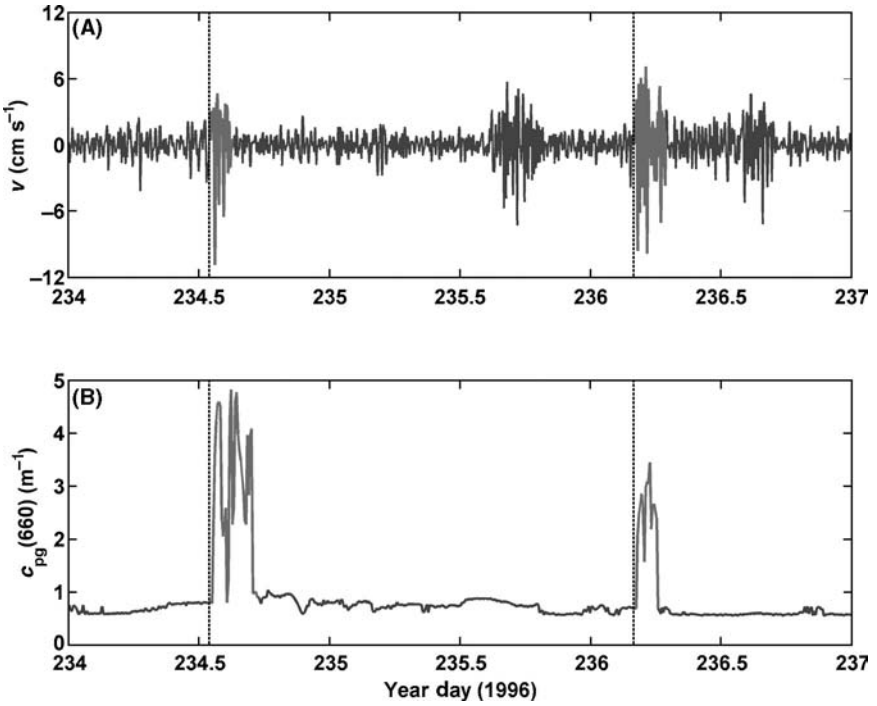

Figure 2.6
Time series of A, bandpassed filtered north-component current velocity measured by a moored acoustic Doppler current profiler; B, beam attenuation coefficient at 660 nm measured by a moored spectral absorption-attenuation meter (ac-9). The subscript pg denotes particulate plus gelbstoff. Data were measured at 52 m (70 m total water depth) between 21 and 24 August 1996 off the coast of Cape Cod, Mass. This figure illustrates the passage of internal solitary waves (ISWs; delineated and highlighted in grey) and the subsequent movement of particulate matter. Note that vertical gradients in particulate matter are important; not all ISWs resulted in an increase in the optical signal.

increases, similar to processes occurring along the US west coast (Pitcher et al., 1993; Pitcher et al., 1998; Pitcher and Calder, 2000). Also parallel with California red tides, Pitcher and Calder (2000) show that South African frontal blooms are transported onshore under certain wind and current conditions to form red tides. Daily shipboard sampling of nearshore physical and biological parameters revealed that phytoplankton community composition in South African embayments is highly dependent on advective processes. Importantly, in regions where year-round upwelling is sporadic, small-scale HABs may form *in situ* when ideal nutrient conditions are met (e.g. coastal New Jersey; Moline et al., 2004).

The physical, chemical and biological characteristics of upwelled water are altered during El Niño events, which occur approximately every three to four years and are largely unpredictable (e.g. Strutton and Chavez, 2000). Although the causes of

El Niño are unknown, many of its effects impact phytoplankton species distribution and the distribution of higher trophic level organisms (Mann and Lazier, 1991). Strutton and Chavez (2000) observed extremely low phytoplankton biomass and productivity in the equatorial Pacific during the 1997–1998 El Niño, one of the strongest on record. Nitrate concentrations were low throughout the upper 100 m of the water column, resulting in chlorophyll concentrations that were less than half of the climatological mean. The effects of El Niño are also observed in eastern Pacific Ocean upwelling regions, which are highly productive areas of the world's oceans. During El Niño, upwelled water along the North and South American west coasts is higher in temperature and lower in nutrients. Oftentimes, warm water harmful algal species flourish in the higher temperature surface waters that accompany El Niño events. Some attribute a *Pseudo-nitzschia australis* bloom and domoic acid event on the US Pacific coast in 1991 to El Niño (Horner et al., 1997). The eastward and northward movement of warm surface waters may have brought toxic diatoms to the US Pacific Northwest, where domoic acid was found in many marine organisms (Horner et al., 1997). Long-term, continuous monitoring efforts are necessary in order to capture these ecologically important, episodic events.

HAB formation is greatly influenced by freshwater runoff into coastal areas in the form of riverine, groundwater, estuarine, or outfall flows. Freshwater plume characteristics are governed by physical processes and greatly influence coastal nutrient dynamics and hence, ecology. Most importantly, freshwater flows are a source of new macro- and micro- nutrients into the coastal ocean (e.g. Mann and Lazier, 1991). The lower salinity freshwater flow into seawater also forms a strong pycnocline and increases stratification of the water column, aiding in the retention of phytoplankton in the high-light surface waters. However, the change of hydrography towards warmer, lower-salinity waters is not conducive to the growth of some toxic phytoplankton species (e.g. *Aureococcus anophagefferens*; Cosper et al., 1989). Buoyancy-driven flows associated with freshwater flows (forced by the horizontal pressure gradient formed by the density difference) may act to advect competing plankton and nutrients to offshore waters, allowing the formation of HABs of phytoplankton species that are tolerant to lower nutrient, higher salinity conditions (e.g. *Gymnodinium mikimotoi* on the north-west European shelf; Lindahl, 1986). However, the turbulence created by buoyancy-driven flows may act to break down stratification, deepen the mixed layer and effectively decrease the light available for photosynthesis, thus inhibiting HAB development. Tidal mixing also generates a great deal of turbulence and sediment resuspension in the coastal ocean, decreasing the light available for phytoplankton utilization. On the other hand, the turbulence may resuspend nutrients from the ocean bottom and lead to the formation of phytoplankton blooms. In summary, coastal ocean processes are extremely complex; time and space scales of variability are relatively short; and forces act simultaneously, resulting in positive and negative feedbacks for primary production.

2.3 Sensor and system technologies relevant to HABs

HAB research must incorporate sensors and systems capable of sampling on multiple and appropriate time and space scales relevant to HAB formation, persistence and destruction (Figure 2.1). The use of a variety of complementary ocean observing

platforms along with data-assimilation models can greatly improve our knowledge and capabilities for making predictions of upper ocean ecology and health of the ocean as well as HABs. Multiple platforms are necessary because of specific platform advantages and limitations (discussed below). Some challenges for monitoring and characterizing HABs are:

- the processes involved occur at several different spatio-temporal scales, are typically nonlinear and coupled through several different multidisciplinary variables;
- physiological and behavioural aspects of oceanographic flora and fauna are inconsistent and unpredictable;
- costs of doing oceanographic measurements from *in situ* platforms are relatively high;
- the assimilation of interdisciplinary data into predictive models is in its infancy.

2.3.1 Sensors related to HAB research

2.3.1.1 Physical sensors

In the past decade, many new instruments for measuring coastal ocean properties have been introduced (e.g. Dickey, 2002). Some of these sensors can be applied to HAB research. Physical instrumentation (e.g. current, temperature and conductivity sensors) has remained relatively unchanged with the exception of size, weight and power requirements and interfacing of instruments. Acoustical methods have been employed in more recently developed current meters (e.g. RD Instruments acoustic Doppler current profiler, ADCP), allowing for accurate, high vertical resolution measurements of current speed and direction (e.g. Dickey et al., 1998*b*). In addition, information about biology (zooplankton biomass and fish) can be inferred from the acoustical signals of these current meters (e.g. Smith et al., 1992; Holliday et al., 1989; Jiang et al., 2007; see Jaffe, Chapter 10 and references therein). High-frequency (HF) radar, e.g. coastal ocean dynamics applications radar (CODAR), has recently been developed for large-scale spatial maps of surface currents. Short- or standard-range HF radar systems can cover roughly 50 km^2 at a resolution of about 1.5 km (Figure 2.7). Long-range systems reach up to 100 km offshore. HF radar uses the Doppler shift principle to determine the surface current from a backscattered radio wave.

2.3.1.2 Optical sensors

Optical instrumentation has seen the largest expansion with regards to technological developments in oceanography (e.g. Dickey, 2001*a*, 2001*b*, 2002, Dickey and Chang, 2001, Chang et al., 2006*b*; Dickey et al., 2006). Up until about 30 years ago, *in situ* optical sensors were generally limited to the Secchi disk, a white disk 25 cm in diameter whose depth of disappearance is defined as the Secchi depth, and broadband scalar irradiance (E_0) or PAR sensors (integrated scalar irradiance from 400–700 nm; see Lewis, 2007; Morel, 2007 – Chapters 6 and 4 this volume). Secchi disk and PAR sensors measure water column optical clarity from the ocean surface and photosynthetically available radiation (PAR), respectively. Although relatively simple, both measurements can provide important information regarding the occurrence of phytoplankton blooms, potentially HABs. For example, Falkowski and Wilson (1992) used a 90-year record of Secchi depth observations in the North Pacific Ocean to determine that small systematic increases in phytoplankton have occurred on the edges of the central ocean gyre, while the gyre core has

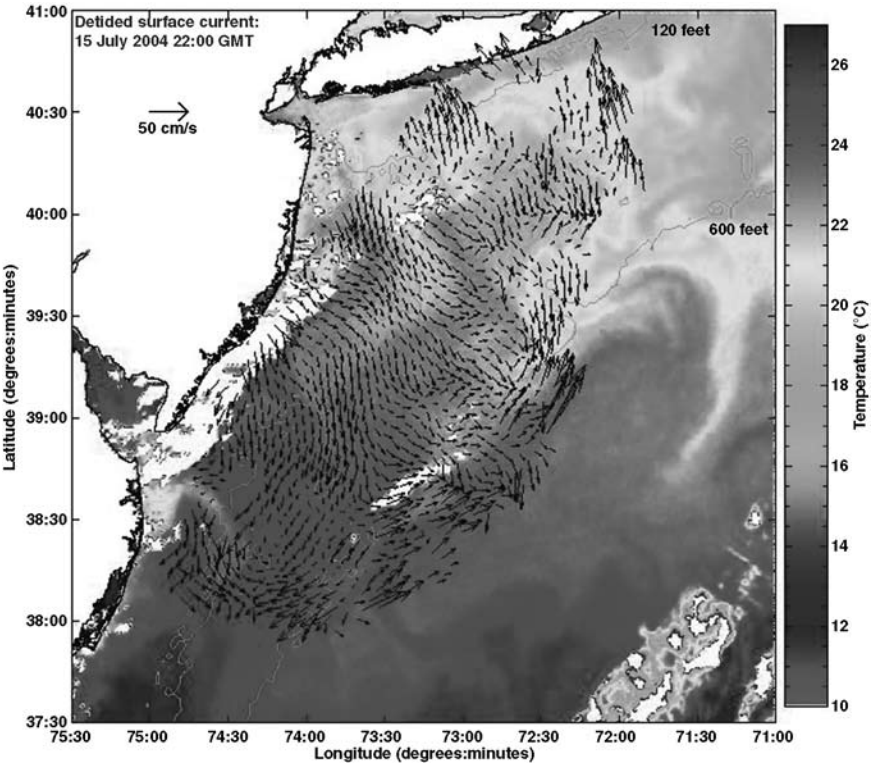

Figure 2.7
Spatial map of surface current vectors (scale at upper left) derived from high-frequency radar measurements overlaid on satellite-derived sea surface temperature from 15 July 2004. The region shown is the Middle Atlantic Bight, US east coast (Long Island at top). Note the highly variable convergence and divergence zones in the current vectors.
Source: courtesy of Josh Kohut and Oscar Schofield, Rutgers University.

undergone a small depletion of phytoplankton. Secchi depth has also provided more than 60 years of water clarity data; these data have been related to eutrophication and the formation of HABs in the Seto Inland Sea, Japan (Yanagi and Okaichi, 1997; also see Cullen et al., 1997).

Sensors analogous to the PAR sensor use flat plate cosine or hemispherical collectors for different measurements or calculations of the apparent optical properties (AOPs; optical properties that depend on the constituents of the aquatic medium and the angular distribution of solar radiation; see Kirk (1994) or Mobley (1994) for definitions of optical properties; see Lewis (2007) and Morel (2007) – Chapters 6 and 4 this volume. Spectroradiometers are radiance and irradiance meters (e.g. Dickey, 2001*b*). Light separation for multispectral sensors is generally achieved using sets of interference filters (usually 10 nm bandwidth) at select wavelengths/wavebands for particular purposes, such as investigating absorption peaks and hinge points for pigment analyses or matching with satellite remote sensing wavelengths (e.g. Sea-viewing

Wide Field-of-view Sensor, SeaWiFS; see Section 2.3.2). A hyperspectral sensor gives continuous spectral coverage over a broad wavelength range (at least over visible wavelengths), with better than 10 nm wavelength resolution (Chang et al., 2004).

Inherent optical properties (IOPs; optical properties that depend only on the aquatic medium itself and are independent of the ambient light field and its geometrical distribution; see Roesler and Boss, 2007 – Chapter 5 this volume) are generally more difficult to measure than AOPs. One of the first IOP sensors to be used in oceanographic research was the beam transmissometer (Bartz et al., 1978). The principle of operation of a beam transmissometer involves the measurement of the proportion of an emitted beam that is lost through both absorption and scattering as it passes through a predetermined path length to a detector. Beam attenuation coefficient (beam c) is derived from beam transmissometer measurements. Beam c has been used to derive (harmful) algal biomass, suspended sediment volume, and concentrations of particulate organic carbon (POC) and productivity in the form of POC (e.g. Bishop, 1999; Dickey and Falkowski, 2002 and references therein).

Within the past decade, *in situ* spectral absorption-attenuation meters have become commercially available (Moore et al., 1992; see Roesler and Boss, 2007 – Chapter 5 this volume). These instruments concurrently measure spectral absorption and attenuation coefficients at up to 90 wavelengths for spectral signatures of both particulate and dissolved material (WET Labs, Inc. ac-9 for nine wavelengths; Pegau and Zaneveld, 1993; Pegau et al., 1995, 1997; and WET Labs, Inc. ac-s for hyperspectral; Zaneveld et al., 2004; Chang et al., 2006*b*). Seawater is pumped through two tubes. The inside of the beam c tube (c-tube) is flat black to minimize reflections, whereas the absorption coefficient tube (a-tube) is *reflective* in order to maximize internal reflection to better estimate absorption. The spectral scattering coefficient is computed from ac-meter data by simply performing the difference $b(\lambda) = c(\lambda) - a(\lambda)$. Absorption-attenuation meter data and spectral decomposition models can be used to provide *in situ* estimates of phytoplankton, detrital and gelbstoff absorption (Roesler et al., 1989; Bricaud and Stramski, 1990; Gallegos and Neale, 2002; Chang and Dickey, 1999; Schofield et al., 2004). Hyperspectral absorption-attenuation meters (ac-s) can in principle be used to isolate pigment peaks for HAB species identification (see Section 2.5.2; Millie et al., 1997; Kirkpatrick et al., 2000; Chang et al., 2004).

Phytoplankton (HAB) biomass is often inferred from measurements of chlorophyll fluorescence (Babin, Chapter 7). *In situ* chlorophyll fluorometers generally employ stimulated fluorescence techniques, exciting phytoplankton with blue light and measuring its light emission in the red, for example excitation/emission (ex/em) wavelengths of, for example, 470/695 nm. Novel *in situ* fluorometers (e.g. WET Labs, Inc. ECOfl3) use different ex/em wavelengths to provide information on, for example CDOM (ex/em = 370/460 nm), fluorescein for dye tracer studies (ex/em = 470/530 nm), or phycoerythrin for red cyanobacteria concentration (ex/em = 540/570 nm). These new spectral fluorometers are relatively small and lightweight and are commercially available.

Backscattering at several different wavelengths or angles can be measured using commercially available, operational instruments that are based on scattering theory and statistical relationships relating scattering at a given angle to the integral over the backward direction (Maffione and Dana, 1997; Boss and Pegau, 2001; see Roesler and Boss, 2007 – Chapter 5 this volume). Particle size distribution, mass concentration, shape and composition (biological versus detrital versus sediment) can be estimated with backscattering and scattering properties, and the ratio of

backscattering to scattering (Ulloa et al., 1994; Twardowski et al., 2001; Babin et al., 2003; Boss et al., 2004*a*, 2004*b*; Roesler and Boss, 2007 – Chapter 5 this volume). *In situ* particle size distributions can also be measured using operational laser (Fraunhofer) diffraction instruments (Sequoia Scientific, Inc. LISST-100; Agrawal and Pottsmith, 1994). Modified versions of these instruments measure particle-settling velocities (Sequoia Scientific, Inc. LISST-ST), which are important for quantifying the vertical movement of phytoplankton. The backscattering and scattering properties of phytoplankton reveal information about cell size and index of refraction (Stramski et al., 2001), which can be used in conjunction with other IOP observations (absorption, scattering and attenuation coefficients) to provide details about *in situ* phytoplankton populations, for example composition, size, morphology and internal structure (Roesler and Boss, 2007 – Chapter 5 this volume). This additional information can help us understand more about the growth and distribution patterns of harmful algal species.

Some HAB species are dinoflagellates that are bioluminescent, meaning that they produce light by a chemical reaction that originates in the organism (e.g. Case et al., 2001). These bioluminescent organisms can be detected *in situ* with bioluminescence sensors (Herren, 2002; Herren et al., 2004). These sensors usually pump water through a baffle, mechanically stimulating the organisms to generate bioluminescence. Optical sensors inside the instrument's chamber then detect the amount of light produced by the organisms. Baffled bioluminescence instruments can operate 24 hours a day, although they are most effective at night, when most bioluminescent species are photoinhibited and reach peak bioluminescence intensities. A major limitation of *in situ* measurements of bioluminescence lies in the separation of phytoplankton bioluminescence signals; these signals can be confounded by bioluminescent bacteria, zooplankton, or jellyfish.

The first generation of bioluminescence sensors were quite large (about the size of an automobile) and could only be used as shipboard samplers (Widder et al., 1993 and references therein). Currently, scientists and engineers are developing portable, lightweight, reduced-power and relatively low-cost optical sensors for oceanographic research. The movement towards smaller sensors coincides with the advancement of autonomous sampling platforms for high spatial and temporal resolution ocean monitoring (see Section 2.3.2).

2.3.1.3 Biological sensors

Many new biological sensors (instruments that measure biological quantities) that are currently transitioning to the operational phase rely on optical principles or techniques. Jaffe (2007 – Chapter 10 this volume) provides an extensive review of optical imaging of plankton. Another example of a biological sensor that employs optics is the flow cytometer. In the flow cytometer, several optical measurements are made as each particle in a water sample passes through a focused laser beam. Light-scattering signals provide information about the distributions of particle size and composition, while fluorescence data allow discrimination between phytoplankton and other particles and identification of major phytoplankton groups, e.g. *Synechococcus*, crytophytes and eukaryotes. Researchers are now deploying flow cytometers for rapid and quantitative measurements of individual suspended microscopic particles for cells in the size range ~0.5–30 μm (Olson et al., 1991; Olson et al., 1993; Vaulot et al., 1995; Vaulot and Marie 1999; Reckermann and Colijn, 2000; Li and Dickie, 2001). Time series of flow

cytometric measurements have contributed to a greater understanding of phytoplankton species succession (Olson et al., 1990; DuRand et al., 2001; Li and Dickie, 2001) and growth processes (DuRand and Olson, 1998; Shalapyonok et al., 1998; André et al., 1999; Jacquet et al., 2001; Shalapyonok et al., 2001; Sosik et al., 2003), which have important implications for HAB research.

Other types of biological sensors that are gaining considerable interest for HAB research are molecular, e.g. deoxyribonucleic acid (DNA), probes (Scholin et al., 2007 – Chapter 11 this volume). Previous molecular analyses of HABs involved several days of cell preparation and high-powered electron microscopy analyses to identify toxic algae. With the advent of *in situ* molecular probes, HAB species can be determined within 4 h of seawater sample collection. These probes can sequence the DNA of a selected phytoplankton and compare its genetic code sequence of nucleotides with that of other related algae. Scholin et al. (1998) are currently developing real-time HAB data collection methods using DNA probes on moorings. More information about molecular probes for HAB research can be found in Scholin et al. (Chapter 11).

2.3.1.4 Chemical sensors

Chemical measurements have greatly improved with technology (e.g. Tokar and Dickey, 2000). Rather than relying on untimely laboratory analyses of bottle samples that may suffer chemical alteration or contamination, *in situ* chemical sensors are being deployed on ship-based vertical profiling packages and more recently, moorings. One of these new chemical sensors is a field-deployable ultraviolet (UV) absorption spectrometer (Satlantic, Inc. In Situ Ultraviolet Spectrometer, ISUS; Johnson and Coletti, 2002). The principle behind the development of the ISUS is optical in nature: nitrate, dissolved in seawater, exhibits a broad absorption maximum centred at ~210 nm. Nitrate absorption competes with the absorption of bromide, a conservative component of sea-salt, and to a lesser extent the carbonate ion (Chang et al., 2004, Figure 4). Advanced spectroscopic deconvolution techniques are used with the ISUS to isolate the nitrate absorption signal to make routine spectral measurements of nutrients (Johnson and Coletti, 2002). Another example of an *in situ* chemical sensor that uses spectrophotometric techniques is the SubChem, Inc. SubChemPak Analyzer. The SubChemPak Analyzer combines flow analytical methodologies of reagents with an absorption detector for rapid *in situ* measurements of dissolved nitrate, nitrite, iron and other nutrients.[8]

One of the main advantages of these *in situ* chemical analyzers is the ability to integrate quantification of ocean chemistry with other more commonly measured oceanographic parameters such as conductivity-temperature-depth (CTD), chlorophyll fluorometers and optical measurements. Interdisciplinary sensor packages that carry chemical sensors may also be towed for under-way sampling, profiled for high vertical-resolution measurements, or deployed on autonomous platforms (e.g. moorings, bottom tripods, autonomous underwater vehicles (AUVs); see Section 2.3.2). Measurements of nutrient concentrations are now possible at temporal and spatial scales relevant to HABs. Challenges with these instruments involve length of deployment, calibration, and storage of reagents (for instruments such as the SubChemPak Analyzer).

[8]http://www.subchem.com/

2.3.2 Sensor platforms

2.3.2.1 Remote sensing systems

Remotely sensed measurements of oceanic properties from satellites or aircraft used for HAB research involve observations that rely on the sun for illumination of the ocean surface. These ocean-colour sensors measure the radiance entering the aperture of the sensor, for example SeaWiFS (satellite) and Portable Hyperspectral Imager for Low Light Spectroscopy (PHILLS; aircraft; Davis et al., 2002). A variety of scanning mechanisms are used to generate two-dimensional fields or images to provide nearly synoptic observations over the oceans (Yoder et al., 2001). Recent reports have summarized many of the salient principles, techniques and applications of ocean-colour remote sensing (e.g. see IOCCG Reports 1–5, 1999, 2000, 2001, 2004, and 2006 respectively).

Ocean-colour data obtained from satellite sensors (e.g. SeaWiFS, Moderate Resolution Imaging Spectroradiometer (MODIS), and several others; see IOCCG Reports 1–5, 1999, 2000, 2001, 2004, and 2006 respectively) are most often used to infer concentrations of biological quantities (e.g. chlorophyll; O'Reilly et al., 1998; Yoder et al., 2001) and other optical information (absorption and scattering coefficients; Figure 2.8). Empirical ocean-colour algorithms are developed to quantify constituents in the water column using wavelength or waveband ratios. Different ratios are employed for different optical parameters, e.g. normalized water-leaving radiance at 490–555 nm ($L_{WN}(490)/L_{WN}(555)$) for chlorophyll *a* concentration and $L_{WN}(443)/L_{WN}(510)$ for dissolved matter or gelbstoff (Kahru and Mitchell, 2001). Several different chlorophyll *a* algorithms exist, applying different wavelengths ratios depending on the water column characteristics (O'Reilly et al., 1998). Analytical or semi-analytical algorithms employ the relationship between remote sensing reflectance and the ratio of backscattering to absorption (or absorption plus backscattering), that is radiative transfer (Lee et al., 2002). Algorithms using ocean-colour measurements of sun-induced fluorescence at wavelengths near 685 nm are proving to be valuable for estimating chlorophyll *a*, especially in coastal waters (IOCCG Report 3, 2001). In addition, remotely sensed optical data can be used to estimate primary productivity (Behrenfeld and Falkowski, 1997; Behrenfeld et al., 2005) and beam attenuation and particle size distribution (Roesler and Boss, 2003).

With the advent of hyperspectral sensors (defined in Section 2.3.1), a single instrument can provide a multitude of wavelengths and wavelength ratios to more accurately resolve a variety of water column constituents. Potentially, hyperspectral technology provides a means for oceanographers to remotely and synoptically classify and quantify complex oceanic environments with respect to particle characteristics, including phytoplankton identification at least by group, and specific chemical compounds (Chang et al., 2004). Recently, hyperspectral remote sensing systems have been used for the identification of red tides and other HABs (Stumpf, 2001), and the characterization of river plumes and fronts in the coastal ocean (Figure 2.8).

It is important to keep in mind that remote sensing, although the only available platform for synoptic measurements is extremely powerful, it can be limited. Cloud cover and coastal fog often obscure remote sensors, making images and data useless for analyses. Importantly, remote sensors measure radiances emitted only over the upper optical depth (Gordon and McCluney, 1975), typically ranging from about 1 m in coastal waters to a maximum of ~35 m in the clearest, open ocean regions. Therefore, only surface HAB species may be detected in remotely sensed images. Due to sensor resolutions, satellite ocean-colour data are often contaminated by land; data are not

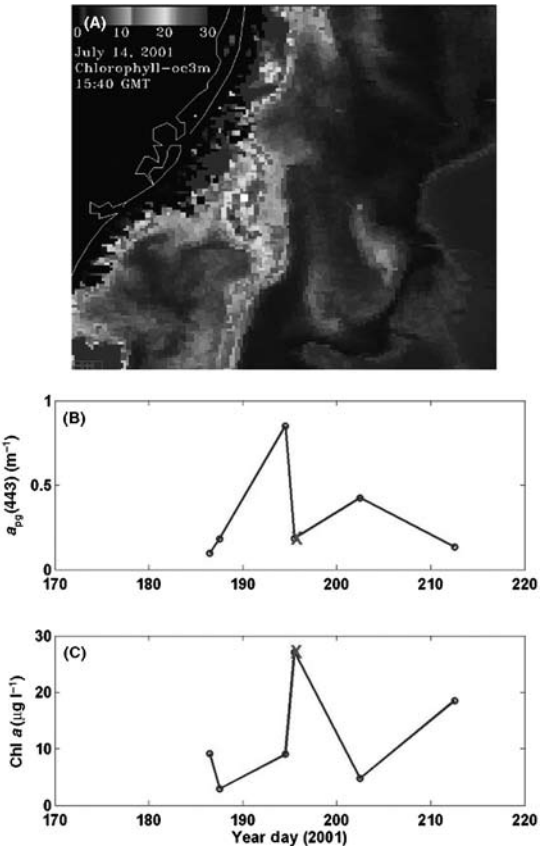

Figure 2.8
A, Moderate Resolution Imaging Spectroradiometer (MODIS) imagery of derived chlorophyll *a* concentration showing a high-biomass filament in the New York Bight on 14 July 2001 (the land mass on the left is coastal New Jersey just north of Cape Hatteras). Time series of B, derived absorption at 443 nm at the location of the white box in the MODIS image; C, derived chlorophyll *a* concentration at the same location. The Xs represent the day and time of image (A). Subscript pg denotes particulate plus gelbstoff. Remote sensing data provides a means to resolve spatial variability and infer important bio-optical parameters.
Source: MODIS imagery and derived bio-optical products were provided by Richard Gould and Robert Arnone, Naval Research Laboratory, Stennis Space Center.

available within about 5 km of coasts. Also, the nature of satellite orbital mechanics imposes restrictions on revisit frequencies, thus ocean-colour data are restricted in terms of temporal coverage. Thus, remote sensing information must be complemented with *in situ* observations (described below) to calibrate remote sensors (Barnes

et al., 2001; Pinkerton et al., 2003), provide continuous time series, and to characterize important subsurface ocean properties.

2.3.2.2 Ships

Ship sampling is the oldest method of gathering oceanographic data, yet still remains a valuable resource for current HAB research in conjunction with modern, technological sampling platforms. Ship sampling provides:

- direct, detailed process-oriented measurements for specific research studies;
- data at multiple depths and over long distances;
- means of deployment of other sampling platforms (such as drifters, floats, AUVs, gliders and moorings).

Sampling via ships may include on-station vertical profiling of instruments or instrument packages; on-station and under-way ship-mounted, tethered or hand-held radiometric measurements; and under-way sampling using flow-through systems (Balch et al., 2001), towed undulating (Barth et al., 1998), and fixed-depth bodies or chains that act as instrument platforms. One of the advantages of ship sampling is that calibrations and cleaning of instruments can be performed between each deployment (profile) to provide more accurate, freshly calibrated, essentially non-biofouled data. A second advantage of ships is that advanced analytical instrumentation that cannot at present be routinely deployed from other *in situ* platforms can be used, for example mass spectrometers, 'clean' methods for ocean chemistry, and radioactivity measurement systems. In addition, ships remain the only feasible platform capable of collecting whole water samples and conducting net tows for timely biological analyses. It is these biological analyses that are essential for complementing continuous, autonomously sampled interdisciplinary observations in order to investigate details of the physiological and behavioural aspects of HABs. Ships have limitations in terms of their high cost, limited availability and restricted synopticity in sampling. Also, they are constrained by meteorological and sea-state conditions.

High costs and limited sampling problems have been resolved with the employment of ship-of-opportunity programmes (e.g. ferries) to make long-term basic measurements along consistent transects. In the Baltic Sea, regular measurements of surface chlorophyll fluorescence, conductivity-temperature and nutrients using a flow-through system are conducted on board cooperating merchant ships.[9] These data have proved invaluable for characterizing the spatial and temporal extent of blooms in Scandinavian waters. The M/S *Scotia Prince* ferry in the Gulf of Maine is equipped with hydrographic, biological, optical and chemical sensors for long-term, continuous measurements to examine factors affecting the distribution of phytoplankton (Balch et al., 2004). Ferrymon, which runs in Pamlico Sound off the coast of North Carolina, regularly collects near-surface temperature, conductivity, dissolved oxygen, pH, turbidity and chlorophyll fluorescence data.[10] These data are telemetered via cellphone technology to Duke University for analyses. Ferrymon activities are used to predict ecosystem responses to changes in Pamlico Sound water quality in an effort to direct coastal management. Alaska State ferries are equipped with instruments to make biophysical observations (hydrography, nutrients and bio-optics) in the Gulf of Alaska to monitor ecosystem changes.[11]

[9]Alg@line; http://www.balticseaportal.fi/
[10]http://www.ferrymon.org/
[11]http://www.pmel.noaa.gov/foci/GEM/alaska_ferry/GEM_ferry.html

2.3.2.3 Moorings and bottom tripods

Moorings and bottom tripods are ideal for HAB monitoring and characterization because these platforms can be used to study environmental changes in the ocean on timescales from minutes to decades. An increasing number of optical, chemical, biological and physical parameters are being measured from these platforms at multiple depths. In addition, researchers are currently developing automatic profiling moorings for high vertical and temporal resolution observations (Donaghay et al., 2003). Another advantage of moorings and tripods is the ability to sample during times of inclement weather and high sea-states. One of the limiting factors for these types of platforms is the great size and weight of moorings along with the high cost of implementation and deployment. Additional future technological advances will allow measurement systems to be more compact and lightweight, less power-hungry and lower in cost (Kaku, 1997; Tokar and Dickey, 2000; Bishop et al., 2001). The greatest disadvantage of these platforms is biofouling of sensors (Lehaitre et al., 2007). Useful data, particularly optical data, from moorings have often been limited to a few months in the open ocean and less in coastal waters (Davis et al., 2000). However, work is progressing to mitigate this problem (Chavez et al., 2000; Manov et al., 2004; Figure 2.9).

Anti-biofouling techniques for optical instrument packages have been effectively implemented (Chavez et al., 2000; Manov et al., 2004). Some of the most useful techniques involve the use of copper and are necessary for long-term deployments of optical sensors (Figure 2.10). Copper significantly reduces marine fouling for long-term bio-optical sensor deployments in the coastal ocean and can effectively replace highly toxic and problem-causing chemical anti-foulants, for example tributyl tin (TBT), bromine and chlorine (reviewed by Manov et al., 2004). Copper shutters that open during sampling and close over radiometric sensors, fluorometers and other optical windows during idle periods, successfully mitigate biofouling on coastal moorings (Chavez et al., 2000; Manov et al., 2004; Figures 2.9, 2.10). Many optical instruments use a flow-through system, thus copper tubing to prevent biological growth in optical systems have been effectively employed. These anti-fouling methods have been shown to increase useful deployment times of moorings from about one month to as long as four months in the coastal ocean (Chang et al., 2001; Chang et al., 2002). Another simple method of reducing biofouling on nearshore coastal moorings is diver servicing or retrieval of optics chains to the deck for cleaning. Many HAB monitoring moorings are or will be deployed within a few kilometres of shore, allowing easy access for regular cleaning of optical windows.

Another advantage of these nearshore observational facilities is in the development and implementation of data telemetry methods using radio frequency technology for real-time or near real-time HAB-related measurements (e.g. the MEPS-Bay system in Nova Scotia, Canada; www.cmep.ca/bay). This is necessary for alerting authorities to the formation and persistence of HABs and for mitigation purposes. Recently, oceanographers have begun to explore the possibilities of using cabled networks for power and communications (fibre optics) to provide researchers and coastal managers with HAB data in real-time or near real-time (e.g. Glenn and Dickey, 2003; National Research Council, 2003). Cabled observatories will provide virtually unlimited power and data communication capabilities, which are especially important for novel biological, optical and chemical sensors that are now being engineered (Scholin et al., 2007 – Chapter 11 this volume) and commercialized. Cables also afford a means for two-way data communication, which facilitates adaptive sampling, for example

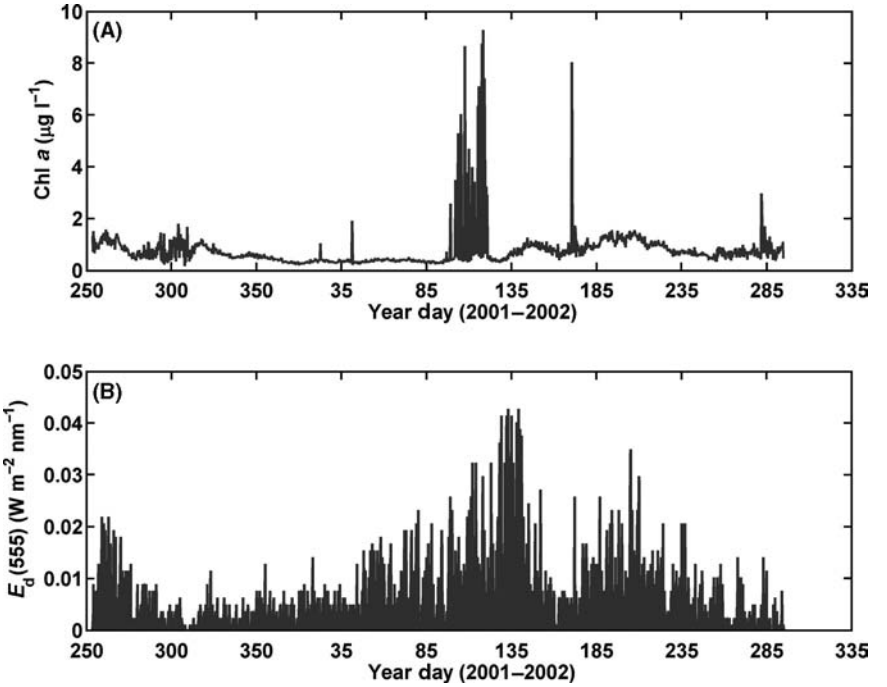

Figure 2.9
Time series of over one year (406 days) of continuous, autonomously collected A, chlorophyll *a* concentration derived from a fluorometer; B, downwelling irradiance at 555 nm measured by a spectral radiometer. Both instruments were equipped with copper shutters to mitigate biofouling. Data were collected at 35 m on a mooring deployed in the Sea of Japan. This long time series captures the spring bloom in late March to late April (starting near Year Day 90 and ending around Year Day 120 in A) and the seasonal variability in solar insolation (low irradiance in winter and high light levels in summer in B).

increasing sampling rates when HABs are detected. The primary disadvantages of cabled networks are the costs of laying cable and the question of obtaining permits through coastal zones to onshore data and power control facilities. To circumvent these limitations, several researchers are exploring the potential for using retired telecommunication cables for ocean observing systems.

Benthic processes relating to HABs may be studied and monitored using instrumentation deployed on bottom tripods in the coastal ocean. Bottom tripods and their instrumentation may be placed in the same environments as moorings using similar suites of sensors, samplers and communication systems deployable from moorings. Geological, biological, physical and optical systems mounted on tripods have been used to investigate sediment and detrital resuspension and settling, bedform formation and movement, bioturbation and flocculation/deflocculation of organic particles (Figure 2.3; Trowbridge and Nowell, 1994; Chang et al., 2001; Hill et al., 2001). *In situ* chemical sensors are currently being deployed near the ocean bottom to investigate nutrient upwelling and resuspension during HAB events. The feasibility of interdisciplinary

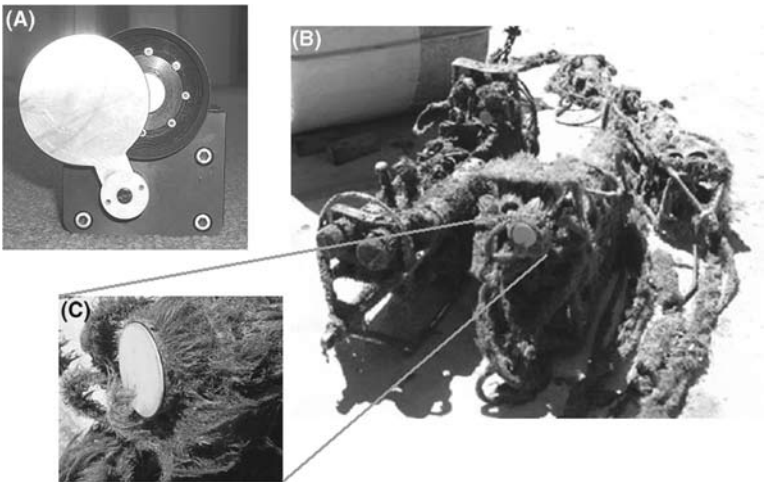

Figure 2.10
A, copper-shuttered hyperspectral radiometer; B, biofouled (macrofouling) interdisciplinary instrument packages, including optical sensors, recovered after a four-month deployment from May to September 2004 in 25 m water depth in the Santa Barbara Channel; C, close-up of the non-biofouled copper shutter of a hyperspectral radiometer. The shutter opens every hour on the hour between 06.00 h and 18.00 h local time just prior to sampling and closes after a few minutes of sampling. This prevented any biological growth on the irradiance detector.

detection systems on stationary platforms for HAB monitoring and research has been discussed by Johnsen and Sakshaug (2000), Cullen et al. (1997), Schofield et al. (1999), Cullen (2007 – Chapter 1 this volume) and Malone (2007 – Chapter 14 this volume).

2.3.2.4 Drifters and floats

Drifters and floats can provide high-resolution spatial data by following water parcels (Abbott et al., 1990; Dickey, 2001*a*). The Lagrangian platforms can provide data in portions of the time-space domain that are inaccessible by satellites, ships and other *in situ* platforms, e.g. under clouds and ice in the Southern and Arctic Oceans. Profiling floats, using buoyancy changes to move vertically, have provided near-real-time interdisciplinary data collected during their rise and descent through the water column (e.g. Mitchell et al., 2000; Bishop et al., 2003). The oceanographic data and Global Positioning System (GPS) data collected on drifters and floats are satellite telemetered after surfacing briefly at prespecified times. Drifter data allow detailed examinations of interdisciplinary processes on short time and space scales and the evaluation of de-correlation scales of chlorophyll and physical variables (Abbott and Letelier, 1998), which is important for the development of observation systems and models. The disadvantages of these platforms are similar to those of moorings and bottom tripods – biofouling and limitations in size, weight, and power of instrumentation. An additional disadvantage of the use of drifters and floats in HAB studies is the presence of boundaries in the coastal ocean. Currents tend to transport these platforms offshore

or onto beaches, away from HABs. However, drifters and floats may be useful for determining physical processes leading to the formation and cessation of HABs (see study by Tester and Steidinger, 1997), in addition to the chemical effects such as particulate organic and inorganic carbon (POC and PIC) production of HABs on regional oceanography (Bishop et al., 2003).

2.3.2.5 Autonomous underwater vehicles, remotely operated vehicles and gliders

Recently, numerous programmes have begun to exploit autonomous underwater vehicles (AUVs), remotely operated vehicles (ROVs) and gliders for coastal ocean scientific studies (Yu et al., 2002), with the potential for HAB research. A description of the history and present and future capabilities of AUVs is provided by Griffiths et al. (2001); AUVs specifically for HAB research are discussed by Griffiths (2007 – Chapter 13 this volume). Modern capabilities of AUVs and ROVs have become possible because of the development of new oceanographic sensors and systems that are relatively small in size, consume moderate power, and can be interfaced to the AUVs, ROVs and gliders. Dynamically diving AUVs are relatively small, lightweight, neutrally buoyant and powered by batteries. Some of the advantages of these autonomous platforms include low cost per deployment, potential to sample in environments generally inaccessible to ships, good spatial coverage and sampling over repeated sections, capability of feature-based or adaptive sampling, and ability for deployment of several vehicles from moorings, ships, offshore platforms and coastal stations. The primary disadvantage of AUVs and ROVs is related to its power consumption. AUVs and ROVs must be recharged regularly and hence, cannot be used for long-term deployments without a docking station. The glider concept uses variable buoyancy control, lift surfaces (wings), a hydrodynamic shape and trajectory control using internal moving mass to control its motion and therefore does not draw as much power as an AUV or ROV. With typical forward speeds of 0.25 m s^{-1}, gliders may be used as long-term virtual moorings or for long transects (Davis et al., 2003). Schofield et al. (2003; 2007 – Chapter 3 this volume) review sampling strategies and 'smart' vehicles with respect to glider technology.

2.4 Sensor and system design of HAB monitoring and assessment programmes

A long-term, interdisciplinary HAB programme is necessary for monitoring and assessment of HAB development, persistence and cessation. Data should be collected at timescales as short as a few hours to the seasonal cycle and spatial scales covering the extent of the HABs out to beyond the continental shelf break. Real-time data telemetry will be essential for early warning of HABs to researchers and responsible authorities. Some important objectives of designing HAB sampling strategies are to:

- develop and implement *in situ* detection and monitoring techniques using a variety of novel interdisciplinary instrumentation and platforms;
- engineer anti-biofouling techniques for long-term deployment of HAB sensors;
- develop and implement real-time telemetry of key data;
- develop and implement web-based adaptive sampling networks, including two-way communication with instrumentation;

- determine threshold values of key HAB parameters to be used for a rapid response alert system prior to HAB formation;
- determine the factors (environmental and anthropogenic, physical, chemical and biological) causing formation, persistence and cessation of HABs;
- monitor the frequency, intensity and duration of HABs;
- provide data for the development of models to predict the occurrence of HABs.

The following suggested techniques would complement existing ship-based and volunteer HAB monitoring efforts, providing shorter temporal scale measurements and more timely and adaptive sampling strategies.

2.4.1 HAB systems and sensors

We advise the use of small, lightweight, relocatable moorings and bottom tripods with interdisciplinary instrument packages deployed in regions of known HAB occurrences (Figures 2.11 to 2.13). These autonomous measurements should be complemented with synoptic measurements (e.g. ocean-colour satellite images) and high spatial resolution measurements to resolve processes associated with HAB development, persistence and cessation (further described below). Bio-optical

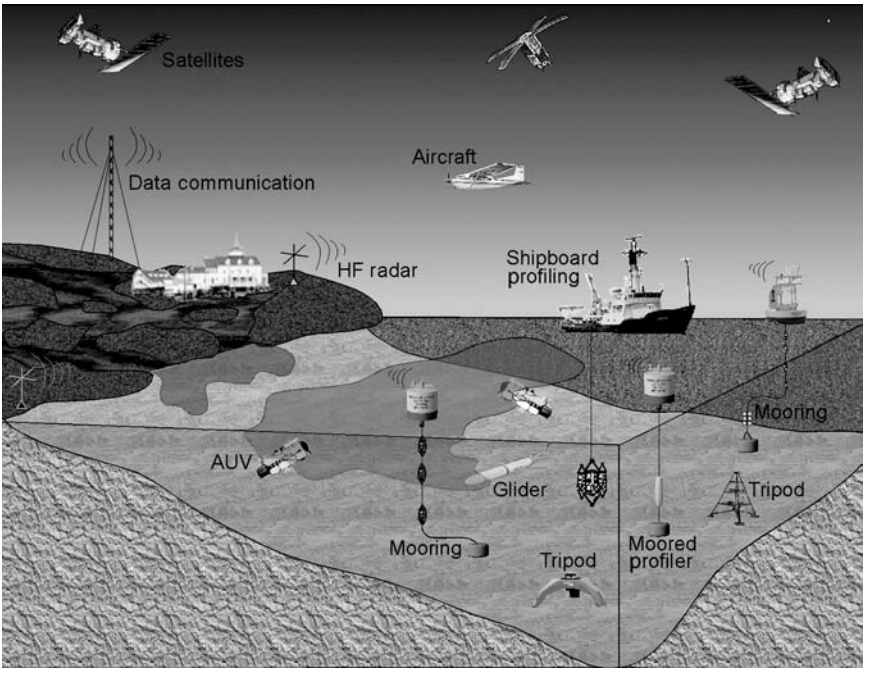

Figure 2.11
Schematic diagram of an ideal interdisciplinary coastal sampling network for harmful algal bloom detection, identification and characterization.

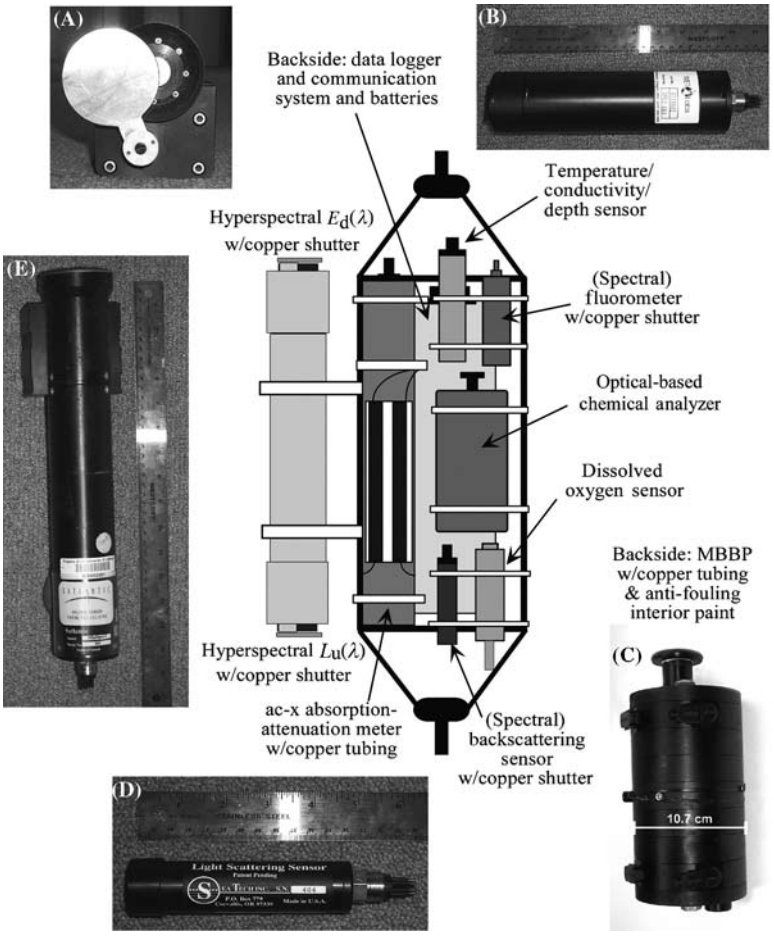

Figure 2.12
(Centre) Schematic diagram of an ideal HAB monitoring mooring instrumentation package and photographs of A, anti-fouling copper shutter system on a Satlantic, Inc. MiniSpec hyperspectral radiometer; B, WET Labs, Inc. single-wavelength ECO fluorometer with copper shutter (left); C, marine bioluminescence bathyphotometer (MBBP); D, WET Labs, Inc. single-wavelength backscattering sensor; E, Satlantic, Inc. MiniSpec hyperspectral radiometer.

instruments equipped with anti-biofouling devices on the moorings will be necessary for detection of HABs and ideally, will include (hyper)spectral absorption-attenuation meters, fluorometers, backscattering sensors and radiometers, and bioluminescence sensors (e.g. marine bioluminescence bathyphotometer, MBBP) (Figure 2.12). New *in situ* optical-based chemical sensors will be necessary for obtaining information about micro- and macronutrients. Dissolved oxygen sensors will be essential for investigating the variability of biological processes in many coastal environments (not everywhere, e.g. Gulf of Maine). Complementary

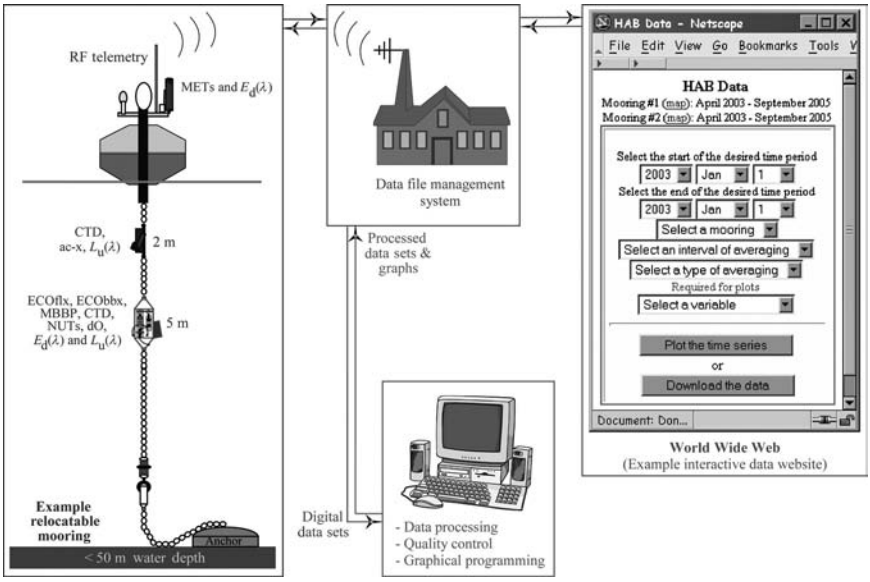

Figure 2.13
Schematic diagram of suggested data communication system: data collection, transmission, processing, graphing and presentation on the internet. RF: radio frequency, METs: meteorological sensors, $E_d(\lambda)$ and $L_u(\lambda)$: radiometers measuring (hyper)spectral downwelling irradiance and upwelling radiance, CTD: conductivity-temperature-depth sensors, ac-x: (hyper)spectral absorption-attenuation meter, ECOflx: (spectral) fluorometer, ECObbx: (spectral) backscattering meter, MBBP: marine bioluminescence bathyphotometer, NUTs: optical-based nutrient analyzer, dO: dissolved oxygen sensor.

hydrographic data should be collected using temperature and conductivity sensors, and meteorological systems and HF-radar and current meters will be deployed for physical data. The sampling rates for all instruments should be hourly or faster with potential for adaptive sampling rates up to several times per minute. Instrumentation packages should be interfaced through a data logger and communication system for data transfer to shore-based computing assets (Figure 2.13).

An automatic data transmission network using cables, radio frequency modems, or satellite telemetry should be used for real-time data collection and transmission. The instruments should be interfaced to a mooring data logger and the communication system (e.g. radio frequency transmitter) attached to the cable or located on the mooring buoy. The data logger will digitize the data before transmission then communicate the data to a shore-based data file management system (Figure 2.13). Computing resources should automatically process the data from its digital format to engineering units. Lastly, a graphical program should automatically convert the data into viewable images and transfer the images onto the internet (Figure 2.13). The data stream from all instruments listed above should also be sent hourly to the website.

A web-based data management system, using JavaScript, will allow users, for example scientists, government health officials (local, state and federal), students and teachers (K-12, college and graduate), and non-governmental organizations to download and view real-time, archived and historical HAB and complementary data. For example, see the Dalhousie University Lunenberg Bay, Nova Scotia coastal observatory data access and visualization site (http://www.cmep.ca/bay).

Data communication should use a system capable of two-way communication from mooring to shore-based computers and vice-versa.[12] Therefore, during times of HAB formation, persistence and cessation, adaptive sampling can be employed to enhance the sampling efforts and ship-based sampling can be coordinated. Sampling rates and instrument gains can be changed when prompted by simple computer commands from shore. Another advantage of real-time data transmission is the ability to check for biofouling of data to schedule diver servicing or instrument/mooring turnarounds.

Integration of detailed ship-based sampling should be employed when HABs are detected in a region. High spatial resolution data collection methods should be used just inside and outside the bloom region (Figure 2.11). A detailed sampling grid within the HAB can be designed according to the along- and cross-shore extent of the HAB; the extent of the HAB may be determined using satellite images if it has a surface expression, is large enough for observation, and has a discernable colour signature. If the HAB is determined to be highly extensive or patchy, measurements can be made along several detailed sampling grids in different locations. Our suggested measurement approach within the detailed sampling grid is to use an AUV or glider together with a vertical profiling instrument package, and whole water sample collection from Niskin bottles deployed from small research boats. Instruments on the AUV or glider could include: (spectral) fluorometer, spectral backscatter and other inherent optical property sensors, rapid chemical analyzer, MBBP, pressure sensor, temperature sensor, conductivity meter, acoustic-based current meter, and GPS. The AUV or glider can operate at pre-programmed speeds and patterns, for example in a zigzag or sawtooth pattern along the detailed sampling grid from the surface to the mixed layer or another depth or at a specified fixed depth (e.g. using artificial intelligence; Schofield et al., 2003). The instruments can sample up to 10 times per second for high spatial and temporal resolution.

The vertical profiling package should be relatively small, lightweight, and deployable from small research boats. Vertical profiles should be obtained at prespecified locations along the detailed sampling grid. Battery-powered instruments on the profiling package could include: hyperspectral IOP and AOP instruments, (spectral) fluorometer, optical-based chemical analyzer, MBBP, pressure sensor, temperature sensor, and conductivity meter. These instruments can profile at <10 cm s^{-1} and should sample several times per second for high vertical resolution (the ac-9 and ac-s have an inherent timescale associated with flushing, and it is longer than this). Niskin bottle samples and plankton samples can be obtained along prespecified sections of the detailed sampling grid, for example at the four corners and at the centre. These water samples should be immediately taken to the laboratory for phytoplankton species identification, nutrient analyses and toxin analysis. Opening and closing nets with 25 μm mesh size can also be attached to the vertical profiling package to collect plankton samples

[12]For example, Woods Hole Oceanographic Institution, Martha's Vineyard Coastal Observatory: http://www.whoi.edu/mvco/

at specific depths (Herren, 2002). The outflow of the MBBP can provide pumped seawater to the net at a rate of 350–400 ml s^{-1} (Herren, 2002). A GPS unit on the small boat can obtain the exact locations of vertical profiles, bottle samples and net tows.

The suggested instrumentation is by no means inexpensive and it is expected that most HAB monitoring and/or research programmes will be unable to put together such an extensive observation system. At a minimum, a HAB programme should have access to large-scale, synoptic observations such as ocean-colour satellite images and their derived product, chlorophyll *a* concentration. Chlorophyll *a* concentration information will at least alert researchers to the formation of blooms in the region of interest and assist in coordination of shipboard sampling efforts with respect to sampling in time and space. Inshore, where ocean-colour satellite data are contaminated by land, a HAB programme should deploy at least one lightweight mooring, within 5 km of shore, for monitoring and characterization purposes. The close proximity to the coastline will facilitate mooring and instrumentation maintenance, including cleaning of optical windows. One instrumentation package, deployed near the surface, should suffice. This package should, at minimum, include: chlorophyll fluorometer, single-wavelength backscattering sensor or beam transmissometer, PAR sensor, dissolved oxygen sensor, temperature sensor, and conductivity meter. Data from these instruments should be real-time telemetered using radio frequency modems, which are relatively inexpensive (about US$3,000). Data from the mooring would be used to monitor the environmental conditions associated with the formation of HABs as well as to develop optical proxies to coordinate and complement extensive shipboard sampling and laboratory analyses. At minimum, shipboard sampling should include a chlorophyll fluorometer, CTD and whole water samples for cell concentration and identification, and nutrient and toxin analyses.

2.4.2 Data analyses

Below, we illustrate potential data analyses for HAB characterization using coastal observation systems. Additional techniques to identify and monitor HABs using *in situ* optical and bio-optical measurements and remote sensing technologies are reviewed by Cullen et al. (1997); Schofield et al., (1999); and Babin, Lewis, Morel, Roesler and Boss, Schofield et al. (2007 – Chapters 7, 6, 4, 5 and 3 this volume).

Statistical analyses can be conducted using mooring time series (or spatial transect) data of interdisciplinary parameters to determine important temporal (spatial) scales of variability (Emery and Thomson, 2001). The most commonly used method is the computation of the power spectral density (PSD) function, which assigns a distribution of power of a given parameter per unit frequency. For example, M2 semidiurnal tidal fluctuations in temperature, for example, can be seen as a peak in the PSD at 1.93 day^{-1} (Figure 2.2A). This can aid in the identification of the principal forcing periods in a region possibly affecting HABs.

A second powerful data analysis technique is autocovariance, which provides information about temporal and spatial scales of decorrelation over a particular time period or spatial domain (Emery and Thompson, 2001). Decorrelation scales are important for the development of adaptive sampling strategies (i.e. where and how often to sample) and models (i.e. time steps and grid spacing).

Importantly, quantification of the relationships between various interdisciplinary parameters can be conducted using most simply linear regression analysis, or coherence and phase or principal component analysis (also called empirical orthogonal function

analysis; see Emery and Thomson, 2001). EOF analysis is an empirical technique used to rank the importance of a set of processes that result in variance of a data set. These methods in general measure the extent to which variables are related to each other over certain temporal or spatial scales. Again, these techniques can be applied to spatial data as well. These statistical methods are extremely useful for identification and quantification of many of the physical and chemical processes (e.g. wind-mixing, waves, tides, river runoff, upwelling, eddies, El Niño events, etc.) important and related to HAB characteristics.

Long-term, continuous, autonomous and interdisciplinary sampling is necessary for understanding HAB dynamics. For example, Figure 2.14 shows a limited set of interdisciplinary HAB-related data collected on an on-going coastal observatory in the Santa Barbara Channel, CA. Two HABs occurred over the time period of this

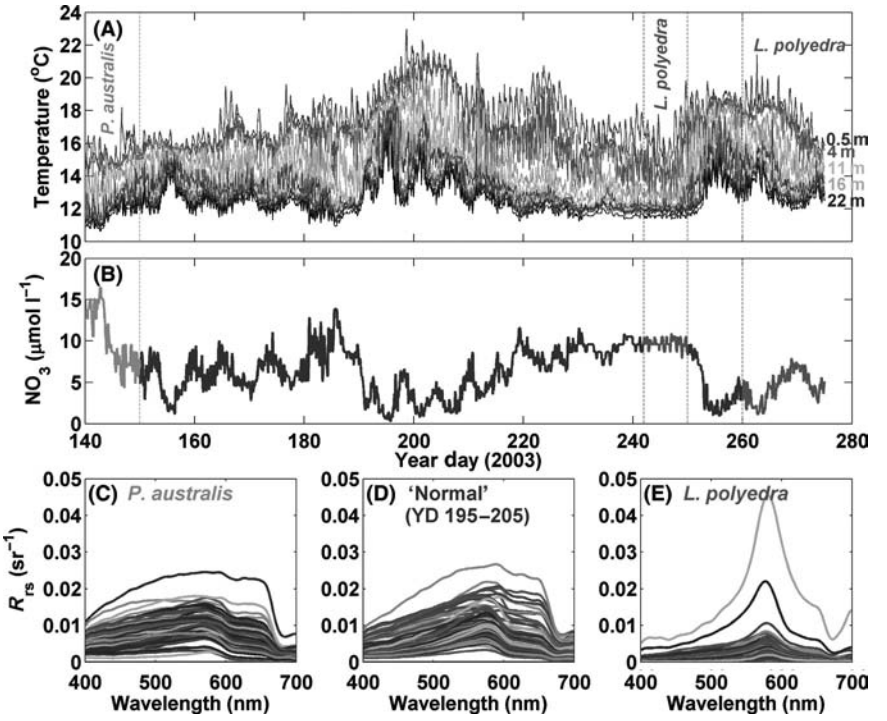

Figure 2.14
Time series of A, temperature collected at about every metre from near surface to 22 m; B, derived nitrate concentration at 22 m (following McPhee-Shaw et al., 2007) from 20 May to 2 October 2003. Remote sensing reflectance spectra computed from hyperspectral radiometer data during C, a *Pseudo-nitzschia australis* bloom (until 30 May); D, conditions not affected by HABs (14–24 July); E, a bloom of *Lingulodinium polyedra* (30 August to 7 September and again 17 September to 2 October). Data were collected on a mooring in the Santa Barbara Channel (25 m water depth). The remote sensing signals during the times of the *L. polyedra* bloom are different from conditions not affected by HABs; this shows promise in using optics for detection and identification of HABs.

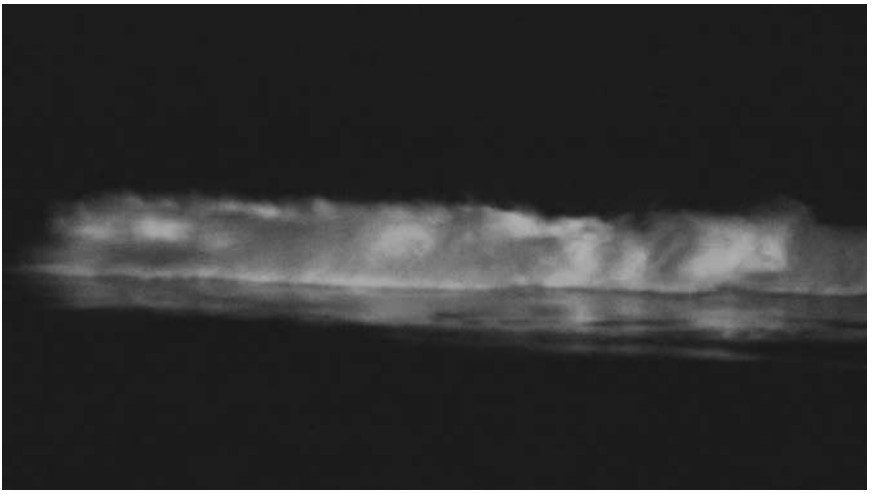

Figure 2.15
Digital photograph (unenhanced) of a breaking wave containing the bioluminescent dinoflagellate species, *Lingulodinium polyedra*, taken along the central coast of California during a red tide in October 2003. *Source*: Image used with permission from Rosalba Dominguez.

particular mooring deployment, a toxic *Pseudo-nitzschia australis* bloom and a bioluminescent bloom of *Lingulodinium polyedra* (Figure 2.15). In April and May 2003, the *P. australis* bloom resulted in a coast-wide domoic acid event and the demise of several sea lions, dolphins and birds (G. Langlois,[13] pers. comm., 2003). The *L. polyedra* bloom occurred from late August to early October 2003; termination of the bloom led to a massive fish kill in nearby Ventura Harbor (Scheibe, 2003). Physical, hydrographic and chemical data help to characterize environmental conditions associated with each HAB. Qualitatively, data suggest that the *P. australis* bloom were associated with higher nutrient conditions whereas the *L. polyedra* blooms were not dependent on nutrients at the surface (Heaney and Eppley, 1981). Also, while *L. polyedra* blooms indeed occurred during times of stratification, waters were stratified during periods when no blooms were present. Therefore, other factors are necessary for the formation of these nuisance blooms.

The value of bioluminescence as an indicator of developing HAB conditions could be determined using coherence analysis between bioluminescence potential and a marker for *L. polyedra* (e.g. cell concentrations determined from water samples). Threshold values of bioluminescence potential coupled with other optical proxies (e.g. phytoplankton absorption at specified wavelengths) should be determined in order to develop rapid response HAB mitigation strategies, that is when threshold values of these parameters are exceeded, HAB investigators are automatically alerted by the web-based data management system. Then, adaptive sampling (whole water sample collection, increased sampling rates, etc.) can commence and responsible authorities notified.

[13]Chief, Marine Biotoxin Monitoring and Control Program, California Department of Health Services, 2151 Berkeley Way, Berkeley, CA 94704.

Complementary shipboard sampling and advanced data analyses (e.g. statistical analyses outlined above) methods can also aid in the quantification of these HAB dynamics. Cross-shelf wind and current velocity and temperature measurements (transected using an AUV, glider, or ship) could have helped determine whether coastal upwelling was related to these blooms. Maps of current velocity (using HF radar) and additional hydrography data could have enabled the observation and quantification of advection and/or freshwater inputs.

Unique optical spectral signals during the times of the HABs show promise in using optics for detection and identification of HABs (Figure 2.14). HAB species identification is possible, in principle, using direct measurements of hyperspectral absorption coefficient or potentially with hyperspectral radiometric measurements (Craig et al., 2006). Radiometric measurements would need to be coupled with remote sensing reflectance inversion models to derive the IOPs (e.g. Roesler and Perry, 1995). Spectral deconvolution procedures would then be followed to arrive at the absorption coefficient for phytoplankton (Schofield et al., 2004 and references therein). Derived hyperspectral absorption data, used in combination with spectral techniques such as derivative analysis (usually the fourth derivative), spectral angle mapping, spectral deconvolution and similarity indices (also called spectral angle mapping in image analysis), can aid in the characterization of marine ecosystems including the detection and identification of HABs (Millie et al., 1995, 1997; Kirkpatrick et al., 2000; Lohrenz et al., 1999); however, to date these methods have required manipulation of samples for spectrophotometry. Spectral analysis, performed on phytoplankton absorption data, can aid in the identification of specific pigment absorption peaks and important wavelength ratios. This method has been shown to be successful for the detection of the red-tide dinoflagellate *Karenia brevis* (Millie et al., 1995; 1997; Kirkpatrick et al., 2000). *K. brevis* can be identified by its accessory pigment, Gyroxanthin–diester, which has unique absorption peaks at 444 nm and 469 nm (Örnólfsdóttir et al., 2003; Chang et al., 2004, Figure 1). Limitations of the above method include:

- It is sometimes necessary and difficult to tune spectral inversion and deconvolution techniques for specific environments;
- Not all HAB species have unique accessory pigments that can be distinguished from other species;
- Some HAB species have toxic and non-toxic states (e.g. *Pseudo-nitzschia australis*);
- Remotely sensed ocean colour validation of the methods presented above have only recently begun (Craig et al., 2006).

The promise and limitations of optical detection systems show that *in situ* optical measurements must be complemented with laboratory-based analyses using microscopic or molecular methods until robust relationships between optical properties and HAB species are quantified. In addition, phytoplankton physiological and physiochemical changes (e.g. nutrient limitation) can be investigated through these complementary laboratory analyses. All collected data should be made available for various biological/chemical/optical/physical data assimilation models for HAB prediction purposes (Franks, 1997; Schofield et al., 1999; Franks, 2007 – Chapter 15 this volume)

2.5 Summary and conclusions

Physical and chemical as well as biological processes are important for understanding, monitoring, and predicting the dynamics of harmful algal blooms. The coastal ocean, where most HABs occur, is considerably more complex than the open ocean as there

is greater diversity of organisms and the time and space scales of variability are shorter. Progress in HAB research will require new interdisciplinary instrumentation, use of a diverse set of emerging observing platforms, and well-integrated observational and modelling efforts. Promising observational tools include:

- hyperspectral optical instrumentation that can be deployed from aircraft, satellites and *in situ* platforms;
- new biological, chemical and optical sensors, many of which have (or soon will have) the capacity to measure on virtually the same time and space scales as physical sensors (e.g. temperature, conductivity, currents);
- several new observing platforms including AUVs, profiling floats and moorings, drifters and gliders;
- real-time two-way data-communication techniques.

Interdisciplinary models are also critical for developing new parameterizations and algorithms that can be applied to complex ecosystems with special focus on HABs. They will also be needed to design optimal sampling arrays. Data assimilation models will be especially important for directing adaptive sampling assets.

At present, most HAB research is response-oriented and is not useful for studying the critical problem of preconditioning of HAB events. Therefore, future focused process studies devoted to HABs need to be done in the context of high-frequency, long time-series observations as the full evolution of a particular HAB events need to be observed and documented. This concept may soon be possible by instrumenting coastal global observing system platforms with key instrumentation to measure variables relevant to the HAB problem and using emerging colour satellites, including those with hyperspectral sensors and high spatial resolution capabilities. Using data assimilation models along with these complementary data sets, it should be possible to quantify ecosystem and HAB variability on time and space scales down to hours and metres and to make plausible predictions of HAB conditions that are useful for environmental management.

References

Abbott, M. R., Brink, K. H., Booth, C. R., Blasco, D., Codispoti, L. A., Niiler, P. P. and Ramp, S. R. 1990. Observations of phytoplankton and nutrients from a Lagrangian drifter off northern California. *J. Geophys. Res.*, 95, pp. 9393–409.

Abbott, M. R., Brink, K. H., Booth, C. R., Blasco, D., Swenson, M. S., Davis, C. O. and Condispoti, L. A. 1995. Scales of variability of bio-optical properties as observed from near-surface drifters. *J. Geophys. Res.*, 100, pp. 13345–67.

Abbott, M. R. and Letelier, R. M. 1998. Decorrelation scales of chlorophyll as observed from bio-optical drifters in the California Current. *Deep Sea Res. II*, 45, pp. 1639–67.

Agrawal, Y. C. and Pottsmith, H. C. 1994. Laser diffraction particle sizing in STRESS. *Cont. Shelf Res.*, 14, pp. 1101–21.

Anderson, D. M. 1995. Toxic red tides and harmful algal blooms: a practical challenge in coastal oceanography. *Rev. Geophys.*, 33, Suppl., pp. 1189–200. (US National Report to IUGG 1991–1994.)

Anderson, D. M., Andersen, P., Bricelj, V. M., Cullen, J. J. and Rensel, J. E. 2001. *Monitoring and Management Strategies for Harmful Algal Blooms in Coastal Waters*. Paris, Intergovernmental Oceanographic Commission of UNESCO, 268 pp. (IOC Technical Series 59.)

Anderson, D. M., Kulis, D. M. and Binder, B. J. 1984. Sexuality and cyst formation in the dinoflagellate *Gonyaulax tamarensis*: cyst yield in batch cultures. *J. Phycol.*, 20, pp. 418–25.

André, J. M., Navarette, C., Blanchot, J. and Radenac, M.-H. 1999. Picophytoplankton dynamics in the equatorial Pacific: growth and grazing rates from cytometric counts. *J. Geophys. Res.*, 104, pp. 3369–80.

Babin, M. 2007. Phytoplankton fluorescence: theory, current literature and *in situ* measurement. In: Babin et al. (eds), op. cit., this volume.

Babin, M., Morel, A., Fournier-Sicre, V., Fell, F. and Stramski, D. 2003. Light scattering properties of marine particles in coastal and open ocean waters as related to the particle mass concentration. *Limnol. Oceanogr.*, 48, pp. 843–59.

Babin, M., Roesler, C. S. and Cullen, J. J. (eds). 2007. *Real-time Coastal Observing Systems for Marine Ecosystem Dynamics and Harmful Algal Blooms: Theory, Instrumentation and Modelling*. Paris, Intergovernmental Oceanographic Commission of UNESCO. (Monographs on Oceanographic Methodology XX.)

Balch, W. M., Drapeau, D., Bowler, B., Booth, E., Goes, J., Ashe, A. and Frye, J. 2004. A multi-year record of optical properties in the Gulf of Maine. I: Spatial and temporal variability. *Progr. Oceanogr.*, 63, pp. 57–98.

Balch, W. M., Drapeau, D. T., Fritz, J. J., Bowler, B. C. and Nolan, J. 2001. Bio-optical backscattering in the Arabian Sea – continuous underway measurements of particulate inorganic and organic carbon. *Deep Sea Res. I*, 48, pp. 2423–52.

Barnes, R. A., Eplee, R. E., Schmidt, G. M., Patt, F. S. and McClain, C. R. 2001. The calibration of SeaWiFS. Part 1: direct techniques. *Appl. Opt.*, 40, pp. 6682–700.

Barth, J. A., Bogucki, D., Pierce, S. D. and Kosro, P. M. 1998. Secondary circulation associated with a shelfbreak front. *Geophys. Res. Lett.*, 25, pp. 2761–64.

Bartz, R., Zaneveld, J. R. V. and Pak, H. 1978. A transmissometer for profiling and moored observations in water. *Ocean Optics V*, *Proc. SPIE*, 160, pp. 102–08.

Behrenfeld, M. and Falkowski, P. G. 1997. Photosynthetic rates derived from satellite-based chlorophyll concentration. *Limnol. Oceanogr.*, 42, pp. 1479–91.

Behrenfeld, M. J., Boss, E., Siegel, D. A. and Shea, D. M. 2005. Carbon-based ocean productivity and phytoplankton physiology from space. *Global Biogeochem. Cy.*, GB1006, doi:10.1029/2004GB002299.

Bianchi, T. S., Engelhaupt, E., Westman, P., Andrén, T., Rolff, C. and Elmgren, R. 2000. Cyanobacterial blooms in the Baltic Sea: natural or human-induced? *Limnol. Oceanogr.*, 45, pp. 716–26.

Bishop, D., Gammel, P. and Giles, C. R. 2001. The little machines that are making it big. *Phys. Today*, 54, pp. 38–44.

Bishop, J. K. B. 1999. Transmissometer measurement of POC. *Deep Sea Res. I*, *46, pp. 353–69.*

Bishop, J. K. B., Guay, C. K., Sherman, J. T., Moore, C. and Davis, R. E. 2003. Prospects for a 'CARGO': a new approach for exploring ocean carbon system variability, In: K. Harada and T. Dickey (eds), *Proc. International Workshop on Autonomous Measurements of Biogeochemical Parameters in the Ocean*. Honolulu, Hawaii. (CD-ROM.)

Bogucki, D., Dickey, T. and Redekopp, L. 1997. Sediment resuspension and mixing through resonantly-generated internal solitary waves. *J. Phys. Oceanogr.*, 27, pp. 1181–96.

Boss, E. and Pegau, W. S. 2001. The relationship of light scattering at an angle in the backward direction to the backscattering coefficient. *Appl. Opt.*, 40, pp. 5503–07.

Boss, E., Pegau, W. S., Lee, M., Twardowski, M. S., Shybanov, E., Korotaev, G. and Baratange, F. 2004*a*. The particulate backscattering ratio at LEO-15 and its use to study particle composition and distribution. *J. Geophys. Res.*, 109(1), C0101410.1029/2002JC001514.

Boss, E., Stramski, D., Bergmann, T., Pegau, W. S. and Lewis, M. 2004*b*. Why should we measure the optical backscattering coefficient? *Oceanogr. Mag.*, 17, pp. 44–49.

Bricaud, A. and Stramski, D. 1990. Spectral absorption coefficients of living phytoplankton and nonalgal biogenous matter: a comparison between the Peru upwelling area and the Sargasso Sea. *Limnol. Oceanogr.*, 35, pp. 562–82.

Burkholder, J. M. and Glasgow, H. B. Jr. 1997. *Pfiesteria piscicida* and other *Pfiesteria*-like dinoflagellates: behavior, impacts, and environmental controls. *Limnol. Oceanogr.*, 42, pp. 1052–75.

California Department of Health Services. 2001. Monthly Biotoxin Report. Environmental Management Branch Marine Biotoxin Monitoring and Control Program, 01–11. Berkeley, Calif., 7 pp.

Case, J. F., Herring, P. J., Haddock, S. H. D., Kricka, L. J. and Stanley, P. E. (eds). 2001. *Bioluminescence and Chemiluminescence 2000*. Singapore, World Scientific Publishing Company.

Chang, G. C. and Dickey, T. D. 1998. Preliminary observations of bio-optical variability associated with internal solitary waves during the Coastal Mixing and Optics experiment. In: T. Duda (ed.), *The 1998 WHOI/IOS/ONR Internal Solitary Wave Workshop: Contributed Papers, WHOI-99-07*. Woods Hole, Mass., Woods Hole Oceanographic Institution, pp. 65–68.

Chang, G. C. and Dickey, T. D. 1999. Partitioning *in situ* total spectral absorption by use of moored spectral absorption – attenuation meters. *Appl. Opt.*, 38, pp. 3876–87.

Chang, G. C. and Dickey, T. D. 2001. Optical and physical variability on time-scales from minutes to the seasonal cycle on the New England shelf: July 1996–June 1997. *J. Geophys. Res.*, 106, pp. 9435–53.

Chang, G. C. and Dickey, T. D. 2004. Coastal ocean optical influences on solar transmission and radiant heating rate. *J. Geophys. Res.*, 109, C01020, doi:10.1029/2003JC001821.

Chang, G. C., Dickey, T. D., Schofield, O., Weidemann, A. D., Boss, E., Pegau, W. S., Moline, M. and Glenn, S. M. 2002. Temporal and spatial scales of physical and bio-optical variability on the New York Bight inner continental shelf. *J. Geophys. Res.*, 107, 3133, doi:10.1029/2001JC001018.

Chang, G. C., Dickey, T. D. and Williams, A. J. 3rd. 2001. Sediment resuspension on the Middle Atlantic Bight continental shelf during Hurricanes Edouard and Hortense: September 1996. *J. Geophys. Res.*, 106, pp. 9517–31.

Chang, G. C., Mahoney, K., Briggs-Whitmire, A., Kohler, D., Mobley, C., Moline, M., Lewis, M., Boss, E., Kim, M., Philpot, W. and Dickey, T. 2004. The new age of hyperspectral oceanography. *Oceanogr. Mag.*, 17, pp. 22–29.

Chang, G. C., Barnard, A. H., McLean, S., Egli, P. J., Moore, C., Zaneveld, J. R. V., Dickey, T. D., and Hanson, A. 2006*a*. In situ optical variability and relationships in the Santa Barbara Channel: implications for remote sensing, *Appl. Opt.*, 45, 3593–3604.

Chang, G. C., Dickey, T., and Lewis, M. 2006*b*. Toward a global ocean system for measurements of optical properties using remote sensing and *in situ* observations, In: J. Gower (ed.), *Remote Sensing of the Marine Environment: Manual of Remote Sensing*, 6, pp. 285–326.

Chavez, F. P., Pennington, J. T., Castro, C. G., Ryan, J. P., Michisaki, R. P., Schlining, B., Walz, P., Buck, K. R., McFayden, A. and Collins, C. A. 2002. Biological and chemical consequences of the 1997–98 El Niño in central California waters. *Progr. Oceanogr.*, 54, pp. 205–32.

Chavez, F. P., Wright, D., Herlien, R., Kelley, M., Shane, F. and Strutton, P. G. 2000. A device for protecting moored spectroradiometers from fouling. *J. Atmos. Ocean. Tech.*, 17, pp. 215–19.

Codd, G. A. 2001. Cyanobacterial toxins: their actions and multiple fates in microbes, animals and plants. *J. Phycol.*, 37, pp. 13.

Cosper, E. M., Dennison, W., Milligan, A., Carpenter, E. J., Lee, C., Holzapfel, J. and Milanese, L. 1989. An examination of the environmental factors important to initiating and sustaining 'brown tide' blooms. In: E. M. Cosper, V. M., Bricelj and E. J. Carpenter (eds), *Novel Phytoplankton Blooms: Causes and Impacts of Recurrent Brown Tides and Other Unusual Blooms*. Berlin, SpringerVerlag, pp. 317–40.

Craig, S. E., Lohrenz, S. E., Lee, Z., Mahoney, K. L., Kirkpatrick, G. J., Schofield, O. M. and Steward, R. G. 2006. Use of hyperspectral remote sensing reflectance for detection and assessment of the harmful alga, *Karenia brevis. Appl. Opt.,* 45, 5414–25.

Cullen, J. J. 2007. Observation and prediction of harmful algal blooms. In: Babin et al. (eds), op. cit., this volume.

Cullen, J. J., Ciotti, A. M., Davis, R. F. and Lewis, M. R. 1997. Optical detection and assessment of algal blooms. *Limnol. Oceanogr.*, 42, pp 1223–39.

Cullen, J. J., Franks, P. J. S., Karl, D. M. and Longhurst, A. 2002. Physical influences on marine ecosystem dynamics. In: Robinson et al. (eds), op.cit., pp. 297–336.

Davis, C., Bowles, J., Leathers, R. A., Korwan, D. R., Downes, T. V., Snyder, W. A., Rhea, W. J., Chen, W., Fisher, J., Bissett, P. W. and Reisse, R. A. 2002. Ocean PHILLS hyperspectral imager: design, characterization, and calibration. *Opt. Expr.*, 10, pp. 210–21.

Davis, R. E., Eriksen, C. C. and Jones, C. P. 2003. Autonomous buoyancy-driven underwater gliders. In: G. Griffiths (ed.), *Technology and Applications of Autonomous Underwater Vehicles*. London, Taylor and Francis, pp. 37–58.

Davis, R. F., Stabeno, P. and Cullen, J. J. 2000. Use of bio-optical measurements from moorings to detect coccolithophore blooms in the Bering Sea. *Ocean Optics XV*, *Proc. SPIE*, US Office of Naval Research, (CD-ROM)

Dickey, T. 1991. The emergence of concurrent high resolution physical and bio-optical measurements in the upper ocean and their applications. *Rev. Geophys.*, 29, pp. 383–413.

Dickey, T. 2001*b*. Sensors: inherent and apparent optical properties. In: J. Steele, S. Thorpe and K. Turekian (eds), *Encyclopedia of Ocean Sciences*. New York, Academic Press, pp. 1313–23.

Dickey, T. 2002. A vision of oceanographic instrumentation and technologies in the early 21st century. In: J. G. Field, G. Hempel and C. P. Summerhayes (eds), *Oceans 2020: Science for Future Needs*. Washington DC, Island Press, pp. 213–56.

Dickey, T. 2003. Emerging ocean observations for interdisciplinary data assimilation systems. *J. Marine Systems*, 40–41, pp. 5–48.

Dickey, T., Lewis, M., and Chang, G. 2006. Bio-optical oceanography: Recent advances and future directions using global remote sensing and *in situ* observations, *Rev. Geophys.*, 44, RG1001, doi:10.1029/2003RG000148.

Dickey, T. and Falkowski, P. 2002. Solar energy and its biological-physical interaction in the sea. In: Robinson et al. (eds), op. cit., pp. 401–40.

Dickey, T., Plueddemann, A. and Weller, R. 1998*b*. Current and water property measurements in the coastal ocean. In: K. H. Brink and A. R. Robinson (eds), *The Sea*. Vol. 10: *The Global Coastal Ocean. Processes and Methods*. New York, John Wiley & Sons, pp. 367–98.

Dickey, T. D. 2001*a*. New technologies and their roles in advancing biogeochemical research. *Oceanogr. Mag.*, 14, pp. 108–20.

Dickey, T. D. and Chang, G. C. 2001. Recent advances and future visions: temporal variability of optical and bio-optical properties of the ocean. *Oceanogr. Mag.*, 14, pp. 15–29.

Dickey, T. D., Chang, G. C., Agrawal, Y. C., Williams, A. J. 3rd and Hill, P. S. 1998*a*. Sediment resuspension in the wakes of Hurricanes Edouard and Hortense. *Geophys. Res. Lett.*, 25, pp. 3533–36.

Donaghay, P. L. and Osborn, T. R. 1997. Toward a theory of biological-physical control of harmful algal bloom dynamics and impacts. *Limnol. Oceanogr.*, 42, pp. 1283–96.

Donaghay, P. L., Sullivan, J. M., Moore, C., Rhoades, B. and McManus, M. 2003. Application of the Ocean Response Coastal Analysis System (ORCAS) to the study of harmful algal blooms. HABWATCH Workshop, Villefranche-Sur-Mer, France, 11–21 June. (Poster)

DuRand, M. D. and Olson, R. J. 1998. Diel patterns in optical properties of the chlorophyte *Nannochloris* sp.: relating individual-cell to bulk measurements. *Limnol. Oceanogr.*, 43, pp. 1107–18.

DuRand, M. D., Olson, R. J. and Chisholm, S. W. 2001. Phytoplankton population dynamics at the Bermuda Atlantic time-series station in the Sargasso Sea. *Deep Sea Res. II*, 48, pp. 1983–2003.

Dzurica, S., Lee, C., Cosper, E. M. and Carpenter, E. J. 1989. Role of environmental variables, specifically organic compounds and micronutrients in growth of the 'brown tide' organism. In: E. M. Cosper, E. J. Carpenter and V. M. Bricelj (eds), *Novel Phytoplankton Blooms: Causes and Impacts of Recurrent Brown Tides and Other Unusual Blooms*. Berlin, Springer-Verlag, pp. 229–42.

Emery, W. J. and Thomson, R. E. 2001. *Data Analysis Methods in Physical Oceanography*, 2nd rev. edn. Amsterdam, Elsevier Science.

Falkowski, P. G. and Wilson, C. 1992. Phytoplankton productivity in the North Pacific ocean since 1900 and implications for absorption of anthropogenic CO_2. *Nature*, 358, pp. 741–43.

Franks, P. J. S. 1997. Models of harmful algal blooms. *Limnol. Oceanogr.*, 42(5), pp. 1273–82.

Franks, P. J. S. 2007. Physics and physical modelling of harmful algal blooms. In: Babin et al. (eds), op. cit., this volume.

Gallegos, C. L. and Neale, P. J. 2002. Partitioning spectral absorption in Case 2 waters: discrimination of dissolved and particulate components. *Appl. Opt.*, 41, pp. 4220–33.

Glenn, S. and Dickey, T. 2003. *Scientific Cabled Observatories for Time Series (SCOTS) Report*. Washington DC, Consortium for Oceanographic Research and Education.

Gordon, H. R. and McCluney, W. R. 1975. Estimation of the depth of sunlight penetration in the sea for remote sensing. *Appl. Opt.*, 14, pp. 413–16.

Griffiths, G. 2007. Glider and autonomous underwater vehicle observing systems. In: Babin et al. (eds), op. cit., this volume.

Griffiths, G., Davis, R., Eriksen, C., Frye, D., Marchand, P. and Dickey, T. 2001. Towards new platform technology for sustained observations, In: C. J. Koblinsky and N. R. Smith (eds), *Observing the Oceans in the 21st Century*. Melbourne, Bureau of Meteorology, GODAE Project Office, pp. 324–38.

Heaney, S. I. and Eppley, R. W. 1981. Light, temperature and nitrogen as interacting factors affecting diel vertical migrations of dinoflagellates in culture. *J. Plankton Res.*, 3, pp. 331–44.

Herren, C. M. 2002. Bioluminescent plankton association with thin layers and marine snow in coastal oceans. Ph.D. thesis, University of California at Santa Barbara.

Herren, C. M., Alldredge, A. L. and Case, J. F. 2004. Coastal bioluminescent marine snow: fine structure of bioluminescence distribution. *Cont. Shelf Res.*, 24, pp. 413–29.

Hill, P. S., Voulgaris, G. and Trowbridge, J. H. 2001. Controls on floc size in a continental shelf bottom boundary layer. *J. Geophys. Res.*, 106, pp. 9543–49.

Holliday, D. V. and Pieper, R. E. 1989. Determination of zooplankton size and distribution with multifrequency acoustic technology. *J. Conseil – Conseil International pour l'Exploration de la Mer*, 46, pp. 52–61.

Horner, R. A., Garrison, D. L. and Plumley, F. G. 1997. Harmful algal blooms and red tide problems on the U.S. west coast. *Limnol. Oceanogr.*, 42, pp. 1076–88.

IOCCG. 1999. Minimum requirements for an operational ocean-colour sensor for the open ocean. A. Morel (ed.), *Report of the International Ocean-Colour Coordinating Group*. Dartmouth, Nova Scotia, International Ocean-Colour Coordinating Group. (Report 1.)

IOCCG. 2000. Status and plans for satellite ocean-colour missions: considerations for complementary missions. J. Yoder (ed.), *Report of the International Ocean-Colour Coordinating Group*. Dartmouth, Nova Scotia, International Ocean-Colour Coordinating Group. (Report 2.)

IOCCG. 2001. Remote sensing of ocean colour in coastal and other optically-complex waters. S. Sathyendranath (ed.), *Report of the International Ocean-Colour Coordinating Group*. Dartmouth, Nova Scotia, International Ocean-Colour Coordinating Group. (Report 3.)

IOCCG. 2004. Guide to the creation and use of ocean-colour, Level-3, binned data products. D. Antoine (ed.), *Report of the International Ocean-Colour Coordinating Group*. Dartmouth, Nova Scotia, International Ocean-Colour Coordinating Group. (Report 4.)

IOCCG. 2006. Remote Sensing of Inherent Optical Properties: Fundamentals, Tests of Algorithms, and Applications. In : Z. Lee (ed.), *Report of the International Ocean-Colour Coordinating Group*. Dartmouth, Nova Scotia, International Ocean-Colour Coordinating Group. (Report 5.)

Jacquet, S., Partensky, F., Lennon, J. and Vaulot, D. 2001. Diel patterns of growth and division in marine picoplankton in culture. *J. Phycol.*, 37, pp. 357–69.

Jaffe, J. S. 2007. Sensing plankton: acoustics and optical imaging. In: Babin et al. (eds), op. cit., this volume.

Jeffrey, S. W., Mantoura, R. F. C. and Wright, S. W. (eds). 1997. *Phytoplankton Pigments in Oceanography*. Paris, UNESCO.

Jiang, S., Dickey, T., Steinberg, D., and Madin, L. 2007. Temporal variability of zooplankton biomass from ADCP backscatter time series data at the Bermuda Testbed Mooring Site, *Deep-Sea Res. I*, 54, pp. 608–36.

Johnsen, G. and Sakshaug, E. 2000. Monitoring of harmful algal blooms along the Norwegian coast using bio-optical methods. *S. Afr. J. Mar. Sci.,* 22, pp. 309–21.

Johnson, K. S. and Coletti, L. J. 2002. *In situ* ultraviolet spectrophotometry for high resolution and long-term monitoring of nitrate, bromide and bisulfide in the ocean. *Deep Sea Res I.*, 49, pp. 1291–305.

Kahru, M. and Mitchell, B. G. 2001. Seasonal and nonseasonal variability of satellite-derived chlorophyll and colored dissolved organic matter concentration in the California Current. *J. Geophys. Res.*, 106, pp. 2517–29.

Kaku, M. 1997. *Visions: How Science Will Revolutionize the 21st Century*? New York, Anchor Books Doubleday.

Kamykowski, D. 1974. Possible interactions between phytoplankton and semidiurnal internal tides. *J. Mar. Res.*, 32, pp. 67–89.

Keafer, B. A. and Anderson, D. M. 1993. Use of remotely-sensed sea surface temperatures in studies of *Alexandrium tamarense* bloom dynamics. In: T. J. Smayda and Y. Shimizu (eds), *Toxic Phytoplankon Blooms in the Sea*. Amsterdam, Elsevier, pp. 763–68.

Kerfoot, J. M., Mahoney, K., Kirkpatrick, G., Lohrenz, S., Moline M. and Schofield, O. 2002. Vertical migration of a toxic *Karenia brevis* red tide and the impact on remote sensing reflectance. *EOS Trans.* AGU/ASLO Ocean Sciences Meeting, Honolulu, Hawaii, 11–15 February.

Kirk, J. T. O. 1994. *Light and Photosynthesis in Aquatic Ecosystems*, 2nd edn. Cambridge, UK, Cambridge University Press.

Kirkpatrick, G. J., Millie, D. F., Moline, M. A. and Schofield, O. 2000. Optical discrimination of a phytoplankton species in natural mixed populations. *Limnol. Oceanogr.*, 45, pp. 467–71.

Lam, C. W. Y. and Ho, K. C. 1989. Red tides in Tolo Harbour, Hong Kong. In: T. Nemoto (ed.), *Red Tides: Biology, Environmental Science, and Toxicology*. New York, Elsevier, pp. 49–52.

Lee, Z. P., Carder, K. L. and Arnone, R. A. 2002. Deriving inherent optical properties from water color: a multi-band quasi-analytical algorithm for optically deep waters. *Appl. Opt.*, 41, pp. 5755–72.

Lehaitre, M., Delauney, L. and Compère, C. 2007. Biofouling and underwater measurements. In: Babin et al. (eds), op. cit., this volume.

Lewis, M. R. 2007. Measurement of apparent optical properties for diagnosis of harmful algal blooms. In: Babin et al. (eds), op. cit., this volume.

Lewis, M. R., Carr, M.-E., Feldman, G. C., Esaias, W. and McClain, C. 1990. Influence of penetrating solar radiation on the heat budget of the equatorial Pacific Ocean. *Nature*, 347, pp. 543–45.

Lewis, M. R., Cullen, J. J. and Platt, T. 1983. Phytoplankton and thermal structure in the upper ocean: consequences of nonuniformity in chlorophyll profile. *J. Plankton Res.*, 88, pp. 2565–70.

Li, W. K. W. and Dickie, P. M. 2001. Monitoring phytoplankton, bacterioplankton, and virioplankton in a coastal inlet (Bedford Basin) by flow cytometry. *Cytometry*, 44, pp. 236–46.

Lindahl, O. 1993. Hydrodynamical processes: a trigger and source for flagellate blooms along the Skagerrak coasts? In: T. J. Smayda and Y. Shimizu (eds), *Toxic Phytoplankton Blooms in the Sea*. Amsterdam, Elsevier, pp. 775–82.

Lohrenz, S. E., Fahnenstiel, G. L., Kirkpatrick, G. J., Carroll, C. L. and Kelly, K. A. 1999. Microphotometric assessment of spectral absorption and its potential application for characterization of harmful algal species. *J. Phycol.*, 35, pp. 1438–46.

Lukatelich, R. J. and McComb, A. J. 1986. Nutrient levels and the development of diatom and blue-green algal blooms in a shallow Australian estuary. *J. Plankton Res.*, 8, pp. 597–618.

Maffione, R. A. and Dana, D. R. 1997. Instruments and methods for measuring the backward-scattering coefficient of ocean waters. *Appl. Opt.*, 36, pp. 6057–67.

Maldonado, M. T., Hughes, M. P., Rue, E. L. and Wells, M. L. 2002. The effect of Fe and Cu on growth and domoic acid production by *Pseudo-nitzschia multiseries* and *Pseudo-nitzschia australis*. *Limnol. Oceanogr.*, 47, pp. 515–26.

Malone, T. C. 2007. Ecosystem dynamics, harmful algal blooms and operational oceanography. In: Babin et al. (eds), op. cit., this volume.

Mann, K. H. and Lazier, J. R. N. 1991. *Dynamics of Marine Ecosystems: Biological-Physical Interactions in the Oceans*. Cambridge, UK, Blackwell Science.

Manov, D. V., Chang, G. C. and Dickey, T. D. 2004. Methods for reducing biofouling of moored optical sensors. *J. Atmos. Ocean. Tech.*, 21, pp. 958–68.

Marasovic, I. 1989. Encystment and excystment of *Gonyaulax polydra* during a red tide. *Estuar. Coast. Shelf Sci.*, 28, pp. 35–41.

Margalef, R., Estrada, M. and Blasco, D. 1979. Functional morphology of organisms involved in red tides, as adapted to decaying turbulence. In: D. L. Taylor and H. H. Seliger (eds), *Toxic Dinoflagellate Blooms*. New York, Elsevier-North Holland, pp. 89–94.

McNeil, J. D., Jannasch, H. W., Dickey, T., McGillicuddy, D., Brzezinski, M. and Sakamoto, C. M. 1999. New chemical, bio-optical and physical observations of upper ocean response to the passage of a mesoscale eddy off Bermuda. *J. Geophys. Res.*, 104, pp. 15537–48.

McPhee-Shaw, E. E., Siegel, D., Washburn, L., Brzezinski, M. and Jones, J. 2007. Mechanisms for nutrient delivery to the inner shelf: observations from the Santa Barbara Channel. *Limnol. Oceanogr.*, (under revision).

Millie, D. F., Kirkpatrick, G. J. and Vinyard, B. T. 1995. Relating photosynthetic pigments and *in vivo* optical density spectra to irradiance for the Florida red-tide dinoflagellate *Gymnodinium breve*. *Mar. Ecol. Progr. Ser.*, 120, pp. 65–75.

Millie, D. F., Schofield, O. M., Kirkpatrick, G. J., Johnsen, G., Tester, P. A. and Vinyard, B. T. 1997. Detection of harmful algal blooms using photopigments and absorption signatures: a case study of the Florida red tide, *Gymnodinium breve*. *Limnol. Oceanogr.*, 42, pp. 1240–51.

Mitchell, B. G., Kahru, M. and Sherman, J. 2000. Autonomous temperature-irradiance profiler resolves the spring bloom in the sea of Japan. *Ocean Optics XV*, *Proc. SPIE*, US Office of Naval Research, (CD-ROM)

Mobley, C. D. 1994. *Light and Water: Radiative Transfer in Natural Waters*. San Diego, Calif., Academic Press.

Moline, M. A., Blackwell, S., Chant, R., Oliver, M. J., Bergmann, T., Glenn, S. and Schofield, O. 2004. Episodic physical forcing and the structure of phytoplankton communities in the coastal waters of New Jersey. *J. Geophys. Res.*, 109, C12504, doi 10.1029/2003JC002071.

Moore, C. C., Zaneveld, J. R. V. and Kitchen, J. C. 1992. Preliminary results from *in situ* spectral absorption meter data. *Ocean Optics XI*, *Proc. SPIE*, 1750, pp. 330–37.

Morel, A. 2007. Introduction to optical properties in the sea: theoretical aspects. In: Babin et al. (eds), op. cit., this volume.

Murakawa, M. 1987. Marine pollution and countermeasures in Japan. *Oceanus*, 30, pp. 55–60.

Nagai, S., Itakura, S., Matsuyama, Y. and Kotani, Y. 2003. Encystment under laboratory conditions of the toxic dinoflagellate *Alexandrium tamiyavanichii* (Dinophyceae) isolated from the Seto Inland Sea, Japan. *Phycologia*, 42, pp. 646–53.

National Research Council. 2003. *Enabling Ocean Research in the 21st Century*. Washington DC, National Academies Press.

Ohlmann, J. C. and Siegel, D. A. 2000 Ocean radiant heating. Part II: Parameterizing solar radiation transmission through the upper ocean. *J. Phys. Oceanogr.*, 30, pp. 1849–65.

Ohlmann, J. C., Siegel, D. A. and Mobley, C. D. 2000. Ocean radiant heating. Part I: Optical influences. *J. Phys. Oceanogr.*, 30, pp. 1833–48.

Okaichi, T. 1989. Red tide problems in the Seto Inland Sea. In: T. Yanagi (ed.), *Sustainable Development in the Seto Inland Sea, Japan – From the Viewpoint of Fisheries*. Tokyo, Terra Scientific Publishing Company, pp. 251–304.

Olson, R. J., Chisholm, S. W., Zettler, E. R., Altabet, M. A. and Dusenberry, J. A. 1990. Spatial and temporal distributions of prochlorophyte picoplankton in the North Atlantic Ocean. *Deep Sea Res.*, 37, pp. 1033–51.

Olson, R. J., Zettler, E. R. and Chisholm, S. W. 1991. Advances in oceanography through flow cytometry. In: S. Demers (ed.), *Particle Analysis in Oceanography*. Berlin, Springer-Verlag, pp. 351–99.

Olson, R. J., Zettler, E. R. and DuRand, M. D. 1993. Phytoplankton analysis using flow cytometry. In: P. F. Kemp, B. F. Sherr, E. B. Sherr and J. J. Cole (eds), *Aquatic Microbial Ecology*. Boca Raton, Fla., Lewis Publishers, pp. 175–86.

O'Reilly, J. E., Maritorena, S., Mitchell, B. G., Siegel, D. A., Carder, K. L., Garver, S. A., Kahru, M. and McClain, C. 1998. Ocean color chlorophyll algorithms for SeaWiFS. *J. Geophys. Res.*, 103, pp. 24937–53.

Örnólfsdóttir, E. B., Pinckney, J. L. and Tester, P. A. 2003. Quantification of the relative abundance of the toxic dinoflagellate, *Karenia brevis* (Dinophyta), using unique photopigments. *J. Phycol.*, 39, pp. 449–57.

Paerl, H. W. 1997. Coastal eutrophication and harmful algal blooms: importance of atmospheric deposition and groundwater as 'new' nitrogen and other nutrient sources. *Limnol. Oceanogr.*, 42, pp. 1154–65.

Parsons, M. L., Dortch, Q. and Turner, R. E. 2002. Sedimentological evidence of an increase in *Pseudo-nitzschia* (Bacillariophyceae) abundance in response to coastal eutrophication. *Limnol. Oceanogr.*, 47, pp. 551–58.

Pegau, W. S., Cleveland, J. S., Doss, W., Kennedy, C. D., Maffione, R. A., Mueller, J. L., Stone, R., Trees, C. C., Weidemann, A. D., Wells, W. H. and Zaneveld, J. R. V. 1995. A comparison of methods for the measurement of the absorption coefficient in natural waters. *J. Geophys. Res.*, 100, pp. 13201–20.

Pegau, W. S., Gray, D. and Zaneveld, J. R. V. 1997. Absorption and attenuation of visible and near-infrared light in water: dependence on temperature and salinity. *Appl. Opt.*, 36, pp. 6035–46.

Pegau, W. S. and Zaneveld, J. R. V. 1993. Temperature-dependent absorption of water in the red and near-infrared portions of the spectrum. *Limnol. Oceanogr.*, 38, pp. 188–92.

Pinkerton, M., Lavender, S. and Aiken, J. 2003. Validation of SeaWiFS ocean color satellite data using a moored databuoy. *J. Geophys. Res.*, 108(C5), doi:10.1029/2000JC000425.

Pitcher, G. C., Boyd, A. J., Horstman, D. A. and Mitchell-Innes, B. A. 1998. Subsurface dinoflagellate populations, frontal blooms and the formation of red tide in the southern Benguela upwelling system. *Mar. Ecol. Progr. Ser.*, 172, pp. 253–64.

Pitcher, G. C. and Calder, D. 2000. Harmful algal blooms of the southern Benguela Current: a review and appraisal of monitoring from 1989 to 1997. *S. Afr. J. Mar. Sci.*, 22, pp. 255–71.

Pitcher, G. C., Horstman, D. A. and Calder, D. 1993. Formation and decay of red tide blooms in the southern Benguela upwelling system during the summer of 1990/91. In: T. J. Smayda and Y. Shimizu (eds), *Toxic Phytoplankton Blooms in the Sea*. Amsterdam, Elsevier, pp. 317–22.

Reckermann, M. and Colijn, F. 2000. Aquatic flow cytometry: achievements and prospects. *Scientia Marina*, 64, p. 151.

Robinson, A. R. and Glenn, S. M. 1999. Adaptive sampling for ocean forecasting. *Naval Res. Rev.*, 51, pp. 26–38.

Robinson, A. R., McCarthy, J. J. and Rothschild B. J. (eds). 2002. *The Sea*. Vol. 12: *Biological-Physical Interactions in the Ocean.* New York, John Wiley & Sons.

Roesler, C. S. and Boss, E. 2003. A novel ocean color inversion model: retrieval of beam attenuation and particle size distribution. *Geophys. Res. Lett.*, 30, 10.1029/2002GL016366.

Roesler, C. S. and Boss, E. 2007. *In situ* measurement of inherent optical properties and potential for harmful algal bloom detection and coastal ecosystem observations. In: Babin et al. (eds), op. cit., this volume.

Roesler, C. S. and Perry, M. J. 1995. *In situ* phytoplankton absorption, fluorescence emission, and particulate backscattering spectra determined from reflectance. *J. Geophys. Res.*, 100, pp. 13279–94.

Roesler, C. S., Perry, M. J. and Carder, K. L. 1989. Modeling *in situ* phytoplankton absorption from total absorption spectra in productive inland marine waters. *Limnol. Oceanogr.*, 34, pp. 1510–23.

Scheibe, J. 2003. Worst may be over in huge fish die-off: severe red tide leaves harbor reeling. *Ventura County Star*, 2 October, p. A01.

Schofield, O., Bergmann, T., Oliver, M., Irwin, A., Kirkpatrick, G., Bissett, W. P. Orrico, C. and Moline, M. A. 2004. Inverting inherent optical signatures in the nearshore coastal waters at the Long Term Ecosystem Observatory. *J. Geophys. Res.*, 109,C12504 doi: 10.1029/2003JC0022071.

Schofield, O., Bosch, J., Glenn, S., Kirkpatrick, G., Kerfoot, J., Lohrenz, S., Moline, M., Oliver, M. and Bissett, P. 2007. Bio-optics in integrated ocean observing networks: potential for studying harmful algal blooms. In: Babin et al. (eds), op. cit., this volume.

Schofield, O., Glenn, S., Bissett, W. P., Frazier, T. K., Iglesias-Rodriguez, D. and Moline, M. A. 2003. Development of regional coastal ocean observatories and the potential benefits to marine sanctuaries. *Mar. Tech. Soc.*, 37, pp. 54–67.

Schofield, O., Grzymski, J., Bissett, W. P., Kirkpatrick, G. J., Millie, D. F., Moline, M. and Roesler, C. S. 1999. Optical monitoring and forecasting systems for harmful algal blooms: possibility or pipe dream? *J. Phycol.*, 35, pp. 1477–96.

Scholin, C., Massion, G., Mellinger, E., Brown, M., Wright, D. and Cline, D. 1998. The development and application of molecular probes and novel instrumentation for detection of harmful algae. *Mar. Tech. Soc.*, 1, pp. 367–70.

Scholin, C. A., Doucette, G. J. and Cembella, A. D. 2007. Prospects for developing mated systems for *in situ* detection of harmful algae and their toxins. In: Babin et al. (eds), op. cit., this volume.

Sellner, K. G. 1997. Physiology, ecology, and toxic properties of marine cyanobacteria blooms. *Limnol. Oceanogr.*, 42, pp. 1089–104.

Shalapyonok, A., Olson, R. J. and Shalapyonok, L. S. 2001. Arabian Sea phytoplankton during Southwest and Northeast Monsoons 1995: composition, size structure and biomass from individual cell properties measured by flow cytometry. *Deep Sea Res. II*, 48, pp. 1231–62.

Shalapyonok, A. A., Olson, R. J. and Shalapyonok, L. S. 1998. Ultradian growth in *Prochlorococcus* spp. *Appl. Environ. Microbiol.*, 64, pp. 1066–69.

Smayda, T. J. 1997. Harmful algal blooms: their ecophysiology and general relevance to phytoplankton blooms in the sea. *Limnol. Oceanogr.*, 42, pp. 1137–53.

Smayda, T. J. 2000. Ecological features of harmful algal blooms in coastal upwelling ecosystems. *S. Afr. J. Mar. Sci.*, 22, pp. 219–53.

Smayda, T. J. 2002. Turbulence, watermass stratification and harmful algal blooms: an alternative view and frontal zones as 'pelagic seed banks'. *Harmful Algae*, 1, pp. 95–112.

Smith, S. L., Pieper, R., Moore, M., Rudstam, L., Green, C., Zamon, J., Flagg, C. and Williamson, C. 1992. Acoustic techniques for *in situ* observations of zooplankton. In: *Archiv fur Hydrobiologie*, Beiheft 36, *Ergebnisse der Limnologie*, 35, pp. 23–43.

Sosik, H. M., Olson, R. J., Neubert, M. G., Shalapyonok, A. A. and Solow, A. R. 2003. Growth rates of coastal phytoplankton from time-series measurements with a submersible flow cytometer. *Limnol. Oceanogr.*, 48, pp. 1756–65.

Stramska, M. and Dickey, T. D. 1992. Variability of bio-optical properties in the upper ocean associated with diel cycles in phytoplankton population. *J. Geophys. Res.*, 97, pp. 17873–87.

Stramski, D., Bricaud, A. and Morel, A. 2001. Modeling the inherent optical properties of the ocean based on the detailed composition of planktonic community. *Appl. Opt.*, 40, pp. 2929–45.

Strutton, P. G. and Chavez, F. P. 2000. Primary productivity in the equatorial Pacific during the 1997–98 El Niño. *J. Geophys. Res.*, 105, pp. 26089–101.

Stumpf, R. P. 2001. Applications of satellite ocean color sensors for monitoring and predicting harmful algal blooms. *Hum. Ecol. Risk Assess.*, 7, pp. 1363–68.

Stumpf, R. P., Culver, M. E., Tester, P. A., Tomlinson, M., Kirkpatrick, G. J., Pederson, B. A., Truby, E., Ransibrahmanakul, V. and Soracco, M. 2003. Monitoring *Karenia brevis* blooms in the Gulf of Mexico using satellite ocean color imagery and other data. *Harmful Algae*, 2, pp. 147–60.

Tester, P. A. and Steidinger, K. A. 1997. *Gymnodinium breve* red tide blooms: initiation, transport, and consequences of surface circulation. *Limnol. Oceanogr.*, 42, pp. 1039–51.

Thompson, R. O. R. Y. 1979. Coherence significance levels. *J. Atmos. Sci.*, 36, pp. 2020–21.

Tokar, J. M. and Dickey, T. D. 2000. Chemical sensor technology – current and future applications. In: M. S. Varney (ed.), *Chemical Sensors in Oceanography*. Amsterdam, Gordon & Breach Scientific Publishers, pp. 303–29.

Trowbridge, J. H. and Nowell, A. R. M. 1994. An introduction to the Sediment Transport Events on Shelves and Slopes (STRESS) program. *Cont. Shelf Res.*, 14, pp. 1057–61.

Turner, J. T. and Tester, P. A. 1997. Toxic marine phytoplankton, zooplankton grazers, and pelagic food webs. *Limnol. Oceanogr.*, 42, pp. 1203–14.

Twardowski, M. S., Boss, E., Macdonald, J. B., Pegau, W. S., Barnard, A. H. and Zaneveld, J. R. V. 2001. A model for estimating bulk refractive index from the optical backscattering ratio and the implications for understanding particle composition in case I and case II waters. *J. Geophys. Res.*, 106, pp. 14129–42.

Ulloa, O., Sathyendranath, S. and Platt, T. 1994. Effect of the particle size-distribution on the backscattering ratio in seawater. *Appl. Opt.*, 33, pp. 7070–77.

Vaulot, D. and Marie, D. 1999. Diel variability of photosynthetic picoplankton in the equatorial Pacific. *J. Geophys. Res.*, 104, pp. 3297–310.

Vaulot, D., Marie, D., Olson, R. J. and Chisholm, S. W. 1995. Growth of *Prochlorococcus,* a photosynthetic prokaryote, in the equatorial Pacific Ocean. *Science*, 268, pp. 1480–82.

Walsh, J. J. and Steidinger, K. A. 2001. Saharan dust and Florida red tides: the cyanophyte connection. *J. Geophys. Res.*, 107, pp. 11597–612.

Widder, E. A., Case, J. F., Bernstein, S. A., MacIntyre, S., Lowenstine, M. R., Bowlby, M. R. and Cook, D. P. 1993. A new large volume bioluminescence bathyphotometer with defined turbulence excitation, *Deep Sea Res. I*, 40, pp. 607–27.

Yanagi, T. and Okaichi, T. 1997. Seto Inland Sea – historical background. In: T. Yanagi (ed.), *Sustainable Development in the Seto Inland Sea, Japan — From the Viewpoint of Fisheries*. Tokyo, Terra Scientific Publishing Company, pp. 9–14.

Yoder, J. A., Moore, J. K. and Swift, R. N. 2001. Putting together the big picture: remote-sensing observations of ocean color. *Oceanogr. Mag.*, 14, pp. 33–40.

Yu, X., Dickey, T., Bellingham, J., Manov, D. and Streitlen, K. 2002. The application of autonomous underwater vehicles for interdisciplinary measurements in Massachusetts and Cape Cod Bays. *Cont. Shelf Res.*, 22, pp. 2225–45.

Zaneveld, J. R. V., Moore, C., Barnard, A. H., Twardowski, M. and Chang, G. C. 2004. Correction and analysis of spectral absorption data taken with the WET Labs ac-s. *Ocean Optics XVII*, *Proc. SPIE*, US Office of Naval Research, (CDROM).

Zingone, A. and Enevoldsen, H. O. 2000. The diversity of harmful algal bloom: a challenge for science and management. *Ocean Coast. Manag.*, 43, pp. 725–48.

3

Bio-optics in integrated ocean observing networks: potential for studying harmful algal blooms

O. Schofield, J. Bosch, S. Glenn, G. Kirkpatrick, J. Kerfoot, S. Lohrenz, M. Moline, M. Oliver and P. Bissett

3.1 Introduction

The problem. *If I were to choose a single phrase to characterize the first century of modern oceanography, it would be a century of under-sampling.* Walter Munk

The new reality. *The ocean sciences are now on the threshold of another major technological advance as the scientific community begins to establish a global, long-term presence in the ocean.* Robert Detrick

Ships have a difficult time sampling the time and space scales relevant for understanding how physics and chemistry regulate marine ecosystems (National Research Council 2000, 2003, Figure 3.1); therefore the biology in the oceans is chronically undersampled. This is a major problem for policy makers and local governments charged with managing coastal resources who are increasingly being asked to develop 'ecosystem-based management' plans (US Ocean Commission on Ocean Policy, 2004). This is especially true in regions where Harmful Algal Blooms (HABs) are present (Hallegraeff, 1993). Ecosystem-based management requires a quantitative understanding of the processes controlling marine food webs. These processes include physical (mixing, stratification, advection) and chemical (micro, macro, and organic nutrients) factors as well as trophic interactions within the marine food webs. These food-web interactions are especially difficult to study as they are modulated by complex climate (global warming, storms, winter cooling/summer heating), pelagic (mixing and stratification), lithospheric (nutrient weathering), and anthropogenic (terrestrially derived macro and micro nutrients, buoyant plumes, human grazing pressures) forcing functions. Understanding these food webs require an integrated view of physics, chemistry, and phytoplankton community dynamics.

Phytoplankton communities often appear to be relatively stable and diverse (the paradox of the plankton, described by Hutchinson, 1961); however the communities occasionally undergo sudden and dramatic fluctuations where the diverse phytoplankton communities shift to rapidly growing monospecific populations. Harmful algal blooms (HABs) are one such manifestation of this phenomena. Theoretical constructs for community shifts have been developed as disturbance hypotheses in ecology (e.g. Paine and Vadas, 1969; Connell, 1978) and catastrophe hypotheses in geology (Berggren and van Couvering, 1984). These theories underlie many of the

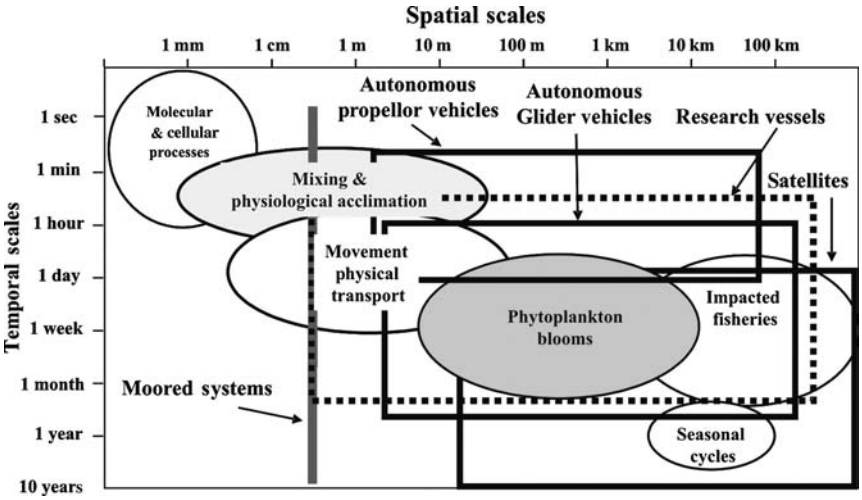

Figure 3.1
The time and space scales relevant for the study of HABs delineated by circles. The squares indicate the time and space scales that can be sampled using the different components central to building an integrated ocean observatory. Note that all available assets are required to span the relevant scales.
Source: modified from Dickey (1993).

conceptual models that are useful in understanding phytoplankton evolution and succession. The essence of these hypotheses is that stochastic as well as periodic environmental fluctuations provide opportunities for some species to temporarily dominate a given assemblage; however, because the environment is dynamic, any competitive advantage afforded to one species or group of species is fleeting (Giller et al., 1994). Given this, identifying the conditions that favour HABs has been a major research effort for the research community; however comprehensive understanding remains elusive due to our limited ability to collect data on ecosystem scales.

Traditional sampling approaches are reactive, slow to respond, and often operate with fixed time and space sampling grids (Figure 3.1). The resulting data do a poor job in resolving the real dynamics of the system and therefore it is not surprising that the causal mechanisms (climate, anthropogenic nutrients, mixing rates, etc.) underlying HAB dynamics remains an active research topic. Recent advances in ocean observation capabilities no longer consign us to operate in an under-sampled environment (Figure 3.2). Ocean observation networks are constructed from multiple platforms and are an operational reality (Smith et al., 1987; Dickey, 1993; Schofield et al., 2002). Platforms available include remote (satellites, aircraft and shore-based), stationary (surface and subsurface), mobile (ships and AUVs), and drifting (surface or vertically mobile) systems, that can provide spatially extensive observational updates on timescales of an hour or better for extended periods (Glenn and Schofield, 2003). These observatories will improve coastal water quality management by providing an environmental context over the ecologically relevant space/timescales in real time to facilitate adaptive sampling of the oceans (Schofield et al., 2003).

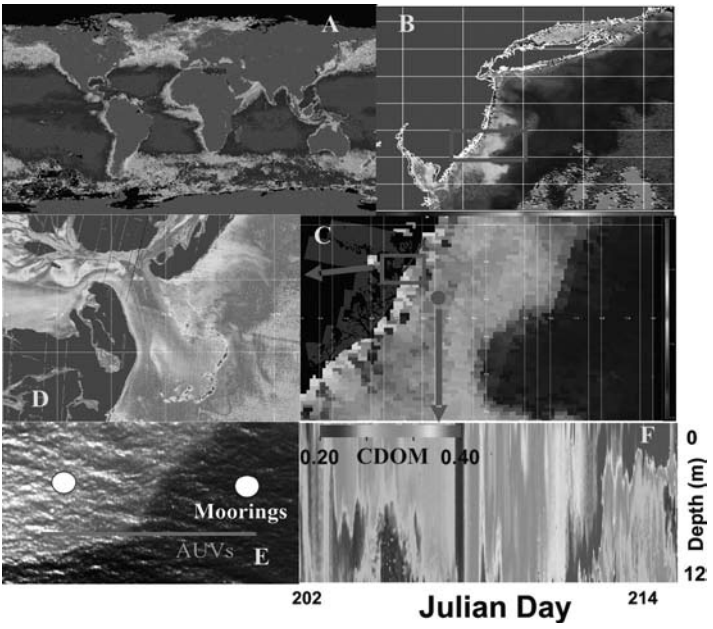

Figure 3.2
The time and space scale variability in ocean colour.
A, annual global chlorophyll *a* map derived from SeaWiFS.[14]
B, backscattering coefficient (wavelength) in summer 2001 in the Mid-Atlantic Bight derived from SeaWiFS.
C, enlarged section of panel B; the satellite's 1 km pixel is clearly visible and illustrates the features in the coastal ocean that are poorly resolved. Note the newer ocean-colour satellites that have spatial resolutions down to 250 km; ocean-colour satellites with 30 m resolution are proposed.
D, enlargement from panel C showing the backscattering coefficient at 442 nm derived from aircraft data. Note the features clearly visible in the aircraft imagery that are missed with the standard 1 km pixels in the satellite imagery.
E, visible image viewed by aircraft, with resolution of the order of tens of metres, showing the dramatic colour change associated with crossing an upwelling front in the Mid-Atlantic Bight. The visible 'greening' of the water is associated with enhanced blue light absorption probably from phytoplankton and/or chromophoric dissolved organic matter (CDOM). This colour shift underlies empirical algorithms for ocean-colour remote sensing.
F, time series of CDOM absorption, estimated from inverting bulk absorption measured with an ac-9 mounted on the Long-term Ecosystem Observatory (LEO) electro-optic fibre-optic cabled seafloor node. This system uses an *in situ* profiling system to obtain both highly resolved depth and time observations. Rapid changes in CDOM concentration are associated with the passage of storms and a large plume of Hudson River water.

[14]seawifs.gsfc.nasa.gov/SEAWIFS.html

Physical measurements (temperature, salinity, currents, wind speed and direction) have long been available to the community; however the ability to make biological measurements has historically been limited. Over the past three decades, optical techniques have made great advances in mapping ocean ecosystems and phytoplankton biology (see e.g. *Limnology and Oceanography,* 1989, 34(8), Mobley, 1994; *Journal of Geophysical Research,* 1995, 100(C7); *Oceanography,* 2004, 17). These optical measurements, while once exotic, have now matured and are available as off-the-shelf technology (Glenn et al., 2004), providing information on the physical, chemical and biological properties in the ocean. Most importantly, these optical measurements are amenable for the growing number of integrated ocean observatories (Glenn et al., 2004). These observing networks offer great potential for HAB research and management by providing (a) a data-rich environment for interpreting bloom dynamics; (b) a means for remote detection of HABs; and (c) a means for adaptive sampling. This chapter will highlight the present capabilities, problems to be overcome, and the potential for optics and integrated ocean observing networks to provide the backbone for developing ecosystem-based management approaches.

3.2 Identifying and tracking water masses and the associated phytoplankton ('where is it in the ocean' problem)

The first problem confronting the researcher and water quality manager is finding, identifying and tracking the HAB events before landfall, which means that it is critical to identify the water mass the algal population is in. Water masses (or water types) have historically been defined by their physical (Helland-Hansen, 1916; Tomczak, 1999) and chemical (Broecker et al., 1985; Weiss et al., 1985; Smethie, 1993; Jenkins, 1980; Jenkins, 1982) properties. These features influence the overall productivity and structure of the biological communities present within the water mass as it is advected by local currents. This movement is regulated by many processes (weather, local topography, river plumes) and therefore tracking a specific water mass (or a HAB population) is difficult using traditional ship-based sampling strategies. Development of approaches that identify and spatially track water masses overtime is one of the central problems confronting the HAB researcher. Such a capability would allow the community to (a) determine water masses that favour HAB initiation; (b) provide a means for tracking specific phytoplankton populations; and (c) identify the environmental conditions and locations that promote the growth of HAB species to be defined.

3.2.1 Current capabilities and obstacles

Two general strategies are currently used to identify water masses. One approach uses clustering techniques to identify water masses based on unique physical, chemical, and biological signatures (Tomczak, 1999). While, traditionally 'conservative' parameters (e.g. temperature and salinity) have been used to identify water masses, developing additional parameters for water mass discrimination based on optical properties shows promise (Oliver et al., 2004*a*). This is not surprising, as optical oceanographers have classified water masses based on their optical properties for decades (Jerlov, 1976; Morel and Prieur, 1977). Optical signatures in coastal systems, where HABs most often occur, reflect the contributions of numerous in-water constituents such as water, phytoplankton, coloured

dissolved organic matter, non-algal particles, and sediment. This complex matrix of materials provides a potential library of parameters that can be effective for discriminating water types if methods can provide reliable estimates of the optically significant constituents present (Kirk, 1994; Kahru and Brown, 1997; Schofield et al., 2004; Sosik, 2007 – Chapter 8 this volume). Given data, the actual classification of water masses is accomplished through a variety of often commercially available mathematical algorithms (Quackenbush, 2001; Martin-Trayovski and Sosik, 2003). The 'art' of using these clustering techniques is that the user is required to define some subjective criteria of what defines a specific water mass (i.e. a certain change in temperature, salinity, optical backscatter etc.). Without guidance the algorithms could potentially designate any difference in the data as a different water mass. These subjective decisions greatly influence the final output of algorithms. Fortunately developments in the field of bioinformatics may provide the foundation for developing objective means to guide these clustering techniques (Yeung et al., 2001; Oliver et al., 2004a, Figure 3.3). These approaches have been demonstrated by short research experiments, but they have yet to be applied operationally.

The difficulty in applying these clustering approaches operationally is 3-fold. First, as these are empirical approaches, local tuning is often required. Second, the choice of appropriate optical input variables is likely to vary with location. For example, optical parameters sensitive to the presence of coloured dissolved organic matter will be effective in delineating river plumes and coastal waters (Bukata et al., 1995; Aarup et al., 1996; Højerslev et al., 1996; Johnsen et al., 2003) but will have little value in offshore continental shelf waters. The third obstacle, arguably the largest, is the limited availability of adequately resolved spatial data.

The second major technique used to identify water masses is based on identifying temporal anomalies in spatial data. This approach differs from the clustering approach as the temporal variations provide the means to identify water mass evolution and episodic events. Deviations of a parameter (chlorophyll *a,* sediment load, etc.) from a climatological or running mean are used to identify a water mass which is experiencing an 'event'. This anomaly can be tracked and adaptively sampled (see below). This approach already anchors operational efforts to delineate toxic *Karenia brevis* in the Gulf of Mexico (Stumpf, 2000). In the Gulf, anomalies are identified as daily chlorophyll *a* imagery is subtracted from a two month running chlorophyll *a* mean. Areas that exhibit a chlorophyll *a* increase of $\geqslant 1\ \mu g\, l^{-1}$ are identified as a water mass that is a potential HAB event. This technique is particularly powerful in delineating episodic blooms of *K. brevis* blooms (Tomilinson et al., 2004). After a bloom has been detected, wind drift models are then used to forecast its potential transport (Stumpf et al., 1998; Culver et al., 2000). Similar to the water mass clustering techniques, the anomaly technique has several problems. First, the approach will identify any episodic events, such as sediment or nepheloid layer resuspension that optically mimic phytoplankton blooms. Local tuning of the temporal averaging is also required. Finally, like the clustering techniques the greatest problem is collecting the spatial and temporal time series of data.

3.2.2 Data sources available for water mass identification and tracking

3.2.2.1 Satellites

To date, remote sensing techniques have been the central tool capable of providing sufficient spatial data for water mass identification on an operational basis (e.g. Figure 3.3). These techniques will expand how satellite data will support HAB

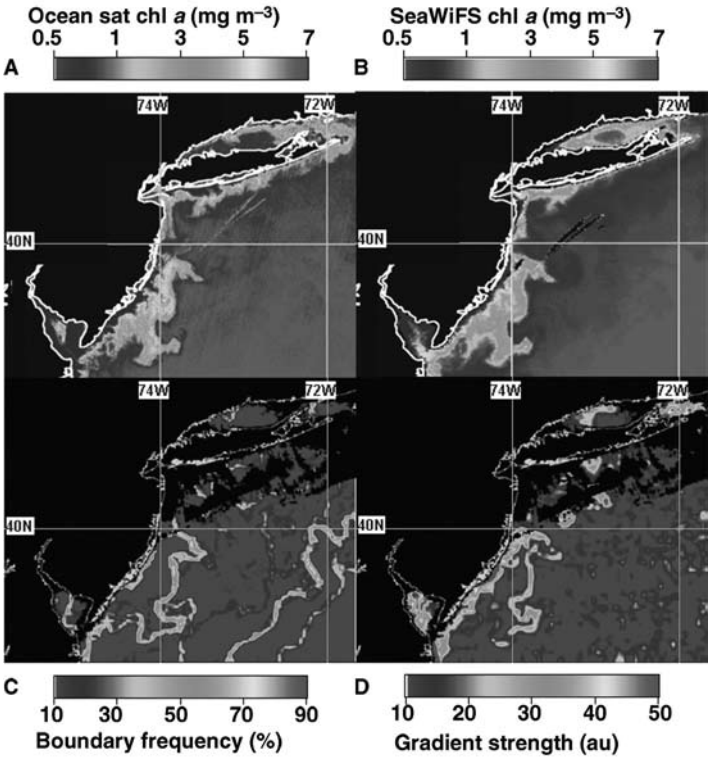

Figure 3.3
Examples of ocean colour and derived water mass imagery in the Mid-Atlantic Bight in summer 2001.
A, image of chlorophyll *a* collected on 2 August, 2001, with the Indian Oceansat satellite which has a spatial resolution of 300 m.
B, image of chlorophyll *a* collected on 2 August 2001 with the American SeaWiFS system.
C, boundary frequency between water masses measured on 2 August 2001. The boundary frequency objectively defines borders between major water masses based on the combined output from an ensemble of clustering algorithms that combines information from sea surface temperature (SST) and spectral reflectance (R_{rs}) (Yeung et al., 2001; Oliver et al., 2004a). These techniques allow the scientist to quantify the most frequently observed borders between water masses. Note that the boundaries of a large coastal bloom, offshore waters and the Gulf Stream are delineated.
D, gradient strengths between the major water masses for 2 August 2001. While the clustering algorithms (Figure 3.C) separate observations into discrete water masses, this does not quantitatively delineate how different the water masses are from one another. Through distance analysis, the relative strengths of these boundaries can be estimated by determining the ratio of the distance between points in parameter space to the distance between points in physical space (Oliver et al., 2004a). In this case, only the edge of the algal bloom represents a significant water mass boundary.

Table 3.1 Current suite of available ocean-colour satellites for HAB biologists

Satellite	Country	of bands	Maximum resolution
SeaWiFS	United States	8	1 km
FY1-D	China	10	1 km
MODIS (aqua,terra)	United States	32	250 m
IRS-P4 (Oceansat)	India	8	300 m

research in future by providing objective tools to analyse available satellite imagery (Cullen et al., 1997; Tester et al., 1998) and this utility will also increase as the number and type of ocean-colour satellites is due to increase in the coming decade (Table 3.1). Remote sensing in coastal waters has historically been hampered by low spatial resolution (1 km or worse) and a limited number of derived proxies that can be used in the water mass identification. Recently launched satellites now have spatial resolutions down to 250 m (Figure 3.2) and these improvements will be especially important in coastal waters where many of the potentially important oceanographic features for understanding HABs occur on spatial scales smaller than one kilometre.

Expanding the number of algorithms that estimate environmental parameters from space is an ongoing process where the parameter of interest (e.g. chlorophyll *a*, sediment or particle concentrations, coloured dissolved organic matter) is related empirically to the light reflectance measured by the satellite. The reflectance is related to the parameter of interest usually by ratioing different wavelengths *or* by inverting the spectral reflectance (R_λ) into absorption (a_λ) and backscattering ($b_{b\lambda}$) values (note $R_\lambda \sim b_{b\lambda}/(a_\lambda + b_{b\lambda})$ (Ruddick et al., 2006 – Chapter 9 this volume). The absorption and backscattering components are proportional to the concentration of the optically active components in the water column, however these proportionalities can be location-dependent thus requiring local tuning (Sosik, 2006 – Chapter 8 this volume).

This iterative tuning of satellite algorithms is sometimes interpreted by some in HAB research and the coastal management community that remote sensing is an immature technology and has only limited value especially as satellites do not provide phytoplankton species specific information. The limitations also imposed by the clouds, limited overhead passes, and limited subsurface data (reflectance signals are exponentially weighted to the surface water signals) have also caused some to dismiss developing remote sensing specifically for HAB research. We believe that this view is unfortunate as the number of and accuracy in the satellite derived products has increased dramatically over the last decade (Table 3.2) and satellites remain one of the only available means to collect sufficient spatial data over relevant ecological scales in near real time. Additionally, they remain one of the few observational tools that permit spatial and temporal hindcast views of environmental parameters leading up to an identified HAB event or HAB 'backtracking'. The spatial data from satellites is thus ideal for water mass identification approaches.

3.2.2.2 Moorings and autonomous vehicles

While satellites provide excellent spatial data for surface waters, the subdaily temporal and subsurface data they provide are limited. Moorings are often used to collect highly resolved time-series measurements and coarse spatial grids can be obtained if

Table 3.2 Some of the available products for the MODIS satellite system, including those still under active development

Parameter
Normalized water-leaving radiance (412, 443, 488, 531, 551, 667, 678 nm)
Chlorophyll *a* + pheopigment (fluorometric, empirical)
Chlorophyll *a* and total pigment concentration (HPLC, empirical)
Chlorophyll fluorescence line height and baseline
Chlorophyll fluorescence efficiency
Total suspended matter concentration in ocean
Pigment concentration in coccolithophore blooms
Detached coccolithophore concentration
Calcite concentration
Diffuse attenuation coefficient at 490 nm
Phycoerythrobilin and Phycourobilin concentration
Chlorophyll *a* concentration (SeaWiFS analogue – OC3M)
Instantaneous photosynthetically available radiation
Instantaneous absorbed radiation by phytoplankton for fluorescence
Gelbstoff absorption coefficient at 400 nm
Phytoplankton absorption coefficient at 675 nm
Total absorption coefficient (412, 443, 488, 531, 551 nm)
Sea surface temperature (day and night), 4 μm and 11 μm
Behrenfeld-Falkowski primary production index
Howard-Yoder-Ryan primary production index
Ocean carbon primary production
New nitrogen production
Export carbon production
Annual chlorophyll *a* concentration
Photosynthetically available radiation
Mixed-layer depth

multiple moorings are deployed; however it should be noted that moorings are expensive and the number that can be deployed is limited. Therefore mooring data needs to be complemented with subsurface spatial data. There is a growing array of autonomous underwater vehicles (AUVs) that are capable of providing subsurface data operationally (Figure 3.4). These platforms matured rapidly in the late 1990s and no longer require dedicated teams of engineers to operate them. The AUVs that are now commercially available include autonomous propeller (Glenn et al., 1998; Blackwell et al., 2003) and non-propeller vehicles (Stommel, 1989; Schofield et al., 2002) (Figures 3.4A, 3.4B). The duration of the AUV lifetimes on a single battery charge varies with platform, however several AUV systems can remain at sea for months at a time. The sampling from these platforms is dense and provides sufficient spatial subsurface data appropriate for water mass identification and classification methods.

The number of physical and bio-optical instruments that have been miniaturized and are now available for AUVs and moorings has dramatically increased in recent years (Figure 3.4C–E). These platforms can currently measure both apparent and inherent optical properties. The IOPs (a is absorption, b is scattering, $c = a + b$, attenuation) are particularly powerful measurements as they are relatively easy to interpret, can be collected even during the night, and can be measured using commercially

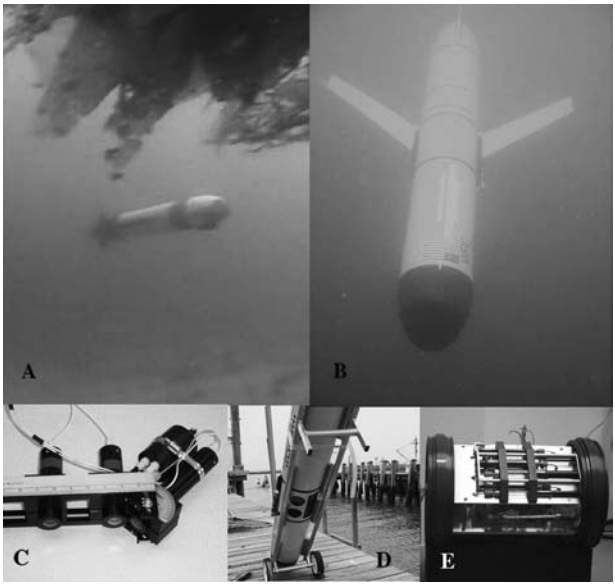

Figure 3.4
Two examples of autonomous vehicles that are commercially available for HAB researchers.
A, propeller class AUVs are operational tools. These systems are highly manoeuvrable and capable of providing high-resolution maps. These systems are capable of carrying a wide range of powerful instruments, with a duration limited to one or two days per battery charge. Shown is a REMUS vehicle as it surveys a kelp garden off southern California.
B, glider class vehicles have no propellers and use buoyancy to provide forward momentum. The lack of a propeller allows for extended missions at sea lasting up to several months per battery charge. Given that the goal is to remain at sea for extended periods, these vehicles cannot carry instruments having high power or frequent maintenance requirements. Shown is a Webb Glider patrolling during a *Karenia brevis* bloom in the Gulf of Mexico. Given the respective strengths and weaknesses of the vehicles, integrated observing networks will require several different classes of vehicles to span the relevant scales.
C, miniaturized attenuation meter before it is integrated into a Webb glider.
D, belly of a Web Glider. The square instrument is an attenuation meter. The circular panels are backscatter and fluorometer sensors.
E, miniaturized hyperspectral spectrometer (liquid guide capillary tube) capable of providing absorption spectra at 0.4 nm resolution.

available instruments (Roesler and Boss, 2007 – Chapter 5 this volume). The AOP measurements are limited to measurements during daylight hours and therefore will not be reviewed extensively in this chapter; however the utility of the AOPs is reviewed in other chapters in this volume (Sosik, 2007 – Chapter 8 this volume).

Absorption measurements provide information on the composition of material present. The great advantage is that total absorption, at any wavelength, is a linear combination of the absorbing constituents, which makes interpretation straightfoward

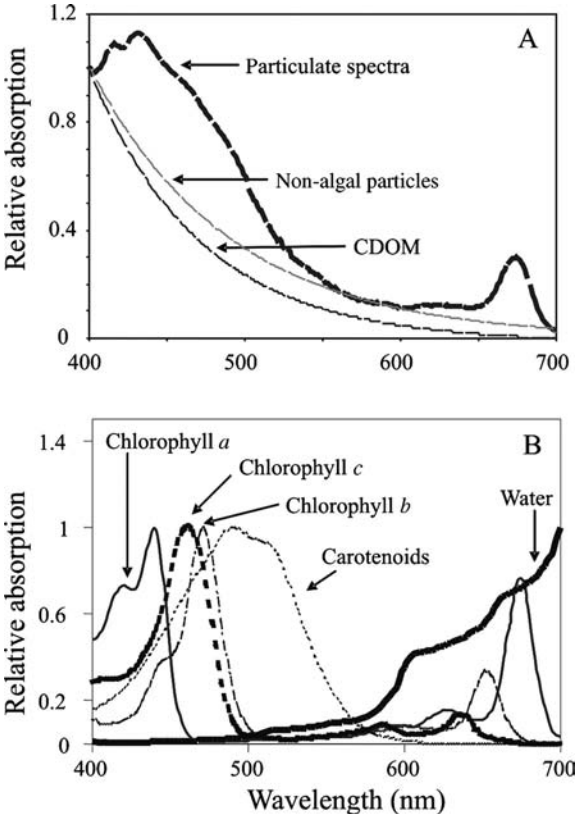

Figure 3.5
A, relative absorption of phytoplankton, CDOM and non-algal particles. B, wavelength dependency for the relative absorption (normalized to the wavelength of peak absorption for each component) of chlorophyll *a*, chlorophyll *b*, chlorophyll *c*, photosynthetic carotenoids, and water. The absorption of light by water in the red wavelengths is 100 times that of chlorophyll *a*.
Sources: adapted from Bidigare et al. (1989); water absorption Pope and Fry (1997).

especially as the spectral absorption (Figuure 3.5A) for water (Pope and Fry, 1997), phytoplankton (Prezelin and Boczar, 1986), chromophoric dissolved organic matter (CDOM, Kalle et al., 1966), and non-algal particles (Kishino et al., 1985) has been characterized. Given this, the bulk absorption signal can be partitioned into the component spectra (Roesler et al., 1989; Chang et al., 1999; Olivier et al., 2004b; Schofield et al., 2004; Figure 3.5). Until the mid-1990s, measurements of absorption were difficult to make because of the low signal in most ocean waters; however instrumentation has improved in the last decade (Zaneveld et al., 1995; Kirkpatrick et al., 2003). These bulk inversion approaches are actively being applied to study *K. brevis* blooms in the Gulf of Mexico from ships (Figures 3.6, 3.7) and recent instrument improvements now allow hyperspectral absorption to be made from AUVs (Figure 3.8).

While parameter maps from inverted absorption measurements are useful for water mass tracking (Figures 3.6, 3.7), can the data be used to identify specific algal HAB taxa? Recent work suggests that this is possible if hyperspectral information is available (Millie et al., 1997; Schofield et al., 1999; Kirkpatrick et al., 2000; Roesler

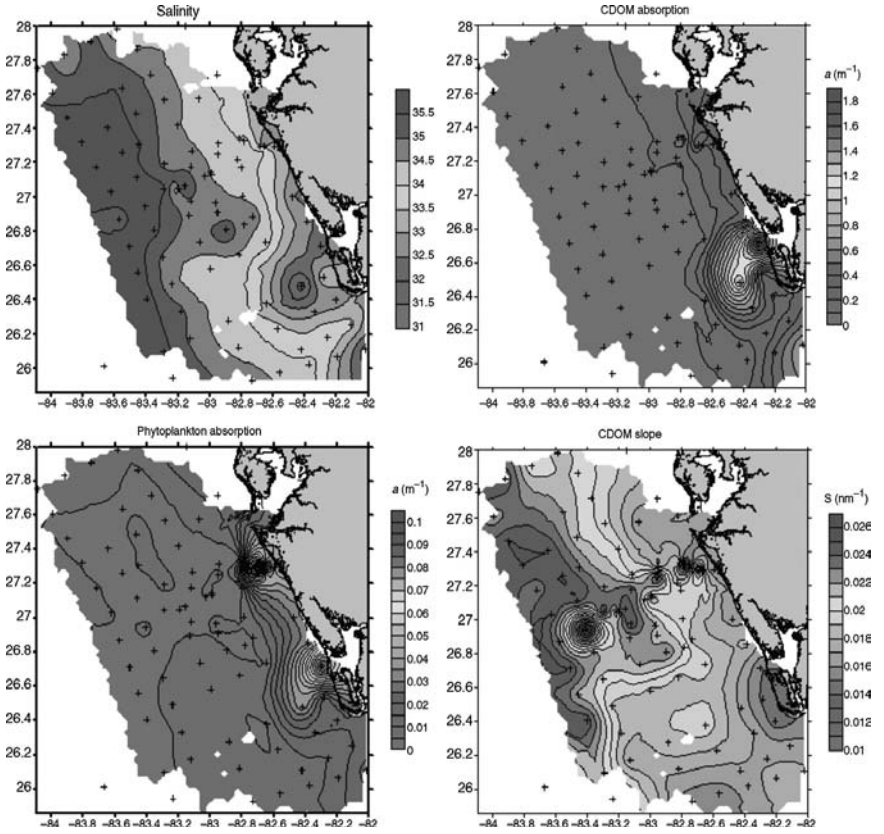

Figure 3.6
Spatial maps of salinity, optically derived maps of CDOM optical weight, phytoplankton optical weight (high values to the south included toxic *K. brevis*), and the exponential spectral slope of the CDOM absorption. The exponential slope for CDOM reflects the composition of the CDOM and low values is often interpreted as freshly derived CDOM (see Carder et al., 1989). The maps of phytoplankton, CDOM, and CDOM slope were all estimated from bulk absorption measurements made with an ac-9 instrument (Zaneveld et al., 1994; Pegau et al., 1995). Often enhanced *K. brevis* cell numbers are associated with river plumes and it has been suggested that blooms may be triggered by nutrient-rich waters near shore that provide a source of nitrogen (in the form of ammonia and/or DON) and/or phosphorus. Numerous culture studies with *K. brevis* have demonstrated the ability of dinoflagellates to use dissolved organic nitrogen for growth (Baden and Mende, 1979; Shimizu and Wrensford, 1993). Because of this the organic rich river water may be an ideal water mass for growth.
Source: Kalle (1996).

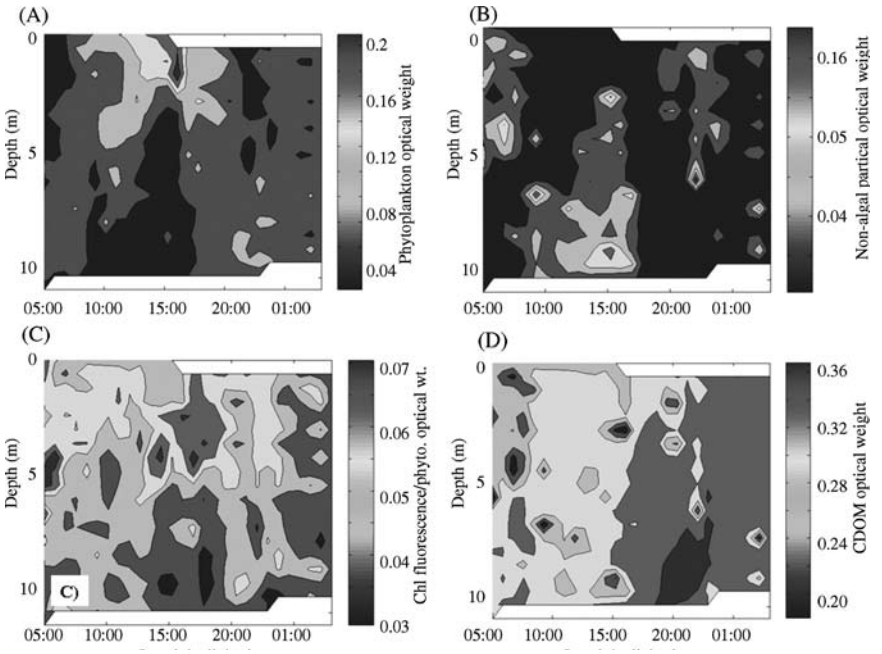

Figure 3.7
An example of IOP measurements during a HAB event which illustrates diel variability in A, phytoplankton; B, non-algal particles; C, chlorophyll fluorescence yields (here estimated as the ratio of chlorophyll fluorescence to phytoplankton optical weight); D, CDOM optical weights (here optical weight refers to the proportion of component absorption to total absorption at 676 nm for phytoplankton and 412 nm for CDOM and non-algal particles, see Schofield et al., 2004) during a Gulf of Mexico cruise in October 2001.
These waters were dominated by the toxic red tide *Karenia brevis* and its vertical migration into surface waters after local noon is clear. Derived swimming speeds compare favourably to measured swimming speeds (approximately 1 m h^{-1}; Heil, 1986). Measurements were made with a WetLabs ac-9 from a ship.

et al., 2005). Hyperspectral inherent optical data has recently become available to the community (e.g., Kirkpatrick et al., 2003), and HAB-specific optical indices can now be developed for operational detection and monitoring under certain conditions or with ancillary data. While a difficult research problem, because HAB species do not generally have optical properties significantly different from their non-HAB-forming relatives, approaches have been developed and demonstrated for some specific cases, notably, natural *K. brevis* populations (Kirkpatrick et al., 2000; Millie et al., 2002). For *K. brevis*, a 'similarity index' is calculated which quantifies the difference between a reference standard (often an absorption spectra from a laboratory culture) and an unknown (a spectrum measured in the field). As small hyperspectral instruments have matured and been integrated into AUVs and moorings, spatial maps of HAB similarity indices are now an operational possibility (Figure 3.8).

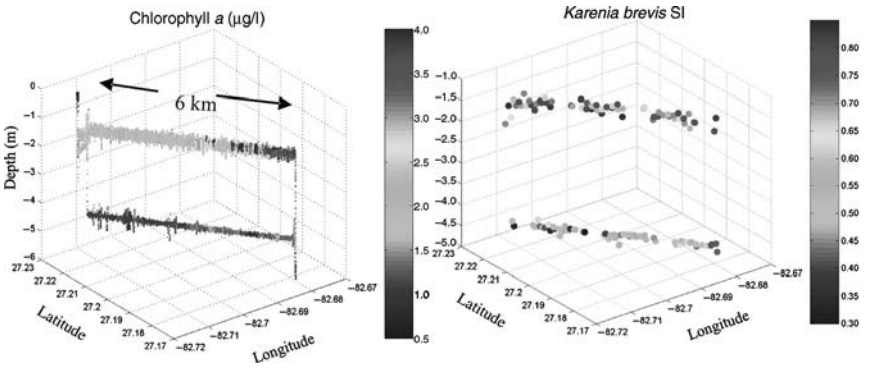

Figure 3.8
Similarity indices (SI) measured with a REMUS vehicle during a red tide in the Gulf of Mexico in winter 2005. The high SI values indicate that a significant fraction of the chlorophyll present is associated with *Karenia brevis*. Note that high SIs, indicating the presence of *K. brevis*, do not necessarily correlate with the highest chlorophyll concentrations measured with the AUV-mounted fluorometer.

While much effort has focused on the interpretation of the absorption data, the other optical measurements such as scattering and attenuation provide information about the nature and concentration of the particles present, which is useful for water-mass tracking and interpreting episodic phenomena (Figure 3.9). The angular distribution of scattered light is a function of particle size and the refractive index (Van der Hulst, 1957; Bricaud et al., 1983; Morel and Bricaud, 1986; Stramski and Kiefer, 1991; see also Morel, 2007, – Chapter 4 this volume); therefore variations in the scattering properties in natural populations can be informative (Roesler and Boss, 2006; Sosik, 2007 – Chapters 5 and 8 this volume). For example, the refractive index can change by over 80% during a 12-hour light cycle due to changes in cellular pigmentation and intracellular compounds (Stramski and Reynolds, 1993; Reynolds et al., 1997). The values of attenuation have been related to the concentration of particulate organic carbon (Bishop, 1986, 1992; Gardner et al., 1993). The wavelength-dependent slope of attenuation has been related to the particle size distribution (Boss et al., 2001; Boss and Pegau, 2001) and combining particle size distribution and angular scattering information allows the estimation of the refractive index of particles (Twardowski et al., 2001), which has been related to the cellular concentration and composition of metabolites in biological particles (Aas, 1996).

Combining optical and hydrographic data collected from satellites, moorings, and AUVs will provide a wealth of data appropriate to that required for HAB research. They, combined with water mass tracking techniques will provide surface and subsurface maps appropriate for tracking a piece of ocean (and the resident phytopl-ankton population) over time. This will improve our ability to know where a population came from, how it is evolving, and where it is heading. The integration of optical data additionally increases the effectiveness of these approaches by providing a detailed biological and chemical context that will assist the HAB researcher not only to track a population over time but allow interpretation of why an event may be occurring.

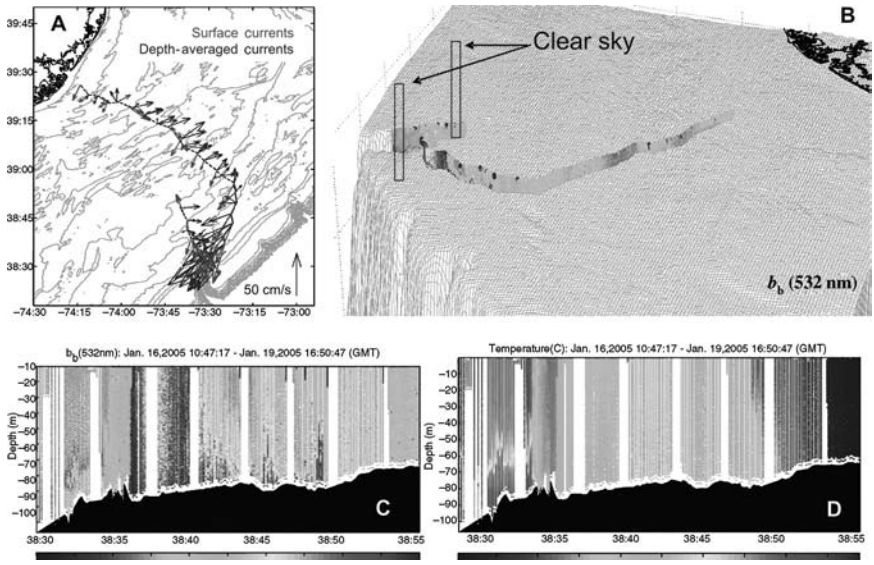

Figure 3.9
Data collected by a long-duration autonomous Webb Glider in the Mid-Atlantic Bight.
A, surface map showing the path flown by the glider. The arrows indicate both depth-averaged (blue) and surface (red) currents during the flight. The glider at the outer shelf edge was advected by a large Nor-Easter storm.
B, map of the optical backscattering coefficient at 532 nm measured with a WetLabs ECO Puck sensor on the glider. The squares indicate times of clear sky during which cloud-free conditions allowed for satellite data to be collected. Note that most of the time during this glider transect, the sky was cloudy, especially during the storm-induced resuspension events, which are indicated by the highest backscatter values on the outer shelf. This illustrates one of the weaknesses of satellite approaches where the presence of clouds can greatly limit the available data.
C, cross-shore transect showing the massive resuspension during the glider transect.
D, corresponding glider map of temperature which does not show as dramatic variations as the particle backscatter. Note the deep warm-water mass when mixed upwards during the resuspension event yields a uniformly warmer water column, which would have been difficult to interpret without the backscattering data.

3.3 Adaptive sampling of HABS ('what is in the ocean' problem)

While optics can provide much useful information, it currently provides little species-specific information. This means that discrete samples still need to be collected to identify what is present within a given water mass or optical feature. Water mass tracking will enable the smart adaptive sampling of the ocean

(Robinson and Glenn, 1999; Schofield et al., 2003). This allows the labour-intensive measurements [detailed biological (productivity or growth parameters, cell cycle phase, toxicity, genomic or proteomic information) or chemical measurements (micronutrients, organic nutrients)] to be made when they will have maximum scientific or management pay-off. This is now possible as modern communication networks allow for two-way communication between shore and ships. Data are combined and then made available often via the internet. This 'net centric' capability will improve as wireless communication networks improve in reliability, range, and bandwidth (Figure 3.10).

The availability of real-time data allows the researcher to adjust sampling strategies to compensate for how the ocean is changing over time. An example of adaptive sampling within an observatory was provided during an experiment in summer 2000. During the experiment, an aircraft observed a turbid feature about 15 km offshore. As the experiment was focused on calibrating hyperspectral sensors, it was important to characterize any optically distinct features present in the ocean. The pragmatic challenge was directing ships that were several hours steam-time away from the feature of interest, which was being advected to a new location by local currents. Note, this challenge is not unlike the challenge facing a water quality manager responding to reports of a HAB offshore. Initial locations of the feature where noted and the surface currents were tracked using the observatory shored based radars as a ship transited to the location (Figure 3.11). The optical features were located within a convergence front and were transported offshore within a meander to the north away from the ship in transit. Communication to direct the ship was facilitated through a network of radio modems, which provided the ship real-time web access to onshore hourly current data. As the ship approached the predicted locations at night, there was no significant bioluminescence in the wake. On reaching the predicted location, bioluminescence appeared in its wake. Vertical profiles exhibited near surface (3 m) and subsurface (12 m) peaks in the bioluminescence (Figure 3.12) with discrete samples identifying the presence of the vertical migrating bioluminescent dinoflagellate *Ceratium fusus*. This red tide, with cell numbers of over several thousand cells per millilitre, was located only within the convergence feature, with bioluminescence and *Ceratium* sp. absent in profiles 1.5 km to the north or south. The front dissipated with a current reversal later in the evening. Thus, the observatory provided information on the transport of the particles allowing the biologists to sample a small biological feature offshore. Traditional ship-based sampling would not have been able to characterize the feature.

3.4 Ocean forecasting (the 'what will happen tomorrow' problem)

Despite improvements in ocean sampling, we will never be able to synoptically sample all the desired biological, chemical, and physical measurements needed to resolve the state and trends of the coastal ocean ecosystem necessary for quantitative 'ecosystem management'. An alternative to measuring all things at all times is to couple an adaptive sampling strategy with mechanistic models in order to resolve the processes that result in a particular ecosystem state, and provide the tools to predict the direction that the ecological system will take. By linking the observation network to the modelling process, there is a refinement of both the data collection and the

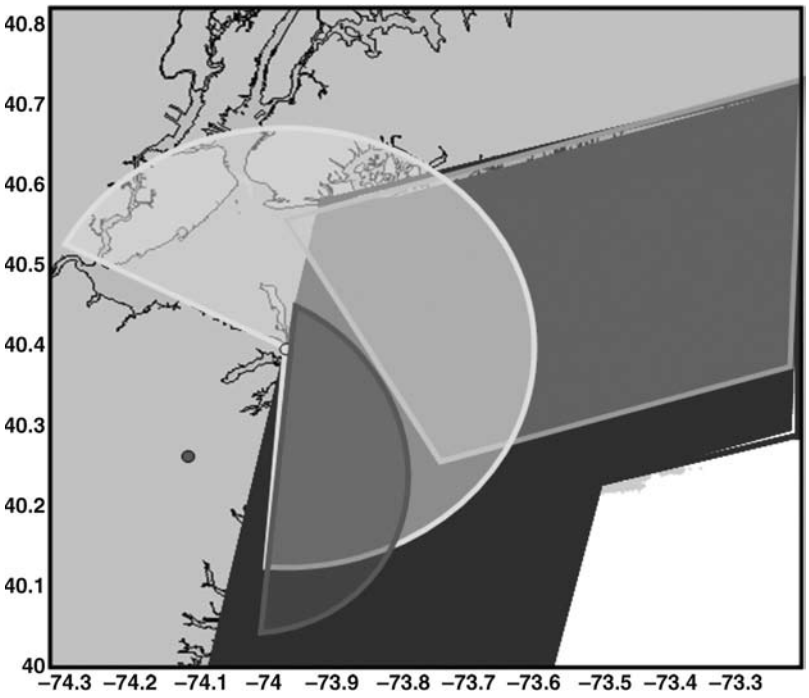

Figure 3.10
Wireless communication networks now allow oceanographers to communicate to shore and other ships in real time. This capability is a transformational advance that allows for adaptive sampling. In many locations communication networks are redundant with many different wireless networks of varying ranges and bandwidths being available. This figure shows the communication capabilities within the nearshore waters of the Mid-Atlantic Bight. The medium grey area represents current wireless coverage using Verizon Inc. National Access capabilities (~100 kbps, coverage up to 20+miles (32 km) off Long Island, less for New Jersey). The dark grey area represents the availability of Verizon Inc. Quick2Net (14.4 kbps, coverage up to 20+miles off both New Jersey and Long Island). The pale grey circular sector represents the range of line-of-sight Radio Modems (~80 kbps, coverage for a 18 mile (29 km) radius centred at Sea Bright Fire Department). Finally the AirNet Communications Wireless Broadband range is represented by the dark grey semi-circle (~1.5 Mbps, coverage 7 miles (11 km) offshore from Sandy Hook). Global coverage is provided by Iridium Satellite communications (2,400 bps, global coverage, data and voice). This provides researchers with a wide range of possibilities of varying bandwidth allowing them to access data.

undestanding of what is required by ecological models. This is illustrated in the simplest form in the equation used to describe the position of a particle at any given time (x):

$$x = x_0 + v_0 t + \frac{1}{2} a_{cc} t^2 \tag{3.1}$$

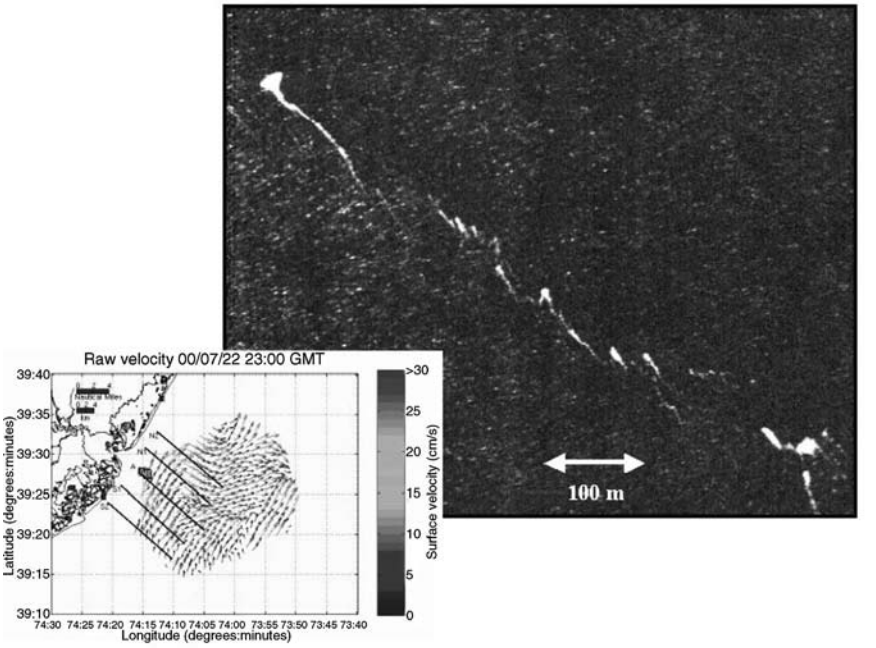

Figure 3.11
An RGB (converted to greyscale) image collected by aircraft showing a small-scale turbid feature about 15 km from shore. The feature was of the order of 1 km to 2 km in size.
Inset: medium-range sea surface current map measured by shore-based radars with the position of the initial aircraft sighting marked by the black circle. The currents, updated every hour, allowed scientists onshore to model the advection pattern of the observed slick and direct the research vessel into position in order to characterize the nature of the material present.

Here x_0 is the initial position of the particle, v_0 is velocity, t is time, and a_{cc} is acceleration. Observations can provide the initial particle positions (x_0) and velocity (v_0), yet models (in this case $F = ma_{cc}$) are used to describe the dynamics of the particle's acceleration (Schofield et al., 2003). If either the model or observing network is missing, the particle's future position will be unknown. Physical measurements for measuring v_0 (Barrick et al., 1887; Glenn et al., 2000; Kohut et al., 2003) and models for measuring a_{cc} (Haidvogel, 2002; Robinson et al., 1999) are relatively mature. Optical measurements will hopefully provide the quantitative measurements of the x_0 and x over time for the biological oceanographer.

Traditionally climatologies have been used to drive ecological models; however, many of the processes of interest are often dominated by episodic events (Giller et al., 1994). These events are better described by ocean nowcast/forecast models (Mooers, 1999) which are rapidly evolving with advances in ocean circulation modelling (Holland and Capotondi, 1996) and data assimilation methods (Dalay, 1991). While biological assimilation modelling systems have long been a research focus (Ishizaka, 1990, Lawson et al., 1995; Fasham and Evans, 1995; Matear, 1995; Robinson et al.,

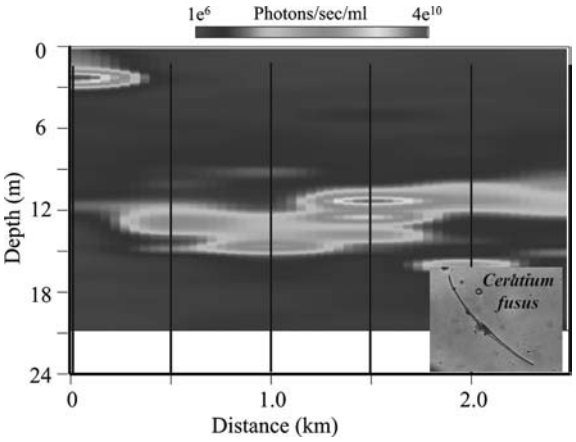

Figure 3.12
Bioluminescence potential measured by a ship-based profiling system after being directed into position by data collected from the sea-surface current data illustrated in Figure 3.11. The bioluminescence (light shades of grey) was due to the dinoflagellate *Ceratium* and it was responsible for the slick observed by the aircraft.

1996), their utility has been hampered by the availability of both the initialization/validation data and parameterization data required by the models.

In the under-sampled ocean, ocean forecast errors are dominated often by uncertainties in the model initialization; therefore ensemble forecasts with differing initial conditions can be used to identify regions where additional data are required. Here the models provide insight into what has not been sampled and guidance for field efforts. With recent advances in our observational capabilities, we are no longer consigned to operate in an under-sampled environment. Ocean observation networks can now provide spatially extensive observational updates on timescales of hours or better (Glenn et al., 1998). This rapid environmental assessment capability changes the paradigm for adaptive sampling and nowcast/forecast modelling. In the well-sampled ocean, forecast errors may now be dominated by uncertainties in the model formulations or boundary conditions, and ensemble forecasts with differing model parameterizations can be used to identify regions in which additional data can be used to keep a model on track. In the time it takes to prepare the ensemble of forecasts for the well-sampled ocean, additional data has arrived, and on-the-fly model-data metrics can be used to quantify which forecast in the ensemble is most accurate. Thus in the well-sampled ocean, the observations improve our understanding of errors associated with fundamental assumptions within biological models.

This new observational paradigm for the well-sampled ocean will be especially important to improving our ability to understanding biological dynamics in coastal ecosystems. A well-sampled ocean provides the means to run ensemble biological forecasts, where the ensemble represents models of varying ecological or physiological complexity. The ocean observatories provide the data to study which of an ensemble of model forecasts best describes reality, which in turn allows us to ask 'why?'. This coupled observation approach will provide researchers with the tools to explore marine ecology in unprecedented detail for the next decade.

3.5 Conclusions

Observation networks will aid efforts to understand HABs as they provide surface and subsurface spatial data in near real-time allowing for water mass tracking and adaptive sampling. The physical data will be complemented with optical data, which provides biological and chemical information. These observations will be coupled to ecological models, providing a tool to improve fundamental understanding of the factors regulating phytoplankton community composition.

References

Aarup, T., Holt, N. and Højerslev, N. K. 1996. Optical measurements in the North Sea-Baltic Sea transition zone. II: Water mass classification along the Jutland west coast from salinity and spectral irradiance measurements.*Cont. Shelf Res.*, 16(10), pp. 1343–53.

Aas, E. 1996. Refractive index of phytoplankton derived from its metabolite composition. *J. Plankton Res.*, 18, pp. 2223–49.

Babin, M., Roesler, C. S. and Cullen, J. J. (eds). 2006. *Real-time Coastal Observing Systems for Marine Ecosystem Dynamics and Harmful Algal Blooms: Theory, Instrumentation and Modelling.* Paris, Intergovernmental Oceanographic Commission of UNESCO. (Monographs on Oceanographic Methodology)

Baden, D. G. and Mende, T. J. 1979. Amino acid utilization by *Gymnodinium breve*. *Phytochemistry*, 18, pp. 247–51.

Barrick, D. E. and Lipa, B. J. 1997. Evolution of bearing determination in HF current mapping radars. *Oceanography*, 10, pp. 72–75.

Berggren, W. A. and van Couvering, J. A. 1984. *Catastrophes and Earth History, the New Uniformitarianism*. Princeton, N.J., Princeton University Press.

Bidigare, R. R., Morrow, J. H. and Kiefer, D. A. 1989. Derivative analysis of spectral absorption by photosynthetic pigments in the western Sargasso Sea. *J. Mar. Res.*, 47, pp. 323–41.

Bishop, J. K. B. 1986. The correction and suspended mass calibration of Sea Tech transmissometer data. *Deep Sea Res.*, 33, pp. 121–34.

Bishop, J. K. B., Smith, R. C. and Baker, K. S. 1992. Springtime distributions and variability of biogenic particulate matter in Gulf Stream warm-core ring 82B and surrounding N.W. Atlantic waters. *Deep Sea Res.*, 39, pp. 295–326.

Blackwell, S., Case, J., Glenn, S. M., Kohut, J., Moline, M. A., Purcell, M., Schofield, O. and von Alt, C. 2003. A new AUV platform for studying near shore bioluminescence structure. In: *12th International Symposium on Bioluminescence and Chemiluminescence*. Singapore, World Scientific Publishing Company, 197–200.

Boss, E., Twardowski, M. S. and Herring, S. 2001. The shape of the beam attenuation spectrum and its relation to the size distribution of oceanic particles. *Appl. Opt.*, 40, pp. 4885–93.

Boss, E. and Pegau, W. S. 2001. The relationship of light scattering at an angle in the backward direction to the backscattering coefficient. *Appl. Opt.*, 40, pp. 5503–07.

Bricaud, A., Morel, A. and Prieur, L. 1983. Optical efficiency factors of some phytoplankters. *Limnol. Oceanogr.*, 28, pp. 816–73.

Broecker, W. S., Takahashi, T. and Takahashi, T. 1985. Sources and flow patterns of deep-ocean waters as deduced from potential temperature, salinity, and initial phosphate concentration. *J. Geophys. Res.*, 90, pp. 6925–39.

Bukata, R. P., Jerome, J. H., Kondratyev, K. Y. and Pozdnyakov, D. V. 1995. *Optical Properties and Remote Sensing of Inland and Coastal Waters.* Boca Raton, Fla., CRC Press, 362 pp.

Chang, G. C. and Dickey, T. D. 1999. Partitioning *in situ* spectral absorption by use of moored spectral absorption-attenuation meters. *Appl. Opt.*, 38, pp. 3876–87.

Connell, J. H. 1978. Diversity in tropical rain forests and coral reefs. *Science*, 199, pp.1302–10.

Cullen, J. J., Ciotti, A. M., Davis, R. F. and Lewis, M. R. 1997. Optical detection and assessment of algal blooms. *Limnol. Oceanogr.*, 42, pp. 1223–39.

Culver, M. E., Soracco, M. P., Stumpf, R. P., Change, P. S. and Steidinger, K. A. 2000. Integrating wind data to determine the influence on movement of a harmful algal bloom event along the northwest coast of Florida. *Proc. Sixth International Conference on Remote Sensing for Marine and Coastal Environments,*. Ann Arbor, Mich.,Verdian ERIM Intl., pp. 25–27.

Dalay, R. 1991. *Atmospheric Data Analysis*. Cambridge, UK, Cambridge University Press.

Dickey, T. 1993. Sensors and systems for sampling/measuring ocean processes extending over nine orders of magnitude. *Sea Tech.*, 34, pp. 47–55.

Fasham, M. J. R. and Evans, G. T. 1995. The use of optimization techniques to model marine ecosystems dynamics at the JGOFS station at 47°N 20°W. *Phil. Trans. Roy. Soc.*, 348, pp. 203–09.

Gardner, W. D., Walsh, I. D. and Richardson, M. J. 1993. Biophysical forcing of particle production and distribution during a spring bloom in the North Atlantic. *Deep Sea Res.*, 40, pp. 171–95.

Giller, P. S., Hildrew, A. G. and Raffaelli, D. G. 1994. *Aquatic Ecology: Scale, Pattern and Process.* New York, Blackwell Scientific Publications.

Glenn, S., Schofield, O., Dickey, T. D., Chant, R., Kohut, Barrier, H., Bosch, J., Bowers, L., Creed, E., Haldeman, C., Hunter, E., Kerfoot, J., Mudgal, C., Oliver, M., Roarty, H., Romana, E., Crowley, M., Barrick, D. and Jones, C. 2004. The expanding role of ocean color and optics in the changing field of operational oceanography. *Oceanography*, 17, pp. 86–95.

Glenn, S. M., Dickey, T. D., Parker, B. and Boicourt, W. 2000. Long term real-time coastal ocean observation networks. *Oceanography*, 13, pp. 24–34.

Glenn, S. M., Haidvogel, D. B., Schofield, O., Grassle, F. J., von Alt, C. J., Levine, E. R. and Webb, D. C. 1998. Coastal predictive skill experiments at the LEO-15 national littoral laboratory. *Sea Tech.*, 39, pp. 63–69.

Glenn, S. M. and Schofield, O. 2003. Observing the oceans from the COOL room: our history, experience, and opinions. *Oceanography*, 16(4), pp. 37–52.

Haidvogel, D. B. and Beckmann, A. 1999. *Numerical Ocean Circulation Modeling*. London, Imperial College Press.

Heil, C. A. 1986. Vertical migration of *Ptycodiscus brevis* (Davis) Steidinger. Master's thesis, University of South Florida, 118 pp.

Helland-Hansen, B. 1916. Nogen hydrogr London. afiske metoder form. *Skand. Naturf. Mote*, pp. 357–59.

Højerslev, N. K., Holt, N. and Aarup, T. 1996. Optical measurements in the North Sea-Baltic Sea transition zone. I: On the origin of the deep water in Kattegat.*Cont. Shelf Res.*, 16(10), pp. 1329–42.

Holland, W. R. and Capotondi, A. 1996. Recent developments in prognostic ocean modeling. In: L. Malanotte-Rizzoli (ed.), *Modern Approaches to Data Assimilation in Ocean Modeling*. Amsterdam, Elsevier Science, pp. 21–56.

Hutchinson, G. E. 1961. The paradox of the plankton. *Amer. Nat.*, 95, pp. 137–40.

Ishizaka, J. 1990. Coupling of coastal zone color scanner data to a physical-biological model of southeastern U.S. continental shelf ecosystems. 3: Nutrient and phytoplankton fluxes and CZCS data assimilation. *J. Geophys. Res.*, 95, pp. 20201–12.

Jenkins, W. J. 1980. Tritium and 3He in the Sargasso Sea. *J. Mar. Res.*, 38, pp. 533–69.

Jenkins, W. J. 1982. Oxygen utilization rates in the north Atlantic subtropical gyre and primary production in the oligotrophic system. *Nature*, 300, pp. 246–49.

Jerlov, N. G. 1976. *Marine Optics*. New York, Elsevier.,

Johnson, D. M., Miller, J. and Schofield, O. 2003. Dynamics and optics of the Hudson River outflow plume. *J. Geophys. Res.*, 108(1–9), 3323, doi:10.1029/2002JC001485.

Kahru, M. and Brown, C. W. 1997. *Monitoring Algal Blooms: New Techniques for Detecting Large-Scale Environmental Change.* New York, Springer-Verlag.

Kalle, K. 1966. The problem of the gelbstoff in the sea. *Oceanogr. Mar. Biol. Rev.*, 4, pp. 91–104.

Kirk, J. T. O. 1994. *Light and Photosynthesis in Aquatic Ecosystems*. Cambridge, UK, Cambridge University Press.

Kirkpatrick, G., Millie, D. F., Moline, M. A. and Schofield, O. 2000. Absorption-based discrimination of phytoplankton species in naturally mixed populations. *Limnol. Oceanography*, 42, pp. 467–71.

Kirkpatrick, G. J., Orrico, C., Oliver, M. J., Moline, M. A. and Schofield, O. 2003. Continuous real-time determination of hyperspectral absorption of colored dissolved organic matter. *Appl. Opt.*, 42, pp. 6564–68.

Kishino, M., Takahashi, M., Okami, N. and Ichimura, S. 1985. Estimation of the spectral absorption coefficients of phytoplankton in the sea. *Bull. Mar. Sci.*, 37, pp. 634–42.

Kohut, J. T. and Glenn, S. M. 2003. Improving HF radar surface current measurements with measured antenna beam patterns. *J. Atmos. Ocean. Tech.*, 20, pp. 1303–16.

Lawson, L. M., Spitz, Y. H., Hofmann, E. E. and Long, R. B. 1995. A data assimilation technique applied to a predator-prey model. *Bull. Math. Biol.*, 57, pp. 593–617.

Martin-Trayovski, L. V. and Sosik, H. M. 2004. Feature-based classification of optical water types in the northwest Atlantic based on satellite ocean color data. *J. Geophys. Res.*, 108, pp. 119.

Matear, R. J. 1995. Parameter optimization and analysis of ecosystem models using simulated annealing: a case study at Station P. *J. Mar. Res.*, 53, pp. 571–607.

Millie, D. F., Schofield, O., Kirkpatrick, G. J., Johnsen, G. and Evens, T. J. 2002. Using absorbance and fluorescence spectra to discriminate microalgae. *Eur. J. Phycol.*, 37, pp. 313–22.

Millie, D. F., Schofield, O., Kirkpatrick, G. J., Johnsen, G., Tester, P. A. and Vinyard, B. T. 1997. Phytoplankton pigments and absorption spectra as potential 'biomarkers' for harmful algal blooms: a case study of the Florida red-tide dinoflagellate, *Gymnodinium breve*. *Limnol. Oceanogr.*, 42, pp. 1240–51.

Mobley, C. D. 1994. *Light and Water: Radiative Transfer in Natural Waters*. San Diego, Calif., Academic Press.

Mooers, N. K. 1999. *Coastal Ocean Prediction.*Washington DC, American Geophysical Union. (Coastal and Estuarine Studies 56.)

Morel, A. and Bricaud, A. 1986. Inherent optical properties of algal cells including picoplankton: Theoretical and experimental results. In: T. Platt, and W. K. W. Li, (eds), *Photosynthetic Picoplankton. Can. Bull. Fish. Aquat. Sci.*, pp. 521–59.

Morel, A. and Prieur, L. 1997. Analysis of variations in ocean color. *Limnol. Oceanogr.*, 22, pp. 709–22.

National Research Council. 2000. *Illuminating the Hidden Planet: The Future of Seafloor Observatory Science.* Washington DC, Ocean Studies Board. (Committee on Seafloor Observatories: Challenges and Opportunities.)

National Research Council. 2004b. *Enabling Ocean Research in the 21st Century: Implementation of a Network of Ocean Observatories,*Washington DC, Ocean Studies Board. (Committee on Seafloor Observatories: Challenges and Opportunities.)

Oliver, M. J., Kohut, J. T., Irwin, A J., Glenn, S. M., Schofield, O., Moline, M. A. and Bissett, W. P. 2004. Bioinformatic approaches for objective detection of water masses. *J. Geophys. Res.*, 109, C07S04, doi:10.1029/2003JC002072.

Oliver, M. W., Schofield, O., Bergmann, T., Glenn, S. M., Moline, M. A., and Orrico,C. 2003. *In situ* optically derived phytoplankton absorption properties in coastal waters and its utility for estimating primary productivity rates. *J. Geophys. Res.*, 109, C07S11, doi:10.1029/2002JC001627.

Paine, R. T. and Vadas, R. L. 1969. The effects of grazing by sea urchins, *Strongylocentrotus spp.*, on benthic algal populations. *Limnol. Oceanogr.*, 14, pp. 710–19.

Pegau, W. S., Cleveland, J. S., Doss, W., Kennedy, D. W. Maffione, R. A., Mueller, J. L., Stone, R., Trees, C. C., Weidemann, A. D., Wells, W. H. and Zaneveld, R. J. V. 1995. A comparison of methods for the measurement of the absorption coefficient in natural waters. *J. Geophys. Res.*, 100, pp. 13201–21.

Pope, R. M. and Fry, E. S. 1997. Absorption spectrum (380–700 nm) of pure water. II: Integrating cavity measurements. *Appl. Opt.*, 33, pp. 8710–23.

Prézelin, B. B. and Boczar, B. A. 1986. Molecular bases of cell absorption and fluorescence in phytoplankton: potential applications to studies in optical oceanography. *Progr. Phycol. Res.*, 4, pp. 350–64.

Quackenbush, J. 2000. Computational analysis of microarray data. *Nat. Rev. Gen.*, 2, pp. 418–27.

Reynolds, R. A., Stramski, D. and Kiefer, D. A. 1997. The effect of nitrogen-limitation on the absorption and scattering properties of the marine diatom *Thalassiosira pseudonana. Limnol. Oceanogr.*, 42, pp. 881–92.

Robinson, A. R., Arango, H. G., Warn-Varnas, A., Leslie, W. G., Miller, A. J., Haley, P. J. and Lozano, C. J. 1996. Real-time regional forecasting. In: L. Malanotte-Rizzoli (ed.), *Modern Approaches to Data Assimilation in Ocean Modeling*. Amsterdam, Elsevier, pp. 377–412.

Robinson, A. R. and Glenn, S. M. 1999. Adaptive sampling for ocean forecasting. *Nav. Res. Rev.*, 51, pp. 26–38.

Roesler, C. S. and Boss, E. 2007. *In situ* measurement of inherent optical properties and potential for harmful algal bloom detection and coastal ecosystem observations. In: Babin et al. (eds), op. cit., this volume.

Roesler, C. S., Etheridge, S. M. and Pitcher, G. C. 2003. Application of an ocean color algal taxa detection model to red tides in the southern Benguela. In: K. A. Steidinger, J. H. Lansdberg, C. R. Tomas, and G. A. Vargo (eds), *Harmful Algae 2002.* Proc. X International Conference on Harmful Algae (20–25 October 2002). St Petersburg, Fla./ Paris, Florida Fish and Wildlife Conservation Commission/Intergovernmental Oceanographic Commission of UNESCO.

Ruddick, K., Lacroix, G., Park, Y., Rousseau, V., De Cauwer, V. and Sterckx, S. 2007. Overview of ocean colour: theoretical background, sensors and applicability to detection and monitoring of harmful algal blooms (capabilities and limitations). In: Babin et al. (eds), op. cit., this volume.

Schofield, O., Bergmann, T., Bisset, W. P., Grassle, F., Haidvogel, D., Kohut, J., Moline, M. A. and Glenn, S. 2002. The long-term ecosystem observatory: an integrated coastal observatory. *J. Ocean. Eng.*, 27, pp. 146–54.

Schofield, O., Bergmann, T., Oliver, M. J., Irwin, A., Kirkpatrick, G., Bissett, W. P., Moline, M. A. and Orrico, C. 2004. Inversion of spectral absorption in the optically complex coastal waters of the Mid-Atlantic Bight. *J. Geophys. Res.*, 109, C12S04, doi:10.1029/2003JC002071.

Schofield, O., Bissett, W. P., Frazer, T. K., Iglesias-Rodriguez, D., Moline, M. A. and Glenn, S. 2003. Development of regional coastal ocean observatories and the potential benefits to marine sanctuaries. *Mar. Tech. Soc.*, 37, pp. 54–67.

Schofield, O., Gryzmski, J., Bissett, W. P., Kirkpatrick, G., Millie, D. F., Moline, M. A. and Roesler, C. 1999. Optical monitoring and forecasting systems for harmful algal blooms: possibility or pipedream? *J. Phycol.*, 35, pp. 125–45.

Shimizu, Y. and Wrensford, G. 1993. Peculiarities in the biosynthesis of brevetoxins and metabolism of *Gymnodinium breve*. In: T. J. Smayda and Y. Shimizu (eds), *Toxic Phytoplankton Blooms in the Sea*. New York, Elsevier, pp. 919–23.

Sosik, H. M. 2007. Characterizing seawater constituents from optical properties. In: Babin et al. (eds), op. cit., this volume.

Stommel, H. 1989. The SLOCUM Mission. *Oceanography*, 1, pp. 22–25.

Smethie, W. M. 1993. Tracing the thermohaline circulation in the western North Atlantic using chlorofluorocarbons. *Progr. Oceangr.*, 31, pp. 51–99.

Smith, R. S., Brown, O. B., Hoge, F. E., Baker, K. S., Evans, R. H., Swift, R. N. and Esaias, W. E. 1987. Multiplatform sampling (ship, aircraft, and satellite) of a Gulf Stream warm core ring. *Appl. Opt.*, 26, pp. 2068–81.

Stramski, D. and Kiefer, D. A. 1991. Light scattering by microorganisms in the open ocean. *Progr. Oceanogr.*, 28, pp. 250–68.

Stramski, D. and Reynolds, R. A. 1993. Diel variations in the optical properties of a marine diatom. *Limnol. Oceanogr.*, 38, pp. 1347–64.

Stumpf, R. P. 2000. Applications of satellite ocean color sensors for monitoring and predicting harmful algal blooms. *Hum. Ecol. Risk Assess.*, 7, pp. 1363–68.

Stumpf, R. P., Ransibrahmanakal, V., Steindinger, K. A., and Tester, P. A. 1998. Observations of sea surface temperature and winds in association with Florida USA red tides (*Gymnodinium breve* blooms). In: B. Reguera, J. Blanco, M. L. Fernández and T. Wyatt, (eds), *Harmful Algae.* Proc. VIII International Conference on Harmful Algae (June 1997, Vigo, Spain). Santiago de Compostela/Paris, Xunta de Galicia/Intergovernmental Oceanographic Commission of UNESCO, pp. 145–48.

Tester, P. A., Stumpf, R. P. and Steindinger, K. A. 1998. Ocean color imagery: what is the minimum potential for early warning? *J. Shellfish Res.*, 17, pp. 1469–71.

Tomczak, M. 1999. Some historical, theoretical and applied aspects of quantitative water mass analysis. *J. Mar. Res.*, 57, pp. 275–303.

Tomlinson, M. C., Stumpf, R. P., Ransibrahmanakul, V., Truby, E. W., Kirkpatrick, G. J., Pederson, B. A., Vargo, G. A. and Heil, C. A. 2004. Evaluation of the use of SeaWiFS imagery for detecting *Karenia brevis* harmful algal blooms in the eastern Gulf of Mexico. *Rem. Sens. Environ.*, 91, pp. 293–303.

Twardowski, M. S., Boss, E., Macdonald, J. B., Pegau, W. S., Barnhard, A. H. and Zaneveld, J. R. V. 2001. A model for estimating bulk refractive index from the optical backscattering ratio and the implications for understanding particle composition in Case I and Case II waters. *J. Geophys. Res.*, 106, pp. 14129–42.

US Commission on Ocean Policy. 2004. *An Ocean Blueprint for the 21st Century.* Final Report of the US Commission on Ocean Policy. National Oceanic and Atmospheric Administration, US Department of Commerce.

van de Hulst, H. C. 1957. *Light Scattering by Small Particles*. New York, John Wiley & Sons.

Weiss, R. F., Bullister, J. L., Gammon, R. H. and Warner, M. J. 1985. Atmospheric chlorofluoromethanes in the deep equatorial Atlantic. *Nature*, 314, pp. 608–10.

Yeung, K. Y., Haynor, D. R. and Ruzzo, W. L. 2001. Validating clustering for gene expression data. *Bioinform.*, 17(4), pp. 309–18.

Zaneveld, J. R. V. 1995. A theoretical derivation of the dependence of the remotely sensed reflectance of the ocean on the inherent optical properties. *J. Geophys. Res.*, 100, pp. 13135–42.

Zaneveld, J. R. V., Kitchen, J. C. and Moore, C. C. 1994. Scattering correction of reflecting tube absorption meter. *Proc. Soc. Photo-Opt. Instrum. Eng.*, 2258, pp. 44–55.

4

Introduction to optical properties in the sea: theoretical aspects

A.Morel

4.1 Introduction

Algal 'bloom', simply defined as a sudden and remarkable increase of phytoplankton abundance, relative to the average level in a given area, has been visually identified for a long time by a change of colour, near the coasts as well as in the open ocean. The colour shift induced by such proliferations can be spectacular. Are these blooms harmful or not is another question, generally not solved by eyes; the indisputable answer will probably always require sampling and specific identification. Anyway, a first step is to detect in an efficient manner the occurrence of blooms, whatever they are, and with this goal optical methods are particularly appropriate (Cullen et al., 1997; Schofield et al., 1999). Indeed, such methods can be remotely operated, may provide quick answer or warning, as well as long-term monitoring. These attributes are shared by optical instruments or techniques operated during regular surveys, by automated mooring deployments for local information, or by remote sensors operated from aircraft or satellite for wider spatial scales. The capabilities and limitations, however, are not the same for *in situ* and remote techniques, and the optical properties involved also differ, although they are related.

The aim of the present chapter is to provide the basic information about these optical properties, by starting with their precise definitions and inter-relationships (exact or approximate). It seems important, particularly for non-specialists, and as an introduction to the other chapters dealing with optical techniques, to first fix a coherent frame (including an accurate vocabulary), before entering into possible applications, and facing the complexity of the real world.

4.2 Bulk properties: inherent and apparent optical properties

The bulk optical properties are those of a medium considered at a macroscopic or large-scale level; in our case the medium comprises water molecules, ions, dissolved compounds, and various particles in suspension. Other optical properties (examined below) can be defined at a microscopic scale, namely at the level of a single particle (e.g. a phytoplanktonic cell). These two classes of properties are obviously related.

Among the bulk properties, a convenient and powerful distinction has been introduced by Preisendorfer (1961) as follows. The Inherent Optical Properties (IOPs) are those properties that depend only on the medium itself, and that exist independently from the way the medium is illuminated. Conversely, the Apparent Optical Properties (AOPs) are those that depend both on the previous IOPs *and* on the geometric structure of the light field incident on, or set up within, the medium. A unique expression, namely the radiative transfer equation (RTE), establishes the exact relationship that links the two classes of properties. Deriving the AOPs from the knowledge of the IOPs combined with boundary conditions (for example, the incident solar radiation, surface roughness) is generally called the direct problem; the inverse problem consists of retrieving the IOPs from measured AOPs under known or assumed illumination conditions. Both problems require the manipulation of the RTE to retrieve accurate or approximate numerical solutions.

4.2.1 Inherent optical properties (IOPs)

The minimal set of independent IOPs comprises the index of refraction, the absorption coefficient, the volume-scattering function and the source function. They are defined below. Other IOPs are derived quantities. They are all wavelength (or frequency) dependent, even if for the sake of simplification, the symbols λ (or ν) are omitted when not specifically needed. The background and the measurement of IOPs in the context of HABs are examined in detail in Roesler and Boss (2007 – Chapter 5 this volume).

4.2.1.1 Index of refraction

The index of refraction n of a medium is the ratio of the velocity c_0 of electromagnetic radiation *in vacuo*, to the velocity c in this medium, so that n is always greater than 1 as c is always smaller than c_0. The frequency ν of the electromagnetic radiation does not change from one medium to another, so that the wavelength changes; the wavelength *in vacuo* is λ_0, with $\lambda_0 = c_0/\nu$, and in another medium is $\lambda = c/\nu$ or $= \lambda_0/n$. Unlike c_0, c generally depends on the frequency. Far from absorption bands, the index is a smooth function of ν (or λ) and increases for decreasing wavelength. This phenomenon is called the 'normal dispersion'. In fact n is the real part of a complex refractive index, introduced at a later stage (see also Appendix 4.1).

At the macroscopic scale and at a fixed λ, n is a constant for water of given salinity and temperature (S and T). Its value (about 1.33 or 1.34 for freshwater and seawater respectively), is known (to six digits) as a function of λ, S, T and pressure (Austin and Halikas, 1976).

Other substances are present as particles in natural waters ('hydrosols'), with refractive indices generally higher than that of water (except bubbles). What is important in Hydrologic Optics is the relative index (n_{subs}/n_{water}), that ranges from 1.15 to 1.22 for mineral substances (apart from opal, with 1.09), and from 1.02 to 1.09, approximately, for watery organic particles, including living cells or derived organic detritus. In contrast, it is equal to 0.75 for air bubbles within a water body. The impact of particles having refractive indices different from their surrounding media is that the light slows down as it enters or travels near the particle; the impact of slowing down is that the light rays are bent and there is a redirection of the incident light field. This is an intuitive approach, not a rigorous explanation.

4.2.1.2 Absorption and scattering

Absorption is a phenomenon by which energy (expressed in joules) carried by electromagnetic radiation disappears, as a result of interaction with matter. According to the energy conservation principle, this amount of energy reappears under another form. The most common form is simply heat (thermalization). Transformation into chemical energy via photochemical reactions is a common pathway in natural environments (e.g. photosynthesis, photodegradation of chemical compounds). The re-emission of radiation at longer wavelengths (Stokes shift) is also another possibility, known as 'inelastic scattering', and corresponds to phenomena such as fluorescence emission (by chlorophyll *a*, for example, or by dissolved organic compound), or to Raman effect by water molecules.

In contrast, the (elastic) scattering phenomenon does not entail any loss of radiant energy; only an angular deviation occurs, namely a redirection of radiation with respect to its initial direction of propagation.

If Φ_0 is the radiant power (also called 'flux', expressed as W or J s^{-1}) incident on a physical body, a fraction Φ_a will be absorbed inside the body, whereas another fraction Φ_b will be scattered out from it. The dimensionless ratios Φ_a/Φ_0 and Φ_b/Φ_0 are called absorptance (A) and scatterance (B), respectively. The ratio $(\Phi_a + \Phi_b)/\Phi_0$ is called attenuance (C) and represents the relative flux lost by the two processes, whereas the transmittance (T) of this body is (1 – C), and represents the quantity $[\Phi_0 - (\Phi_a + \Phi_b)]/\Phi_0$.

A simple and proper definition of the inherent optical coefficients involves these quantities, when considered in a particular geometrical configuration (Figure 4.1A) formed by a narrow collimated beam of monochromatic radiation incident normal

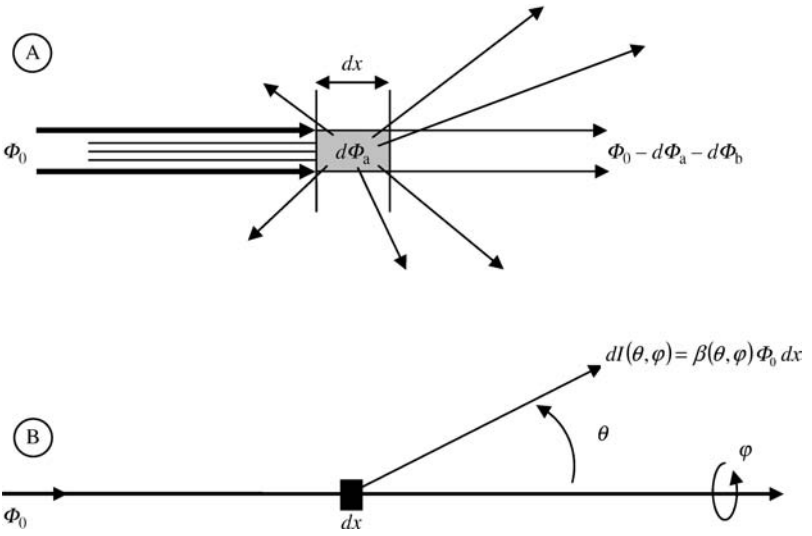

Figure 4.1
A, Schematic geometrical configuration used for the definition of the absorption, scattering and attenuation coefficients, *a* and *b*.
B, the elementary volume (thickness d*x*) is seen as a point source from which originates the scattered radiation in all directions (intensity d*I*).

to an infinitesimally thin layer of medium (thickness dx). The infinitesimally small absorptance and scatterance of such a layer are dA and dB. The absorption and scattering coefficients, a and b respectively, are locally defined as

$$a = \mathrm{d}A/\mathrm{d}x = (\mathrm{d}\Phi_a/\Phi_0)/\mathrm{d}x,$$

and

$$b = \mathrm{d}B/\mathrm{d}x = (\mathrm{d}\Phi_b/\Phi_0)/\mathrm{d}x. \quad (4.1)$$

Both have the dimension of (length)$^{-1}$ and are commonly expressed as m^{-1} in aquatic optics.

Such definitions result from observation: indeed, the absorbed (scattered) power is proportional to the incident power and to the elementary thickness through the coefficient a (b), respectively,

$$\mathrm{d}\Phi_a = a\Phi_0\mathrm{d}x$$

and

$$\mathrm{d}\Phi_b = b\Phi_0\mathrm{d}x. \quad (4.2)$$

The sum $\mathrm{d}\Phi_c = (\mathrm{d}\Phi_a + \mathrm{d}\Phi_b)$ represents the loss of power by absorption and scattering when the beam is passing through the layer. Therefore the elementary *attenuance* dC is related to dx through the attenuation coefficient, $c = (a + b)$ according to

$$\mathrm{d}C = \mathrm{d}\Phi_c/\Phi_0 = -c\mathrm{d}x, \quad (4.3)$$

where the minus sign expresses that $\mathrm{d}\Phi_c$ is a loss for the flux carried by the beam, and thus is a negative quantity. When integrating the above expression over a finite distance x, within a homogeneous medium (i.e. the optical properties are not a function of x), it results in

$$\mathrm{Ln}(\Phi_x/\Phi_0) = -cx \text{ or } \Phi_x = \Phi_0 \exp(-cx), \quad (4.4)$$

where Φ_x is the remaining flux at distance x. This exponential attenuation of light with travelled distance is known as the Beer-Lambert-Bouguer law. The dimensionless product $cx = \tau$ is the 'optical thickness'. Therefore, $\exp(-\tau)$ represents the transmittance along the beam, and conversely $[1 - \exp(-\tau)]$ is its attenuance.

The angular distribution of the scattered power as a result of the primary scattering process (as opposed to multiple scattering process) is described by the volume scattering function (VSF).

The elementary volume (Figure 4.1B), seen from a sufficient distance, acts as a point source radiating in all directions with an intensity $\mathrm{d}I(\theta, \varphi)$ that varies according to the direction (θ, φ), where θ is a polar angle from the direction of propagation of the incident beam, and φ is an azimuth angle. Intensity is the power in a specified direction divided by the elementary solid angle centred on the (θ, φ) direction, so $\mathrm{d}I = \mathrm{d}^2\Phi/\mathrm{d}\Omega$. As for a and b, $\mathrm{d}I(\theta, \varphi)$ is proportional to the incident power and to the

elementary thickness, via an angular scattering coefficient $\beta(\theta, \varphi)$ (units $m^{-1}\,sr^{-1}$), or VSF, so defined as

$$dI(\theta, \varphi) = \beta(\theta, \varphi)\ \Phi_0\ dx. \tag{4.5}$$

For the media and substances considered in hydrologic optics (such as molecules or randomly oriented particles), the scattering phenomenon is assumed to be axially symmetrical (around the initial direction of propagation), so that the dependence vis-à-vis φ disappears, and $d\Omega = 2\pi \sin\theta\, d\theta$. The elementary scattered power in direction θ is

$$d^2\Phi_b = dI(\theta)\, d\Omega = 2\pi \sin\theta\, d\theta\, \beta(\theta, \varphi)\ \Phi_0\, dx. \tag{4.6}$$

The total power lost from the beam by elastic scattering (and thus gained over all other directions from the outer space) is obtained by integrating over the whole space (i.e. over all θ angles from 0 to π)

$$d\Phi_b = \Phi dx\, 2\pi \int_0^{\pi} \beta(\theta) \sin\theta\, d\theta. \tag{4.7}$$

By comparing (4.7) with (4.2), the relationship between the scattering coefficient and the volume scattering function can be derived in a straightforward fashion, and results in

$$b = 2\pi \int_0^{\pi} \beta(\theta) \sin\theta\, d\theta. \tag{4.8}$$

This relationship shows that the angular description of the scattered field requires the knowledge of the $\beta(\theta)$ function, whereas the scattering coefficient b is a derived IOP obtained by integration over the whole space of this function. This integration can be split into two integrals, with θ going from 0 to $\pi/2$, and then from $\pi/2$ to π, leading to the definition of the forward scattering and backscattering coefficients, b_f and b_b, respectively,

$$b_f = 2\pi \int_0^{\pi/2} \beta(\theta)\, \sin\theta\, d\theta \text{ and } b_b = 2\pi \int_{\pi/2}^{\pi} \beta(\theta) \sin\theta d\theta, \tag{4.8′}$$

with $b = b_f + b_b$.

The normalized VSF, denoted $\tilde{\beta}(\theta)$, (units sr^{-1}), or phase function, is obtained by dividing $\beta(\theta)$ by b; therefore its integral over the whole space is unity:

$$1 = 2 \int_0^{\pi} \tilde{\beta}(\theta) \sin\theta d\theta. \tag{4.9}$$

Note that with such a normalization of the VSF, the IOP $\beta(\theta)$ is split into two derived quantities, one describing the magnitude of the phenomenon b, while the other one, $\tilde{\beta}(\theta)$, depicting only the geometrical aspect (i.e. directional redistribution). The forward scattering and backscattering coefficients can be normalized in the same way, b_f/b and b_b/b, leading to the dimensionless quantities $\tilde{b}_f$ and $\tilde{b}_b$, which represent the probabilities of forward or backward scattering, respectively. The ratio b/c provides another dimensionless number ϖ, which represents the probability of photon survival; it is also called the 'single scattering albedo'.

4.2.1.3 Source function

Thermal emission would enter into this category; however, the wavelength domain of the Plank emission is in the infrared (IR); when accounting for the water temperature in natural conditions. In the visible part of the spectrum of interest here, sources only originate from inelastic scattering or bioluminescence. They are described as in (4.8) (subscript em denotes 'emission'),

$$b_{\mathrm{em}} = 2\pi \int_0^{\pi} \beta_{\mathrm{em}}(\theta) \sin\theta \, \mathrm{d}\theta. \tag{4.10}$$

Using the same normalization as in (4.9), $\beta_{\mathrm{em}}(\theta)$ can be written

$$\tilde{\beta}_{\mathrm{em}}(\theta, \lambda) = b_{\mathrm{em}}(\lambda_{\mathrm{ex}} \rightarrow \lambda_{\mathrm{em}}) \, \tilde{\beta}_{\mathrm{em}}(\theta, \lambda), \tag{4.11}$$

where λ_{ex} specifies the wavelength (generally a domain of wavelengths) of radiation able to excite an emission at wavelength λ_{em} (with $\lambda_{\mathrm{ex}} < \lambda_{\mathrm{em}}$). In fact, only a fraction of the absorption coefficient in the λ' domain is devoted to allow a re-emission at λ. In analogy with the elastic process, the source function (4.11) is split into two components, the geometrical one, $\tilde{\beta}_{\mathrm{em}}(\theta, \lambda)$, and a second one that describes the magnitude of the phenomenon via the trans-spectral scattering coefficient, $b_{\mathrm{em}}(\lambda' \rightarrow \lambda)$.

Two distinct physical phenomena give rise to emission in the visible part of the spectrum: the Raman effect by water molecules, and the fluorescence by the algal pigments chlorophyll *a* and phycoerithrin or by chromophoric dissolved organic matter (CDOM). While spontaneous bioluminescence by some organisms yields emission of visible radiation, it does not require a radiative excitation, but a transformation of chemical energy. Bioluminescence may be important in deep water, but generally is insignificant in the upper layers and in day light. Many bioluminescent algal blooms are commonly misnamed 'phosphorescent'. Phosphorescence is a phenomena which, like fluorescence and Raman, requires absorption of light energy, but which differs in that the emission continues after the exciting source is removed. It is of minor significance in the ocean.

The Raman emission is not spectrally fixed. Indeed, the spectral interval (between λ' and λ) corresponds to a constant shift in frequency (related to the rotational/vibrational modes of the H_2O molecule), so that emission can take place at any wavelength λ, provided that energy is available and has been absorbed at the appropriate λ'. Quite different is the fluorescence emission, which is a radiative decay of excited electronic states (from the first excited state to the ground state as far as the chlorophyll *a* molecule is concerned – see Babin, Chapter 7), and thus occurs at fixed wavelengths (λ_{f}) typical of the molecule when excited. The excitation that results from absorption can be more or less efficient, and thus the emission more or less intense, according to the exciting wavelengths (λ'). For example, the chlorophyll *a* molecule, present in all phytoplanktonic species, fluoresces in an approximately spectral Gaussian band about 25 nm wide centred around 685 nm. The excitation spectrum is much wider *in vivo* (say 350–680 nm), as it encompasses not only the absorption spectrum of chlorophyll *a*, but also the absorption spectra of various accessory pigments able to transfer absorbed energy to the chlorophyll *a* molecule. Similar behaviour is observed for the phycobilipigment phycoerithrin found in cyanobacteria and cryptomonads. The dissolved organic matter (also called CDOM, 'yellow substance', 'gelbstoff' or 'gilvin') is composed of a complex mixture of substances, a fraction of which are fluorescent and thus can produce a broadband fluorescence (350–700 nm), depending in magnitude and position on the excitation wavelength.

With reference to (4.11), the Raman scattering phase function $\tilde{\beta}^{R}_{em}(\theta)$ varies according to $(1 + 0.55 \cos^2 \theta)$ (Ge et al., 1993). The fluorescence emission can be assumed to be isotropic, with a constant value independent of θ, $\tilde{\beta}^{f}_{em}(\theta) = (1/4\pi)$ sr^{-1} (see e.g. Gordon et al., 1993). The Raman scattering coefficient $b^{R}_{em}(\lambda' \rightarrow \lambda)$ is a physical property of the water molecule. Its commonly accepted value is $2.6\ 10^{-4}$ m^{-1} (Bartlett et al., 1998) at $\lambda' = 488$ nm (the corresponding emission is around 590 nm); this coefficient varies as $(\lambda')^{-4.775}$. For chlorophyll *a* fluorescence, the excitation spectrum, that is the corresponding coefficient $b^{f}_{em}(\lambda' \rightarrow [685\ nm])$ – where the bracket indicates the whole fluorescent band – spectrally mimics the algal absorption spectrum, with some nuances. They originate from a non-constant capacity of various pigments to transfer excitation to the chlorophyll *a* molecule (the transfer is null for photoprotectant pigments). For this reason, a close kinship exists between the fluorescence excitation spectrum and the action spectrum for photosynthesis.

The quantum yield for fluorescence, ϕ_f, is simply the ratio between the number (or energy) of photons emitted to the number (or energy) of absorbed photons. This yield is about 30% for free chlorophyll *a* molecules (in solution). In natural environments, and when chlorophyll *a* associated with proteins is embedded within the photosynthetic apparatus of living algal cells and is directly involved in the photosynthesis process, ϕ_f decreases down to a few percent (or even < 1% in the highly lit surface layer). As a photo-physiological response of a phytoplankton assemblage, ϕ_f depends on species composition, nutrient status and light availability as well as light history (in this sense, this fluorescence source function is not, strictly speaking, an IOP, whilst the Raman source is a true one). The small fluorescence yield, however, is sufficient to render the sun-induced fluorescence detectable in most oceanic waters within the submarine light field, or even from space (Ruddick et al., 2007 – Chapter 9 this volume).

The Raman source, in spite of being weak, influences the light field, particularly in oligotrophic waters (low chlorophyll concentration) and at depth. In such waters, while the red (solar) light is progressively absorbed, the locally emitted Raman radiation (excited by green radiation) progressively dominates and finally replaces the transmitted flux in this spectral domain.

4.2.1.4 Additivity

A strict additivity governs the IOPs, so that coefficients like *a, b, c* or $\beta(\theta)$ can be split into partial coefficients; each of them corresponds to the various components which contribute to the phenomenon. For the refractive index, the additivity principle (which translates into the application of a linear mixing rule) would hold true if seawater was an ideal solution. This remains a sufficient approximation in most cases.

4.2.1.5 Significance

By virtue of additivity and with the consequential possibility of splitting any IOP into partial contributions, it is clear that the various substances, dissolved or particulate, that are present within the water body can be identified. Their concentration can be assessed if their specific action has been preliminarily studied and quantitatively established (e.g. a 'chl-specific absorption coefficient', or a 'mass-specific scattering coefficient of sediment'). In contrast to this direct link between substances and IOPs, the AOPs cannot be connected directly to the substances, because they depend on the light field and are not additive; thus the inverse problem has to be solved to come back to the IOPs and then to the respective constituents.

4.2.2 Apparent optical properties (AOPs)

When describing the radiant field inside a scattering/absorbing medium, radiance is the fundamental radiometric quantity (units W m^{-2} sr^{-1} where the spectral dependency has been suppressed for notational convenience). It is defined as the power in a specified direction (θ, φ) per unit solid angle and per unit area (therefore radiance is also the intensity per unit area – see above),

$$L(\theta,\varphi) = \mathrm{d}^2\Phi/\mathrm{d}A\mathrm{d}\Omega = (\mathrm{d}I/\mathrm{d}A), \tag{4.12}$$

where the infinitely small area $\mathrm{d}A$ is normal to the beam direction, and where φ and θ are respectively an azimuth angle and a zenith angle, defined in an appropriate coordinate system. All other radiometric quantities derive in some way from this fundamental one. For example, the downwelling irradiance on a horizontal plane, E_d, is the integral of all radiances headed downward from the upper hemisphere ($\Xi_d = 2\pi$ sr) and intercepting an element of the plane surface, so that

$$E_d = \int_{\Xi d} L(\theta,\phi)\cos\theta\,\mathrm{d}\Omega, \tag{4.13}$$

where θ varies from 0 (zenith) to $\pi/2$, and φ varies from 0 (a direction within the horizontal plane selected as origin for azimuth) to 2π. The units are W m^{-2} and the presence of the cosine indicates that each radiance is weighted by the cosine of its incidence angle (θ) onto the horizontal surface. Similarly, an upward irradiance, E_u, can be defined, involving an integration over the lower hemisphere ($\Xi_u = 2\pi$ sr) and $|\cos\theta|$ to keep this quantity as a positive one (as θ varies from $\pi/2$ to π),

$$E_u = \int_{\Xi u} L(\theta,\phi)\cos\theta\mathrm{d}\Omega. \tag{4.13′}$$

If the integration is performed over the whole space (($\Xi = \Xi_d + \Xi_u = 4\pi$ sr), another quantity appears, denoted

$$E = E_d - E_u = \int_{\Xi} L(\theta,\phi)\cos\theta\mathrm{d}\Omega, \tag{4.13″}$$

which represents the 'net downward flux', or the modulus of the vector irradiance, vertically oriented downward. Note that wavelength is omitted in the previous definitions and relationships; however, these quantities are generally employed as spectral quantities, with nm^{-1} (or equivalent) included in their units.

4.2.2.1 Diffuse attenuation coefficients and average cosines

The same reasoning used for the definition of the absorption and scattering coefficients can be re-employed, yet in a different geometrical configuration (Figure 4.2A). A horizontal, infinitely thin layer of absorbing and scattering medium (thickness $\mathrm{d}z$), located at depth z, is considered; it is illuminated from above by (monochromatic) radiances headed downward leading to a certain downward irradiance $E_d(z)$ (4.13). A flat (cosine) collector can measure $E_d(z)$ at z, and also $E_d(z) + \mathrm{d}E_d(z)$ at $z + \mathrm{d}z$. Generally, $\mathrm{d}E_d$ is a negative quantity and represents a decrease (z positive downward), which is proportional to both $\mathrm{d}z$ and E_d through a coefficient denoted K_d (in a way analogous to that used when introducing c via 4.3),

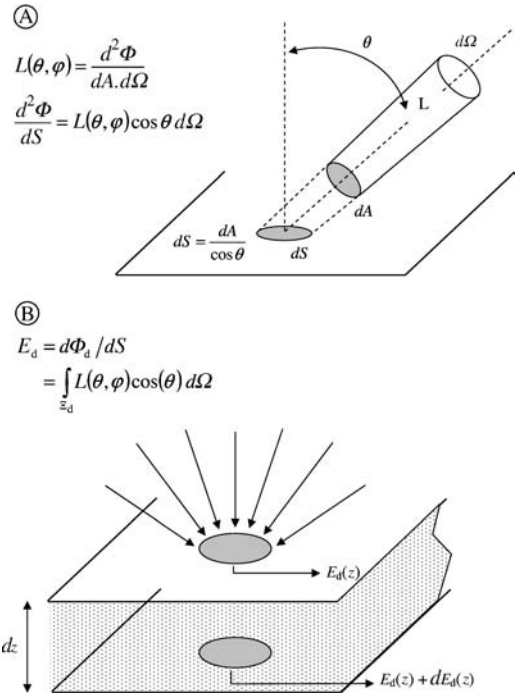

Figure 4.2
A, schematic geometrical configuration used for the definition of radiance; B, plane irradiance and the diffuse attenuation coefficient for downwelling irradiance K_d.

$$dE_d(z) = -K_d(z)E_d(z)dz, \tag{4.14}$$

so that the diffuse attenuation coefficient for downward irradiance is defined (λ omitted) as,

$$K_d(z) = -d[LnE_d(z)]/dz. \tag{4.15}$$

Similar K-coefficients can be defined for any other radiometric quantity, such as E or E_u, or any radiance $L(\theta, \varphi)$, through the same derivative with respect to depth of the neperian (natural) logarithm of this quantity.

By integrating (4.15) over a finite depth interval (e.g. 0–Z), the exponential decrease of irradiance, from $E_d(0)$ to $E_d(Z)$, is expressed as

$$E_d(Z) = E_d(0)\exp[-\int_0^z K_d(z)dz]. \tag{4.16}$$

Such an expression (similar to (4.4)) nonetheless suggests that the K_d coefficient is not constant. Intuitively, K_d must depend (in a certain manner, at present not made explicit) on the inherent coefficients a and b, therefore K_d must change if the medium is not vertically homogeneous. In fact, were the medium homogeneous

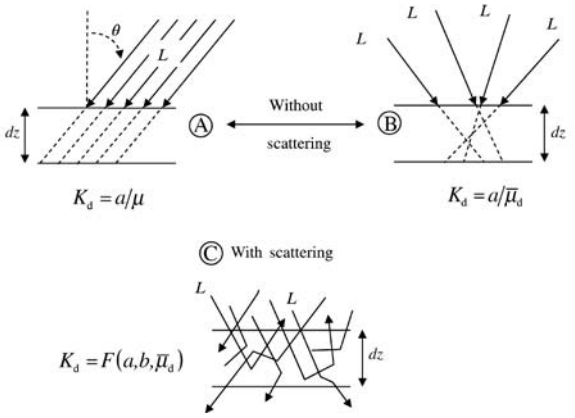

Figure 4.3
A, particular cases of a purely absorbing medium (no scattering) illuminated by parallel slant radiances, or by any other radiance field, B. C, general case of an absorbing and scattering medium; visualization of photon trajectories through the slab.

(i.e. a and b constant), K_d would change as it depends on the geometrical structure of the in-water radiance distribution, which evolves with depth. This is the very reason for having coined the term AOP for such properties.

Some insight into the nature of K_d can be gained by considering a simplified situation (Figure 4.3A) where the radiances headed downward are all originating from the same slant direction (θ), and by assuming in addition that the medium is a purely absorbing one (b negligible compared with a). Note that this hypothetical situation is not far from the real ocean lit by the sun in the near-infrared spectral domain (water absorption is very high, the solar rays are roughly parallel, and the sky radiation is very low). In such a case it is easy to see that the decrease in irradiance, only due to absorption along the slant path ($dl = dz/\cos\theta$) is governed by

$$K_d = a/\mu, \tag{4.17}$$

with $\mu = \cos\theta$. If now the medium is kept unchanged, but the illumination conditions are more complex as a result of variously oriented radiances $L(\theta, \varphi)$ (Figure 4.3B), it is conceivable that such a distribution can be replaced by parallel rays (as above) producing the same effect, provided that an appropriate average angle $\overline{\theta}$ can be found. This angle corresponds to an 'average cosine', $\overline{\mu}_d$, which can be simply obtained through the weighting operation,

$$\overline{\mu}_d = \int_{\Xi d} L(\theta,\phi)\cos\theta\, d\Omega \Big/ \int_{\Xi d} L(\theta,\phi)\, d\Omega. \tag{4.18}$$

The expression for K_d will be as in (4.17), where $\overline{\mu}_d$ (the average cosine for downward irradiance) replaces μ. Another radiometric quantity has been introduced (the denominator in (4.18)), the integral over Ξd ($=2\pi$ sr) of the downward radiance field without the

cosine weighting. This quantity is termed 'scalar downwelling irradiance', $\overset{o}{E}_d$. Similarly, a scalar upward irradiance, $\overset{o}{E}_u$, and an average cosine for the upward irradiance $\overline{\mu}_u$ can be defined. The sum $\overset{o}{E}$ (= $\overset{o}{E}_d$ = $\overset{o}{E}_u$) is the scalar irradiance, directly computable as

$$\overset{o}{E} = \int_{4\pi} L(\theta, \phi) \mathrm{t}\Omega. \tag{4.19}$$

This quantity, $\overset{o}{E}$, actually expresses the total radiant power incident from all directions on a point (it is also called 'flux density'). Note that this point may be a phytoplanktonic cell, and $\overset{o}{E}$ is the appropriate radiometric quantity that describes the radiant energy available for this cell (for photosynthesis, or fluorescence, or dissipative heating).

By considering now the general case of a scattering-absorbing medium (Figure 4.3C), and photons travelling and interacting within the thin layer, three phenomena occur. First, $\overline{\mu}_d$ is modified, and in fact is decreasing with increasing obliquity of the photon paths. Second, due to multiple scattering events, the mean pathlength of photons through the layer is, on average, increased and thus the chance for these photons of being absorbed is also raised, so that K_d becomes larger than in the preceding (purely absorbing) case. Third, some photons, after having wandered inside the layer, are redirected upward and escape from the layer. The result of this bulk backscattering process is to diminish the downward flux, and must translate into an increase of K_d. Finally, K_d appears to be a complex 'mixture' of the IOPs (b, actually $\beta(\theta)$, and a), under the dependence of the geometrical structure of the light field incident onto the slab ($\overline{\mu}_d$). For this reason, even with constant IOPs in the medium, K_d will continue to vary as long as the light field structure changes, with increasing depth for example. At sufficiently large depths, the geometrical structure no longer evolves (Zaneveld, 1989; Morel and Gentili, 2004), so that K_d becomes a constant, takes its 'asymptotic value' and thus becomes a IOP). Outside the asymptotic region, this simple empirical analysis of the light propagation within such a medium cannot go further, and there is no analytical relationship between K_d and the IOPs. Only resorting to the radiative transfer equation (RTE, see below) allows numerical solutions or approximate expressions for K_d as a function of the IOPs to be found.

4.2.2.2 Reflectances

The irradiance reflectance is a dimensionless quantity defined as the ratio of the upward to the downward irradiance at the same level, z,

$$R(\lambda, z) = E_u(\lambda, z)/E_d(\lambda, z). \tag{4.20}$$

If the level considered is '0^-', that is just beneath the surface, the corresponding reflectance $R(\lambda, 0^-)$ describes the capacity of the medium to return radiation towards the atmosphere. The spectral reflectance (at 0^-) describes the intrinsic 'ocean colour' (as it is independent from the spectral composition of the incident solar radiation). This particularly useful AOP can be formally related to IOPs, that is to a and b_b (4.8′), through a generic relationship

$$R(\lambda) = f\{b_b(\lambda)/[a(\lambda) + b_b(\lambda)]\}. \tag{4.21}$$

As R is an AOP, while a and b_b are IOPs, the dimensionless factor f in (4.21) cannot be a constant, but is a varying number that depends on (a) the illumination geometry (essentially on solar zenith angle θ_0, and to some extent on sea-state), and (b) the volume scattering function, in so far as the coefficient b_b does not suffice to describe the scattering pattern. Roughly speaking, f varies between about 0.30 and 0.50, and (as for K_d) can only be obtained by solving the RTE in various specified conditions (Kirk, 1984; Gordon, 1989*b*; Morel and Gentili, 1991).

4.2.2.3 Bidirectional character of marine reflectance

Other reflectances are also used, such as the remote sensing reflectance, R_{RS}, defined just above the interface (denoted 0^+) as

$$R_{RS}(\lambda) = L_w(\lambda, 0^+, \theta, \varphi)/E_d(\lambda, 0^+), \tag{4.22}$$

where $L_w(\lambda, 0^+, \theta, \varphi)$ is a radiance scattered from the ocean interior, and leaving the ocean in a direction $\theta - \varphi$ (i.e. zenith angle, azimuth angle), and $E_d(\lambda, 0^+)$ is the downward irradiance above the surface at the same wavelength. Another related quantity is the 'normalized water-leaving radiance' L_{WN}, defined (Gordon and Clark, 1981) as

$$L_{WN}(\lambda) = R_{RS}(\lambda)F_0(\lambda), \tag{4.23}$$

where $F_0(\lambda)$ is the extraterrestrial solar flux at mean earth–sun distance. Therefore, the normalization corresponds to a hypothetical situation, as L_{WN} represents the radiance which would be measured if the sun were at zenith, and as if the earth was at its mean distance from the sun and in the absence of an intervening atmosphere (in terms of diffuse transmittance supposed to be unity).

The emerging radiance $L_w(\lambda, 0^+, \theta, \varphi)$ originates from an upward radiance (below the surface), denoted $L_u(\lambda, 0^-, \theta', \varphi)$ (where θ' is a nadir angle, related to θ through Snell's law by $\theta' = \sin^{-1}(\sin(\theta/n)$. The remote sensing reflectance (and the normalized water-leaving radiance) has a bidirectional nature. Indeed, radiances L_u and L_w are not constant (the radiance fields are not isotropic); they depend on the direction considered, θ (or θ'), on the sun zenith angle θ_0, and on $\Delta\varphi$, which represents the azimuth difference between the direction considered and that of the sun. Both these angles have to be introduced as additional arguments. The bidirectional effects are described by the variations of a geometric parameter Q, through which any upward radiance is related to the upward irradiance as

$$L_u(\lambda, 0^-, \theta', \Delta\varphi, \theta_0) = E_u(\lambda, 0^-, \theta_0)/Q(\lambda, 0^-, \theta', \Delta\varphi, \theta_0). \tag{4.24}$$

In fact the atmospheric turbidity (depicted by the aerosol optical thickness, τ_a) and the sea state (through the surface slopes related to wind speed W) are other phenomena to be accounted for, so that τ_a and W are other arguments in the above quantities (with a second-order influence, however). For more details on the variations of the f factor and the Q factor, see Chapters 2 and 13 in Mueller and Fargion (2002).

4.2.3 Relationship between AOPs and IOPs: radiance transfer equation

There exists a unique fundamental equation, the radiance transfer equation (RTE), by which the two categories of optical properties are related. This relationship simply expresses that the change of a specific radiance at a depth z, L (z, θ, φ), along an elementary distance $\mathrm{d}z/\cos\theta$ ($\mathrm{d}z$ is the distance along the descending vertical, and θ is the zenith angle) results from attenuation (i.e. a loss) along the elementary slant path and thus involves c, and, from the gain by scattering into the direction of interest (θ, φ), from all other directions about the element. This term involves the radiances from all (θ', φ') directions of the surrounding space ($\Xi' = 4\pi$) combined with the volume scattering coefficient.

This equation is expressed as (λ omitted, as well as the dependency of c and β on depth z),

$$\cos\theta \frac{\mathrm{d}L(z,\theta,\varphi)}{\mathrm{d}z} = -cL(z,\theta,\phi) + \int_{4\pi} \beta(\theta',\phi' \rightarrow \theta,\phi) L(z,\theta',\phi') \mathrm{d}\Omega', \quad (4.25)$$

where the angle between any direction from the surrounding space and the direction of interest is denoted (θ', $\varphi' \rightarrow \theta$, φ). By introducing the normalized VSF, and then dividing by c, it becomes (canonical form):

$$\cos\theta \frac{\mathrm{d}L(\tau,\theta,\phi)}{\mathrm{d}\tau} = -L(\tau,\theta,\phi) + \varpi \int_{4\pi} \tilde{\beta}(\theta',\phi' \rightarrow \theta,\phi) L(\tau,\theta',\phi') \mathrm{d}\Omega', \quad (4.26)$$

where τ (the optical thickness) replaces the geometrical depth (and $\mathrm{d}\tau = c\,\mathrm{d}z$), and the IOPs are all expressed through dimensionless quantities (ϖ and β). Note that as written, the above equation is monochromatic, time-independent, one-dimensional and valid for a passive medium. A source term is to be added on the right of (4.26), when any emission occurs.

The compactness of this integro-differential equation must not give the illusion that its solution is easy. Actually there is no analytical solution. Nevertheless, mathematical and numerical techniques have been developed to derive quasi-exact solutions, which in effect have been revealed to be extremely accurate (Mobley et al., 1993). These numerical tools allow, in particular, the production of 'pseudo-data' regarding all the AOPs, when the IOPs are fixed and the illumination and boundary (e.g. surface roughness, bottom directional albedo) conditions have been specified. Such an approach is at the origin of many studies, by which generated pseudo-data sets of AOPs are statistically studied as function of the input parameters. Such studies lead to approximate and simple expressions relating AOPs and IOPs. In this way, for example, the f factor appearing in (4.21) as well as its variations with sun angle can be elucidated (Morel and Gentili, 1991, 1996). Similarly, the K_d coefficient (4.15) can be explicitly expressed as a function of a and b (or b_b) through useful geometrically dependent relationships (Kirk, 1984; Gordon, 1989*a*).

Another exact relationship, derived by integrating the RTE, and often called in optical oceanography 'Gershun's relationship', expresses the conservation of energy as

$$(\mathrm{d}/\mathrm{d}z)E = -a\overset{\circ}{E}. \quad (4.27)$$

It relates the depth rate of change of the net (vector) irradiance (4.13″) to the scalar irradiance (4.19), via the absorption coefficient. This (negative) rate is equal to the

radiant power locally absorbed, which is expressed by the product $a\,\overset{o}{E}$ (units W m^{-3}). For example, a small portion of this represents the radiant energy captured by phytoplankton at a given wavelength and corresponds to the product $a_\phi(\lambda)\overset{o}{E}(\lambda)$ (where $a_\phi(\lambda)$ is the absorption coefficient of algal pigments). Many variants of the Gershun equation are also in use.

4.3 Bulk IOPs and optical properties of a single particle

As in the definition of the IOPs, it is assumed that parallel rays of monochromatic radiation impinge on a particle (any size, any shape). The geometrical cross-section of this particle, denoted σ_g, is its projected area on the plane of the waves (its 'shadow'). The interaction between the particle and the radiation field is conveniently described by two dimensionless numbers, termed 'efficiency factors', or 'efficiencies', defined as follows: The ratios of the radiative power absorbed within, or scattered by, the particle to the radiative power incident onto its geometrical cross-section define the efficiency factors, Q_a and Q_b respectively. These efficiencies are nothing other than the absorptance and scatterance (Section 4.2.1.2) at the level of a single particle exposed to radiation propagating as plane waves. The sum $(Q_a + Q_b) = Q_c$ is the attenuation efficiency. The products $\sigma_g Q_a$ and $\sigma_g Q_b$ are the absorption and scattering cross-sections (units m^2) of this particle. If now we consider a suspension of these particles (all the same, and either considered spherical or assumed all to be oriented similarly with respect to the incoming beam), with N particles per unit volume (m^{-3}), the bulk optical coefficients of the suspension are simply expressed as the sum of the individual contributions, so that

$$a = \mathrm{N}\,\sigma_g\,Q_a \quad \text{and} \quad b = \mathrm{N}\,\sigma_g\,Q_b, \tag{4.28}$$

or more generally,

$$a,b,c = \int_{\text{all } x} \mathrm{N}(x)\sigma_g(x)\,Q_{a,b,c}(x)\mathrm{d}x, \tag{4.28′}$$

where the particles are of varying size (x is a descriptor of the size), and form a population characterized by a particle number size distribution function N(x). Here, N(x) is the number (per unit volume) of particles having a size within the range ($x \pm \mathrm{d}x/2$). As b can be split into forward and backward components, b_f and b_b, Q_b is also the sum of the two corresponding efficiencies Q_{bf} and Q_{bb}, respectively. In (4.28′) the quantities σ_g and $Q_{a,b,c}$ depend on x, and here lies the interest of this approach. Indeed, whilst the bulk absorption and scattering coefficients, as previously defined, are not directly amenable to theory, the efficiencies can theoretically be predicted and the various cross-sections understood.

4.3.1 Theoretical approaches

4.3.1.1 General considerations

The so-called Mie theory provides an exact solution of the interaction of an electromagnetic field with a dielectric sphere (x in the previous expressions is replaced by diameter D). Not only the $Q_{a,b}(D)$ factors can be derived, but also the VSF. This theory

has been extended later to particles shaped otherwise (cylinders, spheroids etc.). Marine particles, as algal cells and debris, exhibit various shapes. To the extent that they are randomly oriented, a simplified approach consists of considering that, on average, they optically behave as spheres, and thus using Mie theory is an acceptable approximation (more sophisticated approaches have been developed, however, see e.g. Mishchenko et al., 1996). The parameters needed to enter the Mie computations are the relative size, α (with respect to the wavelength) and m, the relative index of refraction (with respect to that of the surrounding medium, i.e. water, n_w). They are thus defined as

$$\alpha = \pi D/\lambda_w, \text{ or } = \pi D n_w/\lambda_0, \tag{4.29}$$

where λ_w and λ_0 are the wavelengths in water and *in vacuo*, respectively, and

$$m = m_s/n_w, \text{ with } m_s = n_s - \mathrm{i}n'_s, \tag{4.29′}$$

and where m_s is the complex index of refraction of the substance forming the sphere (assumed homogeneous). It includes a real part, n_s (see Section 4.2.1.1), and an imaginary part n'_s directly related to the absorption coefficient a_s of the substance forming the particle (see Appendix 4.1), through

$$n'_s = a_s \lambda_0/4\pi. \tag{4.30}$$

Note that in (4.29′) it can safely be assumed that n_w is a purely real number (no absorption). This assumption is valid for the visible spectral domain (even in the red part of the spectrum where water absorption is high, the corresponding imaginary part does not exceed 1–4 10^{-8}). In what follows, m is simply noted as $m = n - in'$ (with $n = n_s/n_w$ and $n' = n'_s/n_w$). Mie theory provides, for spheres of any size and index, exact solutions for the efficiency factors and $\beta(\theta)$ (including the state of polarization of the scattered radiation, whatever the polarization of the incident radiation). Because of their complexity and numerical burden, computations were scarce and restricted to small particles for about 50 years; in the era of computers, they have become progressively more feasible, and are now easily carried out.

When the spherical particles are larger than the wavelength, and provided that their relative index of refraction (m) remains not far from unity, the anomalous diffraction approximation developed by van de Hulst (1957) can apply. This approximation provides the efficiencies (but not the VSF) through much faster computations. The condition of m being close to 1 translates into n_s close to n_w, and n'_s small. For all algal and other biological materials, like heterotrophic marine bacteria, organic detritus, for example, these conditions are amply met (an exception would be the calcite plates of coccolithophorids). Such living particles have a rather high water content (partial volume, $V_w > 50\%$, average 70%), and organic matter is not a highly refringent substance; therefore, their bulk refractive index cannot depart strongly from that of water (Aas, 1981; 1996). In addition, the organic compounds making up the algae (carbohydrates, proteins, lipids) have similar effects on the increment in refractive index, so that their varying proportions are unimportant in fixing the final index. The real part of the relative index ($n = n_s/n_w$) essentially depends on the partial volume of water, V_w, or as well on the carbon concentration within the cellular material, C_C, (as kg C m^{-3}, where m^{-3} refers to cell volume, not medium volume), according to (Morel and Ahn, 1990; Babin et al., 2003).

$$n = 1 + 0.158(1 - V_w) = 1 + 0.233 \times 10^{-3} C_C \quad (4.31)$$

Typical values for algae are around 1.05, corresponding to V_w = 68.5% and C_C = 214 kg C m^{-3}. Deviations with respect to (4.31) are expected as a consequence of the presence of other harder substances forming the external layer, or of gas vacuoles (also because of the influence of absorption on n – see below). Values between 1.01 and 1.07 have been observed for cultivated phytoplankters. Actually, these values were not directly measured by refractometry or immersion techniques (but see Jonasz et al., 1997). Instead, most of them were inferred from inversion of (4.28′), knowing the size function $N(D)$ together with $a(\lambda)$ and $b(\lambda)$, the absorption and scattering spectra (see below).

With their normally high pigment content, algal cells are strongly absorbing bodies. The mean absorption coefficient of the material forming the cells (assumed to be homogeneous) is as high as 10^5 m^{-1} in the (Soret) blue absorption band (440 nm) and in the red absorption band (675 nm) of the chlorophyll molecule; for isolated chloroplasts, even higher a_s values would be appropriate (such high absorption coefficients result because the pathlength is in the cell, or in the chloroplast, not the suspension of cells or chloroplasts). Nevertheless, such high a_s values lead to bulk n'_s values close to or below 10^{-2} (4.30). Therefore, the criterion for using the van de Hulst approximation is well satisfied for unicellular algae, as well as for organic debris and heterotrophic organisms, which are generally less coloured than phytoplankton.

Predictions similar to those (expressed by (4.31)) made for n from the carbon content are also possible regarding n'_s based on the intracellular chlorophyll content. This possibility, however, requires that chlorophyll predominates in fixing the a_s value (4.30). The absorbing effect of other pigments is generally weak near the chlorophyll *a* absorption peak (675 nm), thus a predictive relationship has been proposed for this wavelength (Stramski and Reynolds, 1993; Stramski et al. 2002)

$$n'(674) \approx 7.15\ 10^{-4}\ C_{chl} + \varepsilon, \quad (4.32)$$

where ε is a residual background (≈a few 10^{-4}), and C_{chl} represents the internal chlorophyll *a* concentration within the cellular material. This concentration ranges from less than 1 kg m^{-3} (for diatoms; Bricaud et al., 1988) to more than 15 kg m^{-3} for *Synechococcus* (Morel et al., 1993). Actually, because of the photoacclimation capacity of many phytoplanktonic algae, C_{chl} depends strongly on the light regime and growth conditions.

4.3.1.2 Anomalous diffraction approximation (van de Hulst approximation)

Because this approximation is very useful to interpret the optical behaviour of algal cells, it deserves some additional comments (more detailed presentations and applications to phytoplankton can be found in Morel and Bricaud, 1986; Morel, 1991). In the formulation of this approximation, the relative size and the relative complex refractive index are merged to form two new parameters ρ and ρ', defined as follows:

$$\rho = 2\alpha\,(n - 1) \quad \text{and} \quad \rho' = 4\alpha n'. \quad (4.33)$$

Q_a is an explicit function of ρ', whereas Q_c depends on both ρ and ρ'; the latter appears through the ratio $(1/2)(\rho'/\rho) = n'/(n - 1) = \tan\xi$. The scattering efficiency is then derived by subtraction as $Q_b = Q_c - Q_a$ (see full expressions and figures in Appendix 4.2).

Table 4.1 Typical values of optical parameters at two wavelengths and for three cell sizes

D (μm)	λ (**nm**)	**0.5**	**5**	**50**
α	400	5.26	52.6	526
	700	3.00	30.0	300
ρ (n = 1.05)	400	0.52	5.26	52.6
	700	0.30	3.00	30.0
ρ' (n' = 0.008)	675	0.1	0.996	9.96

Some important consequences result from this simple formulation. If a particle is non-absorbing (e.g. a heterotrophic bacterium, or by approximation an algal cell observed in green light where absorption is minimal, such as at 560 nm), n' and Q_a are zero, so that Q_b and Q_c are identical. Note that in this case the equation expressing Q_c becomes simple (Appendix 4.1). As soon as the particle is no longer purely a body (i.e. Q_a is non-zero), the scattering capacity is lowered. To the extent that Q_c is never enhanced, there is merely a redistribution of attenuation between Q_a and Q_b.

Other important features regarding the efficiencies emerge when the particle become large with respect to wavelength (large α, ρ and ρ' values). In such a situation, Q_c reaches its asymptotic value of 2, whereas Q_a tends towards 1, as does Q_b. The fact that $Q_c = 2$ is often referred to as the 'extinction paradox', as it implies that a particle is able to remove from the incident beam twice the amount of flux it can geometrically intercept. The paradox is only apparent, as diffraction around the particle diverts the (non-incident) radiation stream although it contributes to the total scattered flux originating from the particle.

Typical values of parameters α, ρ and ρ' are provided in Table 4.1 (Appendix 4.2), for spherical (phytoplanktonic) cells with diameters ranging from 0.5 μm to 50 μm; α and ρ are given for the two extreme wavelengths of the visible spectrum; for ρ', the selected wavelength is 675 nm, which corresponds to the red absorption peak of chlorophyll *a*.

4.3.2 Other aspects and consequences of the theory

4.3.2.1 Normal and anomalous dispersion

A perfectly transparent medium has an index of refraction (a pure real number) which slightly and regularly increases as the frequency increases (the wavelength decreases); for example, n_w for seawater (S = 35.00, at 10°C) increases from about 1.337 to 1.351, between 700 nm and 400 nm. This phenomenon is called normal dispersion.

When an absorption band occurs, (centred around a certain frequency ν_0, which corresponds to a natural resonant oscillation of the molecules), the imaginary part of the index is no longer zero and $n'(\lambda)$ exhibits a spectral pattern which is akin to the absorption feature (4.30). In this case, the electromagnetic theory predicts that the real part of the index is perturbed in the vicinity of the absorption band. With respect to its value far from this band (centred on λ_a), $n(\lambda)$ is depressed when $\lambda < \lambda_a$, and then enhanced after the absorption band (with $\lambda > \lambda_a$); $n(\lambda)$ is restored in its initial value exactly in the centre of the band (at $\lambda = \lambda_a$), and far from λ_a in an asymptotic manner. The n and n' spectral profiles are physically related through the anomalous refraction relationship, and mathematically connected (Ketteler-Helmoltz formulae) via the

difference ($v - v_a$) (see Appendix 4.3). Because of the presence of various pigments and various overlapping absorption bands, algal cells present a complex $n'(\lambda)$ spectrum. In turn, these complex features produce fluctuations in the $n(\lambda)$ spectrum (Figure A4.3-2), which are superimposed on the bulk mean value (4.31). This phenomenon has to be accounted for in computations (based on Mie theory or van de Hulst approximation). Indeed, ρ is indirectly connected to ρ' because of the physical interaction between n' and n (e.g. Bricaud and Morel, 1986; Stramski et al., 2001).

4.3.2.2 'Package effect' and 'specific' optical coefficients

From its definition (4.33) and using (4.29) and (4.30), it is easy to see that ρ' also represents the dimensionless quantity ($D\ a_s$), the product of the size and the absorption coefficient of the cellular material.

The efficiency for absorption, Q_a, is only a function of ρ', and this monotonous function starts from zero and increases asymptotically towards 1 (Appendix 4.2). Near zero, when the curve remains sufficiently close to its tangent at the origin, $Q_a \approx (2/3)\ \rho'$. Apart from this limiting case, the curvature induces the so-called 'package effect', that is a nonlinear response of the absorption capacity with respect to either the size or a_s. Indeed, a doubling of D (keeping a_s constant), or as well a doubling of a_s (with D constant) which would result from a doubling of the internal pigment concentration, does not induce a doubling of Q_a, but only an increase in Q_a by a factor less than 2. In the saturating portion of the curve (at high ρ' values), only a little increase can occur. The doubling of a_s may also result from a change in wavelength (without change in pigment or D); it will not be reflected by an identical change in Q_a, which results in 'flattening' the peaks of the spectrum. Because the cellular absorption coefficient (a_s) within phytoplanktonic cells are generally high, the packaging and consequent spectral flattening practically affect all species; although they are reduced, they still affect even the smallest – often heavily pigmented – species, such as *Synechococcus* or *Prochlorococcus* (Morel et al., 1993).

A 'specific' optical coefficient is defined as the optical coefficient that is obtained after it has been normalized with respect to a unit of concentration in a given substance. In spectrophotometry, specific absorption coefficients (or molar 'extinction coefficients' in chemistry) are widely used because they are physical constants, and are characteristic of a given molecule or ion. They allow an unknown concentration to be determined by dividing the measured absorption coefficient of the solution by the specific coefficient. The most commonly specific coefficient used in aquatic optics, is the chlorophyll-specific absorption coefficient. It is denoted $a^*(\lambda) = a_\phi(\lambda)/[\text{chl}]$, where $a_\phi(\lambda)$ is the fraction of the absorption coefficient (of a water body) that is due to the presence of algae, and [chl] represents the chlorophyll concentration within this water (mg m^{-3}); therefore $a^*(\lambda)$ is expressed as $m^2\ mg^{-1}$. By assuming a population of identical cells and using (4.28), also by noting that the concentration [chl] $= NvC_{chl}$, where v represents the volume of the individual cell, and C_{chl} the chlorophyll concentration within the material forming the cell, it follows that (λ omitted),

$$a^*_{susp} = N\sigma_g Q_a / NvC_{chl}. \tag{4.34}$$

For spheres, the σ_g to v ratio is 3/2 D, so that

$$a^*_{susp} = (3/2)Q_a / DC_{chl}. \tag{4.35}$$

The subscript susp specifies that this chlorophyll-specific coefficient may (actually does) differ from one, denoted a^*_{sol}, which would apply if the medium was continuous, or in other words, if the chlorophyll molecules were uniformly distributed within the medium (as in a 'hypothetical' solution). The absorption coefficient of the cellular material (a_s) is proportional to the internal concentration C_{chl}. Any increase in the product (DC_{chl}), and thus an equivalent increase in (Da_s), does not entail an identical increase in Q_a, but generally results in a smaller increase. Therefore a^*_{susp} is no longer a constant (as it is in chemistry, and for true solutions). Actually, it is always smaller (i.e. $a^*_{susp} < a^*_{sol}$) when the absorbing substance is contained within discrete entities, rather than being dissolved. This reduction can be quantitatively expressed by reintroducing in (4.35) the parameter ρ' ($= a_s D$),

$$a^*_{susp} = \frac{3}{2}\frac{Q_a(\rho')}{\rho'}\frac{a_s}{C_{chl}} = Q^*_a(\rho')\frac{a_s}{C_{chl}}, \tag{4.36}$$

which defines a new function $Q^*_a(\rho') = (3/2)\, Q_a(\rho')/\rho'$. A 'solution' would correspond to a situation where $D \to 0$, or $\rho' \to 0$. In such a case $Q_a \approx (2/3)\,\rho'$, so that $Q^*_a \to 1$; therefore $a^*_{sol} = a_s/C_{chl}$ (a relationship that can be straightforwardly obtained). The package effect can be quantified as the ratio

$$a^*_{susp} / a^*_{sol} = Q^*_a(\rho'). \tag{4.37}$$

The Q^*_a function, which decreases from 1 when ρ' (or D) approaches 0 and tends towards 0 when ρ' increases, provides a convenient scale to quantify the package effect. Depending on species and wavelength, Q^*_a values for cultured species range from nearly 1 (no package) to about 0.3 (Morel, 1991), and will probably be less in larger pigmented cells (not studied). Instances of chlorophyll-specific absorption varying in a ratio 1:8, and corresponding $a^*(\lambda)$ spectra are shown in Figure 4.6.

4.3.3 Modelling the optical properties of phytoplanktonic cells

4.3.3.1 Rationale for a model

The usefulness and relevance of a forward model deserves some comments. Why model what can be measured? Actually all the optical properties of algal cells (assumed to be properly isolated or cultured) are not easily accessible for experiments. This is particularly true for the VSF, for the backscattering coefficient (4.8′), and therefore for the contribution of algae to the reflectance spectrum (4.21). Resorting to a theoretical model is necessary and the model must first account for what is measurable before it can be employed for predicting those properties that are not within the reach of experiments. Moreover, when dealing with a natural planktonic community, the effect of the various species on the formation of the bulk optical properties can be estimated if a modelling tool is available to predict the optical behaviour of the main species forming the assemblage (Stramski et al., 2001). Such a tool must be validated before being used. The validation can be made case by case, using various phytoplankters (grown in monospecific culture experiments), and attempting to understand and reconstruct the optical properties that have been determined.

In principle, when the size distribution (expressed with respect to the size parameter, $N(\alpha)$, 4.29), and the spectral values of the complex refractive index, $m(\lambda) = n(\lambda) - in'$, are known, the Mie theory can be applied, and all the desired quantities (the efficiency factors and the VSF) can be derived (at least under the assumption of sphericity and

homogeneity). Practically, only the size distribution, and the optical coefficients $a(\lambda)$ and $b(\lambda)$, via $[c(\lambda) - a(\lambda)]$, can be experimentally determined. There is no direct access to $m(\lambda)$ so that the validation of the tool (measurements versus predictions) is never straightforward.

Briefly the operations are as follows (Bricaud and Morel, 1986). Using $a(\lambda)$ and N(D), (4.28′) can be inverted. In this way, an average efficiency factor for absorption, denoted $\bar{Q}_a(\lambda)$, can be obtained as

$$\bar{Q}_a(\lambda) = a(\lambda) / \int_{allD} N(D)\sigma_g(D)\, dD. \tag{4.38}$$

Note that this quantity is averaged over the entire polydispersed population and would apply to a monodispersed population with all particles having the same (mean) diameter, $\bar{D}$. Then (at each λ value), these 'experimental' $\bar{Q}_a$ values are compared with the 'theoretical' $\bar{Q}_a(\bar{\rho}')$ values (i.e. a convolution of the theoretical Q_a curve with the actual size distribution function). The $\bar{\rho}'$ values are iteratively derived from this comparison. As $\bar{\alpha}$ is known, n' can be obtained (4.33) at each wavelength.

As far as scattering is concerned, an experimental $\bar{Q}_b(\lambda)$ efficiency is computed in the same way as for absorption. Again, the actual value of the real part of the index is *a priori* unknown; it can be written (at each wavelength) $n = 1 + \varepsilon + f(n')$, where the increment ε (4.31) is a floating parameter, whereas the fluctuations due to absorption, denoted $f(n')$, can be assessed through the Ketteler-Helmoltz relationships (Appendix 4.3).

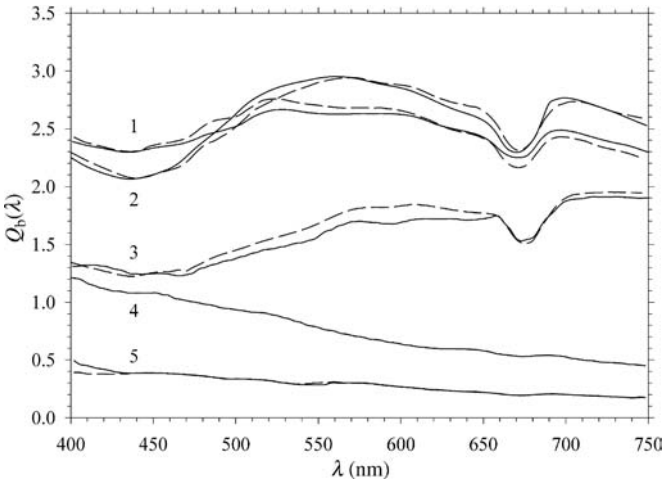

Figure 4.4
Spectral values of the efficiency factor for scattering as derived from scattering measurements, cell sizing and enumeration (solid curves), and corresponding modelled curves (dotted lines, see text). Species identifiers: 1, *Isochrysis galbana*; 2, *Chroomonas fragarioides*; 3, *Prorocentrum micans*; 4, *Anacystis marina*; and 5, *Synechocystis* sp.; with mean sizes 4.45 µm, 5.57 µm, 26.64 µm, 1.43 µm and 1.39 µm respectively, and with mean real part of the index of refraction (i.e. the quantity $1 + \varepsilon$), 1.055, 1.039, 1.045, 1.059 and 1.050 respectively.
Source: adapted from Ahn et al. (1992).

Through a comparison between the experimental $\bar{Q}_b(\lambda)$ efficiency and those derived from theory (Mie or van de Hulst), the value is determined by trial and error until agreement is reached (Figure 4.4). The closure is finally obtained by computing the $\bar{Q}_c(\lambda)$ spectrum and comparing it with the experimental spectrum. The extension consists of computing the VSF and, in corollary, the backscattering probability ($\tilde{b}_b = b_b/b$).

It is important to note that the above method fails if the ε value cannot be determined. This actually happens for large sized cells (when $\bar{\rho} < 15$, approximately), or for wide size distributions, because both these situations lead to a flat Q_c spectrum (with $Q_c \approx 2$), and leave the problem undetermined.

4.3.3.2 Main practical contribution and results from theoretical analysis

Regarding absorption, the essential contribution of theory is to bring to the forefront the existence of the package effect, with its consequence on the chlorophyll-specific absorption coefficient and its possible variations. Reconstruction of absorption spectra of algal cells from the knowledge of their pigment content and composition (via HPLC techniques) must account for this effect. Conversely, a comparison of measured and reconstructed spectra allows this effect to be quantified for natural populations (Bidigare et al., 1990; Nelson et al., 1993).

Other important contributions include the possibility of quantifying the impact of absorption on the refractive index (via the relationships between n and n'), and the capacity for understanding and predicting the features that appear in the scattering spectrum of algae (after having accounted for the n and n' interaction).

According to theory, algal cells scatter light predominantly in the forward direction, as a consequence of their rather large sizes (compared with the wavelength), and low relative index. Between forward (0°) and backward angles (120–180°), the VSF would span 4 to 8 orders of magnitude from the smallest to the largest algal species (Stramski et al., 2001). As a result of such a strong dissymmetry, the backscattering probability for phytoplankton is extremely low (Figure 4.5), of the order of 10^{-3} to 10^{-4}, where the highest values correspond to the tiniest cells. A restricted number of measurements, carried out with various phytoplanktonic species grown in culture, agree with the theoretical predictions (Ahn et al., 1992). Recent field data also confirm these low $\tilde{b}_b$ values (Twardowski et al., 2001).

With such low $\tilde{b}_b$ values, phytoplankton are a weak contributor to the backscattering coefficient of oceanic waters. Therefore, and in reference to (4.21), algae modulate the reflectance spectrum through their absorption coefficient, while the shift in ocean colour due to their presence is paradoxically detectable thanks to the presence of water molecules and other very tiny, mostly unidentified particles, or perhaps bubbles. Indeed, the backscattering probability increases when the size of the particles decreases (and is 1/2 for molecules). They are thus able to return light towards the atmosphere more efficiently than algal cells can do. Detached calcified liths, abundant during *Emiliana huxleyi* blooms, and filamentous cyanobacteria, with gas vesicles providing both buoyancy and enhanced scattering, are notable exceptions to the general rule of low algal $\tilde{b}_b$ values.

As a conclusion, the contribution of theory regarding the backscattering coefficient is currently essential, to the extent that experimental determinations have remained scarce until now. Plausible $\tilde{b}_b$ values are derived from Mie theory, combined with an assumed refractive index and an extrapolated size distribution function towards the small sizes, which at present are not detected by common instrumentation. The impacts

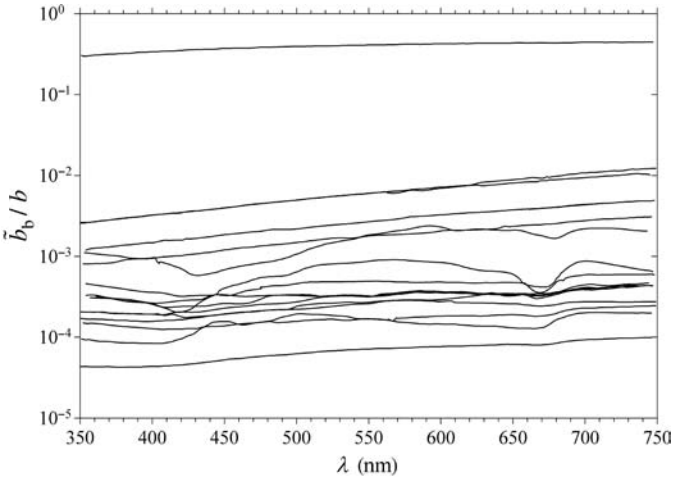

Figure 4.5
Spectral values of the backscattering probability, b_b/b, computed for 16 phytoplanktonic species (size range 0.59–27.6 µm) and for heterotrophic bacteria and viruses ($D = 0.55$ µm and 0.07 µm respectively). The lowest curve corresponds to a diatom (*Chaetoceros curvisetum*) and the highest one to viruses, which almost behave as Rayleigh scatterers (for which b_b/b would be exactly 1/2).
Source: adapted with permission from Stramski et al. (2001).

of absorption on scattering and backscattering are theoretically different; in other words $\tilde{b}_b$ would not be constant along the spectrum. There is experimental confirmation of such an effect *in vitro*, but not yet in field experiments, although the effect of absorption on scattering and backscattering is clearly observed in these experiments.

4.4 Field data and interpretation

4.4.1 Phytoplankton and other particles

Inanimate debris and heterotrophic organisms (viruses, bacteria, flagellates and larger protists) coexist with algal cells in natural waters. In so-called Case 1 waters, phytoplankton and their retinue of material of biological origin are in a first approximation co-varying, and are also the principal agents responsible for variations in optical properties. These waters (about 97% of the ocean) are encountered offshore, and even inshore when the terrestrial influence is negligible.

In contrast, within coastal Case 2 waters influenced by river (glacier) discharges, dissolved coloured (yellow) substances and suspended sediments are also present, and their concentrations vary independently from those of the phytoplankton. Mineral particles (such as in clays) are generally coloured, with an increasing absorption towards the shorter wavelengths (Babin et al., 2003). Sediment resuspension that may occur in shallow waters due to waves, currents and tidal action – also creates Case 2 waters along arid coasts – in the absence of land drainage.

In both Case 1 and Case 2 waters, there is a continuous size distribution of particles ranging from colloids and viruses to fishes and whales, that is spanning 9 to 10 orders of magnitude with respect to size. This distribution is characterized by an increasing number of particles with decreasing size, with a very steep ascending slope (Bader, 1970; Sheldon et al., 1972; Stramski and Kiefer, 1991). At least as a first approximation (but see Risovic, 1993), a power function (a 'Junge' distribution) reproduces this trend and was used for the first calculations dealing with scattering and the VSF (e.g. Morel, 1973; Brown and Gordon, 1974) and is still in use (e.g. Boss et al., 2001). This number size distribution expresses that the number N of particles per unit of volume, in the size interval from x to $x + \mathrm{d}x$, (or $D + \mathrm{dD}$ for spherical particles) depends on the size itself (μm) according to

$$N(x) = Kx^{-j}. \tag{4.39}$$

N is expressed as $\mathrm{m}^{-3}\ \mu\mathrm{m}^{-1}$, K sets the scale of abundance and j is the dimensionless Junge exponent, or the slope of the distribution (in a log-log representation the above expression leads to a straight line and the descending slope is equal to $-j$). The most commonly observed slope values are around -4, which means that there are 10^4 times more particles when the size is decreased by a factor of 10. Superimposed on this general monotonous trend, some features, such as knees and relative maxima, may occur and reveal the dominance of certain size class associated with the presence of particular planktonic species (within a bloom, for example). In any case, when dealing with the optical properties which, to various extents, are sensitive to all kinds of particles, the entire population with its size distribution has to be considered.

4.4.2 Variability of phytoplankton absorption in the natural environment

The varying spectral shape and magnitude of chlorophyll specific algal absorption has been abundantly documented through monospecific culture experiments, and these variations have been in general easily interpreted in the light of theory (pigment composition combined with packaging/flattening effects). The interpretation is more complex when dealing with mixed populations and natural assemblages, as found in oceanic environments (examples in Figure 4.6). In the field, the determination of spectral absorption can be carried out either on the particles retained onto a filter (Trüper and Yentsch, 1967), or directly on the water itself using appropriate equipment (e.g. the ac-9 profiler; Moore et al., 1995; see also Roesler and Boss, 2006 – Chapter 5 this volume). Note that in this case, the effect of absorbing dissolved substances has to be separately determined by repeating the measurement on filtered water (which is now feasible via in situ filtration), in order to assess the particulate absorption.

Whatever the method, phytoplankton and 'non-algal' particles contribute simultaneously to the measured absorption. When using the filter technique, the filter can be soaked in an appropriate solvent to remove pigment from the sample, and then the absorption measurement can be repeated on the extracted filter (Kishino et al., 1985); thus a possibility exists to determine separately the absorption spectrum of non-algal particles and then, by subtraction, to obtain the absorption spectrum of the algal cells only (at least approximately, as cell materials other than pigment, such as cell walls, remain after extraction). Therefore, the particle absorption coefficient, $a_p(\lambda)$, can be split into two partial terms, $a_\phi(\lambda)$ and $a_{NAP}(\lambda)$, corresponding to the phytoplankton compartment (subscript ϕ), and the non-algal particle compartment. The latter consist of

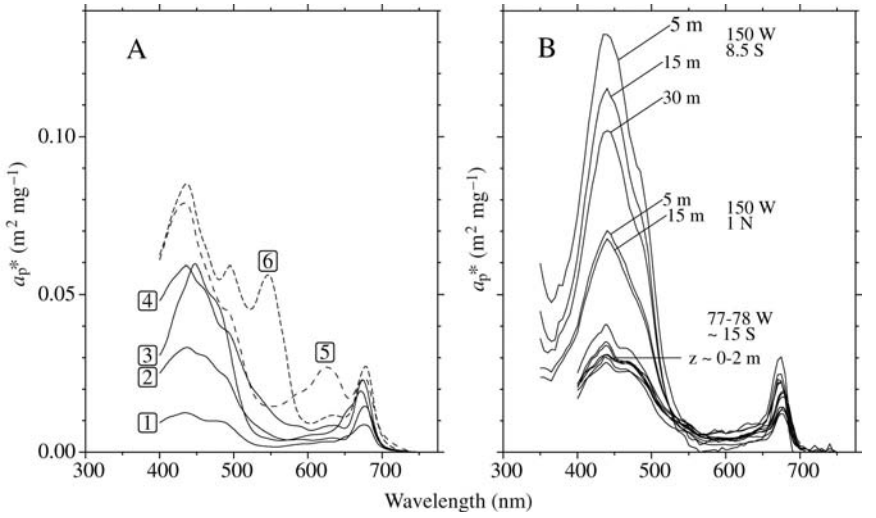

Figure 4.6
A, spectral values of the chlorophyll-specific absorption coefficients, $a^*(\lambda)$, measured on species grown in pure culture: 1, *Dunaliella bioculata*; 2, *Prymnesium parvum*; 3, *Chaetoceros curvisetum*; 4, *Prochlorococcus* sp.; 5, *Anacystis marina*; and 6, *Synechococcus* sp. Note that this coefficient actually is $a_\phi^*(\lambda)$, to the extent that the cultures are free from detritus. B, chlorophyll-specific particle absorption coefficients, $a_p^*(\lambda)$ determined at sea (filter technique) on natural samples at various depths; the spectra have been determined in three locations corresponding, from top to bottom, to oligotrophic, mesotrophic and eutrophic situations, with [chl] = 0.13 mg m^{-3}, 0.35 mg m^{-3} and 3 mg m^{-3}, respectively. Note that this coefficient actually is $a_p^*(\lambda)$, to the extent that the measurements are made using the filter technique, before the Kishino bleaching technique has been applied (see text); thus it involves all kinds of particles, although the contribution appears small in these cases.

living organic particles (e.g. bacteria, small heterotrophs, non-pigmented phytoplankton cellular material), detritus and minerals. These coefficients can be related to (i.e. divided by) the chlorophyll *a* concentration to derive the associate chlorophyll-specific coefficients $a_p^*(\lambda)$, $a_{NAP}^*(\lambda)$ and $a_\phi^*(\lambda)$. The non-algal particulate absorption is generally characterized by a monotonic increase towards the shorter wavelengths (e.g. Roesler et al., 1989; Bricaud et al., 1998), so that the features in the $a_p^*(\lambda)$ spectrum (the presence of maxima and minima) essentially results from the impact of algal absorption (a_ϕ).

By restricting the examination to particle absorption in Case 1 waters, several important features emerge. In a statistical sense, the shape of the $a_p(\lambda)$ spectrum is roughly speaking stable (Garver et al., 1994). This result is consistent with the observation showing that the proportions of the accessory pigments with respect to chlorophyll *a* remain, at least to a first approximation, rather steady (Trees et al., 2000). Nevertheless, within the accessory pigments' pool, significant variations in composition can be detected and interpreted in the context of changing species composition (Claustre, 1994; Vidussi et al., 2001). Exceptions to the general spectral pattern occur when phycobilin pigments are present (as in cyanobacteria) so that peculiar secondary absorption peaks

appear (around 545 nm and 625 nm, associated with phycoerythrin and phycocyanin, respectively. For pure cultures (see Figure 4.6), these peaks are noticeable, while in natural assemblages they are more discreet (Morel, 1997). In the same line, it must be pointed out that common toxic algal species contain the same pigments as do their harmless relatives (McLeroy-Etheridge and Roesler, 1998; but see Millie et al., 1997), so absorption spectra are certainly not a discriminating tool.

In contrast to the spectral shape, the chlorophyll-specific absorption coefficients for total particles or for phytoplankton only, $a^*_p(\lambda)$ and $a^*_\phi(\lambda)$, vary widely in magnitude, and somewhat surprisingly, in a regular manner (Yentsch and Phinney, 1989; Bricaud et al., 1995, 1998). Indeed, $a_p{}^*(\lambda)$ and $a_\phi{}^*(\lambda)$ systematically decrease by about 1 order of magnitude, from oligotrophic to eutrophic waters, namely when the chlorophyll concentration increases from 0.02 to 25 mg m^{-3} (Figure 4.7). Throughout this range, the contribution of $a_{NAP}(\lambda)$ to $a_p(\lambda)$ amounts to an average value of 25–35%. In oceanic waters however, large fluctuations with respect to this mean value (and in both directions) are occasionally observed, either with a reinforced influence of non-algal particles, or conversely an absorption spectrum similar to that of pure cultures. The rather regular decrease of the chl-specific absorption coefficients is in keeping with the package effect and taxonomic changes associated with the trophic status

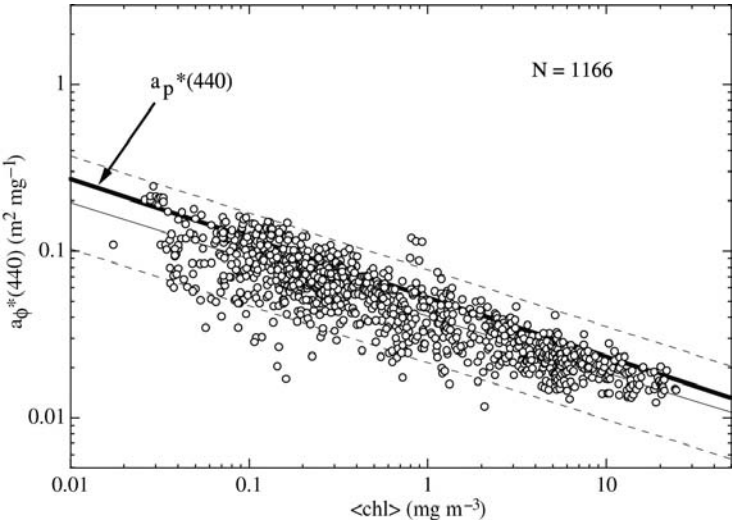

Figure 4.7
Chlorophyll-specific absorption coefficient of algae at the specific wavelength 440 nm, $a_\phi{}^*(440)$, measured in various locations in the world ocean, plotted as a function of [chl] in Case 1 waters ranging from oligotrophic to eutrophic situations.
The heavy line is the regression line ($r^2 = 0.90$) and the prediction interval is shown as dotted lines. The measurements are made using the filter technique, followed by the Kishino bleaching process to derive by difference the absorption by algae only (see text). The $a_p{}^*(440)$ values for the same samples (determined before the bleaching technique is operated), also submitted to the regression analysis, lead to (4.41), represented as a thin line.
Source: redrawn from data in Bricaud et al., 1998, plus additional data.

(Ciotti et al., 2002); the spectral 'flattening' which is also a characteristic of packaging, is also evident and is responsible for an observed regular variation in the normalized particulate absorption spectra (Ciotti et al., 2002; Bricaud et al., 2004). Oligotrophic waters are in general dominated by small sized, mainly prokaryotic cells (picoplankton), whereas eukaryotic nanoplankton and then large microplanktonic cells (diatoms, dinoflagellates) progressively prevail in mesotrophic and eutrophic waters (Malone, 1980). As a result of this change in the mean size, the package effect is more and more pronounced when the chlorophyll concentration in the water body increases, and thus $a_\phi^*(\lambda)$ steadily, albeit nonlinearly, decreases. Power functions are appropriate to reproduce these variations associated with the trophic status (Bricaud et al., 1995; 1998):

$$a_p^*(\lambda) = A_p(\lambda)[\text{chl}]^{-B_p(\lambda)} \text{ and } a_\phi^*(\lambda) = A_\phi(\lambda)[\text{chl}]^{-B_\phi(\lambda)}, \tag{4.40}$$

where the spectral coefficients, $A_p(\lambda)$, are always above $A_\phi(\lambda)$, by about 30% (and up to 100% in the green part of the spectrum, when phytoplankton absorption experiences its minimum); the negative exponents $-B_\phi(\lambda)$ and $-B_p(\lambda)$ are similar, weakly dependent on the wavelength, and of the order of -0.2 to -0.4. The fractional absorption due to particles, that is the product $a_p^*(\lambda) \times [\text{chl}]$, is therefore a nonlinear function of [chl]. At the blue and red absorption maxima (440 nm and 675 nm) for example, it can be fit by the power functions

$$a_p(440) = 0.052[\text{chl}]^{0.64} \text{ and } a_p(675) = 0.020[\text{chl}]^{0.82}, \tag{4.41}$$

and within the 550–620 nm (green-yellow) domain essentially corresponding to the non-algal background,

$$a_p(550,620) \leq 0.01[\text{chl}]^{0.85}. \tag{4.41'}$$

It is worth noting that the exponents vary throughout the spectrum. As a consequence, the shape of the a_p spectrum slightly changes with [chl], and becomes progressively flatter for high chlorophyll concentration. As a result, the change in spectral shape can be related to characteristics of the size distribution of the resident phytoplankton population (Ciotti et al. 2002). Obviously, there are no equivalent expressions for Case 2 waters where absorption may be variously influenced by non-phytoplanktonic particles.

4.4.3 Global particle scattering

In contrast to particulate absorption, which (in Case 1 waters) essentially results from the presence of phytoplankton, scattering originates from all kinds of particles, including the most transparent ones. Therefore, a relationship between b_p and [chl] may exist only if the chlorophyll-bearing particles and the non-algal particles roughly covary (not necessarily in a linear manner). This is approximately true in Case 1 waters, and significant (yet not tight) relationships have been statistically derived from field data over a wide range of chlorophyll concentrations (about 3 orders of magnitude; see Figure 4.8). A general expression, commonly used, is (Gordon and Morel, 1983).

$$b_p(550) = 0.3[\text{chl}]^{0.62}, \tag{4.42}$$

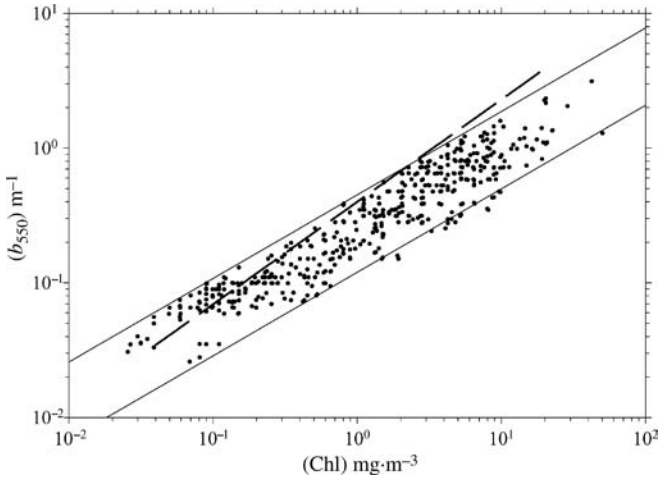

Figure 4.8
Simultaneous determinations of the scattering coefficient at 550 nm and [chl] in Case 1 waters. These 740 data points were used to derive (4.35), and the two parallel lines correspond to the limits of the coefficient, 0.15 and 0.45. The dashed line represents (4.35′), based on recent measurements and considering the upper layer only.
Source: redrawn from Gordon and Morel (1983).

where the leading coefficient actually varies between 0.15 and 0.45 to encompass all the field data in Case 1 waters. In turbid Case 2 waters, scattering is larger, corresponding to a coefficient exceeding 0.45. A relationship, more specifically valid for the upper layer, and based on recent measurements (Loisel and Morel, 1998) is

$$b_p(550) = 0.4\ [\text{chl}]^{0.76}, \qquad (4.42')$$

and is close to the upper limit of the previous expression. It is worth noting that the above relationships are of global nature and useful to distinguish between a wide range of optical environments and trophic levels. Within a region with a narrow range of chlorophyll concentration, or as a function of depth, important departures from the average are to be expected.

The wavelength (550 nm) lies within the absorption minimum of algae, in such a way that the scattering coefficient is minimally affected. Actually, the above coefficients (0.3–0.4, for $\lambda = 550$ nm) are not spectrally constant; for non-absorbing (or weakly absorbing) particles this coefficient is theoretically related to the slope (j) of the Junge size distribution function (4.39). It can be demonstrated (Morel, 1973; see also Boss et al., 2001) that if the particle size distribution encompasses a wide range (e.g. 0.02–200 µm), the coefficient is spectrally varying according to a power law expressed as $\lambda^{(3-j)}$. Therefore, with j around 4, the spectral dependency of the coefficient follows a λ^{-1} law, corresponding to a hyperbolic increase in $b_p(\lambda)$ towards the blue end of the spectrum. With j close to 3, the scattering spectrum would be flat. Actually, such regular patterns are more or less affected by depressions which coincide with the main algal absorption

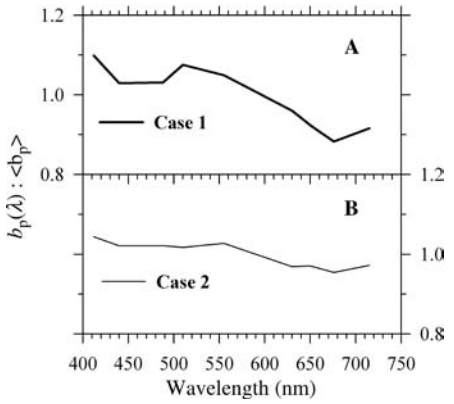

Figure 4.9
Particle scattering spectra normalized by their integral.
A, average spectrum for Case 1 waters (47 separate determinations in Atlantic and Mediterranean Sea).
B, average spectrum for Case 2 waters containing a considerable amount of mineral particles (192 determinations in the English Channel, North Sea, Baltic Sea and in the Rhone river plume in the Mediterranean).
Source: redrawn from Babin et al. (2003).

bands (Figure 4.9), and these will become more pronounced under HAB conditions where phytoplankton dominate the IOPs. These depressions, which obviously are more pronounced in Case 1 waters, tend to vanish in turbid Case 2 waters, inasmuch as absorption is no longer dominated by phytoplankton (Babin et al., 2003). For the same reason, say because the presence of sediments increases b_p independently from [chl], expressions such as (4.41) or (4.41′) are no longer valid in turbid Case 2 waters, so that predicting the scattering coefficient from [chl] becomes infeasible.

In Case 1 waters, particle absorption (4.41) and particle scattering (4.42) exhibit a similar nonlinear dependency (similar exponents) with respect to the chlorophyll concentration. The reasons are not the same, however. Whereas for absorption the package effect was the main reason for the nonlinearity, with respect to scattering, the varying proportions of algal and non-algal particles are more likely the proximate cause. Indeed, when b_p is regressed against the total particulate organic carbon (POC), a quasi-linear relationship emerges (Morel, 1988; Loisel and Morel, 1998); similar relationships for beam attenuation, c_p, have been postulated on a global basis (Mishonov et al., 2003). As POC can be considered as a reliable index of the whole particle population in Case 1 waters (when the contribution by inorganic particles is minimal), the difference in the exponents (from 1 when dealing with POC, down to about 0.7, when dealing with [chl]) indicates that the non-algal particles are in relative proportions more abundant in oligotrophic waters than in eutrophic waters. In other words, the POC/chl ratio decreases between these two trophic situations, as confirmed by direct chemical determinations.

The comparison of these equations (4.1–41′ and 4.2–42′) also shows that in Case 1 waters, particle scattering largely exceeds particle absorption, by a factor ranging from about 5 to 50, depending on the wavelength. In Case 2 waters, particularly in 'sediment-dominated' Case 2 waters, much higher *b*-to-*a* values are the rule.

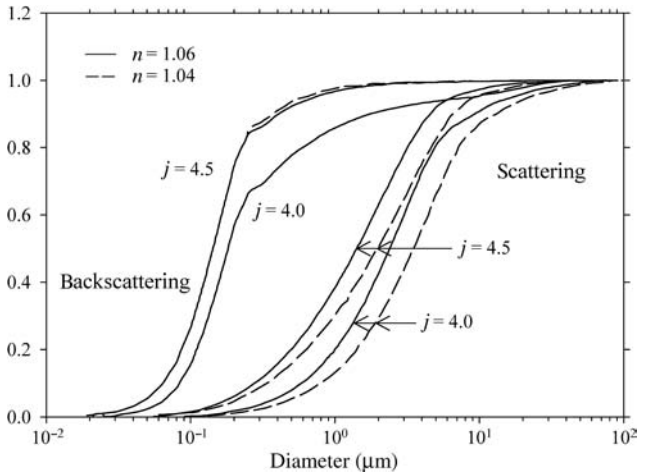

Figure 4.10
Progressive values of the integral (4.28′), when the lower limit is set at 0.01 μm and the upper limit is progressively increased to 200 μm (abscissae). The computed quantities are b and b_b, the scattering and backscattering coefficients; they are normalized with respect to the final values (obtained when $D = 200$ μm); the size distribution, N(D), is the power 'Junge' function (4.32), with $j = 4.0$ and 4.5; two values of the (real) refractive index are considered, as indicated, and are representative of biological material.
Source: redrawn from Morel and Ahn (1991).

Field data (in Case 1 waters) and theoretical predictions regarding total scattering agree rather well (see later, 'closure problem'), and for a simple reason, as follows. With a continuous size distribution as expressed by (4.32), the concept of an average geometrical size for the particle population is meaningless, but from an optical viewpoint, the situation is quite different. Indeed, the behaviour of the Q_b function combined with the size distribution function within (4.28′) results in a conclusion that b is predominantly due to a certain class of particles (Morel, 1973; Morel and Ahn, 1991; Boss et al., 2001). For example, with $j = 4$, the major part (90%) of scattering is due to particles in the size range from about 0.5–10 μm (Figure 4.10). With a mid-point at about 2 μm, 50% of the scattering is due to particles below this size, and 50% to particles above this size, which can be regarded as the average particle size with respect to the scattering process. Actually the mid-point position changes slightly with the j value (increases when j decreases), and with the real part of the index (increases when n decreases). Nonetheless, the most efficient contributors to the formation of scattering remain within this size range, which encompasses most of the photoautotrophic and heterotrophic organisms. As these organisms can be visualized and enumerated, their contribution to scattering can be estimated. Therefore the bulk scattering coefficient can be to a large extent explained.

4.4.4 Backscattering

The same reasoning for the backscattering coefficient (based on (4.28′) and using Q_{bb}, the backscattering efficiency computed through Mie theory) leads to a radically different

conclusion (Morel and Ahn, 1991). Under the same hypotheses (regarding j and n), the most efficient contributors to this coefficient appear to be in the 0.05–0.5 μm size range (Figure 4.10), that is below the current enumeration capability and detection limits of most of the commonly employed techniques.

As mentioned above, field data for the backscattering coefficient are still rather scarce, and systematic studies are in progress. New instruments and techniques are now available (e.g. Maffione and Dana, 1997; Lee and Lewis, 2002; Boss et al. 2004; Roesler and Boss, 2007 – Chapter 5 this volume), and the situation will almost certainly evolve in the near future. The first data in terms of particle backscattering probability (b_{bp} is essentially within the 0.5–2% range) are perfectly coherent with theoretical predictions (e.g. Twardowski et al., 2001; Zhang et al., 2002). However, the variation of this important term along with the chlorophyll concentration, as assumed in reflectance models for Case 1 waters (Gordon et al., 1988; Morel and Maritorena, 2001), remains to be consolidated by systematic field determinations.

4.4.5 IOP closure problem

In principle, the bulk optical IOPs can be explained by the sum of the specific IOPs of each category of materials recognized as being optically significant, combined with the knowledge of their concentrations. The closure is achieved when this operation is successful. Clearly, and within the range of acceptable uncertainties, it is the case when dealing with the absorption coefficient. For the scattering coefficient, the situation is less comfortable. Equations such as (4.42) or (4.42′) empirically express that the bulk scattering coefficient due to particles, b_p, is not a linear function of [chl] in Case 1 waters, and overall is not closely related to variations in [chl]. Experimental (*in vitro*) determinations, as well as theoretical approaches, tend to prove that b^* (the chlorophyll-specific scattering coefficient of algal cells) decreases from small cells to larger cells (Morel, 1987). This result must be accounted for when trying to reconstruct b_p. The contribution by heterotrophs, also assessed on the basis of experiments (bacteria, flagellates and ciliates) can be added. This estimate requires assumptions about the relative numerical abundance of these heterotrophic organisms with respect to that of algae (indeed, quantitative studies of this ecological balance remain scarce). Despite uncertainties and assumptions, such a budget based on the identified components roughly reproduces the average b_p values, as derived from (4.42) (Morel and Ahn, 1991). Actually the sum of these contributions seems to underestimate the field values, which leaves some room for scattering by various debris that is not represented among the identified components.

The same analytical attempt to account for the backscattering coefficient by summing the various contributions, leads to a completely different result and in effect raises a question. The algal compartment has a negligible influence on the backscattering coefficient; heterotrophic bacteria are more efficient contributors to the formation of b_p. Nevertheless, these bacteria and the picoplanktonic species in the same size range (≈0.5 μm), do not seem to account for more than 10% of b_{bp} (e.g. Brown and Gordon, 1973; Morel and Ahn, 1991; Ulloa et al., 1992). Paradoxically, the concentration of phytoplankton, a major product derived from ocean-colour remote sensing, only accounts for less than 5 percent of the particulate backscattering that sets the scale for the water-leaving radiance. As said before, the hardly identifiable, largely unknown submicrometre particles (Koike et al., 1990) may be considered as the dominant contributors to the backscattering coefficient of oceanic waters. The role of bubbles (Zhang et al., 1998, 2002) has also

been put forward for explaining this huge 'missing' backscattering (an increased scattering by algal cells associated with departures from sphericity has also been postulated).

4.5 Optical measurements and monitoring capabilities for HABs

The optical techniques to detect the onset of a bloom and to monitor its development can be operated *in situ* or remotely, from space or from an aircraft. In the first case, the water body is involved down to a depth which depends on the instrumentation arrangement, and it is possible to determine either the IOPs or AOPs. The most straightforward way relies on the use of IOPs directly related with those substances which are present in the water (see Section 4.1.1.4). In the case of remote detection (from satellite, airplane, or from a ship by operating above water measurements), only AOPs can be employed, and specifically the determination of a reflectance is the only parameter available. The solution of the inverse problem is thus necessary, even in a simplified and approximate manner (e.g. (4.21)), which necessarily entails some uncertainties. With such remote techniques, only the upper ocean is involved, with a sensing depth that depends on the wavelength and the water properties. This is a drawback, but, in some circumstances, it may be an advantage. Cyanobacterial blooms, for example, with a dense aggregation of organisms floating at the surface, are accessible to remote detection, even through a simplified approach, thanks to a high reflectivity (e.g. Kahru, 1997; Subramaniam et al., 1999). In contrast, the characterization of organisms, when dispersed and at low concentration within the water column, may remain questionable, or at least, far from providing a quantitative estimate of the importance of a deep bloom.

4.5.1 *In situ* techniques

Stimulated chlorophyll fluorescence, as measured by commercially available sensors and profiling instruments, provides an unambiguous signal attributable to the presence of phytoplankton. The quantitative interpretation of this signal is for many reasons uneasy (Babin, 2007 – Chapter 7 this volume). Nonetheless, in terms of strict detection, this selective response can be immediately interpreted and qualitatively useful.

Absorption measurements are less discriminating or selective than fluorescence. The limitation is particularly severe in Case 2 coastal waters, because of the possible presence of massive amounts of absorbing substances beside phytoplankton. A minimal caution is to determine a base line (for example at 650 nm and 715 nm), above which the absorption peak of chlorophyll (at 675 nm) can be selectively quantified. Although absorption by algae in the blue part of the spectrum (440–490 nm) is larger than at the red (675 nm) peak, this spectral signature is less distinct (even in Case 1 waters) because of interfering absorption by phaeopigments, non-algal particles or CDOM. In Case 2 waters, it can be completely drowned out by the huge absorption background due to high amount of dissolved coloured compounds, debris and sediments.

As a substitute for absorption, the diffuse attenuation coefficient for downwelling irradiance, $K_d(\lambda)$, can be used. Indeed, near the surface, this quantity, with some correction, is almost an inherent property (Gordon, 1989*a*, 1989*b*), according to $\mu_w K_d \cong a + b_b$, where μ_w is the cosine of the underwater sun-zenith angle (after refraction). As b_b is generally very small compared with a, the information provided by K_d is similar

to that discussed above for absorption. The same restrictions apply, and the same need for a choice of appropriate wavelengths persists. The advantage of such a measurement lies in its passive character (the source is the sun), while absorption measurements are an active technique requiring an artificial source and thus more energy (the obvious disadvantage is that the measurement is restricted to daylight hours).

The attenuation (and scattering) coefficients are also rather easily monitored through active techniques, and equipment is commercially available. As stated above, the scattering spectrum is less featured than the absorption spectrum. Because of the approximate compensating effects of absorption and scattering, the attenuation spectrum is quasi-monotonic and not strongly affected by the presence of algae. Information from such measurements cannot be selective; only a global estimate of the particle load is obtained, which in some circumstances (with ancillary information or *a priori* knowledge) may suffice to detect blooms.

If some specific signatures of harmful algae in the UV domain prove to be useful (Kahru and Mitchell, 1998), a dedicated instrumentation must be developed, as measurements in this spectral range are not common practice.

4.5.2 Remote techniques

Remote detection of chlorophyll *a* fluorescence by algae provides an interesting possibility (Gower and Borstad, 1981). In spite of being weak, the sun-induced (or 'natural') fluorescence signal can be detected from an aircraft and even from space. Dedicated satellite-borne instruments are currently in flight (the Medium Resolution Imaging Spectrometer MERIS and the two MODIS sensors). This signal is specific, and can be isolated from the background, thanks to appropriate channels on both sides of the fluorescence emission (for example at 660 nm and 709 nm for MERIS). Such an arrangement allows a baseline to be defined, and the fluorescence line height to be measured above this baseline. Because of the spectral proximity of the three channels, the fluorescence signal is weakly sensitive to inaccuracies that often result from the so-called atmospheric correction (the process by which the atmospheric backscattered signal is removed from the total signal recorded at top-of-atmosphere to derive the marine signal). For various environmental, biophysical and physiological reasons, the translation of the sun-induced fluorescence into a quantitative assessment of the chlorophyll concentration is complex and not free from considerable uncertainties (Sathyendranath, 1986; Babin et al., 1996).

Another characteristic of this kind of detection deserves some comment. The fluorescence signal is emitted near 685 nm, which is a wavelength where water is strongly absorbing. Therefore this signal can only originate from the very upper layer of the ocean. It has been shown (Babin et al., 1996) that in Case 1 waters, z_{90} (the depth of the layer from which 90% of the emerging fluorescence signal originates) is of the order 2–3 m in oligotrophic waters, and reduces to 1 m or less when [chl] reaches or exceeds 10 mg m^{-3}. For the detection of blooms consisting of buoyant algae concentrated in the top layer, this depth limitation is without consequence, but may be a serious drawback if the algal population is vertically dispersed over a thick layer, or if a bloom forms at depth. A potential difficulty is the shift of the fluorescence peak (685–705 nm) which seems to occur in case of very high organism concentration due to reabsorption of the fluoresced light (as in a red tide observed by Gower and Borstad, 1981); the establishment of a reliable baseline would cause a problem in such a case. Also, within dense accumulation of algae, reabsorption of the fluoresced light by adjacent cells results in a quenching effect, making a quantitative interpretation difficult.

The more conventional method for exploiting the information delivered by remote sensors consists of forming the ratio between marine reflectance at two wavelengths (two channels), and to relate such a ratio to [chl]. The rationale for this technique (applicable to Case 1 waters) is contained in (4.16). To the extent that b_b remains small and relatively constant spectrally compared with a, the $R(\lambda)$ spectrum would be a reversed image of the $a(\lambda)$ spectrum. Actually it is not the case, but the smooth spectral shape of $b_b(\lambda)$ is predictable, particularly when b_b is dominated by b_{bw}, (the backscattering coefficient of pure water). Therefore the inverted image of the $R(\lambda)$ spectrum resembles a sloped $a(\lambda)$ spectrum, with the main features preserved. When [chl] increases, absorption in the blue part of the spectrum increases, and reflectance decreases, whereas in the green part, a and thus R are only weakly changing. As a result, the ratio of two reflectances, one in the blue (at 443 nm or 490 nm) and the other in the green (at 560 nm) steadily decreases as [chl] increases. With high concentration, a peak in reflectance develops at the minimum of algal absorption (560–570 nm); the whole reflectance spectrum of eutrophic waters exhibits very low values and the water appears dark and green-brownish in colour. In contrast, oligotrophic waters ([chl] < (0.1 mg m^{-3}) appear bright and purple-blue in colour. This colour results from the combination of a low absorption in the blue part of the spectrum and the high backscattering efficiency of water molecules. Between these two extreme situations, there exists a gradual evolution of the $R(\lambda)$ spectrum with [chl], which can be accurately modelled for Case 1 waters (Figure 4.11), and is the basis for analytical algorithms, known as the 'blue-to-green ratio' technique.

This technique, of general use for Case 1 oceanic waters, fails in most Case 2 waters. The complex assemblages of various absorbing and scattering materials mask the simple evolutions of $a(\lambda)$ and $b_b(\lambda)$, which allow the colour ratio technique to be robust. More or less independently of their algal content, such waters may be very dark, with low $R(\lambda)$ values in the blue, when the yellow substance content is very high, or conversely extremely bright, whitish or turquoise green, when sediments dominate. Other interpretative methods are necessary (IOCCG, 2000); generally they are based on the simultaneous use of all channels, combined with nonlinear optimization techniques or neural network approaches (Sosik, 2007 – Chapter 8 this volume). In any case, the quantification of an algal biomass in the presence of heavy loads of terrigeneous particles and dissolved coloured substances is difficult because of inevitable physical limitations originating from the similarities of intermingled spectral signatures.

4.5.3 Other considerations

The previous considerations derive from a 'classical' optical point of view, and deal with water bodies inhabited by varying phytoplankton populations, in other words, they derive from a '3-D' marine optics approach. The situation may be completely different in some bloom situations. In effect, the distribution of algae may become almost a purely (horizontal) two-dimensional distribution, with a dense accumulation of floating organisms at the surface or a subsurface layer. There are at least two consequences. Firstly, the detection or assessment of such blooms via in-water techniques is obviously impeded; even sampling within the very surface or in a narrow layer may prove to be impractical. The definition of a concentration in such a case is rather difficult (as it is for algae colonies in ice, or for symbiotic zooxanthellae in corals). Secondly, the reasoning used to interpret the remote sensing data becomes obsolete, to the extent that the water itself is no longer an active component of the system (Roesler and

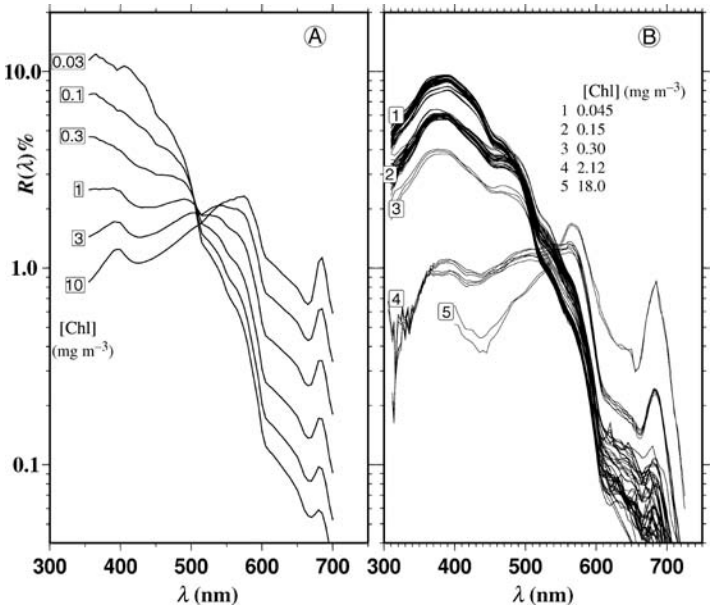

Figure 4.11
A, reflectance spectra, $R(\lambda)$ as in (4.15), produced by a semi-analytical model for Case 1 waters with varying chlorophyll concentrations (Morel and Maritorena, 2001). Note the semilog scale. The natural fluorescence peak (around 685 nm) is modelled by accounting for a varying absorption capacity of algae with [chl] (see Figure 4.7), an incident solar irradiation corresponding to a zenith sun angle of 30° in a clear sky, and by assuming a fluorescence quantum yield equal to 0.8%.
B, reflectance spectra determined at sea in various locations with the chlorophyll concentrations as indicated. The spectra labelled 1, 2 and 3 are for oligotrophic and mesotrophic waters in the central Pacific; the eutrophic waters, 4 and 5, were observed in the Moroccan and Mauritanian upwelling zones.

McLeroy-Etheridge, 1998). For example, the fact that water strongly absorbs the red radiation has a reduced impact on the reflectance, because algae spread out on the surface form a 'carpet' which tends to behave like terrestrial vegetation and mask the water body itself. This explains the possible surprising water colouring (or discoloration), which is visually observed and is at the origin of the term 'red or brown tides'. In effect, red (and near-infrared) radiation can be reflected by such surface assemblages, without being absorbed by water.

Another common aspect of this peculiar horizontal distribution is its patchiness, at scales generally well below the geometrical resolution of remote techniques (except for specialized airborne instruments). Therefore, within a pixel often co-exist signals from the very surface with its algal cover, and from the free water mass deprived from that cover (actually a similar situation occurs in the presence of foam and whitecaps and remains a problem for remote sensing techniques). There is no operational method for the interpretation of such complex radiometric observations and it probably requires a case by case examination and specialized observational platforms.

Appendix 4.1

Meaning of the complex index of refraction

In electromagnetic theory, energy is transported by electromagnetic waves in the direction corresponding to the Poynting vector; in the case of one-dimensional harmonic plane waves, propagating in the x direction, the electric field, E(V m^{-1}), in a plane perpendicular to the Poynting vector, at distance x and time t, is expressed as

$$E(x,t) = E_0 \exp i\,\omega[t - (m/c_0)x]$$

E_0 is a constant and the periodicity with respect to time and distance is expressed by the exponential function, where ω is the angular frequency ($=2\pi/T$, where T is the period),

or $\omega = 2\pi c_0/\lambda_0$. By replacing m by the complex number (n–in')

$$E(x,t) = E_0 \exp \mathrm{i}\omega\{t - [(n - \mathrm{i}n')/c_0]x\}$$

and by taking the real part, it becomes

$$E(x,\mathrm{t}) = E_0 \exp[-\omega(n'/c_0)x]\cos\omega\,[\mathrm{t} - (n/\mathrm{c}_0)x].\,,$$

where the periodic term involves the phase velocity in the medium (c_0/n), whereas the exponential represents a damping factor that affects the initial amplitude E_0, and depends on the distance travelled x and on n'. The flow of energy carried by electromagnetic radiation is proportional to the square of the electric field amplitude, $|E|^2$, then

$$|E|^2 = |E_0|^2 \exp[-2\omega(n'/c_0)x],$$

which in fact is similar to exp(–ax) (4.4), when the scattering coefficient $b = 0$, and the attenuation coefficient c reduces to a, the absorption coefficient. By identifying the terms, we obtain

$$a = 2\omega n'/c_0,$$

$$\text{or } a = 4\pi n'/\lambda_0,$$

and finally (4.30)

$$n' = a\lambda_0/4\pi.$$

In reference to the definition of inherent optical properties (Section 4.2.1), the complex index of refraction, m, represents simultaneously two IOPs (n and a, at a given wavelength), which is possible because a complex number is comprised of two numbers.

Appendix 4.2

Anomalous diffraction approximation (van de Hulst formulae)

The input parameters involved in the computations through this approximation (see also (4.29), (4.29′), (4.33)) are:

$$\rho = 2\alpha(n-1),\ \rho' = 4\alpha n'$$

$$\text{and } \tan\xi = n'/(n-1) = (1/2)(\rho'/\rho)$$

The conditions for applicability of this approximation are: the particles are considered to be homogeneous spheres, n must be close to 1, and n' small.

The efficiencies factors are expressed (van de Hulst, 1957) as

$$Q_c(\rho,\xi) = 2 - 4\exp(-\rho\tan\xi)[(\rho)^{-1}\cos\xi\sin(\rho-\xi) + (\rho)^{-2}\cos^2\xi\cos(\rho-2\xi)] + 4(\rho)^{-2}\cos^2\xi\cos(2\xi)$$

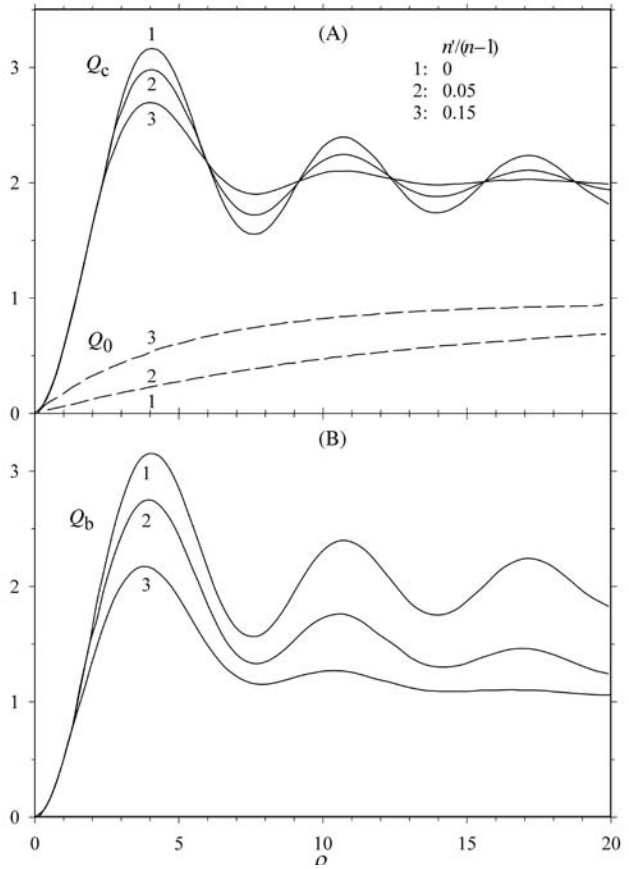

Figure A4.2-1
Variations of the efficiency factors with respect to parameter ρ.
A, Qc and Qa, for increasing absorption (curves 1, 2, 3), as indicated by the ratio $n'/(n-1)$, and starting from zero absorption.
B, Q_b for the same conditions. The asymptotic value for Q_c when ρ increases is 2 in all cases, however, the oscillations are smoothed faster when absorption takes place. The asymptotic values for Q_a and Q_b are in all cases 1 when ρ' is sufficiently large (the corresponding ρ value depends on the n′/(n – 1) ratio).
Source: redrawn from Morel and Bricaud (1986).

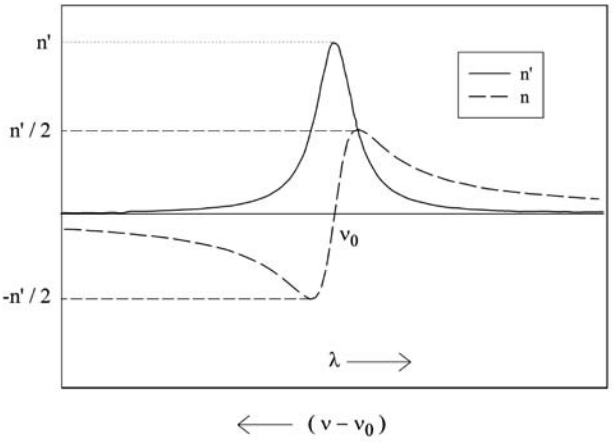

Figure A4.3-1
Variations of the imaginary part of the refractive index for an absorption band (harmonic oscillator with a resonant peak centred on ν_0), and those of the real part (dashed curve). For convenience they are plotted as a function of the wavelength (instead of frequency). Note that the amplitudes of the variations in n' and n are equal, and that the minimum and maximum in n coincide with the half amplitude in n'.

$$Q_a(\rho') = 1 + 2(\rho')^{-1}\exp(-\rho') + 2(-\rho')^{-2}[\exp(-\rho') - 1]$$
$$Q_b(\rho, \rho') = Q_c(\rho) - Q_a(\rho')$$

When there is no absorption $n' = \rho' = \tan\xi = 0$, and $Q_a = 0$ and $Q_c = (\rho) = Q_b(\rho)$ (see curve 1 in Figure A4.2-1),

and $Q_c(\rho)$ reduces to

$$Q_c(\rho') = 2 - (4/\rho)\sin\rho + (4/\rho^2)(1 - \cos\rho).$$

It is worth noting that when ρ and ρ' are large enough (i.e. when the spherical particles are sufficiently large and $n' \neq 0$), $Q_c(\rho)$ tends towards 2, $Q_a(\rho')$ tends towards 1, so that $Q_b(\rho, \rho')$ tends towards 1.

Typical examples of the α, ρ and ρ' values are provided in Table 4.1 for various spherical particles (diameter D)**.** In reference to the evolution of the Q parameters displayed in Figure A4.2-1, simple predictions are possible regarding the spectral shape of the attenuation and scattering coefficients for various phytoplankters. For a small particle (0.5 µm), (a *Prochlorococcus* cell, or a heterotrophic bacterium, for example,), ρ is in the range 0.3 (at 700 nm) to 0.5 (at 400 nm). Remember that for a given size, ρ and λ vary in an inverse manner. Such ρ values correspond to the initial ascending part of the Q_c and Q_b curves, so that the c or b spectra will exhibit a general descending slope from the blue towards the red part of the spectrum (see also Figure 4.4),

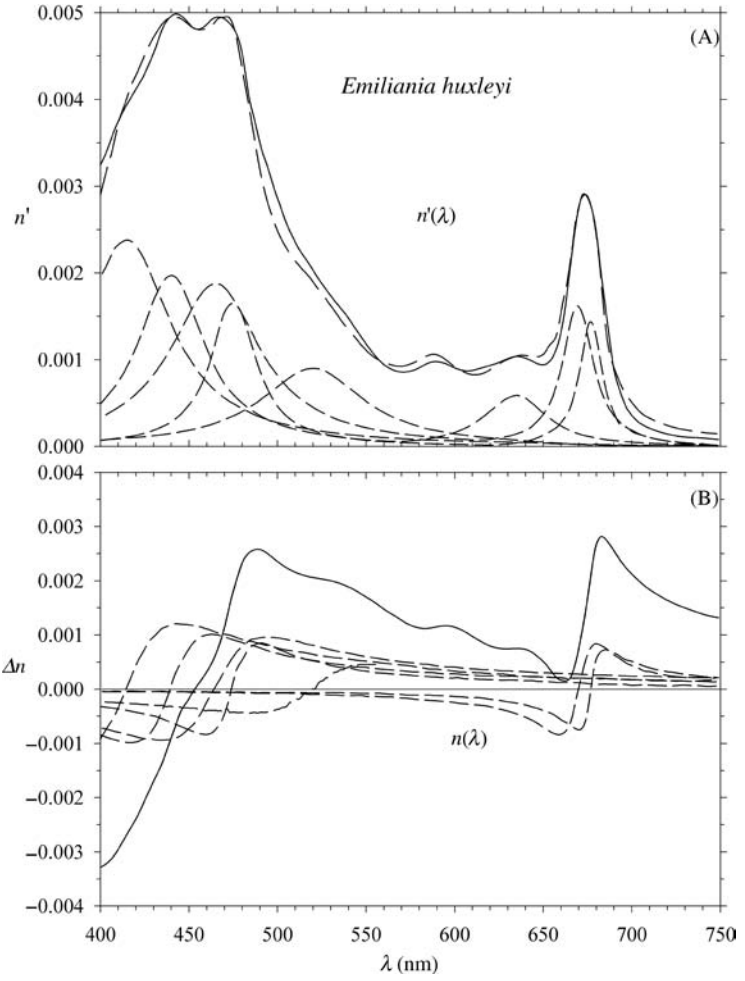

Figure A4.3-2
A, experimental $n'(\lambda)$ spectrum for a phytoplankter (*Emiliana huxleyi*, solid curve), and the reconstructed spectrum (dashed curve) obtained by summing nine separate harmonic oscillators (dotted curves).
B, spectral variations in the real part of the index (solid curve around a background value corresponding to $1 + \varepsilon$), which result from the added effects of the nine oscillators (dashed curves).

notwithstanding some features due to the impact of absorption bands. A converse situation can be observed, with an ascending slope from blue to red, when the ρ values are situated beyond the first maximum of the Q_c and Q_b curves (ρ varying from 4 to 8). A maximum may as well appear in the *c* or *b* spectrum, if the spectral variations in ρ encompass the first maximum (ρ centred on $\cong 4$). Because of the

effect of polydispersion, the other oscillations are barely observable with cultured phytoplankters. For large particles (e.g. with $D = 20$ μm or 50 μm), the Q_c curve becomes flat with a value around the limiting value 2; therefore the *c*-spectrum is also essentially flat, with which eventually the absorption features are superimposed.

These curves correspond to a single particle. For a population of particles of various sizes distributed according a function $N(D)$, a convolution of the previous curves with $N(d)$, transformed into $N(\rho)$, is necessary. The main result of such a convolution is to smooth the oscillations of the Q_c and Q_b curves in an extent which depends of the width on the size distribution function. Often, only the first oscillation and the first maximum remain distinctly marked.

1.9 Appendix 4.3

Anomalous dispersion

An absorption line corresponds to the existence in the medium of oscillators, with a natural resonant frequency, ν_0; this frequency is determined by a possible energy transition, specific of atoms or molecules forming the medium. This phenomenon ideally would lead to a monochromatic absorption line. However, in the close neighbourhood of the resonant frequency, some absorption occurs due to variations in rotational and vibrational energy. The natural broadening of the line and its half width are governed by a damping constant, typical of the involved oscillator. The shape of such an absorption band, once the absorption coefficient is transformed into the imaginary part of the index n', is expressed as

$$n' = K[1 / (1 + u^2)]$$

K represents the line strength, and the variable u is the quantity $(\nu - \nu_0)/\gamma$, where γ accounts for the damping effect. In turn, the correlative change in the real part of the index of refraction is expressed as

$$n' = 1 + \varepsilon - K[u / (1 + u^2)].$$

The term $(1 + \varepsilon)$ represents the value of the real part of the refractive index far from the absorption band, that is within the normal dispersion domain (and also exactly in the centre of the absorption band). These approximate formulae (Ketteler-Helmholtz) suppose that $\Delta\nu = (\nu - \nu_0)$ is small compared with ν_0, which is a safe assumption.

References

Aas, E. 1981. *The Refractive Index of Phytoplankton*. University of Oslo, Norway. (Institute Report Series 112.)

Aas, E. 1996. Refractive index of phytoplankton derived from its metabolite composition. *J. Plankton Res.*, 39, pp. 2223–49.

Ahn, Y. H., Bricaud, A. and Morel, A. 1992. Light backscattering efficiency and related properties of some phytoplankters. *Deep Sea Res.*, 39, pp. 1835–55.

Austin, R. W. and Halikas, G. 1976. *The Index of Refraction of Seawater.* La Jolla, Calif., Scripps Institution of Oceanography. (Reference 76-1.)

Babin, M., Morel, A., Fournier-Sicre, V., Fell, F. and Stramski, D. 2003. Light scattering properties of marine particles in coastal and open ocean waters as related to the particle mass concentration. *Limnol. Oceanog.*, 48, pp. 843–59.

Babin, M., Morel, A. and Gentili, B. 1996. Remote sensing of sea surface sun-induced chlorophyll fluorescence: consequences of natural variations in the optical characteristics of phytoplankton and the quantum yield of chlorophyll *a* fluorescence. *Int. J. Rem. Sens.,* 17, pp. 2417–48.

Babin, M., Roesler, C. S. and Cullen, J. J. (eds). 2006. *Real-time Coastal Observing Systems for Marine Ecosystem Dynamics and Harmful Algal Blooms: Theory, Instrumentation and Modelling*. Paris, Intergovernmental Oceanographic Commission of UNESCO. (Monographs on Oceanographic Methodology)

Bader, H. 1970. The hyperbolic distribution of particle sizes. *J. Geophys. Res.*, 75, pp. 2822–30.

Bartlett, J. S., Voss, K. J., Sathyendranath, S. and Vodacek, A. 1998. Raman scattering by pure water and. seawater. *Appl. Opt.*, 37, pp. 3324–32.

Bidigare, R. R., Ondrusek, M. E., Morrow, J. H. and Kiefer, D. A. 1990. *In vivo* absorption properties of algal pigments. *Ocean Optics X*, *Proc. SPIE*, 1302, pp. 290–302.

Boss, E., Pegau, W. S., Gardner, W. D., Zaneveld, J. R. V., Barnard, A. H., Twardowski, M. S., Chang, G. C. and Dickey, T. D. 2001. Spectral particulate attenuation and particle size distribution in the bottom boundary layer of a continental shelf. *J. Geophys. Res.*, 106, pp. 9509–16.

Bricaud, A., Babin, M., Morel, A. and Claustre, H. 1995. Variability in the chlorophyll-specific absorption of natural phytoplankton: analysis and parameterization. *J. Geophys. Res.*, 100, pp. 13321–32.

Bricaud, A., Claustre, H., Ras, J. and Oubelkheir, K. 2004. Natural variability of phytoplankton absorption in oceanic waters: influence of the size structure of algal populations. *J. Geophys. Res.*, 109, C11010, doi:10.1029/2004JC002419.

Bricaud, A. and Morel, A. 1986. Light attenuation and scattering by phytoplankton cells: a theoretical modeling. *Appl. Opt.*, 25, pp. 571–80.

Bricaud, A., Morel, A., Babin, M., Allali, K. and Claustre, H. 1998. Variations of light absorption by suspended particles with chlorophyll *a* concentration in oceanic (Case 1) waters: analysis and implications for bio-optical models. *J. Geophys. Res.*, 103, pp. 31033–44.

Ciotti, A. M., Cullen, J. J. and Lewis, M. R. 2002. Assessment of the relationships between dominant cell size in natural phytoplankton communities and the spectral shape of absorption coefficient. *Limnol. Oceanogr.*, 47, pp. 404–17.

Coble, P. G., Del Castillo, C. E. B. and Avril, B. 1998. Distribution and optical properties of CDOM in the Arabian Sea during the 1995 Southwest Monsoon. *Deep Sea Res.*, 45, pp. 2195–223.

Cullen, J. J., Ciotti, A. M., Davis, R. F. and Lewis, M. R. 1997. Optical detection and assessment of algal blooms. *Limnol. Oceanogr.*, 42, pp. 1223–39.

Garver, S. A., Siegel, D. A. and Mitchell, B. G. 1994. Variability in near surface particulate absorption spectra: what can a satellite ocean color imager see? *Limnol. Oceanogr.*, 39, pp. 1349–67.

Ge, Y., Gordon, H. R. and Voss, K. J. 1993. Simulation of inelastic scattering contributions to the irradiance field the ocean: variation in Fraunhofer line depths. *Appl. Opt.*, 32, pp. 4028–36.

Gordon, H. R. 1989*a*. Can the Lambert-Beer law be applied to the diffuse attenuation coefficient of ocean water? *Limnol. Oceanogr.*, 34, pp. 1389–409.

Gordon, H. R. 1989*b*. Dependence of the diffuse reflectance of natural waters on the sun angle**.** *Limnol. Oceanogr.*, 34, pp. 1484–89.

Gordon, H. R. and Clark, D. K. 1981. Clear water radiances for atmospheric correction of Coastal Zone Color Scanner imagery. *Appl. Opt.*, 20, pp. 4174–80.

Gordon, H. R. and Morel, A. 1983. *Remote Assessment of Ocean Color for Interpretation of Satellite Visible Imagery. A Review.* New York, Springer-Verlag.

Gordon, H. R., Voss, K. J. and Kilpatrick, K. A. 1993. Angular distribution of fluorescence from phytoplankton. *Limnol. Oceanogr.*, 38, pp. 1582–85.

Gower, J. F. R. and Borstad, G. A. 1981. Use of the *in vivo* fluorescence line at 685 nm for remote sensing surveys of surface chlorophyll *a*. In: J. F. R. Gower (ed.), *Oceanography from Space*. New York, Plenum Press, pp. 329–38.

Gower, J. F. R. and Borstad, G. A. 1991. An exceptional red tide event on the west coast of Canada mapped with AVHRR and imaging spectroscopy. *Proc. International Geoscience and Remote Sensing Symposium, IGARSS'91*, Helsinki.

Jonasz, M., Fournier, G. and Stramski, D. 1997. Photometric immersion refractometry: a method for determining the refractive index of marine microbial particles from beam attenuation. *Appl. Opt.*, 36, pp. 4214–25.

Kahru, M. 1997. Using satellites to monitor large-scale environmental change in the Baltic Sea. In: M. Kahru and C. W. Brown (eds), *Monitoring Algal Blooms: New Techniques for Detecting Large-scale Environmental Change*. New York, Springer-Verlag, pp. 43–61.

Kahru, M. and Mitchell, B. G. 1998. Spectral reflectance and absorption of a massive red tide off southern California. *J. Geophys. Res.*, 103, pp. 21601–09.

Kirk, J. T. O. 1984. Dependence of relationship between inherent and apparent optical properties of water on solar altitude. *Limnol. Oceanogr.*, 29, pp. 350–56.

Kishino, M., Takahashi, M., Okami, N. and Ichimura, S. 1985. Estimation of the spectral absorption of phytoplankton in the sea. *Bull. Mar. Sci.*, 37, pp. 634–42.

Koike, I., Hara, S., Terauchi, T. and Kogure, K. 1990. Role of submicrometer particles in the ocean. *Nature*, 345, pp. 242–44.

Loisel, H. and Morel, A. 1998. Light scattering and chlorophyll concentration in Case 1 waters: a reexamination. *Limnol. Oceanogr.*, 43, pp. 847–58.

Maffione, R. A. and Dana, D. R. 1997. Instruments and methods for measuring the backward-scattering coefficient of ocean waters. *Appl. Opt.*, 36, pp. 6057–67.

Malone, T. C. 1980. *Algal Size*. I: *The Physiological Ecology of Phytoplankton*. Morris, University of California, pp. 433–63.

Malone, T. C. 2007. Ecosystem dynamics, harmful algal blooms and operational oceanography. In: Babin et al. (eds), op. cit., this volume.

McLeroy-Etheridge, S. L. and Roesler, C. S. 1998. Are the inherent optical properties of phytoplankton responsible for the distinct ocean colors observed during harmful algal blooms? *Ocean Optics XIV*, *Proc. SPIE*, 1, pp. 109–16.

Millie, D. F., Schofield, O. M., Kirkpatrick, G. J., Johnsen, G., Tester, P. A. and Vinyard, B. T. 1997. Detection of harmful algal blooms using photopigments and absorption signatures: a case study of the Florida red tide dinoflagellate, *Gymnodinium breve*. *Limnol. Oceanogr.*, 42, pp. 1240–51.

Mishchenko, M. I., Travis, L. D. and Mackowski, D. W. 1996. T-matrix computations of light scattering by non-spherical particles: a review. *J. Quant. Spectros. Radiat. Trans.*, 55, pp. 535–75.

Mobley, C. D. 1993. Comparison of numerical models for computing underwater light fields. *Appl. Opt.*, 32, pp. 7484–505.

Moore, C., Zaneveld, J. R. V. and Kitchen, J. C. 1992. Preliminary results from an *in situ* spectral absorption meter. *Ocean Optics XI*, *Proc. SPIE*, 1750, pp. 330–37.

Morel, A. 1973. Diffusion de la lumière par les eaux de mer: résultats experimentaux et approche théorique. *AGARD Lect. Ser.*, 61, pp. 3.1.1–3.1.76.

Morel, A. 1987. Chlorophyll specific scattering coefficient of phytoplankton, a simplified theoretical approach. *Deep Sea Res.*, 34, pp. 1093–105.

Morel, A. 1988. Optical modeling of the upper ocean in relation to its biogenous matter content. *J. Geophys. Res.*, 93, pp. 10749–68.

Morel, A. 1991. Optics of marine particles and marine optics. In: S. Demers (ed.), *Particle Analysis in Oceanography*. Berlin, Springer-Verlag, pp. 141–88. (NATO Advanced Study Institute Series G27.)

Morel, A. 1997. Consequences of a Synechococcus bloom upon the optical properties of oceanic (Case 1) waters. *Limnol. Oceanogr.*, 42, pp. 1746–54.

Morel, A. and Ahn, Y. H. 1991. Optics of heterotrophic nanoflaggellates and ciliates: a tentative assessment of their scattering role in oceanic waters compared to those of bacterial and algal cells. *J. Mar. Res.*, 49, pp. 177–202.

Morel, A. and Bricaud, A. 1986. Inherent optical properties of algal cells including picoplankton: theoretical and experimental results. In: T. Platt and W. K. W. Li (eds), *Photosynthetic Picoplankton*. *Can. Bull. Fish. Aquat. Sci.*, 214, pp. 521–59.

Morel, A. and Gentili, B. 1991. Diffuse reflectance of oceanic waters: its dependence on sun angle as influenced by the molecular scattering contribution. *Appl. Opt.*, 30, pp. 4427–38.

Morel, A. and Gentili, B. 1996. Diffuse reflectance of oceanic waters. III: Implication of bidirectionality for the remote sensing problem. *Appl. Opt.*, 35, pp. 4850–62.

Morel, A. and Maritorena, S. 2001. Bio-optical properties of oceanic waters: a reappraisal. *J. Geophys. Res.*, 106, pp. 7163–80.

Mueller, J. L. and Fargion, G. S. 2002. *Ocean Optics Protocols for Satellite Ocean Color Sensor Validation*, Revision 3. Greenbelt, Md., NASA Goddard Space Flight Center.

Nelson, N. B., Prézelin, B. B. and Bidigare, R. R. 1993. Phytoplankton light absorption and the package effect in California coastal waters. *Mar. Ecol. Progr. Ser.*, 94, pp. 217–27.

Pegau, W. S., Cleveland, J. S., Doss, W., Dan Kenedy, C., Maffione, R. A., Mueller, J. L., Stone, R., Trees, C. C., Weidemann, A. D., Wells, W. H. and Zaneveld J. R. V. 1995. A comparison of methods for the measurement of the absorption coefficient in natural waters. *J. Geophys. Res.*, 100(C7), pp. 13201–20.

Preisendorfer, R. W. 1961. Application of radiative transfer theory to light measurements in the sea. In: *Radiant Energy in the Sea*. Boulder, Colo., International Union of Geodesy and Geophysics, pp. 11–30. (IUGG Monograph 10.)

Risovic, D. 1993. Two-component model of sea particle size distribution. *Deep Sea Res. I*, 40, pp. 1459–73.

Roesler, C. S. and McLeroy-Etheridge, S. L. 1998. Remote detection of harmful algal blooms. *Ocean Optics XIV*, *Proc. SPIE*, 1.

Sathyendranath, S. 1986. Remote sensing of phytoplankton: a review with special reference to picoplankton. In: T. Platt and W. K. W. Li, (eds), *Photosynthetic Picoplankton*. *Can. Bull. Fish. Aquat. Sci.*, 214, pp. 561–83.

Schofield, O., Gryzmski, J., Bissett, W. P., Kirkpatrick, G., Millie, D. F., Moline, M. A. and Roesler, C. 1999. Optical monitoring and forecasting systems for harmful algal blooms: possibility or pipedream? *J. Phycol.*, 35, pp. 125–45.

Sheldon, R. W., Prakash, A. and Sutcliffe W. H. Jr. 1972. The size distribution of particles in the ocean. *Limnol. Oceanogr.*, 17, pp. 327–340.

Stramski, D., Bricaud, A. and Morel, A. 2001. Modeling the inherent optical properties of the ocean based on the detailed composition of the planktonic community. *Appl. Opt.*, 40, pp. 2929–45.

Stramski, D. and Kiefer, D. A. 1991. Light scattering by microorganisms in the open ocean. *Progr. Oceanogr.*, 28, pp. 343–83.

Stramski, D. and Reynolds, R. A. 1993. Diel variations in the optical properties of marine diatom. *Limnol. Oceanogr.*, 38, pp. 1347–64.

Subramaniam, A., Carpenter, E. J. and Falkowski, P. G. 1999. Bio-optical properties of the marine diazotrophic cyanobacteria *Trichodesmium* spp. II: A reflectance model for remote sensing. *Limnol. Oceanogr.*, 44, pp. 618–27.

Trees, C. C., Clark, D. K., Bidigare, R. R., Ondrusek, M. E. and Mueller, J. M. 2000. Accessory pigments versus chlorophyll *a* concentration within the euphotic zone: a ubiquitous relationship. *Limnol. Oceanogr.*, 45, pp. 1130–43.

Trüper, H. G. and Yentsch, C. S. 1967. Use of glass-fiber filters for the rapid preparation of *in vivo* absorption spectra of phtosynthetic bacteria. *J. Bact.*, 94, pp. 1255–56.

Twardowski, M. S., Boss, E., MacDonald, J. B., Pegau, W. S., Barnard, A. H. and Zaneveld, J. R. V. 2001. A model for estimating bulk refractive index from the optical backscattering ratio and the implications for understanding particle composition in Case I and Case II waters. *J. Geophys. Res.*, 106, pp. 14129–42.

Ulloa, O., Sathyendranath, S. and Platt, T. 1994. Effect of the particle size distribution on the backscattering ratio in seawater. *Appl. Opt*., 33, pp. 7070–77.

van de Hulst, H. C. 1957. *Light Scattering by Small Particles*. New York, John Wiley & Sons.

Vidussi F., Claustre H., Manca, B., Luchetta, A. and Marty, J. C. 2001. Phytoplankton pigment distribution in relation to the upper thermocline circulation in the Eastern Mediterranean Sea during winter. *J. Geophys. Res*., 106, pp. 19939–56.

Yentsch, C. S. and Phinney, D. A. 1989. A bridge between ocean optics and microbial ecology. *Limnol. Oceanogr*., 34, pp. 1694–1705.

Zaneveld, J. R. V. 1989. An asymptotic closure theory for irradiance in the sea and its inversion to obtain the inherent optical properties. *Limnol. Oceanogr*., 34, pp. 1442–52.

Zhang, X., Lewis, M. R. and Johnson, B. 1998. The role of bubbles in the scattering of light in the ocean. *Appl. Opt*., 37, pp. 6525–36.

5

In situ measurement of inherent optical properties and potential for harmful algal bloom detection and coastal ecosystem observations

C. S. Roesler and E. Boss

5.1 Introduction

Until recently, oceanographers and other aquatic scientists depended on simple optical instruments, such as chlorophyll fluorometers and nephelometers or single-wavelength transmissometers, to estimate the respective distributions of phytoplankton and other suspended particles. During the last decade, technological advances and commensurate developments on optical modelling now make it possible to measure *in situ* and interpret the spectral inherent optical properties (IOPs) of the particulate and dissolved constituents of aquatic environments. The capability for estimating biogeochemical properties from optical measurements, which, in combination with moored, profiling and drifting platforms, has opened up new opportunities for studying ecosystem dynamics in general, and harmful algal blooms specifically, on time and space scales that were never before possible (Schofield et al., 2007 – Chapter 3 this volume). The limitations to this approach (i.e. IOP-based biogeochemical proxies) lie in the differences between the IOP theory (covered in Morel, 2007 – Chapter 4 this volume) and the IOP measurement reality that results from the physical and environmental limitations of instrumentation (covered in this chapter), and finally in the assumptions associated with incorporating observations into models (covered in Sosik, 2007 – Chapter 8 this volume).

The inherent optical properties of a medium describe the probability for light absorption and scattering, a and b respectively, and their sum, the beam attenuation c. A consequence of the Beer-Lambert-Buguer law (eg. Shifrin 1988) is that when the medium is a complex mixture of constituents, its bulk IOPs are expressed by the linear sum of the IOPs for each individual constituent:

$$a(\lambda) = \sum_{i=1}^{N} a_i(\lambda) \tag{5.1a}$$

$$b(\lambda) = \sum_{j=1}^{M} b_j(\lambda), \tag{5.1b}$$

where λ is wavelength, i and j indicate the individual constituents and N and M are the total number of absorbing and scattering constituents, respectively. In an aquatic medium, the bulk IOPs are the sum of the IOPs for water itself and all the solutes and

particles contained in it. Because it is an impossible task to measure the IOPs of each individual constituent, components are grouped operationally based on their spectral similarity or defined analytically.

Absorption is operationally separated into particulate and dissolved components where the separation is defined by the nominal pore size of a filter (typically 0.2–0.7 μm).[15] The dissolved fraction, while a very complex mixture of organic molecules, has an absorption spectrum with a relatively invariant spectral shape, decreasing nearly exponentially from the ultraviolet to the red end of the spectrum (Bricaud et al., 1981; Roesler et al., 1989; Babin et al., 2003; Twardowski et al., 2004; Figure 5.1).

The major variation is in the exponential slope coefficient, which responds to changes in composition and size distribution of the organic molecules (Carder et al., 1989; Yakobi et al., 2003; Twardowski et al., 2004). The absorption by particulate material (Figure 5.1) is further separated into phytoplankton and non-algal particles (NAP), the division of which is operationally based on extractive techniques in which the total particulate matter is chemically depigmented and scanned, and the difference between the total particle absorption and the depigmented particle absorption is the *in vivo* absorption by phytoplankton pigments (Ducha and Kubin, 1976; Kishino et al., 1985; Roesler and Perry, 1995). The non-algal particulate matter is composed of the non-pigmented portion of phytoplankton cells, bacteria and zooplankton, detrital material (which leads to the misnomer for this component as detrital absorption) and minerogenic and biogenic inorganic particles. The grouping of these diverse constituents into a single component is in part due to the extractive method separating them from the algal pigments and in part to the similarity in the absorption spectra, which also decays exponentially from blue to red, albeit with a different slope from the dissolved fraction (Iturriaga and Siegel, 1989; Roesler et al., 1989; Morel and Ahn, 1990, 1991). In regions with high minerogenic particle concentrations, separating the NAP absorption into organic and inorganic components has proved difficult because they are spectrally similar in the visible range (Stramski et al., 2001; Babin and Stramski, 2002, 2005) and because chemical or combustive methods to remove the organic material (i.e. Werdell and Roesler, 2003; Etheridge and Roesler, 2004) may not result in additive absorption coefficients (i.e. may not obey (5.1a)). For example, natural inorganic particles, which include both mineralic sediments and biogenic inorganic matter, are also subject to organic coating, causing them to resemble organic particles. Removing the organic coating, which is what may have contributed to the bulk of the *in situ* absorption, may reveal the underlying inorganic particle absorption, which was not necessarily contributing to the original bulk *in situ* absorption. Thus, unlike the extractive

[15] The selection of a single pore size to separate the particulate and dissolved fractions has not been resolved by the community, in part because neither truly removes all the particles from the medium, although obviously the 0.2 μm pore size is closest. However, a 0.7 μm pore size is used to find the total absorption coefficient of a discrete sample analysed spectrophotometrically: particles are concentrated on glass-fibre filters (nominal pore size 0.7 μm) and dissolved samples obtained from the filtrate. Summing the two provides the total absorption. If, however, the 0.2 μm filtrate is used for the dissolved fraction, the total absorption is significantly underestimated by the 0.2–0.7 μm fraction, which contains colloidal particles. *In situ* absorption measurements using the 0.2 μm filter are closer to the particulate/dissolved distinction but cannot hope to compare with discrete samples using the quantitative filter technique (which incorporates a 0.7 μm pore glass-fibre filter) and its filtrate. Thus, to compare *in situ* absorption observations with discrete ones, it is recommended that glass-fibre filters of nominal pore size 0.7 μm be used in both applications, with the understanding that the 'dissolved' fraction contains large colloidal particles, which have their own dynamics separate from particulate and dissolved fractions (e.g. Simeon et al., 2003; Etheridge and Roesler, 2004). Note also that filters are not perfect (eg. Logan 1993) and that filters change their characteristics as a function of use.

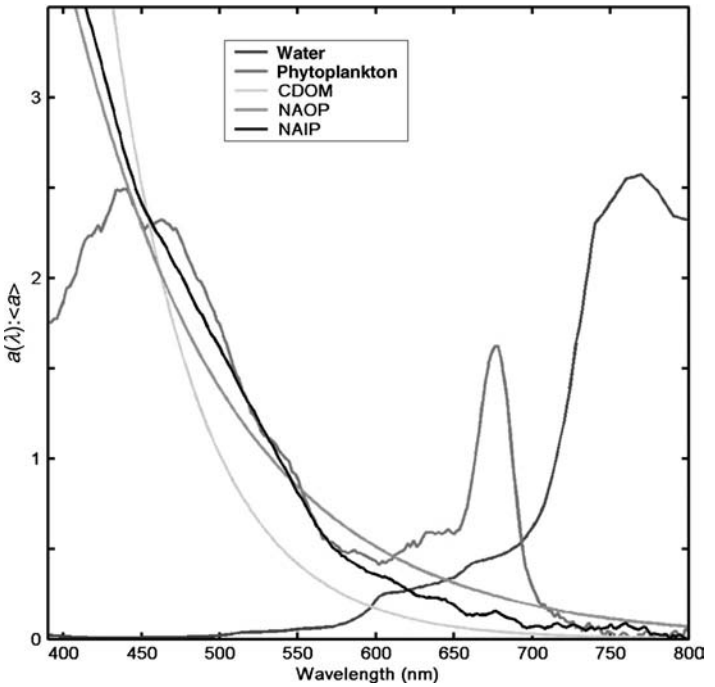

Figure 5.1
Characteristic absorption spectra for bulk seawater constituents normalized to the mean absorption: water, phytoplankton, coloured dissolved matter (CDOM), non-algal particulate organic matter (NAOP), non-algal particulate inorganic matter (NAIP).

technique to separate phytoplankton and non-algal particle absorption, which is additive, the organic and inorganic separation methodology is not additive and the resulting inorganic particle absorption may exceed NAP absorption, may exhibit distinctive peaks associated with minerogenic content (Babin and Stramski, 2002), or may be modified by the impacts of combustion (Babin and Stramski, 2005).

Particle scattering coefficients vary as a function of particle size and composition (the latter of which is manifested by the real and imaginary refractive indices;[16] Figure 5.2). For weakly absorbing particles, the scattering is a smoothly varying function of wavelength, the slope of which is related to the size distribution of the particles and the magnitude of which is a function of the concentration and the real index of refraction (itself a function of wavelength, e.g. Aas, 1996). For strongly absorbing particles such as phytoplankton, models predict that the scattering spectra exhibit distinct minima near the absorption peaks due to anomalous dispersion (van de Hulst, 1957; Morel and Bricaud, 1981; Zaneveld and Kitchen, 1995); such patterns are also observed in natural particle populations (Babin et al., 2002). By definition, the dissolved fraction

[16] Throughout this chapter, the indices of refraction are those relative to pure water. See also Morel (2007) and Lewis (2007) – Chapters 4 and 6 in this volume.

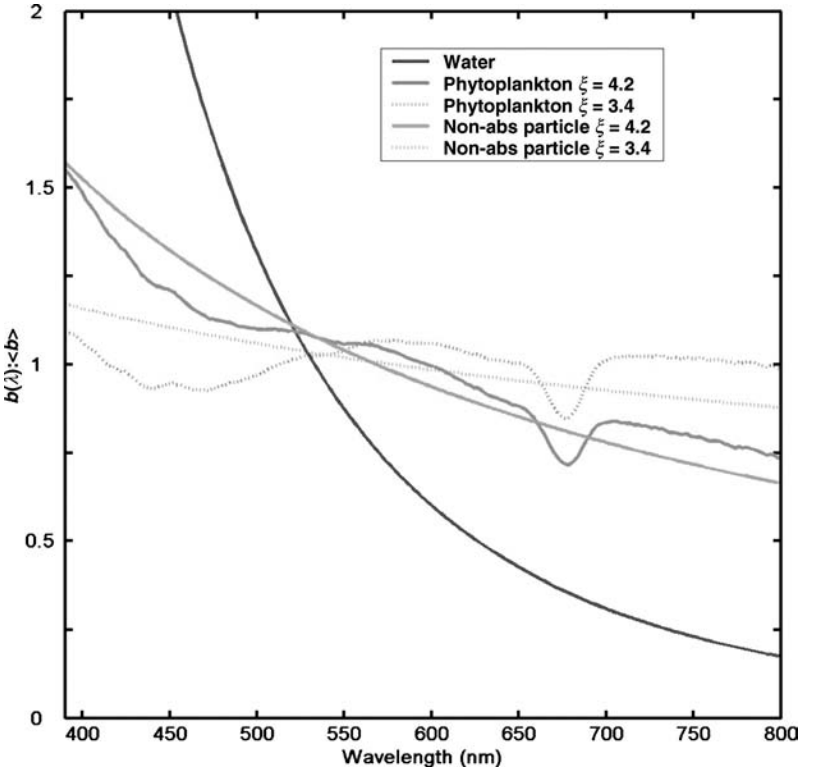

Figure 5.2
Characteristic scattering spectra for major constituents normalized to the mean scattering: water (darkest line), small and large phytoplankton (solid and dashed darker lines, respectively), and small and large weakly absorbing particles (solid and dashed lighter lines, respectively).

would not contribute to scattering other than that due to water itself and dissolved salts because it does not contain particles; however, the filtrate from even a 0.2 μm filter does contain submicrometre colloidal particles that do scatter light, as well as particles larger than the pore size, which pass through the filter due to both flexible pore boundaries and cell walls/membranes (e.g. Logan, 1993; Sosik et al., 2003). The angular dependence of scattering, described by the volume scattering function, also varies as a function of particle size and composition, as outlined in detail below.

To first order, the component IOPs can be decomposed into a multiplicative function of concentration and the concentration-specific IOP:

$$a(\lambda) = a_{\mathrm{w}}(\lambda) + C_{\phi} a^{*}_{\phi}(\lambda) + C_{\mathrm{CDM}} a^{*}_{\mathrm{CDM}}(\lambda) + C_{\mathrm{NAOP}} a^{*}_{\mathrm{NAOP}}(\lambda) + C_{\mathrm{NAIP}} a^{*}_{\mathrm{NAIP}}(\lambda) \quad (5.2a)$$

$$b(\lambda) = b_{\mathrm{w}}(\lambda) + C_{\phi} b^{*}_{\phi}(\lambda) + C_{\mathrm{NAOP}} b^{*}_{\mathrm{NAOP}}(\lambda) + C_{\mathrm{NAIP}} b^{*}_{\mathrm{NAIP}}(\lambda), \quad (5.2b)$$

where C indicates concentration,[17] a^* and b^* are the concentration-specific absorption and scattering coefficients,[18] w and φ indicate water including salts and phytoplankton, CDM indicates non-scattering chromophoric dissolved matter (operationally includes both organic and inorganic matter), and the non-algal particles are presented by both their organic and inorganic constituents (NAOP and NAIP respectively). To second order, these component IOPs vary as a function biogeochemical composition. Such variations are manifested as variations in the spectral shape of a^* and b^*, but may also affect the magnitude. For example, as the phytoplankton species composition and dominant size class change, the spectral shape of a_ϕ^* will vary in response to the changes in the *in vivo* composition and intracellular concentration of pigments (Bricaud et al., 1988; Sathyendranath et al., 1987; Sosik and Mitchell, 1991).

It is the dependence of the component IOPs, and hence the bulk IOPs, on the concentration, composition and size distribution that make them ideal parameters to include in coastal observation systems for monitoring ecosystem dynamics and harmful algal blooms. The recent explosion in opto-electronic technology and the resulting emergence of a suite of *in situ* IOP sensors, which can be deployed on a range of platforms, has yielded the capability, for the first time, of measuring biogeochemical indices at the same time and space scales as hydrographic and hydrodynamic properties, thereby permitting the relationships between environmental conditions and HAB events to be observed and quantified in real time. This capability lies at the heart of employing *in situ* IOP observations as an integral component of HAB detection. The key points are:

1. to measure the IOPs accurately,
2. to optimize the IOP measurements with respect to biogeochemical variability,
3. to quantify the IOP response to biogeochemical variations, and
4. to deconvolve the IOPs into the desired biogeochemical parameters (e.g. generate optical proxies for biogeochemical parameters – Claustre et al., 2000).

This chapter addresses points 1 and 2 in detail using examples from 3, while 4 is the subject of Chapter 8 (Sosik, 2007).

5.2 IOP concepts and measurement theory

The IOPs are defined as those properties describing the probability of photon removal and photon redirection per unit length. As outlined in Chapter 4 (Morel, 2007) these properties are the absorption, scattering and beam attenuation coefficients (a, b and c, respectively), where

$$c = a + b \tag{5.3}$$

and the volume scattering function (VSF; β). The VSF describes the angular distribution of scattering relative to the direction of light propagation θ and azimuthal angle ϕ. The scattering coefficient is the integration of β over all θ and ϕ (i.e. solid angles):

[17] The units on C will vary depending on normalization of the optical property. For example, if a^*_ϕ is the chlorophyll-specific phytoplankton absorption coefficient ($m^2\ mg^{-1}$), C_ϕ would be the chlorophyll concentration ($mg\ m^{-3}$). Likewise if b^*_{NAIP} is the mass-specific inorganic particle scattering coefficient ($m^2\ mg^{-1}$), C_{NAIP} would be the total inorganic particulate mass ($mg\ m^{-3}$).

[18] The concentration-specific component absorption and scattering spectra are determined either from natural samples that have been separated as discussed in the text. or generated in the laboratory from pure cultures (in the case of the phytoplankton component) or pure mineral suspensions (as in the case of NAIP).

$$b = \int_0^{2\pi} \int_0^{\pi} \beta(\theta,\phi) \sin\theta \, d\theta \, d\phi. \tag{5.4a}$$

In natural waters, where particles are assumed to be randomly oriented, azimuthal symmetry is assumed (i.e. scattering independent of ϕ) and the scattering coefficient is represented by:

$$b = 2\pi \int_0^{\pi} \beta \sin\theta d\theta. \tag{5.4b}$$

The backscattering coefficient is the integral of β over the backward hemisphere, relative to the incident radiance (Figure 5.3):

$$b_b = 2\pi \int_{\pi/2}^{\pi} \beta(\theta) \sin\theta \, d\theta. \tag{5.5}$$

The definitions of the IOPs with respect to measurement can be visualized by an infinitesimally thin layer (thickness Δr) of medium illuminated by a plane wave of monochromatic light incident perpendicular to the layer (Figure 5.4). The conservation of power indicates that the fate of the incident radiant flux, Φ_o, on this layer is either absorption, scattering or transmittance, where Φ_A, Φ_B and Φ_T are the absorbed, scattered and transmitted radiant flux, and, by conservation of energy:

$$\Phi_o = \Phi_A + \Phi_B + \Phi_T. \tag{5.6}$$

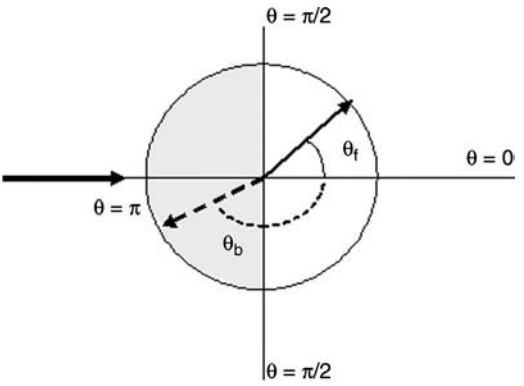

Figure 5.3
Diagram of the scattering angles θ, where the bold arrow at left signifies the incident beam, forward scattering is indicated by the solid arrow and angle θ_f and backscattering by the dashed arrow and angle θ_b. Forward scattering occurs in the forward white hemisphere ($\theta = 0$ to $\pi/2$) while backscattering occurs in the backward shaded hemisphere ($\theta = \pi/2$ to π) and azimuthal symmetry is assumed. In a bulk sense, the symmetry assumption holds in the ocean because, although particles are neither spherical nor homogeneous, they are randomly oriented (a consequence of hydrodynamic turbulence).

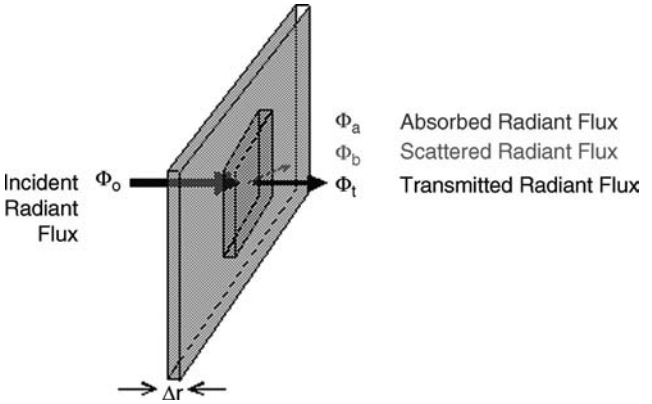

Figure 5.4
Conceptual diagram of radiant flux through an infinitesimal layer of thickness Δr. Energy is conserved such that the incident flux is either scattered by the layer, absorbed by material in the layer, or transmitted through the layer unattenuated.

The absorptance, scatterance and transmittance (A, B and T, respectively) are defined as the fractions of incident power absorbed, scattered and transmitted, and are given by (e.g. Kirk, 1994)

$$A = \frac{\Phi_A}{\Phi_o}, B = \frac{\Phi_B}{\Phi_o} \text{ and } T = \frac{\Phi_T}{\Phi_o}. \tag{5.7}$$

The absorption coefficient, a, is the absorptance per unit distance in the layer, Δr:

$$a = \lim_{\Delta r \to 0} \frac{A}{\Delta r} = \lim_{\Delta r \to 0} \frac{1}{\Delta r}, \tag{5.8}$$

Note the recovery of the far right term where $\Delta\Phi = \Phi A$, the loss of radiant flux over distance Δr, due to absorption ($\Phi_0 - \Phi_T$, for a non-scattering medium), and which in the limit yields

$$\int_0^r a \, \mathrm{d}r = \int_{\Phi(0)}^{\Phi(r)} \frac{1}{\Phi} \mathrm{d}\Phi, \tag{5.9}$$

where $\Phi(0)$ is the incident flux and $\Phi(r)$ is the radiant flux measured at r (ΦT). The absorption coefficient, with units of m^{-1}, is given by

$$a = \frac{-1}{r} \log_e \frac{\Phi(r)}{\Phi(0)}, \tag{5.10}$$

where $\Phi(0) = \Phi$. This equation yields two important pieces of information, first that the absorbed radiant flux is a function of path length (the longer the path, the greater the loss of radiant flux to absorption) and second, that the radiant flux decays exponentially along that path, a fact discussed in Morel, 2007 – Chapter 4 this volume.

Table 5.1 Notation

Symbol	Unit	Definition
A	dimensionless	Absorptance, the fraction of incident radiant power that is absorbed
a	m^{-1}	Absorption coefficient
a^*	$m^2\ mg^{-1}$	Concentration-specific absorption coefficient, e.g. a^*_{φ}, the chlorophyll-specific phytoplankton absorption coefficient has units of m^2 (mg chl)$^{-1}$
a_w, a_p, a_φ, a_{CDM}, a_{NAP}, a_{NAOP}, a_{NAIP}	m^{-1}	Absorption coefficients for water, particles, phytoplankton, CDM, NAP, NAOP, NAIP, respectively
B	dimensionless	Scatterance, the fraction of incident radiant power that is scattered
b	m^{-1}	Scattering coefficient
b^*	$m^2\ mg^{-1}$	Concentration-specific scattering coefficient, e.g. b^*_{NAOP}, might be expressed as the particulate organic carbon-specific scattering coefficient, with units of m^2(mg C)$^{-1}$
b_f, b_b	m^{-1}	Forward and backscattering coefficients, respectively
C	dimensionless	Attenuance, the fraction of incident radiant power that is absorbed or scattered
c	m^{-1}	Beam attenuation coefficient
c_p	m^{-1}	Particle beam attenuation coefficient
CDM (CDOM)		Chromophoric (coloured) dissolved (organic) matter, operationally defined by nominal pore size, generally 0.2–0.7 μm
NAIP		Non-algal inorganic particles, including mineralic sands, clays and biogenic silica and carbonate
NAOP		Non-algal organic particles, including bacteria, zooplankton, detritus
NAP		Non-algal particles, NAOP + NAIP, operationally defined as the particulate material left on a filter after extraction of algal pigments
D	μm	Particle diameter
n, n'		Real and imaginary indices of refraction relative to water
N	Particles m^{-3}	Particle concentration
r	m	Distance
T	dimensionless	Transmittance, the fraction of incident radiant power that is transmitted
β	$m^{-1}\ sr^{-1}$	Volume scattering function

Table 5.1 (*Continued*)

Symbol	Unit	Definition
γ	dimensionless	Slope of the power function fit to spectral particle beam attenuation coefficient
λ	nm	Wavelength
θ	degree	Zenith angle
ϕ	degree	Azimuth angle
$\mathbf{\Phi}$, $\mathbf{\Phi}_o$, $\mathbf{\Phi}_r$, $\mathbf{\Phi}_a$, $\mathbf{\Phi}_b$, $\mathbf{\Phi}_t$	mol photon s^{-1} or watts	Radiant flux, with subscripts o, r, a, b, t indicating incident, at distance *r*, absorbed, scattered, transmitted, respectively
ξ	dimensionless	Slope of the power function fit to particle size distribution, also called Junge slope when equal to 4

Thus, in a scattering medium, the measurement of the absorption coefficient can be determined from observations of the incident radiant flux and the radiant flux that is not lost to absorption over path length *r*, i.e:

$$a = \frac{-1}{r} \log_e \frac{\mathbf{\Phi}_B + \mathbf{\Phi}_T}{\mathbf{\Phi}_o}. \tag{5.11a}$$

If there is no scattering in the medium, the numerator simplifies to the transmitted radiant flux, $\mathbf{\Phi}_T$. Similar arguments hold for the scattering and beam attenuation coefficients as well as the VSF:

$$b = \frac{-1}{r} \log_e \tag{5.11b}$$

$$c = \frac{-1}{r} \log_e \frac{\mathbf{\Phi}_T}{\mathbf{\Phi}_o} = \frac{-1}{r} \log_e T \tag{5.11c}$$

$$\beta(\bar{\theta}) = \frac{\int_{\phi_1}^{\phi_2} \int_{\theta_1}^{\theta_2} \beta(\theta') \sin\theta' \, d\theta' \, d\phi'}{\int_{\phi_1}^{\phi_2} \int_{\theta_1}^{\theta_2} \sin\theta' \, d\theta' \, d\phi'} = \frac{-1}{r\Delta\Omega} \log_e \frac{\mathbf{\Phi}_o - \mathbf{\Phi}_{B'}}{\mathbf{\Phi}_o}, \tag{5.11d}$$

.

$$\text{and } \Delta\Omega \equiv \int_{\phi_1}^{\phi_2} \int_{\theta_1}^{\theta_2} \sin\theta' \, d\theta' \, d\phi'.$$

Equation (5.11c) indicates that the beam attenuation coefficient is theoretically related to transmittance *T*. However, because *T* is a relative quantity, it is usually reported as a percentage and reported with the path length over which it was measured (i.e. 77% transmission in a 25 cm path, relative to water). The integral on the left of the equal sign in (5.11d) is the scattering coefficient within a solid angle ($\Delta\Omega$) defined by

the ranges θ_1 to θ_2 and ϕ_1 to ϕ_2, and $\Phi_{B'}$ is the scattered radiant flux integrated over all angles except for the solid angle defined by the range θ_1 to θ_2 and ϕ_1 to ϕ_2.

The key to accurate measurements of these IOPs is the capability to configure instrumentation such that the appropriate radiant flux components are accounted for. The key to accurate interpretation of these IOPs with respect to biogeochemical information is in part dependent on the resolution and limitations of *in situ* IOP measurement and in part on the sensitivity of the measured coefficients to variations in the biogeochemical properties.

One theoretical tool used to study the interaction of light and matter is Mie theory, which yields the IOPs associated with monochromatic light impinging on a homogeneous sphere of a given size and complex refractive index (Mie, 1908). The real part of the index of refraction indicates how the speed of light changes between the particle and the medium while the imaginary part is proportional to the wavelength times the absorption of the material (e.g. van de Hulst, 1957; Morel, 2007 – Chapter 4, Appendix 4.2 this volume). Such modelling has been found to be very useful in interpreting *in situ* IOPs (e.g. Morel, 1973; Gordon, 1974; Twardowski et al., 2001) as well as predicting IOPs for which no measurement was available (e.g. backscattering in Stramski and Kiefer, 1991). It is noteworthy, however, that the limitations imparted by the assumption of sphericity (Bohren and Hufmann, 1983) and homogeneity (Bricaud et al., 1992; Kitchen and Zaneveld, 1992; Zaneveld and Kitchen, 1995) have not been fully investigated for oceanic particles (but see Calvano et al., 2007).

Throughout this manuscript we will assume a simple theoretical size distribution of idealized particles given by a power-law (sometimes referred to as hyperbolic or Junge-like) function, described by:

$$N(D)\,\mathrm{d}D = C_N D^{-\xi} \tag{5.12}$$

where D is diameter (m), $N(D)$ is the number of particles per volume in the interval between D and $D + \mathrm{d}D$ (particles $\mathrm{m}^{-3}\ \mu\mathrm{m}^{-1}$), C_N is a constant proportional to the particle concentration (particles m^{-3}) and ξ is the power-law slope (dimensionless). Equation (5.12) has been found to capture much of the first order variability observed in oceanic particles size distributions for the range of particles most likely to affect the IOPs (Bader, 1970; Morel, 1973; and see discussion in Stramski and Kiefer, 1991 and Twardowski et al., 2001), although this cannot be verified quantitatively for particles below ~0.5 μm, due to the difficulty in detecting them with routine instrumentation. One example where the power-law distribution is not a good approximation of the oceanic particle size distribution (PSD) is during monospecific algal blooms when the algal cell size distribution is better predicted by a Gaussian or lognormal distribution and this distribution skews the total PSD away from the power-law shape. In two illustrative examples below we will superimpose a Gaussian population of phytoplankton on top of a background hyperbolic distribution (e.g. Bricaud et al., 1995) to demonstrate the impact of a bloom on IOPs.

5.3 IOP measurement reality

It should be stated up front that it is *impossible* to measure the IOPs as defined theoretically in the previous section due to errors incurred by physical and electronic limitations in instrumentation; for example, transmitted photons cannot be detected in the absence

of near forward scattered photons because of the limitation on the size of the detector solid angle. That said, IOPs can be estimated with significant accuracy with proper instrument characterization and corrections for limitations. The instrument elements of interest are the source beam, the sample compartment or interrogation volume, and the detector, the configurations of which determine which IOP is being measured and what corrections have to be applied (e.g. Bricaud et al., 1995; Mueller et al., 2003).

5.3.1 Beam attenuation coefficients measured with c-meters (transmissometers)

The ideal instrument configuration for measuring the beam attenuation coefficient should meet a number of criteria so that the measurement follows the theoretical constraints. The source beam should comprise a plane wave such that all photon rays are traveling parallel to one another. The beam width should be as small as possible relative to the instrument length (Tyler et al., 1974), yet large relative to the detector field-of-view and the size of the suspended particles (Shifrin 1988) to avoid edge effects. The geometric path length should be of an appropriate length for the water type so that the sample is optically dilute (i.e. in which multiple scattering is negligible, for example a 5 cm path for turbid coastal waters and a 25 cm path for clear oceanic waters). The detector should have an infinitely small acceptance angle to exclude far-forward scattered light. While most of these configuration constraints can be achieved, there are physical limitations to the detector acceptance angle and thus some portion of the forward scattered beam is collected as transmitted flux. The magnitude of this error is a function of the acceptance angle of the detector and the shape of the volume scattering function for the medium. In the ocean, the volume scattering function undergoes the greatest rate of increase with decreasing scattering angle (e.g. far-forward scattered light; Figure 5.5) and thus this error can be very significant, as demonstrated below, section 5.5.8 and instrument-to-instrument comparisons of beam attenuation

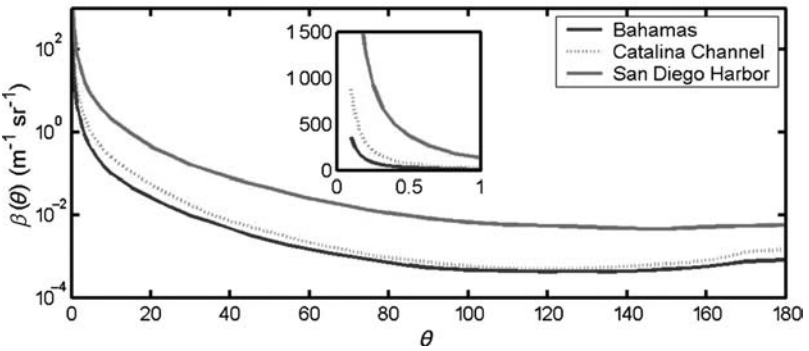

Figure 5.5
Volume scattering functions (VSFs) observed for natural waters from three optically diverse environments: clear open ocean Bahamas (bottom), coastal Catalina Channel (middle), and turbid San Diego Harbor (top). *Inset*: the VSFs for the first degree of forward scattering on a linear scale. Beam transmissometers have finite acceptance angles that capture this far forward scattered light and attribute it to unattenuated flux.
Source: data from Petzold (1972).

Table 5.2 Configuration specifications for commercially available beam attenuation meters

Instrument	Beam source	Beam width (mm)	Acceptance angle (°)	Path length (cm)
AlphaTracka transmissometer	Light emitting diode (LED)	15	0.86	5
SeaTech transmissometer	Collimated incandescent bulb	7	1.5	25
Sequoia LISST	Solid state diode laser	6	0.069(B), 0.006(F)	5, 10
WET Labs ac9, acs	Collimated incandescent bulb	10	0.93	25, 10
WET Labs cstar	LED	10	1.2	25, 10

can be very difficult if they have different detector geometry (Voss and Austin, 1993; Pegau et al., 1995, Boss and slade, 2006).

Here we consider some *c*-meter examples: the AlphaTracka, the Sequoia LISST (Laser In Situ Scattering and Transmissometer) and the WET Labs ac-9 and c-star (the nine- and single-wavelength versions, respectively) (Table 5.2). The configurations of the instruments are quite different and thus quantitative comparisons yield large differences with respect to magnitude, but will yield similar qualitative or relative results, assuming no change in particle size distribution (PSD). The degree of accuracy and the need for correction depend on whether the derived beam attenuation coefficient is being used for radiative transfer modelling (Gordon, 1993) or for the detection of suspended particulate matter. In the former case, calculation of the radiance distribution requires very high accuracy in the derived IOPs while calculations of irradiance, reflectance and diffuse attenuation are insensitive to small variations in the acceptance angle of beam attenuation. The sensitivity required for the detection of particulate matter is further explored in this chapter. As a rule, however, beam attenuation coefficients should always be reported with configuration information, particularly the detector acceptance angle (Pegau et al., 1995). The difference in the derived beam attenuation coefficients for natural waters can be as high as 15% between the ac-9 and the LISST (for particles with a refractive index of $1.05 + i\,0.001$ and a size distribution approximated by a power-law with a slope of 4). The instrument with the smallest detection angle, the LISST, yields the largest *c* coefficient, and yet even this instrument can significantly underestimate the theoretical beam attenuation coefficient. However, using a single instrument, the relative estimates of the beam attenuation coefficient can be very powerful with regards to detecting the magnitude and variability of suspended particulate material. The differences between instrumentation are attributed to trade offs between size, weight, spectral resolution, power and the needs of the user.

Ideally the optical path length (i.e. the distance that photons travel between source and detector) is equal to the geometric path length of the sample compartment, so that all the photons that reach the detector are unscattered and none of the scattered photons reach the detector. In optically thick media, photons can undergo multiple scattering. In this case the optical path length of the multiply-scattered photon exceeds the geometric path length (Figure 5.6), thus photons have a greater probability of being scattered or absorbed, a process that leads to an overestimated attenuation coefficient. Conversely, some

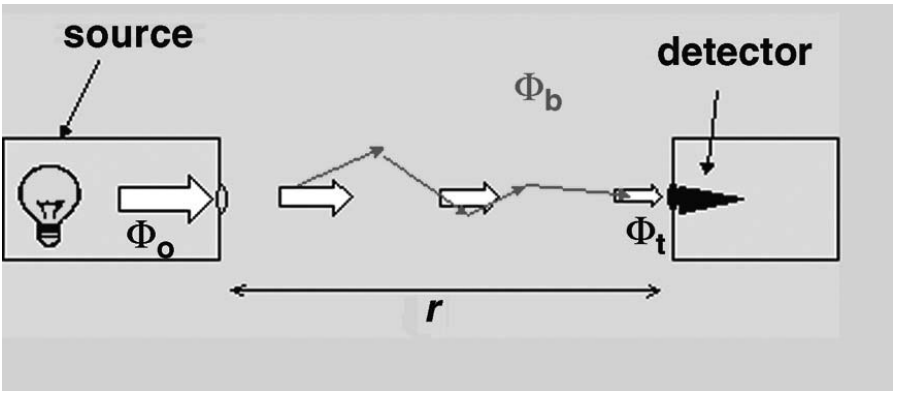

Figure 5.6
Conceptual diagram of the radiant flux in a beam transmissometer in which incident flux Φ_o is multiply scattered (grey arrows Φ_b) or transmitted (white arrows Φ_t) into the detector. In this case the geometric path length r is smaller than the optical path length for some photons, described by the sum of the grey arrows.

portion of the multiply-scattered photons can enter the detector, appearing unattenuated, a process that leads to an underestimated attenuation coefficient. These are difficult phenomena to correct for (van de Hulst, 1957) and it is best to control the optical thickness of the measurement by controlling the geometric path length (i.e. choosing a shorter path length instrument for more turbid waters) so that the instrument response is linear with particle concentration. A rule of thumb suggested by van de Hulst (1957) to ensure single scattering, is to maintain the configuration such that the product $cr < 0.1$ (where r is the geometric path length). This criterion is very restrictive and was determined analytically using a VSF for molecular suspension (which are very flat in the forward angles). The VSFs for aquatic particles tend to be much more peaked in the forward direction (Figure 5.5) and thus the criterion can be relaxed. The criterion for a specific environment can be determined by measuring the IOPs of a dilution series of the particles under consideration and quantifying the range of linear response of the IOP versus particle concentration. Indeed, we observe the response of beam transmissometers to be linear with concentration even for cr significantly exceeding 1 (Doxaran et al., 2006).

5.3.2 Absorption coefficients measured with the ac-9 or acs

Currently there is only one commercially available *in situ* absorption meter that measures absorption based on (5.11a) (Zaneveld et al., 1990; Moore et al., 1992). Other instrumentation exists to derive absorption from hybrid or apparent optical properties, but these approaches will not be treated here. Absorption measured with the WET Labs ac-9 or acs, the hyperspectral version of the 9- wavelength instrument is similar to a beam attenuation measurement, with the exception that the configuration is optimized to collect scattered light (Figure 5.7), the majority of which, for natural particulate populations, will be in the forward direction. This is achieved through a quartz sampling tube, which reflects forward scattered light back into the sample path, and a diffuser in front of the detector to collect the forward scattered light. However, not all the scattered light is collected, and from (5.11a) it is clear that the amount of scattering that is not detected leads

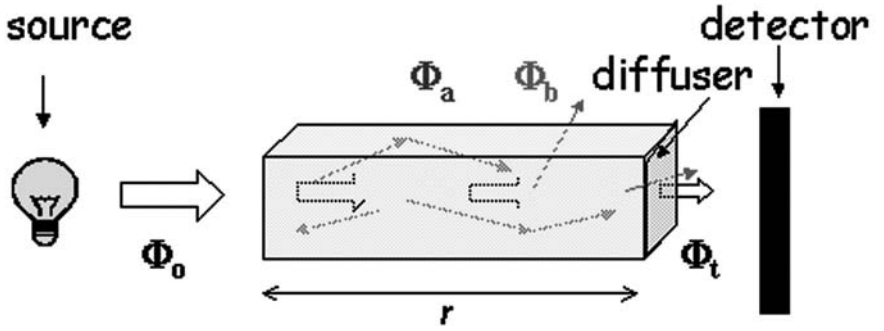

Figure 5.7
Conceptual diagram of the radiant flux in a reflecting tube absorption meter in which incident flux is absorbed, transmitted, scattered into the detector, reflected off the side walls into the detector, scattered out of the cuvette, or multiply scattered.

to a direct overestimation of the absorption coefficient by attributing scattered flux to absorbed flux. It is that portion of the scattering function approximately at angles exceeding 40° (i.e. the back- and side-scattered light) that is not detected (Kirk, 1992). Scattering can impact the estimation of absorption in other ways. Similar to the case for beam attenuation, when the sample is highly concentrated, the beam can undergo multiple scattering events along the path length, which increases the probability of absorption, leading to overestimation. These errors can be corrected to varying degrees of accuracy depending on the availability of ancillary data (Section 5.4).

5.3.3 Scattering coefficients

Scattering coefficients, measured according to (5.11b) are difficult to quantify due to the near impossibility of independently detecting the absorbed flux (c.f. an instrument that measures scattering directly has recently been designed, e.g. Musser et al., 2004). For these reasons, scattering coefficients are generally derived by difference between the measured beam attenuation and the absorption coefficients (5.3). In the absence of independent estimates of absorption, the scattering coefficient can be derived from the beam attenuation coefficient at a wavelength for which absorption by dissolved and particulate materials is assumed negligible (e.g. 650 nm to 660 nm or in the near-infrared >720 nm, depending on seawater composition). Thus all the caveats for attenuation measurements apply to this approach.

There is a distinction between sensors that measure the scattering coefficient or the volume scattering function at a defined θ and φ from those that measure some aspect of scattering as a means to assess total particle concentration or total suspended load (Table 5.3). These latter sensors are often called turbidity meters or nephelometers, which express values in units of NTU (nephelometric turbidity units) or FTU (formazine turbidity units). These units are based on a suspension of polymerized hexamethylenetetramine and hydrazine sulfate under strictly controlled conditions. These units cannot be directly converted into IOP units of m^{-1}, and are quantitatively useful only for a specific population of non-natural particles (e.g. Gibbs, 1974*a*, 1974*b*). So when two different brands of turbidity meters are calibrated with the same calibration suspension, they should not

Table 5.3 Instrumental configuration of commercially available turbidity and scattering sensors. All beams are divergent (see Figure 5.8), but differ in whether they have a narrow (<45°) or wide (>45°) solid angle.

Instrument	**Beam width**	**Detector acceptance angle(s) and FOV (°)**	**Wavelength (nm), λ**
D&A Tech OBS	Narrow	140 to 160	875 (LED)
HOBILabs Hydroscat	Narrow	140 ± 10	2 or 6 selectable filters
SeaPoint turbidometers	Wide	15 to 150	880 (LED)
WET Labs NTU	Narrow	140 ± 10	700 (LED)
WET Labs LSS*	Wide	45 to 145	880 (LED)
WET Labs ECObb	Narrow	117 ± 10°	470, 528, 660, 800 (LED)
WET Labs ECOvsf	Narrow	110, 125, 150 ± 10	470, 528, 660, 800 (LED)

* No longer commercially available.

be expected to provide the same output in the natural environment because they generally have different configurations. The signals from certain of these instruments may be converted to IOPs if appropriately calibrated for particle concentration, composition, and size distribution using appropriate calibration standards (e.g. beads of known optical properties, Zaneveld et al., 1980). Detailed knowledge of the source and detector's fields-of-view are needed for such calibrations, but the calibrations will not necessarily apply to natural particles. These sensors tend to be more economical and if the user's application is to discern some aspect of total suspended load, such as suspended particle mass or concentration without the need to compare to results obtained with another type of instrument, they might provide a reasonable option compared with IOP sensors.

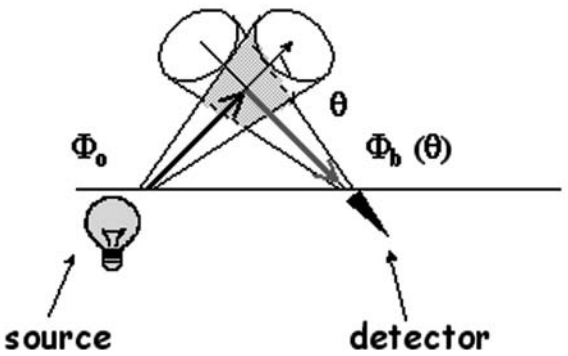

Figure 5.8
Conceptual diagram of a single-angle backscattering sensor. The incident irradiance Φ_o is a divergent beam with a known solid angle (upward bold arrow), the detector likewise has a known detection solid angle. The detected scattered flux Φ_b (downward bold arrow) occurs about the central backscattering angle θ, within a volume (grey) defined by the intersection of the incident and detected solid angles. The geometric path length is defined by the sum of the geometric lengths of the bold arrows. *Source*: simplified from Maffione and Dana (1997).

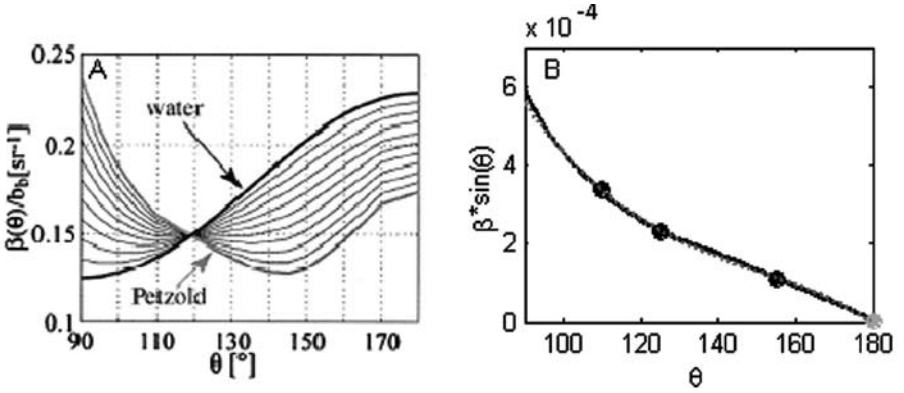

Figure 5.9
A, relationship between the normalized volume backscattering function and backscattering angle for a range of volume scattering functions from pure water to Petzold's San Diego Harbor (see Figure 5.5) (from Boss and Pegau, 2001). The angle at which they intersect is ~117°.
B, graphical representation of the calculation of the backscattering coefficient from three point observations at discrete angles as in (5.5), the integration of the product of the volume scattering function β, and the sin of the scattering angle θ, shown here for a typical oceanic VSF (black). Observational detection angles of the WET Labs ECO-VSF meter (black symbols), and the data point at 180° (grey symbol), which is necessarily zero because sin(180°) = 0. A third-order polynomial fit to the four data points (dotted line) is used in the integration over θ to determine the backscattering coefficient.

Measurements of the VSF or portions of the VSF are achieved with a set of divergent-beam/small-angle-detector pairs at a range of angles (e.g. Figure 5.8 for scattering). Attenuation occurs along the path and must be corrected for, either with observations or approximations, otherwise the backscattering is underestimated by the measurement due to attenuation along the scattered path.

Complete VSF measurements are not routinely made and there is no commercially available instrumentation yet, although some are likely in the next five years. Selected *in situ* VSF observations made with the General Angle Scattering Meter (GASM) in the early 1970s (Petzold, 1972) are still used today in radiative transfer modelling because of the dearth of publicly available VSF observations. GASM resolved the VSF at 1° resolution from 10° to 170° and at 532 nm. New technology (Lee and Lewis, 2003) has an angular resolution of 0.3° at a single wavelength, but is not yet commercially available.

The backscattering coefficient is currently determined from one or more measurements of the VSF at $\theta > 90°$. A single angle measurement of the backscattering has been found to be significantly related to the integrated backscattering coefficient (Oishi, 1990; Maffione and Dana, 1997; Boss and Pegau, 2001; Sullivan et al., 2005) (Figure 5.9A). The exact angle that minimizes the error depends on whether the instrument omits or includes the pure water backscattering signal (e.g. for the WET Labs and HOBI Labs instruments, respectively). When the backscattering is measured at multiple angles (e.g. 3, as is the case the WET Labs ECO-VSF), the backscattering coefficient is computed, via (5.5), by integrating the function $\beta \sin\theta$ over $\theta = \pi/2$ to π.

As the observations are only made at three angles (110°, 125° and 150°), a polynomial is fit to those three data points. Noting that the $\sin(\theta = \pi) = 0$, a fourth point at 180° can be included for a total of 4 points in the polynomial fit (Figure 5.9B). A third-order polynomial is the lowest order polynomial providing the best fit to the VSF in the backward direction (M. Twardowski, pers. comm.).

5.4 Calibrations, characterizations and corrections

5.4.1 Absolute calibrations, biogeochemical calibrations, tracking

Each commercially available IOP instrument undergoes careful absolute calibration procedures to convert the detected analogue or digital signal into IOP units (e.g. m^{-1} or m^{-1} sr^{-1}, see discussion in Cullen and Davis, 2003). Often included in these calibrations are the processing steps required to account for the errors associated with non-ideal configurations. In other applications these steps may require separate processing by the user. A secondary calibration may also be applied, either by the factory, or by the user, in which either the signal or the derived IOP is related to some scalar biogeochemical property or concentration such as total suspended solids, particle concentration or chlorophyll concentration. These calibrations are generally based on many more assumptions, the details of which are covered by Sosik (2007) in Chapter 8. Finally, ancillary calibration procedures may be employed, not to derive absolute IOP units but to track changes in the instrumentation between absolute calibrations. This tracking procedure might be necessary in situations of long deployments, cruises or experiments when absolute calibration might be difficult (calibration standard difficult to obtain) or impossible (*in situ* deployment). This type of tracking might be done by looking at the time series of the dark signal or air calibration. The configuration of the instrument, the suite of corrections and the absolute calibration are what determine good quality quantitative observations from qualitative or uncalibrated ones. There are many instruments available, all with techniques for corrections and calibrations; however, understanding the sensitivity and robustness of the observations is necessary for obtaining optical observations that translate into IOPs which are comparable between sampling dates, between instruments and between investigators.

Absolute calibration requires some sort of reference material either to obtain a known signal (i.e. a scattering surface of known reflectance used to calibrated the scattering sensors) or to obtain an absolute signal relative to the reference for which the IOPs are known (i.e. relative to a pure water reference). Independent means of assessing the purity of the calibration material is vital for obtaining accurate absolute calibrations. For example, a Spectralon® plate, with known reflectance, does degrade with time and exposure to light. Optically pure water can be a problem to make and maintain, even in the laboratory, due to its high reactivity with other substances and its tendency to form highly scattering micro bubbles.

Ideally, instruments should be calibrated by the manufacturer or a certified or well experienced laboratory before and after each deployment or cruise. Practically, however, this may not be possible and the user must develop an independent calibration and tracking protocol. Unavoidable sources of instrument variations with time include changes in lamp output magnitude and spectral dependence, detector degradation and response, and filter degradation and response. With careful protocols, these can be tracked and quantified and the data can be corrected. Avoidable sources

of instrument variation include dirty instrumentation, incorrect configurations and inappropriate blanks. Often these are not quantifiable and accurate data can never be recovered (Cullen and Davis, 2003).

A sample observational protocol for an ac-9 is as follows:

1. Obtain factory air and pure water calibration.
2. Clean instrument tubes and optical windows with a solvent such as ethanol and lens paper.
3. Perform air and pure water calibrations on the benchtop with instrument in a vertical position, using the appropriate factory calibration. Values should be within instrument specifications of zero.[19]
4. Place instrument in its deployment configuration (i.e. strapped to cage or frame). Repeat steps 2 and 3. The air and pure water calibrations should be within factory specifications of those derived in step 3. If not, check that the optical alignment has not been changed by deployment configuration (it is recommended that only one end of the instrument is tightly strapped to prevent bending).
5. Repeat steps 2 and 4 daily during observational programme, if possible, noting the potential difficulty in obtaining absolute calibrations. In addition, if possible, perform daily measurement with a 0.2 micron filter placed on the intake of the a and c tubes at depth. Deviations from an exponential function in specific wavelengths are likely due to problems with the calibration values at these wavelengths.
6. Perform a final air and pure water calibration and compare them to the pre-deployment values (when confident about laboratory set-up, pure water facilities and procedures), otherwise obtain factory air and pure water calibration post deployment to ensure robust comparisons with pre-deployment values.
7. If post-deployment calibrations are significantly different from pre-deployment values, analyse the time course of air and pure water calibrations to quantify drift or step-functions in instrument response. If deployment does not permit a time course of pure water or air calibrations, as shown in Figure 5.10, examine the raw data for features consistent with a step function or trend. Using the pre- and post-calibration values, construct an appropriate time course of factory calibration to apply to *in situ* data (Figure 5.10).

5.4.2 Environmental sensitivity

Electronic instrumentation often exhibits sensitivity to ambient temperature. Optical instruments that depend on precise alignment may also exhibit sensitivity to ambient pressure. While these are often well characterized or controlled by the factory, it is a source of potential variability that is worth verifying as there may be some residual effects. The severity of this error depends on the deployment platform. Profiling instruments that pass through a sharp thermocline, or profile to great depths are more likely to yield

[19]A newly calibrated instrument should ideally measure the absorption and attenuation of pure water within the instrument specifications (e.g. ± 0.005 m^{-1}). However, calibrations are very sensitive to instrument position and some changes may occur in transit. If only one wavelength is significantly different from the calibration (i.e. >0.1 m^{-1} in both a and c), this may indicate a filter malfunction. When a and c measurements at all wavelengths are significantly different from zero, this may indicate a detector or lamp malfunction. Checking for stability over the course of a few days may indicate that the instrument underwent some drift in transit and that a new pure water calibration, performed in the laboratory, is necessary. Over longer timescales the ac-9 calibration does change as a function of time (order 0.02 m^{-1}/200 days), see Twardowski et al. (1999), and care must be taken to do periodic calibrations to keep track of this drift.

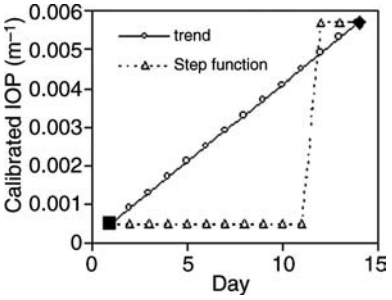

Figure 5.10
Hypothetical time course in pure water IOP observations relative to pre-deployment factory calibration. An observed linear trend between pre- (filled square) and post- (filled diamond) deployment factory calibration is given by circles, a step function is given by triangles. These daily observations would indicate how to apply factory calibrations to deployment observations during post-processing: a linear interpolation between the pre- and post-deployment calibrations or the pre-deployment calibration until day 11 and the post-deployment calibration from days 12 to 15.

problem data because of the mismatch between the profiling speed and the time for the instrument to reach thermal equilibrium. These artifacts can be quantified with careful characterization in the laboratory and can become part of the data processing sequence as long as time-dependent hysteresis is not significant or profiling speeds are very slow.

A second order of environmental sensitivity is that of the reference or calibration material. For example, pure water absorption and scattering properties are both temperature and salinity dependent and this dependence has been well quantified (Morel, 1974; Pegau and Zaneveld, 1993; Pegau et al., 1997). Therefore, a factory calibration with 25 C pure water will not be the same as a calibration with 10 C pure water, nor would the calibration for 33 PSU water be the same as that for pure water. Thus, the dependence of the reference material IOPs on temperature must be quantified in addition to the instrument response to temperature, salinity and pressure (i.e. the dependence of the pure water running through the sample compartment or the sample volume *and* the dependence of the instrument *in* water of a temperature different from room temperature). Generally the variations in water optical properties as a function of temperature, salinity and pressure are at specific wavelengths associated with the harmonic absorption features of water (most notably ~600 nm, ~665 nm and ~740 nm, Pope and Fry, 1999), while the instrument-dependence will be different at all wavelengths depending on instrument electronics and the thermal properties of the instrument material.

5.4.3 From raw data to calibrated and corrected *in situ* IOPs, example with the ac-9

An example of the steps required to derive accurate IOPs from ac-9 observations is given in this section. It is often difficult to discern problem data from real-time profiles or time-series observations at a single wavelength, thus it is recommended that the user examine the spectral data in real time as well. All raw data are binned such that each bin represents an independent observation as follows. The flow tube residence time is determined by the ratio of the volume of the flow tubes and the flow rate through the

tube (~50 ml for 0.8 cm-wide and 25 cm-long tubes). The latter can be performed in the field or in the laboratory with the instrument and pump connected; collect the outflow from the sample tubes, noting the time of the collection. Calculate the flow rate from the quotient of the volume collected and the time of the collection (~2.8 L min^{-1} depending on the pump and tubing configuration). Knowing the sampling rate of the instrument (6 Hz) one can determine how many realizations must be binned to derive an independent observation *in situ*. Using a SeaBird pump in the field typically requires binning approximately six realizations (depending on the pump settings), using restricted gravity flow in the laboratory typically requires binning approximately 36 realizations. These computations are critical for observing fine scale features in the field so as to prevent the signal from a large anomalous particle to be interpreted as a 'thin layer'. Additionally, binning reduces the error associated with the fact that different parcels of water flow through the absorption and attenuation tubes due to small scale patchiness in the environment. All the following calibrations and corrections are performed on binned data only.

In the following example, a profile of beam attenuation and absorption was measured in stratified coastal waters. The raw observations, calibrated relative to pure water with the pre-deployment factory calibration, do not provide any evidence or problem data (Figure 5.11A, B). However, examination of the spectral values at discrete depths indicates that the pre-deployment calibrations may not be accurate (Figure 5.11 C, D, symbols). The expectation is that the spectral attenuation is a smoothly varying function (i.e. the 555 nm channel is anomalous) and that the absorption resembles

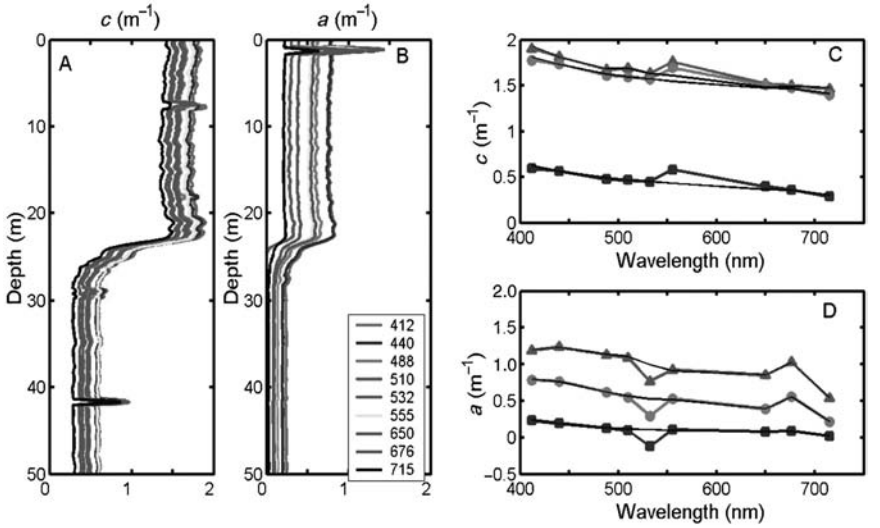

Figure 5.11
Example of observed attenuation and absorption measured with an ac-9 in stratified coastal waters. Depth profiles of raw A, attenuation; B, absorption observations using a pre-deployment factory calibration at nine wavelengths.
C, D, attenuation and absorption spectra, respectively, taken from discrete depths within and below the mixed later and at the 2 m absorption peak. Spectra corrected for post-deployment calibrations shown in black lines.

an exponential function associated with NAP or CDM with or without the impacts of phytoplankton pigments (again the strong dip at 555 nm is not characteristic of either; note that the calibration errors do not necessarily have to occur at the same wavelengths for *a* and *c* as they do in this case if the problem is related to the detector or sample tubes). If only the surface spectra displayed this spectral irregularity, and it was not consistently at the same wavelengths, bubbles might be suspected. Application of current calibration coefficients (derived from shipboard calibrations or from pre- and post-deployment factory calibrations as in Figure 5.10) result in spectral coefficients that behave as predicted (Figure 5.11C, D, black lines).

After the appropriate calibrations are applied to the observations, absorption and attenuation must be corrected for variations in the absorption by pure water due to differences between the temperature and salinity of the *in situ* water and that used in the factory or laboratory calibrations. Using the algorithms of Pegau et al. (1997), the corrected spectra are obtained (Figure 5.12A, shown for absorption only). In this case the *in situ* water was more saline and colder than the pure water used to calibrate the instrument (0 PSU and ~25 C). This correction is applied to both the absorption and attenuation coefficients over the visible spectrum, although for this particular filter configuration, only the values at 715 nm exhibit significant effects. This correction

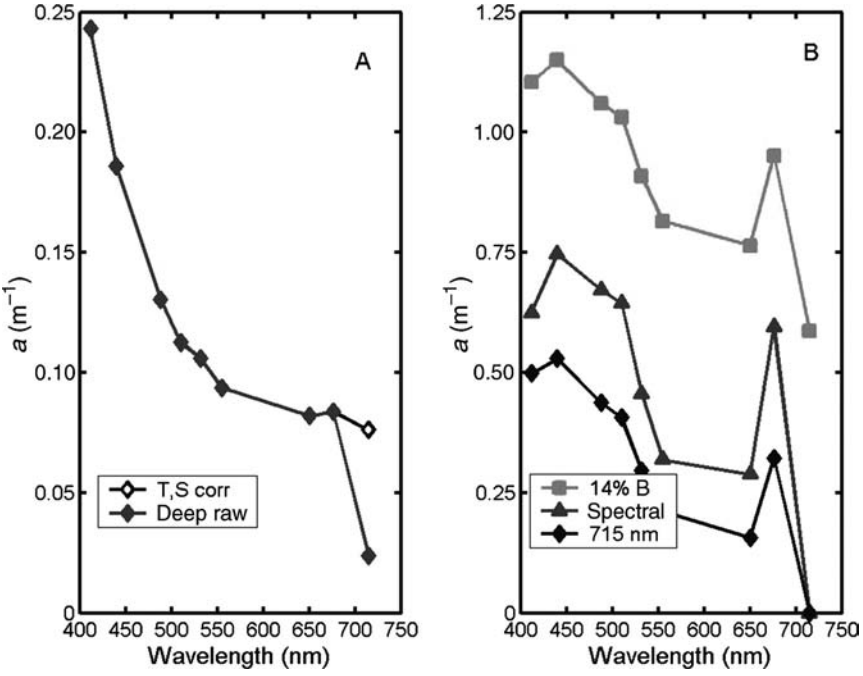

Figure 5.12
A, absorption spectrum from the deep layer, as in Figure 5.11D, before and after temperature and salinity correction (filled diamond and open diamond, respectively).
B, absorption spectrum from the absorption peak in Figure 5.11D, after applying post-calibrations and temperature and salinity corrections, corrected for scattering by three different models. See text for details.

is especially critical for the absorption observations because some scattering correction schemes hinge on the observed value of absorption at 715 nm (Zaneveld et al., 1994) and thus any error due to temperature or salinity will propagate to the other wavelengths via the scattering correction.

In the absence of synchronous CTD measurements with IOP measurements, an accurate temperature correction can be obtained using the spectral attenuation measurements alone. The spectral behaviour of beam *c* has been well documented to be a smoothly varying function of wavelength for multispectral aquatic measurements with wide spectral windows around each wavelength (e.g. Voss, 1992; Boss et al., 2001*a*). Similar to the spectrum for absorption shown in Figure 5.12A, the 715 nm value falls away from the curve described by the other eight wavelengths. Using a power-law spectral fit to the eight wavelengths of observed beam *c*, the value at 715 nm can be predicted. The difference between this predicted value and the observed value is the correction in *a* (715) due to temperature and salinity variations. This can then be used to correct the observed absorption spectrum (and, interestingly, the *in situ* temperature can be determined from the absorption correction).

The final step is the scattering correction applied to the absorption observations to account for the losses due to scattering out of the detector (Figure 5.7). There has been no consensus on how to correct the absorption for scattering losses (Kirk, 1992; Zaneveld et al., 1994; Bricaud et al., 1995; Roesler, 1998). Methods range from subtracting the observed offset in the absorption at 715 nm, consistent with that done in spectrophotometry (Babin and Stramski, 2002), to subtracting a percentage of the spectral scattering coefficient. Below are three models for scattering correction:

$$a(\lambda) = a_{\text{meas}}(\lambda) - a_{\text{meas}}(715) \tag{5.13a}$$

$$a(\lambda) = a_{meas}(\lambda) - n\%^{*}[c(\lambda) - a_{meas}(\lambda)] \tag{5.13b}$$

$$a(\lambda) = a_{\text{meas}}(\lambda) - a_{\text{meas}}(715)^{*}\frac{c(\lambda) - a_{\text{meas}}(\lambda)}{c(715) - a_{\text{meas}}(715)} \tag{5.13c}$$

where $a(\lambda)$ is the scattering-corrected spectral absorption, $a_{\text{meas}}(\lambda)$ is the measured spectral absorption, after calibrations and temperature-salinity corrections have been applied, and $c(\lambda)$ is the measured spectral attenuation after calibrations and temperature-salinity corrections have been applied. It is clear that the nature of the scattering correction is critical to interpretation of the spectral absorption coefficients (Figure 5.12B).

Both the 13a and 13c scattering corrections imply that there is no non-water absorption at 715 nm. Babin and Stramski (2002), using an integrating sphere and spectrophotometry, conclusively demonstrated that there is minimal absorption at 715 nm by particulate material, including inorganic particles, in a range of natural waters. This suggests the observed signal $a_{\text{m}}(715)$ is due to scattering alone and that the absorption at 715 nm should be zero. This would indicate that the percent of *b* correction (5.13b) is not appropriate because it results in a non-zero value for absorption at 715 nm, and further suggests that a constant percentage of the scattering is lost to the detector, when instead this percentage would strongly depend on the angular dependence of the VSF.[20] That leaves the spectrally independent and spectrally dependent corrections ((5.13a) and (5.13c) respectively). Observations and modelling of the optical properties

of both weakly and strongly absorbing particles (Stramski and Mobley, 1997 compilations) indicate that scattering is spectrally dependent except for extreme cases of large polydispersed (varied size distribution), weakly absorbing particles in which b is spectrally flat. The model given by (5.13c), which essentially removes a fraction of the spectral scattering, scaled to the measured absorption at 715 nm, accounts for both types of particles. The error in (5.13c) is that portion of the scattering losses that are due to backscattering. For some strongly absorbing particles, the spectral shape of the backscattering may be different from the spectral shape of total scattering. However, based on a few studies and data sets, the spectral backscattering to scattering ratio seems to be relatively independent of wavelength in natural waters (e.g. Ulloa et al., 1994; Twardowski et al., 2001).

5.5 Instrument sensitivity to particle characteristics

Interpretation of observed IOPs with respect to the underlying biogeochemical properties of oceanic substances requires an understanding of how the IOPs vary in response to changes in particle properties and how accurately instrumentation resolves those changes. In this section, we simulate IOP variability as a function of particle concentration, composition (as revealed by the real refractive index), and size distribution (Bricaud et al., 1986). We end with a simulation of the development of two algal blooms of two very different algal species. In the first set of these simulations, we compute the volume scattering function for populations of spherical particles that have defined concentrations, defined refractive indices, and sizes that are Z to obey power-law particulate size distributions that obey the power-law function with defined slopes ξ, and an upper size of 200 m (Figure 5.13).[21] Except in the case of examining the response to particle concentration, the simulated volume scattering functions have been normalized to the integrated particle volume, thus removing the biomass effects on the observations. We then compute the beam attenuation coefficient that would be observed by two commercially available instruments, the Sequoia LISST and the WET Labs ac-9. In general, as particle concentration increases, the absorption, scattering and attenuation coefficients increase, and if all else is held constant, they increase linearly with concentration. This provides the robust approach to estimating particle or dissolved concentrations with

[20]Some authors suggest that there is non-zero absorption in the range of 715 nm, although methodological errors might explain their observations. If this is found to be true in the future, additional work on scattering corrections will be necessary as attributing all the a (715) signal to scattering will lead to underestimated absorption coefficients.

[21]A specific note about microbubbles in the aquatic environment: it has been suggested that such bubbles are responsible for significant brightening of ocean-colour radiance as measured by satellite and airborne sensors because the backscattering by particles cannot seem to account for the predicted backscattering coefficient derived from ocean colour (see discussion in Stramski et al., 2004). The IOPs of microbubbles can be modelled very accurately using Mie theory (Zhang et al., 1998) as they are homogeneous spherical particles with size distributions predicted from wind speed and a known index of refraction relative to water of 0.75. However, measuring the IOPs of microbubbles is not trivial. First, because the presence of a ship may artificially introduce bubbles into the surface layer and, second, because any manipulation of the sample, such as drawing it through a sample chamber as in the case of an ac-9, can modify the natural population. Flat-face sensors, such as the Hydroscat and ECO-series, provide the most robust means of sensing natural bubble populations. Bubbles are not included in the following simulations.

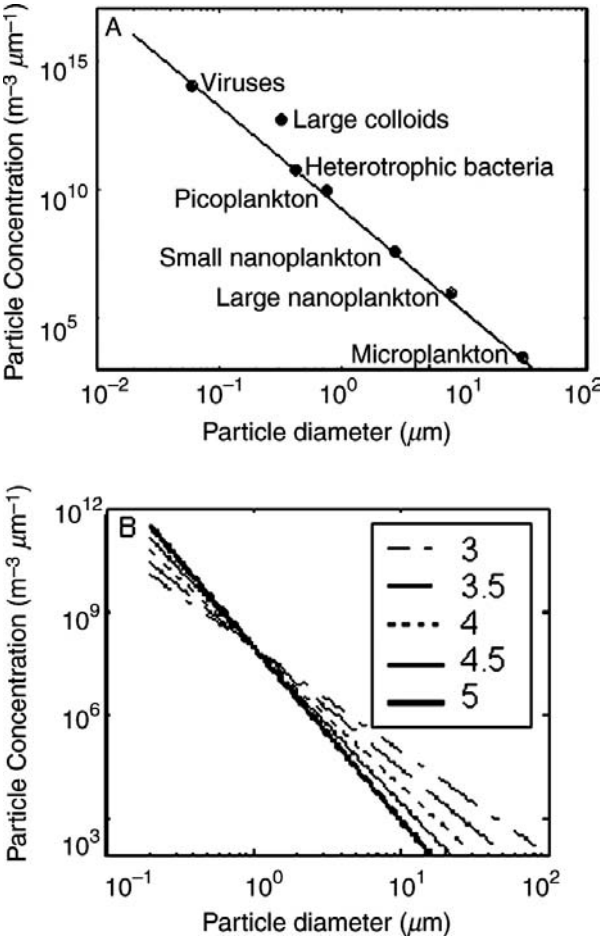

Figure 5.13
A, size distribution for oceanic particles. Solid line represents a Junge slope of 4. Particle concentration units are differential with respect to size interval.
B, range of particle size distributions as in A, for Junge slopes ranging from 3 to 5 used in simulations in the following figures.
Source: Stramski and Kiefer (1989).

IOP measurements. Particle attenuation and scattering also increase as the index of refraction increases, which is the basis for using IOP measurement to estimate particle composition. Finally, particle IOPs are significantly influenced by particle size distribution, but not in a predictable or linear manner. In Section 5.5.7 we address specifically which particles (in terms of size) are responsible for scattering and attenuation and thus which impact IOP measurements made with specific instrumentation.

5.5.1 IOP measurement sensitivity to particle concentration

The VSF for a population of weakly absorbing particles with refractive index of 1.05 + i 0.001, obeying a power-law size distribution (eqn. 12) with $\xi = 4$ is shown in Figure 5.14A. This would correspond to a mixed population of organic particles at any wavelength or phytoplankton at a wavelength at which they are weakly absorbing (e.g. ~555 nm or ~650 nm). The concentration values vary 50-fold on an arbitrary scale. The far-forward scattering function is shown on a linear scale in the inset. The beam attenuation coefficients that would be measured with a Sequoia LISST and a WET Labs ac-9 are within 0.09% and 5.85% of theoretical values, respectively, and the measured beam c is linearly related to the particle concentration (Figure 5.14B). The instrumental underestimation of beam c is due to the finite acceptance angles (Table 5.2), with the ac-9 exhibiting the largest underestimation due to its larger detection angle.

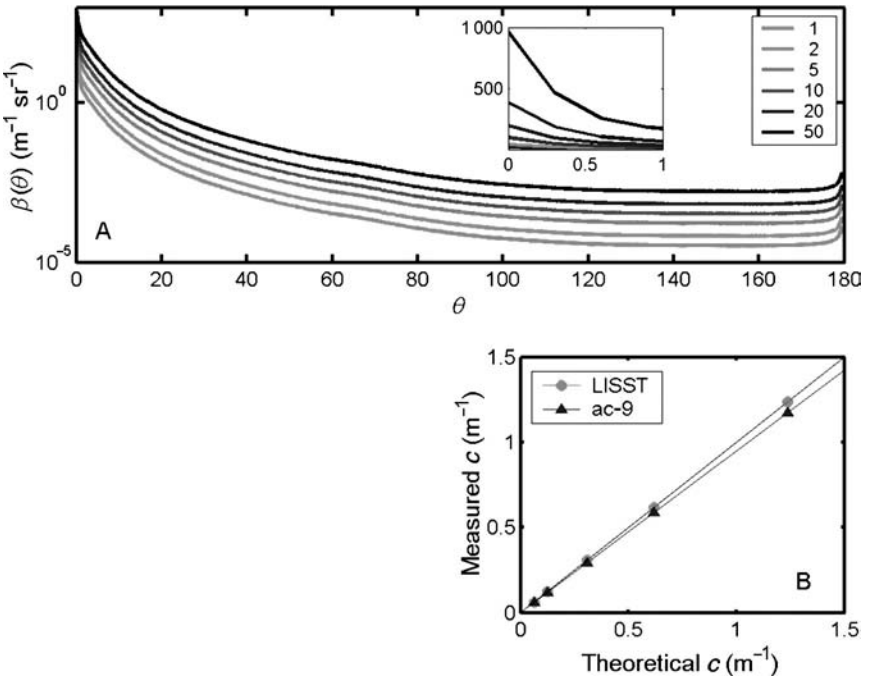

Figure 5.14
A, volume scattering functions for a range of particle concentrations (1–50 arbitrary units) for particles obeying a Junge distribution with slope of 4 and refractive index of 1.05 + i 0.001.
B, modelled values for beam attenuation coefficient coefficients for the samples in A that would result from measurements made with a LISST and an ac-9 versus the theoretical beam attenuation coefficients, given their detection angle responses.

5.5.2 IOP measurement sensitivity to composition (real refractive index)

The VSF for a population of weakly absorbing particles (imaginary refractive index of 0.001), obeying a power-law size distribution with $\xi = 4$ with real refractive indices varying from 1.01 to 1.22 is shown in Figure 5.15A. While there is a crossover in the VSF functions at approximately 0.5°, with the low refractive index particles exhibiting higher scattering at angles <0.5°, the magnitude is not very different to the high refractive index particles. Thus for both instruments the measured beam *c* values are within 2% of the theoretical values (Figure 5.15B). This range in real refractive indices spans particles from phytoplankton to minerals, respectively, with non-algal organic particles in between (Stramski et al., 2001). As the magnitude of refractive index increases, particles of a given size scatter more. Thus for a constant particle volume and particle size, suspended mineral particles are more scattering than organic non-algal particles, which, in turn, are more scattering than phytoplankton cells. This range in real refractive index induces more than an order of magnitude variation in the beam attenuation

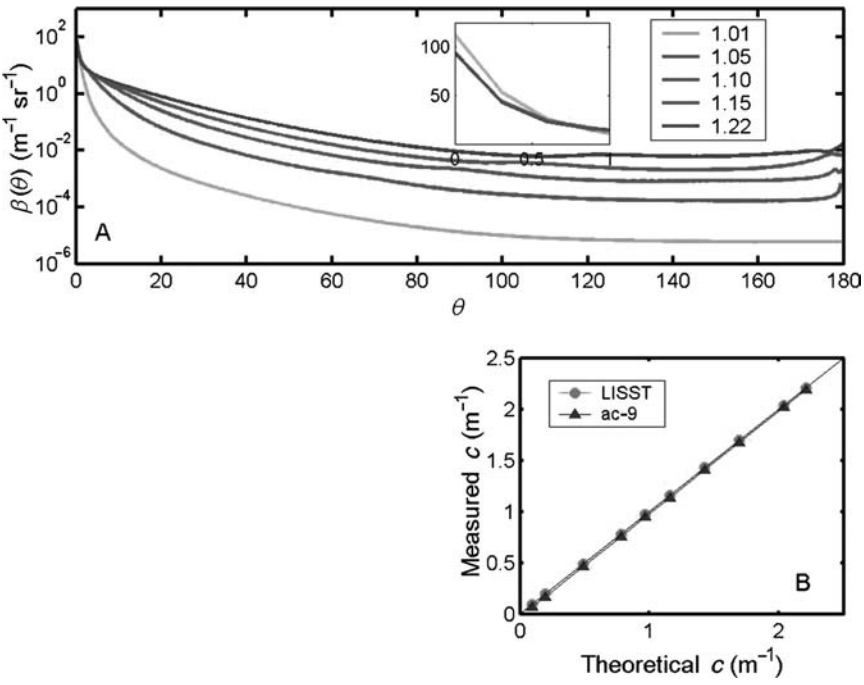

Figure 5.15
A, volume scattering functions for particles with a range of real refractive index, obeying a Junge distribution with slope of 4 and imaginary refractive index of 0.001. Curves have been normalized to total particle volume to remove the effects of biomass.
Inset: first degree of resolution on a linear scale.
B, beam attenuation coefficients for the samples in A that would result from measurements made with the two instruments versus the theoretical values, as in Figure 5.14.

coefficient for a constant particle volume (so mineral particles will scatter >10 times as much as the equivalent phytoplankton particles). This order of variation due to particle composition is comparable to that observed for a order of magnitude variation in concentration of particles with a single index of refraction. Normalizing beam attenuation by total particle volume (i.e. m^{-1} (m^3 particles per m^3 of water)$^{-1}$) provides a quantity similar to the mass-specific beam attenuation and allows us to study changes in IOPs that are independent of total concentration. This clearly demonstrates that particle composition has an impact on the observed beam *c* values that are comparable to large changes in particle concentration and thus interpreting changes in the beam attenuation coefficient as purely a change in the suspended load can be significantly in error. Diel variations in cell-specific beam *c* have been observed in phytoplankton cultures and in the field. These are attributed to diel variations in the cellular refractive index caused by changes in cell composition in response to growth and division or to nutrient stress (Cullen and Lewis, 1995; Stramski et al., 1995; Stramski, 1999; Stramski et al., 2002).

5.5.3 Instrument sensitivity to particle size distribution

The particle size distribution, described by the power-law distribution function (Figure 5.13B), induces complex variations in the volume scattering function (Figure 5.16A). When the power-law PSD exponent ξ is small, a value of 3, the particle population is composed of a larger portion of large particles compared with a larger exponent of 5, for which the population has proportionally more smaller particles. At small angles, the VSFs exhibit a crossover between populations of particles obeying a power-law PSD slope of 3 and those obeying a power-law PSD slope of 5 (while keeping to total particulate volume or mass constant). Because both instruments collect the scattering at small angles, the curve associated with the power-law PSD slope of 4 yields the largest integral and thus the largest *c* value per volume. Thus the magnitude of the normalized beam *c* undergoes a nonlinear change as a function of the PSD slope, whereby the attenuation per volume is largest for particles with $\xi = 4$, and it decreases as the slope of the particle size distribution increases to 5 or decreases to 3 (Figure 5.16B). Because of the detection angle of the ac-9, such an instrument is likely to display a stronger nonlinear behaviour when compared with the LISST, and for these simulations the difference can approach 6%.

The WET Labs ac-9 is currently the only commercial instrument that measures the spectral beam *c* coefficients. By removing the effects of water via the calibration procedure, and removing the effects of absorption by CDM, the particle beam attenuation, c_p, is computed. The spectral distribution of particle beam attenuation is a smoothly varying function of wavelength (Voss, 1992) and has been found to be well described by a power-law function of wavelength (Diel and Haardt, 1980; Boss et al., 2001*a*, 2001*b*):

$$c_p(\lambda) = c_p(\lambda_0)\left(\frac{\lambda}{\lambda_0}\right)^{-\gamma} \tag{5.14}$$

where λ_0 is a reference wavelength and γ describes the spectral slope of the power function. An exact linear relationship between the exponent of the beam attenuation coefficient γ, and the power-law exponent of the PSD ξ, has been demonstrated using Mie theory for non-absorbing, homogeneous spherical particles (Volz, 1954; Morel, 1973; Diehl and

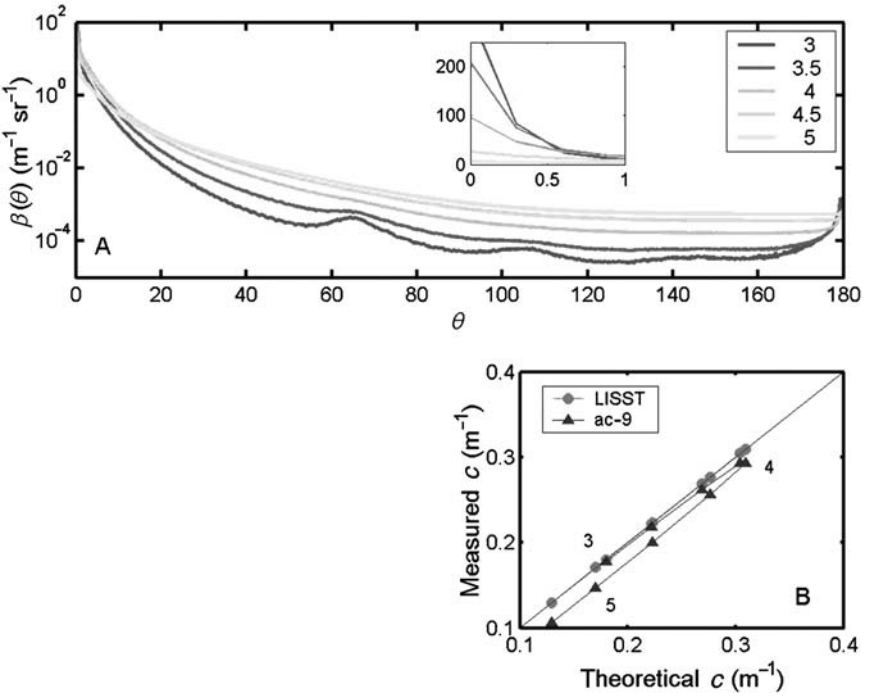

Figure 5.16
A, volume scattering functions for particles obeying the Junge distribution with a range of slopes and with a refractive index of 1.05 + i 0.001. Curves have been normalized to total particle volume to remove the effects of biomass.
Inset: first degree of resolution on a linear scale. Note the VSF crossover occurs in the far-forward scattering, with the Junge slope of 3 (dominance by larger particles) exhibiting the strongest scattering at the smallest angles and the Junge slope of 5 (dominance by smaller particles) the strongest side and backscattering.
B, beam attenuation coefficients for samples in A that would result from measurements made with the two instruments versus the theoretical values, as in Figure 5.14. The values of the Junge slope are indicated, showing the hysteresis. The maximal value of beam c occurs at a Junge slope of 4.

Haardt, 1980) when the size distribution is considered from zero to infinity. Approximations to this relationship for limited size ranges were made by Boss et al. (2001*b*) such that:

$$\xi = \gamma + 3 - 0.5 \exp(-6\gamma) \tag{5.15}$$

where the right-hand term accounts for the size range approximation. Thus a flat beam c spectrum ($\gamma = 0$), is associated with a small power-law PSD exponent, that is larger particle dominance; when the beam c spectrum decreases from blue to red ($\gamma = 1$), this is associated with larger power-law slope or smaller particle dominance. This relationship

performed well for the range of ξ found in the ocean, and for absorbing particles and non-spherical particles. This model has been successfully applied to particles in the benthic boundary layer on the continental shelf (Boss et al., 2001*a*) and to a monospecific algal bloom of *Prorocentrum micans* (Etheridge et al., 2002) a successful phytoplankton community in Long Island Sound (Etheridge and Roesler, 2004) and to a range of oceanic conditions (Oubelkheir et al., 2005).

5.5.4 Forward volume scattering function meter sensitivity

The Sequoia LISST is currently the only commercially available technology for measuring the volume scattering function in the forward direction (Agrawal and Pottsmith, 2000) (Figure 5.17). A collimated laser beam enters the sample chamber in which it is scattered by suspended particles. Photons are scattered at an angle θ relative to the incident direction and pass through a lens so that they are focused onto a ring detector. Photons scattered at small angles (i.e. 0.1°) are focused at small radial distances from the centre of the detector while photons that are scattered at large angles (i.e. ~15°) are focused at large radial distances from the centre of the detector. The detector is composed of 32 discrete concentric ring detectors such that each detector receives scattered flux from discrete scattering angles relative to the incident irradiance. The discretized detection angles range logarithmically from either 0.0135° to 8° or 0.0269° to 15° (in water) depending on the model type. The detected scattered signal is dominated by diffraction rather than refraction, and the shape of the VSF is relatively insensitive to refractive index (Figure 5.15A) but very sensitive to particle size distribution (Figure 5.16A). This makes it possible to use the far-forward VSF to estimate the shape of the particle size distribution for particles without accounting for their refractive index (composition). Using look up tables generated for hundreds of possible size distributions, the measured VSF is inverted to predict particle size distributions at 32 logarithmically spaced intervals from approximately 1.25–250 μm or 2.5–500 μm, respectively (Y. Agrawal, pers. comm.). Extensive testing using calibration beads (Slade, and Boss, 2006.) suggests that the polarization of the laser beam does not contribute a significant uncertainty to the measurement of the near-forward VSF with the LISST (which is defined for an unpolarized beam; Figure 5.17B).

5.5.5 Backward volume scattering meter sensitivity

There are currently two major types of commercially available backscattering meters that detect within narrow angular ranges. One technology detects backscattering at a single backward angle (e.g. HOBI Labs Hydroscat and WET Labs ECObb) with multiple or single-wavelength configurations (Figure 5.18). The other technology is a single-wavelength sensor that detects backscattering at three angles (nominally 110°, 125° and 150°) (Figure 5.19). Multiple sensors with different wavelength light-emitting diodes (LEDs) can be used to gain spectral information. The backscattering coefficient can be derived from observations made with both of these technologies (see Section 5.3.3), based on different assumptions. The sensitivity of these instruments to particle characteristics is demonstrated in Figures 5.14 to 5.16 in the backscattering angles. To first order, the backscattering increases as the concentration of particles increases. To second order, backscattering increases as the real refractive index increases and as the imaginary refractive index decreases (i.e. weakly absorbing particles are more efficient backscatters compared with strongly absorbing particles because photons that enter particles are more likely to be absorbed and thus are not available to be backscattered), and the slope of the

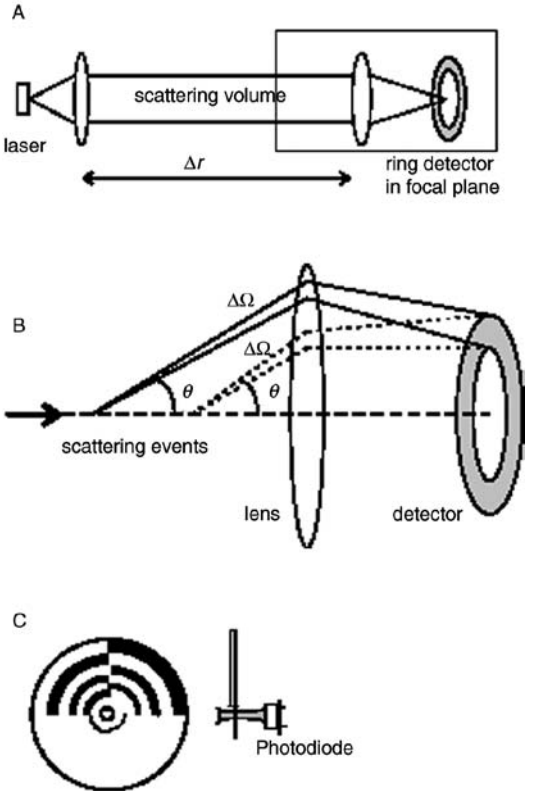

Figure 5.17
Conceptual diagrams of the Sequoia LISST, which measures the VSF in the far forward direction at 32 angular intervals.
A, laser passes through a lens into the sample compartment, called the scattering volume.
B, scattering events within the scattering volume cause photons to pass through a lens such that all scattering events along the optical path at angle θ are focused onto the detector at the same radial distance from the centre of the detector, regardless of where in the sample chamber they occur.
C, the detector consists of 32 concentric ring detectors arranged in quarter-circle arcs, each a defined radial distance from the centre and thus each associated with a unique forward scattering angle θ.
Source: LISST manual.

power-law size distribution increases (more small particles) (Stramski and Kiefer, 1991; Stramski et al., 2004). Thus variations in the backscattering signal, like the beam attenuation, are not purely a function of particulate suspended load, but also of the particle composition and size.

The effects of particle characteristics on backscattering have been described by Twardowski et al. (2001) who derived the theoretical relationship between the particle backscattering ratio (essentially the efficiency of particle backscattering, given by the

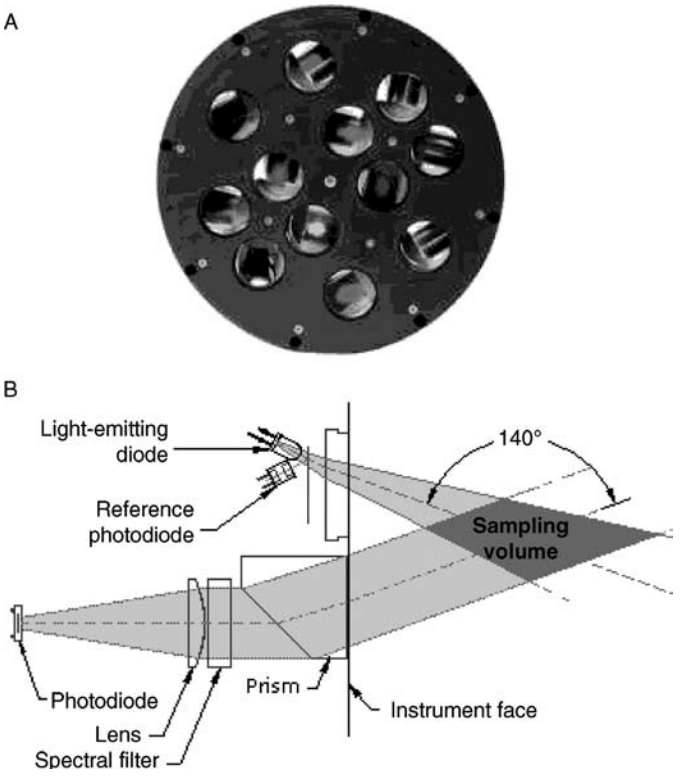

Figure 5.18
Configuration of HOBI Labs Hydroscat-6.
A, top view of sensor head showing the six source/detector pairs.
B, side view of instrument showing cross-section of one source beam from the LED, the detection field-of-view (arrows) and the intersection, which is the backscattering sampling volume.
Source: HOBI Labs website (www.hobilabs.com).

ratio of particle backscattering to particle scattering) and the power-law exponent and real refractive index (Figure 5.20). Superimposed on the theoretical nomogram, they plotted *in situ* observations from the Gulf of California. Data clusters were associated with specific regions of the water column for which the dominant particle type could be identified. These particle types included algal cells (data from the subsurface chlorophyll fluorescence maximum), non-algal organic particles (from the water column well below the euphotic zone, >100 m), and inorganic particles (from the resuspended nepheloid layer). This approach is a useful one for determining the bulk particle composition from observations of the particle backscattering and particle scattering coefficients (in both cases the effect of water are removed, either by correction or by calibration) and to a lesser degree, the power-law exponent. Algal cells, and other strongly absorbing particles, exhibit the lowest backscattering ratios (~0.5%) due to their large water content (Aas, 1996), while other weakly absorbing organic and detrital particles have

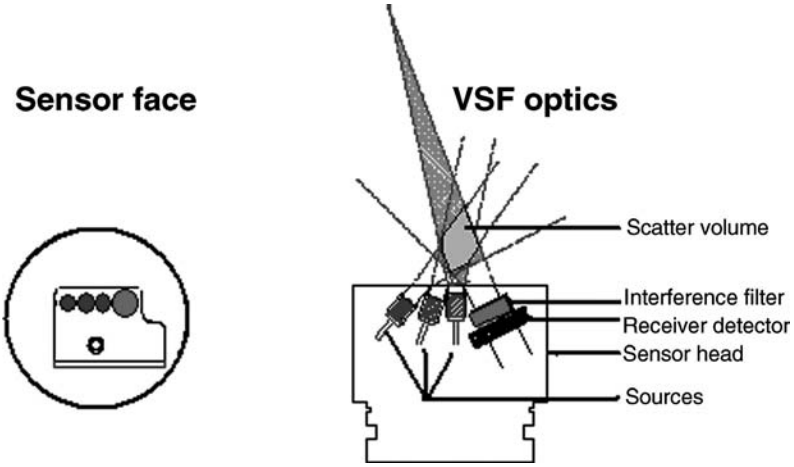

Figure 5.19
Conceptual diagram of the sensor head (left) and cross-section (right) of WET Labs ECOvsf showing the three LEDs and the single detector. The LEDs emit light at three different angles relative to the sensor head and relative to the single detector leading to detection of backscattering centred at 110°, 125° and 150°, from top to bottom, respectively.
Source: ECOvsf manual.

higher ratios (near 1%) and inorganic particles have the highest ratios (~2%). Boss et al. (2004), however, found that absorption impacts the backscattering coefficient of highly refractive particles more than lesser refractive particles, adding some uncertainty to our ability to invert for the index of refraction of these particles in the wavelengths were they may strongly absorb, for example in the blue. Thus for equivalent particle concentration and size, strongly absorbing algal cells will exhibit lower backscattering coefficients than will non-algal particles (organic and inorganic). This is in part what leads to a darkening of the water during algal blooms compared with episodes of sediment resuspension, which brightens the water.

5.5.6 Sensitivity of side or wide angle scattering meters (turbidometers, nephelometers)

Sensors designed to detect side angles or wide angle scattering have been used historically to quantify the suspended particle mass (Table 5.3), although it has been recognized for years that the utility was dependent on careful calibration with a known scattering suspension or *in situ* particles (Gibbs, 1974*a*, 1974*b*) because of the dependence of the magnitude of the side scattering on, not only particle concentration, but particle composition (real refractive index) and size distribution. An elegant demonstration of the correct calibration procedure was provided by Baker et al. (2001) for the WET Labs LLS. Their application of the technology was to study the suspended particles of the deep sea hydrothermal plumes, which have relatively low suspended loads (<0.1 mg l^{-1}) but with variable composition and size distributions. Raw voltages from 19 instruments were intercalibrated using a formazine standard. Clay suspensions

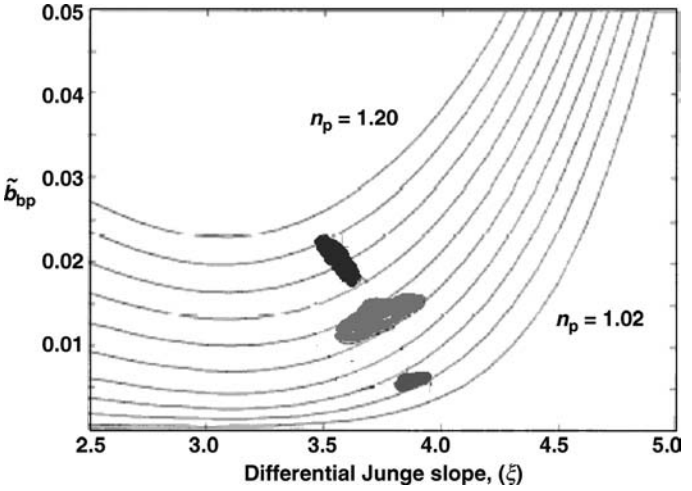

Figure 5.20
Theoretical relationship between the particle backscattering ratio and the Junge slope of particle size distribution with lines of constant real refractive index varying from 1.02 to 1.20. Superimposed are data clusters for *in situ* observations of particle backscattering ratio and the Junge slope (determined from c_p observations and (5.14) and (5.15)), taken from the subsurface chlorophyll maximum (lowest), deep-water column (middle), and benthic nepheloid layer (highest). The three data clusters are dominated by algal particles, non-algal organic particles and mineral particles, with backscattering ratios of approximately 0.005, 0.0125 and 0.02, respectively.
Source: modified from Twardowski et al. (2001).

of discrete size distributions (Figure 5.21A) were used to quantify the LSS response as a function of concentration (Figure 5.21B). A different standard curve was observed for each suspension of clay with different PSD. The slope of the standard curve, the concentration-specific backscattering coefficient (denoted K_{bs} in the original paper, b^*_b in the notation herein), when plotted as a function of the mean diameter for its respective clay suspension, displayed a Gaussian dependence (Figure 5.21C). Thus the response of the LSS varies significantly with particle size under a constant composition. The utility of this approach is the capability of quantifying the scattering response separately to concentration, composition and size distribution. However, *in situ*, additional IOP measurements would be needed to elucidate the cause of a specific change in the signal of a specific IOP (e.g. concentration, composition or size distribution).

5.5.7 What are the particles responsible for scattering in the ocean?

Having analysed the IOP response to particle characteristics and the instrument response to IOP variability, it is useful to step back and ask which particles dominate the *in situ* IOP observations. Here we examine a beam transmissometer (ac-9), a wide angle scattering sensor (LSS), and a single angle backscattering sensor (ECObb). Figure 5.22 shows the theoretical instrumental response as a function of particle size

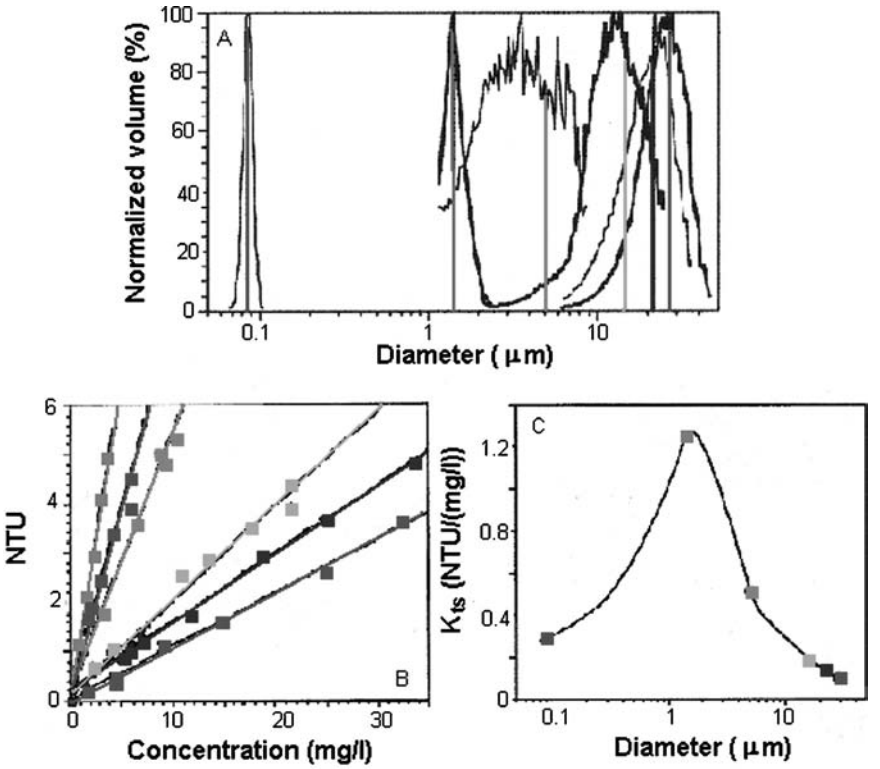

Figure 5.21
Example of the characterization of the WET Labs LSS sensor using dilutions of inorganic clay particles of known size distribution.
A, size distribution of six clay-particle suspensions, determined by Coulter Counter. Vertical lines indicate modal diameter for each suspension.
B, LSS response (NTU) to dilutions of the six suspensions, each represented by data points along a line colour-coded to the size distribution as in A. The slope of the line is the concentration-specific backscattering coefficient, K_{bs} $(\text{NTU mg l}^{-1})^{-1}$.
C, dependence of the concentration-specific backscattering coefficient K_{bs} on the mean particle diameter for each suspension, data points colour-coded as in A and B. This demonstrates that the LSS is most sensitive to particles in the size range 1 μm and less sensitive to both larger and smaller particles.
Source: modified from Baker et al. (2001).

for a range of real refractive indices. This figure is generated by computing the volume scattering function of a population of particles of a specific diameter and integrating that volume scattering function over the theoretical detection angles of each sensor. This is done for populations of particles of each discrete diameter value. Finally, the instrumental response has been normalized to the total particle volume so that we are looking at the response to a given, or known, particle volume, which is packaged into particles of diameter *D*. Thus, numerous small particles have the same volume of a few large particles. This approach is taken because of the use of scattering sensors to derive

volumetric biogeochemical proxies for total suspended solids (TSS) or total particulate organic carbon concentration (POC), neither of which contains size distribution information.

The volume-specific scattering response generally increases with refractive index for all particle sizes, as expected. However, the response of beam *c* to particle size is also a strong function of real refractive index. For beam *c* (Figure 5.22A), the strongest response is for a particle volume composed of 1 μm diameter particles of real refractive index 1.24 (as might be found for some clay suspensions). If the particles have a low real refractive index of 1.05 (typical for phytoplankton), it is the 5 μm diameter particles that yield the strongest mass specific response. Wide angle scattering response (Figure 5.22B) is dominated by the submicrometre particles of diameter ~0.5 μm (which would include microbubbles which have a refractive index of 0.75) with monotonically decreasing response to real refractive index. The particle volume-specific single angle backscattering response (Figure 5.22C) demonstrates a complex dependence on particle diameter. For any given refractive index, it is the small particles of diameter ~0.2 μm (clay and virus particles), that yield the strongest response and certainly the particle suspensions characterized by diameters <3 μm (which would include bacteria and picoplankton) have the highest specific backscattering signal. These results are consistent with those of Morel and Ahn (1991), Stramski and Kiefer (1991) and Baker et al. (2001) who found, respectively, that (a) the backscattering ratio declines, for monodispersed[22] populations, as particle size increases from 0.1 μm and is lower than that for polydispersed populations, (b) total scattering is dominated by particles in the range 1−10 μm and (c) backscattering is dominated by 0.1−1 μm particles. Note that Figure 5.22 provides the shape of the relative contribution of each size class to the respective IOP for particles obeying a power-law PSD with $\xi = 4$.

In terms of phytoplankton, only the very small picoplankton would be significant contributors to the particle backscattering. Larger phytoplankton are inefficient backscatterers because of their larger size and because of their strong absorption (imaginary refractive indices). However, it is important to note that they become more important backscatterers at wavelengths for which their absorption is minimal (generally the green region of the spectrum) and thus can still have a significant impact, particularly at the high concentrations that would be encountered during some HABs. In addition, non-sphericity is known to increase backscattering compared with what would be estimated for spherical particles, as assumed in our calculations (Bohren and Singham, 1991, Calvano et al., 2007).

While these simulations yield much information regarding scattering dependence on size and refractive index as well as instrument response, there are relatively few *in situ* examples for these dependencies. One approach is to measure the backscattering coefficient on a discrete water sample (must be a large volume to prevent scattering contamination by sidewall vessels), then to sequentially filter the water through smaller and smaller pore sizes, measuring the backscattering coefficient on each sequential suspension. In this way it is possible to separate the total backscattering coefficient into contributions by particles within each size interval. This approach to test these dependencies was conducted on water collected over a tidal cycle in the Damariscotta River Estuary, Maine using the WET labs ECOvsf. For this particular experiment

[22] Monodispersed refers to the population size distribution, dominated by particles within a narrow size range, as in a monospecific algal bloom. In contrast, polydispersed indicates a population comprised of particles with a large size range.

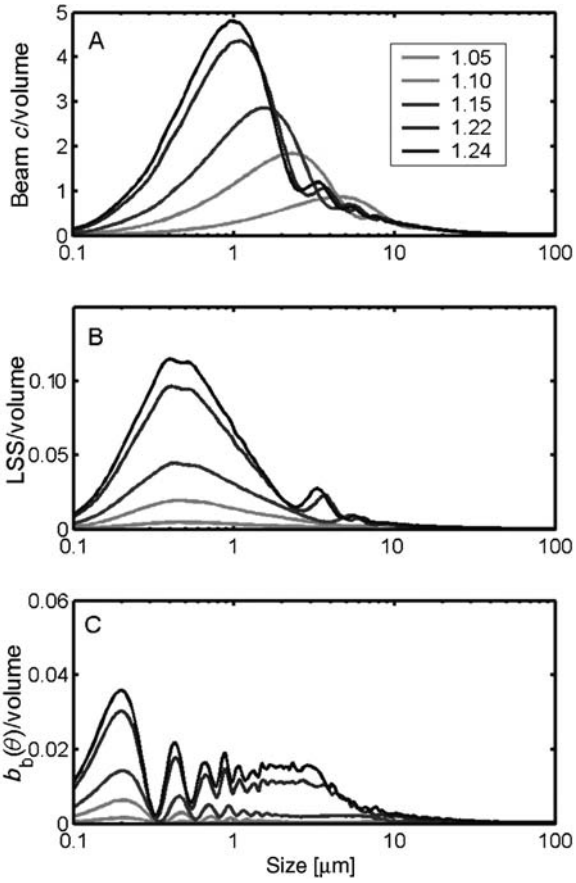

Figure 5.22
Particle volume-specific instrument response as a function of particle diameter for A, beam transmissometer; B, wide-angle scattering sensor; C, single-angle backscattering sensor, as a function of particle refractive indices (ranging 1.05 to 1.24). As particle refractive index increases, all scattering properties increase. Beam *c* is most sensitive to highly refractive (i.e. mineralic) particles in the range 1 µm. For less refractive particles (i.e. phytoplankton), beam *c* is most sensitive to particles of diameter 5 µm. Wide-angle side scattering is most sensitive to particles in the size range 0.5 µm, regardless of refractive index although the response increases with refractive index. Backscattering is most sensitive to small particles of order 0.2 µm although the relationship is complex and particles up to 5 µm are effective backscatterers.

the size fraction 3−10 µm was found to contribute approximately 50% to the total backscattering coefficient (Figure 5.23). These results were consistent throughout the tidal cycle. In keeping with the results of the simulation in Figure 5.22, it confirms that the particles in this size range are efficient backscatterers and were numerous in these waters.

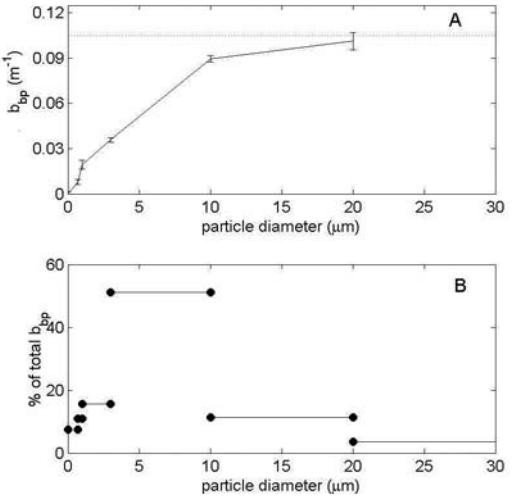

Figure 5.23
Example of the contribution of particles within discrete size ranges to the total particle backscattering for natural waters.
A, cumulative backscattering as a function of particle diameter for discrete size intervals. The total particle backscattering coefficient is indicated by the dotted line (~0.105 m^{-1}) and error bars indicate ±1 standard deviation of >300 realizations.
B, percentage contribution to total backscattering by each size interval. A whole water sample collected from the Damariscotta River Estuary was size fractioned (ranges indicated by bars) and the backscattering of each fraction was measured with a WET Labs ECOvsf sensor (440 nm). For this particular sample, which is consistent with other collected during a 24-hour time-series experiment, the particles in the 3–10 μm size range dominated the backscattering coefficient. This results in part from their particle-specific backscattering efficiency (modelled in Figure 5.22) and their *in situ* concentration relative to particles in the other size intervals.

5.5.8 What is the IOP measurement response to algal blooms?

The above discussion has centred on the sensitivity of IOP measurements by *in situ* sensors to weakly absorbing particles (non-pigmented particles with low imaginary refractive indices) in order to aid in the interpretation of *in situ* IOP observations under typical oceanic conditions. How does the picture change in the presence of intense algal blooms? In this section we investigate how phytoplankton impact the IOPs and provide two specific examples for blooms of *Prorocentrum micans*, a 27 μm diameter dinoflagellate that causes red tides in coastal Gulf of Maine waters and elsewhere. *Aureococcus anofragefferens* is a 2 μm pelagophyte that causes brown tides in Long Island inlets and is related to the organisms causing brown tides along the Texas Gulf Coast and the west coast of South Africa.

Phytoplankton impact IOPs greatly because their spectrally varying imaginary refractive index n', which is a consequence of their specific pigments. These impacts

include variations in both the magnitude and spectral shape of the absorption and scattering spectra. Particle absorption varies spectrally, and the spectral shape changes from the exponentially decaying function of wavelength, typical of non-algal particles, to spectrally complex as the proportion of phytoplankton cells increases relative to non-algal particles (e.g. Bricaud and Stramski, 1990; Garver et al., 1994; Cleveland, 1995; Sosik et al., 2001; Babin et al., 2003) (Figure 5.24A). Within the phytoplankton component of the particulate matter, the spectral shape changes as pigment ratios vary in response to species composition (e.g. Sathyendranath et al., 1987; Bricaud et al., 1988; Hoepffner and Sathyendranath, 1991; Allali et al., 1997; Bricaud et al., 1998) (Figure 5.24B). Finally, within a single pigment-based algal taxonomic group, the spectral shape of the phytoplankton absorption varies in response to algal cell size and nutrient and light conditions due to packaging of the pigment within the cell (Morel and Bricaud, 1981; Sosik and Mitchell, 1991) (Figure 5.24C).

All these sources of variability will impact the interpretation of *in situ* IOP observations during high concentration algal blooms. One of the characteristics of HABs that is often observed is the dominance of a single species over other species in the community (Cullen, 2006 – Chapter 1 this volume). Here we present two examples. The first case is a bloom of *Prorocentrum micans* observed off the Bigelow Laboratory dock in West Boothbay Harbor, Maine (USA) in 2001 (Etheridge et al., 2002). Chlorophyll concentrations for the bloom of the 27 µm modal diameter cell exceeded 100 mg chl m^{-3}. The observed IOPs for this bloom are shown in Figure 5.25. The absorption shows some flattening of the blue peak due to strong pigment packaging (the specific absorption coefficient at 676 nm was 0.0075 m^2 mg^{-1}). The spectral slope of the particulate beam *c* was flat, consistent with dominance by large particles, and the spectral dependence of the scattering and backscattering demonstrated the anomalous dispersion, that is depressed scattering, associated with absorption peaks. The backscattering ratio was ~0.2% consistent with large, strongly absorbing algal cells.

The bloom resulted in red discoloration of the water (Figures 5.26A, 5.26B). This was not because of a specific pigmentation of *P. micans*, but rather the combination of strong absorption in the blue and green wavelengths (400–550 nm) and spectrally flat backscattering (Figures 5.25A, 5.25D). The coastal waters of the Gulf of Maine are characterized by high CDM absorption, originating from the many freshwater inputs. This and the very high *P. micans* absorption in combination with water absorption, resulted in an absorption minimum that was shifted to approximately 600–650 nm, which in combination with the red enhanced backscattering spectrum yielded reflectance maxima in the spectral range 600–700 nm, or a reddish ocean (Etheridge et al., 2002).

The second case is that of an *Aureococcus anophagefferens* bloom observed in Quantuck Bay, Long Island, New York in 2000 (Etheridge and Roesler, 2004). In contrast to the IOPs for the large *P. micans* bloom, the IOPs for the 2 µm diameter *A. anophagefferens* exhibited strongly peaked absorption (chlorophyll specific absorption at 676 nm ~0.2 m^2 mg^{-1}), spectrally decreasing particulate beam attenuation and scattering spectra, and backscattering ratios of ~1%, all consistent with strongly absorbing small algal particles. Like the Gulf of Maine, the waters in Long Island Sound are also typically green due to strong CDM absorption. However, the differences between the *A. anophagefferens* absorption compared with that of *P. micans* in the blue/green region of the spectrum (i.e. less green absorption relative to blue) in combination with an order of magnitude increase in the red-enhanced backscattering coefficients are sufficient

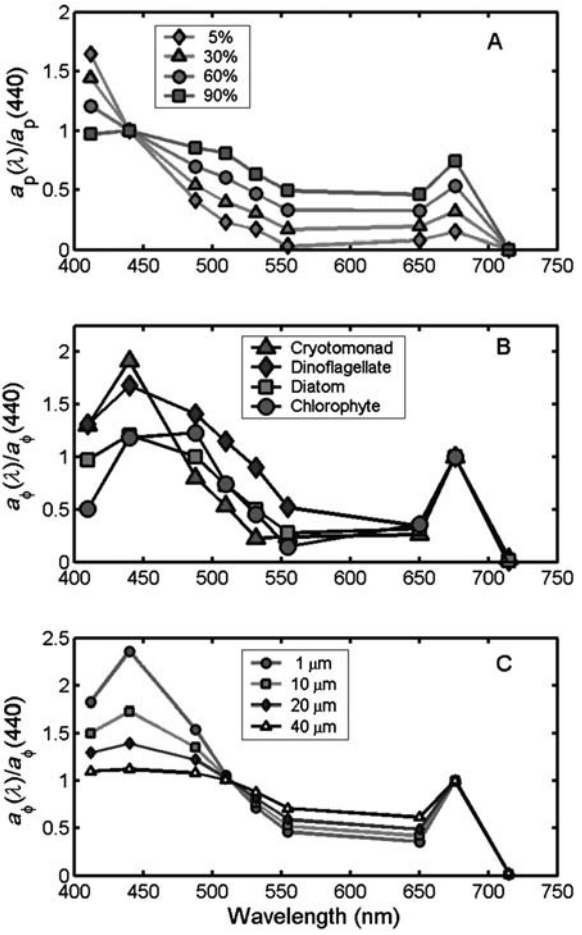

Figure 5.24
Spectral absorption variations associated with phytoplankton properties as would be observed with an ac-9.
A, particulate absorption simulated as a function of percentage of algal contribution relative to non-algal particles, scaled to 440 nm. As the contribution by phytoplankton to the total particle absorption decreases, the spectral shape becomes more exponential like that of non-algal particle absorption (see Figure 5.1).
B, spectral phytoplankton absorption for four algal taxa, measured in culture, scaled to 440 nm. The variations in the absorption spectral shapes are caused by variations in pigment composition between the taxa.
C, spectral phytoplankton absorption simulated for a single pigment composition as a function of algal cell diameter (micrometres), scaled to 440 nm. As the cell size increases, the absorption efficiency at each wavelength decreases, leading to flattened absorption peaks, a process called pigment packaging.
Source: Morel and Bricaud (1981).

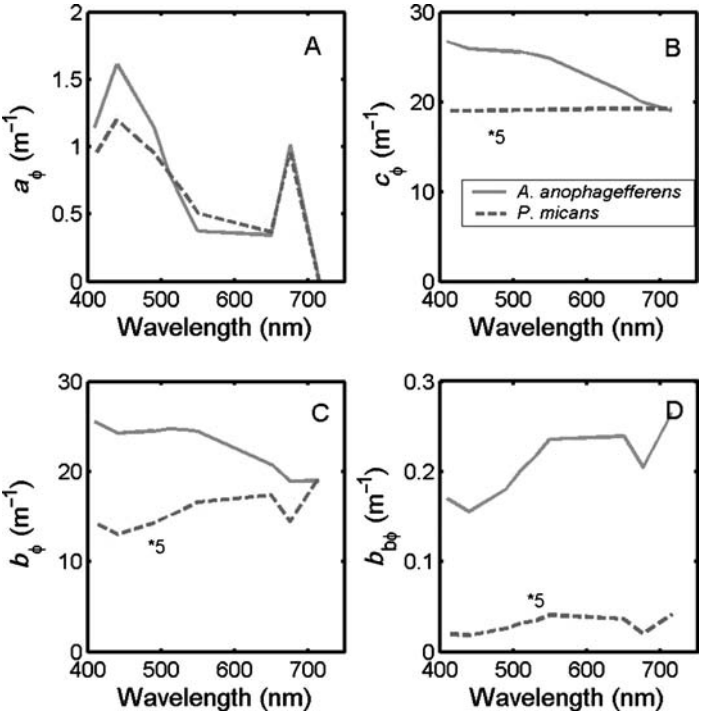

Figure 5.25
Measured inherent optical properties of two algal blooms, *Prorocentrum micans* (red) in the Gulf of Maine and *Aureococcus anophagefferens* (brown) in Long Island Sound. The algae were of sufficient concentrations to turn the water respectively red and brown. The *a* and *c* coefficients were measured with an ac-9, and used to derive *b*. The measured IOPs and particle size distributions were used to estimate indices of refraction at the ac-9 wavelengths and backscattering was determined using Mie modelling. Note that the *P. micans* values in B, C and D have been multiplied by 5 for ease of resolving spectral shapes.

to change the colour of the water to brown, instead of red (Figure 5.26C). Measured radiance reflectance spectra for the brown tide bloom exhibited a broad flat maximum over the range 550–700 nm compared with the more narrowly peaked spectrum with a maximum of 600 nm observed for *P. micans*.

If we consider a monitoring programme that includes IOP observations, how are these two very different blooms resolved by the observations? Against a background of organic particles characterized by a refractive index of 1.05 + i 0.001 and a power-law PSD slope of 4, typical of coastal to oceanic waters, we simulated the development of a bloom by allowing greater proportions of the total particle volume (which was held constant) to be attributed to superimposed monodispersed algal cells. The phytoplankton were modelled as homogeneous spheres with PSDs described by Gaussian distributions with size ranges of 25 μm ± 15 μm and 2.5 μm ± 1.5 μm, respectively, and with refractive indices of $1.02 > n'$ (where n' was determined from the absorption coefficients in Figure 5.25A

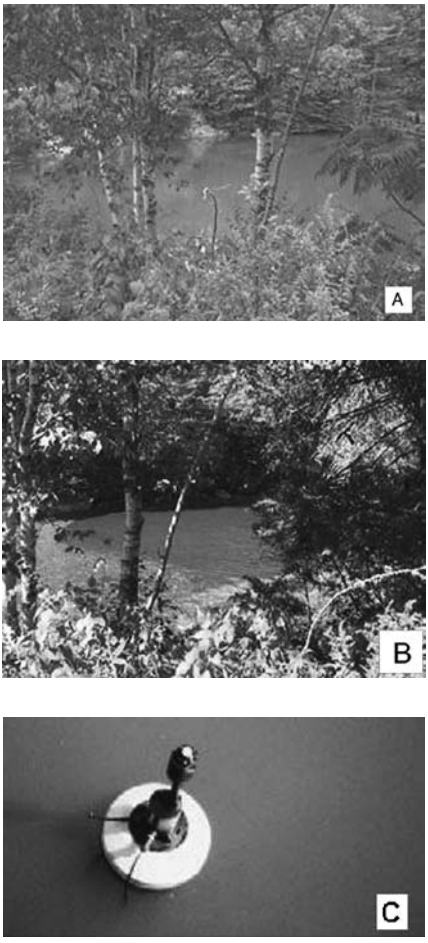

Figure 5.26
Examples of water discoloration during the monospecific HABs in Figure 5.25.
A, B, views of coastal waters near Bigelow Laboratory for Ocean Sciences, West Boothbay Harbor, Maine, in October 1999, (A) prior to and (B) during the *P. micans* bloom. The water is characteristically green due to high CDOM absorption and red during the bloom from the enhanced blue-green absorption and red backscattering of the *P. micans* cells.
Source: photos courtesy of M. Keller.
C, brown water associated with the *Aureococcus anophagefferens* bloom in Quantuck Bay, Long Island, New York, in June 2000.
Source: photo courtesy of S. Etheridge.

and the PSD, Morel and Bricaud, 1981). The VSF for the *P. micans* bloom simulation indicates that as the proportion of the total volume attributed to the large, strongly absorbing algal cells increases, the far-forward scattering at angles <1° also increases because larger particles diffract light more efficiently than small particles (Figure 5.27A). How-

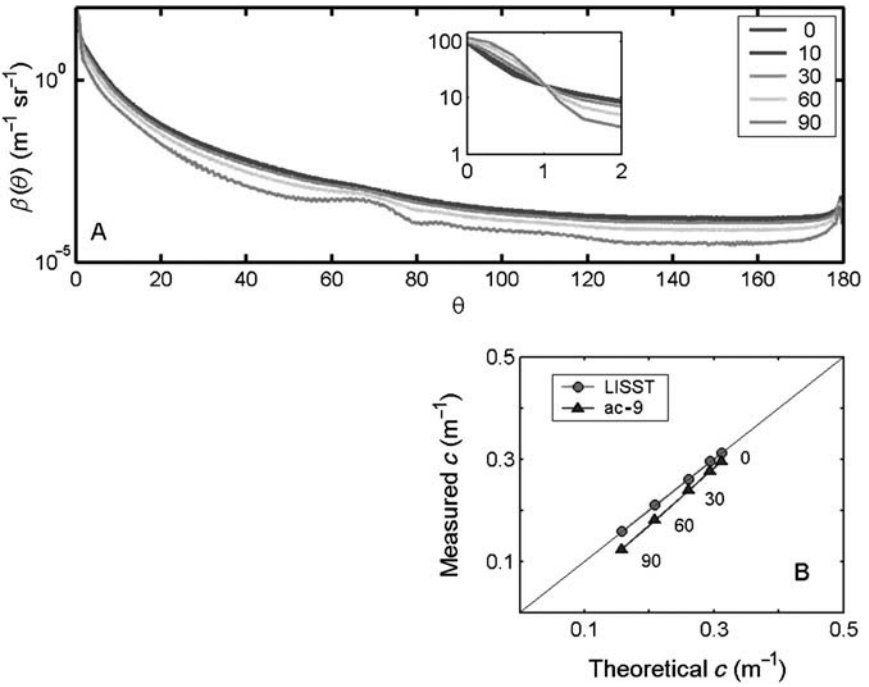

Figure 5.27
A, volume scattering functions computed for particles with refractive index 1.05 + i 0.001, a Junge slope of 4 with increasing proportions of *P. micans* cells from 0% to 90% of total particle volume. The total particle volume was held constant, only the proportions change.
Inset: first 2° of resolution.
B, modelled values for beam attenuation coefficient versus theoretical values for the two instruments as in Figures 5.14 to 5.16. As the proportion of *P. micans* increases, beam attenuation coefficients decrease, because phytoplankton are less efficient attenuaters than other weakly absorbing particles.

ever, at angles >1°, scattering decreases because large absorbing particles are ineffective scatterers per volume (photons entering the particles tend to be absorbed before they are scattered out of the particle). Thus the total scattering, beam attenuation and backscattering coefficients all *decrease* as the proportion of *P. micans* cells increases (Figure 5.27B).

The scenario is different for the *A. anophagefferens* bloom (Figure 5.28). The VSF exhibits two crossovers as a function of the proportion of algal cells to the total particle volume increases, one at approximately 0.7° and a second at approximately 20°. In this case the diffraction scattering at angles <0.7° decreases as the relative concentration of *A. anophagefferens* increases because these cells are less efficient scatters per unit volume. However, between 0.7° and 20°, the scattering increases with increasing cell proportions. At backscattering angles, the algae are again inefficient backscatterers because of their strong absorption and low refractive index. When the VSF is integrated over all angles it is found that the total scattering and therefore attenuation coefficients increases with in-

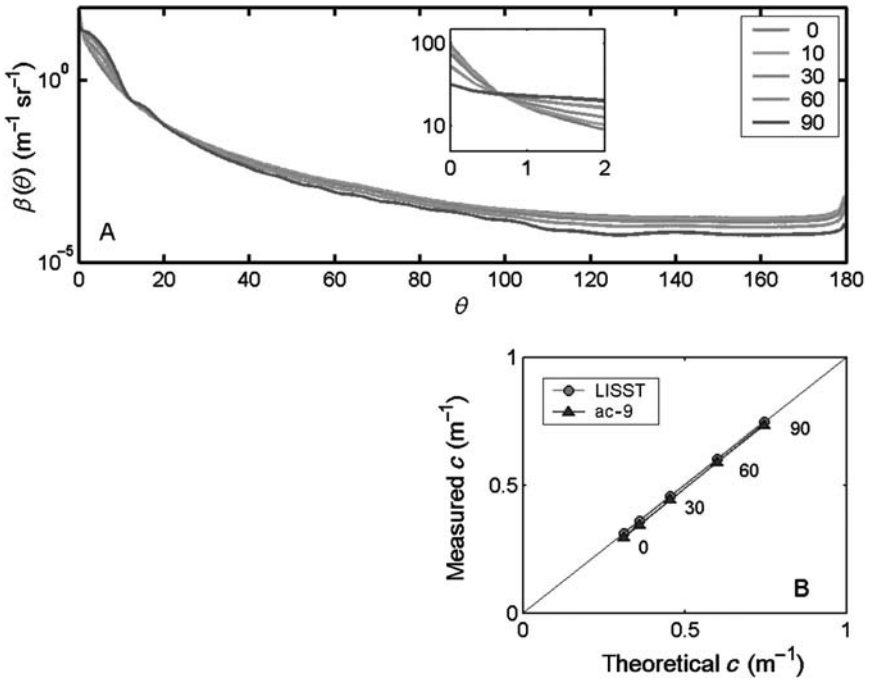

Figure 5.28
A, volume scattering functions computed for particles with refractive index 1.05 + i 0.001, a Junge slope of 4 with increasing proportions of *Aureococcus anophagefferens* cells from 0% to 90% of total particle volume. The total particle volume has been held constant, only the proportion of *A. anophagefferens* cells relative to background particles changes.
Inset: first 2° of resolution.
B, modelled values for beam attenuation coefficient versus the theoretical values for the two instruments as in Figure 5.27. As the proportion of *A. anophagefferens* increases, beam attenuation coefficient per particle volume increases as the small *A. anophagefferens* cells are more efficient attenuaters than the larger background particles (which might consist of larger cells, aggregates, detrital matter, suspended sediments).

creasing proportions of *A. anophagefferens* to the total particle population (Figure 5.28B). However, the backscattering coefficient, as for the case of *P. micans*, decreases as the cell proportion increases. The backscattering coefficient for *A. anophagefferens* is nearly an order of magnitude greater than that for the same particle volume of *P. micans*, consistent with observations that backscattering is dominated by small particles, even if they are absorbing particles. So for equivalent algal cell volumes, HABs dominated by small cell species will yield brighter waters than those dominated by large cell species if all other components are constant. Yet HABs yield darker waters than those without high concentrations of algal cells because phytoplankton are less efficient backscatterers than are the more weakly absorbing non-algal particles for the same particle volume concentration.

5.6 Employing IOP sensors in a coastal monitoring programme

The utility of using *in situ* observations of IOPs in a coastal monitoring programme has been demonstrated above as they can provide information regarding particle concentration and composition, once the instruments are characterized and calibrated to adequate standards. An understanding of the sources of variability in the constituent-specific optical properties, and an understanding of the instrument-specific response to those variabilities are both necessary to interpret *in situ* observations. While no single IOP model will be applicable to all algal blooms, *in situ* IOP observations can contribute important information as blooms initiate and develop. These include detection of (a) changes in the proportion of algal absorption to total absorption, (b) changes in the spectral slope of the beam attenuation to indicate bulk particle size changes, (c) changes in the bulk backscattering ratio to indicate changing dominance by algal particles, and (d) changes in near forward VSF indicating changes in the bulk size distribution. The nature of the HAB problem (Cullen, 2007 – Chapter 1 this volume) will help to dictate which IOPs will be the most useful. Ancillary measurements of physical and chemical parameters (e.g. temperature, salinity, radiance, turbulence levels, nutrients, pigments) can greatly supplement the IOP measurement to narrow down the probable cause of the change in IOP.

5.6.1 HAB scenario 1: high algal biomass caused by the target species

For a HAB problem in which any increase in particle attenuation is due to the cells themselves or due to covarying particles, a simple beam transmissometer or scattering sensor might be sufficient for early detection. This is the case for *Aureococcus anophagefferens* in Long Island Sound embayments (Figures 5.29A, 5.29B). However, when monitoring such situations with a full suite of IOP sensors, obtaining more information regarding the ecosystem is possible. This was found for two embayments in Long Island Sound

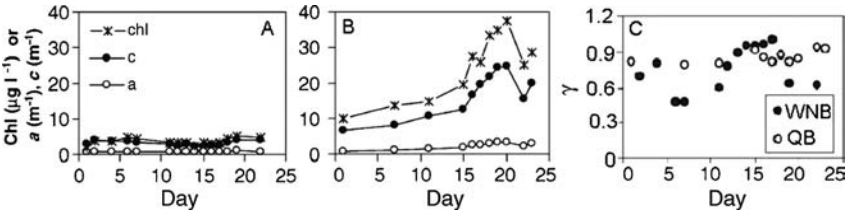

Figure 5.29
Time series of IOP observations during a brown-tide bloom, Long Island, N.Y. (Etheridge and Roesler, 2004): beam attenuation, absorption and chlorophyll from A, West Neck Bay; B, Quantuck Bay; C, slope of the particle beam attenuation coefficient (γ) for both sites. The phytoplankton community varied in both particle size and pigment composition at WNB although the bulk concentration remained stable. In contrast, a bloom of *Aureococcus anophagefferens* developed at QB as indicated by the increase in the IOP magnitudes and chlorophyll concentration. The indicator of size distribution remained invariant and indicative of small particles, consistent with the *A. anophagefferens* cell size (<3 μm). These results were verified by microscopy and size fractionated HPLC pigment analyses.

in 2000 (Etheridge and Roesler, 2004). Recurrent brown tide blooms had previously been found in West Neck Bay; for the field programme Quantuck Bay was used as the control environment against which the developing brown tide would be viewed. Time-series IOP observations were made in two different embayments, contrary to previous observations, the brown tide developed in Quantuck Bay and not in West Neck Bay (Figures 5.29A, 5.29B). Estimations of the particle size distribution derived from the spectral slope of beam *c* indicated that the bay with the *A. anophagefferens* bloom was dominated by smaller particles consistently over the three-week period while large variations in the estimated particle size slope were observed in the bay without the brown tide (Figure 5.29C). Size fractionated HPLC pigment analyses and microscopy verified that the non-brown tide phytoplankton community was highly variable in both size and pigment-based taxonomy although the bulk biomass (as estimated by chlorophyll concentration and particulate beam *c*) remained nearly constant in contrast the brown-tide phytoplankton community was dominated by *A. anophagefferens* with virtually no other contributions by other species throughout the bloom. Thus the spectral beam *c* observations contributed significantly to understanding both the biomass aspects of the bloom but also the composition phytoplankton composition in both bays.

5.6.2 HAB scenario 2: high algal biomass, in which target species just one member of the population

For productive waters with high algal concentrations that are occasionally plagued by blooms of toxic or harmful species, more information than biomass is required. If the targeted species is recurrent and its optical and size properties are known, the spectral IOPs may provide indicators of the target species against the background of the phytoplankton community. In this case, instrumentation to detect particle size distribution and spectral absorption properties may be advantageous. This is the case for *Karenia brevis* off the coast of Florida and *Alexandrium* sp. or *Dinophysis* sp. off the coast of South Africa. Detecting a target species among a general population of phytoplankton using the IOPs is likely to depend on the capability for *in situ* hyperspectral absorption and algorithms to identify particular features associated with pigment composition (Schofield et al., 1999). This approach has been implemented on the West Florida Shelf using two different *in situ* technologies: a hyperspectral absorption/attenuation meter (WET Labs acs; Craig et al., 2006) and a liquid waveguide capillary cell spectrometer (LWCC, essentially a hyperspectral spectrophotometer with ~1 nm resolution; Kirkpatrick et al., 2003) in combination with an algorithm called a similarity index (essentially the goodness of fit between the measured absorption spectrum and that associated with the target species). Results suggest that the fraction of chlorophyll associated with *K. brevis* is significantly related to the similarity index derived from LWCC absorption measurements (Kirkpatrick et al., 2000). Recently this spectrometer has been deployed on a glider platform to retrieve three dimensional distributions of *K. brevis* (Schofield et al., 2004).

5.6.3 HAB scenario 3: low algal biomass or target species never dominates population

In coastal waters where seasonal algal blooms occur but the target species never reaches high-biomass conditions and thus never contributes significantly to the bulk optical properties, IOP observations alone cannot identify the target species of interest. If however, unique behavioural or ecological patterns, such as vertical migration or

co-occurrence of target species with other taxa that *are* optically detectable, can result in the development of optical proxies indicating the likely presence of the target species. This is the case with *Alexandrium fundyense* in the Gulf of Maine. For example, *in situ* observations of spectral or hyperspectral absorption, in combination with optically based estimates of size distribution, can be used to identify species succession from large diatom communities to dinoflagellates to smaller flagellates, indicating when *Alexandrium* sp. are likely to be found (see Section 5.6.4).

5.6.4 Temporal variations in ecosystem structure inferred from *in situ* IOP observations

An example of the type of time-series observations that are available with moored IOP instrumentation is taken from the Gulf of Maine Ocean Observing System (GoMOOS) programme. IOP and hydrographic observations of an autumn transition period in the coastal Gulf of Maine waters are shown in Figure 5.30. These observations are from one of 10 moorings deployed in the Gulf of Maine, which report real-time hourly observations of meteorologic, hydrographic and optical conditions. In autumn 2002, the coastal waters were undergoing destratification, with mixing events occurring the third week of August and the second week of September, separated by restratification, and a final mixing at the beginning of October, which resulted in complete destratification (Figure 5.30A).

Associated with these changes in the thermal structure were significant changes in the optical properties (Figures 5.30B to 5.30F). The spectral absorption coefficients, measured with an ac-9 at ~3 m, were deconvolved into contributions by the major absorbing constituents (Roesler et al., 1989). The standard deconvolution model, which depends on an *a priori* determination of the 440 nm:676 nm ratio for absorption by phytoplankton, was found to converge only if two different ratios were used for the first part and the last part of the time series (1.9, 1.6 respectively). These yielded two very different spectral shapes for the phytoplankton absorption (Figures 5.30E, 5.30F respectively). Incorporating these two phytoplankton absorption spectral shapes, plus the absorption spectral shapes for NAP and CDM (i.e. Figure 5.1), a linear least-squares minimization to the total absorption time series was obtained. The resulting time series of the magnitude of constituent absorption at 440 nm indicates that a_{CDM} is relatively invariant for this time period, while a_{NAP} is negligible until mid-November, when it increases dramatically.

The first component of phytoplankton absorption is associated with the small algal blooms that occur in response to the series of destratification/stratification events until mid-October. Once the water column becomes destratified, and presumably well-mixed, the second phytoplankton component becomes dominant. While there was no *in situ* validation, the spectral shapes of these two components are consistent with these observations, the first exhibiting strong peaks, characteristic of phytoplankton growing near the surface in a stratified high-light environment; the second exhibiting strong pigment packaging characteristic of light-limited cells in a deeply mixing water column.

The particle backscattering ratio (Figure 5.30C), which is indicative of particulate composition, is consistent with the particulate composition obtained by absorption inversion. Periods of algal blooms are associated with low backscattering ratios, while the transition from the high concentrations of the high-light adapted phytoplankton to lower concentrations of the low-light adapted phytoplankton with some contributions

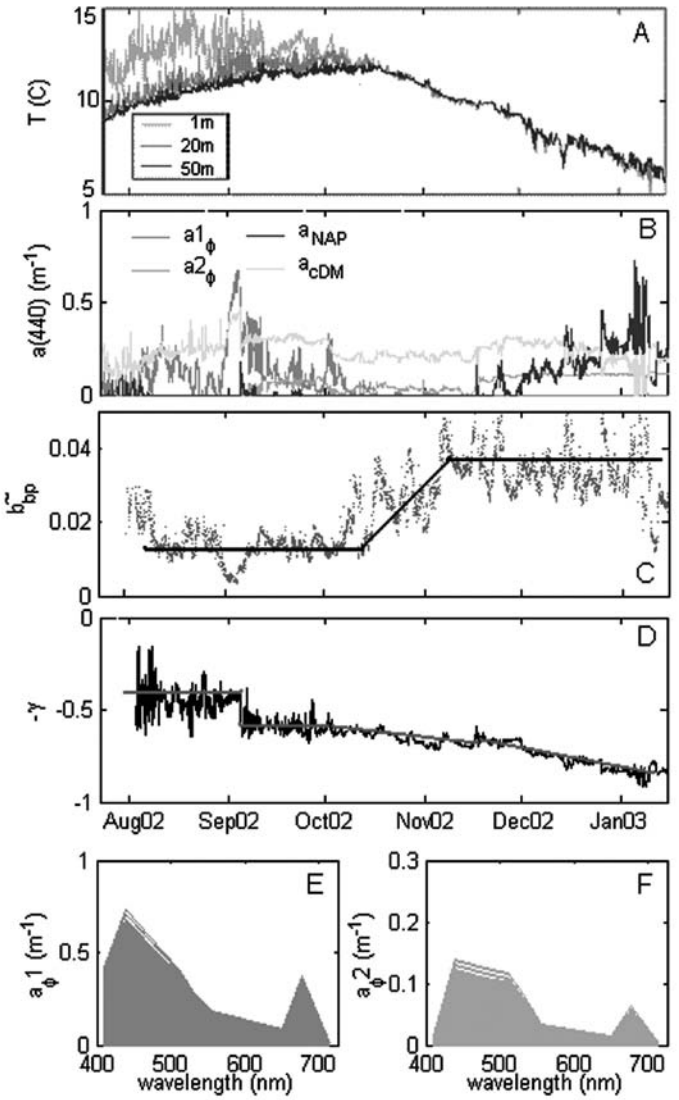

Figure 5.30
Real-time hourly observations of temperature, IOPs and derived optical properties for the period August 2002 to January 2003 from the Eastern Maine Coastal Current, Gulf of Maine.
A, temperature at 0 m, 20 m and 50 m.
B, component absorption (440 nm, derived from total measured absorption, see text for details).
C, particle backscattering ratio (660 nm).
D, spectral slope of particle attenuation -γ.
E, F, spectral shape of two phytoplankton absorption components, the temporal pattern for each shown in B. See text for details.
Source: Roesler and Barnard (2003).

by NAP, is associated with backscattering ratios characteristic of more detrital organic particles. Finally, the increase in the NAP absorption component is associated with high backscattering ratio values, consistent with inorganic particles. The spectral slope of the particle attenuation spectrum γ is initially ~0.4, indicating larger particle dominance until the decline of the large bloom (Figure 5.30D). The value decreases to ~0.6 as the proportion of high-light adapted cells declines. The slope continues to decrease as the particulate pool changes composition to the low-light adapted algal population and finally to the inorganic particle population composed of smaller particles (steeper PSD exponent).

Analysis of residual (detided) currents at this mooring (data not shown) indicate that this period of increasing inorganic particles is associated with strong offshore currents. The inshore region is known for deep tidal mixing, which during destratified periods resuspends sediments into the surface layer, which would then be transported offshore past the mooring. The combination of hydrographic and optical observations, complete with analysis of derived optical properties allows the structure of the dissolved and particulate pools (including phytoplankton, other organic and inorganic particles) to be characterized on highly resolved times scales. Such an approach, when applied to a HAB situation can provide information not only on algal absorption properties, but co-occurring particulate and dissolved matter and variations in particle size distribution. As outlined in the three HAB scenarios above, this may provide direct information on the HAB itself, or ancillary information about the ecosystem as a whole with which to interpret HAB dynamics. While biofouling of optical instrumentation is of great concern in moored situations, great strides have been made in reducing biofouling with copper coatings, tubing and shutters (Chang and Dickey, 2007; Lehaitre et al., 2007 – Chapters 2 and 12 this volume) Additionally, employing multiple optical sensors to derive redundant optical properties yields a method for *in situ* validation: phytoplankton concentration via fluorometry and absorption (e.g. by decomposition or the magnitude of the absorption at 676 nm), or particle composition via absorption deconvolution and particle backscattering ratios, and particle size distribution via LISST and spectral c_p.

5.7 State-of-the-art and future *in situ* IOP observations

In situ analysis of seawater to further discern particle specific IOPs has lead to some unique observations about the concentration, composition and distribution of algal groups. One type of manipulation is *in situ* size fractionation, in which filter cartridges are placed at the intake port of the ac-9 (Roesler et al., 1997; Boss et. al.,2007). By choosing the filter size carefully, the target species in question can be isolated from the bulk particles and the optical properties monitored for changes in concentration. Other manipulations might be chemical, such as acidification of the water sample to dissolve carbonate cell walls (Balch et al. 1999). This approach has been used to detect the presence of coccolithophorids *in situ*. A third manipulation is pressurization to burst gas vacuoles associated with cyanobacteria such at *Trocodesmium* spp. (Subramanian et al., 1999) to identify their presence *in situ*.

A promise for the future is the detection of pigment based taxonomic groups based on hyperspectral absorption observations. While the absorption ratios detected at ac-9 wavelengths are sufficient to resolve major groups (Figure 5.24B), the aim is that with increased spectral resolution, even finer distinctions can be made. This is the basis for

the 'breve-buster' discussed in Section 5.6.2. The 0.5 m path length Liquid Waveguide Capillary Cell and *in situ* size fractionation to examine the high-resolution absorption properties of *Karenia brevis*-sized particles, which in combination with the similarity index algorithm (Millie et al., 1997), appears to detect the presence of *K. brevis* (Kirkpatrick et al., 2000). This instrumentation package is currently being deployed aboard an AUV, which provide high-resolution observations in three dimensions.

One of the major underlying assumptions in many of the simulations and interpretations of optical proxies is that of particle sphericity. Future commercial VSF and polarized scattering sensors will further increase the information on underlying constituents facilitating and providing more robust inversions than currently available. In particular, polarized scattering contains additional information on the shape of underlying particles currently unavailable (Geller et al., 1985; Hovenier et al., 2003).

Finally, the near future is exploding with the miniaturization of optical sensors. This miniaturization will lead to the incorporation of optical sensors on a range of platforms that have remained elusive due to size, mass and power constraints. These include gliders, drifters and floats (Rudnick and Perry, 2003; Griffiths, 2007 – Chapter 13 this volume). Sensor miniaturization is currently being employed in the development of hybrid sensors such as those that detect both fluorescence and backscattering in a can the size of a hockey puck (WET Labs). The explosion of observational platforms and optical instrument development in combination with optical theory will lead to detection of oceanic constituents on time and space scales that are currently only a dream.

References

Aas, E. 1996. Refractive index of phytoplankton derived from its metabolite composition. *J. Plankton Res.*, 18, pp. 2223–49.

Agrawal, Y. C. and Pottsmith, H. C. 2000. Instruments for particle size and settling velocity observations in sediment transport. *Mar. Geol.*, 168, pp. 89–114.

Allali, K., Bricaud, A. and Claustre, H. 1997. Spatial variations in the chlorophyll-specific absorption coefficients of phytoplankton and photosynthetically active pigments in the Equatorial Pacific. *J. Geophys. Res.*, 102, pp. 12413–23.

Babin, M., Morel, A., Fournier-Sicre, V., Fell, F. and Stramski, D. 2002. Light scattering properties of marine particles in coastal and oceanic waters as related to the particle mass concentration. *Limnol. Oceanogr.*, 48, pp. 843–59.

Babin, M., Roesler, C. S. and Cullen, J. J. (eds). 2006. *Real-time Coastal Observing Systems for Marine Ecosystem Dynamics and Harmful Algal Blooms: Theory, Instrumentation and Modelling*. Paris, Intergovernmental Oceanographic Commission of UNESCO. (Monographs on Oceanographic Methodology)

Babin, M. and Stramski, D. 2002. Light absorption by aquatic particles in the near-infrared spectral region. *Limnol. Oceanogr.*, 47, pp. 911–15

Babin, M. and Stramski, D. 2005. Variations in the mass-specific absorption coefficient of mineral particles suspended in water. *Limnol. Oceanogr.*, 49, pp. 756–767.

Babin, M., Stramski, D., Ferrari, G. M., Claustre, H., Bricaud, A., Obolensky, G. and Hoepffner, N. 2003. Variations in the light absorption coefficients of phytoplankton, nonalgal particles, and dissolved organic matter in coastal waters around Europe. *J. Geophys. Res.*, doi:10.1029/2001JC000882.

Bader, H. 1970. The hyperbolic distribution of particle sizes. *J. Geophys. Res.*, 75, pp. 2823–30.

Baker, E. T., Tennant, D. A., Feely, R. A., Lebon, G. T. and Walker, S. L. 2001. Field and laboratory studies on the effects of particle size and composition on optical backscattering measurements in hydrothermal plumes. *Deep Sea Res. I*, 48, pp. 593–604.

Balch, W. M., Drapeau, D. T., Cucci, T. L., Vaillancourt, R. D., Kilpatrick, K. A. and Fritz, J. J. 1999. Optical backscattering by calcifying algae – separating the contribution by particulate inorganic and organic carbon fractions. *J. Geophys. Res.*, 104, pp. 1541–58.

Bohren, C. F. and Huffman, D. R. 1983. *Absorption and Scattering of Light by Small Particles*. New York, John Wiley & Sons.

Bohren, C. F. and Singham, S. B. 1991. Backscattering by nonspherical particles: a review of methods and suggested new approaches. *J. Geophys. Res.*, 96, pp. 5269–77.

Boss, E. and Pegau, W. S. 2001. Relationship of light scattering at an angle in the backward direction to the backscattering coefficient. *Appl. Opt.*, 40, pp. 5503–07.

Boss, E., Pegau, W. S., Gardner, W. D., Zaneveld, J. R. V., Barnard, A. H., Twardowski, M. S., Chang, G. C. and Dickey, T. D. 2001*b*. The spectral particulate attenuation and particle size distribution in the bottom boundary layer of a continental shelf. *J. Geophys. Res.*, 106, pp. 9509–16.

Boss, E., Twardowski, M. S. and Herring. S. 2001*a.* The shape of the beam attenuation spectrum and its relation to the size distribution of oceanic particles. *Appl. Opt.*, 40, pp. 4885–93.

Boss E., Pegau, W. S., Lee, M., Twardowski, M. S., Shybanov, E., Korotaev, G. and Baratange, F. 2004. The particulate backscattering ratio at LEO 15 and its use to study particles composition and distribution. *J. Geophys. Res.*, 109(C1), doi:C0101410.1029/2002JC001514.

Boss, E., Collier, R., Larson, G., Fennel, K., and Pegau, W. S., 2007. Measurements of spectral optical properties and their relation to biogeochemical variables and processes in Crater Lake National Park, OR. *Hydrobiologia,* 574, pp. 149–159.

Bricaud, A., Bedhomme, A. L. and Morel, A. 1988. Optical properties of diverse phytoplankton species: experimental results and theoretical interpretation. *J. Plankton Res.*, 10, pp. 851–73.

Bricaud, A., Morel, A., Babin, M., Allali, K. and Claustre, H. 1998. Variations of light absorption by suspended particles with the chlorophyll *a* concentration in oceanic (Case 1) waters: analysis and implications for bio-optical models. *J. Geophys. Res.*, 103, pp. 31033–44.

Bricaud, A., Morel, A. and Prieur, L. 1981. Absorption by dissolved organic matter of the sea (yellow substance) in the UV and visible domains. *Limnol. Oceanogr.*, 26, pp. 43–53.

Bricaud, A., Morel, A. and Prieur, L. 1986. Optical efficiency factor of some phytoplankters. *Limnol. Oceanogr.*, 28, pp. 816–32.

Bricaud, A., Roesler, C. S. and Zaneveld, J. R. V. 1995. *In situ* methods for measuring the inherent optical properties of ocean waters. *Limnol. Oceanogr.*, 40, pp. 393–410.

Bricaud, A. and Stramski, D. 1990. Spectral absorption coefficients of living phytoplankton and nonalgal biogenous matter: a comparison between the Peru upwelling area and the Sargasso Sea. *Limnol. Oceanogr.*, 35, pp. 562–82.

Bricaud, A., Zaneveld, J. R. V. and Kitchen, J. C. 1992. Backscattering efficiency of coccolithophorids: use of a three-layered sphere model. *Ocean Optics XI*, *Proc. SPIE*, 1750, pp. 27–33.

Carder, K. L., Steward, R. G., Harvey, G. R. and Ortner, P. B. 1989. Marine humic and fulvic acids: their effects on remote sensing of ocean chlorophyll. *Limnol. Oceanogr.*, 34, pp. 68–81.

Chang, G. C. and Dickey, T. D. 2007. Interdisciplinary sampling strategies for detection and characterization of harmful algal blooms. In: Babin et al. (eds), op. cit., this volume.

Claustre, H., Fell, F., Oubelkheir, K., Prieur, L., Sciandra, A., Gentili, B. and Babin, M. 2000. Continuous monitoring of surface optical properties across a geostrophic front: biogeochemical inferences. *Limnol. Oceanogr.*, 45, pp. 309–21.

Clavano, W., Boss, E. and Karp-Boss, L., 2007. Inherent optical properties of non-spherical marine-like particles – from theory to observations. *Oceanography and Marine Biology: An Annual Review,* 45, pp. 1–38.

Cleveland, J. S. 1995. Regional models for phytoplankton absorption as a function of chlorophyll *a* concentration. *J. Geophys. Res.*, 100, pp. 13333–44.

Craig, S., Lohrenz S., Lee, Z., Mahoney, K., Kirkpatrick, G., Schofield, O. and Steward, R., 2006. Use of hyperspectral remote sensing reflectance for detection and assessment of the harmful alga, Karenia brevis. *Applied Optics* 45, pp. 5414–5425.

Cullen, J. J. 2007. Observation and prediction of harmful algal blooms. In: Babin et al. (eds), op. cit., this volume.
Cullen, J. J. and Davis, R. F. 2003. The blank can make a big difference in oceanographic measurements. *Limnol. Oceanogr. Bull.*, 12, pp. 29–35.
Cullen, J. J. and Lewis, M. R. 1995. Biological processes and optical measurements near the sea surface: some issues relevant to remote sensing. *J. Geophys. Res.*, 100, pp. 13255–266.
Diehl, P. and Haardt, H. 1980. Measurement of the spectral attenuation to support biological research in a 'plankton tube' experiment. *Oceanol. Acta*, 3, pp. 89–96.
Ducha, J. and Kubin, S. 1976. Measurement of *in vivo* absorption spectra of microscopic algae using bleached cells as a reference sample. *Arch. Hydrobiol. Suppl.*, 49, pp. 199–213.
Etheridge, S. M. 2002. Ecophysiology and optical detection of harmful algal blooms. Ph.D. thesis, Storrs, University of Connecticut, 184 pp.
Etheridge, S. M. and Roesler, C. S. 2004. Temporal variations in phytoplankton, particulates, and colored dissolved organic material based on optical properties during a Long Island brown tide compared to an adjacent embayment. *Harmful Algae*, 3, pp. 331–42.
Etheridge, S. M., Roesler, C. S., Franklin, H. M. and Boss, E. 2002. Do bio-optical parameters and relationships apply to extreme algal blooms? *Ocean Optics XVI*, *Proc. SPIE*.
Garver, S. A., Siegel, D. A. and Mitchell, B. G. 1994. Statistical variability of near-surface particulate absorption spectra: what can a satellite ocean color imager see? *Limnol. Oceanogr.*, 39, pp. 1349–67.
Geller, P. E., Tsuei, T. G. and Barber , P. W. 1985. Information content of the scattering matrix for spheroidal particles. Applied Optics 24, pp. 2391–2396.
Gibbs, R. J. 1974*a*. Principles of studying suspended materials in water. In: R. J. Gibbs (ed.), op. cit., pp. 3–15.
Gibbs, R. J. (ed.). 1974*b*. *Suspended Solids in Water*. New York, Plenum Press.
Gordon, H. R. 1974. Mie theory models of light scattering by ocean particulates. In: R. J. Gibbs (ed.), op. cit., pp. 73–80.
Gordon, H. R. 1993. Sensitivity of radiative transfer to small-angle scattering in the ocean: quantitative assessment. *Appl. Opt.*, 32, pp. 7505–11.
Griffiths, G. 2007. Glider and autonomous underwater vehicle observing systems. In: Babin et al. (eds), op. cit., this volume.
Hovenier, J. W., Volten, H., Muñoz, O., van der Zande, W. J. and Waters, L. B. F. M., 2003. Laboratory studies of scattering matrices for randomly oriented particles: potentials, problems, and perspectives. Journal of Quantitative Spectroscopy and Radiative Transfer 79–80, pp. 741–755.
Hoepffner, N. and Sathyendranath, S. 1991. Effect of pigment composition on absorption properties of phytoplankton. *Mar. Ecol. Progr. Ser.*, 73, pp. 11–23.
Iturriaga, R. and Siegel, D. A. 1989. Microphotometric characterization of phytoplankton and detrital absorption properties in the Sargasso Sea. *Limnol. Oceanogr.*, 34, pp. 1706–26.
Kirk, J. T. O. 1992. Monte Carlo modeling of the performance of a reflecting tube absorption meter. *Appl. Opt.*, 31, pp. 6463–68.
Kirk, J. T. O. 1994. *Light and Photosynthesis in Aquatic Ecosystems*. Cambridge, UK, Cambridge University Press.
Kirkpatrick, G., Millie, D., Moline, M. and Schofield, O. 2000. Optical discrimination of a phytoplankton species in natural mixed populations. *Limnol. Oceanogr.*, 45, pp. 467–71.
Kirkpatrick, G. J., Orrico, C., Moline, M. A., Oliver, M. and Schofield, O. M. 2003. Continuous hyperspectral absorption measurements of colored dissolved organic material in aquatic systems. *Appl. Opt.*, 42, pp. 6564–68.
Kishino, M., Takahashi, M., Okami, N. and Ichimura, S. 1985. Estimation of the spectral absorption coefficients of phytoplankton in the sea. *Bull. Mar. Sci.*, 37, pp. 634–42.
Kitchen, J. and Zaneveld, J. R. V. 1990. On the non-correlation of the vertical structure of light scattering and chlorophyll *a* in Case I waters. *J. Geophys. Res.*, 95, pp. 20237–46.
Kitchen, J. C. and Zaneveld, J. R. V. 1992. A three-layered sphere model of the optical properties of phytoplankton. *Limnol. Oceanogr.*, 37, pp. 1680–90.

Lee, M. E. and Lewis, M. R. 2003. A new method for the measurement of the optical volume scattering function in the upper ocean. *J. Atmos. Ocean. Tech*., 20, pp. 563–71.

Lehaitre, M., Delauney, L. and Compère, C. 2007. Biofouling and underwater measurements. In: Babin et al. (eds), op. cit., this volume.

Logan, B. E. 1993. Theoretical analysis of size distributions determined using screens and filters. *Limnol. Oceanogr*., 38, pp. 372–81.

Maffione, R. A. and Dana, D. R. 1997. Instruments and methods for measuring the backward-scattering coefficient of ocean waters. *Appl. Opt*., 36, pp. 6057–67.

Mie, G. 1908. Beiträge zur Optik trüber Medien, speziell kolloidaler Metallösungen. *Ann. Physik*, 4, pp. 377–455.

Millie, D., Schofield, O. M., Kirkpatrick, G. J., Johnsen, G., Tester, P. A. and Vinyard, B. T. 1997. Detection of harmful algal blooms using photopigments and absorption signatures: a case study of the Florida red tide, *Gymnodinium breve*. *Limnol. Oceanogr*., 42, pp. 1240–51.

Moore, C., Zaneveld, J. R. V. and Kitchen, J. C. 1992. Preliminary results from an *in situ* spectral absorption meter. *Ocean Optics XI*, *Proc. SPIE*, 1750, pp. 330–37.

Morel, A. 1973. Diffusion de la lumière par les eaux de mer: résultats experimentaux et approche théorique. *AGARD Lect. Ser*., 61, pp. 3.1.1–3.1.76.

Morel, A. 1974. Optical properties of pure water and pure seawater. In: N. G. Jerlov and E. S. Nielsen (eds), *Optical Aspects of Oceanography.* San Diego, Calif., Academic Press, pp. 1–24.

Morel, A. 2007. Introduction to optical properties in the sea: theoretical aspects. In: Babin et al. (eds), op. cit., this volume.

Morel, A. and Ahn, Y.-H. 1990. Optical efficiency factors of free living marine bacteria: influence of bacterioplankton upon the optical properties and particulate organic carbon in oceanic waters. *J. Mar. Res*., 48, pp. 145–75.

Morel, A. and Ahn, Y.-H. 1991. Optics of heterotrophic nanoflagellates and ciliates: a tentative assessment of their scattering role in oceanic waters compared to those of bacterial and algal cells. *J. Mar. Res*., 49, pp. 177–202.

Morel, A. and Bricaud, A. 1981. Theoretical results concerning light absorption in a discrete medium, and application to specific absorption by phytoplankton. *Deep Sea Res*., 28A, pp. 1375–93.

Mueller J. L., Fagion, G. S., McClain, C. R., Pegau, W. S., Zaneveld, J. R. V., Mitchell, B. G., Kahru, M., Wieland, J. and Stramska, M. 2003. Ocean optics protocols for satellite ocean color sensor validation. In: *Inherent Optical Properties: Instruments, Characterizations, Field Measurements and Data Analysis Protocols*. (NASA/TM-2003-211621/Rev4-Vol.IV.)

Musser, J., Fry, E., Gray, D., Kattawar, G., Lu, Z. and Xianzhen, Z. X. 2004. Direct measurement of the integrated scattering coefficient *b*. *Ocean Optics XVII*, *Proc. SPIE*, XX.

Oishi, T. 1990. Significant relationship between the backward scattering coefficient of sea water and the scatterance at 120°. *Appl. Opt*., 29, pp. 4658–65.

Oubelkheir, K., Claustre, H., Babin, M., Sciandra, A., 2005. The comparative bio-optical and biogeochemical properties of contrasted trophic regimes. *Limnology and Oceanography*, 50 (6), pp. 1795–1809.

Pegau, W. S., Gray, D. and Zaneveld, J. R. V. 1997. Absorption and attenuation of visible and near-infrared light in water: dependence on temperature and salinity. *Appl. Opt*., 36, pp. 6035–46.

Pegau, W. S. and Zaneveld, J. R. V. 1993. Temperature-dependent absorption of water in the red and near-infrared portions of the spectrum. *Limnol. Oceanogr*., 38, pp. 188–92.

Pegau, W. S., Zaneveld, J. R. V. and Voss, K. J. 1995. Towards closure of the inherent optical properties of natural waters. *J. Geophys. Res*., 100(C7), pp. 13193–99.

Petzold, T. J. 1972. *Volume Scattering Functions for Selected Ocean Waters*. La Jolla, Calif., Scripps Institution of Oceanography, 79 pp. (SIO Ref. 72–78.)

Roesler, C. S. 1998. Theoretical and experimental approaches to improve the accuracy of particulate absorption coefficients derived from the quantitative filter technique. *Limnol. Oceanogr*., 43, pp. 1649–60.

Roesler, C. S. and Barnard, A. H. 2003. Temporal variability in ecosystem structure in the Eastern Maine Coastal Current as observed by the Gulf of Maine Ocean Observing System (GOMOOS). *ASLO Aquatic Science Meeting*. Salt Lake City, UT.

Roesler, C. S. and Perry, M. J. 1995. *In situ* phytoplankton absorption, fluorescence emission, and particulate backscattering spectra determined from reflectance. *J. Geophys. Res.* , 100(C7), pp. 13279–94.

Roesler, C. S., Perry, M. J. and Carder, K. L. 1989. Modeling *in situ* phytoplankton absorption from total absorption spectra. *Limnol. Oceanogr.*, 34, pp. 1512–25.

Roesler, C. S., Simeon, J. and Talbot, M. C. 1997. Variability in vertical distributions of size-fractioned component absorption and scattering coefficients in shallow continental shelf waters. *ASLO/AGU Ocean Sciences*, Santa Fe, N.M.

Rudnick, D. L. and Perry, M. J. (eds). 2003. *ALPS: Autonomous and Lagrangian Platforms and Sensors.* Workshop Report. www.geo-prose.com/ALPS.

Sathyendranath, S., Lazarra, L. and Prieur, L. 1987. Variations in the spectral values of specific absorption of phytoplankton. *Limnol. Oceanogr.*, 32, pp. 403–15.

Schofield, O., Bosch, J., Glenn, S., Kirkpatrick, G., Kerfoot, J., Lohrenz, S., Moline, M., Oliver, M. and Bissett, P. 2006. Bio-optics in integrated ocean observing networks: potential for studying harmful algal blooms. In: Babin et al. (eds), op. cit., this volume.

Schofield, O., Glenn, S., Kirkpatrick, G., Jones, C. and Twardowski, M. 2004. Measuring mesoscale *in situ* optics of the continental shelves with autonomous Webb gliders. *Ocean Optics XVII*, *Proc. SPIE*.

Schofield, O., Gryzmski, J., Bissett, W. P., Kirkpatrick, G., Millie, D. F., Moline, M. A. and Roesler, C. 1999. Optical monitoring and forecasting systems for harmful algal blooms: possibility or pipedream? *J. Phycol.*, 35, pp. 125–45.

Shifrin, K., 1988. Physical Optics of Ocean Water. *Am. Inst. of Phys.* N.Y. pp. 285.

Simeon, J., Roesler, C. S., Pegau, W. S. and Dupouy, C. 2003. Sources of spatial variability in light absorbing components along an equatorial transect from 165°E to 150°W. *J. Geophys. Res.*, 108(C10), 3333, doi:10.1029/2002JC001613.

Sosik, H. M. 2007. Characterizing seawater constituents from optical properties. In: Babin et al. (eds), op. cit., this volume.

Sosik, H. M., Green, R. E., Pegau, W. S. and Roesler, C. S. 2001. *J. Geophys. Res.*, 106, pp. 9455–72.

Sosik, H. M. and Mitchell, B. G. 1991. Absorption, fluorescence and quantum yield for growth in nitrogen-limited *Dunaliella tertiolecta*. *Limnol. Oceanogr.*, 36, pp. 910–21.

Sosik, H. M, Olson, R. J., Neubert, M. G., Shalapyonok, A. and Solow, A. R. 2003. Growth rates of coastal phytoplankton from time-series measurements with a submersible flow cytometer. *ASLO Aquatic Sciences Meeting*, Salt Lake City, UT.

Stramski, D. 1999. Refractive index of planktonic cells as a measure of intracellular carbon and chlorophyll *a* content. *Deep Sea Res.*, 46, pp. 335–51.

Stramski, D., Boss, E., Bogucki, D. and Voss, K. J. 2004. The role of seawater constituents in light backscattering in the ocean. *Progr. Oceanogr.*, 61(1), pp. 27–55.

Stramski, D., Bricaud, A. and Morel, A. 2001. Modeling the inherent optical properties of the ocean based on the detailed composition of the planktonic community. *Appl. Opt.*, 40, pp. 2929–45.

Stramski, D. and Kiefer, D. A. 1991. Light scattering by microorganisms in the open ocean. *Progr. Oceanogr.*, 28, pp. 343–83.

Stramski, D. and Mobley, C. D. 1997. Effects of microbial particles on oceanic optics: a database of single-particle optical properties. *Limnol. Oceanogr.*, 42, pp. 538–49.

Stramski, D., Sciandra, A. and Claustre, H. 2002. Effects of temperature, nitrogen, and light limitation on the optical properties of the marine diatom *Thalassiosira pseudonana*. *Limnol. Oceanogr.*, 47, pp. 392–403.

Stramski, D., Shalapyonok, A. and Reynolds, R. A. 1995. Optical characterization of the oceanic unicellular cyanobacterium *Synechococcus* grown under a day-night cycle in natural irradiance. *J. Geophys. Res.*, 100(C7), pp. 13295–307.

Subramaniam, A., Carpenter, E. J. and Falkowski, P. G. 1999. Bio-optical properties of the marine diazotrophic cyanobacteria *Trichodesmium* spp. II: A reflectance model for remote-sensing. *Limnol. Oceanogr.*, 44, pp. 618–27.

Twardowski, M. S., Boss, E., MacDonald, J. B., Pegau, W. S., Barnard, A. H. and Zaneveld, J. R. V. 2001. A model for estimating bulk refractive index from the optical backscattering ratio and the implications for understanding particle composition in Case I and Case II waters. *J. Geophys. Res.*, 106, pp. 14129–42.

Twardowski, M. S., Boss, E., Sullivan, J. M. and Donaghay, P. L. 2004. Reanalysis of the use of an exponential model to describe the spectral shape of absorption by chromophoric dissolved organic matter (CDOM). *Mar. Chem.*, 89, pp. 69–88.

Twardowski, M. S., Sullivan, J. M., Donaghay, P. L. and Zaneveld, J. R. V. 1999. Microscale quantification of the absorption by dissolved and particulate material in coastal waters with an ac-9. *J. Atmos. Ocean. Tech.*, 16, pp. 691–707.

Tyler, J. E., Austin, R. W. and Petzold, T. J. 1974. Beam transmissometers for oceanographic measurements. In: R. J. Gibb (ed.), op. cit., pp. 51–60.

Ulloa O., Sathyendranath, S. and Platt, T. 1994. Effect of the particle-size distribution on the backscattering ratio in seawater. *Appl. Opt.*, 33, pp. 7070–77.

van de Hulst, H. C. 1957. *Light Scattering by Small Particles*. New York, John Wiley & Sons.

Volz, F. 1954. Die Optik und Meterologie der Atmospharischen Trubung. *Ber. Dtsch. Wetterdienstes*, 2, p. 3047.

Voss, K. J. 1992. A spectral model of the beam attenuation coefficient in the ocean and coastal areas. *Limnol. Oceanogr.*, 37, pp. 501–09.

Voss, K. J. and Austin, R. W. 1993. Beam-attenuation measurement error due to small-angle scattering acceptance. *J. Atmos. Oceanic Tech.*, 10, pp. 113–21.

Werdell, P. J. and Roesler, C. S. 2003. Remote assessment of benthic substrate composition in shallow waters using multispectral reflectance. *Limnol. Oceanogr.*, 48, pp. 557–67.

Yacobi, Y. Z, Alberts, J. J., Takacs, M., McElvaine, M., 2003. Absorption spectroscopy of colored dissolved organic carbon in Georgia (USA) rivers: the impact of molecular size distribution. Limnology and Oceanography, 62(1), pp. 41–46.

Zaneveld, J. R. V., Bartz, R. and Kitchen, J. C. 1990. A reflective-tube absorption meter. *Proc. SPIE*, 1302, pp. 124–36.

Zaneveld, J. R. V. and Kitchen, J. C. 1995. The variation in the inherent optical properties of phytoplankton near an absorption peak as determined by various models of cell structure. *J. Geophys. Res.*, 100, pp. 13309–20.

Zaneveld, J. R. V., Kitchen, J. C. and Moore, C. C. 1994. Scattering error correction of reflecting-tube absorption meters. *Ocean Optics XII*, *Proc. SPIE*, 2258, pp. 44–55.

Zaneveld, J. R. V., Spinrad, R. W. and Bartz, R. 1980. Optical properties of turbidity standards. *Ocean Optics VI*, *Proc. SPIE*, 208, pp. 159–68.

Zhang, X., Lewis, M. R. and Johnson, B. 1998. The role of bubbles in the scattering of light in the ocean. *Appl. Opt.*, 37, pp. 6525–36.

6

Measurement of apparent optical properties for diagnosis of harmful algal blooms

M. R. Lewis

6.1 Introduction

Dense surface accumulations or blooms of algae have been noted since antiquity by a change in the colour of the sea. The effect can be spectacular; the wine-dark seas of Homer, the descriptions of discolorations of rivers by Aristotle, and the lurid biblical chronicles of waters turning to blood all probably have their origins in algal blooms.

The 'colour' of the ocean is one example of a number of 'apparent optical properties' (AOP; see Morel, 2007 – Chapter 4 this volume) that can potentially be used to detect the presence of high concentrations of algae and perhaps to diagnose the specific nature of the organisms forming the blooms (Cullen et al., 1997; Schofield et al., 1999). Such properties can be measured remotely by automated ocean observatories, aircraft or satellites, and may provide a capability for rapid detection as well as a basis for long-term monitoring and potentially for prediction.

The objective of this chapter is to provide basic definitions and information about apparent optical properties (AOPs) and their observation. While such definitions and interrelationships may be tedious, it is particularly important in order to enable the collection of the most useful and accurate data as possible, with the goal of making unambiguous interpretations about the ecosystem. Finally, this chapter describes approaches and applications, not just in the theoretical framework, but in the complexity of the real world.

6.2 Apparent optical properties (AOPs): theoretical considerations

6.2.1 Basic radiometric quantities

The fundamental radiometric property is the spectral radiance distribution ($L(\theta, \varphi, \lambda)$), with units of J m^{-2} s^{-1} sr^{-1} nm^{-1} (W m^{-2} sr^{-1} nm^{-1}) or quanta $\cdot$ m^{-2} s^{-1} sr^{-1} nm^{-1}), described as the radiant power (or photon flux) in a specified zenith (θ) and azimuth (φ) direction per unit solid angle, per unit area normal to the incident beam at a given wavelength (λ) (Kirk, 1994; Mobley, 1994; Morel, 2007 – Chapter 4 this volume). It represents the angular and spectral structure of the light field. Of course, it varies with time, with location, and with depth as well in the real ocean, as it results from the modification of the incident radiance field by the sea surface, the inherent optical properties of the ocean interior, and the reflectivity of the sea bottom.

All other radiometric quantities derive from the radiance distribution. In particular, the various irradiances are derived by weighted integration of the radiance field over defined solid angles. The downwelling ($E_d(\lambda)$, units of W m^{-2} nm^{-1} or photons m^{-2} s^{-1} nm^{-1}) and upwelling ($E_u(\lambda)$, same units) plane irradiances are given as the cosine-weighted integration of the radiance distribution over the upper (downwelling) and lower (upwelling) hemispheres, respectively. These hemispheres are separated by a horizontal surface oriented normal to the local gravity vector. The plane irradiances are useful to define the flux of energy across a given depth horizon in the ocean. Specifically,

$$E_d(\lambda) = \int_{\Xi d} L(\theta, \varphi, \lambda) \cos\theta \, d\Omega, \tag{6.1}$$

where θ varies from 0 (zenith) to $\pi/2$, φ varies from 0 (a direction within the horizontal plane selected as the origin for azimuth) to 2π and the integration is taken over the upper hemisphere ($\Xi_u = 2\pi$ sr). Photons traveling straight down would be weighted twice as much as photons arriving at 60° to the horizontal surface.

Similarly, the upwelling spectral plane irradiance E_u can be defined by integration over the lower hemisphere(($\Xi_u = 2\pi$ sr) and with $|\cos\theta|$ to keep this quantity as a positive one (as θ varies from $\pi/2$ to π),

$$E_u(\lambda) = \int_{\Xi u} L(\theta, \varphi, \lambda) |\cos\theta| d\Omega. \tag{6.2}$$

The net downward irradiance ($E(\lambda) = E_d(\lambda) - E_u(\lambda)$, units of W m^{-2} nm^{-1} or photons m^{-2} s^{-1} nm^{-1}) represents the vertical component of the irradiance vector and is given by the difference between the upward and downward irradiances, or the cosine weighted integral over all solid angles ($\Xi = \Xi_d + \Xi_u = 4\pi$ sr). It represents the net flux of energy across a given depth.

A further quantity of biogeochemical and physical interest is the scalar irradiance ($E_o(\lambda)$, units of W m^{-2} nm^{-1} or photons m^{-2} s^{-1} nm^{-1}), which results from the unweighted integration of radiance over all hemispheres. Every photon of a given wavelength, irrespective of its direction of travel, is treated equally in this definition, and it is of particular importance for photosynthesis studies where the algal cell is sensitive only to the magnitude and not the directionality of the incoming photon flux.

Another derived quantity of interest results from spectral integration of the irradiances over the wavebands active in photosynthesis, generally taken as the interval from 350 or 400 nm to 700 nm or 750 nm. All the above irradiances can be spectrally integrated, to provide a measurement of photosynthetically available radiation (PAR, units of W m^{-2} or photons $\cdot m^{-2}$ s^{-1}). This is typically given as the integrated scalar irradiance over this waveband.

6.2.2 Derived radiometric quantities

6.2.2.1 Diffuse attenuation coefficients

The diffuse attenuation coefficients describe the rate of change in radiances or the various irradiances taken in a particular direction, For example, the nadir radiance (photons traveling directly up in the ocean) is of particular interest for the remote

sensing problem, and is denoted here as the 'upwelling radiance', $L_u(\lambda, z)$. This quantity diminishes with depth as

$$\frac{dL_u(\lambda,z)}{dz} = -K_L L_u(\lambda, z), \tag{6.3}$$

where K_L is the diffuse attenuation coefficient for upwelling radiance, and where inelastic scattering processes have been neglected (Morel, 2007 – Chapter 4 this volume). This implies,

$$K_L(\lambda, z) = -\frac{d[\ln(L_u(\lambda,z))]}{dz}. \tag{6.4}$$

Similar *K*-coefficients can be defined for any other radiometric quantity, such as $E_d(\lambda, z)$ or $E_u(\lambda, z)$ (K_d, K_u, respectively) or for any radiance $L(\theta, \varphi, \lambda, z)$, through the same derivative with respect to depth of the neperian (natural) logarithm of this quantity. Note that as the diffuse attenuation coefficients are functions of apparent optical properties, they are AOPs as well, and will change with changes in the radiance distribution. They are also functions of the inherent optical properties (specifically *a* and *b*) and exhibit a spectral dependence.

Equation (6.3) can be integrated over a finite depth interval (0 to *Z*, for example), and results in an exponential decrease of radiance, from $L_u(\lambda, 0)$ to $L_u(\lambda, Z)$. This can be expressed as

$$L_u(\lambda, Z) = L_u(\lambda, 0)\exp[-\int_0^Z K_L(\lambda, z)dz]. \tag{6.5}$$

Such an expression (or similar ones for the various irradiances) makes explicit the depth dependence of the *K* coefficients. To the extent that the radiance distribution at the surface changes with time (such as with changes in the solar zenith angle, surface roughness, or changes in the cloud cover), or to the extent that the inherent optical properties change, the diffuse attenuation coefficients will vary with time as well. Note that even with vertically uniform IOPs, the radiance distribution will vary with depth, and hence so will the diffuse attenuation coefficient. More detail is given in Morel (2007 – Chapter 4 this volume). For example, the diffuse attenuation coefficient for downward irradiance is closely aligned with the absorption coefficient, *a*, and is often expressed as,

$$K_d(\lambda) \approx \frac{a(\lambda)}{\mu_d(\lambda)}, \tag{6.6}$$

where $\mu_d(\lambda)$ is the average cosine for the downward spectral radiance distribution and where backscattering is considered small relative to absorption. However, we repeat here the conclusion that no simple analytical relationship exists between *K* and the IOPs. Numerical solutions to the radiative transfer equation (RTE) can only provide approximate expressions or parameterizations for *K* as a function of the IOPs as seen in (6.6). With this caveat in mind however, it should be noted that an argument has been made that for sun angles greater than 30° above the horizon, and for situations where scattering is small in comparison with absorption, the diffuse attenuation coefficients

can be considered as somewhat independent of the radiance distribution and can be denoted as 'quasi-inherent' optical properties.

6.2.2.2 Reflectances

The irradiance reflectance is a dimensionless quantity defined as the ratio of the upward to the downward irradiance at the same depth, z,

$$R(\lambda, z) = E_u(\lambda, z)/E_d(\lambda, z). \tag{6.7}$$

The spectral reflectance just below the sea surface (0^-) describes the intrinsic 'ocean colour' as it is effectively free from contributions from the surface Fresnel reflectance and is independent from the spectral composition of the incident solar radiation. As with the diffuse attenuation coefficients, the reflectance depends on both the inherent optical properties and the radiance distribution, and is often parameterized as

$$R(\lambda) = f\{b_b(\lambda)/[a(\lambda) + b_b(\lambda)]\}. \tag{6.8}$$

where the dimensionless factor f in (6.5) accommodates, among other things, the radiance distribution. The situation is actually more complex, as the reflectance relates in some weighted sense to vertical variations in the inherent optical properties (specifically the volume scattering coefficient) and the varying radiance distribution. The factor f is often taken to be from about 0.30 to 0.50, and (as for K_d) can only be obtained by numerical solutions of the RTE in various specified conditions (Kirk, 1984; Gordon, 1989*a*; Morel and Gentili, 1991).

The reflectance can as well be defined just above the sea surface (i.e. 0^+). In this case, the radiance field propagating in the upward direction in the ocean interior is first reduced as one crosses the air/sea interface, and then increased as a result of photons specularly scattered upward from the ocean surface. The downward irradiance is likewise taken above the interface. The reflectance above the ocean surface is often termed the 'albedo' by the climate community, who refer to that portion of the upwelling irradiance from the ocean interior as the 'underlight'.

The remote sensing reflectance R_{RS} is defined just above the interface as

$$R_{RS}(\lambda) = L_w(\theta, \varphi, \lambda, 0^+)/E_d(\lambda, 0^+), \tag{6.9}$$

where $L_w(\theta, \varphi, \lambda, 0^+)$, called the 'water-leaving spectral radiance', is the radiance scattered from the ocean interior, and leaving the ocean in a direction θ, φ (i.e. zenith angle, and azimuth angle), and $E_d(\lambda, 0^+)$ is the downward irradiance above the surface at the same wavelength. Often, the direction taken is assumed to be normal to the ocean surface, hence the nadir water-leaving radiance. The water-leaving radiance relates to the upwelling radiance, $L_u(\theta', \varphi, \lambda, 0^-)$, (where θ' is a nadir angle, related to θ through Snell's law by $\theta' = \sin^{-1}(\sin\theta/n)$, where n is the real refractive index of the seawater medium). Another related quantity is the 'normalized water-leaving radiance' L_{WN}, defined (Gordon and Clark, 1981) as,

$$L_{WN}(\lambda) = R_{RS}(\lambda)\, F_0(\lambda), \tag{6.10}$$

where $F_0(\lambda)$ is the extraterrestrial solar flux at the given wavelength at the mean earth–sun distance. Therefore, L_{WN} represents the radiance which would be measured if the

sun were at zenith, and as if the earth was at its mean distance from the sun and in the absence of an intervening atmosphere. The utility of L_{WN} is generally within the remote sensing field (Ruddick et al., 2007 – Chapter 9 this volume).

6.3 Measurement and interpretation of AOPs in the ocean

Optical methods to detect the onset of a bloom and to monitor its development can be applied *in situ* or from above the surface of the sea, from an aircraft or from space. The first case has the advantage of measuring throughout the water column, to a greater or lesser extent depending on the particular instrumentation used, and the platforms on which the instruments are deployed. Generally, both IOPs and AOPs can be measured, which aids in the interpretation of the AOPs. In the case of above-water remote detection (from satellite, airplane, or from a ship making above water measurements), only AOPs, and specifically only reflectance, can be measured.

The influence of harmful algal populations on the optical properties of the sea is however, directly tied to variations in the IOPs (Schofield et al., 2007; Morel, 2007; Roesler and Boss, 2007; Sosik, 2007 – Chapters 3, 4, 5 and 8 this volume). However, it is often methodologically useful to employ instruments that measure the AOPs, and to invert these using approximations of the radiative transfer equation to retrieve the IOPs and then to diagnose constituent dynamics. Measurements of AOPs have a longer history (at least 70 years) and there is a much richer data set on such apparent optical properties than inherent optical properties which have only been extensively made with any rigour in the last decade. Furthermore, unlike current measurements of inherent properties (scattering in particular) the fundamental measurements of radiance and irradiance are directly traceable to agreed and readily available international standards appropriate for use in the oceanographic environment. Measurements of irradiance taken at a given location and at a given time are directly comparable to those taken at different locations and times; the same cannot be said for fluorescence (Babin, 2007 – Chapter 7 this volume) or for actual measurements of IOPs (Roesler and Boss, 2007 – Chapter 5 this volume), due to physiological variations in the former and to instrumental constraints in both the former and latter. Another advantage of the measurement of apparent optical properties lies in its passive character (the source is the sun), while absorption and scattering measurements represent active techniques requiring an artificial source and thus more energy. For the derivation of diffuse attenuation and reflectance, a further real advantage is that in principal, only relative measurements are required (e.g. measuring the vertical gradient in irradiance), and hence precise, but not necessarily accurate, measurements can provide useful information from their vertical gradients. On the other hand, passive measurement of apparent optical properties cannot be made under low illumination, such as at night or when the sun is low on the horizon, and is subject to many potential sources of environmental variation and uncertainty. Finally, measurements of radiance and irradiance, and the derivation of diffuse attenuation coefficients and reflectances, have been extensively examined by the oceanographic community and have resulted in a consensus with respect to a detailed set of protocols and approaches for design, characterization, calibration, at-sea deployment, and data analyses of instruments for the measurement of ocean AOPs (Mueller and Fargion, 2003).

In what follows, instrumentation for the measurement of AOPs is described, some of their sources of error discussed, and lastly some discussion is given relating to the

detection and monitoring of harmful algal blooms. The reader should note the excellent series of Technical Memoranda published by the SeaWiFS Project Office, which provides much more detailed descriptions of instrument requirements, their characterization and calibration, and the recommended protocols for deployment at sea.

6.3.1 Instrumentation and observations

6.3.1.1 Radiance

As seen in Section 6.2.1, radiance is the fundamental radiometric property; given the full radiance distribution, $L(\theta, \varphi, \lambda, z)$, and its variation with respect to depth, all the more commonly used AOPs (irradiances, reflectances, diffuse attenuation coefficients) can be derived. In principle (but not yet in practice), the vertical variation in the full radiance distribution could be used to estimate the absorption coefficient through the Gershun relation, and c, as well as β through inversion of the radiative transfer equation.

Radiance is routinely measured at sea, albeit at a single or few angles. For a single angle measurement, a 'Gershun tube' and appropriate stops provide a narrow acceptance angle (<10° ~0.1 sr) of the fore-optics, which limits the subtended solid angle viewed by a (typically silicon) photodetector (Figure 6.1A). Restricting the field-of-view limits the number of photons impinging on the detectors, and hence the ability to measure with an acceptable signal-to-noise ratio. Thus a tradeoff is necessary between angular resolution and signal strength. Filters can be used to provide defined spectral bands. These can be matched to those used on specific orbiting satellites, and provide the highest radiometric performance in terms of bandpass definition and out-of-band performance. Clusters of such single waveband instruments are called 'multi-channel' radiance sensors. Recently, high-performance gratings coupled with advanced detector arrays have been used to provide radiance measurements with a high degree of spectral resolution (<5 nm). These so-called 'hyperspectral' measurements open the door to the use of analytical spectroscopy of spectral radiance at sea; such techniques are particularly relevant to the diagnosis of characteristics of harmful algal blooms (Roesler and Boss, 2003; Chang et al., 2004; Lorenz et al., 2004; Figure 2). Again tradeoffs are required: the higher spectral resolution is an advantage in constraining algorithms for the retrieval of constituents because of increased degrees of freedom, but the radiometric performance is somewhat less, and the ability to detect low photon flux across the visible spectrum is diminished relative to filter-based single detector instruments. A key metric is the signal-to-noise ratio, which must be achieved over the high dynamic range required to cover the range of oceanic conditions. Dynamic ranges of >20 bits can be achieved with individual silicon photodetectors; this results in a capability to profile irradiance reliably to the equivalent depth of the 0.01% light level under cloudy skies, while maintaining a desirable high sampling frequency (6–10 Hz). Hyperspectral instruments, because of their nature and the reduced photon flux into narrow spectral bands, are not as capable, and generally rely on longer integration times (upwards to 8 seconds or more) to achieve equivalent signal-to-noise performance.

Single angle radiance sensors are most often deployed in a nadir viewing arrangement such that only the upwelling radiance originating from directly below the platform is measured. While it is arguably an important viewing angle for remote sensing applications, the angular structure of the radiance field in the ocean is complex, and depends on the geometry of illumination as modified by the sea surface and also on the IOPs in the ocean (Morel and Gentili, 1996).

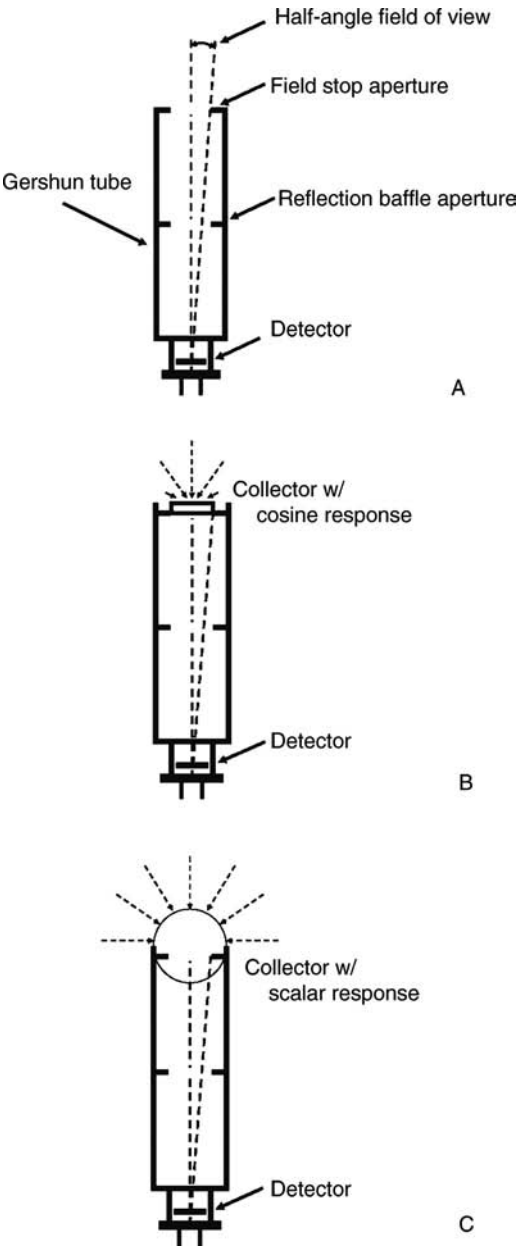

Figure 6.1
Schematic diagrams of optical instruments for the measurement of A, radiance; B, planar irradiance; C, scalar irradiance.

Measurements of the full angular distribution of the radiance field are far fewer than the measurement of upwelling spectral radiance taken at nadir. Older observations (e.g. Smith et al., 1970) made use of photographic measurements with 'fish-eye' lenses to determine the radiance distribution, and others used multiple single angle devices deployed either sequentially at different angles, or as arrays (Jerlov, 1976; Aas and Højerslev, 1999). Modern techniques make use of improved optics and replace film with digital imaging techniques (e.g. Voss, 1989). A prime difficulty is the enormous dynamic range of the radiance distribution in the downward direction, which can vary by a factor of $>10^6$ from the direction of the sun's disk to the edge of the field.

To illustrate the measurement of radiance, two examples of the vertical distribution of nadir radiance are given in Figure 6.2. The first (6.2A) is taken from the South Pacific Gyre, in some of the clearest ocean waters with concentrations of chlorophyll ~0.02 mg m^{-3}. The second is from a eutrophic marine inlet (Bedford Basin, Nova Scotia) during a local algal bloom in the spring, where the estimated chlorophyll concentration is approximately 20 mg m^{-3}. There are numerous features to note in these spectra. First is the differential spectral filtering that occurs in the two water bodies, with the maximum in upwelling radiance in the violet in the South Pacific waters, and distinctly in the green in the Bedford Basin profile. Second, although the incident irradiance is quite different between the two stations (see Figure 6.3), the decrease in the radiance with depth is much more rapid in the coastal station than in the open ocean, and the magnitude of the upwelled flux relative to the downward flux is much reduced. Finally, the peak observed at ~680 nm in the coastal station is due to the 'natural' or solar-stimulated fluorescence emitting from the dense algal population (Babin 2007, Chapter 7 this volume). The shift in colour from blue to green and the rate of decrease of radiance can both be used as diagnostics of the concentration of phytoplankton in the upper ocean.

6.3.1.2 Irradiance

Given a measurement of the full radiance distribution, there would be no need for special instruments for the measurement of irradiance; the radiance field could be integrated directly over all angles. However, the difficulties of making such measurements routinely has resulted in the development and deployment of a wide variety of instruments which carry out the required angular integration through the use of specialized optical collector systems.

The measurement of downwelling irradiance on a horizontal plane, $E_d(\lambda)$ (6.1) or the upwelling irradiance, $E_u(\lambda)$ (6.2), both require specialized collectors that weight the incoming radiance by the cosine of their angle of incidence on the plane of the detector, generally deployed normal to the gravity vector. These collectors, often called diffusers, are flat white plates that rest above the photodetectors, which measure the incoming light in the same fashion as radiance detectors (Figure 6.1B). In a similar fashion to the radiance detectors, irradiance sensors can be deployed in an array (multichannel), or using a single aperture to collect light for spectral dispersal (hyperspectral, Figure 6.3). The net downward flux is just the difference in the measured downwelling and upwelling fluxes.

Irradiance collectors designed to weight all incoming photons equally measure scalar irradiance ($\mathring{E}(\lambda)$). In practice, this means that the surface of the collectors must present normal incidence to all directions; the collector or diffuser is therefore spherical and is sometimes referred to as a '4π' collector. Measurements can be made separately

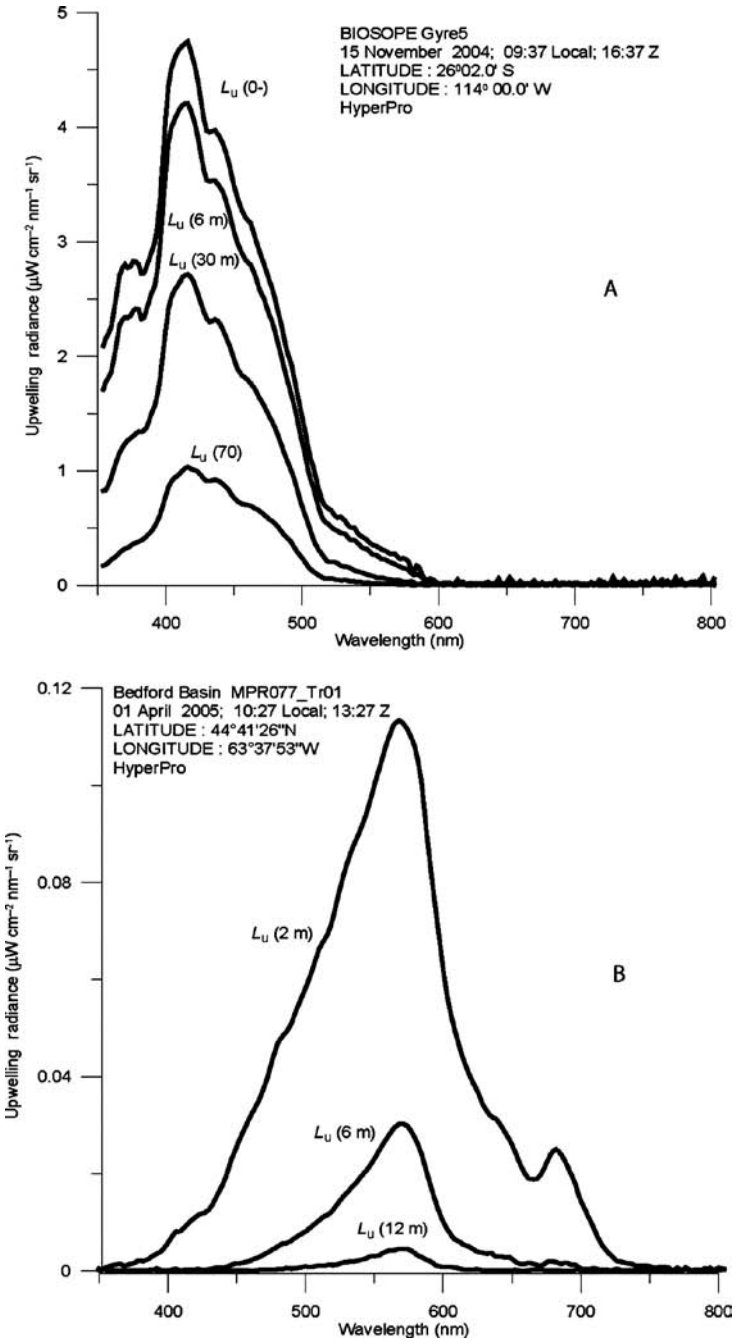

Figure 6.2
Measured spectral distribution of upwelling radiance at various depths in the water in A, ultra-oligotrophic South Pacific; B, coastal algal bloom.

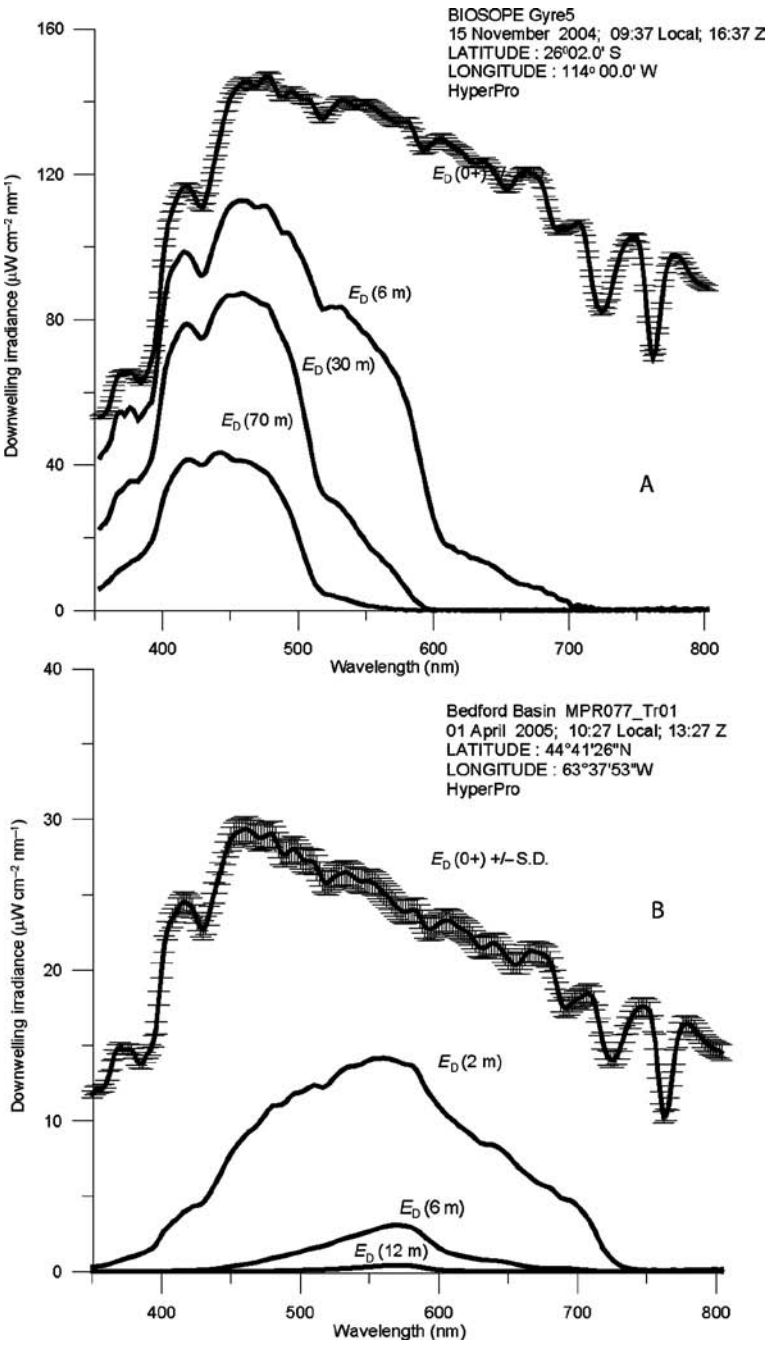

Figure 6.3
Measured spectral distribution of downwelling irradiance above the surface and at various depths in the water at the same stations as Figure 6.2.

for the upward or downward hemisphere (Figure 6.1C) for greatest accuracy when properly shielded, or a single spherical detector can be used, but which will have a null in the direction where the cable or fibre enters the sphere. Both single-wavelength and multi-wavelength sensors can in principle be deployed.

The vertical distributions of irradiance at the two index stations above are presented in Figure 6.3. The surface spectra are similar in shape, albeit with a much reduced flux at the higher latitude station, and a perceptible increase in the relative proportion of red wavelengths in the cloudy northern case. The variation in the surface irradiance over the course of the profile is small in both cases (a desirable, even necessary situation) as indicated by the standard deviation of downward flux at the surface. As one proceeds deeper into the water in both locations, wavelengths in the red and infrared are rapidly attenuated, largely because of the high absorption coefficient of seawater. For the 'blue water' station, the energy becomes progressively restricted to a relatively narrow spectral interval in the blue-violet, and significant ultraviolet radiation is noted to a depth of 70 m. In the 'green water' station, the ultraviolet and blue wavelengths are rapidly removed by a combination of phytoplankton pigments and chromophoric dissolved organic matter (CDOM; Siegel et al., 2002). The resulting spectrum is peaked in the far green. Note that, as with the radiance distribution, the magnitude of downwelling irradiance decreases much faster in the coastal station than in the open sea.

6.3.1.3 Photosynthetically available radiation (PAR)

A special case, applicable again in principle to all the above designs for both radiance and irradiance, is the situation where the filter set and detector are chosen to weight all incoming photons from 400 nm (or 350 nm) to 700 nm equally (because photon energy decreases with wavelength, the sensitivity in energy terms must increase in a linear fashion with respect to the wavelength). Such a broadband detector is most commonly associated with the spherical scalar collector to provide a measurement of 'PAR'. The application is generally for photosynthesis studies where the justification is that algal cells are not sensitive to the geometrical orientation of light, and where any photon in the visible band is potentially available to effect photosynthetic charge separation (but see discussion on the difference between photosynthetically available versus photosynthetically usable radiation in Morel, 1978).

6.3.2 Derived radiometric quantities

Measurements of irradiance and radiance can be used to form other important AOPs such as the diffuse attenuation coefficient (for up/downwelling radiance or irradiance or scalar irradiance, see (6.3)), the reflectances and normalized water-leaving radiances (6.7) to (6.10), and the average cosines.

6.3.2.1 Diffuse attenuation

The diffuse attenuation coefficient requires that measurements be made at multiple depths within the water column, and the local vertical gradient in irradiance (or radiance) computed (see (6.3) to (6.5)). This is carried out using a variety of different platforms (see below). As a substitute for absorption, the diffuse attenuation coefficient for downwelling irradiance, $K_d(\lambda)$, can be used. Indeed, near the surface, this quantity with some correction is almost an inherent property ('quasi-inherent') (Gordon,

1989*b*), according to $\mu_w K_d \cong (a)$, where μ_w is the cosine of the underwater sun-zenith angle (after refraction), and where scattering is small in comparison with absorption. Although it is not strictly correct, there is a long history of treating K_d as the additive sum of constituent parts, in the same way as done for absorption above and a tabulation of K_d as a function of wavelength and chlorophyll concentration has been carried out by Morel and Maritorena (2001) based on statistical analysis of a large number of irradiance profiles. It should be noted however, that such statistical tabulations assume that water and chlorophyll (and its co-varying properties) are the predominant contributor to variations in IOPs. Although such an assumption generally breaks down in the optically complex near-coastal waters, it may continue to have validity even for intense blooms of algae in the inshore (Ciotti et al., 1999).

Given a measurement of the vertical distribution of radiance or irradiance, it remains to determine the optimal method for the determination of the diffuse attenuation coefficients. In ideal conditions (no clouds (or complete overcast), flat sea, homogeneous vertical distribution of IOPs, etc.) it would seem to be fairly straightforward; in fact, given its apparent nature and a host of factors mentioned below, it is more difficult.

Examples of the vertical profiles of selected wavelengths of irradiance are shown in Figure 6.4, again with the open ocean and coastal stations shown for comparison. The individual lines correspond to wavelengths of 450 nm (blue), 550 nm (green) and 650 nm (red). It is clear that while the curves are approximately linear at least locally, there are strong vertical variations in the slopes (diffuse attenuation coefficients), and it is also clear that there are strong spectral dependencies, which vary as the amount of chlorophyll increases.

The recommended (Mueller et al., 2003) approach to the estimation of the diffuse attenuation coefficient is to first normalize the profile data at each wavelength with respect to the surface irradiance at the same wavelength, measured above the surface simultaneously with the profile. In the examples provided (Figure 6.4), the surface reference at 550 nm is shown as the dotted line for reference. For these examples, there is little change, but note the apparent decrease in the rate of decline in irradiance at depth as the surface values increase slightly at the blue water station. If no normalization was carried out, this would be interpreted as an artificial decrease in the attenuation coefficient. In the presence of clouds moving across the sky during the profile, it is often impossible to adequately normalize the data, as the surface reference is spatially separated from the profile location, and in any event small clouds cast shadows underwater that are not vertically uniform.

The next step would be to fit the data to equations of the form of (6.5), recognizing that the K profile is not uniform due to changes in both the radiance distribution and in the inherent optical properties. The traditional approach (Smith and Baker, 1984) is to subset the data into blocks of a few metres (generally more for blue water, less for green), and compute the local slope of the logarithmic decline in irradiance at a particular waveband using least-squares regression. The interval over which the computation is taken determines the vertical resolution in the K profile, so in principle, one would like to make this as small as possible without introducing a large amount of uncertainty in the estimated slopes. An alternative integral method exists but is not in general use (Mueller and Austin, 1995).

Figure 6.5 shows measurements of the spectral distribution of the diffuse attenuation coefficient for both upwelling radiance and downward irradiance, again for the same stations as above, and for the upper layer (40 m for the open ocean station, 6 m

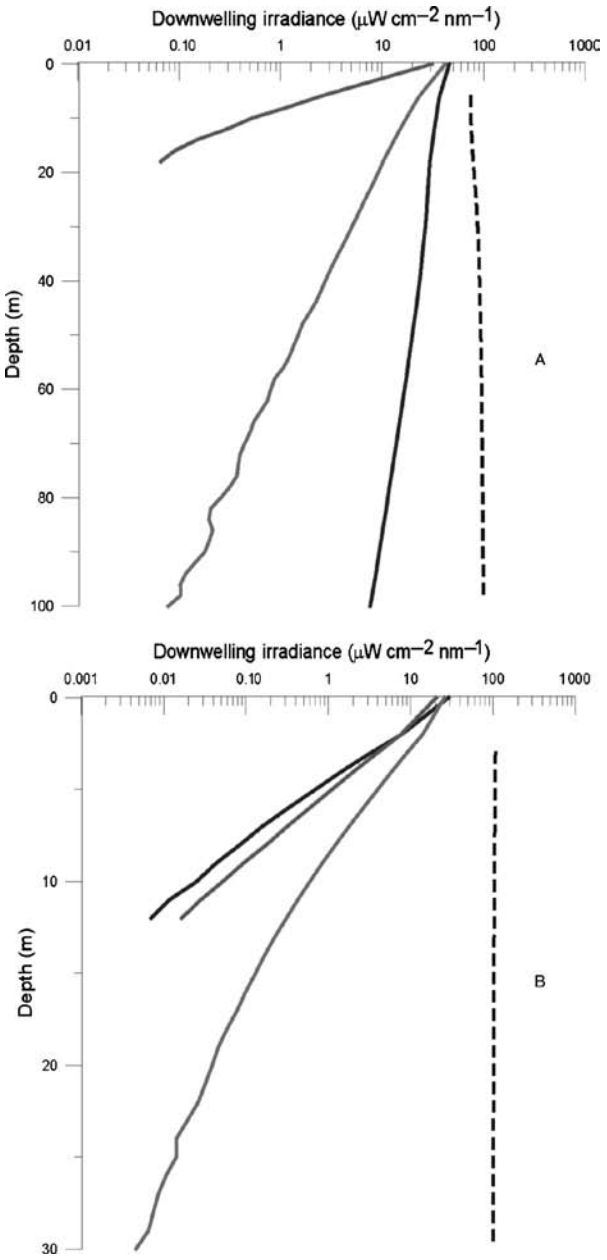

Figure 6.4
Profiles of downward irradiance for selected wavelengths in the two stations in Figures 6.2 and 6.3. The blue lines reference 443 nm, green 555 nm and red 650 nm. The above-water irradiances (555 nm), measured at the same time and normalized to their mean value during the profile, are also given as dotted lines.

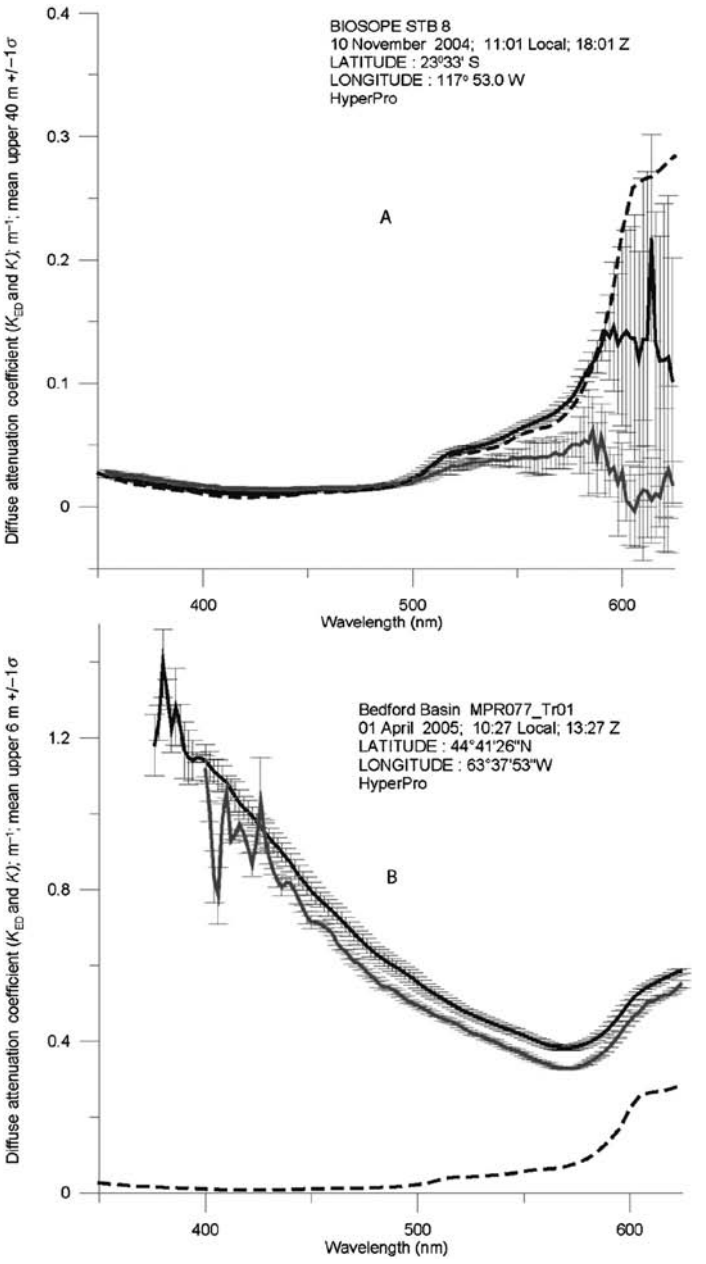

Figure 6.5
Computed diffuse attenuation coefficient (±1 standard deviation) for downwelling irradiance (upper line, solid) and upwelling nadir radiance (lower line, solid) for the two stations given in Figures 6.2 to 6.4. The dotted black line depicts theoretical values for pure seawater from Morel and Maritorena (2001).

for the coastal one). For reference, the estimated value for pure ocean water in the absence of particulate or dissolved contaminants is given as a dotted line (Morel and Maritorena, 2001). For the blue water station, the estimated diffuse attenuation coefficients over the blue and green part of the spectrum are not distinguishable from theoretical values for pure seawater. The measured values towards the red are noisier, and in fact are less than those of pure water. This results from the high water attenuation in these bands, and the dominance of Raman scattered radiance, which essentially adds energy into this spectral band from other wavebands (Morel, 2007 – Chapter 4 this volume). The observations of diffuse attenuation from the coastal station are almost 2 orders of magnitude higher, and demonstrate a dramatic difference in the spectral shape. Here, the blue wavebands are strongly attenuated by phytoplankton and CDOM, the former of which contributes to the red as well.

6.3.2.2 Reflectances

Reflectances, the ratio of the upwelling to the downwelling irradiances (see (6.7)), can be measured in the water using either separate instruments simultaneously, or sequentially with the same instrument turned upside down to measure the upwelled irradiance after a measure of the downwelling flux is made at the same depth. In the latter case, no absolute calibration is really needed as the same sensor is used to measure both the downward and upward irradiance. Such a condition can only be realistically met if the surface illumination conditions are rather stable between measurements, such as with a clear sky or with total overcast conditions. Normally, separate sensors are used, with one oriented up and the other down. In such a case, very accurate relative (and preferably absolute) calibrations are required. Sensors should be spectrally matched, and ideally collocated with respect to time and depth.

It is often of interest to estimate the reflectance (6.7) or the upwelling radiance just below the sea surface, based on measurements taken in the water, and propagated to the sea surface in post-processing. Generally (although see below) it is not easy to make the appropriate measurements anywhere close to the interface. One approach is to make measurements of upwelling radiance (or irradiance), and downwelling irradiance at a number of depths and propagate them to the surface; because of the presence of waves, valid observations may only exist some distance from the surface. From these measurements, the spectral diffuse attenuation coefficients are first estimated based on (6.4). This estimate is based on a block of data as near the surface as practically possible. The diffuse attenuation coefficients are then used in a predictive sense to estimate the value of the upwelling radiance or irradiance at the bottom of the air/sea interface by effectively extrapolating the logarithmic profile. This is often difficult to accomplish, particularly in the presence of a significant sea, and is exceptionally difficult to do in general for wavelengths > 650 nm given the contribution by Raman scattering (see Figure 6.4). At this point, the spectral reflectance, or the remote sensing reflectance, can be determined just below the sea surface (0^-).

A second approach is to attempt to make measurements of the upwelling radiance (or irradiance) as close as practical to the sea surface using a float or buoy to keep the sensors both aligned with respect to the vertical, and in a fixed vertical position. It is possible to carry such a deployment, even in moderate seas; however, even for sensors fixed 10 cm below the surface, it is necessary to correct for attenuation to the sea surface for greatest accuracy, particularly in turbid coastal waters. Without a full profile, the attenuation coefficient must in this case be estimated from the ratio of upwelling radiance (ocean colour), and empirical algorithms relating this ratio to diffuse attenuation

coefficients then used as a predictor for the propagation problem. For Case 1 waters, and even for most coastal environments, this works with acceptable accuracy, although it will not be as accurate in sediment laden waters, or locations with extremely high CDOM concentrations. The downwelling irradiance used for normalization can be taken from sensors mounted above the sea surface, with appropriate Fresnel reflectivity applied, generally 2–4%, depending on the solar zenith angle.

This general approach can be continued to provide an estimate of the remote-sensing reflectance or normalized water-leaving radiances above the surface (see Eq. 6.9 and 6.10). This will require a means to propagate the radiance through the sea/air interface. For photons travelling upward, the transmitted fraction is given as $t(\theta) \sim (1 - \rho(\theta',\theta)/n^2$, where the Fresnel reflectance ρ is a function of the incident (θ') and refracted (θ) angles related by Snell's law. Photons striking the sea surface from below at angles greater than ~48° are totally reflected back into the ocean interior. For the usual case where one is interested in normal incidence, $t(\theta) \sim 0.54$. The remote sensing reflectance can then be formed using a measurement of downwelling irradiance taken above the sea surface, and the normalized water-leaving radiance computed by multiplication by a suitable $F_0(\lambda)$ (e.g. Thuillier et al., 2003).

In some cases, it may be desirable to estimate in-water optical properties solely from measurements taken above the surface. For example, ships of opportunity can be instrumented (Balch et al., 2004), or instruments deployed on buoys, docks or towers. These instruments by their nature are restricted to direct measurement of AOPs only, and specifically the reflectance of the sea surface. With such remote techniques, only the upper layer is involved, with a thickness that depends on the wavelength and the water properties. A good rule of thumb is that 90% of the signal observed above the surface originates from the top third of the euphotic zone; this might be 70 m in the open ocean or a few metres in the productive coastal waters. While this is certainly a drawback for characterization of organisms dispersed and at low concentration within the water column or quantitatively estimating the importance of a deep bloom, in some circumstances, it may be an advantage. Cyanobacterial blooms, for example, with a dense aggregation of organisms floating at the surface, are accessible to remote detection, even through a simplified approach thanks to a high reflectivity (e.g. Kahru, 1997). Such methods however, are powerful in examination of horizontal spatial variability with the extreme example being satellite remote sensing of the surface of the sea.

Narrow field-of-view sensors can be deployed above the surface of the ocean looking down to evaluate the upwelling radiances. Such instruments can be single-look devices – for example a nadir viewing radiance sensor looking down at the sea surface – or imaging sensors that capture some components of the upwelling radiance distribution. There are several classifications of such sensors, including 'framing imagers' similar to a camera, 'pushbroom scanners' that image a single line and build an image from sequential along-track lines, and 'whiskbroom' scanners that use a moving optical system to measure radiance along a cross track line perpendicular to the direction of the platform motion, and then use the motion of the platform to build up the second along track dimension.

Irradiance sensors as well can be deployed above the sea surface, and are usually used to measure the downward irradiance for normalization of the measured upwelling radiance or irradiance, as discussed above. This paired measurement results in the estimation of the reflectance of the sea surface. Note that only approximately half of the measured upward radiance derives from the ocean interior, with the other half deriving from Fresnel reflectance of the sea surface; as one approaches grazing incidence

measurements, this percentage falls to zero. The reflectance of sun and sky from the sea surface must be minimized, and in any event corrected for, to be able to use such measurements routinely for the diagnosis of variations in the optical properties of the sea.

Figure 6.6 clearly demonstrates the influence of phytoplankton absorption on the spectral distribution of the reflectance, $R(\lambda, 0^-)$, as estimated from a free-fall profile of upwelling radiance (see Figure 6.7) and a ship-mounted instrument to measure the downwelling irradiance. The reflectance from the clearest ocean waters shows a maximum reflectance in the UV, and appears bright and purple-blue in colour. In

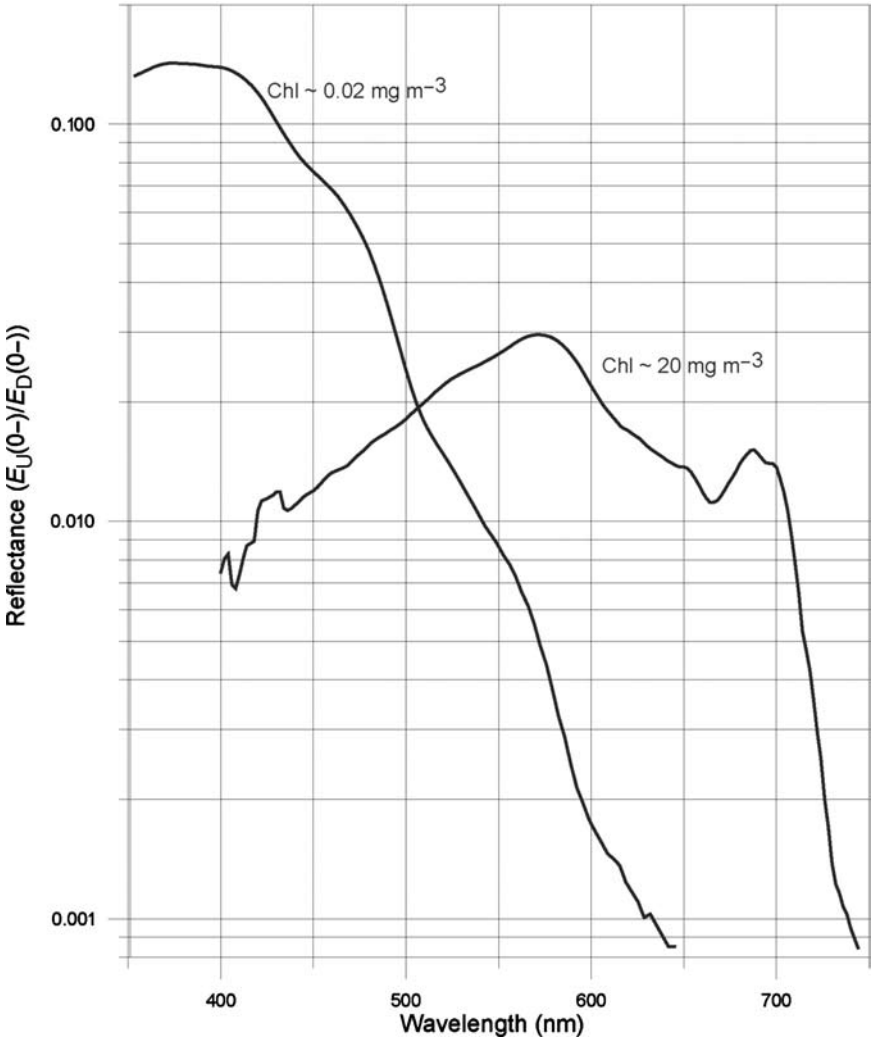

Figure 6.6
Hyperspectral reflectance estimated just below the surface based on the data given in Figures 6.2 and 6.3.

the coastal station, the amplitude of the reflectance is decreased by almost an order of magnitude. The peak reflectance is strongly shifted to the green (the minimum in phytoplankton absorption), and the chlorophyll fluorescence band near 680 nm is evident. The agreement between these observationally based data and the theoretical reflectances (Morel, 2007 – Figure 4.11 this volume) is excellent.

However, it can be seen from (6.8) that the retrieval of information on phytoplankton (or other constituents) is not as straightforward from reflectance as from diffuse attenuation. There are two reasons for this. First, the variation in f (and Q) with respect to surface illumination, with sea-state, and with the inherent optical properties (mostly β) is not straightforward, although tabulations (valid for Case 1 waters only) have been carried out (Morel and Gentilli, 1996; Mueller and Fargion, 2002). Second, we are less able to dispense so easily with the backscattering coefficient as above, and must deal explicitly with its variation as a function of constituents, albeit in an empirical fashion. Some relief can be had through the formation of reflectance ratios (often in use for the interpretation of remotely sensed ocean-colour data, see Ruddick et al., 2007 – Chapter 9 this volume). To the extent that b_b remains small compared with a, and relatively constant (spectrally), the $R(\lambda)$ spectrum would be an inverted view of the $a(\lambda)$ spectrum. Such a case can be seen by comparison of Figures 6.6 and 6.5. At low chlorophyll concentrations, the reflectance spectrum is dominated by the absorption (and to an extent, the high backscattering) of pure seawater, whereas the increased pigment load increases the absorption in the blue to blue-green and results in the dominance of green wavelengths in the reflectance spectrum. Between the two extreme situations seen in Figure 6.6, there exists a gradual evolution of the $R(\lambda)$ spectrum along with changes in the chlorophyll concentrations, which is the basis for analytical algorithms, such as the 'blue-to-green ratio' technique (see also Kahru and Mitchell, 1998).

The situation is more complex in most coastal environments, where contributions to absorption and scattering devolve from a diversity of particulate and dissolved sources. In particular, high concentrations of CDOM increase absorption in the UV and blue, and result in little energy scattered upward in these wavebands (see Figures 6.5B, 6.6B). Highly scattering waters – such as cases with high suspended sediments, or in Arctic waters dominated by glacial 'flour', or in cases where coccolithophorids are blooming, or in places with high rates of bubble injection – the enhanced scattering drives the reflectances up, resulting often in a turquoise colour to the sea as viewed from above. In such cases, the accurate derivation of the contribution from phytoplankton pigment, and the diagnosis of algal dynamics, is a problem.

6.3.2.3 Secchi disk

One would be remiss in writing a review of optical properties and instruments if one did not mention one of the earliest instruments to be deployed for the measurement of AOPs, the Secchi disk. The disappearance of the white (or otherwise) disk as it is lowered from the side of the ship, and viewed by the observer looking down from above, has a long and rich history in oceanography (Tyler, 1968). The Secchi depth (the depth at which the disk is no longer visible) is a rather complex AOP; the interpretation includes the physiological response of the human eye and the characteristics of the disk, in addition to the IOPs and the radiance distribution. Nonetheless, the measurement has lasting value; the calibration coefficient has not changed in the century and a half, and it is economical and easy to use. Lewis et al. (1988) were able to make use of this to produce a global map of estimated upper-ocean optical properties and chlorophyll concentrations from the world Secchi depth database, and Falkowski and Wilson

(1992) examined a 90-year record to deduce long-term trends in the concentration of chlorophyll in the North Pacific Ocean. Specifically with respect to harmful algae, a 60-year record of the Secchi depth has been used with great success to monitor the changing nature of Japan's Seto Inland Sea (Yanagi and Okaichi, 1997; Cullen, 2007 – Chapter 1 this volume).

6.3.3 Issues with respect to the measurement of in-water AOPs

There are a number of issues surrounding the accurate measurement and interpretation of AOPs in natural ocean waters. These have received intense scrutiny, with an ultimate goal to provide reliable in-water optical observations to support ocean monitoring and satellite ocean-colour programmes. The end result of this community investigation is a remarkably complete set of protocols and recommendations for the characterization, calibration, deployment and analysis of AOP data (Mueller and Austin, 1995; Mueller and Fargion, 2002; Mueller et al., 2003).

6.3.3.1 Calibration/characterization issues

The characterization and calibration of instruments used at sea includes a number of aspects, treated in detail in Mueller et al. (2003). Characterization of AOP instruments includes definition of spectral responsivity, signal-to-noise ratios, field-of-view (radiance) and cosine response (irradiance), immersion coefficients (Tyler and Smith, 1970), spectral bandpass and stray light, and many other aspects. The adequate characterization of dark signals (including their temperature dependence) is particularly important as it provides a blank which needs to be subtracted prior to detailed processing. Calibration issues involve reference of instrument response to standards traceable to national primary standard repositories (e.g. US National Institute for Standards and Technology). The highest possible accuracy and precision result from adequate attention paid to all these details; laboratory intercomparison studies have documented current accuracies to better than 5% absolute. Any errors here propagate to applications of optical diagnosis of natural water bodies. As a general rule, these characterizations and calibrations require extensive optical laboratories and are the responsibility of the instrument manufacturer; the user should however, be aware of these, and insist on compliance with the community consensus protocols (Mueller et al., 2003). Calibrations should be carried out both before and after deployment; for the greatest accuracies, field stability monitors are available to track calibration deviations over the course of a cruise.

A particular issue should be mentioned with respect to the use of 'PAR sensors' (see above) for quantitative radiometry. Because of the wide bandpass used with such instruments (nominally 400–700 nm), any deviations between the spectrum of the lamp used to calibrate the instrument and the spectrum of the light field one measures at sea introduces unacceptably high errors, which are not correctable. This effect exists to a much lesser extent for instruments with narrow bandpass filters as well, but is in principle correctable (Marshall and Smith, 1990). As a general rule, it is recommended that PAR be estimated from the spectral integration over the visible based on measurements using narrowband multichannel or hyperspectral radiometers.

6.3.3.2 Environmental issues

More of a problem in a general sense are the issues surrounding measurement of optical properties under the unforgiving conditions at sea. Even the most accurate and precise instrument will fail to provide useful data and information unless adequate care is

taken with deployment methodologies and proper accounting is made for environmental variability. The ocean is inherently a difficult environment to conduct research, and optical observations are particularly susceptible.

Temporal variations in solar radiation

The most obvious source of variability in the measurement of properties that depend on the radiance distribution is the input spectral radiance distribution from sun and sky. The two end members are the easiest to deal with: the situation of a cloudless sky, and relatively clear atmosphere, and at the other extreme, complete overcast conditions. Both result in radiance fields which, while very different, are similar in that they are relatively stable over the timescale of a typical observation of the upper ocean (tens of minutes). Unfortunately for the optical oceanographer, such conditions are not as common as the situation where scattered clouds of various types are present and where they are actively moving across the sky. The resulting variability over a measurement sequence can often render the observations of little value. With respect to measurements taken aboard ship, one can time the measurements (or try to do so) such that little variability exists in the downward radiance field, but for observations on unmanned platforms such as buoys or autonomous underwater vehicles (AUV), this variability must be faced in post-processing.

In the event that an above-water radiometer is available during a profile, this record can be used to normalize the subsurface values to a common incident irradiance condition (Smith and Baker, 1984; see above discussion). A similar correction can be applied to surface observations from floats or buoys. One must be careful however, as temporal variations in the light field observed at the surface may lead (or lag) those at significant depths when the solar zenith angle is more than a few degrees. It may be possible to temporally smooth the above water record to filter high-frequency (period <15 seconds) variations. Care should be taken as well to ensure that the surface reference sensor is not blocked from viewing the entire sky, and that it is not contaminated by reflection from ship surfaces. Generally, the recommendation is to place the reference sensor at the highest point on the ship to avoid these problems. Gimballed sensors, if properly designed, can potentially avoid large errors due to ship movements.

Sea state

Given suitable sky radiance distributions, one would desire to make profiles of upwelling radiance and downwelling irradiance in the upper ocean, and to compute the attenuation coefficient(s) and reflectances for the diagnosis of sources of optical variability. In many cases, these values are used to propagate radiance and irradiance in some sense to and through the sea surface to provide a reference point for above water observations from aircraft or satellite. Under calm conditions and with solar zenith angles less than 60°, this approach works nicely. However, the agitation of the local sea and the presence of significant swell introduces enhanced variability in scattering through bubble injection (e.g. Zhang et al., 1998, 2002), and a highly variable radiance field caused by the successive focusing and defocusing of surface waves at a range of scales (Zaneveld et al., 2001*a*).

The influence of surface waves on the optical fluctuations in the near-surface layer has been extensively examined by Walker (1994). This is a very difficult problem to deal with; the variations are not linear, so that simple averaging in time is not fully appropriate, and some recourse must be had to computations of radiative transfer, constrained with both observations (perhaps deeper in the water column) and assumptions regarding

vertical homogeneity. Multiple casts can provide statistics on derived quantities such as attenuation coefficients, which can then be used to establish confidence limits (Zaneveld et al., 2001*a*); in general, estimates of the diffuse attenuation coefficient for upward radiance are not nearly as contaminated as those for downwelling irradiance. Enhanced variability in reflectances (and normalized water-leaving radiances) occurs as well as a result of a roughened sea-surface (Zaneveld et al., 2001*b*, see below).

The injection of bubbles is a different problem as this changes (locally) the inherent optical properties (scattering in particular) rather than only altering the radiance distribution as is the case for surface gravity and capillary waves. Bubble clouds injected as a result of breaking waves increase the total scattering coefficient, and alter the angular distribution to enhance the backscattering ratio (Zhang et al., 1998, 2002; Stramski and Tegowski, 2001). As a result, the attenuation coefficient is increased, as is the reflectance. The resulting small-scale spatial variability introduces uncertainty in the scaling up of discrete optical profiles to the larger scale associated with aircraft or satellite images, and as above, multiple realizations of vertical profiles may permit confidence intervals to be established on estimated AOPs.

Shadowing and reflection

If this was not enough, the measurement of radiances and irradiances themselves introduce modifications of the radiance field, potentially leading to error. Most notable is the 'shading' effect of the instrument mass which decreases the radiance field in the shadow zone below an instrument, particularly when it aims at nadir. The magnitude of this effect to first order depends on the product of the diameter of the instrument (r) to the absorption coefficient of the wavelength of interest (a); the effect is most pronounced for red wavelengths in most ocean and coastal waters at low solar zenith angles (Gordon and Ding, 1992; Leathers et al., 2004). Not only the diameter, but also the height of the instrument and any supporting structure also affects the in-water radiance distribution (e.g. Piskozub et al., 2000). In recent years, manufacturers have progressively decreased the diameter of oceanographic optical instruments which minimizes this effect; nonetheless, correction procedures are necessary under some circumstances.

To first order, the approach of Gordon and Ding (1992) appears to be satisfactory at least for clear to moderately turbid waters ($a \cdot r < 0.5$; $b \leq a$; Mueller et al., 2003). Here, the correction term ε for a radiance sensor of radius r is given as $\sim 1 - \exp(-\kappa' ar)$, which simplifies to $\kappa' ar$ for small values of the non-dimensional product of the instrument radius and the attenuation coefficient. The term κ' varies inversely as a function of solar zenith angle (actually as a function of the refracted angle in water). To fix an order of magnitude of the error, consider two instruments, one with diameter 6 cm and another that is 30 cm. For the clearest of ocean waters, and with the sun near zenith (20°), the error in measuring upwelling radiance with the smaller instrument is less than 2% over the waveband 350–600 nm, but climbs to ~7% at 700 nm. Errors in measurement of upwelling irradiance are less, and are under 4% over all visible wavelengths. However, an instrument of 30 cm diameter would only have errors less than 2% for wavelengths less than 500 nm, and unacceptably high values in the red (>30% at 700 nm). For bloom situations (chl ~30 mg m^{-3}), the error becomes very high for both, with errors >2% over all wavelengths for the smaller instrument, and ranging from 13% to 35% for the larger one. For such turbid waters, it may prove better to use fibre-optic probes situated away from the main body of the instrument to reduce the error to acceptable values.

At a larger scale, the presence of the research vessel (or buoy platform) itself introduces optical artefacts. A large shadow region develops in the opposite direction to the sun, and near the ship, direct reflection from the hull becomes a significant contributor to the radiance distribution. Proper orientation of the ship during optical deployments helps this situation, as does the deployment using a 'free-fall' strategy away from the ship (Waters et al., 1990, see below) or use of remotely operated vehicles (ROV).

Bottom reflection

Significant errors can occur in the estimation of attenuation and reflectance values when measurements are taken in optically shallow regions, that is, where light reflected from the sea bottom is a significant component of the upwelling flux. Here, the complications of surface roughness and instrument shading are compounded by the variable reflectances of the sea bottom, and the often undulating sea floor. A recent entire issue of *Limnology and Oceanography* was dedicated to these situations.[23] Although these represent extraordinarily complex environments, the use of optical probing has enormous practical application here.

Biofouling

A problem that is of particular interest for the establishment of long-term moored or floating optical measurement platforms is biofouling. This is an involved and complex topic, always a factor in deployments greater than a few days in productive waters. Current approaches include copper shutters and mechanical brushes (Chavez et al., 2000, Manov et al., 2004; Chang and Dickey, 2007 – Chapter 2 this volume; Lehaitre et al., 2007 – Chapter 12 this volume), but for optimal results, periodic (weeks) cleaning of *in situ* optical instrumentation is recommended. In practice, and particularly in the highly variable coastal regime, it is often difficult to discriminate between local real changes in optical properties and biofouling influences.

Surface reflectivity

A solution to the biofouling problem is to make measurements from above the surface of the ocean. In addition to the issues discussed above for in-water measurements, interpretation of the observations of upwelling radiance and irradiance above the sea surface demand additional consideration. Many of these have been discussed elsewhere (Hooker et al., 2002) and included in the published set of provisional operational protocols (Mueller et al., 2003).

First, even in the absence of an intervening atmosphere, correction must be made to the measured radiance to account for direct reflectance from sun and sky ('glint'). To first order, this can be minimized by looking at the sea surface away from the direct sun reflection, or by masking data taken near the same azimuthal angle as the sun. For flat seas and a stable platform, correction can then be made for sky reflection by measuring the downward radiance in the same azimuthal plane, and in the complementary angle to that directed downward at the sea surface. The magnitude of the scattered skylight can then be estimated. Such techniques, when carefully applied, can result in highly accurate estimations of the water-leaving radiances from a measurement taken above the sea surface (Hooker et al., 2002).

[23] *Light in Shallow Waters*, 48, 2003.

However, such conditions are not always (or not usually) met: platforms are not stable, the sea surface can be rough and occasionally covered with whitecaps and foam, and the sky radiance distribution can be complex in the presence of patchy clouds. Control over azimuthal pointing (i.e. relative to the angle of the sun) may not always be optimal. Turbid waters are a particular problem in many respects (Toole et al., 2000). Derivation of an appropriate average can be quite difficult under such conditions, and the routine use of such observations challenging. For example, considering all sources of error, Toole et al. (2000) estimated uncertainties of 12–24% for estimates of remote sensing reflectances based on in-water profiles, and as much as 45% for measurements taken above the surface.

Measurements taken at higher altitudes from aircraft or satellite can average over small-scale variability due to waves, bubbles and foam, but have additional concerns, foremost the 'correction' for atmospheric scattering which accounts for as much as 95–98% of the signal for measurements taken at top-of-atmosphere. Platform and sensor attitudes become important, and must be convoluted with estimates of the angular distribution of the water-leaving radiances for appropriate normalization (Morel and Gentili, 1996). Further discussion of remote sensing issues and topics may be found in Ruddick et al. (2007 – Chapter 9 this volume).

6.3.4 Platforms used for the measurement of optical properties at sea

In the last few years, an interesting range of platforms has been developed or modified for in-water optical oceanographic instrumentation that augments more conventional ship-based measurements (Dickey et al., 2006, Twardowski et al., 2005). These can be thought of as complementary, as each has its own temporal and spatial scales over which the observations can be made. Sampling strategies that integrate multiple platforms can therefore be very effective (e.g. Dickey et al., 2006; Chang and Dickey, Chapter 2). This section describes the general types of platforms available and provides some examples of using these platforms for remote sensing related applications.

6.3.4.1 Deployment from research vessels

Optical measurements traditionally have been made from research ships. This remains a useful platform, and one that comes into its own when optical observations are coupled with other biogeochemical measurement programmes to investigate specific processes at sea (Sosik, 2007 – Chapter 8 this volume). Optical instruments can be deployed as sensors integrated into larger systems such as CTD and rosette, a situation which is now standard practice, although care needs to be taken to avoid ship shadow or hull reflectance. Generally, this involves deployment of instruments on the sunlit side of the ship. The optimal approach is to maneuver the measurement vehicle away from the ship by 100 m or so. This can be done by active means (e.g. ROV under propulsion), or more commonly by 'fishing' a tethered free-fall device until it is removed from the ship, and then allowing the platform to fall freely while measuring the optical profile (Waters et al., 1990). The data used in Figures 6.2 to 6.6 are from such a free-fall device which can be seen in its deployed configuration in Figure 6.7.

As mentioned above, instruments can be deployed as a tethered surface float (TSRB) which allows measurements of upwelling radiance and irradiance to be made very near the surface. An example of such a deployment is shown in Figure 6.8, where the upwelling sensors are located approximately 8 cm below the air/sea interface.

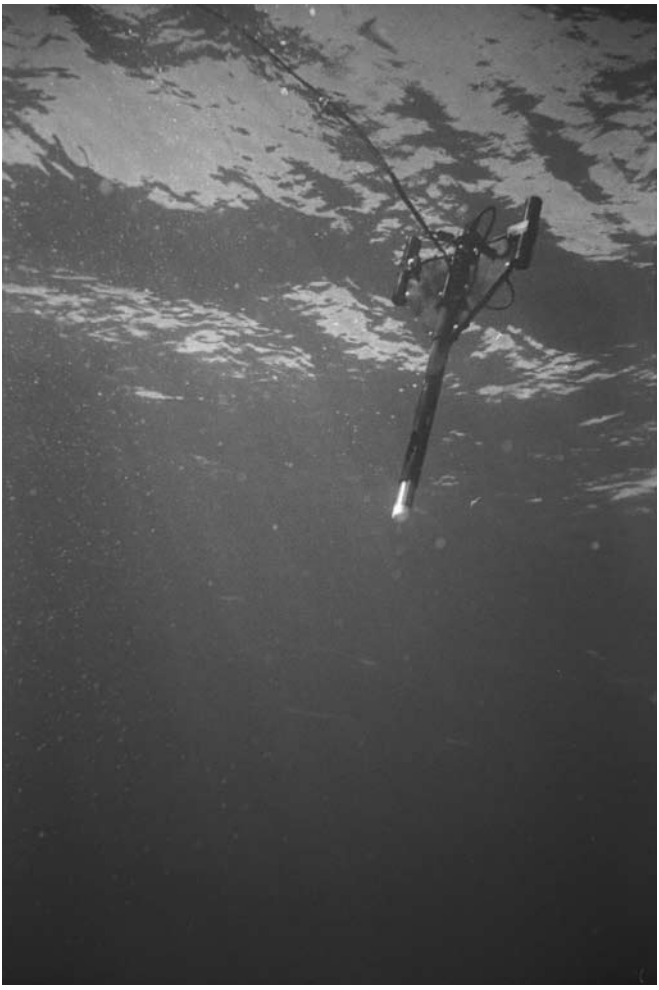

Figure 6.7
Free-fall platform for the measurement of apparent optical properties in the sea.

6.3.4.2 Deployment from moored arrays

While shipboard measurements are typically the highest quality, the restrictions on long-term station occupation have driven requirements for moored platforms that can collect optical data over longer periods of time (Lewis and McLean, 1999; Dickey et al., 2006). Furthermore, potential biases associated with restrictions on sampling during heavy weather are reduced. The pioneering BioWatt and Bermuda testbed moorings (Dickey et al., 2006) represented the first achievement of long time-series observations of optical variability. Many such moored systems now exist (e.g. Clark et al., 1997, Chavez et al., 1999; Dickey et al., 2006); Canada, Europe, Japan and the United States all have ambitious plans to instrument the coastal regions with both cabled and radio-telemetry ocean

Figure 6.8
Surface buoy platform for the measurement of upwelling irradiance and radiance just below (6–8 cm) the sea surface.

observation systems. Both IOP and AOP instruments are appropriate for such platforms, where they can be deployed in a vertical array, or on autonomous bottom or surface-mounted profiling winch systems. As a result, all the potential deployment options for the measurement of radiance and irradiance (sensors at fixed depths, sensors mounted above water, profiling) are possible. Such moored optical systems are susceptible to biofouling, however, and much successful effort has gone into the development of effective means to minimize this interference for time periods as long as six months to a year (Chavez et al., 2000; Manov et al., 2004). Such moorings can be operated to provide information in near real time, a distinct advantage for early warning systems for harmful algal blooms, and furthermore can be configured to carry out adaptive sampling strategies cued by specific environmental factors and events such as red-tide indicators.

6.3.4.3 Deployment from autonomous mobile platforms

In recent years, there has been a surge in the development of new autonomous vehicles for the measurement of a wide range of oceanographic properties. These include profiling floats under the global ARGO programme (e.g. Wilson, 2000), the use of powered AUVs with conventional propulsion methods (Griffiths et al., 2001; Griffiths, 2007 – Chapter 13 this volume) and hybrid vehicles such as gliders that combine the buoyancy control of profiling floats with mechanisms for controlling the vertical position of the vehicle (e.g. Davis et al., 2002). Optical instruments have seen limited but growing deployment on such platforms. The few missions to date however have offered an unprecedented view of ocean optical variability. For example, passive irradiance sensors have been used to generate time series of the spectral attenuation coefficient from profiling floats in the Japan Sea (Mitchell et al., 2000). Irradiance sensors on the REMUS autonomous vehicle have mapped optical variability in the coastal zone (Brown et al., 2004; Figure 9B). Future plans to populate the global ocean with profiling floats may well include optical sensors as a core payload. Some

minor challenges exist (e.g. orientation issues on gliders) but the mass, power and data metrics for irradiance and radiance sensors are well within platform constraints at present.

6.3.4.4 Nekton of opportunity

A novel approach to the profiling of underwater optical properties has emerged through efforts to instrument freely swimming organisms in the sea. Such efforts have been successful with marine mammals, turtles, sharks, rays, pelagics, groundfish and

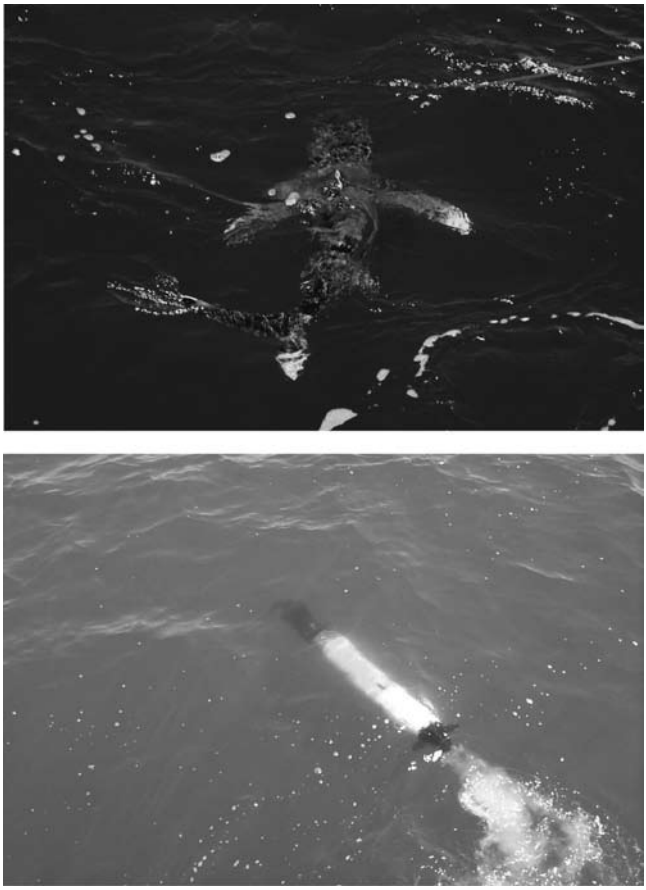

Figure 6.9
Two varieties of autonomous platform used for optical measurements. The rich blue of the oligotrophic waters contrasts with the oceanic white-tip shark, a species being used as a data collection platform by surgically implanted devices. The dark green waters of the coastal environment are a backdrop for the REMUS autonomous vehicle, which has been used for the measurement of the three-dimensional optical structure of the coastal ocean.

whales (Figure 6.5A). The optical characteristics of a given area, albeit roughly, have been determined by the incorporation of 'light' sensors into tags that also log pressure and temperature. Conversely, the light data has been used to geolocate the 'platform' in time through the estimation of the daylight extent and precession (Sibert and Nielsen, 2001). While such instruments cannot be used for the most accurate work in optical oceanography, they are potentially useful in defining spatial and temporal variations in the penetration of light in the sea (Figure 6.9A).

6.4 Apparent optical properties in the context of monitoring harmful algal blooms

It is clear from the above that measurements of apparent optical properties hold promise for the detection of high concentrations of algae, which, under some circumstances, may be considered harmful in some sense. The addition of high concentrations of algal particles to natural water bodies, along with other associated particulates and dissolved material, enhances both absorption and scattering, in a spectrally selective fashion. These changes in IOPs propagate within the context of the radiative transfer equation to cause observable changes in AOPs as well, particularly the diffuse attenuation and reflectance. As a result, observations of the distribution in time and space of the optical properties of the upper ocean remain the best means for detection of potentially harmful blooms of algae. The development of management support systems to permit the routine monitoring, detection and perhaps prediction of such blooms requires care, and optical instruments can be only one component of an overall observation and prediction strategy. Except in special circumstances, algae that form harmful blooms do not have unique spectral signatures in either absorption or scattering; as a result, while optical measurements themselves can provide detection capability, local knowledge, ancillary observations and direct chemical measurements will be required to provide definitive evidence supporting the existence and evolution of harmful concentrations of algae. An integrated, extensive and ongoing ocean observation system is therefore a valuable, necessary, but not sufficient component of an overall management strategy for natural water bodies.

References

Aas, E. and Højerslev, N. K. 1999. Analysis of underwater radiance observations: apparent optical properties and analytical functions describing the angular radiance distribution. *J. Geophys. Res.*, 104, pp. 8015–24.

Babin, M. 2007. Phytoplankton fluorescence: theory, current literature and *in situ* measurement. In: Babin et al. (eds), op. cit., this volume.

Babin, M., Roesler, C. S. and Cullen, J. J. (eds). 2006. *Real-time Coastal Observing Systems for Marine Ecosystem Dynamics and Harmful Algal Blooms: Theory, Instrumentation and Modelling*. Paris, Intergovernmental Oceanographic Commission of UNESCO. (Monographs on Oceanographic Methodology.)

Balch, W. M., Drapeau, D. T., Bowler, B. C., Booth, E. S., Goes, J. I., Ashe, A. and Frye, J. M. 2004. A multi-year record of hydrographic and bio-optical properties in the Gulf of Maine. I: Spatial and temporal variability. *Progr. Oceanogr.*, 63, pp. 57–98.

Brown, C. A., Huot, Y., Purcell, M. J., Cullen, J. J. and Lewis, M. R. 2004. Mapping coastal optical and biochemical variability using an autonomous underwater vehicle and a new bio-optical inversion model. *Limnol. Oceanogr. Meth.*, 2, pp. 262–81.

Chang, G. C. and Dickey, T. D. 2007. Interdisciplinary sampling strategies for detection and characterization of harmful algal blooms. In: Babin et al. (eds), op. cit., this volume.

Chang, G., Mahoney, K., Briggs-Whitmore, A., Kohler, D., Mobley, C., Lewis, M., Moline, M., Boss, E., Kim, M., Philpot, W. and Dickey, T. 2004. The new age of hyperspectral oceanography. *Oceanography*, 17, pp. 16–23.

Chavez, F. P., Strutton, P. G., Friederich, G., Feely, R. A., Feldman, G. C., Foley, D. C. and McPhaden, M. J. 1999. Biological and chemical response of the equatorial Pacific Ocean to the 1997–98 El Nino. *Science*, 286, pp. 2126–31.

Chavez, F. P., Wright, D., Herlien, R., Kelley, M., Shane, F. and Strutton, P. G. 2000. A device for protecting moored spectroradiometers from fouling. *J. Atmos. Ocean. Tech*., 17, pp. 215–19.

Ciotti, A. M., Cullen, J. J. and Lewis, M. R. 1999. A semi-analytical model of the influence of phytoplankton community structure on the relationship between light attenuation and ocean color. *J. Geophys. Res*., 104, pp. 1559–78.

Ciotti, A. M., Lewis, M. R. and Cullen, J. J. 2002. Assessment of the relationships between dominant cell size in natural phytoplankton communities and the spectral shape of the absorption coefficient. *Limnol. Oceanogr*., 47, pp. 404–17.

Clark, D., Gordon, H. R., Voss, K. J., Ge, Y., Broenkow, W. and Trees, C. 1997. Validation of atmospheric correction over the oceans. *J. Geophys. Res*., 102, pp. 17209–17.

Cullen, J. J. 2007. Observation and prediction of harmful algal blooms. In: Babin et al. (eds), op. cit., this volume.

Cullen, J. J., Ciotti, A. M., Davis, R. F. and Lewis, M. R. 1997. Optical detection and assessment of algal blooms. *Limnol. Oceanogr*., 42, pp. 1223–39.

Davis, R. E., Eriksen C. C. and Jones, C. P. 2002. Autonomous buoyancy-driven underwater gliders. In: G. Griffiths (ed.), *The Technology and Applications of Autonomous Underwater Vehicles*. London, Taylor and Francis, pp. 37–58.

Dickey, T., Lewis, M. and Chang, G. 2006. Optical oceanography: Recent advances and future directions using global remote sensing and *in situ* observations. *Rev. Geophys.* 44 pp. 1–39.

Falkowski, P. G. and Wilson, C. 1992. Phytoplankton productivity in the North Pacific Ocean since 1900 and implications for absorption of anthropogenic CO_2. *Nature*, 358, pp. 741–43.

Gordon, H. R. 1989*a*. Dependence of the diffuse reflectance of natural waters on the sun angle. *Limnol. Oceanogr*., 34, pp. 1484–89.

Gordon, H. R. 1989*b*. Can the Lambert-Beer law be applied to the diffuse attenuation coefficient of ocean water ? *Limnol. Oceanogr.*, 34, pp. 1389–1409.

Gordon, H. R. and Clark, D. K. 1981. Clear water radiances for atmospheric correction of Coastal Zone Color Scanner imagery. *Appl. Opt.*, 20, pp. 4174–80.

Gordon, H. R. and Ding, K. 1992. Self-shading of in-water optical instruments. *Limnol. Oceanogr*., 37, pp. 491–500.

Griffiths, G. 2007. Glider and autonomous underwater vehicle observing systems. In: Babin et al. (eds), op. cit., this volume.

Griffiths, G., Davis, R., Eriksen, C., Frye, D., Marchand, P. and Dickey, T. 2001. Towards new platform technology for sustained observations. In: C. J. Koblinsky and N. R. Smith (eds), *Observing the Oceans in the 21st Century*. Melbourne, Bureau of Meteorology, GODAE Project Office, pp. 324–38.

Hooker, S. B., Lazin, G., Zibordi, G. and McLean, S. 2002. An evaluation of above- and in-water methods for determining water-leaving radiances. *J. Atmos. Ocean. Tech*., 19, pp. 486–515.

Jerlov, N. G. 1976. *Marine Optics*. New York, Elsevier.

Kahru, M. 1997. Using satellites to monitor large-scale environmental change: A case study of canobacteria blooms in the Baltic Sea. In: M. Kahru and C. W. Brown (eds), *Monitoring Algal Blooms: New Techniques for Detecting Large-scale Environmental Change*. New York, Springer-Verlag, pp. 43–61.

Kahru, M. and Mitchell, B. G. 1998. Spectral reflectance and absorption of a massive red tide off southern California. *J. Geophys. Res.*, 103, pp. 21601–09.

Kirk, J. T. O. 1984. Dependence of relationship between inherent and apparent optical properties of water on solar altitude. *Limnol. Oceanogr.*, 29, pp. 350–56.

Kirk, J. T. O. 1994. *Light and Photosynthesis in Aquatic Ecosystems*, 2nd ed. New York, Cambridge University Press.

Leathers, R. A., Downes, T. V. and Mobley, C. 2004. Self-shading correction for oceanographic upwelling radiometers. *Opt. Exp.*, 12, pp. 4709–18.

Lehaitre, M., Delauney, L. and Compère, C. 2007. Biofouling and underwater measurements. In: Babin et al. (eds), op. cit., this volume.

Lewis, M. R., Kuring, N. and Yentsch, C. 1988. Global patterns of ocean transparency. *J. Geophys. Res.*, 93, pp. 6847–56.

Lewis, M. R. and McLean, S. D. 1999. Optical observations for operational oceanography. *Backscatter*, 10, pp. 22–25.

Lohrenz, S. E., Fahnenstiel, G. L., Kirkpatrick, G. J., Carroll, C. L. and Kelly, K. A. 1999. Microphotometric assessment of spectral absorption and its potential application for characterization of harmful algal species. *J. Phycol.*, 35, pp. 1438–46.

Manov, D., Chang, G. and Dickey, T. 2004. Methods for reducing biofouling of moored optical sensors, *J. Atmos. Ocean. Tech.*, 21, pp. 957–67.

Mitchell, B. G., Kahru, M. and Sherman, J. 2000. Autonomous temperature-irradiance profiler resolves the spring bloom in the Sea of Japan. *Ocean Optics XV*, *Proc.* Monaco, Oct. 2000.

Mobley, C. D. 1994. *Light and Water*: *Radiative Transfer in Natural Waters*. San Diego, Calif., Academic Press.

Morel, A. 1978. Available, usable, and stored radiant energy in relation to marine photosynthesis. *Deep Sea Res.*, 25, pp. 673–88.

Morel, A. 2007. Introduction to optical properties in the sea: theoretical aspects. In: Babin et al. (eds), op. cit., this volume.

Morel, A. and Gentili, B. 1991. Diffuse reflectance of ocean waters: its dependence on sun angle as influenced by the molecular scattering contribution. *Appl. Opt.*, 30, pp. 4427–38.

Morel, A. and Gentili, B. 1996. Diffuse reflectance of oceanic waters. III: Implication of bidirectionality for the remote sensing problem. *Appl. Opt.*, 35, pp. 4850–62.

Morel, A. and Maritorena, S. 2001. Bio-optical properties of oceanic waters: a reappraisal. *J. Geophys. Res.*, 106, pp. 7163–80.

Mueller, J. L. and Austin, R. W. 1995. *Ocean Optics Protocols for SeaWiFS validation, Revision 1*, Vol. 25. In: S. B. Hooker, E. R. Firestone and J. G. Acker (eds), NASA Tech. Memo. 104566. Greenbelt, Md., NASA Goddard Space Flight Center.

Mueller, J. L. and Fargion, G. S. 2002. *Ocean Optics Protocols for Satellite Ocean Color Sensor Validation, Revision 3*. Greenbelt, Md., NASA Goddard Space Flight Center.

Mueller, J. L., Fargion, G. S. and McClain, C. R. (eds). 2003. *Ocean Optics Protocols For Satellite Ocean Color Sensor Validation, Revision 4*, Vol. IV. Greenbelt, Md., NASA Goddard Space Flight Center.

Piskozub, J., Weeks, A. R., Schwarz, J. N. and Robinson, I. S. 2000. Self-shading of upwelling irradiance for an instrument with sensors on a sidearm. *Appl. Opt.*, 39, pp. 1872–78.

Roesler, C. S. and Boss, E. 2007. *In situ* measurement of inherent optical properties and potential for harmful algal bloom detection and coastal ecosystem observations. In: Babin et al. (eds), op. cit., this volume.

Ruddick, K., Lacroix, G., Park, Y., Rousseau, V., De Cauwer, V. and Sterckx, S. 2007. Overview of ocean colour: theoretical background, sensors and applicability to detection and monitoring of harmful algal blooms (capabilities and limitations). In: Babin et al. (eds), op. cit., this volume.

Schofield, O., Bosch, J., Glenn, S., Kirkpatrick, G., Kerfoot, J., Lohrenz, S., Moline, M., Oliver, M. and Bissett, P. 2007. Bio-optics in integrated ocean observing networks: potential for studying harmful algal blooms. In: Babin et al. (eds), op. cit., this volume.

Schofield, O., Gryzmski, J., Bissett, W. P., Kirkpatrick, G., Millie, D. F., Moline, M. A. and Roesler, C. 1999. Optical monitoring and forecasting systems for harmful algal blooms: possibility or pipedream? *J. Phycol.*, 35, pp. 125–45.

Sibert, J. R. and Nielsen, J. L. (eds). 2001. *Electronic Tagging and Tracking in Marine Fisheries*. Proc. Symp. Tagging and Tracking Marine Fish with Electronic Devices. Honolulu, Hawaii, Kluwer Academic Publishers.

Siegel, D. A., Maritorena, S., Nelson, N. B., Hansell, D. A. and Lorenzi-Kayser, M. 2002. Global distribution and dynamics of colored dissolved and detrital organic materials. *J. Geophys. Res.*, 107, pp. 3228–42.

Smith, R. C., Austin, R. W. and Tyler, J. E. 1970. An oceanographic radiance distribution camera system. *Appl. Opt.*, 9(9), pp. 2015–22.

Smith, R. C. and Baker, K. 1984. Analysis of ocean optical data. *Ocean Optics VIII*, *Proc. SPIE*, 478, pp. 119–26.

Sosik, H. 2007. Characterizing seawater constituents from optical properties. In: Babin et al. (eds), op. cit., this volume.

Stramski, D. and Tegowski J. 2001. Effects of intermittent entrainment of air bubbles by breaking wind waves on ocean reflectance and underwater light field. *J. Geophys. Res.*, 106, (C12) 31345–31360.

Thuillier, G., Herse, M., Simon, P. C., Labs, D., Mandel, H., Gillotay, D. and Foujols, T. 2003. The solar spectral irradiance from 200 to 2400 nm as measured by the SOLSPEC spectrometer from the ATLAS 1-2-3 and EURECA missions. *Sol. Phys.*, 214, pp. 1–22.

Twardowski, M. S., Lewis, M. R., Barnard, A. H. and Zaneveld, J. R. V. 2005. In-water instrumentation and platforms for ocean color remote sensing applications. In: R. Miller, C. Del-Castillo and B. McKee (eds), *Remote Sensing of Coastal Aquatic Environments*. New York, Kluwer Academic Publishers.

Tyler, J. E. 1968. The secchi disc. *Limnol. Oceanogr.*, 13, pp. 1–6.

Tyler, J. E. and Smith, R. C. 1970. *Measurement of Spectral Irradiance Underwater*, XII. New York, Gordon & Breach Science Publishers.

Voss, K. J. 1989. Electro-optic camera system for measurement of the underwater radiance distribution. *Opt. Eng.*, 28, pp. 241–47.

Walker, R. E. 1994. *Marine Light Field Statistics*. New York, John Wiley & Sons.

Waters, K., Smith, R. C. and Lewis, M. R. 1990. Avoiding ship-induced light-field perturbation in the determination of oceanic optical properties. *Oceanography*, 3, pp. 18–21.

Wilson, S. 2000. Launching the ARGO armada. *Oceanus*, 42, pp. 17–19.

Yanagi, T. and Okaichi, T. 1997. Seto Inland Sea – historical background. In: T. Okaichi and T. Yanagi (eds.), *Sustainable Development in the Seto Inland Sea, Japan – From the Viewpoint of Fisheries*. Tokyo, Terra Scientific Publishing Company, pp. 9–14.

Zaneveld, J. R. V., Boss, E. and Barnard, A. H. 2001*a*. The influence of surface waves on measured and modeled irradiance profiles. *Appl. Opt.*, 40(9), pp. 1442–49.

Zaneveld, J. R. V., Boss, E. and Hwang, P. A. 2001*b*. The influence of coherent waves on the remotely sensed reflectance. *Opt. Exp.*, 9, pp. 260–66.

Zhang, X., Lewis, M. R. and Johnson, B. 1998. The influence of bubbles on scattering of light in the ocean. *Appl. Opt.*, 37, pp. 6525–36.

Zhang, X., Lewis, M. R., Lee, M., Johnson, B. and Korotaev, G. 2002. The volume scattering function of natural bubble populations. *Limnol. Oceanogr.*, 47, pp. 1273–82.

7

Phytoplankton fluorescence: theory, current literature and *in situ* measurement

M. Babin

7.1 Introduction

The measurement of chlorophyll *a* (chl *a*) *in vivo* fluorescence was introduced in oceanography by Lorenzen (1966) to monitor changes in phytoplankton biomass. It is now routinely measured at sea using various kinds of commercial benchtop and *in situ* sensors (fluorometers, radiance and irradiance meters, flow cytometers), and can even be remotely detected at the sea surface from an aircraft or satellite (Gower and Borstad, 1981). Two ocean-colour sensors currently detect sea surface chl *a* fluorescence from space (MODIS and MERIS). Over time, chl *a* fluorometry has become a major tool in biological oceanography, especially for mapping the spatial distribution of phytoplankton at various scales, and for monitoring temporal fluctuations in phytoplankton biomass. Sun-induced chl *a* fluorescence has also been used to estimate primary production (Kiefer et al., 1989).

In the late 1970s and during the 1980s, protocols previously developed in plant physiology for measuring the so-called 'variable fluorescence' were introduced in oceanography to study and monitor phytoplankton photosynthesis (Cullen and Renger, 1979; Kolber et al., 1990). This fluorometry approach allows a more mechanistic interpretation of changes in photosynthesis. The use of variable fluorescence to estimate primary production was also proposed (e.g. Kolber and Falkowski, 1993). Commercial variable-fluorescence sensors are now available, including an *in situ* profiler appropriate for autonomous deployments.

This chapter reviews the different fluorescence-based approaches used in oceanography, with special emphasis on those that are appropriate for autonomous deployment and for which commercial sensors are available. Also provided is the theoretical background necessary to understand what the different fluorescence sensors actually measure, and to interpret fluorescence signals in terms of phytoplankton biomass and photosynthesis. Although many commercial sensors are mentioned, my intention was to provide examples rather than an exhaustive list.

For more detailed reviews on chl *a* fluorescence and photosynthesis, see Clayton (1980), Krause and Weis (1991), Falkowski and Raven (1997) and Hall and Gao (1999), and the website of Govindjee.[24]

[24]http://www.life.uiuc.edu/govindjee/

7.2 Theoretical background

7.2.1 Fluorescing properties of chlorophyll *a*

Chlorophyll *a* absorbs light in the blue and red parts of the visible electromagnetic spectrum (Figure 7.1). The red absorption band, which is centred at 662 nm when chlorophyll *a* is dissolved in acetone, corresponds to an electronic transition from the ground to the first excited state of the chl *a* molecule (Figure 7.2). The blue absorption band is centred at 430 nm in acetone and corresponds to an electronic transition from the ground to the second excited state (Figure 7.2, see also Figure 2.3 in Falkowski and Raven, 1997). Each electronic state is characterized by a number of substates that correspond to different molecular vibrational and rotational energy. This is why the absorption occurs in wide wavebands rather than distinct lines. A transition down from the second to the first excited state generally occurs through thermal decay within less than a picosecond. In solution, the transition down from the first to the ground state can lead to the re-emission of a photon of lower energy (i.e. longer wavelength), or also through thermal decay. The re-emission of a photon is called *fluorescence* or *phosphorescence*. Because fluorescence occurs much faster (*c.* 15 nanoseconds) than phosphorescence (*c.* 1 ms), it accounts for nearly all photon re-emission. Fluorescence by chl *a* in acetone is spectrally characterized by a main peak centred at 668 nm and a secondary

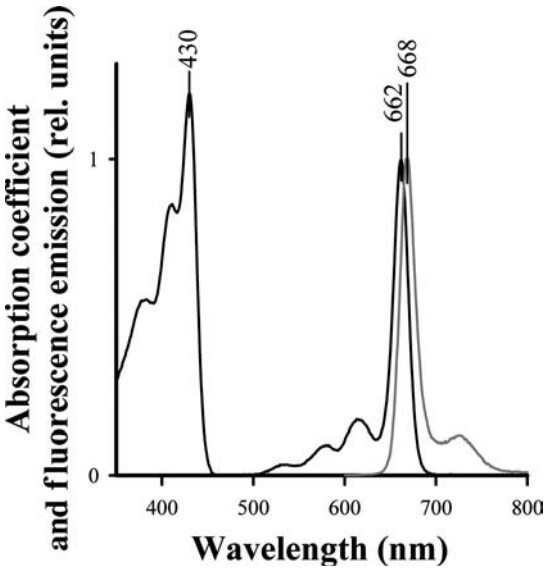

Figure 7.1
Spectra of light absorption (black line) and of fluorescence emission (grey line) by pure chlorophyll *a* dissolved in acetone. Note that the fluorescence spectrum is more or less a mirror image of the absorption spectrum in the red spectral range, shifted towards longer wavelengths. This phenomenon is called the Stokes shift. It results from losses of energy during the transition from excited to ground state (see Figure 7.2 and related text).

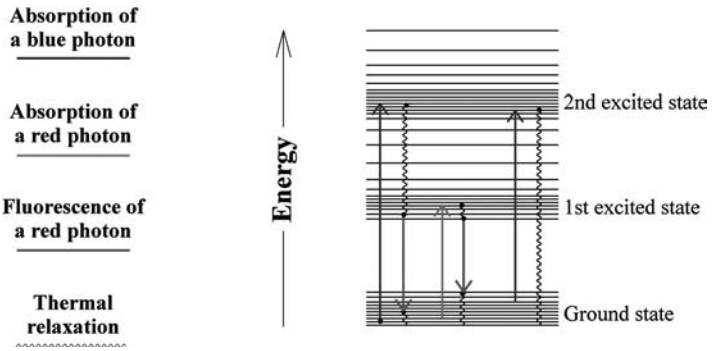

Figure 7.2
Energy levels and different types of transitions between electronic excited states, when a photon is absorbed by chlorophyll *a*.

shoulder at 710 nm (Figure 7.1). The quantum yield of fluorescence (ϕ_F) is defined as the fraction of absorbed photons re-emitted as fluorescence. It is approximately 30% for chl *a* in acetone, which means that the remaining 70% of absorbed photons lead to thermal decay. At very high chl *a* concentration, fluorescence is visible to the naked eye, as shown in Figure 7.3.

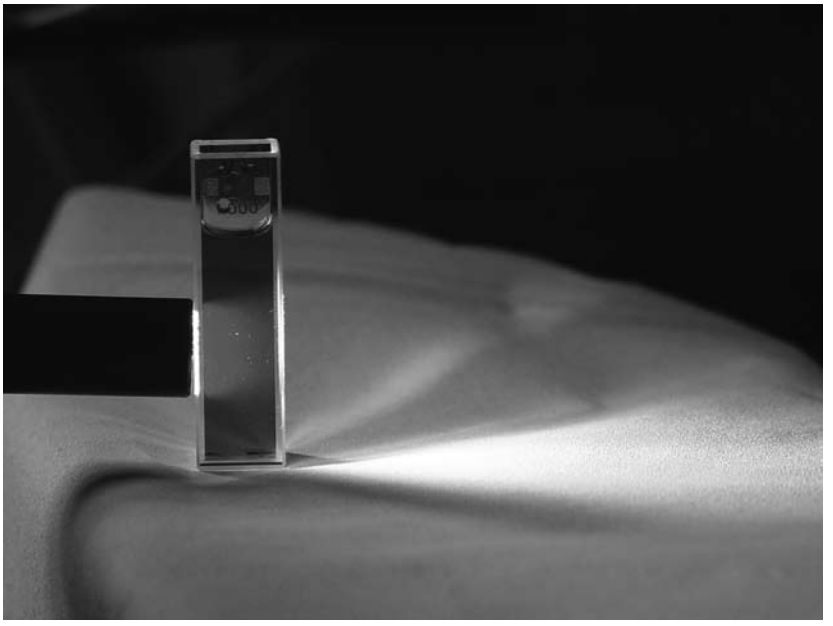

Figure 7.3
Fluorescence (gray) emitted by chlorophyll *a* dissolved in pure acetone, when induced using a beam of white light.

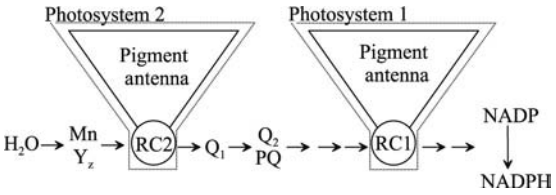

Figure 7.4
Schematic representation of the light reactions of photosynthesis in plants. The arrows indicate the flow of electrons (see text). Mn and Y_z constitute the water-splitting complex from which RC2 extracts electrons, and which in turn extracts electrons from water. It involves a molecule of tyrosine (Y_z) and a cluster of four manganese atoms (Mn). Q_1 (more commonly denoted Q_A) is the primary electron acceptor from RC2. The plastoquinone Q_2 (more commonly denoted Q_B) is the secondary electron acceptor. It is a mobile molecule that, once reduced by Q_1 and protonated twice, moves away from Q_1 and is replaced by another oxidized Q_2 from of a pool (PQ) of several plastoquinone molecules present in the lumen.

7.2.2 Functional organization of photosynthetic apparatus

The light reactions of photosynthesis in oxygenic photoautotrophs are very roughly schematized in Figure 7.4. These reactions occur within the thylakoid membrane located in the chloroplasts.[25] The whole photosynthetic apparatus can be seen as a set of elements, so-called *photosynthetic units*. Each photosynthetic unit is composed of two *photosystems* (PS1 and PS2), associated with an electron transport chain. Each photosystem is composed of a matrix of pigments bound to proteins, the *pigment antenna*, and *reaction centre* (RC1 or RC2, respectively). Together, the two photosystems promote the photochemical reaction that leads to the reduction of $NADP^+$ and the phosphorylation of ADP, using the free energy of photons absorbed by pigments. NADPH and ATP are then used in the dark reactions of photosynthesis to reduce carbon. In linear electron flow (the main pathway), the energy of two photons (one per reaction centre, RC1 and RC2) is necessary to reduce one molecule of $NADP^+$ into NADPH, and four such events are necessary to oxidize two molecules of H_2O and produce one molecule of O_2. Therefore, the minimum photon requirement for the production of one molecule of O_2 is eight, and the theoretical maximum quantum yield of oxygen photosynthetic production is thus 0.125 mol O^2 $(\text{mol photon})^{-1}$.

At room temperature, *most of chl a's fluorescence originates from PS2*. Therefore, the following discussion is mainly focused on PS2. Its functional structure is shown in Figure 7.5. In addition to chl *a*, the pigment antenna of PS2 contains accessory pigments: other chlorophylls, carotenoids and phycobilins. The composition is specific to phytoplankton taxa (reviewed by Jeffrey and Vesk, 1997). Among accessory pigments, the *light-harvesting* ones transfer nearly 100% of their excitation energy (a so-called *exciton*) to chl *a* when they absorb a photon. Once located in chl *a*, the exciton can be transferred to the reaction centre, or lead to the re-emission of a photon as fluorescence or to thermal decay.

[25]In prokaryotic oxygenic photoautotrophs, the thylakoid membranes are free in the cell, i.e. not embedded in chloroplasts.

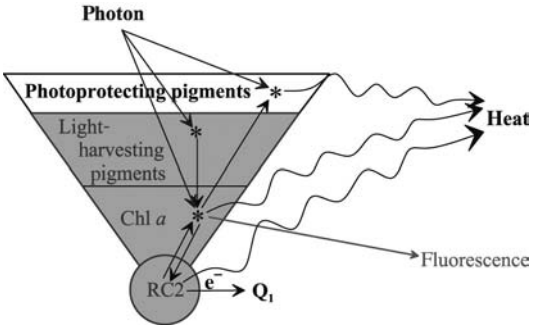

Figure 7.5
Simplified representation of the functional organization of PS2.

The *xanthophylls*, a family of carotenoids, often play a role of *photoprotection* against excessive irradiance in plants (Demmig-Adams, 1990). In chlorophytes, the three xanthophylls zeaxanthin, antheraxanthin and violaxanthin associated with the PS2 pigment antenna are involved in a cycle. Indeed, they can be enzymatically inter-converted back and forth by de-epoxidation and epoxidation, respectively, following the sequence zeaxanthin ↔ antheraxanthin ↔ violaxanthin. High irradiance, and the correlated build-up of a proton gradient across the thylakoid membrane (ΔpH),[26] stimulates the de-epoxidation pathway that leads to the formation of zeaxanthin. While violaxanthin can in some cases act as a light harvesting pigment, i.e. transfer its excitation energy to chl *a*, zeaxanthin and antheraxanthin are involved in the photoprotection of the photosynthetic apparatus. It has been hypothesized that zeaxanthin and antheraxanthin can trap the excitation energy of chl *a* and dissipate this energy as heat (see reviews by Owens, 1995; Yamamoto and Bassi, 1996). In chromophytes (chlorophyll *c* containing phytoplankton), an analogue cycle with two xanthophylls, diadinoxanthin and diatoxanthin, has been shown to be involved in photoprotection (Olaizola and Yamamoto, 1994). In the latter cycle, diatoxanthin is the photoprotecting member.

Photoprotection related to the xanthophyll cycle takes place when the light reactions are in excess of the capacity of the dark reactions (moderate to high irradiance), and prevents damage from occurring in the photosynthetic apparatus. The response of the xanthophyll cycle to irradiance changes can be fast through epoxidation/de-epoxidation (minutes), and slow through variations in the pool size of xanthophylls-cycle pigments (hours to days) (see review by Lavaud et al., 2004). An increase in the pool size provides a greater capacity to the fast response.

The reaction centre is the site where the energy of absorbed photon is converted into chemical energy. The RC2 core consists of a chl *a* dimer (so-called P_{680}). The main molecular components of RC2 are two major proteins, D1 and D2. These proteins are complexed to P_{680} as well as to some of the electron carriers.

In brief, the different possible fates of the energy of an absorbed photon in PS2 are the following (see Figure 7.5 and Gilmore and Govindjee, 1999, for a more detailed description):

[26]Protons formed by water splitting in PS2 and proton transport by the plastoquinone pool accumulate in the lumen when their production exceeds the rate of ADP/Pi recycling by the dark reactions of photosynthesis.

1. the energy of a photon absorbed by a photoprotecting pigment is dissipated as heat;
2. the energy of a photon absorbed by a light harvesting pigment is transferred by resonance to antenna chl *a*;
3. the energy of a photon absorbed by a light harvesting pigment and then transferred to chl *a*, or of a photon directly absorbed by chl *a* is either (a) dissipated as heat, directly or through de-excitation by a photoprotecting pigment, (b) used for the re-emission of a red photon (fluorescence), or (c) transferred to P680 in the RC2;
4. the energy of a photon transferred by antenna chl *a* to RC2 or of a photon directly absorbed by P680 is either (a) used to transfer an electron to (i.e. to reduce) the first electron acceptor, [27] Q_1, when the latter is not already in a reduced state (it is then said to be 'open'), (b) back-transferred to antenna chl *a* when Q1 is already in a reduced state (it is then said to be 'close'), or (c) dissipated as heat if RC2 is damaged;
5. the fate of a photon back-transferred from RC2 to the pigment antenna is as in 4.

7.2.3 Simple model describing variations in quantum yield of photosystem 2 fluorescence at room temperature

The flux of *in vivo* fluorescence emitted by an elementary volume (F: µmol photons m^{-3} s^{-1}) can be expressed by the following equation[28] (Falkowski and Kiefer, 1985; Babin et al., 1996*a*):

$$F = PAR\ [chl\,a]\ \bar{a}^*\ Q_a^*\phi_F \tag{7.1}$$

where PAR (µmol photons m^{-2} s^{-1}), which stands for photosynthetically available radiation, is the scalar irradiance integrated between 400 nm and 700 nm, [chl *a*] (mg m^{-3}) is the concentration of chl *a*, $\bar{a}^*$ (m^2 mg^{-1}) is the chl *a*-specific spectrally averaged absorption coefficient of phytoplankton weighted by the irradiance spectrum, Q_a^* (dimensionless) is the fluorescence intracellular reabsorption factor, and ϕ_F [mol emitted photons (mol absorbed photons)$^{-1}$] is the quantum yield of *in vivo* fluorescence. While the product PAR [chl *a*] $\bar{a}^*$ reflects the amount of light absorbed by phytoplankton, ϕ_F indicates the fraction that is converted to fluorescence, and Q_a^* the fraction of that fluorescence that is not reabsorbed within the cells (Collins et al., 1985).

$\bar{a}^*$ is defined as

$$\bar{a}^* = \frac{\int_{400}^{700} a_\phi^*(\lambda)\, \mathring{E}(\lambda)\, d\lambda}{PAR} \tag{7.2}$$

where $a_\phi^*(\lambda)$ (m^2 mg^{-1}) is the chl *a*-specific absorption coefficient of phytoplankton, and $\mathring{E}(\lambda)$ is the scalar irradiance (µmol photons m^{-2} s^{-1}). The variations in the $a_\phi^*(\lambda)$ spectrum are due to changes in pigment composition, intracellular pigment concentration and

[27] The first electron acceptor from RC2 is commonly denoted Q_A, where Q stands for 'quencher'. In this chapter, the symbol Q_1 is used instead of Q_A to avoid confusion with the reabsorption factor, Q_a^*.
[28] For simplicity, the spectral dependency of some terms is not explicitly expressed in this equation.

cell size, among species and in response to environmental factors such as light and nutrients (see Morel, 2007; Roesler and Boss, 2007; Sosik, 2007 – Chapters 4, 5 and 8 this volume, and references therein). $\overline{a}^*$ variations are due to changes both in the magnitude of $a_\phi^*(\lambda)$, and in the matching between the spectra of $a_\phi^*(\lambda)$ and $E^o(\lambda)$. In open ocean (Case 1) waters, the typical range of variations in $\overline{a}^*$ is 0.005–0.05 $m^2\ mg^{-1}$ at the sea surface (Babin et al., 1996*a*). It is certainly much larger when considering vertical variations, and in coastal (Case 2) waters where the shape of the $E^o(\lambda)$ spectrum is more variable.

Q_a^* can be expressed as (Morel and Bricaud, 1981)

$$Q_a^* = \frac{a_\phi^*(\mathrm{em})}{a_{sol}^*(\mathrm{em})}, \tag{7.3}$$

where em represents the wavelength range of fluorescence emission (centred around ~685 nm, with a half-height width of ~25 nm for the main band), and a_{sol}^* is the *in vivo* chlorophyll-specific absorption coefficient of unpackaged phytoplankton pigments (i.e. in solution). Intracellular reabsorption of fluorescence results from the overlap between the red absorption band (maximum centred at 675 nm) and the fluorescence emission band of chl *a* (see Figure 7.6; and Collins et al., 1985). In theory, Q_a^* can vary between 0 and 1, but in the marine environment, the range of variations is 0.2–1 at 685 nm (Babin et al., 1996*a*), depending on the intracellular pigment concentration (i.e.

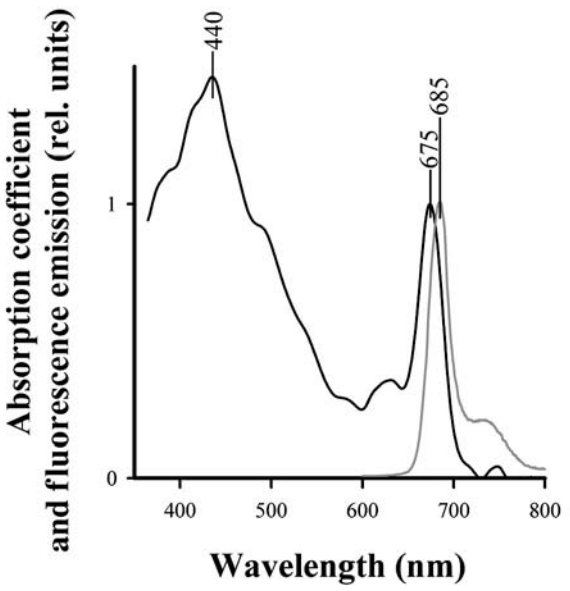

Figure 7.6
Example of *in vivo* absorption (black line) and fluorescence emission (grey line) spectra measured on the diatom *Thalassiosira pseudonana*. Note that, *in vivo*, absorption and fluorescence bands are systematically shifted towards longer wavelengths (see Figure 7.1).

how tightly the pigments are packaged) and on cell diameter (Morel, 2007 – Chapter 4 this volume).

ϕ_F can be expressed with the following simplified model[29,30] (but see Lavergne and Trissl, 1995, and Kramer et al., 2004, for more detailed models of fluorescence):

$$\phi_F = \frac{\sigma_{PS2}^{opt}}{\sigma_{PSU}} \left[\frac{q_P \; k_F}{k_F + k_D + k_P} + \frac{(1-q_P)k_F}{k_F + k_D} \right] \quad , \tag{7.4}$$

where σ_{PS2}^{opt} is the optical absorption cross-section of PS2 (m^2 photon^{-1}), σ_{PSU} is the optical absorption cross-section of a photosynthetic unit (m^2 photon^{-1}), k_F, k_D and k_P are the rate constants (s^{-1}) of fluorescence, thermal dissipation and photochemistry (i.e. charge separation), and q_P is the 'open' fraction of RC2s (dimensionless). The first term on the right of (7.4) represents the fraction of light absorbed by PS2 antenna while the second term represents the quantum yield of an average RC2. In the marine environment a typical range of variation for ϕ_F is 0.005–0.05 mol emitted photons (mol absorbed photons)$^{-1}$ (Kishino et al. 1984; Maritorena et al. 2000; Morrison, 2003).

σ_{PSU} represents the absorption cross-section of photosynthetic units. It is calculated from

$$\sigma_{PSU} = \frac{\overline{a}^*}{n_{PS2}}, \tag{7.5}$$

where n_{PS2} is the number of photosynthetic units. n_{PS2} experimentally corresponds to the number of oxygen-evolving RC2 per unit chl *a*. Its units are therefore O_2 (mg chl *a*)$^{-1}$, or photons (mg chl *a*)$^{-1}$ if four photons are assumed to be necessary for evolving one O_2 molecule. σ_{PSU} accounts for absorption by chl *a* and accessory pigments of both PS1 and PS2, collectively referred to as *photosynthetic pigments*, by photoprotecting pigments, and by all other *non-photosynthetic pigment*s. Here, we define non-photosynthetic pigments as those pigments that absorb light but do not transfer energy to chl *a* (see Figure 7.7) In addition to photoprotecting pigments, they essentially include pheopigments, β-carotene[31] and zeaxanthin[32] in prokaryotic phytoplankton (e.g. cyanobacteria and *Prochlorococcus* sp.). σ_{PS2}^{opt} represents the absorption by chl *a* and accessory pigments associated with PS2 only ($\sigma_{PS2}^{opt} < \sigma_{PSU}$). It excludes absorption by all other pigments. So, the ratio $\sigma_{PS2}^{opt} / \sigma_{PSU}$ varies with the PS1-PS2 absorption stoichiometry and the relative abundance of non-photosynthetic pigments (Lutz et al., 1998, 2001).

[29]For simplicity, the optical cross-sections in this and the following equations (except when otherwise stated) are, as for $\overline{a}^*$ (see (7.1) and (7.2)), expressed as averages over the whole visible range, weighted by the irradiance spectrum.

[30]This equation is valid for the 'puddle' model, where each RC2s is assumed to have its own separate pigment antenna. In the 'lake' model, all RC2s are assumed to share pigment antennas.

[31]β-carotene is thought to be involved in the de-excitation of active forms of oxygen that occur under high light and produce damage to the cell.

[32]In prokaryotic phytoplankton, zeaxanthin is often present in larger concentration than chl *a*. However, it is located in the cell wall. Therefore, it does absorb light but cannot transfer energy to chl a. At the same time, it cannot accept energy from chl *a* to dissipate it as heat, as occurs when a xanthophylls cycle is present. The role of zeaxanthin in prokaryotic phytoplankton is still unknown at this time.

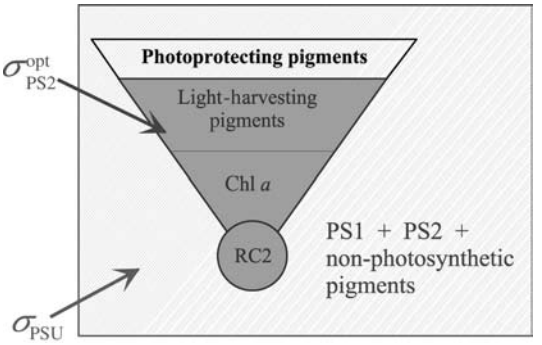

Figure 7.7
Schematic representation of the PSU and PS2 absorption cross-sections.

7.2.4 Photochemical and non-photochemical quenching of fluorescence

In (7.4), the open fraction of RC2s, q_P, varies as a function of ambient light. If light is delivered as a flash short enough to induce a single photosynthetic event (i.e. shorter than about 100 μs), the relationship between q_P and the quantum energy of the flash (ε, photons m^{-2}) follows a cumulative one-hit Poisson function (the so-called 'target theory') (Mauzerall and Greenbaum, 1993):

$$q_P = e^{-\sigma^{eff}_{PS2}\,\varepsilon} \tag{7.6}$$

where σ^{eff}_{PS2} is the effective absorption cross-section of PS2, that is the absorption cross-section for only the photons that lead to charge separation in RC2 ($\sigma^{eff}_{PS2} < \sigma^{opt}_{PS2}$). If light is delivered continuously, q_P can be expressed as (Dubinsky et al., 1986; but see Zonneveld, 1997; Han, 2001, for other models):

$$q_P = e^{-\sigma^{eff}_{PS2}\,\tau_P\,PAR} \tag{7.7}$$

where τ_p(s) is defined as the turnover time for electron transport through the electron carrier chain.[33,34] According to (7.4), when q_P increases, ϕ_F decreases. This decrease of ϕ_F related to photochemistry is generally referred to as 'photochemical quenching' of fluorescence. By analogy, any decrease of ϕ_F not related to photochemistry is referred to as 'non-photochemical quenching' of fluorescence. Non-photochemical quenching involves different causes and mechanisms that lead to an increase in thermal dissipation of absorbed energy within the PS2 pigment antenna and RC2 (k_D in (7.4)).

[33]When photosynthesis is stimulated by repeated single-turnover saturating flashes and the period between the flashes is progressively decreased, at some period the yield of photosynthesis per flash starts to decrease because the electron transport chain becomes saturated and, therefore, limited by the rate of reactions downstream of RC2. τ_p approximately corresponds to that period value. The rationale for using τ_p in (7.7) is that, when multiplied by the continuous irradiance PAR, it provides the amount of photons per time steps within which the target theory applies. In other words, it allows the continuous-light problem to be reduced into the light-flash one. Kolber and Falkowski (1993) interpret τ_p as the time necessary for an electron to be transferred from the first electron donor, water, to the final acceptor, carbon – τ_p is typically a few milliseconds.

[34]This equation is valid for the 'puddle' model (see Note 29).

A qualitative differentiation between different types of non-photochemical quenching is often made from the relaxation kinetics of non-photochemical quenching when a sample is placed in the dark or dim light. Three relaxation phases are generally observed (Krause and Weis, 1991). The first one lasts from seconds to a few minutes and indirectly results from the build-up of a proton gradient across the thylakoid membrane (ΔpH) under high irradiance (accumulation of protons in the lumen). This type of non-photochemical quenching is referred to as 'energy-dependent' quenching and denoted q_E. The increase in ΔpH under high irradiance stimulates the de-epoxidation of violaxanthin (or diadinoxanthin) into antheraxanthin and zeaxanthin (or diatoxanthin). The latter pigments are probably the direct cause of q_E as they trap the energy of singlet-state excited chl *a* and dissipate it as heat (see e.g. review by Yamamoto and Bassi, 1996). q_E can lead to a decrease of up to 90% in ϕ_F and, thereby, serve as a highly efficient and dynamic way to down-regulate transfer of excess energy to RC2 under high irradiance. The second phase in non-photochemical quenching relaxation, denoted q_T, lasts 5–20 min and is generally associated with so-called 'state transitions'. Historically, the term 'state transition' has been used to designate the relative changes in the absorption cross-sections of PS1 and PS2 observed in response to changes in the spectrum of ambient light. The mechanism behind this phenomenon consists in the detachment and attachment of pieces of the PS2 pigment antenna under high- and low-irradiance conditions, respectively. Detachment and attachment would result from the enzyme-driven phosphorylation and dephosphorylation of the antenna proteins, respectively, and would be regulated by the reduction level of the plastoquinone pool (see review by Aro and Ohad, 2003). That is, under high irradiance, the increase in the reduction level of the plastoquinone pool would stimulate phosphorylation of antenna proteins and vice versa. It is unclear whether or not such changes in σ_{PS2}^{opt} are always associated with inverse complementary changes in PS1 absorption cross-section. q_T can decrease ϕ_F by up to 20% (see discussion on this topic in Falkowski and Raven, 1997). Finally, the third phase of non-photochemical quenching relaxation, denoted q_I, lasts several tens of minutes to a few hours (see e.g. Oliver et al., 2003) and is related to photoinhibition,[35] which is photo-damage in the photosynthetic apparatus. According to the current understanding about the nature of photoinhibition, the D1 protein in RC2 would be the main target (see reviews by Aro et al., 1993, 1999). Therefore, the rate of q_I relaxation would be a function of the rate of D1 repair. In the marine environment, q_I may be responsible for decreases in ϕ_F of up to 40% (see e.g. Falkowski et al., 1995).

7.2.5 Transient changes in fluorescence

When a photosynthetic organism is suddenly transferred from dark to light, the flux of *in vivo* fluorescence (and ϕ_F) experiences several typical transient changes. The number and magnitude of these transients depend on the energy and duration of light exposure. Each of these transients reflects a specific process of photosynthesis. The analysis of these transients is useful for the interpretation of variations in F (or ϕ_F) obtained using various measurement protocols. Figure 7.8 shows two idealized examples of so-called 'induction curves' obtained on samples transferred from dark to continuous moderate (non-saturating) and high (saturating) irradiance.

[35]The term 'photoinhibition' is sometimes used to refer to any decrease in the quantum yield of photosynthesis resulting from exposure to excess light, and often also to designate such decreases specifically related to structural damage in the photosynthetic apparatus. In this review, we use the latter definition.

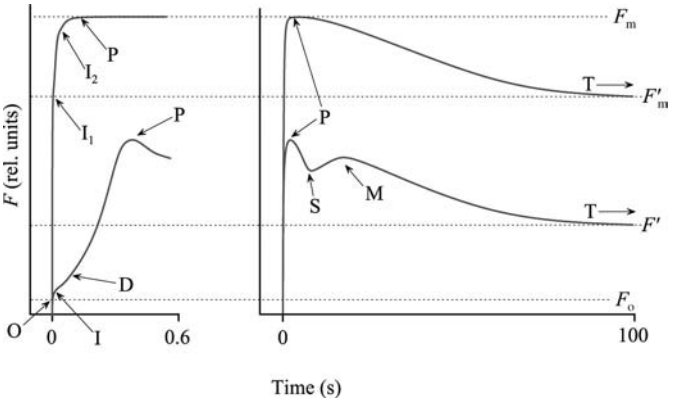

Figure 7.8
Idealized fluorescence induction curves. The two panels show the same curves, but for two different time ranges. In both panels, the upper curve is obtained on exposure to high, saturating light, while the lower curve is obtained on exposure to moderate, non-saturating light. The letters indicate different phases described in the text.

The different transients obtained in the former case, identified by conventional letters, are related to the following processes (more details available in Govindjee and Satoh, 1986; Geider and Osborne, 1992; Govindjee, 1995; Stirbet et al., 1998; Lazar, 1999):

O — When light is turned on, F shows a quasi-instantaneous rise to the O level. This fluorescence originates from the antenna and occurs before migration of energy to the reaction centres. This signal is generally referred to as 'minimum fluorescence' and denoted F_o (and correspondingly ϕ_{Fo}).

O–I — F then rises within 30–100 ms to an inflection. The O–I rise results from the progressive reduction of Q_1 (see Figure 7.4) and the associated closure of the reaction centres. In (7.4), this rise corresponds to a decrease in q_P, i.e. a decrease of photochemical quenching.

I–D — After I, the F increase slows down until D (for dip). The I–D transient results from the onset of Q_1 reoxidation by plastoquinones.

D–P — F then rises within ~100 ms to a plateau (P). This increase in F results from the completion of Q_1 reduction to the maximum level under these light conditions. It is faster than during the I–D transient because Q_1 reduction is faster than its reoxidation by plastoquinones.

P–S–M–T — F then experiences a number of transients related to the reoxidation of Q_1 allowed by the initiation of carbon fixation, and to non-photochemical quenching. It reaches a steady-state value after minutes to a few hours, denoted F'.

When a photosynthetic organism is transferred from the dark to saturating irradiance, some of the transients described above vanish. F goes from O to I in two steps (I_1 and I_2). I_1 is reached within less than 1 ms and results from the rapid reduction of Q_1. F then goes from I_1 to I_2 within ~100 ms. According to Schreiber and Krieger (1996), this rise results from the relaxation of a special type of non-photochemical

quenching that takes place in dark conditions. F then reaches the P level after full reduction of Q_1. P corresponds to 'maximum fluorescence', denoted F_m, obtained when photochemical quenching (and thus q_p) becomes null. After minutes to hours, F finally reaches a steady value (F_m') once non-photochemical quenching is in place.

7.3 Protocols for measurement of *in vivo* phytoplankton fluorescence; use of chl *a* fluorescence to study phytoplankton ecophysiology

There are a number of chl *a* fluorescence measurement protocols used in oceanography for different purposes, at different time and space scales, and from different platforms. This section describes, for these different approaches, the basic principles, typical instruments, and the measurement protocols. It also discusses the underlying assumptions and provides commented examples.

7.3.1 'Standard' fluorometry for determination of biomass *in vivo*

7.3.1.1 Basic principle

The assumption that justifies this approach is straightforward: if PAR is generated using a constant artificial source and the product $\overline{a} * Q_a^* \phi_F$ in (7.1) is assumed to be constant, then F is proportional to [chl *a*].

7.3.1.2 Instruments and protocols

The most common use of *in vivo* chl *a* fluorescence in oceanography is for simple and instantaneous estimates of phytoplankton biomass. There are two types of fluorometer frequently used in oceanography for estimating phytoplankton biomass: the flow-through benchtop and the *in situ* versions.

Figure 7.9 shows the optical set-up of the benchtop field fluorometer commercialized by Turner Designs Inc. (Sunnyvale, California). The main features are:

- low-pressure mercury vapour lamp (4 watts) that produces continuous light of moderate energy
- blue (340–500 nm) filter for the excitation of the seawater sample
- red (680 nm) band filter for the collection of the fluorescence signal
- photomultiplier tube as detector
- dual-beam optics to correct for drifts in the lamp output and/or detector sensitivity (represented by the light pipe in Figure 7.9).

As in most systems measuring fluorescence, the excitation and detection optics are at a right angle from each other. While the old Model 10 was fully analogical, the new Model 10-AU is programmable, has a digital output, and has an optional internal data logger. It can be used for discrete sample analysis and for continuous-flow monitoring. The dynamic range is such that it allows operation over any natural range of chl *a* concentrations.

As for any measurement of *in vivo* chl *a* fluorescence, the determination of a blank is a critical step (Cullen and Davis, 2003). The only appropriate blank is an *in situ* water sample filtered just before analysis through a glass-fibre filter (e.g. Whatman

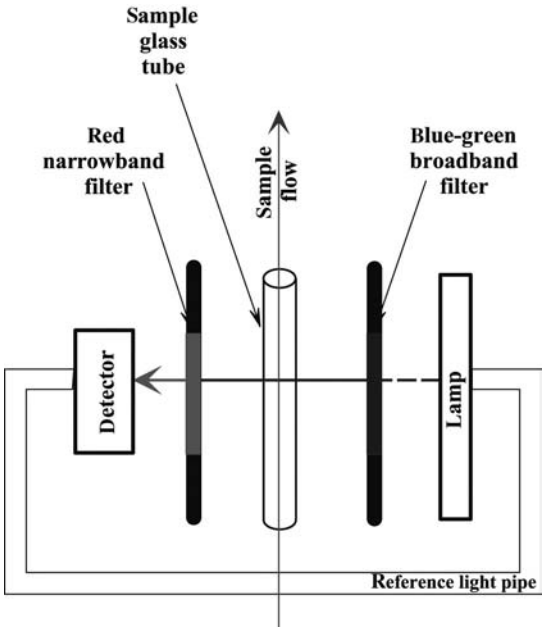

Figure 7.9
Optical set-up of a typical benchtop fluorometer, such as Turner Designs Model 10. Note that the excitation and detection optics are in fact at a right angle.

GF/F) or other kinds of filters with pore size smaller than 0.45 µm (e.g. Whatman Nuclepore® 0.2 µm). When using a given type of filter, it is important to make sure that it does not release any fluorescing substance during filtration. This can be done by measuring the signal of pure water passed through the filter, or by comparing the signal measurements done on a given sample passed through different types of filter (e.g. glass-fibre filter versus polycarbonate membrane).

Although *in vivo* fluorescence in fact provides qualitative information about phytoplankton biomass, a calibration of the system can be carried out to convert the fluorometer raw output into [chl *a*] values. The calibration procedure simply consists of comparing the fluorometer output with chemical determinations of [chl *a*] on common samples. For measurements in the natural environment, it is preferable to use samples from the study area to perform the calibration, rather than phytoplankton cultures, to account for natural variations in pigment composition and packaging. Indeed, a local calibration maximizes the likelihood that the assumption made in Section 7.3.1.1 holds.

The optical set-up of typical underwater fluorometer is similar to that of the flow-through fluorometer described above, except that the exciting source is a Xenon lamp or LED's that produce short and intense flashes. The sampled water volume is defined by the intersection between the cone of the exciting beam, and the cone seen by the

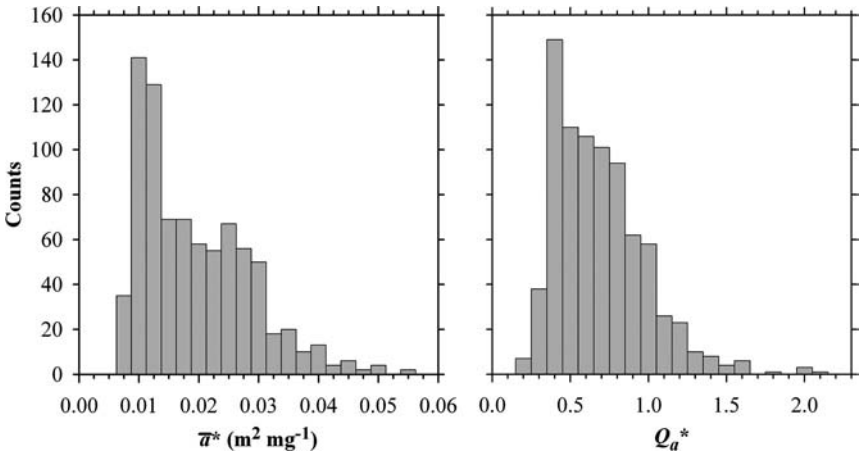

Figure 7.10
Frequency distributions for $\overline{a}^*$ and Q_a^* in oceanic waters.
Source: redrawn from Babin et al. (1996*a*).

detection optics. This type of profiler can be operated from surface down to several hundreds or thousands of metres, depending on the brand and model. As with many profiling instruments, it can be interfaced with a CTD sensor.

7.3.1.3 Validity of underlying assumptions

As mentioned above, this approach relies on the assumption that the product $\overline{a}^* \, Q_a^* \, \phi_F$ is constant. Figure 7.10 shows frequency distributions for $\overline{a}^*$ and Q_a^* observed in the open ocean waters of different basins (Babin et al., 1996*a*). Both $\overline{a}^*$ and Q_a^* vary over nearly an order of magnitude.[36] While sea-surface $\overline{a}^*$ variations result from changes in pigment composition and pigment packaging (see reviews by Morel, 2007; Roesler and Boss, 2007; Sosik, 2007 – Chapters 4, 5 and 8 this volume), variations in Q_a^* result from the latter only. To first order, $\overline{a}^*$ and Q_a^* covary with [chl *a*]. These statistical relationships are well represented by power laws. At regional scales, however, these relationships are often invalid (see e.g. Babin et al., 2003). So, at a large scale, the variations in $\overline{a}^*$ and Q_a^* may simply make the relationship between F and [chl *a*] (under the assumption of constant PAR) nonlinear (Ostrowska et al., 2000*a*, 2000*b*). But from region to region, this relationship may change significantly.

One simple way to determine whether variations in ϕ_F affect F v. [chl *a*] is to look at time series over periods of time so short that it can be assumed that $\overline{a}^*$ and Q_a^* do not vary significantly. Using a benchtop fluorometer, Kiefer (1973) observed diel variations in F that spanned over more than a factor of 4. Loftus and Seliger (1978) and Abbott et al. (1982) found that F varies inversely with ambient irradiance at very short timescales (e.g. minutes) as a result, for example, of cloud passage

[36]Note that in Babin et al. (1996), $\overline{a}^*$ was computed using an irradiance spectrum representative of ocean surface. The proper $\overline{a}^*$ value for fluorometer should be computed using the spectrum of the excitation source in (7.2).

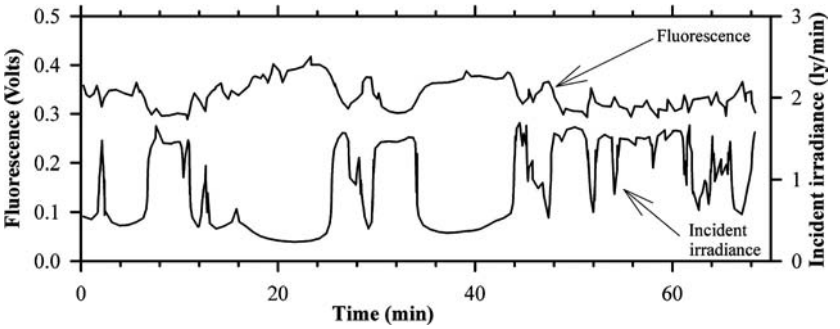

Figure 7.11
Temporal changes in the fluorescence signal measured at 35 m using an *in situ* fluorometer in Lake Tahoe (USA).
Source: redrawn from Abbott et al., (1982).

(see Figure 7.11). These typical variations in ϕ_F mainly result from non-photochemical quenching induced by the recent exposure to ambient light.

The characteristics of excitation light and its impact on ϕ_F is an important aspect of *in vivo* chl *a* fluorometry (Cullen et al., 1988, Neale et al., 1989). Figure 7.12

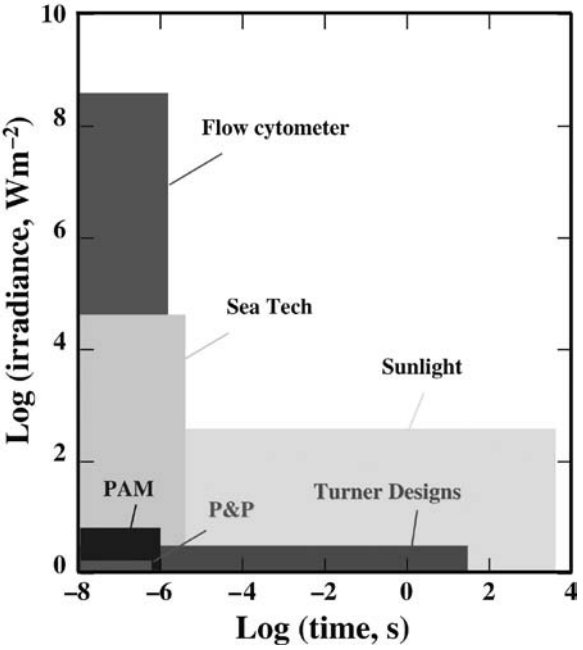

Figure 7.12
Energy versus duration for various excitation sources. Note that the Sea Tech fluorometer is an analogue to the Aquatracka Mk III. P&P Stands for pump-and-probe (see text below).
Source: courtesy of J. J. Cullen.

shows a diagram of energy versus duration for the excitation sources of different types of fluorometers used in oceanography (some of them are described later). When considering at the same time a typical fluorescence induction curve such as the one shown in Figure 7.8, the 'type' of fluorescence measured using a given excitation source can be determined. In the case of the benchtop fluorometer commercialized by Turner Designs Inc., the weakness of the source is such that F_o is most probably measured in most conditions (Neale et al., 1989; but see Section 7.3.3.2). In the case of the underwater fluorometer Aquatracka Mk III, which produces short (microseconds) and intense flashes (in the profiling mode, each sample 'sees' one flash), the measured

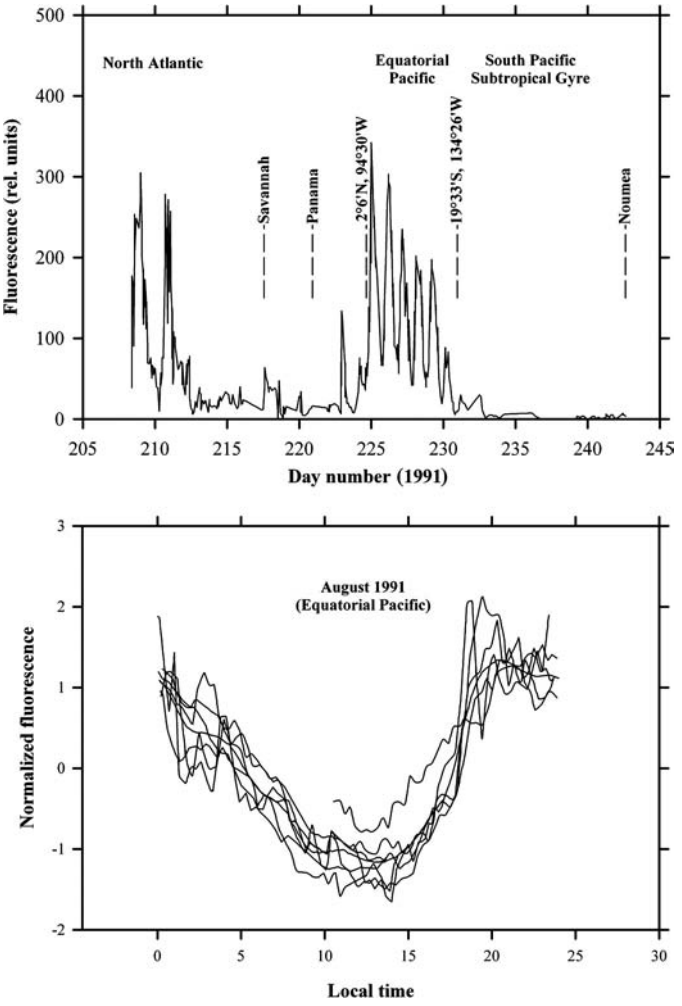

Figure 7.13
Changes in surface *F* measured using a benchtop fluorometer with a flow-through sampling system along a track between New Caledonia and Le Havre (France).
Source: redrawn from Dandonneau and Neveux (1997).

signal probably corresponds to a level located between F_o and F_m mostly determined by photochemical quenching.

Another critical aspect of *in vivo* fluorometry is the spectrum of the excitation source. It must cover a spectral range in the blue and green domains large enough to cover the absorption bands of most phytoplankton groups. This is especially important for phycobilin-containing groups because the latter pigment absorbs in the green, rather than in the blue as chlorophylls and carotenoids do (see e.g. Beutler et al., 2003).

7.3.1.4 Examples

To illustrate the kind of observations that can be made with fluorometers, as well as the difficulties generally associated with their interpretation, two examples are presented. In the first one, under way subsurface measurements were carried out by Dandonneau and Neveux (1997) using a benchtop fluorometer (Turner Model 112 equipped with a flow-through cuvette) onboard a ship of opportunity steaming from New Caledonia in the Pacific to Le Havre in France (through the Panama Channel). The observed fluorescence trace shows large regional variations in *F*, certainly related to changes in phytoplankton biomass (Figure 7.13). It also shows, however, more than 4-fold diel variations in *F* resulting from non-photochemical quenching. This pattern is especially clear in the Equatorial Pacific. On the bottom panel of Figure 7.13, the daily *F* traces observed in the Equatorial Pacific superimpose nicely after normalization. They all exhibit a minimum around noon. Obviously, it can be difficult to distinguish spatial from diel variation patterns when their scales coincide.

In the second example, Claustre et al. (1999) examined the temporal variations in the *F* vertical profile over five consecutive days, in the subtropical Pacific (Figure 7.14). These profiles were characterized by a deep chlorophyll maximum at a depth that varied between 50 m and 80 m over time because of internal waves, and by *F* surface minima around noon most probably resulting from non-photochemical

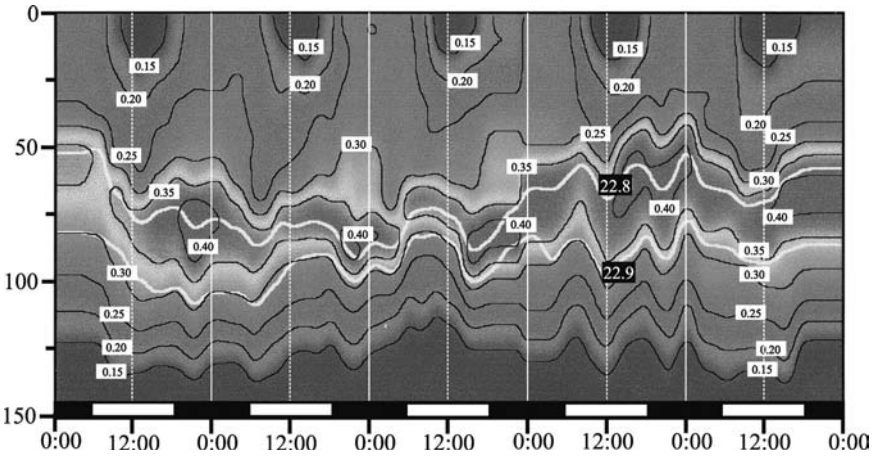

Figure 7.14
Temporal changes over five days in the vertical profile of chl *a* fluorescence measured with an underwater fluorometer at 5°S 150°W in the Pacific ocean.
Source: redrawn from Claustre et al., 1999.

quenching of fluorescence. Obviously, the day and night F vertical profiles were significantly different close to the surface. Nevertheless, the position of the deep chlorophyll maximum could be monitored at high temporal and vertical resolution.

These two examples illustrate the fact that horizontal and vertical patterns in phytoplankton biomass estimated from chl *a* fluorescence can be strongly affected by non-photochemical quenching. Therefore, they must be interpreted with caution. Simultaneous observations of irradiance may help separate the fluorescence quenching effect from the biomass effect.

It is worth noting that the calibration of fluorometers is a particular problem in the case of sustained observation on moorings over long periods of time, or on autonomous moving platforms (e.g. gliders, floats) over large distances. Is it better to calibrate a fluorometer at time zero (for a mooring) or at initial station (as in a glider) and then interpret six months or hundreds of kilometres of variability relative to that single point, or to calibrate relative to a culture, the conditions of which are controlled and repeatable? It is certainly an important issue with respect to *in situ* observing platforms.

7.3.2 Spectrofluorometry

7.3.2.1 Basic principle

When fluorescence is measured on a given sample of photosynthetic organism using a monochromatic beam of irradiance $E(\lambda_{ex})$, and λ_{ex} is varied throughout the visible range, then changes in F as a function of λ_{ex} are proportional to spectral changes in σ_{PS2}^{opt} as

$$\frac{F(\lambda_{ex})}{E(\lambda_{ex})} = [\text{chl}\,a]\;\; a^*(\lambda_{ex})\;\; Q_a^*\;\; \phi_F(\lambda_{ex}) \tag{7.8}$$

and when combining (7.8) with (7.4) and (7.5):

$$\frac{F(\lambda_{ex})}{E(\lambda_{ex})} = [\text{chl}\,a]\;\; Q_a^*\;\; n_{PS2}\;\; \sigma_{PS2}^{opt}(\lambda_{ex})\;\; \left[\frac{q_P\;k_F}{k_F + k_D + k_P} + \frac{(1-q_P)\;k_F}{k_F + k_D}\right] \tag{7.9}$$

so that, assuming that [chl *a*], Q_a^*, n_{PS2} and the k term in (7.9) do not vary during the measurement:

$$\frac{F(\lambda_{ex})}{E(\lambda_{ex})} \propto \sigma_{PS2}^{opt}(\lambda_{ex}) \tag{7.10}$$

The $F(\lambda_{ex})$ spectrum is referred to as an *excitation spectrum* (Figure 7.17) It is often used to infer the absorption spectrum of photosynthetic pigments (e.g. Mitchell and Kiefer, 1988; Sakshaug et al., 1991; Sosik and Mitchell, 1995). When applied on natural water samples it has the advantage of providing a specific phytoplankton signal even in the presence of other absorbing substances (e.g. Desiderio et al., 1997; see also Morel, 2007; Sosik, 2007 – Chapters 4 and 8 this volume).

Spectrofluorometry is also used to determine the spectral shape of fluorescence emission, generally referred to as the *emission spectrum* (Figure 7.18). In that case, the wavelength of $E(\lambda_{ex})$ is fixed, and that of emission scanned to obtain $F(\lambda_{em})$. The emission spectrum allows detection of the presence of other fluorescing pigments in addition to chl *a* (e.g. Cowles et al., 1993). The only such phytoplankton pigments are

the phycobilins, mostly phycoerythrin and phycocyanin, that absorb light around 550 nm and 620 nm, and fluoresce around 575 nm and 650 nm, respectively (reviewed by Prézelin and Boczar, 1986). Cyanobacteria and Cryptophytes are the main taxa containing phycobilins.

7.3.2.2 Instruments and protocols

The optical set-up of a standard commercial benchtop spectrofluorometer is sketched in Figure 7.15. It is generally composed of an exciting source coupled to a monochrometer, a sample compartment for standard 1 cm glass cuvettes, and a monochrometer coupled to a detector that collects fluorescence. A fraction of the exciting light beam is diverted to a reference detector before the sample. This reference beam allows the measurement of $E(\lambda_{ex})$ in relative units when a so-called 'quantum counter' is placed in front of the reference detector. A quantum counter is a dye solution that has the following properties: it absorbs nearly all light in the spectral range of interest; it has a fluorescence quantum yield constant over the spectral range of interest; and it is stable over time. The quantum counter intercepts the reference beam and only transmits its own fluorescence to the reference detector at a fixed wavelength. Therefore, the measured signal does not depend on spectral variations in the sensitivity of the detector. Moreover, because the quantum yield of the quantum counter is spectrally constant (i.e. it does not depend on the energy of photons), it does provide a measure of $E(\lambda_{ex})$ in relative quantum units (see Hofstraat et al., 1992, for more details), which is appropriate for the normalization of chl *a* fluorescence. Common solutions used as quantum counters include Rhodamine-B, Basic Blue-3 and Oxazine-170. The latter two are especially convenient because they allow measurement over a wider spectral range (255–700 nm) compared with Rhodamine-B (UV-600 nm) (Kopf and Heinze 1984). Note that to cover that range in $F(\lambda_{ex})$, chl *a* fluorescence must be detected in the region of the near-IR maximum around 730 nm (see Figure 7.6) (e.g. Neori et al., 1988). To obtain an emission spectrum spectrally calibrated in relative units,

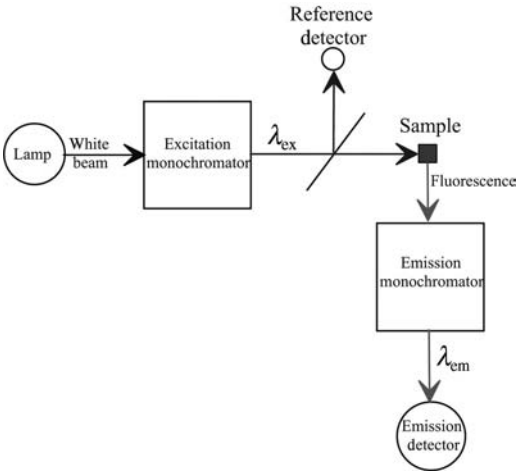

Figure 7.15
Optical set-up of a typical benchtop spectrofluorometer.

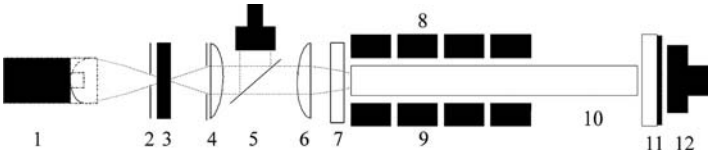

Figure 7.16
Optical set-up of the submersible spectrofluorometer Safire® (WET Labs Inc., Oregon, USA). 1, flash lamp; 2, aperture; 3, interference filter; 4, plano-convex lens; 5, beam splitter/ref. det.; 6, plano-convex lens; 7, pressure window; 8, 9, detector arrays; 10, flow tube; 11, pressure window/diffuser; 12, absorption detector.

a standard lamp is generally used to derive the sensitivity spectrum of the detector (Hofstraat et al., 1992).

A fixed-band underwater spectrofluorometer is now commercialized by WET Labs Inc. (Oregon, USA) under the brand name Safire®. The optical set-up of this instrument is illustrated in Figure 7.16. The excitation optics include a flash lamp and a filter wheel that holds 6 narrowband interference filters. The emission optics include 16 detectors combined with different narrowband interference filters, and positioned at the periphery of a glass tube through which seawater is continuously pumped. So, the Safire measures fluorescence at 6 excitation and 16 emission wavelengths, at a sampling rate of 5 Hz. In addition, it can measure side-scattering at the 6 wavelengths where $\lambda_{ex} = \lambda_{em}$ (Roesler and Boss, 2007 – Chapter 5 this volume). The Safire allows the acquisition of detailed vertical fluorescence profiles as well as high-resolution time series of spectral fluorescence properties (Desiderio et al., 1997). Another submersible spectrofluorometer, the FluoroProbe 2 (bbe Moldaenke GmbH, Kiel-Kronshagen, Germany), is now available on the market.

7.3.2.3 Validity of underlying assumptions

When using $F(\lambda_{ex})$ to infer $\sigma^{opt}_{PS2}(\lambda)$ or to estimate the absorption spectrum of photosynthetic pigments, it is assumed that the ratio in (7.9) (ratio of rate constants) does not vary while scanning the visible spectrum. This assumption is incorrect when $E(\lambda_{ex})$ is in a range such that q_p varies (i.e. F is between F_o and F_m). In that case, spectral changes in $E(\lambda_{ex})$ and/or in $\sigma^{opt}_{PS2}(\lambda)$ lead to variations in q_p. To avoid such changes, a common approach consists of poisoning the sample with 3′-(3,4-dichlrophenyl)-1′,1′-dimethyl urea (DCMU). DCMU prevents the reoxidation of Q_1 and, thereby, maintains all RC2 closed. That way, q_p equals zero and F_m is measured (Neori et al. 1986). DCMU can be dissolved in methanol or ethanol[37] and then introduced in the sample at a final concentration of 50–100 μM.

There are two problems in trying to infer the absorption coefficient for photosynthetic pigments from the fluorescence excitation spectrum. The first one is that excitation spectra need to be expressed in absorption or specific absorption units [m^{-1}

[37]Note that, to avoid adverse effects by the solvent, the DCMU solution must be concentrated enough to obtain the desired final concentration in the sample by introducing only a small volume (<1% of the sample volume).

or m^2 (mg chl *a*)$^{-1}$, respectively]. As proposed by Sakshaug et al. (1991), this can be achieved by scaling the excitation spectrum to measured a_ϕ at 675 nm. The underlying assumption is that $a_\phi(\lambda)$ in the spectral region of the chl *a* red absorption band always represents only photosynthetic pigments. The second problem in using the excitation spectrum to infer photosynthetic pigment absorption is that the former reflects absorption only by pigments associated with PS2. As a result, the excitation spectrum sometimes poorly represents absorption by all photosynthetic pigments (see example below and Lutz et al., 1998, 2001).

7.3.2.4 Examples

Figure 7.17 shows absorption and excitation spectra measured on *Cryptomonas* sp. by Sciandra et al. (2000). The excitation spectrum was scaled to absorption at 675 nm. In the blue region (up to 520 nm), $a_\phi(\lambda)$ is larger than absorption inferred from fluorescence probably because of the presence of non-photosynthetic carotenoids (α-carotene and/or alloxanthin). In the green region (520–600 nm), however, absorption inferred from fluorescence is much larger than $a_\phi(\lambda)$. This is certainly because *Cryptomonas* sp. contains large amounts of phycoerythrin only associated with PS2 (Prézelin and Boczar, 1986). This example illustrates the difficulty in relying on excitation spectra to infer absorption by all photosynthetic pigments, especially when dealing with phycobilin-containing phytoplankton species.

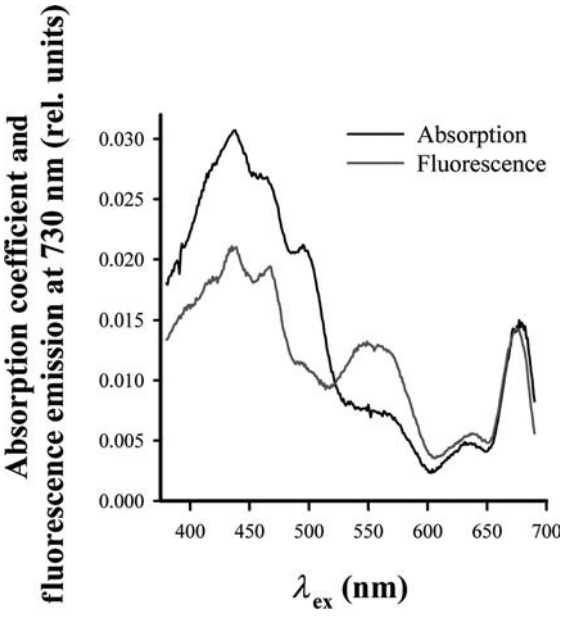

Figure 7.17
Absorption and fluorescence excitation spectra of *Cryptomonas* sp.
Fluorescence was detected around 730 nm. Both spectra were scaled to be equal at 675 nm.
Source: data obtained during study described by Sciandra et al. (2000).

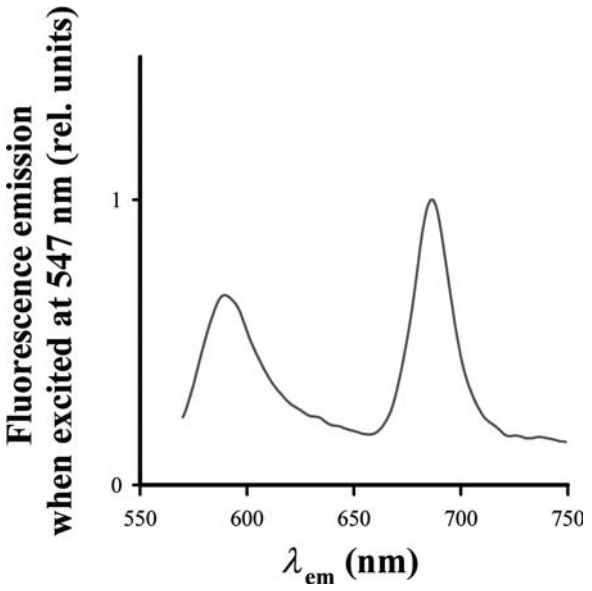

Figure 7.18
Fluorescence emission spectrum of *Cryptomonas* sp. Fluorescence was excited around 547 nm.
Source: data obtained during study described by Sciandra et al. (2000).

Figure 7.18 shows the emission spectrum of *Cryptomonas* sp. It illustrates very clearly the distinct fluorescence bands of phycoerythrin and chl *a*. The specific fluorescence emission properties of phycobilin-containing phytoplankton are also commonly exploited in flow cytometry, most often to distinguish cyanobacteria from other picoplankton species (see review by Olson et al., 1991).

The use of excitation and emission fluorescence spectra to discriminate phytoplankton groups in natural waters has been first proposed by Yentsch and Phinney (1979) (see also Yentsch and Yentsch, 1985). Recently, the feasibility of this approach has been demonstrated by Beutler et al. (2002, 2004).

7.3.3 Variable fluorescence

7.3.3.1 Basic principle

The quantum yields of maximum and minimum fluorescence, ϕ_{Fm} and ϕ_{Fo} respectively, can be expressed as:

$$\phi_{Fm} = \frac{\sigma_{PS2}^{opt}}{\sigma_{PSU}} \quad \frac{k_F}{k_F + k_D} \tag{7.11}$$

$$\phi_{Fo} = \frac{\sigma_{PS2}^{opt}}{\sigma_{PSU}} \quad \frac{k_F}{k_F + k_D + k_P} \tag{7.12}$$

When replacing ϕ_F by ϕ_{Fm} and ϕ_{Fo} in (7.1) to obtain the expressions for F_m and F_o, respectively, the following equation can be derived:

$$\frac{F_v}{F_m} = \frac{k_P}{k_D + k_F + k_P} = \phi_P^{max} \tag{7.13}$$

where F_v is variable fluorescence defined as $F_m - F_o$, and ϕ_P^{max} is the maximum quantum yield for energy conversion in RC2. The following may also be obtained from (7.1) and (7.4):

$$\frac{F_m' - F'}{F_v'} = q_P \tag{7.14}$$

Note that in (7.14) steady-state fluorescence values are used.[38] By fitting (7.6) to experimental q_P versus ε data, σ_{PS2}^{eff} can be derived.

There are now a number of measurement protocols and commercial instruments that allow the experimental determination of ϕ_P^{max}, σ_{PS2}^{eff} and q_P on natural phytoplankton samples. In limnology and oceanography, ϕ_P^{max} and σ_{PS2}^{eff} have been used as indexes of photoinhibition, nutrient limitation and photoacclimation. Together with q_P, they are also used to estimate primary production (Oquist et al., 1982; Kolber and Falkowski, 1993; Suggett et al., 2001).

7.3.3.2 Instruments and protocols

Use of DCMU

As mentioned above, DCMU prevents the reoxidation of Q_1 and, thereby, maintains all RC2 closed, in which case $q_P = 0$ and F_m is measured. In the late 1970s and early 1980s, several groups started to use DCMU on natural phytoplankton samples in order to derive variable fluorescence (e.g. Cullen and Renger, 1979; Roy and Legendre, 1979; Vincent et al., 1984). Fluorescence measurements have generally been achieved using Turner Designs benchtop or flow-through fluorometers. A first measurement is generally made after dark – adapting the sample for 30 min in order to relax energy-dependent and state-transition non-photochemical quenching (q_E and q_T). Given the low power on these fluorometers, this first measurement is assumed to represent F_o. A second measurement is then made after the addition of DCMU to obtain F_m. In the case of low-light acclimated phytoplankton cells, it is safer to verify that F_o is actually measured. This can be done by conducting on a given sample a series of few measurements of F_o and F_m, while increasingly attenuating the excitation light source of the fluorometer using neutral filters. F_o is actually measured when F_v/F_o no longer increases by further attenuating the fluorometer excitation light source.

Pulse amplitude modulation

The pulse amplitude modulation (PAM) fluorometer was introduced by Schreiber (1986) and is now commercialized in various models (benchtop, submarine, imager) by Heinz Walz GmbH (Effeltrich, Germany). The FL200-F benchtop fluorometer commercialized by Photon Systems Instruments (Brno, Czech Republic) can be

[38] Steady-state fluorescence values are obtained under ambient light for F_m' and F', and immediately after sample collection and isolation in the dark for F_o'.

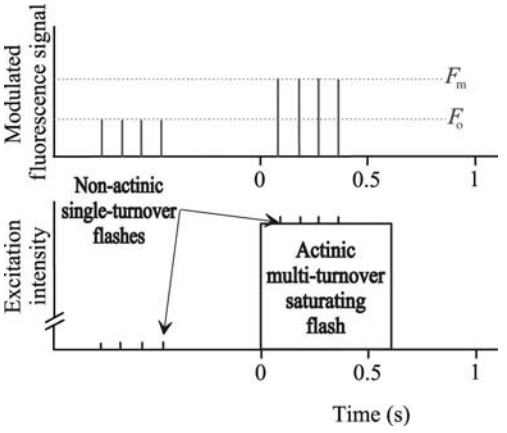

Figure 7.19
Common measurement protocol applied to measure F_o and F_m with PAM fluorometer.

used to make similar measurements. The measurement protocol typically followed to determine F_o and F_m using the PAM fluorometer is sketched in Figure 7.19. Prior to measurement, the sample is generally dark-adapted for 30 min to relax q_E and q_T. The sample is then exposed to a short series of weak and short (~10 μs) flashes. These flashes, often referred to as 'probe flashes', do not induce any fluorescence quenching (neither photochemical nor non-photochemical) and, therefore, provide a measurement of F_o in the dark adapted state. The sample is then exposed to a saturating actinic[39] flash. That flash lasts around 600 ms. It thus produces multiple photosynthetic events (or turnovers), that is multiple successive charge separations at each RC2. During the actinic flash, the sample is, at the same time, exposed to probe flashes. The electronics of the PAM fluorometer are such that it only records the modulated part of the detected fluorescence, i.e. that induced by the probe flashes, and observed on top of the constant fluorescence background from the actinic flash. This measurement corresponds to F_m.

Pump-and-probe

Pump-and-probe (P&P) fluorometry was introduced by Mauzerall (1972), and then intensively used to study phytoplankton photosynthesis in the laboratory and at sea by Paul Falkowski's group (e.g. Falkowski et al., 1986; Kolber et al., 1990). Two commercial P&P fluorometers are currently available. One is made by Heinz Walz GmbH as an accessory of the PAM fluorometer. The other one is the FL200-F benchtop fluorometer made by Photon Systems Instruments.

The most significant differences between the P&P and the common (i.e. multiturnover) PAM protocols are, in P&P: (a) the use of a single-turnover actinic flash, and (b) the application of actinic flashes of variable energies (Figure 7.20). First, the measurement of F_o is made as described above for the PAM fluorometer. Then the sample

[39]Actinic radiant energy is energy that produces a photochemical effect (e.g. visual, chemical). In the study of photosynthesis, actinic radiant energy produces changes in the state of the photosynthetic apparatus, such as for example the redox level of some electron carriers (e.g. plastoquinone pool). Actinic energy can be saturating, but not necessarily. Probe flashes are not actinic.

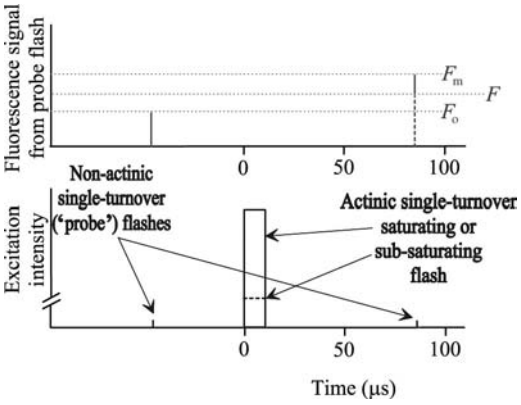

Figure 7.20
Pump-and-probe (P&P) measurement protocol to measure F_o, F and F_m.

is exposed to a short (~10 µs) saturating actinic flash (so-called 'pump' flash), and a probe flash is applied about 80 µs later to measure F_m. The 80 µs delay is necessary for all RC2s to become closed (i.e. Q_1 reduced) after the pump flash. After that delay, the plastoquinones begin reoxidizing Q_1. The pump flash produces a single turnover because it is shorter than 80 µs. A 600 ms actinic flash as in the PAM protocol produces multiple turnovers because it is much longer than that delay. By varying the energy of the pump flash, F can be measured at levels intermediate between F_o and F_m. This is how σ_{PS2}^{eff} can be derived using the P&P protocol (see (7.14)).

Fast repetition rate

The fast repetition rate (FRR) fluorometry protocol was first described in detail by Kolber et al. (1998). This protocol was developed as an alternative to P&P for fast measurements of F, F_o, F_m and few other parameters. It is especially appropriate for

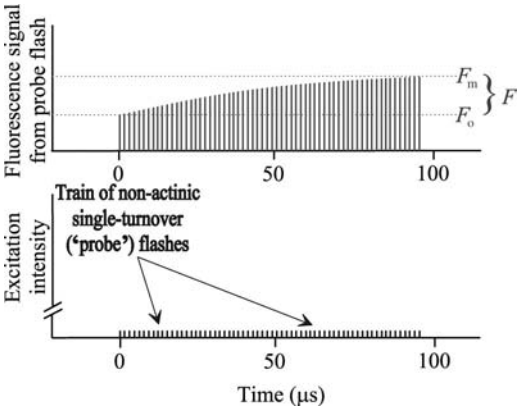

Figure 7.21
Fast repetition rate (FRR) measurement protocol.

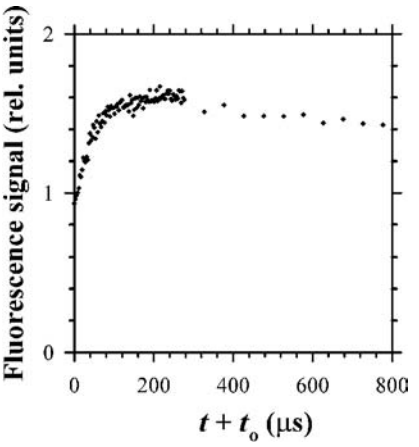

Figure 7.22
Example of a fluorescence saturation curve measured with the FASTtracka® in the Mediterranean Sea (September 1999). Each data point represents the fluorescence signal measured with one probe flash. The abscissa indicates the time elapsed after the first flash.

high-frequency measurements in oceanography. The first FRR fluorometer to be commercialized was the FASTtracka® I (Chelsea Technologies Group, Surrey, United Kingdom). This underwater instrument allows high-resolution sampling over vertical profiles as well as under way when attached to a towed vehicle. It also has an autonomous mode for deployment, for example, on moorings. An improved version of that sensor, the FASTtracka II, is now available. Additionally, a highly sensitive benchtop fluorometer that uses a protocol similar to the FRR one, the fluorescence induction and relaxation technique (FIRe) (Gorbunov and Falkowski, 2004), has recently been commercialized by Satlantic Inc. (Halifax, Canada).

The FRR protocol is sketched in Figure 7.21. The sample is exposed to a series (e.g. 100) of short (~1 µs) and weak consecutive flashes, at a frequency of about 0.35 MHz, over an interval of about 280 µs. The virtue of these flashes is double: first they progressively populate the RC2 (i.e. reduce Q_1), and second, they each serve as probe flashes to measure the fluorescence signal. After this first 280 µs period, the sample is exposed to a series (e.g. 20) of flashes at lower frequency (~20 kHz) to determine the turnover time of Q_1 reoxidation by the plastoquinone pool (τ_Q; *s*). An example of FRR measurement is shown in Figure 7.22. To derive F_o, F_m and σ^{eff}_{PS2}, a model described by Kolber et al. (1998) is fitted to the experimental data. The FASTtracka performs measurements within a dark chamber through which seawater flows, as well as in a 'light' chamber where the sensed seawater volume is exposed to ambient light conditions. In both cases, there is no dark adaptation. Therefore, steady-state fluorescence is actually measured (F', F_o' and F_m') which includes all non-photochemical quenching processes.

7.3.3.3 Validity of underlying assumptions

The values of F_m measured with the multi-turnover and DCMU protocols are generally higher than those obtained with the single-turnover ones (P&P and FRR) by up to 40% (i.e. Schreiber and Krieger 1996, Kromkamp and Forster 2003), although the

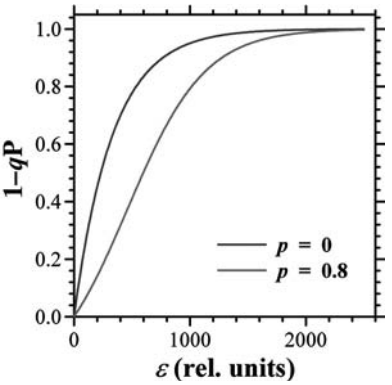

Figure 7.23
Examples of relationships between the number of closed RC2 as a function of flash energy, calculated with (7.8) (equivalent to $p = 0$), and with Equations 8 and 1 from Kolber et al. (1998) with $p = 0.8$. The latter high p value was used to better illustrate the sigmoid shape of the curve. The same σ_{PS2}^{eff} value was used to calculate both curves.

extent of this difference is much smaller under some conditions (e.g. Suggett et al., 2003). The F_v/F_m values obtained using the former two protocols are found to agree well (e.g. Parkhill et al., 2001). According to Schreiber and Krieger (1996), the former two measure I_2 in the fluorescence induction curve, while the latter two measure I_1 (see Section 7.2.5 and Figure 7.8). Various arguments have been put forward to defend I_1 or I_2 as the best F_m value to be used for calculating F_v/F_m (for example Kolber et al., 1998; Schreiber and Krieger, 1996). The debate is still open. One clear advantage of the single-turnover protocols is that they additionally allow σ_{PS2}^{eff} determinations, and the rapidity of FRR fluorometry is especially appropriate for *in situ* oceanographic applications.

Equation (7.6) is valid under the assumption that no transfer of excitons occurs from closed to open RC2.[40] When such transfers occur[41] (so-called 'interconnectivity'), F_o and F_m do not change, but F is affected and the relationship between q_P and ε becomes sigmoid rather than exponential (see Figure 7.23). Consequently, (7.6) cannot be fitted to the experimental P&P data to derive σ_{PS2}^{eff}. The model developed by Kolber et al. (1998), based on that from Lavergne and Trissl (1995), to fit the FRR data includes an interconnectivity parameter, p, that theoretically varies between 0 (no interconnectivity) and 1 (full interconnectivity), and in reality may vary between 0 and 0.6 under variable environment conditions (Vassiliev et al. 1995). An adequate retrieval of this parameter when fitting Kolber et al.'s model to experimental FRR data is critical, as it affects the retrieval of all other parameters (F, F_o, F_m and σ_{PS2}^{eff}). When the saturation curve derived by FRR fluorometry (Figure 7.22) is noisy, as is often the case in low chl *a* environments, the retrieval of p becomes difficult. To circumvent this problem, Suggett et al. (2001) chose to fix this parameter at a value of 0.3. A sensitivity analysis where different fixed p (0–0.6) values have been adopted for processing actual FASTtracka data from the Mediterranean Sea, suggests that the use of different fixed p

[40]This corresponds to the 'puddle' model.
[41]This corresponds to a 'connected unit' model.

values leads to variations in F_v/F_m of 20% on average (Babin, unpublished). Because the actual variability of p in the natural environment is unknown, it is at present unclear whether or not the use of a fixed p of 0.3 leads to significant error in the retrieval of the other fluorescence parameters. When biomass is high, as in phytoplankton culture, p is retrieved with good confidence, and F_v/F_m compares very well with that measured using pump-and-probe fluorometry (Bruyant et al., 2005).

Laney (2003) recently published a detailed study on the different sources of experimental and computational errors associated with the data provided by the FASTtracka FRR fluorometer commercialized by Chelsea Technologies Group. He emphasized two major problems: first, the instrument response function[42] (IRF) varies from one gain to another, and second, the data-processing software provided by the manufacturer produces systematic biases in the retrieval of the fluorescence parameters (F_v/F_m, σ_{PS2}^{eff}, p and τ_Q). To resolve the first problem, the IRF must be characterized using a dye solution separately for each of the five built-in gains. To resolve the second problem, Laney (2003) developed and successfully tested a new processing software.[43]

While phaeophytin is typically present at low levels compared with chl *a* in open ocean waters (Trees et al., 2000), this is not the case for coastal waters. Phaeophytin contributes to fluorescence detected around 685 nm. More specifically, it contributes to F_o and F_m, but not to F_v as it is not involved in photosynthesis. As a result, the presence of phaeophytin in seawater leads to an underestimate of ϕ_P^{max} (7.13). Fuchs et al. (2002) have shown than when the phaeophytin to total pigment ratio is 0.7, a realistic value in coastal waters, ϕ_P^{max} can be underestimated by 25%. Fuchs et al. (2002) were able to predict the impact of phaeophytin on ϕ_P^{max} based on seawater pigment composition. They also found that the measurement of σ_{PS2}^{eff} is not affected by the presence of phaeophytin.

7.3.3.4 Examples

Figure 7.24 shows the changes in variable fluorescence (in this case expressed as F_v/F_o and denoted $\Delta\phi_{sat}$) over a vertical section located through an eddy in the subtropical Pacific. This Figure also shows the distribution of chl *a* concentration, temperature and nitrate concentration. These results were published by Falkowski et al. (1991) who argued that the highest variable fluorescence values observed close to the surface around 25 km result from the eddy pumping of nitrate to the surface. Higher chl *a* concentration and lower temperature were also observed in that area. Behrenfeld et al. (1996) and Behrenfeld and Kolber (1999) interpreted changes in variable fluorescence observed in the Pacific and Southern Ocean as an indication of iron limitation.

The relationship between variable fluorescence and nitrate concentration has been documented by several laboratory and field studies (Kolber et al., 1988; Kolber et al., 1990; Babin et al., 1996*b*). A recent laboratory study by Parkhill et al. (2000) has shown however that under nutrient limited balanced growth, variable fluorescence remains at maximum value even under nutrient limited, but balanced growth, conditions. Parkhill et al. (2000) suggested that the decrease in variable fluorescence under nitrogen limitation may occur only under unbalanced growth.

[42]The FASTtracka fluorometer shows a systematic artefactual transient in the measured fluorescence signal over the series of ~100 flashes used to close reaction centres. This artefact can be observed using a fluorophore solution that shows no variable fluorescence (e.g. extracted chl *a*, rhodamine B). In the FASTtracka manufacturer's protocol, this transient is characterized at a single gain and a instrument response function (IRF) is produced to correct actual data for this problem.

[43]The software can be downloaded from: http://picasso.oce.orst.edu/ORSOO/FRRF/

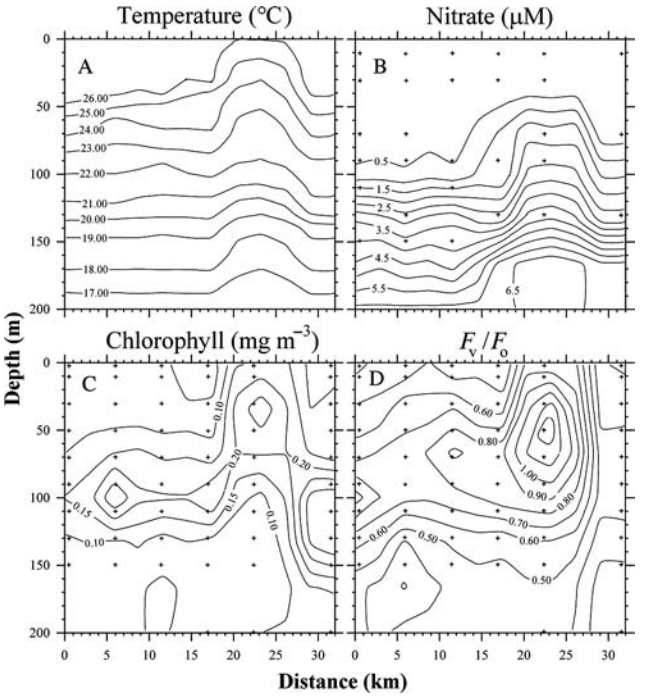

Figure 7.24
Changes in temperature, nitrate concentration, chl *a* concentration, and variable fluorescence (expressed here as F_v/F_o) over a vertical section across an upwelling eddy in the subtropical Pacific.
Source: reproduced from Falkowski et al. (1991).

7.3.4 Sun-induced chlorophyll fluorescence

Spectra of downward and upward irradiance measured at depth in natural waters typically feature a peak around 685 nm (Figure 7.25). This peak corresponds to the *in vivo* emission of chl *a* fluorescence by phytoplankton (Morel and Prieur, 1977; Neville and Gower, 1977; Gordon, 1979). It is also present in radiance and reflectance spectra. As depth increases, the fluorescence peak in the upward irradiance spectrum becomes better defined with a smaller background (Figure 7.26). This is because, close to the surface, upward irradiance in this spectral region results from both elastic backscattering of sun radiant energy and chl *a* fluorescence (inelastic scattering). With increasing depth, the sun radiant energy is quickly absorbed by pure seawater (water has a high absorption coefficient in the red spectral region), while chl *a* fluorescence is still present as a result of light absorption by phytoplankton in the blue part of the spectrum where vertical attenuation of light is generally weaker. At depth, however, some background in upward irradiance still exists in addition to chl *a* fluorescence. This background irradiance results from Raman (inelastic) scattering by pure seawater stimulated by light around 555 nm, a wavelength where vertical attenuation is weaker than around 685 nm (Maritorena et al., 2000). Raman scattering accounts for up to 20–40% of total upward irradiance at 685 nm, and in some cases it dominates the signal (Morrison, 2003).

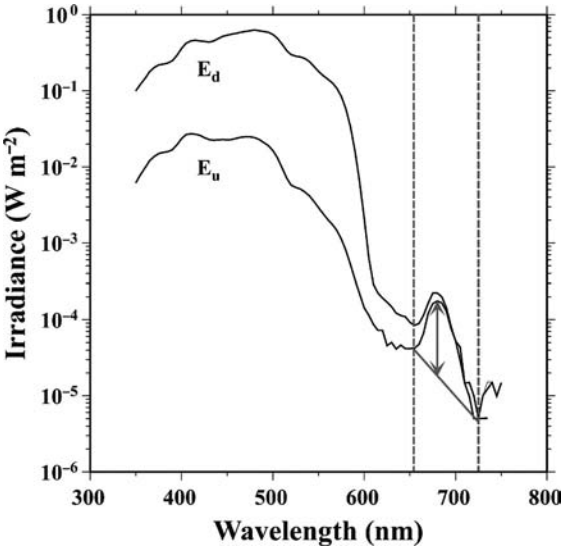

Figure 7.25
Examples of downward and upward irradiance spectra measured at 31.6 m in the subequatorial Pacific, with [chl *a*] = 0.09 mg m^{-3}. The solid grey line depicts the baseline defined by $E_u(\lambda)$ at two adjacent wavelengths (vertical dashed lines), and the double-headed arrow depicts the fluorescence line height (see text).
Source: reproduced from Maritorena et al. (2000).

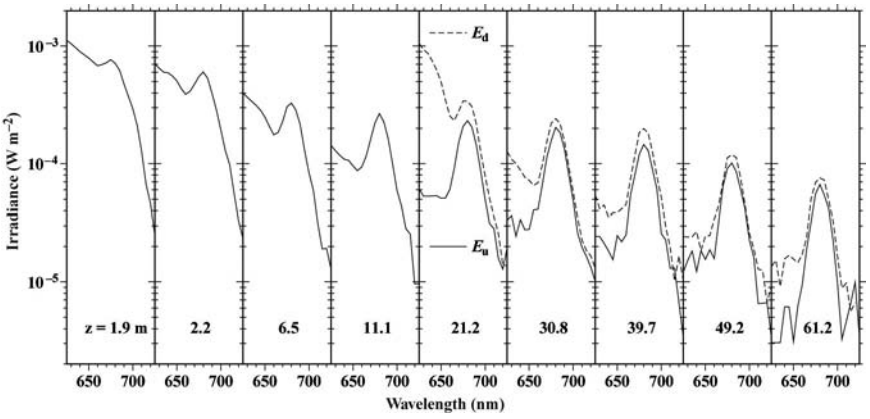

Figure 7.26
Examples of downward and upward irradiance spectra measured at different depths in the equatorial Pacific, with [chl *a*] = 0.25 ± 0.02 mg m^{-3} over that whole depth range.

The variations in the *in vivo* emission of chl *a* fluorescence by phytoplankton as observed in the *in situ* radiant field can be described by the following expression:

$$\mathrm{d}L_{\mathrm{F}}(z) = \frac{1}{4\pi}\ \mathrm{PAR}(z)\ [\mathrm{chl}\,a]\ \bar{a}^{*}(z)\ Q_{a}^{*}\ \phi_{\mathrm{F}}\ e^{-[a_{\lambda_{\mathrm{em}}} + K(\mathrm{PAR})]\,\ell}\ \mathrm{d}\ell\,, \quad (7.15)$$

where $L_{\mathrm{F}}(z)$ is the part of radiance due to chl *a in vivo* fluorescence measured at nadir and depth z and originating from a thin layer at distance ℓ below the sensor, $a_{\lambda\mathrm{em}}$ is the total absorption coefficient[44] of seawater over the wavelengths of chl *a in vivo* fluorescence, and K(PAR) is the vertical attenuation coefficient for scalar irradiance over the 400–700 nm spectral range. When integrating (7.15) over ℓ from 0 to ∞, the following equation is obtained:

$$L_{\mathrm{F}}(z) = \frac{1}{4\pi}\ \mathrm{PAR}(z)\ [\mathrm{chl}\ a]\ \bar{a}^{*}(z)\ Q_{a}^{*}\ \phi_{\mathrm{F}}\ [a_{\lambda_{em}} + K(\mathrm{PAR})]^{-1} \quad (7.16)$$

Here, it is assumed that [chl *a*], $\bar{a}^{*}$, Q_{a}^{*}, and ϕ_{F} are vertically constant over the ℓ range seen by the sensor. This assumption is often valid because 90% of the signal comes from less than 2 m below the sensor due to strong absorption by water in this waveband. But strong vertical variations in both [chl *a*] and ϕ_{F} can be observed, especially close to sea surface in the case of ϕ_{F}, as a result of non-photochemical quenching. If $\bar{a}^{*}$, Q_{a}^{*}, and ϕ_{F} are spatially constant, and $a_{\lambda\mathrm{em}}$ and K(PAR) are known [measured or expressed as a function of [chl *a*] as is generally the case in open ocean Case 1 waters, then:

$$[\mathrm{chl}\ a] = f\left(\frac{L_{\mathrm{F}}}{\mathrm{PAR}(z)}\right) \quad (7.17)$$

L_{F} can be measured using underwater spectrometers. The PNF-300 underwater spectrometer, commercialized by Biospherical Instruments Inc. (San Diego, Calif., USA), is specifically designed for the measurement of so-called 'natural' fluorescence (Kiefer et al., 1989). In fact, it measures vertical profiles of nadir radiance around 685 nm [$L_{\mathrm{u}}(685)$] and of PAR. When using this instrument, it is assumed that below a few metres depth, $L_{\mathrm{F}} \sim L_{\mathrm{u}}(685)$. L_{F} can also be measured using the underwater spectroradiometers commercialized by different companies (e.g. Biospherical Instruments Inc.; HOBI Labs, USA; Satlantic Inc., Canada; Trios GmbH, Germany). The advantage of spectroradiometers over single-wavelength radiometers is that L_{F} (or irradiance and reflectance equivalents) can be extracted from the $L_{\mathrm{u}}(\lambda)$ spectrum using a baseline (Maritorena et al. 2000) or a modelling (Morrison, 2003) approach. The baseline approach is illustrated in Figure 7.25. It simply consists in subtracting from $L_{\mathrm{u}}(685)$ a background signal determined by linear interpolation between $L_{\mathrm{u}}(\lambda)$ at two wavelengths on each side of the fluorescence peak. This approach is often referred to as the 'fluorescence line height' (FLH) technique. It is now applied to reflectance spectra measured from space using the MODIS (NASA) and MERIS (ESA) sensors (e.g. Gower et al., 2004). Its use from space is attractive because, in coastal (Case 2) waters, it provides a more specific signal of chl *a* than the traditional blue-to-green reflectance ratio (Ruddick et al., 2007 – Chapter 9 this volume).

[44]Around 685 nm, the total absorption coefficient of seawater largely results from absorption by pure water, except at very high chl *a* concentrations.

7.3.4.1 Validity of underlying assumptions

The major difficulties in using FLH to estimate chl *a* concentration are the following:

- ϕ_F is highly variable in the natural environment. According to the observations of Maritorena et al. (2000) and Morrison (2003) in the Pacific and Atlantic, respectively, ϕ_F varies from around 0.005–0.05 mol emitted photons (mol absorbed photons)$^{-1}$. The small values are generally observed close to surface when non-photochemical quenching is maximal. Therefore, the assumption of constant ϕ_F is obviously a problem.
- It is well known that K(PAR) also varies greatly at sea. However, it can easily be measured *in situ*. For remote sensing applications, K(PAR) cannot be measured but, because it strongly covaries with [chl *a*] (Morel, 1988), FLH remains well correlated with [chl *a*] despite K(PAR) variability. In Case 2 waters, however, K(PAR) is poorly correlated with [chl *a*]. Consequently, the large variations in PAR, and the changes in the spectral shape of E(λ) that affect $\overline{a}^*$ (see (7.2)), cannot be accounted for (Fisher and Kronfeld, 1990). So, the variability in the apparent optical properties of Case 2 waters is such that the interpretation of FLH variations is a problem.
- It has been shown by Gower et al. (1999) that the chl *a* fluorescence peak in reflectance spectra moves from 685 nm to more than 700 nm as [chl *a*] and/or turbidity increase. This apparent shift in the fluorescence peak position results from the occurrence, in high chl *a* and turbid waters, of an elastic scattering peak around 700 nm. Scattering by phytoplankton and suspended particles, which is more or less spectrally neutral over the limited spectral range between 680 nm and 700 nm, forms a peak because backscattered light is strongly absorbed below 700 nm by chl *a*, and highly absorbed above 700 nm by pure water. The problem may strongly compromise the baseline approach used to derive FLH (Gower et al., 1999). To circumvent that problem, the solution may be a full inversion of the reflectance spectrum into inherent optical properties and fluorescence (Roesler and Perry, 1995; Morrison, 2003).

7.3.4.2 Examples

Only a few studies have included true attempts to estimate [chl *a*] using sun-induced chl *a* fluorescence. For example, Kiefer et al. (1989) and Chamberlin et al. (1990) used the PNF-300 fluorometer (or a precursor of it) to measure $L_u(683)$ and PAR profiles. When comparing estimated with measured [chl *a*] on limited data sets from Case 1 waters, they obtained an R^2 of around 0.9. This result is apparently very good. But it can be expected that when applied to a larger data set that covers several seasons and locations, this approach provides much poorer results. This is even worse in coastal waters. Nevertheless, the FLH deserves further studies as it is a promising approach and, perhaps, the most interesting approach for remote sensing of [chl *a*] in coastal waters. Recently, Gower and Borstad (2004) published a study suggesting that [chl *a*] can be retrieved within a factor of about 4 from the fluorescence signal measured by the satellite sensor MODIS. Huot et al. (2005) conducted a detailed analysis of the FLH signal measured by MODIS over the Pacific and Indian Ocean.

7.4 Use of chlorophyll fluorescence to estimate primary production

7.4.1 Variable fluorescence

Kolber and Falkowski (1993) proposed a model for estimating primary production (i.e. the instantaneous gross rate of carbon fixation by phytoplankton) from variable fluorescence information obtained from *in situ* FRR fluorometry. The main equation of their model, partly based on the famous study of Genty et al. (1989), is the following:

$$P = 10^{-6}\,[\mathrm{chl}\,a]\;n_{\mathrm{PS2}}\;\mathrm{PAR}\;\sigma_{\mathrm{PS2}}^{\mathrm{eff}}\;q_P\;\frac{\phi_{\mathrm{P}}^{\max}}{0.65}\;\phi_{\mathrm{e}}(\mathrm{PAR})\;PQ^{-1}, \tag{7.18}$$

where P is the rate of carbon fixation (µmol C s^{-1} m^{-3}), ϕ_e is the quantum yield of electron transport for O_2 evolution in RC2 [mol O_2 (mol photon)$^{-1}$], and PQ is the photosynthetic quotient [mol O_2 (mol C)$^{-1}$]. $\phi_p^{max}/0.65$ is an estimate of the fraction of RC2s that is functional[45] (see Kromkamp and Forster, 2003, and references therein for the correspondence between (7.18) and the equations of Genty et al., 1989).

According to the model of Kolber and Falkowski (1993), ϕ_e can be expressed as:

$$\phi_{\mathrm{e}} = 0.25 \qquad \text{if PAR}\,\sigma_{\mathrm{PS2}}^{\mathrm{eff}}\;q_p \le 1/\tau_{\mathrm{p}}$$

$$\phi_{\mathrm{e}} = 0.25/\mathrm{PAR}\;\sigma_{\mathrm{PS2}}^{\mathrm{eff}}\;q_{\mathrm{p}}\;\tau_{\mathrm{p}} \qquad \text{if PAR}\;\sigma_{\mathrm{PS2}}^{\mathrm{eff}}\;q_{\mathrm{p}} > 1/\tau_{\mathrm{p}}. \tag{7.19}$$

Equation (7.18) can be interpreted as follows:

- the product [chl *a*] n_{PS2} represents the concentration of RC2s in seawater,
- the product PAR σ_{PS2}^{eff} represents the amount of light absorbed by PS2s per unit time,
- the product $q_P(\phi_P^{max}/0.65)$ ϕ_e represents the photochemical yield in terms of oxygen,
- and PQ converts oxygen into carbon.

σ_{PS2}^{eff}, q_P and ϕ_P^{max} are determined *in situ* from FRR observations. [chl *a*] and PAR can be easily measured, or estimated using other *in situ* sensors. Kolber and Falkowski (1993) proposed an approach for estimating τ_p at a given location (not depth-resolved). It is based on deriving E_k from the q_P vertical profile. E_k is the PAR value at which the photosynthetic rate approaches saturation. Then τ_P can be derived from the following expression:

$$\tau_{\mathrm{P}} = \frac{1}{E_{\mathrm{k}}\;\sigma_{\mathrm{PS2}}^{\mathrm{eff}}}. \tag{7.20}$$

Note that the FRR protocol allows τ_Q (see Section 7.3.3.2) to be determined but not τ_p (Kolber et al., 1998). The other quantities in (7.18) have to be assumed constant (see e.g. Suggett et al., 2001) as their measurement on natural phytoplankton is difficult or not currently possible (but see Suggett et al., 2004, for n_{PS2}).

[45] This fraction is also sometime expressed as $(F_v/F_o)/1.8$ (see e.g. Babin et al., 1996b).

Kolber and Falkowski (1993) compared primary production estimated from FRR fluorometry using their model, with primary production measured using the commonly used radiocarbon technique. The intercept and slope of the linear regression were close to 0 and 1, respectively, and the value of R^2 was 0.67. Similar results were obtained by Suggett et al. (2001).

As recognized by both Kolber and Falkowski (1993) and Suggett et al. (2001), the most significant weaknesses of this approach are the following:

FRR fluorometry in fact measures the photosynthetic activity at the scale of photosynthetic units, while at sea the pool size of photosynthesizing matter is in fact quantified in terms of bulk chl *a* concentration. n_{PS2} is the variable required to convert from a single photosynthetic unit to a whole phytoplankton community in seawater. But n_{PS2} is known to vary over at least a factor of 5 (e.g. Dubinsky et al., 1986) among phytoplankton species and in response to changes in environmental factor (mostly light and nutrients), and it is currently not possible to measure n_{PS2} on natural samples because of the low sensitivity of available measurement protocols (but see Suggett et al. 2004). To estimate primary production from FRR fluorometry measurements, constant n_{PS2} values have thus been used (e.g. Kolber and Falkowski 1993, Suggett et al. 2001). An incorrect n_{PS2} value leads to proportionally incorrect estimates of primary production.

In order to actually reflect the functional fraction of RC2s, ϕ_P^{max} must be measured after 30 min of dark adaptation to relax q_E and q_T ($(F_m - F_o)/F_m$ must be measured). In practice, this cannot be achieved *in situ* using the FASTtracka fluorometer ($(F_m' - F_o')/F_m'$ is in fact measured). As a result, the ϕ_P^{max} measured *in situ* in the dark chamber of the FASTtracka is smaller than it should be, especially close to the sea surface (but see discussion on the usefulness of ϕ_P^{max} in Kromkamp and Forster, 2003).

The use of (7.19) relies on the estimate of E_k made with the approach proposed by Kolber and Falkowski (1993), which provides a single value for the entire water column where phytoplankton are present. It has been shown by several studies that E_k is highly variable with depth (up to more than an order of magnitude), especially in well stratified systems (e.g. Babin et al., 1996*b*). In Kolber and Falkowski's model, an incorrect value of E_k affects the estimates of primary production at high irradiance (above E_k).

The photosynthetic quotient, *PQ*, is known to vary between about 1 and 1.4 mol C (mol O_2)$^{-1}$ mostly as a function of the type of nitrogen available in seawater (Laws, 1991). It is lowest when ammonium dominates, and highest when nitrate is the main source because the cell must reduce nitrate to ammonium with electrons produced by the light reactions of photosynthesis. Compared the other sources of error mentioned above, *PQ* is not a major one. Its value can be adjusted based on climatologic knowledge of the sampled ocean system.

There are a number of other potential problems with the assumptions made in Kolber and Falkowski's model (e.g. spectral nature of σ_{PS2}^{eff}, energy losses between RC2 and the dark reactions of photosynthesis). Nevertheless, this approach can still be considered promising, and attractive as an alternative to the use of isotopes, which have their own assumptions and limitations. This is especially true in the context of autonomous observation.

7.4.2 Sun-induced chlorophyll fluorescence

Kiefer et al. (1989) proposed a simple model that allows estimation of primary production from sun-induced chl *a* fluorescence. It can be summarized by the following equations:

$$P = \mathrm{PAR}\ [\mathrm{chl}\,a]\ \bar{a}^*\ \phi_C \tag{7.21}$$

where ϕ_C is the quantum yield of carbon fixation (moles of carbon fixed per mole of absorbed photon). By combining (7.1) and (7.21), the following is obtained:

$$P = F \frac{\phi_C}{Q_a(\lambda_{em})\ \phi_F} \tag{7.22}$$

The ratio ϕ_C/ϕ_F is known to be highly variable because of photochemical and non-photochemical quenching (Kiefer and Reynolds, 1992; Westberry and Siegel, 2003). To convey the complexity of this ratio, we can express it with the formalism proposed by Kolber and Falkowski (1993) together with (7.4) and (7.5):

$$\frac{\phi_C}{\phi_F} = q_P \frac{\phi_P^{max}}{0.65} \phi_e(\mathrm{PAR})\ PQ^{-1} \left[\frac{q_P\ k_F}{k_F + k_D + k_P} + \frac{(1-q_P)\ k_F}{k_F + k_D} \right]^{-1}. \tag{7.23}$$

Chamberlin et al. (1990) presented an empirical relationship between ϕ_C/ϕ_F and PAR. With the above model (7.22) and that relationship, they obtained an R^2 of 0.9 when comparing fluorescence-based primary production with measured primary production in different ocean systems. Stegmann et al. (1992) obtained similar results in the Equatorial Pacific. Westberry and Siegel (2003) obtained much poorer results on a time series in the Sargasso Sea.

The sun-induced chl *a* fluorescence approach for estimating primary production suffers from some of the difficulties experienced by variable-fluorescence. It is not, however, sensitive to uncertainties in n_{PS2}. But it does not account for photochemical quenching while the variable-fluorescence approach does. Additionally, it may be more sensitive to non-photochemical quenching (c.f. ratio in (7.23)). When comparing the two fluorescence-based methods discussed here for estimating primary production, Kiefer and Reynolds (1992) found R^2 values of 0.74 and 0.86 with FLH and FRR approaches, respectively, when comparing with radiocarbon-based measurements of primary production. This unique comparison suggests that the FRR-fluorometry approach is a slightly better predictor of radioisotope-estimated production.

7.5 Conclusion

The most significant use of *in vivo* chl *a* fluorescence in oceanography is made for rapidly detecting and quantifying phytoplankton biomass. Chl *a in vivo* fluorescence is a specific marker of phytoplankton, and it can be detected with high sensitivity. There are several sensors on the market for this application, both benchtop and underwater instruments, and some of them are relatively inexpensive. Temporal and spatial variability is a major feature of coastal ecosystem and harmful algal bloom (HAB) dynamics. Chl *a in vivo* fluorescence can be used to monitor this variability at all significant spatial (e.g. cell, community, ocean basins) and temporal scales. Because it is not species-specific, it is useful in the monitoring and study of HABs species that dominate biomass. The horizontal subsurface thin layers formed by a high concentration of a given phytoplankton species (e.g. *Pseudo-nitzschia* sp.; Rines et al., 2002) is a good example of an application where the signal of *in vivo* chl *a* fluorescence can be used to study their formation and outbreak as a function of physical and chemical conditions.

In vivo phytoplankton spectral fluorescence properties allow, to some extent, the discrimination between phytoplankton groups (e.g. Beutler et al., 2002). This is especially true when phycobilin-containing species are present. *In situ* autonomous spectrofluorometers (e.g. Safire, FluoroProbe 2) and flow cytometers (e.g. CytoBuoy) are now available on the market. As standard fluorometers, *in situ* spectrofluorometers allow intensive sampling at all temporal and spatial scales relevant to the study and monitoring of phytoplankton blooms, including HAB. Additionally it does provide information on taxonomic composition of phytoplankton communities. This information is certainly not as specific as that provided by molecular tools (Scholin et al., 2007 – Chapter 11 this volume). But this shortcoming is largely compensated by the amount of information generated over a broad spectrum of temporal and spatial scales.

The variable fluorescence approach is powerful and can still be considered as promising. It provides information on the status of the photosynthetic apparatus that can be related to the light history of phytoplankton cells and to the impact of nutrients. Variable fluorescence data remain, however, difficult to interpret. The estimate of primary production is an attractive use of fluorescence. But further studies are needed to establish the actual strengths and weaknesses of these approaches. All the problems and limitations associated with the FRR approach need to be quantified and the main assumptions must be verified. There are a number of encouraging initiatives currently pursuing this goal (e.g. Laney, 2003; Suggett et al., 2004). Variable fluorescence techniques may provide a mean to study phytoplankton bloom dynamics at a more physiological level. Combined with the capability of exploring all temporal and spatial scales of blooms, this tool may become a major element of observing systems for HABs.

A common strength of the fluorescence techniques described in this chapter is that they can be deployed from virtually all platforms appropriate for autonomous operation, including ships of opportunity (e.g. ferries), moorings, autonomous underwater vehicles, floats and satellites. The latter is especially attractive because HABs often develop in coastal waters where the use of fluorescence may contribute a lot in the use of remotely sensed ocean colour.

Table 7.1 List of symbols

Symbol	Definition	Units
[chl *a*]	In-water concentration of chlorophyll *a*	mg m^{-3}
λ	Wavelength	nm
λ_{em}	Wavelength of fluorescence emission	nm
λ_{ex}	Wavelength of exciting irradiance	nm
F	Flux of *in vivo* fluorescence emitted by an elementary volume	µmol photons m^{-3} s^{-1}
F'	Flux of *in vivo* fluorescence emitted by an elementary volume, specifically under steady state conditions	µmol photons m^{-3} s^{-1}
F_m	Maximum flux of *in vivo* fluorescence measured when all reaction centres are closed	µmol photons m^{-3} s^{-1}
F_m'	Maximum flux of *in vivo* fluorescence measured when all reaction centres are closed, specifically under steady state conditions	µmol photons m^{-3} s^{-1}
F_o	Minimum flux of *in vivo* fluorescence measured when all reaction centres are open	µmol photons m^{-3} s^{-1}
F_o'	Minimum flux of *in vivo* fluorescence measured when all reaction centres are open, specifically under steady state conditions	µmol photons m^{-3} s^{-1}
PAR	Photosynthetically available radiation	µmol photons m^{-2} s^{-1}
E_k	PAR value at which the photosynthetic rate approaches saturation	µmol photons m^{-2} s^{-1}
$\mathring{E}$	Scalar irradiance	µmol photons m^{-2} s^{-1}
L_F	Part of radiance due to chl *a in vivo* fluorescence	µmol photons m^{-2} s^{-1} sr^{-1}
L_u	Upward radiance	µmol photons m^{-2} s^{-1} sr^{-1}
ε	Quantum energy of a flash	Photons m^{-2}
$\overline{a}^*$	Chlorophyll-specific, spectrally averaged absorption coefficient of phytoplankton weighted by the irradiance spectrum, see (7.2)	$m^2 mg^{-1}$
a_ϕ^*	Chlorophyll-specific absorption coefficient of phytoplankton	m^2 mg^{-1}
a_{sol}^*	*In vivo* chlorophyll-specific absorption coefficient of unpackaged phytoplankton pigments	m^2 mg^{-1}
$a_{\lambda em}$	Absorption coefficient of seawater over the spectral range of chl *a in vivo* fluorescence emission	m^{-1}
Q_a^*	Fluorescence intracellular reabsorption factor	dimensionless
K	Vertical attenuation coefficient for scalar irradiance	m^{-1}
σ_{PS2}^{opt}	Optical absorption cross-section of photosystem 2	m^2 photon^{-1}
σ_{PS2}^{eff}	Effective absorption cross-section of photosystem 2	m^2 photon^{-1}

(Continued)

TABLE 7.1 *(Continued)*

Symbol	Definition	Units
σ_{PSU}	Optical absorption cross-section of a photosynthetic unit	m^2 photon^{-1}
ϕ_F	Quantum yield of fluorescence	mol emitted photons (mol absorbed photon)$^{-1}$
ϕ_{Fm}	Maximum quantum yield of fluorescence	mol emitted photons (mol absorbed photon)$^{-1}$
ϕ_{Fo}	Minimum quantum yield of fluorescence	mol emitted photons (mol absorbed photon)$^{-1}$
ϕ_P^{max}	Maximum quantum yield for energy conversion in RC2 (photochemistry)	mol photons used for charge separation (mol absorbed photon)$^{-1}$
ϕ_e	Quantum yield of electron transport for O_2 evolution in RC2	mol O_2 (mol photon)$^{-1}$
q_P	Fraction of 'open' RC2	dimensionless
k_x	Rate constant of chl *a* de-excitation processes, the subscript *x* is F for fluorescence, D for thermal decay, and P for photochemistry (or charge separation)	s^{-1}
n_{PS2}	Number of oxygen-evolving RC2 per unit chl *a*	O_2 (mg chl *a*)$^{-1}$ or photons (mg chl *a*)$^{-1}$
τ_P	Turnover time for electron transport through PS2	s
τ_Q	Turnover time of Q_1 reoxidation by the plastoquinone pool	s
PQ	Photosynthetic quotient	mol O_2 (mol C)$^{-1}$
RC1	Reaction centre 1	
RC2	Reaction centre 2	
PS1	Photosystem 1	
PS2	Photosystem 2	
q_E	Energy-dependent non-photochemical quenching	
q_T	State-transition related non-photochemical quenching	
q_I	Photoinhibition-related non-photochemical quenching	

References

Abbott, M. R., Richerson, P. J. and Powell, T. M. 1982. *In situ* response of phytoplankton fluorescence to rapid variations in light. *Limnol. Oceanogr.*, 27, pp. 218–25.

Aro, E.-M. and Ohad, I. 2003. Redox regulation of thylakoid protein phosphorylation. *Antiox. Redox Signal.*, 5, pp. 55–67.

Aro, E. M., Virgin, I. and Andersson, B. 1993. Photoinhibition of Photosystem. II: Inactivation, protein damage and turnover. *Biochim. Biophys. Acta*, 1143, pp. 113–34.

Babin, M., Morel, A., Claustre, H., Bricaud, A., Kolber, Z. and Falkowski, P. G. 1996*b*. Nitrogen- and irradiance-dependent variations of the maximum quantum yield of carbon fixation in eutrophic, mesotrophic and oligotrophic marine systems. *Deep Sea Res.*, 43, pp. 1241–72.

Babin, M., Morel, A. and Gentili, B. 1996*a*. Remote sensing of sea surface sun-induced chlorophyll fluorescence: consequences of natural variations in the optical characteristics of phytoplankton and the quantum yield of chlorophyll *a* fluorescence. *Int. J. Rem. Sens.*, 17, pp. 417–48.

Babin, M., Roesler, C. S. and Cullen, J. J. (eds). 2007. *Real-time Coastal Observing Systems for Marine Ecosystem Dynamics and Harmful Algal Blooms: Theory, Instrumentation and Modelling*. Paris, Intergovernmental Oceanographic Commission of UNESCO. (Monographs on Oceanographic Methodology.)

Babin, M., Stramski, D., Ferrari, G. M., Claustre, H., Bricaud, A., Obolensky, G. and Hoepffner, N. 2003. Variations in the light absorption coefficients of phytoplankton, nonalgal particles, and dissolved organic matter in the coastal waters around Europe. *J. Geophys. Res.*, 108, 3211, doi: 3210.1029/2001JC000882.

Behrenfeld, M. J., Bale, A. J., Kolber, Z., Aiken, J. and Falkowski, P. G. 1996. Confirmation of iron limitation of phytoplankton photosynthesis in the equatorial Pacific Ocean. *Nature*, 383, pp. 508–11.

Behrenfeld, M. J. and Kolber, Z. 1999. Widespread iron limitation of phytoplankton in the South Pacific Ocean. *Science*, 283, pp. 840–43.

Beutler, M., Wiltshire, K. H., Arp, M., Kruse, J., Reineke, C., Moldaenke, C. and Hansen, U. P. 2003. A reduced model of the fluorescence from the cyanobacterial photosynthetic apparatus designed for the *in situ* detection of cyanobacteria. *Biochim. Biophys. Acta*, 1604, pp. 33–46.

Beutler, M., Wiltshire, K. H., Meyer, B., Moldaenke, C., Lüring, C. and Meyerhöfer, M. 2002. A fluorometric method for the differentiation of algal populations *in vivo* and *in situ*. *Photosynth. Res.*, 72, pp. 39–53.

Beutler, M., Wiltshire, K. H. Reineke, C. and Hansen, U. P. 2004. Algorithms and practical fluorescence models of the photosynthetic aparatus of red cyanobacteria and Cryptophyta designed for the fluorescence detection of red cyanobacteria and cryptophytes. *Aquat. Microb. Ecol.*, 35, pp. 115–29.

Bruyant, F., Babin, M., Genty, B., Prasil, O., Behrenfeld, M. J., Claustre, H., Bricaud, A., Garczarek, L., Holtzendorff, J., Koblizek, M., Dousova, H. and Partensky, F. 2005. Diel variations in the photosynthetic parameters of *Prochlorococcus* strain PCC 9511: combined effects of light and cell cycle. *Limnol. Oceanogr.*, 50, pp. 850–63.

Chamberlin, W. S., Booth, C. R., Kiefer, D. A., Morrow, J. H. and Murphy, R. C. 1990. Evidence for a simple relationship between natural fluorescence, photosynthesis and chlorophyll in the sea. *Deep Sea Res.*, 37, pp. 951–73.

Clayton, R. K. 1980. *Photosynthesis: Physical Mechanisms and Chemical Patterns*. Cambridge, UK, Cambridge University Press.

Collins, D. J., Kiefer, D. A. Soohoo, J. B. and Mcdermid, I. S. 1985. The role of reabsorption in the spectral distribution of phytoplankton fluorescence emission. *Deep Sea Res.*, 32, pp. 983–1003.

Cowles, T. J., Desiderio, R. A. and Neuer, S. 1993. *In situ* characterization of phytoplankton from vertical profiles of fluorescence emission spectra. *Mar. Biol.*, 115, pp. 217–22.

Cullen, J. J. and Davis, R. F. 2003. The blank can make a big difference in oceanographic measurements. *Limnol. Oceanogr. Bull.*, 12, pp. 29–35.

Cullen, J. J. and Renger, E. H. 1979. Continuous measurement of the DCMU-induced fluorescence response of natural phytoplankton populations. *Mar. Biol.*, 53, pp. 13–20.

Cullen, J. J., Yentsch, C. M., Cucci, T. L. and Mcintyre, H. L. 1988. Autofluorescence and other optical properties as tools in biological oceanography. *Ocean Optics IX*, *Proc. SPIE*, pp. 149–56.

Dandonneau, Y. and Neveux, J. 1997. Diel variations of *in vivo* fluorescence in the eastern equatorial Pacific: an unvarying pattern. *Deep Sea Res. I*, 44, pp. 1869–80.

Demmig-Adams, B. 1990. Carotenoids and photoprotection in plants: a role for the xanthophyll zeaxanthin. *Biochim. Biophys. Acta*, 1020, pp. 1–24.

Desiderio, R. A., Moore, C., Lantz, C. and Cowles, T. J. 1997. Multiple excitation fluorometer for *in situ* oceanographic applications. *Appl. Opt.*, 36, pp. 1289–96.

Dubinsky, Z., Falkowski, P. G. and Wyman, K. 1986. Might harvesting and utilization by phytoplankton. *Plant Cell Physiol.*, 27, pp. 1335–49.

Falkowski, P. G., Fujita, Y., Ley, A. and Mauzerall, D. 1986. Evidence for cyclic electron flow around photosystem II in *Chlorella pyrenoidosa*. *Plant Physiol.*, 81, pp. 310–12.

Falkowski, P. G., Greene, R. and Kolber, Z. 1995. Light utilization and photoinhibition of photosynthesis in marine phytoplankton. In: N. R. Baker and J. R. Bowyer (eds), *Photoinhibition of Photosynthesis from Molecular Mechanisms to the Field. Environmental Plant Biology*. Abingdon, UK, Bios Scientific Publishers, pp. 407–32.

Falkowski, P. G. and Kiefer, D. A. 1985. Chlorophyll *a* fluorescence in phytoplankton: relationship to photosynthesis and biomass. *J. Plankton Res*, 7, pp. 715–31.

Falkowski, P. G. and Raven, J. A. 1997. *Aquatic Photosynthesis*. Malden, Mass., Blackwell Sciences.

Falkowski, P. G., Ziemann, D., Kolber, Z. and Bienfang, P. K. 1991. Role of eddy pumping in enhancing primary production in the ocean. *Nature*, 352, pp. 55–58.

Fischer, J. and Kronfeld, U. 1990. Sun-stimulated chlorophyll fluorescence. Part 1: Influence of oceanic properties. *Int. J. Rem. Sens.*, 11.

Fuchs, E., Zimmerman, R. C. and Jaffe, J. S. 2002. The effect of elevated levels of pheophytin in natural water on variable fluorescence measured from phytoplankton. *J. Plankton Res.*, 24, pp. 1221–29.

Geider, R. J. and Osborne. B. A. 1992. *Algal Photosynthesis*. New York, Chapman & Hall.

Genty, B., Briantais, J. M. and Baker, N. R. 1989. The relationship between the quantum yield of photosynthetic electron transport and quenching of chlorophyll fluorescence. *Biochim. Biophys. Acta*, 990, pp. 87–92.

Gilmore, A. M. and Govindjee. 1999. How higher plants respond to excess light: energy dissipation in photosystem II. In: G. S. Singhal, R. Renger, S. K. Sopory, K. D. Irrgang and Govindjee (eds), *Concepts in Photobiology: Photosynthesis and Photomorphogenesi*s. Narosa Publishing House.

Gorbunov, M. Y. and Falkowski, P. G. 2004. Fluorescence induction and relaxation (FIRe) technique and instrumentation for monitoring photosynthetic processes and primary production in aquatic ecosystems. In: A. van der Est and D. Bruce (eds), *Photosynthesis: Fundamental Aspects to Global Perspectives.* Proc. 13th International Congress of Photosynthesis. XX, Allen Press.

Gordon, H. R. 1979. Diffuse reflectance of the ocean: the theory of its augmentation by chlorophyll *a* fluorescence at 685 nm. *Appl. Opt.*, 18, pp. 1161–66.

Govindjee. 1995. Sixty-three years since Kautsky: chlorophyll *a* fluorescence. *Aus. J. Plant Physiol.*, 22, pp. 131–60.

Govindjee and Satoh, K. 1986. Fluorescence properties of chlorophyll *b*- and chlorophyll *c*-containing algae. In: Govindjee, J. Amesz and D. C. Fork (eds), *Light Emission by Plant and Bacteria*. New York, Academic Press, pp. 497–538. (Cell Biology: a series of monographs.)

Gower, J. F. R. and Borstad, G. A. 1981. Use of *in vivo* fluorescence line at 685 nm for remote sensing surveys of surface chlorophyll *a*. In: J. F. R. Gower (ed.), *Oceanography from Space.* New York, Plenum Press, pp. 329–38.

Gower, J. F. R. and Borstad, G. A. 2004. On the potential of MODIS and MERIS for imaging chlorophyll fluorescence from space. *Int. J. Rem. Sens.*, 25, pp. 1459–64.

Gower, J. F. R., Brown, L. and Borstad, G. A. 2004. Observation of chlorophyll fluorescence in west coast waters of Canada using the MODIS satellite sensor. *Can. J. Rem. Sens.*, 30, pp. 17–25.

Gower, J. F. R., Doerffer, R. and Borstad, G. A. 1999. Interpreation of the 685 nm peak in water-leaving radiance spectra in terms of fluorescence, absorption and scattering, and its observation by MERIS. *Int. J. Rem. Sens.*, 20, pp. 1771–86.

Hall, D. O. and Rao, K. 1999. *Photosynthesis*, 6th ed. Cambridge , UK, Cambridge University Press.

Han, B. P. 2001. Photosynthesis-irradiance response at physiological level: a mechanistic model. *J. Theor. Biol.*, 213, pp. 121–27.

Hofstraat, J. W., Rubelowsky, K. and Slutter, S. 1992. Corrected fluorescence excitation and emission spectra of phytoplankton: toward a more uniform approach to fluorescence measurements. *J. Plankton Res.*, 14, pp. 625–36.

Huot, Y., Brown, C. A. and Cullen, J. 2005. New algorithms for MODIS sun-induced chlorophyll fluorescence and a comparison with present data products. *Limnol. Oceanog. Meth.*, 3, pp. 108–30.

Jeffrey, S. W. and Vesk, M. 1997. Introduction to marine phytoplankton and their pigment signatures. In: S. W. Jeffrey, R. F. C. Mantoura and S. W. Wright (eds), *Phytoplankton Pigments in Oceanography*. Paris, Intergovernmental Oceanographic Commission of UNESCO, pp. 37–84. (Monographs on Oceanographic Methodology.)

Kiefer, D. A. 1973. Fluorescence properties of natural phytoplankton populations. *Mar. Biol.*, 22, pp. 263–69.

Kiefer, D. A., Chamberlin, W. S. and Booth, C. R. 1989. Natural fluorescence of chlorophyll *a*: relationship to photosynthesis and chlorophyll concentration in the western South Pacific gyre. *Limnol. Oceanogr.*, 34, pp. 868–81.

Kiefer, D. A. and Reynolds, R. A. 1992. Advances in understanding phytoplankton fluorescence and photosynthesis. In: P. G. Falkowski and A. D. Woodhead (eds), *Primary Productivity and Biogeochemical Cycles in the Sea*. New York, Plenum Press, pp. 155–74.

Kishino, M., Sugihara, S. and Okami, N. 1984. Estimation of quantum yield of chlorophyll *a* fluorescence from the upward irradiance spectrum in the sea. *La Mer*, 22, pp. 233–40.

Kolber, Z. and Falkowski, P. G. 1993. Use of active fluorescence to estimate phytoplankton photosynthesis *in situ*. *Limnol. Oceanogr.*, 38, pp. 1646–65.

Kolber, Z., Prasil, O. and Falkowski, P. G. 1998. Measurements of variable chlorophyll fluorescence using fast repetition rate techniques: defining methodology and experimental protocols. *Biochim. Biophys. Acta*, 1367, pp. 88–106.

Kolber, Z., Wyman, K. and Falkowski, P. G. 1990. Natural varaibility in photosynthetic energy conversion efficiency: a field study in the Gulf of Maine. *Limnol. Oceanogr.*, 35, pp. 72–79.

Kolber, Z., Zehr, J. and Falkowski, P. G. 1988. Effects of growth irradiance and nitrogen limitation on photosynthetic energy conversion in photosystem II. *Plant Physiol.*, 88, pp. 923–29.

Kopf, U. and Heinze, J. 1984. 2,7-Bis(diethylamino)phenazoxonium chloride as a quantum counter for emission measurements between 240 and 700 nm. *Anal. Chem.*, 56, pp. 1931–35.

Kramer, D. M., Johnson, G., Kiirats, O. and Edwards, G. E. 2004. New fluorescence parameters for the determination of Q_A redox state and excitation energy fluxes. *Photosynth. Res.*, 79, pp. 209–18.

Krause, G. H. and Weis, E. 1991. Chlorophyll fluorescence and photosynthesis: the basics. *Ann. Rev. Plant Physiol. Plant Mol. Biol.*, 42, pp. 313–49.

Kromkamp, J. C. and Forster, R. M. 2003. The use of variable fluorescence measurements in aquatic ecosystems: differences between multiple and single turnover measuring protocols and suggested terminology. *Eur. J. Phycol.*, 38, pp. 103–12.

Laney, S. R. 2003. Assessing the error in photosynthetic properties determined by fast repetition rate fluorometry. *Limnol. Oceanogr.*, 48, pp. 2234–42.

Lavaud, J., Rousseau, B. and Etienne, A. L. 2004. General features of photoprotection by energy dissipation in planktonic diatoms (Bacillariophyceae). *J. Phycol.*, 40, pp. 130–37.

Lavergne, J. and Trissl, H. W. 1995. Theory of fluorescence induction in photosystem. II: Derivation of analytical expressions in a model including exciton-radical-pair equilibrium and restricted energy transfer between photosynthetic units. *Biophys. J.*, 68, pp. 2474–92.

Laws, E. A. 1991. Photosynthetic quotients, new production and net community production in the open ocean. *Deep Sea Res.*, 38, pp. 143–67.

Lazar, D. 1999. Chlorophyll *a* fluorescence induction. *Biochim. Biophys. Acta*, 1412, pp. 1–28.

Loftus, M. E. and Seliger, H. H. 1975. Some limitations of the *in vivo* fluorescence technique. *Chesapeake Sci.*, 16, pp. 79–92.

Lorenzen, C. J. 1966. A method for the continuous measurement of *in vivo* chlorophyll concentration. *Deep Sea Res.*, 13, pp. 223–27.

Lutz, V. A., Sathyendranath, S., Head, E. J. H. and Li, W. K. W. 1998. Differences between *in vivo* absorption and fluorescence excitation spectra in natural samples of phytoplankton. *J. Phycol.*, 34, pp. 214–27.

Lutz, V. A., Sathyendranath, S., Head, E. J. H. and Li, W. K. W. 2001. Changes in the *in vivo* absorption and excitation spectra with growth irradiance in three species of phytoplankton. *J. Plankton Res.*, 23, pp. 555–69.

Maritorena, S., Morel, A. and Gentili, B. 2000. Determination of the fluorescence quantum yield by oceanic phytoplankton in their natural habitat. *Appl. Opt.*, 39, pp. 6725–37.

Mauzerall, D. 1972. Light-induced changes in *Chlorella*, and the primary photoreaction for the production of oxygen. *Proc. Natl. Acad. Sci.*, 69, pp. 1358–62.

Mauzerall, D. and Greenbaum, N. L. 1989. The absolute size of a photosynthetic unit. *Biochim. Biophys. Acta*, 974, pp. 119 – 40.

Melis, A. 1999. Photosystem-II damage and repair cycle in chloroplasts: what modulates the rate of photodamage *in vivo*. *Trends Plant Sci.*, 4, pp. 130–35.

Mitchell, B. G. and Kiefer, D. A. 1988. Chlorophyll *a* specific absorption and fluorescence excitation spectra for light-limited phytoplankton. *Deep Sea Res.*, 35, pp. 639–63.

Morel, A. 1988. Optical modeling of the upper ocean in relation to its biogenous matter content (Case 1 water). *J. Geophys. Res.*, 93, pp. 10749–68.

Morel, A. 2007. Introduction to optical properties in the sea: theoretical aspects. In: Babin et al. (eds), op. cit., this volume.

Morel, A. and Bricaud, A. 1981. Theoretical results concerning light absorption in a discrete medium, and application to specific absorption of phytoplankton. *Deep Sea Res.*, 28, pp. 1375–93.

Morel, A. and Prieur, L. 1977. Analysis of variations in ocean color. *Limnol. Oceanogr.*, 22, pp. 709–22.

Morrison, J. R. 2003. *In situ* determination of the quantum yield of phytoplankton chlorophyll *a* fluorescence: a simple algorithm, observations, and a model. *Limnol. Oceanogr.*, 48, pp. 618–31.

Neale, P. J., Cullen, J. J. and Yentsch, C. M. 1989. Bio-optical inferences from chlorophyll *a* fluorescence: what kind of fluorescence is measured in flow cytometry? *Limnol. Oceanogr.*, 34, pp. 1739–48.

Neori, A., Vernet, M., Holm-Hensen, O. and Haxo, F. T. 1986. Relationship between action spectra for chlorophyll *a* fluorescence and photosynthetic O_2 evolution in algae. *J. Plankton Res.*, 8, pp. 537–48.

Neori, A., Vernet, M., Holm-Hensen, O. and HAXO, F. T. 1988. Comparison of chlorophyll far-red and red fluorescence excitation spectra with photosynthetic oxygen action spectra for photosystem II in algae. *Mar. Ecol. Progr. Ser.*, 44, pp. 297–302.

Neville, R. A. and Gower, J. F. R. 1977. Passive remote sensing of phytoplankton via chlorophyll *a* fluorescence. *J. Geophys. Res*., 82, pp. 3487–93.

Olaizola, M. and Yamamoto, H. Y. 1994. Short-term responses of the diadinoxanthin cycle and fluorescence yield in *Chaetoceros muelleri* (Bacillariophyceae). *J. Phycol*., 30, pp. 606–12.

Oliver, R. L., Whittington, J., Lorenz, Z. and Webster, I. T. 2003. The influence of vertical mixing on the photoinhibition of variable chlorophyll *a* fluorescence and its inclusion in a model of phytoplankton photosynthesis. *J. Plankton Res*., 25, pp. 1107–29.

Olson, R. J., Zettler, E. R., Chisholm, S. W. and Dusenberry, J. A. 1991. Flow cytometry in oceanography. In: S. Demers (ed.), *Particle Analysis in Oceanography*. Springer-Verlag, pp. 351–402. (NATO Advanced Study Institute Series G: Ecological Sciences.)

Öquist, G., Hagström, Å., Alm, P., Samuelsson, G. and Richardson, K. 1982. Chlorophyll *a* fluorescence, an alternative method for estimating primary production. *Mar. Biol*., 68, pp. 71–75.

Ostrowska, M., Majchrowski, R., Matorin, D. N. and Wozniak, B. 2000*a*. Variability of specific fluorescence of chlorophyll in the ocean. Part 1: Theory of classical *in situ* chlorophyll fluorometry. *Oceanologia*, 42, pp. 203–19.

Ostrowska, M., Matorin, D. N. and Ficek, D. 2000*b*. Variability of the specific fluorescence of chlorophyll in the ocean. Part 2: Fluorometric method of chlorophyll *a* determination. *Oceanologia*, 42, pp. 221–29.

Owens, T. G. 1995. Excitation energy transfer between chlorophylls and carotenoids. A proposed molecular mechanism for non-photochemical quenching. In: N. R. Baker and J. R. Bowyer (eds), *Photoinhibition of Photosynthesis from Molecular Mechanisms to the Field. Environmental Plant Biology*. Abingdon, UK, Bios Scientific Publishers, pp. 95–110.

Parkhill, J. P., Maillet, G. and Cullen, J. J. 2001. Fluorescence-based maximal quantum yield for photosystem II as a diagnostic of nutrient stress. *J. Phycol*., 37, pp. 517–29.

Prézelin, B. B. and Boczar, B. A. 1986. Molecular bases of cell absorption and fluorescence in phytoplankton: potential applications to studies in optical oceanography. In: F. Round and D. Chapman (eds), *Progress in Phycological Research*. Bristol, UK, Biopress, pp. 349–464.

Rines, J. E. B., Donaghay, P. L., Dekshenieks, M. M. and Sullivan, J. M. 2002. Thin layers and camouflage: hidden *Pseudo-nitzschia* populations in a fjord in the San Juan Islands, Washington, USA. *Mar. Ecol. Progr. Ser*., 225, pp. 123–37.

Roesler, C. S. and Boss, E. 2007. *In situ* measurement of inherent optical properties and potential for harmful algal bloom detection and coastal ecosystem observations. In: Babin et al. (eds), op. cit., this volume.

Roesler, C. S. and Perry, M. J. 1995. *In situ* phytoplankton absorption, fluorescence emission, and particulate backscattering spectra. *J. Geophys. Res*., 100, pp. 13279–94.

Roy, S. and Legendre, L. 1979. DCMU-enhanced fluorescence as an index of photosynthetic activity in phytoplankton. *Mar. Biol*., 55, pp. 93–101.

Ruddick, K., Lacroix, G., Park, Y., Rousseau, V., De Cauwer, V. and Sterckx, S. 2007. Overview of ocean colour: theoretical background, sensors and applicability to detection and monitoring of harmful algal blooms (capabilities and limitations). In: Babin et al. (eds), op. cit., this volume.

Sakshaug, E., Johnsen, G., Andresen, K. and Vernet, M. 1991. Modeling of light-dependent algal photosynthesis and growth: experiments with the Barents Sea diatoms *Thalassiosira nordenskioeldii* and *Chaetoceros furcellatus*. *Deep Sea Res*., 38, pp. 415–30.

Scholin, C. A., Doucette, G. J. and Cembella, A. D. 2007. Prospects for developing automated systems for *in situ* detection of harmful algae and their toxins. In: Babin et al. (eds), op. cit., this volume.

Schreiber, U., Bilger, W. and Schliwa, U. 1986. Continuous recording of photochemical and non-photochemical quenching with a new type of modulation fluorometer. *Photosynth. Res*., 10, pp. 51–62.

Schreiber, U. and Krieger, A. 1996. Two fundamentally different types of variable chlorophyll fluorescence *in vivo*. *FEBS Lett*., 397, pp. 131–35.

Sciandra, A., Lazzara, L., CLaustre, H. and Babin, M. 2000. Responses of the growth rate, pigment composition and optical properties of *Cryptomonas* sp. to light and nitrogen stresses. *Mar. Ecol. Progr. Ser.*, 201, pp. 107–20.

Sosik, H. M. 2007. Characterizing seawater constituents from optical properties. In: Babin et al. (eds), op. cit., this volume.

Sosik, H. M. and Mitchell, B. G. 1995. Light absorption by phytoplankton, photosynthetic pigments and detritus in the California current system. *Deep Sea Res. I*, 42, pp. 1717–48.

Stegmann, P. M., Lewis, M. R., Davis, C. O. and Cullen, J. J. 1992. Primary production estimates from recordings of solar-stimulated fluorescence in the Equatorial Pacific at 150°W. *J. Geophys. Res.*, 97, pp. 627–38.

Stirbet, A., Govindjee, B., Strasser, J. and Strasser, R. J. 1998. Chlorophyll *a* fluorescence induction in higher plants: modelling and numerical simulation. *J. Theor. Biol.*, 193, pp. 131–51.

Suggett, D., Kraay, G., Holligan, P., Davey, M., Aiken, J. and Geider, R. J. 2001. Assessment of photosynthesis in a spring cyanobacterial bloom by use of a fast repetition rate fluorometer. *Limnol. Oceanogr.*, 46, pp. 802–10.

Suggett, D., Oxborough, K., Baker, N. R., Mcintyre, H. L., Kana, T. M. and Geider, R. J. 2003. Fast repetition rate and pulse amplitude modulation chlorophyll *a* fluorescence measurements for assessment of photosynthetic electron transport in marine phytoplankton. *Eur. J. Phycol.*, 38, pp. 371–84.

Suggett, D. J., Macintyre, H. L. and Geider, R. J. 2004. Evaluation of biophysical and optical determinations of light absorption by photosystem II in phytoplankton. *Limnol. Oceanogr. Meth.*, 2, pp. 316–32.

Trees, C. C., Clark, D. K., Bidigare, R. R., Ondrusek, M. E. and Mueller, J. L. 2000. Accessory pigments versus chlorophyll *a* concentration within the euphotic zone: a ubiquitous relationship. *Limnol. Oceanogr.*, 45, pp. 1130–43.

Vassiliev, I. R., Kolber, Z., Wyman, K., Mauzerall, D., Shukla, V. K. and Falkowski, P. G. 1995. Effects of iron limitation on photosystem II composition and light utilization in *Dunaliella tectiolecta*. *Plant Physiol.*, 109, pp. 963–72.

Vincent, W. F., Neale, P. J. and Richerson, P. J. 1984. Photoinhibition: algal responses to bright light during diel stratification and mixing in a tropical alpine lake. *J. Phycol.*, 20, pp. 201–11.

Westberry, T. K. and Siegel, D. A. 2003. Phytoplankton natural fluorescence variability in the Sargasso Sea. *Deep Sea Res. I*, 50, pp. 417–34.

Yamamoto, H. Y. and Bassi, R. 1996. Carotenoids: localization and function. In: D. R. Ort and C. F. Yocum (eds), *Oxygenic Photosynthesis: the Light Reactions. Advances in Photosynthesis*. New York, Kluwer Academic Publishers.

Yentsch, C. S. and Phinney, D. A. 1985. Spectral fluorescence: a taxonomic tool for studying the structure of phytoplankton populations. *J. Plankton Res.*, 7, pp. 617–32.

Yentsch, C. S. and Yentsch, C. M. 1979. Fluorescence spectral signatures: the characterization of phytoplankton populations by the use of excitation and emission spectra. *J. Mar. Res.*, 37, pp. 471–83.

Zonneveld, C. 1997. Modeling the effects of photoadaptation on the photosynthesis-irradiance curve. *J. Theor. Biol.,* 186, pp. 381–88.

8

Characterizing seawater constituents from optical properties

H. M. Sosik

8.1 Introduction

Most of the variability in the optical properties of the upper ocean is due to changes in the concentration and type of constituents present in the water. The optically important constituents are often of interest to ecologists and biogeochemists and include coloured dissolved organic matter, plankton and suspended sediments. Particularly in coastal waters, a wide range of dynamic processes contribute to changes in these constituents and, as a consequence, optical properties are highly variable in space and time.

In practice, understanding what drives observed optical variability is a challenging problem. Most of the constituents that contribute to optical variability are difficult to measure directly and the potential for deriving information about them from optical properties motivates much of the research in ocean optics. Optical properties can be readily measured from platforms as diverse as moorings, autonomous vehicles and earth-orbiting satellites, making them accessible at a wide range of space and timescales. To the extent that reliable relationships between constituents and optical properties can be determined, information on constituent characteristics may be available at the same set of scales.

This chapter offers an overview of current knowledge about relationships between marine optical properties and seawater constituents. It is not an exhaustive review of this rapidly advancing topic but instead provides some historical context and an introduction to recent developments through selected examples from observational studies. Where applicable, examples have been chosen to highlight links between optical properties and phytoplankton, and harmful algal bloom (HAB) taxa, in particular.

8.2 Overview of IOP variability

Inherent optical properties (IOPs) depend only on the properties of the medium and its constituents (Preisendorfer, 1976; Kirk, 1994) and they include spectral absorption and scattering coefficients ($a(\lambda)$ and $b(\lambda)$, respectively, where λ represents wavelength) (see Table 8.1 for notation summary). The fundamental IOPs are the absorption coefficient and the volume scattering function, as various scattering coefficients (e.g. total, backward) can be determined by integration of the volume scattering function over the appropriate angles (see Morel, 2007 – Chapter 4 this volume – for more details). Measurements of the volume scattering function for natural waters are not commonly made, so this discussion is restricted to scattering coefficients.

Table 8.1 Notation

Symbol	Definition
IOP	Inherent optical property
AOP	Apparent optical property
Chl	Chlorophyll *a* concentration, mg m^{-3}
CDOM	Chromophoric dissolved organic matter
NAP	Non-algal particles
CDM	CDOM + NAP
POC	Particulate organic carbon
PIC	Particulate inorganic carbon (calcium carbonate)
a	Absorption coefficient, m^{-1}
b	Scattering coefficient, m^{-1}
c	Beam attenuation coefficient, m^{-1}
b_b	Backscattering coefficient, m^{-1}
a_x, b_x, c_x, $b_{b,x}$	Optical coefficients where x is a particular seawater constituent; x is replaced by p, CDOM, w, ph or NAP, respectively designating particles, CDOM, water, phytoplankton and NAP
a_x^*,b_x^*	Constituent-specific optical coefficients, $m^2\ mg^{-1}$
b_b	Backscattering ratio (b_b/b), dimensionless
λ	Wavelength, nm
z	Depth, m
S	Spectral slope for CDOM or NAP, nm^{-1}
γ	Hyperbolic spectral slope, dimensionless
$a_{<ph>}(\lambda)$	Normalized phytoplankton absorption coefficient, dimensionless
$\mathbf{a}_x$	Absorption basis vector (spectral shape) for constituent x, dimensionless
$\mathbf{b}_x$	Scattering basis vector for constituent x, dimensionless
A_x	Optical property amplitude for component x, m^{-1}
$\mathbf{a}_{<pico>}$	Absorption basis vector for picophytoplankton, dimensionless
$\mathbf{a}_{<micro>}$	Absorption basis vector for microphytoplankton, dimensionless
F	Dominant cell size index (amplitude), dimensionless
L_u	Upwelling radiance, W $m^{-2}\,nm^{-1}\,sr^{-1}$
E_d	Downwelling irradiance, W $m^{-2}\,nm^{-1}$
E_u	Upwelling irradiance, W $m^{-2}\,nm^{-1}$
$\bar{\mu}_d$	Average cosine for downwelling irradiance, dimensionless

Table 8.1 *(Continued)*

Symbol	Definition
$\bar{\mu}_u$	Average cosine for upwelling irradiance, dimensionless
K_d	Diffuse attenuation coefficient for downwelling irradiance, m^{-1}
K_w	Diffuse attenuation coefficient associated with water, m^{-1}
K^*_{chl}	chl - specific diffuse attenuation coefficient, $m^2\ mg^{-1}$
R_{rs}	Remote sensing reflectance, sr^{-1}
R	Irradiance reflectance, dimensionless

An important characteristic of IOPs is that they are additive. This means that, for a seawater sample containing a mixture of constituents, the absorption and scattering coefficients of the various constituents are independent, and the total coefficient can be determined by summation. This fact arises from the definition of IOPs with respect to collimated light. As discussed by Roesler and Boss (2007 – Chapter 5 this volume) current methods to measure IOPs can only approximate ideal light field and collection geometry, so corrections are sometimes required to obtain adequate estimates of true IOPs.

To explain natural variability in total IOPs and to derive estimates of ecologically and biogeochemically relevant constituents from measured IOPs, it is useful to identify categories of constituents, each of which makes a distinct contribution to the total IOPs. Typically, categories are selected on the basis of a combination of operational and functional criteria. For total $a(\lambda)$, for example, Prieur and Sathyendranath (1981) suggested partitioning into contributions from water $a_w(\lambda)$, chromophoric dissolved organic matter (CDOM) $a_{CDOM}(\lambda)$, phytoplankton $a_{ph}(\lambda)$ and non-algal particles (NAP) $a_{NAP}(\lambda)$:

$$a(\lambda) = a_w(\lambda) + a_{CDOM}(\lambda) + a_{ph}(\lambda) + a_{NAP}(\lambda). \tag{8.1}$$

Similar summations can be applied to other IOPs such as $b(\lambda)$, backscattering $b_b(\lambda)$ and the beam attenuation coefficient $c(\lambda)$, which is defined as the sum

$$c(\lambda) = a(\lambda) + b(\lambda). \tag{8.2}$$

It should be emphasized that (8.1) represents an example set of constituent categories, and the concept can be generalized to as many levels as practical or important for specific problems; in principle, different taxa of phytoplankton can be included as separate terms on the right-hand side or NAP can be separated into organic and inorganic forms, for example.

The concept of a constituent-specific optical coefficient can also be useful for understanding and predicting optical variability. A specific coefficient is one that is normalized by an index of concentration for the constituent of interest. A common example is chlorophyll-specific phytoplankton absorption:

$$a^*_{ph}(\lambda) = \frac{a_{ph}(\lambda)}{\mathrm{Chl}}, \tag{8.3}$$

where Chl indicates the chlorophyll *a* concentration in the water. Other examples include carbon-specific scattering coefficients for phytoplankton or mass-specific scattering coefficients for mineral particles. Specific coefficients are useful because variation in the total mass of constituents is the first order source of variability in absolute IOPs. This means that, typically, specific coefficients are less variable than absolute ones, with the residual variability in specific coefficients due to differences in the characteristics of material within a particular category (e.g. changes in species composition in the phytoplankton or changes in the chemical composition or structure of mineral particles).

Linear spectral mixing is another concept that has been used to help characterize and explain IOP variability. In its simplest form, this approach can be used to represent optical contributions of two constituents, each of which has a distinct spectral shape. For example, one may consider that total particle backscattering ($b_{b,p}(\lambda)$) results from backscattering by two pools of particles, one with characteristic spectral shape $\mathbf{b_{b1}}$ and the other with shape $\mathbf{b_{b2}}$:

$$b_{b,p}(\lambda) = A_1\mathbf{b_{b1}} + A_2\mathbf{b_{b2}} \tag{8.4}$$

In this expression, $\mathbf{b_{b1}}$ and $\mathbf{b_{b2}}$ represent wavelength-dependent basis vectors that describe the spectral shape of backscattering associated with particle type 1 and 2, respectively; these basis vectors are scaled to be non-dimensional. A_1 and A_2 represent the amplitudes of the scattering by particle types 1 and 2 respectively; these are scalars and thus do not vary with wavelength. If assumptions can be made concerning the relevant basis vectors and the bulk IOP is measured at multiple wavelengths, then statistical methods can be used to estimate the unknown amplitude terms in a linear mixing model such as that expressed in (8.4). The approach can be generalized to any number of terms, but unique solutions for the amplitudes depend on the spectral distinctness of the basis vectors and require at least as many spectral bands as basis vectors.

As indicated in (8.1), water molecules are important light absorbers and additionally they contribute to light scattering. Water itself is not, however, an important source of variability in IOPs in marine waters. There are some variations in spectral light attenuation by 'pure' water depending on factors such as temperature and salinity (see Pegau et al., 1997, for example), but, for the purposes of describing variations in the optical properties of the ocean, these effects are small and are not discussed further here. The following sections focus on particular water constituents and their effects on IOPs.

8.2.1 Absorption

8.2.1.1 CDOM

For optical oceanographers and many marine chemists, CDOM is operationally defined by its passage through a small pore size filter (usually 0.2 μm) and its ability to absorb visible and ultraviolet radiation. CDOM is a poorly characterized portion of the total dissolved organic matter (DOM) pool and there are no routine analytical techniques for chemically quantifying total CDOM; for this reason, CDOM is frequently quantified in terms of its measurable optical properties (i.e. absorption or fluorescence). Especially in coastal waters with substantial riverine inputs, absorption by CDOM can be very high compared with other constituents, and so it influences the quantity and colour of light penetrating into and reflecting from the upper ocean. Even in the open ocean, however, absorption by CDOM cannot be neglected (Nelson et al., 1998).

CDOM absorption is characterized by smoothly varying spectral dependence with amplitude tending to increase exponentially towards blue and ultraviolet wavelengths. For this reason its contribution to absorption is usually represented by an exponential function:

$$a_{\mathrm{CDOM}}(\lambda) = a_{\mathrm{CDOM}}(\lambda_0)\mathrm{e}^{-S(\lambda-\lambda_0)}, \tag{8.5}$$

where λ_0 represents a reference wavelength and S is the slope of the exponential increase with decreasing wavelength (Bricaud et al., 1981). Both the amplitude and the spectral slope of a_{CDOM} depend on the composition of the dissolved organic matter pool and this in turn depends on a variety of source and sink processes. Terrestrial input, primarily from riverine sources, is significant; in addition, other processes including photooxidation (enhanced by CDOM's strong ultraviolet absorption) and local microbial activity can lead to production or loss of different forms of CDOM. These are discussed in more detail below.

CDOM fluorescence can be used as a proxy for a_{CDOM}. This topic will not be discussed further here, except to note that, as reviewed by Blough and Del Vecchio (2002), the relationship between CDOM fluorescence and absorption is complex, so regionally and temporally specific relationships must be established empirically.

8.2.1.2 Phytoplankton

As photosynthetic organisms, phytoplankton contain high concentrations of pigments that harvest energy from sunlight. These pigments consist of different chlorophylls and carotenoids (and, in certain taxa, biliproteins) present in varying amounts (Jeffrey and Vesk, 1997) and each type of pigment has particular spectral properties that lend phytoplankton their characteristically featured absorption spectra. Due to the ubiquitous presence of chlorophylls, absorption peaks at blue (~440 nm) and red wavelengths (~675 nm) are always present, with the blue peak broadened and enhanced by accessory pigments (Bidigare et al., 1990; see also Morel, 2007 – Chapter 4 this volume; Roesler and Boss, 2007 – Chapter 5 this volume). Pigment composition, and thus general light absorption characteristics, are partly constrained by phylogeny (Jeffrey and Vesk, 1997), but there are also important variations associated with environmental factors that affect growth (e.g. Kana et al., 1988; Sosik and Mitchell, 1991). Pigment composition and physiological status also affect the amount of light energy absorbed by phytoplankton that is reemitted as fluorescence at red wavelengths (discussed in detail in Babin, 2007 – Chapter 7 this volume).

The first order source of variation in light absorption by phytoplankton is total biomass and this, of course, depends on complex ecological and environmental factors that regulate phytoplankton growth and loss rates. Secondary effects with important consequences for how phytoplankton absorb light include variations in intracellular pigment concentration and composition and variations in cell size and shape; size and shape directly impact pigment package effects (e.g. Morel and Bricaud, 1981*a*, 1986).

8.2.1.3 Non-algal particles

Marine particles besides phytoplankton are also known to absorb light. In natural samples it is difficult to separate the broad category of NAP into its different contributors, which can include heterotrophic organisms such as bacteria and micrograzers, other organic particles of a detrital nature such as faecal pellets and cell debris, and

various mineral particles of both biogenic (e.g. calcite liths and shells) and terrestrial (e.g. clays and sand) origin. In comparison with phytoplankton, much less is known about the optical properties of these particles, but some generalizations have emerged.

In particular, in coastal and open ocean waters total NAP absorption tends to exhibit an absorption spectrum that monotonically increases with decreasing wavelength, similar in form to that observed for CDOM (e.g. Iturriaga and Siegel, 1989; Roesler et al., 1989; Sosik and Mitchell, 1995; Nelson et al., 1998). Consequently, a_{CDOM} can be replaced by a_{NAP} in (8.5) to provide an adequate description of NAP absorption. Despite the similar functional form found for a_{NAP} and a_{CDOM}, S values are generally not the same for these two pools, with lower values typically characteristic of particles (Roesler et al., 1989; Bricaud and Stramski, 1990; Nelson and Guarda, 1995; Bricaud et al., 1998). These observations are based on the operational definition of NAP absorption as that which is retained on a filter and not extractable by methanol following the method first proposed by Kishino et al. (1985). Because of the similar spectral character of CDOM and NAP, for some applications these pools have been combined into a single class, referred to as coloured detrital matter (CDM; which is technically a misnomer as it also includes living and inorganic matter), whose absorption follows (8.5) with a composite S parameter that will vary with the relative contributions of CDOM and NAP (Roesler et al., 1989; Siegel and Michaels, 1996; Garver and Siegel, 1997; Carder et al., 1999).

In some waters absorption by inorganic particles may also be significant, but this topic has not been well studied. Work is under way to characterize the absorption properties of specific types of mineral particles that may be important in marine systems (Babin and Stramski 2004; Stramski et al., 2004).

8.2.2 Scattering and backscattering

All particulate material whose index of refraction differs from the surrounding medium will scatter light. The amount of scattering is influenced by particle size and shape and by any absorption that occurs within the particle. In contrast to absorption, scattering is not completely characterized simply by specifying its wavelength dependence; it also has angular dependence. Total scattering is summed over all possible scattering angles, but it is also possible to define scattering coefficients over particular angular subsets. Backscattering, which is simply scattering integrated over the backward hemisphere with respect to the direction of light incidence (see Morel, 2007 – Chapter 4 this volume – for details), is a quantity that has received a lot of attention due to its importance for ocean-colour interpretation (see Section 8.4.2). As for total scattering, backscattering depends on particle concentration, size, shape and complex refractive index. Theoretical considerations show that backscattering is generally enhanced relative to forward scattering as particle size decreases, so different particles may dominate total scattering and backscattering in natural waters.

Although the dependence of light scattering on particle size, shape and refractive index is complex, some generalizations can be made on the basis of Mie theory, which applies to homogeneous, spherical particles (see e.g. Morel and Bricaud, 1986). For a given wavelength, scattering by polydisperse particles tends to increase with average particle size and with the average real part of the refractive index, so highly refractive mineral particles scatter more light than a population of bacteria of similar concentration and size distribution, for example. Furthermore, the wavelength dependence of the scattering cross-section tends to be steeper for smaller particles. Because of its

extreme small size (usually defined $<0.2\ \mu$m) and relatively dilute nature (compared with water molecules, for example), light scattering by CDOM can be neglected (see e.g. analyses by Ulloa et al., 1994; Babin et al., 2003*a*).

Mie theory indicates that scattering of idealized (homogeneous and spherical) non-absorbing particles varies with wavelength in a manner that depends systematically on particle size and refractive index. The wavelength dependence is often represented according to

$$b_{\mathrm{p}}(\lambda) = b_{\mathrm{p}}(\lambda_0)\left(\frac{\lambda}{\lambda_0}\right)^{-\gamma}, \tag{8.6}$$

where λ_0 is a reference wavelength and γ represents a hyperbolic slope (Morel and Bricaud 1981*b*; Morel 1988). For scattering by particles that are small relative to the wavelength of light (e.g. bacteria), γ is approximately 2, whereas for larger particles γ approaches 0 (Morel and Ahn, 1990, 1991; Ahn et al., 1992). For polydisperse particles whose abundance increases with decreasing size according to a power law ('Junge' distribution), (8.6) has also been shown to hold (e.g. Boss et al., 2001*a*). Furthermore, (8.6) is useful for absorbing particles whose imaginary refractive index varies monotonically with wavelength (Stramski et al., 2001). If (8.6) is considered for backscattering by small monodisperse particles, γ approaches 0 (e.g. Ahn et al., 1992); whereas, Ulloa et al. (1994) have shown that, for polydisperse particles with a Junge-type size distribution, the backscattering ratio

$$\tilde{b}_{\mathrm{b,p}}(\lambda) = \frac{b_{\mathrm{b,p}}(\lambda)}{b_{\mathrm{p}}(\lambda)} \tag{8.7}$$

is spectrally neutral, so that $b_{\mathrm{p}}(\lambda)$ and $b_{\mathrm{b,p}}(\lambda)$ have the same γ. Non-absorbing particles and Junge-type size distributions are special cases, however, and in general $\tilde{b}_{\mathrm{b,p}}(\lambda)$ should be considered highly dependent on particle size and refractive index.

In phytoplankton cells, absorption by pigments reduces scattering preferentially at wavelengths where absorption is higher. For these and other absorbing particles, simple generalizations about spectral shape of $b_{\mathrm{p}}(\lambda)$, $b_{\mathrm{b,p}}(\lambda)$, and $\tilde{b}_{\mathrm{b,p}}(\lambda)$ cannot be made and a wide range of shapes are possible depending on the combination of particle size and complex refractive index (e.g. Bricaud et al., 1983; Bricaud and Morel, 1986; Stramski and Kiefer, 1991; Ahn et al., 1992; Stramski et al., 2001), as well as other factors such as particle shape and heterogeneity (Zaneveld and Kitchen, 1995; Gordon and Du, 2001).

For typical particle properties encountered in ocean waters, the functional form of (8.6) can reasonably be applied to $c_{\mathrm{p}}(\lambda)$, even when some of the underlying assumptions are relaxed. This has recently been discussed in detail by Boss et al. (2001*a*).

8.3 Relationships between IOPs and constituents

This section contains selected examples of documented relationships between IOPs and seawater constituents. Some emphasis is on studies in coastal waters, but reference to key work in open ocean waters is included as well. Not only do open ocean 'end-members' often influence coastal systems, but investigations of open ocean 'Case 1'

(Morel and Prieur, 1977) waters often set the context for characterizing more complex 'Case 2' coastal regions.

8.3.1 Chlorophyll

Since the pioneering work of Yentsch (1960, 1962), which documented that phytoplankton pigments have a significant effect on light attenuation in aquatic ecosystems, there has been a great deal of work relating optical variability to Chl. Due to its ubiquitous presence in phytoplankton and its relative ease of measurement (e.g. Yentsch and Menzel, 1963; Holm-Hansen et al., 1965), Chl is the most commonly used index of phytoplankton biomass. Especially for open ocean conditions and for absorption coefficients, relationships with Chl have been able to explain a large amount of the observed variance.

8.3.1.1 Particle absorption

Perhaps the most reliable optical relationships have been documented between chlorophyll and particle absorption [$a_p(\lambda) = a_{ph}(\lambda)+a_{NAP}(\lambda)$] for Case 1 waters. Not surprisingly, this is especially true for $a_{ph}(\lambda)$, which in general is positively, although nonlinearly, correlated with Chl (Figure 8.1A). As described in Section 8.2.1, second-order variations in $a_{ph}(\lambda)$ can be examined by considering Chl-specific absorption (8.3). Notably, a variety of studies in natural waters have suggested that $a^*_{ph}(\lambda)$ values tend to be inversely related to Chl (e.g. Mitchell and Kiefer, 1988; Yentsch and Phinney, 1989; Bricaud and Stramski, 1990; Carder et al., 1991; Babin et al., 1995; Sosik and Mitchell, 1995). Bricaud et al. (1995*b*) synthesized a large data set and proposed that a power law could adequately describe this dependence across a wide range of ocean regions:

$$a^*_{ph}(\lambda) = A(\lambda)\,\mathrm{Chl}^{B(\lambda)}, \tag{8.8}$$

where parameters $A(\lambda)$ and $B(\lambda)$ are statistically determined (Figure 8.1B). There is no mechanistic basis for this particular mathematical formulation and others have been proposed (e.g. Cleveland, 1995; Lutz et al., 1996; Ciotti et al., 1999). As recently reviewed by Bricaud (2002), there is currently little consensus with respect to details of the various $a_{ph}(\lambda)$ and Chl relationships that have been published.

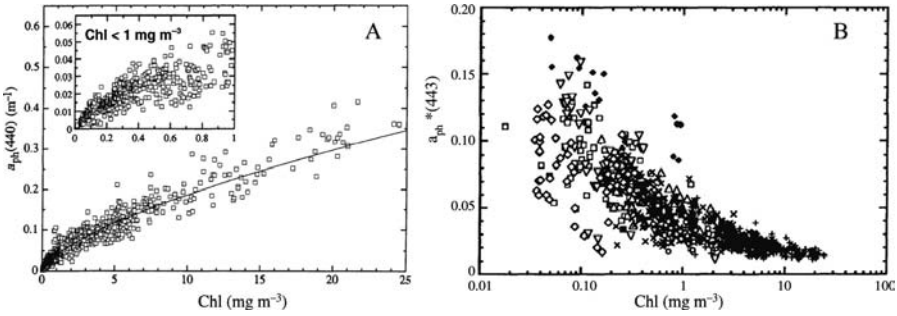

Figure 8.1
Dependence of A, $a_{ph}(440)$; B, $a^*_{ph}(44$; on Chl for a wide range of Case 1 waters. The curve in A represents a least-squares power law fit.
Source: Bricaud et al. (1995*b*).

As mentioned in Section 8.2.2, substantial variations in $a^*_{ph}(\lambda)$ are expected due to differences in accessory pigment composition and in cell size. The applicability of relationships such as that expressed by (8.8) suggests that, in natural systems, there is a general co-variation between these cell properties and bulk Chl for example, smaller cells (with associated higher $a^*_{ph}(\lambda)$) tend to dominate in oligotrophic (i.e. low Chl) waters (see Ciotti et al., 1999 for more discussion of this topic). This is consistent with well-documented changes in planktonic community structure with trophic status (e.g. Yentsch and Phinney, 1989; Chisholm, 1992).

Despite these generalizations, it is not surprising that some variance in $a_{ph}(\lambda)$ and $a^*_{ph}(\lambda)$ cannot be explained simply by Chl. In fact, there is substantial unexplained variance in the global relationships examined by Bricaud et al. (1995*b*). Cleveland (1995) examined regional dependence in more detail and suggested that temperate and subtropical regions are statistically similar, but that different parameterization is required for subpolar waters. In addition, there is evidence that seasonally (Nelson and Guarda 1995) and regionally (Lutz et al., 1996; Reynolds et al., 2001) varying parameterization may be required for certain areas, and some studies of coastal areas have shown no dependence of $a^*_{ph}(\lambda)$ on Chl, within the observed dynamic range (Hoepffner and Sathyendranath, 1992). The importance of changes in accessory pigment composition (which does not necessarily covary with Chl) in explaining natural variability in $a^*_{ph}(\lambda)$ has been emphasized in several studies (e.g. Sosik and Mitchell, 1995; Allali et al., 1997). Some variations in the accessory pigment-to-chlorophyll ratios can be attributed to differences among species, while others arise from physiological responses such as photoacclimation.

In a follow-up study to their work on $a_{ph}(\lambda)$, Bricaud et al. (1998) examined patterns of variability in $a_p(\lambda)$ with respect to Chl. They reported that a similar functional form (i.e. (8.8) with $a^*_p(\lambda)$ replacing $a^*_{ph}(\lambda)$ can be useful. Their findings suggest that, for Case 1 waters, $a_{NAP}(\lambda)$ is roughly proportional to $a_p(\lambda)$, with NAP making an average contribution of 27%. Earlier observations (Bricaud and Stramski, 1990) suggested that the ratio $a_{NAP}(\lambda)/a_p(\lambda)$ might increase at lower Chl, however, more extensive studies by Cleveland (1995) and Bricaud et al. (1998) reported that, while observed variance in the ratio is high, there is no apparent trend as a function of Chl. Some observations do suggest that there are systematic deviations from the average 25–30% contribution for NAP in certain regions, including areas of the Southern Ocean (Sosik et al., 1992) and the equatorial Pacific (Bricaud et al., 1998). For Case 2 waters with significant resuspension effects or terrigenous sources of NAP, there is no expectation that $a_{NAP}(\lambda)$ will be proportional to $a_p(\lambda)$, and systematic relationships have not been described.

8.3.1.2 Beam attenuation, scattering and backscattering

To the extent that Chl represents an index of particle load, positive correlations may be expected with $c(\lambda)$, $b(\lambda)$ and $b_b(\lambda)$. These relationships have been explored principally because of their practical implications for Chl retrieval from satellite ocean-colour data (e.g. Gordon and Morel, 1983; Gordon et al., 1988). Early observational work summarized in Gordon and Morel (1983) suggested that, for Case 1 waters spanning a wide range of Chl, $b_p(550)$ tends to be positively correlated with Chl in a nonlinear manner that can be statistically described with a power law similar to (8.8) (but with $b_p(550)$ replacing $a^*_{ph}(\lambda)$). Voss (1992) and more recently Loisel and Morel (1998) used new observations of c_p to reevaluate this type of relationship; their

findings confirm the early generalization but also emphasize that a large amount of variance in particle scattering or attenuation cannot be explained simply on the basis of Chl (Figure 8.2). In Case 2 waters, scattering that is uncorrelated with Chl can be due to contributions of materials such as suspended sediments (e.g. Gould et al., 1999; Sosik et al., 2001), but even under Case 1 conditions, there can be important effects of non-phytoplankton scatterers such as heterotrophic organisms, particulate detritus, minerals and bubbles (e.g. Morel and Ahn, 1990; Stramski et al., 2001; Green et al., 2003*a*). Furthermore, scattering-to-chlorophyll relationships are expected to be influenced by variations in cellular carbon-to-chlorophyll (which in turn affects complex refractive index) associated with interspecific differences and photoacclimation in phytoplankton (Morel, 1987; Stramski and Morel, 1990). These effects should be evident in natural observations (e.g. Kitchen and Zaneveld, 1990; Loisel and Morel, 1998), but they cannot be unambiguously diagnosed with scattering measurements alone.

The relationship between $b_{b,p}(\lambda)$ and Chl is even more complex and a global synthesis of observations has not been put forward, though there is some evidence that Chl can explain a portion of the variability in $b_{b,p}(\lambda)$ on a regional basis (Balch et al., 2001; Reynolds et al., 2001). Models have been proposed that represent Chl dependence in such a way that $b_{b,p}(\lambda)$ amplitude increases with increasing Chl, while

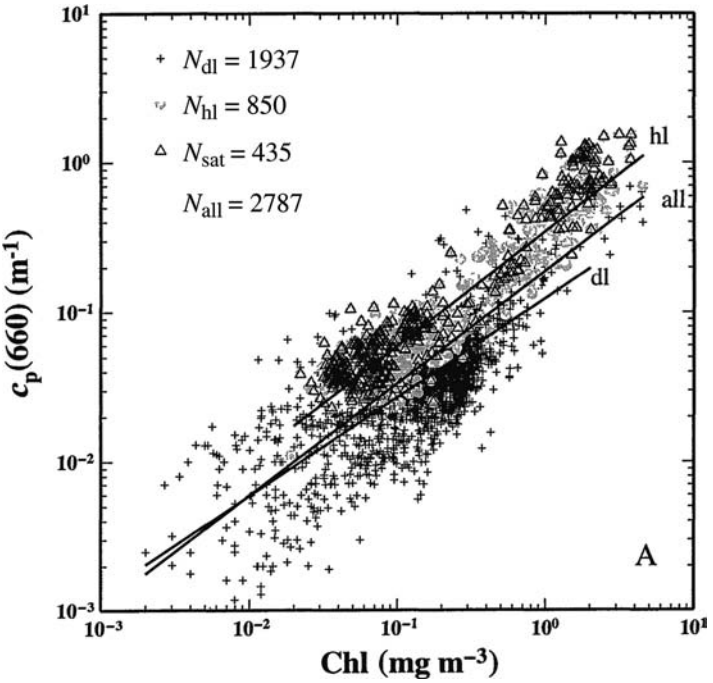

Figure 8.2
Dependence of $c_p(660)$ on Chl for a wide range of Case 1 waters. Lines indicate linear regression results, with separate lines for subsets of points from the upper layer with homogeneous Chl (hl) and from the deeper layer (dl).
Source: Loisel and Morel (1998).

the spectral slope (γ in a function of the form given by (8.6)) decreases with Chl (Gordon et al., 1988; Morel, 1988; Morel and Maritorena, 2001). Morel and Maritorena (2001) reviewed published approaches to this problem and concluded that consensus is not yet evident. Indeed, this may be an elusive goal as various lines of evidence from theoretical and observational studies suggest that, typically, phytoplankton are not an important source of $b_{b,p}(\lambda)$ variability in natural waters (Ahn et al., 1992; Stramski et al., 2001; Green et al., 2003a). Exceptions to this generalization occur in waters dominated by phytoplankton taxa with internal gas vacuoles (e.g. *Trichodesmium* sp.; Subramaniam et al., 1999) or that produce coccoliths (e.g. *Emiliania huxleyi*; Holligan et al., 1983; Balch et al., 1991). Some intriguing recent observations suggest that, during blooms of the red-tide species *Karenia brevis*, $_{b,p}(\lambda)$ varies with Chl in a manner that differs from non-bloom conditions (Cannizzaro et al., 2007) (Figure 8.3). It is probable, however, that this reflects not the *K. brevis* cells directly, but rather some other constituent that covaries with the blooms.

Because the angular distribution of scattered light depends on the properties of the particles (i.e. size, shape and composition), indices such as the dimensionless backscattering ratio, $\tilde{b}_{b,p}$ (8.7), have also been examined with respect to dependence on Chl. While there is no simple theoretical motivation for such a relationship, one may be expected given systematic shifts in the particle composition in planktonic systems as a function of trophic status, for which Chl can be a general indicator (as discussed above, for example, in the case of observed $a^*_{ph}(\lambda)$ dependence on Chl). Inferences from analysis of other optical properties (e.g. Gordon et al., 1988; Morel, 1988; Morel and Maritorena, 2001) and, more recently, direct scattering observations

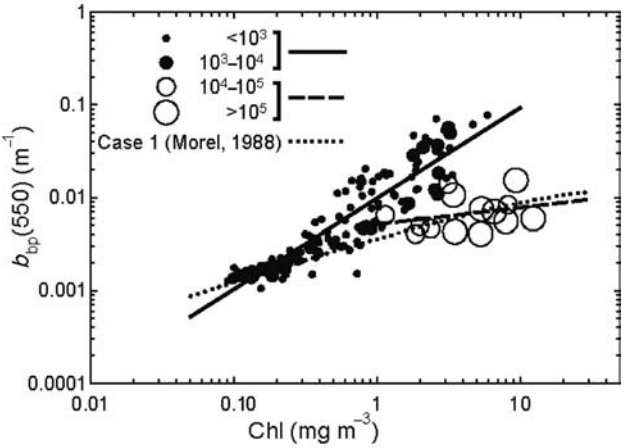

Figure 8.3
Dependence of $b_{b,p}(550)$ on Chl for the West Florida shelf during *K. brevis* bloom and non-bloom conditions. Symbols indicate ranges of observed cell concentration for *K. brevis* (cell l^{-1}) and the Case 1 water Chl-dependent $b_{b,p}(550)$ model of Morel (1988) is shown for comparison. Lines show regression results for different ranges of cell concentration and the model of Morel (1988).
Source: Cannizzaro et al. (2007).

(Twardowski et al., 2001) suggest that $\tilde{b}_{b,p}(\lambda)$ is often lower in high-chlorophyll waters (Figure 8.4). This is consistent with a trend towards more relative backscattering by large, low refractive index particles (e.g. phytoplankton cells) under eutrophic conditions. Nonetheless, variance in $\tilde{b}_{b,p}(\lambda)$ that is not explained by Chl remains high (Figure 8.4).

For scattering in general, and backscattering especially, lack of routine measurement capabilities has limited knowledge of patterns and sources of natural variability. With the recent introduction of new sensor technologies (Moore et al., 1992; Maffione and Dana, 1997; Moore et al., 2000), this situation is changing and new studies further exploring the dependence of scattering properties on water constituents are emerging (e.g. Twardowski et al., 2001; Chang et al., 2002; Babin et al., 2003*a*; Boss et al., 2007). This is an active area of research that is beginning to elucidate how changes in particle load and particle characteristics (i.e. size and complex refractive index) combine to determine natural light scattering properties (see below).

8.3.1.3 CDOM

Principally in an effort to simplify interpretation of remotely sensed ocean colour, there have been attempts to explain variability in the magnitude of a_{CDOM} on the basis of Chl (or a_{ph}). Some empirical results show a positive relationship (i.e. higher a_{CDOM} with higher Chl), but relationships between a_{CDOM} and Chl depend strongly on location and, as first documented by Bricaud et al. (1981), unexplained variance can be very high. In a recent example, Ciotti et al. (1999) used a linear relationship with $a_{ph}(443)$ to parameterize $a_{CDOM}(443) + a_{NAP}(443)$ in a semi-analytical model for optical properties. They found, however, that a separate 'high-CDOM' relationship was necessary for a Canadian coastal embayment, compared with coastal waters off Oregon. Moreover, for the high-CDOM case, the explained variance was very low (<10%). In a different study involving Southern Ocean waters, Reynolds et al. (2001)

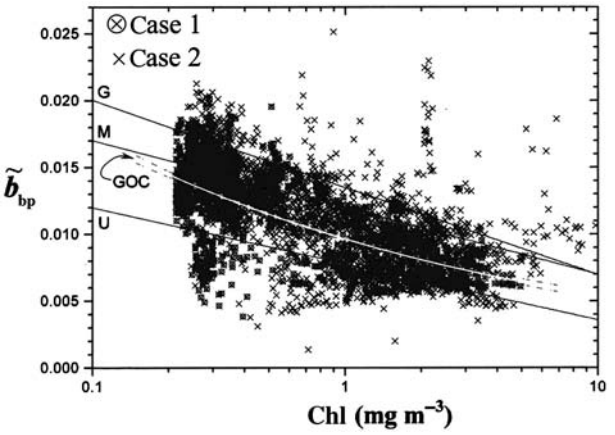

Figure 8.4
Dependence of $\tilde{b}_{b,p}$ on Chl observed in Case 1 and Case 2 waters from the Gulf of California. GOC indicates the least-squares hyperbolic fit and G, M and U show the model relationships proposed by Gordon et al. (1988), Morel (1988) and Ulloa et al. (1994), respectively.
Source: Twardowski et al. (2001).

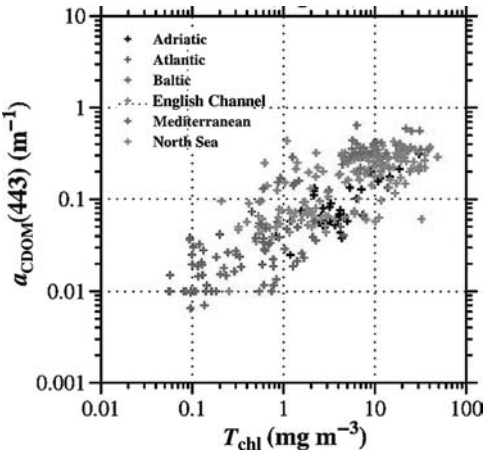

Figure 8.5
Dependence of $a_{CDOM}(443)$ on Chl observed for a wide range of European coastal waters.
Source: Babin et al. (2003*b*).

showed that 55% of the variance in $a_{CDOM}(400)$ could be predicted from Chl with a power law (i.e. (8.8) with $a_{CDOM}(400)$ replacing $a^*_{ph}(\lambda)$). This approach may be least applicable for oligotrophic open ocean waters since, as reported by Nelson et al. (1998), there is no evidence of covariation between a_{CDOM} and Chl for seasonal variations in the Sargasso Sea. Probably the most complicated conditions exist over a range of coastal water types. Babin et al. (2003*b*) have emphasized this for European waters; their observations showed covariation between $a_{CDOM}(443)$ and Chl across the full dynamic range observed but also that unexplained variance can be high and that site-to-site differences are substantial (Figure 8.5). Taken together, these studies emphasize that relationships between a_{CDOM} and Chl or a_{ph} should not be assumed, and site-specific empirical verification is required before this approach can be useful.

8.3.2 CDOM and salinity

The limited capability of chlorophyll to explain variability in a_{CDOM} in many coastal locations can be understood by considering the importance of freshwater sources of CDOM. Some of the most compelling evidence for this comes from studies that document a strong correlation between a_{CDOM} and salinity. Recently, Blough and Del Vecchio (2002) reviewed knowledge about CDOM in coastal waters, including a synthesis of salinity relationships (Figure 8.6). It is apparent from these results that freshwater typically exhibits much higher values of a_{CDOM} (10 m^{-1} or greater at 355 nm) than oceanic waters (0.1 m^{-1} or less at 355 nm) and that, for many systems, first order variations in a_{CDOM} result from near-conservative mixing between freshwater and marine end members. It is also evident that the freshwater end members vary dramatically from system to system. At this time, generalizations about this variability are lacking and regional characterization is necessary to define the expected relationship between CDOM and salinity.

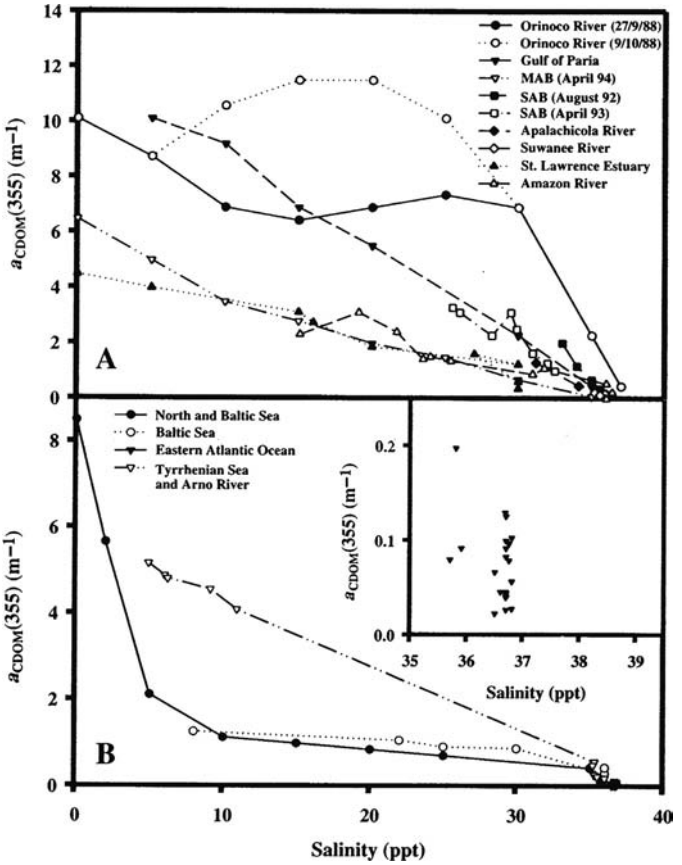

Figure 8.6.
Dependence of $a_{CDOM}(355)$ on salinity compiled from investigations of many riverine to coastal ocean systems.
Source: Blough and Del Vecchio (2002).

Relationships between a_{CDOM} and salinity are more complicated in coastal systems with mixing of more than two important water masses, as has been postulated to explain the nonlinear relationships for the North and Baltic Sea observations of Højerslev et al. (1996), for example, and the Orinoco River outflow studied by Blough et al. (1993) (Figure 8.6). Additional sources of complexity can arise from *in situ* production and loss processes. The best documented of these is photochemical oxidation, which is expected to vary seasonally in its importance. A variety of studies have shown lower a_{CDOM} for a given salinity in summer surface waters compared with other times of year and depths (e.g. Vodacek et al., 1997; Boss et al., 2001*b*), and incubation experiments have shown high rates of DOM photochemical oxidation (Kieber et al., 1990; Miller and Zepp, 1995).

Notwithstanding the strong inverse correlations between CDOM and salinity often observed over large salinity gradients, it is important to emphasize that in many locations freshwater inputs do not control CDOM variability. At salinities >~35 there is no correlation with salinity (Figure 8.6, inset). In fact, efforts to detect terrestrial

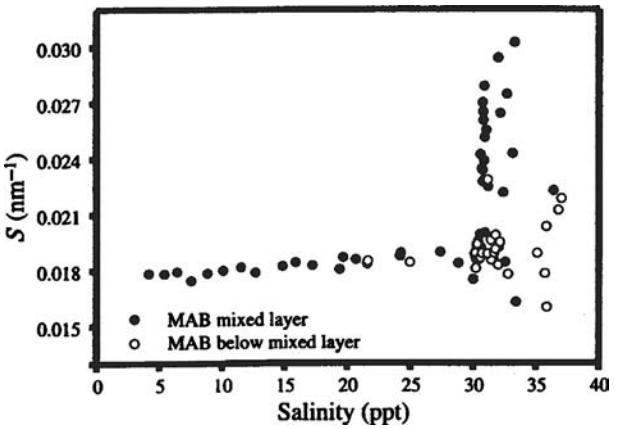

Figure 8.7
Dependence of S for a_{CDOM} on salinity observed during a transect from Delaware Bay into the continental shelf waters of the Middle Atlantic Bight. *Source*: Blough and Del Vecchio (2002).

DOM markers in the open ocean have suggested that terrestrial DOM contributes minimally in open ocean environments (Opsahl and Benner 1997). Blough and Del Vecchio (2002) point out that, given present-day annual riverine inputs and no oceanic losses, the open ocean would reach freshwater a_{CDOM} levels in ~35,000 years. The observed large a_{CDOM} gradient between freshwater and the open ocean can only be maintained if there are loss processes acting with timescales of the order of 100 years. Observations suggest that *in situ* microbial processes must be a net source of marine a_{CDOM} (Nelson et al., 1998; Twardowski and Donaghay, 2001) and that photochemical degradation of terrestrial CDOM must be significant (see review by Mopper and Kieber, 2002).

Whereas the magnitude of a_{CDOM} tends to decrease with increasing salinity, the spectral slope tends to increase (Figure 8.7). This is probably indicative of different CDOM composition. Carder et al. (1989), for example, showed that S values are higher for marine fulvic acids than for marine humic acids. Observed S values range approximately 3-fold (~0.01–0.03 nm^{-1}), with typical values of 0.015 nm^{-1} for coastal waters and 0.025 nm^{-1} for open ocean waters (Blough and Del Vecchio, 2002). There is also evidence that S values increase in response to photodegradation of CDOM (Vodacek et al., 1997; Twardowski and Donaghay, 2002). Note that care should be taken in applying (8.5) and comparing S values from different studies owing to effects of curve fitting procedure and choice of wavelength range. As detailed in Blough and Del Vecchio (2002), nonlinear curve fitting over the full ultraviolet and visible spectrum may provide the most robust and intercomparable results, while recent work by Twardowski et al. (2004) suggests that a hyberbolic model (following the form of (8.6)) may be preferable to the exponential (8.5) most commonly used to date.

8.3.3 CDOM and DOC

Dissolved organic carbon (DOC) represents an important component of the marine carbon budget and variations in its concentration are of broad interest to ecologists and geochemists. Indices of the coloured portion of DOC may be assessed from platforms

that include aircraft and earth-orbiting satellites (e.g. Vodacek et al., 1995; Siegel et al., 2002), but CDOM reflects a variable fraction of the total DOM pool and consequently relationships between CDOM properties and DOC continue to be investigated.

For coastal environments that experience freshwater influence, positive and generally linear relationships between DOC and CDOM absorption (or CDOM fluorescence) have been documented. For example, Vodacek et al. (1997) showed this for transects from Delaware Bay to the Sargasso Sea (Figure 8.8A). For river-influenced regions, these relationships typically show a high positive intercept for DOC, indicating a background level of non-coloured material. Ferrari (2000) has suggested, however, that this may not be the case for more oceanic waters (see Figure 8.8B). It is noteworthy that, in contrast to findings for coastal waters, Nelson et al. (1998) and Nelson and Siegel (2002) have shown that DOC and CDOM absorption are completely uncorrelated in the subtropical Sargasso Sea (Figure 8.8C). Even for a single coastal region, the relationship between DOC and CDOM cannot be assumed to be stable because the two can be differentially affected by source and loss processes. In the observations of Vodacek et al. (1997), for example, photodegradation of CDOM probably caused the lower CDOM levels relative to DOC in summer surface waters when compared with spring, late autumn, and also with summer samples from below the mixed layer (Figure 8.8A).

Some recent studies have suggested that CDOM absorption properties can be used to diagnose the occurrence and distribution of some different forms of CDOM containing compounds. At least two broad classes of DOM have been proposed to occur and be differentiable in marine systems: relatively refractory (slow average turnover rate) low molecular weight compounds and more labile high molecular weight compounds (e.g. Santschi et al., 1995; Guo et al., 1996). These pools are expected to have different absorption efficiency and spectral character. For coastal waters off Washington, Twardowski and Donaghay (2002) suggest that lower a_{CDOM} amplitudes and especially higher S values are characteristic under situations when there have been cumulative effects of photooxidation, and low molecular weight compounds are expected to dominate. For Equatorial Pacific waters, Simeon et al. (2003) measured two fractions of CDOM, <0.2 μm and 0.2–0.7 μm, and showed that the smaller sized material typically dominated in deep waters and exhibited higher S values compared with the larger size class in surface waters, which may be strongly influenced by biological production of labile DOM (e.g. Santschi et al., 1995).

8.3.4 SPM, POC and PIC

For most optical techniques, it is not possible to measure separately the contributions of different types of particles to the bulk signal from a water volume. For this reason many researchers have examined the relationships between optical properties, especially light scattering, and various indices of total particle load. The case of chlorophyll (discussed above) is one example, but other indices can be more appropriate depending on the environment or problem of interest. Almost without exception, these approaches have been empirical in nature with applications ranging from studies of plankton ecology to bottom boundary layer dynamics to pollution monitoring.

8.3.4.1 Beam attenuation, scattering and backscattering

Optically calibrated scattering coefficients are difficult to measure directly, so observations relating to particle load have typically been based on $c(\lambda)$ measurements at

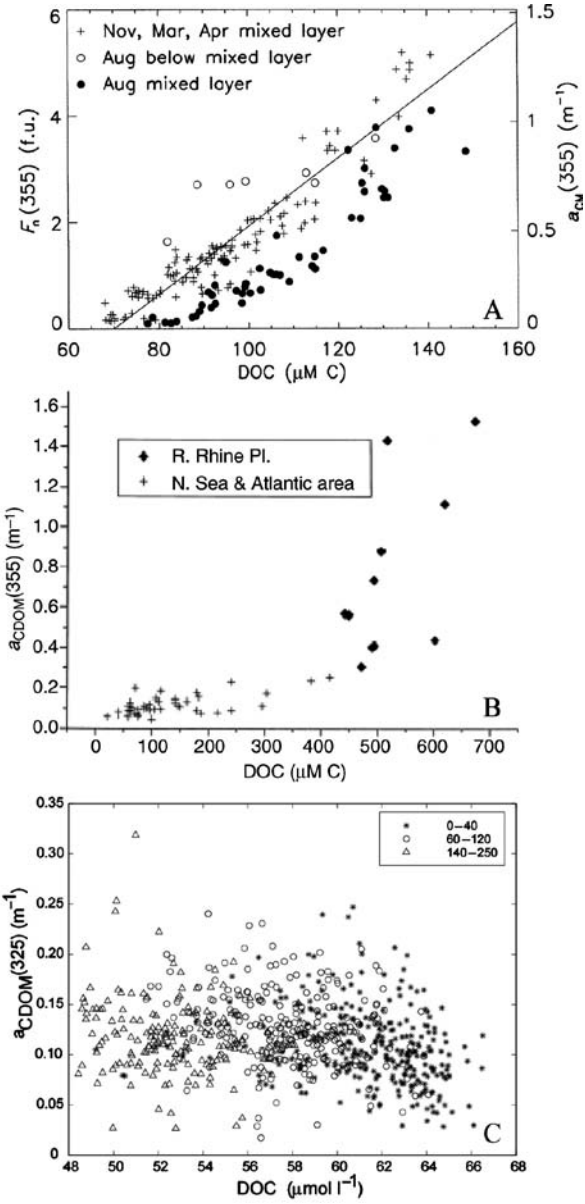

Figure 8.8
Dependence of A, CDOM fluorescence (left *y*-axis) and $a_{CDOM}(355)$ (right *y*-axis) on DOC observed during transects from Delaware Bay across the continental shelf and into the eastern Sargasso Sea;
B, $a_{CDOM}(355)$ on DOC in the Rhine River plume and other European coastal waters;
C, $a_{CDOM}(325)$ on DOC at the BATS station in the Sargasso Sea. Legend in C indicates sampling depth (m).
Sources: A, Vodacek et al. (1997); B, Ferrari (2000); C, Nelson and Siegel (2002).

wavelengths where either $a(\lambda) - a_w(\lambda)$ is presumed to be small or $a(\lambda) - a_w(\lambda)$ is also measured (such as with an ac-9 meter, see Roesler and Boss, 2007 – Chapter 5 this volume).

Total suspended particulate matter (SPM) is a common currency that is usually expressed as dry weight of particles (per unit water mass or volume) and is also referred to by different terms including seston and total suspended solids. Typically, SPM is taken to include mineral particles and plankton, as well as organic particles of detrital nature. Positive correlations between SPM and $b(\lambda)$ (or c at 660 nm) have been documented under a variety of coastal (e.g. Baker and Lavelle, 1984; Gardner et al., 2001; Babin et al., 2003*a*; Bergmann et al., 2004) and open ocean conditions (e.g. Gordon and Morel, 1983; Bishop, 1986; Gundersen et al., 1998) (Figure 8.9). Although scattering relationships with SPM are expected to be less variable than those with total particle volume or surface area (Carder et al., 1974), in general, SPM-specific $b_p(\lambda)$ (or $c(\lambda)$) coefficients,

$$b_p^*(\lambda) = \frac{b_p(\lambda)}{\mathrm{SPM}}, \tag{8.9}$$

are not expected to be constant for natural particles (e.g. Baker and Lavelle, 1984). This is reflected in empirical relationships that differ among regions, because of differences in particle properties including composition and size distribution. Some systematic variations in $b_p^*(\lambda)$ have been documented; most notably, typical values are approximately twice as high in the open ocean as in coastal waters (Bishop 1986; Babin et al., 2003*a*). This particular finding is consistent with the conclusion that, compared with coastal waters, scattering properties of open ocean waters depend more on organic particles. Notwithstanding the general correlations that are typically found, variability in b_p that

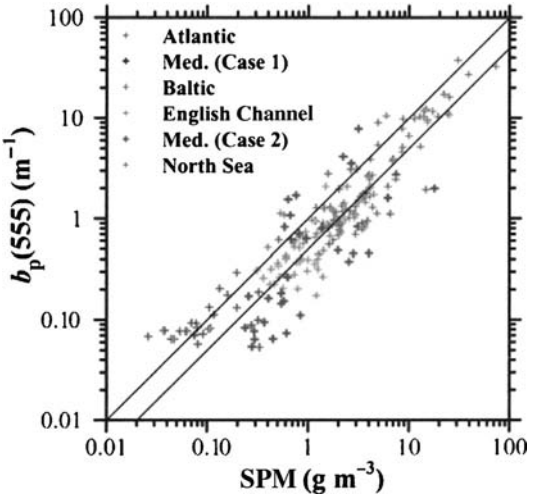

Figure 8.9
Dependence of $b_p(555)$ on SPM observed for a wide range of European coastal waters. Lines indicate 1:1 and 1:2.
Source: Babin et al. (2003*a*).

cannot be explained by SPM can be high even within local environments, and even with modern measurement and calibration techniques (e.g. Babin et al., 2003*a*) (Figure 8.9).

The heterogeneous nature of natural particle pools presents a major limitation on the generality of relationships between SPM and optical properties. There are some analytical techniques that allow subcategories of SPM to be quantified, and under certain conditions these can help to explain variability in optical properties. Particulate organic carbon (POC) concentration is one such index, which reflects contributions both from living organisms and detrital material, and its relationship with light scattering has been extensively explored, primarily for Case 1 waters. Positive linear correlations between b_p, c_p or $b_{b,p}$ and POC have been documented for regional studies within a variety of open ocean environments (e.g. Gardner et al., 1993; Gundersen et al., 1998; Bishop, 1999; Claustre et al., 1999; Stramski et al., 1999). Within coastal waters the relative organic content of the particle pool can be highly variable and, in general, substantial variability in scattering cannot be easily related to POC (e.g. Gardner et al., 2001; Babin et al., 2003*a*) (Figure 8.10B).

Across a broad range of Case 1 conditions, the general dominance of organic particles leads to $b_p(660)$ or $c_p(660)$ exhibiting a near linear dependence on POC (Loisel and Morel, 1998; Bishop et al., 1999) (Figure 8.10A). In part because NAP (especially detritus) make a substantial (40–50%) contribution to c_p in these environments (DuRand and Olson, 1996; Chung et al., 1998; Claustre et al., 1999; Green et al., 2003*a*), POC is expected to explain more overall variability than chlorophyll. Even for POC within Case 1 waters, however, unexplained variability exists (Figure 8.10A), presumably associated with changes in particle properties such as size distribution and pigmentation. Within surface waters in these environments, $c_p(660)$ often exhibits regular diel variations that have been used to estimate daily production or growth rates (e.g. Siegel et al., 1989; Cullen et al., 1992; DuRand and Olson, 1996; Claustre et al., 1999); these approaches are also limited by species-dependent or size-dependent variability in POC- or cell-specific scattering (e.g. DuRand and Olson, 1996).

For the special case of coccolithophore blooms, light scattering by mineral particles can dominate and particulate inorganic carbon (PIC) concentration can explain a substantial part of the variability in light scattering. This has been especially well documented in observational studies during blooms in the North Atlantic where b_p dependence on PIC can be near linear (Ackleson et al., 1994; Balch et al., 1996) (Figure 8.11). Balch et al. (2001) have recently developed an empirical approach for deriving simultaneous estimates of POC and PIC from continuous b_b observations, by alternating between measurements with and without acid pretreatment (which dissolves the particulate calcium carbonate). In addition, Guay and Bishop (2002) have developed an approach to quantify PIC on the basis of attenuation measurements with polarized light; this method should be readily adaptable for submersible applications with a modified transmissometer. Even though these new approaches may effectively separate b_p or $b_{b,p}$ associated with calcium carbonate, absolute accuracy for optical estimates of constituent concentrations such as POC and PIC will still depend on natural variability in specific scattering properties; as mentioned above, these in turn are functions of the distributions of particle composition, size and shape. For this reason, spatially and temporally explicit empirical relationships remain essential for the highest accuracy.

In general, $b_{b,p}(\lambda)$ is thought to depend strongly on the abundance of submicrometre detrital and mineral particles (e.g. Stramski and Kiefer, 1991; Stramski et al.,

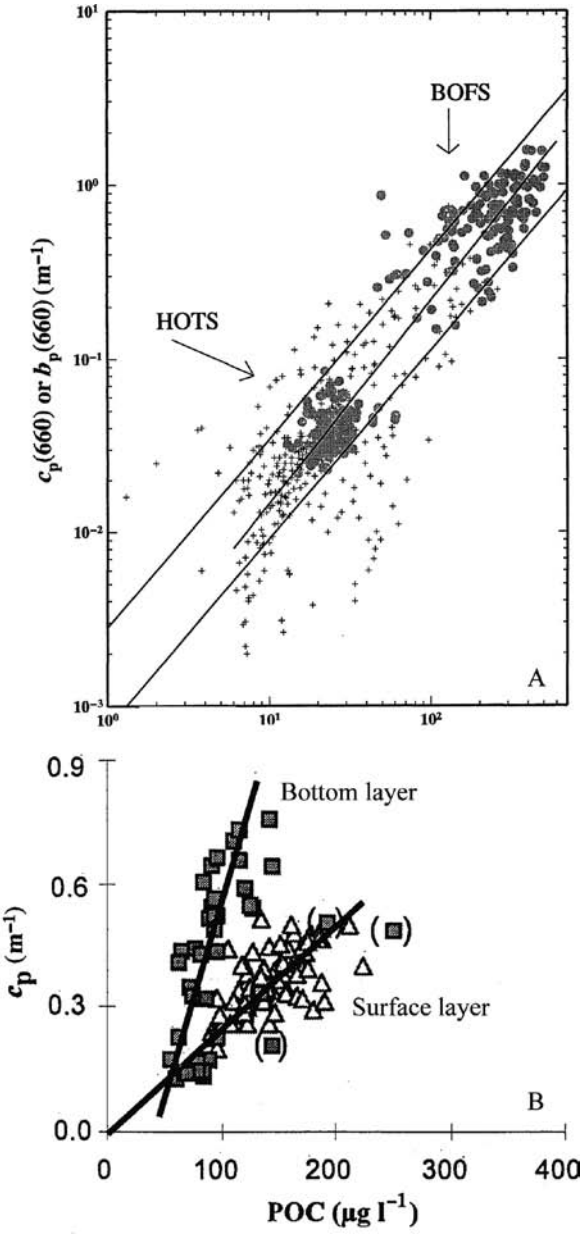

Figure 8.10
Dependence of $c_p(660)$ on POC observed for A, Case 1 waters in the Pacific (HOTS) and Atlantic (BOFS); B, New England continental shelf waters during stratified summer conditions. The line in B and the central line in A are regression results, and the upper and lower lines in A bound approximate Case 1 conditions (see Loisel and Morel, 1998, for details). *Sources*: A, Loisel and Morel (1998); B, Gardner et al. (2001).

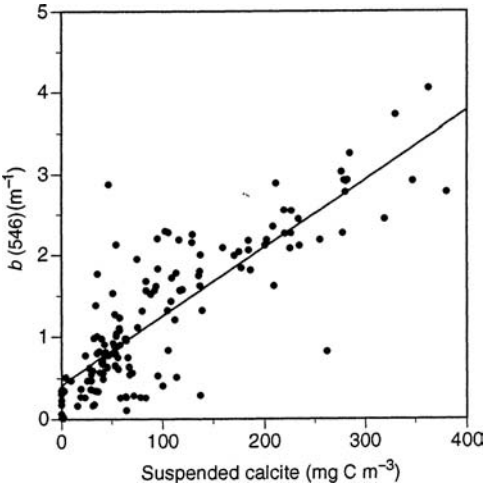

Figure 8.11
Dependence of $b(546)$ on PIC during an *E. huxleyii* bloom in the North Atlantic. The line represents the linear regression result.
Source: Balch et al. (1996).

2001; Green et al., 2003*a*), although observational studies of these particles and their optical properties barely exist. Besides exceptional conditions such as coccolithophore blooms discussed above, generalizations about $b_{b,p}(\lambda)$ dependence on particle load (or perhaps more appropriately, indices of <1 μm particle load) are currently lacking.

8.3.4.2 Absorption

Direct relationships between absorption coefficients and indices of particle load such as SPM and POC have not received much attention, principally because Chl is convenient to measure and, under many circumstances, known to explain a majority of the variability in $a_p(\lambda)$. As described above (Section 8.3.1), for Case 1 waters $a_{NAP}(\lambda)$ tends to roughly covary with $a_{ph}(\lambda)$ (Bricaud et al., 1998). In Case 2 waters, however, $a_{NAP}(\lambda)$ can be more important than $a_{ph}(\lambda)$ and the sources of NAP can be decoupled from processes that lead to variability in Chl. For European coastal waters, $a_{NAP}(\lambda)$ has been shown to exhibit an overall correlation with SPM, although site-specific variations in the relationship show influences of high detrital versus high mineral loads (Bowers et al., 1996; Babin et al., 2003*a*). More detailed interpretation of these kinds of observations is limited by lack of knowledge of the ranges and sources of variability in specific absorption coefficients for different types of NAP, and by lack of routine analytical methods to separate different types of NAP.

8.3.5 Particle size distribution, refractive index and pigmentation

Whereas the magnitude of absorption and scattering coefficients depend to first order on the total amount of constituents in the water, other characteristics including spectral shapes and ratios such as $\tilde{b}_{b,p}$ are more strongly influenced by the type of constituents present. As reviewed above, light scattering and absorption properties

of particles depend on their size and complex refractive index, as well as on their shape and internal structure. The real part of the refractive index primarily governs scattering processes and is controlled by the density and composition of the particle (i.e. relative amounts of water, protein, calcite, quartz, etc.). The imaginary part governs absorption and depends strongly on the structure of pigment molecules. On the basis of theoretical understanding, combined with observational studies, some approaches have emerged that rely on distinctive optical properties to infer characteristics of the heterogeneous pool of natural particles.

8.3.5.1 Beam attenuation, scattering and backscattering

Mie theory provides a basis for understanding how different types of particles may result in distinctive spectral shapes and ratios of optical coefficients (see Bohren and Hoffman, 1983, for more details on Mie theory). Strictly, the theory applies only to homogeneous spherical particles and its forward application for a mixed assemblage of particles requires complete knowledge of the distributions of particle size and complex refractive index. Nonetheless, general inferences about the type of particles that dominate in different natural particle assemblages can be made by comparison to theoretical results (e.g. Bricaud et al., 1995*a*; Gould et al., 1999). Babin et al. (2003*a*), for example, examined the spectral shape of $b_p(\lambda)$ and $b_p(\lambda)$:$c_p(\lambda)$ to identify Case 2 coastal European waters likely to be dominated by mineral particles and readily distinguished them from nearby Case 1 waters where phytoplankton play a dominant role (Figure 8.12). Barnard et al. (1998) examined a large spectral IOP data set from diverse environments (Cases 1 and 2) and quantified overall linear dependencies between IOPs at different wavelengths; this global result can provide a framework for comparison with local-to-regional scale spectral properties that may reflect different or site-specific patterns of constituent variability.

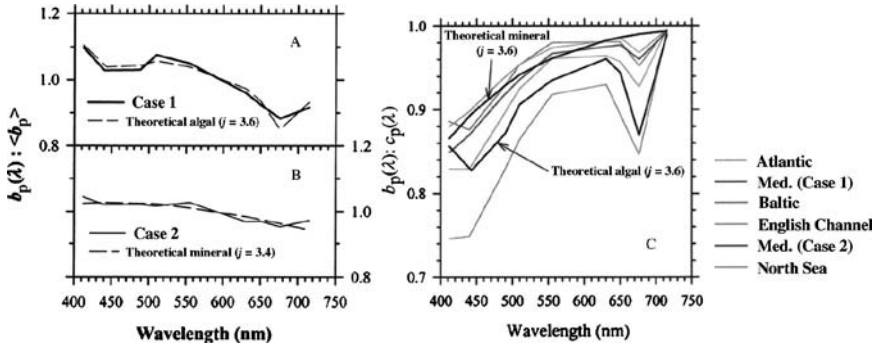

Figure 8.12
Mean normalized spectral shape for $b_p(\lambda)$ observed from diverse European coastal environments with A, Case 1; B, Case 2 waters. C, mean ratios of $b_p(\lambda)$ to $c_p(\lambda)$ for each of the regions examined. For comparison, results from Mie theory are also shown for Junge-distributed (slope indicated by *j* values) particles with refractive indices typical for algae and minerals.
Source: Babin et al. (2003*a*).

There is an extensive literature on inversion methods aimed at explicitly quantifying bulk (or composite) particle properties, such as refractive index and size distribution, from light scattering (e.g. Brown and Gordon, 1974; Zaneveld et al., 1974; Kitchen et al., 1982; Bricaud et al., 1995*a*; see also review by Zaneveld et al., 2002). For example, Mie theory and observational evidence support a relatively simple relationship between the Junge slope of the particle size distribution and the spectral shape of $c(\lambda)$ (Morel, 1973; Boss et al., 2001*c*; Boss et al., 2001*a*). Twardowski et al. (2001) have built on this and developed a method that also provides bulk real refractive index estimates from IOPs that can now be measured with *in situ* sensors, that is $c(\lambda)$ and $\tilde{b}_{b,p}(532)$. Their method cannot be used to separate precisely the contributions of different types of particles in a mixture, but it can discriminate situations dominated by different broad classes of particle type. Boss et al. (2004), for example, used the approach in eastern US inner shelf waters to identify a range of bulk refractive index conditions from low values (~1.02–1.08, relative to water), indicative of phytoplankton dominance, to high values (~1.1–1.2), indicative of mineral particles (Figure 8.13). In addition to some sensitivity to violation of the assumptions of Mie theory, the approach of Twardowski et al. (2001) has other caveats, including sensitivity to lack of knowledge of particle absorption properties (imaginary refractive index) and the assumption that the particle size distribution is hyperbolic (which may be violated during near monospecific blooms, for example) (Boss et al., 2004).

Flow cytometry is one method that allows the light scattering properties of individual marine particles to be rapidly and quantitatively assessed, and thus allows distributions of properties to be observed. The method also allows differentiation of phytoplankton from NAP (e.g. Green et al., 2003*b*). Ackleson and Spinrad (1988) first showed that Mie theory-based scattering inversion methods could be applied to flow

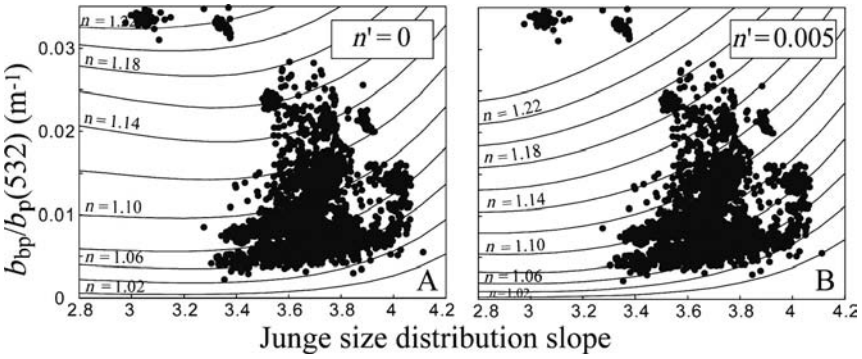

Figure 8.13
Backscattering ratio $\tilde{b}_{b,p}(532) = b_{bp}/b_p(532)$ as a function of the Junge slope of the particle size distribution. Data points correspond to *in situ* results from continental shelf waters off New Jersey, USA, with Junge slopes estimated from the spectral slope of $c(\lambda)$ (see Boss et al., 2004, for details). Variations in bulk refractive index can be constrained by comparison to contour lines, which show Mie theory for a range of real refractive indices (n) and for A, non-absorbing particles or B, absorbing particles with imaginary refractive index (n') equal to 0.005. Real refractive indices of 1.02–1.08 are characteristic of phytoplankton, whereas higher values suggest the presence of mineral particles.
Source: Boss et al. (2004).

cytometry data for marine particles. Green et al. (2003*a*, 2003*b*; Green and Sosik, 2004) refined the approach and used it to derive particle size and refractive index distributions for different types of particles in natural samples, including various groups of microorganisms, mineral particles and detrital particles. Although flow cytometric approaches have advantages over bulk methods such as that of Twardowski et al. (2001) because detailed distributions can be explicitly derived, their application is not practical for rapid *in situ* sampling and is subject to the same limitations associated with Mie theory assumptions.

8.3.5.2 Absorption

In general, different chromophore and pigment molecules have different spectral absorption properties, and bulk $a_p(\lambda)$ reflects a composite spectrum of the summed contributions from all absorbing molecules present. For phytoplankton in particular, the pigments and their absorption properties are relatively well described and this has been exploited for interpretation of $a_{ph}(\lambda)$ observations from natural samples. An important category of methods for this relates to deriving information about the presence of certain taxonomic groups; these are discussed in detail in the following section. In addition to depending on phylogeny, however, pigment composition is also subject to physiological regulation and, under some circumstances, it may be possible to infer acclimation status from effects on $a_{ph}(\lambda)$. Eisner et al. (2003) have shown how this can be applied with high resolution vertical profiles in coastal waters of the north-west USA. They developed a spectral slope index for blue-to-green wavelengths of $a_p(\lambda)$ that reflected the ratio of photoprotective carotenoids to photosynthetic carotenoids in the phytoplankton (Figure 8.14). In their study over a few days, the slope index exhibited variability related to changes in stratification and incident light that is consistent with photoacclimation responses in the phytoplankton. In most cases, it will be challenging to separate these effects from those associated with changes in species composition, and this approach may not work well except at some local scales.

In addition to depending on pigment composition, the spectral shape of $a_{ph}(\lambda)$ is also sensitive to cell size. This results from pigment package effects whereby large cells and those with high internal concentrations of pigment exhibit lower absorption per pigment molecule and flatter spectra compared with smaller, less pigmented cells (e.g. Morel and Bricaud, 1981*a*, 1986). As discussed in Section 8.3.1, this effect probably contributes to the observed global trend for $a^*_{ph}(\lambda)$ to be higher in low-chlorophyll waters. Recently, Ciotti et al. (2002) have explored this idea through analysis of $a_{ph}(\lambda)$ from a range of environmental conditions. Their results showed that $a_{ph}(\lambda)$ spectral shape varied in a regular fashion with dominant cell size in natural phytoplankton assemblages, with dominant cell size able to explain 80% of the variability in spectral shape. On the basis of these findings, they developed a spectral mixing model to estimate a community level cell size index from analysis of $a_{ph}(\lambda)$ shape ($a_{<ph>}(\lambda)$, i.e. after normalization to its mean). In a manner analogous to that discussed in Section 8.2.1 for (8.4), the model represents an estimated normalized spectrum, $\hat{a}_{<ph>}(\lambda)$, as a linear sum of two basis vectors:

$$\hat{a}_{<ph>}(\lambda) = F\ \mathbf{a}_{<pico>} + (1-F)\mathbf{a}_{<micro>}, \tag{8.10}$$

where the basis vectors, $\mathbf{a}_{<pico>}$ and $\mathbf{a}_{<micro>}$, are the normalized $a_{ph}(\lambda)$ values observed for extreme cases of picophytoplankton and microphytoplankton dominated waters,

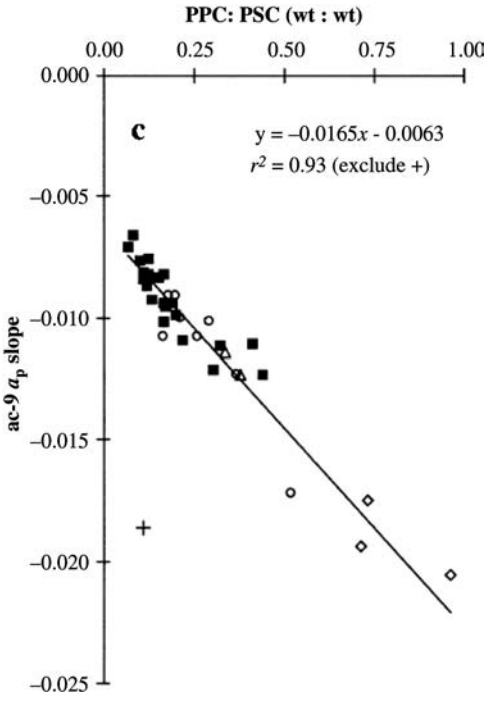

Figure 8.14
Dependence of slope index for $a_p(\lambda)$ (=[a_p(488) – a_p(532)]:[a_p(676)(488–532 nm)]) on the ratio of photoprotective carotenoids to photosynthetic carotenoids (PPC:PSC) derived from observations over several days in coastal waters of the north-west USA. The line represents the linear regression result.
Source: Eisner et al. (2003).

respectively. F ($S_{<f>}$ in the original terminology of Ciotti et al. (2002)) is a dimensionless community size index, which varies from 0 (microplankton dominated) to 1 (picoplankton dominated). The value of F for any spectrum can be selected so that it results in minimized residuals between the estimated and measured $a_{<ph>}(\lambda)$ (Figure 8.15). As pointed out by Ciotti et al. (2002), the residuals themselves can also provide information about physiological and/or taxonomic variability; for example, perhaps revealing the presence of a bloom species with distinctive pigmentation. While values of F cannot be unambiguously interpreted in terms of taxonomic composition in an assemblage, they may provide an ecologically relevant index for applications such as trophic models and estimation of biogeochemical fluxes.

8.3.6 Phytoplankton community composition

Size structure in the phytoplankton can be an informative index of community structure; however, there are many applications for which more detailed taxonomic information is desirable. Optical properties can provide some insights into taxonomic composition of a phytoplankton assemblage, but there are critical limitations for

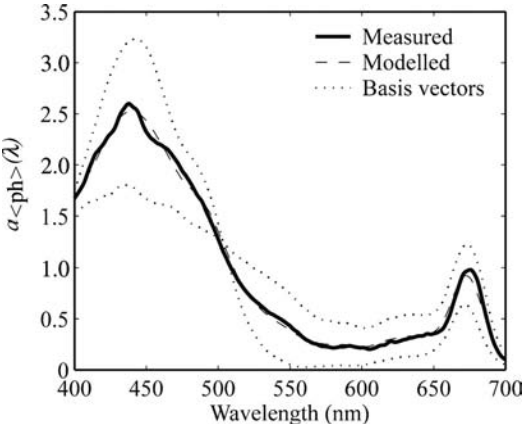

Figure 8.15
Linear spectral mixing model results estimate a phytoplankton community size index (F) from normalized $a_{ph}(\lambda)$ measured for inner shelf waters of New England during summer. The two basis vectors ('pico' and 'micro') used in the model are shown for comparison. For this example, the retrieved value of F is 0.51, indicating that the phytoplankton community is dominated by nanoplanktonic cells. See text and Ciotti et al. (2002) for model details.

all approaches, and definitive identification and enumeration at the species or genus level is not possible for many taxa without high-quality cell-imaging techniques.

Most approaches to derive information about different groups of phytoplankton from IOPs are based on absorption properties. The underlying principle is that the spectral character of absorption is strongly dependent on pigment composition, which in turn varies across taxonomic groups (Jeffrey and Vesk, 1997). Details of pigment composition derived from high-performance liquid chromatography (HPLC) can be used to characterize contributions of different algal classes to total Chl (e.g. Mackey et al., 1996). Hoepffner and Sathyendranath (1993) describe a decomposition method to estimate pigment composition from $a_{ph}(\lambda)$, allowing estimates of algal class contributions to be made without the need for more time-consuming HPLC. HPLC-based methods can only be used to discriminate classes or pigment groups (i.e. chlorophytes from diatoms from dinoflagellate, etc.), because marker pigments are generally not genus or species specific; in addition, accuracy is limited by overlap in pigment occurrence among groups and natural plasticity in pigment ratios within groups (e.g. Goericke and Montoya 1998). In addition to these caveats, spectral absorption-based approaches are further limited because some pigments that are chemically distinct have very similar absorption spectra (Bidigare et al., 1990) (i.e. diatoms may not be distinguishable from dinoflagellates despite differences in carotenoids). Indeed, distinct accessory pigment effects can be difficult to detect in natural spectra (Garver et al., 1994), and these methods require further study and careful evaluation of uncertainties.

Related spectral methods to characterize phytoplankton composition on the basis of fluorescence instead of absorption have also been proposed (e.g. Yentsch and Phinney, 1985; Beutler et al., 2002). Chlorophyll fluorescence is highly specific to phytoplankton and it reflects effects of absorption by various photosynthetic pigments,

so fluorescence excitation spectra may be decomposed to estimate the contributions of different algal groups in a mixture. Beutler et al. (2002) used a linear spectral mixing model to do this, where the basis vectors were derived from a spectral library spanning a variety of phytoplankton species. Decomposition methods for fluorescence and absorption spectra have similar limitations with respect to taxonomic specificity and accuracy (e.g. SooHoo et al., 1986), but fluorescence may have greater potential for *in situ* applications due to its sensitivity and lower interference from other constituents such as CDOM and NAP. New sensors for this kind of analysis are now becoming readily available.

Different types of absorption-based approaches rely on quantitative techniques such as derivative analysis to emphasize aspects of spectra associated with pigment composition (e.g. Millie et al., 1997) or discriminant analysis to classify spectra according to taxonomic group (e.g. Johnsen et al., 1994). The derivative approach has been most notably applied to the problem of detecting the presence of the red-tide dinoflagellate *K. brevis* in mixed assemblages. Millie et al. (1997) used the fourth derivative of absorption spectra and derived a 'similarity index' to quantify the comparison between known spectra for *K. brevis* and 'unknown' spectra for mixtures of species that may include *K. brevis*. This similarity index has been shown to be a reliable indicator for the biomass of *K. brevis* in natural samples from areas where *K. brevis* is known to bloom (Millie et al., 1997; Schofield et al., 1999; Kirkpatrick et al., 2000) (Figure 8.16). Work is under way to adapt this method to a liquid capillary waveguide application that provides high sensitivity suitable for natural cell abundances (Kirkpatrick et al., 2000). The apparent utility of this spectral approach for detection of *K. brevis* seems to be linked to the species' role as a high-light adapted organism

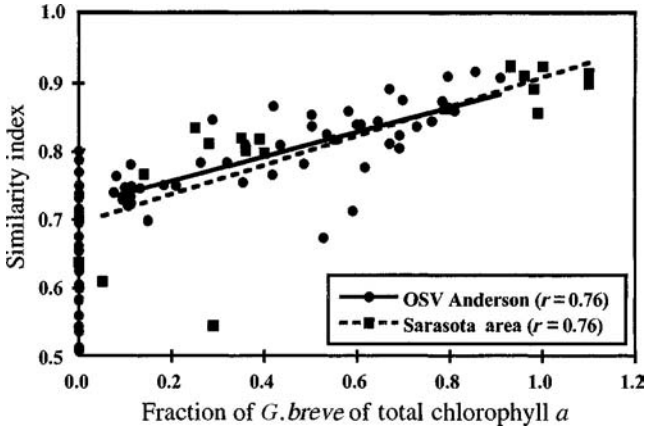

Figure 8.16
Similarity index (reflecting a comparison on fourth derivatives of normalized $a_p(\lambda)$ as described in Kirkpatrick et al. (2000)) between known *K. brevis* spectra and those for natural samples collected in the Gulf of Mexico, as it varies with the fraction of Chl attributed to *K. brevis* (previously designated *G. breve*). Lines show linear regression results for offshore (OSV Anderson) and nearshore (Sarasota) data.
Source: Kirkpatrick et al. (2000).

that forms near-monospecific blooms (Schofield et al., 1999). Recent evidence suggests that this method may have broader applicability for discriminating taxonomic groups (Millie et al., 2002).

For selected phytoplankton taxa, light scattering properties can be indicative of bloom effects. As described above (Section 8.3.1), this applies to taxa such as *Trichodesmium*, which form high concentration blooms of cells with gas vacuoles, and *E. huxleyi*, which produce high concentrations of calcium carbonate coccoliths. In practice, the presence of these blooms is most often detected through the influence of high scattering magnitude on apparent optical properties as discussed below (Section 8.5.4).

Flow cytometry is a specialized optical technique that has been used extensively to enumerate and characterize different types of phytoplankton (Olson et al., 1993; Reckermann and Colijn, 2000). This method is fundamentally different from those discussed in the rest of this chapter because it is based on light scattering and fluorescence measurements resolved for individual particles within a mixture, rather than depending on a single measurement of the bulk mixture. Despite this difference, flow cytometry is still subject to many of the same limitations with respect to the capability to discriminate taxa. It is routinely possible to enumerate separately *Prochlorococcus*, *Synechococcus,* coccolithophores, and pennate diatoms, while other groups can only be classified roughly according to cell size (e.g. Olson et al., 1989; Olson et al., 1990). With recent developments in flow cytometers, capabilities now exist for automated measurements of phytoplankton communities with submersible instruments (Dubelaar and Gerritzen, 2000; Olson et al., 2003; Sosik et al., 2003).

8.4 Overview of AOP variability

Apparent optical properties (AOPs) are determined by the IOPs and by the geometric characteristics of a natural light field (Preisendorfer, 1976; Kirk, 1994). They depend strongly enough on the IOPs that they can be characteristic of a water body and its constituents, but light field geometry must also be taken into account to completely explain their variability. AOPs are determined from measurements of radiometric quantities such as downwelling or upwelling plane irradiance, $E_d(\lambda)$ and $E_u(\lambda)$ respectively, and upwelling radiance $L_u(\lambda)$ (see Lewis, 2007 – Chapter 6 this volume – for more details). The following sections focus on how particular IOPs and seawater constituents affect AOPs.

8.4.1 Diffuse attenuation and reflectance

One of the most commonly determined AOPs is the diffuse attenuation coefficient for downwelling irradiance, $K_d(\lambda)$, which is simply the exponential rate of change in $E_d(\lambda)$ with depth z:

$$K_d(z,\lambda) = -\frac{1}{E_d(\lambda)}\frac{dE_d(z,\lambda)}{dz} = -\frac{d\left\{\ln\left[E_d(z,\lambda)\right]\right\}}{dz}. \qquad (8.11)$$

Similar diffuse attenuation coefficients can be defined for vertical profiles of any radiometric quantity – $E_u(z, \lambda)$, $L_u(z, \lambda)$, etc. The IOP dependence of $K_d(z, \lambda)$ can be considered by expressing the directionality of the light field in terms of the average cosine of the zenith angle for downwelling irradiance, $\bar{\mu}_d$, and for upwelling irradiance, $\bar{\mu}_u$, so that

$$K_{\mathrm{d}}(z,\lambda) = \frac{a(z,\lambda) + b_{\mathrm{b}}(z,\lambda)}{\bar{\mu}_{\mathrm{d}}(z)} - \frac{b_{\mathrm{b}}(z,\lambda)}{\bar{\mu}_{\mathrm{u}}(z)} R(z,\lambda), \tag{8.12}$$

where $R(\lambda)$ represents irradiance reflectance (Preisendorfer, 1961, as cited in Kirk 1994).

Spectral reflectance is another frequently measured AOP, one which is of immediate interest for ocean-colour remote sensing. Irradiance reflectance is determined according to

$$R(\lambda) = \frac{E_{\mathrm{u}}(\lambda)}{E_{\mathrm{d}}(\lambda)}, \tag{8.13}$$

while 'remote-sensing' reflectance is typically defined as radiance reflectance above the sea surface:

$$R_{\mathrm{rs}}(\lambda) = \frac{L_{\mathrm{u}}(0^+,\lambda)}{E_{\mathrm{d}}(0^+,\lambda)}, \tag{8.14}$$

where $L_{\mathrm{u}}(0^+,\lambda)$ and $E_{\mathrm{d}}(0^+,\lambda)$ are quantities determined just above the air-water interface ($z = 0^+$). These reflectance quantities can be viewed as depending on IOPs according to

$$R(\lambda) = f \frac{b_{\mathrm{b}}(\lambda)}{a(\lambda) + b_{\mathrm{b}}(\lambda)}, \tag{8.15}$$

(shown for the example of $R(\lambda)$), where f is only approximately constant and in general varies with the angular distribution of the light field (e.g. Kirk, 1984; Morel and Gentili, 1991).

Because of their dependence on the angular distribution of the light field, AOPs for different constituents are not additive and, in the strictest sense, it is not valid to consider contributions of one constituent independent of others. Nonetheless, for some applications, $K_{\mathrm{d}}(\lambda)$ has been considered to be a 'quasi-inherent' optical property and has been approximated according to a sum of components, and constituent-specific $K_{\mathrm{d}}(\lambda)$ values have also been introduced. In a classic example where this was applied to natural water bodies, Smith and Baker (1978) proposed the relationship

$$K_{\mathrm{d}}(\lambda) = K_{\mathrm{w}}(\lambda) + \mathrm{chl}\ \ K^{*}_{\mathrm{chl}}(\lambda) + K_X(\lambda), \tag{8.16}$$

where the three terms on the right represent approximate contributions from pure seawater, from material correlated with Chl, and from other material (i.e. uncorrelated with Chl); in direct analogy with (8.3), $K^{*}_{\mathrm{chl}}(\lambda)$ is the specific coefficient for the Chl component.

8.5 AOP relationships and examples

This section contains selected examples of documented relationships between AOPs and seawater constituents. Some emphasis is placed on quantities related to phytoplankton biomass and community composition, but other constituents are discussed where appropriate. The examples highlighted are intended to be illustrative but in no way exhaustive, considering the long history and many directions of research on these topics.

8.5.1 Chlorophyll and IOPs from irradiance

Especially in Case 1 waters, particle absorption is an important source of variability in $K_d(\lambda)$, so it is not surprising that relationships with Chl have proved robust. Morel (1988) proposed that the nonlinear dependence of $K_d(\lambda)$ on Chl could be represented by a modification to (8.16):

$$K_d(\lambda) = K_w(\lambda) + \chi(\lambda)\,\mathrm{Chl}^{e(\lambda)}, \tag{8.17}$$

where $\chi(\lambda)$ and $e(\lambda)$ were determined statistically for a large data set of Case 1 waters and have recently been updated (Morel and Maritorena, 2001). It is important to note that this relationship is based on a statistical analysis and does not imply that chlorophyll-containing particles are the only source of variability in $K_d(\lambda)$. Even for open ocean waters, there is strong evidence suggesting that CDM (mostly CDOM) affects seasonal patterns in $K_d(\lambda)$ (Siegel and Michaels 1996), and anomalous CDM content causes some apparent Case 1 locations to deviate from general parameterizations of (8.6) (see e.g. Morel and Maritorena, 2001, Figure 7, Mediterranean waters). To the extent that CDM effects are correlated with Chl, they are implicitly included in (8.17), but uncorrelated effects contribute to observed variance that is not explained by the equation. In coastal waters, major CDM sources, such as resuspension and riverine input, are often uncoupled from processes contributing to changes in Chl, so variability in $K_d(\lambda)$ is even more complex. Nonetheless, local-to-regional characterization of these effects can be made, and AOPs such as $K_d(\lambda)$ can be useful for long-term monitoring

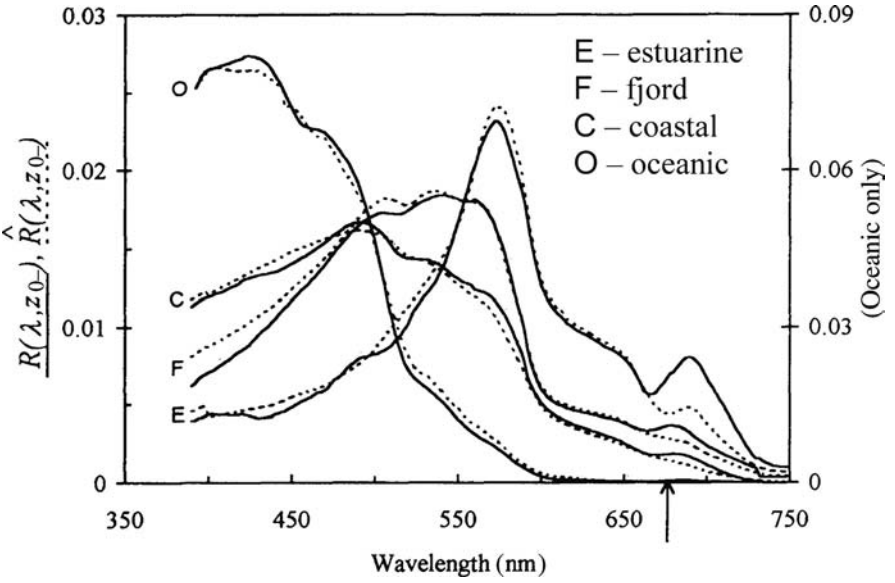

Figure 8.17
Observed (solid lines) and inversion model results (dashed lines) for reflectance spectra from a variety of water types off the north-west USA. *Source*: Roesler and Perry (1995).

and early warning for blooms of algal species that contribute significantly to total Chl (Cullen et al., 1997).

Principally because widespread availability of *in situ* instrumentation for measuring IOPs is a relatively recent trend, there has been longstanding interest in analytical approaches for estimating absorption and scattering from irradiance observations (e.g. Zaneveld, 1974; Gordon et al., 1975; Kirk, 1984). These approaches remain of interest as AOPs can often be measured more easily and inexpensively than IOPs. On the basis of radiative transfer simulations, Gordon (1991), for example, proposed an inversion method to estimate $a(\lambda)$, $b(\lambda)$, and $b_b(\lambda)$ from a combination of $K_d(\lambda)$ and $R(\lambda)$ observations, given clear sky conditions and a vertically homogeneous ocean with no inelastic scattering. Subsequently, efforts have been made to reduce uncertainties in these types of inversions despite variable sky conditions, the presence of vertical stratification, variable scattering phase functions, effects of Raman scattering, and a wide range of Case 1 to Case 2 conditions (e.g. Gordon and Boynton, 1997, 1998; Loisel and Stramski, 2000; Stramska et al., 2000; Boynton and Gordon, 2002). Gordon (2002) provides an exceptional review of the history and current status of developments in this area.

By extension of the information summarized in Section 8.3, it should be possible to derive details about water constituents from IOPs that are in turn derived from AOP inversion. It is also possible to use semi-analytical approaches for direct retrieval of constituent properties from radiometric observations. Brown et al. (2004), for example, have used irradiance spectra to estimate simultaneously a_{ph} and a_{CDM} at characteristic wavelengths. A distinguishing feature of their approach is that it does not require vertical profiles, and thus can be applied to time-series irradiance observations collected from fixed-depth moored sensors or to horizontally resolved irradiance observations collected from a towed or self-propelled vehicle. As a second example, Ciotti et al. (1999) have developed a model representing diffuse attenuation coefficients and ratios of upwelling radiance in different wavebands that depends on chlorophyll and includes explicit parameterization of changes in pigment packaging, accessory pigmentation, CDOM absorption, detrital particle absorption and particle scattering. These types of approaches demonstrate the potential to derive information about constituent quantities and characteristics from AOPs. Other relevant examples are included in the following section.

8.5.2 Chlorophyll and IOPs from surface reflectance

A noteworthy subset of AOP inversion approaches relies only on surface reflectance observations; these have received a great deal of attention due to their relevance for remote sensing applications. The dependence of reflectance on IOPs, as expressed in (8.15), reveals that reflectance spectra contain information about the underlying constituents contributing to light absorption and backscattering. This has been the basis for a variety of reflectance inversion approaches developed to derive IOP or constituent estimates. The simplest are purely empirical algorithms to estimate a single constituent (e.g. Chl) from spectral ratios (e.g. Gordon et al., 1983; O'Reilly et al., 1998). More complex formulations directly use analytical expressions, such as (8.15), combined with some empirical knowledge concerning constituent IOP characteristics. In some cases, these semi-analytical inversion approaches rely on selected spectral ratios for separating constituent properties (e.g. Carder et al., 1999; Morel and Maritorena, 2001; Lee et al., 2002), while others use absolute magnitude in all available spectral

bands (e.g. Sathyendranath et al., 1989; Doerffer and Fischer, 1994; Roesler and Perry, 1995; Hoge and Lyon, 1996; Garver and Siegel, 1997; Gould et al., 2001; Reynolds et al., 2001). Furthermore, some models use a reflectance expression directly comparable with (8.15) and some assume a quadratic dependence on $\frac{b_b(\lambda)}{a(\lambda)+b_b(\lambda)}$, as proposed by Gordon et al. (1988). Semi-analytical reflectance inversion models usually provide estimates of several properties. For example, it is possible to simultaneously retrieve Chl, $a_{CDM}(\lambda)$, and $b_b(\lambda)$ (e.g. Maritorena et al., 2002) (also see example in Figure 8.18).

Developments are proceeding rapidly on the topic of inverse models of surface reflectance and there is currently no consensus as to which approach is best, especially for coastal waters. In fact, it is unlikely that a single approach will work best for all applications. It is beyond the scope of this chapter to discuss and compare all existing approaches. In what follows, we focus instead on an example that typifies some general

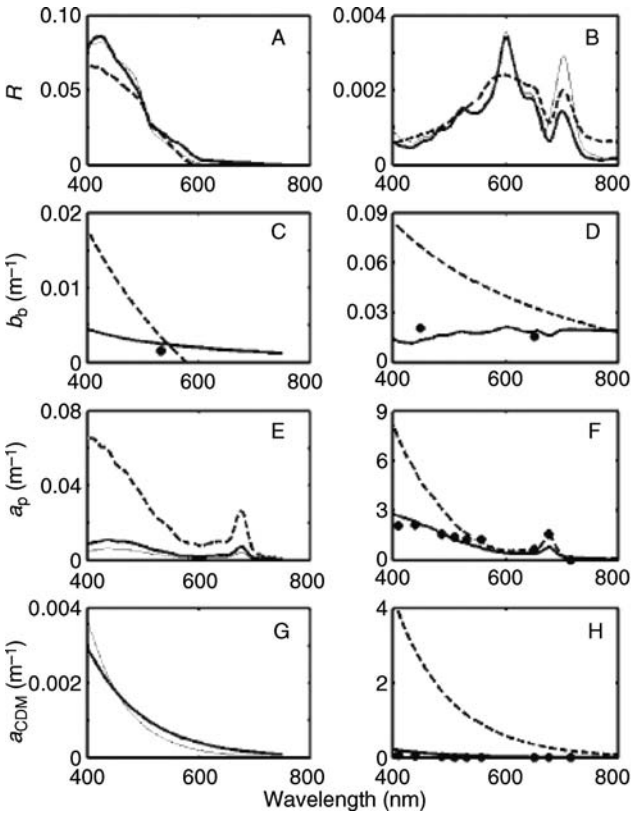

Figure 8.18
Observations (thin solid lines and symbols) and inversion results from the Roesler and Perry (1995) 'standard' model (dashed lines) and from the Roesler and Boss (2003) '*c*-model' (thick solid line), for coastal waters off Oregon (left column) and off South Africa (right column).
Source: Roesler and Boss (2003).

aspects of the problem and that has also been recently applied to analysis of mixed species phytoplankton blooms.

8.5.2.1 Reflectance inversion example

The model of Roesler and Perry (1995) describes irradiance reflectance and includes effects of absorption by phytoplankton, CDOM and NAP, and backscattering by two types of particle qualitatively described as 'large' and 'small'. The basic model follows (8.15) with $a(\lambda)$ and $b(\lambda)$ determined according to linear mixing:

$$a(\lambda) = A_{\mathrm{ph1}}\mathbf{a_{ph1}} + A_{\mathrm{NAP1}}\mathbf{a_{NAP1}} + A_{\mathrm{CDOM1}}\mathbf{a_{CDOM1}} + a_{\mathrm{w}}(\lambda) \tag{8.18}$$

and

$$b_{\mathrm{b}}(\lambda) = A_{\mathrm{bb1}}\mathbf{b_{b1}} + A_{\mathrm{bb2}}\mathbf{b_{b2}} + b_{\mathrm{b,w}}(\lambda). \tag{8.19}$$

As in (8.4), the As here represent amplitudes for each component; and $\mathbf{a_{ph1}}$, $\mathbf{a_{NAP1}}$, $\mathbf{a}_{\mathrm{CDOM1}}$, $\mathbf{b_{b1}}$ and $\mathbf{b_{b2}}$ represent spectral basis vectors for each type of absorber (phytoplankton, NAP, CDOM) and two types of particulate backscatters. For the model application described by Roesler and Perry (1995), $\mathbf{a_{ph1}}$ was fixed at an average shape derived from a series of direct observations in coastal waters; $\mathbf{a_{NAP1}} + \mathbf{a_{CDOM1}}$ were assumed to follow a non-dimensional form of (8.5), with a fixed S value taken from published observations; and $\mathbf{b_{b1}}$ and $\mathbf{b_{b2}}$ were set according to a non-dimensional version of (8.6) with $\gamma = 0$ and -1, respectively, to approximate backscattering contributions by pools of 'large' and 'small' (relative to the wavelength) particles. The five amplitudes (A_{ph1}, A_{NAP1}, A_{CDOM1}, A_{bb1}, A_{bb2}) are estimated with least-squares regression to minimize the residuals between measured and modelled reflectance spectra. This approach can be used to reproduce measured reflectance spectra for a variety of waters ranging from estuarine to open ocean (Figure 8.17).

Many semi-analytical reflectance models are similar to that of Roesler and Perry (1995) and the parameterization of backscattering is an important source of error in these models. As explained in Section 8.2.3, there are well-documented deviations from the form of (8.6) for strongly absorbing particles such as phytoplankton. This may not be a problem in open ocean waters where most of the backscattering is not from phytoplankton cells, but, under bloom conditions in coastal waters, it may be critical for IOP retrieval from inverse methods. Recently, Roesler and Boss (2003) have introduced a new approach that does not require a simple constraint on the shape of the backscattering spectrum. Their model is similar to that of Roesler and Perry (1995) except that (8.6) is used for only one type of particulate backscatterer. The spectral basis vector for these particles $\mathbf{b_{b1}}$ is specified assuming that $c_{\mathrm{p}}(\lambda)$ follows a power function similar to (8.6) and that $b_{\mathrm{p}}(\lambda)$ and $b_{\mathrm{b,p}}(\lambda)$ have the same spectral shape (i.e. $\tilde{b}_{\mathrm{b,p}}$ as defined in (8.7) is independent of wavelength). This leads to

$$\mathbf{b_{b1}} = \frac{A_{\mathrm{cp1}}\mathbf{c_{p1}} - A_{\mathrm{ph1}}\mathbf{a_{ph1}} - A_{\mathrm{NAP1}}\mathbf{a_{NAP1}}}{A_{\mathrm{b1}}}, \tag{8.20}$$

which is a non-dimensional form of $c_p(\lambda) - a_p(\lambda)$. In Roesler and Boss (2003), the basis vectors $\mathbf{a_{ph1}}$ and $\mathbf{a_{NAP1}}$ were specified as in Roesler and Perry (1995) and the basis vector for beam attenuation was taken as

$$\mathbf{c_{p1}} = \left(\frac{\lambda}{\lambda_0} \right)^{-\gamma} . \tag{8.21}$$

This latter assumption is based on the observations that variations in the functional form of the spectral dependence for $c_p(\lambda)$ are more restricted than for $b_{b,p}(\lambda)$, and that spectral variations in $b_{b,p}$ are weak. An interesting feature of this model is that inversion for IOPs produces not only the more standard $a(\lambda)$ and $b_b(\lambda)$ retrievals, but also $c(\lambda)$ estimates.

Roesler and Boss (2003) applied this 'c-model' to invert measured $R(\lambda)$ for IOPs, with γ and five amplitude terms derived by least-squares minimization. They also compared results to those for the standard Roesler and Perry (1995) model in which the basis vectors for particle backscattering are taken to follow simple power laws, that is as in (8.6). From this analysis, it was evident that both models can reproduce the major features of measured $R(\lambda)$ for different water types, although the *c*-model performed better for fine details (Figures 8.18A, 8.18B). The *c*-model markedly outperformed the standard model in IOP retrieval (Figures 8.18C to 8.18H). Because inversion of the *c*-model provides estimates of $c(\lambda)$ amplitude and spectral slope (γ), there is potential for obtaining information about the shape of the particle size distribution (see Section 8.3.5 and Boss et al., 2001*a*, for example). Further assessment of this and related models, especially comparison of retrieval results with independent measurements for a variety of water types, is currently needed.

8.5.3 Empirical algorithms for SPM, POC and PIC

Besides those for retrieving Chl (discussed in Sections 8.5.1 and 8.5.2), empirical algorithms relating SPM to AOPs have been most widely pursued. As reviewed by Kirk (1994), there have been a number of efforts to derive total SPM from remotely sensed reflectance, most developed for local or regional application in coastal or inland waters. Some approaches are based on reflectance intensity at red or near-infrared wavelengths, whereas others depend on changes in spectral shape, and applications have been developed for satellite-based sensors including Landsat, AVHRR, CZCS, SeaWiFS and others. In general, differences in particle size and composition can be extreme and, because this leads to large variations in mass-specific scattering, a universal empirical algorithm for SPM is unlikely to emerge.

Some recent efforts have focused on the potential for particular subcategories of SPM to be retrieved from remotely sensed reflectance. Stramski et al. (1999) used empirical relationships between $R(555)$ and $b_b(510)$ and between POC and $b_{b,p}(510)$ for Southern Ocean waters to derive seasonal POC maps from SeaWiFS observations. This approach has been further developed for application in the Mediterranean (Loisel et al., 2001) and another related empirical approach (on the basis of a correlation between POC and SeaWiFS-derived normalized water-leaving radiance at 555 nm) has been proposed for the South Atlantic (Mishonov et al., 2003). Loisel et al. (2002) have used satellite-based observations to examine global patterns of seasonality in $b_{b,p}(490)$ and to estimate the global surface POC pool. While these methods may yield acceptable results for many oceanic conditions, their accuracy will undoubtedly be compromised

under certain situations common in coastal waters, including those with high loads of mineral particles. In fact, even within two regions of the Southern Ocean, Stramski et al. (1999) observed significant differences in the relationship between POC and $b_{b,p}(510)$.

A second subcategory of SPM that is amenable to remote sensing is PIC, specifically particulate calcite present in coccoliths produced during *E. huxleyi* or other coccolithophore blooms. Semi-analytical models can be formulated to include the effects of calcite-specific scattering (Gordon et al., 1988; Ackleson et al., 1994; Tyrell et al., 1999; Smyth et al., 2002), although multiple constituent retrievals can be a problem in these applications. Gordon et al. (2001) developed an approach to map PIC on the basis of red and near-infrared SeaWiFS bands, combined with an experimentally determined relationship between $b_b(\lambda)$ and coccolith calcite concentration. This approach has the advantage of being relatively independent of effects of Chl and CDOM absorption. Regardless of the algorithm form, retrieval of PIC depends on knowledge of calcite-specific backscattering (Balch et al., 1991; Balch et al., 1996; Voss et al., 1998) and natural variability within and between species may ultimately constrain accuracy (Balch et al., 1999).

8.5.4 Phytoplankton community composition

The possibility that information about the taxonomic composition of phytoplankton may be retrieved from analysis of AOPs, especially reflectance, is attractive to plankton ecologists. If robust techniques for this can be developed, then spatially and temporally resolved maps of community structure may be derived from satellites, vertical moorings and other platforms.

In a strict sense, this goal remains elusive, and for the same reasons as for IOPs there is no theoretical or empirical evidence to suggest that it can ever be achieved with the rigour of other more conventional methods for quantitatively describing community structure, such as microscopy and molecular genetic analyses. Nevertheless, there are several well-documented circumstances under which AOPs can be used to provide information about occurrence and distribution of particular bloom taxa.

8.5.4.1 Empirical algorithms for particular taxa

The most successful efforts to quantify the occurrence of particular types of phytoplankton from AOPs have been based on empirical analysis of surface reflectance properties. Blooms of taxa associated with distinctive light-scattering properties, such as the coccolithophore *E. huxleyi* and the filamentous cyanobacterium *Trichodesmium* sp., can be detected in satellite imagery. *E. huxleyi* blooms and their associated highly scattering coccoliths produce milky white patches visible from space (e.g. Holligan et al., 1983) and empirical classification algorithms that are based on spectral water-leaving radiance have been used to map global bloom distribution (Brown and Yoder 1994; Iglesias-Rodríguez et al., 2002). *Trichodesmium* blooms also produce distinctive highly reflective, discoloured patches that have been identified empirically in ocean color images (Subramaniam and Carpenter, 1994; Subramaniam et al., 2002). For the purpose of detecting both *E. huxleyi* and *Trichodesmium*, efforts to develop analytical models for remote sensing reflectance have begun to be explored (Ackleson et al., 1994; Subramaniam et al., 1999; Tyrell et al., 1999). Local- or region-specific approaches may also be effective for discriminating waters dominated by different

taxonomic groups; for example, as shown by Bergmann et al. (2004) for diatom- versus cryptophyte-dominated communities in Lake Michigan. For taxa of special interest, such as the red-tide dinoflagellate *K. brevis* common on the west Florida coast, remote sensing algorithms have been used to monitor possible blooms in the context of historical knowledge about bloom seasonality and distribution (Stumpf, 2001). For the case of *K. brevis* off Florida, further work to develop a more explicit taxon-specific approach is also being pursued since these blooms have been shown to have different chlorophyll-specific scattering from other waters in the region (e.g. Cannizzaro et al., 2004).

Most efforts to detect particular taxa on the basis of AOPs rely on distinctive scattering characteristics; however, absorption properties may also be useful for some cases. Kahru and Mitchell (1998) have exploited characteristic absorption features at ultraviolet (UV) wavelengths to identify red-tide blooms from $R_{rs}(\lambda)$ observations extending into the UV. They showed that these bloom species off southern California exhibit enhanced UV absorption (at 380 nm; associated with micosporine-like amino acids) compared with background conditions, and this can be readily detected in reflectance band ratios. Currently, this kind of approach cannot be implemented for satellite imagery because the sensors lack UV bands, but future ocean-colour missions may include such a capability. Another possibility is that effects of the characteristic absorption peaks associated with phycobiliproteins in cyanobacteria may be detectable in AOPs (Sathyendranath et al., 1994), although this may only be practical under extreme bloom conditions (Morel, 1997).

8.5.4.2 Reflectance inversion to retrieve multiple taxa

Especially for application to phytoplankton blooms composed of multiple taxa, an important limitation of the reflectance inversion approaches discussed in Section 8.5.2 is that they typically assume a single fixed spectral basis vector for $a_{ph}(\lambda)$. As the shape of $a_{ph}(\lambda)$ is known to vary with factors such as pigment content and cell size, this simplification may lead to errors in retrieved constituent IOPs. To address this problem in the case of some specific bloom waters, Roesler et al. (2003) introduced a replacement for the first term in (8.18) that accounts for five separate basis vectors:

$$a_{\mathrm{ph}}(\lambda) = \sum_{i=1}^{5} A_{\mathrm{phi}} \mathbf{a_{phi}}, \tag{8.22}$$

where, as above, the amplitudes, A_{phi}, are estimated and the basis vectors, $\mathbf{a_{phi}}$, are specified *a priori*, in this case, for each phytoplankton type *i*. For application to red-tide bloom waters off South Africa, Roesler et al. (2004) determined $\mathbf{a_{phi}}$ from a combination of microscopic and spectrophotometric analysis of various particle size fractions from discrete water samples. They then inverted $R(\lambda)$ measurements to estimate the separate contributions of diatoms, dinoflagellates (except *Dinophysis*), *Dinophysis*, *Mesodinium* and chlorophytes during evolution of a red-tide bloom (Figure 8.19). This is a compelling demonstration of the possibility to retrieve taxonomic information about phytoplankton community structure from remote sensing measurements; however, it is important to recognize that this goal was possible because the basis vectors for $a_{ph}(\lambda)$ were carefully determined from water samples collected during the bloom. Moreover, the example comes from bloom conditions under which phytoplankton dominated both the IOPs and AOPs. Further research is required to determine how broadly this promising approach can be applied.

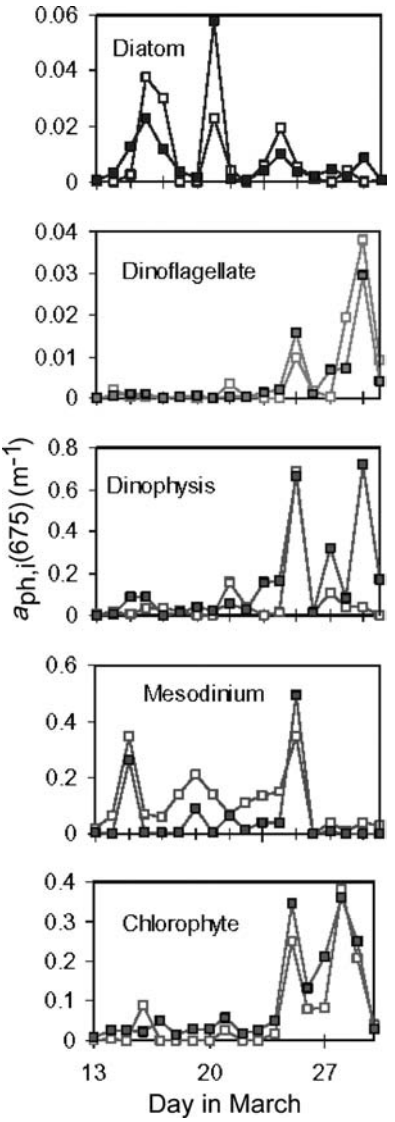

Figure 8.19
Contributions of different phytoplankton groups to total $a_{ph}(675)$ during a bloom sequence in South African coastal waters estimated from microscopic observations (open symbols) and from the reflectance inversion model (solid symbols) of Roesler et al. (2004). See text for details.
Source: Roesler et al. (2004).

8.6 Optical properties and HABs – summary comments

In assessing the relationships between HABs and optical properties, it is critical to consider that spatial, temporal and ecological characteristics of HABs vary dramatically and in ways that have optical implications. For example, some taxa form near monospecific blooms of such an extent that they dominate the phytoplankton biomass over large space and timescales. In some other cases, such as the one presented in Section 8.5.4, mixed species blooms can be responsible for total biomass that is so high that the absorption and scattering associated with phytoplankton exceeds that for other particulate and dissolved material. In these cases, bulk IOPs and AOPs have great potential to provide information about bloom dynamics, and a wide range of measurement approaches from microscale IOP meters (Roesler and Boss, 2007 – Chapter 5 this volume) to regional scale remote sensing of surface AOPs (Ruddick et al., 2007 – Chapter 9 this volume) are useful. Even in these cases, however, extracting information about specific bloom taxa from bulk optical properties remains a research topic.

Another extreme are spatially and temporally localized HABs where a single species increases in abundance, yet remains a small portion of the total phytoplankton biomass. In some cases these blooms can even be localized to thin (meter-scale or less) subsurface vertical layers. These are generally not amenable to detection by satellite or airborne remote sensing. Direct optically based detection of these HAB species *in situ* requires specialized techniques under development such as cell-level imaging or optical indicators linked with molecular probing (see e.g. Scholin et al., 2007 – Chapter 11 this volume). For these types of HAB, more conventional optical approaches may be most appropriate for general characterization of the environmental conditions under which the HAB phenomena occur.

Cullen (2007 – Chapter 1 this volume) proposes a classification system for HABs that is based on environmental and ecological characteristics, some of which have a direct bearing on optical consequences. This kind of assessment should be a first step in identifying which of the optical techniques and measurement approaches reviewed here may be effective components of an ocean observing system for HAB monitoring and research. Depending on the HAB problem of interest, the goals for an observing system may span from environmental characterization to species-specific detection to prediction of bloom transport and fate (Schofield et al., 2007 – Chapter 3 this volume). It cannot be overstated that no one approach or set of approaches can be recommended for all types of HABs. Informed choices must be made about sampling strategy, including which properties to target and the appropriate space and timescales for observation. The knowledge summarized here about advantages and limitations of various optical approaches for providing information on seawater constituents should be an important consideration in making these decisions.

8.7 Conclusion – opportunities and challenges

The optical properties of seawater depend on so many characteristics of the water's constituents that the problem of their interpretation presents at once great opportunities and great challenges. If the relationships between optical properties and constituent properties were very simple, then the potential for insights would be well constrained but relatively limited. In fact, the complexity of factors contributing to optical

variability currently limits the accuracy with which we can extract information about ecological and biogeochemical properties from optical observations. At the same time, the potential to derive new and more accurate information continues to be alluring.

The present state of this field is strengthened by several lines of theoretical underpinning and by observational generalizations that have emerged over years of inquiry. These foundations provide a ready frame of reference for investigating exceptions and intriguing results that continue to defy easy interpretation, such as the optical properties of near-monospecific phytoplankton blooms. Developments in this area are proceeding rapidly and we can continue to look forward to new and fundamental insights.

Potential ecological applications for optical observations span a great range of space and timescales, as well as requiring various degrees of accuracy and specificity. This means that general conclusions about current status and future needs and potential are difficult to make. For many of the examples presented in this chapter, there are well documented relationships between optical properties and constituents that are evident when the full range of observed variability (a 'global' data set) is considered. When these relationships are examined in closer detail, however, it is common to find that the global generalization does not apply at many smaller scales. At the same time, there are a variety of cases where local (in space or time) relationships between optical properties and constituent properties can be well defined and understood. These can be exploited for many important applications, but not indiscriminately extrapolated to larger or different scales.

In the end, the choice of relevant optical properties and interpretation approaches must depend on the problem of interest. In many cases, difficulties or limitations with interpretation are more than offset by the sampling advantages. Almost without exception, ecologists do not have tools or methods for sampling quantities of interest in the ocean over the scales and with the resolution that important questions require. Optical properties that are practical to measure at timescales ranging from microseconds to years and on space scales from micrometres to thousands of kilometres have great appeal. A model that will probably continue to be productive is that of local-to-regional scale optical sampling, combined with periodic or intermittent (perhaps guided) discrete sampling for detailed analysis of constituents or properties of interest.

References

Ackleson, S. G., Balch, W. M. and Holligan, P. M. 1994. The response of water-leaving radiance to particulate calcite and pigment concentration: a model for Gulf of Maine coccolithophore blooms. *J. Geophys. Res.*, 99, pp. 7483–500.

Ackleson, S. G. and Spinrad, R. W. 1988. Size and refractive index of individual marine particulates: a flow cytometric approach. *Appl. Opt.*, 27, pp. 1270–77.

Ahn, Y. H., Bricaud, A. and Morel, A. 1992. Light backscattering efficiency and related properties of some phytoplankters. *Deep Sea Res.*, 39, pp. 1835–55.

Allali, K., Bricaud, A. and Claustre, H. 1997. Spatial variations in the chlorophyll-specific absorption coefficients of phytoplankton and photosynthetically active pigments in the equatorial Pacific. *J. Geophys. Res.*, 102, pp. 12413–23.

Babin, M. 2007. Phytoplankton fluorescence: theory, current literature and *in situ* measurement. In: Babin et al. (eds), op. cit., this volume.

Babin, M., Morel, A., Fournier-Sicre, V., Fell, F. and Stramski, D. 2003*a*. Light scattering properties of marine particles in coastal and open ocean waters as related to the particle mass concentration. *Limnol. Oceanogr.*, 48, pp. 843–59.

Babin, M., Roesler, C. S. and Cullen, J. J. (eds). 2007. *Real-time Coastal Observing Systems for Marine Ecosystem Dynamics and Harmful Algal Blooms: Theory, Instrumentation and Modelling*. Paris, Intergovernmental Oceanographic Commission of UNESCO. (Monographs on Oceanographic Methodology.)

Babin, M., Stramski, D., Ferrari, G. M., Claustre, H., Bricaud, A., Obolensky, G. and Hoepffner, N. 2003*b*. Variations in the light absorption coefficients of phytoplankton, nonalgal particles, and dissolved organic matter in coastal waters around Europe. *J. Geophys. Res.*, 108, 3211, doi:3210.1029/2001JC000882.

Babin, M. and Stramski, D. 2004. Variations in the mass-specific absorption coefficient of mineral particles suspended in water. *Limnol. Oceanogr.*, 49, pp. 756–67.

Babin, M., Therriault, J. C., Legendre, L., Nieke, B., Reuter, R. and Condal, A. 1995. Relationship between the maximum quantum yield of carbon fixation and the minimum quantum yield of chlorophyll *a in vivo* fluorescence in the Gulf of St. Lawrence. *Limnol. Oceanogr.*, 40, pp. 956–68.

Baker, E. T. and Lavelle, J. W. 1984. The effect of particle size on the light attenuation coefficient of natural suspensions. *J. Geophys. Res.*, 89, pp. 8197–203.

Balch, W. M., Drapeau, D. T., Cucci, T. L., Vaillancourt, R. D., Kilpatrick, K. A. and Fritz, J. J. 1999. Optical backscattering by calcifying algae: separating the contribution of particulate inorganic and organic carbon fractions. *J. Geophys. Res.*, 104, pp. 1541–58.

Balch, W. M., Drapeau, D. T., Fritz, J. J., Bowler, B. C. and Nolan, J. 2001. Optical backscattering in the Arabian Sea – continuous underway measurements of particulate inorganic and organic carbon. *Deep Sea Res. I*, 48, pp. 2423–52.

Balch, W. M., Holligan, P. M., Ackleson, S. G. and Voss, K. J. 1991. Biological and optical properties of mesoscale coccolithophore blooms in the Gulf of Maine. *Limnol. Oceanogr.*, 36, pp. 629–43.

Balch, W. M., Kirkpatrick, K. A., Holligan, P., Harbour, D. and Fernandez, E. 1996. The 1991 coccolithophore bloom in the central North Atlantic. 2: Relating optics to coccolith concentration. *Limnol. Oceanogr.*, 41, pp. 1684–96.

Barnard, A. H., Pegau, W. S. and Zaneveld, J. R. V. 1998. Global relationships of the inherent optical properties of the oceans. *J. Geophys. Res.*, 103, pp. 24955–68.

Bergmann, T., Fahnenstiel, G., Lohrenz, S., Millie, D. and Schofield, O. 2004. The impacts of recurrent resuspension events and variable phytoplankton community composition on remote sensing reflectance. *J. Geophys. Res.*, 109, C10S15, doi:10.1029/2002JC001575.

Beutler, M., Wiltshire, K. H., Meyer, B., Moldaenke, C., Lüring, C., Meyerhöfer, M., Hansen, U. P. and Dau, H. 2002. A fluorometric method for the differentiation of algal populations *in vivo* and *in situ*. *Photosyn. Res.*, 72, pp. 39–53.

Bidigare, R. R., Ondrusek, M. E., Morrow, J. H. and Kiefer, D. 1990. *In vivo* absorption properties of algal pigments. *Ocean Optics X*, *Proc. SPIE*, 1302, pp. 290–302.

Bishop, J. K. B. 1986. The correction and suspended matter calibration of Sea Tech transmissometer data. *Deep Sea Res.*, 33, pp. 121–34.

Bishop, J. K. B. 1999. Transmissometer measurement of POC. *Deep Sea Res. I*, 46, pp. 353–69.

Bishop, J. K. B., Calvert, S. E. and Soon, M. Y. S. 1999. Spatial and temporal variability of POC in the northeast Subarctic Pacific. *Deep Sea Res. II*, 46, pp. 2699–733.

Blough, N. V. and Del Vecchio, R. 2002. Chromophoric DOM in the coastal environment. In: D. A. Hansell and C. A. Carlson (eds), *Biogeochemistry of Marine Dissolved Organic Matter*. New York, Academic Press, pp. 509–46.

Blough, N. V., Zafiriou, O. C. and Bonilla, J. 1993. Optical absorption spectra of waters from the Orinoco River outflow: terrrestrial input of colored organic matter to the Caribbean. *J. Geophys. Res.*, 98, pp. 2271–78.

Bohren, C. F. and Hoffman, D. R. 1983. *Absorption and Scattering of Light by Small Particles*. New York, John Wiley & Sons.

Boss, E., Pegau, W. S., Gardner, W. D., Zaneveld, J. R. V., Barnard, A. H., Twardowski, M. S., Chang, G. C. and Dickey, T. D. 2001*c*. Spectral particulate attenuation and particle

size distribution in the bottom boundary layer of a continental shelf. *J. Geophys. Res.*, 106, pp. 9509–16.

Boss, E., Pegau, W. S., Lee, M., Twardowski, M., Shybanov, E., Korotaev, G. and Baratange, F. 2004. Particulate backscattering ratio at LEO 15 and its use to study particle composition and distribution. *J. Geophys. Res.*, 109(C1), doi:10.1029/2002JC001415.

Boss, E., Pegau, W. S., Zaneveld, J. R. V. and Barnard, A. H. 2001*b*. Spatial and temporal variability of absorption by dissolved material at a continental shelf. *J. Geophys. Res.*, 106, pp. 9499–507.

Boss, E., Twardowski, M. S. and Herring, S. 2001*a*. Shape of the particulate beam attenuation spectrum and its inversion to obtain the shape of the particulate size distribution. *Appl. Opt.*, 40, pp. 4885–93.

Bowers, D. G., Harker, G. E. L. and Stephan, B. 1996. Absorption spectra of inorganic particles in the Irish Sea and their relevance to remote sensing of chlorphyll. *Int. J. Rem. Sens.*, 17, pp. 2449–60.

Boynton, G. C. and Gordon, H. R. 2002. Irradiance inversion algorithm for absorption and backscattering profiles in natural waters: Improvements for clear waters. *Appl. Opt.*, 41, pp. 2224–27.

Bricaud, A. 2002. Inherent optical properties of particles in Case 1 waters: The various parameterizations and their consistency. *Ocean Optics XVI*, *Proc.* pp. 1–8.

Bricaud, A., Babin, M., Morel, A. and Claustre, H. 1995*b*. Variability in the chlorophyll-specific absorption coefficients of natural phytoplankton: Analysis and parameterization. *J. Geophys. Res.*, 100, pp. 13321–32.

Bricaud, A. and Morel, A. 1986. Light attenuation and scattering by phytoplankton cells: a theoretical modeling. *Appl. Opt.*, 25, pp. 571–80.

Bricaud, A., Morel, A., Babin, M., Allali, K. and Claustre, H. 1998. Variations of light absorption by suspended particles with chlorophyll *a* concentration in oceanic (Case 1) waters: analysis and implications for bio-optical models. *J. Geophys. Res.*, 103, pp. 31033–44.

Bricaud, A., Morel, A. and Prieur, L. 1981. Absorption by dissolved organic matter of the sea (yellow substance) in the UV and visible domains. *Limnol. Oceanogr.*, 26, pp. 43–53.

Bricaud, A., Morel, A. and Prieur, L. 1983. Optical efficiency factors of some phytoplankters. *Limnol. Oceanogr.*, 28, pp. 816–32.

Bricaud, A., Roesler, C. and Zaneveld, J. R. V. 1995*a*. *In situ* methods for measuring the inherent optical properties of ocean waters. *Limnol. Oceanogr.*, 40, pp. 393–410.

Bricaud, A. and Stramski, D. 1990. Spectral absorption coefficients of living phytoplankton and non-algal biogenous matter: a comparison between the Peru upwelling area and the Sargasso Sea. *Limnol. Oceanogr.*, 35, pp. 562–82.

Brown, C. A., Huot, Y., Purcell, M. J., Cullen, J. J. and Lewis, M. R. 2004. Mapping coastal optical and biogeochemical variability using an Autonomous Underwater Vehicle (AUV) and a new bio-optical inversion algorithm. *Limnol. Oceanogr. Meth.*, 2, pp. 262–81.

Brown, C. W. and Yoder, J. A. 1994. Coccolithophorid blooms in the global ocean. *J. Geophys. Res.*, 99, pp. 7467–82.

Brown, O. B. and Gordon, H. R. 1974. Size-refractive index distribution of clear coastal water particulates from light scattering. *Appl. Opt.*, 13, pp. 2874–81.

Cannizzaro, J. P., Carder, K. L., Chen, R. F., Heil, C. A. and Vargo, G. A. 2007. A novel technique for detection of the toxic dinoflagellate, *Karenia brevis*, in the Gulf of Mexico from remotely sensed ocean color data. *Cont. Shelf Res.*

Carder, K. L., Betzer, P. R. and Eggimann, D. W. 1974. Physical, chemical, and optical measures of suspended-particle concentrations: their intercomparison and application to the West African Shelf. In: R. J. Gibbs (ed.), *Suspended Solids in Water*. New York, Plenum Press, pp. 173–93.

Carder, K. L., Chen, F. R., Lee, Z. P. and Hawes, S. K. 1999. Semianalytic moderate-resolution imaging spectrometer algorithms for chlorophyll *a* and absorption with bio-optical domains based on nitrate-depletion temperatures. *J. Geophys. Res.*, 104, pp. 5403–21.

Carder, K. L., Hawes, S. K., Baker, K. A., Smith, R. C., Steward, R. G. and Mitchell, B. G. 1991. Reflectance model for quantifying chlorophyll *a* in the presence of productivity degradation products. *J. Geophys. Res.*, 96, pp. 20599–611.

Carder, K. L., Steward, R. G., Harvey, G. R. and Ortner, P. B. 1989. Marine humic and fulvic acids: their effects on remote sensing of ocean chlorophyll. *Limnol. Oceanogr.*, 34, pp. 68–81.

Chang, G. C., Dickey, T. D., Schofield, O. M., Weidemann, A. D., Boss, E., Pegau, W. S., Moline, M. A. and Glenn, S. M. 2002. Nearshore physical processes and bio-optical properties in the New York Bight. *J. Geophys. Res.*, 107, 3133, doi:3110.1029/2001JC001018.

Chisholm, S. W. 1992. Phytoplankton size. In: P. G. Falkowski and A. D. Woodhead (eds), *Primary Productivity and Biogeochemical Cycles in the Sea*. New York, Plenum Press, pp. 213–37.

Chung, S. P., Gardner, W. D., Landry, M. R., Richardson, M. J. and Walsh, I. D. 1998. Beam attenuation by microorganisms and detrital particles in the equatorial Pacific. *J. Geophys. Res.*, 103, pp. 12669–81.

Ciotti, A. M., Cullen, J. J. and Lewis, M. R. 1999. A semi-analytical model of the influence of phytoplankton community structure on the relationship between light attenuation and ocean color. *J. Geophys. Res.*, 104, pp. 1559–78.

Ciotti, A. M., Lewis, M. R. and Cullen, J. J. 2002. Assessment of the relationships between dominant cell size in natural phytoplankton communities and the spectral shape of the absorption coefficient. *Limnol. Oceanogr.*, 47, pp. 404–17.

Claustre, H., Morel, A., Babin, M., Cailliau, C., Marie, D., Marty, J. C., Tailliez, D. and Vaulot, D. 1999. Variability in particle attenuation and chlorophyll fluorescence in the tropical Pacific: scales, patterns, and biogeochemical implications. *J. Geophys. Res.*, 104, pp. 3401–22.

Cleveland, J. S. 1995. Regional models for phytoplankton absorption as a function of chlorophyll *a* concentration. *J. Geophys. Res.*, 100, pp. 13333–44.

Cullen, J. J. 2007. Observation and prediction of harmful algal blooms. In: Babin et al. (eds), op. cit., this volume.

Cullen, J. J., Ciotti, A. M., Davis, R. F. and Lewis, M. R. 1997. Optical detection and assessment of algal blooms. *Limnol. Oceanogr.*, 42, pp. 1223–39.

Cullen, J. J., Lewis, M. R., Davis, C. O. and Barber, R. T. 1992. Photosynthetic characteristics and estimated growth rates indicate grazing is the proximate control of primary production in the equatorial Pacific. *J. Geophys. Res.*, 97, pp. 639–54.

Doerffer, R. and Fischer, J. 1994. Concentrations of chlorophyll, suspended matter, and gelbstoff in Case II waters derived from satellite coastal zone color scatter data with inverse modeling methods. *J. Geophys. Res.*, 99, pp. 6457–7466.

Dubelaar, G. B. J. and Gerritzen, P. L. 2000. CytoBuoy: a step forward towards using flow cytometry in operational oceanography. *Scientia Marina*, 64, pp. 255–65.

DuRand, M. D. and Olson, R. J. 1996. Contributions of phytoplankton light scattering and cell concentration changes to diel variations in beam attenuation in the equatorial Pacific from flow cytometric measurements of pico-, ultra- and nanoplankton. *Deep Sea Res. I*, 43, pp. 891–906.

Eisner, L. B., Twardowski, M. S., Cowles, T. J. and Perry, M. J. 2003. Resolving phytoplankton photoprotective: photosynthetic carotenoid ratios on fine scales using *in situ* spectral absorption measurements. *Limnol. Oceanogr.*, 48, pp. 632–46.

Ferrari, G. M. 2000. The relationship between chromophoric dissolved organic matter and dissolved organic carbon in the European Atlantic coastal area and in the West Mediterranean Sea (Gulf of Lions). *Mar. Chem.*, 70, pp. 339–57.

Gardner, W. D., Blakey, J. C., Walsh, I. D., Richardson, M. J., Pegau, S., Zaneveld, J. R. V., Roesler, C., Gregg, M. C., MacKinnon, J. A., Sosik, H. M. and Williams, A. J. 3rd. 2001. Optics, particles, stratification, and storms on the New England continental shelf. *J. Geophys. Res.*, 106, pp. 9473–97.

Gardner, W. D., Walsh, I. D. and Richardson, M. J. 1993. Biophysical forcing of particle production and distribution during a spring bloom in the North Atlantic. *Deep Sea Res. II*, 40, pp. 171–95.

Garver, S. and Siegel, D. 1997. Inherent optical property inversion of ocean color spectra and its biogeochemical interpretation. 1: Time series from the Sargasso Sea. *J. Geophys. Res.*, 102, pp. 18607–25.

Garver, S. A., Siegel, D. A. and Mitchell, B. G. 1994. Statistical variability of near-surface particulate absorption spectra: what can a satellite ocean color imager see? *Limnol. Oceanogr.*, 39, pp. 1349–67.

Goericke, R. and Montoya, J. P. 1998. Estimating the contribution of microalgal taxa to chlorophyll *a* in the field-variations of pigment ratios under nutrient- and light-limited growth. *Mar. Ecol. Progr. Ser.*, 169, pp. 87–95.

Gordon, H. R. 1991. Absorption and scattering estimates from irradiance measurements: Monte Carlo simulations. *Limnol. Oceanogr.*, 36, pp. 769–77.

Gordon, H. R. 2002. Inverse methods in hydrologic optics. *Oceanologia*, 44, pp. 9–58.

Gordon, H. R. and Boynton, G. C. 1997. Radiance irradiance inversion algorithms for estimating the absorption and backscattering coefficients of natural waters: homogeneous waters. *Appl. Opt.*, 36, pp. 2636–41.

Gordon, H. R. and Boynton, G. C. 1998. Radiance irradiance inversion algorithm for estimating the absorption and backscattering coefficients of natural waters: vertically stratified water bodies. *Appl. Opt.*, 37, pp. 3886–96.

Gordon, H. R., Boynton, G. C., Balch, W. M., Groom, S. B., Harbour, D. S. and Smyth, T. J. 2001. Retrieval of coccolithophore calcite concentration from SeaWiFS imagery. *Geophys. Res. Lett.*, 28, pp. 1587–90.

Gordon, H. R., Brown, O. B., Evans, R. H., Brown, J. W., Smith, R. C., Baker, K. S. and Clark, D. K. 1988. A semianalytic radiance model of ocean color. *J. Geophys. Res.*, 93, pp. 10909–24.

Gordon, H. R., Brown, O. B., and Jacobs, M. M. 1975. Computed relationships between the inherent and apparent optical properties of a flat homogeneous ocean. *Appl. Opt.*, 14, pp. 417–27.

Gordon, H. R., Clark, D. K., Brown, J. W., Brown, O. B., Evans, R. H. and Broenkow, W. W. 1983. Phytoplankton pigment concentrations in the Middle Atlantic Bight: comparison of ship determinations and CZCS estimates. *Appl. Opt.*, 22, pp. 20–36.

Gordon, H. R. and Du, T. 2001. Light scattering by nonspherical particles: application to coccoliths detached from *Emiliana huxleyi*. *Limnol. Oceanogr.*, 46, pp. 1438–54.

Gordon, H. R. and Morel, A. 1983. *Remote Assessment of Ocean Color for Interpretation of Satellite Visible Imagery. A Review*. New York, Springer-Verlag.

Gould, R. W. Jr, Arnone, R. A. and Martinolich, P. M. 1999. Spectral dependence of the scattering coefficient in Case 1 and Case 2 waters. *Appl. Opt.*, 38, pp. 2377–83.

Gould, R. W. Jr, Arnone, R. A. and Sydor, M. 2001. Absorption, scattering, and remote-sensing reflectance relationships in coastal waters: testing a new inversion algorithm. *J. Coast. Res.*, 17, pp. 328–41.

Green, R. E. and Sosik, H. M. 2004. Analysis of apparent optical properties and ocean color models using measurements of seawater constitutents in New England continental shelf surface waters. *J. Geophys. Res.*, 109, C03026, doi:03010.01029/02003JC001977.

Green, R. E., Sosik, H. M. and Olson, R. J. 2003*a*. Contributions of phytoplankton and other particles to inherent optical properties in New England continental shelf waters. *Limnol. Oceanogr.*, 48, pp. 2377–91.

Green, R. E., Sosik, H. M., Olson, R. J. and DuRand, M. D. 2003*b*. Flow cytometric determination of size and complex refractive index for marine particles: comparison with independent and bulk estimates. *Appl. Opt.*, 42, pp. 526–41.

Guay, C. K. H. and Bishop, J. K. B. 2002. A rapid birefringence method for measuring suspended $CaCO_3$ concentrations in seawater. *Deep Sea Res. I*, 49, pp. 197–210.

Gundersen, J. S., Gardner, W. D., Richardson, M. J. and Walsh, I. D. 1998. Effects of monsoons on the seasonal and spatial distributions of POC and chlorophyll in the Arabian Sea. *Deep Sea Res. II*, 45, pp. 2103–32.

Guo, L., Santschi, P. H., Cifuentes, L. A., Trumbore, S. E. and Southon, J. 1996. Cycling of high-molecular-weight dissolved organic matter in the Middle Atlantic Bight as revealed by carbon isotopic (^{13}C and ^{14}C) signatures. *Limnol. Oceanogr.*, 41, pp. 1242–52.

Hoepffner, N. and Sathyendranath, S. 1992. Bio-optical characteristics of coastal waters: absorption spectra of phytoplankton and pigment distribution in the western North Atlantic. *Limnol. Oceanogr.*, 37, pp. 1660–79.

Hoepffner, N. and Sathyendranath, S. 1993. Determination of the major groups of phytoplankton pigments from the absorption spectra of total particulate matter. *J. Geophys. Res.*, 98, pp. 22789–803.

Hoge, F. E. and Lyon, P. E. 1996. Satellite retrieval of inherent optical properties by linear matrix inversion of oceanic radiance models: an analysis of model and radiance measurement errors. *J. Geophys. Res.*, 101, pp. 16631–48.

Højerslev, N. K., Holt, N. and Aarup, T. 1996. Optical measurements in the North Sea-Baltic Sea transition zone. I. On the origin of the deep water in the Kattegat. *Cont. Shelf Res.*, 16, pp. 1329–42.

Holligan, P. M., Viollier, M., Harbour, D. S., Camus, P. and Champagne-Philippe, M. 1983. Satellite and ship studies of coccolithophore production along a continental shelf edge. *Nature*, 304, pp. 339–42.

Holm-Hansen, O., Lorenzen, C. J., Holmes, R. W. and Strickland, J. D. H. 1965. Fluorometric determination of chlorophyll. *J. Cons. Int. Explor. Mer*, 30, pp. 3–15.

Iglesias-Rodríguez, M. D., Brown, C. W., Doney, S. C., Kleypas, J., Kolber, D., Kolber, Z., Hayes, P. K. and Falkowski, P. G. 2002. Representing key phytoplankton functional groups in ocean carbon cycle models: Coccolithophorids. *Global Biogeochem. Cy.*, 16, 1100, doi: 1110.1029/2001GB001454.

Iturriaga, R. and Siegel, D. A. 1989. Microphotometric characterization of phytoplankton and detrital absorption properties in the Sargasso Sea. *Limnol. Oceanogr.*, 34, pp. 1706–26.

Jeffrey, S. W. and Vesk, M. 1997. Introduction to marine phytoplankton and their pigment signatures. In: S. W. Jeffrey, R. F. C. Mantoura and S. W. Wright, (eds), *Phytoplankton Pigments in Oceanography: Guidelines to Modern Methods*. Paris, UNESCO, pp. 37–84.

Johnsen, G., Samset, O., Granskog, L. and Sakshaug, E. 1994. *In vivo* absorption characteristics in 10 classes of bloom-forming phytoplankton: taxonomic characteristics and responses to photoadaptation by means of discriminant and HPLC analysis. *Mar. Ecol. Progr. Ser.*, 105, pp. 149–57.

Kahru, M. and Mitchell, B. G. 1998. Spectral reflectance and absorption of a massive red tide off southern California. *J. Geophys. Res.*, 103, pp. 21601–09.

Kana, T. M., Glibert, P. M., Goericke, R. and Welschmeyer, N. A. 1988. Zeaxanthin and β-carotene in *Synechoccus* WH7803 respond differently to irradiance. *Limnol. Oceanogr.*, 33, pp. 1623–27.

Kieber, R. J., Zhou, X. and Mopper, K. 1990. Formation of carbonyl compounds from UV-induced photodegradation of humic substances in natural waters: fate of riverine carbon in the sea. *Limnol. Oceanogr.*, 35, pp. 1503–15.

Kirk, J. T. O. 1984. Dependence of relationship between inherent and apparent optical properties of water on solar altitude. *Limnol. Oceanogr.*, 29, pp. 350–56.

Kirk, J. T. O. 1994. *Light and Photosynthesis in Aquatic Ecosystems*. Cambridge, UK, Cambridge University Press.

Kirkpatrick, G. J., Millie, D. F., Moline, M. A. and Schofield, O. 2000. Optical discrimination of a phytoplankton species in natural mixed populations. *Limnol. Oceanogr.*, 45, pp. 467–71.

Kishino, M., Takahashi, N., Okami, N. and Ichimura, S. 1985. Estimation of the spectral absorption coefficients of phytoplankton in the sea. *Bull. Mar. Sci.*, 37, pp. 634–42.

Kitchen, J. C. and Zaneveld, J. R. V. 1990. On the non-correlation of the vertical structure of light scattering and chlorophyll *a* in Case I waters. *J. Geophys. Res.*, 95, pp. 20237–46.

Kitchen, J. C., Zaneveld, J. R. V. and Pak, H. 1982. Effect of particle size distribution and chlorophyll content on beam attenuation spectra. *Appl. Opt.*, 21, pp. 3913–18.

Lee, Z. P., Carder, K. L. and Arnone, R. A. 2002. Deriving inherent optical properties from water color: a multiband quasi-analytical algorithm for optically deep waters. *Appl. Opt.*, 41, pp. 5755–72.

Lewis, M. 2007. Measurement of apparent optical properties for diagnosis of harmful algal blooms. In: Babin et al. (eds), op. cit., this volume.

Loisel, H., Bosc, E., Stramski, D., Oubelkheir, K. and Deschamps, P. Y. 2001. Seasonal variability of the backscattering coefficient in the Mediterranean Sea based on satellite SeaWiFS imagery. *Geophys. Res. Lett.*, 28, pp. 4203–06.

Loisel, H. and Morel, A. 1998. Light scattering and chlorophyll concentration in Case 1 waters: a reexamination. *Limnol. Oceanogr.*, 43, pp. 847–58.

Loisel, H., Nicolas, J. M., Deschamps, P. Y. and Frouin, R. 2002. Seasonal and inter-annual variability of particulate organic matter in the global ocean. *Geophys. Res. Lett.*, 29, doi:10.1029/2002GL015948.

Loisel, H. and Stramski, D. 2000. Estimation of the inherent optical properties of natural waters from the irradiance attenuation coefficient and reflectance in the presence of Raman scattering. *Appl. Opt.*, 39, pp. 3001–11.

Lutz, V. A., Sathyendranath, S. and Head, E. J. H. 1996. Absorption coefficient of phytoplankton: regional variations in the North Atlantic. *Mar. Ecol. Progr. Ser.*, 135, pp. 197–213.

Mackey, M. D., Mackey, D. J., Higgins, H. W. and Wright, S. W. 1996. CHEMTAX – a program for estimating class abundances from chemical markers: application to HPLC measurements of phytoplankton. *Mar. Ecol. Progr. Ser.*, 144, pp. 265–83.

Maffione, R. A. and Dana, D. R. 1997. Instruments and methods for measuring the backward-scattering coefficient of ocean waters. *Appl. Opt.*, 36, pp. 6057–67.

Maritorena, S., Siegel, D. A. and Peterson, A. R. 2002. Optimization of a semianalytical ocean color model for global-scale application. *Appl. Opt.*, 41, pp. 2705–14.

Miller, W. L. and Zepp, R. G. 1995. Photochemical production of dissolved inorganic carbon from terrestrial organic matter: significance to the oceanic organic carbon cycle. *Geophys. Res. Lett.*, 22, pp. 417–20.

Millie, D. F., Schofield, O. M. E., Kirkpatrick, G. J., Johnsen, G. and Evens, T. J. 2002. Using absorbance and fluorescence spectra to discriminate microalgae. *Eur. J. Phycol.*, 37, pp. 313–22.

Millie, D. F., Schofield, O. M., Kirkpatrick, G. J., Johnsen, G., Tester, P. A. and Vinyard, B. T. 1997. Detection of harmful algal blooms using photopigments and absorption signatures: a case study of the Florida red tide dinoflagellate, *Gymnodinium breve*. *Limnol. Oceanogr.*, 2, pp. 1240–51.

Mishonov, A. V., Gardner, W. D. and Richardson, M. J. 2003. Remote sensing and surface POC concentration in the South Atlantic. *Deep Sea Res. II*, 50, pp. 2997–3015.

Mitchell, B. G. and Kiefer, D. A. 1988. Variability in pigment specific particulate fluorescence and absorption spectra in the northeastern Pacific Ocean. *Deep Sea Res.*, 35, pp. 665–89.

Moore, C. C., Twardowski, M. S. and Zaneveld, J. R. V. 2000. The ECO VSF – a sensor for determination of the volume scattering function in the backward direction. *Ocean Optics XV*, *Proc.* p. 1.

Moore, C., Zaneveld, J. R. V. and Kitchen, J. C. 1992. Preliminary results from an in-situ spectral absorption meter. *Ocean Optics XI*, *Proc. SPIE*, 1750, pp. 330–37.

Mopper, K. and Kieber, D. J. 2002. Photochemistry and the cycling of carbon, sulfur, nitrogen and phosphorus. In: C. A. Carlson (ed.), *Biogeochemistry of Marine Dissolved Organic Matter*. New York, Academic Press, pp. 456–508.

Morel, A. 1973. Diffusion de la lumière par les eaux de mer. Résultats expérimentaux et approche théorique. In: *Optics of the Sea. AGARD Lect. Ser.*, 61, pp. 3.1.1–3.1.76.

Morel, A. 1987. Chlorophyll-specific scattering coefficient of phytoplankton. A simplified theoretical approach. *Deep Sea Res.*, 34, pp. 1093–105.

Morel, A. 1988. Optical modeling of the upper ocean in relation to its biogenous matter content (case I waters). *J. Geophys. Res.*, 93, pp. 10749–68.

Morel, A. 1997. Consequences of a *Synechococcus* bloom upon the optical properties of oceanic (Case 1) waters. *Limnol. Oceanogr.*, 42(8), pp. 1746–54.

Morel, A. 2007. Introduction to optical properties in the sea: theoretical aspects. In: Babin et al. (eds), op. cit., this volume.

Morel, A. and Ahn, Y. H. 1990. Optical efficiency factors of free-living marine bacteria: influence of bacterioplankton upon the optical properties and particulate organic carbon in oceanic waters. *J. Mar. Res.*, 48, pp. 145–75.

Morel, A. and Ahn, Y. H. 1991. Optics of heterotrophic nanoflagellates and ciliates: a tentative assessment of their scattering role in oceanic waters compared to those of bacterial and algal cells. *J. Mar. Res.*, 49, pp. 177–202.

Morel, A. and Bricaud, A. 1981*a*. Theoretical results concerning light absorption in a discrete medium, and applications to specific absorption of phytoplankton. *Deep Sea Res.*, 28A, pp. 1375–93.

Morel, A. and Bricaud, A. 1981*b*. Theoretical results concerning the optics of phytoplankton, with special reference to remote sensing applications. In: J. F. R. Gower (ed.), *Oceanography from Space*. New York, Plenum Press, pp. 313–27.

Morel, A. and Bricaud, A. 1986. Inherent optical properties of algal cells including picoplankton: Theoretical and experimental results. In: T. Platt and W. K. W. Li (eds), *Photosynthetic Picoplankton*. *Can. Bull. Fish. Aquat. Sci.*, 214, pp. 521–59.

Morel, A. and Gentili, B. 1991. Diffuse reflectance of oceanic waters: Its dependence on sun angle as influenced by the molecular scattering contribution. *Appl. Opt.*, 30, pp. 4427–38.

Morel, A. and Maritorena, S. 2001. Bio-optical properties of oceanic waters: a reappraisal. *J. Geophys. Res.*, 106, pp. 7163–80.

Morel, A. and Prieur, L. 1977. Analysis of variations in ocean color. *Limnol. Oceanogr.*, 22, pp. 709–22.

Nelson, J. R. and Guarda, S. 1995. Particulate and dissolved spectral absorption on the continental shelf of the southeastern United States. *J. Geophys. Res.*, 100, pp. 8715–32.

Nelson, N. B. and Siegel, D. A. 2002. Chromophoric DOM in the open ocean. In: C. A. Carlson (ed.), *Biogeochemistry of Marine Dissolved Organic Matter*. New York, Academic Press, pp. 547–78.

Nelson, N. B., Siegel, D. A. and Michaels, A. F. 1998. Seasonal dynamics of colored dissolved material in the Sargasso Sea. *Deep Sea Res. I*, 45, pp. 931–57.

Olson, R. J., Chisholm, S. W., Zettler, E. R., Altabet, M. A. and Dusenberry, J. A. 1990. Spatial and temporal distributions of prochlorophyte picoplankton in the North Atlantic Ocean. *Deep Sea Res.*, 37, pp. 1033–51.

Olson, R. J., Shalapyonok, A. A. and Sosik, H. M. 2003. An automated submersible flow cytometer for pico- and nanophytoplankton: FlowCytobot. *Deep Sea Res. I*, 50, pp. 301–15.

Olson, R. J., Zettler, E. R. and Anderson, O. K. 1989. Discrimination of eukaryotic phytoplankton cell types from light scatter and autofluorescence properties measured by flow cytometry. *Cytometry*, 10, pp. 636–43.

Olson, R. J., Zettler, E. R. and DuRand, M. D. 1993. Phytoplankton analysis using flow cytometry. In: P. F. Kemp, B. F. Sherr, E. B. Sherr and J. J. Cole (eds), *Handbook of Methods in Aquatic Microbial Ecology*. Boca Raton, Fla., Lewis Publishers, pp. 175–86.

Opsahl, S. and Benner, R. 1997. Distribution and cycling of terrigenous dissolved organic matter in the ocean. *Nature*, 386, pp. 480–82.

O'Reilly, J. E., Maritorena, S., Mitchell, B. G., Siegel, D. A., Carder, K. L., Garver, S. A., Kahru, M. and McClain, C. R. 1998. Ocean color chlorophyll algorithms for SeaWiFS. *J. Geophys. Res.*, 103, pp. 24937–53.

Pegau, W. S., Deric, G. and Zaneveld, J. R. V. 1997. Absorption and attenuation of visible and near-infrared light in water: dependence on temperature and salinity. *Appl. Opt.*, 36, pp. 6035–46.

Preisendorfer, R. W. 1961. Application of radiative transfer theory to light measurements in the sea. In: *Radiant Energy in the Sea*. Boulder, Colo., International Union of Geodesy and Geophysics, pp. 11–30. (IUGG Monograph 10.)

Preisendorfer, R. W. 1976. *Hydrologic Optics, Volume V. Properties*. Honolulu, Hawaii, US Department of Commerce, National Oceanic and Atmospheric Administration, Environmental Research Laboratories.

Prieur, L. and Sathyendranath, S. 1981. An optical classification of coastal and oceanic waters based on the specific spectral absorption curves of phytoplankton pigments, dissolved organic matter, and other particulate materials. *Limnol. Oceanogr.*, 26, pp. 671–89.

Reckermann, M. and Colijn, F. (eds). 2000. Aquatic flow cytometry: achievements and prospects. *Scientia Marina*, 64(2), pp. 117–268.

Reynolds, R. A., Stramski, D. and Mitchell, B. G. 2001. A chlorophyll-dependent semianalytical reflectance model derived from field measurements of absorption and backscattering coefficients within the Southern Ocean. *J. Geophys. Res.*, 106, pp. 7125–38.

Roesler, C. S. and Boss, E. 2003. Spectral beam attenuation coefficients retrieved from ocean color inversion. *Geophys. Res. Lett.*, 30, 1468, doi:1410.1029/2002GL016185.

Roesler, C. S. and Boss, E. 2007. *In situ* measurement of inherent optical properties and potential for harmful algal bloom detection and coastal ecosystem observations. In: Babin et al. (eds), op. cit., this volume.

Roesler, C. S., Etheridge, S. M. and Pitcher, G. C. 2004. Application of an ocean color algal taxa detection model to red tides in the southern Benguela. In: K. A. Steidinger, J. H. Lansdberg, C. R. Tomas and G. A. Vargo (eds), *Harmful Algae 2002.* Proc. X International Conference on Harmful Algae (20–25 October 2002). St Petersburg, Fla./Paris, Florida Fish and Wildlife Conservation Commission/Intergovernmental Oceanographic Commission of UNESCO, pp. 303–305.

Roesler, C. S., Perry, M. J. and Carder, K. L. 1989. Modeling *in situ* phytoplankton absorption from total absorption spectra in productive inland marine waters. *Limnol. Oceanogr.*, 34, pp. 1510–23.

Roesler, C. S. and Perry, M. J. 1995. *In situ* phytoplankton absorption, fluorescence emission, and particulate backscattering spectra determined from reflectance. *J. Geophys. Res.*, 100, pp. 13279–94.

Ruddick, K., Lacroix, G., Park, Y., Rousseau, V., De Cauwer, V. and Sterckx, S. 2007. Overview of ocean colour: theoretical background, sensors and applicability to detection and monitoring of harmful algal blooms (capabilities and limitations). In: Babin et al. (eds), op. cit., this volume.

Santschi, P. H., Guo, L., Baskaran, K. M., Trumbore, S., Southon, J., Bianchi, T. S., Honeyman, B. and Cifuentes, L. 1995. Isotopic evidence for the contemporary origin of high-molecular weight organic matter in oceanic environements. *Geochim. Cosmochim. Acta*, 59, pp. 625–631.

Sathyendranath, S., Hoge, F. E., Platt, T. and Swift, R. N. 1994. Detection of phytoplankton pigments from ocean color: improved algorithms. *Appl. Opt.*, 33, pp. 1081–89.

Sathyendranath, S., Prieur, L. and Morel, A. 1989. A three-component model of ocean colour and its application to remote sensing of phytoplankton pigments in coastal waters. *Int. J. Rem. Sens.*, 10, pp. 1373–94.

Schofield, O., Bosch, J., Glenn, S., Kirkpatrick, G., Kerfoot, J., Lohrenz, S., Moline, M., Oliver, M. and Bissett, P. 2007. Bio-optics in integrated ocean observing networks: potential for studying harmful algal blooms. In: Babin et al. (eds), op. cit., this volume.

Schofield, O., Grzymski, J., Bissett, W. P., Kirkpatrick, G., Millie, D. F., Moline, M. and Roesler, C. S. 1999. Optical monitoring and forecasting systems for harmful algal blooms: possibility or pipe dream? *J. Phycol.*, 35, pp. 1477–96.

Scholin, C. A., Doucette, G. J. and Cembella, A. D. 2007. Prospects for developing automated systems for *in situ* detection of harmful algae and their toxins. In: Babin et al. (eds), op. cit., this volume.

Siegel, D. A., Dickey, T. D., Washburn, L., Hamilton, M. K. and Mitchell, B. G. 1989. Optical determination of particulate abundance and production variations in the oligotrophic ocean. *Deep Sea Res.*, 36, pp. 211–22.

Siegel, D. A., Maritorena, S., Nelson, N. B., Hansell, D. A. and Lornenzi-Kayser, M. 2002. Global distribution and dynamics of colored dissolved and detrital organic materials. *J. Geophys. Res.*, 107, 3228, doi:3210.1029/2001JC000965.

Siegel, D. A. and Michaels, A. F. 1996. Quantification of non-algal light attenuation in the Sargasso Sea: implications for biogeochemistry and remote sensing. *Deep Sea Res. II*, 43, pp. 321–45.

Simeon, J., Roesler, C., Pegau, W. S. and Dupouy, C. 2003. Sources of spatial variability in light absorbing components along and equatorial transect from 165°E and 150°W. *J. Geophys. Res.*, 108, 3333, doi:3310.1029/2002JC001613.

Smith, R. C. and Baker, K. S. 1978. Optical classification of natural waters. *Limnol. Oceanogr.*, 23, pp. 260–67.

Smyth, T. J., Moore, G. F., Groom, S. B., Land, P. E. and Tyrell, T. 2002. Optical modeling and measurements of a coccolithophore bloom. *Appl. Opt.*, 41, pp. 7679–88.

SooHoo, J. B., Kiefer, D. A., Collins, D. J. and McDermid, I. S. 1986. *In vivo* fluorescence excitation and absorption spectra of marine phytoplankton. I: Taxonomic characteristics and responses to photoadaptation. *J. Plankton Res.*, 8, pp. 197–214.

Sosik, H. M., Green, R. E., Pegau, W. S. and Roesler, C. S. 2001. Temporal and vertical variability in optical properties of New England shelf waters during late summer and spring. *J. Geophys. Res.*, 106, pp. 9455–72.

Sosik, H. M. and Mitchell, B. G. 1991. Absorption, fluorescence and quantum yield for growth in nitrogen limited *Dunaliella tertiolecta*. *Limnol. Oceanogr.*, 36, pp. 910–21.

Sosik, H. M. and Mitchell, B. G. 1995. Light absorption by phytoplankton, photosynthetic pigments, and detritus in the California Current System. *Deep Sea Res.*, 42, pp. 1717–48.

Sosik, H. M., Olson, R. J., Neubert, M. G., Shalapyonok, A. A. and Solow, A. R. 2003. Growth rates of coastal phytoplankton from time-series measurements with a submersible flow cytometer. *Limnol. Oceanogr.*, 48, pp. 1756–65.

Sosik, H. M., Vernet, M. and Mitchell, B. G. 1992. A comparison of particulate absorption properties between high- and mid-latitude surface waters. *Antarct. J. Unit. States*, 27, pp. 162–64.

Stramska, M., Stramski, D., Mitchell, B. G. and Mobley, C. D. 2000. Estimation of the absorption and backscattering coefficients from in-water radiometric measurements. *Limnol. Oceanogr.*, 45, pp. 628–41.

Stramski, D., Bricaud, A. and Morel, A. 2001. Modeling the inherent optical properties of the ocean based on the detailed composition of the planktonic community. *Appl. Opt.*, 40, pp. 2929–45.

Stramski, D. and Kiefer, D. A. 1991. Light scattering by microorganisms in the open ocean. *Progr. Oceanogr.*, 28, pp. 343–83.

Stramski, D. and Morel, A. 1990. Optical properties of photosynthetic picoplankton in different physiological states as affected by growth irradiance. *Deep Sea Res.*, 37, pp. 45–266.

Stramski, D., Reynolds, R. A., Kahru, M. and Mitchell, B. G. 1999. Estimation of particulate organic carbon in the ocean from satellite remote sensing. *Science*, 285, pp. 239–42.

Stramski, D., Wozniak, S. B. and Flatau, P. J. 2004. Optical properties of Asian mineral dust suspended in seawater. *Limnol. Oceanogr.*, 49, pp. 749–55.

Stumpf, R. P. 2001. Application of satellite ocean color sensors for monitoring and predicting harmful algal blooms. *Hum. Ecol. Risk Assess.*, 7, pp. 1363–68.

Subramaniam, A., Brown, C. W., Hood, R. R., Carpenter, E. J. and Capone, D. G. 2002. Detecting *Trichodesmium* blooms in SeaWiFS imagery. *Deep Sea Res. II*, 49, pp. 107–21.

Subramaniam, A. and Carpenter, E. J. 1994. An empirically derived protocol for the detection of blooms of the marine cyanobacterium *Trichodesmium* using CZCS imagery. *Int. J. Rem. Sens.*, 15, pp. 1559–69.

Subramaniam, A., Carpenter, E. J. and Falkowski, P. G. 1999. Bio-optical properties of the marine diazotrophic cyanobacteria *Trichodesmium* spp. II: A reflectance model for remote sensing. *Limnol. Oceanogr.*, 44, pp. 618–27.

Twardowski, M. S., Boss, E., Macdonald, J. B., Pegau, W. S., Barnard, A. H. and Zaneveld, J. R. V. 2001. A model for estimating bulk refractive index from the optical backscattering ratio and the implications for understanding particle composition in case I and case II waters. *J. Geophys. Res.*, 106, pp. 14129–42.

Twardowski, M. S., Boss, E., Sullivan, J. M. and Donaghay, P. L. 2004. Modeling the spectral shape of absorption by chromophoric dissolved organic matter. *Mar. Chem.*, 89, pp. 69–88.

Twardowski, M. S. and Donaghay, P. L. 2001. Separating *in situ* and terrigenous sources of absorption by dissolved materials in coastal waters. *J. Geophys. Res.*, 106, pp. 2545–60.

Twardowski, M. S. and Donaghay, P. L. 2002. Photobleaching of aquatic dissolved materials: absorption removal, spectral alteration, and their interrelationship. *J. Geophys. Res.*, 107, doi:10.1029/1999JC000281.

Tyrell, T., Holligan, P. M. and Mobley, C. D. 1999. Optical impacts of oceanic coccolithophore blooms. *J. Geophys. Res.*, 104, pp. 3223–41.

Ulloa, O., Sathyendranath, S. and Platt, T. 1994. Effect of the particle-size distribution on the backscattering ratio in seawater. *Appl. Opt.*, 33, pp. 7070–77.

Vodacek, A., Blough, N. V., DeGrandpre, M. D., Peltzer, E. T. and Nelson, R. K. 1997. Seasonal variation of CDOM and DOC in the Middle Atlantic Bight: terrestrial inputs and photooxidation. *Limnol. Oceanogr.*, 42(4), pp. 674–86.

Vodacek, A., Hoge, F. E., Swift, D. G., Kungel, J. K., Peltzer, E. T. and Blough, N. V. 1995. The use of *in situ* and airborne fluorescence measurements to determine UV absorption coefficients and DOC concentrations in surface waters. *Limnol. Oceanogr.*, 40, pp. 411–15.

Voss, K. J. 1992. A spectral model of the beam attenuation coefficient in the ocean and coastal areas. *Limnol. Oceanogr.*, 37, pp. 501–09.

Voss, K. J., Balch, W. M. and Kirkpatrick, K. A. 1998. Scattering and attenuation properties of *Emiliania huxleyi* cell and their detached coccoliths. *Limnol. Oceanogr.*, 43, pp. 870–76.

Yentsch, C. S. 1960. The influence of phytoplankton pigments on the colour of sea water. *Limnol. Oceanogr.*, 7, pp. 1–9.

Yentsch, C. S. 1962. Measurement of visible light absorption by particulate matter in the ocean. *Limnol. Oceanogr.*, 7, pp. 207–17.

Yentsch, C. S. and Menzel, D. W. 1963. A method for the determination of phytoplankton and phaeophytin by fluorescence. *Deep Sea Res.*, 10, pp. 221–31.

Yentsch, C. S. and Phinney, D. A. 1985. Spectral fluorescence: an ataxonomic tool for studying the structure of phytoplankton populations. *J. Plankton Res.*, 7, pp. 617–32.

Yentsch, C. S. and Phinney, D. A. 1989. A bridge between ocean optics and microbial ecology. *Limnol. Oceanogr.*, 34, pp. 1694–1705.

Zaneveld, J. R. V. 1974. New developments of the theory of radiative transfer in the oceans. In: N. G. Jerlov and E. S. Nielsen (eds), *Optical Aspects of Oceanography*. New York, Academic Press, pp. 121–34.

Zaneveld, J. R. V. and Kitchen, J. C. 1995. The variation in the inherent optical properties of phytoplankton near an absorption peak as determined by various models of cell structure. *J. Geophys. Res.*, 100, pp. 13309–20.

Zaneveld, J. R. V., Roach, D. R. and Pak, H. 1974. The determination of the index of refraction distribution of oceanic particulates. *J. Geophys. Res.*, 79, pp. 4091–95.

Zaneveld, J. R. V., Twardowski, M. S., Shifrin, K. S., Pegau, W. S., Boss, E. and Zolotov, I. 2002. Inversion of light scattering measurements to obtain biogeochemical parameters. *Ocean Optics XVI, Proc.* pp. 1–19.

9

Overview of ocean colour: theoretical background, sensors and applicability to detection and monitoring of harmful algal blooms (capabilities and limitations)

K. Ruddick, G. Lacroix, Y. Park, V. Rousseau, V. De Cauwer and S. Sterckx

9.1 Introduction – coming of age of ocean colour

9.1.1 Objective, scope and contents

Anecdotal and journalistic references to harmful algal blooms often report the impact on water colour, using terms such as 'red tide'. Indeed probably the earliest recording (Exodus 7: 20–21) of a harmful algal bloom (HAB) remarks that the waters 'turned to blood'. A few thousand years later, photoelectric devices have replaced the human eye as detector, allowing a transition from subjective and descriptive observations to detailed and quantitative information on water constituents. The objective of this chapter is to summarize the status of optical remote sensing of HABs by reviewing ocean-colour theory and giving an overview of available systems. Applications of optical remote sensing to the monitoring of HABs are reviewed, noting capabilities and limitations, and future perspectives are discussed.

The scope of this chapter, as given by the title 'ocean colour', covers passive systems for optical remote sensing using the sun as direct light source (Mobley, 1994). While the term 'optical remote sensing' could be considered to cover a wide variety of sensors, including the human eye, airborne photographic cameras, shipborne above-water radiometers, and others, the scope here is limited to sensors providing digital image-based information, thus covering essentially satellite and airborne radiometers. The focus is on reflectance-based techniques because of their overwhelming importance in the available data stream. However, it is noted that some information on phytoplankton (without specific relevance to HABs) can be retrieved from remote sensing of sun-stimulated fluorescence (Babin, 2005; Gower et al., 1999). Active remote sensing systems based on, for example, laser-induced fluorescence (Hoge and Swift, 1981) are excluded. Applications are drawn mainly from marine waters because of the user interest and experience there though the validity of the theory and systems to estuarine and inland waters is also considered. The applications described in this chapter are drawn essentially from HAB studies. However, the theory described as well as many of the remarks made are relevant both to HABs and to the much wider field of ecosystem dynamics. In fact, as discussed in detail below, ocean colour is used primarily for algae bloom (AB) detection and generally requires supplementary information from

seaborne measurements or expert knowledge for determination of the harmfulness of the event. The question 'Is the AB a HAB?' is a major challenge for the ocean-colour technique.

The definition of 'harmful' in this context is left to others (Cullen, 2007 – Chapter 1 this volume; GEOHAB, 2001; Graneli et al., 1998). This chapter thus covers a wide range of algal species with very different severities of impact.

The content has been selected to provide the theory relevant to understanding the basic principles of ocean-colour observations and an appreciation of the current capabilities and limits of these tools for HAB detection. The target readership is students and potential end-users of coastal observation systems who should thus acquire sufficient knowledge for the initiation and use of such observing tools. Thus, the focus is on general principles of ocean-colour remote sensing and a broad understanding of processes with emphasis on their spectral reflectance, loosely termed as 'colour'. Optical remote sensing specialists who require a more detailed description of radiative transfer theory and especially the complications of interacting processes, such as multiple scattering, and second-order optical effects, should consult the references in the appropriate sections. Readers with no interest in the details of ocean-colour theory and data processing may skip Sections 9.2, 9.3.1 and 9.3.2 but are strongly advised to be aware of the variety of methods presented in Sections 9.3.3, 9.3.4 and 9.3.5 and especially of their limitations. It is common for products from the main ocean-colour sensors to give very different results in coastal waters even for data acquired almost simultaneously (De Cauwer et al., 2004).

Key questions to be answered in this chapter include:

- What is ocean colour?
- What sensors are available and suitable for HAB detection?
- What information can be obtained from such sensors?
- What are the limitations of the ocean-colour technique for HAB detection?
- What future developments can be expected?

9.1.2 Historical perspective

The technological basis for marine applications of ocean-colour remote sensing began to emerge in the 1960s and 1970s with airborne studies aimed at chlorophyll detection (Clarke et al., 1970). At this time one of the first satellite HAB detections was made (of *Nodularia spumigena* in the Baltic) using Landsat MSS (Öström, 1976). During the 1960s and 1970s the fundamental theoretical basis also emerged for marine radiative transfer (Preisendorfer, 1961) and, in particular, for the relationship between spectral radiance or reflectance at the sea surface and phytoplankton pigments (Morel and Prieur, 1977). The latter study proposed an optical classification of waters into 'Case 1', where scattering in the water arises mainly from phytoplankton particles, and 'Case 2' where inorganic particles are significant. In practice, Case 1 waters are generally deep, relatively clear oceanic waters whereas most coastal waters fall into the Case 2 class. The feasibility of satellite remote sensing of chlorophyll at least for Case 1 waters was finally established by studies based on the Coastal Zone Colour Scanner (CZCS) which flew aboard the Nimbus-7 satellite for the period 1978–86 for example (Gordon et al., 1983; Smith and Wilson, 1981). At this time the theoretical basis for optical remote sensing, including atmospheric correction, was becoming better established (Gordon and Morel, 1983). Delays in the launch of follow-up sensors led

to a gap in the stream of satellite ocean-colour data and a consequent lack of applications and research funding as well as relatively slow progress in optical remote sensing theory – a Dark Age for ocean colour. Finally a new generation of ocean-colour sensors was heralded with the launch of the Ocean Color and Temperature (OCTS) and POLDER-1 sensors aboard ADEOS-1, and the MOS sensor aboard IRS-1 in 1996 and a turning point for ocean colour was reached with the long-awaited launch of the Sea-viewing Wide Field-of-view Sensor (SeaWiFS) aboard SeaStar/Orbimage-2 in 1997. At last the scientific community had easy access to well-calibrated and supported multispectral optical remote sensing data of the entire world and could develop, test and exploit algorithms for mapping chlorophyll *a* concentration as well as other products related to optical properties.

9.1.3 Post-SeaWiFS revolution in optical remote sensing for coastal waters

Originally designed for global carbon cycle and climate change studies, SeaWiFS has spectral bands suitable for atmospheric correction and chlorophyll *a* retrieval in Case 1 waters, is tilted to avoid sunglint and combines solar, lunar and vicarious calibration methods. Thanks to the high quality of the data source and open policies for data distribution to researchers (until 2005) and for the SeaDAS image processing software, SeaWiFS has rapidly become popular with ocean-colour researchers. This is attested by the large number of authorized SeaWiFS users (over 2,000 in 2003) and the frequent appearance of imagery at scientific conferences.

In order to assess use of satellite imagery by the wider public of marine scientists, a survey has been made of 50 papers per year from 1992 to 2002 taken from four key coastal oceanography journals: *Journal of Geophysical Research*, *Continental Shelf Research*, *Journal of Marine Systems* and the (ex-Netherlands) *Journal of Sea Research*. Of the 550 papers considered, 14% presented satellite imagery in some way. Of these about one quarter related to ocean-colour imagery (in decreasing order of importance: CZCS, SeaWiFS, OCTS, AVHRR, airborne), nearly one half to thermal infrared imagery (primarily AVHRR) and the remainder to various active radar instruments (TOPEX/Poseidon, ERS-SAR, etc.). Interestingly, even for the years 2000–2002 a mere five out of 150 papers presented SeaWiFS imagery, suggesting that ocean colour still has fairly limited penetration in the domain of coastal oceanography. Despite such low figures for peer-reviewed publications it seems that ocean-colour imagery is appearing more and more frequently in scientific conferences and on the internet.

Since 1997 many more ocean-colour sensors with a variety of characteristics (see Section 9.4 and Figure 9.1) have been launched or planned. While no single system guarantees a long-term source of ocean-colour data the success of SeaWiFS and the promise of the well-supported MODIS and MERIS sensors has stimulated rapid progress in processing algorithms and the confidence necessary for planning operational monitoring of chlorophyll by satellites.

As a consequence of this post-SeaWiFS revolution in the availability of ocean-colour data (and to a lesser extent the significant increases in computing power) the improvements to processing algorithms have been considerable over the last eight years. Atmospheric correction routines have become more and more complex in the effort to continually reduce uncertainties for example by detailed consideration of

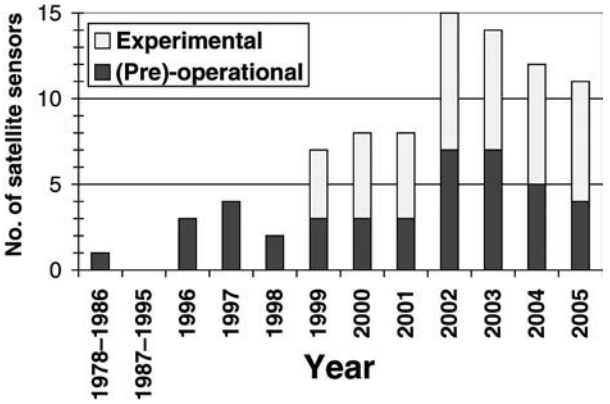

Figure 9.1
Number of functioning ocean-colour sensors in space. A distinction is made between sensors with a well-documented chlorophyll product, termed here '(pre-)operational' in terms of HAB detection, and other sensors, considered by the International Ocean-Colour Coordinating Group (IOCCG) at the time of writing as ocean-colour sensors and termed here 'experimental'. All other sensors, including some hyperspectral sensors with potential phytoplankton applications such as Hyperion and CHRIS, and those with established suspended-matter mapping capabilities such as AVHRR, SPOT and Landsat, have been excluded. See Section 9.4 for details.

multiple scattering, turbid water effects, absorbing aerosols, etc. The retrieval of marine parameters has similarly become more complex especially for coastal waters where uncertainties remain high.

9.2 Radiative transfer theory – from sun to sensor via phytoplankton (or not)

9.2.1 Summary of light paths from sun to sensor

An ocean-colour remote sensor measures radiance, a vector quantity defined operationally by (Mobley, 1994) as the radiant energy measured per unit time per unit surface area of collector per unit solid angle field-of-view per unit wavelength and with typical units mW m^{-2} nm^{-1} sr^{-1}. Radiance is measured by converting light energy reaching it from discrete fields of view (one narrow solid angle per image pixel) into an electrical signal. This electrical signal is digitized and transmitted back to earth for calibration and processing. While the origin of this light energy is supposed here to be the sun (excluding such processes as bioluminescence) the passage of light from sun to sensor occurs through the medium of the atmosphere and the ocean where various electromagnetic interactions may occur. The fraction of light reaching the sensor after interaction at some stage with marine particles, such as phytoplankton, contains

information about how those particles scattered or absorbed light. The objective of ocean-colour remote sensing is to extract useful information, such as the concentration and if possible an indication of the composition of these particles, from the total light received. In the HAB context, the concentration of chlorophyll *a* and, if possible, an indication of phytoplankton species composition or harmfulness are the relevant parameters.

The electromagnetic interactions between sun and sensor can be conveniently decomposed (Sturm, 1980) into absorption and scattering events occurring in the medium of the atmosphere or of the sea or at the air/sea interface. This decomposition is illustrated in Figure 9.2, which shows the photon paths reaching the sensor in the simple case where only one scattering event has occurred – this is called the single-scattering approximation (SSA). Even in this simple case many photons originally following such trajectories will be absorbed by molecules or particles in the atmosphere or the sea. Indeed the 'missing light' caused by preferential absorption for photons of certain wavelengths by phytoplankton pigments is a vital source of information. Of course, reality is more complicated than this SSA picture because photons reaching the sensor may have undergone multiple scattering interactions in the atmosphere, in the sea and at the air/sea interface (Gordon and Morel, 1983).

A useful indication of the importance of the various processes is provided by (Sturm, 1980) who considered typical satellite remote sensing conditions (sun/viewing geometry and sea and atmosphere composition). This study estimated that between 1% and 35% of the received signal contains information about the composition of the sea, while the fraction of the signal corresponding to last scattering in the atmosphere and at the air/sea interface is estimated as 64–97% and 1–2% respectively. These ranges are useful for building intuition, though may of course be exceeded in extreme cases, such as very turbid water, viewing in the direction of sun glitter, etc., as well as in less

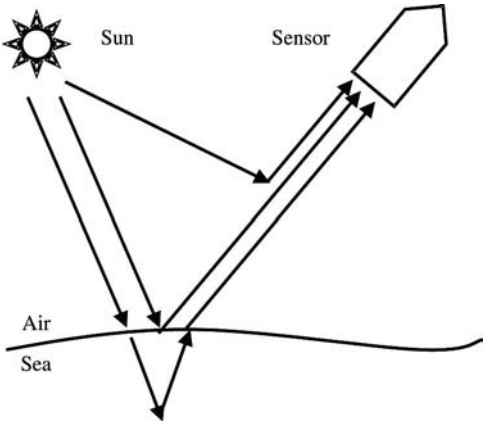

Figure 9.2
Trajectories of photons reaching the sensor after a single scattering interaction. All these trajectories are subject to possible absorption, which varies significantly as a function of wavelength.

extreme cases such as cloudy conditions, where ocean-colour remote sensing by satellite is impossible.

In this section the important optical processes are described and illustrated with emphasis on their spectral reflectances. In Section 9.3 the algorithms for inverting the received signal to remove or correct for the unwanted effects of the atmosphere and the air/sea interface and to yield the desired marine parameter(s) are reviewed.

9.2.2 Definitions and terminology

9.2.2.1 Decomposition of radiances

The theory of marine and atmospheric optics can be decomposed into the consideration of distinct processes. As these processes interact in the general multiple scattering case, a number of alternative decompositions could be envisaged and indeed in the specialized literature a dedicated decomposition is often chosen to isolate a single process that is studied in detail subject to certain approximations. However, an ocean-colour processing algorithm requires a systematic decomposition of all processes. This decomposition may be documented explictly in papers and reports or may be implicit in the implementation of an algorithm in a computer code. In this chapter a systematic decomposition is defined, which covers all possible sun-sensor photon paths while grouping them in a way suitable for calculation in Section 9.3. The price for adopting such a decomposition is the need to introduce and define appropriate terminology, which may seem unwieldy. However, this need to (re)define terms for each ocean-colour study becomes apparent from a review of the available literature where different definitions or approximations may be used for the same terminology. The terminology used here is defined in this section and summarized in Table 9.1.

Table 9.1 Notation used for apparent optical properties, geometrical parameters, inherent optical properties and other parameters used in the optical model. TOA denotes top-of-atmosphere. Superscripts in […] are dropped after definition.

Symbol	Name	Units	Definition
$L_{\mathrm{tot}}^{\mathrm{TOA}}$ and $\rho_{\mathrm{tot}}^{\mathrm{TOA}}$	Total radiance and reflectance at TOA	mW m^{-2} nm^{-2} sr^{-1} and –	(9.1) and (9.4)
$L_{\mathrm{path}}^{\mathrm{TOA}}$	Atmospheric path radiance at TOA	mW m^{-2} nm^{-1} sr^{-1}	(9.1)
$L_{\mathrm{int}}^{\mathrm{TOA}}$ and $\rho_{\mathrm{int}}^{\mathrm{TOA}}$	Air/water interface reflection radiance and reflectance at TOA	mW m^{-2} nm^{-1} sr^{-1} and –	(9.1) and (9.4)
$L_{\mathrm{w}}^{\mathrm{TOA}}$	Water-leaving radiance at TOA	mW m^{-2} nm^{-1} sr^{-1}	(9.1)
L_{w}^{0+} and $\rho_{\mathrm{w}}^{[0+]}$	Water-leaving radiance and reflectance above-water	mW m^{-2} nm^{-1} sr^{-1} and –	(9.6)
$L_{\mathrm{a}}^{\mathrm{TOA}}$ and $\rho_{\mathrm{a}}^{[\mathrm{TOA}]}$	Aerosol radiance and reflectance at TOA	mW m^{-2} nm^{-1} sr^{-1} and –	(9.2) and (9.4)

Table 9.1 (*Continued*)

Symbol	Name	Units	Definition
L_r^{TOA} and $\rho_r^{[TOA]}$	Rayleigh (air molecule) radiance and reflectance at TOA	mW m^{-2} nm^{-1} sr^{-1} and –	(9.2) and (9.4)
L_{ar}^{TOA} and ρ_{ar}^{TOA}	Aerosol-Rayleigh multiple scattering radiance and reflectance at TOA	mW m^{-2} nm^{-1} sr^{-1} and –	(9.2) and (9.4)
L_g^{TOA}	Sunglint radiance at TOA	mW m^{-2} nm^{-1} sr^{-1} and –	(9.3)
L_{wc}^{TOA}	Whitecap radiance at TOA	mW m^{-2} nm^{-1} sr^{-1} and –	(9.3)
L_g^{0+} and ρ_g^{0+}	Sunglint radiance and reflectance above-water	mW m^{-2} nm^{-1} sr^{-1} and –	(9.3) and (9.7)
L_{wc}^{0+} and ρ_{wc}^{0+}	Whitecap radiance and reflectance above-water	mW m^{-2} nm^{-1} sr^{-1} and –	(9.3) and (9.7)
T_v	Diffuse atmospheric transmittance for water-leaving radiance (sea to sensor)	–	(9.9)
T_0	Diffuse atmospheric transmittance for downwelling irradiance (sun to sea)	–	(9.10)
$t_{oz}^{0,v}$	Two-way ozone atmospheric transmittance for irradiance	–	After (9.11)
r_{sky}	Reflectance factor for sky radiance at air/sea interface	–	After (9.12)
θ_o	Solar zenith angle	–	Fig. 9.8
θ_v	Sensor zenith angle	–	Fig. 9.8
$\Delta\phi$	Relative sensor-sun azimuth angle	–	Fig. 9.8
θ_- and θ_+	Atmospheric scattering angles	–	(9.14)
λ	Wavelength of light	nm (but μm in (9.14))	
W	Wind speed at 10 m above sea level	ms^{-1}	

(*Continued*)

Table 9.1 (*Continued*)

Symbol	Name	Units	Definition
a, a_w, a_ϕ and a_Y	Absorption coefficients: total, pure water, phytoplankton and yellow substance	m^{-1}	(9.27)
b_b, b_{bw}, b_{bC} and b_{bNC}	Backscattering coefficients: total, pure water, phytoplankton and other particles	m^{-1}	(9.28)
C	Concentration of chlorophyll *a*	mg m^{-3}	
k	Exponential slope for yellow substance absorption	nm^{-1}	(9.34)
n	Power law exponent for (non-covarying) particulate backscatter	–	(9.33)
v	Power law exponent for phytoplankton backscatter	–	(9.31)
f'	Reflectance model factor	–	(9.26)
Q	Ratio of irradiance to radiance (below water)	–	(9.26)
$\Re$	Air/water interface reflection and refraction factor	–	(9.26)

In this chapter the radiance detected by the sensor is decomposed according to the number and type of scattering events that photons reaching the sensor have undergone (in any order) in their trajectory from sun to sensor. Such scattering events can occur in the atmosphere, at the air-water interface or in the water.

The radiance reaching the sensor at top-of-atmosphere (TOA), L_{tot}^{TOA}, can then be decomposed as

$$L_{tot}^{TOA} = L_{path}^{TOA} + L_{int}^{TOA} + L_{w}^{TOA}, \tag{9.1}$$

where the atmospheric path radiance, L_{path}^{TOA}, is defined for photons which have undergone at least one scattering in air and none in water, L_{int}^{TOA} for exactly one scattering at the air/sea interface and none in air or water and L_{w}^{TOA} for photons that have scattered at least once in the water. The path radiance is further decomposed as

$$L_{\text{path}}^{\text{TOA}} = L_{\text{a}}^{\text{TOA}} + L_{\text{r}}^{\text{TOA}} + L_{\text{ar}}^{\text{TOA}}, \tag{9.2}$$

where $L_{\text{r}}^{\text{TOA}}$ denotes photons that have been scattered at least once by air molecules (Rayleigh scattering) but not by aerosol particles, $L_{\text{a}}^{\text{TOA}}$ denotes photons that have been scattered at least once by aerosol particles but not by air molecules, and $L_{\text{ar}}^{\text{TOA}}$ represents photons where at least one of each type of scattering has occurred.

$L_{\text{int}}^{\text{TOA}}$ is decomposed into foam or whitecap radiance $L_{\text{wc}}^{\text{TOA}}$, for which the only scattering event is at foam and sunglint radiance $L_{\text{g}}^{\text{TOA}}$, for which the only scattering event is specular reflection of direct sunlight:

$$L_{\text{int}}^{\text{TOA}} = L_{\text{g}}^{\text{TOA}} + L_{\text{wc}}^{\text{TOA}}. \tag{9.3}$$

All other air/sea interface reflections, including skylight reflection, are defined within $L_{\text{path}}^{\text{TOA}}$ or $L_{\text{w}}^{\text{TOA}}$.

9.2.2.2 Normalization and reflectance

In order to relate radiance measurements to the properties of viewed matter, it is more useful to normalize radiance by a suitably chosen downwelling irradiance (or 'spectral downward plane irradiance'), defined (Mobley, 1994) as the integral over all downward directions of the radiance multiplied by the cosine of the corresponding zenith angle. Normalization of detected light (radiance in the case of a remote sensor, radiance or irradiance for an underwater sensor) by illuminating light (usually downwelling irradiance) yields a reflectance. Reflectance is an apparent optical property because of its dependence on the ambient light field. However, if the normalization is appropriately chosen this dependence will be weak and the reflectance will be essentially related to the desired inherent optical properties of the medium, be it sea or atmosphere. In the marine optics literature, many different normalizations have been proposed yielding alternative definitions for reflectance. As examples, the upward light can be measured as radiance or irradiance, the upward light and the normalizing irradiance can be considered at the top-of-atmosphere, just above water or just below water, normalizing irradiance can be downwelling or total scalar (isotropic integral over all solid angles including upward). Corrections can be made for atmospheric transmittances, air/sea interface and/or bidirectional effects, etc. Corresponding terminology includes 'subsurface irradiance reflectance', 'remote sensing reflectance', 'normalized water-leaving reflectance', yet such terms are not always uniformly used and need to be clearly defined in each study.

In this chapter the total, path, Rayleigh, aerosol, aerosol-Rayleigh and air/sea interface reflectances (at the TOA), ρ_{tot}, ρ_{r}, ρ_{a}, ρ_{ar}, ρ_{int} are defined by normalization with top-of-atmosphere downwelling irradiance, $E_{\text{d}}^{\text{TOA}}$. Thus,

$$\left(\rho_{\text{tot}}^{\text{TOA}}, \rho_{\text{r}}^{\text{TOA}}, \rho_{\text{a}}^{\text{TOA}}, \rho_{\text{ar}}^{\text{TOA}}, \rho_{\text{int}}^{\text{TOA}}\right) = \frac{\pi}{E_{\text{d}}^{\text{TOA}}}\left(L_{\text{tot}}^{\text{TOA}}, L_{\text{r}}^{\text{TOA}}, L_{\text{a}}^{\text{TOA}}, L_{\text{ar}}^{\text{TOA}}, L_{\text{int}}^{\text{TOA}}\right), \tag{9.4}$$

where the top-of-atmosphere downwelling irradiance is given by

$$E_{\text{d}}^{\text{TOA}} = E_0 \cos\theta_0, \tag{9.5}$$

where E_0 is the extraterrestrial solar irradiance (corrected for variations in sun-earth distance) and θ_0 is the solar zenith angle.

In contrast, the water-leaving reflectance ρ_w^{0+} is more conveniently defined by multiplying the (just) above-water water-leaving radiance L_w^{0+} by π (thus converting from radiance-type units of mW m^{-2} nm^{-1} sr^{-1} to irradiance-type units of mW m^{-2} nm^{-1}) and normalizing by the above-water downwelling irradiance E_d^{0+}.

Thus,

$$\rho_w^{0+} = \frac{\pi L_w^{0+}}{E_d^{0+}}, \tag{9.6}$$

and similarly,

$$\left(\rho_g^{0+}, \rho_{wc}^{0+}\right) = \frac{\pi}{E_d^{0+}}\left(L_g^{0+}, L_{wc}^{0+}\right), \tag{9.7}$$

Then the simple addition of detected radiances expressed by (9.1) and (9.2) gives after normalization, and dropping wavelength-dependence of all quantities in the notation,

$$\rho_{tot}^{TOA} = \rho_r^{TOA} + \rho_a^{TOA} + \rho_{ar}^{TOA} + \rho_{int}^{TOA} + T_0 T_v \rho_w^{0+}, \tag{9.8}$$

where T_v is the diffuse atmospheric transmittance for water-leaving radiance from sea to sensor (v for 'viewing') as defined by (Yang and Gordon, 1997):

$$T_v = \frac{L_w^{TOA}}{L_w^{0+}}, \tag{9.9}$$

and T_0 is the diffuse atmospheric transmittance for downwelling irradiance from sun to sea as defined by (Gordon et al., 1988b):

$$T_0 = \frac{E_d^{0+}}{E_d^{TOA}} \tag{9.10}$$

It is noted that diffuse atmospheric transmittance, an apparent optical property of the entire atmosphere here, can be defined in a variety of ways according to the radiance or irradiance quantity that is being transmitted, and alternative definitions and/or terminology may occur in certain references. Moreover these quantities are not to be confused with the direct atmospheric transmittance for specular reflection of sunlight (sunglint).

While important for an accurate determination of properties such as chlorophyll concentration, the newcomer to ocean colour will be relieved to learn that while the atmospheric path radiance is never negligible the diffuse atmospheric transmittances usually have values between 0.8 and 1.0, except at distinct wavelengths relating to gaseous absorption (e.g. oxygen absorption at 762 nm) and at large viewing or sun angles. Thus, a simpler intuitive picture can be established of the ocean-atmosphere system by imagining perfect atmospheric transmittances $T_v = T_0 = 1.0$ in (9.8).

9.2.3 Atmospheric scattering and absorption processes

The importance of atmospheric scattering and absorption processes in contributing to the at-sensor signal (TOA for satellites) implies that quantitative information about the sea can be obtained only after a rather precise atmospheric correction. Indeed, while significant progress has been made in this respect over the last 20 years, poor

atmospheric correction is, along with the difficulty of distinguishing between phytoplankton absorption and yellow substance absorption in coastal waters, the main cause of severe errors or complete failures in satellite remote sensing of chlorophyll *a*. It is not uncommon for an apparently small error in atmospheric correction to be amplified to give errors in chlorophyll *a* retrieval of an order of magnitude.

Atmospheric scattering occurs by interaction of light with air molecules, which because of their small size compared with the wavelength of light can be represented by Rayleigh scattering theory, and with aerosol particles, which can be approximated by Mie scattering theory. These processes are generally referred to as Rayleigh scattering and aerosol scattering respectively. A detailed treatment of these and other atmospheric radiative transfer processes can be found in (Thomas and Stamnes, 1999). For the purposes of illustrating the colour of these processes, in this section the simple case of the single scattering approximation is considered where photons reaching the sensor have undergone only one scattering event. For correction of such effects in ocean-colour imagery to yield water-leaving reflectance a more accurate consideration is required as outlined in Section 9.3.

9.2.3.1 Rayleigh scattering

For single Rayleigh scattering in the atmosphere and neglecting polarization-related wavelength dependency of the Rayleigh scattering phase function, $p_r(\theta_0,\theta_v,\Delta\phi)$, the Rayleigh reflectance, ρ_r, can be given as a first approximation by (Gordon et al., 1988*a*):

$$\rho_r = \frac{t_{oz}^{0,v}(\lambda,\theta_0,\theta_v)\tau_r(\lambda)p_r(\theta_0,\theta_v,\Delta\phi)}{4\cos\theta_0\cos\theta_v}, \tag{9.11}$$

where θ_0 and θ_v are the solar and sensor zenith angles, $t_{oz}^{0,v}(\lambda,\theta_0,\theta_v)$ is the transmittance associated with the reduction of irradiance by two trips through the ozone layer, $\tau_r(\lambda)$ is the Rayleigh scattering optical thickness and

$$p_r(\theta_0,\theta_v,\Delta\phi) = P_r(\theta_-) + \left[r_{sky}(\theta_0) + r_{sky}(\theta_v)\right]P_r(\theta_+) \tag{9.12}$$

where r_{sky} is the air/sea interface reflectance factor (equal to the Fresnel reflection coefficient for a flat sea) and $P_r(\alpha)$ is the Rayleigh scattering phase function,

$$P_r(\alpha) = \frac{3}{4}\left[1+\cos^2\alpha\right], \tag{9.13}$$

for a general scattering angle, α. θ_- and θ_+ are the scattering angles for the cases without air/sea interface scattering and with a single reflection at the air/sea interface respectively and can be calculated geometrically from

$$\cos\theta_\pm = \pm\cos\theta_0\cos\theta_v - \sin\theta_0\sin\theta_v\cos\Delta\phi, \tag{9.14}$$

where $\Delta\phi$ is the relative azimuth angle between sun and sensor. The convention chosen here for definition of relative azimuth angle is the angle subtended at the target pixel by the vertical half-planes containing the sun and the sensor (see also Figure 9.8). Thus, $\Delta\phi = 0°$ for viewing away from the sun and $\Delta\phi = 180°$ for viewing towards the sun.

If ozone absorption is ignored ($t_{oz}^{0,v} = 1$) then (9.11) permits a decomposition of Rayleigh reflectance into a factor which depends only on the geometry of sun and sensor and the factor $\tau_r(\lambda)$, which defines completely the spectral shape or colour of the process. The latter has been estimated as (Hansen and Travis, 1974):

$$\tau_r(\lambda) = \frac{P_{atm}}{P_{atm0}} * 0.008569\,\lambda^{-4}\,(1 + 0.0113\,\lambda^{-2} + 0.00013\,\lambda^{-4}), \qquad (9.15)$$

where P_{atm} is the actual atmospheric pressure (a measure of the number of air molecules in a vertical column of the atmosphere), $P_{atm0} = 1013.25$ mbar is a standard atmospheric pressure, and the wavelength λ is expressed in micrometres (μm).

Figure 9.3 shows the Rayleigh reflectance calculated from (9.11) to (9.15) for viewing angles typical of ocean-colour sensors, for sun zenith angles of 20°, 40° and 60°, for a sun-sensor relative azimuth angle of 90° and for a sky reflectance factor calculated for a flat sea following (Mobley, 1994). It is noted that the calculation of Rayleigh reflectance with these equations is not of sufficient accuracy for atmospheric correction (see Section 9.3), which requires the use of atmospheric radiative transfer codes taking account of effects such as multiple scattering, polarization, rough sea, etc. However, these equations give a first approximation of the Rayleigh reflectance and are useful to establish an intuitive understanding of how this will vary with wavelength and geometry. Thus, from Figure 9.3 it is clear that Rayleigh reflectance increases for large viewing angles. This can be seen as brightening of the edges of an image and is caused by lengthening of the air mass through which scattering can occur, as indicated by the factor $1/\cos\theta_v$ in (9.11). The Rayleigh reflectance generally increases for increasing sun zenith angle because of the $1/\cos\theta_0$ normalization factor in (9.11), although changes in scattering angle may counteract or amplify to some extent this tendency.

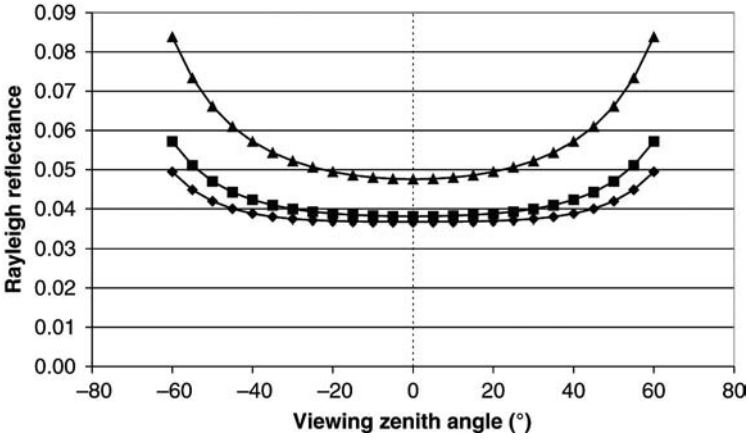

Figure 9.3
Rayleigh reflectance at 555 nm calculated from (9.11) for viewing angles typical of ocean-colour sensors and sun zenith angles of 20° (lower line, diamonds), 40° (squares) and 60° (triangles).

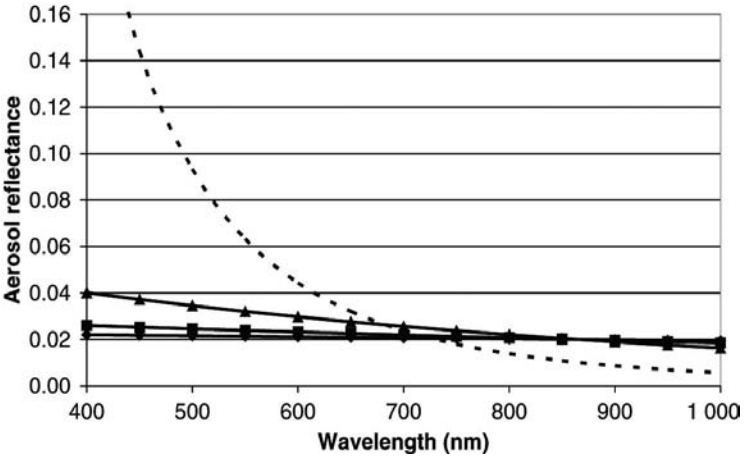

Figure 9.4
Aerosol reflectance spectra for typical maritime (diamonds), coastal (squares) and tropospheric (triangles) aerosol types and geometry and for an arbitrarily chosen $\rho_a(865\text{nm}) = 0.02$. For comparison the Rayleigh reflectance spectra corresponding to the case, $\theta_v = 45°$, $\theta_o = 60°$, $\Delta\varphi = 90°$ of Figure 9.3 is shown as a dashed line.

The wavelength dependence of Rayleigh reflectance is very strong – the factor λ^{-4} dominates in (9.15) – giving particularly large reflectances in the blue. This is illustrated together with aerosol reflectance in Figure 9.4.

9.2.3.2 Aerosol scattering

Light scattered into the sensor viewing direction by particles in the atmosphere is also significant. In contrast to Rayleigh scattering, which is determined essentially by geometry and atmospheric pressure, aerosol reflectance varies considerably in time and space because of variations in the concentration and type of particles in the atmosphere. For example, concentration variations of an order of magnitude can occur during a day owing to advection of aerosols by winds, with atmospheric fronts giving particularly strong variations. Similarly, aerosols may consist of water droplets, desert or volcanic dust, particles emitted by industrial or domestic activities, etc. The prevailing mixture of aerosol type depends on proximity to the respective sources and wind patterns, relative humidity, etc. The diversity of origin is matched by a diversity of optical properties because of different refractive index, size distribution, shape, altitude, etc. Formally these can be expressed by representing the aerosol reflectance, ρ_a, with a SSA (Gordon and Wang, 1994*b*) as a function of aerosol single-scattering albedo, $\omega_a(\lambda)$, aerosol optical thickness, $\tau_a(\lambda)$, and aerosol scattering phase function, $P_a(\alpha, \lambda)$

$$\rho_a = \frac{\omega_a(\lambda)\tau_a(\lambda)P_a(\theta_0, \theta_v, \Delta\phi, ,}{4\cos\theta_0\cos\theta_v}, \tag{9.16}$$

where

$$p_a(\theta_0, \theta_v, \Delta\phi, \lambda) = P_a(\theta_-, \lambda) + \left[r_{sky}(\theta_0) + r_{sky}(\theta_v) \right] P_a(\theta_+, \lambda). \quad (9.17)$$

In contrast to the calculation of Rayleigh refectance, the factors in (9.16) cannot be calculated *a priori* on the basis of known parameters. However, for any specified pixel in an ocean-colour image (i.e. fixed geometry and aerosol optical properties), the wavelength dependence of aerosol reflectance can be expected to follow a simple functional form of the type

$$\rho_a(\lambda) = \rho_a(\lambda_0) e^{c(\lambda - \lambda_0)}, \quad (9.18)$$

where λ_0 is a specified wavelength and c is a factor that depends on the viewing geometry and the aerosol type (Gordon and Wang, 1994*b*).

The wavelength dependance of aerosol reflectance is plotted in Figure 9.4 for various values of c and for $\rho_a(865\,\text{nm}) = 0.02$. This arbitrarily chosen value of $\rho_a(865\,\text{nm})$, and those for c, have a magnitude that is possible for ocean-colour situations (Viollier et al., 1980). However, for reasons described above variability is high (e.g. factor 10) and Figure 9.4 should be seen as an illustration of the colour of aerosol reflectance rather than the magnitude. The figure shows that aerosol reflectance has smooth, almost linear spectral form with colour varying from white aerosols typical of a maritime atmosphere ($c \approx 0$) to aerosols with stronger blue reflection.

9.2.3.3 Atmospheric absorption

Transparency of the atmosphere is necessary for satellite remote sensing. This transparency is quantified by variously defined transmittances, which depend on

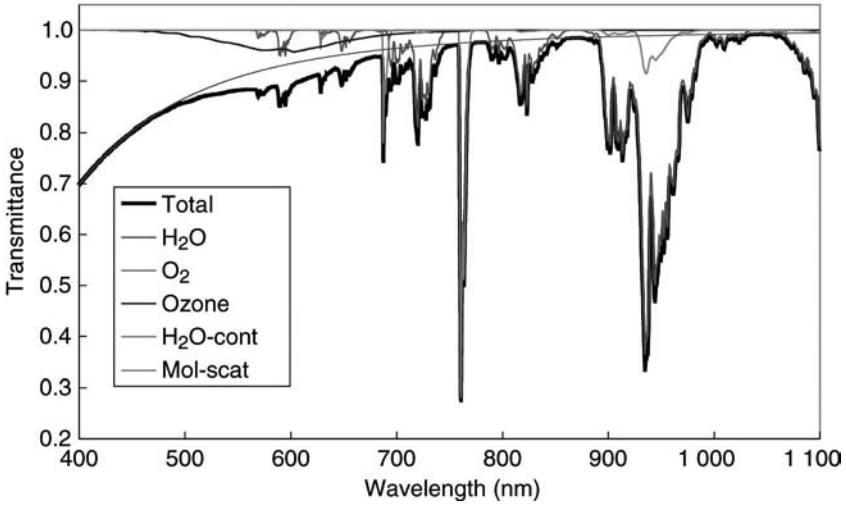

Figure 9.5
Light transmittance spectra for total atmospheric column. Contributions of molecular (water vapour, oxygen, ozone) absorption and molecular scattering are also shown.

absorption and broadband scattering in the atmosphere, with transmittance equal to one indicating perfect transparency. Ocean-colour sensors are designed to use wavelengths located in spectral windows where atmospheric transparency is high. However, some gaseous absorption is unavoidable because of the finite bandwidth (e.g. 10–20 nm at full-width-half-maximum) of sensors and the complexity of the atmospheric absorption spectra. Atmospheric molecules like water vapour (H_2O), ozone (O_3) and oxygen (O_2) are the most important absorbers in the visible and near-infrared. Line absorption data for atmospheric molecules has been compiled in the High Resolution Transmission Molecular Absorption database (Rothman et al., 1998). For water vapour, in addition to discrete molecular absorption lines, there is continuum absorption over the whole spectrum. Figure 9.5 shows the atmospheric transmittance computed from LOWTRAN (Kneizs et al., 1983) for the US standard atmosphere model for a vertical path. For non-vertical viewing or solar illumination the length of photon paths through the atmosphere increases with a factor $1/\cos\theta$, where θ is the viewing or sun zenith angle, and the transmittance decreases accordingly (Viollier et al., 1980).

Weak absorption by ozone takes place over the entire visible range and needs to be accounted for in ocean-colour data processing. Furthermore, depending on the choice of spectral position, ocean-colour bands can be affected by absorption due to oxygen (e.g. near 762 nm) or water vapour (e.g. near 710 nm). Ozone concentration, atmospheric pressure and relative humidity are used for the correction of absorption due to atmospheric ozone, oxygen and water vapour, respectively.

9.2.4 Air/sea interface reflection

Light that passes through the atmosphere can be either reflected or refracted (transmitted) at the air/sea interface because of the difference in dielectric constants of air and water. The refracted light interacts with the water column and some is scattered back to the atmosphere. This water-leaving radiance is discussed in Section 9.2.5. As sketched in Figure 9.6, light reflected at the air/sea interface is considered via three distinct processes: A, reflection of skylight; B, reflection of direct sunlight by the water surface (sunglint); and C, reflection of direct sunlight by whitecaps. This decomposition into reflection of direct and diffuse light facilitates calculation of the respective atmospheric transmittances. The current section focuses on the reflection coefficient of the air/sea interface as relevant for processes A and B, and on variation of the whitecap reflectance with wind speed and sea/air temperature difference, process

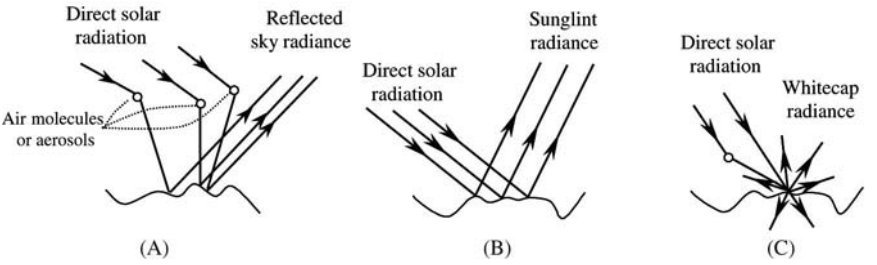

Figure 9.6
Sketch of A, sky reflection; B, sunglint; C, whitecap reflection on the air/sea interface.

C. Correction for these effects is incorporated in ocean-colour data processing chains, as outlined in Section 9.3.2.

9.2.4.1 Reflected skylight and sky reflectance factor

Reflected skylight is considered in Section 9.2.3 via the extra terms in (9.12) and (9.17) for aerosol and Rayleigh scattering and in general, skylight effects are accounted for in ocean-colour processing (the inverse problem of Section 9.3.2) by look-up tables for the aerosol or Rayleigh scattering. However, reflected skylight is considered separately in this subsection because it is useful for processing seaborne radiance data measured just above water (Mueller et al., 2000). The angular distribution of reflected light depends on both the angular distribution of incident light and the geometry of the surface wave pattern. This is represented by the sky reflectance factor, r_{sky}, which is defined as $r_{sky} = L_{ref}(\theta_v, \phi_v) / L_{sky}(\pi - \theta_v, \phi_v)$, where L_{ref} and L_{sky} are the reflected sky radiance and the incident sky radiance respectively. For a definition of r_{sky} taking account of detector field-of-view (see Mobley, 1999). The variation of r_{sky} as function of θ_v is shown in Figure 9.7 for varying wind speed. The reflectance of a perfectly flat surface, the Fresnel reflectance, is also plotted for comparison. This figure shows that the sky reflection increases as sensor zenith angle increases basically according to the Fresnel reflection law, dramatically so for $\theta_v > 50^\circ$. Increasing wind speed increases/decreases the sky reflectance for moderate/high sensor zenith angles respectively. Assuming wavelength-independence of the refractive index, r_{sky} can also be considered as independent of wavelength. The reflected skylight just above the water will, thus, have the same colour as the incident skylight.

Figure 9.7 has been made with the assumption of unpolarized light and a uniform sky radiance distribution. For a more accurate assessment of r_{sky}, both polarization and a more realistic sky radiance distribution should be considered. In these calculations, the multiple reflection between facets and the shadow effect have also been ignored. These effects may become significant for high sensor zenith angle (Gordon and Wang, 1992; Mobley, 1994; Nakajima and Tanaka, 1983).

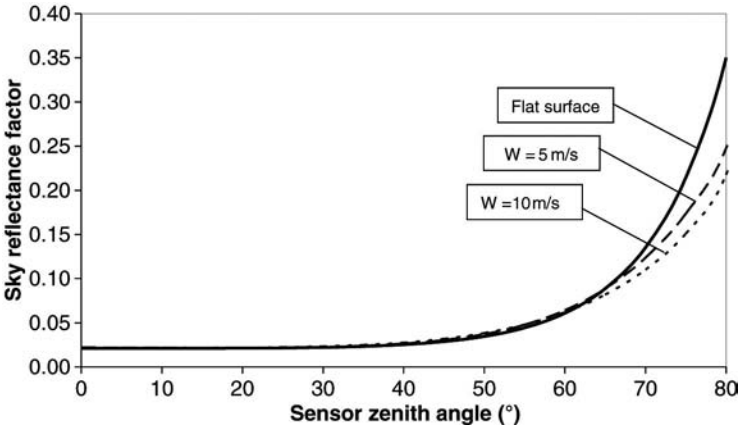

Figure 9.7
Sky reflectance factor for flat and wind-roughened surfaces with wind speed 5 m/s or 10 m/s, assuming a uniform distribution of sky radiance.

9.2.4.2 Sunglint

In contrast to skylight reflection, sunglint reaches the sensor only for viewing zenith angle equal to the sun zenith and for 180° relative azimuth angle between sun and sensor, for the case of a flat 'mirror-like' sea. For windy conditions the sea surface becomes roughened and viewing directions close to this critical sunglint viewing direction also receive sunglint. In ocean-colour images sunglint can be seen as a very bright patch, whose size increases with increasing wind speed. Some sensors (see Table 9.2) avoid sunglint by tilting away from the sun.

The sunglint reflectance, ρ_g^{0+} is defined in (9.7) as the ratio of the glint radiance and the downwelling irradiance just above the water and the angular geometry is illustrated in Figure 9.8.

ρ_g^{0+} is given by (Cox and Munk, 1954) as

$$\rho_g^{0+} = \frac{\pi \rho_F(\omega) P_s(\theta_0, \phi_0, \theta_v, \phi_v; W)}{4 \mu_v \mu_0 \cos^4(\theta_n)}, \tag{9.19}$$

where $\theta_0, \phi_0, \theta_v, \phi_v$ are the solar zenith angle, the solar azimuth angle, the sensor nadir angle and the sensor azimuth angle, respectively; $\rho_F(\omega)$ is the Fresnel reflectance; $P_s(\theta_0, \phi_0, \theta_v, \phi_v, W)$ is the probability of surface slope for which the incident ray with direction (θ_0, ϕ_0) is reflected to the direction (θ_v, ϕ_v); W is the wind speed 10 m above the sea surface, ω is half of the angle between the vectors of surface to sun and surface to sensor, μ_v and μ_o are the cosines of θ_v and θ_o. The wind-direction independent surface slope distribution function $P_s(\theta_0, \phi_0, \theta_v, \phi_v, W)$ is approximated by

$$P_s(\theta_0, \phi_0, \theta_v, \phi_v, W) = \frac{1}{\pi \sigma^2} \exp\left(-\frac{\tan^2 \theta_n}{\sigma^2} \right), \tag{9.20}$$

where $\sigma^2 = 0.003 + 0.512 W$. A more general surface slope distribution accounting for the wind direction can be found in Cox and Munk (1954).

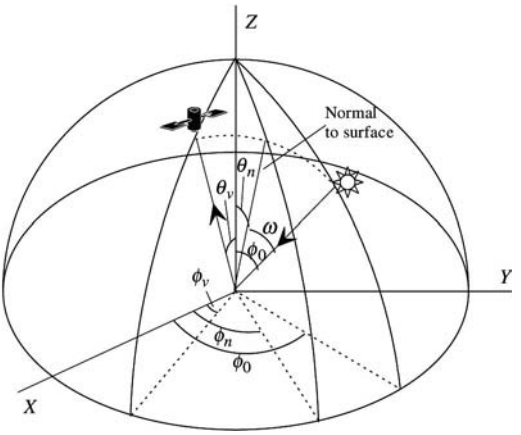

Figure 9.8
Definition of angles related to sun/sensor configuration and the normal vector to the wind-blown surface.

The angles ω, θ_n and ϕ_n in the above equations are given by

$$\cos(2\omega) = \cos\theta_v \cos\theta_0 + \sin\theta_v \sin\theta_0 \cos(\phi_v - \phi_0) \tag{9.21}$$

$$\theta_n = \cos^{-1}\left(\frac{\cos\theta_v + \cos\theta_0}{2\cos\omega}\right)$$

$$\cos\phi_n = \frac{\sin\theta_0 \cos\phi_0 + \sin\theta_v \cos\phi_v}{2\cos\omega \sin\theta_n}$$

$$\sin\phi_n = \frac{\sin\theta_0 \sin\phi_0 + \sin\theta_v \sin\phi_v}{2\cos\omega \sin\theta_n}.$$

In Figure 9.9, calculations of ρ_g^{0+} with this model are shown for five azimuth angles, for $\theta_0 = 30^\circ$ and W = 10m/s. The glint reflectance with $\Delta\phi = 45^\circ$ is much smaller that the reflectance with $\Delta\phi = 90^\circ$ or $\Delta\phi = 135^\circ$ for the sensor zenith angle 5° – 40°. This is easily understood because in the latter case the sensor is looking more towards the sun. For relative azimuth angles of 90° or greater with respect to sun and moderate wind speeds, the sunglint reflectance is typically the largest contribution to top-of-atmosphere reflectance. In such a case ocean-colour imagery will be degraded or even rendered unusable. Assuming wavelength-independence of the refractive index, ρ_g^{0+} can also be considered to be independent of wavelength. The sunglint just above water will thus have the same colour as the incident sunlight.

Many sunglint correction algorithms use similar equations to those presented here, although the slope distribution may be considered as a function of wind direction. As new techniques using laser and radar are developed, more measurements of the surface slope distribution are being reported (Hwang and Shemdin, 1988; Liu et al., 1997). These results validated the much older Cox and Munk model or extended it to negative air – sea temperature, high wind speed or low sun elevation. However, such improvements are not yet widely employed in ocean-colour processing, to our knowledge.

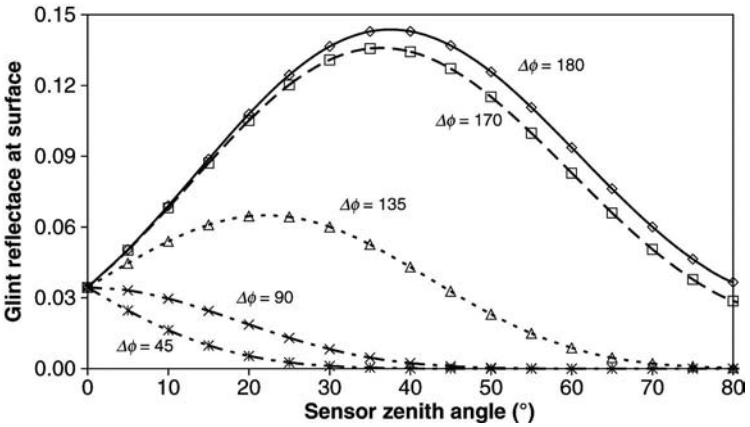

Figure 9.9
Glint reflectance versus sensor zenith angle in degrees for various azimuth angles with sun zenith angle of 30° and wind speed of 10 m/s.

9.2.4.3 Whitecap reflectance

The whitecap reflectance can be estimated from

$$\rho_{wc}^{0+} = f_{wc}\rho_{eff}\ (\lambda) \tag{9.22}$$

where f_{wc} is the fractional coverage of whitecaps, ρ_{eff} is the effective albedo and $f(\lambda)$ is a spectral factor (Koepke, 1984). The formula for f_{wc} proposed by Monahan and O'Muircheartaigh (1986) is

$$f_{wc} = 1.95 \times 10^{-5} W^{2.55} \exp(0.0861\Delta T) \tag{9.23}$$

where ΔT is sea – air temperature difference in °C. For effective albedo, (Koepke, 1984) showed

$$\rho_{eff} = 0.22 \pm 0.11 \tag{9.24}$$

(Frouin et al., 1996) parameterized the spectral factor as:

$$f(\lambda) = 1 \text{ for } \lambda < 0.6\,\mu\text{m} \text{ and } f(\lambda) = \exp[-p(\lambda - 0.6)^q] \text{ for } \lambda > 0.6\,\mu\text{m}, \tag{9.25}$$

with $p = 1.75 \pm 0.48$ and $q = 0.99 \pm 0.05$. This $f(\lambda)$ parameterization gives a significant reduction in reflectivity at near-infrared bands which is in contradiction to earlier results of (Whitlock et al., 1982) but is consistent with (Moore et al., 2000). The above model gives $\rho_{wc}^{0+} = (0.0015, 0.0013)$ and $(0.0043, 0.0036)$ at (400–600 nm, 700 nm) for W = 10 m/s and 15 m/s respectively.

It is noted that the whitecap reflectance expressed by these equations may be a poor estimate of reality in many cases because of the dynamic nature of whitecap formation and ageing (Koepke, 1984; Monahan and O'Muircheartaigh, 1986). The effect of whitecap reflectance on atmospheric correction has been studied for remote sensing applications by (Gordon and Wang, 1994*a*).

9.2.5 Marine reflectance

For HAB detection it is, of course, the water-leaving reflectance that contains potentially useful information. The interaction of light with seawater, including dissolved and particulate constituents, can be considered by applying radiative transfer equations where interactions are represented by inherent optical properties such as the total absorption coefficient and volume scattering function. Approximate solutions of the radiative transfer equations have been obtained (Gordon et al., 1975; Kirk, 1981; Morel and Prieur, 1977) allowing water-leaving reflectance to be expressed as a function of total absorption coefficient $a(\lambda)$, and total backscattering coefficient $b_b(\lambda)$. In this section such an approximate solution is presented in order to illustrate briefly the spectral shape of water-leaving reflectance and its variation with chlorophyll concentration C, and other factors. Methods to invert the water-leaving reflectance spectrum to give C are reviewed in Section 9.3.3. As the purpose here is to give a first impression of the colour of processes, in this section it is assumed that the water column is vertically homogeneous (Philpot, 1987; Vasilkov et al., 1999) and that bottom reflection (Ackleson, 2003), Raman emission (Haltrin and Kattawar, 1993; Sugihara et al., 1984),

phytoplankton fluorescence (Babin et al., 1996; Carder and Steward, 1985; Gower et al., 1999) and yellow substance fluorescence (Hoge et al., 1993) are neglected. For a more detailed description of inherent and apparent optical properties of water (including fluorescence) the reader is referred to the references and the other chapters of this volume (Babin, 2007; Morel, 2007; Roesler and Boss, 2007; Schofield et al., 2007; Sosik, 2007 – Chapters 7, 4, 5, 3 and 8 respectively).

Using the model of (Morel and Gentili, 1996), but expressing for the water-leaving reflectance $\rho_w(\lambda)$ rather than the subsurface irradiance reflectance

$$\rho_w(\lambda) = \pi \frac{f'}{Q} \Re \frac{b_b}{a + b_b}, \tag{9.26}$$

where f' varies (Morel and Gentili, 1991) with sun zenith angle and weakly with inherent optical properties, Q is the ratio of irradiance to radiance just beneath the air/sea interface, and the term $\Re$ (Morel and Gentili, 1996) represents reflection and refraction effects at the air/sea interface and depends primarily on θ_v and sea state and weakly on θ_0. The decomposition of total absorption and backscatter coefficients into components relating to water constituents can be performed in various ways depending on the desired product(s). For the present study targeting chlorophyll *a* concentration in coastal waters, the following decomposition is adopted:

$$a(\lambda) = a_w(\lambda) + a_\phi(\lambda) + a_Y(\lambda) \tag{9.27}$$

$$b_b(\lambda) = b_{bw}(\lambda) + b_{bC}(\lambda) + b_{bNC}(\lambda) \tag{9.28}$$

where a_ϕ is the phytoplankton absorption coefficient, a_Y is the absorption coefficient of all dissolved and non-phytoplanktonic particulate matter, termed 'total yellow substance', a_w is the coefficient of pure water for which tabulated data are available in Buiteveld et al. (1994), b_{bw} is the backscatter coefficient of seawater (Morel, 1974)

$$b_{bw}(\lambda) = 0.5 * 0.00288 * \left(\frac{\lambda}{500\,\text{nm}}\right)^{-4.32}, \tag{9.29}$$

where b_{bC} is the backscatter coefficient of phytoplankton (and covarying detrital particles), and b_{bNC} is the backscatter coefficient of all other (non-covarying) particulate matter. Phytoplankton absorption can be parameterized (Bricaud et al., 1998) as a function of chlorophyll by:

$$a_\phi = A_\phi(\lambda) C^{E_\phi(\lambda)}, \tag{9.30}$$

where C is the chlorophyll *a* concentration and A_ϕ and E_ϕ are empirical constants derived from measurements. Phytoplankton backscatter can be parameterized by (Morel and Maritorena, 2001) as

$$b_{bC}(\lambda) = \{0.002 + 0.01 * [0.50 - 0.25 \log C]\} * \left(\frac{\lambda}{550\,\text{nm}}\right)^{v} * 0.416\, C^{0.766}, \tag{9.31}$$

where v is an exponent which is zero for $C > 2$ mg m^{-3} but negative for lower C:

$$v = 0.5 * (\log_{10} C - 0.3) \quad \text{for } 0.02 < C < 2 \text{ mg m}^{-3}. \tag{9.32}$$

Backscatter from other particles can be represented spectrally via the form (Morel and Prieur, 1977):

$$b_{\text{bNC}}(\lambda) = b_{\text{bNC}}(550 \text{ nm}) \left(\frac{\lambda}{550 \text{ nm}} \right)^{-n}, \tag{9.33}$$

where the exponent n has been measured for a variety of marine particles by for example (Babin et al., 2003*a*).

Yellow substance absorption can be represented by a form (Roesler et al., 1989; Sathyendranath et al., 1989):

$$a_{\text{Y}}(\lambda) = a_{\text{Y}}(440 \text{ nm}) \text{e}^{-k(\lambda - 440 \text{nm})}, \tag{9.34}$$

where k depends on the type of yellow substance(s) that are present and particularly the ratio of particulate to dissolved yellow substance. Measurements of k for non-algae particles and for coloured dissolved organic matter are presented in Babin et al. (2003*b*) and the references therein.

9.2.5.1 Case 1 phytoplankton-dominated water

Using these parameterizations, water-leaving reflectance is presented in Figure 9.10 for conditions typical of Case 1 phytoplankton dominated waters. A high-biomass case $C = 10$ mg m^{-3} is also included for comparison with the Case 2 examples shown in Section 9.2.5.2, although it is noted that the parameterizations used for phytoplankton absorption and backscatter have been designed generally for lower C. In this model increasing chlorophyll affects reflectance both via backscatter and absorption. The increase in backscatter increases reflectance without changing spectral shape as can be seen for the range 600–800 nm where total absorption is almost independent of C. For increasing C, the increase in absorption tends to decrease reflectances as well as changing the spectral shape particularly in the range 400–550 nm.

For high-biomass HABs, chlorophyll concentrations could be much greater than the $C = 10$ mg m^{-3} case considered in Figure 9.10. In such cases the reliability of the present model is in doubt. However, it is clear at least that in such cases the reflectance in the red and near-infrared will continue to increase as C increases and the local minimum near 670 nm will become more pronounced.

A more complete and accurate treatment of Case 1 waters with consideration of lower concentrations more typical of deep oceanic waters can be found in (Morel and Maritorena, 2001) – see especially Figure 8 of that paper.

9.2.5.2 Case 2 phytoplankton with yellow substance

The conditions illustrated in Figure 9.10 are typical of high-biomass phytoplankton blooms in open ocean waters. However, for coastal waters where HAB applications predominate both yellow substance and backscatter from tripton can be significant giving very different magnitude and spectral shape for $\rho_{\text{w}}(\lambda)$. This is illustrated in

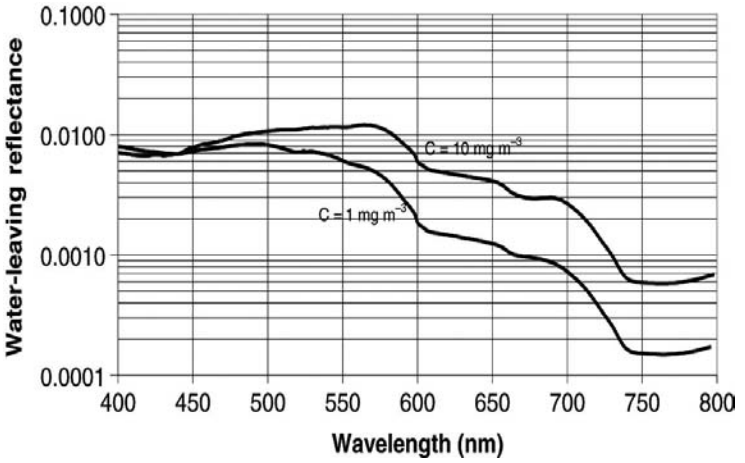

Figure 9.10
Water-leaving reflectance estimated using (9.26) to (9.34) for typical Case 1 phytoplankton-dominated conditions using $C = (1, 10)$ mg m^{-3}, $a_Y(440\text{ nm})$ (0.014, 0.056) m^{-1}, $f'/Q = 0.09$, $\Re = 0.53$, $b_{bNC}(550\text{ nm}) = 0$ and $k = 0.014\,\text{nm}^{-1}$.

Figure 9.11 where the same model is used as for Fig. 9.10 except that a non-zero b_{bNC} and high a_Y are used.

Figures 9.10 and 9.11 both include a case with $C = 10$ mg m^{-3} and $a_Y(440\text{nm}) = 0.056$ m^{-1} but for different $b_{bNC}(550\text{ nm})$ and hence backscatter difference of a factor of nearly 50. Comparing these, the magnitude of reflectance is different by a factor varying spectrally between about 10 and 50 depending mainly on the importance

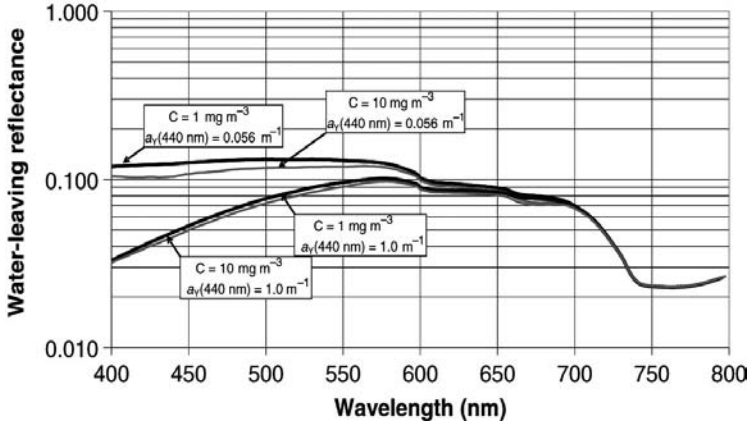

Figure 9.11
Water-leaving reflectance estimated using (9.26) to (9.34) for various Case 2 water types (phytoplankton, tripton and yellow substance) using $C = 1$ and 10 mg m^{-3}, $a_Y(440\text{ nm}) = 0.056$ and 1.0 m^{-1}, $f'/Q = 0.09$, $\Re = 0.53$, $b_{bNC}(550\text{ nm}) = 0.5$ m^{-1}, $n = 0$ and $k = 0.014$ nm^{-1}.

of the 'saturation' nonlinearity of (9.26) for high b_b. While it is noted that the model (9.26) is less reliable for such high b_b, reflectance spectra of such shape and magnitude are commonly found in turbid coastal waters (e.g. Gons, 1999; Whitlock et al., 1981). An important feature of Figure 9.11 is that $\rho_w(\lambda)$ is almost independent of C and $a_Y(440\text{ nm})$ for $\lambda > 700$ nm, as absorption from pure water and backscatter from non-phytoplanktonic particles are the dominant optical properties there. Moreover, while $\rho_w(\lambda)$ varies with both C and $a_Y(440\text{ nm})$ for $400\text{ nm} < \lambda < 550$ nm, $\rho_w(\lambda)$ is almost independent of $a_Y(440\text{ nm})$, but sensitive to variations in C for $650\text{ nm} < \lambda < 700$ nm. These properties can be exploited in the design of chlorophyll retrieval algorithms as described in Section 9.3.3. In addition to C, $a_Y(440\text{ nm})$ and $b_{bNC}(550\text{ nm})$ variations, differences in n and k will also affect $\rho_w(\lambda)$ via spectrally-smooth variations without significantly affecting the wavelength ranges where $\rho_w(\lambda)$ is sensitive to C and $a_Y(440\text{ nm})$ variations.

9.3 Inverse ocean-colour problem – from ocean colour back to phytoplankton

From the previous section it is clear that many processes contribute to the ocean-colour signal recorded by a remote sensor. Most of these processes contain no useful information regarding marine phytoplankton and are considered as noise, which must be removed. The task of the ocean-colour algorithm is to work back from the detected signal, removing or correcting for atmospheric and air/sea interface effects and distinguishing between the desired phytoplankton-related information and other marine signals. This process is variously known as 'inversion' or 'retrieval' and can be carried out with a variety of optical approximations and mathematical techniques. The inverse problem and typical approaches are summarized in this section.

In most processors the inversion of the at-sensor signal is achieved in two steps. First, in the 'atmospheric (and air/sea interface) correction' step, the radiance measured by the sensor is decomposed into the useful signal consisting of photons that have travelled through the marine medium and the noise arising from detected photons reaching the sensor via other paths, particularly via scattering in the atmosphere. Then, in the marine optics step, the marine signal, usually in the form of a water-leaving reflectance spectrum, is processed to yield the desired geophysical parameter(s) such as chlorophyll *a* concentration.

This decomposition into atmospheric and marine optics is natural and efficient provided the two components can indeed be calculated *with sufficient accuracy* independently, that is if the decomposition can be achieved without the need for approximations, which significantly degrade the calculations. Otherwise it is necessary to perform a multivariate inversion for the combined sea-atmosphere system. This question to couple or not to couple the sea and the atmosphere in the inversion procedure is addressed in Section 9.3.1. The rest of this section is then based on the assumption that some decoupling (either full or iterative) is implemented.

9.3.1 To couple or not to couple?

Should inversion of the at-sensor signal be achieved by coupling or decoupling the marine and atmospheric component signals? The first step in answering this question is to consider the atmosphere and air/sea interface components. It is clear from the

definition of L_{path} and L_{int} that these are entirely independent of the marine conditions and are identical for a black sea or for a reflective sea. Thus, any atmospheric radiative transfer simulations for calculation of these components can be performed for a perfectly absorbing sea as in (Antoine and Morel, 1998). Aspects of the atmospheric correction, such as the Rayleigh reflectance, which require only geometric and auxiliary (i.e. non-reflectance) data clearly pose no problem of sea-atmosphere coupling. However, calculation of the aerosol reflectance and hence the Rayleigh-aerosol reflectance requires use of the sensor reflectance data, as these cannot be estimated with sufficient accuracy by other means. It is therefore necessary to distinguish between the marine and atmospheric contributions to the sensor reflectance data, at least insofar as necessary for calculation of the aerosol reflectance. An approach that has been employed successfully for relatively clear water (Gordon and Wang, 1994*b*) and that avoids multivariate inversion of the coupled atmosphere-marine problem, is to approximate the water-leaving reflectance in the NIR (near-infrared e.g. SeaWiFS 765 nm and 865 nm bands) as zero. Thus, the atmospheric signal can be isolated there and used to calculate near-infrared aerosol reflectance and aerosol-Rayleigh reflectance. With the further assumption that the entire aerosol reflectance spectrum can be defined uniquely and accurately from the near-infrared reflectances, then this spectrum can be calculated for all wavelengths by spectral extrapolation from the near-infrared to the blue using typical aerosol models.

In this attempt to avoid coupling of the atmosphere and marine optical problems, the two assumptions of negligible NIR water-leaving reflectance and unique and accurate spectral extrapolation of aerosol reflectance from the NIR to the blue have been introduced. The approach therefore becomes inaccurate or fails when either of these assumptions is not valid. For sufficiently turbid waters, as found in many coastal regions, the assumption of negligible NIR water-leaving reflectance is clearly not valid (see references cited below). This has stimulated a variety of approaches, as follows:

- The coupled sea-atmosphere system (or the sea-aerosol subsystem) can be considered together using an integrated multivariate inversion approach. Thus a solution is sought for a set of water and atmospheric parameters (e.g. aerosol optical thickness, chlorophyll concentration, yellow substance absorption and suspended particulate matter concentration) by inverting for all parameters simultaneously. Applications of such an approach are given by Doerffer and Fischer (1994), Land and Haigh (1996) and Neumann et al. (1995).
- The coupled sea-atmosphere system can be considered by successive iterations between a marine inversion and an atmospheric inversion. For example, in a first iteration atmospheric parameters are calculated assuming zero NIR water-leaving radiance. On the basis of this first atmospheric correction the marine parameters are calculated and used to estimate non-zero NIR water-leaving radiances, which are then used for a second, improved atmospheric correction. Applications of such an approach for SeaWiFS and MERIS are given by Arnone et al. (1998) and Moore et al.(1999) using a Case 2 water marine model, and by Siegel et al. (2000) for a Case 1 water marine model. For CZCS similar iterative approaches were adopted to deal with the more severe case of non-zero water-leaving radiance at 670 nm in CZCS processing (Aarup et al., 1990; Bricaud and Morel, 1987; Gould and Arnone, 1994; Mueller, 1984; Smith and Wilson, 1981; Viollier and Sturm, 1984).
- Decoupling of the sea-atmosphere system can be obtained even for turbid water by exploiting the fact that the water-leaving reflectance spectrum in the NIR has

a very well-defined colour because reflectance is there approximately inversely proportional to the pure water absorption spectrum. As this colour is very different from that of the aerosol reflectance spectrum (almost white) the aerosol and water reflectances can be simply decomposed analytically. Applications of such an approach are given for SeaWiFS by (Hu et al., 2000; Ruddick et al., 2000) and an early precursor is described for CZCS by (Guan et al., 1985).

No consensus has yet been reached on which approach is to be preferred, though some considerations are given here. Assuming that all inversion procedures use the same underlying (forward) optical model, and that this model corresponds perfectly to reality and has a unique inverse solution, then the fully coupled, the iteratively coupled and the decoupled methods should give the same solution, albeit at potentially different computational speeds. Differences, however, may be expected in the following cases:

- The need to decompose into separate ocean and atmosphere problems may require extra approximations to be applied in the decoupled approach. For example (Ruddick et al., 2000) and (Hu et al., 2000) assume some spatial homogeneity of aerosol Angstrom coefficient. If such approximations are not appropriate for a given image then the quality of the solution obtained can be degraded.
- If the underlying forward model does not correspond perfectly to reality then the solutions that will be returned by the different approaches may be different as may be solutions returned by different methods from the same family of approaches.
- If the problem does not have a unique solution, but multiple solutions which are equally valid in terms of the available reflectance data then the choice of method may influence which solution will be returned. Again, but here for the fully coupled and iteratively coupled approaches, further assumptions may be made to better constrain solutions by removing degrees of freedom of the system, e.g. by setting aerosol Angstrom coefficient *a priori* (Doerffer and Fischer, 1994; Neumann et al., 1995).

Leaving aside computational time, careful analysis of all methods suggests that 'to couple or not to couple?' is not the important question. What is important is the validity of approximations that are made in the underlying optical model of any specific implementation and whether the spectral information available at the sensor is sufficient to distinguish between the relevant processes and their associated unknown parameters. Regarding the latter, it seems that for many coastal waters with independently varying phytoplankton, inorganic suspended matter, CDOM, aerosol concentration and aerosol type the selected bands of current sensors are insufficient to uniquely define the parameters associated with these factors. Even if the atmosphere and marine systems can be sufficiently decoupled, for example by exploiting systematic differences in the NIR, a similar problem of insufficient information may be encountered though more critically in inversion of the marine optics model. In this respect it is clear that advantages can be expected from sensors with more spectral bands chosen to provide independent information.

9.3.2 Atmosphere and air/sea interface correction

The SeaWiFS processing chain provides an excellent example of how the inverse ocean-colour problem can be handled. The component algorithms are well-documented and their implementation in the processing code is distributed in the SeaDAS software (version 4.0), thus providing a complete definition of some of the details that are not

covered in the supporting peer-reviewed papers. The main steps in this atmospheric correction, which treats pixels independently, can be summarized as follows:

- The calibrated TOA reflectance, $\rho_{\mathrm{tot}}^{\mathrm{TOA}}(\lambda)$, is first corrected for whitecap reflectance using formulae similar to those of Section 9.2.4.3, but propagated to the TOA using estimates of diffuse transmittances.
- Next a correction is made for ozone absorption by calculating the two-way transmittance, $t_{\mathrm{oz}}^{0,\mathrm{v}}$, based on auxiliary measurements (or climatological data) for ozone.
- The Rayleigh reflectance, $\rho_r^{\mathrm{TOA}}(\lambda)$, is then calculated from geometry and atmospheric pressure using a model similar to (9.11) to (9.15), except that this is implemented in the form of look-up tables generated by highly accurate atmospheric radiative transfer simulations rather than from more approximate analytical functions. $\rho_r^{\mathrm{TOA}}(\lambda)$ is removed from the ozone- and whitecap-corrected $\rho_{\mathrm{tot}}^{\mathrm{TOA}}(\lambda)$ to give Rayleigh-corrected reflectances.
- Further corrections are made for oxygen absorption (765 nm band) and for sunglint. The latter correction uses the model of (Cox and Munk, 1954) as described in Section 9.2.4.2 with auxiliary wind-speed data. An iterative estimate of aerosol optical thickness is used to calculate the diffuse transmittances needed to propagate $\rho_{\mathrm{g}}^{0+}(\lambda)$ to $\rho_{\mathrm{ar}}^{\mathrm{TOA}}(\lambda)$ as described in (Wang and Bailey, 2001). Regions of high sunglint are flagged as inappropriate for ocean-colour processing.
- At the near-infrared wavelengths 765 nm and 865 nm, the water-leaving reflectance is assumed zero and the ratio of the Rayleigh-corrected reflectances at these two bands is used to deduce the aerosol spectral shape as represented by the 'epsilon' parameter defined by $\varepsilon^{765\,\mathrm{nm},865\,\mathrm{nm}} = \rho_{\mathrm{a}}^{765\,\mathrm{nm}}/\rho_{\mathrm{a}}^{865\,\mathrm{nm}}$ for a single-scattering approximation (Gordon and Wang, 1994*b*). This is compared with the $\varepsilon^{765\,\mathrm{nm},865\,\mathrm{nm}}$ tabulated for a range of aerosol models using atmospheric radiative transfer simulations. A weighted combination of the two best-fitting aerosol models is selected and used to represent fully the optical properties of aerosols in the pixel. Aerosol reflectances are then calculated for a fully multiple-scattering case for all wavelengths providing the terms $\rho_{\mathrm{a}}^{\mathrm{TOA}}(\lambda$ and $\rho_{\mathrm{ar}}^{\mathrm{TOA}}(\lambda)$ that must be eliminated from (9.8). Generalizations of this approach for turbid waters are described in Section 9.3.1.
- With full knowledge of the aerosol properties, Rayleigh scattering and the absorption from various atmospheric gases (ozone, water vapour, oxygen) the diffuse atmospheric transmittances, $T_0(\lambda)$ and $T_v(\lambda)$, can be calculated giving the water-leaving reflectance spectrum.

Similar procedures are applied to MODIS and MERIS data in the corresponding processing facilities. The MODIS atmospheric correction algorithm is described by Gordon and Voss (1999). MERIS algorithms are described in a series of Algorithm Theoretical Basis Documents (ATBD) (Meris Team, 2000) and corresponding papers by, for example, Antoine and Morel (1999) for atmospheric correction over Case 1 waters, Moore et al. (1999) for calculation of turbid water effects on the atmospheric correction, and others.

9.3.3 Retrieval of chlorophyll concentration and other phytoplankton-related parameters

Phytoplankton is most commonly quantified from conventional measurement techniques via the concentration of chlorophyll *a*, *C*. Most ocean-colour algorithms have, therefore, also targeted this parameter and this has been the main source of information

to date for HAB applications (see Section 9.5). Chlorophyll retrieval algorithms are reviewed in Sections 9.3.3.1–9.3.3.3. However, there is considerable interest in a HAB context in going further than C and attempting to distinguish in some way phytoplankton species composition. Such approaches are described in Sections 9.3.4 and 9.3.5. For certain applications, including global climate change and fisheries resources, primary production is also an ocean-colour parameter of interest – however, this is of less direct interest in the HAB context and is therefore not treated here.

9.3.3.1 Chlorophyll retrieval from blue-green ratios

The development and testing of algorithms for chlorophyll retrieval in Case 1 waters over 30 years has led to operational generation of ocean-colour chlorophyll products from sensors such as SeaWiFS, MODIS and MERIS. Reasonable consensus has been reached regarding optimal algorithm design with most operational ocean-colour C products being derived from a function of the ratio of water-leaving reflectance at a blue and a green band. For example, the MERIS Case 1 water algal pigment index product (Morel and Antoine, 2000) is defined via

$$\log_{10} C = \sum_{x=0}^{m} A_m (\log_{10} \rho_{443,555})^x \tag{9.35}$$

where

$$\rho_{443,555} = \frac{\rho_w(443\ \text{nm})}{\rho_w(555\ \text{nm})} \tag{9.36}$$

and A_m is a set of empirical coefficients. A number of similar band ratio algorithms are reviewed by O'Reilly et al. (1998). Their study concluded with the suggestion of a modified cubic polynomial algorithm for SeaWiFS using wavelengths chosen from the maximum of $\rho_{443,555}$, $\rho_{490,555}$ and $\rho_{510,555}$ in order to adapt to a wide range of C. All such algorithms fail in waters where optical constituents such as coloured dissolved organic matter or non-algae particles significantly affect the water colour at blue and green wavelengths. Thus, for most coastal HAB situations these algorithms are unlikely to give reliable results and may give totally erroneous products.

9.3.3.2 Chlorophyll retrieval from red-NIR ratios

As shown in Figure 9.11, reflectance spectra are affected by red chlorophyll absorption around 665 nm almost independently of any yellow substance. Algorithms for C have been designed for coastal and inland waters to take advantage of this feature (Dekker, 1993; Gons, 1999; Mittenzwey et al., 1992) by considering a ratio of reflectances within and just outside the red chlorophyll absorption wavelengths e.g. $\rho_{664,709}$. Sensitivity studies (Ruddick et al., 2001) show that such algorithms are suitable for high C and high b_b conditions and may, thus, be appropriate for many high-biomass HABs in turbid coastal and inland waters. For low C the ratio becomes less sensitive to C variations (Hoogenboom et al., 1998*a*) and for low b_b the reflectance magnitude at such wavelengths becomes small and difficult to accurately measure. Such algorithms have been tested for seaborne and airborne reflectance spectra though satellite data with appropriate wavelengths have only recently become available. For conditions where chlorophyll fluorescence is also significant at the wavelengths considered, suitable modifications are needed for the red-NIR band ratios algorithms.

9.3.3.3 Chlorophyll retrieval from multiband inversion algorithms

The algorithms of the preceding sections are applicable only for certain optical water types because of the assumptions and approximations made explictly or implicitly in their derivation. Using only a limited number of well-chosen wavelengths, these band ratio algorithms typically ignore much of the available ρ_w spectra. In view of the rapid expansion in spectral resolution and with the objective of deriving C retrieval algorithms with more general applicability new multiband inversion algorithms have been developed. The numerical methods used in such algorithms are diverse (Burenkov et al., 1985; Chami et al., 2002; Doerffer and Fischer, 1994; Hoge and Lyon, 1996; Hoogenboom et al., 1998b; Schiller and Doerffer, 1999; Sugihara et al., 1985; Vasilkov, 1997), as is the corresponding terminology, which includes neural networks, matrix inversion, least-squares inversion, spectral fitting, genetic programming, etc. However, most of these algorithms consist essentially of a forward optical model, which can be used to simulate $\rho_w(\lambda)$ from input such as C, b_b(550 nm) and a_Y(440 nm), and a numerical method that fits, usually according to a least-squares norm, the observed $\rho_w(\lambda)$ to the simulated $\rho_w(\lambda)$. C is then given by the best-fitting forward model input data set. Some approaches use all available bands, while others are restricted to the most appropriate bands.

These multiband algorithms are still a matter of considerable research. However, such an approach has already been applied for the Case 2 water global processing chain for MERIS data (Doerffer and Schiller, 1997) and improvements of this class of algorithms are to be expected in the coming years. While algorithm diversity at present seems greatest in terms of the choice of numerical fitting method, it is the validity of the forward optical model that should be most important in determining whether retrieved C will be appropriate for any given optical conditions.

9.3.3.4 Fluorescence-based algorithms

Phytoplankton can also be detected via sun-stimulated fluorescence (Babin et al., 1996; Gower et al., 1999). While no cases of satellite HAB detection by fluorescence have yet been reported, fluorescence does provide extra information on phytoplankton that could be detected by ocean colour. Moreover chlorophyll retrieval by the methods reported in Sections 9.3.3.2 and 9.3.3.3 might in some cases be degraded if the contribution of fluorescence to the water-leaving reflectance spectrum is not considered.

9.3.4 Beyond chlorophyll retrieval using reflectance spectra: is the AB a HAB?

While chlorophyll algorithms could be in some circumstances sufficient for detection and mapping of high-biomass (HB) HAB species, it is essential in many HAB events to assess the concentration and geographical distribution of only the harmful species. In these cases, an effective detection at the species level and discrimination from other species is required for their observation from ocean-colour techniques.

Among emerging technologies applicable to HABs detection at the species level, the development of taxa-specific ocean-colour algorithms is promising (Chang and Dickey, 2005; Cullen, 2007 – Chapter 1 this volume; Cullen et al., 1997; Schofield et al., 1999; Sosik, 2007 – Chapter 8 this volume). This methodology relies on the use of specific inherent optical properties (SIOPs), in particular the specific absorption

spectra and spectral backscattering of harmful species. From this, specific algorithms can be developed for the direct identification of HAB species as reviewed in the following subsections.

With knowledge of the species present it is possible to estimate HAB cell counts from the satellite-derived chlorophyll concentrations using empirical formulae (e.g. Rousseau et al., 1990). Alternatively *in situ* cell count data could be simply superimposed on satellite chlorophyll maps as in NOAA's Coastwatch service (see Case 1 of Table 9.4).

9.3.4.1 Pigment absorption and backscattering spectra

The taxa-specific absorption spectral shapes reflect the presence and/or a specific combination of different accessory chlorophylls and carotenoids (Johnsen et al., 1994; Schofield et al., 2007 – Chapter 3 this volume). These pigments have been recognized as valuable chemotaxonomic tools to distinguish taxa (Jeffrey, 1997; Jeffrey and Vesk, 1997; Johnsen et al., 1994). As harmful phytoplankton species generally belong to several distinct phytoplankton classes (Cullen, 2007 – Chapter 1 this volume; Zingone and Enevoldsen, 2000), the use of their specific pigment composition and related absorption spectra offers possibilities for distinguishing them from other phytoplankton (Cullen, 2007 – Figure 1.7 this volume).

Identification of the spectral absorption spectra of HAB organisms can be obtained from both pure cultures of harmful species (Johnsen et al., 1994) or from *in situ* measurements on natural populations (e.g. Chang and Dickey, 2007 – Chapter 2 this volume; Liew et al., 1999; Millie et al., 1997). From this, different analytical techniques are used for recovering specific pigments from absorption spectra. The fourth-derivative of the particulate absorption spectra (Figure 1.7, Chapter 1) has been used to resolve the positions of absorption maxima attributable to specific pigments (Bidigare et al., 1989; Millie et al., 1997; Schofield et al., 2007 – Chapter 3 this volume). The contribution of various pigments to absorption spectra can also be retrieved using Gaussian curve deconvolution techniques (Hoepffner and Sathyendranath, 1991; Stuart et al., 1998). From the analyses of absorption spectra, taxa-specific algorithms can be developed to detect harmful species.

A well-known case concerns the red-tide dinoflagellate *Karenia brevis* (formerly *Gymnodinium breve*, a neurotoxic shellfish poisoning). A carotenoid, the gyroxanthin-diester was identified as specific of this organism (Millie et al., 1995; Millie et al., 1997). On this basis, a processing algorithm using a similarity index based on the comparison of the fourth derivative of the particulate absorption spectrum of an unknown sample to that of *G. breve* was developed (Millie et al., 1997). This algorithm was successfully applied for detection of this dinoflagellate in natural, mixed phytoplankton communities (Kirkpatrick et al., 2000). Use of such chemotaxonomical information in the formulation of taxa-specific ocean-colour algorithms is however difficult because this accessory pigment does not have unique absorption properties. The absorption spectrum of gyroxanthin-diester is indeed nearly identical to other xanthophylls (Kirkpatrick et al., 2000).

It is noted, however, that successful testing of such taxa-specific algorithms using total phytoplankton (or particulate) absorption spectra or simulated reflectance data as input and with perfect knowledge of the species that may be present and their SIOPs does not imply that these algorithms will be successful when used with satellite-derived ocean-colour data. The latter case is much more difficult because of the need

to first isolate the phytoplankton optical properties from other optical components that affect the water-leaving reflectance and because of the possible uncertainties generated by imperfect atmospheric correction. For example, fourth-derivative methods have never to our knowledge been tested with real atmospherically corrected data and may be particularly sensitive to small errors that cause spectral noise. Moreover, there may be multiple solutions to the problem of inverting water-leaving reflectance spectra (Sydor et al., 2004). One example of the separation of algal classes by applying a singular value decomposition technique to measured reflectance spectra is documented by (Liew et al., 1999) though it is not clear to what extent such results depend on the training set used and whether the same classification success will hold more generally.

In situ measurements of inherent optical properties (IOPs) including backscattering to scattering ratio and volume scattering function can provide information on, for example, the proportion of backscattering by algal particles and on the bulk size distribution of particles (Roesler and Boss, 2007 – Chapter 5 this volume). However, the use of such differences in scattering properties alone to provide species information from optical remote sensing data is not proven and is likely to be very difficult in waters with particles of potentially different origin.

9.3.4.2 Trichodesmium

An algorithm specific to the nitrogen-fixing cyanobacteria *Trichodesmium* has been developed. This cyanobacteria species forms massive blooms in oligotrophic tropical and subtropical waters (and is sometimes but not always classified as harmful). This algorithm uses (fluorescence-modulated) backscattering and absorption spectra and is successful in identifying *Trichodesmium* blooms in CZCS imagery (Subramaniam et al., 1999*a*). In this algorithm, the spectral dependence of the chlorophyll-specific absorption cross-sections and the spectral dependence of the chlorophyll-specific backscatter cross-sections are used (Subramaniam et al., 1999*b*).

9.3.4.3 Nodularia spumigena

Detection of *Nodularia spumigena* in the Baltic Sea relies on the high reflectance of the positively buoyant cyanobacteria filaments formed at the surface layer in the latter stages of the bloom (Kahru, 1997). Surface blooms can be observed at visible and near-infrared wavelengths even with broadband satellite sensors such as AVHRR (Kahru, 1997) and with even low-sensitivity sensors such as Landsat (Öström, 1976) and without the need for accurate atmospheric correction or sophisticated bio-optical algorithms. These detections do require, however, *a priori* knowledge of the blooming species and the ecosystem.

9.3.4.4 Phycocyanin

An algorithm specific to the pigment phycocyanin has been developed (Simis et al., 2005) and tested with MERIS imagery (Gons et al., 2005). This is based on phycocyanin absorption at 620 nm. The absorption of chlorophyll *a* at this wavelength complicates retrieval though the method shows clear promise for turbid, cyanobacteria-dominated waters.

9.3.4.5 UV-absorbing compounds

A promising technique for mapping the distribution of red tides relies on the detection of ultra-violet (UV) absorbing substances. These molecules, known as mycosporine-like amino-acids (MAAs), are synthesized by phytoplankton cells and are considered as a physiological adaptation to UV radiation exposure by providing efficient photoprotection (Vernet et al., 1994). Synthesis and excretion of MAAs, characterized by a maximum UV absorption at 360 nm, has been shown for the red-tide dinoflagellate *Lingulodinium polyedra* (formerly *Gonyaulax polyedra*) exposed to UV radiation (Vernet and Whitehead, 1996). On this basis, a massive *Lingulodinium polyedra* red tide was remotely detected off Southern California from measurements of reflectance into the UV spectral range (340–380 nm) by (Kahru and Mitchell, 1998). They consequently developed an in-water algorithm for the detection of red tides and differentiation from other phytoplankton blooms. This algorithm is applicable to remote sensing if the signal-to-noise ratio and atmospheric correction are sufficient to retrieve the dynamic range of water-leaving radiance. The problem encountered in the detection of red tides by their MAAs absorption is the interference of absorption by detrital and dissolved organic matter which also strongly absorb in the UV region (Kahru and Mitchell, 1998). The detection of UV-absorption compounds is limited to availability of UV spectral bands on ocean-colour sensors, the first example of which was the 380 nm band of the Global Imager (GLI) ocean-colour sensor on board the Japanese ADEOS-II spacecraft (IOCCG, 1998). Use of such optical properties is restricted to high-biomass and phototactic or surface HAB organisms such as some dinoflagellates (Schofield et al., 1999) and cyanobacteria (Kahru and Mitchell, 1998).

9.3.4.6 Limitations and perspectives

Based on the identification of specific optical properties, taxa specific algorithms have been developed and are now being tested for the detection of HABs. Clearly, the measurement and interpretation of SIOPs should have a central role in future research related to HAB detection. The identification of spectral signatures of the different harmful species remains a limiting step in the development of this technology. Besides traditional spectrophotometric techniques using an integrating sphere, the development of *in situ* hyperspectral measurements of IOPs will contribute significantly to this research (Millie et al., 1997; Roesler and Boss, 2007 – Chapter 5 this volume). It remains to be seen whether successes in distinguishing between phytoplankton groups on the basis of *in situ* absorption measurements can be reproduced for the much more difficult problem when only remotely sensed reflectance spectra are available.

9.3.5 Beyond chlorophyll retrieval with a little help

Research on species-specific absorption spectra and their impact on remotely sensed reflectance spectra will continue with the aim of using the ocean-colour tool for more than just chlorophyll retrieval. However, ocean colour should not be considered as a stand-alone tool for HAB detection and monitoring. As seen in the following section on reported applications and in the final discussion on possibilities and limitations, ocean colour is very powerful for detection of ABs or 'potential HABs' because remote sensing can cover very much larger areas than

seaborne measurements and does this very systematically (except when clouds prevent). However, it is generally difficult to determine the harmfulness of a detected AB by ocean colour alone. This limitation leads naturally to the combination of ocean colour with supplementary information from seaborne measurements or from expert knowledge of the region. For example, operational HAB bulletins such as NOAA's Coastwatch system use ocean colour for AB detection, but add information on phytoplankton species cell counts to assess harmfulness. Quoting (Stumpf, 2001) 'imagery can provide a means of identifying blooms that should be sampled, and can also identify areas where *K. brevis* is not located, owing to the lack of chlorophyll. Imagery can also provide an estimate of the extent of a bloom in areas of low chlorophyll'. The number of locations where potentially expensive *in situ* measurements are needed can be considerably reduced if the ocean-colour information is used to define the bloom extent.

Returning to ocean colour, more information regarding a (H)AB can be obtained by a multitemporal analysis. For example, NOAA's Coastwatch system compares chlorophyll concentration from the most recent image with mean chlorophyll from the preceding three months (Stumpf, 2001). High anomalies are classified as 'probably *K. brevis*'. Thus, an AB is considered not just via the instantaneous chlorophyll concentration but also by the temporal change in concentration. Again, however, the harmfulness of the AB is not determined by ocean colour but requires additional *in situ* information.

In addition to the combination of ocean-colour imagery with *in situ* measurements the role of subjective expert analysis should not be underestimated. A marine biologist with experience of a certain region will generally know at what time and in what locations harmful species are likely to occur even though it may be difficult to translate such knowledge or intuition into a computer programmable algorithm. An operational HAB bulletin will generally require a subjective analysis of ocean-colour imagery and other data before information is released to the press and the public, especially in view of the unnecessary panic and subsequent loss of credibility that can result from false alerts. Thus, NOAA's Coastwatch HAB bulletins include a summary 'conditions report' in addition to detailed imagery, measurements and scientific analysis in much the same way as a weather forecast would. For example, a typical such report reads: 'A harmful algal bloom has been identified off Saratosa … Patchy low to moderate impacts are expected at the beach throughout Wednesday morning … Reports of discoloured water are possible.'

Finally, it is intriguing to note that an experienced marine biologist will often 'know' what species dominates a bloom just by looking at it from a ship or an aircraft. This is probably partly a result of inductive reasoning: if a certain species has bloomed at the same time and in the same place in previous years then that species is likely to reoccur. However, it is also possible that human observers are using more than just radiometric (colour) information but also spatial (shape) information at scales unresolved by satellite data. For example, some phytoplankton may form stripes near the surface because of small-scale interactions between hydrodynamics and the species-dependent swimming or buoyancy of phytoplankton – see (Franks, 2007 – Chapter 15 this volume) and references cited therein. Other species may generate foam or other surface accumulations which are identifiable to a trained human observer even though they could not be distinguished from other phenomena by spatially averaged radiometric information. For example, Langmuir circulation, whitecaps, boat wakes and surface foam originating from phytoplankton may all look the same to a satellite with 1 km spatial resolution, but an oceanographer or sailor will easily distinguish between the various phenomena.

9.4 Sensors and platforms – choosing the right tool for the job

In this section the available ocean-colour remote sensors are reviewed from the point of view of the user. How appropriate are these tools for doing the job of detecting harmful algae blooms?

Over the last few years the number of available satellite-based ocean-colour sensors has increased dramatically (Figure 9.1). Additionally many other satellite-based optical sensors, which were not designed for ocean colour, (e.g. AVHRR, SPOT, Landsat) have visible bands sufficiently sensitive to detect certain marine phenomena such as very high suspended matter concentrations or floating layers of algae. If the latter are included then the user is confronted with an array of thirty or more possible data sources. Theoretically, a user could combine the strong points of each data source, for example the higher spatial resolution of one sensor could be essential for obtaining details close to the coast or in estuaries and inland waters, while another sensor with a wider swath would show the spatial extent of a bloom. Similarly, in regions where cloudiness is frequent but has high variability over a day the combination of sensors with different overpass times raises the probability of obtaining a useful image on any given day. However, in practice the cost (human resources, computer equipment, data) of setting up and maintaining real-time HAB detection systems for handling a wide variety of data sources necessitates a restriction to a small number of remote sensors. The optimal number in most cases is one (or zero!), though more advanced systems may consider two as a worthwhile number while research users could consider more on a less systematic and non-real-time basis. In view of this, the current section will not review all possible sensors but will concentrate on a very limited number of particularly promising sensors.

9.4.1 Platform characteristics and impact on applications – satellite and airborne systems

A remote sensor must be mounted on a platform, which provides power and communications and ensures that the sensor is directed towards a useful target at least some of the time. Such a platform could be a moving ship, a coastal tower, an offshore platform, a tethered balloon, a powered aircraft, a spaceborne satellite, etc. In practice, for the detection of HABs, the latter two platforms have been used almost exclusively to date because viewing from high altitude from a moving platform gives wider spatial coverage. This section therefore concentrates on the technical characteristics of these two types of platform.

While satellite platforms offer data at a global scale according to a systematic time schedule and with highly centralized data processing and distribution, airborne platforms offer the alternative of a more user-specific service at a regional scale. Data acquisition can be organized flexibly both in time and space, limiting operations to certain periods of the year or even to unpredictable events determined at short notice and allowing fast revisit. The lower altitude of airborne platforms allows a much higher spatial resolution to be achieved, typically metre-scale or less. Moreover the possibility of underflying clouds can be a very considerable advantage for airborne systems in many regions with frequent cloud cover. Accompaniment by a trained human observer may add texture and shape information as well as offering some real-time flexibility in data acquisition. Of course, the flexibility of airborne systems carries its disadvantages. Organization of data acquisition and processing of data are more labour-intensive and offer less scope

for economies of scale than satellite systems. The user must, therefore, assess the costs and benefits of the available systems and choose accordingly for a specific application.

9.4.1.1 Satellite platforms

The following technical characteristics of satellite platforms may affect the suitability of a remote sensor for a given HAB application:

- *Longevity*: One advantage of satellite systems is the possibility of obtaining data of reasonably homogeneous quality over a relatively long time-frame, typically a few years or possibly decades as achieved for terrestrial and meteorological applications by the NOAA-AVHRR and Landsat series. Related to longevity is the level of commitment and support provided to the platform by the owner, usually a national or international space agency though possibly a private company. This commitment is necessary to ensure that any applications developed for a specific data source will be sustainable in the long term.
- *Orbit*: All current satellite platforms for ocean-colour sensors orbit the earth in polar or near-polar sun-synchronous orbits with the exception of the Taiwanese OCI sensor which has a low inclination orbit. These orbits offer a view of usually the entire earth over a certain timeframe with repetition of imagery at regular intervals. For the user the orbit, combined with the swath of the sensor (see Section 9.4.2), will determine the frequency at which the desired target will be viewed. This frequency may vary from two or three images per day to one image every few days. As regards choice of orbit, it is interesting to note for the future that a geostationary orbit, as adopted currently for certain meteorological satellites, would offer the alternative prospect of near-continuous monitoring of a certain region of the earth.
- *Pointability/tilt*: Current ocean-colour sensors operate typically according to a fixed viewing programme. In some cases the platform or sensor can be periodically reoriented e.g. tilting to avoid sunglint or to perform a lunar calibration in the case of SeaWiFS. User-requested pointability of the platform is currently not possible for ocean-colour sensors, however, has been implemented successfully for certain terrestrial applications, for example, by the SPOT series.
- *Multi-sensor synergy*: It may be interesting in some applications to combine data of different types, e.g. ocean colour and radar for surface roughness or thermal infrared for sea surface temperature. Some minor advantage may be afforded in this respect by mounting different sensors on the same platform, thus ensuring perfect simultaneity of the data sources. However, such synergistic applications are generally limited and can often be achieved by data from separate platforms separated in time by up to a few hours. In practice, it is the cost and operational considerations (power requirements, vulnerability, punctuality, data transmission, economies of scale, etc.) for the platform operator that dominate the issue of the number of sensors a satellite should carry. It is interesting to note in this respect a possible trend towards smaller, single-sensor satellites or constellations of such sensors for future systems.
- *Data storage/transmission*: Though less critical for the 'mainstream' platforms considered here, some ocean-colour sensors are still limited to some extent by the amount of data that can be stored onboard and/or transmitted per orbit. In such cases the platform/sensor operator may need to prioritize according to which

regions of the world and/or which spatial resolution will be used for acquisition. For real-time HAB detection the speed of data transmission and ground segment processing is also a key factor.

9.4.1.2 Airborne platforms

For satellite systems the platform is typically unique and is owned and/or operated by a national or international space agency. The marginal cost of adding a new user or new region is small compared with the set-up costs for the mission. In contrast, the market for airborne systems is very differently structured and a much greater variety and number of airborne platforms, suitable also for terrestrial applications, are available. These may be owned and operated by national government agencies or may be rented with or without associated sensors and data processing services from private companies. The choice of platform is then dictated less by technical characteristics of the platform than by cost of the system (which is usually borne directly by the user) and by operational, practical and local considerations such as range/autonomy, crew, preferred altitude (compromise between resolution and swath), overlaps with other, possibly terrestrial, remote sensing activities, etc. However, it is worth noting that platform *stability* is an important technical consideration in the choice of platform. Spatial distortion of airborne remote sensing data caused by side winds and air turbulence can be a problem, particularly in the across-track direction due to the aircraft roll. Such geometric distortions need to be corrected in the post-processing of data using sensor attitude (roll, pitch, yaw) and position information measured inflight with an inertial navigation system (INS) in combination with a global positioning system (GPS). The use of a stabilized platform will reduce such distortions facilitating the data processing and improving image quality.

9.4.2 Sensor characteristics and impact on applications

While platform characteristics affect primarily the frequency (and cost) of data, the usefulness of information that can be extracted from a system is mainly a function of the sensor characteristics as follows:

- *Spectral bands*: the number, location and width of spectral bands is crucial in determining whether a sensor will be able to detect HAB-related phenomena. Sensors, such as AVHRR, LANDSAT, SPOT and ASTER, with a limited number (e.g. one to three) of broad bands in the visible part of the spectrum may be suitable for detecting strong backscatter from the sea and thus for mapping regions of high suspended matter (Stumpf and Pennock, 1989). However, in coastal waters backscatter is not generally well correlated with phytoplankton and more bands are needed in order to distinguish absorption features in the reflectance spectrum. For Case 1 waters, IOCOG (1998) suggest that three reasonably narrow (bandwidth 20 nm or preferably 10 nm) visible bands (e.g. 443 nm, 490 nm, 560 nm) are necessary for chlorophyll detection in open ocean waters in addition to two NIR bands (e.g. 750 nm, 870 nm) for atmospheric correction. For coastal waters many more bands are desirable in order to separate the optical effects of phytoplankton, yellow substance and inorganic suspended matter (see Sections 9.2.5 and 9.3.3). For example, a 412 nm band may help to distinguish between yellow substance and phytoplankton absorption though uncertainties in

atmospheric correction (and vicarious calibration) of such a band may be a problem. For turbid coastal waters with strong backscatter, extra bands within and just outside the red chlorophyll absorption maximum (e.g. 670 nm and 710 nm) may allow chlorophyll absorption to be isolated from yellow substance absorption (see Section 9.3.3 and references therein). Provided sun-induced fluorescence can be distinguished from spectral variation of absorption, bands located at and around the chlorophyll *a* fluorescence emission peak (e.g. 685 nm and 710 nm) may yield information on phytoplankton concentration – see IOCCG (1999) and references therein. Owing to extra difficulties in decoupling the marine reflectance from aerosol reflectance in turbid water (Section 9.3.1) further NIR and/or red bands may be useful to improve atmospheric correction. Looking further ahead, discrimination between phytoplankton species, if feasible, will clearly require extra spectral information e.g. in the 480–560 nm range for cyanobacteria. In fact, the most promising approach to solving many of the retrieval problems in coastal waters is often to add spectral resolution. It is reasonable to say that the future for optical remote sensing of coastal waters is hyperspectral.

- *Spatial resolution*: In the perspective of HAB detection in coastal waters the spatial resolution of 1 km typical of many ocean-colour sensors is appropriate for large-scale blooms. However, sensors with a higher spatial resolution (e.g. 300 m for MERIS) may offer new possibilities for small-scale HAB events such as occur in estuaries and large lakes, although new problems including adjacency effects may then be encountered. If much higher spatial resolution is required then airborne sensors are required unless a satellite-based sensor with much coarser spectral resolution is sufficient (e.g. SPOT). For oblique, off-nadir viewing, e.g. at the edge of a broad swath image, spatial resolution becomes coarser and geometrical distortion of pixels can increase.
- *Swath*: The swath or width of an image determines not only the size of a region that can be covered. For HAB detection the swath of 1,000 km or more on most ocean-colour sensors is considerably larger than the region affected. More critically though, swath will affect the frequency at which images can be acquired and is in this respect more important than the repeat cycle of sun-synchronous platforms. An instrument with broad swath can image a region on successive orbits with spatially separated tracks. For example, SeaWiFS imagery for southern North Sea waters (latitude 52°N) is available once or twice daily (e.g. at about 12:00 local solar time and sometimes about 13:30) whereas MERIS with a narrower swath will image the region two to three times less frequently. However, data quality for broad swath instruments is expected to degrade for large viewing zenith angles because of higher errors in atmospheric correction.
- *Calibration and validation*: Although much more difficult to determine objectively, the efforts that the sensor operators have taken to control in-flight calibration and product validation clearly affect data quality and suitability. Calibration is typically achieved by combination of a number of approaches including preflight laboratory measurements, on-board calibration lamps, in-flight sun and/or moon viewing, and vicarious calibration, the use of ground-based radiometric measurements extrapolated to the sensor altitude. An example of such an approach is provided by the SeaWiFS calibration plan (McClain et al., 1992). Product validation is typically achieved through a distributed network of research institutions performing measurements under the coordination of the sensor operator according to standardized protocols (Doerffer, 2002; Fargion and Mueller, 2000).

Regular calibration and validation workshops are organized to track any changes in sensor performance and identify weaknesses in processing algorithms. At the first level the atmospheric correction is validated by comparing satellite and seaborne water-leaving reflectance/radiance data. At a second level chlorophyll products are validated with similar comparison. The SeaWiFS specification (Hooker et al., 1993) of 5% for absolute radiometric accuracy of water-leaving radiance and 35% for chlorophyll provides a useful indication of target accuracy for products. However, it is clear that such accuracies are very difficult to achieve in coastal waters because of high uncertainties in both atmospheric correction and chlorophyll retrieval.

- *Support*: A related factor which may make the difference between success and failure of ocean colour for HAB applications is the level of user support provided with data. In this respect the larger space agencies typically provide the best service. The case of SeaWiFS is particularly noteworthy because free and well-supported image processing software is made available to data users via the SeaDAS initiative.
- *Artefacts*: Many other details of sensor design and performance may be of relevance (usually negative) in specific cases. While the subject is too vast to detail here, artefacts relating to straylight within the sensor, saturation, noise, insufficient sensitivity, striping/banding, smile and isolated band failure/drift have been found for various ocean-colour sensors. Many such artefacts can be detected easily by visual inspection of instantaneous images before corrections and filtering have been applied to hide them.
- *Price*: Commercialization of ocean-colour imagery is still relatively limited. Most space agencies provide data free of charge or at very low cost for research use. As applications mature and HAB detection systems become more operational users may be required to pay for satellite data. As an example, SeaWiFS data for 1997–2004 were available free of charge for research use (but subject to a two-week embargo) under a data-buy contract between NASA and Orbimage, the satellite constructor. SeaWiFS data for commercial and real-time use and post-2004 data must be purchased from Orbimage. Similar arrangements are planned or being implemented for other sensors, e.g. MERIS, though MODIS is freely available for all applications. For long-term investment in applications, a clear pricing policy is important for users.

9.4.3 Summary of current and historical satellite and airborne sensors

Most operational HAB detection systems will concentrate on the one or two most appropriate sensors for the job. The rapid expansion in available satellite-based ocean-colour sensors thus implies a need to choose. The criteria for this choice will typically be cost (of data and, more importantly, of any computing or human resources necessary to exploit it), availability of data and product quality. Thus, in this section attention is restricted to only those sensors for which a well-documented chlorophyll product is easily available for most of the world – such sensors are summarized in Table 9.2. These sensors are considered to be well-calibrated and well-supported. For information on more research-oriented or regional ocean-colour sensors the reader is referred to the many websites carrying such information, especially that of the International Ocean-Colour Coordinating Group (IOCCG), which has provided much of the information in this section.[46]

[46] www.ioccg.org

Table 9.2 Summary of historical and current ocean-colour sensors for which a well-documented chlorophyll product exists for most of the world. The equator crossing time is given in local solar time, the spatial resolution is given at nadir for the chlorophyll bands (in the case of sensors with multiple resolution). The number of spectral bands is separated into visible (400–700 nm), near-infrared (700–1,100 nm) and other (mainly thermal infrared). The sources of information include the International Ocean-Colour Coordinating Group (IOCCG, 1998) and the hardcopy references therein as well as the IOCCG and sensor agency websites. Sensors still functioning in 2005 are given as 'current'

Sensor	**CZCS**	**OCTS**	**POLDER -1**	**MOS-IRS**	**SeaWiFS**	**MODIS TERRA**	**MERIS**	**MODIS AQUA**	**GLI**	**POLDER -2**
Satellite	Nimbus-7	ADEOS-1	ADEOS-1	IRS-P3	OrbView-2 Sea Star	EOS-AM1	Envisat-1	EOS-PM1	ADEOS-2	ADEOS-2
Agency	NASA	NASDA	CNES	DLR	OSC/ NASA	NASA	ESA	NASA	NASDA	CNES
Start	1978	1996	1996	1996	1997	1999	2002	2002	2002	2002
End	1986	1997	1997	2004	Current	Current	Current	Current	2003	2003
Time (h)	12:00	10:41	10:41	10:30	12:00	10:30	10:00	13:30	10:30	10:30
Resolution (m)	825	700	~6500	500	1100	1000	300	1000	1000	6000
Swath (km)	1566	1400	2400	200	2806	2330	1150	2330	1600	2400
VIS/NIR/ other bands	4/1/1	6/2/4	5/4/0	8/9/1	6/2/0	11/5/20	8/7/0	11/5/20	16/8/12	5/4/0
Spectral Coverage (nm)	443-11500	412-12050	443-910	408-1600	412-865	412-14235	412-900	405-14385	375-12500	443-910
Tilt (degrees)	±20	±20	Variable	No	±20	No	No	No	±20	Variable

Table 9.3 Summary of current airborne sensors suitable for HAB detection

Sensor	DAIS 7915	CASI-2	AISA	AVIRIS	HYMAP
Field of view	±26°	±27.2°		±15°	±35°
Pixels per line	512	512	500	614	
VIS/NIR/other bands	e.g. 32/0/47	Up to 288	Up to 244	Up to 224	100-200
Spectral Coverage (nm)	400-12670	405-950	400-970	400-2500	400-2500

Table 9.2 contains the most important technical characteristics of the current satellite missions and Table 9.3 gives information on the most appropriate airborne sensors.

9.4.4 Future systems

As becomes clear from scanning oceanography journals (Section 9.1) and websites describing marine applications the delay between launch of a satellite and maturity of an application is considerable. Within the first two years of a satellite mission products are generally unstable and incompletely validated hampering the development of applications. Looking to other fields of satellite remote sensing such as use of AVHRR for sea surface temperature and Landsat for terrestrial applications, it may take even decades for applications to reach maturity and for satellite data to become a standard source of information. Combining such considerations with the considerable uncertainties surrounding the launch date and performance of even sensors that are already well under development it is clear that the user interest in future sensors is limited. In this section an exhaustive consideration of future ocean-colour sensors is, thus, not attempted however three promising future perspectives are noted:

- The development of medium-resolution (e.g. 1 km) geostationary systems offers the potential for much better temporal coverage than from polar-orbiting platforms, thus allowing fast dynamics of HAB events to be monitored or, in areas of scattered clouds, raising the probability of useful imagery. As an example, the proposed NOAA-NASA geostationary and pointable Special Events Imager could offer multispectral imagery every 10 min for a swath of 300 km at spatial resolution of 300 m.
- Over a 10–20 year time frame, the development of Unmanned Airborne Vehicles (UAV) may offer similar advantages over polar-orbiting platforms. As an example, the Pegasus UAV under development in Europe consists of a solar HALE (High Altitude Long Endurance) carrier operating at about 18 km whose payload will include multispectral optical and thermal digital cameras. This could be positioned semi-permanently over a region of interest allowing imaging many times a day for the few days of a typical HAB event.
- Hyperspectral sensors are already standard for airborne optical remote sensing, which is well suited for high-resolution monitoring of HABs in small areas (lakes, estuaries, etc.), albeit at considerable cost. Over the next few years the number of *hyperspectral space-borne sensors* is likely to increase rapidly. They will provide significant advantages over existing multispectral satellite sensors particularly in optically complex waters.

9.5 Applications of optical remote sensing to HAB detection

9.5.1 Ocean colour as a tool for HAB detection

Reports of HAB events have increased dramatically during the last decade (Hallegraeff, 1993). There is therefore scientific and public concern about the need for quantitative, cost-effective methods to detect and characterize the spatial and temporal variability of HABs in order to predict and mitigate such harmful events. The geographical extent and magnitude of HABs events have usually been assessed from seaborne monitoring and occasionally with numerical models (Johannessen et al., 1989). However, *in situ* data from ship-based or mooring-based observation programmes are generally not suitable for monitoring the bloom distribution at spatial and temporal scales relevant to HABs. Remote sensing from airborne or spaceborne sensors therefore offers the potential for improving the detection and mapping of these harmful events. However, ocean-colour data are still used relatively infrequently in HAB detection and management. In a recent study on HAB management for aquaculture farms, (Kallee, 2002) found that fish farmers in general wanted advance warning of a forthcoming HAB. However, only two (one in Norway, one in Chile) of the 12 organizations that responded, stated that they used remote sensing to detect HABs. In this section a number of past and present applications of ocean colour to HAB detection and mapping are reviewed, giving an impression of the capabilities and limitations of this tool. The point of view of the HAB detection user is given in more detail in Pitcher et al. (2007 – Chapter 21 this volume).

9.5.2 Description of past and present uses of ocean colour in HAB studies

Table 9.4 gives an overview of key characteristics of some of the best-documented cases of HAB detection. Where possible, a peer-reviewed publication is given as reference source. However, as the subject matter goes beyond research and even extends to public news bulletins, in many cases information is available only in the form of grey literature including conference proceedings and technical reports and in the form of websites (consulted originally in February–March 2003 and updated in February 2005). In this section, the scope of the chapter has been widened from ocean colour to cover also thermal infrared remote sensing of sea surface temperature (SST). Various correlations between phytoplankton and SST may exist depending on the local oceanographic conditions. For example, water masses with different nutrient concentrations may be correlated with SST, especially for the case of river plumes. Alternatively, a high-biomass HAB may increase heat absorption in the near surface layer (Kahru et al., 1993). Consequently, the tracking of water masses by SST has proved useful in a number of HAB cases. As satellite sensors have been available for SST mapping for decades and are well-established, their use can be seen as a precursor of the more directly relevant information that more recent ocean-colour sensors can be expected to produce.

Until now, most applications of remote sensing for HAB detection were based on the spatial and temporal near-surface chlorophyll concentrations and *a priori* knowledge of the blooming species (Graneli et al., 1998). As an example, ocean-colour data have been used for estimating the geographical extent of high-biomass blooms of diatoms and *Phaeocystis globosa* off the Dutch coast (Holligan et al., 1989) and have proved

Table 9.4 Characteristics of some well-documented cases of HAB detection by remote sensing

Case (see below)	Species	Region	R/S parameter/ Information	Remote sensors	Integration
1.	*Karenia brevis*	Gulf of Mexico	Chl, SST	SeaWiFS, AVHRR	*In situ*, meteo, other satellite R/S
2	*Nodularia spumigena*	Baltic Sea	Reflectance, SST, Chl	AVHRR, CZCS, TM/MSS, SeaWiFS, MODIS	*In situ*, ships of opportunity, observer reports
3	*Gymnodinium* sp.	Chiloe Archipelago	Brown patches	Airborne	*In situ*
4	*Chattonella verruculosa*	Denmark and Norway	Chl, SST	SeaWiFS, AVHRR, MERIS	*In situ*, modelling
5	*Karenia mikimotoi*	English Channel	Chl, SST	SeaWiFS, AVHRR	*In situ*, modelling
6	*Phaeocystis globosa*	North Sea	Chl, SST	CZCS, AVHRR	

1. NOAA's Coastwatch programme provides information on the location and extent of HABs in the Gulf of Mexico (SW coast of Florida) since 1999 (Stumpf and Culver, 2002). Their HAB bulletins are available at http://www.csc.noaa.gov/crs/habf/index.html and are sent during bloom events to interested users by e-mail. The concentration of cell counts is represented in categories from 'Present' ($<10^3$ cell/l) to 'High' ($>10^6$ cell/l). An expert judgement of the HAB situation is provided in a 'Condition report'. An example of the satellite imagery used is given in Figure 9.12.
2. High-biomass blooms of the toxic cyanobacteria *Nodularia spumigena* have been detected for the Baltic Sea by satellites on the basis of high reflectance (Öström, 1976) and satellite data have been used to investigate interannual ecosystem variability (Kahru, 1997; Kahru et al., 1994; Kahru et al., 2000). Near-real-time HAB monitoring is carried out within the Alg@line project (Rantajärvi, 2003) using a variety of seaborne measurements and observations with some satellite imagery support and reports are published on the internet (Baltic Sea Portal on http://www.fimr.fi)
3. Airborne observations in the Chiloé Archipelago (Chile) showed brown patches which accompanied salmon kills at acquaculture sites in the inland waters of Chile (Clément et al., 2000) attributed to *Gymnodinium* sp. Ocean-colour imagery is used (Clément, pers. comm.) to determine the chlorophyll distribution.
4. Operational monitoring of the Norwegian 1998 bloom of *Chattonella verruculosa*, which coloured water brown, is reported by Pettersson et al. (2000*b*). SeaWiFS imagery was considered to give a good representation of the shape and size of the bloom, although possible contamination of the chlorophyll products by inorganic suspended sediments is noted. The Harmful Algae Bloom Monitoring service of Norway set up within the framework of the DeciDe-HAB Project (Pettersson et al., 2000*a*) diffuses the ALGEINFO bulletins that give current information on the algal situation in Norwegian waters from March to October (see http://www.nersc.no/Decide-HAB/).
5. A bloom of the toxic flagellate *Karenia Mikimotoi* was found in seaborne measurements in the English Channel in summer 2003. Satellite chlorophyll imagery showed displacement of the bloom over a six-week period (Vanhoutte-Brunier et al., 2004).
6. CZCS chlorophyll images from 1980 are presented for Danish coastal waters by Holligan et al., (1989) to show the distribution and dynamics of phytoplankton populations, composed of diatoms and *Phaeocystis globosa*, a high-biomass mucilagenous species.

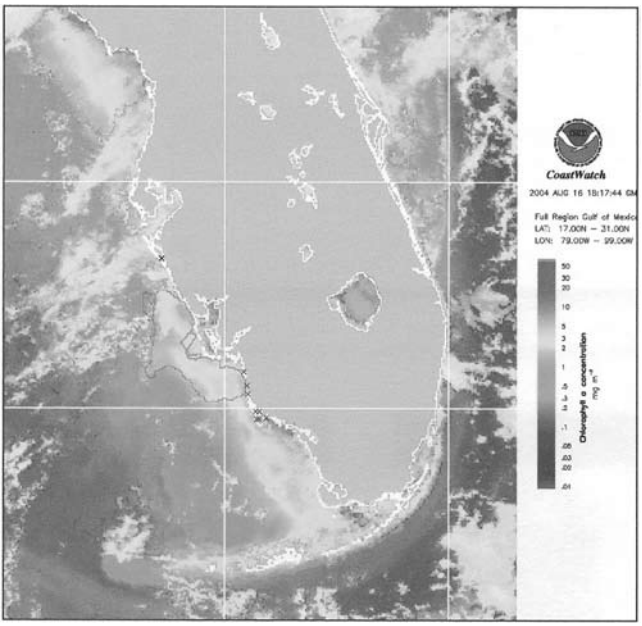

Figure 9.12
Satellite imagery section of a sample HAB bulletin (19 August 2004) from NOAA Coastwatch. Satellite-derived chlorophyll concentration from SeaWiFS is given in the colour scale with the red polygon on the West Florida coast marking a possible HAB region (considered as 'low to moderate probability' in this case). *In situ* sampling stations are given as crosses denoting that HABs were not present in cell concentration sampling data. *Source*: Information courtesy of Florida Fish and Wildlife Conservation Commission and NOAAHAB Forecasting System. Image courtesy of Orbimage, Inc. and NOAA Coastwatch.

valuable for monitoring of the dynamics and the advection of blooms (Pettersson et al., 2000b). Blooms of the raphidophyte *Chattonella vericulosa* were mapped in the same manner in coastal waters of Denmark and Norway. In Florida, blooms of the red-tide-forming dinoflagellate *Karenia brevis* (formerly called *Gymnodinium breve*) were also successfully detected via chlorophyll with the CZCS, at cell densities (10^4 –10^5 cells/l) 1 or 2 orders of magnitude less than that detectable by the human eye (>10^6 cells/l) (Tester and Steidinger, 1997).

Alternatively, satellite SST images have been used to describe HAB dynamics on the basis of the distribution of water masses and hydrographic features such as upwellings, fronts and eddies. Accumulations of *Karenia brevis* off the west coast of Florida, for example, have been shown to be closely coupled to the intrusions of the Loop Current onto the Florida shelf (Tester and Steidinger, 1997). SST images can be used for detecting water masses of different temperature (Johannessen et al., 1989; Kahru, 1997), where temperature may be correlated with the presence of HABs. Such is the case in Galicia where SST images are used to predict the shoreward advection of the dinoflagellate *Gymnodinium catenatum*, which causes significant damage in mari-culture (Fraga et al., 1988). In Norway, remotely sensed SST have been used to follow

the movement of fronts and other physical features where HAB species accumulate (Pettersson et al., 2000*c*). In this way, satellite SST images can be used as an early warning system on the basis of statistical correlations established between the presence of physical oceanographic features and HAB events.

Most reported observations concern high-biomass blooms recorded at the surface of coastal waters, presumably owing to the impact on human activities there. Very few examples of detection of HAB by satellites have been reported for offshore waters or open sea. HABs also occur in rivers and lakes (Paerl et al., 2001). For such regions the spatial resolution of satellite sensors has historically been a severe limitation. Applications are reported though for airborne sensors (Dekker and Donze, 1994; Hunter et al., 2004; Jupp et al., 1994; Sathyendranath et al., 1997; Richardson and Kruse, 1999) and new and future satellite sensors with higher spatial resolution (e.g. the 300 m of MERIS and the 250 m of MODIS) that may open new perspectives.

Until now, remote sensing has been used mostly in conjunction with *in situ* data of phytoplankton cell density and species, eco-physiological studies of HAB, ecological modelling or optical in-water observations (Cullen et al., 1997). Taken together, these tools constitute a complementary approach essential to a thorough understanding of HAB dynamics (Schofield et al., 1999). Models can predict several other parameters which are necessary for the understanding of spreading and decay of blooms (Pettersson et al., 2000*c*).

9.6 Conclusions: place of ocean colour in systems for the detection and monitoring of ecosystem dynamics and HABs

9.6.1 Possibilities and limitations

This chapter has reviewed the theoretical basis for detection of ABs or 'potential HABs' by ocean colour. An analysis of past and present applications shows two main uses of ocean colour:

- High-biomass surface blooms can be detected directly and mapped in space and time via chlorophyll *a* concentration provided ocean-colour sensors and algorithms are sufficient to overcome problems of atmospheric correction and chlorophyll retrieval in coastal waters. In some cases of high-reflectance blooms, spatial mapping of bloom extent can be achieved even without atmospheric correction or chlorophyll retrieval algorithms (Kahru, 1997). Ocean-colour imagery is an element of near real-time HAB warning systems that are starting to emerge in regions where economic resources are threatened.
- Less directly, ocean colour and thermal infrared imagery are used to map water masses, which may be correlated in some way with the presence of HABs and, therefore, indicate the spatial extent of HAB processes.

In both cases, ocean colour is not used independently but in conjunction with expert knowledge of the region, *in situ* monitoring techniques and sometimes with numerical models (McGillicuddy et al., 2007 – Chapter 16 this volume).

The following limitations of the ocean-colour technique are noted:

- Cloudy conditions prevent satellite ocean-colour remote sensing and for some regions are sufficient to eliminate the technique. Low-altitude airborne ocean-colour remote sensing may provide an alternative for the small regions typically

of interest in a HAB perspective. However, cloudiness is the main unavoidable limitation of the ocean-colour technique in the long term.

- In coastal waters imperfect atmospheric correction and the difficulty of distinguishing between phytoplankton and non-phytoplankton optical properties can seriously degrade chlorophyll products. Such degradation is not always obvious to the user of ocean-colour images and can lead to misinterpretation of the HAB situation. The need for *in situ* measurements to check ocean-colour data quality in all cases is clear. Careful study of papers on the subject shows that the analysis of HAB extent and dynamics based on ocean-colour imagery often relies on asynchronous, circumstantial or anecdotal evidence of HABs and is thus of dubious quality.
- The ocean-colour technique is essentially limited to surface blooms of sufficiently high biomass to make a discernible difference to surface reflectance. For HAB species which are toxic at low concentrations and which occur at the same time as other non-HAB species with higher concentration the ocean-colour technique will be of little use. In general the ocean-colour technique is powerful for AB detection but the question of whether the AB is a HAB typically requires supplementary information, for example, from a limited number of seaborne measurements or expert knowledge of the region.

9.6.2 Challenges and opportunities

What developments can be expected over the next 10 years? Judging from the pace of ocean-colour progress over the last 10 years, the easy answer is that changes will be enormous. In 1993, there were no satellite ocean-colour sensors, the internet was only just beginning to develop, and ocean colour was a topic restricted mainly to North American and European research institutes. In 2003 there were seven well-supported ocean-colour sensors and many smaller, regional or experimental missions. Thanks to advances in computer technology and helped by the SeaWiFS and SeaDAS projects ocean-colour data are now being analysed, by researchers, throughout the world, with considerable activity in Asia. Dissemination of information has been revolutionized by the use of e-mail and the internet and the distribution of HAB bulletins to a wide public is now rapid and cheap. In the light of these radical changes it is clearly hazardous to predict future developments. However, the following factors are likely to influence progress:

- Economic pressures on space agencies to show a return for public investment will shape the availability and price of ocean-colour data. The effect of such pressures is highly unpredictable and subject to national and international policy decisions. Will the price of data from the (pre-)operational ocean-colour sensors be low to encourage greater use and economy of scale, or high to reflect the cost of acquisition? Will single-country ocean-colour missions continue to proliferate in response to specific needs or to ensure political independence, or will the number of ocean-colour sensors be reduced to a few well-supported international missions with a long-term plan to ensure continuity? Will large multi-sensor missions be replaced by smaller, cheaper, dedicated ocean-colour missions? None of these questions has obvious answers though it is clear that ocean colour is now here to stay.
- The needs of users will also shape developments. The continued development of coastal aquaculture and fisheries to respond to food needs, particularly in developing countries, is likely to expand the interest in HAB detection systems.

- As far as technology is concerned the improvement of sensors, especially by enhancing spectral resolution and signal-to-noise ratio, will undoubtedly continue. It is clear that the future for optical remote sensing of coastal waters is hyperspectral and that atmospheric correction and chlorophyll retrieval will be improved by the use of extra spectral information.
- The improved spectral resolution and sensitivity of sensors may also facilitate efforts to go beyond chlorophyll detection to the identification of phytoplankton species, possibly by considering photoacclimation or other pigment-specific processes. However, the application of species-specific algorithms based on absorption or scattering properties to atmospherically corrected ocean-colour data is likely to be much more of a problem than the use of such algorithms with absorption spectra input.
- The improved imaging frequency of future geostationary and UAV platforms will be useful for operational HAB detection applications.
- Chlorophyll-retrieval algorithms for coastal waters will continue to improve especially for the multiband algorithms which can exploit more fully multispectral or hyperspectral data. The further development of image quality indicators (e.g. the MERIS level 2 product flags) should reduce the possible misinterpretation of data by users, increasing reliability and user confidence.

References

Aarup, T., Groom, S. and Holligan, P. M. 1990. The processing and interpretation of North Sea CZCS imagery. *Neth. J. Sea Res.*, 25, pp. 3–9.

Ackleson, S. G. 2003. Light in shallow waters: a brief research review. *Limnol. Oceanogr.*, 48, pp. 323–28.

Antoine, D. and Morel, A. 1998. Relative importance of multiple scattering by air molecules and aerosols in forming the atmospheric path radiance in the visible and near infrared parts of the spectrum. *Appl. Opt.*, 37, pp. 2245–59.

Antoine, D. and Morel, A. 1999. A multiple scattering algorithm for atmospheric correction of remotely sensed ocean colour (MERIS instrument): principle and implementation for atmospheres carrying various aerosols including absorbing ones. *Int. J. Rem. Sens.*, 20, pp. 1875–916.

Arnone, R. A., Martinolich, P., Gould, R. W., Stumpf, R. and Ladner, S. 1998. Coastal optical properties using SeaWiFS. *Ocean Optics XIV*, *Proc. SPIE*, 1, pp. 1–14.

Babin, M. 2007. Phytoplankton fluorescence: theory, current literature and *in situ* measurement. In: Babin et al. (eds), op. cit., this volume.

Babin, M., Morel, A., Fournier-Sicre, V., Fell, F. and Stramski, D. 2003*a*. Light scattering properties of marine particles in coastal and open ocean waters as related to the particle mass concentration. *Limnol. Oceanogr.*, 28, pp. 843–59.

Babin, M., Morel, A. and Gentilli, B. 1996. Remote sensing of sea surface sun-induced chlorophyll fluorescence: consequences of natural variations in the optical characteristics of phytoplankton and the quantum yield of chlorophyll *a* fluorescence. *Int. J. Rem. Sens.*, 17, pp. 2417–48.

Babin, M., Roesler, C. S. and Cullen, J. J. (eds). 2007. *Real-time Coastal Observing Systems for Marine Ecosystem Dynamics and Harmful Algal Blooms: Theory, Instrumentation and Modelling*. Paris, Intergovernmental Oceanographic Commission of UNESCO. (Monographs on Oceanographic Methodology.)

Babin, M., Stramski, D., Ferrari, G. M., Claustre, H., Bricaud, A., Obolensky, G. and Hoepffner, N. 2003*b*. Variations in the light absorption coefficients of phytoplankton,

nonalgal particles and dissolved organic matter in coastal waters around Europe. *J. Geophys. Res.*, 108, 3211, doi:3210.1029/2001JC000882.

Bidigare, R. R., Morrow, J. H. and Kiefer, D. A. 1989. Derivative analysis of spectral absorption by photosynthetic pigments in the western Sargasso Sea. *J. Mar. Res.*, 47, pp. 323–41.

Bricaud, A. and Morel, A. 1987. Atmospheric corrections and interpretation of marine radiances in CZCS imagery: use of a reflectance model. *Oceanolog. Acta*, pp. 33–50.

Bricaud, A., Morel, A., Babin, M., Allali, K. and Claustre, H. 1998. Variations of light absorption by suspended particles with chlorophyll *a* concentration in oceanic (Case 1) waters: analysis and implications for bio-optical models. *J. Geophys. Res.*, 103, pp. 31033–44.

Buiteveld, H., Hakvoort, J. M. H. and Donze, M. 1994. The optical properties of pure water. *Ocean Optics XII*, *Proc. SPIE*, 2258, pp. 174–83.

Burenkov, V. I., Vasilkov, A. P. and Stephantsev, L. A. 1985. Retrieval of spectral inherent optical properties of seawater from the spectral reflectance. *Oceanology*, 25, pp. 49–54.

Carder, K. L. and Steward, R. G. 1985. A remote-sensing reflectance model of a red-tide dinoflagellate off west Florida. *Limnol. Oceanogr.*, 30, pp. 286–98.

Chami, M., Robilliard, D. and Fonlupt, C. 2002. Inversion of oceanic constituents in Case I and II waters with genetic programming algorithms. *Appl. Opt.*, 41, pp. 6260–75.

Chang, G. C. and Dickey, T. D. 2007. Interdisciplinary sampling strategies for detection and characterization of harmful algal blooms. In: Babin et al. (eds), op. cit., this volume.

Clarke, G. K., Ewing, G. C. and Lorenzen, C. J. 1970. Spectra of backscattered light from the sea obtained from aircraft as a measure of chlorophyll concentration. *Science*, 167, pp. 1119–21.

Clement, A., Seguel, M., Arzul, G., Guzman, L. and Alarcon, C. 2000. Widespread outbreak of a haemolytic, ichthyotoxic *Gymnodinium* sp. in Southern Chile. In: G. M. Hallegraeff, S. I. Blackburn, C. J. Bolch and R. J. Lewis (eds), *Harmful Algal Blooms*. Paris, Intergovernmental Oceanographic Commission of UNESCO.

Cox, C. and Munk, W. 1954. Measurements of the roughness of the sea surface from photographs of the sun's glitter. *J. Opt. Soc. Am.*, 44, pp. 834–50.

Cullen, J. J. 2007. Observation and prediction of harmful algal blooms. In: Babin et al. (eds), op. cit., this volume.

Cullen, J. J., Ciotti, A. M., Davis, R. F. and Lewis, M. R. 1997. Optical detection and assessment of algal blooms. *Limnol. Oceanogr.*, 42, pp. 1223–39.

De Cauwer, V., Ruddick, K., Park, Y., Nechad, B. and Kyramarios, M. 2004. Optical remote sensing in support of eutrophication monitoring in the Southern North Sea. European Association of Remote Sensing Laboratories, *EARSeL e-Proc. 3*, pp. 208–21.

Dekker, A. G. 1993. Detection of water quality parameters for eutrophic waters by high resolution remote sensing. Ph.D. thesis, Vrije Universiteit Amsterdam.

Dekker, A. G. and Donze, M. 1994. Imaging spectrometry as a research tool for inland water resources analysis. In: J. Hill and J. Mégier (eds), *Imaging Spectrometry – a Tool for Environmental Observations*. Dordrecht, Netherlands, Kluwer Academic Publishers, pp. 295–317. (ECSC-EEC-EAEC.)

Doerffer, R. 2002. *Protocols for the Validation of MERIS Water Products*. Geesthacht, Germany, GKSS Forschungszentrum Geesthacht/MERIS-ESL.

Doerffer, R. and Fischer, J. 1994. Concentrations of chlorophyll, suspended matter, gelbstoff in case II waters derived from satellite coastal zone color scanner data with inverse modeling methods. *J. Geophys. Res.*, 99, pp. 7457–66.

Doerffer, R. and Schiller, H. 1997. *Pigment Index, Sediment and Gelbstoff Retrieval from Directional Water Leaving Radiance Reflectance Using Inverse Modelling Technique*. Geesthacht, Germany, GKSS Forschungszentrum Geesthacht, p. 83.

Fargion, G. S. and Mueller, J. L. (eds). 2000. *Ocean Optics Protocols for Satellite Ocean Color Sensor Validation, Revision 2*. Washington DC, National Aeronautical and Space Administration NASA report TM-2000-209966, p. 184.

Fraga, S., Anderson, D. M., Bravo, I., Reguera, B., Steindinger, K. A. and Yentsch, C. M. 1988. Influence of upwelling relaxation on dinoflagellates and shellfish toxicity in Ria de Vigo, Spain. *Estuar. Coast. Shelf Sci.*, 27, pp. 349–61.

Franks, P. J. S. 2007. Physics and physical modelling of harmful algal blooms. In: Babin et al. (eds), op. cit., this volume.

Frouin, R., Schwindling, M. and Deschamps, P. Y. 1996. Spectral reflectance of sea foam in the visible and near-infrared: *In situ* measurements and remote sensing implications. *J. Geophys. Res.*, 101, pp. 14361–71.

Geohab. 2001. *Global Ecology and Oceanography of Harmful Algal Blooms, Science Plan*. Baltimore/Paris, Scientific Committee on Oceanic Research/Intergovernmental Oceanographic Commission of UNESCO, p. 87.

Gons, H. J. 1999. Optical teledetection of chlorophyll *a* in turbid inland waters. *Environ. Sci. Tech.*, 33, pp. 1127–33.

Gons, H. J., Hakvoort, H., Peters, S. W. M. and Simis, S. G. H. 2005. Optical detection of cyanobacterial blooms. In: J. Huisman, H. C. P. Matthijs and P. M. Visser (eds), *Harmful Cyanobacteria*. Berlin, Springer-Verlag, pp. 177–99.

Gordon, H. R., Brown, J. W. and Evans, R. H. 1988*a*. Exact Rayleigh scattering calculations for use with the Nimbus-7 Coastal Zone Color Scanner. *Appl. Opt.*, 27, pp. 862–71.

Gordon, H. R., Brown, O. B., Evans, R. H. Brown, J. W., Smith, R. C., Baker, K. S. and Clark, D. K. 1988*b*. A semianalytical radiance model of ocean color. *J. Geophys. Res.*, 93, pp. 10909–24.

Gordon, H. R., Brown, O. B. and Jacobs, M. M. 1975. Computed relationships between inherent and apparent optical properties of a flat, homogeneous ocean. *Appl. Opt.*, 14, pp. 417–27.

Gordon, H. R., Clark, D. K., Brown, J. W., Brown, O. B., Evans, R. H. and Broenkow, W. W. 1983. Phytoplankton pigment concentrations in the Middle Atlantic Bight: comparison of ship determinations and CZCS estimates. *Appl. Opt.*, 22, pp. 20–36.

Gordon, H. R. and Morel, A. Y. 1983. *Remote Assessment of Ocean Color for Interpretation of Satellite Visible Imagery. A Review.* New York, Springer-Verlag.

Gordon, H. R. and Voss, K. J. 1999. MODIS Normalized Water-leaving Radiance Algorithm Theoretical Basis Version 4.

Gordon, H. R. and Wang, M. 1992. Surface roughness considerations for atmospheric correction of ocean colour sensors. I: The Rayleigh-scattering component. *Appl. Opt.*, 31, pp. 4247–60.

Gordon, H. R. and Wang, M. 1994*a*. Influence of oceanic whitecaps on atmospheric correction of ocean-color sensors. *Appl. Opt.*, 33, pp. 7754–63.

Gordon, H. R. and Wang, M. 1994*b*. Retrieval of water-leaving radiance and aerosol optical thickness over the oceans with SeaWiFS: a preliminary algorithm. *Appl. Opt.*, 33, pp. 443–52.

Gould, R. W. and Arnone, R. A. 1994. Extending Coastal Zone Color Scanner estimates of the diffuse attenuation coefficient into Case II waters. *Ocean Optics XII*, *Proc. SPIE*, 2258, pp. 704–10.

Gower, J. F. R., Doerffer, R. and Borstad, G. A. 1999. Interpretation of the 685 nm peak in water-leaving radiance spectra in terms of fluorescence, absorption and scattering, and its observation by MERIS. *Int. J. Rem. Sens.*, 20, pp. 1771–86.

Graneli, E., Codd, G. A., Dale, B., Lipiatou, E., Maestrini, S. Y. and Rosenthal, H. 1998. *EUROHAB Science Initiative: Harmful Algal Blooms in European Marine and Brackish Waters*. Brussels, European Communities, p. 93.

Guan, F. M., Pelaez, J. and Stewart, R. H. 1985. The atmospheric correction and measurement of chlorophyll concentration using the Coastal Zone Color Scanner. *Limnol. Oceanogr.*, 30, pp. 273–85.

Hallegraeff, G. M. 1993. A review of harmful algal blooms and their apparent global increase. *Phycologia*, 32, pp. 79–99.

Haltrin, V. I. and Kattawar, G. 1993. Self-consistent solutions to the equation of transfer with elastic and inelastic scattering in oceanic optics. 1: Model. *Appl. Opt.*, 32, pp. 5356–67.

Hansen, J. E. and Travis, L. D. 1974. Light scattering in planetary atmospheres. *Space Sci. Rev.*, 16, pp. 527–610.

Hoepffner, N. and Sathyendranath, S. 1991. Effect of pigment composition on absorption properties of phytoplankton. *Mar. Ecol. Progr. Ser.*, 73, pp. 11–23.

Hoge, F. E. and Lyon P. E. 1996. Satellite retrieval of inherent optical properties by linear matrix inversion of oceanic radiance models: an analysis of model and radiance measurement errors. *J. Geophys. Res.*, 101, pp. 16631–48.

Hoge, F. E. and Swift, R. N. 1981. Airborne simultaneous spectroscopic detection of laser-induced water Raman backscatter and fluorescence from chlorophyll *a* and other naturally occuring pigments. *Appl. Opt.*, 20, pp. 3197–205.

Hoge, F. E., Vodacek, A. and Blough, N. V. 1993. Inherent optical properties of the ocean: retrieval of the absorption coefficient of chromophoric dissolved organic matter from fluorescence measurements. *Limnol. Oceanogr.*, 38, pp. 1394–402.

Holligan, P. M., Aarup, T. and Groom, S. B. 1989. The North Sea satellite colour atlas. *Cont. Shelf Res.*, 9, pp. 665–765.

Hoogenboom, H. J., Dekker, A. G. and Althuis, I. J. A. 1998*a*. Simulation of AVIRIS sensitivity for detecting chlorophyll over coastal and inland waters. *Rem. Sens. Environ.*, XX, pp. 333–40.

Hoogenboom, H. J., Dekker, A. G. and Haan, J. F. D. 1998*b*. Retrieval of chlorophyll and suspended matter from imaging spectrometry data by matrix inversion. *Can. J. Rem. Sens.*, 24, pp. 144–52.

Hooker, S. B., Mcclain, C. R. and Holmes, A. 1993. Ocean Color Imaging: CZCS to SeaWiFS. *Mar. Tech. Soc.*, 27, pp. 3–15.

Hu, C., Carder, K. L. and Muller-Karger, F. 2000. Atmospheric correction of SeaWiFS imagery over turbid coastal waters: a practical method. *Rem. Sens. Environ.*, 74, pp. 195–206.

Hunter, P. D., Tyler, A. N., Willby, N. J., Gilvear, D. J., Preston, T., Présing, M., Toth, V. and Green, M. 2004. Monitoring eutrophic shallow lake environments through airborne remote sensing and *in situ* spectroradiometery: the Norfolk Broads, UK, and Lake Balaton, Hungary. *Proc. Airborne Research & Survey Facility Biannual Workshop*.

Hwang, P. A. and Shemdin, O. H. 1988. The dependence of sea surface slope on atmospheric stability and swell conditions. *J. Geophys. Res.*, 93, pp. 13903–12.

IOCCG. 1998. Minimum requirements for an operational, ocean colour sensor for the open ocean. Dartmouth, Nova Scotia, International Ocean-Colour Coordinating Group/Scientific Committee on Oceanic Research, 1, p. 50.

IOCCG. 1999. Status and plans for satellite ocean colour missions: considerations for complementary missions. Dartmouth, Nova Scotia, International Ocean-Colour Coordinating Group/Scientific Committee on Oceanic Research, 2, p. 43.

Jeffrey, S. W. 1997. Application of pigment methods to oceanography, In: Jeffrey et al., op. cit., pp. 127–66.

Jeffrey, S. W., Mantoura, R. F. C. and Wright, S. W. (eds). 1997. *Phytoplankton Pigments in Oceanography*. Paris, Intergovernmental Oceanographic Commission of UNESCO, pp. 127–66. (Monographs on Oceanographic Methodology 10.)

Jeffrey, S. W. and Vesk, M. 1997. Introduction to marine phytoplankton and their pigment signatures. In: Jeffrey et al., op. cit., pp. 37–84.

Johannessen, J. A., Johannessen, O. M. and Haugan, P. 1989. Remote sensing and model simulation study in the Norwegian coastal current during the algal bloom in May 1988. *Int. J. Rem. Sens.*, 10, pp. 1893–906.

Johnsen, G., Samset, O., Granskog, L. and Sakshaug, E. 1994. *In vivo* absorption characteristics in 10 classes of bloom-forming phytoplankton: taxonomic characteristics and responses to photoadaptation by means of discriminant and HPLC analysis. *Mar. Ecol. Progr. Ser.*, 105, pp. 149–57.

Jupp, D. L. B., Kirk, J. T. O. and Harris, G. P. 1994. Detection, identification and mapping of cyanobacteria – using remote sensing to measure the optical quality of turbid water. *Aust. J. Mar. Freshwat. Res.*, 45, pp. 801–28.

Kahru, M. 1997. Using satellites to monitor large-scale environmental change: a case study of cyanobacteria blooms in the Baltic Sea. In: M. Kahru and C. W. Brown (eds), *Monitoring*

Algal Blooms: New Techniques for Detecting Large-Scale Environmental Change. New York, Springer-Verlag, pp. 43–61.

Kahru, M., Horstmann, U. and Rud, O. 1993. Cyanobacterial blooms cause heating of the sea surface. *Mar. Ecol. Progr. Ser.*, 101, pp. 1–7.

Kahru, M., Hortsmann, U. and Rud, O. 1994. Satellite detection of increased cyanobacteria blooms in the Baltic Sea: Natural fluctuation or ecosystem change? *Ambio*, 23, pp. 469–72.

Kahru, M., Leppänen, J. M., Rud, O. and Savchuk, O. P. 2000. Cyanobacteria blooms in the Gulf of Finland triggered by saltwater inflow into the Baltic Sea. *Mar. Ecol. Progr. Ser.*, 207, pp. 13–18.

Kahru, M. and Mitchell, B. G. 1998. Spectral reflectance and absorption of a massive red tide off southern California. *J. Geophys. Res.*, 103, pp. 21601–09.

Kallee, C. U. 2002. Living with harmful algal blooms: HAB management for acquaculture farms. Master's thesis, University of Oldenburg, Germany.

Kirk, J. T. O. 1981. Monte Carlo study of the underwater light field in, and relationships between optical properties of, turbid yellow waters. *Aust. J. Freshwat. Res.*, 32, pp. 517–32.

Kirkpatrick, G. J., Millie, D. F., Moline, M. A. and Schofield, O. 2000. Optical discrimination of a phytoplankton species in natural mixed populations. *Limnol. Oceanogr.*, 45, pp. 467–71.

Kneizs, F. X., Shettle, E. P., Gallery, W. O., Chetwynd, J. H. A. L. W., Selby, J. E. A., Clough, S. A. and Fenn, R. W. 1983. *Atmospheric Transmittance/Radiance: Computer Code LOWTRAN 6.* Hanscom AFB, Mass., US Air Force Geophysics Laboratory.

Koepke, P. 1984. Effective reflectance of whitecaps. *Appl. Opt.*, 23, pp. 1816–24.

Land, P. E. and Haigh, J. D. 1996. Atmospheric correction over Case 2 waters with an iterative fitting algorithm. *Appl. Opt.*, 35, pp. 5443–5451.

Liew, S. C., Lin, I. I., Kwoh, L. K., Holmes, M., Teo, S., Gin, K. and Lim, H. 1999. Spectral reflectance signatures of case II waters: potential for tropical algal bloom monitoring using satellite ocean colour sensors. *Proc. 10th JSPC/VCC Joint Seminar on Marine and Fisheries Sciences.*

Liu, Y., Yan, W. T. L. X. H. and Hwang, P. A. 1997. The probability density function of the ocean surface slopes and its effects on radar backscatter. *J. Phys. Oceanogr.*, 27, pp. 782–97.

McClain, C. R., Esaias, W. E., Barnes, W., Guenther, B., Endres, D., Hooker, S., Mithcell, G. and Barnes, R. 1992. SeaWiFS Calibration and Validation Plan. Volume 3 NASA technical memorandum 104566. NASA Goddard Space Flight Center, p. 41.

McGillicuddy, D. J. Jr, Anderson, D. M., Stock, C. A., Lynch, D. R. and Townsend, D. W. 2007. Modelling blooms of *Alexandrium fundyense* in the Gulf of Maine. In: Babin et al. (eds), op. cit., this volume..

Meris Team. 2000. *MERIS Level 2 Algorithms Theoretical Basis Document.* Report PO-TN-MEL-GS-0005, MERIS Expert Support Laboratories.

Millie, D., Kirkpatrick, G. J. and Vinyard, B. T. 1995. Relating photosynthetic pigments and *in vivo* optical density spectra to irradiance for the Florida red-tide dinoflagellate *Gymnodinium breve*. *Limnol. Oceanogr.*, 42, pp. 1223–39.

Millie, D. F., Scofield, O. M., Kirkpatrick, G. J., Johnson, G., Tester, P. A. and Vinyard, B. T. 1997. Detection of harmful algal blooms using photopigments and absorption signatures. A case study of the Florida red tie dinoflagellate, *Gymnodinium breve*. *Limnol. Oceanogr.*, 42, pp. 1223–39.

Mittenzwey, K. H., Gitelson, A. A., Ullrich, S. and Kondratiev, K. Y. 1992. Determination of chlorophyll *a* of inland waters on the basis of spectral reflectance. *Limnol. Oceanogr.*, 37, pp. 147–49.

Mobley, C. D. 1994. *Light and Water: Radiative Transfer in Natural Waters*. New York, Academic Press.

Mobley, C. D. 1999. Estimation of the remote-sensing reflectance from above-surface measurements. *Appl. Opt.*, 38, pp. 7442–55.

Monahan, E. C. and O'Muircheartaigh, I. G. 1986. Whitecaps and the passive remote sensing of the ocean surface. *Int. J. Rem. Sens.*, 7, pp. 627–42.

Moore, G. F., Aiken, J. and Lavender, S. J. 1999. The atmospheric correction of water colour and the quantitative retrieval of suspended particulate matter in Case II waters: application to MERIS. *Int. J. Rem. Sens.*, 20, pp. 1713–34.

Moore, K. D., Voss, K. J. and Gordon, H. R. 2000. Spectral reflectance of whitecaps: their contribution to water-leaving radiance. *J. Geophys. Res.*, 105, pp. 6493–99.

Morel, A. 1974. Optical properties of pure water and sea water. In: N. G. Jerlov and E. Steeman-Nielsen (eds), *Optical Aspects of Oceanography*. New York, Academic Press. pp. 1–24.

Morel, A. 2007. Introduction to optical properties in the sea: theoretical aspects. In: Babin et al. (eds), op. cit., this volume.

Morel, A. and Antoine, D. 2000. MERIS Algorithm Theoretical Basis Document 2.9: Pigment index retrieval in Case 1 waters. Villefranche sur Mer, France, Laboratoire de Physique et Chimie Marines, p. 26.

Morel, A. and Gentili, B. 1991. Diffuse reflectance of oceanic waters: its dependence on sun angle as influenced by the molecular scattering contribution. *Appl. Opt.*, 30, pp. 4427–38.

Morel, A. and Gentili, B. 1996. Diffuse reflectance of oceanic waters. III: Implications of bidirectionality for the remote sensing problem. *Appl. Opt.*, 35, pp. 4850–62.

Morel, A. and Maritorena, S. 2001. Bio-optical properties of oceanic waters: a reappraisal. *J. Geophys. Res.*, 106, pp. 7163–80.

Morel, A. and Prieur, L. 1977. Analysis of variations in ocean color. *Limnol. Oceanogr.*, 22, pp. 709–22.

Mueller, J. L. 1984. Effects of water reflectance at 670 nm on Coastal Zone Color Scanner (CZCS) aerosol radiance estimates off the coast of central California. *Ocean Optics VII*, *Proc. SPIE*, XX, pp. 179–86.

Mueller, J. L., Davis, C., Arnone, R., Frouin, R., Carder, K., Lee, Z. P., Steward, R. G., Hooker, S., Mobley, C. D. and Mclean, S. 2000. Above-water radiance and remote sensing reflectance measurements and analysis protocols. In: *Ocean Optics Protocols for Satellite Ocean Color Sensor Validation Revision 2.* Washington DC, National Aeronautical and Space Administration, pp. 98–107.

Nakajima, T. and Tanaka, M. 1983. Effect of wind-generated waves on the transfer of solar radiation in the atmosphere-ocean system. *J. Quant. Spectros. Radiat. Trans.*, 29, pp. 521–37.

Neumann, A., Krawczyk, H. and Walzel, T. 1995. A complex approach to quantitative interpretation of spectral high resolution imagery. *Proc. Third Thematic Conference on Remote Sensing for Marine and Coastal Environments*. Ann Arbor, Mich., Environmental Research Institute of Michigan, pp. 641–52.

O'Reilly, J. E., Maritorena, S., Mitchell, B. G., Siegel, D. A., Carder, K. L., Garver, S. A., Kahru, M. and McClain, C. 1998. Ocean color chlorophyll algorithms for SeaWiFS. *J. Geophys. Res.*, 103, pp. 24937–53.

Öström, B. 1976. Fertilization of the Baltic by nitrogen fixation in the blue-green alga *Nodularia spumigena*. *Rem. Sens. Environ.*, 4, pp. 305–10.

Paerl, H. W., Fulton, R. S., Moisander, P. H. and Dyble, J. 2001. Harmful freshwater algal blooms, with an emphasis on cyanobacteria. *Sci. World*, 1, pp. 76–113.

Peterson, D. L., Brass, J. A., Smith, W. H., Langford, G., Wegener, S., Dunagan, S., Hammer, P. and Snook, K. 2003. Platform options of free-flying satellites UAVs or the International Space Station for remote sensing assessment of the littoral zone. *Int. J. Rem. Sens.*, 24, pp. 2785–804.

Pettersson, L. H., Durand, D., Groom, S., Lavender, S., Svendsen, E., Noji, T. and Søiland, H. 2000*a*. DeciDe for near-real-time use of ocean color data in management of toxic algae blooms. University of Bergen, Norway, Nansen Environmental and Remote Sensing Center, p. 19. (Analysis Document.)

Pettersson, L. H., Durand, D., Johannessen, O. M., Svendsen, E., Soiland, H. and Regner, P. 2000*b*. Satellite observations and model predictions of toxic algae bloom in coastal waters. *Proc. 28th International Symposium on Remote Sensing of the Environment*, p. 4.

Pettersson, L. H., Durand, D. D., Svendsen, E., Noji, T., Søiland, H., Groom, S. and Lavender, S. 2000*c*. DeciDe for near-real-time use of ocean color data in management

of toxic algae blooms. University of Bergen, Norway, Nansen Environmental and Remote Sensing Center, p. 30. (Specification, Definition and Design Document.)

Philpot, W. D. 1987. Radiative transfer in stratified waters: a single-scattering approximation for irradiance. *Appl. Opt.*, 26, pp. 4123–32.

Pitcher, G. C., Bernard, S. and Fawcett, A. 2007. Real-time coastal observing systems for ecosystem dynamics and harmful algal blooms: needs and expectations of users. In: Babin et al. (eds), op. cit., this volume.

Preisendorfer, R. W. 1961. Application of radiative transfer theory to light measurements in the sea. In: *Radiant Energy in the Sea*. Boulder, Colo., International Union of Geodesy and Geophysics, pp. 11–30. (IUGG Monograph 10.)

Rantajärvi, E. 2003. *Alg@line in 2003: 10 Years of Innovative Plankton Monitoring and Research – an Operational Information Service in the Baltic Sea*. Helsinki, Finnish Institute of Marine Research, p. 55.

Reinersman, P. N. and Carder, K. L. 1995. Monte Carlo simulation of the atmospheric point-spread function with an application to correction for the adjacency effect. *Appl. Opt.*, 34, pp. 4453–71.

Richardson, L. L. and Kruse, F. A. 1999. Identification and classification of mixed phytoplankton assemblages using AVIRIS image-derived spectra. *AVIRIS Proc. 1999*. Pasadena, Calif., California Institute of Technlogy, Jet Propulsion Laboratory, pp. 99–17.

Roesler, C. S. and Boss, E. 2007. *In situ* measurement of inherent optical properties and potential for harmful algal bloom detection and coastal ecosystem observations. In: Babin et al. (eds), op. cit., this volume.

Roesler, C. S., Perry, M. J. and Carder, K. L. 1989. Modeling *in situ* phytoplankton absorption from total absorption spectra in productive inland marine waters. *Limnol. Oceanogr.*, 34, pp. 1510–23.

Rothman, L. S., Rinsland, C. P., Goldman, A., Massie, S. T., Edward, D. P., Flaud, J. M. Perrin, A., Camy-Peyret, C., Dana, V., Mandin, J. Y., Schroeder, J., McCann, A., Gamache, R. R., Wattson, R. B., Yoshino, K., Chance, K. V., Jucks, K. W., Brown, L. R., Nemtchinov, V. and Varanasi, P. 1998. The HITRAN molecular spectroscopic database and HAWKS (HITRAN atmospheric workstation): 1996 edition. *J. Quant. Spectrosc. Radiat. Trans.*, 60, pp. 665–710.

Rousseau, V., Mathot, S. and Lancelot, C. 1990. Calculating carbon biomass of *Phaeocystis* sp. from microscopic observations. *Mar. Biol.*, 107, pp. 305–14.

Ruddick, K. G., Gons, H. J., Rijkeboer, M. and Tilstone, G. 2001. Optical remote sensing of chlorophyll *a* in Case 2 waters using an adaptive two-band algorithm with optimal error properties. *Appl. Opt.*, 40, pp. 3575–85.

Ruddick, K. G., Ovidio, F. and Rijkeboer, M. 2000. Atmospheric correction of SeaWiFS imagery for turbid coastal and inland waters. *Appl. Opt.*, 39, pp. 897–912.

Sathyendranath, S., Prieur, L. and Morel, A. 1989. A three-component model of ocean colour and its application to remote sensing of phytoplankton pigments in coastal waters. *Int. J. Rem. Sens.*, 10, pp. 1373–94.

Sathyendranath, S., Subba Rao, D. V., Chen, Z., Stuart, V., Platt, T., Budgen, G. L., Jones, W. and Vass, P. 1997. Aircraft remote sensing of toxic phytoplankton blooms: a case study from Cardigan River, Prince Edward Island. *Can. J. Rem. Sens.*, 23, pp. 15–23.

Schiller, H. and Doerffer, R. 1999. Neural network for emulation of an inverse model operational derivation of Case II water properties from MERIS data. *Int. J. Rem. Sens.*, 20, pp. 1735–46.

Schofield, O., Bosch, J., Glenn, S., Kirkpatrick, G., Kerfoot, J., Lohrenz, S., Moline, M., Oliver, M. and Bissett, P. 2007. Bio-optics in integrated ocean observing networks: potential for studying harmful algal blooms. In: Babin et al. (eds), op. cit., this volume.

Schofield, O. J., Gryzmski, J., Bissett, W. P., Kirkpatrick, G., Millie, D. M., Moline, M. A. and Roesler, C. 1999. Optical monitoring and forecasting systems for harmful algal blooms: possibility or pipedream? *J. Phycol.*, 35, pp. 1477–96.

Siegel, D. A., Wang, M., Maritorena, S. and Robinson, W. 2000. Atmospheric correction of satellite ocean color imagery: the black pixel assumption. *Appl. Opt.*, 39, pp. 3582–91.

Simis, S. G. H., Peters, S. W. M. and Gons, H. J. 2005. Remote sensing of the cyanobacterial pigment phycocyanin in turbid inland water. *Limnol. Oceangr.*, 50, pp. 237–45.

Smith, R. C. and Wilson W. H. 1981. Ship and satellite bio-optical research in the California Bight. In: J. F. R. Gower (ed.), *Oceanography from Space*. New York, Plenum Press, pp. 281–94.

Sosik, H. M. 2007. Characterizing seawater constituents from optical properties. In: Babin et al. (eds), op. cit., this volume.

Stuart, V., Sathyendranath, S., Platt, T., Maass, H. and Irwin, B. 1998. Pigments and species composition of natural phytoplankton populations: effect on the absorption spectra. *J. Plankton Res.*, 20, pp. 187–217.

Stumpf, R. P. 2001. Applications of satellite ocean color sensors for monitoring and predicting harmful algal blooms. *Hum. Ecol. Risk Assess.*, 7, pp. 1363–68.

Stumpf, R. P. and Culver, M. A. 2002. Forecasting of harmful algal blooms in the Gulf of Mexico. *Proc. 7th International Conference on Remote Sensing for Marine and Coastal Environments*, p. 4.

Stumpf, R. P. and Pennock, J. R. 1989. Calibration of a general optical equation for remote sensing of suspended sediments in a moderately turbid estuary. *J. Geophys. Res.*, 94, pp. 14363–71.

Sturm, B. 1980. The atmospheric correction of remotely sensed data and the quantitative determination of suspended matter in marine water surface layers. In: A. P. Cracknell (ed.), *Remote Sensing in Meteorology, Oceanography and Hydrology*. Chichester, UK, Ellis Horwood, pp. 163–97.

Subramaniam, A., Carpenter, E. and Falkowski, P. 1999*a*. Bio-optical properties of the marine diazotrophic cyanobacteria *Trichodesmium* spp. II: A reflectance model for remote sensing. *Limnol. Oceanogr.*, 44, pp. 618–27.

Subramaniam, A., Carpenter, E., Karentz, D. and Falkowski, P. 1999*b*. Bio-optical properties of the marine diazotrophic cyanobacteria *Trichodesmium* spp. I: Absorption and photosynthetic action spectra. *Limnol. Oceanogr.*, 44, pp. 608–17.

Sugihara, S., Kishino, M. and Okami, N. 1984. Contribution of Raman scattering to upward irradiance in the sea. *J. Oceanogr. Soc. Jpn*, 40, pp. 397–404.

Sugihara, S., Kishino, M. and Okami, N. 1985. Estimation of water quality parameters from irradiance reflectance using optical models. *J. Oceanogr. Soc. Jpn*, 41, pp. 399-406.

Sydor, M., Gould, R. W., Arnone, R. A., Haltrin, V. I. and Goode, W. 2004. Uniqueness on remote sensing of the inherent optical properties of ocean water. *Appl. Opt.*, 43, pp. 2156–62.

Tester, P. A. and Steidinger, K. A. 1997. *Gymnodinium breve* red tide blooms: initiation, transport and consequences of surface circulation. *Limnol. Oceanogr.*, 42, pp. 1039–51.

Thomas, G. E. and Stamnes, K. 1999. *Radiative Transfer in the Atmosphere and Ocean*. Cambridge, UK, Cambridge University Press.

Vanhoutte-Brunier, A., Lyons, S., Fernand, L., Cugier, P., Menesguen, A. and Gohin, F. 2004. Modelling the *Karenia mikimotoi* bloom that occurred in the western English Channel during summer 2003.

Vasilkov, A. P. 1997. A retrieval of coastal water constituent concentrations by least-square inversion of a radiance model. *Proc. Fourth Internatonal Conference on Remote Sensing for Marine and Coastal Environments*. Ann Arbor, Mich., Environmental Research Institute of Michigan, pp. 107–16.

Vasilkov, A. P., Burenkov, V. I. and Ruddick, K. G. 1999. The spectral reflectance and transparency of river plume waters. *Int. J. Rem. Sens.*, 20, pp. 2497–508.

Vernet, B., Brody, E. A. Holm-Hansen, O. and Mitchell, B. G. 1994. The response of Antarctic phytoplankton to ultraviolet light: absoprtion, photosynthesis and taxonomic compounds. *Antarct. Res. Ser.*, 62, pp. 143–58.

Vernet, M. and Whitehead, K. 1996. Release of ultraviolet-absorbing compounds by the red tide dinoflagellate *Gonyaulax polyedra*. *Mar. Biol.*, 127, pp. 35–44.

Viollier, M. and Sturm, B. 1984. CZCS data analysis in turbid coastal waters. *J. Geophy. Res.*, 89, pp. 4977–85.

Viollier, M., Tanr, D. and Deschamps, P. Y. 1980. An algorithm for remote sensing of water color from space. *Boundary-Layer Meteorol.*, pp. 247–67.

Wang, M. and Bailey, S. W. 2001. Correction of sun glint contamination on the SeaWiFS ocean and atmospheric products. *Appl. Opt.*, 40, pp. 4790–98.

Whitlock, C. H., Bartlett, D. S. and Gurganus, E. A. 1982. Sea foam reflectance and influence on optimum wavelength for remote sensing of ocean aerosols. *Geophys. Res. Lett.*, 9, pp. 719–22.

Whitlock, C. H., Poole, L. R., Usry, J. W., Houghton, W. M., Witte, W. G., Morris, W. D. and Gurganis, E. A. 1981. Comparison of reflectance with backscatter and absorption parameters for turbid waters. *Appl. Opt.*, 20, pp. 1696–703.

Yang, H. and Gordon, H. R. 1997. Remote sensing of ocean color: assessment of water-leaving radiance bidirectional effects on atmospheric diffuse transmittance. *Appl. Opt.*, 36, pp. 7887–97.

Zingone, A. and Enevoldsen, H. O. 2000. The diversity of harmful algal blooms: a challenge for science and management. *Ocean Coast. Manag.*, 43, pp. 725–48.

10

Sensing plankton: acoustics and optical imaging

J. S. Jaffe

10.1 Introduction

Planktonic communities are ubiquitous and diverse assemblages of organisms, which play a key role in structuring pelagic ecosystems. Photosynthetic phytoplankton, discussed elsewhere in this volume, play a key role as they support oceanic food webs and alter the biogeochemical cycling of nutrients and carbon in the ocean. Planktonic animals, or zooplankton, serve as a link between primary production by unicellular phytoplankton and higher trophic levels such as pelagic fish stocks, many of which are commercially exploited. The environmental and biological factors controlling the distribution and population dynamics of pelagic communities is a central goal of biological oceanography. The importance of understanding the abundance, dynamics and interactions of planktonic organisms with increased spatial and temporal resolution has led to the development and application of improved sensors to observe and quantify them. As documented in this volume, harmful algal blooms (HABs) can exert a dominant (and harmful) influence on pelagic ecosystems via the consumption of nutrients, the production of toxins, and the creation of anoxic conditions. The precise mechanism and how dynamics of these food webs are affected is of great interest. Here, we consider the development of technology to study and understand HABs with the ultimate goal of perhaps mitigating their effects.

In considering the relationship of HABs to zooplankton it will be necessary to understand the effects of both HABs on zooplankton and the effects of zooplankton on HABs. Although we have much to learn, initial efforts in these areas by Turner et al. (2000) and Buskey (2003) have helped to determine the relationship of phytoplankton to zooplankton and leave many questions for future work. Perhaps some of the technologies described in this chapter will be useful in order to unravel interesting aspects of these ecosystems.

This chapter aims to provide a contemporary review of acoustic technologies that have been developed for monitoring zooplankton. In addition, a survey of underwater optical imaging of both zooplankton and phytoplankton is presented. As a general outline, first, a review of the basic physics of sound scattering from zooplankton is presented. This is followed by an introduction to the propagation of light in the sea and its special relevance to underwater optical imaging. The background information is presented to give a good idea of the underlying physical and environmental principles that form the basis for the current generation of underwater systems. A survey of these systems, which includes many examples of contemporary underwater acoustical and optical systems, is presented. These systems range from commercially available

conventional off-the-shelf technology (COTS) to one-of-a-kind instruments that may someday transition into the standard repertoire of oceanographic facilities.

There is, in fact, no perfect technology for observing zooplankton in the sea. Optical techniques offer the highest possible resolution and present the data in a form that is readily interpretable by humans, due to our extensive experience with visual observation. Acoustics offers the possibilities for longer-range imaging of these animals, however suffers from a lack of specificity, a non-intuitive basis for scattering strength, and a lack of knowledge of the multidimensional features of the scattering functions. On the most basic level, the net techniques that have been used for many years offer the highest observational accuracy in permitting species identification, however they suffer from problems associated with avoidance, the inability to non-invasively obtain certain classes of animal, and biases that depend on the size and swimming speeds of the animals.

Taken together, these three techniques are the standard repertoire for observing the animals. Each has significant strengths but also significant weaknesses. Taken together, however the methods can complement each other. In the case of acoustics, due to the ease of creating, recording and processing sound, there has been a proliferation in the use of acoustical techniques for sensing zooplankton. Several excellent surveys of sound scatter by organisms in the sea and the contemporary instruments, which have evolved to sense zooplankton (Griffiths et al., 2002), (Foote and Stanton, 2000), have been written. In addition, there are textbooks that consider the use of acoustics for fisheries assessment (McClennan and Simmonds, 1992). A book on acoustical oceanography (Medwin and Clay, 1998) describes both fisheries and zooplankton acoustics along with the basic physics of sound and sound propagation in the sea.

In the case of optics, the ever rapid development of advanced recording, processing and algorithmic techniques has fostered a recent generation of optical zooplankton observational equipment. A recent book chapter (Foote, 2000) and a review of zooplankton survey techniques (Wiebe and Benfield, 2003) describe many of the contemporary systems that are available. The interested reader is referred to these articles for further information and perhaps, a different view of these topics from those of this author.

10.2 Physics

In this section the basic physics of the process of sound scattering from organisms is reviewed, with special emphasis on applications to zooplankton. This is followed by a discussion of the properties of light propagation and scattering and the principles of underwater imaging.

10.2.1 Foundations of acoustical sensing of zooplankton

In order to understand the possibilities for using sonar in assessing the distribution, abundance, and behaviour of zooplankton, the general principles of active sonar systems should be considered. The general set-up, as illustrated in Figure 10.1, consists of a set of electronics for both transmitting and receiving the sonar signal. These are then connected to a transducer that transforms the electrical signal into a sound wave. This wave then propagates into the medium where it is both attenuated and scattered. On scatter from an organism of interest, the sound is then transformed back from a pressure wave into an electrical signal that is recorded and analysed.

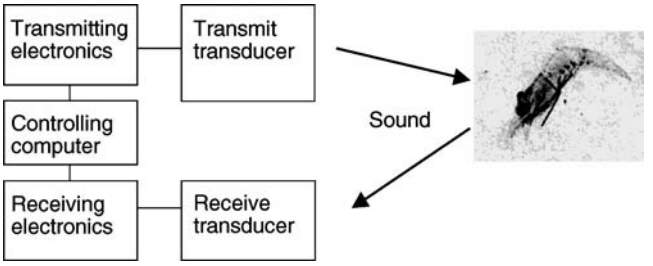

Figure 10.1
Basic components of a sonar system for recording reflections from zooplankton.

In considering both the production and receipt of sound, there are standard texts that discuss the basic principles of sonar systems and their implementation (Urick, 1983; Kino, 1987). Briefly, the sonar equation is the standard mathematical vehicle by which the delectability of animals can be determined. A general formulation of this equation for a single frequency that relates the intensity (I_{rcvd}) of the received sound (watts m^{-2}) to the acoustic power which has been transmitted (W_{xmit}) in watts by an omnidirectional source for a single target at range r from the source as:

$$I_{\text{rcvd}} = \frac{W_{\text{xmit}} e^{-2ar}}{r^4} \frac{\sigma}{4\pi}. \tag{10.1}$$

Here, a is the absorption coefficient for the specific frequency of interest (ordinarily considered to be only a function of the state of the water) and σ is referred to as the acoustic cross-section (units m^2). Pressure levels at the receiver can be computed from the relationship between the intensity and pressure. As pressure is a time-varying quantity, the root-mean-square pressure (p_{rms}) is a more meaningful parameter that can be related to the average intensity using

$$< I > = \frac{p_{\text{rms}}^2}{\rho c}. \tag{10.2}$$

When the pressure is in pascals, the density of the media (water), ρ is in kg m^{-3}. c is the velocity of sound in the media (m s^{-1}), accounting for a non-omnidirectional source can be accomplished in a straightforward manner.

The equation illustrates the general features of almost every remote sensing system in which the radiation that has been produced is both exponentially attenuated (due to absorption) and spherically spread (a consequence of conservation of the energy). Although (10.1) is certainly the most intuitively appealing, most sonar engineers prefer to cast the equation into logarithms and reference the source levels to micropascals. The interested reader is referred to standard texts for the details. For our purpose here the important parameter is the relationship between the target strength (TS) and the acoustic cross-section. The relationship is

$$\text{TS} = 10 \log \frac{\sigma}{4\pi}. \tag{10.3}$$

Note that this implies an exponential scale for TS. We also remark that target strength can be related to the fraction of sound scattered by a target as

$$\mathrm{TS} = 10 \log \frac{I_{\mathrm{refl}}}{I_{\mathrm{inc}}}, \tag{10.4}$$

where I_{inc} and I_{refl} are the incident and reflected intensities of the sound field. One important detail, often overlooked, is that the incident sound level is taken at the organism. However, the reflected sound level is usually referred to at 1 m range. Probably the most intuitive way to think of TS is as the logarithm (to base 10) of the fraction of energy that is reflected by the target. Target strength of -60 dB therefore implies that 10^{-6} of the energy incident on the target will be reflected. As this is a typical value for a large zooplankter, the characterization of animal reflectivity *in situ* can be a challenging endeavour.

In many situations the reflections from individual animals cannot be discerned and the sonar system is operated in a mode called echo integration. In this mode the recorded energy is the result of the reflection from the myriad of organisms that are in the sonar beam. The higher the diversity of scattering types (defined below), the more difficult the data are to interpret. In the most difficult situations, empirical relationships can be established which relate the integrated energy to animal abundance; however, their validity needs to be determined by ancillary methods such as net tows.

A more general approach considers the scattering function β (here we use β in order to be consistent with the optical theory presented below) as a function of the orientation of the target relative to the incident and reflected sound. Figure 10.2A demonstrates that in the most general formulation, this is a four-dimensional function. As this function can be very complex (and perhaps rarely measured), some type of simplification is typically made in order to reduce its dimensionality. A common one is that the source and receiver are collocated as shown in Figure 10.2B. This is referred to as a monostatic apparatus and is by far the most common way to measure backscatter from animals. Assuming that the source and receiver are collocated leaves only two remaining degrees of freedom; the orientation of the animal (θ_i, φ_i).

One of the earliest theoretical formulations of zooplankton scattering was the fluid filled sphere, treated by Anderson (1950). This spherically symmetric function was computed (by two computers, in this case people) as a function of the product of the equivalent spherical radius, *r,* and the wave number of the incident sound,

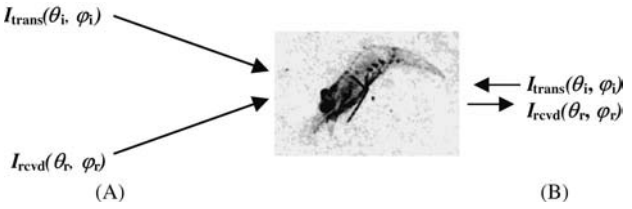

Figure 10.2
Illustration of the geometrical origin of the four-dimensional scattering function $\beta(\theta_i, \varphi_i, \theta_r, \varphi_r)$. The angles (θ_i, φ_i) and (θ_r, φ_r) are the relative angles between a coordinate framework fixed to the animal orientation and the angles of incidence and reflection, where θ_i and φ_r are the polar and azimuthal angles. A, bistatic configuration; B, monostatic configuration ($\theta_i = \theta_r$, $\varphi_i = \varphi_r$).

$k = 2\pi/\lambda$. Since then, increasingly sophisticated models of acoustic backscatter have evolved, taking into consideration the relevant symmetry and acoustical properties of the organisms under consideration. As zooplankton present a great variety of body morphologies and compositions, measurement of even a representative number of scattering functions presents a great challenge. In addition, the necessity of understanding their angle-dependent scatter, hopefully *in situ*, presents an added layer of complication. In some sense, due to these facts, there has been a substantial interest in modelling zooplankton scattering with the hope that such models could 'fill in the gaps' between the necessity for measurement and the need to reconcile any given acoustical experiment with an understanding of the composition of the volume under consideration.

One area that has seen much research has been the modelling of scattering from elongated fluid filled bodies. These efforts have been primarily aimed at understanding the scattering from krill. In a series of articles that span over a decade, Stanton and colleagues have formulated both simple (Stanton et al., 1993) and more complex models (Lavery et al., 2002) in order to understand the scattering from these organisms. A recent review summarizes efforts and outlooks at modelling the scattering from these animals (Stanton and Chu, 2000). As one example, Figure 10.3 shows acoustic backscatter target strength versus $k = 2\pi r/\lambda$, the ratio of equivalent radius to wavelength multiplied by 2π, for the deformed fluid cylinder (Stanton et al., 1993*b*) as a function of animal orientation. The graph was produced using assumptions about the two important parameters of material composition: animal density contrast (ratio of animal density to that of the surrounding water, $g = 1.06$) and sound speed contrast (ratio

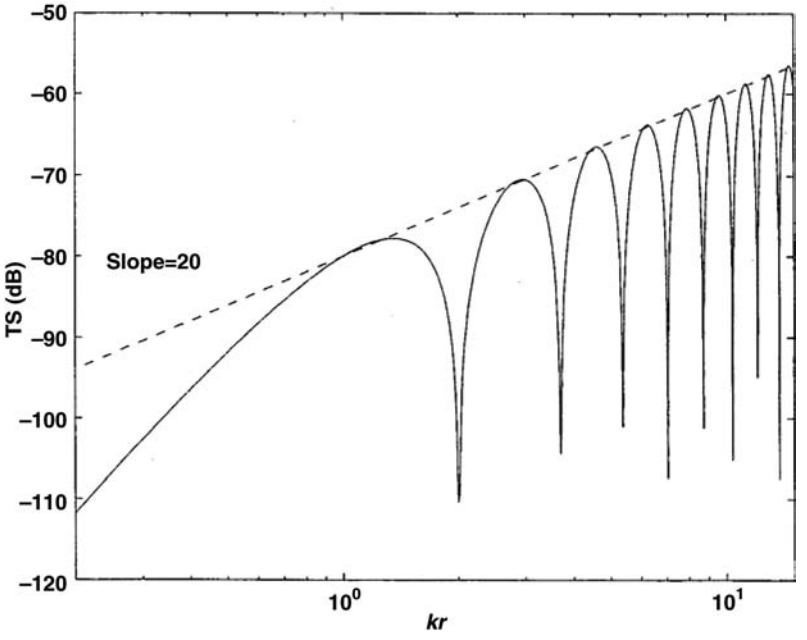

Figure 10.3
Backscatter target strength (TS) versus *kr* for the bent cylinder model of Stanton (1993*b*) as computed by Demer (1994) at 420 kHz.

of sound speed in the animal to that of the surrounding water, $h = 1.06$) (Demer, 1994). The product of these parameters gh is called the acoustic impedance (similar to the refractive index in optics). Greater values of acoustic contrast lead to higher reflectivity (again similar to the refractive index in optics). The assumed values for these parameters were subsequently validated.

The graph clearly shows a transition from a steeper region (at low kr) where a small increase in kr will result in a larger increase in scattering (approximately proportional to incident frequency f raised to the fourth power) to a more gently increasing region where the slope asymptotes to 20 (due to the dependence on cross-sectional area). The former area is called the Rayleigh regime and the larger kr region is called the geometrical or geometric scattering regime. The nulls, or deep areas of low backscatter, are due to coherent interference between different parts of the body. Most system designers interested in detecting single species try to 'tune' their wavelengths so that kr is greater than or equal to one as this leads to an efficient use of power (however see discussion below on multispectral imaging) with a minimum of attenuation due to absorption. As such, the $kr = 1$ point is often a design goal for the systems. So, for example, considering a 1.13 mm copepod of equivalent spherical radius $r = 0.2$ (McGehee et al., 2003) the $kr = 1$ implies that a wavelength of $\lambda = 1.25$ mm, or a frequency (assuming $f\lambda =$ 1,500 m/s) of $f = 1.2$ MHz should be used. The equivalent spherical radius is that value of r in the spherical model which best matches the observed frequency spectrum from the more complex organism. It is because of the low backscatter target strength of animals that are small relative to the wavelength of the sound that low frequency sonars are of little use in detecting small organisms, unless their abundance is extremely high. The interested reader should be aware that many graphs of target strength are really the 'reduced target strength' which subtracts a quantity of 10 log L^2 from the displayed quantity (Lavery et al., 2002). Here L is the 'equivalent' length of the animal, a number similar to the equivalent spherical radius, which accounts for the systematic change in target strength as a function of animal length.

Considering the variety of zooplankton, it is clear that a wide number of morphological traits need to be considered. Zooplankton comprise over 30 phyla with diverse body plans. Some of the more important are the crustacean zooplankton (euphausiids, copepods), the gelatinous forms (salps, medusae), animals with hard shells (pterapods) and zooplankton with gas inclusions (siphonophores). Certainly, the broad classes of animals can be used to predict backscattering, however, in each case the prediction of sound backscattering will probably be dependent on the details of animal morphology and composition. Animal composition will also change based on physiological condition and lipid reserves, and perhaps other environmental factors. It certainly remains an open issue to determine the applicability of the existing models to the variety of zooplankton that populate the sea.

Griffiths et al. (2002) note that several classes of animal sound scattering models have been considered: fluid-like (euphausiids, copepods), animals with hard shells (pterapods), and animals with gas inclusions (siphonophores). An added complication in the case of animals with gas inclusions is that there is a resonance frequency for the bubble. However, even far away from this resonance peak, the presence of a gas-filled inclusion will produce a large degree of backscattering. Figure 10.4 summarizes a comparison of the target strengths of a number of animals computed using a variety of scattering models. The graph makes it clear that the simple interpretation that acoustic scattering is proportional to animal abundance or biomass is not possible for diverse assemblages of animals. In one recent example of the difficulties associated with a simplistic

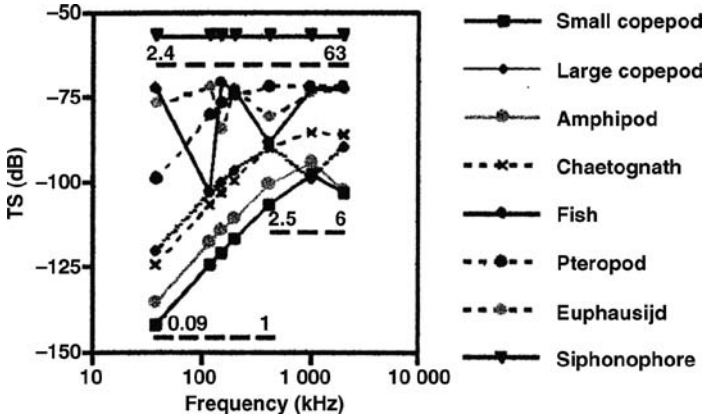

Figure 10.4
Set of curves depicting the backscatter target strength (TS) dependency on frequency as a function of animal type.
Source: Griffith (2002).

approach, it was noted that the scattering from pterapods in a given field trial dominated the acoustic backscattering even though they comprised only 0.1% of the individuals (Griffiths, 2002). These facts are in agreement with modelling and measurements by Stanton et al., where it was shown that the frequency-dependent scattering from a 21.8 mm decapod shrimp was extremely similar in magnitude (excepting fine structure) to a 1.9 mm gastropod. The authors remark that the echo energy per unit quantity of biomass of the 2 mm-long gastropod is about 19,000 times that of the 30 mm-long salp. This, of course, underscores the need for additional sampling schemes such as net tows, or independent optical imaging of the animals as discussed below.

An interesting option, extensively considered by Holliday over several decades (Holliday and Pieper, 1989, 1995), is to use multiple frequencies (narrowband) of interrogation. As the reflected energy is approximately a linear superposition of the frequency dependent scattering from the animals, providing the individual scattering functions are linearly independent, in principle, an inversion can be performed to compute the relative contributions of each component. As part of this work, it was revealed that the inversion is ill-posed, however by positively constraining the solution, it was demonstrated that it is possible to compute the relative contributions of the different scatterers, even in underdetermined systems. The efficacy of such a technique is a function of the frequency bands that have been chosen and the equivalent spherical radii of the particles. A poor choice of frequencies may render the inversion impossible, while a good choice will promote success. Greenlaw and Johnson (1983) considered the mathematical theory related to the 'inverse' problem of computing animal abundances as a function of animal type from the collected multiple frequency backscatter data.

One further complication that should be considered in any attempt to perform a 'routine' survey is the effect introduced by animal orientation on backscattering. Figure 10.5 shows the result of comparison of a computer model of the backscattering from a euphausiid (source/receiver at the same location) with recorded data (McGehee et al., 1998) as the animal orientation changes from 'head on' to a side view. The figure

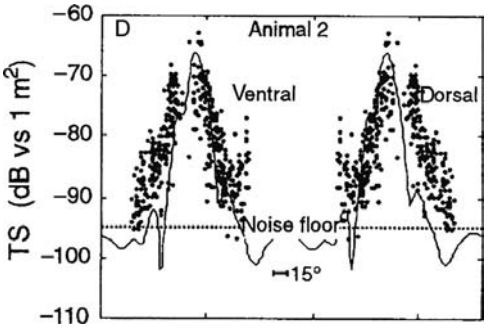

Figure 10.5
Laboratory measurements of backscattered target strength (TS) (dots) and model predictions (solid line) versus animal orientation of *Euphausia superba* at 120 kHz.
Source: McGehee (1998).

illustrates that the increase in the effective cross-sectional area normal to the beam direction is greatly reduced for the head-on view (0°) with respect to broadside at 90° and 270° (~25 dB). Moreover this effect can be large for small changes in tilt angle, resulting in a large change in the amount of reflected energy. Complications due to this effect in the field are particularly severe for elongated animals that do not have gas inclusions (e.g. euphausiids). Recent studies by Warren et al. (2002) have confirmed these observations and also extended them to the study of elastic-shelled organisms. Increased knowledge of animal orientation or 'behaviour' is thus a prerequisite for higher accuracy in echo sounder survey results.

In considering the common methods that are used for 'observing' the animals, we remark that there are two traditional modes for performing sonar studies: echo integration and echo counting. In the echo integration mode, the volume backscattering is recorded and animal abundance is then estimated using either a single frequency or multiple frequency inversion. In the echo counting mode, the reflections from individual animals are recorded and the number of animals can be inferred from the multiplicity of traces. In practice, problems with the echo counting approach arise when animal densities become high because the multitude of reflections can 'saturate' the echo-counting technique and individual traces may no longer distinguishable. In this case, the total energy in the recorded sound is related to the abundance of animals using some type of linear relationship (McClennan and Simmonds, 1992). This relationship forms the basis for many fisheries abundance estimates and there is a large literature dealing with this methodology and the types of corrections that are needed under various operating conditions.

The user of any acoustic system for estimating zooplankton abundance and/or behaviour has many factors to contend with. In environments where there is low species diversity, the interpretation of acoustic backscattering data can be greatly simplified. However, the interpretation of the data still requires the consideration of animal size and orientation. In many 'real world' situations, the diversity of animal species can be high and thus, acoustics seems to be most valuable when accompanied by other methods for constraining the interpretation of the reflected energy. Animal identification can be

accomplished with net tows (with all the associated issues related to avoidance, etc.), or optical imaging methods. The optical methods have their own set of related issues (small interrogation volumes, reactions of the animals to lights, etc.). The following section considers the use of optical imaging and its implementation in observing zooplankton.

10.2.2 Principles of underwater optical imaging

The basic principles of underwater light propagation and its ramifications for underwater optical imaging have been known for some time now and the use of optical imaging systems for underwater sensing, exploration and discovery are commonplace to every diver or snorkeller who has marvelled at the underwater landscape. Starting with the pioneering work of Siebert Duntley (1963) who was originally at the Massachusetts Institute of Technology and then the director of the Scripps Visibility Lab, a number of researchers have been involved in the advancement of underwater imaging (Mertens, 1970; Smith, 1984; Dolin and Levin, 1991). Recently, Jaffe et al. (2002) have reviewed the status of the contemporary field of underwater optical imaging. Briefly, the modern revolution in new and affordable optical components has given underwater optical engineers the opportunity to create a whole new generation of such systems.

On a basic level, one usually discriminates between 'passive' and 'active' imaging systems. In the case of passive systems, the imager does not illuminate the subject matter. Thus, some other source of light, either ambient or other, is necessary. In the case of active imaging systems, the imager itself generates the light. Although passive systems can be substantially less invasive than active ones, unfortunately, except in some of the clearest waters, these systems are not capable of producing images of zooplankton. That this can be true in many cases is likely because these animals place a premium on being transparent, or difficult to see, in order to avoid predators. Consequently, in every case that this author can identify, imaging systems for optically observing underwater zooplankton all use an 'active' source of illumination. This source can be either a CW (continuous wave) light source such as an underwater flashlight, a strobe light, or some type of laser, either pulsed or CW. Many of these systems are reviewed in the section on applications, however first some physics.

The propagation of light underwater can be described in a straightforward way via the concept of radiance. Simply put, radiance is the three-dimensional directional intensity of light propagation at a given location and time. Given that radiance is the state variable for optical radiation, the radiant distribution (which also considers polarization) describes everything that is knowable about an optical experiment. As this quantity is spatially, spectrally and temporally variable, its measurement provides quite a challenge for the underwater instrument designer. As covered by Morel (2007) and Lewis (2007), Chapters 4 and 6 this volume, many sensors have been devised to permit the measurement of either this quantity or one of its moments. Cameras measure radiant energy by integrating radiance over each pixel in the camera.

A considerable simplification in understanding the performance of underwater illumination systems can be accomplished by categorizing the different components of the image. Figure 10.6 shows that the light that has arisen from an artificial source can suffer several fates: (a) absorption by the intervening water or the subject; (b) scattering from the intervening water; (c) reflection from the subject; (d) scattering in the intervening water after reflection by the target. The goal of any underwater imaging system is to maximize the contribution of reflection while at the same time minimizing the other three effects.

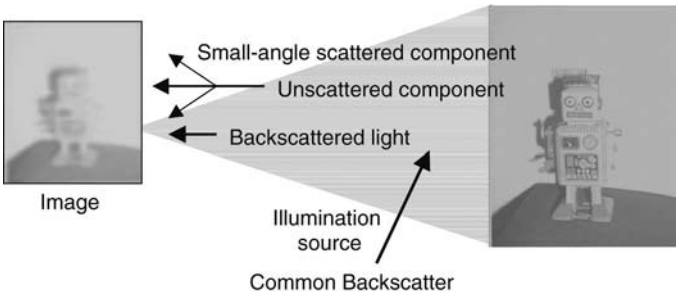

Figure 10.6
Schematic of an underwater imaging system and the components of an image that result from a categorization of the retrieved light.

The environmental parameters that describe the propagation of light determine how well one can see. These parameters are the absorption and scattering of the water and the reflectivity of the subject. Although these parameters have been measured in some cases, the details of every environmental situation can play a predominant role in determining the outcome of an underwater optical imaging experiment. This is because, not surprisingly, the ocean can maintain large gradients in absorbers and scatterers (at for example, density discontinuities, or near the sea floor) that can also vary in time. Absorption, a, is a scalar. However, the more complicated situation of scattering must be described by a vector function that indicates the degree of scattered light as a function of incident angle and observation angle, $\beta(\theta_i, \varphi_i, \theta_r, \varphi_r)$. In most cases, in the water column, this function can be considered to be cylindrically symmetric (as above for acoustics), which reduces the dimensionality of the problem, however still leaves $\beta(\theta)$, the volume scattering function (VSF), to be measured.

An additional complication, which can be exploited in many situations, is the possibility of the absorbed light being re-radiated in some form. This can be via fluorescence or Raman scattering. Both elastic scattering (at the same wavelength of the incident light) and inelastic scattering (at some other, typically longer wavelength) can play a substantial role in the observations of an underwater optical imaging system.

The design of 'efficient' underwater optical imaging systems can be aided by the development of computer models which can, in large part, mimic the propagation of light underwater and predict the outcome of a given situation. The computer model permits the user to place both cameras and lights at different locations with various orientations with respect to the subject matter. Predictions from the system can then be produced which will indicate the properties of the image field. This naturally assumes that the environment has been adequately characterized with respect to absorption and volume scattering. Although many absorption measurements have been performed and can be found in standard texts on underwater optics (Jerlov, 1976; Kirk, 1994; Shifrin, 1988), information about the scattering function is rarely available. A web-based resource for underwater optical parameters is now available.[47] The site contains many observations which can be used for obtaining absorption and scattering values which can be used to predict the quality of underwater images. Although there have been relatively few measurements of the volume scattering function, a unique set of data (Petzold, 1972) have been used for many years and produce quite believable results when used in under

[47] http://wood.jhuapl.edu/

water models (McGlamery 1975; Jaffe, 1990; Jaffe et al., 1998*b*) and recent technological advances have yielded instrumentation so that volume scattering function observations will hopefully be routine in the near future (Roesler and Boss, 2007 – Chapter 5 this volume). The models can range from Monte Carlo simulations, which keep track of every photon, to those that use a semi-analytic formulation (Zege et al., 1991). The conventional formulation for understanding image propagation uses concepts from linear systems theory (Gonzalez and Wintz, 1987). This approach has been validated using Monte Carlo modelling (Jaffe, 1995) and also semi-analytic formulations (Zege et al., 1991) for 'reasonable' numbers of scattering lengths. The index which quantifies image blurring, the point spread function, describes the transformation in radiance distribution that occurs from object to image due to the small-angle scattering. Limited experimental determinations of these functions have been made and several parameterizations exist (Mertens and Replogle, 1977; Voss, 1991*a*, 1991*b*; McLean and Voss, 1991). Unfortunately, there have been relatively few situations where the results of the models have been compared with the output of the camera systems when a complete environmental and instrumental suite of parameters was known. Nevertheless, in many cases, especially system design, the models can be used in a comparative sense, weighing the relative advantages and disadvantages of different geometries as a function of environment.

In considering the special case of the underwater imaging of zooplankton, a great unknown can be the animals' reflectivity. Many of the animals are transparent; this presumably conferring reduced visibility from predators. Therefore, for the most part, zooplankton imaging system designers typically use an empirical approach via the collection of animals and the experimentation with different imaging geometries. In some of these imaging systems a kind of 'dark field' mode is used which images the scattered light (Davis et al., 1992; Strickler, 2000), however avoids the unscattered beam.

One desirable trait of an underwater imaging system is to possess a degree of 'non-invasiveness', especially if behavioural observations are desired. This can be quite difficult for underwater optical imaging, as the options for propagating light over long distances are limited and for systems that are in close proximity, the animals are sensitive to hydrodynamic disturbances. Moreover, high light levels might affect the animals' behaviour. The underwater lighting system designer whose goal is to image zooplankton needs to trade off all these factors.

10.3 Applications: with special relevance to real-time sensing

In the previous sections both the underlying physics for sound and light propagation in the sea have been discussed. In the next several sections, the practical implementation of such systems is described. In keeping with the general theme of this volume, we concentrate our efforts on describing systems that have some type of capability for reporting their data in real time.

10.3.1 Acoustical systems for sensing zooplankton

Although there are a multitude of commercial acoustic systems that have been used in order to monitor fish, the commercial use of acoustics for monitoring zooplankton has been limited. This is probably due to the limited commercial marketplace for these animals. In turn, this has limited the types of acoustics systems that can be purchased off-the-shelf for measuring acoustic reflections from zooplankton.

Table 10.1 Categorization of acoustic systems, showing examples where commercial systems are available (commercial) and N/K: not known to have been built. Authors' names are associated mainly with research systems

	Single beam	**Split beam**	**Dual beam**	**Multi beam**
Single frequency	Commercial	Commercial	Commercial	Commercial FTV: Jaffe (1995)
Multiple frequency	Maps/Taps: Holliday et al. Griffiths (1997)	Wiebe (1997, 2002) Demer (1999)	Wiebe (1994)	N/K
Wideband system	Commercial (SciFish) Stanton (1998) Foote (1998)	N/K	N/K	N/K

In looking at the practical realizations of the acoustics we note that there are several different types of systems that have been used. One way of categorizing these systems is to consider both the number of beams and the number of frequencies that the system employs. Table 10.1 contains a list of systems known to this author. The notation commercial means that commercial versions of the system are available. N/K indicates that, to the knowledge of this author, there has not been either a research or commercial system used with these features.

10.3.1.1 Single frequency systems

Certainly, the simplest type of system uses a single frequency and a single beam. In this category, one can find many of the economical consumer oriented acoustical systems for detecting fish. Unfortunately, the use of these systems for scientific purposes has been hindered by a lack of calibration, which, in turn, prohibits their detection voltages from being turned into quantitative biomass.

One system that is widespread in the oceanographic fleet is the acoustic Doppler current profiler (ADCP). The system, manufactured by RDI instruments of San Diego, allows the user to estimate the underwater, range-dependent, vector-valued current velocity. It works by sending four beams of sound into the water and subsequently measuring the range-dependent Doppler shift and hence, from the four beams, some estimate of the vector-valued current.

As these systems have become standard equipment for much of the oceanographic fleet, the possibility for using them to estimate biomass is appealing. In a classic study, Flagg and Smith (1989) used such a system to estimate zooplankton biomass. Although this early work attracted much attention, the difficulties of using such a system for quantitative estimation of animal abundance have precluded their routine use in the field. Thus, despite the fact that these systems operate at several frequencies, many of which are suitable for zooplankton, the systems have been used mostly for qualitative estimation of animal abundance. Nevertheless, the existence of concurrent information about both the physics (currents) and biology (animal abundance) presents interesting opportunities for analysis.

Both dual beam and split beam systems have been quite popular for several decades. The systems have similar goals in that, as the sound fields that are projected by

a sonar vary as a function of projection and receiving angle, the position of the animal must be known in order to estimate the intensity of sound that is in incident on it so that the fraction of sound reflected (and hence the target strength) can be inferred. Both of these types of system are routinely calibrated and their field use has resulted in many quantitative measurements. The split beam systems split a disk into four quadrants which each listen to the received signal. The time delay between quadrants is used to discern the direction that the sound is coming from. In dual beam systems the transmit and receive beam patterns (the intensity of sound with respect to direction) are cylindrically symmetric and the ratio between the intensity of the received sound for each target is used to locate the target and unambiguously allow the determination of target strength.

In comparing the performance advantages of the systems, Ehrenberg (1979) considered the relative advantages of split beam and dual beam systems from a signal processing point of view. The conclusions, at that time, supported the idea that the split beam systems were more robust in estimating animal position. This was especially true in the presence of other, possibly interfering targets. This may, in fact, explain the preponderance of split beam systems that are currently in use. There are several companies that manufacture bioacoustic systems (Simrad (Norway), Reson A/S (Denmark), Biosonics (Seattle, USA), Hydroacoustic Technology Inc. (Seattle, USA)). The systems can be purchased with a range of frequencies, some of which are suitable for observing zooplankton. Our purpose here is not to perform an exhaustive review of these systems and their use in zooplankton acoustics, but rather to alert the reader to the existence of such systems. Further information can be found in the article by Foote and Stanton (2000).

Multibeam systems offer an interesting set of advantages when considering field-of-view and the amount of power that can be projected. As the acoustic reflectivity of zooplankton is typically low, these systems can offer substantial advantages for mapping these low-reflectivity targets when a larger field-of-view is desired. Several commercial systems exist that were designed for multibeam bathymetry (Simrad, Norway and Reson, Denmark). The Simrad SM2000 system operates at a frequency of 200 kHz and projects sound in a plane that is 120° wide by 1.5° or 3°. The receiver beam forms the sound into 128 beams, each of a width of 1.5°. The system has been used to map schools of herring off Nova Scotia with interesting capabilities to map three-dimensional distributions of animals (Mayer, 2002). Several examples of the use of the Reson system, which operates at a frequency of 455 kHz with 60 beams each of width 1.5° have illustrated its utility in characterizing the three-dimensional distributions of animals (Gerlotto, 1998, 1999). To date, however, neither system has been used to characterize zooplankton distributions.

One multibeam system which has been used to map the behaviour of euphausiids and copepods is the FishTV system (Jaffe et al., 1995). Only two of these systems have been produced, one operating at a frequency of 435 kHz and the other at 1.57 MHz. Both systems incorporate similar designs and use multiple projectors that operate sequentially and are accompanied by parallel receipt. The 435 kHz system has a field-of-view of 16° by 16° and can map the reflections of 50–100 animals m^{-3} (De Robertis, 2001) with a localization capability of one cm at frame rates of up to 4 Hz. At close range, the system records reflections from 4 m^3 volume. A set of experiments in Saanich Inlet over two consecutive summer seasons resulted in the observation of several hundred thousand trajectories of the dominant taxa: euphausiids. The results have provided interesting information about the activity levels of the animals in the daytime

(Jaffe et al., 1999) and the trajectories of the animals during their vertical migration (De Robertis et al., 2003). The 1.57 MHz system has been used to track copepods as small as 1–2 mm in the Gulf of Eilat (Genin et al., 2005).

10.3.1.2 Multifrequency systems

The use of multiple narrowband frequencies in order to obtain more information than is available with a single frequency is a strategy for mapping animals that has been pursued by several groups. In one frequency regime (400 kHz–3 MHz) a series of instruments by Holliday and associates over the last few decades has been used to estimate the size distribution of small animals (1 cm–200 μm). In another frequency regime, there have been several systems whose design goals have been to map larger zooplankton (0.5 cm and larger) over larger volumes. As discussed above, the goal of these investigators has been to characterize animal size and, perhaps animal type, as a function of location.

Holliday and Pieper (1995) document many of the field situations that they have encountered with the MAPS system (at 21 frequencies) and the BITS system (at 165 kHz and 1.1 MHz). In the use of two frequencies, the requirements for reasonable inversions can be quite stringent. These include the existence of a single size organism that dominates the scatter at both frequencies, the existence of a validated model and other provisos that essentially imply that the animal densities are not so high as to introduce nonlinearities in the inversion process.

The latest version of the systems, TAPS™ uses between four and eight frequencies. The system was designed to increase the discrimination in size over that of the BITS system without requiring the use of the large number of transducers that are used in the MAPS.

Holliday et al. (2003) describe the deployment of an 8-frequency version of the TAPS™ system that was extensively used in a series of studies in a shallow fjord in northern Puget Sound (between Seattle, WA, United States and Victoria, BC, Canada). During summer 1998 several multifrequency acoustical zooplankton sensors (TAPS™) were deployed. The sensor measured volume scattering strengths at 100 kHz, 265 kHz, 300 kHz, 700 kHz, 1,850 kHz and 4,230 kHz with a 12.5 cm range resolution. The authors state that 'useful' results were obtained at ranges up to 20 m or 30 m (presumably with the lower frequencies). This new spatial resolution permitted the users to record a great deal of fine structure that existed in the water column. Inverse calculations for animal abundance as a function of equivalent size indicated that one of the 'thin' layers seen was dominated by 1.2 mm copepods. Additional observations indicated the presence of mysid-shaped animals concentrated in an adjoining but distinct thin layer.

In looking at other multifrequency systems, the Biomapper system of Wiebe et al. (1997) operating at two frequencies of 120 kHz and 420 kHz was used extensively in mapping plankton distributions in the vicinity of Georges Bank. The authors state 'acoustics was used for *first-order* estimates of the biomass of various taxa assuming that the proportions of taxa remained constant at constant depth'. Building on experiences from the first BIOMAPPER system (and also a system called the Greene Bomber which employed a dual beam transducer operating at 420 kHz) the Woods Hole group has fabricated a new system, BIOMAPPER II (Wiebe et al., 2002). The acoustics for the system was manufactured by HTI (Seattle, USA)

and it uses five upward-looking and five down-looking sonars at frequencies of 43 kHz, 120 kHz, 200 kHz, 420 kHz and 1,000 kHz. The system is well integrated with the resident vehicle and is completely digitally integrated into the complete package. Other examples of multifrequency systems are those of Foote (1998) and Griffiths et al. (1997).

Note also that various users have combined multiple frequency split and dual beam systems themselves by simply deploying the various frequency systems together. The table here considers examples of systems where there has been a 'tight integration' of the various frequencies so that identical volumes that have been insonified can be judged.

The conclusions of these workers seem to support the idea that there is, in fact, no ubiquitous solution to the acoustic detection of plankton. It seems, rather that based on the complexity of the scattering of the animals in a given ecosystem, the number of frequencies that are needed to describe the spatially dependent density of animals needs to be 'tuned'. That is not to say that valuable information cannot be obtained from acoustics, but rather that the users of such systems must carefully choose their frequencies and inversion techniques based on the dominant taxa at the site of interest.

10.3.1.3 Broadband systems

The use of broadband sound is an area that holds much promise for zooplankton acoustics. One example of broadband sound use in the laboratory was by Chu and Stanton (1998), who showed that they could judge the size of the animals using a linear modulated FM chirp from 300 kHz to 700 kHz. Certainly, the coherent processing of broadband reflections represents a frontier that has great potential for providing valuable information about animal type. In addition, if the reflections were resolvable such that broadband sonar can be operated in an echo-counting mode, it is possible that the features of the reflected waveforms will allow a higher degree of inference than the multiple (narrow bandwidth) sonars. A commercial system currently available from Scientific Fishery Systems Inc. (Scifish, 2003), Anchorage, Alaska, uses a continuous sound source from 110 kHz to 190 kHz. The manufacturer states that the system has been used successfully to classify among 20 different types of riverine and pelagic fish species.

10.3.1.4 Prospects for real-time acoustical monitoring of zooplankton

With special regard to the subject of this volume, we note that there are several examples of the use of acoustical systems for real-time monitoring of zooplankton. In addition, the current trends in increased electronic power storage and processing efficiency lead to optimistic conclusions about the future of such devices.

Concerning projects and equipment that have already been accomplished, the multifrequency systems of Holliday and co-workers have been used on moorings for many years. The BITS system was placed on a mooring on the northern edge of the San Pedro Basin near the shelf slope break near Los Angeles, California. First installed in autumn 1992, the system was composed of a two-frequency echo sounder. In one of the extended deployments, it was deployed on a mooring for nearly nine months. The system collected meteorological data on wind speed, light level and a two-way packet radio communication system was used to automatically download the data to a shore station within line-of-sight of the mooring. The system of Holliday et al. (2003)

that was deployed in Puget Sound is another example of the use of these TAPS™ like systems on moorings. D. V. Holliday and colleagues (D. V. Holliday et al., 2005) have also deployed an eight frequency TAPS™ system (TAPS™ 8) on a biophysical mooring in the Gulf of Alaska. The system can discriminate animals into multiple-size classes between 250 μm to 25 mm in total length by sampling a 2 l volume at a range of 1.5 m from the transducers. The lower frequencies were also used to estimate animal abundances at ranges as far as 15 m. The system is designed to autonomously record data from the mooring over an almost six-month period.

ADCPs have been extensively used on moorings, however, as explained above, the information currently available from these instruments has been primarily qualitative. In one example, F. Nilsen and colleagues (University of Bergen) used moored ADCPs in order to analyse the daily vertical zooplankton migration in connection with mixed layer dynamics. Other opportunities currently being explored by several groups includes the deployment of either dual or split beam systems on moorings, and the adaptation of modern consumer-level fish finders to remote moorings (D. V. Holliday, pers. comm.).

Future methods for acoustic surveys might incorporate different types of collection geometries or use more information. An interesting demonstration of multifrequency recordings from individuals (Demer, 1999) demonstrated that several animal types resident in the Antarctic ecosystem (euphausiids, siphonophores, myctophids) could be spatially discriminated (in some cases) using this approach. Alternative future methods could incorporate phase-coherent processing of wideband echoes from individuals. Other alternatives would be to use Doppler processing techniques in order to glean information about those animals that actively propel themselves (Holliday, 1974, 1977).

One interesting idea, which has seen little application, has been to use a 'true' underwater acoustic imaging system to 'see' the animals. An early use by Barans and Holliday (1983) showed that, in fact, a high-resolution side-scan system could be used for imaging bottom fish. Currently, the DIDSON system of Belcher (Belcher, 2003) is being experimented with in order to monitor the length of fish that are progressing through a hydroelectric dam bypass. The extension of these methods to 'imaging' of underwater zooplankton presents substantial challenges, especially when considering the high resolution that will be needed and the low reflectivity of many of the animals. As one final opportunity, it is possible that other aspects of the scattered field, such as forward or side scattering, might provide additional information that could be used to improve species discrimination.

10.3.2 Optical imaging of zooplankton

The use of optical systems for observing zooplankton has been successful in many situations and a variety of systems have been used for either routine survey or animal identification. In the case of survey, one must be prepared to argue that the assessment of animal populations is insensitive to the collection equipment. In some situations, both animal identification and abundance can often be judged. However, the small volumes required to obtain the resolution needed for animal identification can be partially compensated for by the use of fast frame rates and rapid surveys. Note that neither the optical plankton counter (OPC) nor the laser optical plankton counter (LOPC) are considered here as they are not 'imaging' systems. The interested reader is referred

to the article by Wiebe and Benfield (2003) and references therein for information on this system.

10.3.2.1 Video Plankton Recorder (VPR)

One system that has been used extensively in the field to image zooplankton is the Video Plankton Recorder (VPR; Davis et al., 1994). This uses forward scattered light to image animals that are nearly transparent. Several cameras image several volume sizes simultaneously to provide information on different scales. The VPR is an underwater microscope with a coupled video system that can be towed through the water column to make observations of small organisms in the approximate size range 0.2 –20 mm. Examples of animals which can be imaged are copepods, hydroids and medusa. The quality of the images is generally sufficient to distinguish among species, and the same images can be classified automatically, as by a trained neural network, even at a video-image acquisition rate of 60 frames per second (60 Hz). Automated classification has the benefit of reducing the vast quantity of data to a description of the patterns of concentration (Tang et al., 1998).

The VPR was developed during the US GLOBEC Georges Bank Regional Program (Davis et al., 1996; Benfield et al., 1996; Ashjian et al., 2001). Over the course of several years, the system provided extremely valuable data on the distribution of mesozooplankton at the George's Bank region. Recently, (2001, 2002), it has been used in conjunction with the BIOMAPPER II system in the Antarctic.

10.3.2.2 ZooVis system

A new system by Benfield (2001) uses a strobed sheet of white light. The system promises to yield images of zooplankton over an image field-of-view of 12 cm with a resolution of 50 μm. The zooplankton imaging and visualization system is a profiling instrument designed to collect quantitative images of mesozooplankton to depths of 250 m. The camera is aimed downward into a sheet 12 cm wide and 3 cm deep. By setting the depth of field to match or slightly exceed the depth of the light sheet, only targets that are in focus are illuminated.

10.3.2.3 Underwater Video Profiler system

The Underwater Video Profiler system (Gorsky et al., 1992) is an imaging system that consists of a Hi-8 video camera (with ultimate 512 by 512 resolution), controlling and data logging unit, batteries and several lighting systems. The lighting systems can either be a collimated light field in front of the camera, which images 0.28 l via a 1.5 cm illumination sheet used for particle distributions, or a second system that uses four spotlights to image a volume of 70 l of water. System calibration yielded a detection size of 100 μm. The system was designed for recording information about zooplankton and has been used successfully to image a variety of animals. In a typical deployment, the system was lowered at a rate of 1 m s^{-1} via a tether that resulted in a vertical sampling interval of 4 cm. Stemmann et al. (2000) present the results of a survey in the north-west Mediterranean of particles greater than 150 μm. Several oceanographic studies illustrate the success of the system in the western Mediterranean (Baussant et al., 1993; Gorsky et al., 2002) and the north Mediterranean (Gorsky et al., 2000). Figure 10.7 illustrates a collection of images taken with this system.

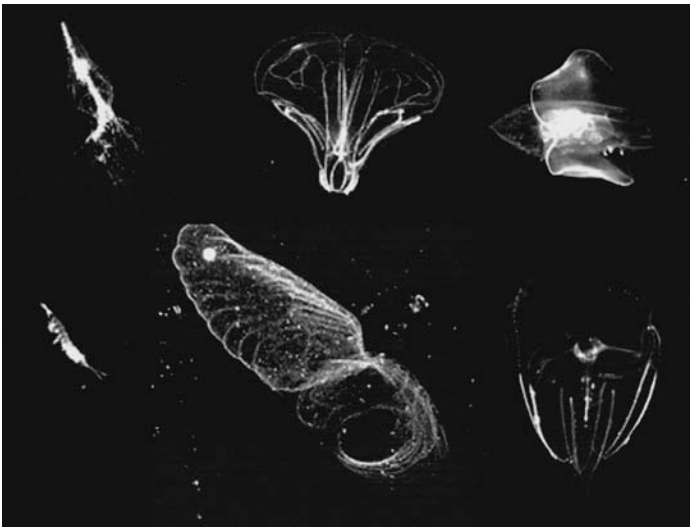

Figure 10.7
Collection of macrozooplankton taken with the UVP from the north-east Atlantic, recorded during the French Pomme oceanographic cruise in 2001.
Source: Gorsky, pers. comm.

10.3.2.4 3D Zooplankton Observatory

A system recently designed and built by Strickler and Hwang (2000) for obtaining information about three-dimensional trajectories of zooplankton (3D Zooplankton Observatory) uses Schlieren imaging in conjunction with multiple cameras in order to obtain orthogonal projections of animals in a 1 l volume. The system permits the viewing of aquatic organisms ranging from phytoplankton to fish and promises to provide interesting information about zooplankton behaviour in the laboratory.

10.3.2.4 Prospects for real-time imaging of zooplankton

Perhaps all the systems considered in this section have the capability for real-time imaging of zooplankton. In the case of the VPR system, the Autonomous Vertically Profiling Plankton Observatory (AVPPO) has been designed to collect data on the vertical position and taxonomic composition of plankton, together with ancillary environmental data. The system consists of the Video Plankton Recorder, which is buoyant, a transmissometer, fluorometer, downwelling light sensor, conductivity, temperature, absorption and scattering meter and an ADCP at 1.2 MHz that is used in an up-looking mode. Deployed at 100 m, the device can operate in currents of up to 4 knots and medium seas (10–20 ft/3–6 m surface waves). It is autonomous and can profile up to 500 times at a user-defined interval of days to weeks.

In a typical use, the VPR is released and being buoyant it floats to the surface. It is then retrieved from the surface by a winch at a rate of 10 cm s^{-1}. Both video and environmental data are recorded. The system has the capability of transmitting a subset of the data to shore via a cellphone link. It has been deployed on Georges Bank, and

as part of the Frontprogram[49] between Montauk Point and Block Island and between Stellwegen Bank and Scituate (USA).

There is no doubt that the other systems considered in this section: ZooVis, UVP and the 3D Zooplankton Observatory, could be configured to operate in a real-time mode on moorings. As these systems have a very small volume of interrogation, the most advantageous use would be in an environment where the systems were profiling (as above) or in areas where there was adequate current to transport a volume of water through the field-of-view. As a final note, one should be aware of problems of avoidance by plankton. A general question arises about the non-invasiveness of any technology that uses light and creates a hydrodynamic disturbance. Thus, the user of any such system should consider the effects of their experimental configuration on the animals. From a hydrodynamic point of view, the deployment of such systems in a mode where they are either LaGrangian or 'downstream', that is it is desirable that their imaging volume looks ahead of their hydrodynamic disturbance. In the case of light exposure, either the attraction or repulsion of zooplankton to light indicates that it is probably best to use a short exposure time on a 'fresh' volume of interrogation if non-invasiveness is desired. This is not to say that valuable information cannot be collected from systems that use continuous illumination, but rather that such users should take into consideration the effects of such systems on the animals and on the types of conclusions that they are making.

10.3.3 Optical imaging of phytoplankton

In the previous section the underwater optical imaging of zooplankton was considered. Here, we survey a set of optical imaging systems that have the ability to observe phytoplankton. The demands on the use of underwater optical imaging systems for observing phytoplankton are very similar to what might be considered in the construction of a high-magnification underwater microscope. If a true image of the organisms is desired then, considering that the cells sizes range from micrometres to tens of micrometres, the resolution needed would be at minimum several micrometres. As previously discussed, as light can be both attenuated and scattered, the observation of minute detail from cells that are suspended in water and therefore *in situ* can be challenging.

10.3.3.1 Holographic imaging

A promising technique that has seen great progress in the last decade is underwater holography. Holographic imaging uses coherent light scattered from a collection of underwater particles which is recorded on high-resolution film to create an interferogram, or coding, of the three-dimensional volume. The technique can be used in either an 'in-line' or 'off-axis-holography' which are different geometric configurations (Figure 10.8). In the 'in-line' case, the scattered light is allowed to constructively and destructively interfere with the light that is unscattered. The 'in-line' technique seems to work best when the water is only weakly scattering. As such, the scattered light can be combined with another, internally generated beam which coherently interferes with the scattered light.

Given the image of the interferogram, the three-dimensional volume can be reconstructed via either analogue or digital techniques. In the analogue method, an optical bench is used to physically reconstruct the three-dimensional volume that is then typically imaged with a digital camera. In the digital technique, the

[49] http://nopp.uconn.edu

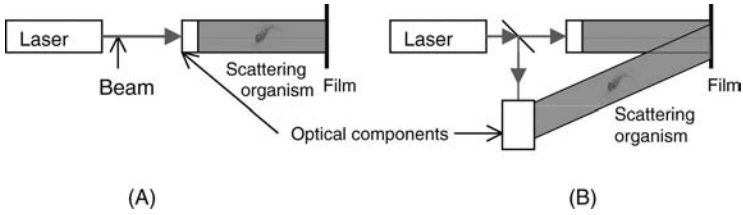

Figure 10.8
Basic geometry of A, in-line hologram; B, off-axis hologram.

raw interferogram is digitized and the necessary image transforms are performed in order to synthesize the three-dimensional image in the computer.

One potential disadvantage of the method is that prodigious amounts of data are produced and have to be processed, so automated analysis of such data is imperative. A recent review of underwater holographic imaging principles and implementation by Hobson and Watson (2002) is recommended for further reading.

One of the first contributions to *in situ* holography was from Carder (1979). In the United States, a group that worked on underwater holograms for some time was under the supervision of A. J. Acosta at the California Institute of Technology. Several Ph.D. theses were authored in this area (O'Hern et al., 1988). In the last few years, a group at Johns Hopkins University have developed an *in situ* holography system that uses an in-line configuration in order to record coherent interference patterns that can be reassembled into three-dimensional volumes (Katz et al., 1999; Malkiel et al., 1999). A laboratory system that uses both in-line and off-line geometries has also been used extensively in the laboratory to measure the fluid fields around copepods. The system uses a ruby laser with an in-line recording configuration and has a sample volume of 732 ml. The reconstructed images have a resolution ranging from 10–20 μm for spherical particles and 3 μm for linear particles that lie within 100 mm from the film (in the plane of the camera imaging plane).

Most recently, a group in Aberdeen (UK) has succeeded in deploying an underwater holographic imaging system that uses both in-line and off-axis geometry in order to form a set of images (Hobson and Watson, 1999; Watson et al., 2001). The system uses a pulsed Nd:YAG laser system which has the capability of very short exposure times which permits system operation in moderate flows. The interested reader should beware that the resolution usually quoted by the creators of such systems is the transverse or side to side (relative to the beam propagation direction). Hobson and Watson (2002) have noted that there is a fundamental limit to the axial resolution (along the beam axis) of such systems so that for a given system resolution of 5 μm, the depth of focus for a frequency doubled Nd-YAG laser-recorded holograph is 47 μm. One way around this complication is to fabricate a system that permits two orthogonal views of the subject (Sheng, 2003).

A system recently tested by Owen and Zozulya (2000) uses digital recording techniques and thus circumvents some of the complexities associated with film. The required digital image reconstruction techniques were developed and used to go directly from the camera image to the three-dimensional volumes. The authors demonstrate resolution to 5 μm in small volumes and the technique seems to have promise because of the compactness of the instrument and its capability to circumvent some of the issues relating to the recording media.

10.3.3.2 Flow cam

A system that has been developed to image organisms from the sea is the Flow Cam system by Fluid Imaging Technologies (Boothbay, ME, USA). The system, based on flow cytometry technology, works by pumping samples through a relatively small volume that has both illumination and high-resolution optics incident upon it. Having a small volume of interrogation allows the optics to be optimized for excellent image capability; however, this precludes using the system for imaging the *in situ* distribution of animals and therefore restricts the system's use to analysis of samples that have been collected. The system has been used to image particles as large as 1 mm with a resolution of almost micrometres. The system comes in both a 'lab bench' model for analysing retrieved samples and there is also a Submersible FloCAM System that can analyse particles from 5–1,000 μm with a processing rate of up to 10 ml/min. An interesting aspect of the system is that the manufacturers provide a suite of software programs that can be used to both examine and search the database of inferred particle characteristics.

10.3.3.3 FIDO-Φ

FIDO-Φ is a system designed to image the location and abundance of phytoplankton in volumes of approximately 0.5 l. The system does not 'image' individual phytoplankton per se, however, it records either the scattered or fluoresced light from a volume that has been illuminated with a sheet of light 5–7 mm thick and subtends an angle of approximately 30°. In a typical application an area of 25 cm by 25 cm at a range of 80 cm is viewed from a low-light level CCD camera.

Palowitch and Jaffe (1993, 1995) demonstrated a laboratory-based system for imaging the spatial distribution of phytoplankton, which was subsequently used by Jaffe et al. (1998) and Franks et al. (2001) in the ocean in both a monochromatic and multispectral mode. Although this original system was tethered, in 2001 a new autonomous profiling system was used to collect information to 100 m depth on consecutive deployments. Preliminary processing of the data has revealed a large degree of spatial heterogeneity on scales of tens of centimetres. The primary advantages of the device are its ability to assay modestly large volumes (when compared with a conventional fluorometer) and to record the spatial organization of phytoplankton in their native, *in situ* environment.

10.4 Combining acoustics and optics

As considered above, the lower frequency acoustical techniques for sensing zooplankton (50–200 kHz) have the advantage that they can be used at moderate distances (tens to hundreds of metres) and survey large volumes. On the other hand, optical methods can be used for definitive animal identification (providing the magnification is large enough and the water clear). In consideration of this, several investigators have either deployed or synthesized *in situ* devices that attempt to capitalize on the advantages of both optical and acoustical modalities. As these sensing methodologies are complementary, they can work together to permit a much more specific and valid set of inferences to be made. In the opinion of this author, acoustics holds the promise of true non-invasiveness whereas optics holds the promise of a detailed view of the organisms. The use of optics and acoustics in support of each other is documented in this section.

Over several field seasons, a very thorough set of surveys of the George's Bank area were performed using both acoustic and optical techniques. One of the acoustic systems used was the Biomapper (Wiebe, 1997), complemented by the Video Plankton Recorder. In addition, extensive net tows were performed in order to provide yet another degree of characterization. The advantage of the VPR, relative to the net tows, is that the device provides an instantaneous view of animals in its vicinity. As is widely appreciated, net tows integrate over the survey volumes. In the presence of high spatial variability, the VPR can provide a degree of information that is not attainable with either acoustics or with the nets. In this set of surveys the optical information was used to complement the acoustic data, but as the two platforms were being used from two different ships the correspondence between the two was rather a problem. This motivated the development of the new BIOMAPPER II system (Wiebe, 2002), as described above. The system also has a VPR system mounted right on its bow so that some of the problems of judging animal correspondences that were encountered with the previous system could be avoided. Hopefully, the *in situ* identification of animals by the VPR and its coupling with the acoustics will permit the inference of animal taxa to the volumes that are being surveyed by acoustics but have not been imaged with the VPR system.

An example of an *in situ* optical imaging system that was coupled to a system to measure target strengths at multiple frequencies (24 kHz and 120 kHz) is documented by Warren and Stanton (2001). The authors deployed the systems on an ROV that was allowed to drift with the current for short periods of time and thus be relatively non-invasive. Gas-bearing siphonophores were optically imaged and corresponding target strengths were recorded. Although exact correspondences between organism and image were not achieved, a great deal of *in situ* target strength information was recorded which indicated that the siphonophores had large target strengths. A downward-looking sonar at a frequency of 120 kHz permitted the correlation between a more traditional echo-sounding system and the *in situ* sensors.

The OASIS system combines the FishTV multibeam sonar system with a sensitive high-resolution CCD camera. Using the system, exact correspondence between

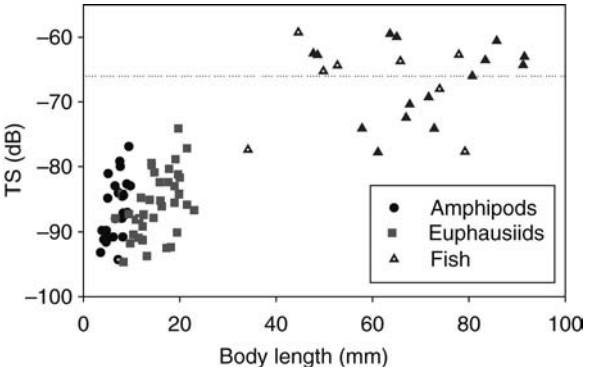

Figure 10.9
Animal body length versus observed *in situ* target strength as a function of animal taxa.
Source: Jaffe et al. (1998*c*).

animal taxa, orientation, and backscatter intensity was obtained (Jaffe et al., 1998*c*). A special location, the 'magic voxel', was identified and when an animal was positioned in this exact three-dimensional spot (as sensed by the acoustics system) an optical image was taken using a red-filtered strobe light for illumination. Deployment of the system over several weeks from a ship moored in Saanich Inlet, British Columbia, resulted in somewhat greater than 100 optical images of animals with coincident target strength information. In order to promote non-invasiveness, a current vane was placed on the armature so that, in adequate current flow, the system could be pointed 'upstream', thus reducing the hydrodynamic signature on the volume being imaged. Behavioural observations of the animal in three dimensions, in real time, were consistent with the conjecture that they were unaware of the device. Figure 10.9 shows a plot of target strength versus taxa and size for the animals which were simultaneously optically imaged and whose *in situ* target strength was recorded.

10.5 Summary and conclusions

The use of acoustics and optical imaging for monitoring *in situ* zooplankton has been discussed. In addition, optical imaging of phytoplankton has been considered. A basic presentation of the underlying physical principals of systems for achieving this purpose has been made and a number of systems have been highlighted.

In the case of zooplankton, the primary contention is that the 'perfect' system for measuring zooplankton abundance and distribution does not exist. It is also somewhat unfortunate that taken together, the acoustical systems, the optical systems, and the net tow systems (not covered here), do not completely fill all the gaps. As all oceanographers know, the ocean is a space and time varying volume that can change rapidly. The characterization of large volumes at even moderate resolution remains a challenge.

The newest generation of deployment opportunities has however great potential to enhance our view of oceanic processes. As demonstrated here, autonomous profiles, whether conducted from a vehicle or a mooring, hold great promise. In addition, the newest generation of Autonomous Vehicles may permit a higher degree of space-time sampling than heretofore possible. The recent demonstration of the Autosub-II system (Brierly et al., 2002), which was deployed in the Antarctic and equipped with multiple frequency split beam sonars in order to detect the locations of euphausiids under ice at ranges of up to 27 km from the ice edge, is an excellent example of the new opportunities that these platforms present.

What can one say to the interested oceanic ecologist about which types of system are ideal for a given situation? In one set of circumstances, ecosystems with high species and morphological diversity, even the multifrequency systems would not be a good choice. As inferred by Holliday and Pieper (1995) the use of very few frequencies can only be conclusive in the presence of very low diversity. For the two frequencies, only one dominant organism is necessary. The higher the diversity, the more frequencies will be needed. However, it cannot be said that for *any* given ecosystem, the use of a great many frequencies will provide an unambiguous outcome. Indeed it is likely that, given the current methods, obtaining animal abundance and species or even taxa identification simultaneously is not possible without using either optical or net tow techniques to supplement this information.

It seems therefore that a prerequisite to using acoustics is to have a certain amount of knowledge about what might be encountered in the field. This type of information

can be obtained from both optical imaging and net tows. Afterwards, some guess can be made about an optimal acoustical package for survey and the range of acoustic frequencies can then be specified. Sample inversions should then be tried under assumptions about species diversity and location that allow the user to gain experience about what results the field expeditions may yield.

In the realm of new instruments, it is the firm belief of this author that broadband echo-counting sonars which can obtain wideband spectra from individuals have the potential to greatly increase our ability to infer species and size. In addition, the prospects for using multistatic scatter in order to deduce animal size seem plausible. This will be especially valuable when coupled with the *in situ* measurement of scattering functions with exact optical measurement of taxa and orientation. In the realm of optics, perhaps the newest generation of very low-light cameras coupled with infrared light will permit a new non-invasive and unambiguous view of these animals in their natural habitat.

References

Anderson, V. C. 1950. Sound scattering from a fluid sphere. *J. Acoust. Soc. Am.*, 22, pp. 426–31.

Ashjian, C. J., Davis, C. S., Gallager S. M. and Alatalo, P. 2001. Distribution of plankton, particles, and hydrographic features across Georges Bank described using the Video Plankton Recorder. *Deep Sea Res. II*, 48(1–3).

Babin, M., Roesler, C. S. and Cullen, J. J. (eds). 2006. *Real-time Coastal Observing Systems for Marine Ecosystem Dynamics and Harmful Algal Blooms: Theory, Instrumentation and Modelling*. Paris, Intergovernmental Oceanographic Commission of UNESCO. (Monographs on Oceanographic Methodology.)

Barans, C. A. and Holliday, D. V. 1983. A practical technique for assessing some snapper/grouper stocks. *Bull. Mar. Sci.*, 33(1).

Baussant, T., Gasser, B., Gorsky, G. and Kantidakis, A. 1993. Mesopelagic micronekton and macrozooplankton observed by echosounding, multiple-net sampling and video profiling across the Almeria-oran front (W. Mediterranean sea). *Ann. Inst. Oceanogr.*, 69(1).

Belcher, E. R. 2003. http://www.apl.washington.edu/programs/DIDSON/DIDSON.html

Benfield, M. C., Davis, C. S., Wiebe, P. H., Gallager, S. M., Lough, R. G. and Copley, N. J. 1996. Video plankton recorder estimates of copepod, pteropod and larvacean distributions from a stratified region of Georges bank with comparative measurements from a MOCNESS sampler. *Deep Sea Res. II*, 43(7–8).

Benfield, M. C., Schwehm, C. J. and Keenan, S. F. 2001. ZOOVIS: a high resolution digital camera system for quantifying zooplankton abundance and environmental data. *Proc. American Society of Limnology and Oceanography, 2001 Aquatic Sciences Meeting*, Albuquerque, NM, 12–17 February.

Brierley, A. S., Fernandes, P. G., Brandon, M. A., Armstrong, F., Millard, N. W., McPhail, S. D., Stevenson, P., Pebody, M., Perrett, J., Squires, M., Bone, D. G. and Griffiths, G. 2002. Antarctic krill under sea ice: elevated abundance in a narrow band just south of ice edge. *Science*, 295, p. 5561.

Buskey, E. J., Deyoe, H., Jochem, F. J. and Villareal, T. A. 2003. Effects of mesozooplankton removal and ammonium addition on planktonic trophic structure during a bloom of the Texas 'brown tide': a mesocosm study. *J. Plankton Res.*, 25(2).

Carder, K. L. 1979. Holographic microvelocimeter for use in studying ocean particle dynamics. *Opt. Eng.*, 18.

Chu, D. Z. and Stanton, T. K. 1998. Application of pulse compression techniques to broadband acoustic scattering by live individual zooplankton, *J. Acous. Soc. Am.*, 104(1).

Davis, C. S., Gallager, S. M., Marra, M. and Stewart, W. K. 1996. Rapid visualization of plankton abundance and taxonomic composition using the video plankton recorder, *Deep Sea Res. II*, 43(7–8).

Davis, C. S., Gallager, S. M. and Solow, A. R. 1992. Microaggregations of oceanic plankton observed by towed video microscopy. *Science*, 257.

Demer, D. A. 1994. Accuracy and precision of echo integration of surveys of Antarctic krill. Ph.D. thesis, University of California San Diego, Scripps Institution of Oceanography.

Demer, D. A., Soule, M. A. and Hewitt, R. P. 1999. A multiple-frequency method for potentially improving the accuracy and precision of *in situ* target strength measurements, *J. Acous. Soc. Am*., 105(4).

De Robertis, A. 2001. Validation of acoustic echo counting studies of zooplankton behavior, *ICES J. Mar. Sci.*, 58.

De Robertis, A., Schell, C. and Jaffe, J. S. 2003. Acoustic observation of the swimming behavior of the euphausiid *Euphausia pacifica* Hansen. *ICES J. Mar. Sci*.

Dolin, L. S. and Levin, I. M. 1991. *Manual of Underwater Vision Theory*. Leningrad, Gidroatomizdat.

Duntley, S. Q. 1963. Light in the sea. *J. Opt. Soc. Am*., 53(2).

Ehrenberg, J. E. 1979. A comparative analysis of *in situ* methods for directly measuring the acoustic target strength of individual fish. *IEEE J. Ocean. Eng.*, 4(4).

Flagg, C. N. and Smith, S. L. 1989. On the use of the acoustic Doppler current profiler to measure zooplankton abundance, *Deep Sea Res.*, 36.

Foote, K. F. 2000. Optical methods. In: Harris et al. (eds), op cit.

Foote, K. F. and Stanton, T. K. 2000. Acoustical methods. In: Harris et al. (eds), op cit.

Foote, K. G. 1998. Broadband acoustic scattering signatures of fish and zooplankton (BASS). *Proc. 3rd European Marine Science and Technology Conference*, Lisbon, 23–27 May 1998.

Franks, P. J. S. and Jaffe, J. S. 2001. Microscale distributions of phytoplankton: initial results from a two-dimensional imaging fluorometer, OSST. *Mar. Ecol. Progr. Ser*., 220.

Genin, A., Jaffe, J. S., Reef, R., Richter, C. and Franks, P. J. S. 2005. Swimming against the flow: a mechanism of zooplankton aggregation. *Science*.

Gerlotto, F., Hernandez, C. and Linares, F. 1998. Experiences with multibeam sonar in shallow tropical waters. *Fish. Res.*, 35(1–2).

Gerlotto, F., Soria, M. and Freon, P. 1999. From two dimensions to three: the use of multibeam sonar for a new approach in fisheries acoustics. *Can. J. Fish. Aquat. Sci*., 56(1).

Gonzalez, R. C. and Wintz, P. 1987. *Digital Image Processing*, 2nd ed. Reading, Mass., Addison-Wesley.

Gorsky, G., Aldorf, C., Kage, M., Picheral, M., Garcia, Y. and Favole, J. 1992. Vertical distribution of suspended aggregates determined by a new underwater video profiler, *Ann. Inst. Oceanogr.*, 68(1–2).

Gorsky, G., Picheral, M. and Stemmann, L. 2000. Use of the Underwater Video Profiler for the study of aggregate dynamics in the North Mediterranean. *Estuar. Coast. Shelf Sci*., 50(1).

Gorsky, G., Prieur, L., Taupier-Letage, I., Stemmann, L. and Picheral, M. 2002. Large particulate matter in the Western Mediterranean. I: LPM distribution related to mesoscale hydrodynamics. *J. Mar. Syst*., 33.

Greenlaw, C. F. and Johnson, R. K. 1983. Multiple frequency acoustical estimation. *Biol. Oceanogr.*, 2.

Griffiths, G., Fielding, S. and Roe, H. S. J. 2002. Biological-physical-acoustical interactions. In: A. R. Robinson, J. J. McCarthy and B. J. Rothschild (eds), *The Sea.* Vol. 12: *Biological-Physical Interactions in the Ocean*. New York, John Wiley & Sons, pp. 441–74.

Griffiths, G., Harris, A. J. K. Mansfield, R. Somers, M. L. Crisp, N. A. H. S., Roe, J. and Smith, B. V. 1997. A multi frequency echo sounder for use within a towed undulating vehicle to study oceanic zooplankton abundance. *Proc. 7th International Conference on Electronic Engineering in Oceanography*, Southhampton, UK.

Harris, R. P., Wiebe, P. H., Lenz, J., Skjodal, H. R. and Huntley, M. (eds). 2000. *ICES Zooplankton Methodology Manual*. New York, Academic Press.

Hobson, P. R. and Watson, J. 1999. Accurate three-dimensional metrology of underwater objects using replayed real images from in-line and off-axis holograms, *Meas. Sci. Tech.*, 10(12).

Hobson, P. R. and Watson, J. 2002. The principles and practice of holographic recording of plankton. *J. Opt. A: Pure Appl. Opt.*, 4(4).

Holliday, D. V. 1974. Doppler structure in echoes from schools of pelagic fish. *J. Acoust. Soc. Am.*, 55(6).

Holliday, D. V. 1977. Two applications of the Doppler effect in the study of fish schools, Rapp. R. v. Reun. Cons. *Int. Explor. Mer*, 170.

Holliday, D. V. and Pieper, R. E. 1989. Determination of zooplankton size and distribution with multifrequency acoustic technology, *J. Conseil – Conseil International pour l'Exploration de la Mer*, 46.

Holliday, D. V. and Pieper, R. E. 1995. Bioacoustical oceanography at high frequencies. *ICES J. Mar. Sci.*, 52.

Holliday, D. V., Donaghay, P. L., Greenlaw, C. F., McGehee, D. E., McManus, M. M., Sullivan, J. M. and Miksis, J. L. 2003. Advances in defining fine- and micro-scale pattern in marine plankton. *ICES J. Mar. Sci.*

Holliday, D. V., Napp, J. M., Greenlaw, C. F. and Stabeno, P. J., 2005. Intra- and Interannula measurements of zooplancton biomass in the Gulf of Alaska using bioacoustical sensors, *J. Acoust. Soc. Am.*, 118 (3).

Jaffe, J. S. 1990. Computer modeling and the design of optimal underwater imaging systems. *IEEE J. Ocean. Eng.*, 15(2).

Jaffe, J. S. 1995. Monte Carlo modeling of underwater-image formation: validity of the linear and small-angle approximations. *Appl. Opt.*, 34(24).

Jaffe, J. S., Franks, P. J. S. and Leising, A. W. 1998*a*. Simultaneous imaging of phytoplankton and zooplankton distributions. *Oceanography*, 11(1).

Jaffe, J. S., McLean, J. Strand, M. P. and Moore, K. D. 2002. Underwater optical imaging: status and prospects. *Oceanography*, 14(3).

Jaffe, J. S., Moore, K. D., Ochoa, B. L., Zawada, D. and Zege, E. 1998*b*. Underwater optical imaging: new hardware and software. *Sea Tech*.

Jaffe J. S., Ohman, M. D. and De Robertis, A. 1998*c*. OASIS in the sea: measurement of the acoustic reflectivity of zooplankton with concurrent optical imaging. *Deep Sea Res. II*, 45(7).

Jaffe, J. S., Ohman, M. D. and De Robertis, A. 1999. Sonar estimates of daytime activity levels of *Euphausia pacifica* in Saanich Inlet. *Can. J. Fish. Aquat. Sci.*, 56(11).

Jaffe J. S., Reuss, E., Mcgehee, D. and Chandran, G. 1995. FTV – a sonar for tracking macrozooplankton in three dimensions, *Deep Sea Res. I*, 42(8).

Jerlov, N. G. 1976. *Marine Optics*, 2nd rev. edn. Amsterdam/New York, Elsevier Scientific.

Katz, J., Donaghay, P. L., Zhang, J., King, S. and Russell, K. 1999. Submersible holocamera for detection of particle characteristics and motions in the ocean. *Deep Sea Res.*, 1, p. 46.

Kino, G. S. 1987. *Acoustic Waves, Devices, Imaging and Analog Signal Processing*. XX, Prentice-Hall. (Signal Processing Series, edited by A. V. Oppenheim.)

Kirk, J. T. O. 1994. Light and photosynthesis in aquatic ecosystems, 2nd ed. Cambridge, UK, Cambridge University Press.

Lavery A. C., Stanton, T. K., McGehee, D. E. and Chu, Dezhang. 2002. Three-dimensional modeling of acoustic backscattering from fluid-like zooplankton. *J. Acous. Soc. Am.*, 111(3).

MacLennan, D. N. and Simmonds, E. J. 1992. *Fisheries Acoustics*. New York, Chapman & Hall. (Fish and Fisheries Series 5.)

Malkiel, E., Alquaddoomi, O. and Katz, J. 1999. Measurements of plankton distribution in the ocean using submersible holography. *Meas. Sci. Tech.*, 10(12).

Mayer, L., Li, Y. C. and Melvin, G. 2002. 3D visualization for pelagic fisheries research and assessment. *ICES J. Mar. Sci.*, 59(1).

McGehee, D. E., Benfield, M., Holliday, V. and Greenlaw, C. 2003. Advanced multifrequency inversion methods for classifying acoustic scatterers. http://zooplankton.lsu.edu/scattering_models/MultifreqInverseMethods.html.

McGehee, D. E., O'Driscoll, R. L. and Traykovski, L. V. M. 1998. Effects of orientation on acoustic scattering from Antarctic krill at 120 kHz. *Deep Sea Res. II*, 45(7), pp. 1273–94.

McGlamery, B. J. 1975. A computer model for underwater camera systems. *Opt. Eng.*, 14(4).

McLean, J. W. and Voss, K. J. 1991. Point spread functions in ocean water: comparison between theory and experiment. *Appl. Opt.*, 30(15).

Medwin, H. and Clay, C. S. 1998. *Fundamentals of Acoustical Oceanography*. Boston, Academic Press.

Mertens, L. E. 1970. *In Water Photography, Theory and Practice*. New York, John Wiley & Sons.

Mertens, L. E. and Replogle, F. S. Jr. 1977. Use of point spread and beam spread functions for analysis of imaging systems in water. *J. Opt. Soc. Am.*, 67(1).

O'Hern T. J., d'Agostino, L. and Acosta, A. J. 1988. Comparison of holographic and Coulter counter measurements of cavitation nuclei in the ocean. *J. Fluid. Eng.*, 110(2).

Owen R. B. and Zozulya, A. A. 2000. In-line digital holographic sensor for monitoring and characterizing marine particulates. *Opt. Eng.*, 39(8).

Palowitch, A. W. and Jaffe, J. S. 1993. Three-dimensional ocean chlorophyll distributions from underwater serial-sectioned fluorescence images. *Appl. Opt.*, 33(14).

Palowitch, A. W. and Jaffe, J. S. 1995. Optical serial sectioned chlorophyl-*a* microstructure. *J. Geophys. Res.*, 100(7).

Petzold, T. J. 1972. *Volume Scattering Function for Selected Ocean Waters*. La Jolla, Calif., Scripps Institution of Oceanography.

Scifish. 2003. www.scifish.com.

Sheng, J., Malkiel, E. and Katz, J. 2003. Single beam two-views holographic particle image velocimetry. *Appl. Opt.*, 42(2).

Shifrin, K. S. 1988. *Physical Optics of Ocean Water*. New York, American Institute of Physics.

Smith, P. F. 1984. *Underwater Photography*. XX, Van Nostrand Reinhold Company Inc.

Stanton, T. K. and Chu, D. Z. 2000. Review and recommendations for the modelling of acoustic scattering by fluid-like elongated zooplankton: euphausiids and copepods. *ICES J. Mar. Sci.*, 57(4).

Stanton, T. K., Chu, Dezhang, Wiebe, P. H. and Clay, C. S. 1993*b*. Average echoes from randomly oriented random-length finite cylinders: zooplankton models. *J. Acous. Soc. Am.*, 94(6).

Stanton, T. K., Clay, C. S. and Chu, Dezhang. 1993*a*. Ray representation of sound scattering by weakly scattering deformed fluid cylinders: simple physics and application to zooplankton. *J. Acous. Soc. Am.*, 94(6).

Stanton, T. K., Wiebe, P. H., Chu, D. Z., Benfield, M. C., Scanlon, L., Martin, L. and Eastwood, R. L. 1994. On acoustic estimates of zooplankton biomass. *ICES J. Mar. Sci.*, 51(4).

Stemmann, L., Picheral, M. and Gorsky, G. 2000. Diel variation in the vertical distribution of particulate matter (>0.15 mm) in the NW Mediterranean Sea investigated with the Underwater Video Profiler. *Deep Sea Res. I*, 47(3).

Strickler, J. R. and Hwang, J. S. 2000. Matched spatial filters in long working distance microscopy of phase objects. In: P. C. Cheng, P. P. Hwang, J. L. Wu, G. Wang and H. Kim (eds), *Focus on Modern Microscopy*. River Edge, N.J., World Scientific Publishing.

Tang, X. O., Stewart, W. K., Vincent, L., Huang, H., Marra, M., Gallager, S. M. and Davis, C. S. 1998. Automatic plankton image recognition. *Artif. Intell. Rev.*, 12(1–3).

Turner, J. T., Doucette, G. J., Powell, C. L., Kulis, D. M., Keafer, B. A. and Anderson, D. M. 2000. Accumulation of red tide toxins in larger size fractions of zooplankton assemblages from Massachusetts Bay. *Mar. Ecol. Progr. Ser.*, 203.

Urick, R. J. 1983. *Principles of Underwater Sound*. XX, McGraw-Hill.

Voss, K. J. 1991*a*. Variation of the point spread function in the Sargasso Sea. SPIE, 1537, *Underwater Imaging, Photography, and Visibility*.

Voss, K. J. 1991*b*. Simple empirical model of the oceanic point spread function. *Appl. Opt.*, 30(18).

Warren, J. D., Stanton, T. K., Benfield, M. C., Wiebe, P. H., Chu, D. and Sutor, M. 2001. *In situ* measurements of acoustic target strengths of gas-bearing siphonophores. *ICES J. Mar. Sci.*, 58(4).

Warren, J. D., Stanton, T. K., McGehee, D. E. and Chu, D. 2002. Effect of animal orientation on acoustic estimates of zooplankton properties. *IEEE J. Ocean. Eng*.

Watson, J., Alexander, S., Craig, G., Hendry, D. C., Hobson, P. R., Lampitt, R. S., Marteau, M. M., Naried, H., Player, M. A., Saw, K. and Tipping, K. 2001. Simultaneous in-line and off-axis subsea holographic recording of plankton and other marine particles. *Meas. Sci. Tech*., 12.

Wiebe, P. H. and Benfield, M. C. 2003. From the Hensen net toward four-dimensional biological oceanography. *Progr. Oceanogr*., 56(1).

Wiebe, P. H. and Greene, C. H. 1994. The use of high frequency acoustics in the study of zooplankton spatial and temporal patterns. *Proc. NIPR Symposium on Polar Biology*, 7.

Wiebe, P. H., Stanton, T. K., Benfield, M. C., Mountain, D. G. and Greene, C. H. 1997. High-frequency acoustic volume backscatter in the Georges Bank coastal region and its interpretation using scattering models. *IEEE J. Ocean. Eng*., 22(3), pp. 445–64.

Wiebe, P. H., Stanton, T. K., Greene, C. H., Benfield, M. C., Sosik, H. M., Austin, T. C., Warren, J. D. and Hammer, T. 2002. BIOMAPER-II: an integrated instrument platform for coupled biological and physical measurements in coastal and oceanic regimes. *IEEE J. Ocean. Eng*., 27(3).

Zege, E. P., Ivanov, A. P. and Katsev, I. L. 1991. *Image Transfer Through a Scattering Medium*. New York, Springer Verlag.

11

Prospects for developing automated systems for *in situ* detection of harmful algae and their toxins

C. A. Scholin, G. J. Doucette and A. D. Cembella

11.1 Introduction

Many methods for identifying harmful algal bloom (HAB) species and their toxins are amenable to automation. Other chapters in this volume concentrate on the use of optical sensors as a means of detecting organisms based on their intrinsic biophysical characteristics. Here, we focus specifically on techniques that target molecular markers as indicators of species identity and toxicity at the cellular level. The approaches used to detect these molecules include:

- application of probes (e.g. lectins, antibodies, DNA, receptors) that bind to unique 'molecular signatures' of given organisms and toxins;
- sample fractionation protocols that involve sequential separation and detection of specific molecules based on their inherent physical and chemical properties;
- methods wherein fractionation procedures and molecular probes are used concurrently.

The aim is to examine the potential for developing novel instrumentation that enables unattended *in situ* application of these techniques and employs telemetry for reporting results in real time. Although such instrumentation is not yet available to the general oceanographic and marine science community, a number of research programmes are providing a glimpse of how this goal might soon be achieved. From this perspective, we consider the challenges involved in detecting a wide array of organisms and bioactive compounds in natural samples and outline the current approaches. Furthermore, we define the technological constraints associated with automating these methods for field deployment, specifically with respect to unattended sample collection, processing and signal transduction. Finally, we focus on a newly developed, experimental platform designed to use molecular probe technology for the concurrent *in situ* detection of HAB species and their toxins, describing recent research activities and plans for implementing this technology in the near future.

11.1.1 Need for detection of HAB species and toxins *in situ*

Development of methods and instruments suitable for detecting HAB species and phycotoxins *in situ* is dictated by regulatory, management and research requirements. The ability to provide coastal resource managers with advanced warning of bloom development or the presence of harmful species and their toxins at low but potentially problematic concentrations would clearly enhance HAB research, management and mitigation

efforts. This is especially true if a network of sensors was available for conducting synoptic analyses and thus minimizing the need for ship-based sample collection. The same technology would also be useful for triggering 'event response' field surveys. Ultimately, arrays of *in situ* sensors could provide the data-streams needed to drive biophysical models designed to forecast the development or movement of a bloom event. This capability would offer new opportunities for mitigating the profound ecosystem and economic impacts associated with HABs (e.g. Hoagland et al., 2002).

11.1.2 Diversity of HAB species and their toxins

Only a few dozen of the thousands of algal species present in the oceans are considered harmful and/or toxic (Smayda, 1997). Nevertheless, the HAB species of concern to either human or ecosystem health constitute a diverse array of taxa representing most major classes of microalgae, such as dinoflagellates, diatoms, raphidophytes, chrysophytes, prymnesiophytes and pelagophytes, plus other protistan groups (e.g. silicoflagellates and ciliates) and even prokaryotes (certain cyanobacteria; see Cullen, 2007 – Chapter 1 this volume). Species belonging to these phylogenetically distinct groups encompass many sizes, shapes, cell wall types, pigment compositions, optical properties, genetic signatures and nutritional modes, and they occur across a wide range of habitats from the pelagic zone to the benthos, including epiphytic and epizootic taxa. Harmful effects can be expressed through a variety of mechanisms, such as damage to fish gills, oxygen depletion, release of harmful metabolites (e.g. ammonia), light attenuation and production of toxins. Recent comprehensive reviews of HAB species, their associated toxins, and environmental and human health consequences are found elsewhere (Van Dolah, 2000*a*, 2000*b*; Landsberg, 2002; Hallegraeff et al., 2003; Sellner et al., 2003).

The phycotoxins are often grouped according to the various intoxication syndromes they cause, including paralytic shellfish poisoning (PSP; caused by saxitoxin and derivatives), neurotoxic shellfish poisoning (NSP; caused by brevetoxins), amnesic shellfish poisoning (ASP; caused by domoic acid), diarrhetic shellfish poisoning (DSP; caused by okadaic acid/dinophysistoxins), azaspiracid poisoning (AZP; caused by azaspiracids), ciguatera fish poisoning (CFP; caused by ciguatoxins) and cyanobacterial toxin poisoning (CTP; caused by microcystins/anatoxins/cylindrospermopsin, etc.).

Phycotoxins produced by eukaryotic microalgae and cyanobacteria are extremely diverse, varying both chemically (e.g. molecular weight, polarity, solubility, etc.) and biologically (e.g. toxicity, pharmacologic target, etc.). Several reviews of harmful eukaryotic microalgae (Bates, 1998; Cembella, 1998; Wright and Cembella, 1998) and cyanobacteria (Carmichael, 2001) considered the ecophysiological role or human health effects of these toxins, while other recent treatments have highlighted the structural-functional relationships and biosynthesis of these compounds (e.g. Shimizu, 2000; Cembella, 2003). In any case, the properties and structures of different phycotoxins provide 'chemical signatures' that potentially can be used to reveal the presence of some HAB organisms. Therefore, the toxin section of this review concentrates on detection methods suitable for use with natural samples, emphasizing both particulate and dissolved phases.

11.1.3 Challenges associated with detecting HAB species and their toxins

Harmful algal species have historically been distinguished based on differences in cell morphology and ultrastructure using light- and electron microscopy. However,

traditional detection methods that rely on microscopy can be logistically difficult to implement when hundreds of samples must be processed soon after collection and in a very short period. Some HAB species exert their negative effects only upon reaching high cell concentrations, which can result in discoloration of the water (e.g. red tide). These high-biomass blooms have been associated with severe impacts, such as destruction of benthic habitat through excessive light attenuation (e.g. *Aureococcus*, Bricelj and Lonsdale, 1997) and fish kills (e.g. *Karenia*, Steidinger et al., 1998; *Heterosigma*, Taylor, 1993), which can result from direct toxicity, physical damage, or a combination thereof. For such high-biomass blooms, particularly when cells are aggregated primarily at or near surface and the bloom is virtually monospecific, direct optical observations provide a very tractable means of detecting bloom events (Cullen, 2007; Schofield et al., 2007 – Chapters 1 and 3 this volume). Nevertheless, discriminating 'harmful' from 'benign' blooms that can occur in the same region is critical (e.g. blooms of *Pseudo-nitzschia*; e.g. Bates et al., 1993; Scholin et al., 2000), yet such distinction is not usually practical based on remote and/or *in situ* optical sensors.

Other HAB species exert harmful effects at concentrations far below those that lead to visually discoloured water and may represent only a small fraction of the total number of cells present in the environment. For example, toxigenic species of the marine dinoflagellates *Alexandrium* and *Dinophysis* can cause toxicity in pelagic and benthic food webs even at concentrations below 10^3 cells l^{-1}. Such 'blooms' of *Alexandrium* and *Dinophysis* seldom dominate phytoplankton assemblages, and because they may be concentrated in thin subsurface layers or, alternatively, highly dispersed throughout the upper water column (Anderson, 1998; Maestrini, 1998), they can be quite recalcitrant to detection by remote and *in situ* optical sensing systems. A further complication arises from the fact that certain populations of a given 'toxigenic' taxon may vary in the amount of toxin per cell in response to fluctuating environmental regimes (e.g. Pan et al., 1998; Cembella et al., 1998; Scholin et al., 2000), or toxicity may be restricted to only certain species or 'strains' of species as those organisms are defined morphologically. (e.g. Bates, 1998; Lundholm et al., 2003). To address these challenges, researchers have explored the use of molecular markers as a basis for detecting HAB species and toxins (Anderson, 1995; see Section 11.2). While molecular markers do offer advantages for discriminating between organisms at levels not possible using optical approaches, there nonetheless remain many technical considerations that must be taken into account to use such signatures as the basis for developing instruments meant to function *in situ*. For example, the definition of a 'species', the physiological status of a cell, and the choice of assay format (e.g. whole-cell versus cell-free) all introduce analytical biases, factors that ultimately affect how well a given assay appears to perform for a given target in a particular geographical region under a range of variable, natural conditions.

Recognition of organisms loosely referred to as 'species' and 'strains' is central to the development and application of molecular probes and therefore deserves further consideration. Researchers have long recognized that groups of organisms defined on the basis of molecular characteristics, such as toxins, cell surface antigens, or DNA sequences, are not always consistent with the same groups as defined by cell morphology. For example, molecular characterization of the *Alexandrium tamarense/catenella/fundyense* species complex (Scholin, 1998) revealed many distinct strains (hypothesized geographic races) that share an overlapping set of morphological features. Despite this understanding, there is still no internationally adopted standard for recognizing molecularly divergent strains of the same species (defined morphologically), nor

an accepted standard for referring to strains that are morphologically separable but considered 'molecularly indistinguishable'. One difficulty lies in the fact that morphological characteristics can result from the expression of multi-gene complexes modified by the environment, whereas taxonomic molecular probes are typically targeted to a small and probably unrelated portion of the genome (e.g. segments of hypervariable domains of the large- and small-subunit ribosomal RNA molecules [LSU, SSU rRNA] and the genes that encode them [rDNA]). The genes that enable phycotoxin production are presumbably subject to different selective pressures and they may even be derived from endosymbionts or via other lateral gene transfers. Concepts relating to the definition of species therefore have a profound impact on the design and application of molecular-based assays for HAB research and monitoring. For example, there are *no* 'species-specific' molecular probes for *A. tamarense, A. catenella* or *A. fundyense*, as these species are defined based on cell morphology. There are, however, 'geographic race' or region-specific probes. This presents a challenge in attempting to validate the utility of molecular-based assays, particularly when working with natural samples where multiple geographic races of a target species could co-occur. Problems with nomenclature aside, the lesson learned thus far is that distinct 'populations' of a given species may exist at the molecular level. Similarly, groups of species that are considered morphologically, and thus taxonomically, distinct may be very similar or even identical based on selected molecular characteristics. These scenarios must be taken into account when designing and evaluating species-specific molecular-based detection systems and relating results of such tests to traditional, internationally accepted methods for identifying species that are based on microscopy (for a detailed example of this see Lundholm et al., 2003).

Another important consideration is determining to what extent the physiological status of cells influences their recognition by species-specific molecular probes. Studies of *Karenia mikimotoi* (syn. *Gymnodinium mikimotoi*, *G. nagasakiense*, *G. aureolum*), *Alexandrium fundyense*, *Pseudo-nitzschia multiseries* and *Heterosigma akashiwo* involving antibodies targeting cell surface antigens and oligonucleotides targeting rRNA sequences demonstrate that cell physiology affects the reactivity of these probes (for details see e.g. Vrieling et al., 1997; Anderson et al., 1999; Bates et al., 1999; Tyrrell et al., 2000; Peperzak et al., 2001). The degree to which probe reactivity is influenced by physiological status (nutrient limitation, light regime, growth stage in culture) depends on the type of probe employed as well as species-specific and methodological variables. For example, quantitation of *A. tamarense* and *A. ostenfeldii* cells in mixed natural assemblages from the North Sea, comparing whole-cell hydridization of filtered cells using species-specific rRNA-targeted probes with careful counts by the classic Utermöhl inverted-microscope method, revealed a substantial underestimate of cell concentration for both species by the probe method relative to the conventional optical counting technique, possibly because the rRNA content of some cells was low (for details see John et al., 2003). Such discrepancies also depend greatly on whether probes are applied to intact cells or to cell homogenates, as these approaches do not strictly measure the same thing, in turn making it difficult to quantitatively relate results obtained by one method versus the other when a wide range of sample types is considered (e.g. Scholin et al., 1999).

Culture studies provide an invaluable source of information for gauging the limitations of species-specific molecular detection strategies. Yet such investigations alone are not sufficient to determine whether a given approach is acceptable for routine use on natural samples in a region. For example, cross-reactivity tests using cultured taxa survey only a small fraction of naturally occurring species. Similarly, as a cultured

strain is not necessarily representative of a given species in all geographical areas, the absence of observed cross-reactions in culture studies does not guarantee that a detection method is taxon-specific with respect to the diversity of organisms and compounds found in nature. Also, the range of environmental variables (physical, chemical, biological) examined in laboratory cultures clearly does not encompass all conditions to which natural populations are exposed and may even exceed boundaries typical of natural conditions. Consequently, assessing the utility of novel molecular detection strategies depends a great deal on direct testing of natural samples and establishing validation methods relevant to the range of conditions and sample types likely to be encountered during routine research and monitoring activities.

There are also many issues to be addressed when developing detection techniques for phycotoxins, particularly when rapid diagnostics and near real-time results are required. The broad chemical and structural diversity of phycotoxins, coupled with differences in intrinsic potency and their susceptibility to biotransformation, accounts for many of the challenges associated with the detection of these compounds. Each of the phycotoxin classes comprise a suite of structurally similar analogues that typically share a common pharmacologic target and mode of action (Shimizu, 1996, 2000), yet can vary widely in their intrinsic toxic potencies (Lewis, 1995; Fernández et al., 2003). Among the phycotoxin classes, the molecular weights of specific analogues can vary by more than 2 orders of magnitude, for example from domoic acid (*c.* 300 Da) to maitotoxin (*c.* 32,000 Da), and the solubility spectrum ranges from hydrophilic to lipophilic (Van Dolah, 2000*b*; Quilliam, 2003*b*). Additional complicating factors for the detection and quantitation of phycotoxins in natural samples include:

- occurrence of certain toxins in particulate (i.e. associated with intact cells or other particulate material) form and/or dissolved in seawater (Bates, 1998; Pan et al., 2001);
- highly variable levels of cellular toxins depending on the nutritional status of the population (Cembella, 1998);
- formation of structurally related catabolites and adducts during trophic transfer (frequently with higher or lower toxicity than the original toxin molecule; Bricelj and Shumway, 1998; Poli et al., 2000; Teegarden and Cembella, 1996);
- the potential for some sample types (e.g. plankton, fish, seawater, etc.) to interfere with certain detection methods (Lefebvre et al., 1999; Quilliam, 2003*b*);
- the current lack of a universal extraction and clean-up method for all phycotoxins from a variety of sample types.

In addition, the release of phycotoxins in dissolved form into the surrounding water (e.g. Landsberg, 2002) and subsequent chemical alterations of that extracellular toxin (Quilliam, 1996; Quilliam and Ross, 1996) pose many challenges for detecting and quantifying these metabolites. Although some of these issues must be taken into account regardless of the technique employed to detect a toxin (e.g. variation in cellular toxin content), other problems can be minimized or even eliminated by selection of the appropriate detection method. For example, approaches based on the detection of toxic activity rather than toxin structure can deal effectively with biotransformations, as any accompanying changes in toxicity are actually integrated into the measurement being reported (see below for details). On the other hand, particular approaches lend themselves better to automation or remote deployments, or for detection of certain phycotoxin classes, so the application (i.e. regulatory, monitoring, research, etc.) generally drives the decision regarding the method of choice.

11.2 Molecular methods for detecting HAB species and toxins

11.2.1 Targets and tools for detecting HAB species

There are several approaches for identifying harmful algal species in natural samples:

- direct visualization of individual cells using microscopy (e.g. Sournia, 1978; Hall, 1999);
- portable and *in situ* sensors capable of detecting optical features of cells (e.g. Gentien et al., 1995; Kirkpatrick et al., 2000; Sellner et al., 2003; Flow Cytometer And Microscope;[50] CytoBuoy;[51] see also Schofield et al., 2007 – Chapter 3 this volume);
- molecular probes that reveal individual taxa (e.g. Scholin et al., 2002).

This section focuses on the latter strategy, in particular detection of cell surface moieties and nucleic acids (RNA and DNA). Each of these molecular targets can be visualized and/or quantified using combinations of biochemical techniques and application of lectin, antibody or nucleic acid probes coupled with an appropriate signal transduction system. Reviews of these techniques, protocols and use case scenarios for application are found elsewhere (e.g. Anderson, 1995; Scholin and Anderson, 1998; Rhodes et al., 1998*a*; Litaker and Tester, 2002; Scholin et al., 2002). Techniques that show a strong potential for use in near real-time detection systems that are either human-assisted (e.g. shipboard, dockside, etc.) or deployed for remote operation *in situ* (i.e. in-water, unattended) are emphasized here.

11.2.1.1 Cell surface and intracellular biomarkers: lectins and antibodies

Lectins and antibodies are commonly used to reveal cell surface moieties diagnostic of particular HAB species and strains. Lectins are non-enzymatic secreted proteins (commonly glycoproteins) that bind to specific sugar residues. Potential binding sites associated with microalgae include cell-surface glycoproteins, polysaccharides and chitin (Sengbusch and Müller, 1983; Waite et al., 1995; Hori et al., 1996). Many fluorescently labelled lectins are commercially available (Scholin et al., 2002). These probes have been used to differentiate among algal species and even between strains of the same species (Costas et al., 1993; Costas and Rodas, 1994), employing epifluorescence microscopy, or more rarely flow cytometry, to detect labelled cells. Typcially, a suite of lectins is applied to empirically reveal unique binding patterns that discriminate species of interest from other non-target organisms. Lectin-based identification has been incorporated into some harmful algal monitoring programmes (Rhodes et al., 1995, 1998*b*; Cho et al., 1998, 2000, 2001); however, this technique is not in widespread use because accurate identification usually requires application of multiple lectins with different specificities, binding profiles may vary depending on the geographical origin of the organisms in question, and some species show altered lectin-binding profiles depending on growth rate and physiological condition. Despite these limitations, lectin-based identification methods are relatively simple and rapid so long as care is taken to ensure that labelling patterns are reliable indicators of given species in well-defined geographical regions (Scholin et al., 2002).

[50]FLOWCAM: www.fluidimaging.com
[51]www.cytobuoy.com

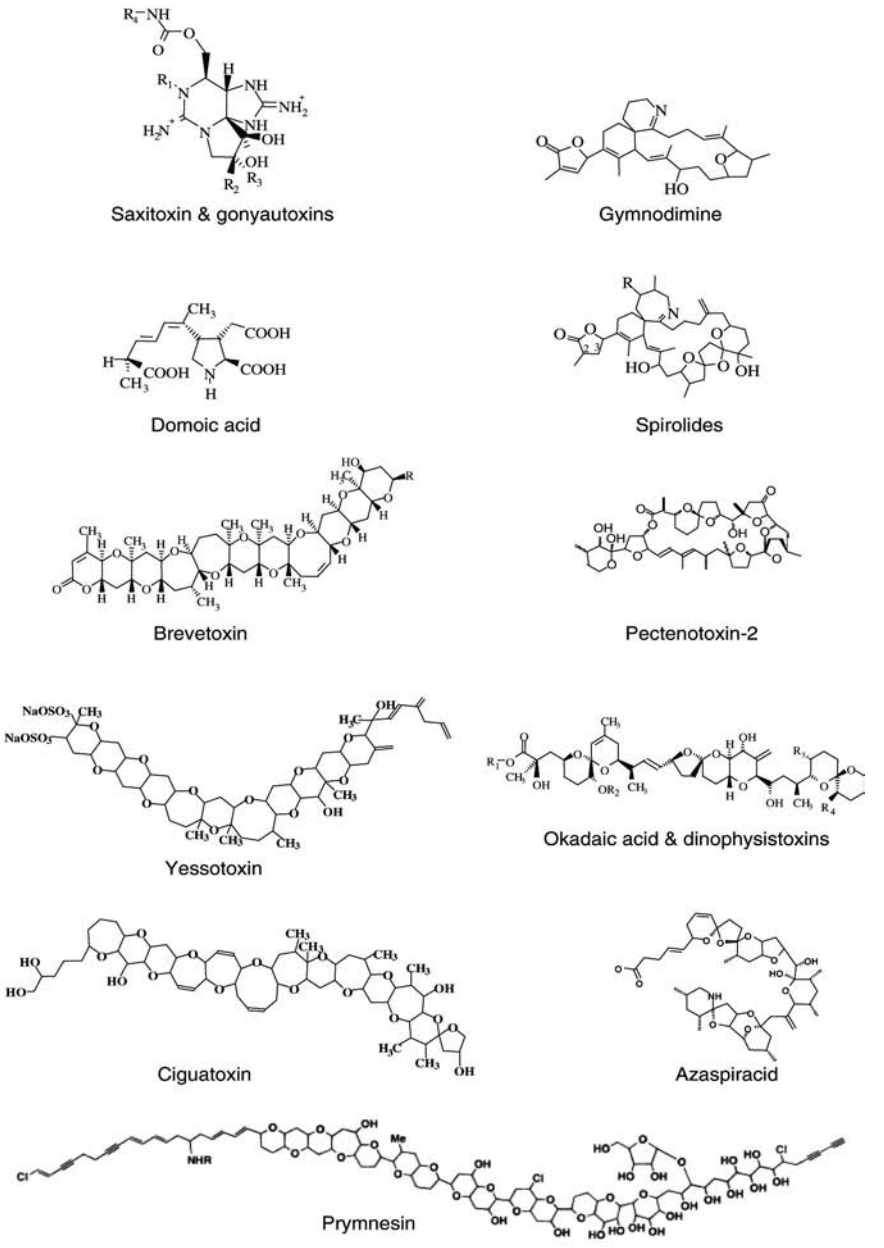

Figure 11.1
Examples of chemical structures of various phycotoxins produced by eukaryotic microalgae, including hydrophilic N-containing neurotoxins (saxitoxin analogues, domoic acid), ladder-frame polyethers (brevetoxin-B, yessotoxin, ciguatoxin), cyclic imine toxins (spirolides, gymnodimine, pinnatoxin), linear and macrocyclic polyethers (okadaic acid, pectenotoxin-2) and hybrid forms (azaspiracid and prymnesin).

Within the last decade, antibodies have also been used for discriminating among algal taxa (Vrieling and Anderson, 1996) and they are now applied routinely in a number of research and monitoring programmes. Numerous antibodies have been developed against cell surface antigens that are specific for a wide range of harmful taxa (Anderson, 1995; Scholin and Anderson, 1998). These taxa include various dinoflagellates (e.g. *Alexandrium* spp.: Sako et al., 1993; Adachi et al., 1993; *Karenia* spp. [as *Gymnodinium nagasakiense* or *Gyrodininium aureolum*]: Nagasaki et al., 1991; Vrieling et al., 1994; Peperzak et al., 2001), diatoms (e.g. *Pseudo-nitzschia* spp.: Bates et al., 1993; Peperzak et al., 2001), raphidophytes (e.g. *Chattonella* spp.: Uchida et al., 1989) and pelagophytes (e.g. *Aureococcus anophagefferens*: Anderson et al., 1990, 1993).

Preserved, intact cells of the target organism or cellular subfractions (e.g. surface membranes, thecal plates and cell coating, mucus layers, etc.) are used as an immunogen to generate antisera. The resulting antibodies are produced against one (monoclonal) or more (polyclonal) unidentified antigens present on the cell surface at the time of harvesting and may include polysaccharides (Ross and Bates, 1996), proteins (Nagasaki et al., 1991), lipopolysaccharides (Schmidt et al., 1980), or combinations thereof. Antibodies are screened for reactivity against the target species, as well as against a range of closely and distantly related microalgal taxa to confirm the specificity of the recognition. In addition, as the composition of cell surface antigens may vary with physiological status, antibody screening should include confirmatory testing against the target species grown under different culture conditions (e.g. Anderson et al., 1999; Peperzak et al., 2000).

At present, detection of antibody-cellular antigen reactions typically relies on a fluorophore-based reporting system and epifluorescence microscropy or flow cytometry, an approach collectively termed *immunofluorescence*. Application of this technique to microalgae and specifically to HAB taxa has been extrensively reviewed (e.g. Vrieling and Anderson, 1996; Scholin et al., 2002). It should be noted that while antibodies have also been produced against *intracellular* targets (e.g. tubulin, rubisco [ribulose bisphosphate carboxylase], PCNA [proliferating cell nuclear antigen]) in microalgae (Lin and Carpenter, 1996) and certain phycotoxins within harmful species (Anderson and Cheng, 1988; Lawrence and Cembella, 1999), in all these cases the focus was directed primarily towards ecophysiological characteristics rather than species identification.

Application of antibody probes for identifying HAB taxa in natural samples has favoured probes targeting cell surface antigens, probably reflecting their ease of preparation and the absence of a requirement for cell permeabilization. The potential role of automated flow cytometric methods in immunofluorescence-based detection of HAB taxa has been explored in several studies with cultured and natural populations (reviewed by Peperzak et al., 2000). For example, Vrieling et al. (1995) found that antibody-labelled cells of the ichthyotoxic dinoflagellate, *Karenia mikimotoi* (as *Gyrodinium aureolum*), collected from the North Sea could be identified via flow cytometry. However, quantification relative to conventional optical microscope counts was poor due to loss of cells during sample processing, an observation also reported for natural populations of other species (e.g. *Alexandrium* spp.; Sako et al., 1996). Thus, while immuno-flow cytometry shows promise for automated detection of HAB species, the loss of cells during antibody staining and other practical limitations, such as the cost, processing time, and availability of suitably specific antibodies, remain obstacles.

An alternative immunological approach based on a high throughput, enzyme-linked immunosorbant assay (ELISA) incorporating a monoclonal antibody against the brown tide pelagophyte *Aureococcus anophagefferens* has been successfully employed

in monitoring programmes in the north-eastern USA (Caron et al., 2003). Beyond this one case, however, ELISA-based methods for cell detection have seen little use, probably because of difficulties associated with sample handling and processing, the potential for increased background (i.e. lower signal-to-noise ratio) when biomass is highly concentrated in an effort to reveal rare target cells, and the availability of other methods that offer opportunities to detect multiple species in a single sample (e.g. DNA probe arrays).

11.2.1.2 Nucleic acids

Nucleic acids constitute a class of target molecule that has been used extensively for discriminating between and among HAB taxa. In particular, the rDNA cistron and expressed rRNAs have been employed widely for this purpose. Extensive public domain sequence databases[52] are available for rRNA genes, permitting robust comparisons of sequence data. Ribosomal gene sequences contain regions that range from highly conserved to highly variable, providing resolution from broad phylogenetic groupings to increasingly narrower taxa such as genera, species, and in some cases unique strains. The high copy number of rRNA per cell makes it an attractive hybridization target. Although rRNA sequences are very useful genetic markers, they do not always provide a basis for distinguishing between and among populations and strains of the same species. As a result, other gene sequences and genomic approaches are being adopted by researchers. For example, Bolch et al. (1999) have used the phycocyanin intergenic spacer region to reveal differences among species of the toxigenic cyanobacterial genus *Nodularia*, Dyble et al. (2002) have studied genes involved in nitrogen metabolism as a basis for discriminating among isolates of the cyanobacterium *Cylindrospermopsis raciborskii*, and Zhang and Lin (2002) have targeted the mitochondrial cytochrome *b* gene to detect *Pfiesteria piscicida*. Alternative genomic strategies that do not depend on the conservative properties of single genes for taxon discrimination are also increasingly available. For example, RAPD (random amplification of polymorphic DNA; Berg et al., 1994) assays could prove useful for discriminating between organisms at the subspecific and population level; however, this technique is somewhat compromised by the lack of stability and reproducibility. Another more robust alterative, AFLP (amplified fragment length polymorphism) can effectively discriminate among members of a major species complex within *Alexandrium* (John et al., 2004), but its use is at present confined to the laboratory and not obviously amenable to field deployment for natural populations.

Nucleic acid probes may be applied in either whole-cell or cell-free formats. The whole-cell approach has typically involved use of oligonucleotides that target rRNA sequences found inside the cell. This method is referred to as fluorescence *in situ* hybridization (FISH) and is similar to protocols for applying lectins and antibodies. Microalgal cells labelled using the FISH method can be examined directly by epifluorescence microscopy or analysed by flow cytometry (e.g. Peperzak et al., 2001). Laser scanning solid phase cytometry (Chemunex, France), which involves scanning of fluorescently-tagged cells captured on filter membranes, rather than in suspension as for flow cytometry, is a recently introduced alternative detection method for FISH-labelled cells. Protocols are being developed for application of this semi-automated method in detecting harmful species such as *Alexandrium minutum* and *Pseudo-nitzschia* spp., ultimately within the context of routine HAB monitoring programmes (Eller and Medlin, 2002).

[52]For example, rdp.cme.msu.edu/html/

The whole-cell hybridization approach has been developed and applied extensively for the detection of many harmful algae, including dinoflagellates (e.g. *Alexandrium* spp.: Adachi et al., 1996; *Dinophysis* spp.: Rehnstam-Holm et al., 2002; *Karenia* spp.: Mikulski et al., 2005; *Pfiesteria* spp.: Rublee et al., 1999; Litaker et al., 2002), diatoms (e.g. *Pseudo-nitzschia* spp.: Scholin et al., 1997; Miller and Scholin, 1996, 1998, 2000; Peperzak et al., 2001), and raphidophytes (e.g. *Heterosigma akashiwo*: Tyrrell et al., 2001; *Fibrocapsa japonica*: Tyrrell et al., 2001; *Chattonella subsalsa*: Tyrrell et al., 2001). The FISH technique is used routinely for identifying *Alexandrium* spp. and *Pseudo-nitzschia* spp. in the national HAB monitoring programme in New Zealand (Rhodes et al., 1998*a*, 1998*b*, 2000, 2001). Probes for additional HAB species present in the coastal waters of New Zealand, including *Karenia* spp., *Heterosigma* and *Fibrocapsa*, are currently being tested (Rhodes et al., 2000, 2002).[53] Other countries are also exploring the use of FISH probes as a means of enhancing routine phytoplankton monitoring programmes (e.g. Cho et al., 2002). Species-specific rRNA-targeted FISH probes for co-occurring populations of *A. tamarense* and *A. ostenfeldii*, which produce different toxins and are difficult to resolve by casual optical microscopic observations as performed in routine HAB monitoring programmes, have proved to be effective in taxonomic discrimination of *Alexandrium* in the North Sea (John et al., 2003) and in coastal Nova Scotian embayments related to aquaculture (Rafuse et al., 2003). Nevertheless, quantative analysis by FISH probes must be interpreted with several caveats, including possible loss of cells during sample processing and the fact that the abundance of ribosomes within a cell can vary in proportion to growth rate, which alters the label intensity of individual cells (e.g. Anderson et al., 1999; Peperzak et al., 2000). Weakly labelled cells may be difficult to visualize, count, and discriminate from other material in natural samples, leading to underestimates of cell abundance.

In contrast to methods that rely on labelling whole cells, where cells must remain intact throughout the labelling procedure, techniques for the application of probes to cell-free extracts begin with cell disruption. Signature molecules are liberated and may undergo some selective purification and/or enzymatic amplification (such as the polymerase chain reaction, PCR) prior to detection. Cell-free assays generally offer greater throughput and potential for detecting simultaneously many more molecular signatures in a single sample than techniques based on intact cells. The most prevalent techniques for detecting HAB taxa in the cell-free format include sandwich hybridization (SH) and methods involving PCR (e.g. Scholin et al., 2002; Litaker and Tester, 2002).

The SH detection approach is applicable to both DNA and RNA (e.g. Van Ness and Chen, 1991, Medlin et al., 2002), but for HAB research has more commonly been directed to rRNA targets. The SH technique as developed by Scholin et al. (1996, 1999) relies on chemical lysis of the algal cells to release the target molecule (i.e. rRNA), followed by binding of the target in the crude homogenate by a taxon-specific 'capture' probe immobilized on a solid support (e.g. bead, membrane, etc.). Hybridization of a 'signal' probe to another region of the immobilized rRNA follows the capture step, and results of the assay are recorded using one of several reporting systems (i.e. absorbance, fluorescence, chemiluminesence, etc.; Scholin et al., 1996). While the SH method precludes the direct microscopic observation of labelled target cells, this technique does allow for rapid, high throughput sample processing and is highly amenable to automation. To date, however, SH reagent 'kits' as described by Scholin et al. (1999,

[53]www.cawthron.org.nz/phytoplankton_lab.htm

2002) have at times proved difficult to obtain consistently from a commercial vendor (e.g. Saigene Corp.) with a vested interest in envrironmental research and monitoring, thereby limiting widespread testing and application of this technique. Other methods that use the SH concept but that are based on fibre-optic coupled probes and fluorescence detection schemes are emerging as an active area of research (e.g. Ferguson et al., 2000; Anderson et al., unpublished) as well as electrochemical-based signal transduction (e.g. Medlin et al., 2002; see also Alderon Biosciences).[54]

In its current iteration, the SH method as used by Scholin et al. (1999) employs a robotic sample processor, a 96-well plate-based format and a colorimetric signal-reporting system. This assay is currently being evaluated by New Zealand researchers with the aim of incorporating it into their existing phytoplankton monitoring programmes (Rhodes et al., 2000 and unpublished). The SH technique has been applied to the detection of diatoms (*Pseudo-nitzschia* spp.; Scholin et al., 1996, 1997, 1999), raphidophytes (*Heterosigma*, *Fibrocapsa*, *Chattonella*; Tyrell et al., 2000, 2002; Tyrrell, unpublished), and dinoflagellates (*Alexandrium* spp., *Karenia* spp. and a *Pfiesteria*-like organism isolated in Florida; Scholin, Anderson, Haywood and Steidinger, unpublished).

A number of investigators are testing the SH approach against results obtained by direct counts of unlabelled or labelled cells (i.e, whole-cell assay) in comparative studies of natural HAB populations, such *Alexandrium* spp. (e.g. Anderson et al., 2002; Anderson et al., 2005), *Pseudo-nitzschia* spp. (e.g. Parsons et al., 1999; Scholin et al., 1999, 2000), *Heterosigma* (Tyrrell et al., 2001, 2002; O'Halloran et al., 2006), *Fibrocapsa* (Tyrrell et al., 2001; Rhodes et al., unpublished), and *Karenia* (Haywood et al., 2002). A fully deployable field system based on the SH technique (i.e. Environmental Sample Processor, ESP), is currently being explored for remote, near real-time detection of several HAB species, groups of marine bacteria, and invertebrate larvae (see Section 11.4; Scholin et al., 1998; Goffredi et al., 2006).

Detection methods for HAB taxa that employ PCR also require binding of complementary strands of nucleic acids. The PCR technique makes it possible to enzymatically amplify defined fragments of the target organism's genome (e.g. Innis et al., 1995). Assays based on PCR require primers (i.e. oligonucleotides), extraction of nucleic acids from samples, an enzymatic reaction mixture, and application of one or more thermocycling protocols. Protocols for end-point PCR, real-time PCR, and PCR heteroduplex mobility assays are reviewed by Scholin et al. (2002). PCR-based techniques for detecting and discriminating between and among HAB species are becoming increasingly common (e.g. *Alexandrium* spp.: Penna and Magnani, 1999, 2000; *Karenia* [as *Gymnodinium*)]: Godhe et al., 2001; *Pfiesteria* spp.: Bowers et al., 2000, Coyne et al., 2001; Rublee et al., 1999, 2001; Saito et al., 2002; Zhang and Lin, 2002; *Cylindrospermopsis*: Dyble et al., 2002; *Microcystis*: Ouellette et al., 2002). PCR methods are highly sensitive and have been employed to detect single vegetative cells and cysts of harmful species (Bolch, 2001). Moreover, recent developments in real-time PCR have yielded portable instrumentation suitable for field applications[55] that will probably be incorporated into HAB monitoring and research programmes in the near future.

In addition to optical-based reporting systems, detection of nucleic acids can also be accomplished electrochemically (reviewed by Wang, 2002*a*). 'Lab-chips' that

[54]www.alderonbiosciences.com
[55]For example, Cepheid, Sunnyvale, California: www.cepheid.com

incorporate electrochemical-based detection of target nucleic acids in array formats are commercially available (e.g. eSensor, Motorola Life Sciences). Electrochemical reporting systems are projected by some to be essential for developing a new generation of devices that make portable, field-based detection of harmful algal species tractable (e.g. Litaker et al., 2002; Medlin et al., 2002). At this time, however, requirements for preparing samples (e.g. cell homogenization, nucleic acid purification, PCR amplification, etc.) for detection with electrochemical transducers are best met in a conventional laboratory setting, but this situation is likely to change in the near future.

11.2.2 Approaches for HAB toxin detection

11.2.2.1 Background

As a first approach to designing a detection system for a particular group of marine microalgal toxins, it is important to consider the targeted molecules' structural homologies (e.g. for immunodiagnostic methods), mode of action (e.g. for receptor and ion-channel assays), and physico-chemical properties (e.g. for chromatographic separation and subsequent optical, electrochemical, or mass-specific detection). For example, some of the diverse phycotoxins produced among marine microalgae (Figure 11.1) may be structurally characterized as: (a) linear and cyclic amines, e.g. domoic acid and spirolides, respectively; (b) linear and macrocyclic polyethers, e.g. okadaic acid/dinophysistoxins and pectenotoxins, respectively; (c) ladder-frame polyethers, e.g. ciguatoxins and brevetoxins; and (d) guanidine derivatives (saxitoxin and analogues), and these properties can be exploited to help 'tune' detection strategies that favour one class of toxins over another. Access to purified toxin standards remains an essential element for developing, refining and validating phycotoxin detection methods suitable for use with a wide range of sample types. At present, methods for detecting phycotoxins can be grouped into three general categories: chemical analyses (Luckas et al., 2003; Quilliam, 2003*a*, 2003*b*), *in vitro* assays (Cembella et al., 2003) and *in vivo* assays (Fernández et al., 2003). Extensive reviews of those methods are found elsewhere (see relevant chapters in Botana, 2000, Hallegraeff et al., 2003), but reflect primarily a regulatory perspective for phycotoxins occurring in seafood and not a view towards *in situ* detection of these toxins in plankton and seawater samples – the main subject of the following discussion. While *in vivo* mammalian bioassays exist for several of the major toxin groups (Fernández et al., 2003), this approach shows no immediate potential for high throughput, automated, or *in situ* application and is thus beyond the scope of this chapter.

11.2.2.2 Chemical analyses

Toxin detection based on strict chemical analyses typically requires the steps of extraction, 'clean-up', and concentration prior to carrying out the analytical procedure. Currently there is no single, universal extraction method for chemical analysis of phycotoxins given their diversity in molecular weight, polarity, solubility and stability properties, and *in situ* concentrations in different types of samples. Further analytical complications are presented by salt effects for toxins dissolved in seawater, as well as lipid and protein interference from biological samples. Most extraction and 'clean-up' methods for phycotoxin analysis have been developed in favour of natural products chemistry or regulatory aspects of these toxins in shellfish or

finfish tissues, where lipid removal ('defatting') and/or protein precipitation are often required. Fortunately, plankton matrices are much more amenable to simple extraction protocols and preparation is often limited simply to a molecular weight cut-off (e.g. 10,000 Da) or restrictive pore-diameter (e.g. 0.45 μm) filtration step prior to analysis.

Over the past two decades, the chemical analysis of phycotoxins has usually been carried out by instrumental techniques involving high-performance liquid chromatography (LC) as a separation method, coupled with UV, diode array spectral scanning, or fluorescence as optical detection systems, and (rarely) electrochemical detection. Recent advances in column separation chemistries and physical properties (e.g. microbore columns) now provide high-resolution LC separation of both polar and non-polar phycotoxin components – often in a single sample.

A critical limitation of optically based LC-detection systems for phycotoxin analysis is that the detection and correct identification of the component is dependent on somewhat non-specific physico-chemical properties (fluorescence emission or absorbance at a particular wavelength) and a coincident retention time corresponding to an analytical standard. Thus, these systems are best suited to phycotoxin analysis targeting known toxin constituents and for which there exists certified analytical standards – conditions that are not always met in research applications. Without extensive pre-concentration (e.g. via solid-phase extraction and subsequent solvent evaporation), optical detection limits of conventional LC systems, usually in the micro- to nanomolar concentration range for underivatized analytes, are inadequate for the direct *in situ* analysis of phycotoxins in seawater or in individual, putatively toxic cells.

Pre-column fluorescence derivatization techniques have been successfully applied to the analysis of phycotoxins in pooled plankton cells (usually at least about 100 cells required) isolated by manual micropipette from natural plankton assemblages, such as the DSP toxins found in *Dinophysis* spp. (Lee et al., 1989). Such pre-column derivitization procedures are quite tedious and prone to artefacts, as well as being limited to only those toxin constituents that react with the fluorochrome. Sorting flow cytometry can be used to separate and concentrate putatively toxigenic cells from mixed cultures and natural plankton assemblages based on the inherent and apparent optical properties of target speices, and/or by some type of molecular probe-based fluorochrome-labelling. Such methods have proved useful for subsequent toxin analysis in the plankton, particularly in grazing experiments (Cembella and Turner, unpublished). After sorting, the pooled cells can be subjected to LC analysis with detection by optical methods (e.g. post-column fluorescence detection of saxitoxin analogues) or mass spectrometry (e.g. the detection of spirolides in *Alexandrium ostenfeldii* cells, Cembella et al., 1999).

Mass spectrometry (MS), which provides a highly specific, mass-based detection of analytes, particularly when coupled with LC separation methods, has proved revolutionary for the identification and quantification of phycotoxins in a variety of sample types (Quilliam, 1996, 2003*a*, 2003*b*). Other separation technologies, such as capillary electrophoresis (CE) (Zhao et al., 1997), have also been successfully integrated with MS for the detection of phycotoxins, but their use has typically been restricted to the analysis of semi-purified extracts and concentrated toxin standards. The development of sophisticated injection interfaces for MS (e.g. the SCIEX Ion-Spray™ system) that permit input of the analyte to the mass spectrometer detector after ionization at atmospheric pressure now allows (with appropriate mobile phase modifiers) the analysis of virtually all the known phycotoxins from plankton matrices. Detection

in MS systems is based on a highly specific property of each toxin – the mass:charge ratio (*m*/*z*) – which is then integrated with the retention time or migration time of individual components separated by LC or CE systems, respectively. This approach usually provides for the unequivocal identification of phycotoxins in natural samples by exact matching of the *m*/*z* and retention time with analytical toxin standards. Further confirmatory evidence of correct toxin identification in natural samples is possible when LC and MS systems are operated in tandem mode to fragment toxin molecules into a cascading series of diagnostic daughter ions (i.e. LC-MS/MS or even -MS/MS/MS; e.g. Bargu et al., 2002). The latter is especially critical when dealing with putatively harmful species not previously known to be toxic in a given region (e.g. Pan et al., 2001).

The concentration dependent and mass-detection limits of MS systems have been reduced dramatically in recent years – it is now feasible to detect picomolar concentrations and subnanogram amounts of low molecular weight phycotoxins in microalgal extracts. Recently, Cembella et al. (1999) showed the feasibility of detecting the spirolides produced by <50 cells isolated manually and then pooled from field populations and cultures of *Alexandrium ostenfeldii* by applying a novel microextraction technique. With the innovative application of hydrophilic interaction liquid ion chromatography (HILIC) coupled to MS (Figure 11.2), Quilliam (2003*b*) has demonstrated the near-simultaneous resolution of more than a dozen phycotoxin components representing four major toxin groups from a common matrix in a single chromatographic run (*c*. 30 min) (Figure 11.3). Recent improvements in micro-extraction techniques and high-resolution MS now permit the analysis of certain phycotoxins (e.g. spirolides) in a *single cell* of *A. ostenfeldii* (Quillian, Aasen and Cembella, unpublished). Such developments are truly exciting, with the near-term prospects of detecting complete toxin spectra from individual cells in a single analytical event, opening the possibility of doing direct genetic diversity analysis of toxin production in field populations. Analytical instrumentation for phycotoxin detection, such as LC-FD and LC-MS systems, is rarely mobilized from central laboratories and shipboard applications are uncommon. Although the size, cost and robustness of MS detectors have previously restricted their use to the laboratory, new innovations are proving that this should be the case in future. Many modern instruments are now physically robust and stable enough (e.g. to fluctuations in line voltage and power spikes) to be operated reliably on board ship, and technological advancements have resulted in substantial reductions in size, price and performance capabilities, such that single quadrupole benchtop MS detectors are approaching the price of high-end fluorescence detection systems.

Shipboard operation of LC instruments is now quite feasible and has been employed to generate near-real-time data for certain phycotoxins. Despite certain limitations, primarily analytical and hardware costs, there have been a few very successful applications of LC with fluorescence detection (FD) and LC-MS instrumentation to conduct profiling of toxins in plankton from the water column, albeit from discrete samples (Cembella et al., 2002). Cembella and co-workers (Figure 11.4) have also produced spatio-temporal profiles of PSP toxins and spirolides, revealing seasonal variations in *Alexandrium* spp. in a coastal embayment in Nova Scotia, Canada. Similarly, Hummert et al. (2002) employed shipboard LC to demonstrate PSP toxin diagenesis with depth in the North Sea and, in a related joint study, shipboard analysis of phycotoxins in plankton was shown to substantiate the enumeration of *A. ostenfeldii* and *A. tamarense* cells (John et al., 2003).

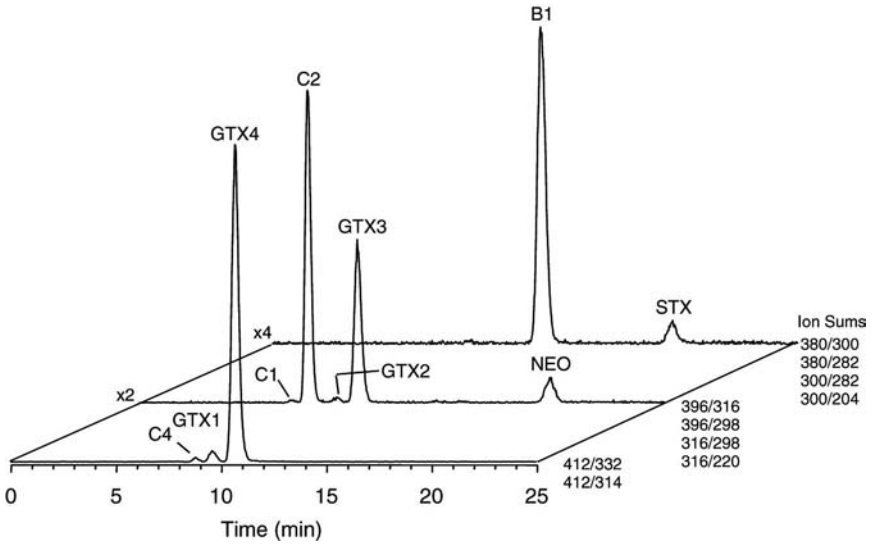

Figure 11.2
Analysis of of PSP toxins in plankton samples by hydrophilic interaction liquid ion-chromatography (HILIC) coupled with detection by ion-spray mass spectrometry (MS) in selected reaction monitoring (SRM) mode. *Alexandrium tamarense* samples were collected from Shelburne Harbour, Nova Scotia (2000) during a major fish kill incident of farmed Atlantic salmon (*Salmo salar*). Chromatographic separation was achieved by gradient elution on a TosoHaas Amide-80 microbore analytical column (250 mm by 2 mm) with a mobile phase consisting of 60–90% CH_3CN, 2 mM $HCOONH_4$, pH 3.5 (HCOOH). The HILIC method exploits two selectivity mechanisms: (a) hydrophilic interactions cause selective partitioning of the analytes into a stagnant enriched aqueous layer on surface of the stationary phase; (b) ion exchange interactions enhance selectivity according to molecular charge and polarity. *Source*: chromatogram reproduced with permission from Quilliam et al. (2001).

Robotics, autosamplers and column-switching technology allow for automated sample preparation and on-line clean-up, pre- or post-column derivatization, and unattended sample injection for continuous operation. Nevertheless, a current limitation of all LC methods is the requirement for sequential sample analyses, typically with a refractory period between discrete samples when operating in gradiant separation mode to return the system to initial conditions. Even under optimal circumstances, this limits the analytical processing of samples to no more than a few dozen per 24 hour period. Thus, while advances in LC instrumentation and column technology continue to reduce the time of analysis and the use of programmed autosamplers has automated sample injection, truly high throughput analysis is restricted to those with access to multiple instruments operating simultaneously (an expensive proposition).

Current MS systems for phycotoxin analysis are still far removed from the ultimate requirements for 'real-time' observations and measurements of phycotoxins

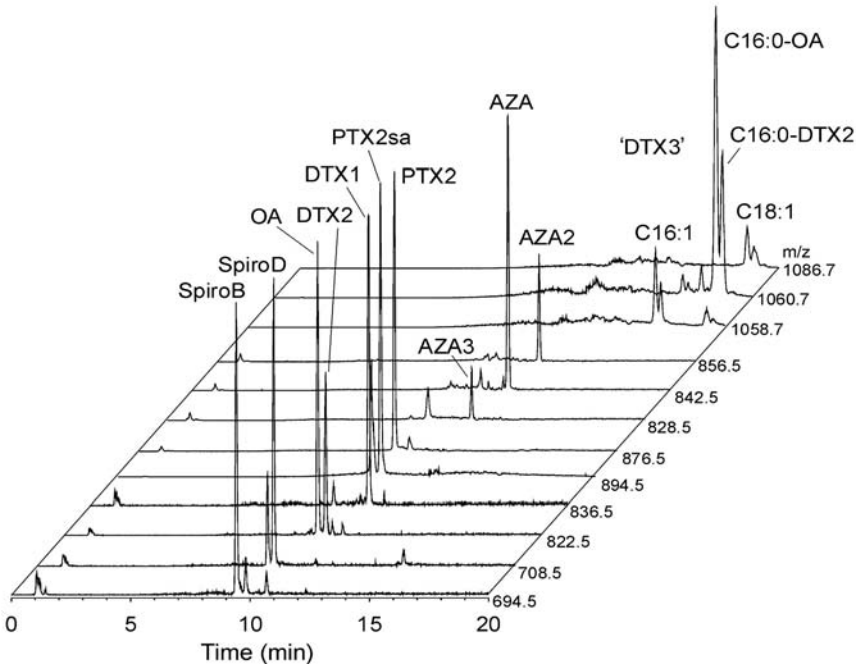

Figure 11.3
Universal analytical method applicable for the detection and quantification of marine phycotoxins in a single chromatographic injection. The toxins present in the mussel tissue matrix in the chromatogram shown here include spirolides (spiroB/D), okadaic acid (OA), dinophysistoxins (DTX1/2), pectenotoxins (PTX2 and PTX2sa), azaspiracids (AZA) and acyl esters of OA and DTX2 ('DTX3'). Toxin components are resolved by gradient elution on a Hypersil-BDS-C8 microbore analytical column (50 mm by 2 mm) with a mobile phase consisting of 5–100% CH_3CN, 2 mM $HCOONH_4$, 50 mM HCOOH at a flow rate of 0.2 ml min^{-1}. Detection is by ion-spray mass spectrometry (MS) with atmospheric pressure ionization (API) and selected reaction monitoring (SRM) of key molecular ions of known mass-charge (*m/z*) ratio in positive ion mode (either $[M+H]^+$ or $[M+NH_4]^+$). This general method has been applied to the analysis of plankton extracts on board ship but is not configured to provide real-time or continuous data. *Source*: chromatogram reproduced with permission from Quilliam et al. (2001).

in situ. At present, there remain physical limitations in flow splitting (MS injection systems and detectors normally handle only nanolitres) for both direct injection and LC separation prior to MS detection. On-line sample processing, such as the pre-concentration of dissolved toxins from seawater matrices and extraction of toxins from plankton collected directly from the water column, is not yet feasible. Nonetheless, with the design of toxin-specific sorbents such as molecularly imprinted polymers (MIPs, see Section 11.2.2.3), currently showing great promise for the selective

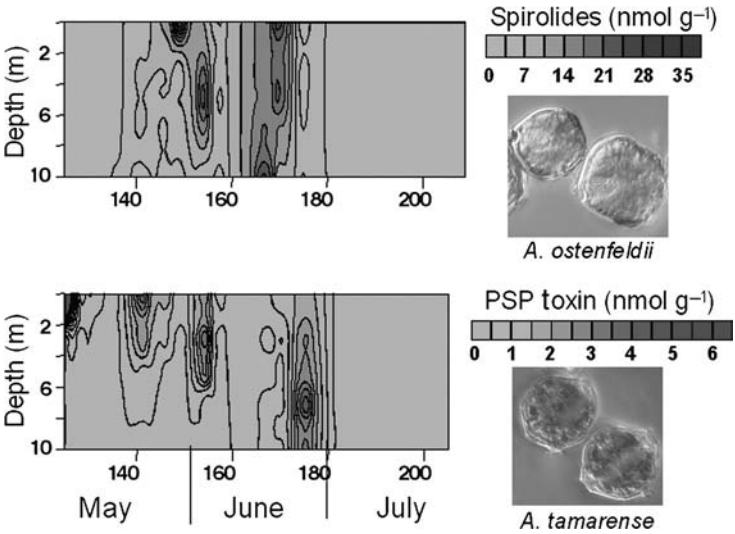

Figure 11.4
High-resolution toxin-specific analytical methods can be used to map spatio-temporal variations in toxin content in the plankton and associated bloom dynamics in relation to physical and chemical parameters. In this study on Graves Shoal (1998), along the eastern shore of Nova Scotia, liquid chromatography with fluorescence detection (LC-FD) and mass spectrometry (LC-MS) were employed to determine changes in the vertical distribution of PSP toxins and spirolides, respectively, over time in the water column. The units for the contour plots represent total net toxin (nmol) per gram wet weight of total net plankton material (>20 μm) collected by pump.
Source: Cembella et al., previously unpublished data.

removal of domoic acid dissolved in seawater using a solid phase extraction approach (Doucette, Piletsky and Ramsdell, unpublished), development of on-line applications should progress rapidly.

Moreover, small, modular mass spectrometers are being developed for oceanographic and underwater use. For example, researchers at the Center for Ocean Technology[56] have successfully incorporated these instruments (Figure 11.5) into autonomous underwater vehicles (AUVs). Prototype testing of AUVs fitted with MS capabilities is under way, with developmental efforts focused primarily on natural and anthropogenic organics (e.g. volatile organic compounds and dissolved gases). The system as currently configured is limited to the detection of compounds having masses up to a maximum of 300 amu (atomic mass units) (Langebrake, 2003) and thus not practical for use with phycotoxins, which generally exceed 300 amu. However, the potential for subsequent iterations of underwater MS systems to accommodate existing methods for certain phycotoxins, especially those known to occur dissolved in seawater (e.g. domoic acid), suggests that AUV-mounted mass spectrometers could be configured for real time, *in situ* toxin detection once appropriate sample collection, concentration and clean-up procedures are in place.

[56]cot.marine.usf.edu/

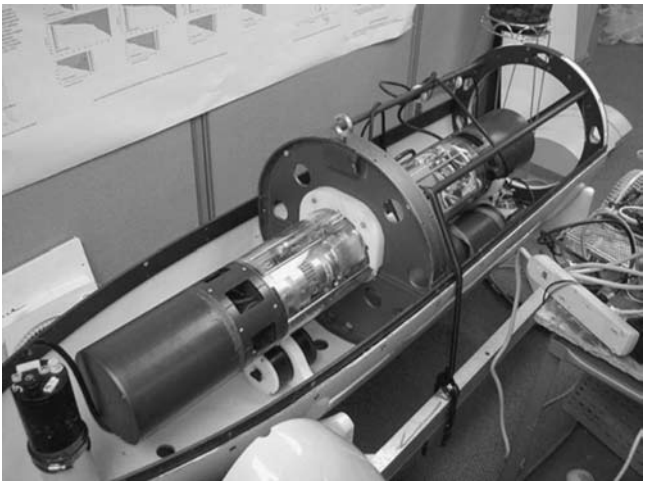

Figure 11.5
Underwater quadrupole mass spectrometer contained in an autonomous underwater vehicle developed by the Center for Ocean Technology (COT). This first deployable version was designed to detect and quantify volatile organic compounds and dissolved gases. Capabilities for tracing both anthropogenic and natural chemicals (e.g. HAB toxins) using networks of AUVs are the focus of ongoing and future developmental efforts.
Source: photo courtesy of D. Fries, COT.

11.2.2.3 In vitro assays

Background

The remaining group of HAB toxin detection methods consists of *in vitro* assays, which can be categorized into either functional- or structural-based approaches. The former rely on detection of biochemical activity of a toxin, whereas the latter depend on recognition of features of chemical structure at the molecular level. Both types of *in vitro* assays for HAB toxins have been reviewed recently (Towers and Garthwaite, 2001; Van Dolah and Ramsdell, 2001; Cembella et al., 2003). There are advantages and disadvantages to assays based on either approach and no single method provides results that satisfy all potential end-users. Chosing one technique over another is often driven by the type of information desired, the users' expertise and preference, and the utility of the method relative to the task at hand (e.g. laboratory-based analyses of few samples versus field-based analyses of many samples in a short period). Both functional and structural *in vitro* assays are susceptible to artefacts associated with non-specific interactions not related to toxins in question and this possibility must be accounted for in assay design and implementation.

Functional assays are based on interactions of toxins that bind to specific biological receptors or that interfer with enzyme function, and the avidity of those interactions provides an integrated measure of the potency of toxin(s) in a sample. That is, these assays yield estimates of 'net toxicity' for all toxins and their derivatives in a sample that are bound by the same receptor type or interfere with the same enzyme.

The same is true for toxins that are structurally modified through natural processes such as biotransformation, provided that receptor recognition remains unaltered. An important limitation for functional assays is that these methods cannot yield definitive toxin identification. For example, testing an extract containing several saxitoxin derivatives would yield a response reflective of the integrated toxic potency of that mixture, but that determination provides no information as to which specific saxitoxin derivatives are present. Moreover, taking this last case one step further, other known (e.g. tetrodotoxin, the puffer fish toxin) or unknown toxic components that express a similar mode of action (in this case Na^+-channel blocking) would also contribute to the assay response, so results must be interpreted as 'saxitoxin equilvalents' or 'Na^+-channel blocking activity' and not a specific amount of saxitoxin per se.

By comparison, structural assays (e.g. immunoassays) require the conformational interaction of a toxin with a recognition factor (e.g. antibody) and are thus highly susceptible to structural modifications of toxin molecules. These assays generally display a high degree of specificity for the toxin class against which they were designed, and so results of this type of assay can to some extent be interpreted more rigorously than those obtained using functional assays. Nevertheless, detection of multiple derivatives of a given toxin, or a distinctly different but structurally related toxin, can still occur depending on the degree to which the assay recognition factor (e.g. antibody) cross-reacts with the structurally distinct, 'non-target' molecules. For example, certain anti-ciguatoxin antibodies will also cross-react with brevetoxins because they share some common features in the ladder-frame architecture of the polyether rings (Baden and Adams, 2000). So while structural assays have the *potential* to yield more specific information regarding toxin composition compared with functional assays, caution must still be exercised in interpreting those results because cross-reactions are possible.

Functional assays

Functional assays developed for the detection of HAB toxins include cytotoxicity tests (e.g. Manger et al., 1995), enzyme inhibition assays (e.g. Della Loggia et al., 1999), reporter gene assays (Fairey et al., 1999) and receptor binding assays (e.g. Van Dolah et al., 1994). In some cases these tests have been calibrated against regulatory methods used in HAB toxin monitoring programmes (e.g. Suarez-Isla et al., 1997). However, some of the key benefits of these assays, such as providing a means to estimate total toxic activity and thereby protect consumers from eating contaminated seafood, actually become impediments when attempting to format these assays for autonomous, in-water applications. In particular, maintaining the biological activity of a cell line or a receptor preparation (required for toxin recognition) for extended periods of time under conditions encountered outside the laboratory (e.g. variable temperature) remains a major challenge. Nonetheless, a recent report describing the development of a portable microelectrode array recording system for cultured neuronal networks (Figure 11.6) capable of detecting a broad range of neurotoxins indicates that such impediments can be overcome to some extent (Pancrazio et al., 2003). Investigators have demonstrated previously that neuronal networks cultured on microelectrode arrays are able to form functional and stable synaptic connections (Gross, 1994). Extracellular recordings from such excitable cells permit non-invasive, long-term measurements of cellular signaling activity (e.g. action potentials or spikes) that can be monitored via the microelectrode array, thereby yielding unique, physiologically relevant responses to a given toxin exposure. While several operational aspects of the system still require modification (e.g. extending the length of time the cultured cells can be maintained

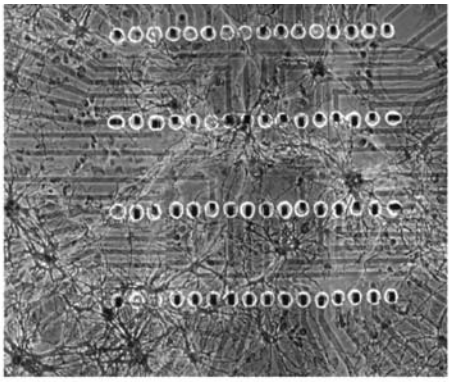

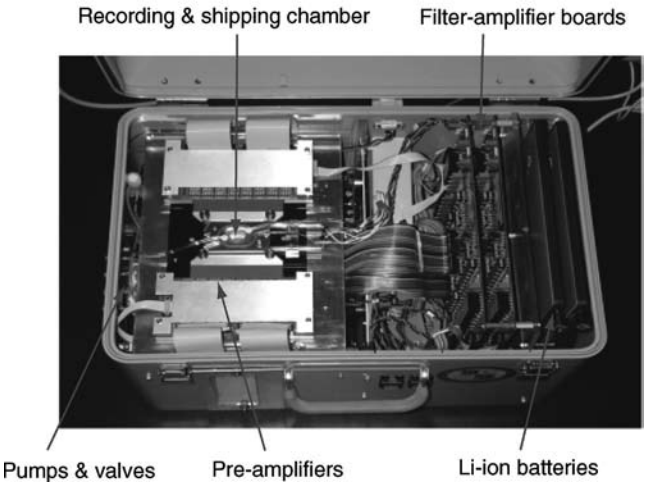

Figure 11.6
Upper panel: neuronal network derived from embryonic mouse tissue cultured over a microelectrode array 52 days *in vitro*; recording area 0.8 mm^2. The black dots visible on the array are microelectrode recording sites. Lower panel: portable microelectrode array recording system contained within an aluminum carrying case (45 cm (l) by 30 cm (w) by 40 cm (h)) and weighing 15 kg, including rechargeable lithium ion battery packs.
Source: photos courtesy of J. Pancrazio, Naval Research Laboratory.

prior to use, providing an appropriate sample collection and processing 'front-end' for delivering samples, etc.), cultured neuronal networks are becoming better positioned to provide rapid, function–based toxin detection that should be amenable to integration into autonomous devices, although deployment on *in situ* platforms remain somewhat questionable.

Other function-based methods, including receptor assays for both domoic acid (Powell et al., 2002) and PSP toxins (saxitoxin analogues; Powell and Doucette, 1999) conducted in the laboratory, have been used to test samples collected autonomously and stored onboard the Environmental Sample Processor (ESP) platform. Results of these assays showed toxin levels varying proportionally with the abundance of associated HAB species as determined by sandwich-hybridization and whole-cell assays (for details see Section 11.4.2).

Ultimately, integrated detection of both HAB species and toxins is essential for the accurate assessment of HAB-related risks and to studies of HAB population dynamics, given the potential for wide fluctuations in per cell toxin content as a function of variable physiological status and genetic composition (see Section 11.3.1.1).

Structural assays

In comparison to the functional approach, structure-based assays, such as immunoassays, are collectively robust techniques that lend themselves well to use in the field and probably to future applications on in-water, autonomous platforms. Antibody-based assays (e.g. enzyme-linked immunosorbent assays or ELISAs) have been developed for a variety of HAB toxins and several of these tests exist as advanced prototypes (β-tested) or are available commercially (Cembella et al., 2003; Naar et al., 2002). Most ELISA testing for algal toxins is currently performed in the laboratory, generally in a high throughput 96-well plate format. An ELISA microplate assay for PSP toxins based on a polyclonal antibody to saxitoxin, but with broad cross-reactivity to other PSP toxin analogues (Laycock et al., 2001), has been used to detect the presence of these toxins in a fish-kill incident linked to a bloom of *Alexandrium tamarense* (Cembella et al., 2002). Nevertheless, application of toxin-specific ELISA assays to natural phytoplankton assemblages is still rare. An adaption of this technology has been incorporated into a lateral flow immunochromatographic (LFI) assay, providing a single test (±) for PSP toxins in a format similar to that of home pregnancy test kits (Figure 11.7). The Jellett Rapid Test for PSP toxins (previously marketed as the MIST Alert™) was originally designed for toxic extracts of shellfish and has undergone extensive testing against the AOAC (1990) mouse bioassay, currently the regulatory standard for PSP toxin testing (Jellett et al., 2002; Mackintosh and Smith, 2002). This rapid (<10 min) and portable qualitative immunoassay test is amenable to field use on crude extracts (described in detail in Cembella et al., 2003) and is available commercially from Jellett Rapid Testing.[57] Via a slight modification, including dilution of the sample in an proprietary buffer, the LFI test strip has been evaluated successfully to monitor PSP toxin content in *Alexandrium tamarense* throughout a culture cycle (Silva et al., 2001). Furthermore, the test has been extensively validated against many toxic strains of PSP toxin-producing species from diverse geographical populations, including non-toxic controls, with no evidence of sample matrix effects, false positive, or false negative responses (Rafuse et al., 2004). The Jellett Rapid Test for PSP toxins was tested in tandem with a related LFI for domoic acid (previously marketed as the MIST Alert™ for ASP) in field populations of *Alexandrium* and *Pseudo-nitzschia* species in Nova Scotia, Canada. The test was found to yield results consistent with toxic species abundance and chemical analysis of phytoplankton toxins (Figure 11.8). The portability and ease of sample preparation and interpretation of the LFI assay system make it suitable for the rapid screening of certain algal toxins in field settings, although the sample throughput and quantification capabilities are limited.

[57]www.jellett.ca

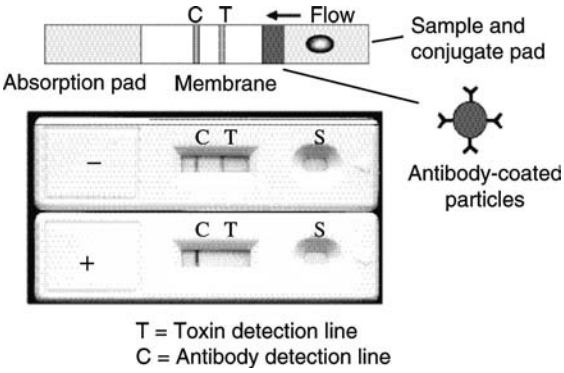

Figure 11.7
Jellett Rapid Test for PSP toxins (formerly the MIST Alert™ kit for PSP toxins) developed by Jellett Rapid Testing, showing cassettes with positive (upper) and negative (lower) test strips. No T line indicates that toxin is present in a sample, while a visible T-line indicates a toxin level below detection limit. The C line is a control showing that the reagents have been sufficiently activated to provide a valid test result. The regulatory limit for PSP toxins is 80 μg STX eq. 100 g^{-1} tissue.
Source: courtesy of J. Jellett, Jellett Rapid Testing.

As one promising alternative to the traditional plate-based ELISA approach, antibodies specific for algal toxins have been immobilized on gold-coated sensor chips with an embedded microfluidic flow system. The specific interaction between the antibodies and immobilized toxin changes the refractive index of the chip surface, and that change is detected using an optical sensor and the principle of surface plasmon resonance (SPR; e.g. Figure 11.9). Assays conducted in this inhibition format are completed within minutes and a single chip can be regenerated hundreds of times with no loss of performance. A SPR-based assay has been developed for domoic acid (Traynor et al., 2002), validated against the standard HPLC regulatory method, and is now being implemented by the Northern Ireland Food Standards Agency (FSA) shellfish toxin monitoring programme (Traynor et al., 2006). Further modifications to this method have lowered the limit of detection (<1 ng ml^{-1}) and demonstrated its utility for detecting DA in plankton and seawater (Doucette et al., 2005). Other researchers employing a different antibody and DA immobilization protocol have designed a similarly sensitive SPR-based method, although the effects of biological matrices on toxin detection were not examined (Yu et al., 2005). While gaining acceptance in the area of algal toxin detection, current SPR-based applications are confined to the laboratory. However, small, field-portable platforms incorporating SPR technology are now becoming available and aimed at allowing this approach to be implemented for real-time or near-real-time field detection of analytes.[58] Further technological advances will be required to adapt SPR instruments for in-water deployments, in particular making the system less susceptible to mechanical vibration and swings in ambient temperature.

In contrast to the antibodies noted above, there are naturally occurring proteins that bind selected algal toxins with similarly high affinity and have thus been used as

[58]For example, www.ti.com/snc/products/sensors/spreeta.htm

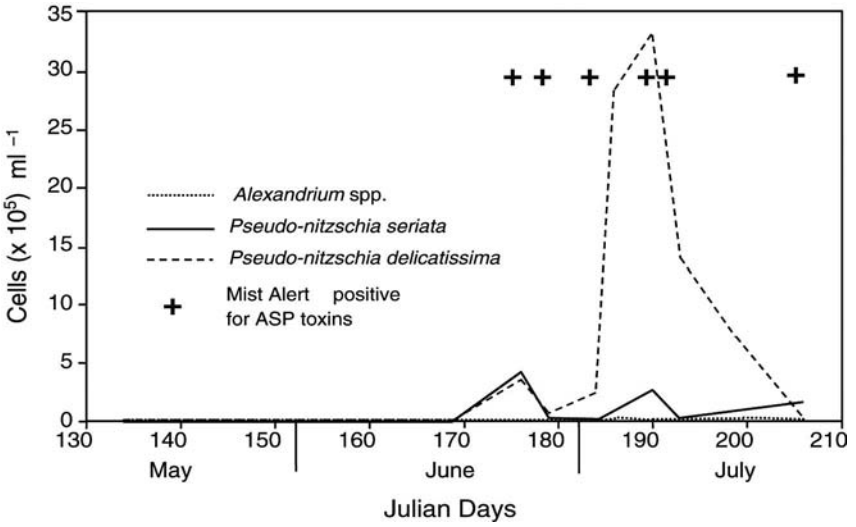

Figure 11.8
Application of the MIST Alert™ for PSP and ASP toxins to mixed phytoplankton assemblages collected by vertical net tow (20 µm mesh) from Ship Harbour, Nova Scotia (2001). Cell concentrations of *Alexandrium* spp., *Pseudo-nitzschia seriata* and *P. delicatissima* identified by TEM (transmission electron microscopy) and counted by phase contrast microscopy are given for the net tow concentrate. Positive results (+) from the MIST Alert™ are indicated only for ASP toxin (detection limit: approximately 10 pmol for domoic acid) because cell concentrations of *Alexandrium* were too low to yield PSP toxin levels above detection for the immunodiagnostic test (approximately 20 pmol STX eq.).
Source: Cembella et al., previously unpublished data.

the basis for another class of structure-based assays. The best example of such a protein is saxiphilin. Originally isolated from the plasma of the bullfrog, *Rana catesbeiana* (Li and Moczydlowski, 1991) and later from the circulatory fluids of a number of other vertebrate as well as invertebrate species (Llewellyn et al., 1997), this hydrophilic protein and its various isoforms have a subnanomolar affinity for saxitoxin and several of its derivatives, and has been incorporated into a high-throughput, radiometric-based assay (Llewellyn et al., 1998). The assay has performed well in comparison with other techniques (e.g. HPLC, mouse bioassay; Llewellyn et al., 2001) and was recently reformatted with a colorimetric endpoint analogous to a conventional ELISA assay (L. Llewellyn, pers. comm.), making this approach more amenable to portable, field-based applications. The saxiphilin-based assay is classed here as a structural rather than functional type because this protein has no demonstrated biological function in the organisms from which it has been isolated, some of which are terrestrial invertebrates having no known contact with potential PSP toxin sources.

One of the most novel approaches to phycotoxin detection involves a relatively new, biomimetic sensor technology based on 'molecular imprinting' (Ramström and Ansell, 1998). This technology involves the formation of cavities in a polymer with

Figure 11.9
Left panel: Biacore 3000 system, which incorporates a label-free, surface plasmon resonance biosensor technology in order to monitor the progress of biomolecular interactions in real time. This system has been used as a platform to develop an antibody-based test for the algal toxin, domoic acid (DA). DA is immobilized on a gold-coated sensor chip (right panel) containing an embedded microfluidic system (image underlying chip). A mixture of DA-specific antibody and sample is delivered to the monitored surface of the sensor chip and the binding of free antibody (i.e. antibody not already bound to DA contained in the sample) to the immobilized DA is measured based on resonance changes detected at the chip surface and quantified using a calibration curve produced with standard reference material.

the correct shape and functionality to specifically bind a target analyte, thus yielding an artificial receptor. The first attempt to employ molecular imprinting in phycotoxin detection was directed at the cyanobacterial toxin, microcystin-LR (Chianella et al., 2003). A computer model optimized the composition of the molecularly imprinted polymer (MIP), which then served both as a sensing element in a piezoelectric sensor and also as a solid phase extraction (SPE) material for pre-concentrating the toxin. The MIP-SPE cartridge was capable of pre-concentrating microcystin-LR up to 500-fold from tap water (98% recovery rate) prior to detection on a MIP piezoelectric sensor (94% accuracy at 95 nM). Notably, a MIP film for domoic acid has been synthesized recently and grafted onto a toxin sensor chip for use in a SPR-based application; however, the lower limit of detection was somewhat inferior (*c.* 5-fold) compared with a monoclonal antibody, and biological samples have yet to be tested with this method

(Lotierzo et al., 2004). A MIP-based solid phase extraction cartridge has also undergone preliminary testing for selective removal and concentration of DA from a seawater matrix, with recovery values thus far averaging 84% (Doucette, Piletsky and Ramsdell, unpublished). Such encouraging results indicate that additional development of phycotoxin detection and clean-up methods based on molecular imprinting are warranted.

11.3 Technological requirements for remote detection of HAB species and toxins

11.3.1 Background

The preceding sections have outlined a number of methods for detecting HAB species and toxins that are applicable to analysis of field samples. Each method has specific requirements that must be met in order to carry out the analytical or assay procedure. For example, the selection of appropriate sample volumes, the steps taken to concentrate target organisms, extraction and clean-up protocols, the choice of reagents for preserving, extracting, amplifying and detecting targeted taxa and toxins, options for signal transduction, etc., are all quite well understood for laboratory procedures. This is an essential foundation on which conception, design and development of novel sensors is based. Moreover, a detailed description of the functional requirements associated with a given detection methodology is a primary source of information for assessing whether that technique is more or less suited for automation and deployment on remote platforms.

Regardless of the particular method in question, all instruments envisioned must function in the context of the natural environment in an unattended fashion, in some cases subsurface, for extended periods of time under variable conditions not found in the laboratory, and provide data that can be readily integrated with other systems such as those providing contextual information (temperature, salinity, chlorophyll fluorescence, etc.). From that perspective, in the following section we consider some of the overarching functional requirements and technological hurdles faced when projecting development of instruments that will use molecular detection techniques for HAB taxa and toxins onboard autonomous platforms.

11.3.2 Challenges associated with integrating sample collection and processing

Development of molecular assays for detecting HAB taxa and toxins have evolved largely from biomedical applications, so current advances in the field of biomedical diagnostics point to a vision of what may soon become applicable to autonomous, *in situ* HAB detection systems. The development of molecular diagnostic equipment that is portable, battery operated and requires little training to use successfully is a major focus of research in support of the biomedical industry and is also a primary aim in the design of test systems for HAB research and monitoring. 'Point-of-care-diagnostics', as referred to in the biomedical realm, promises to yield assays far smaller and easier to apply than those of the present generation, and this trend will certainly create exciting options for developing biosensors with ocean science applications (e.g. Wang, 2002*a*, 2000*b*). Devices based on micro-, nanofluidic and micro-electromechanical systems (MEMS), sometimes referred to as 'lab chips', are especially promising in this regard.

Many efforts to develop lab-chip technology have focused on specific detection techniques, methods of signal transduction and means of producing individual sensor components themselves. A growing number of companies offer equipment that automates sample processing and detection of molecular signatures found in complex sample matrices. There are also microsensor chip arrays coupled to mass spectrometry techniques, e.g. MALDI (matrix assisted laser desorption interference) that may prove to be valuable for rapid, automated toxin detection and for toxin gene expression studies in the near future. All these advances offer an encouraging vision of emergent molecular detection technologies as viable sensors for autonomous platforms from both science (analytical potential) and engineering (small size and low power) perspectives. Nevertheless, much of the supporting instrumentation needed to control these devices and analyse resulting data is not yet suited to autonomous, extended operation in the ocean.

The nature and amount of sample material required for analysis are two of the key considerations that set detection of HAB species and toxins apart from the vast majority of analytes targeted in biomedical diagnostics. For many biomedical applications, sample sizes are extremely small (e.g. drop of blood, skin swab, single hair) and the molecules of interest (e.g. metabolite, pathogen, defective gene) vary against a relatively constant and well-defined background. This makes integration of sample collection, processing, and analytical functions into a very small form factor quite tractable. In contrast, due to the potentially low absolute abundances of HAB taxa and toxins, the merger of micro- and nanofluidic scale sensors and autonomous ocean observation platforms requires hardware that accomodates much larger sample volumes and for rendering them to a state appropriately matched to the input needs of the sensor (i.e. restricted particle size, microlitre or nanolitre sample volumes, etc.). Particle size range encountered in natural samples is also an important consideration. This, too, further affects the design of systems for automating sample collection and sample processing prior to final analysis on a small, micro- or nanofluidic device. Finally, seawater is not a constant and necessarily well-defined matrix – variations in salinity, temperature, and organic composition may cause interference with certain methods, which must be compensated for in extraction and sample processing.

11.3.3 Importance of integrating detection of HAB species and toxins

Wide variations are known to occur in toxin synthesis and catabolism through the cell cycle, as a function of changes in physiological state, as well as within and among geographical populations of even the same species (e.g. Bates, 1998; Cembella, 1998; Wright and Cembella, 1998). The partitioning of toxins between particulate and extracellular dissolved forms may also vary substantionally as a function of growth rate and cell physiological status (Quilliam, 1996; Pan et al., 2001), and it is likely that certain lipophilic toxin components exist in colloidal or micellar forms in the water column, particularly during bloom senescence. For some toxic species, it is possible to detect cells in the apparent absence of any particulate or dissolved toxin they may be capable of producing. Therefore, concurrent measurements of species presence/abundance and toxicity are critical to understanding mechanisms underlying HAB dynamics and for making predictions as to where and when HABs might affect the health of humans and aquatic ecosystems. Striking examples of variation in cellular toxicity have been observed during *Pseudo-nitzschia australis* blooms in Monterey Bay, California. Concurrent measurements of domoic acid and cell concentrations yielded estimates of

domoic acid per cell that differed by about 20-fold in 1996 and 10-fold in 1998 (Scholin et al., 1999, 2000). Similarly, detection of domoic acid by immunodiagnostic assay (Mist Alert™) and instrumental methods showed particulate toxin concentrations associated with a concurrent bloom of two *Pseudo-nitzschia* species – one putatively toxic and the other non-toxic – in a Nova Scotian embayment (Figure 11.8). Clearly, an integrated approach involving detection of phycotoxins as well as the corresponding toxigenic organisms is highly desirable when considering the development of novel instrumentation for unattended, *in situ* applications.

11.3.4 Common sample collection, processing and analyte detection themes

Many of the diagnostic procedures for detecting HAB species and toxins share an overlapping set of requirements. For example, many assays require relatively large sample volumes. Organisms of interest may be present at concentrations <100 cells per litre, usually requiring sample volumes of at least 100 ml to ensure that at least a few target cells are captured. Sample volumes >1 l are more practical to capture target organisms that are rare or to obtain sufficient biomass of very low-toxicity cells. Even for those organisms that occur at very high concentrations, millilitres of sample are needed to acquire a representative group of organisms from a discrete point in time and space. The fact that some species also occur in thin layers further highlights challenges associated with obtaining appropriate samples that are central to research and resource management interests (e.g. Rines et al., 2002).

Protocols for processing samples prior to conducting various assays are very similar. Operationally, these methods can be divided into those that rely on maintaining cell integrity (whole-cell assays) and those that require cell disruption (cell-free assays). After the initial steps of sample collection and concentration, a method-dependent subset of relatively generic procedures follows: application of a series of reagents in a timed sequence, temperature modulation, chromatographic and/or solid phase extraction chemistries, filtration, and so on. Some procedures separate target molecules based on their physical properties (e.g. size, hydrophobicity, chemically reactive groups), others rely on intermolecular reactions (e.g. antibody/antigen binding, nucleic acid hybridization, enzyme mediated processes), and some use a combination of these methods. Detection and quantification of target molecules also relies on a relatively generic set of signal transduction modalities, in particular optical or electrochemical sensors. Thus, it is reasonable to assume that a single electromechanical device should be capable of detecting multiple molecular signatures, some simultaneously. Indeed, many projected applications of *in situ* 'molecular sensors' will demand an ability to detect multiple taxa and chemical compounds simultaneously, as researchers and resource managers are rarely concerned with only a single HAB taxon or toxic compound in a given region.

11.3.5 Case for sample archival

Development of novel sensors that take advantage of molecular detection techniques and that function autonomously, *in situ*, are well within the realm of possibility and are fast becoming a reality. However, validation of assays run on these platforms, as well as routine interpretation of test results, will depend on the assay format used (whole-cell versus cell-free) and some information regarding the nature of samples encountered. For example, detection of species in the whole-cell format requires that

the probe access target molecules and that those molecules are present in sufficient quantity to visualize the cell above background. Furthermore, the cell must remain intact from sample collection through processing and be recognized as consistent with the morphology of the target organism. Anything that obscures target cells from view will affect results of whole-cell assays (e.g. Scholin et al., 1999; Tyrrell et al., 2001, 2002), so even if a target cell is present in a sample it may not always be detected using the whole-cell approach.

When using cell-free detection schemes, the presence and abundance of a targeted species is inferred based on detecting and quantifying a specific signature molecule. Similar to the whole-cell method, results of cell homogenate-based assays are operationally defined. Samples containing target cells that are healthy and free-living, versus those samples that contain target cells that are dead, trapped in organic matter (e.g. faecal pellets), or recently consumed by predators, could all yield a positive reaction signaling the presence of a target taxon. When viewing such samples under the microscope one would draw significantly different conclusions as to what species are in fact present – in the first case, target organisms are clearly visible and can be enumerated, while in the second they are not and therefore would be considered 'absent'. The more sensitive the cell homogenate assay and the more stable the target molecule, the more likely that such discrepancies will arise and potentially confound efforts to determine the efficacy of a given assay. Major disagreements between results of assays targeting intact cells and 'signatures of cells' are thus possible and should be expected when analysing natural samples. The transfer of toxins through the food web is a vivid illustration of this phenomenon if one considers the toxin a specific indicator of cell presence and abundance. For these reasons, it is highly desirable to incorporate sample archival capability onboard autonomous platforms, so that apparent discrepancies between whole-cell and cell-free assays conducted *in situ* can be studied in detail by alternative methods in a well-equipped laboratory.

11.3.6 Need for sensor arrays and time-series analyses

Researchers have long recognized the need for making routine, synoptic measurements of both species and toxins at multiple stations in order to better understand how alterations of the physical and chemical environment drive bloom formation, maintenance and termination. The development of HABs can occur over large geographical areas that do not necessarily coincide with regions where harmful effects are exerted because of bloom advection and dispersion (see also Cullen, 2007 – Chapter 1 this volume). In addition to fluctuations in toxigenic cell concentration, the cellular toxin content may also vary dramatically in time and space over the bloom cycle. Therefore, most applications that strive to predict the onset, fate and toxicity of HABs require a comprehensive and well-distributed network of sampling sites, as well as the capability to detect target organisms and their toxins at very low concentrations, even when they are embedded in a complex sample matrix. Ideally, synoptic sampling and time-series analyses would provide information on trends and spatial relationships that will make it possible to identify and map the distribution of HAB organisms and their associated toxicty well in advance of potential problems they may cause. Contextual sensors, such as temperature, salinity, nutrients, bulk optical properties, etc., are essential for placing the organisms and toxins detected remotely in an appropriate environmental framework. There have been a few successful attempts to map the spatio-temporal variation of toxins (e.g. Figure 11.4) and the causative species in the water column throughout a complete bloom cycle. In some cases the accompanying

physical parameters (temperature, salinity, density) have also been profiled, but the total number of observational nodes has always been fewer than desired to define the bloom in mesoscale time-space. Consequently, monitoring and study of HABs using novel sensors will probably be achieved by a combination of fixed (moorings, pier pilings, etc.) and mobile observational nodes (ships, autonomous vehicles, and personnel that may access sampling sites from shore). It is highly unlikely that a single instrument and a restricted set of analytical procedures will provide this capability in full.

11.4 Environmental sample processor: automated, *in situ* detection of HAB species and toxins

Instruments that allow molecular probe detection technologies to be deployed autonomously, *in situ*, are just beginning to emerge. For example, workers at the University of South Florida are developing the Autonomous Microbial Genosensor (AMG), a device that aims to use an isothermal RNA-specific amplification technology as a basis for detecting RNA viruses and HAB species (Casper et al., 2004; J. Paul, pers. comm.). The first field trials of the AMG were scheduled for March 2005.

In a separate but parallel effort, scientists and engineers at the Monterey Bay Aquarium Research Institute (MBARI) have developed the Environmental Sample Processor (ESP; Scholin et al., 1998, 2001; Figure 11.10). First fielded in 2000, the ESP was specifically designed with eye towards detecting HAB taxa and toxins. In this section we review the ESP system, provide examples of some of the data obtained from prototype instruments, and outline plans for its further development. While this section focuses on the ESP, note that development of such in-water systems is an active area of research and in coming years their designs and analytical capabilities are likely to evolve rapidly. Details concerning the ESP are provided here to illustrate one possible solution to the many challenges faced when attempting to deploy molecular probe technologies in a remote context.

The ESP was conceived as a generic platform to collect discrete samples of water, concentrate particulates in those samples onto user-selected solid supports, automate pre-programmed chemical processing and limited analysis of material collected, and telemeter the resulting data to ship or shore. Current sample processing options automated by the ESP include, but are not limited to:

- preservation of microorganisms (particulate matter) for light and electron microscopy;
- preservation of microorganisms (particulate matter) for nucleic acid and toxin analyses;
- application of molecular probes (DNA, antibody) for identification of specific organisms using whole cell formats;
- application of molecular probes (DNA, antibody) using cell homogenate formats, the latter including nucleic acid extraction and development of custom DNA probe arrays for real-time detection of multiple organisms simultaneously, as well as toxin extraction and ELISA-based tests for toxin detection.

The ESP is deployed in tandem or directly bundled with other instrument packages, such as a conductivity, temperature and depth (CTD) recorder, chlorophyll fluorescence sensor, etc. The first ESP prototypes built were referred to as 'first generation' or 1G ESPs. Development and application of a 'second generation' or 2G ESP is under way.

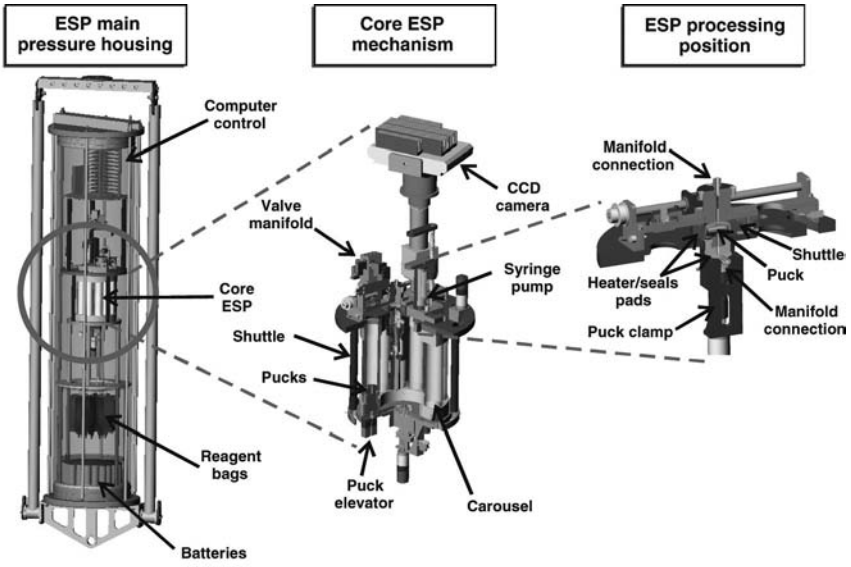

Figure 11.10
Major components of the first generation (1G) ESP system fitted for autonomous, subsurface operation. Left panel: view of the entire ESP in its pressure housing (see Figure 11.13 for a schematic of the ESP mooring). Centre panel: view of the core mechanical and fluidic components of the ESP. Right panel: close-up cutaway of the ESP 'processing position', the part of the instrument where pucks (see Figure 11.11) are clamped and used to filter water samples and carry out chemical processing of particulates retained from those samples.

11.4.1 1G ESP functionality

The 1G ESP (Figure 11.10) consists of five major subsystems: carousel, puck shuttle, clamp, syringe pump and CCD camera. The carousel stores up to 100 'pucks' or carriers that accommodate a wide variety of user-defined 25 mm diameter filters or chemically adsorptive media. Pucks are highly configurable for performing different types of analyses supported by the ESP architecture (Figure 11.11). A linear shuttle is used to move a puck from the carousel to the processing position where it is sealed in a clamp, thus providing connections to the valve manifolds. The clamp seals have embedded heater pads for temperature control from ambient to ~100°C at any time during a protocol. The shuttle is also used to move pucks to an imaging station where a CCD camera records results of DNA probe array assays. A syringe pump draws in seawater samples and dispenses the required reagents. The syringe pump is capable of mixing and dispensing fluid volumes from ~100 µl to ~25 ml. Modular valving supports use of up to 16 different custom-defined reagents. Additional valves allow the syringe pump to pull reagents 'top-to-bottom' or to push reagents 'bottom-to-top' across the filter or adsorptive medium contained in a puck. Reagents can also be trapped in a puck so that specific reactions can occur in a relatively small volume (e.g. 250 µl) over an extended period. Target molecules eluted from one puck may be pulled into the syringe pump

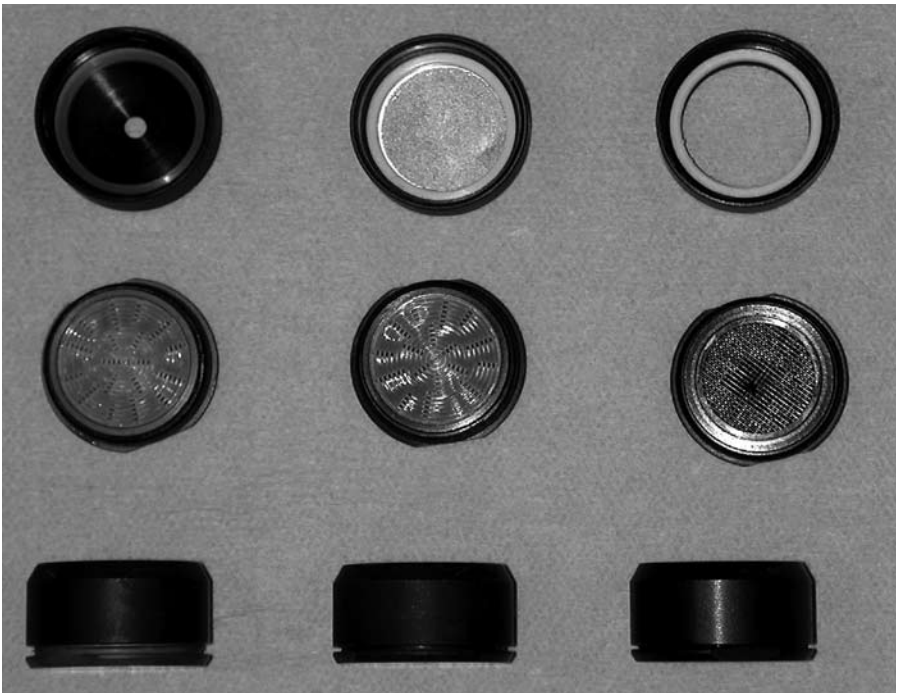

Figure 11.11
ESP 'pucks' that hold 25 mm user-defined media. Pucks are highly configurable for performing different types of analyses, but all conform to common outer envelope (bottom). The three pucks shown are used for (L to R) creating cell homogenates, archiving cells for microscopy and developing DNA probe arrays. All use a common core processor, the 1G ESP.

and used in a protocol requiring a different filter medium (e.g. DNA probe arrays for use in sandwich hybridization reactions). Processed or spent pucks are unloaded into an empty carousel tube. Waste may be discharged overboard or captured onboard in a dedicated reservoir. Users control the ESP through a simple ASCII text-based language that defines the sequence of steps emulated by the instrument based on a hierarchy of subroutines. A number of subroutine macros can be called from a higher-level macro. For example, a high-level ESP 'mission macro' specifies times that the instrument will be activated, a series of subroutines the user wants to execute at that time (e.g. collect a sample for a probe array, develop an array, archive a sample, etc.), and finally a 'sleep' command to place the instrument on stand-by until the next designated sampling period. In this fashion, users can specify different suites of real-time analyses (e.g. develop arrays that target different groups of species) or different types of sample archivals (e.g. whole cell, nucleic acid, toxin, etc.) over the course of a deployment.

Two 1G ESP prototypes have been built thus far. One instrument was designed as a laboratory benchtop development platform and is suitable for shipboard applications. The second 1G ESP was fitted for *in situ*, subsurface, autonomous operation. Examples illustrating tests of these prototypes are given in Sections 11.4.2 and 11.4.3.

11.4.2 Field test of the shipboard 1G ESP prototype

The shipboard ESP prototype was deployed in Monterey Bay, California, during August 2000 (Figure 11.12). The device was programmed to generate cell homogenates (crude cell lysates) and develop prototype DNA probe arrays designed to simultaneously reveal the presence of several different harmful algal species in near real-time. The same instrument was also used to archive discrete samples for a diverse set of post-deployment processes: (a) whole-cell hybridization; (b) domoic acid and saxitoxin assays; and (c) construction of rDNA clone libraries. The following results summarize the DNA probe arrays, whole-cell probing and toxin analyses, emphasizing two different toxigenic phytoplankton species: the diatom *Pseudo-nitzschia australis* and the dinoflagellate *Alexandrium catenella*.

In the example shown in Figure 11.12, samples collected at various locations (Figure 11.12A) contained different suites of species and toxins. For example, neither *P. australis* nor *A. catenella* were detected in Samples 2–4 (ESP2–4) albeit at different concentrations, as indicated by the variable intensity associated with the *P. australis*-specific probe on the DNA probe array. *A. catenella* was detected only on an array in Sample 4 (ESP4) (Figure 11.12B). Samples archived for whole cell (Miller and Scholin, 2000) and toxin receptor binding assays (Powell and Doucette, 1999) enabled post-deployment validation of the probe array data collected in real time. Examples of the whole cell analyses are shown in the lowest series of images in Figure 11.12B (frames 1a–4a). Immediately after development of an oligonucleotide array, the ESP was programmed to concentrate and preserve an aliquot of the same sample used to generate the array. The ESP1 sample (Figure 11.12A) showed no reactivity with the probe array, and so in whole-cell analysis was treated with a 'universal probe' that targets SSU rRNAs common to all species. That sample was collected near a site of upwelling where centric diatoms and heterotrophic dinoflagellates were abundant, as is clear from the epiflourescence micrograph Figure 11.12B, frame 1). In contrast, the probe array developed from the ESP2 sample indicated the presence of *P. australis*. The corresponding archived whole-cell sample was therefore processed using a probe that targets *P. australis* and results were consistent with that prediction (Figure 11.12B, frame 2). Similarly, the probe array developed from the ESP3 sample indicated that *P. australis* was very abundant and the corresponding whole-cell probe analysis also agreed with that observation (Figure 11.12B, frame 3). Lastly, the probe array developed from the ESP4 sample indicated the presence of both *P. australis* and *A. catenella*. In this case, the archived whole-cell sample was processed with a probe specific for *A. catenella*, confirming the presence of that species (Figure 11.12B, frame 4). In that same sample, one can also see the faint outline of large pennate diatoms (not labelled by the '*A. cat*' probe), the probable source of the *P. australis* signal seen on the corresponding probe array.

These simple, prototype oligonucleotide array tests prove that simultaneous detection of multiple HAB species in a single sample is possible, providing a basis for inferring what suite of toxins might also be present. To test this idea, the ESP was programmed to collect an aliquot of the same sample used to generate the probe arrays and used for whole-cell probing. Based on results of the probe tests, the resulting 'toxin archive' filters were screened for either domoic acid or saxitoxin activity using a receptor binding technique (Lefebvre et al., 1999; Powell and Doucette, 1999). Results for samples ESP1, ESP2 and ESP3 showed a gradient of domoic acid activity that parallel

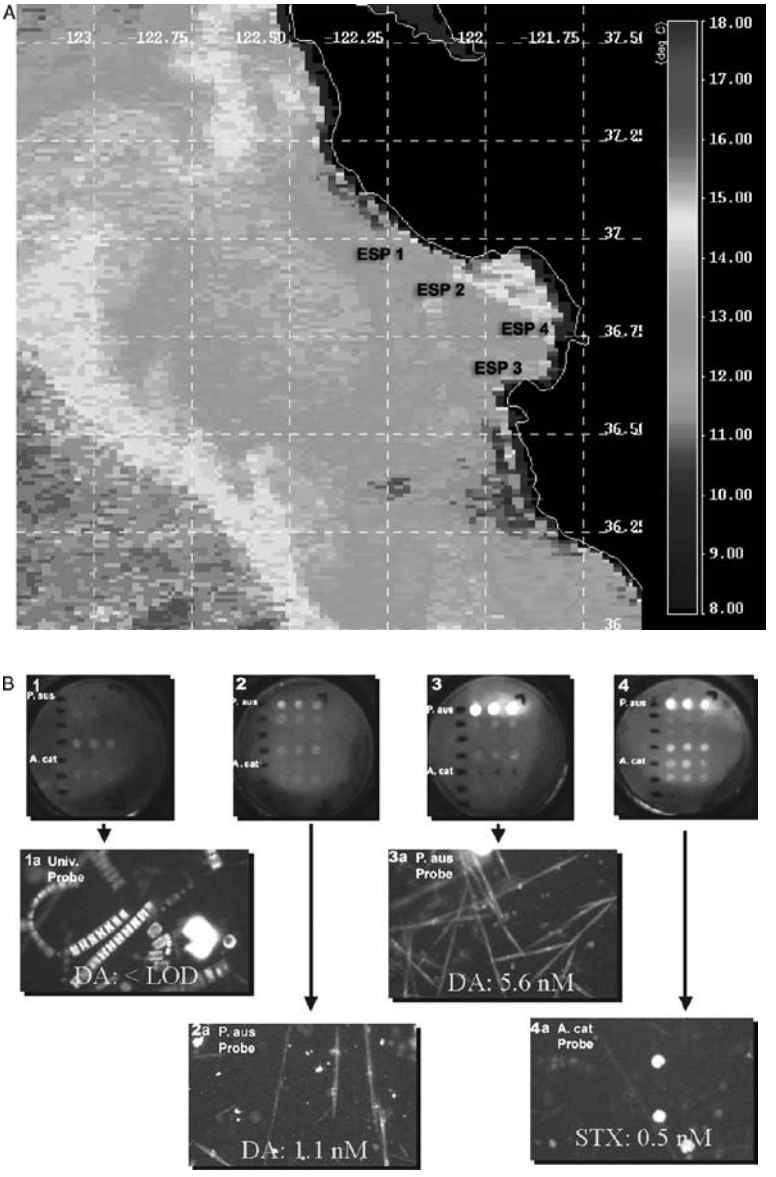

Figure 11.12
Examples of data obtained using the shipboard ESP in Monterey Bay, California. A, sea surface temperature and locations of sampling stations (ESP 1-4). B, images of the oligonucleotide probe arrays (centre frames) and micrographs showing results of fluorescent *in situ* hybridization assays (lower frames). Domoic acid and PSP toxin activity associated with a sample is printed at the foot of the micrographs. Locations of probes for

(Continued)

Figure 11.12 (*continued*)
P. australis and *A. catenella* on the arrays, spotted in triplicate, are denoted *P. australis* and *A. catenella* respectively. To develop a oligonucleotide probe array, the ESP collected 400 ml of seawater, concentrated particles >~5 μm onto a 25 mm Durapore filter, homogenized material retained in 1.5 ml of lysis reagent, and the resulting sample homogenate was drawn into the syringe. The sample collection puck was replaced with a puck carrying a custom-printed oligonucleotide probe array. The sample homogenate was passed over that array, followed by a sequence of reagents that reveal rRNA molecules retained at specific locations on the array grid using the principles of sandwich hybridization (Scholin et al., 1996, 1997, 1999). An image of the resulting array was recorded using the ESP's CCD camera. For whole cell hybridization, a 50 ml sample was passed through a 3 μm pore size polycarbonate filter and the particles retained were treated with a saline ethanol solution for 1 hour then dried (Miller and Scholin, 2000). The preserved, dried sample was stored onboard the ESP. Following deployment, the ESP was programmed to process the archived samples using fluorescent *in situ* hybridization after Miller and Scholin (2000). Once the hybridization process was complete, the sample filter was recovered and viewed using conventional epifluorescence microscopy. In the examples shown here, several different rRNA probes were used: Univ. (targets rRNA from all organisms), *P. aus* (targets rRNA specific to *P. australis*), and *A. catenalla* (targets rRNA specific to *A. catenella*; see Miller and Scholin, 1998). Samples archived for toxin analysis consisted of 750 ml aliquots concentrated onto GF/F filters stored dry onboard the ESP, then recovered post-deployment and held at –20°C until tested using a receptor binding technique for either domoic acid or saxitoxin (Lefebvre et al. 1999; Powell and Doucette 1999).

observations of the abundance of *P. australis* (Figures 11.12A, 11.12B, frames 1–3). Similarly, *A. catenella*, a suspected PSP toxin producer, was detected in sample ESP4; results of the toxin analysis confirmed that saxitoxin activity was also present in that sample (Figures 11.12A, 11.12B, frame 4).

11.4.3 Field test of the moored, subsurface ESP prototype

The *in situ* ESP was deployed in the Gulf of Maine in May 2001 with the objective of detecting *Alexandrium fundyense*. This species is often concentrated alongshore with the onset of downwelling favourable winds (Franks and Anderson, 1992*a*, 1992*b*); therefore, the ESP was deployed in an embayment within Casco Bay, Maine, where these cells might accumulate under such conditions. The instrument was moored in ~30 m of water with the sample processor module immobilized at 5 m (at low tide) and tethered to a surface float (Figure 11.13). Chlorophyll fluorescence and CTD sensors were attached to the ESP housing; the data obtained from these sensors along with times that the ESP was programmed to sample are shown in Figure 11.14A. During the deployment, a short burst of downwelling winds was experienced and the effect on the physical properties of the water column was apparent. Following this transition, *A. tamarense* cells were transported to the mooring site with a concentration of approximately 1–200 l^{-1}. A series of prototype, hand-spotted DNA probe arrays developed subsurface by the ESP demonstrate the appearance of this species at the mooring (Figure 11.14B, centre panel). At the same time the ESP was sampling, developing prototype

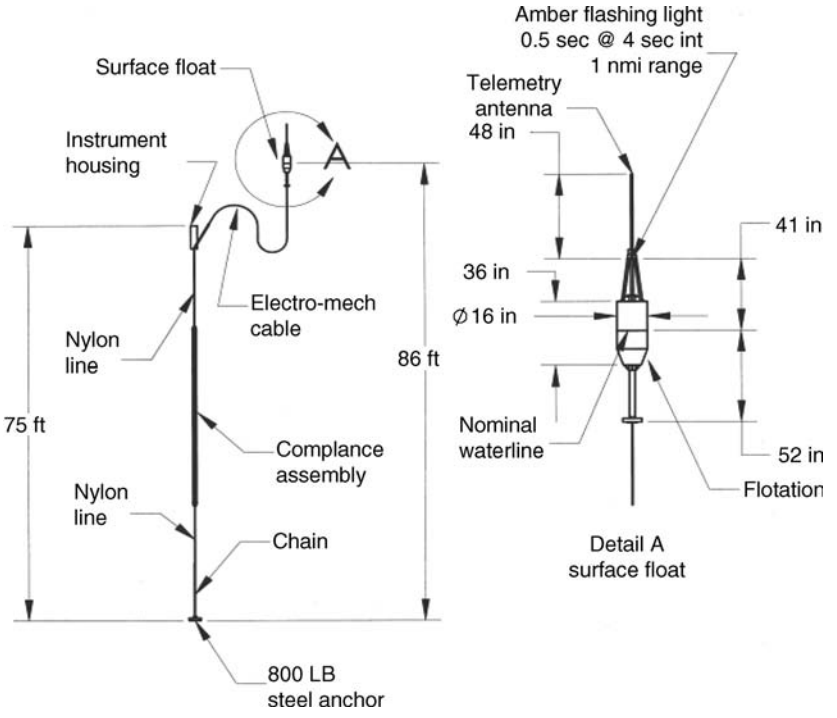

Figure 11.13
Example of mooring configuration for the 1G ESP. The depths of the mooring anchor, tether and ESP are adjustable. The ESP is held at a fixed depth from the bottom, so the actual depth of the instrument relative to the surface will vary in response to tidal fluctuations, storm surge, etc.

DNA probe arrays, and sending data to shore via radio modem, a ship-based crew used a profiling CTD to characterize the water column and Niskin bottles to collect water samples at a depth and location near that of the ESP mooring. Samples collected manually were then tested for the presence of *A. tamarense*, *P. australis* and *P. multiseries/pseudodelicatissima* cells using a benchtop version of the sandwich hybridization chemistry emulated by the ESP (Scholin et al., 1999) (Figure 11.15C, lower panel). Although *A. tamarense* cells accumulated in Casco Bay during this period, concentrations were not great enough to warrant public health warnings and shellfish bed closures. Low numbers of *P. australis* also appeared to be present in one of the samples. *P. multiseries and P. pseudodelicatissima* cells were not detected by the ESP nor in samples collected onboard ship and processed manually. To our knowledge, this is the first example of autonomous, subsurface, DNA probe-based detection of HAB species.

Protocols for printing DNA probes have been refined since the 2001 test deployment (Figure 11.15). An x, y, z translation table is now used to deposit 'probe ink' at specified locations on the array surface. The current arrays are fitted with probes for several species of harmful algae representing three different algal classes. The repertoire of rRNA-targeted probes is currently being expanded to include additional HAB species, bacteria and invertebrate larvae.

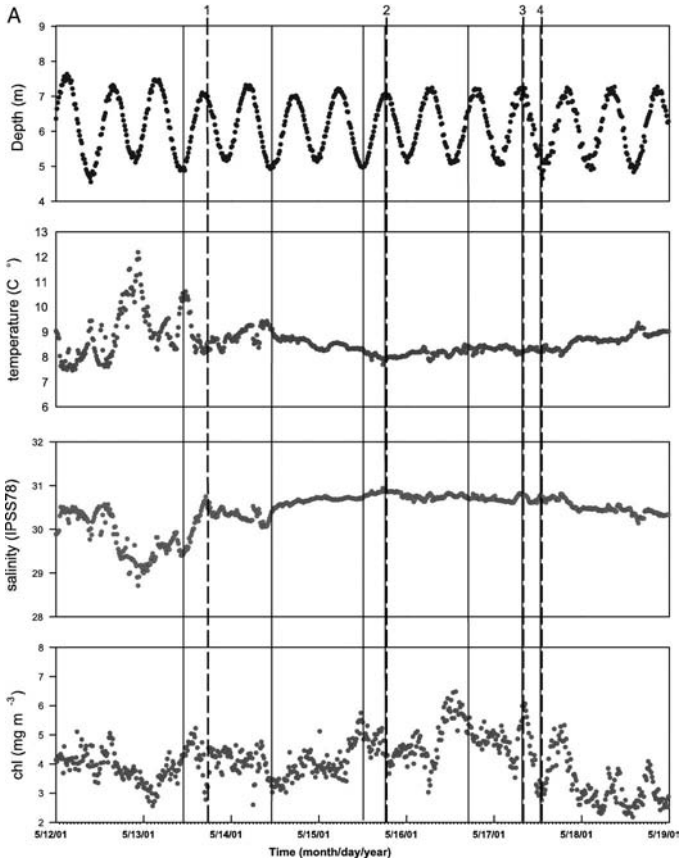
A
1
2
3
4
Depth (m)
temperature (C °)
salinity (IPSS78)
chl (mg m -3)
5/12/01
5/13/01
5/14/01
5/15/01
5/16/01
5/17/01
5/18/01
5/19/01
Time (month/day/year)

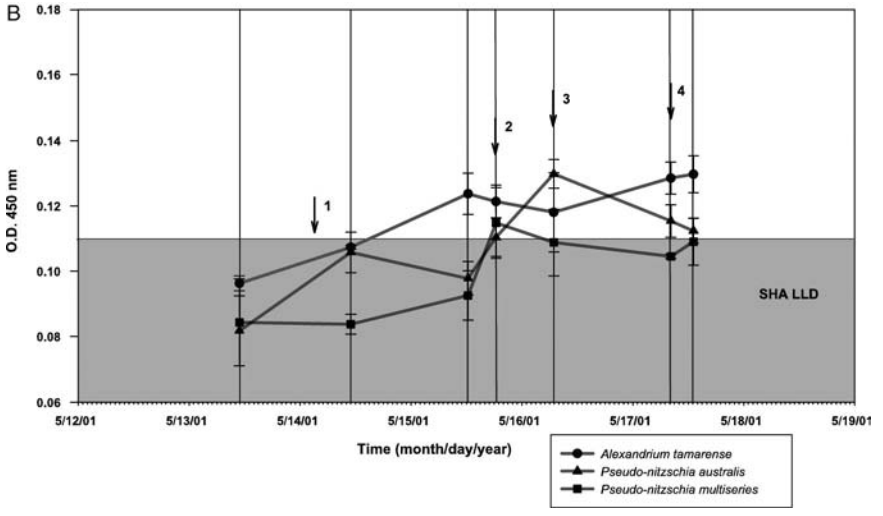
B
O.D. 450 nm
0.18
0.16
0.14
0.12
0.10
0.08
0.06
1
2
3
4
SHA LLD
5/12/01
5/13/01
5/14/01
5/15/01
5/16/01
5/17/01
5/18/01
5/19/01
Time (month/day/year)
Alexandrium tamarense
Pseudo-nitzschia australis
Pseudo-nitzschia multiseries

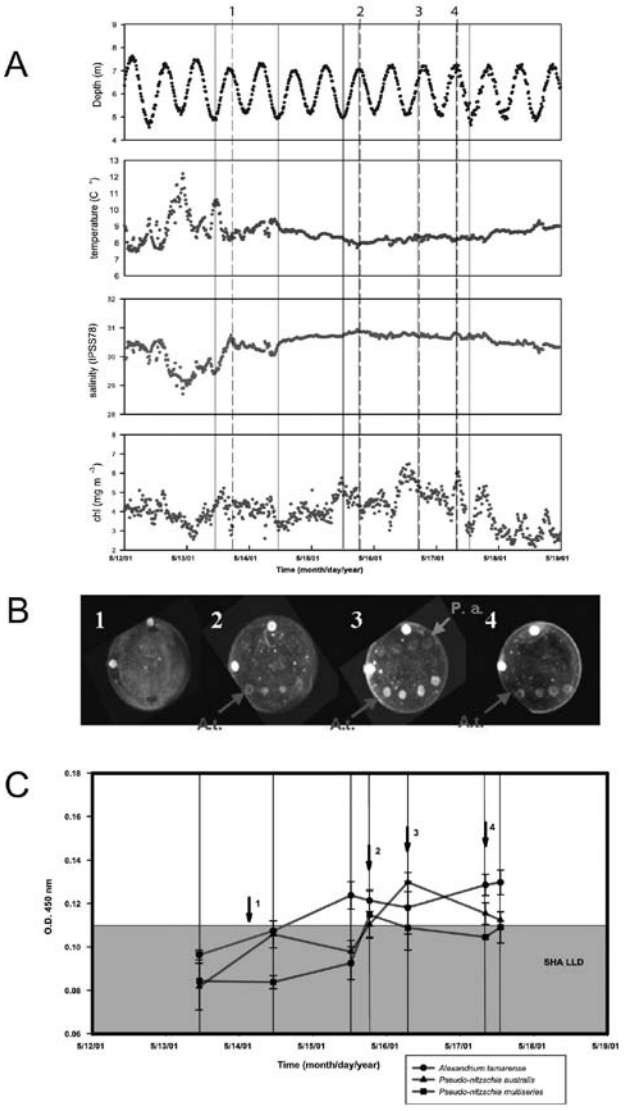

Figure 11.14 Examples of data obtained using the *in situ* ESP in Casco Bay, ME. A, depth, temperature, salinity, and chlorophyll fluorescence recorded on board the ESP during the deployment. Dashed black lines 1–4 show ESP sampling times that correspond to probe array images in (B); blue solid lines indicate when water samples were collected from a depth and position near the ESP mooring using Niskin bottles on a hydrowire. B, prototype DNA probe arrays developed on board the ESP (as in Figure 11.2); the two bright spots at top and left are registration marks; probes for *P. australis* (above), *P. multiseries/ pseudodelicatissima* (centre) and *A. tamarense* (below) are hand-spotted in quadruplicate. Arrays 1–4 correspond numerically to the same numbers shown on (A, dashed lines) and (C, arrows). C, results of benchtop sandwich hybridization assays (SHA; Scholin et al., 1999) for Niskin bottle samples collected at times shown in (A); probes used for that assay are the same as those spotted onto the arrays. Shaded area, non-detection range; values above that indicate a positive reaction; red, *A. tamarense*; green, *P. australis*; purple, *P. mulitiseries/pseudodelicatissima*.

11.4.4 2G ESP development plan

The existing 1G ESP has worked successfully on several, limited test deployments with extensive support by the original MBARI science/engineering design team. The 2G ESP will build on the same design concepts already validated in the existing units, incorporating changes to make it much more robust, compact and user friendly. The

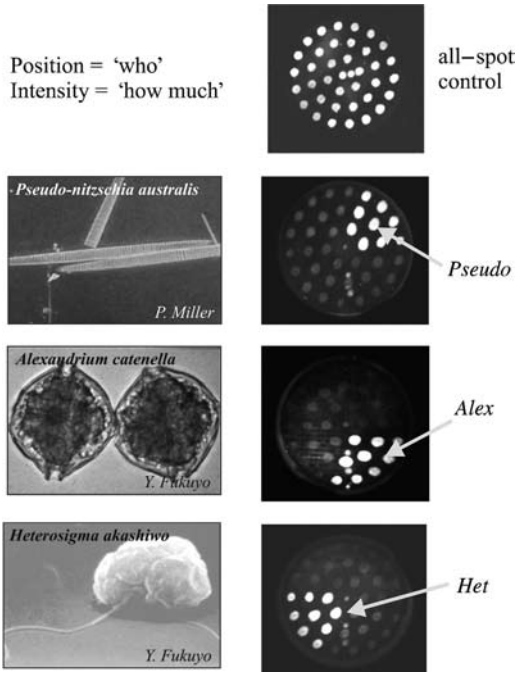

Figure 11.15
Custom, prototype DNA probe arrays printed on filters and developed in the ESP. Images show target organisms and corresponding array image. *Source*: Scholin, unpublished; images of cells kindly provided by Miller and Fukuyo.

overall goal in designing the 2G ESP is to produce a system that can be successfully deployed for a variety of applications on a routine basis by a team of trained technicians, thus making it accessible to a much larger group of users than is possible at present. A major effort is being made to reduce the size, complexity and power consumption of the instrument, and to take advantage of microfluidic-scale detection technologies. There will also be an effort to provide space and appropriate electrical, software and fluid connectivity to support the addition of future sample and analytical 'modules'. The first 2G ESP was scheduled to begin operation mid-2005.

11.5 Conclusions and future prospects

Molecular diagnostics are increasingly being introduced into HAB research and monitoring programmes, but these tools are far from universally available and are not uniformly applied even within the HAB research community. Introduction of novel technologies for taxon- and toxin-specific detection into a regulatory framework, which involves human health and has implications for national and international commerce, will always be subject to a legislative lag phase, as well as to extensive validation trials. In many cases, this may involve approval and certification, such as by evaluation

panels of the Association of Official Analytical Chemists, the World Health Organization, national regulatory authorities (e.g. US Food and Drug Administration), or supranational trading consortia (e.g. European Union, the Asia-Pacific Economic Cooperation (APEC), etc.). Among the more than 50 countries that maintain HAB surveillance programmes, only a handful (e.g. Norway, New Zealand) actually use toxic cell concentration and plankton toxicity data *directly* for regulatory purposes, such as the closure of shellfish beds and early warning to fish aquaculturists. Nevertheless, such long-term concerns should not discourage scientists and engineers from attempting to design and implement advanced sensor technology for bloom monitoring and dynamics studies.

Such systems can serve a multitude of functions:

- early warning systems for aquaculturists, fisheries personnel and related regulatory agencies;
- acquistion of long-term continous data sets for hindcast and data assimilation modelling;
- provision of strategic advice on location-specific bloom probabilities for site-selection and coastal zone management;
- rapid screening technology to reduce the regulatory burden of conventional monitoring based on mammalian bioassays and instrumental analysis;
- assistance to scientists in determining cause and effect relationships in bloom dynamic studies;
- facilitation of studies on environmental effects of HABs;
- public education and awareness of coastal environmental issues through documentaries, webcasts and website information.

For the next decade, we expect that many of these automated real-time bloom or toxin detection systems will have to be operated in parallel with more traditional methods until scientists, environmental managers, regulatory authorities and even the general public become more comfortable with the robustness of these systems, as well as the reliability and accuracy of the data. For example, whole-cell protocols for harmful algae and cell-free methods for both these organisms and their toxins are often employed in a complementary fashion. Whole-cell-based applications provide a basis for visualizing specific cells that harbour and express molecular signatures of interest, whereas cell-free formats allow for detecting a suite of molecular and chemical signatures, but with no reference to organism morphology. Miniaturized analytical systems that meet functional requirements imposed by whole-cell and cell-free molecular detection methods are under active development and in some cases are already commercialized. Nonetheless, bringing these advancements to bear on autonomous platforms applied to environmental research and monitoring requires sample collection and processing schemes that differ substantially from those currently used or envisioned for biomedical tests.

It must, therefore, be emphasized that in addition to detection methods for harmful algal species and their toxins, parallel development of technologies for the collection and concentration of these potentially dilute analytes is essential. As discussed above, wide fluctuations in the abundance of algal species and toxin levels over a range of temporal/spatial scales are well documented and can pose a challenge to obtaining sufficient material for analysis. For example, sensitive technologies (e.g. LC-MS) offer the prospect of near-simulaneous toxin detection, even in *individual* cells, for a multitude of toxins from different toxin classes, but these 'universal toxin detection systems' would have to be complemented with universal extraction and clean-up methods to achieve *in situ* toxin detection systems.

To fully realize the potential for *in situ* detection for a range of applications, the research, engineering, industry, resource management, and regulatory communities must strike up a dialogue to identify users' needs, the most appropriate technologies to obtain these data, and the most efficient means to manufacture and bring to market reliable products that meet those demands. In contrast to measuring many physical and chemical properties associated with a water mass (e.g. temperature, conductivity, alkalinity, etc.), none of the approaches for detecting HAB species and their toxins based on molecular characteristics are instantaneous. Samples must be collected and processed in order to reveal the target organisms and/or toxins of interest. The amount of time required for processing samples and the equipment needed varies greatly depending on assay format (whole-cell or cell-free), the nature of the target molecule itself, and details of the analytical methods employed. Therefore, near-term, *in situ* application of 'biosensors' as considered here will probably be tightly integrated with, and to some extent controlled by, other physico-chemical sensors. The latter sensors will probably be used to trigger a molecular analytical event in response to a contextual, hierarchical set of environmental variables readily detectable at high frequency and previously identified as indicators of conditions favourable for HAB formation. Despite the challenges that lie ahead, the development of sensors based on molecular biological techniques is progressing rapidly and holds great promise for application on autonomous platforms.

References

Adachi, M., Sako, Y. and Ishida, Y. 1996. Identification of the toxic dinoflagellates *Alexandrium catenella* and *A. tamarense* (Dinophyceae) using DNA probes and whole cell hybridization. *J. Phycol.*, 32, pp. 1049–52.

Anderson, D. M. 1995. Identification of harmful algal species using molecular probes: an emerging perspective. In: P. Lassus, G. Arzul, E. Erard, P. Gentien and C. Marcaillou (eds), *Harmful Marine Algal Blooms*. Paris, Technique et Documentation-Lavoisier/Intercept Ltd, pp. 3–13.

Anderson, D. M. 1998. Physiology and bloom dynamics of toxic *Alexandrium* species, with emphasis on life cycle transitions. In: Anderson et al. (eds), op. cit., pp. 29–48.

Anderson, D. M., Cembella, A. D. and Hallegraeff, G. M. (eds). 1998. *Physiological Ecology of Harmful Algal Blooms*. Heidelberg, Springer-Verlag. (NATO Advanced Study Institute Series 41.)

Anderson, D. M. and Cheng, T. P. O. 1988. Intracellular localization of saxitoxins in the dinoflagellate *Gonyaulax tamarensis. J. Phycol.*, 24, pp. 17–22.

Anderson, D. M., Keafer, B. A., Kulis, D. M., Connell, L. and Scholin, C. A. 2003. Application of molecular probes in studies of *Alexandrium* in the Gulf of Maine: success and problem areas. In: K. A. Steidinger, J. H. Lansdberg, C. R. Tomas and G. A. Vargo (eds), *Harmful Algae 2002.* Proc. X International Conference on Harmful Algae (20–25 October 2002). St Petersburg, Fla./Paris, Florida Fish and Wildlife Conservation Commission/Intergovernmental Oceanographic Commission of UNESCO, p. 14. (Abstract)

Anderson, D. M., Kulis, D. and Cosper, E. M. 1990. Immunofluorescent detection of the brown tide organism *Aureococcus anophagefferens*. In: E. M. Cosper, V. M. Bricelj and E. J. Carpenter (eds), *Novel Phytoplankton Blooms: Causes and Impacts of Recurrent Brown Tides and Other Unusual Blooms*. Berlin, Springer-Verlag, pp. 213–28.

Anderson, D. M., Kulis, D. M., Doucette, G. J., Gallagher, J. C. and Balech, E. 1994. Biogeography of toxic dinoflagellates in the genus *Alexandrium* from the northeastern United States and Canada. *Mar. Biol.*, 120, pp. 467–78.

Anderson, D. M., Kulis, D. M., Keafer, B. A. and Berdalet, E. 1999. Detection of the toxic dinoflagellate *Alexandrium fundyense* (Dinophyceae) with oligonucleotide and antibody probes: variability in labeling intensity with physiological condition. *J. Phycol.*, 35, pp. 870–83.

Anderson, D. M., Kulis, D. M., Keafer, B. A., Gribble, K. E., Marin, R. and Scholin, C. A. 2005. Identification and enumeration of *Alexandrium* spp. from the Gulf of Maine using molecular probes. *Deep Sea Res. II*, 52, pp. 2467–2490.

AOAC. 1990. Paralytic shellfish poison. Biological method. Final action. In: K. Hellrich (ed.), *Official Methods of Analysis*, 15th edn. Arlington, Va., Association of Official Analytical Chemists, Sec. 959.08, pp. 881–82.

Babin, M., Roesler, C. S. and Cullen, J. J. (eds). 2006. *Real-time Coastal Observing Systems for Marine Ecosystem Dynamics and Harmful Algal Blooms: Theory, Instrumentation and Modelling*. Paris, Intergovernmental Oceanographic Commission of UNESCO. (Monographs on Oceanographic Methodology.)

Baden, D. G. and Adams, D. J. 2000. Brevetoxins: chemistry, mechanism of action, and methods of detection. In: L. M. Botana (ed.), *Seafood and Freshwater Toxins: Pharmacology, Physiology and Detection*. New York, Marcel Dekker, pp. 505–32.

Bargu, S., Powell, C. L., Coale, S. L., Busman, M., Doucette, G. J. and Silver, M. J. 2002. Krill: a potential vector for domoic acid in marine food webs. *Mar. Ecol. Progr. Ser.*, 237, pp. 209–16.

Bates, S. S. 1998. Ecophysiology and metabolism of ASP toxin production. In: Anderson et al. (eds), op. cit., pp. 405–26.

Bates, S. S., Garrison, D. L. and Horner, R. A. 1998. Bloom dynamics and physiology of domoic-acid-producing *Pseudo-nitzschia* species. In: Anderson et al. (eds), op. cit., pp. 267–92.

Bates, S. S., Leger, C., Keafer, B. A. and Anderson, D. M. 1993. Discrimination between domoic-acid-producing and non-toxic forms of the diatom *Pseudonitzschia pungens* using immunofluorescence. *Mar. Ecol. Progr. Ser.*, 100, pp. 185–95.

Bates, S. S., Scholin, C. A., Ferguson, M. and Leger, C. 1999. Application of ribosomal RNA-targeted probes to detect *Pseudo-nitzschia multiseries* and *P. pungens* in Atlantic Canadian waters. *Can. Tech. Rep. Fish. Aquat. Sci.*, 2261, pp. 63–67.

Berg, D. E., Akopyants, N. S. and Kersulyte, D. 1994. Fingerprinting microbial genomes using the RAPD or AP-PCR method. *Meth. Mole. Cell. Biol.*, 5, pp. 13–24.

Bolch, C. J. S. 2001. PCR protocols for genetic identification of dinoflagellates directly from single cysts and plankton cells. *Phycologia*, 40, pp. 162–67.

Bolch, C. J. S., Orr, P. T., Jones, G. J. and Blackburn, S. I. 1999. Genetic, morphological and toxicological variation among globally distributed strains of *Nodularia* (Cyanobacteria). *J. Phycol.*, 35, pp. 339–55.

Botana, L. M. (ed.). 2000. *Seafood and Freshwater Toxins: Pharmacology, Physiology and Detection*. New York, Marcel Dekker.

Bowers, H. A., Tengs, T., Glasgow, H. B. Jr, Burkholder, J. M., Rublee, P. A. and Oldach, D. W. 2000. Development of real-time PCR assays for rapid detection of *Pfiesteria piscicida* and related dinoflagellates. *Appl. Environ. Microbiol.*, 66, pp. 4641–48.

Bricelj, V. M. and Lonsdale, D. J. 1997. *Aureococcus anophagefferens*: cause and ecological consequences of brown tides in US mid-Atlantic coastal waters. *Limnol. Oceanogr.*, 42, pp. 1023–38.

Bricelj, V. M. and Shumway, S. E. 1998. Paralytic shellfish toxins in bivalve mollusks: occurrence, transfer kinetics, and biotransformation. *Rev. Fish. Sci.*, 6, pp. 315–83.

Carmichael, W. W. 2001. Health effects of toxin-producing cyanobacteria: the CyanoHABs. *Hum. Ecol. Risk Assess.*, 7, pp. 1393–407.

Caron, D. A., Schaffner, R. A., Moran, D. M., Dennett, M. R., Lonsdale, D. J., Gobler, C. J., Nuzzi, R. and McLean, T. I. 2003. Development and application of a monoclonal antibody technique for counting *Aureococcus anophagefferens*, an alga causing recurrent brown tides in the northeastern United States. *Appl. Environ. Microbiol.*, 69, pp. 5492–502.

Casper, E. T., Paul, J. H. and Smith, M. C. 2004. Concentration, detection and quantification of enteroviruses in marine coastal environments by real-time NASBA. In*: ASLO/TOS Ocean Research 2004 Conference, 15–20 February 2004, Honolulu, Hawaii*, p. 26. (Abstract)

Cembella, A. D. 1998. Ecophysiology and metabolism of paralytic shellfish toxins in marine microalgae. In: Anderson et al. (eds), op. cit., pp. 381–404.

Cembella, A. D. 2003. Chemical ecology of eukaryotic microalgae in marine ecosystems. *Phycologia*, 42, pp. 420–47.

Cembella, A. D. and Destombe, C. 1996. Genetic differentiation among *Alexandrium* populations from eastern Canada. In: T. Yasumoto, Y. Oshima and Y. Fukuyo (eds), *Harmful and Toxic Algal Blooms*. Paris, Intergovernmental Oceanographic Commission of UNESCO, pp. 447–50.

Cembella, A. D., Doucette, G. J. and Garthwaite, I. 2003. *In vitro* assays for phycotoxins. In: G. M. Hallegraeff et al. (eds), op. cit., pp. 297–345.

Cembella, A. D., Lewis, N. I. and Quilliam, M. A. 1999. Spirolide composition in micro-extracted pooled cells isolated from natural plankton assemblages and from cultures of the dinoflagellate *Alexandrium ostenfeldii*. *Nat. Tox.*, 8, pp. 1–10.

Cembella, A. D., Quilliam, M. A., Lewis, N. I., Bauder, A. G., Dell'Aversano, C., Thomas, K., Carver, C., Jellett, J. and Cusack, R. R. 2002. The toxigenic marine dinoflagellate *Alexandrium tamarense* as the probable cause of enhanced mortality of caged salmon in Nova Scotia. *Harmful Algae*, 26, pp. 1–13.

Chianella, I., Piletsky, S. A., Tothill, I. E., Chen, B. and Turner, A. P. F. 2003. MIP-based solid phase extraction cartridges combined with MIP-based sensors for the detection of microcystin-LR. *Biosens. Bioelectron.*, 18, pp. 119–27.

Cho, E. S., Hur, H. J., Byun, H. S., Lee, S. G., Rhodes, L. L., Jeong, C. S. and Park, J. G. 2002. Monthly monitoring of domoic acid producer *Pseudo-nitzschia multiseries* (Hasle) Hasle using species-specific DNA probes and WGA lectins and abundance of *Pseudo-nitzschia* species (Bacillariophyceae) from Chinhae Bay, Korea. *Bot. Mar.*, 45, pp. 364–72.

Cho, E. S., Park, J. G., Oh, B. C. and Cho, Y. C. 2001. The application of species-specific DNA-targeted probes and fluorescently tagged lectins to differentiate several species of *Pseudo-nitzschia* (Bacillariophyceae) in Chinhae Bay, Korea. *Sci. Mar.*, 65, pp. 207–14.

Cho, E. S., Rhodes, L. L. and Cho, Y. C. 2000. Comparative lectin binding patterns of *Cochlodinium polykrikoides* Margalef in field and culture. *J. Kor. Soc. Oceanogr.*, 35, pp. 153–57.

Cho, E. S., Seo, G. W., Lee, S. G., Kim, H. G., Lee, S. J., Rhodes, L. L. and Hong, Y. K. 1998. Application of FITC-conjugated lectin probes for the recognition and differentiation of some Korean coastal red tide microalgae. *J. Fish. Sci. Tech.*, 1, pp. 250–54.

Coyne, K. J., Hutchins, D. A., Hare, C. E. and Cary, S. C. 2001. Assessing temporal and spatial variability in *Pfiesteria piscicida* distributions using molecular probing techniques. *Aquat. Microb. Ecol.*, 24, pp. 275–85.

Della Loggia, R, Sosa, S. and Tubaro, A. 1999. Methodological improvement of the protein phosphatase inhibition assay for the detection of okadaic acid in mussels. *Nat. Tox.*, 7, pp. 387–92.

Doucette, G. J., Traynor, I. M., King, K. L., Mikulski, T. M. and Elliott, C. T. 2005. A surface plasmon resonance-based immunobiosensor for domoic acid: applications for diverse sample matrices. *Marine and Freshwater Toxins Analysis*: 1st Joint Symposium and AOAC Task Force Meeting, 11–14 April 2005, Baiona, Spain. (Poster)

Dyble, J., Paerl, H. W. and Neilan, B. A. 2002. Genetic characterization of *Cylindrospermopsis raciborskii* (Cyanobacteria) isolates from diverse geographic origins based on *nifH* and *zcpcBA*-IGS nucleotide sequence analysis. *Appl. Environ. Microbiol.*, 68, pp. 2567–71.

Eller, G. and Medlin, L. 2002. Molecular probes for the rapid detection of toxin marine microalgae. In: K. A. Steidinger, J. H. Lansdberg, C. R. Tomas and G. A. Vargo (eds), *Harmful Algae 2002.* Proc. X International Conference on Harmful Algae (20–25 October 2002). St Petersburg, Fla./Paris, Florida Fish and Wildlife Conservation Commission/Intergovernmental Oceanographic Commission of UNESCO, p. 83. (Abstract)

Fairey, E. R., Edmunds, J. S. G., Deamer-Melia, N. J., Glasgow, H. Jr, Johnson, F. M., Moeller, P. R., Burkholder, J. M. and Ramsdell, J. S. 1999. Reporter gene assay for fish-killing activity produced by *Pfiesteria piscicida*. *Environ. Health Perspect.*, 107, pp. 711–14.

Ferguson, J. A., Steemers, F. J. and Walt, D. R. 2000. High-density fiber-optic DNA random microsphere array. *Anal. Chem.*, 72, pp. 5618–24.

Fernández, M. L., Richard, D. J. A. and Cembella, A. D. 2003. *In vivo* assays for phycotoxins. In: Hallegraeff et al. (eds), op. cit., pp. 347–80.

Field, K. G., Olsen, G. J., Lane, D. J., Giavannoni, S. J., Ghiselin, M. T., Raff, E. C., Pace, N. R. and Raff, R. A. 1988. Molecular phylogeny of the animal kingdom. *Science*, 239, pp. 748–53.

Franks, P. J. S. and Anderson, D. M. 1992*a*. Alongshore transport of a toxic phytoplankton bloom in a buoyancy current: *Alexandrium tamarense* in the Gulf of Maine. *Mar. Biol.*, 112, pp. 153–64.

Franks, P. J. S. and Anderson, D. M. 1992*b*. Toxic phytoplankton blooms in the southwestern Gulf of Maine: testing hypotheses of physical control using historical data. *Mar. Biol.*, 112, pp. 165–74.

Gentien, P., Lunven, M., Le Haitre, M. and Duvent, J. L. 1995. *In situ* depth profiling of particle sizes. *Deep Sea Res*., 42, pp. 1297–312.

Godhe, A., Otta, S. K., Rehnstam-Holm, A. S, Karunasagar, I. and Karunasagar, D. I. 2001. Polymerase chain reaction in detection of *Gymnodinium mikimotoi* and *Alexandrium minutum* in field samples from southwest India. *Mar. Biotech*., 3, pp. 152–62.

Goffredi, S. K., Jones, W., Scholin, C., Marin, R., Hallam, S. and Vrijenhoek, R. C. 2006 Molecular detection of marine larvae. *Mar. Biotech.,* 8, pp. 149–160.

Gross, G. W. 1994. Internal dynamics of randomized mammalian neuronal networks in culture. In: D. A. Stenger and R. M. McKenna (eds), *Enabling Technologies for Cultured Neural Networks*. New York, Academic Press, pp. 277–317.

Hall, S. 1999. Volunteer phytoplankton program. In: J. L. Martin and K. Haya (eds), *Proc. Sixth Canadian Workshop on Harmful Marine Algae*. *Can. Tech. Rep. Fish. Aquat. Sci*., 2261, p. 30.

Hallegraeff, G. M., Anderson, D. M. and Cembella, A. D. (eds). 2003. *Manual on Harmful Marine Microalgae*. Paris, Intergovernmental Oceanographic Commission of UNESCO. (Monographs on Oceanographic Methodology 11.)

Hasle, G. R. 1995. *Pseudo-nitzschia pungens* and *P. multiseries* (Bacillariophyceae): nomenclatural history, morphology, and distribution. *J. Phycol.*, 31, pp. 428–35.

Haywood, A. J., Scholin, C. A., Marin, R. III, Rhodes, L. L. and Steidinger, K. A. 2002. Whole cell and sandwich hybridization assays for *Karenia brevis* and related species. In: K. A. Steidinger, J. H. Lansdberg, C. R. Tomas and G. A. Vargo (eds), *Harmful Algae 2002.* Proc. X International Conference on Harmful Algae (20–25 October 2002). St Petersburg, Fla./Paris, Florida Fish and Wildlife Conservation Commission/Intergovernmental Oceanographic Commission of UNESCO, p. 123. (Abstract)

Hoagland, P., Anderson, D. M., Kaoru, Y. and White, A. W. 2002. The economic effects of harmful algal blooms in the United States: estimates, assessment issues, and information needs. *Estuaries*, 25, pp. 819–37.

Hori, K., Ogata, T., Kamiya, H. and Mimuro, M. 1996. Lectin-like compounds and lectin receptors in marine microalgae: haemaglutination and reactivity with purified lectins. *J. Phycol.*, 32, pp. 783–90.

Hummert, C., Ruehl, A., Reinhardt, K., Gerdts, G. and Luckas, B. 2002. Simultaneous analysis of different algal toxins by LC-MS. *Chromatographia*, 5, pp. 673–80.

Innis, M. A., Gelfand, D. H. and Sninsky, J. J. (eds). 1995. *PCR Strategies*. San Diego, Calif., Academic Press.

Jellett, J. F., Roberts, R. L., Laycock, M. V., Quilliam, M. A. and Barrett, R. E. 2002. Detection of paralytic shellfish poisoning toxins in shellfish tissue using Mist Alert™, a new rapid test, in parallel with the regulatory AOAC mouse bioassay. *Toxicon*, 40, pp. 1407–25.

John, U., Cembella, A., Hummert, C., Elbrächter, M., Groben, R. and Medlin, L. K. 2003. Discrimination of the toxigenic dinoflagellates *Alexandrium tamarense* and *A. ostenfeldii* in co-occurring natural populations from Scottish coastal waters. *Eur. J. Phycol.*, 38, pp. 25–40.

John, U., Groben, R., Beszteri, B. and Medlin, L. 2004. Utility of amplified fragment length polymorphisms (AFLP) to analyse genetic structure within the *Alexandrium tamarense* species complex. *Protist*, 155, pp. 169–79.

Hallegraeff, G. M., Anderson, D. M. and Cembella, A. D. (eds). 2003. *Manual on Harmful Marine Microalgae*. Paris, Intergovernmental Oceanographic Commission of UNESCO. (Monographs on Oceanographic Methodology 11.)

Kirkpatrick, G. J., Millie, D. F., Moline, M. A. and Schofield, O. M. 2000. Optical discrimination of a phytoplankton species in natural mixed populations. *Limnol. Oceanogr.*, 45, pp. 467–71.

Landsberg, J. H. 2002. The effects of harmful algal blooms on aquatic organisms. *Rev. Fish. Sci.*, 10, pp. 1–113.

Langebrake, L. C. 2003. AUV sensors for marine research. In: G. Griffiths (ed.), *Technology and Applications of Autonomous Underwater Vehicles*. London, Taylor and Francis, pp. 245–77.

Lawrence, J. E. and Cembella, A. D. 1999. An immunolabelling technique for the localization of diarrhetic shellfish toxins in individual microalgae. *Phycologia*, 38, pp. 60–65.

Laycock, M. V., Jellett, J. F., Belland, E. R., Bishop, P. C., Thériault, B. L., Russell-Tattrie, A. L., Quilliam, M. A., Cembella, A. D. and Richards, R. C. 2001. Mist Alert™: a rapid assay for paralytic shellfish poisoning toxins. In: G. M. Hallegraeff, S. I. Blackburn, C. J. Bolch and R. J. Lewis (eds), *Harmful Algal Blooms 2000*. Paris, Intergovernmental Oceanographic Commission of UNESCO, pp. 254–56.

Lee, J. S., Igarashi, T., Fraga, S., Dahl, E., Hovgaard, P. and Yasumoto, T. 1989. Determination of diarrhetic shellfish toxins in various dinoflagellate species. *J. App. Phycol.*, 1, pp. 147–52.

Lefebvre, K. A., Powell, C. L. Busman, M., Doucette, G. J., Moeller, P. D. R., Silver, J. B., Miller, P. E., Hughes, M. P., Singaram, S., Silver, M. W. and Tjeerdema, R. S. 1999. Detection of domoic acid in northern anchovies and California sea lions associated with an unusual mortality event. *Nat. Tox.*, 7, pp. 85–92.

Lewis, R. J. 1995. Detection of ciguatoxins and related benthic dinoflagellate toxins: *in vivo* and *in vitro* methods. In: G. M. Hallegraeff, D. M. Anderson and A. D. Cembella (eds), *Manual on Harmful Marine Microalgae*. Paris, Intergovernmental Oceanographic Commission of UNESCO, pp. 135–61.

Li, Y. and Moczydlowski, E. 1991. Purification and partial sequencing of saxiphilin, a saxitoxin-binding protein from the bullfrog, reveals homology to transferrin. *J. Biol. Chem.*, 266, pp. 15481–87.

Lin, S. and Carpenter, E. J. 1996. An empirical protocol for whole-cell immunofluorescence of marine phytoplankton. *J. Phycol.*, 32, pp. 1083–94.

Litaker, R. W., Sundseth, R., Wojciechowski, M., Bonaventura, C., Henkens, R. and Tester, P. 2001. Electrochemical detection of DNA or RNA from harmful algal bloom species. In: G. M. Hallegraeff, S. I. Blackburn, C. J. Bolch and R. J. Lewis (eds), *Harmful Algal Blooms 2000*. Paris, Intergovernmental Oceanographic Commission of UNESCO, pp. 242–45.

Litaker, R. W. and Tester, P. A. 2002. Molecular methods for detecting and characterizing harmful phytoplankton. In: C. J. Hurst, R. L.Crawford, G. R. Knudsen, M. J. McInerney and L. D. Stetzenbach (eds), *Manual of Environmental Microbiology*, 2nd edn. Washington DC, ASM Press, pp. 342–53.

Litaker, R. W., Vandersea, M. W., Kibler, S. R., Madden, V. J., Noga, E. J. and Tester, P. A. 2002. Life cycle of the heterotrophic dinoflagellate *Pfiesteria piscicida* (Dinophyceae). *J. Phycol.*, 38, pp. 442–63.

Llewellyn, L. E., Bell, P. M. and Moczydlowski, E. G. 1997. Phylogenetic survey of soluble saxitoxin-binding activity in pursuit of the function and molecular revolution of saxiphilin, a relative of transferrin. *Proc. Roy. Soc. Lond. Ser. B, Biol. Sci.*, 264, pp. 891–902.

Llewellyn, L. E., Doyle, J., Jellet, J., Barrett, R., Alison, C., Bentz, C. and Quilliam, M. 2001. Measurement of paralytic shellfish toxins in molluscan extracts: comparison of the microtitre plate saxiphilin and sodium channel radioreceptor assays with mouse bioassay, HPLC analysis and a commercially available cell culture assay. *Food Additives and Contaminants*, 18, pp. 970–80.

Llewellyn, L. E., Doyle, J. and Negri, A. P. 1998. A high-throughput, microtiter plate assay for paralytic shellfish poisons using the saxitoxin-specific receptor, saxiphilin. *Anal. Biochem.*, 261, pp. 51–56.

Lotierzo, M., Henry, O. Y. F., Piletsky, S., Tothill, I., Cullen, D., Kania, M., Hock, B. and Turner, A. P. F. 2004. Surface plasmon resonance sensor for domoic acid based on grafted imprinted polymer. *Biosens. Bioelectron.*, 20, pp. 145–52.

Luckas, B., Hummert, C. and Oshima, Y. 2003. Analytical methods for paralytic shellfish poisons. In: Hallegraeff et al. (eds), op. cit., pp. 191–209.

Lundholm, N., Moestrup, Ø., Hasle, G. R. and Hoef-Emden, K. 2003. What is *Pseudo-nitzschia pseudodelicatissima*? – a study of the *P. pseudodelicatissima/cuspidata* complex (Bacillariophyceae). *J. Phycol.*, 39, pp. 797–813.

Lundholm, N. Moestrup, Ø., Kotaki, Y., Scholin, C. and Miller, P. 2006. Inter- and intraspecific variation of the *Pseudo-nitzschia*-complex (Bacillariophyceae) illustrated by rRNA probes, morphological data and phylogenetic analyses identification of *P. decipiens* and *P. dolorosa* spp. Nov. *J. Phycol.*, 42, pp. 464–481.

Mackintosh, F. H. and Smith, E. A. 2002. Evaluation of Mist Alert™ rapid test kits for the detection of paralytic and amnesic shellfish poisoning toxins in shellfish. *J. Shellfish Res.*, 21, pp. 455–60.

Maestrini, S. 1998. Bloom dynamics and ecophysiology of *Dinophysis* spp. In: Anderson et al. (eds), op. cit., pp. 243–66.

Manger, R. L., Leja, L. S., Lee, S. Y., Hungerford, J. M., Hokama, Y., Dickey, R. W., Granade, H. R., Lewis, R., Yasumoto, T. and Wekell, M. M. 1995. Detection of sodium channel toxins: directed cytotoxicity assays of purified ciguatoxins, brevetoxins, saxitoxins, and seafood extracts. *J. Assoc. Offic. Anal. Chem. Int.*, 78, pp. 521–27.

Marquette, C. A., Coulet, P. R. and Blum, L. J. 1999. Semi-automated membrane based chemiluminescent immunosensor for flow injection analysis of okadaic acid in mussels. *Anal. Chim. Acta*, 398, pp. 173–82.

Medlin, L. K., Kerkmann, K., Huljic, S., Eller, G. and Lange, M. 2002. Application of molecular probes for the detection of harmful algae on DNA-microchips. In: K. A. Steidinger, J. H. Lansdberg, C. R. Tomas and G. A. Vargo (eds), *Harmful Algae 2002.* Proc. X International Conference on Harmful Algae (20–25 October 2002). St Petersburg, Fla./Paris, Florida Fish and Wildlife Conservation Commission/Intergovernmental Oceanographic Commission of UNESCO, p. 193. (Abstract)

Mikulski, C. M., Morton, S. and Doucette, G. J. 2005. Development and application of LSU rRNA probes for *Karenia brevis* in the Gulf of Mexico, USA. *Harmful Algae*, 4, pp. 49–60.

Miller, P. E. and Scholin, C. A. 1996. Identification of cultured *Pseudo-nitzschia* (Bacillariophyceae) using species-specific LSU rRNA-targeted fluorescent probes. *J. Phycol.*, 32, pp. 646–55.

Miller, P. E. and Scholin, C. A. 1998. Identification and enumeration of cultured and wild *Pseudo-nitzschia* (Bacillariophyceae) using species-specific LSU rRNA-targeted fluorescent probes and filter-based whole cell hybridization. *J. Phycol.*, 34, pp. 371–82.

Miller, P. E. and Scholin, C. A. 2000. On detection of *Pseudo-nitzschia* species using rRNA-targeted probes: sample fixation and stability. *J. Phycol.*, 36, pp. 238–50.

Naar, J., Weidner, A. and Baden, D. 2002. Competitive ELISA – an accurate, quick and effective tool to monitor brevetoxins in environmental and biological samples. In: K. A. Steidinger, J. H. Lansdberg, C. R. Tomas and G. A. Vargo (eds), *Harmful Algae 2002.* Proc. X International Conference on Harmful Algae (20–25 October 2002). St Petersburg, Fla./ Paris, Florida Fish and Wildlife Conservation Commission/Intergovernmental Oceanographic Commission of UNESCO, p. 210. (Abstract)

Nagasaki, K., Uchida, A. and Ishida, Y. 1991. A monoclonal antibody which recognizes the cell surface of red tide alga *Gymnodinium nagasakiense*. *Nippon Suisan Gakk.*, 57, pp. 1211–14.

O'Halloran, C., Silver, M. W., Holman, T. R. and Scholin, C. A. 2006. *Heterosigma akashiwo* in central California waters. *Harmful Algae*, 5, pp. 124–132.

Ouellette, A. J. A., Boyer, G. L. and Wilhelm, S. W. 2002. Quantitative PCR and sequence analysis for determination of microbial community structure and the detection of toxic *Microcystis* in Lake Erie. In: K. A. Steidinger, J. H. Lansdberg, C. R. Tomas and G. A. Vargo (eds), *Harmful Algae 2002.* Proc. X International Conference on Harmful Algae (20–25 October 2002). St Petersburg, Fla./Paris, Florida Fish and Wildlife Conservation Commission/Intergovernmental Oceanographic Commission of UNESCO, p. 222. (Abstract)

Pan, Y., Bates, S. and Cembella, A. D. 1998. Environmental stress and domoic acid production by *Pseudo-nitzschia*: a physiological perspective. *Nat. Tox.*, 6, pp. 127–35.

Pan, Y., Parsons, M. L., Busman, M., Moeller, P. D. R., Dortch, Q., Powell, C. L. and Doucette, G. J. 2001. *Pseudo-nitzschia* sp. cf. *pseudodelicatissima* – a confirmed producer of domoic acid from the northern Gulf of Mexico. *Mar. Ecol. Progr. Ser.*, 220, pp. 83–92.

Pancrazio, J. J., Gray, S. A., Shubin, Y. S., Kulagina, N., Cuttino, D. S., Shaffer, K. M., Eisemann, K., Curran, A., Zim, B., Gross, G. W. and O'Shaughnessy, T. J. 2003. A portable microelectrode array recording system incorporating cultured neuronal networks for neurotoxin detection. *Biosens. Bioelectron.*, 18, pp. 1339–47.

Parsons, M. L., Scholin, C., Doucette, G., Fryxell, G. A., Dortch, Q. and Soniat, T. M. 1999. *Pseudo-nitzschia* species (Bacillariophyceae) in Louisiana coastal waters: molecular probe field trials, genetic variability and domoic acid analyses. *J. Phycol.*, 35, pp. 1368–78.

Penna, A. and Magnani, M. 1999. Identification of *Alexandrium* (Dinophyceae) species using PCR and rDNA-targeted probes. *J. Phycol.*, 35, pp. 615–21.

Penna, A. and Magnani, M. 2000. A PCR immunoassay method for the detection of *Alexandrium* (Dinophyceae) species. *J. Phycol.,* 36, pp. 1183–86.

Peperzak, L., Sandee, B., Scholin, C., Miller, P. and Van Nieuwerburgh, L. 2001. Application and flow cytometric detection of antibody and rRNA probes to *Gymnodinium mikimotoi* (Dinophyceae) and *Pseudo-nitzschia multiseries* (Bacillariophyceae). In: G. M. Hallegraeff, S. I. Blackburn, C. J. Bolch and R. J. Lewis (eds), *Harmful Algal Blooms 2000*. Paris, Intergovernmental Oceanographic Commission of UNESCO, pp. 206–09.

Peperzak, L., Vrieling, E. G., Sandee, B. and Rutten, T. 2000. Immuno flow cytometry in marine phytoplankton research. *Scientia Marina*, 64, pp. 165–81.

Poli, M. A., Musser, S. M., Dickey, R. W., Eilers, P. P. and Hall, S. 2000. Neurotoxic shellfish poisoning and brevetoxin metabolites: a case study from Florida. *Toxicon*, 38, pp. 981–93.

Powell, C. L. and Doucette, G. J. 1999. A receptor binding assay for paralytic shellfish poisoning toxins: recent advances and applications. *Nat. Tox.*, 7, pp. 393–400.

Powell, C. L., Ferdin, M. E., Busman, M., Kvitek, R. G. and Doucette, G. J. 2002. Development of a protocol for determination of domoic acid in the sand crab (*Emerita analoga*): a possible new indicator species. *Toxicon*, 40, pp. 481–88.

Quilliam, M. A. 1996. Liquid chromatography-mass spectrometry of seafood toxins. In: D. Barcelo (ed.), *Applications of LC-MS in Environmental Science*. Amsterdam, Elsevier, pp. 415–44.

Quilliam, M. A. 2003*a*. Chemical methods for lipophilic shellfish toxins. In: Hallegraeff et al. (eds), op. cit., pp. 211–45.

Quilliam, M. A. 2003*b*. Chemical methods for domoic acid, the amnesic shellfish poisoning (ASP) toxin. In: Hallegraeff et al. (eds), op. cit., pp. 247–65.

Quilliam, M. A., Hardstaff, W. R., Ishida, N., McLachlan, J. L., Reeves, A. R., Ross, N. W. and Windust, A. J. 1996. Production of diarrhetic shellfish poisoning (DSP) toxins by *Prorocentrum lima* in culture and development of analytical methods. In: Yasumoto et al., (eds), op. cit., pp. 289–92.

Quilliam, M. A. and Ross, N. W. 1996. Analysis of diarrhetic shellfish poisoning toxin and metabolites in plankton and shellfish by ion-spray liquid-chromatography mass spectrometry. In: A. P. Snyder (ed.), *Biochemical and Biotechnological Applications of Electrospray Ionization Mass Spectrometry*. Washington DC, American Chemical Society, pp. 351–64.

Rafuse, C., Cembella, A, Laycock, M. and Jellett, J. 2006. Rapid monitoring of toxic phytoplankton and zooplankton with a lateral-flow immunochromatographic assay for ASP and PSP toxins. In: K. Steidinger et al. (eds), *Proc. Tenth International Conference on Harmful Algal Blooms*, pp. 309–311.

Ramstrom, O. and Ansell, R. J. 1998. Molecular imprinting technology: challenges and prospects for the future. *Chirality*, 10, pp. 195–209.

Rehnstam-Holm, A. S., Godhe, A. and Anderson, D. M. 2002. Molecular studies of *Dinophysis* (Dinophyceae) species from Sweden and North America. *Phycologia*, 41, pp. 348–57.

Rhines, J. E .B., Donaghay, P. L., Dekshenieks, M. M., Sullivan, J. M. and Twardowski, M. S. 2002. Thin layers and camouflage: hidden *Pseudo-nitzschia* spp. (Bacillariophyceae) populations in a fjord in the San Juan Islands. Washington, USA. *Mar. Ecol. Progr. Ser.*, 225, pp. 123–37.

Rhodes, L. L. 1998. Identification of potentially toxic *Pseudo-nitzschia* Bacillariophyceae in New Zealand coastal waters using lectins. *New Zeal. J. Mar. Freshwat. Res.*, 32, pp. 537–44.

Rhodes, L., Haywood, A., Adamson, J. and Scholin, C. 2002. DNA probes in whole cell format for the detection of *Karenia* species in New Zealand waters. In: K. A. Steidinger, J. H. Lansdberg, C. R. Tomas and G. A. Vargo (eds), *Harmful Algae 2002.* Proc. X International Conference on Harmful Algae (20–25 October 2002). St Petersburg, Fla./Paris, Florida Fish and Wildlife Conservation Commission/Intergovernmental Oceanographic Commission of UNESCO, p. 242. (Abstract)

Rhodes, L. L., Haywood, A. J. and Fountain, D. W. 1995. FITC-conjugated lectins as a tool for differentiating between toxic and non-toxic marine dinoflagellates. *New Zeal. J. Mar. Freshwat. Res.*, 29, pp. 359–65.

Rhodes, L., Mackenzie, A. L., Kaspar, H. F. and Todd, K. E. 2001. Harmful algae and mariculture in New Zealand. *ICES J. Mar. Sci.*, 58, pp. 398–403.

Rhodes, L., Scholin, C. and Garthwaite, I. 1998*a*. *Pseudo-nitzschia* in New Zealand and the role of DNA probes and immunoassays in refining marine biotoxin monitoring programmes. *Nat. Tox.*, 6, pp. 105–11.

Rhodes, L., Scholin, C., Garthwaite, I., Haywood, A. and Thomas, A. 1998*b*. Domoic acid producing *Pseudo-nitzschia* species educed by whole cell DNA probe-based and immunochemical assays. In: B. Reguera, J. Blanco, M. L. Fernández and T. Wyatt (eds), *Harmful Algae*. Proc. VIII International Conference on Harmful Algae (June 1997, Vigo, Spain). Santiago de Compostela/Paris, Xunta de Galicia/Intergovernmental Oceanographic Commission of UNESCO, pp. 274–47.

Rhodes, L., Scholin, C., Tyrrell, J., Adamson, J. and Todd, K. 2000. The integration of DNA probes into New Zealand's routine phytoplankton monitoring programmes. In: G. M. Hallegraeff, S. I. Blackburn, C. J. Bolch and R. J. Lewis (eds), *Harmful Algal Blooms 2000*. Paris, Intergovernmental Oceanographic Commission of UNESCO, pp. 429–32.

Ross, N. W. and Bates, S. S. 1996. Electro-immunoblotting characterization of *Pseudo-nitzschia multiseries* and *P. pungens* antigens recognized by antibodies directed against whole cells. *J. Appl. Phycol.*, 8, pp. 51–58.

Rublee, P. A., Kempton, J., Schaefer, E., Burkholder, J. M., Glasgow, H. B. Jr and Oldach, D. 1999. PCR and FISH detection extends the range of *Pfiesteria piscicida* in estuarine waters. *Virginia J. Sci.*, 50, pp. 325–36.

Rublee, P. A., Kempton, J. W., Schaefer, E. F., Allen, C., Harris, J., Oldach, D. W., Bowers, H., Tengs, T., Burkholder, J. M. and Glasgow H. B. 2001. Use of molecular probes to assess geographic distribution of *Pfiesteria* species. *Environ. Health Perspect.*, 109, pp. 765–67.

Saito, K., Drgon, T., Robledo, J. A. F., Krupatkina, D. N. and Vasta, G. R. 2002. Development of standard and quantitative-competitive PCR-based diagnostic assays for *Pfiesteria piscicida* targeted to the non-transcribed spacer of rDNA. In: K. A. Steidinger, J. H. Lansdberg, C. R. Tomas and G. A. Vargo (eds), *Harmful Algae 2002.* Proc. X International Conference on Harmful Algae (20–25 October 2002). St Petersburg, Fla./Paris, Florida Fish and Wildlife Conservation Commission/Intergovernmental Oceanographic Commission of UNESCO, p. 248. (Abstract)

Sako, Y., Adachi, M. and Ishida, Y. 1993. Preparation and characterization of monoclonal antibodies to *Alexandrium* species. In: T. J. Smayda and Y. Shimizu (eds), *Toxic Phytoplankton Blooms in the Sea*. Amsterdam, Elsevier, pp. 87–93.

Sako, Y., Murakami, T., Adachi, M., Uchida, A., Ishida, Y., Yamaguchi, M. and Takeuchi, T. 1996. Detection of the toxic dinoflagellate *Alexandrium* species by flow cytometry using a monoclonal antibody. In: Yasumoto et al., (eds), op. cit., pp. 463–66.

Scholin, C., Marin, R., Miller, P., Doucette, G., Powell, C., Howard, J., Haydock, P. and Ray, J. 1999. Application of DNA probes and a receptor binding assay for detection of *Pseudo-nitzschia* (Bacillariophyceae) species and domoic acid activity in cultured and natural samples. *J. Phycol.*, 35, pp. 1356–67.

Scholin, C., Massion, G., Mellinger, E., Brown, M., Wright, D. and Cline, D. 1998. The development and application of molecular probes and novel instrumentation for detection of harmful algae. *Ocean Community Conference '98 Proceedings, 1.* Marine Technology Society, pp. 367–70.

Scholin, C. A. 1998. Morphological, genetic and biogeographic relationships of *Alexandrium tamarense*, *A. catenella* and *A. fundyense*. In: Anderson et al. (eds), op. cit., pp. 13–27.

Scholin, C. A. and Anderson, D. M. 1998. Detection and quantification of HAB species using antibody and DNA probes: progress to date and future research objectives. In: B. Reguera, J. Blanco, M. L. Fernández and T. Wyatt (eds), *Harmful Algae*. Proc. VIII International Conference on Harmful Algae (June 1997, Vigo, Spain). Santiago de Compostela/Paris, Xunta de Galicia/Intergovernmental Oceanographic Commission of UNESCO, pp. 253–57.

Scholin, C. A., Buck, K. R., Britschgi, T., Cangelosi, J. and Chavez, F. P. 1996. Identification of *Pseudo-nitzschia australis* (Bacillariophyceae) using rRNA-targeted probes in whole cell and sandwich hybridization formats. *Phycologia*, 35, pp. 190–97.

Scholin, C. A., Gulland, F., Doucette, G. J., Benson, S., Busman, M., Chavez, F. P., Cordaro, J., Delong, R., Devogelaere, A., Harvey, J., Haulena, M., Lefebrve, K., Lipscomb, T., Loscutoff, S., Lowenstine, L. J., Marin, R. III, Miller, P. E., McLellan, W. A., Moeller, P. D. R., Powell, C. L., Rowles, T., Silvagni, P., Silver, M., Spraker, T., Trainer, V. and Van Dolah, F. M. 2000. Mortality of sea lions along the central California coast linked to a toxic diatom bloom. *Nature*, 403, pp. 80–84.

Scholin, C. A., Massion, E. I., Wright, D. K., Cline, D. E., Mellinger, E. and Brown, M. 2001. Aquatic autosampler device. (US Pat. 6187530.)

Scholin, C. A., Miller, P., Buck, K., Chavez, F., Harris, P., Haydock, P., Howard, J. and Cangelosi, G. 1997. Detection and quantification of *Pseudo-nitzschia australis* in cultured and natural populations using LSU rRNA-targeted probes. *Limnol. Oceanogr.*, 42, pp. 1265–72.

Scholin, C. A., Vrieling, E., Peperzak, L., Rhodes, L. and Rublee, P. 2003. Detection of HAB species using lectin, antibody and DNA probes. In: Hallegraeff et al. (eds), op. cit., pp. 131–63.

Sellner, K. G., Doucette, G. J. and Kirkpatrick, G. 2003. Harmful algal blooms: causes, impacts, and detection. *J. Ind. Microbiol. Biotech.*, 30, pp. 383–406.

Sengbusch, P. V. and Müller, U. 1983. Distribution of glycoconjugates at algal cell surfaces as monitored by FITC-conjugated lectins. Studies on selected species from *Cyanophyta, Pyrrhophyta, Raphidophyta, Euglenophyta, Chromophyta* and *Chlorophyta. Protoplasma*, 114, pp. 103–13.

Shimizu, Y. 1996. Microalgal metabolites: a new perspective. *Ann. Rev. Microbiol.*, 50, pp. 431–65.

Shimizu, Y. 2000. Chemistry and mechanism of action. In: L. M. Botana (ed.), *Seafood and Freshwater Toxins: Pharmacology, Physiology and Detection*. New York, Marcel Dekker, pp. 151–72.

Silva, M. A., Jellett, J. F., Laycock, M. V., Quilliam, M. A. and Cembella, A. D. 2001. Phytoplankton monitoring using a rapid field test: Mist Alert™ for Paralytic Shellfish Poisons. In: J. N. C. Whyte (ed.), *Proc. Seventh Canadian Workshop on Harmful Marine Algae*. *Can. Tech. Rep. Fish. Aquat. Sci.*, 2386, pp. 28–34.

Smayda, T. J. 1997. Bloom dynamics: physiology, behavior, trophic effects. *Limnol. Oceanogr.*, 42, pp. 1132–36.

Sournia, A. 1978. *Phytoplankton Manual*. Paris, Intergovernmental Oceanographic Commission of UNESCO, 337 pp. (Monographs on Oceanographic Methodology 6.)

Steidinger, K. A., Vargo, G. A., Tester, P. A. and Tomas, C. R. 1998. Bloom dynamics and physiology of *Gymnodinium breve* with emphasis on the Gulf of Mexico. In: Anderson et al. (eds), op. cit., pp. 133–53.

Suarez-Isla, B. A., Sierralta, J., Compagnon, D., Fonseca, M. and Loyola, H. 1997. Real life strategies for red tide management in Chile: systematic application of receptor-based radioassays for PSP and ASP toxins in international seafood safety programs. *Proc. Eighth International Conference on Harmful Algae*, Vigo, Spain. (Abstract)

Taylor, F. J. R. 1993. Current problems with harmful phytoplankton blooms in British Columbia waters. In: T. J. Smayda and Y. Shimizu (eds), *Toxic Phytoplankton Blooms in the Sea*. Amsterdam, Elsevier, pp. 699–704.

Teegarden, G. J. and Cembella, A. D. 1996. Grazing of toxic dinoflagellates, *Alexandrium* spp., by adult copepods of coastal Maine: implications for the fate of paralytic shellfish toxins in marine food webs. *J. Exp. Mar. Biol. Ecol.*, 196, pp. 145–76.

Towers, N. R. and Garthwaite, I. 2001. Biological assay and detection methods for marine 'shellfish' toxins. In: E. Massaro (ed.), *Neurotoxicology Handbook*, Vol. 1. London, Humana Press, pp. 269–91.

Traynor, I. M., Crooks, S. H. R., Plumpton, L. and Elliott, C. T. 2002. Detection of the marine toxin domoic acid in bivalve molluscs by immunobiosensor. 4th International Symposium on Hormone and Veterinary Drug Residue Analysis, 4–7 June 2002, Antwerp, Belgium. (Poster)

Traynor, I. M., Plumpton, L., Fodey, T. L., Higgins, C. and Elliott, C. T. 2006. Immunobiosensor detection of domoic acid as a screening test in bivalve molluscs: comparsion with liquid chromatography-based analysis. *J. Assoc. Offic. Anal. Chem.*, pp. 868–872

Tyrrell J. V., Bergquist, P. R., Bergquist, P. L. and Scholin, C. A. 2001. Detection and enumeration of *Heterosigma akashiwo* and *Fibrocapsa japonica* (Raphidophyceae) using rRNA-targeted oligonucleotide probes. *Phycologia*, 40, pp. 457–67.

Tyrrell, J. V., Connell, L. B. and Scholin, C. A. 2002. Monitoring for *Heterosigma akashiwo* using a sandwich hybridization assay. *Harmful Algae*, 1, pp. 205–14.

Uchida, A., Nagasaki, K., Hiroishi, S. and Ishida, Y. 1989. The application of monoclonal antibodies to an identification of *Chattonella marina* and *Chattonella antiqua*. *Nippon Suisan Gakk.*, 55, pp. 721–25.

Van Dolah, F. M. 2000*a*. Marine algal toxins: origins, health effects, and their increased occurrence. *Environ. Health Perspect.*, 108S, pp. 133–41.

Van Dolah, F. M. 2000*b*. Diversity of marine and freshwater algal toxins. In: L. M. Botana (ed.), *Seafood and Freshwater Toxins: Pharmacology, Physiology and Detection*. New York, Marcel Dekker, pp. 19–43.

Van Dolah, F. M., Finley, E. L., Haynes, B. L., Doucette, G. J., Moeller, P. D. and Ramsdell, J. S. 1994. Development of rapid and sensitive high throughput assays for marine phycotoxins. *Nat. Tox.*, 2, pp. 189–96.

Van Dolah, F. M. and Ramsdell, J. S. 2001. Review and assessment of *in vitro* detection methods for algal toxins. *J. Assoc. Offic. Anal. Chem.*, 84, pp. 1617–25.

Van Ness, J. and Chen, L. 1991. The use of oligonucleotides probes in chaotrope-based hybridization solutions. *Nucleic Acids Res.*, 19, pp. 5143–51.

Vrieling, E. G. and Anderson, D. M. 1996. Immunofluorescence in phytoplankton research – application and potential. *J. Phycol.*, 32, pp. 1–16.

Vrieling, E. G., Gieskes, W. W. C., Rademaker, R. W. M., Vriezekolk, G., Peperzak, L. and Veenhuis, M. 1995. Flow cytometric identification of the ichthyotoxic dinoflagellate *Gyrodinium aureolum* in the central North Sea. In: P. Lassus, G. Arzul, E. Erard, P. Gentien and C. Marcaillou-Le Baut (eds), *Harmful Marine Algae*. Paris, Technique et Documentation-Lavoisier/Intercept, pp. 743–48.

Vrieling, E. G., Koeman, R. P. T., Scholin, C. A., Scheerman, P., Peperzak, L., Veenhuis, M. and Gieskes, W. W. 1996. Detection of a domoic acid-producing *Pseudo-nitzschia* species

in the Dutch Wadden Sea by electron microscopy and molecular probes. *Eur. J. Phycol.*, 31, pp. 333–40.

Vrieling, E. G., Peperzak, L., Gieskes, W. W. C. and Veenhuis, M. 1994. Detection of the ichthyotoxic dinoflagellate *Gyrodinium* cf. *aureolum* and morphologically related *Gymnodinium* species using monoclonal antibodies: a specific immunological tool. *Mar. Ecol. Progr. Ser.*, 103, pp. 165–74.

Vrieling, E. G., Van de Poll, W. H., Vriezekolk, G. and Gieskes, W. W. C. 1997. Immunoflow cytometric detection of the ichthyotoxic dinoflagellates *Gyrodinium aureolum* and *Gymnodinium nagasakiense*: independence of physiological state. *Neth. J. Sea Res.*, 37, pp. 91–100.

Waite, A. M., Olson, R. J., Dam, H. and Passow, U. 1995. Sugar-containing compounds on the cell surfaces of marine diatoms measured using concanavalin A and flow cytometry. *J. Phycol.*, 31, pp. 925–33.

Wang, J. 2002*a*. Electrochemical nucleic acid biosensors. *Anal. Chim. Acta*, 469, pp. 63–71.

Wang, J. 2002*b*. Portable electrochemical systems. *Trends Anal. Chem.*, 21, pp. 226–32.

Wright, J. L. C. and Cembella, A. D. 1998. Ecophysiology and biosynthesis of polyether marine biotoxins. In: Anderson et al. (eds), op. cit., pp. 427–51.

Yasumoto, T., Oshima, Y. and Fukuyo, Y. (eds). 1996. *Harmful and Toxic Algal Blooms*. Paris, Intergovernmental Oceanographic Commission of UNESCO.

Yu, Q., Chen, S., Taylor, A. D., Homola, J., Hock, B. and Jiang, S. 2005. Detection of low-molecular-weight domoic acid using surface plasmon resonance sensor. *Sensor. Actuator. B Chem.*, 107, pp. 193–201.

Zhang, H. and Lin, S. 2002. Detection and quantification of *Pfiesteria piscicida* by using the mitochondrial cytochrome *b* gene. *Appl. Environ. Microbiol.*, 68, pp. 989–94.

Zhao, J. Y., Thibault, P. and Quilliam, M. A. 1997. Analysis of domoic acid and isomers in seafood by capillary electrophoresis. *Electrophoresis*, 18, pp. 268–76.

12

Biofouling and underwater measurements

M. Lehaitre, L. Delauney and C. Compère

12.1 Introduction

Biofouling has long been considered as a limiting factor in ocean monitoring requiring the placement of any materials under water. Many potential solutions to this problem have been proposed but none seems to be universally applicable.

Much emphasis has been laid on the fouling of ship hulls. The strong hydrodynamic effect on tankers increases payload and surface roughness of the hull, leads to speed reduction and additional fuel consumption, but in the long term, corrosion induced on metallic-based material is also significant.

The need to monitor the marine environment within global earth observation systems requires more and more continuous field observations of marine environments worldwide. During the last 20 years, many monitoring stations have been developed aiming at either collecting field data to calibrate satellite observations or simply for coastal water quality assessment. Most of them are surface buoys or subsurface moorings, located in the euphotic zone, which is known to be the most heterogeneous and complex ocean space. These systems are now equipped with sophisticated sensing equipment; sensors, housings and support structures are subject to the same fouling problems as ship hulls. Emphasis has to be put on the long-term quality of measurements that may face very short-term biofouling effects.

This situation is very complex and must be approached simultaneously in two ways: by the improvement of knowledge of biofouling kinetics and by the development of prevention strategies. These two approaches have often been followed separately, resulting in the impression that the problem persists in spite of numerous solutions being available.

Biofouling can be considered as a noise for measurement purposes in a similar way to other physical perturbations. The challenge is to define exactly what are the potential noise inputs in each application in order to arrive efficiently at the most accurate output value. Biofouling is part of the environment to be observed, so it is very difficult to decorrelate this particular process from the natural evolution of the medium. Care must be taken in the choice of a prevention as it can also strongly influence locally the environment to be monitored.

Throughout this chapter, the authors keep in mind this difficulty and attempt to give users the state of the art on different prevention strategies and guidelines to choosing the most relevant for their application.

12.2 Biofouling basics

When a structure is immersed in seawater, it is rapidly covered by unavoidable fouling. This growth is a complex phenomenon and much remains to be understood. In marine environments, over 400 organisms are related to fouling problems. Organisms may be divided according to their size into micro-organisms (or so called biofilm, slime, micro-fouling) and macro-fouling.

The succession of fouling organisms is generally considered in five main stages (Figure 12.1):

- the first event is the adsorption of organic and inorganic macromolecules immediately after immersion, forming the primary film;
- second, the transport of microbial cells to the surface, and immobilization of bacteria on the surface;
- in the third stage, the bacterial attachment to the substratum is consolidated through extracellular polymer production, forming a microbial film on the surface;
- the fourth stage corresponds to the development of a more complex community with the presence of multicellular species, microalgae, debris, sediments, etc. on the surface;
- the last stage is the attachment of larger marine invertebrates such as barnacles, mussels and macro-algae.

However, even if numerous real-life experiments on materials immersed in seawater have been carried out, the existence of a pattern for the attachment of micro-fouling followed by macro-fouling has been called into question. And it now seems that some of these stages may occur in parallel or may be missing. From Roberts (Roberts et al., 1991), macro-organisms do not necessarily need the presence of a biofilm on a surface to settle.

12.2.1 Micro-fouling

12.2.1.1 Mechanisms of biofilm formation

The first step of biofilm formation, occurring within minutes of immersion, corresponds to the adsorption of organic macro-molecules (e.g. exopolymers, proteins, humic acids) and/or inorganic molecules such as salts and silts, already present in the environment or produced by the micro-organisms (Baier et al., 1972; Compère et al., 2001). These adsorbed molecules form a conditioning layer. This non-continuous layer

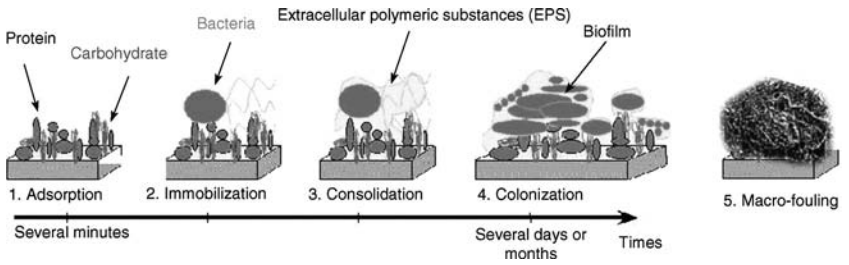

Figure 12.1
Stages of biofilm formation.
Sources: Characklis (1990); Rubio (2002).

(Walls et al., 1998; Pradier et al., 2000) induces modifications of the surface properties surface tension, surface energy (Fletcher et al., 1985; Zisman et al. 1964), polarity, wettability which will permit subsequent adhesion (Phase 1, Figure 12.1).

The bacterial adhesion itself occurs in two stages a few minutes to hours after immersion (Marshall et al., 1971; Powell et al., 1983; Robb, 1984; Rubio, 2002). The bacterial attachment to the substratum is at first reversible but becomes irreversible due to the secretion of extracellular polymers (acid polyaccharides) developing polymeric bridging between the cell and the substratum (Féra, 1985). The reversible adhesion of micro-organisms refers to weak interactions between the cells and the support, (Phase 2, Figure 12.1). The micro-organisms are at least 3 nm from the substratum and may be easily detached by simple rinsing. Two theories are generally considered to describe and predict attachment of micro-organisms on solid surfaces: the DVLO theory, named after the authors, Derjaguin, Verwey, Landau, Oberbeck (Derjaguin et al. 1941; Verwey et al., 1948); and the theory based on thermodynamics (Bos et al., 1999). The DVLO theory involves electrostatic interactions and Van Der Waals forces to explain the reversible adhesion without considerations of acid-basic interactions. The thermodynamic approach neglects the electrostatic interactions and considers the bacterial adhesion as an equilibrium and is based on the free energy of adhesion (Pethica et al., 1980).

The irreversible attachment of micro-organisms involves high-energy interactions (Phase 3, Figure 12.1). These forces include dipole-dipole interactions, Debye interactions, ion-dipole interactions, hydrogen bonds and polymeric bridging. Extracellular structures such as polysaccharides or proteins have multiple roles, permitting the irreversible attachment as well as the retention of nutrients, organic and inorganic substances, in their immediate environment. An example of marine bacteria entrapped in extracellular polymers after attachment on a stainless-steel surface is shown in Figure 12.2 (Rubio, 2002).

Once film attachment has occurred and if the physico-chemical conditions at the interface are adequate, bacteria grow on the surfaces as micro-colonies (Mills et al., 1981). Very rapidly (within a few days), a film includes unicellular algae (diatoms) in the euphotic zone.

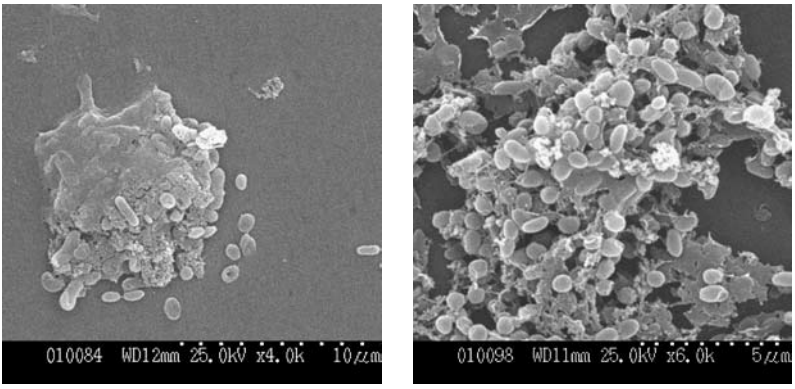

Figure 12.2
Marine bacteria entrapped in their own exopolymers after attachment on stainless-steel surfaces.
Source: Rubio (2002).

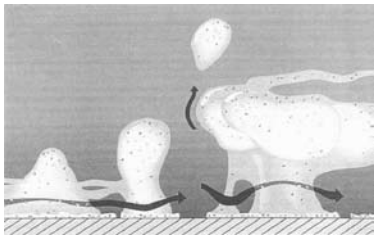

Figure 12.3
Conceptual model of the architecture of bacterial biofilms formed by *Pseudomonas aeruginosa*.
Source: Costerton (1995).

12.2.1.2 Properties of a biofilm

Recent imaging devices, such as confocal scanning laser microscopy and atomic force microscopy, have provided detailed information on biofilm architecture and structure. The conceptual model of the architecture of a single-species biofilm, developed by Costerton et al. (1995), is currently adopted, Figure 12.3. Biofilms are complex structures made from cells and aggregates or micro-colonies of bacteria. These are located in a random way in a highly hydrated polymeric matrix (80–95% water) with pores, voids through which nutrient flow has been measured (Stoodley et al., 1994).

One important characteristic of biofilms is their heterogeneity (spatial and temporal). Figure 12.3 clearly depicts the water channels and heterogeneity characteristic of a mature biofilm with detachment of cell clusters. The primary film is itself non-continuous on a surface, some regions may remain bare, while others are covered with a film as observed in Figure 12.4. This atomic force microscopy image was obtained during *in situ* measurements in natural seawater after 48 hours immersion, using conditions under which the probe (typically called the tip, because it literally is a sharp metallic tip) did not displace the particles.

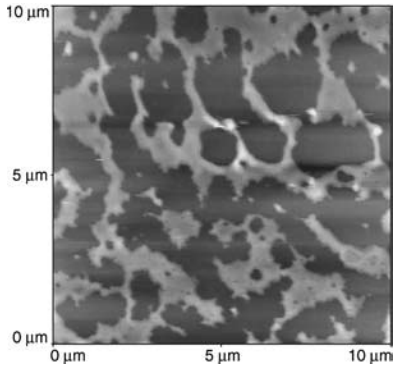

Figure 12.4
Atomic force microscopy *in situ* images obtained on glass microscope slides after 48 hours –immersion in natural seawater at Brest.
Source: image courtesy of M. Walls, CECM-CNRS, Vitry, France.

A biofilm appears rapidly in a very stratified form, with different morphologies of bacteria (generally, cocci and rod shapes near the surface and filamentous forms in the uppermost layers), diatoms, debris, ciliated organisms, skeletons and some aggregates of particulate matter, dispersed on the surface (Figure 12.5).

Biofilm thickness may vary from a few micrometres to a few centimetres depending on the medium composition, the substratum nature, the microbial strains present and the time. As shown in Figure 12.3, this thickness is not homogeneous on a surface. Thus, the dissolved oxygen content may vary significantly through a biofilm: some regions are anaerobic whereas others are aerobic. The concentration of oxygen can even become sufficiently low for anaerobic bacteria to grow. They use sulphate instead of oxygen in their metabolism to develop, generally at the interface with the substratum, while oxygen will be used at the interface with the medium in the metabolism of aerobic micro-organisms. The presence of microalgae will cause photosynthetic activity with oxygen production. As with the oxygen content, the pH is not uniform

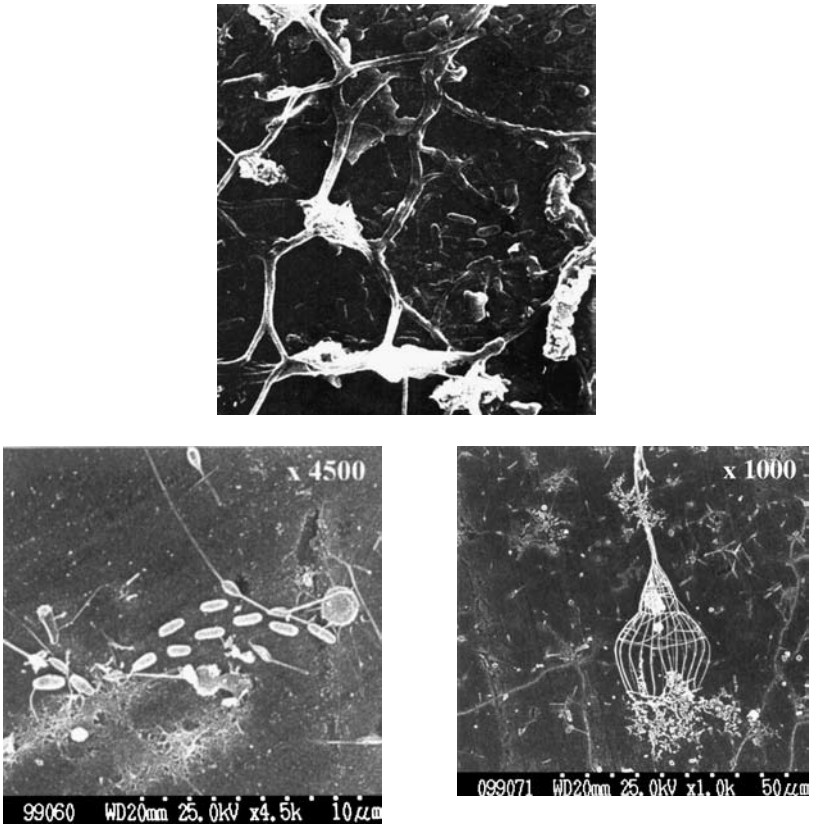

Figure 12.5
Biofilm on stainless-steel surfaces after one month of immersion in natural seawater at Brest. Observations with a scanning electron microscope.
Source: Le Bozec (2002).

through a biofilm due to the acid production by certain bacteria. Thus the presence of a biofilm may create chemical conditions totally different from those of the medium. In contrast to the open sea, pH, dissolved oxygen content, and the concentrations of metallic cations and other ions may vary considerably at the substratum-biofilm interface. This is particularly important if a biofilm is present on the sensitive part of a sensor.

12.2.2 Characteristics of macro-organisms

Macro-fouling is generally of greater concern than micro-fouling for offshore structures, ships and oceanographic instruments due to its larger contribution to weight or hydrodynamic loading. It may be of many types, plants or animals, and is generally classified into 'soft' and 'hard' fouling. The hard species present a solid skeleton such as a shell or a calcareous tube (e.g. calcareous algae, barnacles, mussels, tubiculous worms) that protects the body within, whereas the soft species such as some sponges, anemones and bryozoa have no such protection. However, the texture of these soft organisms may greatly vary, from very pliable to quite rigid bodies. Table 12.1 summarizes the main organisms into these two categories.

Mussels and barnacles are very common hard foulers. Mussels generally settle between 0–20 m deep and may colonize a structure in large beds within the first years of immersion. Many organisms, such as seaweeds, hydroids and soft corals, may overgrow mussel beds. As shown in Figure 12.6, the barnacle species are found in a depth range from the splash zone down to about 20 m and some forms are found deeper, from 60 m to 210 m. Other hard foulers, such as oysters and aggregate tubeworms, may lead to major problems of fouling.

Algae, hydroids and anemones are found through a large depth range. Some of them may reach very large size, *Branchiocerianthus imperator*, the biggest known hydroid, has polyps 2 m high (OECD, 1986).

Even if the sensitive part of a sensor is locally protected against marine growth with an antifouling strategy, and appears perfectly clean, biofouling of adjacent surfaces with large macro-organisms may interfere with the measurement. Accumulation of debris from macrofouling may be observed in an instrument housing and may contribute to spiking of a fluorescence measurement, for example. Large colonization with macro-organisms may modify the environment surrounding the sensors and in such a situation the measurements may be erroneous, for example, the presence of algae that produce or consume oxygen.

Table 12.1 Main hard and soft marine growths

Hard fouling	**Soft fouling**
Mussel	Seaweed
Barnacle	Hydroid
Oyster	Soft coral
Tubeworm	Sponge
Encrusting sponge	Anemone

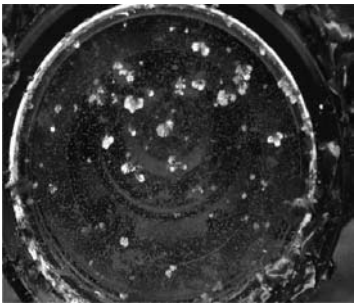

Figure 12.6
Poly(methylmethacrylate) (PMMA) windows after two months exposure in natural seawater.
Source: Festy et al. (1998).

12.2.3 Factors influencing biofouling growth

The biofouling development on a surface is the net result of several physical, chemical and biological factors:

- temperature, conductivity, pH, dissolved oxygen content, organic material content;
- nature of the substratum, roughness, surface charge, hydrophobicity/hydrophilicity;
- hydrodynamic conditions;
- location, season, depth.

12.2.3.1 Geographical location

From literature on the marine growth in tropical, subtropical and temperate areas, it appears that fouling is dependent on location. Fouling is generally more intense in tropical locations probably due to the continuous process of breeding and the warmer temperature of seawater. Some organisms may also adjust to different environmental conditions and extend over large areas such as North Polar regions to the Mediterranean, whereas others are limited to a very restricted region. However, important differences may be observed in neighbouring areas due to hydrological or biological conditions. For example, according to Forteath et al. (1984), it is not possible to predict the fouling communities on the basis of geographical location in the North Sea. In some cases, neighbouring structures may have completely different fouling communities (Kingsbury, 1981).

The geographical impact on biofouling has been demonstrated through a field experiment on a glass window settled in three different European waters (Baltic Sea, Atlantic coastal ocean and Bosphorus strait), Figure 12.7. The test was performed during the same period (six weeks of exposure between May and July 2002) on three similar deployments. The biofouling nature and the window coverage were completely different from one site to the others due to the local environmental conditions (weather, water temperature and salinity).

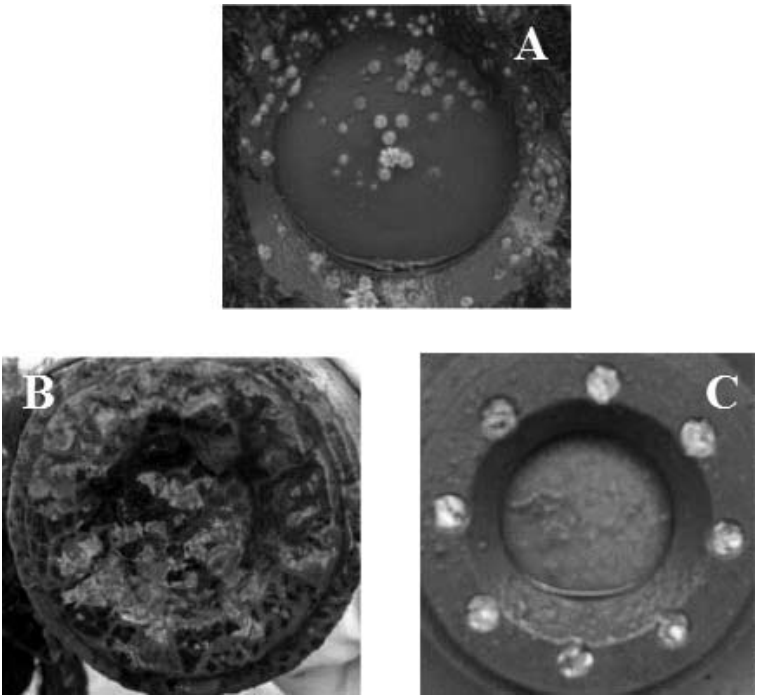

Figure 12.7
Glass windows after six weeks exposure in natural seawater between May and July 2002 at 2 m depth. A, Atlantic; B, Bosphorus; C, Baltic
Source: courtesy of EC-MISPEC project partners.

12.2.3.2 Distance from shore

Many fouling organisms drift with the currents from the shoreline to structure sites. Some larvae, such as barnacles and mussels, need three weeks or more to feed and grow during a swimming stage before settling as soon as they reach a suitable substratum. During this pelagic stage, they may drift away from their originating point.

12.2.3.3 Depth

Physico-chemical parameters of seawater such as salinity, temperature, organic content and light penetration can vary strongly with depth, and these changes greatly affect the type and growth of fouling. As the rate of fouling is generally more important in zones near the shore, it also decreases with increasing depth at any location. Very little information on the distribution of bacterial diversity and on biofilm formation on materials in deep sea environments is available (Venkatesan, 2003; Luna, 2004).

The density of bacteria (Amran et al., 2003) on glass slides after 14 months' immersion at 2,400 m depth (Astronomy with a Neutrino Telescope and Abyss environmental RESearch project: ANTARES) is similar to those observed on samples exposed for one to two weeks in shallow waters at similar temperatures (around 13–15 °C). This may be explained by the poor quantity of organic matter at these depths (2,400 m).

The bacteria observed in the deep sea are smaller than those observed at shallow depths and they seem to produce less exopolymers (Amran et al., 2003).

Macro-fouling is generally more important in the 0–40 m range, a zone rich in plankton and with high light levels. Most algae are photosynthetic and can only survive in those regions having adequate light. However mussels, barnacles, tubeworms, ascidians and hydrozoans, which take their energy from organisms and particles present in the sea and do not need light, may cause fouling at great depths. Thus, the consequences of increasing depth are usually a modification of the dominant species and a reduction in thickness. At depths below 150 m, the physico-chemical parameters of seawater (nutrients, salinity, temperature) are generally similar in any ocean, hence the same organisms are often observed at such depths as long as the bottom is geologically similar.

12.2.3.4 Temperature and season

Temperature and season play an important role in fouling composition. The bacterial colonization on surfaces immersed in natural seawater presents large seasonal fluctuations. The temperature seems to be the significant parameter. An increase in a community's growth rate is generally observed with an increase in temperature. In temperate or cold waters, most spawning and fouling growth occurs from April to September, although in tropical locations it occurs all year round at a high and constant level. Some soft marine species also die back during the winter period and survive in a planktonic form.

12.2.3.5 Water current and tidal conditions

The settlement of some organisms is strongly dependent on the water currents (wind-driven and residual), which bring the larvae from the shore to the site. Some currents bring larvae to the shore from offshore. Algae are strongly influenced by the degree of exposure to wave wash. Some species are strongly influenced by water movement. For example, the sensitivity of hydroids to water movement has been widely demonstrated (Riedl, 1971). They orientate their colonies perpendicular to the main direction of flow, allowing a greater supply of oxygen and food. Morphological variations are also observed between superficial colonies and hydroids settled at lower depths because of different water movements.

12.2.3.6 Water quality

Salinity

The total salinity of seawater is about 35 PSU. In enclosed seas, it can exceed 40 PSU, if the evaporation is higher than the fresh water input (example: Red Sea), and it can be less than 10 PSU when fluvial inputs are important (Baltic Sea). In some estuaries, the salinity may be lower than 10 PSU, especially for rivers subject to extreme climatic conditions such as tropical monsoons; important quantities of fresh water are then produced. This factor will therefore influence the biological species as a function of the location. Some organisms, such as tubeworms, are quite tolerant to a wide range of salinity (2–40%), temperature and oxygen concentration fluctuations.

Light

Light is an essential influence on the phytal system. It is the primordial source of energy at the root of the food chain of the surface ecosystem following this

simplified scheme: primary producers (phytoplankton, algae), primary consumers (worms, molluscs, small crustaceans), secondary consumers (cirripedia, ascidians) and tertiary consumers (crabs, shrimps, fishes). A theory exists that proposes a relation between the type of habitat and the algae phylogeny. It suggests the apparition of cyanobacteria (formerly called blue-green algae), red algae and brown algae first, followed by green, with more and more efficient performance in the use of photosynthesis as they settle on the surface of waters. Red algae are generally present in the infralittoral, whereas brown algae tend to appear in the intertidal area and green algae are ubiquitous. It also seems that, as light is degraded in energy and composition with depth, its use only by chlorophyll for photosynthesis is not possible. Accessory pigments are thus necessary to capture energy. These pigments include phycoerythrin for red algae, phycocyanin for cyanobacteria and fucoxanthin for brown algae. The connection between depth and distribution of algae – green, brown, red and blue-green species from the surface towards deep waters – is not however systematically observed.

The algae avoid too intense light. They generally develop in coastal regions, in depth ranges of 0–40 m. Biofouling from algae will vary regionally, but will probably have an effect in some regions (i.e. Equatorial Pacific). Whatever latitude, the light penetration around a structure may be disturbed by water turbidity, in particular the natural presence of organic material, plankton or pollutants due to human activities. In addition, it has been shown that the *Laminaria* gametophytes are able to survive six months in darkness. The distributions of algae are determined by multiple factors: presence of pigment, hydrodynamics, nutrients, nature of substrate, etc. According to their pigments, the species are adapted to the use of the available light radiation according to the filter constituted by the water mass, and develop in more or less deep water.

The relation between depth and the presence of invertebrates is more closely related to food availability than to the direct action of light. Exposure to sunlight, very strong and constant in the intertropical regions, is weak and periodic in the polar regions. Thus, for example, this factor will have consequences on the composition of the animals found on structures in the equatorial zone and in the North Sea.

Nutrients

A low seawater flow rate will initially support the formation of a biofilm on a surface, but will limit its growth at a later stage. On the other hand, strong flow rates and thus significant shear forces on the surfaces will slow down bacterial adhesion but allow the fast growth of biofilm due to a significant contribution of nutrients.

The organic matter produced by plants serves as food for animals. Living micro-organisms (bacteria, protozoa, diatoms) or detritus (dead animals or microscopic plants such as phytoplankton) brought by currents may also constitute nutrition for sessile animals. Coastal waters are generally richer than oceanic waters due to domestic or industrial effluents. Thus sites located near shore generally present higher fouling rates. Moreover, coastal masses contain more quantities of fouling larvae than ocean waters.

Silt

The presence of silt may considerably modify the type and composition of fouling in very closed geographical locations. The accumulation of silt may prevent the attachment of many organisms (Ghobashy et al., 1980). As an example, some species, such as

the hydroid *Tubularia larynx*, have difficulties attaching to silt-covered surfaces; others such as the solitary tubeworms or bryozoans can survive in such conditions.

12.2.3.7 Other factors

Chemical signals

Many factors, such as the physico-chemical parameters of seawater described above, salinity, temperature, season, light and organic matter in seawater, influence the settlement of species on artificial substrates. But natural marine products seem to induce larvae attachment, these chemical cues being released from adults or prey organisms. Fusetani (1997) has identified a few compounds that induce larval settlement and metamorphosis. A number of recent papers report the important role of biofilms on the settlement of organisms (e.g. Dahms, 2004; Banks, 2002). Strathmann and Branscomb et al. (1979) proposed that microbial cues help larvae to identify a valuable site of settlement. Important seasonal variations in the effects of biofilming cues on the larval attachment of certain marine species have been observed by Wieczorek et al. (1996). But these results are not yet completely explained; inhibitory or facilitatory settlement conditions appear to be a function of the season for some species.

Competition between species

Some species have difficulties in colonizing a surface when suitable space is limited on the structure (Forteath, 1983). This is the case for example in the North Sea for the hydroid *Tubularia larynx*, which grows during summer and has a die-back period in winter. During autumn other species may colonize and overgrow the surface, and the following summer this hydroid will be unable to settle. The deployment date considerably influences the resulting dominant fouling species (Forteath, 1983).

Human activities

Some fouling organisms may have been transported by ships. Vessels may bring spores and larvae from site to site. Acute and severe modifications of the environmental parameters may rapidly change the community structure. Disturbances caused by human activities, such as the use of chemical cleaning with antifouling agents at the time of installation, may have important effects on marine growth.

Eashwar and colleagues (1995) studied the interrelation of cathodic protection (CP) and marine macro-fouling, and showed with laboratory and field experiments that the settlement is greatly enhanced by CP. Calcareous organisms (barnacles, oyster, calcareous algae) are more important on cathodically protected structures than on unprotected substrata. The CP provokes an alcalinization at the metal/seawater interface and then promotes the precipitation of calcareous deposits. These deposits could favour the settlement because of the increasing surface roughness or enhance the shell growth of oysters, barnacles for example, with the high availability of calcium ions.

Nature of substratum

Various factors of the material surface affect the bacterial colonization rate: surface charge (Kerr et al., 1998*b*), surface roughness (Kerr et al., 1999*a*; Scheuerman et al., 1998), hydrophobicity and nature of the material. As an example, for short exposure, polyethyl terephtalate (PET) offers better biofouling resistance than poly(methylmethacrylate) (PMMA) due to different surface properties (Kerr et al., 2001).

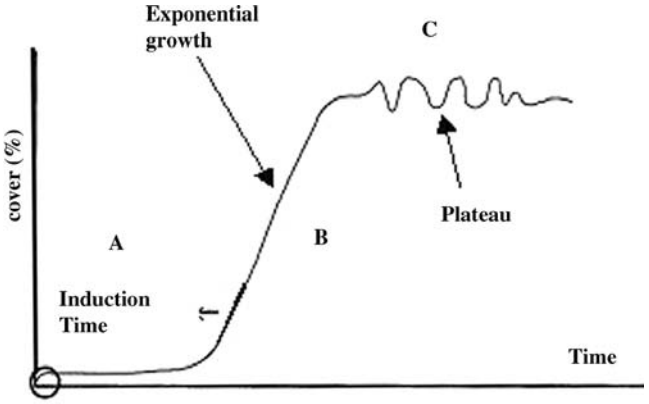

Figure 12.8
Biofilm growth.
Source: Characklis (1990).

12.2.4 Tentative modelling of biofouling

Biofilm development is described by Characklis et al. (1990) with a sigmoidal function, Figure 12.8. The shape of this curve is more or less similar in any case. The evolutions may be different on each of the three characteristic parts of the curve (A, B, C).

The first characteristic, A, is usually presented as the delay, and certainly the most important parameter used to qualify the fouling occurrence. It will be representative of a particular situation depending on the local environmental growth conditions. The situation is completely different from tropical areas to northern seawaters, as well as for the same site when considering the different seasons. This delay time also depends on the type of organisms.

The B region is roughly the growth rate which can be simply characterized as a slope. Similarly to the A parameter, the slope can be more or less sharp in relation to the environment.

The C plateau corresponds to the maximum coverage of a structure or of measurement interface for marine sensor.

As mathematical models would be useful for equipment end-users, Breur (2001) used the Netherlands Organisation for Applied Scientific Research (TNO) data for the development of a model for fouling growth in temperate marine waters. He showed that it is possible to estimate the fouling rate of eight organisms such as barnacles, mussels and macroalgae. Logistic growth, which results in a S-curved growth, was assumed to estimate the growth curve of fouling organisms. However, validation of the models through other series of experimental data would be necessary.

Figure 12.9 shows the envelope of mean biofouling development on glass at three European sites: Millport (UK), and a combined mean biofilm growth for the Den Helder (Netherlands) and Cascais (Portugal) sites based on mean measurements of the percentage of surface area covered by eukaryotic fouling organisms.

The methods for the quantitative analyses of marine growths have been standardized in the offshore petroleum sector according to the Marine Technology Directorate (Anon., 1992). The average thickness of hard and soft organisms are calculated

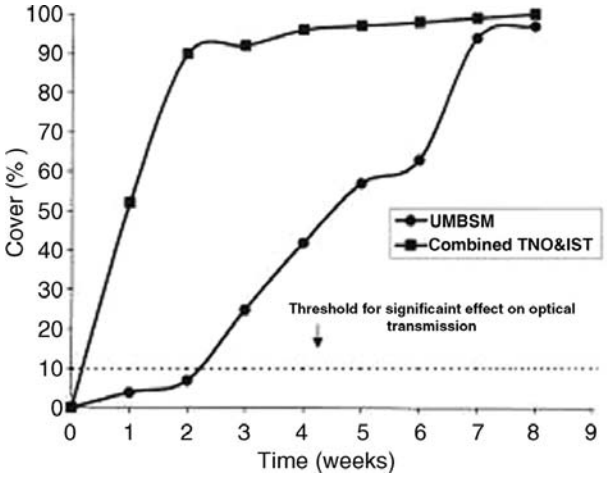

Figure 12.9
Envelope of mean biofouling development on glass at three European sites: Millport (UMBSM-UK), and combined Den Helder (TNO-Netherlands) and Cascais (IST-Portugal) sites.
Source: BROS Final Report (1998).

separately. Thus, forecasts of fouling thickness on a platform are estimated. However, important discrepancies may be observed between forecasts and real values. They are essentially due to the lack of precise knowledge on the successive stages of settlement of fouling organisms as a function of geographical location, physico-chemical parameters, and to unexpected events such as storms.

12.3 Biofouling effects on oceanographic measurements

The ocean plays a major role in the understanding of the earth's evolution. Several major international programmes have been launched to increase knowledge of the interaction between ocean and atmosphere (World Ocean Circulation Experiment, WOCE; Global Ocean Ecosystems Dynamics, GLOBEC; Global Ocean Observing System, GOOS; Integrated Ocean Observing System, IOOS) or about the impact of human activity in coastal zones. Even if it is still necessary to continue improving the essential work on short-term local processes, it becomes more and more crucial to obtain long-term observations of the open ocean or coastal areas.

Marine instrumentation is evolving efficiently from a technological point of view with respect to energy consumption, data storage capacity or transmission, data quality and calibration protocols. The conjunction between the increasing number of available *in situ* measurement techniques and the demand for offshore autonomous operation have made biofouling one of the major problems for long-term *in situ* monitoring.

Biofouling effects on marine instrumentation are numerous: hydrodynamic screening, reduction of thermal exchanges, modifications of interfacial properties so crucial for any transducers, as well as additional corrosion or bio-degradation of the

supports. The emphasis must be on the relation between the biofouling structure and the physico-chemical principles applied to underwater oceanographic measurements. Sometimes, short-term biofouling effects can be sensed, even if not subjectively visible. As stated above, biofouling is fully dependent on the environment to be observed, so it must be considered as a parameter more or less detectable according to the principle and sensitivity of the instrument. Marine instrumentation is based either on extrinsic or intrinsic configuration, representing direct interaction on a water volume or not.

Many kinds of sensors are used and it is not the purpose of this chapter to present in detail all the different types, but to describe briefly the principles of different sensors in order to analyse the effect of fouling on the measurements.

12.3.1 Extrinsic instrumentation

Extrinsic instrumentation means that the measurement is achieved on a volume of water. The signal carrier is always travelling through the water path. Optics and acoustics are the most predominant fields of application. Although they are often based on similar instrumental configurations, they are rather different in their physical characteristics.

12.3.1.1 Optics and bio-optics

For several international programmes on the Global Ocean, optics play an important role as they are now essential for ocean assessment through inherent (IOP) and apparent (AOP) optical properties of waters (McLeroy-Etheridge and Roesler, 1998; Mobley, 1994). Much work (Van de Hulst, 1980; Van de Hulst, 1981; Zaneveld, 1994; Morel, 1994; Roesler, 1998; see also Roesler and Boss, 2007 – Chapter 5 this volume) has been done on the fundamental equation $c = a + b$ relating the light beam attenuation c to coefficients a and b for absorption and scattering respectively (m^{-1}).

Due to the high electromagnetic frequency of light, the sensitivity to any obstacles along an optical path is probably much higher than for any other field of physics. This is particularly critical in the case of very low attenuation values.

Instruments such as transmissometers, nephelometers or absorption spectrometers (Claustre et al., 2000; Zaneveld, 1994; Chang and Dickey, 1999) have been rigorously designed to correspond as closely as possible to the theory. Looking at the biofouling influencing factors presented in Section 12.2.3, it can be asserted that optics sensitivity will be strongly affected by a structured organic layer growing continuously in the field of measurement.

Nature of substratum

Transparent interfaces are always needed. Borosilicate glass windows (PMMA) are generally used, having a more suitable refractive index for underwater applications. Assessments have been carried out showing differences in the fouling kinetics of several materials such as glasses (borosilicate: a very common material for high-quality optical components in the visible range, CaF_2 crystal, sapphire), polymer or quartz (BROS, 1998).

Structure of biofilm

The heterogeneity of the biofilm appears even in the first stage of growth. As it is difficult to de-correlate the biofouling from the suspension, the limits of the instrument

are generally estimated by the user when a baseline drift is sensed. The particulate form provided by the organisms settled on the window, for example, is no more than a complex organic scattering interface located in the optical field of the measurement. The density and size range of the organisms are continuously evolving at a rate depending on environmental parameters.

Nature of biofilm

As the biofilm is composed of bacteria to phytoplankton, as well as polymeric substances, it will influence absorption measurements. This will have a double bias effect, not only on the transmitted signal losses, but also on the spectral response as the biofilm is acting as a filter. The strong absorption of biofilm components such as chl *a* or other pigments will mask those of the suspension. Fluorescence biomass estimation will suffer a sensitivity reduction. Concerning the description of different methods given by Lewis (2007 – Chapter 6 this volume), improvements in data processing are now available. Even if some improvements have been proposed to better discriminate the organisms' absorption response in conjunction with scattering measurements (Roesler and Zaneveld, 1994), this is still an important problem. The biofouling effect must be strongly avoided during early field experiments.

Instrumental set-up

Many optical instruments are based on a free-flowing cell limited by two window interfaces. The hydrodynamics of the set-up will have a critical influence. Turbulent flow near the windows or the material used for the housing may increase biofilm formation. Entrapped nutrients in turbulent flow conditions close to a measuring cell will attract organisms, which will find environmental conditions conducive to attachment. Care thus has to be taken when handling instruments at sea, and a judicious orientation will sometimes limit the biofouling rate.

Macro-fouling

When the macro-fouling stage is reached, the measurement availability may still be subject to questions. It is important to understand that local protection focused on the measurement will not prevent macro-fouling on the surrounding of the instrument. A micro-environment that will not be perceived in terms of fouling will nevertheless provide strong bias in the observation, which will not be the true water-mass image.

The A, B and C parameters of biofouling (Figure 12.8) are never taken into account during the calibration, but they are however fully included in the data. It is vital to estimate a biofouling parameter that would represent a coverage percentage related to an admissible percentage of reduction in measurement quality. The curve in Figure 12.10B shows that only a few hours would be sufficient to reduce the transmission value more than 10%. This was completely dependent on the growth kinetics of the location, and could be completely different in another region.

The failure of a transmissometer deployed at 2,400 m depth at a site located 20 nautical miles offshore from La Seyne sur Mer in the French Mediterranean (ANTARES project) was blamed on biofouling of the optical windows. The direct measurements of loss of transmissivity of glass spheres were complemented by studies of the biofouling on glass slides, and by a detailed study of sedimentation at the site. Scanning electron microscopy (SEM) observations of the glass slides indicated that the percentage of surface area covered by fouling was low and it was more likely that the light attenuation was due to build-up of loosely adhered particles (Amran et al., 2003).

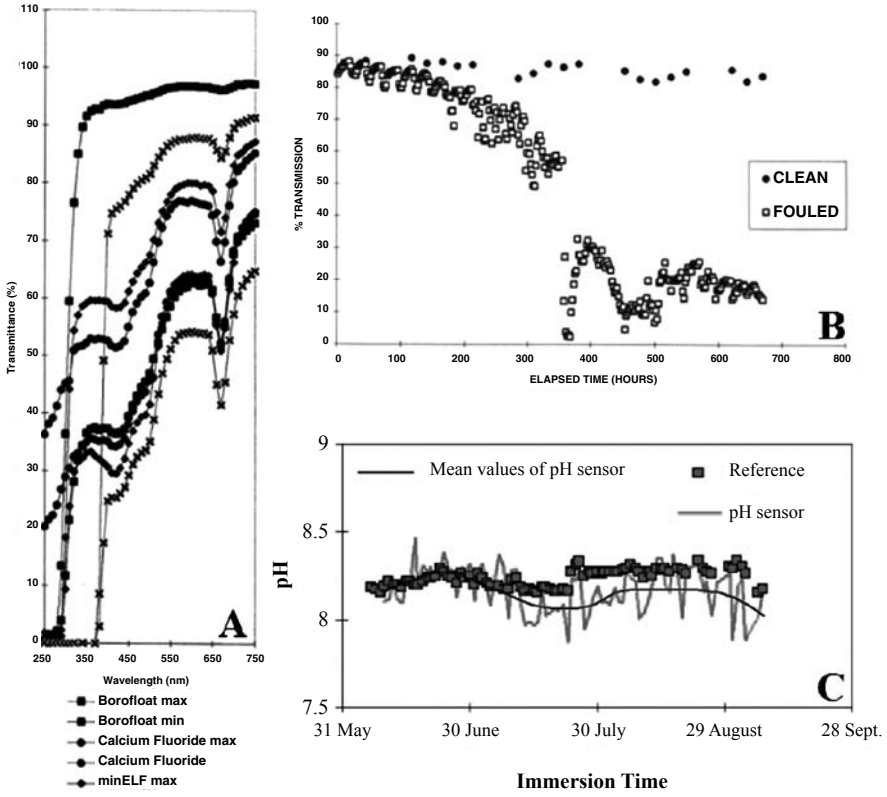

Figure 12.10
A, transmission spectra of different glasses before (max) and after (min) exposure. Lowering of beam transmission at 670 nm corresponds to the presence of chlorophyll *a* in the organisms settling on different surfaces. The samples were exposed for three weeks on the island of Cumbrae (Scotland), from 27 August 1997.
Source: after Parr et al., BROS (1998).
B, biofouling effect on transmission of light measurements: one transmissometer is continuously immersed in natural seawater and the other stored in freshwater and placed in seawater for 20 min per day to record the data.
Source: Kerr et al. (1998*b*).
C, biofouling effect on pH measurements. Comparison between *in situ* measurements with a continuously immersed glass electrode and measurements performed in the laboratory on seawater samples.
Source: IFREMER data.

12.3.1.2 Imagery

Imagery is not currently used for long-term monitoring, except for some applications in the offshore industry. Biofouling will produce a reduction in contrast, progressively reaching the complete disappearance of any structural forms under observation. However it is a very convenient tool for biofouling assessment as attention can be focused on a specific interface. The basic parameter of surface coverage is easily established at a level depending on the spatial resolution of the detector. Some applications in oceanography (Gorsky et al., 2000; Lunven et al., 2003) show that species in suspension are sometimes identified (zooplankton) by their shape or motion, requiring the highest frame quality.

12.3.1.3 Acoustic

Acoustic equipment has been particularly concerned with biofouling for a long time because transducers are always hull-mounted and permanently immersed in subsurface water layers. Although cleaning the hull is not only required for acoustic transducers, the basic characteristics of any echo sounder are to some degree altered when a biological layer is formed in the field of propagation.

One of the most important parameters (Brekhovskikh et al., 1982) is the optimum acoustic impedance *Zo* given by the relation:

$Zo = ro*c$ (Rayl)	ro (kg m^{-3}) is the volumetric mass fully dependent on the nature of the particular layer.
	c (m s^{-1}) is the celerity, directly related to Young's elastic modulus of the layer.

In a similar way as with optics, the biofouling layer evolution in front of the transducer is continuously providing an impedance mismatching effect, which affects the initial propagation field. During the last two decades, a new generation of current meters based on the acoustic Doppler effect have been developed for underwater long-term applications. They are devoted to the long-term monitoring of coastal hydrology and sediment transport studies. Having a higher frequency range (>100 kHz) than conventional sonar (a few kilohertz), they are more sensitive to biofouling. Such equipment is usually settled on the seabed of shallow estuaries or along harbour navigation channels, areas that are particularly exposed to biofouling. This also concerns the acoustic data transceivers that are now replacing cable links. Usually requiring sharp spatial directivity, especially in shallow waters, strong biofouling acts as an absorber and a scattering interface, broadening the emission and detection solid angles.

12.3.1.4 Electric

Electric fields are not widely used in underwater volume sensing, but are the reference in the measurement of salinity by conductivity (Figure 12.11) value of free flowing water sample. The principle is to measure the current through a previously defined resistance given by a volume of water (Aminot et al., 1983). Electric measurement is sometimes used for current water-flow. In these two examples, a biological layer on the electrode or inside the coil will have an impact both on the referenced geometrical shape of the sample and the dielectric properties of the interfaces. All the calibration parameters will quickly be obsolete, inducing strong bias in data accuracy.

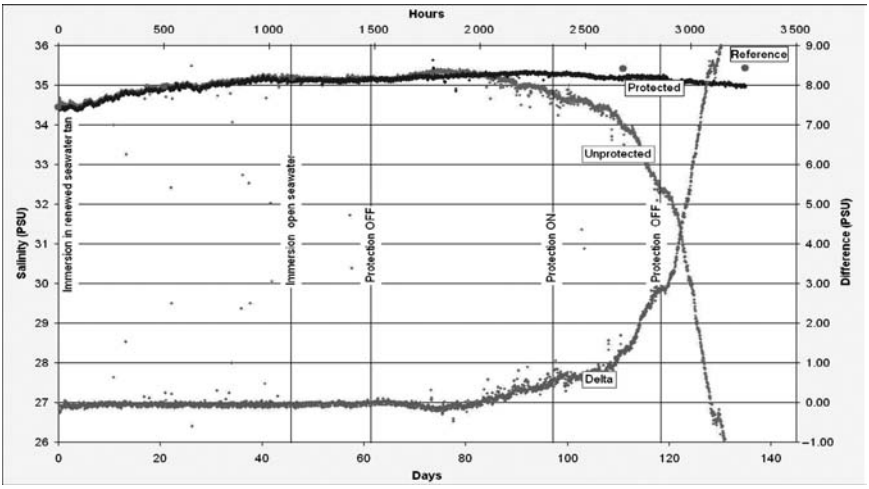

Figure 12.11
Biofouling effect on conductivity measurements. Comparison between *in situ* measurements with a continuously immersed conductivity sensor (unprotected) and measurements performed in the laboratory on seawater samples (reference). The dark grey line corresponds to the measurements obtained with a protected conductivity sensor with active chlorine generation. *Source*: IFREMER data.

12.3.2 Intrinsic instrumentation

Intrinsic instrumentation is mainly based on transducer principles, which means that there is no direct interaction between the signal and the medium. The parameters to be measured are obtained via a composite interface through which the signal carrier is modulated by a selective interaction of the water content. Diffusion of chemical molecules through a membrane is often encountered but the structural modification of an interface by adsorption or affinity is also appearing along with the increase in biosensing.

12.3.2.1 Chemical sensors

It would be very difficult to demonstrate in detail the biofouling effects for this entire class of sensors but obviously any additional layer on a transducer will generate a strong bias in the response. In addition to the basic mask, via the effect of the biological layer, it will also act very quickly on the measurement significance. The presence of biofilms will generate a micro-environment at the sensing interface. The most common example is the dissolved oxygen measurement. The exchanges in the near field of the sensor will be mainly due to the specific concentration of organisms on the interface. This also concerns pH or redox sensors and all electrochemical sensors.

For example, Figure 12.10C shows a shift of pH measurements after two weeks immersion, in comparison with reference measurements performed in the laboratory with a calibrated sensor and water samples collection. The biofouling effect can be estimated and a limit of acceptability established.

12.3.2.2 Biosensors

The previous comments also apply to biosensing, particularly concerning the detection of toxic algae (Scholin et al., 2000, 2007 – Chapter 11 this volume). This type of sensor is relatively new and field experience is lacking. The first known experience is for short periods and the use of micro-fluidic systems for the future must be assessed to estimate the level of difficulty.

12.4 Biofouling: an additional background noise

No instruments or physico-chemical sensors will escape biofouling interference and the complexity of the problem will never be solved completely. It is absolutely necessary to keep in mind that a compromise has always to be found and this requires a clear expression of needs from the user rather than looking for a simple or perfect solution.

In the particular case of measurement it is very important to keep to a signal analysis approach. For example, biofouling should be considered as a noise signal for the measurement with the particularity of being non-stationary, i.e. function of many parameters such as time, weather, water quality and water depth. The introduction of such an additional interference could be represented as follows:

If A is the parameter to be measured through the biofilm layer ('green box'), it becomes B and the calibration of the sensor or instrument will deliver exactly B. The solution to this problem is to find an anti-fouling 'black box' which would normally act as the inverse transfer function of the initial biofouling green box to recover the true parameter A.

This is not easy as the biofouling green box is potentially virtual as long as the anti-fouling black box is efficient. As nothing is perfect, the choice and evaluation of an anti-fouling strategy will be extremely difficult because of the absence of a well-established relation to the quality of measurement expected by users. For example, an application simply requiring an underwater image of a known structure will not have the same requirement as a biologist who needs morphological details. In the first case the user may accept a reduction in data quality whereas the second will be more demanding. Most of the time the appreciation of the biofouling is fully subjective, and the noise approach must be necessary for sensing measurements, but it is rarely proposed as it is difficult to define a clear signal-to-noise (S/N) ratio that could be related to biofouling.

Following the simple descriptive scheme presented above, if the complementarity between green and black boxes is not guaranteed, the introduction of the green box could be more critical than the biofilm itself.

A recommendation would be to carry out, for each sensor to be used in a region or period where strong biofouling effect is expected, some field assessments to find the exact threshold under which the available quality requirement is not satisfied. As it is difficult to provide this kind of qualification for each sensor or instrument, a characterization and classification of the biofouling for a typical area over a year would probably give more precise information to help the user. It would allow the best approach to be selected from the different protection methods presented in the next section.

12.5 Biofouling prevention strategy and measures

An anti-fouling strategy has been developed for the shipping industry using a simple economic point of view. Assessments were based on the simple evaluation of the cleaning quality of large surfaces of material which are generally metal alloys. This has been first extended to marine instrumentation without any care, but experience has shown that the strategy must focus on the measurement considerations rather than of keeping the equipment clean. This is implying that any anti-fouling method must be fully related to the quality of measurement and the eventual adverse effects of anti-fouling strategies on the measured parameters must be evaluated. Regarding what is offered on the market, it became necessary to propose a classification of the existing methods to give the user a better orientation for choosing the most convenient one. Manov et al. (2003) present a recent evaluation of different antifouling solutions for optical instrumentation; *in situ* optical measurements from field tests are presented. Numerous strategies can be considered to prevent biofilm development. For relatively limited surfaces, which is the case of the majority of sensors, the strategies can be first classified in two main groups: passive and active methods. A third one would be eventually proposed even if it is not specifically a class but mainly a combination of the two previous ones.

12.5.1 Passive strategy

The passive strategies are characterized by the fact they do not require any external energy. Inside the passive strategy class, a subdivision can be made depending on the mode of action which can be either surface or volume efficient.

12.5.1.1 Volumetric biocide release

This means that the biocide release is assumed to render the close environment of the sensing head continuously protected against any start of biofouling. The basic effect is mainly to increase the delay time A, Figure 12.8, until the biocide release is over, often followed by a slower kinetics slope B, Figure 12.8.

- For a long time anti-fouling paints have been widely used whereby the biocide is directly issued from the ship hull for protection. For example, strong efficient organotin antifouling compounds are known to release a high level of toxic metallic ions into the water. The impact on the environment is so critical that its use is now strictly prohibited by international regulation (directive No. 89/677/CEE). In the past, many marine instruments used TBT-based paints such as acoustic Doppler current profilers (ADCPs). Alternatives to TBT paints include copper-based coatings and silicon-based paints. However, the toxicity of copper to aquatic organisms is well established (Cu II) and animals exposed to high copper concentration had high levels of DNA damage (Luoma et al., 1998). Furthermore, cupric oxide may impede system performance or damage surrounding metallic components due to corrosion. Innovative research is targeting a biological approach to solve the environmental problem such as the development of marine paints based on enzymes as antifouling agents (Schneider et al., 2000).
- The windows of transmissometers may also be surrounded by a porous plastic ring impregnated with a biocide such as trialkyltin to reduce fouling. Antifouling

rings fitted around the sensors have been used on all Sea Tech transmissometers since 1994 (Strahle et al., 1994). The toxin slowly leaches into the water in front of the transmissometer window. Another example is given by the MicroCAT's internal-field conductivity cell of Sea-Bird which is protected against fouling. A plastic cup with threaded cover at each end of the cell retains the anti-foul material, a tributyltin oxide (TBTO). The toxin quantity is typically sufficient for at least two year's deployment. The International Maritime Organization (IMO) ban applies only to paint containing TBTO and does not apply to TBTO in its pure chemical form, as used by Sea-Bird.

12.5.1.2 Surface biocidity

Optical sensors are probably the equipment most sensitive to biofouling and, as described above, the optical path and interfaces must be strictly free of any additional layer. Several strategies are proposed to overcome the difficulty in maintaining the optical properties of each interface.

- The nature of the substratum has been mentioned as a factor influencing biofouling. Numerous works are carried out on low surface-energy coating systems. These materials do not prevent fouling from settling and growing on a surface, but the fouling is easily removed. Even it is not an anti-fouling technique, commercially available glasses such as Borofloat® (BROS Final Report, 1998) provide a delay in the biofilm growth compared with a simple borosilicate. Borofloat® contains boron oxide, which could enhance the fouling resistance due to tin residues from manufacturing. Due to the slight presence of bactericidal molecules on the surface, the efficiency remains very limited in time with most of the effect on the kinetics slope B, Figure 12.8.
- In a similar way, work has been done on biocidal coatings which are mainly doped with toxic compounds (boron oxide, Cu, CuAs, Ag), (Meinema et al., 1998). The optical properties are more or less affected by this process. Biofouling resistance of transparent polymers is increased after soaking in surfactants solutions (Kerr et al., 2001). The presence of surfactants alters the surface energy of the polymers.
- Hydrophobicity of materials by specific coating on PMMA has also been studied. This does not prevent biofouling but, combined with water jet or wiper, the layer can easily be removed (BROS Final Report, 1998).
- Surface actions are now also encountered for chemical sensing with the development of antifouling membranes; antifouling substances are embedded directly into the silicone during fabrication (Capsum, international patent pending).
- Nanotechnologies are also offering prospective solutions by polymeric nanothreads (in nanometre range) bonded on transparent surfaces or on surface-directed developments such as nanopatterned surfaces (Curtis et al., 2001). Recently, nanoscale porous membranes have been gaining attention as options to replace commercially available polymeric membranes to render them less susceptible to fouling. A permanent charge is induced on these membranes by ion implantation (Jones, 2002).

12.5.2 Active strategy

Active strategies, in opposition to passive techniques, are those which operation must be controlled according to sequential protocol. Such antifouling systems are

often managed directly by the instrument which includes cleaning phases in the measurement sequences. They are based on different principles using volumetric or surface action. The prevention remains however energy dependent and consequently temporally limited.

12.5.2.1 Volumetric action mode for sensor

- One antifouling strategy is retraction of the sensitive elements into an inert or biocide-filled chamber between measurements (WET Labs. Inc., Chang and Dickey, 2007 – Chapter 2 this volume). This means that sensitive surfaces are only exposed to a biofouling environment for a few minutes (Remote In-situ Monitoring of Aquatic Resources (RIMAR) project). This technique seems efficient both for copper biocide effect and the management of the on/off shuttering. It is for the moment the longest field experience which is suitable for the particular Photosynthetic Active Radiation (PAR) and fluorescence sensors.
- Copper is currently used in a variety of ways, such as copper-based shutters (Bioshutter for Satlantic instruments), copper-based alloy screens at inlets for flow-through type devices (filtering inlet of the MAREL coastal water monitoring system) or around the probe body (Ocean Seven 301 multiparameter CTD probe from Idronaut). While the copper electrodes are generally used to reduce macro-fouling, an attempt to reduce biofilm formation on optical surfaces was made in the BROS project (Head and Davenport, 1997). The released bivalent Cu2+ is able to influence the enzyme and respiration system (Breur, 2001) and has a toxic effect on many marine organisms. The efficiency of copper ions is influenced by many parameters such as the electrochemical potential and the chemical composition of seawater. The dissolution rate of copper electrodes may be controlled using engineered power supply such as the Cathelco system. From the literature, it appears that a few milligrams per litre of copper ions are enough to show mortality effects.

12.5.2.2 For flow-through systems

Flow-through configurations can be encountered either for simple instrument or complex multi-sensor systems.

- Several instrument manufacturers (Sea-Bird, WET Labs Inc.) are developing products based on automated water circulation, sequentially managed or not, which combine passive biocide releasing or washing phases within the flow-through protocol (Woerther, 1999; Woerther et al., 1998).
- A coastal monitoring buoy has been developed in France, the MAREL network (Woerther 1999; Woerther et al., 1998), which is based on an online settlement of sensors along a water pumping circuit. Managed with an hourly acquisition frequency for a two-month free-operation mode, the system is equipped with a controlled chlorine generator which allows adjustment of the biocide concentration.

12.5.2.3 Surface action mode

This action mode class is essentially concerned with sensors and instruments, simply because prevention has to be focused directly on the interface measurement head.

- Wipers are used on the optical windows of different sensors to reduce fouling (Clean SweepTM wiper for turbidity, chlorophyll, DO, pH from YSI, Bio-wiperTM from

WET Labs. Inc.) or on membranes (Electrode Cleaning System (ECS) for dissolved oxygen sensors from Foxboro®). These techniques are not recommended for processes that contain suspended abrasive materials.

- Shutters and essentially copper shutters (Barnard and Roesler, 2004; Manov et al., 2003) are routinely used by WET Labs. Inc., HOBILabs and Satlantic. The shutter covers the optical surfaces and opens only during measurements.
- Water jetting is also used as an antifouling technology. Water is forced across a surface under high pressure to generate sufficient shear forces to remove the biofilm. As explained in Section 12.2.3.5, an increase of fluid circulation may enhance the quantity of available nutrients, thus water jetting can be associated with biocides (BROS Final Report, 1998) or used with hydrophobic coatings.
- Ultrasonic surface excitation may prevent biofouling by using a piezoelectric film to generate ultrasound (Latour, 1998). A dielectric material having a permanent internal electrostatic field (electret) may be applied on optical materials. The frequency scale, energy level and number of electrets need to be adapted to obtain a curative effect on fouling without any risk of structural damage.
- Anti-fouling gatekeepers may be placed at the input of a sensor system (Sea-Bird conductivity cell). The anti-foulant is an expendable device that is installed on each end of the conductivity cell, so that any water that enters the cell is treated.
- Specific coating having electrically conductive properties and light transparency such as SnO_2 (Festy et al., 1998) seems to be interesting for optical windows. A very low surface chlorine generation can be managed sequentially according to specific user requirements, (Figures 12.12, 12.13).
- Ultraviolet radiation (UVR) is widely used in food protection. Deep UV (<300 nm) is the most efficient range to produce the maximum biocide effect, but it also has serious drawbacks for organic materials such polymers. A patent (Patent WO03065032, system and method for preventing fouling in sensors) concerning the use of UV radiation to reduce fouling in a water quality monitoring system was recently deposited (Stuart, 2003). The water quality monitoring system comprises a housing having an interior cavity for a monitoring sensor and ultraviolet light sources designed to be operable within the interior cavity.

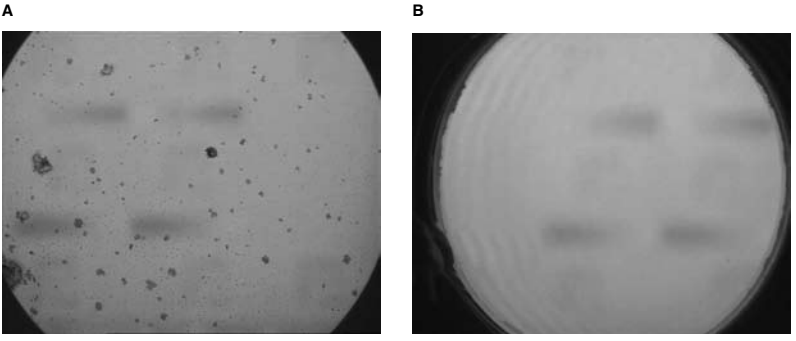

Figure 12.12
Field observations of biofouling at the window interface of a video camera after two months of exposure. Views from inside: A, unprotected; B, with SnO_2 coating active chlorine generation.
Source: IFREMER data.

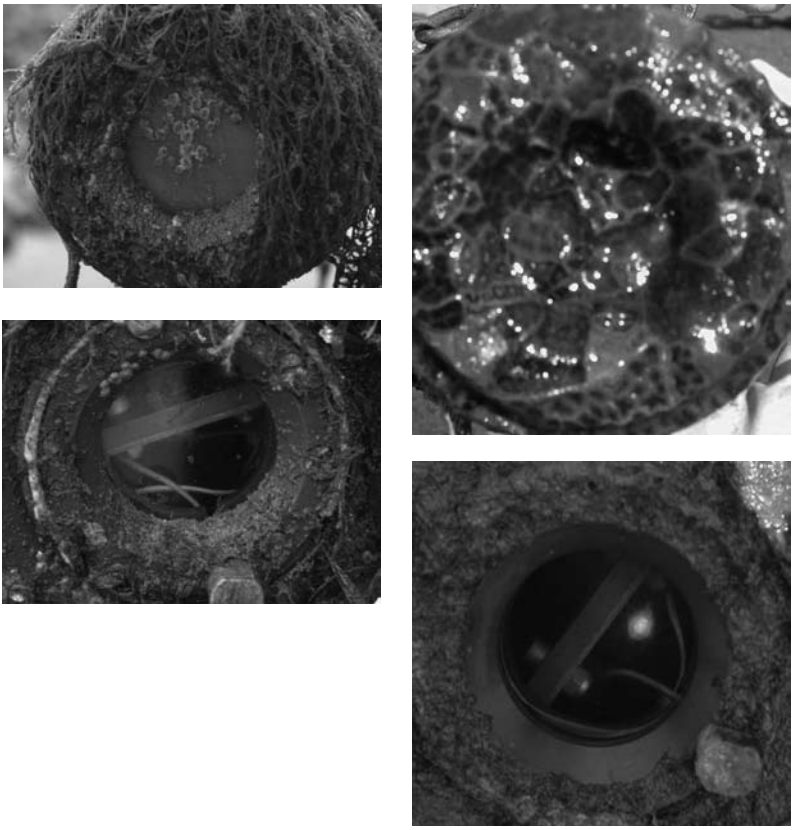

Figure 12.13
Comparative experiment on optical windows after nine weeks simultaneous exposition: left, Atlantic Ocean; right, Bosphorus Strait; above, non-protected and below, surface chlorine generation.
Source: courtesy of EC-MISPEC project.

- Most bacteria are known to have negative surface charges, and polarizing a transparent indium/tin oxide semi conductor deposited on glass at negative potentials creates a negative electrical residual charge and thus prevents cell first adhesion (Kerr et al., 1999b). Patent applications based on this principle regularly appear but no use of these methods in practice has been reported.

12.5.3 Adverse effects

Selection of antifouling strategies depends on the data quality objectives and is site-specific, depending on local conditions. Special care must be taken to avoid adverse effects because surface treatments of an optical window may modify the interfacial properties. Electrodes in the vicinity of a conductivity sensor may perturb measurement. Biocide molecules can interfere with an oxygen sensor membrane or induce

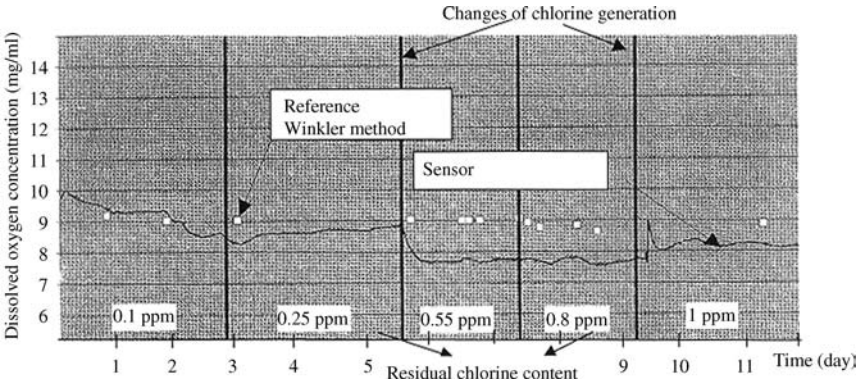

Figure 12.14
Adverse effects of high chlorine generation on dissolved oxygen measurements.
Source: IFREMER data.

local water property modifications. An example of adverse effect on measurements is given in Figure 12.14; in case of high chlorine generation (residual chlorine content 0.55 ppm) in the vicinity of an oxygen sensor, the dissolved oxygen measurements are no longer comparable with reference measurements performed in the laboratory on seawater sampling using the Winkler method.

A major dilemma for users is to try to improve their observation tools in terms of reliability and quality of measurement while it is clear that no perfect solution against biofouling is available. The main reason is that biofouling must be seen as part of the measurement. A major effort to qualify the biofouling kinetics is required to sharpen the strategy, entailing more rigorous assessment work on different prevention methods. Several programmes have been funded by the EC to improve knowledge and help users. Initiatives such as EC-project EVR1-2001-00034 BRIMOM (Biofouling Resistant Infrastructure for Measuring, Observing and Monitoring) will provide basic recommendations to European research infrastructures to improve the reliability of oceanographic data. The delivery of this project will consist of a set of specific technologies to be applied to different types of underwater instruments.

When considering the biofouling effect as part of the measurement, the user responsible for data quality also needs to integrate this parameter in the same way as any other signal bias source (e.g. stability, power consumption limits external parameter influences). Only scientific considerations are presented here but economic factors must also be taken into account, either for the user or the provider who must be aware of the market. An inefficient strategy could have a negative effect on the overall product. The effort to qualify and guarantee the efficiency of a protection method, which will not always be absolutely necessary, will increase the cost of the measurement. Organization and experience are required to help find the most convenient solution for each particular case.

12.6 Provisional tools for decision-making

The extreme diversity of anti-fouling methods and the complexity of ensuring the quality of long-term monitoring justify a minimum of guidelines to find convergence between local field peculiarities and the most suitable strategies.

As we have shown, many anti-fouling strategies are now available. They are all more or less efficient, often depending on external factors directly related to the particular application. These factors may include the experiment duration, climate, location, all of which are normally known by the user. These affect the complexity of the system as well as the possible increase in cost, implying that care should be taken with the choice to be made. It is for example unnecessary to implement sophisticated protection if the application does not require it because the quality of measurement will not be affected by biofouling during the period of operation. All available techniques of protection are time limited and this must be taken into account by the user and projected onto an estimation of the possible fouling evolution during the working period. Most of the time the user is fully dependent on optional arbitrary solutions proposed by manufacturers. The decision to choose a particular strategy must be the responsibility of the user who must define accurately the frame of use. As it is never easy to anticipate possible interference from biofouling, the user needs some basic help in taking the most relevant decision.

Biofouling can be modelled for application to a specific location according to information given by the user, who must have a clear enough idea of the simplified

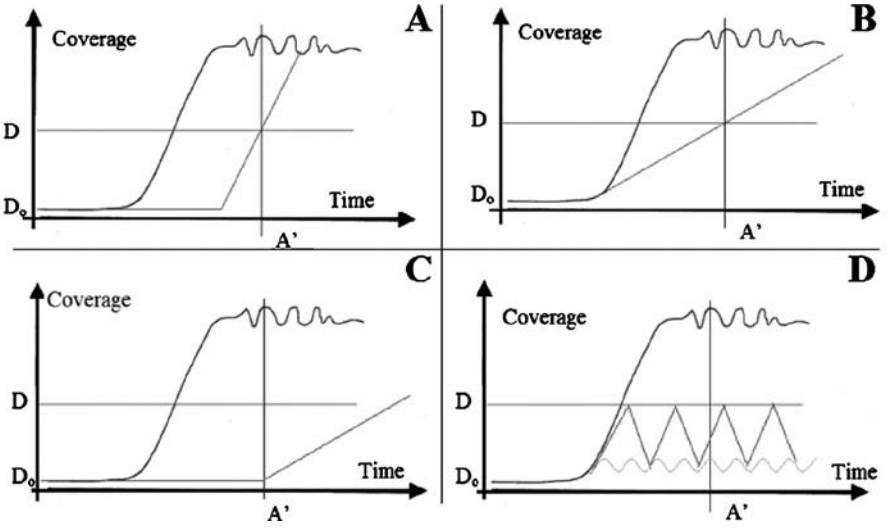

Figure 12.15
Proposed solutions to satisfy users' data quality requirements. A and B can be achieved with passive techniques, C and D require an active strategy.
A, biofouling can be delayed
B, growth rate is reduced by biocide releasing
C, D must be equal to D_0 during the experiment
D, biofouling can be removed or limited

biofouling kinetics representation either from experience or from an environmental database of the specific area.

From the basic curve in Figure 12.8, the user must plot the two essential parameters leading to the data quality requirement for the application. For simplification the two parameters are designated D and A'. D is the admitted threshold corresponding to the level of fouling coverage having no influence on the expected measurement quality. This can be assimilated as a S/N ratio in conformity with the instrument calibration. The A' value represents the time of the experiment. This gives a rectangular area in which the biofouling evolution must be maintained naturally or controlled by a prevention strategy.

The D value can be D_0, which is the highest requirement level of prevention. Keeping D_0 over a long period will be difficult and limits the number of potential solutions.

Inside the defined area, several methods can be available to the user, who will then be able to choose the best solution according to the particular constraints of the application (e.g. cost, technical considerations).

The different situations described in Figure 12.15 show that several solutions can fulfil a specific need.

The main difficulty for the moment is that users have generally no clear idea of the required D value. For a long time this value has been roughly estimated at the end of the field experiment. In addition to work in modelling the kinetics, some structured assessments are needed for any type of instrument to optimize this approach.

The ideal approach may be subject to random errors due to a poor estimate of the growth kinetics or the choice of protection. The conception of a biofouling sensor could be an interesting alternative in helping the user to determine the limit of reliability of the data file. It would also be simpler and perfectly adequate for shorter experiments conducted during low biofouling conditions.

12.7 Conclusion

Marine biofouling is a natural process occurring in the ocean as soon as a substratum is lowered or moored underwater.

Biofouling is part of the measurement and must be considered along with any other source of signal bias. Thus the user must first clearly define the data quality requirements for the application. Second, the acceptable level of noise due to biofouling must be established, and finally the most convenient antifouling strategies must be determined for each particular case during a rigorous qualification phase. Special care must be taken in the choice of an antifouling strategy as it can also strongly modify the local environment to be monitored.

References

Aminot, A. and Chaussepied, M. 1983. *Manuel des analyses chimiques en milieu marin*. Centre National pour l'Exploitation des Océans/Banco National de Dados Oceanográficos Documentation.

Amram, P. et al. (ANTARES collaboration). 2003. Sedimentation and fouling of optical surfaces at the ANTARES site. *Astropart. Phys.*, 19, pp. 253–67.

Anon. 1992. *Appraisal of Marine Growth on Offshore Structures*. UK Marine Technology Directorate, 92/102.

Babin, M., Roesler, C. S. and Cullen, J. J. (eds). 2006. *Real-time Coastal Observing Systems for Marine Ecosystem Dynamics and Harmful Algal Blooms: Theory, Instrumentation and Modelling*. Paris, Intergovernmental Oceanographic Commission of UNESCO. (Monographs on Oceanographic Methodology XX.)

Baier, R. E. 1972. *Proc. Third International Congress on Marine Corrosion and Fouling*. Gaithersburg, Md., National Bureau of Standards, pp. 633–39.

Banks, P. D. and Brown, K. M. 2002. Hydrocarbon effects on fouling assemblages: the importance of taxonomic differences, seasonal, and tidal variation. *Mar. Environ. Res.*, 53, pp. 311–26.

Barnard, A. and Roesler, C. 2004. The use of multi-parameter bio-optical instrument systems for long-term observations of ecosystem community structure. *ASLO/TOS Ocean Research 2004 Conference*, 15–20 February 2004, Honolulu, Hawaii.

Bos, R., Van der Mei, H. C. and Busscher, H. J. 1999. Physico-chemistry of initial microbial adhesive interactions-its mechanisms and methods for study. *FEMS Microbiol. Rev.*, 23, pp. 179–230.

Brekhovskikh, L. and Lysanov, Yu. 1982. *Fundamentals of Ocean Acoustics*. Berlin, Springer-Verlag.

Breur, R. 2001. Fouling and Bioprotection of Metals, Monitoring and Control of Deposition Processes in Aqueous Environments, Ph.D. thesis, TNO Industrial Technology.

BROS. 1998. Biofouling Reduction on Optical Systems. Final report, Vols I and II, 1 February 1996–31 July 1998. (Contract MAS3-CT95-0028.)

Characklis, W. G. 1990. Microbial fouling and microbial biofouling control. In: W. G. Characklis and K. C. Marshall, *Biofilms*. New York, John Wiley & Sons, pp. 523–634.

Chang, G. C. and Dickey, T. D. 1999. Partioning *in situ* total spectral absorption by use of moored spectral absorption-attenuation meters, *Appl. Opt.*, 38(18), pp. 3876–87.

Chang, G. C. and Dickey, T. D. 2007. Interdisciplinary sampling strategies for detection and characterization of harmful algal blooms. In: Babin et al. (eds), op. cit., this volume.

Claustre, H., Fell, F., Oubelkheir, K., Prieur, L., Sciandra, A., Gentilli, B. and Babin, M. 2000. Continuous monitoring of surface optical properties across a geostrophic front: biogeochemical inferences. *Limnol. Oceanogr.*, 45(2), pp. 309–21.

Compère, C., Bellon-Fontaine, M. N., Bertrand, P., Costa, D., Marcus, P., Poleunis, C., Pradier, C. M., Rondot, B. and Walls, M. G. 2001. Kinetics of conditioning layer formation on stainless steel immersed in seawater. *Biofouling*, 17(2), pp. 129–45.

Costerton, D. E., Lewandowski, Z., Caldwell, D. E., Korber, D. R. and Lappin-Scott, H. M. 1995. Microbial biofilms. *Ann. Rev. Microbiol.*, 45, pp. 711–45.

Curtis, A. and Wilkinson, C. 2001. Nanotechniques and approaches in biotechnology. *Trends Biotech.*, 19, pp. 97–101.

Dahms, H. U., Dobretsov, S. and Qian, P. Y. 2004. *J. Exp. Mar. Biol. Ecol.*, Vol 313, pp. 191–209.

Derjaguin, B. V. and Landau, I. 1941. *Acta Physicochim. URSS*, 14, pp. 633–62.

Eashwar, M., Subramanian, G., Chandrasekaran, P., Manickam, S. T., Maruthamuthu, S. and Balakrishnana, K. 1995. The interrelation of cathodic protection and marine macrofouling. *Biofouling*, 8, pp. 303–12.

Fera, P. 1985. Étude expérimentale de la colonisation par les bactéries de surface immergées en milieu marin. Thesis, Université Bretagne Occidentale, France.

Festy, D., Le Bras, S., Clegg, M., Lacotte, N., Lehaitre, M., Menlove, R. and Sebastiao, P. 1998. Biofilm prevention on optics by chlorine compound generation on tin oxide coating. *Ocean 98*, Nice, France.

Fletcher, M. and Pringle, J. H. 1985. *J. Colloid Interface Sci.*, 104(1) pp. 5–14.

Forteath, G. N. R., Picken, G. B. and Ralph, R. 1983. Interaction and competition for space between fouling organisms on the Beatrice oil platforms in the Moray Firth, North Sea. *Int. Biodeterioration Bull.*, pp. 45–52.

Forteath, G. N. R., Picken, G. B. and Ralph, R. 1984. Patterns of macrofouling on steel platforms in the central and northern North Sea. In: J. R. Lewis and A. D. Mercer,

Corrosion and Marine Growth on Offshore Structures. London/Chichester, Society of Chemical Industry/Ellis Horwood.

Fusetani, N. 1997. Marine natural products influencing larval settlement metamorphosis of benthic invertebrates. *Curr. Org. Chem.*, 1, pp. 127–52.

Ghobashy, A. F. A. and El-Komy, M. M. 1980 Fouling in the southern region of the Suez Canal. *Hydrobiol. Bull.*, 14(3), pp. 179–85.

Gorsky, G., Picheral, M. and Stemmann, L. 2000. Use of the underwater video profiler for the study of aggregate dynamics in the North Mediterranean. *Estuar. Coast. Shelf Sci.*, 50, pp. 121–28.

Head, R. and Davenport, J. 1997. The use of copper electrodes to reduce biofilm formation on optical surfaces. In: J. Wimpenny, P. Handley, P. Gilbert, H. Lappin-Scott and M. Jones (eds), *Biofilms: Community Interactions and Control*. London, Bioline, pp. 287–92.

Jones, K. L. 2002. Nanoporous membrane materials. *National Nanofabrication Users Network Abstracts*, *Biol. Chem.*, p 15.

Kerr, A., Beveridge., C. M., Cowling, M. J., Hodgkiess, T., Parr, A. C. S. and Smith, M. J. 1999*a*. *Biol. Assoc. UK*, 79, pp. 357–59.

Kerr, A., Cowling, M. J., Beveridge, C. M., Smith, M. J. and Parr A. C. S. 1998. The early stages of marine biofouling and its effect on two types of optical sensors. *Environ. Int.*, 4(3), pp. 331–43.

Kerr, A., Hodgkiess, T., Cowling, M. J., Beveridge, C. M., Smith, M. J. and Parr, A. C. S. 1998. A novel technique to prevent bacterial fouling, using imposed surface potential. *J. Appl. Microbiol*, 85, pp. 1067–72.

Kerr, A., Hodgkiess, T., Cowling, M. J., Smith M. J. and Beveridge, C. M. 1999*b*. Effect of galvanically induced surface potentials on marine fouling. *Lett. Appl. Microbiol.*, 29(1), pp. 56–60.

Kerr, A., Smith, M. J., Cowling, M. J. and Hodgkiess, T. 2001. The biofouling resistant properties of six transparent polymers with and without pre-treatment by two antimicrobial solutions. *Mater. Des.*, 22, pp. 383–92.

Kingsbury, R. W. S. M. 1981. Marine fouling of North Sea installations. *Marine Fouling of Offshore Structures*. Society for Underwater Technology, Conference Session 1.

Latour, M. 1998. Mechanical vibrations induced on elastic structures by piezopolymer transducers. Progress in electrets. *IEEE Trans. Dielectrics Electrical Insulation*, 5(1), pp. 40–44.

Lewis, M. R. 2007. Measurement of apparent optical properties for diagnosis of harmful algal blooms. In: Babin et al. (eds), op. cit., this volume.

Luna, G. M., Dell'Ano, A., Giuliano, L. and Danovaro, R. 2004. Bacterial diversity in deep Mediterranean sediments: relationship with the active bacterial fraction and substrate availability. *Environ. Microbiol.*, 6(7), pp. 745–53.

Lunven, M., Gentien, P., Kononen, P., Le Gaul, E. and Daniélou, M. M. 2003. *In situ* video and diffraction analysis of marine particles. *Estuar. Coast. Shelf Sci.*

Luoma, S. N., Steinert, S., Streib-Montee, R. and Weis, P. 1998. The effects of copper on marine organisms. In: P. F. Seligman and A. Zirino (eds), *Chemistry, Toxicity and Bioavailability of Copper and its Relationship to Regulation in the Marine Environment*. Arlington, Va., US Office of Naval Research. (Workshop Report, Technical Document 3044.)

Manov, D. V., Chang, G. C. and Dickey, T. D. 2004. Methods for reducing biofouling of moored optical sensors. *J. Atmos. Ocean. Tech.*, 21, pp. 958–68.

Marshall, K. C., Stout, R. and Mitchell, R. 1971. *J. Gen. Microbial.*, 68, pp. 337–48.

McLeroy-Etheridge, S. L. and Roesler, C. S. 1998. Are the inherent optical properties of phytoplankton responsible for the distinct ocean colors observed during harmful algal blooms? *Ocean Optics XIV*, *Proc. SPIE*, 1, pp. 109–16.

Meinema, H. A., Rentrop, A. C. H., Breur, A. H. J. and Ferrari, G. M. 1998. Development of organic-inorganic hybrid coatings with anti-fouling properties for application on optical

underwater instruments. *Proc. 2nd International Conference on Coatings on Glass (ICCCG)*, Saarbrucken, Germany, 6–10 September 1998.
Mills, A. L. and Maubrey, R. 1981. *Micro. Ecol.*, 7, pp. 315–22.
Mobley, C. D. 1994. *Light and Water: Radiative Transfer in Natural Waters*. New York, Academic Press.
Morel, A. 1994. Optics from the single cell to the mesoscale. In: R. W. Spinrad, L. K. Carder and M. J. Perry (eds), *Ocean Optics*. Oxford, Clarendon Press, pp. 93–106.
Oecd. 1986. *Catalogue of Main Marine Fouling Organisms*. Paris, Organisation for Economic Co-operation and Development.
Pethica, B. A. 1980. Microbial and cell adhesion. In: R. C. W. Berkeley, J. M. Lynch, J. Melling, P. R. Rutter and D. Vincent (eds), *Microbial Adhesion to Surfaces*. Chichester, UK, Ellis Horwood, pp. 19–45.
Powell, M. S. and Slater, N. K. H. 1983. *Biotech. Bioeng.*, 25, pp. 891–900.
Pradier, C. M., Bertrand, P., Bellon-Fontaine, M. N., Compère, C., Costa, D., Marcus, P. Poleunis, P., Rondot, B. and Walls, M. G. 2000. Adsorption of proteins on an AISI 316 stainless steel surface in natural seawater, *Surf. Interface Anal.*, 30, pp. 45–49.
Riedl, R. 1971. Water movement, 5.3. Animals. In: O. Kinne (ed.), *Marine Ecology*. London, Wiley Interscience, pp. 1123–56.
Robb, I. D. 1984, Stereo-biochemistry and function of polymers. In: K. C. Marshall (ed.), *Microbial Adhesion and Aggregation (Dahlem Konferenzen)*. Berlin, Springer-Verlag, pp. 39–49.
Roberts, D., Rittschof, D., Holm, E. and Schmidt, A. R. 1991. *J. Exp. Mar. Biol. Ecol.*, 150, pp. 203–21.
Roesler, C. S. 1998. Theoretical and experimental approaches to improve accuracy of particulate absorption coefficients derived from the quantitative filter technique. *Limnol. Oceanogr.*, 43, pp. 1649–60.
Roesler, C. S. and Boss, E. 2007. *In situ* measurement of inherent optical properties and potential for harmful algal bloom detection and coastal ecosystem observations. In: Babin et al. (eds), op. cit., this volume.
Roesler, C. S. and Zaneveld, J. R. V. 1994. High resolution vertical profiles of spectral absorption, attenuation, and scattering coefficients in highly stratified waters. *Ocean Optics XII*, *Proc. SPIE*, 2258, pp. 309–19.
Rubio, C. 2002. Thesis, Université de Paris VI.
Scheuerman, T. R., Camper, A. K. and Hamilton, M. A. 1998. Effects of substratum topography on bacterial adhesion, *J. Colloid Interface Sci.*, 208, pp. 23–33.
Scholin, C. A. 2000. Application of DNA probes for detection of harmful algae, *J. Shellfish Res*, 19(1), p. 637.
Schneider, I. and Allermann, K. 2000. Antifouling paint composition comprising rosin and enzyme. PCT application (PCT/DK01/00202). BioLocus ApS.
Stoodley, P., deBeer, D. and Lewandowski, Z. 1994. *Z. Appl. Environ. Microbiol.*, 60, pp. 2711–16.
Strahle, W. J., Perez, C. and Martini, M. A. 1994. Antifouling leaching technique for optical lenses. *Proc. OCEANS OSATES '94 Conference 2*, Institute of Electrical and Electronic Engineers–Oceanic Engineering Society (IEEE–OES), pp. 710–715.
Strathmann, R. R. and Branscomb, E. S. 1979. Adequacy of cues to favourable sites used by settling larvae of two intertidal barnacles. In: S. E. Stanczyk (ed.), *Reproductive Ecology of Marine Invertebrates*. University of South Carolina, pp. 77–89. (Library in Marine Sciences 9.)
Stuart, G. 2003. System and method for preventing fouling in sensors. Patent WO03065032.
Van de Hulst, H. C. 1980. *Multiple Light Scattering*. New York, Academic Press.
Van de Hulst, H. C. 1981. *Light Scattering by Small Particles*. New York, Dover Publications.
Venkatesan, R., Dwarakadasa, E. S. and Ravindran, M. 2003. Biofilm formation on structural materials in deep sea environments. *Indian J. Eng. Mater. Sci.*, 10, pp. 486–91.
Verwey, E. J. W. and Overbeek, J. T. G. 1948. *Theory of the Stability of Lyophobic Colloids*. Amsterdam, Elsevier.

Walls, M. G., Rondot, B., Costa, D., Pradier, C. M., Marcus, P., Bellon-Fontaine, M. N., Compère, C. and Guezennec, J. 1998. The BASIS group. A study of the initial stages of biofilm formation on stainless steel immersed in sea water. In: L. Faria (ed.), *Proc. Euromat 98 (Materials in Oceanic Environment)*. Lisbon, Sociedade Portuguesa de Materiais, 1, pp. 421–30

Wieczorek, S. K., Murray, A. W. A. and Todd, C. D. 1996. Seasonal variation in the effects of hard substratum biofilming on settlement of marine invertebrate larvae. *Biofouling*, 10(4), pp. 309–30.

Woerther, P. 1999. Coastal environment of the Seine bay area monitored by a new French system of automated measurement stations. *Proc. EUROGOOS Second International Conference*, Rome.

Woerther, P. and Grouhel, A. 1998. Automated measurement network for the coastal environment. OCEANS 98, IEEE Conference and Exhibition, Nice, Franch.

Zaneveld, J. R. 1994. Optical closure: from theory to measurement. In: R. W. Spinrad, L. K. Carder and M. J. Perry (eds), *Ocean Optics*. Oxford, UK, Clarendon Press, pp. 59–72.

Zisman, W. A. 1964. *Adv. Cem. Ser.*, 43, pp. 1–51.

13

Glider and autonomous underwater vehicle observing systems

G. Griffiths

13.1 Introduction

Gliders and propeller-driven autonomous underwater vehicles (AUVs) are examples of how advances in technology can deliver new sampling tools to the marine scientist. These vehicles exist today in many forms, in academic research establishments, in the military and in commercial service. While still in development in some respects, the technology is sufficiently mature to have become a mainstay of the offshore survey industry in several deep-water parts of the world. It is applying this new technology to the study of harmful algal blooms (HABs) that remains a challenge for the marine science community, not the technology of the autonomous vehicle per se.

AUVs and gliders have been proposed as components of coastal and open ocean observing systems at many workshops, conferences and symposia (e.g. IOC, 1998; Jahnke et al., 2002; Dickey, 2002). More specifically, many authors have called for technological innovations to improve our understanding of HABs (e.g. Zingone et al., 2000; Roelke and Buyukates, 2001; van Dolah et al., 2001). This chapter describes the present state of development of gliders and AUVs and, in describing a number of scientific investigations carried out with these vehicles, attempts to provide a reasoned view of how this particular new technology may aid the study of HABs. Throughout, the aim is to avoid giving the reader the impression that AUVs are a solution to all their data-gathering needs for physical and biochemical measurements in the coastal ocean. Rather, these new platforms can only ever be part of a solution within an integrated observing system. The challenge of developing suitable sensors for use on small, battery-powered vehicles is enormous. Longhurst's caution on keeping a proper perspective on the real outcomes from new technology in the study of marine life underpins this chapter (Longhurst, 2000).

This chapter is organized as follows. Section 13.2 outlines the types of autonomous underwater vehicles in use today. Section 13.3 examines the general problem of sampling a water space in which changes occur over a range of time and space scales. A simple metric for estimating the information obtained from surveys as a function of survey speed and area coverage is discussed. Using this metric, the relative efficiencies of different autonomous vehicles and sampling strategies are examined. Section 13.4 explores some of the key technical issues facing the user of autonomous vehicles for the study of HABs. Examples are given of relevant new sensors that have been designed for use in AUVs or have been modified for autonomous use. Section 13.5 provides several examples of science outcomes from present-generation AUVs that have some lessons for the use of this new technology in the study of HABs. These include applications

that have tested hypotheses (process studies) and prototypical examples relevant to use within sustained observing systems. Section 13.6 outlines some of the existing barriers to take-up: scientific, technical, economic, logistical and legal, with some suggestions for how these barriers might be overcome.

13.2 The family of underwater vehicles

The family of autonomous underwater vehicles spans a size range from ~1 m to ~10 m in length and in mass from less than 50 kg to 10,000 kg. Representative examples of different types are shown in Figure 13.1. As a general rule, the larger vehicles are able to cover longer ranges, although one class of vehicle – the underwater gliders – achieve long range despite their small size. This is solely because they travel at low speed and the power consumption of their control systems and sensors has been minimized. The only essential difference between gliders and propeller-driven vehicles is the mechanism for conversion of stored energy to forward motion. In gliders, electrical energy from the batteries is used within a pump to effect a change in the buoyancy and orientation of the vehicle, the change in buoyancy is converted to forward motion with lift surfaces i.e. wings. In a propeller driven vehicle, a motor replaces the pump and a rather different type of lift surface, the propeller, replaces the wings.

An important class of AUV for potential use in observing HABs is the semi-submersible. The advantage being a far longer range and higher speed compared with underwater vehicles, achieved at comparable or less cost. This advantage comes from the use of an internal combustion engine as the power source, made possible because air is available via a snorkel. A disadvantage is that the semi-submersible operates close to the sea surface, hence it cannot provide vertical profiles other than via remote sensing instruments (e.g. currents and acoustic backscatter from an ADCP) or via subsidiary towed undulators (Ferguson, 2003).

Autonomous surface vehicles (ASVs) may also be an effective solution for monitoring HABs. They share the high speed and endurance of the semi-submersible; they can be of even lower cost, but may pose more of a navigation hazard in many parts of the world. Despite their simpler requirements for navigation, power source and data communications, it appears that civil ASV technology is not as advanced as that for AUVs (Griffiths et al., 2001).

An alternative to the free-roaming autonomous vehicle for some applications is the moored profiler. These one-dimensional AUVs crawl up and down a moored guide wire. They have the potential to provide repeated profiles at a single location over an extended time, making data transmission to and from shore possible. Costs are lower than for an AUV because the control systems are far simpler. Cumulative profiling distances of 1,000 km are possible on a single battery module in deep ocean instruments, for example, 2,500 up-down profiles over 200 m at a speed of 0.3 m s^{-1} (Doherty, 1999). For use in continental shelf waters, the SeaHorse mooring (Greenan et al., 2004) uses a surface moored buoy that extracts energy from the surface waves to power a package that climbs up and down the mooring line.

Free-fall and tethered profilers also have an important role to play in the study of bio-optical, biophysical and biochemical interactions in the sea. They have been particularly effective in the study of thin layers in coastal waters. The profilers developed

Figure 13.1
Examples of several types of autonomous underwater vehicle (AUV).

and described by Hanson and Donaghay (1998) combine sensors for temperature, conductivity, fluorescence with Wet Labs' ac-9 spectral absorption and attenuation meter and chemical measurements of dissolved oxygen, pH, nitrite and iron II. At a fall rate of 1–2 m/min, the chemical sensors are able to resolve changes in the vertical on the scales of 10–20 cm.

13.3 4-D sampling using underwater vehicles

AUVs have the potential to contribute information to four-dimensional (where the dimensions are latitude, longitude, depth and time) views of the physical, biochemical and optical ocean and coastal environment relevant to the study of HABs.

Quite how AUVs can contribute that important information can be established by considering what processes and properties are relevant to the dynamics of HABs and how AUVs can be used to study those processes or properties. Other chapters in this volume contain the detail on processes and properties, while Chang (2003) provides a summary, but to illustrate how AUVs can contribute, consider the examples in Table 13.1.

Table 13.1 Properties and processes relevant to HAB dynamics and how AUVs can contribute information

Property or process	**Relevant chapters**	**How AUVs can contribute**
Underwater light field	Lewis (6), Roesler and Boss (5), Cullen (1)	Measurements of radiance and irradiance, spectral distribution, absorption, attenuation etc., including vertical profiles and spatial distribution, contemporaneously with other measurements.
Physical forcing, thermal structure, density gradients, turbulence	Franks (15), Chang and Dickey (2)	Can provide vertical sections and horizontal maps of physical properties including temperature, salinity, turbulence while also gathering bio-optical and other measurements. Minimal disturbance to phenomena being studied.
Distribution of nutrients and micro-nutrients	Chang and Dickey (2)	Emerging capability to carry fast sensors for estimation of some nutrients e.g. nitrate, phosphate and iron.
Distribution, abundance and species composition of phytoplankton	Roesler and Boss (5), Babin (7), Morel (4), Chang and Dickey (2)	Single-wavelength fluorometers widely used on AUVs, and variable fluorescence instruments could be carried in principle. Care needed to ensure information for proper interpretation is also gathered, e.g. to estimate fluorescence yield, avoidance/estimation of quenching, actual species composition. Flow cytometry within AUVs is in its infancy, promising but not yet delivering within an autonomous instrument species identification using neural network or other techniques.

Table 13.1 *(Continued)*

Property or process	Relevant chapters	How AUVs can contribute
Distribution, abundance and species composition of zooplankton and fish	Jaffe (10)	Larger AUVs can carry sensors for observing acoustic backscatter at multiple frequencies. Inversion of backscatter to species composition and abundance not straightforward, and may not always be possible. Useful observations in areas with limited and known species present.
Variation of the above in space and time	This chapter	Biological distributions are patchy; surveys with single or multiple vehicles, along set grids, or using measurements of properties by the sensors on the vehicle to adapt the survey pattern can lead to improved descriptions of the spatial and temporal patchiness of HABs, compared with what could be obtained using fixed instruments on moorings. Telemetry of data summaries to shore, and retasking from shore, perhaps using directions based on the results of simulation models assimilating previous data offers new observation capabilities.

The potential indicated in the table may be realized through careful design of sampling schemes that recognize the limitations of the technology, both of the vehicle and of the sensors it will carry. As low-cost AUVs become available, it will become feasible to use multiple vehicles undertaking coordinated missions to mitigate some of the restrictions of an individual vehicle.

13.3.1 Performance metrics for AUV surveys

Present-day limitations, for example in the energy available in autonomous vehicles and the lack of *in situ* sensors for many, if not most, of the biochemical parameters of interest mean that this emerging technology is restricted in its application. There are also economic factors at play. Very few AUVs are in routine production, let alone being manufactured in quantity (considered as over 100 per year). Hence, economies of scale have yet to be realized. These technical and economic limitations have a direct impact on the present-day utility of these sampling platforms.

The energy limitation leads directly to a restricted range of spatial scales over which observations can be made. For example, a large propeller-driven AUV with a range of 500 km between refuelling could map an area 45 km by 45 km with survey

lines 5 km apart. Over a continental shelf, such a survey could provide high resolution in the vertical (~0.1 m) for physical and optical properties and for chlorophyll fluorescence, coupled with an along-track horizontal resolution of less than 700 m if using a saw-tooth profile pattern. However, the cross-track resolution would barely satisfy the Nyquist criterion for resolving physical or biological variability at the Rossby radius (of the order of 10 km). Cross-track biological patchiness at scales of less than 10 km would not be resolved. By reducing the area covered to 20 km by 20 km, with tracks 1 km apart, cross-track patchiness at scales of 2 km and above could be resolved.

This spatial coverage issue is even more acute for small propeller-driven AUVs, with typical operating ranges of the order of 50 km. Only by operating at very slow speed (typically 0.25 m s^{-1}rather than the 1.5–2.5 m s^{-1} typical of propeller-driven vehicles) can small AUVs achieve long range. To date, such slow-speed, long-range vehicles have used hydrodynamic lift from wings and a buoyancy change engine as their propulsor, rather than the propeller commonly found on higher speed vehicles. Termed 'gliders', these buoyancy change vehicles have theoretical ranges in excess of 1,000 km (Davis et al., 2003).

It is precisely because of the interdependence of range, speed and spatial sampling that survey design is so important when using AUVs. Willcox et al. (2001) derived performance metrics (ε) for the spatial (ε_λ) and temporal (ε_τ) errors for a survey in the horizontal plane over an area dominated by wave-like structures:

$$\varepsilon_\lambda = \left[\frac{\lambda_s^2}{\lambda_0^2 + \lambda_s^2} \right]^{1/2} \tag{13.1}$$

$$\varepsilon_\tau = \left[1 + \frac{2\tau_0}{\tau_s} (e^{-\tau_s/2\tau_0} - 1) \right], \tag{13.2}$$

where τ_0 is a temporal correlation scale, τ_s is the time taken for the survey, λ_0 is a spatial correlation length scale and λ_s the survey spatial resolution, where λ_s is twice the leg spacing for a 'lawnmower' type of survey to satisfy the Nyquist sampling criterion of requiring at least two samples at the highest frequency to be resolved.

The combined survey error is:

$$\varepsilon_{tot} = \varepsilon_\lambda + \varepsilon_\tau - \varepsilon_\lambda \varepsilon_\tau \tag{13.3}$$

which on substituting for ε_λ and ε_τ from (13.1) and (13.2) gives:

$$\varepsilon_{tot} = \left[1 + \frac{2\tau_0}{\tau_s} (e^{-\tau_s/2\tau_0} - 1) \right] - \frac{2\tau_0}{\tau_s} \left[\frac{\lambda_s^2}{\lambda_0^2 + \lambda_s^2} \right]^{1/2} \left(e^{-\tau_s/2\tau_0} - 1 \right) \tag{13.4}$$

When ε_{tot} approaches one, little information on the true spatial and temporal properties of the process is obtained. Conversely, as ε_{tot} approaches zero the survey approaches a true snapshot without temporal or spatial blurring.

In some applications, it may be advantageous to use an autonomous vehicle as a virtual mooring, that is, the vehicle remains at one location in the horizontal, but may alter its depth; for example, it may spiral from the sea surface to the bottom (Griffiths et al., 2002). In this case the spatial error metric ε_λ will be one, there will be no spatial

information, but the temporal error metric ε_τ will be a minimum. A suitable survey timescale to use in (13.4) would be the time taken to perform one vertical profile.

13.3.2 Simulation

Using this error metric we can assess how different autonomous vehicles may be suited to particular monitoring or mapping requirements as part of a HAB study. In this simple example, three different vehicle types are considered, each capable of operating over a range of at least 100 km:

- a buoyancy-driven glider operating at a speed of 0.3 m s^{-1};
- a propeller-driven AUV operating at 2 m s^{-1};
- an autonomous surface vehicle (ASV) operating at 6 m s^{-1}.

The task for the simulation is to survey an area of 30 km^2 where the spatial correlation length scale of the dominant process is 5 km and the temporal correlation scale is 6 hours. These temporal and spatial scales are sufficiently fine to resolve fluorescence changes due to phytoplankton growth and solar radiation and physical changes due to semi-diurnal tidal currents. Abbott et al. (1995) using observations from bio-optical drifters in filaments of the California coastal current showed that fluorescence variability on scales of less than 10 km was important (their Fig. 4) and that variance spectra showed peaks down to 6 hours (their Fig. 13). Of course, variability does also occur on smaller scales than considered in this simulation, but those chosen illustrate what can be done using single or small fleets of gliders or AUVs. The analysis method can be applied to smaller scales.

From the error metric simulation we can estimate the optimum combination of spatial resolution and overall survey time for the different vehicles. For a rectangular lawnmower survey in the horizontal plane over an area A, with legs spaced at $\lambda_s/2$, to be completed in time τ_s, the vehicle must travel at a speed of:

$$V = \frac{2A}{\lambda_s \tau_s} + \frac{2\sqrt{A}}{\tau_s} \tag{13.5}$$

Rearranging (5) to give λ_s as a function of speed:

$$\lambda_s = \frac{2A}{\tau_s V} \Bigg/ \left(1 - \frac{2\sqrt{A}}{\tau_s V}\right) \tag{13.6}$$

Contours of the combined survey error metric ε_{tot} are shown in Figure 13.2 as a function of τ_s and λ_s. Superimposed are three lines, showing the operating areas of the three vehicle types listed above. The operating area in each case is the area to the right of the line labelled with the vehicle type. That is, each vehicle may travel slower than set out above, but not faster. For the ASV there is a minimum in the combined error metric at ε_{tot}~0.28. This occurs at a spatial resolution of ~700 m and a survey time of just less than 4½ hours. Over this time the vehicle would have travelled some 96 km. In the case of the underwater AUV the minimum error metric is higher, at ε_{tot}~0.45, achieved at a spatial resolution of 1,100 m and a survey time of nearly 9 hours. The AUV would have covered 64 km in this time. For a single glider, the combined error metric in this simulation is high, at a minimum of ε_{tot}~0.79, achieved at a spatial resolution of ~2,500 m and a survey time of a little over 31 hours, with the vehicle covering 34 km. In this particular example, the glider would provide very little information on

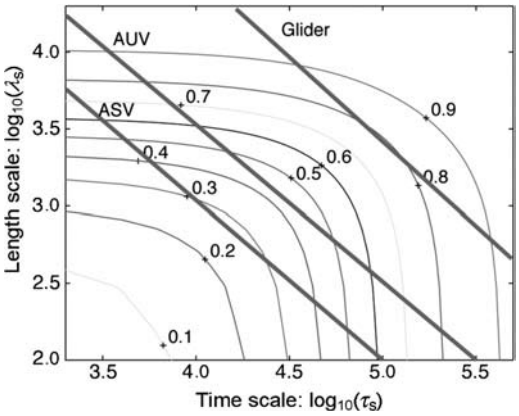

Figure 13.2
Survey error metric (ε_{tot} (13.4)) as a function of spatial resolution (λ_s) and temporal resolution (τ_s) for an example process with a spatial correlation length scale of 5 km, a temporal correlation length scale of 6 hours and a survey area of 30 km^2. As ε_{tot} approaches 1.0, little useful information is obtained. The three sloping lines represent the error metric for surveys that could be conducted by three vehicles: a glider moving at 0.3 m s^{-1}, an AUV at 2 m s^{-1} and an autonomous surface vehicle (ASV) operating at 5 m s^{-1}. Each vehicle shows a (different) optimum combination of duration and spatial resolution for minimum error.

the temporal or spatial patterns of the process. However, that is not to say that it would not provide information on the absence or presence of a bloom and details of its vertical distribution relative to temperature and salinity, for example.

The survey error metric can also be used to explore the benefits of using more than one vehicle in a survey. If, for example, five gliders were to be deployed to survey the 30 km^2 area, each tackling 6 km^2, then the minimum error metric would drop to ε_{tot}~0.55 at a spatial resolution of 1,200 m and a total survey time of 14 hours. Thus a group of gliders would lead to a faster survey, with a higher spatial resolution and a lower error metric. In terms of economics, for this simple case of a snapshot survey, the purchase cost of five gliders would not be too dissimilar to the purchase cost of an AUV capable of 64 km range at 2 m s^{-1}. Where the gliders would provide additional benefit is in their ability to remain operating for hundreds of kilometres over 30 days or more, an option that would be far more costly on an AUV.

There is considerable scope to expand the error metric approach to remove the need for the simplifying assumptions made here (and in Wilcox et al., 2001). Chief among these in the HAB case is to use better descriptions of the spatial and temporal features of interest, and their interactions with physical oceanographic conditions such as tides, mean currents and mixed layer depths in three dimensions.

13.3.3 Adaptive sampling

Regular grid-based or lawnmower sampling may not be the most effective use of autonomous vehicles, given the limitations discussed in Sections 13.3.1 and 13.3.2. By

exploiting the ability of autonomous vehicles to use the data they are gathering to alter their survey plans and strategies, it becomes possible to devise adaptive sampling schemes that make better use of the range and endurance of the AUV. This work is in its infancy, but elements of the systems and algorithms required have been designed and tested. For example, coordinating control strategies for collective behaviour of AUVs and gliders, drawing inspiration from bacterial chemotaxis, have been proposed and developed (Bachmayer and Leonard, 2002).

One of the key requirements is for the mission controller of the AUV to be able to replan the mission based on sensor data. That is, the mission controller itself must be adaptive. An early implementation of adaptive control on an AUV was described by Farrell and Clauberg (1993). Theoretical and algorithm development continued within the context of Concurrent Mapping and Localisation (CML) for example Smith et al. (1997), often with bathymetry as the survey variable. CML techniques allow the vehicle to build up a map of its position and of environmental variables, and to use the information subsequently to refine the mission track. For example, if, on its pre-programmed track, the vehicle identifies a valley in the seafloor, it modifies its track to optimize the recorded data, such as by altering its depth, reducing and or reorienting its track spacing. Clearly, the problems in developing search algorithms for a time-varying field such as chlorophyll fluorescence that may be advecting through the area are more complex than for bathymetry.

As a step towards this goal, *in situ* demonstrations of mapping chemical substances with AUVs have been made. These have ranged from simple pre-programmed mapping (Fletcher, 2001) to vehicle track alteration based on a simple threshold of concentration of a rhodamine dye observed with a fluorometer (Arrieta, 2003).

13.4 Key technologies

The key technologies for AUVs relevant to the study of HABs include, *inter alia*, energy storage, mission control, mission programming, navigation, communications and sensors. While pressure vessel technology is a key issue for deep-diving AUVs it is less of a problem for the depth range of interest to the study of HABs.

13.4.1 Energy storage

The low specific energy density of present-day energy storage technology is a serious limitation for all-electric AUVs, that is, for vehicles that operate fully submerged (Abu Sharkh et al., 2003). Taking lithium-ion rechargeable cells as an example of an advanced, yet readily available and reasonably safe battery chemistry, the energy density of about 540–650 kJ kg^{-1} is far less than that achievable from an internal combustion engine at about 3,000–6,000 kJ kg^{-1} for air-breathing Stirling and Diesel engines as used in semi-submersibles or ASVs. Lithium-ion cells that can be recharged over 500 times are a cost-effective option for underwater vehicles when the expected number of full-range missions exceeds 50–100, to amortize the high capital cost. If fewer missions are planned or expected over the life of the vehicle, then primary manganese alkaline cells can provide similar energy density at a lower cost. Conversely, if range is of paramount importance, and cost is a lesser consideration, primary lithium batteries are available with energy densities of over 1,000 kJ kg^{-1}. Using these cells would more than double the range of a vehicle that used primary manganese alkaline cells, but at about 10 times the cell cost. Because currently available gliders usually operate with

less on-board energy than propeller-driven AUVs, primary lithium batteries can be cost-effective for these vehicles. Contrary to the impression sometimes given, underwater gliders may be less efficient than propeller-driven vehicles in their conversion of electric energy to thrust (that is, newtons per watt); it is primarily their low speed and low power control and sensor systems that gives them their extended endurance.

Much attention is focused on fuel cell technology for energy storage for electric vehicles and for consumer products such as laptop computers. Breakthroughs in fuel cell technology will undoubtedly work their way through for use in AUVs, but there is one crucial difference. Fuel cells for automotive and consumer applications use oxygen from the surrounding air. Underwater, the oxygen for a fuel cell must be provided from an on-board store, for example via decomposition of a compound such as hydrogen peroxide or by carrying cryogenic liquid oxygen. This leads to additional challenges to ensure safe operation, even in the event of mishaps. A compromise is the semi-fuel cell, which can use dilute oxidants. Here, the safety problems are more manageable, but not entirely absent. Developers of aluminium-oxygen semi-fuel cells expect to reach energy densities of about 1,000 kJ kg^{-1} by 2007 (Adams, 2002).

An alternative approach to seeking higher energy density batteries is to refuel the vehicle during its missions. Docking stations have been developed that enable a vehicle to engage with a mooring, upload data that it has collected, download new mission instructions, and recharge its on-board batteries (Galletti di Cadilhac and Brighenti, 2003). Although docking technology is in its infancy, it is seen as important to AUV and hybrid AUV/ROV users in the offshore energy business and is therefore likely to develop quickly (Marty, 2004). If it were strategically important to routinely monitor an area for HABs, then deploying a docking station to extend AUV endurance would be an option worthy of consideration. Such a docking station could also provide scientific measurements. In some circumstances, its energy could come from the environment, e.g. through solar or wave power.

13.4.2 Mission control and mission programming

AUVs have seen their greatest commercial success in surveys of properties, e.g. bathymetry and stratigraphy, which do not change over the time of the survey. Such surveys can readily be achieved using pre-programmed regular grids that do not require complex mission control strategies. In essence, the mission controller executes a linear list of commands to traverse between pre-programmed waypoints; reaching a waypoint is an event, which triggers the vehicle to head towards the next waypoint. There is no need in such a controller for conditional branches (if-then-else logic) or for the vehicle itself to determine course or mission changes between waypoints, other than to avoid obstacles.

In contrast, AUVs tasked with surveying fields that change in time and in space will need more complex mission control strategies. This is not just an energy issue (as discussed in Section 13.3.3) but adaptive tasking may be necessary for the vehicle to maintain its sampling within the field of interest. For example, a pre-programmed survey grid may be of little value if the phytoplankton patch being studied advects through the predetermined survey area. In this case, a Lagrangian approach to survey design and mission control might be preferable. One approach to achieving this would be for the vehicle navigation system to use speed through the water, rather than speed over the ground, resulting in navigation relative to the (moving) water rather than the (fixed) ground.

The ability of a glider to follow a pre-programmed survey grid is limited when working in an area where the currents, from tides or from density gradients, approach

or exceed the forward speed of the vehicle. One approach to minimize this problem is to design the survey grid with *a priori* knowledge of the currents at the site. A second approach is to use the measurements from the glider, especially the difference between dead-reckoned and actual position at each surfacing, to modify the mission plan. If neither approach is capable of producing a survey grid that meets the requirements, there has to be a question over the suitability of a low-speed glider for the task.

13.4.3 Navigation

AUVs operating in coastal waters can pose a hazard to navigation by other users. This is especially true for unattended AUV missions, where no support vessel may be in attendance. An important factor in mitigating this hazard is accurate knowledge of the position of the AUV. All AUVs operate with dead-reckoning navigation between navigation fixes. These fixes update the dead reckoning, thereby avoiding the unchecked growth in position errors. Navigation fixes can be obtained from GPS satellites when the AUV is on the surface. With Selective Availability turned off, GPS accuracy of about 10 m for 95% of the time would suffice in most circumstances, but there may be occasions when higher accuracy would be needed. In this case, the vehicle would need to be fitted with a Differential GPS (DGPS) system.

If the vehicle is operating routinely in an area it may be practical to augment GPS position fixes with those from an underwater long-baseline acoustic navigation system (LBL). A particularly effective implementation of LBL for use in continental shelf waters is the GPS-buoy system that integrates surface buoys equipped with DGPS and acoustic transponders (Coudeville and Thomas, 1998).

Recent developments in fibre-optic gyrocompasses and in acoustic Doppler velocity logs have led to significant improvements in the accuracy of dead reckoning for AUVs. If the vehicle is within bottom track range of the seabed, which may be 200–400 m depending on the operating frequency of the Doppler log, then position error of less than 0.2% of the track covered is possible. That is, if navigation fixes from GPS or LBL were 20 km apart, the maximum position error would be 40 m.

13.4.4 Communications

AUVs vary in their ability to communicate real-time results to the user. At one extreme, it is standard practice with the Hugin 3000 vehicle for the support vessel to maintain continuous acoustic communication with the AUV throughout its mission (Jalving et al., 2003). The other extreme is complete lack of communication, as for the Autosub missions under sea ice (Brierley et al., 2002). Most AUV missions use a communications strategy between these two extremes. Limited-range acoustic communication is often used to ensure that a vehicle is working correctly after launch, and that the initial part of the mission is proceeding to plan. Acoustic communications can also be important prior to recovering the vehicle, especially if there is any uncertainty as to the vehicle's position, for example after a long period submerged. However, this type of operation, where the horizontal operating range from the AUV to the support vessel may be several km, usually restricts the bandwidth of the acoustic system to less than 10 kbits s^{-1}.

AUVs, when on the surface, can make effective use of satellite communication. The ARGOS system provides a very low data rate (with four, 256-bit messages every few hours possible, depending on latitude) but it also provides an important location capability that may be needed if the AUV mission does not go to plan. Higher data rates can be achieved using data communications satellite systems such as Orbcomm

and Iridium. Both of these systems offer two-way transmission, which can be used for updating the mission plans of the AUV. Demonstration missions have been completed using these satellites. For example, in April 1999 missions, the Autosub vehicle used Orbcomm to send email messages with status data to its home base. These messages were automatically translated into cellphone text messages and relayed to the engineers on shore waiting for the vehicle to complete its mission. Such text messaging is now also possible for ARGOS.

The Iridium system offers higher data rates (up to 2,400 baud, with a typical throughput of 180 bytes per second) at reasonable costs (€0.001 per byte). Experiments with Iridium transmitters on profiling floats were made in 2002, with encouraging results (Riser, 2002) and in 2004 the technology was in routine use within gliders by many groups. The communication bandwidth offered by Iridium makes it possible to send selected data in compressed form from the vehicle when on the surface to a shore laboratory for analysis and interpretation followed by possible amendments to the vehicle's mission using the reverse communication channel (Fiorelli et al., 2003).

13.4.5 Sensors

For both small and large AUVs the tasks that they can tackle in studying HABs are constrained by the sensor suite that the vehicles can carry. Clearly, large AUVs can carry all the instruments that a small AUV can carry, and so these are discussed first.

Miniature *in situ* sensors exist for the physical parameters temperature, conductivity and pressure, and short-range, high-frequency acoustic Doppler current profilers have been fitted to vehicles less than 2 m long. A range of small, low-power consumption optical sensors is now available for use in gliders and larger AUVs. For example, the Environmental Characterization Optics (ECO) Pucks™ from WetLabs[59] includes single-wavelength fluorometers appropriate for chlorophyll *a*, coloured dissolved organic matter, phycoerythrin or phycocyanin; and several combined sensors for measuring fluorescence and scattering at different wavelengths and scattering angles. These share a common size, 63 mm diameter and 50 mm long and consume an average power of less than 1 W. Several of these sensors and similar have been carried on gliders and other small vehicles (for example, Creed et al., 2002; Schofield et al., 2003; Schofield et al., 2007 – Chapter 3 this volume).

More complex instruments can be fitted to the larger AUVs, for example:

- *Nutrient sensors*: an UV-absorption spectrometer that can be used to estimate dissolved nitrate concentration has been tested on Autosub (Griffiths et al., 2000) and an instrument based on the same technique has been used on towed undulators (Johnson and Coletti, 2002) and is now available from Satlantic, Inc. The advantage of measuring nutrients using physical phenomena (such as optical absorption) is the fast response (less than 1 s) compared with wet-chemical techniques (tens of seconds to minutes). This is especially important when the vehicle is used to obtain vertical profiles. Taking a typical vertical profiling speed of 0.3 m s^{-1} for an AUV, a wet-chemical sensor with a 60 s response time would give a vertical resolution of 18 m, hardly adequate for studies of nutrient distributions in coastal waters.
- *Nutrient analyzers*: based on wet chemical techniques may be employed. These have been used successfully on moorings, vertical profilers and tow-yo devices (Hanson, 2000; SubChem Systems, Inc.).

[59]http:// www.wetlabs.com/products/eflcombo/pucks.htm

- *Pump and probe fluorometry*: a fast repetition rate fluorometer has been used successfully on towed undulating vehicles to provide information on the primary production parameters, e.g. the photosynthetic competence (Fv/Fm), Allen et al. (2002). This technology could be used on a large AUV, but no such example is known at the time of writing. Caution is needed over using sensors that may be sold as sensors of primary production. Users need to understand the assumptions behind the measurements and the limitations of existing instruments, (Babin, 2007; Morel, 2007 – Chapters 7 and 4 this volume).
- *Flow cytometry*: is a powerful technique that measures scattering and fluorescence from individual particles. It is widely used in laboratory-based phytoplankton research (Yentsch, 1990) as it can determine the composition of mixed phytoplankton populations rapidly. The sample fluid is coaxially surrounded by a clean sheath fluid and directed through an orthogonal tightly focused laser beam. As the particles pass through the laser beam singly they can be counted and sized. Information on light scattering and fluorescence can be used to separate phytoplankton cells from detritus. An *in situ* cytometer originally developed for moored applications (Dubelaar et al., 1999) has been fitted to an AUV, Figure 13.3. The instrument can operate to 250 m, recycling its sheath fluid and can measure particles with effective spherical diameters of 2–500 μm (Tarran et al., 2001). Another *in situ* flow cytometer, the FlowCytobot, has been developed and used offshore, in conjunction with, but not on, an AUV (Olson et al., 2003).

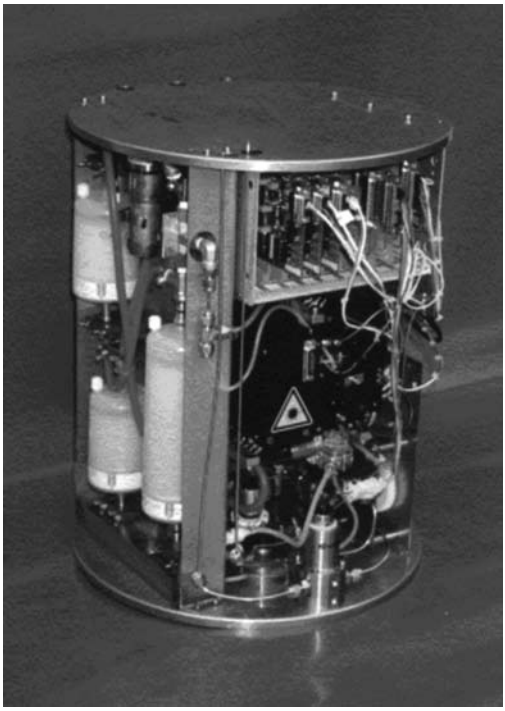

Figure 13.3
Cytosub flow cytometer as used in the Autosub AUV in May 2001.
Source: courtesy Plymouth Marine Laboratory.

- *Water samplers*: with the paucity of sensors for nutrients and other chemical substances, and the need to collect water samples to study the microbiology, an apparatus that can allow the vehicle to collect water samples is of value. Such devices are available commercially. One example can take up to 50 samples on command and store them in 250 ml sterile plastic bags. These bags may be distributed throughout a free-flooding vehicle. If the need is to take samples for later analysis of dissolved gasses, then gas-tight metalized bags are available.[60]
- *Mass spectrometer*: a quadrupole mass spectrometer has been developed specifically for use on AUVs (Fries et al., 2001; Short et al., 2001). Early versions had a depth limit of less than 100 m due to the membrane in the introduction probe. The instrument has a mass range of 2–200 amu and a detection limit of about 1 part per billion, making it suitable for biologically important gasses such as carbon dioxide, methane, methyl iodide and methyl bromide, but not for detecting larger molecules such as algal toxins (Scholin et al., 2007 – Chapter 11 this volume).
- *Zooplankton sensors*: A number of sensors are available that enable an AUV to make observations on zooplankton. The optical plankton counter (OPC) has become a common instrument within towed undulators for obtaining size and abundance information on particles from 100 μm to 20 mm (Herman, 1992; Jaffe, 2007 – Chapter 10 this volume). The OPC uses a single light sheet spanning a narrow rectangular opening to size and count particles passing through. Langebrake (2003) describes a dual light-sheet plankton counter, developed for use on an AUV, that uses orthogonal sheets of light that measure the length of a particle in two dimensions, which overcomes the assumption of symmetry in the OPC instrument.
- The *shadowed image particle profiling evaluation recorder* (SIPPER) instrument has also been developed for use on AUVs (Samson et al., 2000). It uses two high-speed line scan cameras and collimated laser generated light sheets to image particles passing through the device. Two-dimensional imaging is possible, and the data may be processed to provide a three-dimensional reconstruction of sampled particles. Figure 13.4 shows a collage of example shadowgraphs from SIPPER.
- A number of *acoustic instruments* exist that may be carried by AUVs to observe acoustic backscatter (Griffiths et al., 2002). While acoustics is undoubtedly a powerful qualitative tool for the study of zooplankton behaviour and abundance, there are major challenges to inferring biomass, let alone species composition and size, within mixed populations. Nevertheless, in areas where only a few species of zooplankton dominate the biomass, acoustic instruments on AUVs have proved effective in quantitative studies. For example, in a study of the distribution of *Euphausia superba* in relation to the ice edge in the Weddell Sea, the Autosub AUV carried upward-looking 38 kHz and 120 kHz scientific echo sounders to estimate abundance and species (Brierley et al., 2002). Experiments have also taken place with 38 kHz fisheries echo sounders on AUVs to demonstrate their capability as low-noise platforms for acoustic fish stock assessment surveys, where the stock was dominated by a single species, here herring, with well known acoustic properties (Fernandes and Brierley, 1999; Fernandes et al., 2001). Experiments such as those described by Jaffe (Chapter 10) have helped to establish the acoustic properties of target species, through combining accurate acoustic measurements with species recognition using optical imaging.

[60]For example, http://www.polymerpkg.com/Specialty.htm

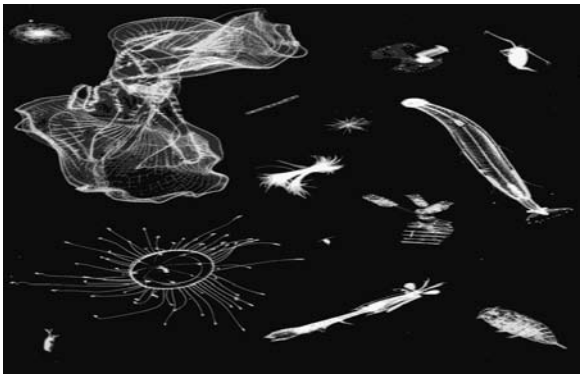

Figure 13.4
Mosaic of individual shadowgraphs of zooplankton obtained with the SIPPER imaging system that can be mounted on an AUV.
Source: courtesy of College of Marine Science, University of South Florida.

13.5 Applications of AUVs in coastal waters

The foundations have been laid for the use of AUVs in studies of harmful marine microalgae. Technology developments in sensors and vehicles over the last decade, as outlined in this section, have reached the point when it is practical to expect results of true scientific value from experiments based on data collection from AUVs. The cost effectiveness of using AUVs continues to improve as vehicles become available from several companies. This is especially true of vehicles designed for use in coastal waters.

The examples described in this section are meant to provide illustrations of the types of missions that have been carried out by AUVs that are deemed relevant in one way or another, to the study of HABs. The reader is asked to recognize that, at the time of writing, there have been very few publications in the scientific literature of the results of observations of HABs from autonomous underwater vehicles. The examples below have been chosen to demonstrate that:

- low cost (<€80,000) AUVs with bio-optical sensors can be deployed for extended periods and telemeter synopses of results to shore (Section 13.5.1);
- AUVs can provide bio-optical measurements with sufficiently high spatial sampling to resolve plankton patchiness on length scales of 1 km and above in coastal waters (Section 13.5.2);
- *in situ* flow cytometry is now a reality, allowing *in situ* quantitative measurements (cells per ml) and demarcation into species or groups (Section 13.5.3);
- experiments to test hypotheses on plankton population distributions can be devised, where the use of AUVs removes many of the constraints that would be present in shipboard or moored observations (Section 13.5.4);
- over small areas, repeated surveys by AUVs can be used to provide a number of virtual time-series stations, including for the study of turbulence (Section 13.5.5);
- adaptive sampling of the environment is close to being achieved, where the sampling tracks of the vehicle are determined by the variable(s) being studied (Section 13.5.6).

13.5.1 Underwater gliders in the Gulf of Mexico

Slocum gliders have been used extensively within multidisciplinary experiments at the LEO-15 site off New Jersey (Schofield et al., 2002). In these deployments, of up to 10 days, the gliders were fitted with combined dual-wavelength optical backscatter and single channel fluorescence sensors (HydroScat-2). More recently, similar gliders have been deployed to study algae off the west coast of Florida. These deployments made headlines in the general and scientific press.[61] The articles referred to a joint experiment lasting three days between the Mote Marine Laboratory, Sarasota, Florida, and the Coastal Ocean Observation Laboratory of Rutgers University, New Jersey. The gliders were deployed to demonstrate the feasibility of obtaining prior warning of offshore blooms of *Karenia brevis*, a toxin-producing dinoflagellate. *Karenia brevis* blooms are known to drift onshore, where they endanger shellfish farms and, within sea spray, the organism is an irritant to the human respiratory system. Such blooms therefore impact the local aquaculture economy, human health and tourism.

Figure 13.5A shows the particle load inferred from optical backscatter at 670 nm and Figure 13.5B chlorophyll fluorescence collected from a HydroScat-2 sensor on a Slocum glider during a red-tide event off Sarasota, Florida, in January 2003. High optical backscatter within 3 m of the seabed showed that abiotic particles were present in significant abundance, while the highest chlorophyll fluorescence extended to 6 m off the seabed (from Schofield et al., 2003).

Following the successful demonstration missions, gliders were deployed in summer and autumn 2003, when *Karenia brevis* blooms were possible. The vehicles were equipped with an optical phytoplankton detector (BreveBuster) developed by the Mote Marine Laboratory (Kirkpatrick et al., 2003). Vehicles were directed into areas where satellite imagery has shown elevated levels of chlorophyll. Missions of typically 30 days will be possible, with synopses of the data being transmitted ashore via satellite telemetry.

13.5.2 Phytoplankton patchiness

The autonomous vehicle Odyssey (Bellingham, 1997) has been used to study plankton patchiness and its relationship to physical processes in Massachusetts and Cape Cod Bays, on the east coast of the USA (Yu et al., 2002). Chlorophyll fluorescence and infrared optical backscatter were the bio-optical sensors and a CTD provided the physical data. A prototype 150 kHz phased array ADCP was also carried on the vehicle to measure current profiles and acoustic backscatter. The experiment was part of a larger programme–the Littoral Ocean Observing and Predicting System (LOOPS). The scientific focus of LOOPS was zooplankton patchiness, but observation and modelling of phytoplankton were necessary components of the holistic approach (Robinson et al., 1999). The scientific plan for LOOPS called attention to that fact that HABs have occurred in Massachusetts and Cape Cod bays (Robinson, 1998).

The AUV was operated mainly as a profiler, following a sawtooth pattern between the surface and a few metres off the seabed (typically at 20–60 m depth). The sawtooth pattern produced a horizontal resolution varying from typically 120 m at mid-depth to 240 m near the sea surface and seabed. The vertical resolution was of the order of 0.1 m.

[61]For example, *Florida Today*, 16 January 2003; *Nature Science Update*, 23 January 2003.

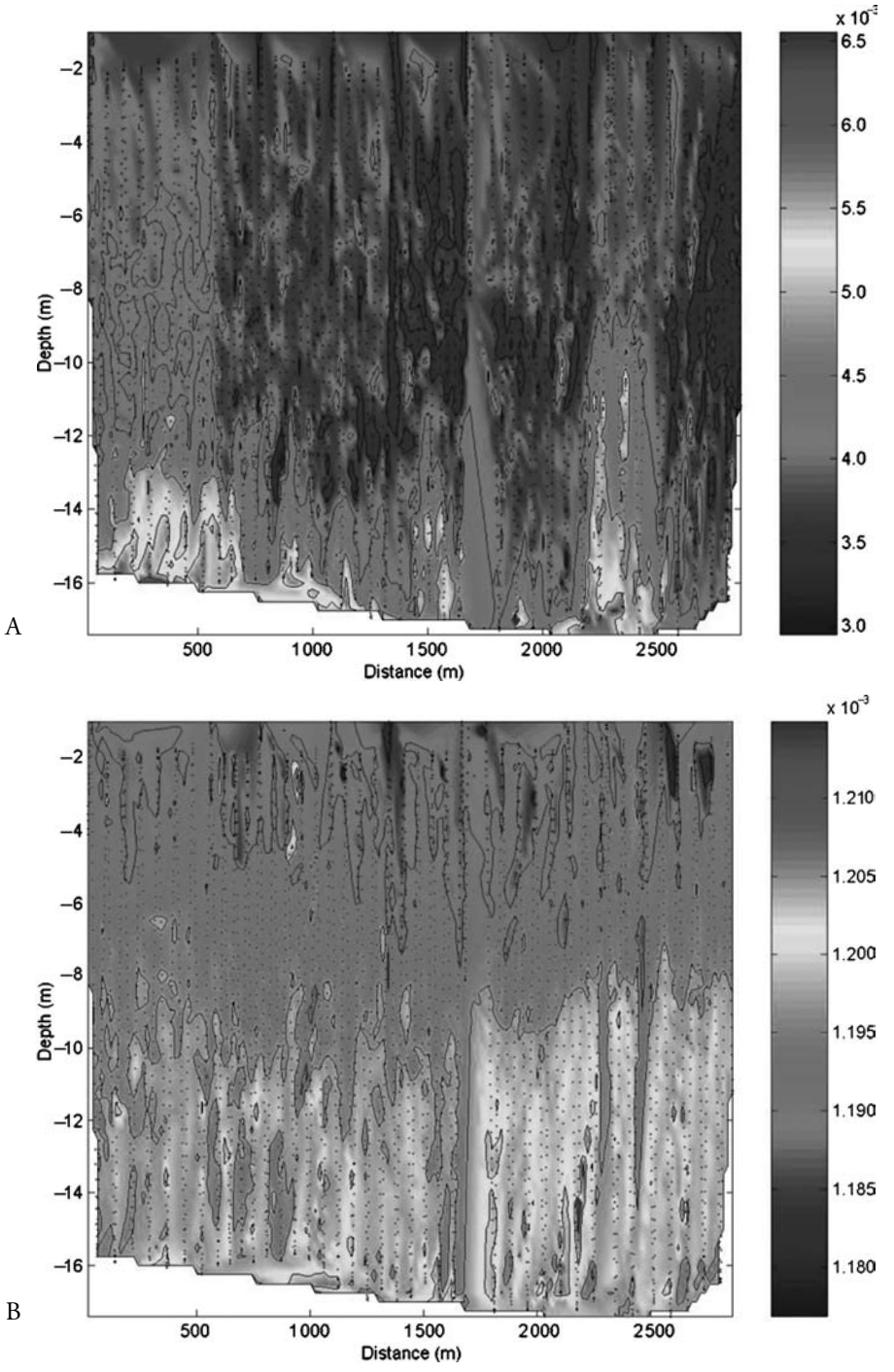

Figure 13.5
Vertical contour sections of A, optical backscatter at 670 nm; B, chlorophyll fluorescence (in relative units) from a Slocum glider on 16 January 2003 off Sarasota, Florida.
Source: courtesy of Rutgers University, Institute of Marine and Coastal Sciences.

The ability of the AUV to gather biophysical data is well illustrated in Figure 13.6. Over a 9 km section the physical regime described in Yu et al. (2002) changed from strongly stratified at the centre of Cape Cod Bay to upwelling near the coast at Race Point at the tip of Cape Cod, as indicated by the density shown in Figure 13.6C. Measurements from the fluorometer showed a pronounced subsurface fluorescence maximum at 17–22 m in the stratified region, the fluorescence over this depth range being over three times that in the upper 10 m, Figure 13.6E. Within two profiles (about 240 m) the vertical structure of the chlorophyll distribution changed, commensurate with the physical change from stratified to upwelling. In the upwelling region, the pronounced chlorophyll peak subsided, and the ratio of chlorophyll concentration at 20 m to the upper 10 m changed from 3:1 to about 1.2:1.

In addition to delineating this change in inferred chlorophyll distribution relating to physical conditions, the Odyssey AUV survey was able to obtain an estimate of the autocorrelation length scale of plankton patchiness. Vertically averaged fluorescence was calculated, the horizontal mean was removed, and the autocorrelation calculated as a function of distance. For the section described above, the autocorrelation function had its first zero crossing at 450 m, which, on the assumption of sine wave like periodicity, the authors interpreted to represent an apparent plankton patchiness scale of about 1.8 km (Yu et al., 2002). The scale was apparent rather than real because of the relatively low forward speed of the AUV (~1.5 m s^{-1}) leading to a degree of Doppler shifting of the true scale. From estimates of the advection speed of patches within the survey area, the estimated true patchiness length scale was 3.6 km.

13.5.3 *In situ* analytical flow cytometry from an AUV

Analytical flow cytometry provides a method of determining the composition of phytoplankton populations based on simultaneous measurement of fluorescence and light scatter on single particles at high speed (Burkill and Gallienne, 2001; Sosik, 2007 – Chapter 8 this volume). Some cytometers determine size through time-resolved optical measurements as well as through single measurements of light scattering (Burkill and Gallienne, 2001). The multi-parameter data from flow cytometry is well suited to analysis using decision-making algorithms such as neural networks (Frankel et al., 1989; Boddy et al., 2000) to provide automatic identification to species or functional group. Until the advent of an *in situ* flow cytometer in the late 1990s and an AUV with sufficient payload space to carry it, flow cytometry at best required gathering individual water samples for sample-by-sample analysis on a research vessel, or preserving the samples for later analysis on shore.

A fully self-contained flow cytometer, based on time-resolved cytometric analysis technology originally developed for environmental monitoring from a moored buoy (Dubelaar et al., 1999), has been deployed from the Autosub AUV. Its first deployment was in May 2001 off the Isles of Scilly, south-west coast of the UK (Tarran et al., 2001). The vehicle also carried an ac-9 scattering and absorption meter (described by Roesler and Boss, 2006 – Chapter 5 this volume) an Aquamonitor water sampler, dual CTDs (fitted with dissolved oxygen and fluorescence sensors) and an acoustic Doppler current profiler. The study used these instruments to examine 'the relationships between inherent optical properties, phytoplankton community structure and the abundance of suspended particles in the size range 3–500 μm' (Cunningham et al., 2003). At the time of the experiment there were two distinct areas of different biological activity in

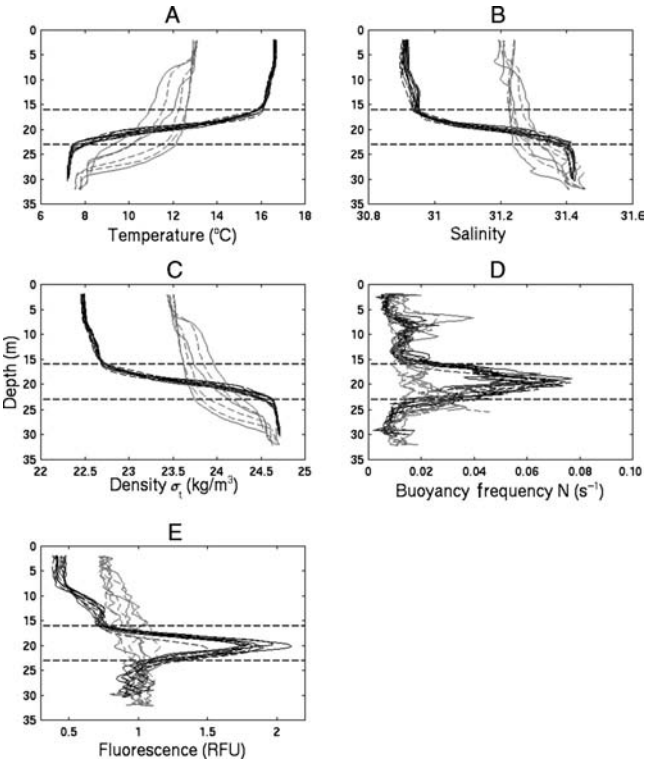

Figure 13.6
A, temperature; B, salinity; C, density; D, buoyancy frequency; E, chlorophyll fluorescence (in relative units) across a 9 km section in Cape Cod Bay taken by the Odyssey AUV in September 1998. The profiles in black were from the strongly stratified region near the centre of Cape Cod Bay, while the profiles in grey were from the region of upwelling near the coast at Race Point at the tip of Cape Cod. The transition between these two regions occurred within two profiles (about 240 m).
Source: Yu et al. (2002).

the area: a coccolithophore bloom in the western approaches to the English Channel and a mixed population of diatom chains and *Phaeocystis* colonies around the Scillies (Cunningham et al., 2003). An illustration of the colour of the sea within the coccolithophore bloom can be seen in Figure 13.7A, at the time of an Autosub launch.

As the AUV made *in situ* measurements, contemporaneous remote sensing of the sea surface was possible from a CASI radiometer (Wilson, 1997) on an aircraft from the UK Environment Agency. Furthermore, the lack of cloud enabled SeaWiFS satellite images of ocean colour to be obtained through collaborative work with the NERC Remote Sensing Unit at Plymouth Marine Laboratory, Figure 13.7B.

Figure 13.7C shows the layers of information at different scales that were obtained from the satellite imagery and the flow cytometer. The satellite image shows the Isles of Scilly in black, and regions of high chlorophyll in green. AUV transect

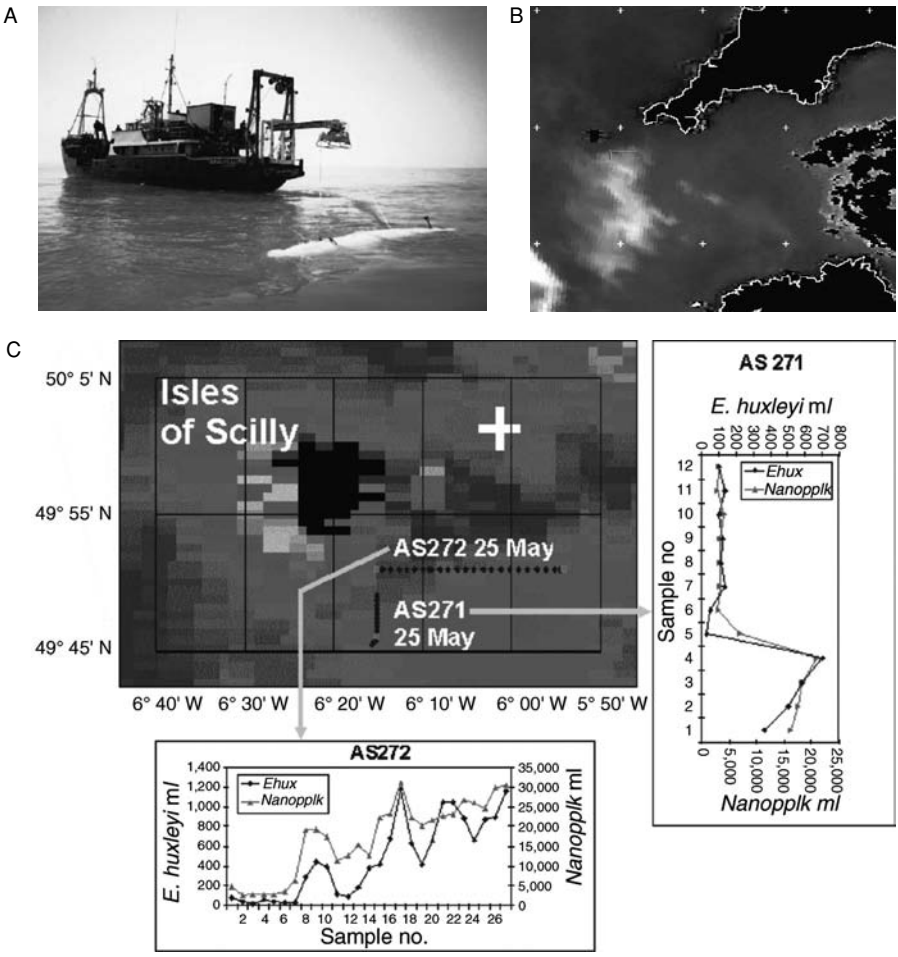

Figure 13.7
Autosub AUV after deployment from the RV *Terschelling*.
A, in a cocolithophore bloom off the Isles of Scilly in May 2001;
B, SeaWiFS satellite image of the area on the same day, with the cocolithophore bloom visible to the south of the islands, and the two Autosub tracks shown in blue;
C, small-area view of the SeaWiFS data colour-coded for chlorophyll (high in green, low in blue) with the tracks of the Autosub AUV on two transects. Counts of nanophytoplankton and *E. huxleyi* cells on each transect are also shown. SeaWiFS data received at NERC receiving station, Dundee, UK, and processed at the Plymouth Marine Laboratory. *Source*: SeaWiFS data courtesy of NASA SeaWiFS Project and Orbimage.

AS272 on 25 May 2001 from west to east took the AUV from a region of low chlorophyll as seen from the contemporaneous satellite image (blue) through a small 'peninsula' of higher chlorophyll, into a lower region, and then into a larger patch of high chlorophyll. From the flow cytometer on the AUV, counts of cells per ml were obtained for the coccolithophore *Emiliania huxleyi* and for nanophytoplankton

(Cunningham et al., 2003). There is a high degree of agreement between the remote sensed and *in situ* measurements. The 'peninsula' of higher chlorophyll seen in the satellite image corresponds to the peaks in *E. huxleyi* and nanophytoplankton in samples 8–10. The same degree of agreement was also present on the previous south-north leg AS271.

This experiment has demonstrated that the combination of AUV and advanced *in situ* biological instrumentation can yield quantitative results that complement and give rigour to remote sensed observations.

13.5.4 Zooplankton abundance and distribution

High-frequency acoustics can provide information on zooplankton abundance and distribution (Jaffe, Chapter 10). The technique is amenable to use on AUVs as present generation echo sounders are reasonably compact with average power consumption below 100 W. However, the sounders are not yet small enough or low enough power to be used on gliders.

Quantitative estimates of zooplankton biomass and limited discrimination to species has been achieved using high-frequency acoustics in certain environments, for example off South Georgia (Brierley et al., 1999). Extending the technique to environments with more diverse zooplankton populations is the goal of a number of groups (e.g. Holliday and Pieper, 1995; Martin et al., 1996; Wiebe et al., 1996). Interaction with zooplanktonic grazers is a factor in the net growth performance of HABs (Fiedler, 1982; Zingone and Enevoldsen, 2000). Hence, broad area surveys of zooplankton abundance, patchiness and behaviour may contribute to integrated biophysical studies. AUVs make excellent platforms for carrying high-frequency echosounders because of their low self-noise and the fact that they operate well away from the acoustically noisy sea surface (Griffiths et al., 2001).

Brierley et al. (2002) described the results from using high-frequency echosounders on the Autosub AUV in the Weddell Sea in early 2001. Their experiment was designed to test the null hypothesis that the presence of sea-ice cover had no affect on the biomass density of Antarctic krill (*Euphausia superba*) in underlying waters. As well as demonstrating the use of an AUV for acoustic observations of zooplankton, this exemplar demonstrates how an AUV can be used, in conjunction with a ship, to test a well-posed null hypothesis.

The experiment design required the AUV and the ship carry exactly the same instrumentation (38 kHz and 120 kHz scientific echo sounders). The AUV tracks ran south at 150 m depth from open water, under the marginal ice zone and under the more consolidated pack ice. Meanwhile the ship ran reciprocal transects to the north, in open water. Thus the quiet AUV, with its echosounders looking up, made measurements without disturbing the environment. That would not have been the case had the ice strengthened ship carried out the sea-ice transect. In all, six transects in and out of the pack ice were made spanning 5° of longitude.

Using established techniques for identifying which echoes came from *Euphausia superba* based on the difference between mean volume backscatter strength (MVBS) at 38 kHz and 120 kHz, and accepted relationships between MVBS and *Euphausia superba* biomass (Brierley et al., 1999), vertically integrated biomass density (g m^{-2}) was obtained as a function of position from the ice edge, Figure 13.8. The results were clear; krill were concentrated between 1 km and 13 km south of the ice edge. Krill densities were five times greater within this band than in open water to the north of the ice edge.

13.5.5 Mapping variations in turbulence over linear sandbanks in the coastal zone

There remains uncertainty about what role turbulence may play in connection with HABs (Kiørboe, 1993; Sullivan and Swift, 2003). Zingone (2003) points out the apparent contradiction that '(while) turbulence is considered to prevent dinoflagellate blooms ... a number of harmful dinoflagellates proliferate in frontal or upwelling zones'. In coastal waters, knowledge of circulation patterns and turbulence generation related to seabed morphology may therefore be important to understanding HAB phenomena. In areas such as the southern North Sea, linear sand ridges are prominent topographic features on the seabed. For example, Broken Bank, 100 km off the UK east coast, is 41 km long by 5 km wide, with an asymmetric cross-section. Its north-eastern slope is steep, while its south-western slope is gentle. Gradients in bottom shear stress result in sediment transport that maintains the bank and leads to local mean circulation cells superimposed on the tidal currents around the banks.

Using tens of sets of seabed moored instruments to study the spatial variations in circulation and turbulence along and across these banks would be expensive. In an experiment using the Autosub AUV in August 1999 Voulgaris et al. (2001) demonstrated the ability of an autonomous vehicle to mimic a set of virtual seabed moorings across Broken Bank.

Equipped with acoustic Doppler current profilers and acoustic velocimeters for both mean current and turbulence measurements, the AUV mission lasted 70 hours. Each (semidiurnal) tidal cycle the vehicle made 11 transects across the Bank, following the topography at a height of 4 m in water depths of 15 m to 37 m. The data reduction process provided information on the tidal and residual current within 15 segments across the Bank, each segment being sampled 11 times within the tidal cycle. The segment spacing was conditional on the slope – segments near the crest were closely spaced, at 40 m, while those on the swales of the Bank spanned 250 m.

Figure 13.9 shows the results for the M2 tidal component and for the residual circulation. Both show the effect of the crest of the Bank. The direction of the tidal flow veers clockwise approaching the crest from the swales of the Bank, followed by a sudden change anticlockwise as the crest is passed. In the along-ridge direction a clockwise residual flow existed, while across the ridge, the residual flow diverged. The latter is consistent with theories of flow divergence because of density gradients due to more sediment being in suspension near the crest of sandbanks (Sannay et al., 2004).

13.5.6 Towards adaptive AUV missions in coastal waters

Within the SUMARE project of the European Union's Fifth Framework programme, the AUV Mauve has been used for bathymetric survey of sand exploitation in Belgian coastal water. Although the focus has not been on surveys of plankton and plankton patchiness, elements of the research programme are relevant to the study of HABs using autonomous vehicles.

Mauve is a small, low-cost and reconfigurable AUV developed specifically to work in coastal seas. As such, it is a small, torpedo-like vehicle, 1.80 m long with a weight of approximately 30 kg in air. Mauve has a reconfigurable scientific payload, including temperature, conductivity, turbidity and fluorescence sensors, with another payload including an altimeter and an obstacle avoidance sensor. Navigation of the vehicle relies on dead reckoning and long base line systems using two acoustic beacons.

A

B

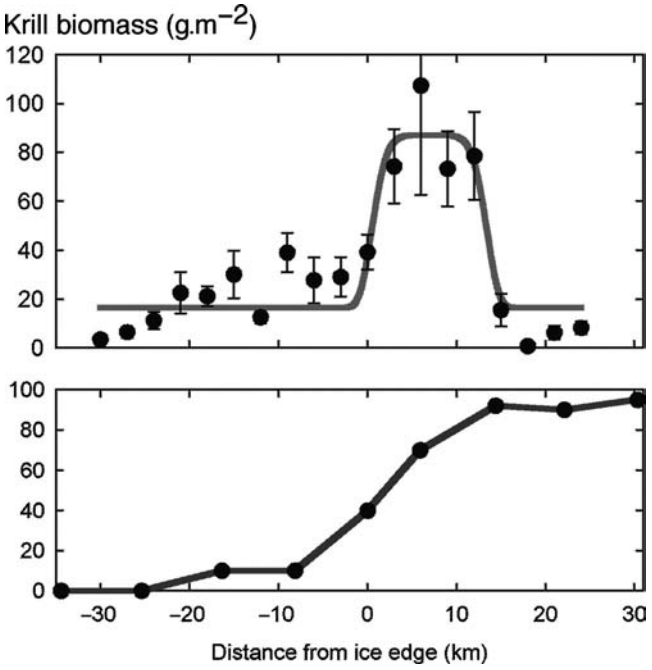

Figure 13.8
Quantitative information on zooplankton distribution and abundance has been obtained from AUVs.
A, the Autosub AUV was deployed north of the marginal ice zone in the Weddell Sea and made repeated transects under the pack ice to the south. B, using a dual frequency echosounder, estimates of krill biomass were made in relation to the position of the ice edge, where the line indicates ice concentration. Significantly higher krill biomass was observed within a band 1–13 km south of the ice edge, where the ice edge is taken to be the position of 50% ice concentration. The line is a modified normal regression function fitted to the biomass data, while the error bars indicate ±1 standard error of the mean.
Source: Brierley et al. (2002).

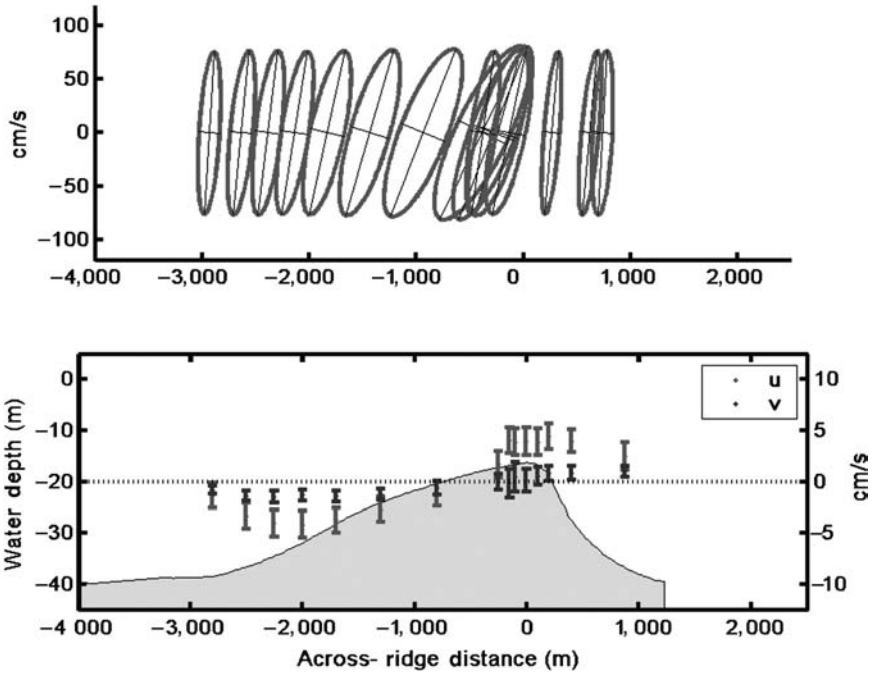

Figure 13.9
Example of how an AUV can be used to simulate a series of moored stations. Upper panel shows the M2 tidal current ellipses in grey at 15 virtual stations across a sandbank in the North Sea, with the spacing of the stations reduced near the crest of the bank. The major and minor axes are shown in black. The major axis shows the direction of the flood and ebb currents, and how this direction changes, veering clockwise over the ridge. The lower panel shows the residual current distribution across the bank, that is, with the tidal components removed. Points in light grey are the along-bank component of current, dark grey the across bank. The error bars are ±1 standard error of the mean. The variation of the two current components is consistent with a clockwise circulation of the mean flow. *Source*: courtesy of University of South Carolina.

The vehicle can cruise at 2 m s^{-1} for almost 4 hours. The most innovative aspect of the SUMARE project is the use of the adaptive sampling concept and its implementation in the Mauve AUV through specific guidance algorithms. The AUV can decide for itself, using the newly acquired data, where is the more appropriate place, and what is the best way to sample in order to achieve the objective of the mission. Progress to date has included development of novel environment descriptions for situations where identification of features is difficult, using the technique of random closed set statistics. While this has been applied to the study of maerl deposits on the seabed off Scotland (Rolfes and Rendas, 2001), the work may be transposable to navigation relative to biological distributions.

13.6 Removing the barriers to widespread use

13.6.1 Scientific barrier

One barrier to the adoption of new technology can be the conservatism of users. This is often understandable. Experiments at sea are expensive and time-consuming; the desire to be sure that data are collected may conflict with the wish to try out new technology or methods. Users may have memories of developers and supporters of a new technology overstressing its advantages. This can lead to severe difficulties. Longhurst (2000) eloquently sets out many of the issues to do with new sensors for marine life. His key points are worth summarizing here. First, his general caution: 'Several authors urge the deployment of new technologies ... and in all there is in my opinion a lack of realism about what they measure'. Second, a caveat on remote sensing: 'All remote sensing techniques require validation', with a stronger caveat when that sensing involves living organisms 'particular caution on any claim to detect and identify marine species without capturing the organism'. Third, a plea for researchers to consult the literature (much of which may not be available on-line), they should realize the 'importance of what is in the literature using data gathered using established techniques such as nets'.

Many of his arguments could be adapted to refer to AUV rather than sensor technology, for example, ensuring realism in mission planning and expectation, ensuring appropriate experiment design and appropriate sensors. Nevertheless, there is a growing presence in the peer-reviewed literature of results from AUV missions, many of which could not have been obtained using other technology. Furthermore, reviewers of proposals requesting funding for experiments and data gathering using AUVs now have access to the results of previous campaigns, to the methods that have achieved results, and to a knowledge base of which sensors will work on these vehicles on which to base their assessments. This recent diffusion of knowledge about what has been, and what can be, achieved with the new technology will help remove the barrier and reduce the difference in perception between the new user and the technology proponent.

13.6.2 Technical barriers and need for technical support

There are no real technical barriers, as such, to using autonomous vehicles to gather information relevant to the study of HABs. Rather, further developments are likely to target weaknesses in currently available AUVs. One important area of weakness is reliability, particularly when required to undertaken frequent missions or when making major alterations to the payload. Only if reliability can be improved will it become cost-effective to use expensive high-energy density secondary cells, such as lithium polymer, to improve the range and power available for sensors.

Knowledgeable technical staff will be needed to deploy, support, maintain and develop AUVs and gliders used in marine science. The scale of effort depends on the complexity of the vehicle. While one person may well be able to provide the technical support for a fleet of several purchased gliders, a large purpose-built AUV such as Autosub needs a team of six and a minimum of four staff at sea to support 24-hour operation.

Studying HABs will not tax several areas of technical difficulty for AUVs, such as lightweight pressure vessel design; buoyancy compensation; precise (5 m) navigational accuracy or real-time acoustic communication. The major challenges are not to do with the vehicle and its systems for autonomous operation, rather the challenges

lie with developing capable and appropriate sensors. These new sensors may include molecular probes (Scholin et al., 2007 – Chapter 11 this volume), with electrochemical detection; miniature fast-response nutrient sensors; video image capture and automated analysis; miniature fast repetition rate fluorometers and more capable underwater mass spectrometers.

13.6.3 Economic barriers

An important barrier to take-up of AUV technology that must be removed is the high cost of today's most capable vehicles. These tend to be large, if only because many of the sensors that are available for biochemical measurements are themselves large at this stage of development. The full construction cost of an AUV such as Autosub is of the order of £1 million, without science sensors. Large AUVs tend to require support teams of four to six people, they require launch and recovery systems that may cost £150,000, freight may involve three 20 ft (6 m) containers, energy cost on primary batteries is high at about £20 per kilometre. Smaller vehicles will have lower costs, they are generally simpler, carry fewer instruments, are easier to handle and use less energy.

With new manufacturers entering the AUV marketplace, competition is very likely to increase cost-effectiveness over the next five years. It is also probable that manufacturers will themselves, or through specialist service providers, provide either a complete service to users or lease out vehicles. In the case of a full service, users will not themselves need to invest capital in purchasing complete AUV systems, neither will they need to build up the technical knowledge to operate and maintain the vehicles. Service providers will then carry the risk of delivering the data to users.

The technical developments discussed previously will lead to the availability of medium-sized (2–4 m long, 0.2–0.4 m in diameter) vehicles with effective biochemical sensors. As an example of a future AUV and sensor package, the University of South Florida (USF) has invested in a 0.32 m diameter Bluefin AUV. It will be used extensively in the Gulf of Mexico. The vehicle will be fitted with a MIPPER (miniature SIPPER) zooplankton imager currently under development at USF. MIPPER will have a much higher resolution but a smaller sample tube, 3 cm by 3 cm against 10 cm by 10 cm for SIPPER. This instrument is designed to be much less expensive (it only has one light sheet) and small enough to fit inside the new generation of vehicles.

13.6.4 Logistical barriers

While autonomous vehicles, by their very nature, can be independent of deployment platforms, until very recently, most AUV deployments have been from ships. While necessary during the development of large vehicles, or those intended for open ocean operations, ship logistics add considerable cost to AUV operations.

Notwithstanding the legal issues surrounding the use of AUVs, operating these vehicles in the coastal zone can be made less costly if missions could be shore-based. In this case, the logistics are far simpler. Prudence suggests that a guard vessel may be required during the initial launch and transit phase, and during return transit and recovery. However, this vessel may be small, it need not have the capacity to carry the AUV or have specialist equipment installed.

The feasibility of shore launch, suggested procedures and a comparative risk analysis have been discussed in Griffiths et al. (1998). The example given was an AUV mission that left a quiet Scottish harbour under the escort of a small inflatable boat. The new generation of small AUVs such as the REMUS (Purcell, 2000), Mauve and Gavia

lend themselves well to shore-based operations. It is feasible to transport these vehicles to the site of interest by automobile and to launch them either from an inflatable boat or manually from the shore by just one or two people (Figure 13.1).

It is important to obtain insurance cover for AUV operations. While cover against loss is advisable, it is essential to obtain cover against possible damage to the property of third parties. Despite being a relatively young technology in the hands of users, insurance cover for operating AUVs is readily available and has proved cost-effective for many operators (Edwards, 2000).

13.6.5 Legal issues

AUVs are not explicitly referred to at present in either English or international maritime law (Brown, 2003). It is therefore a matter of opinion as to whether AUVs are or are not subject to existing national and international laws governing, for example, safe navigation at sea. While the lack of specific mention of AUVs can lead to doubt, there are certain obligations when deploying equipment into the sea for marine scientific research. Brown (2003) points out that Article 261 (of the UN Convention on the Law of the Sea) requires that,'The deployment and use of any type of scientific research installations or equipment shall not constitute an obstacle to established international shipping routes'. A pre-programmed AUV with limited collision avoidance systems, operating unattended near shipping lanes (e.g. English Channel, North Sea, entrances to major ports, etc.) would need to have its missions carefully planned to avoid interference with shipping. For an AUV undertaking adaptive missions, perhaps in a Lagrangian frame of reference, tracking blooms in coastal waters, the legal difficulties could be even greater.

In an exhaustive study of the use of AUVs, Brown and Gaskell (2000) have detailed the issues and provided a framework for users to consider their obligations. An AUV in coastal waters on missions that involve significant time at or near the surface may raise issues of salvage. This may occur because the vehicle has truly been lost and then found by a salvor, or there may be a case of false salvage. That is, the AUV was not out of control, causing a danger or in danger itself, but merely seeming to be passive, for example when drifting on the surface awaiting a satellite navigation fix. Brown and Gaskell (2001) have provided concise answers to such questions and how to avoid confusion in the first place.

References

Abbott, M. R., Brink, K. H., Booth, C. R, Blasco, D., Swenson, M. S., Davis, C. O. and Codispoti, L. A. 1995. Scales of variability of bio-optical properties as observed from near-surface drifters. *J. Geophys. Res.*, 100(7), pp. 13345–67.

Abu Sharkh, S. M., Griffiths, G. and Webb, A. T. 2003. Power sources for unmanned underwater vehicles. In: G. Griffiths (ed.), *Technology and Applications of Autonomous Underwater Vehicles*. London, Taylor and Francis, pp. 19–35.

Adams, M. 2002. Aluminium energy semi-fuel cell systems for underwater applications: the state of the art and the way ahead. *Proc. IEEE Workshop on AUV Power Sources*, San Antonio, Texas, June 2002, pp. 85–88.

Allen, J. T., Cornell, V., Moore, C. M., Crisp, N. and Dunning, J. 2002. Operational oceanography with the new SeaSoar undulator. *Sea Tech.*, 43(4), pp. 35–40.

Arrieta, R. 2003. Plume tracking with the Remus vehicle. *Proc. Workshop on 'ADCPs in Action'*, San Diego, March 2003. Abstract at http://www.rdinstruments.com/adcps_action/adcp03review.html (Accessed December 2004.)

Babin, M., Roesler, C. S. and Cullen, J. J. (eds). 2006.*Real-time Coastal Observing Systems for Marine Ecosystem Dynamics and Harmful Algal Blooms: Theory, Instrumentation and Modelling*. Paris, Intergovernmental Oceanographic Commission of UNESCO. (Monographs on Oceanographic Methodology.)

Bachmayer, R. and Leonard, N. E. 2002. Vehicle networks for gradient decent in a sampled environment.*Proc. IEEE Conference on Decision and Control,* pp. 112–17.

Boddy, L., Morris, C. W., Wilkins, C.W., Al-Haddad, L., Tarran G., Jonker, R. R. and Burkill, P. H. 2000. Identification of 72 phytoplankton species by radial basis function neural network analysis of flow cytometric data. *Mar. Ecol. Progr*., 195, pp. 47–59.

Brierley, A. S., Fernandes, P. G., Brandon, M. A., Armstrong, F., Millard, N. W., McPhail, S. D., Stevenson, P., Pebody, M., Perrett, J. R., Squires, M., Bone, D. G. and Griffiths, G. 2002. Antarctic krill under sea ice: elevated abundance in a narrow band just south of ice edge. *Science*, 295, pp. 1890–92.

Brierley, A. S., Watkins, J. L., Goss, C., Wilkinson, M. T. and Everson, I. 1999. Acoustic estimates of krill density at South Georgia, 1981 to 1998. *CCAMLR Science*, 6, pp. 47–57.

Brown, E. D. and Gaskell, N. J. J. 2000. Report on the law, state practice and procedure relating to autonomous underwater vehicles. London, Society for Underwater Technology, 200 pp., apps.

Brown, E. D. and Gaskell, N. J. J. 2001. Questions and answers on the law, state practice and procedure relating to autonomous underwater vehicles. London, Society for Underwater Technology, 82 pp.

Burkill, P. H. and Gallienne, C. P. 2001. Optical particle characterisation by flow cytometry, plankton counters and other techniques. In: J. Steele, S. Thorpe and K. Turekian (eds), *Encyclopedia of Ocean Sciences*. New York, Academic Press, pp. 2040–2048.

Chang, G., Dickey, T., Jiang, S., Manov, D. and Spada, F. 2003. In: M. Kawasaki, N. Asgrriz and R. Anthony (eds), *Optical Methods for Interdisciplinary Research in the Coastal Ocean, Recent Research Developments in Optics*. Homewood, Ill., Research Signpost Publishing, Chap. 15, pp. 249–70.

Coudeville, J. M. and Thomas, H. 1998. A primer: using GPS underwater. *Sea Tech*., 39, pp. 31–34.

Creed, E. L., Mudgal, C., Glenn, S. M., Schofield, O. M., Jones. C. P. and Webb, D. C. 2002. Using a fleet of Slocum battery gliders in a regional scale coastal ocean observatory. *Proc. IEEE Conference Oceans 2002*, 1, pp. 320–24.

Cunningham, A., McKee, D., Craig, S., Tarran, G. and Widdicombe, C. 2003. Fine-scale variability in phytoplankton community structure and inherent optical properties measured from an autonomous underwater vehicle. *J. Mar. Sys*., 43, 1–2, pp. 51–59.

Davis, R. E., Eriksen, C. C. and Jones, C. P. 2003. Autonomous buoyancy-driven underwater gliders. In: G. Griffiths (ed.), *Technology and Applications of Autonomous Underwater Vehicles*. London, Taylor and Francis, pp. 37–58.

Dickey, T. D. 2002. A vision of oceanographic instrumentation and technologies in the early twenty-first century. In: J. G. Field, G. Hempel and C. P. Summerhayes (eds), *Oceans 2020 – Science, Trends and the Challenge of Sustainability*. Washington DC, Island Press, pp. 209–54.

Doherty, K. W., Frye, D. E., Liberatore, S. P. and Toole, J. M. 1999. A moored profiling instrument. *J. Atmos. Ocean. Tech*., 16, pp. 1816–29.

Dubelaar, G. B., Gerritzen, P. L., Beeker, A. E. R., Jonker, R. R. and Tangen, K. 1999. Design and first results of the CYTOBUOY: an autonomous flow cytometer with wireless data transfer for *in situ* analysis of marine and fresh waters. *Cytometry*, 37, pp. 247–54.

Edwards, S. R. P. 2000. AUVs. How do you insure them? *Int. Ocean Syst. Des*., 4, pp. 10–12.

Farrell, J. and Clauberg, B. 1993. Issues in the implementation of an indirect adaptive control system. *IEEE J. Ocean. Eng*., 18, pp. 311–18.

Ferguson, J. S. 2003. Semi-submersible AUVs. In: G. Griffiths (ed.), *Technology and Applications of Autonomous Underwater Vehicles*. London, Taylor and Francis, pp. 227–43.

Fernandes, P. G. and Brierley, A. S. 1999. Using an autonomous underwater vehicle as a platform for mesoscale acoustic sampling in the marine environment. *ICES CM 1999/M:01*, 16 pp.

Fernandes, P. G., Brierley, A. S., Simmonds, E. J., Millard, N. W., McPhail, S. D., Armstrong, F., Stevenson, P. and Squires, M. 2000. Fish do not avoid survey vessels. *Nature*, 404, pp. 35–36.

Fiedler, P. C. 1982. Zooplankton avoidance and reduced grazing responses to *Gymnodinium splendens* (Dinophyceae). *Limnol. Oceanogr.*, 27(5), pp. 961–65.

Fiorelli, E., Bhatta, P., Leonard, N. E. and Shulman, I. 2003. Adaptive sampling using feedback control of an autonomous underwater glider fleet. *Proc. 13th Unmanned Untethered Submersible Technology Symposium*, New Hampshire, August 2003, unpaginated.

Fletcher, B. 2001. Chemical plume mapping with an autonomous underwater vehicle. *Proc. Oceans 2001*, Hawaii. MTS/IEEE.

Frankel, D. S., Olson, R. J., Frankel, S. L. and Chisholm, S. W. 1989. Use of a neural net computer system for analysis of flow cytometric data of phytoplankton populations. *Cytometry*, 10(5), pp. 540–50.

Fries, D. P., Short, T., Langebrake, L. C., Patten, J. T., Kerr, M. L., Kibelka, G., Burwell, D. C. and Jalbert, J. C. 2001. In-water field analytical technology: underwater mass spectrometry, mobile robots, and remote intelligence for wide and local area chemical profiling. *Field Analyt. Chem. Tech.*, 5, pp. 121–30.

Galletti di Cadilhac, R. and Brighenti, A. 2003. Docking systems. In: G. Griffiths (ed.), *Technology and Applications of Autonomous Underwater Vehicles*. London, Taylor and Francis, pp. 93–108.

Greenan, B. J. W., Petrie, B. D., Harrison, W. G. and Oakey, N. S. 2004. Are the spring and fall blooms on the Scotian Shelf related to short-term physical events? *Cont. Shelf Res.*, 24, pp. 603–25.

Griffiths, G., Davis, R. E., Eriksen, C. C., Frye, D. E., Marchand, P., Dickey, T. and Weller, R. 2001. Towards new platform technology for sustained observations. In: C. J. Koblinsky and N. R. Smith (eds), *Observing the Oceans in the 21st Century*. Melbourne, Bureau of Meteorology, GODAE Project Office, pp. 324–37.

Griffiths, G., Enoch, P. and Millard, N. W. 2001. On the radiated noise of the Autosub autonomous underwater vehicle. *ICES J. Mar. Sci.*, 58, pp. 1195–200.

Griffiths, G., Fielding, S. and Roe, H. S. J. 2002. Biological-physical-acoustical interactions. In: A. R. Robinson, J. J. McCarthy and B. J. Rothschild (eds), *The Sea.* Vol. 12: *Biological-Physical Interactions in the Ocean*. New York, John Wiley & Sons, pp. 441–74.

Griffiths, G., Knap, A. and Dickey, T. 2000. The autonomous vehicle validation experiment. *Sea Tech.*, 41, pp. 35–43.

Griffiths, G., McPhail, S. D., Rogers, R. and Meldrum, D. T. 1998. Leaving and returning to harbour with an autonomous underwater vehicle. *Proc. Oceanology International '98*, Brighton. New Malden, UK, Spearhead Exhibitions, 3, pp. 75–87.

Hanson, A. K. 2000. A new *in situ* chemical analyzer for mapping coastal nutrient distributions in real time. *Proc. IEEE Conference Oceans 2000*, 3, pp. 1975–82.

Hanson, A. K. and Donaghay, P. L. 1998. Micro- to fine-scale chemical gradients and layers in stratified coastal waters. *Oceanography*, 11(1), pp. 10–17.

Herman, A. 1992. Design and calibration of a new optical plankton counter capable of sizing small zooplankton. *Deep Sea Res.*, 39, pp. 395–415.

Holliday, D. V. and Pieper, R. E. 1995. Bioacoustical oceanography at high frequencies. *ICES J. Mar. Sci.*, 53, pp. 279–96.

IOC. 1998. The GOOS Prospectus 1998. Paris, Intergovernmental Oceanographic Commission of UNESCO.

Jahnke, R., Atkinson, L. Barth, J., Chavez F., Daly, K., Edson, J., Franks, P., O'Donnell, J. and Schofield, O. 2002. Coastal ocean processes and observatories: advancing coastal research. *Report of the CoOP Observatory Science Workshop*, 7–9 May 2002, Savannah, Georgia, USA. (Skidaway Institute of Oceanography Technical Report TR-02-01.)

Jalving, B., Vestgård, K. and Storkersen, N. 2003. Detailed seabed surveys with AUVs. In: G. Griffiths (ed.), *Technology and Applications of Autonomous Underwater Vehicles*. London, Taylor and Francis, pp. 179–201.

Johnson, K. S. and Coletti, L. J. 2002. *in situ* ultraviolet spectrophotometry for high resolution and long-term monitoring of nitrate, bromide and bisulfide in the ocean. *Deep Sea Res*., 49, pp. 1291–1305.

Kiørboe, T. 1993. Turbulence, phytoplankton cell size, and the structure of pelagic food webs. *Adv. Mar. Biol*., 29, pp. 1–72.

Kirkpatrick, G. J., Orrico, C., Moline, M. A., Oliver, M. J. and Schofield, O. 2003. Continuous hyperspectral absorption measurements of colored dissolved organic material in aquatic systems. *Appl. Opt*., 42(33), pp. 6564–68.

Langebrake, L. 2003. AUV sensors for marine research. In: G. Griffiths (ed.), *Technology and Applications of Autonomous Underwater Vehicles*. London, Taylor and Francis, pp. 245–77.

Longhurst, A. R. 2000. Letter to the Editor. *Oceanography*, 13(2), pp. 3–4.

Martin, L. V., Stanton, T. K., Wiebe, P. H. and Lynch, J. F. 1996. Acoustic classification of zooplankton. *ICES J. Mar. Sci*., 53, pp. 217–24.

Marty, P. 2004. SWIMMER, ALIVE … the dawn of intervention AUVs. *Proceedings UUVS 2004*, Spearhead Exhibitions Ltd., Richmond, Surrey, unpaginated.

Olson, R. J., Shalapyonok, A. and Sosik, H. M. 2003. An automated submersible flow cytometer for analysing pico- and nanophytoplankton: FlowCytobot. *Deep Sea Res.*, 50, pp. 301–15.

Purcell, M. von Alt, Allen, C., Austin, B., Forrester, T., Goldsborough, N. and Stokey, R. 2000. New capabilities of the REMUS autonomous underwater vehicle. *Proc. IEEE Conference Oceans 2000*, 1, pp. 147–51.

Riser, S. 2002. Iridium communications and ARGO floats. Section 4.1. http://www-argo.ucsd.edu/iast4.pdf (Accessed December 2004.)

Robinson, A. R. 1998. Scientific plan for the LOOPS Massachusetts Bay sea trial MBST-98. http://people.deas.harvard.edu/~robinson/, Recent Work link, then MBST-98 (Accessed December 2004.)

Robinson, A. R., Bellingham, J. G., Chryssostomidis, C., Dickey, T. D., Levine, E., Petrikalakis, N., Porter, D. L., Rothschild, B. J., Schmidt, H., Sherman, K., Holliday, D. V. and Atwood, D. K. 1999. Real-time forecasting of the multi-disciplinary coastal ocean with the Littoral Ocean Observing and Predicting System (LOOPS). *Proc. Third Conference on Coastal Atmospheric and Oceanic Prediction Processes*, New Orleans, La., American Meteorological Society.

Roelke, D. and Buyukates, Y. 2001. The diversity of harmful algal bloom-triggering mechanisms and the complexity of bloom initiation. *Hum. Ecol. Risk Assess*., 7 pp. 1347–62.

Rolfes, S. and Rendas, M. J. 2001. Statistical environment representation for navigation in natural environments. *Proc. 9th International Symposium on Intelligent Robotic Systems*, Toulouse, France, 18–20 July 2001.

Samson, S., Langebrake, L. C., Lembke, C., Patten, J. and Russell, D. 2000. Design and current results of a high-resolution Shadowed Image Particle Profiling and Evaluation Recorder. *Proc. Oceanology International 2000*. New Malden, UK, Spearhead Exhibitions. unpaginated.

Sannay, R., Voulgaris, G., Trowbridge, J. H. and Warner, J. C. 2004. *Tidal and residual currents over asymmetric sandbanks. American Geophysical Union*, Fall Meeting 2004, abstract OS21B-1234.

Schofield, O., Bergmann, T., Bissett, P., Grassle, J. F., Haidvogel, D. B., Kohut, J., Moline, M. and Glenn, S. M. 2002. The long-term ecosystem observatory: an integrated coastal observatory. *IEEE J. Ocean. Eng*., 27(2), pp. 146–54.

Schofield, O., Kerfoot, J., Creed, E., Mudgal, C., Glenn, S. M., Jones, C., Webb, D., Kirkpatrick, G. and Twardowski, M. 2003. Current status of the COOL fleet of Webb Slocum gliders. Data and information at http://marine.rutgers.edu/cool/glider/florida/DailyFieldWork.html (Accessed December 2004.)

Short, R., Fries, D., Kerr, M. L., Toler, S., Lembke, C., Byrne, R. and Wenner, P. 2001. Underwater mass-spectrometers for *in situ* chemical analysis of the hydrosphere. *Am. Soc. Mass Spectrom*., 12, pp. 676–82.

Smith, C. M., Leonard, J. J., Bennett, A. A. and Shaw, C. 1997. Feature-based concurrent mapping and localization for autonomous underwater vehicles. *Proc. Oceans 1997*. 2, Marine Technology Society/Institute of Electrical and Electronic Engineers, pp. 896–901.

Sullivan, J. M. and Swift, E. 2003. Effects of small-scale turbulence on net growth rate and size of ten species of marine dinoflagellates. *J. Phycol.*, 39, pp. 83–94.

Tarran, G. A., Burkilli, P. H., Cunningham, A., Dubelaar, G. B. J. and Gerritzen, P. L. 2001. Cytosub: an *in situ* flow cytometer for analysing phytoplankton with the Autosub AUV, In : International Workshop on Autonomous measurements of Biogeochemical Parameters in the Ocean, Plymouth, 2001, abstracts, Plymouth, University of Plymouth, 2001, unpaginated

Van Dolah, F. M., Roelke, D. and Greene, R. M. 2000. Health and ecological impacts of harmful algal blooms: risk assessment needs. *Hum. Ecol. Risk Assess.*, 7, pp. 1329–45.

Voulgaris, G., Trowbridge, J. H. and Terray, E. 2001. *Spatial Variability of Bottom Turbulence over a Linear Sand Ridge: Mooring Deployment and Survey Cruise Report*. RRS Challenger, Cruise Number 146 Broken Bank, North Sea, UK, 17–28 August 1999. Woods Hole, Mass., Woods Hole Oceanographic Institution, 41 pp. (Technical Report WHOI-2001-09.)

Wiebe, P. H., Mountain, D. G., Stanton, T. K., Greene, C. H., Lough, G., Kaartvedt, S., Dawson, J. and Copley, N. 1996. Acoustical study of the spatial distribution of plankton on Georges Bank and the relationship between volume backscattering strength and the taxonomic composition of the plankton. *Deep Sea Res.*, 43, pp. 1971–2001.

Willcox, J. S., Bellingham, J. G., Zhang, Y. and Baggeroer, A. B. 2001. Performance metrics for oceanographic surveys with autonomous underwater vehicles. *IEEE J. Ocean. Eng.*, 26, pp. 711–25.

Willcox, J. S., Zang, Y., Bellingham, J. G. and Marshall, J. 1996. AUV survey design applied to oceanic deep convection. *Proc. Oceans 1996.* Fort Lauderdale, Marine Technology Society/Institute of Electrical and Electronic Engineers, pp. 949–54.

Wilson, A. K. 1997. An integrated data system for airborne remote sensing. *Int. J. Rem. Sens.*, 18(9), pp. 1889–901.

Yu, X., Dickey, T., Bellingham, J. G., Manov, D. and Streitlien, K. 2002. The application of autonomous underwater vehicles for interdisciplinary measurements in Massachusetts and Cape Cod Bays. *Cont. Shelf Res.*, 22, pp. 2225–45.

Zingone, A. 2003. Harmful algal blooms: keys to understanding of phytoplankton ecology. At http://www.ioc.unesco.org/icam/processes24.doc (Accessed December 2004.)

Zingone, A. and Enevoldsen, H. O. 2000. The diversity of harmful algal blooms: a challenge for science and management. *Ocean Coast. Manag.*, 43, pp. 725–48.

14

Ecosystem dynamics, harmful algal blooms and operational oceanography

T. C. Malone

14.1 Oceanography and stewardship of marine ecosystems

On 31 July 2003, 33 nations and the European Union declared their commitment to develop a comprehensive, coordinated and sustained Global Earth Observation System of Systems (GEOSS) as the means 'to monitor continuously the state of the earth, to increase understanding of dynamic earth processes, to enhance prediction of the earth system, and to further implement our international environmental treaty obligations'.[62] On 16 February 2005, a 10-year international implementation plan for GEOSS was adopted by 60 countries and the European Commission. The Global Ocean Observing System (GOOS) is the ocean and coastal contribution to the GEOSS.

GOOS is being designed and implemented to provide data and information on marine systems needed to achieve six related societal goals:

- Improve predictions of weather variability and climate change;
- Mitigate the effects of natural hazards (e.g. tropical cyclones) more effectively;
- Improve the safety and efficiency of maritime operations;
- Minimize public health risks;
- Protect and restore healthy ecosystems more effectively;
- Sustain living marine resources.

Achieving these goals requires the development of 'operational' oceanography that will enable continuous and sustained provision of reliable data on the oceans for rapid detection and timely predictions of changes in physical, biogeochemical and ecological states of marine and estuarine systems. Operational physical oceanography is rapidly developing for the purposes of predicting climate change, forecasting marine weather and natural hazards, and improving maritime services (goals 1–3). In contrast, the development of operational capabilities for those goals that require observations and models of the biogeochemistry and ecology of marine systems is in its infancy (goals 4–6).

Harmful algal blooms (HABs) affect public health, the structure and function of marine ecosystems, and the sustainability of living marine resources. Thus, the development of operational capabilities for rapid detection and timely predictions of HABs is a high priority for GOOS. This contribution provides an overview of GOOS and, in this context, general requirements for developing operational capabilities for an ecosystem-based approach to managing and mitigating the effects of HABs.

[62] http://earthobservations.org/

14.1.1 Climate, people and coastal ecosystems

The cumulative effects of natural hazards, human activities and climate change are, and will continue to be, most pronounced in the coastal zone where people and ecosystem goods and services are most concentrated, exposure to natural hazards is greatest, and inputs of energy and matter from land, sea and air converge (Costanza et al., 1993; McKay and Mulvaney, 2001; Nicholls and Small, 2002; Small and Nicholls, 2003). The changes occurring in coastal waters ('phenomena of interest') affect public health and wellbeing, the safety and efficiency of marine operations, and the capacity of ecosystems to support goods and services including the sustainability of living marine resources and biodiversity (Table 14.1). Although the phenomena of interest tend to be local in scale, they are occurring in coastal ecosystems worldwide and are often local expressions of larger-scale variability and change (Figure 14.1) including the following:

- basin scale changes in ocean-atmosphere interactions, e.g. El Niño Southern Oscillation (ENSO), North Atlantic Oscillation (NAO) and Pacific Decadawl Oscillation (PDO) (Barber and Chavez, 1986; Wilkinson et al., 1999; Arcos et al., 2001; Koblinsky and Smith, 2001; Lipp et al., 2001; Beaugrand et al., 2002; Francis et al., 1998);

Table 14.1 Examples of the drivers of change (forcings) and associated phenomena of interest in coastal marine ecosystems that are the subject of the Integrated Ocean Observing System (IOC, 2003). Forcings and phenomena of interest that are related to or may increase the probability of HABs and human exposure to algal toxins are italicized.

	Forcings of interest
'Natural'	*Global warming*, sea level rise
	Natural hazards (extreme weather, seismic events)
Anthropogenic	*Currents*, *waves*, *tides* and storm surges
	River and groundwater discharges, sediment inputs
	Alteration of hydrological and nutrient cycles
	Inputs of chemical contaminants and human pathogens
	Harvesting natural resources (living and non-living)
	Physical alterations of the environment
	Introduction of non-native species
	Phenomena of interest
Climate and weather	*Variations in sea surface temperature; surface fluxes of momentum, heat and fresh water*; sources and sinks of carbon; sea ice
Marine operations	Variations in water level, bathymetry, *surface winds, currents and waves*; sea ice; susceptibility to natural hazards
Natural hazards	Storm surge and coastal flooding; coastal erosion; public safety and property loss
	Risk of exposure to human pathogens, chemical contaminants, and *biotoxins* (contact with water, aerosols, seafood consumption)
Public health	*Habitat modification, loss of biodiversity, cultural eutrophication, harmful algal events, invasive species*, chemical contamination, diseases in and mass mortalities of marine organisms
Healthy ecosystems	*Fluctuations in spawning stock size*, recruitment and natural mortality; changes in areal extent and condition of essential habitat; food availability
Living marine resources	*Aquaculture production and water quality*

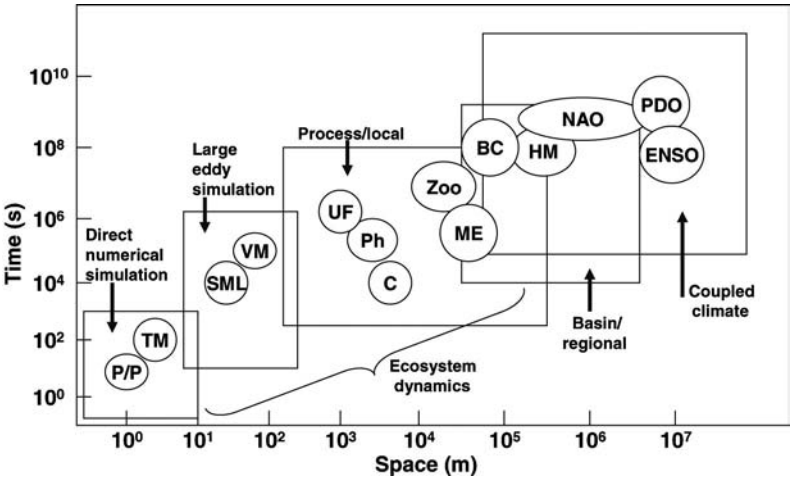

Figure 14.1
Time-space scales of marine processes and models that link global climate dynamics on large scales to the population dynamics of phytoplankton on the smaller scales of biomass accumulation and trophic interactions within ecosystems. The rectangles approximate the time-space scales encompassed by global ocean-climate and basin scale models (coupled climate, basin/regional) and smaller scale models of ecosystem dynamics ranging from the mesoscale (e.g. tidal and upwelling fronts and associated phytoplankton and zooplankton aggregations) to the scales of turbulent mixing and predator-prey interactions.
BC, boundary currents; C, convection; ENSO, El Niño-Southern Oscillation; HM, horizontal migration; ME, mesoscale eddies; NAO, North Atlantic Oscillation; PDO, Pacific Decadal Oscillation; Ph, phytoplankton; P/P predator/prey; TM: turbulent mixing; SML, surface mixed layer; UF, upwelling front; VM, vertical migration; Zoo, zooplankton.
Source: modified from Montua et al. (2002).

- human alterations of the environment, exploitation of living resources, and introductions of non-native species (Peierls et al., 1991; Carlton, 1996; Vitousek et al., 1997; Hallegraeff, 1998; GESAMP, 2001; Myers and Worm, 2003);
- natural hazards (Michaels, et al., 1997; Flather, 2000);
- global climate change (Barry et al., 1995; Najjar et al., 1999; Levitus et al., 2000).

In terms of human alterations, Jackson et al. (2001) and Lenihan et al. (2001) recently argued that over-fishing is not only the first major human perturbation of coastal ecosystem dynamics, it exacerbates the effects of nutrient pollution, contributes to habitat loss and associated loss of biodiversity, and increases the susceptibility of coastal ecosystems to invasive species, HABs and outbreaks of disease. Given the reality that such anthropogenic effects occur in the context of natural variability and change, mitigating and managing the effects HABs depend on the ability to distinguish local expressions of large-scale changes from local sources of variability and change. This can only be achieved through comparative analysis of observations made over a broad spectrum of scales (local to global) in different locations (Duarte, 1992).

14.1.2 Ecosystem dynamics and harmful algal blooms

Changes in the occurrence and magnitude of HABs reflect interactions between the structure and function of coastal ecosystems, the external forcings that impinge on them, and the population dynamics of HAB species that inhabit them. Local responses of biological populations to basin scale forcings such as ENSO, PDO and NAO appear to involve all trophic levels with response times generally increasing with trophic level, organism size and generation time (Francis et al., 1998). Such a pattern is consistent with the 'bottom-up' effects of nutrients and light that propagate through food webs from primary producers to higher order predators. Changes in predation may also exert 'top-down' effects that cascade to lower trophic levels (Carpenter, 1988; Abreu et al., 1994; Vanni and Layne, 1997; Heath and Houde, 2001). Thus, the rapid decline (90%) in biomass of large marine predators (including tuna, marlin, swordfish, cod, halibut, shark) during the last half of the twentieth century (Myers and Worm, 2003) has profound implications in terms of the structure and function of ecosystems, including possible increases in HABs due to changes in grazing patterns that may favour HA species (Busky and Stockwell, 1993; Jackson et al., 2001; Lenihan et al., 2001).

Given the convergence of basin scale forcings, fishing pressure and land-based inputs of nutrients in coastal waters, the cumulative effects of changes in the balance between top-down and bottom-up processes are likely to be especially pronounced in coastal systems. Fronts, eddies, buoyant plumes, multi-layered flow regimes, and interactions between benthic and pelagic communities in coastal marine and estuarine ecosystems enhance nutrient cycling and phytoplankton productivity and may promote the growth of harmful algae (Smayda, 1989; Jumars, 1993; Hood et al., 1999; Chapelle et al., 2000; Anderson et al., 2002). An example is the northern Adriatic Sea (Figure 14.2) which has experienced an apparent decadal scale shift from frequent HABs to the occurrence of mucilage events. With its long history of overfishing and nutrient pollution (Malone et al., 1999), such shifts in the products of community metabolism may reflect the importance of ecosystem dynamics in modulating relationships between sources (nutrient inputs) and sinks (accumulations of organic matter) leading to different outcomes (HABs or mucilage) (Fonda Umani, pers. comm.). Examples such as this reflect a cascading hierarchy of nonlinear physical-chemical-biological interactions that can be represented by robust models of ecosystem dynamics (Baretta et al., 1995; Nihoul and Djenidi, 1998; Moll and Radach, 2001; Hofman and Lascara, 1998; Kudela and Chavez, 2000; Hofmann and Friedrichs, 2002; Mantua et al., 2002; Robinson and Lermusiaux, 2002).

14.1.3 Ecosystem-based management

Successful prevention, control and mitigation of the environmental effects of human activities, natural hazards and climate change depend on the capacity to anticipate changes with sufficient lead-time to make informed decisions with desired outcomes (Clark et al., 2001). To this end, ecosystem-based management, which considers the effects of human activities in the context of natural variability, is emerging as a unifying approach to environmental protection, resource management, land-use planning and environmental engineering (NRC, 1999; Sherman and Duda, 1999; UNEP, 2001; Cicin-Sain and Knecth, 1998). Implementing such a strategy requires the capability to engage in *adaptive management*, a decision-making process that depends on reliable, routine and rapid detection of changes in the condition or state of coastal ecosystems. As

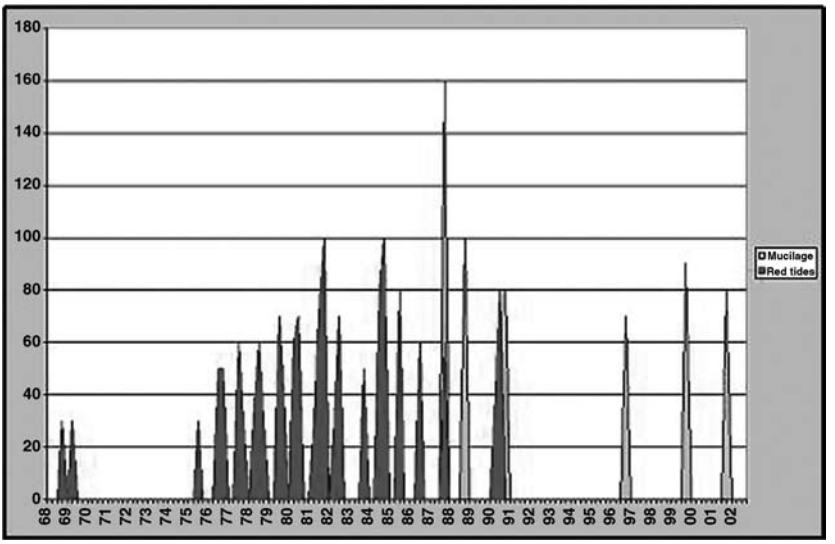

Figure 14.2
Time series of HABs and mucilage events in the northern Adriatic Sea. Red tides, which were most frequent during the late 1970s and 1980s, decreased during the late 1980s as mucilage events became more prevalent. It has been hypothesized that the transition from HABs to mucilage events is related to large outbreaks of gelatinous zooplankton in the early 1980s. This set in motion a cascade of effects beginning with accumulations of phytoplankton biomass, subsequent increases in the frequency and spatial extent of anoxia, benthic mortalities and lower filtration rates by benthic organisms. The resulting increase in pools of dissolved organic carbon provided the substrate for the formation of large mucilage mats.
Source: S. Fonda Umani, pers. comm.

indicated by recent attempts to quantify the condition of coastal marine and estuarine ecosystems on regional to global scales, *we do not have this capability today* (Malone, 2003).

Ecosystem-based approaches are especially important in coastal waters where the combined effects of habitat alterations, land-based inputs of nutrients and contaminants, over fishing, harmful algal blooms, and invasive species are most severe (Botsford et al., 1997). Effective ecosystem-based management of HABs and their effects depends on rapid assessments and timely predictions. Rapid assessment requires improved observing capabilities that increase the speed and accuracy with which changes in the distributions of key environmental parameters and of HA species are detected. Timely predictions require both improved data assimilating models of ecosystem dynamics and observations to parameterize and initialize them (Figure 14.3). The emergence of operational oceanography (Section 14.3) and the science of ecological forecasting

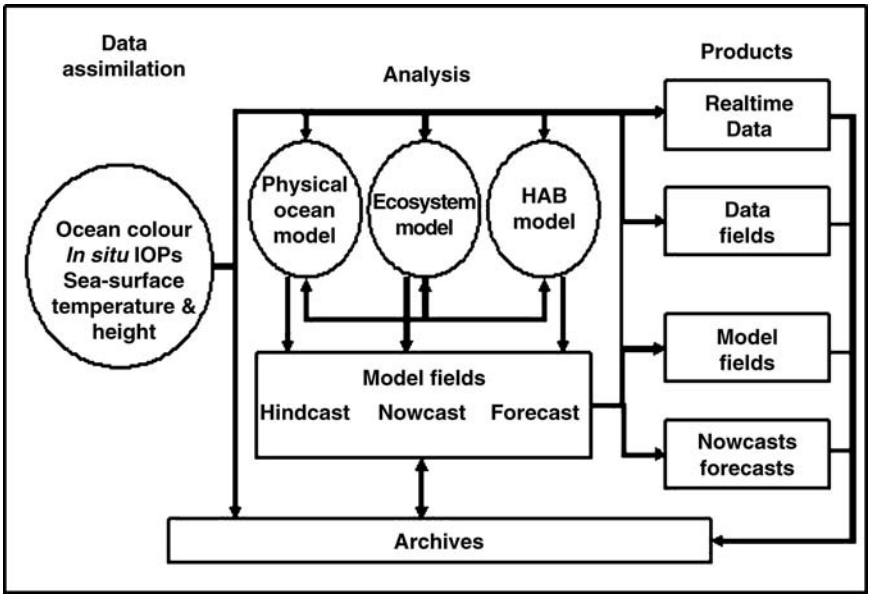

Figure 14.3
Near real-time estimates of physical, chemical and biological fields are becoming feasible as ocean prediction models are developed. These models produce predictions and data-driven simulations by linking dynamics and observations via the assimilation of observations into numerical models. One example is the Advanced Fishery Management Information System designed to produce nowcasts and forecasts of fish distributions in the Gulf of Maine and Georges Banks (Sundermeyer, 2001). Similar models for HABs are being developed that use the spectral distribution of light energy (IOPs), ocean colour, nutrient concentrations, sea surface temperature, and sea surface height to drive coupled physical, nutrient-phytoplankton-zooplankton (ecosystem) and population (HAB) models to predict the abundance and distribution of pigmented HA species (e.g. Schofield et al., 1999).

(Clark et al., 2001; Hofmann and Friedrichs, 2002) are important steps towards achieving these objectives.

Forecasting skill will improve as the 'slow' variables that portend or initiate changes are determined and techniques for their rapid detection are developed (Clark et al., 2001). For example, the combined effects of nutrient enrichment from land-based sources (primarily non-point inputs of nutrients from fertilizers) and overfishing oyster stocks have been shown to result in a massive spring diatom bloom that fuels the development of summer anoxia in Chesapeake Bay (Malone et al., 1996; Newell, 1988; Jackson et al., 2001). In cases such as this, projections of future patterns of land use based on the constraints of geomorphology, land-cover, distance from market centres, and agricultural practices (e.g. fertilizer production and use) could inform predictions of nutrient pollution and associated loss of habitat and changes in carrying capacity for fish production (Robertson et al., 2000; Tilman et al., 2001). Likewise, given the cross-disciplinary effects of temperature (e.g. water density, rates of chemical reactions

and biological processes, biogeography), it is likely to be an important slow variable on scales of decades to centuries.

Correlations between temperature cycles and the occurrence of HA species suggest that global warming may be an important slow variable. For example, based on sediment records, it has been predicted that global warming could result in the return of *Pyrodinium bahamense* to Australian waters (McMinn, 1989) and cause increases in the frequency of *Gymnodinium catenatum* blooms along the Galician coast (Fraga and Bakun, 1993). Blooms of *Pyrodinium bahamense* in the Philippines and *Dinophysis* spp. in Scandinavian waters have been correlated with positive temperature anomalies associated with the El Niño Southern Oscillation (Maclean, 1989) and the North Atlantic Oscillation (Belgrano et al., 1999), respectively. Although temperature may be a proxy for more complex causal relationships, documenting relationships such as these may lead to the development of process-based models for HAB prediction.

14.2 Managing HABs in an ecosystem context

14.2.1 The HAB challenge

14.2.1.1 HAB species

The majority of HAB species are dinoflagellates from four orders (Dinophysiales, Gymnodiniales, Peridiniales, Prorocentrales) and most toxic species are from four genera (*Alexandrium, Dinophysis, Gymnodinium, Prorocentrum*). At the same time, HA species (roughly 225 species from 12 taxonomic classes of algae) exhibit a wide variety of life-cycle strategies, trophic types, physiology, behaviour, morphology and harmful effects (Pfiester and Anderson, 1987; Hallegraeff, 1993; Richardson, 1997; Zingone and Enevoldsen, 2000; Anderson et al., 2002). Likewise, although most toxic species are from four genera, the diversity of species and toxins is high (nearly 100 species from eight classes; at least 20 different toxins that cause PSP alone).

For the purposes of management, HAB species can be divided into two broad categories, those that cause harm through the production of toxins and those that cause harm through excessive accumulations of biomass (Malone et al., 1996; Anderson et al., 2002). Although most species in both groups are pigmented and cause problems when they bloom, many are not pigmented and some have toxic effects at low cell densities, that is they can cause harm without blooming or without a detectable pigment signature (e.g. *Alexandrium tamarense, Pfiesteria piscicida, Protoperidinium* sp.).

14.2.1.2 Environmental regulation

Phytoplankton blooms are natural phenomena, and the same environmental characteristics of coastal ecosystems that enhance nutrient cycles and primary production (benthic-pelagic coupling, proximity to land-based inputs of nutrients, constraints of geomorphology on dispersion), also promote HABs. The frequency and magnitude of HABs can be enhanced by a variety of human activities including nutrient pollution (Howarth et al., 2000; Anderson et al., 2002), overfishing (Newell, 1988), global warming (e.g. McMinn, 1989; Fraga and Bakun, 1993) and introductions of non-native HA species (Carlton, 1996; Hallegraeff, 1998). Thus, it has been argued that there has been a global increase in the occurrence of HABs in recent decades and that this trend is related to human alterations of marine ecosystems (Anderson, 1989;

Smayda, 1989; Hallegraeff, 1993). However, Wyatt (1995) compared the time and space scales of observation and modelling required to test this hypothesis to the corresponding availability of data and models. He concluded that, although there are a number of locations where monitoring and modelling have detected trends within specific ecosystems (Table 14.2), only the continuous plankton recorder surveys (Warner and Hays, 1994) and global climate models (Stammer et al., 2001) operate on the time-space scales required to test the 'global spreading' hypothesis. Furthermore, understanding the relationship between human activities and HABs will require comparative analysis of observations made over a broad spectrum of scales (local to global) in different locations (Duarte, 1992).

Like all phytoplankton, the abundance of HAB species at any point in time and space is a function of the balance between local rates of growth and mortality; physical processes that transport, concentrate and disperse cells; and vertical movements of cells related to swimming, sinking and buoyancy control (Donaghay and Osborn, 1997; Richardson, 1997; Anderson et al., 2002). Species-specific growth rates are governed by genetics and environmental factors including temperature, salinity, turbulence, nutrients and light energy. Mortality rates are governed by grazing, viral infections, cell lysis and stresses relating to small-scale physical shear. Woods (2002) has articulated the challenge of predicting HABs in terms of building models based on 'biological primitive equations' equivalent to those for physics and chemistry. Given that species succession reflects species-specific responses to physical processes from turbulent scales to advective transport, the development of models that predict the occurrence of HABs with known certainty is not a trivial undertaking (Mantua et al., 2002).

Although the interactions among environmental and genetic factors that select for particular HA species are not well understood, the physical conditions under which HABs occur are well documented. HABs tend to occur in layers of low turbulent intensity (as defined by Sanford, 1997), in buoyant plumes, in fronts, or in systems that are poorly flushed when these features are associated with high nutrient inputs (inorganic and organic) that increase nutrient availability, changing nutrient ratios, or both (Donaghay and Osborn, 1997; Andersen et al., 2002). Results of culture experiments suggest that changing nutrient supplies and ratios also influence the production and toxicity of secondary metabolites produced by some species, e.g. enhanced saxitoxin production by *A. tamarense* when growth is P-limited than when N-limited (Boyer et al., 1987); enhanced production of domoic acid by *Pseudo-nitzschia multiseries* when Si-limited (Bates et al., 1991), enhanced production of okadaic acid by *D. acuminata* when N-limited than when P-limited (Johansson et al., 1996; Johansson and Granéli, 1999); and enhanced production of brevetoxin by *K. brevis* when exposed to elevated concentrations of urea (Shimizu et al., 1993). Thus, although the population dynamics of HA species differ substantially among taxa, interactions between changing physical and nutrient regimes appear to be generally important in regulating distribution, abundance and toxicity of most HA species.

As discussed by Donaghay and Osborn (1997), the interaction of biological and physical processes in regulating the development and impacts of HABs varies over a continuum of scales from accumulations of biomass in poorly flushed systems subject to high nutrient inputs (long residence time of water) to accumulations of biomass within thin layers or discontinuities. Examples of the former include seasonal to interannual blooms of *Aureococcus anophagefferens* in Laguna Madre, Texas and coastal bays of Long Island, NY (Cosper et al., 1989; Busky and Stockwell, 1993). Examples

Table 14.2 Examples of time-series observations of HABs, HAB toxins or HAB affects (mass mortalities) from coastal ecosystems

Location	Variables measured	First year
Canada:	PSP	1942
east coast	PSP	1950
west coast		
Finland:	Phytolankton	1968
Gulf of Finland	Mortalities	1984
all		
France:	Mortalities	1976
all	*Gyrodinium*	1980
	DSP	1983
	PSP	1984
Germany:	Phytoplankton species	1962
German Bight		
HELCOM:	Phytoplankton	1979
Baltic Sea		
Italy:	HA species	1968
Adriatic Sea		
Norway:	PSP	1962
Oslo fjord	Mortalities	1966
all	*Gyrodinium*	1981
	PSP	1982
	Dinophysis	1984
	DSP	1984
Portugal:	PSP	1986
all	Phytoplankton	1987
	DSP	1987
Spain:[1]	PSP	1976
Galicia	Phytoplankton	1977
	DSP	1982
	Dinophysis	1985
Sweden:	PSP	1982
west coast	DSP	1984
	Phytoplankton	1989
United States:	PSP	1958, 1972
east coast	Phytoplankton	1958
west coast	PSP	1962, 1978, 1980
Gulf of Mexico	Mortalities	1989
west Florida shelf	NSP	1978
	Mortalities	1980
	Red tides	1878

[1] The EU has established a Community Reference Laboratory (CRL) for handling problems associated with HAB toxins in seafood. Located in Vigo, Spain, the CRL works with representatives from National Reference Laboratories (NRL) within the EU and associated ICES countries to develop recommendation to the EU Commission on issues such as which toxins to prioritize, maximum tolerance concentrations of toxins in seafood, and methods of analysis. *Source*: modified from ICES (1991).

of the latter include blooms of *Gymnodinium catenatum* and *Dinophysis acuminata* in Spanish *rias* (Fraga et al., 1988; Figueiras et al., 1998; Sordo et al., 2001), subsurface blooms of *Gyrodinium aureolum* and *Chrysochromulina polylepsis* in the pycnocline of Scandinavian waters (Dundas et al., 1989; Bjornsen and Nielsen, 1991), blooms of *Gyrodinium aureolum* along convergent fronts (Pingree et al., 1975), and blooms of *Alexandrium tamarense* in buoyant plumes in the Gulf of Maine (Franks and Anderson, 1992). Seasonal accumulations of diatom-biomass in Chesapeake Bay (Malone et al., 1996) and large-scale HABs, such as the 1976 *Ceratium tripos* bloom in the Middle Atlantic Bight (Malone, 1978; Falkowski et al., 1980; Boesch and Rabalais, 1991) provide intermediate examples. In these cases long residence times and nutrient enrichment support growth-dependent increases in biomass on timescales of days to weeks, while two-layered, estuarine circulation concentrates biomass to levels that can not be accounted for by autochthonous growth on timescales of weeks to months.

14.2.2 Managing HABs

An important goal of HAB research and monitoring is to provide the knowledge, data and information needed to protect public health and sustain the capacity of marine ecosystems to support goods and services. Ecosystem-based management strategies are aimed at preventing HABs before they occur (e.g. reduce nutrient loading), mitigating their effects (e.g. close shellfish beds, close beaches, move net pens of cultured salmon), and controlling them once they occur (reducing their magnitude, containing their distribution). Achieving these objectives requires the development of three related capabilities for both implementing adaptive management and assessing their efficacy:

- more rapid detection of HA species and toxins;
- timely predictions of where and when HABs are likely to occur;
- timely forecasts of their trajectories in time and space.

As target species and the environmental conditions that promote their growth, biomass accumulation and toxicity differ from place to place, requirements (variables to measure, time and space scale of measurement, acceptable time lags between occurrence, detection and prediction, models) for ecosystem-based management will also change. However, although a variety of factors influence the dynamics of HABs (including grazing, life cycles strategies, vertical migrations), it is also clear that initiation, growth, maintenance and termination of many HA species are governed by the interplay between nutrient enrichment and changing physical regimes. Thus, progress towards the development of effective adaptive management practices will probably be most rapid for those HA species that are pigmented, occur frequently in particular locations (hot spots), and respond to changing nutrient fields and physical regimes in terms of the frequency and magnitude of blooms (as indicated by increases in biomass and pigment concentration).

14.3 Operational oceanography

An operational system is one in which the provision of reliable data and derived products (e.g. GIS products, alerts, forecasts) and services is routine, guaranteed, and sustained at rates and in forms specified by user groups (e.g. public health ministries, water quality and coastal zone managers, tourist industry). The observing system for the World Weather Watch is an example of such a system in that it efficiently links

measurements of meteorological variables to numerical models for the singular purpose of providing nowcasts and forecasts of the weather on local to global scales. With an important exception, a similar system is being developed for the oceans (Global Ocean Observing System, GOOS).[63] As described in Section 14.3.1, the exception is that GOOS is to be a multidisciplinary system (measurements of meteorological, physical, biological, chemical and geological variables on local to global scales) that serves a much greater diversity of data and information for multiple purposes.

Sustained, long-term, high-resolution time-series measurements and large-scale, spatially synoptic observations of the oceans are required for both research and operational oceanography:

- research to resolve and understand the effects of human activities and natural sources of variability and change (Duarte, 1992; Francis and Hare, 1994; McKay and Mulvany, 2001) and
- operational oceanography to provide reliable and repeated estimates of physical, chemical and biological fields and associated model-based early warnings and predictions (Nowlin et al., 1996; Stel et al., 1997; Malone and Cole, 2000; Flather, 2000).

In the case of HABs, early warnings and timely forecasts will require near real-time observations of geophysical (near surface wind vectors; sea surface temperature, salinity, currents and waves; vertical distribution of density), chemical (nutrients), and optical properties (see Chapters 3–13, this volume); data assimilation schemes; and operational models of coupled physical-ecological processes. In this regard, the importance of accurately simulating time-dependent variability in the physical environment on scales from metres to hundreds of kilometres cannot be overemphasized.

14.3.1 Global Ocean Observing System (GOOS)

14.3.1.1 Purpose

The mandate to establish a Global Ocean Observing System was articulated and ratified as an international consensus in 1992 with the signing of the Framework Convention on Climate Change and the Programme of Action for Sustainable Development at the UN Conference on Environment and Development (UNCED) (IOC, 1998).[64] The latter calls for the establishment of a GOOS that will enable effective management and sustainable use of the marine environment and its natural resources. GOOS is an important component of the Integrated Global Observing Strategy (IGOS)[65,66] and the oceans and coasts component of the Global Earth Observing System of Systems (GEOSS).

GOOS is developing as a global network that systematically acquires and disseminates data and information based on requirements specified by groups that use, depend on, manage or study marine and estuarine systems (IOC, 1998). The observing system consists of two related and convergent modules:

- an open ocean module concerned primarily with detecting and predicting natural hazards and changes in the ocean-climate system and their effects on marine operations and services;[67]

[63] http://ioc.unesco.org/goos/docs/GOOS_125_COOP_Plan.pdf
[64] http://ioc.unesco.org/goos/Prospe98/Contents.html
[65] http://ioc.unesco.org/goos/docs/GOOS_066_act.pl.htm
[66] http://ioc.unesco.org/igospartners/
[67] See GOOS websites for further information: http://ioc.unesco.org/goos/

- a coastal module concerned primarily with effects of human activities, natural hazards and climate change on public health risks, the condition of coastal marine and estuarine ecosystems, and the living resources they support.

Achieving the goals of GOOS requires the development of operational oceanography for rapid detection and timely prediction of a broad spectrum of phenomena (Table 14.1). Although each goal has unique requirements for data and information, they have many data needs in common. Likewise, the requirements for data communications and management are similar across all six goals. Thus, an integrated approach to the development of a multiuse, multidisciplinary observing system is feasible, sensible and cost-effective.

14.3.1.2 An end-to-end system

Rapid detection and timely prediction depend on the establishment of an observing system that efficiently links measurements and modelling via integrated data communications and management. The system must be sustained (permanent) to provide continuity and to capture the spectra of variability that characterize the marine environment and the organisms that inhabit it. It must be integrated to provide spatially and temporally synoptic observations of physical, chemical and biological variables to achieve multiple objectives encompassed by the six goals. Linking user needs to measurements requires an efficient and managed flow of data and information among three essential subsystems (Figure 14.4):

- A monitoring subsystem (networks of platforms and sensing techniques) to measure variables on time-space scales required to assess the state of marine ecosystems and to rapidly detect and predict changes in or the occurrence of priority phenomena of interest (Table 14.1);

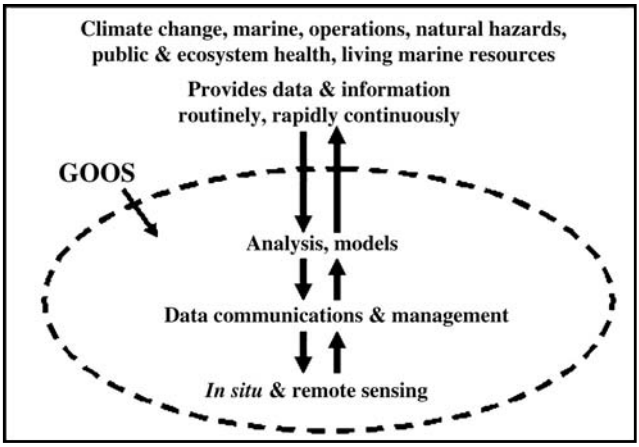

Figure 14.4
The observing system consists of three, closely linked subsystems. Implementation and development of these as a system is driven by user requirements, technical capabilities, and sustainable investments in infrastructure (capitalization) and operations (including the required technical expertise). Note that, depending on capabilities and needs, user groups may directly access data and information from any one or all of the subsystems.

- A data communications network and management subsystem that provides rapid access to diverse data from many sources;
- A data-assimilation and analysis (conceptual, statistical and numerical models; geographical information systems) subsystem for the provision of data and information in formats and at rates specified by the users.

Together, the subsystems constitute an 'end-to-end' system designed to provide data and information for informed decisions on timescales required to achieve desired affects and to evolve in response to the changing needs of multiple user groups.

14.3.2 Coastal Module of GOOS

14.3.2.1 Regional observing systems and the Global Coastal Network

The Integrated Design Plan for the Coastal Module of GOOS (IOC, 2003) calls for establishing regional coastal ocean observing systems (RCOOSs) worldwide (Figure 14.5) and, through this process, the development of a Global Coastal Network (GCN). The GCN will (a) measure, manage and analyse common variables needed by all or most coastal nations and regions; (b) establish a sparse network of sentinel and reference stations for early detection of the effects of land-based inputs (e.g. freshwater, sediments and nutrients) and basin scale variability (e.g. El Niño-Southern Oscillation, North Atlantic Oscillation, Pacific Decadal Oscillation); and (c) apply internationally accepted standards and protocols for measurements, data telemetry, data management and modelling.

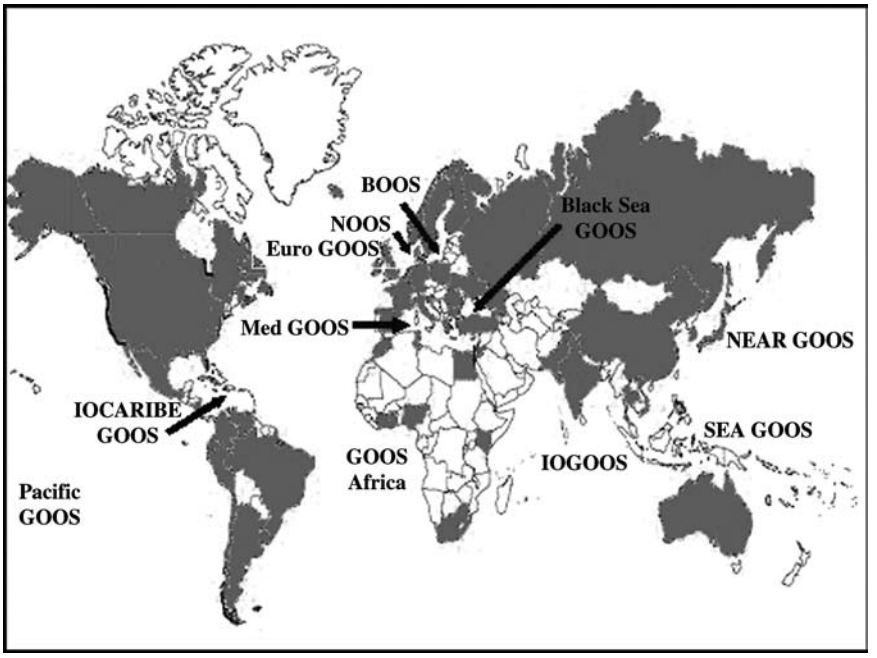

Figure 14.5
As of 2003, Global Ocean Observing System Regional Alliances and countries with national GOOS Programmes are forming worldwide.

Table 14.3 Provisional list of common variables recommended to be measured as part of the global coastal system. The procedure used to develop this list is described in the integrated design plan in detail. In brief, this is the minimum set of variables needed to detect or predict a maximum number of the phenomena of interest. Rankings were weighted based on user group and model

Physical	Chemical	Biological
Sea level	Sediment organic content	Benthic biomass
Temperature	Dissolved inorganic nitrogen,	Phytoplankton
Salinity	phosphorus, silicon	biomass
Currents	Dissolved oxygen	Faecal indicators
Surface waves		
Bathymetry		
Shoreline position		
Sediment grain size		
Attenuation of solar radiation		

The provisional common variables include geophysical variables (temperature, salinity, currents, waves, sea level, shoreline position, bathymetry, sediment grain size), chemical variables (dissolved inorganic nutrients, dissolved oxygen, sediment organic content), biological variables (faecal indicators, phytoplankton biomass, benthic biomass) and biophysical variables (optical properties). Depending on national and regional priorities, GRAs may increase the resolution at which the common variables are measured, supplement common variables with the measurement of additional variables and provide data and information products that are tailored to the requirements of stakeholders in the respective regions.

Observational elements that are to be linked to form an integrated system of observations include (a) coastal networks for near-shore observations; (b) the global network of coastal tide gauges; (c) fixed platforms, moorings, drifters and underwater vehicles for *in situ* measurements; (d) research and survey vessels, volunteer observing ships; (e) remote sensing from satellites and aircraft; research and survey ships; and (f) remote sensing from land-based platforms, e.g. high-frequency radar.

14.3.2.2 Towards operational marine ecology

During the decade since UNCED in 1992, substantial progress has been made in the design and implementation of the open ocean module (Koblinsky and Smith, 2001). In contrast, although a high priority of the international community, development of the coastal module has been slow. This is due in part to two related limitations: first, the lack of capacity to rapidly and routinely detect changes in those phenomena of interest that require measurements of biological and chemical variables; and second, the lack of operational ecosystem-based models required to predict the occurrence of or changes in ecological phenomena of interest. Thus, improving the GOOS through the incorporation of elements for operational marine ecology depends on major advances on at least three research fronts:

- development of integrated data communications and management systems that provide rapid access to diverse data from many sources;
- development of *in situ* and remote sensing techniques for near real-time provision of data on key biological and chemical variables;

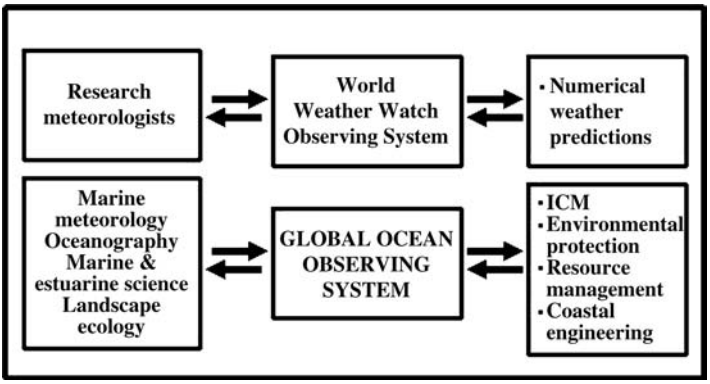

Figure 14.6
The global atmospheric observing system of the World Weather Watch (WWW) is the kind of operational, end-to-end system that GOOS is envisioned to be. Just as weather nowcasts and forecasts are not possible without sustained observations and operational models, implementation of ecosystem-based, adaptive management practices will not be possible without operational models of marine ecosystems and uninterrupted provision of oceanographic data required to initialize and up-date model runs. However, the analogy ends there as GOOS will serve a broad diversity of multidisciplinary data and information and its development will require a broader base of scientific disciplines.

- development of data-assimilation techniques and coupled physical-ecological models that can be run in an operational mode. Harmful algal blooms are an important case in point.

Just as advances in science and technology will enable advances in operational capabilities of GOOS, the sustained provision of data and information by GOOS will enable advances in science and technology (Figure 14.6). Development of synergy between research and operational capabilities will enhance the value of investments in science and technology. It will also stimulate advances in public understanding of the oceans by providing a 'window' to the sea for more timely visualization of change and its consequences. Such a synergy between research, public awareness, and the evolution of GOOS must be cultivated and sustained to achieve its full benefits.

More effective linkages are needed between advances in science and technology and the development of operational capabilities. To this end, a continuum of activities from research to operational marine ecology should be institutionalized to ensure timely use of new technologies and knowledge for improving operational capabilities of GOOS (Nowlin et al., 2000; Nowlin and Malone et al., 2005). These can be summarized as follows:

1. Research projects and programmes of finite duration are the ultimate source of new technologies (platforms, sensors, measurement protocols, data telemetry, etc.) and knowledge (e.g. models).
    - Research programmes that provide the scientific foundations for implementing and improving the coastal module of GOOS include coastal LTERs, LOICZ, GLOBEC and GEOHAB. The broad goals these programmes

are to improve understanding of long-term ecological phenomena across national and regional boundaries, promote comparability of observations, and encourage data exchange (International LTER); determine the fluxes of materials (emphasis on water, sediments, and carbon, nitrogen and phosphorus compounds) into, within, and from coastal ecosystems (LOICZ); understand and model the effects of physical forcings on the distribution, diversity and productivity of animal populations (zooplankton in particular) in marine ecosystems (GLOBEC); and improve the prediction of harmful algal events by determining the mechanisms underlying their population dynamics through interdisciplinary research, modelling, and an enhanced observational network (GEOHAB).

2. Pilot projects of finite duration are needed to gain community acceptance of new techniques and knowledge through repeated testing designed to demonstrate their utility and sustainability in a routine, operational mode.
    - To be designated a GOOS Pilot Project, projects must target high-priority elements for building the fully integrated system based on existing capabilities and user needs. Proposed projects must (a) specify how the project is likely to contribute to the development of GOOS, (b) describe the benefits to potential user groups, (c) specify objectives and milestones, (d) describe project management and performance metrics (e.g. feasibility and impact, improving existing elements of the IOOS, product development); and (e) specify goals that can be achieved within a specified, finite period (e.g. three to five years).
    - The Global Ocean Data Assimilation Experiment (GODAE) High Resolution Sea Surface Temperature (GHRSST) is an example of a pilot project established to give international focus and coordination to the development of a new generation of global, multi-sensor, high-resolution, SST products.[68] In this decade (2003–2013), enhanced ocean sampling from satellites (e.g. ENVISAT, EOS, ADEOS, MSG) and *in situ* platforms (e.g. Argo floats) is expected. GHRSST will capitalize on these developments to demonstrate the benefits of integrated global ocean SST products. The goal is to rapidly and periodically provide high-resolution (time and space) SST products that meet the needs of GODAE, the scientific community, operational users and climate applications on a global scale.
    - Activities that are directly relevant to the development of operational capabilities for detecting and predicting HABs include the Global Information Service for the European Coastal Environment (Coast Watch),[69] Real-time Ocean Services for Environment and Security (ROSES),[70] and the Gulf of Mexico HABSOS project discussed below (Section 14.4.2).
3. Pre-operational projects of finite duration are needed to ensure that incorporation into the observing system leads to a value-added product (more cost-effective than functioning in isolation) and to ensure that incorporation does not compromise the integrity and continuity of existing data streams and product delivery.
    - Candidates for pre-operational projects must (a) meet all the criteria for selection as a pilot project, (b) justify selection as a pre-operational project in

[68] www.bom.gov.au/bmrc/ocean/GODAE/
[69] http://www.coastwatch.info/
[70] http://roses.cls.fr/

terms of how it will improve the value added nature of GOOS, (c) document capabilities in terms of sustainability on timescales specified by the users, (d) involve collaboration among research and operational groups and be endorsed by operational groups and potential users, and (e) describe procedures by which the system or elements of the system will be incorporated into the operational observing system.

- The Mediterranean Forecasting System (MFS)[71] is an example of an end-to-end pre-operational project (Pinardi et al., 2007 – Chapter 20 this volume).
- It is a collaboration between environmental agencies of Cyprus, Egypt, France, Greece, Italy, Israel, Malta, Spain, Norway and the United Kingdom. The overarching goal is the prediction of marine ecosystem variability from sea surface temperature, salinity and currents to primary production on timescales of days to months. The scientific rationale for the system is based on the hypothesis that coastal hydrodynamics and ecosystem fluctuations are intimately connected to the large-scale general circulation. The emphasis to date has been on demonstrating the utility of near real time (NRT) forecasts of basin scale currents. NRT data from networks of voluntary observing ships (SST, SSS), moored autonomous *in situ* sensors (temperature, salinity, currents), satellites (sea surface height, SST) and data assimilation techniques are used to produce three-, five- and ten-day forecasts for three-month periods for the entire basin.

4. The evolution of the operational system is driven by the requirements of user groups and occurs through the selective incorporation of elements that have been tested pre-operationally.
    - To be established as part of the operational system, that meet the criteria for pre-operational designation must (a) demonstrate compliance with GOOS design principles; (b) be endorsed by operational and user communities; (c) be cost-effective; and (d) document affordability and readiness (required assets are available including technical support; availability of instrumentation, computing power, etc.).
    - The Baltic Operational Observing System (BOOS) is a collaboration between government agencies of the countries surrounding the Baltic Sea (Germany, Poland, Lithuania, Latvia, Estonia, Russian Federation, Finland, Sweden, Denmark) that are responsible for monitoring and modelling the Baltic and for providing marine forecasts and other services for the marine industry, environmental organizations and other end users.[72] Through the shared use of infrastructure, expertise and data, the goals of BOOS are to: (a) improve services to meet the requirements of environmental and maritime user groups; (b) increase the cost-effectiveness of investments in ocean observations; (c) further develop the market for operational oceanographic products by identifying new customers; (d) provide high-quality data and long time series required to advance the scientific understanding of the Baltic Sea; and (e) provide data and forecasts to protect the marine environment, conserve biodiversity, and monitor climate change and variability.

Existing elements or systems (regardless of origin or sponsorship) may be considered for any stage if they meet the relevant requirements.

[71] www.cineca.it/mfspp
[72] www.boos.org/

14.3.2.3 Phased implementation

Recognizing that (a) all the major goals of GOOS should be addressed from the beginning and (b) current operational capabilities from sensors to models dictate an initial emphasis on marine services, natural hazards and climate prediction, implementation of GOOS will be an evolutionary process that incorporates biological and chemical variables as new technologies, knowledge and operational models are developed (Figure 14.7). Phased implementation of the coastal module will be guided by the following considerations:

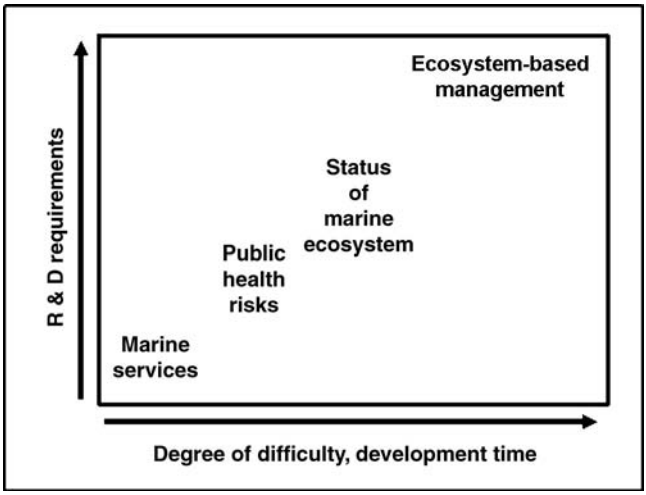

Figure 14.7
Time-dependent development of a fully integrated observing system. Predictions of most of the phenomena of interest require the same physical and meteorological data acquired for marine services and forecasting natural hazards. Those elements of an operational observing system required for improved marine services and forecasts of natural hazards are more developed (including the required operational models) than those required for ecosystem-based management. Capabilities to assess public health risks and the status of marine ecosystems are somewhere in between. Given current capabilities and the importance of physical processes to the phenomena of interest relevant to the goals of ecosystem health and living marine resources, initial development of the global system will target the measurement and processing of physical variables as well as those biological and chemical variables that can be measured routinely and for which products can be clearly defined. To the extent that they are operational, non-physical variables should now be incorporated into the observing system (e.g. chlorophyll fluorescence, dissolved oxygen). As technologies and procedures for rapid measurement and analysis of additional biological properties (e.g. phytoplankton species, zooplankton abundance, fish abundance, concentrations of pathogens, biomarkers) and chemical properties (e.g. nutrients, pesticides, PAHs) are developed, they will be incorporated into the system to achieve regional priorities and meet the needs of user groups.

- Safe and efficient coastal marine operations and the mitigation of natural hazards require accurate nowcasts and timely forecasts of storms, extent of coastal flooding, currents and sea state. The geophysical fields that must be estimated and assimilated in near real time include barometric pressure, surface wind vectors, atmospheric deposition, air and water temperature, sea level, stream flows, surface currents and waves, and ice extent.
- In addition to rapid detection of changes geophysical fields above, mitigating the effects of natural hazards and reducing public health risks also requires a predictive understanding of the effects of habitat loss and modification (barrier islands, tidal wetlands, sea grass beds, etc.) on the susceptibility of coastal ecosystems and human populations to them. Minimizing public health risks and protecting and restoring coastal ecosystems require additional observations of public risk factors (e.g. faecal indicators, seafood contamination) and indicators of ecosystem health (e.g. species of harmful algae, habitat modification, oxygen depletion, non-indigenous species) (Table 14.1). Relevant variables include salinity; habitat extent and condition; concentrations of nutrients, suspended sediments, phytoplankton biomass, contaminants, biotoxins and pathogens; attenuation of visible light; and the distribution and abundance plant and animal species.
- In addition to sustained data streams on the state of marine ecosystem, the demands of protecting living marine resources and managing harvests (of wild and farmed stocks) in an ecosystem context (adaptive management) require timely information on population (stock) abundance, distribution, age (size) structure, fecundity, recruitment rates, migratory patterns and mortality rates (including catch statistics).

14.4 Developing ecological capacity

Two quite different but related activities are summarized below to illustrate current capabilities that should be developed and integrated into the coastal module of GOOS to improve capacity to detect and predict HABs. The surveys conducted with the continuous plankton recorder (CPR), under the auspices of the Sir Alister Hardy Foundation for Ocean Science, are pre-operational and ready to be integrated into GOOS as an operational element. The Harmful Algal BloomS Observing System (HABSOS) is a pilot project of the US GOOS Programme. This is but one example of similar projects that are currently being developed around extensive time-series measurements of HA species (Table 14.2), e.g. EuroHAB (Graneli et al., 1998).

14.4.1 Continuous Plankton Recorder (CPR) Surveys[72]

As noted by Wyatt (1995), the continuous plankton recorder programme (Warner and Hays, 1994) is the only observational effort that operates on scales that can provide biological data needed to test the hypothesis that the frequency and magnitude of HABs are increasing on a global scale. Although the technology needs updating, the continuous plankton recorder is expected to become an important operational element of GOOS on a global scale. Sir Alister Hardy initiated the CPR surveys in 1931 (Hardy, 1935) and, with the exception of the Second World War years, surveys have been conducted by ships-of-opportunity in the North Atlantic and North Sea at roughly monthly intervals ever since. Under the direction of the Sir Alister Hardy Foundation for Ocean Science (SAHFOS), the survey adopted an open access data policy in 1999

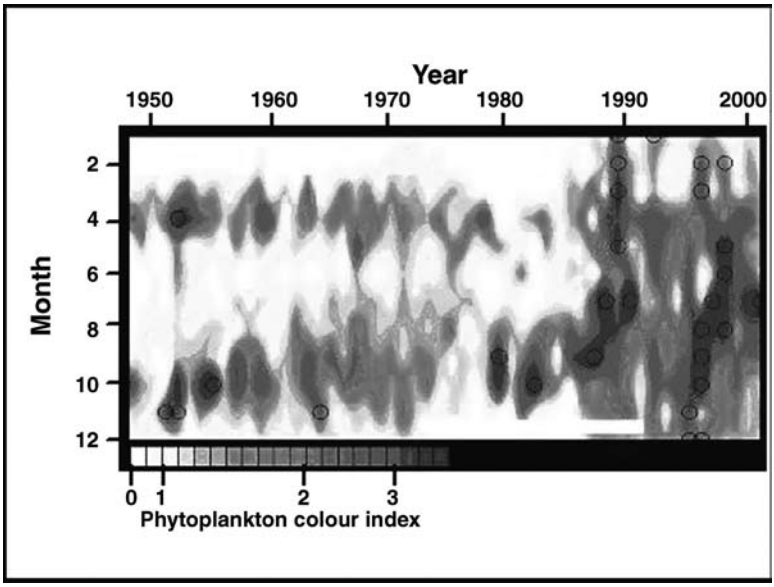

Figure 14.8
The time series of monthly mean values of the CPR colour index in the central North Sea shows a dramatic increase in phytoplankton biomass in the late 1980s. Circles denote colour indices greater than 2 standard deviations above the long-term monthly mean.

consistent with GOOS design principles (IOC, 1998). The survey, which collects data on the abundance and distribution of over 450 phytoplankton and zooplankton taxa, provides the only measure of the state of marine plankton communities on ocean basin and decadal timescales (Reid et al., 1998; Beaugrand et al., 2002). For example, the CPR colour index, a measure of phytoplankton biomass, for the North Sea from 1948 to 2000 shows a dramatic increase during the early 1980s (Figure 14.8), primarily due to increases in the summer biomass of flagellates. The database also includes information on major HA species in the region (Table 14.4) that show interannual variations and trends in abundance (Figure 14.9).

There is a clear need to incorporate existing CPR surveys into regional observing systems; to provide more rapid access to CPR data for purposes of ecosystem-based management of fisheries, HABs and invasive species; and to expand the programme into other regions. In regard to the latter, CPRs are or will soon be in use in the Baltic (as part of the Baltic Operational Observing System), Gulf of Guinea (Large Marine Ecosystem Programme), Indian Ocean (Indian Ocean GOOS), Mediterranean (MedGOOS), north Pacific (PICES), and the Southern Ocean (International LTER). GRAs are encouraged to embrace these efforts and to incorporate the data streams into integrated data communications and management to enable rapid access and analysis.

[73] www.sahfos.org, www.npm.ac.uk/sahfos/

Table 14.4 Examples of known harmful phytoplankton taxa recorded by the CPR survey in the North Atlantic and North Sea at a meso- to macro-scale with a temporal resolution of one month

Taxa	Harmful effects	Initiated time series
Ceratium furca	Oxygen depletion	1948
Coscinodiscus wailesii	Mucilage production	1977(invasive species)
Dinophysis spp.	DSP	1948
Gonyaulax spp.	Unspecified toxicity	1965
Noctiluca scintillans	Discoloration, oxygen depletion	1981
Phaeocystis spp.	Foam, mucilage production; Hypoxia, Anoxia	1948
Prorocentrum micans	DSP, discoloration, oxygen depletion	1948
Pseudo-nitzschia spp.	ASP	1948
Cylindrotheca closterium	Foam, mucilage production	1948
Chaetoceros spp.	Clogs gills	1948
Skeletonema costatum	Clogs gills	1948

14.4.2 Gulf of Mexico HABSOS Pilot Project[73]

The Harmful Algal BloomS Observing System (HABSOS) project was launched in 2000 following a 1997 workshop on harmful algal bloom forecasting and a 2000 workshop on linking management requirements to the development of GOOS (Fisher et al., 2003; Stumpf et al., 2003). The goal of HABSOS is to create the capacity to provide an internet-based data communications and management system for collecting, processing and disseminating data and information in the form of (a) early HAB alerts (detecting new blooms); (b) frequent updates of the locations of existing blooms; (c) timely forecasts of HAB trajectories and the time and location of HAB land falls; and (d) probabilities that a bloom will occur based on environmental conditions. HABSOS is designed and implemented as a proof of concept, user-driven project. To this end, the project is a partnership involving US federal (Environmental Protection Agency, EPA; National Oceanic and Atmospheric Administration, NOAA; Naval Oceanographic Office) and state (Florida, Alabama, Mississippi, Louisiana, Texas) agencies, academic marine research laboratories in the USA and Mexico, and industries working in the Gulf of Mexico. Current primary users are federal, state and local resource and environmental managers and scientists.

The Gulf of Mexico has many features that make this region suitable for a pilot project that can rapidly develop into an operational system. These include the following:

- There is a long history of monitoring HABs (Figure 14.10) and associated shellfish bed closures.
- Although home to 30 or more toxic species, *Karenia brevis* (formerly *Gymnodinium breve*) has by far the greatest impact in the region in terms of human health, mass mortalities of marine organisms, and shellfish-bed closures (Steidinger et al., 1997).
- *K. brevis* can be detected by both remote and autonomous *in situ* sensing (Schofield et al., 1999; Hu et al., 2003; Stumpf et al., 2003). It is pigmented with concentrations of chlorophyll *a* and cells correlated over the dynamic range

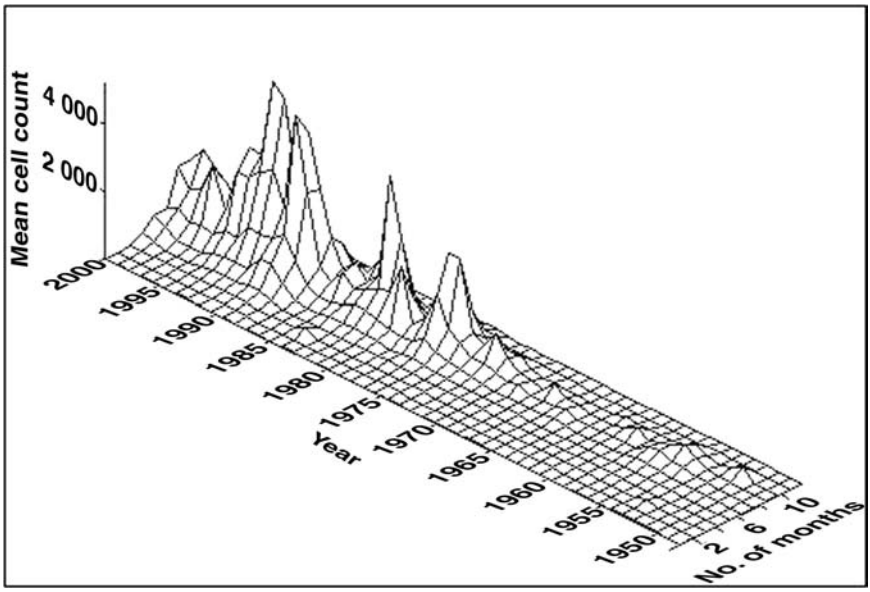

Figure 14.9
Monthly mean cell counts per sample (integrated over 20 nautical miles) of *Prorocentrum micans* in the North Sea. Peaks were recorded in 1975–76 and 1982 followed by a sustained period of high cell densities beginning in the late 1980s, coincident with the sudden increase in the chlorophyll index. Although *P. micans* may not be toxic itself, it is a good indicator of the presence of *Dinophysis acuminata*, which is toxic at low cell densities (Johns et al., 2003).

of concentrations typically found in the Gulf (<1–20 μg chl^{-1}); it has a surface expression and can be detected remotely; and it has a specific signature of inherent optical properties that allows recognition by *in situ* optical instrumentation (Stumpf et al., 2003).

- *K. brevis* blooms are a regional problem, i.e. they are not confined to one state but are often transported across state jurisdictions (e.g. Tester et al., 1991; Stumpfet al., 2003).
- *K. brevis* blooms occur most frequently during late summer and autumn when diatom biomass tends to be low and *K. brevis* often dominates the chlorophyll *a* field (Kusek et al., 1999).
- Blooms of *Trichodesmium* spp., a genus of cyanobacteria with an optical signature (phycobilins) different from that of *K. brevis* (Subramaniam and Carpenter, 1994), often precede *K. brevis* blooms (Walsh and Steidinger, 2001).
- The frequency and timing of blooms may be a useful indicator of global warming (Tester et al., 1993).

A comprehensive review of the occurrence of *K. brevis* blooms, the biology and ecology of *K. brevis* and its impacts (real and perceived) is given by Kusek et al. (1999).

A climatological approach to detecting chlorophyll *a* anomalies that are most likely caused by *K. brevis* (75% of the time during 1999 through 2001) has been developed by Stumpf (2001) and used to provide early warnings of new blooms, to

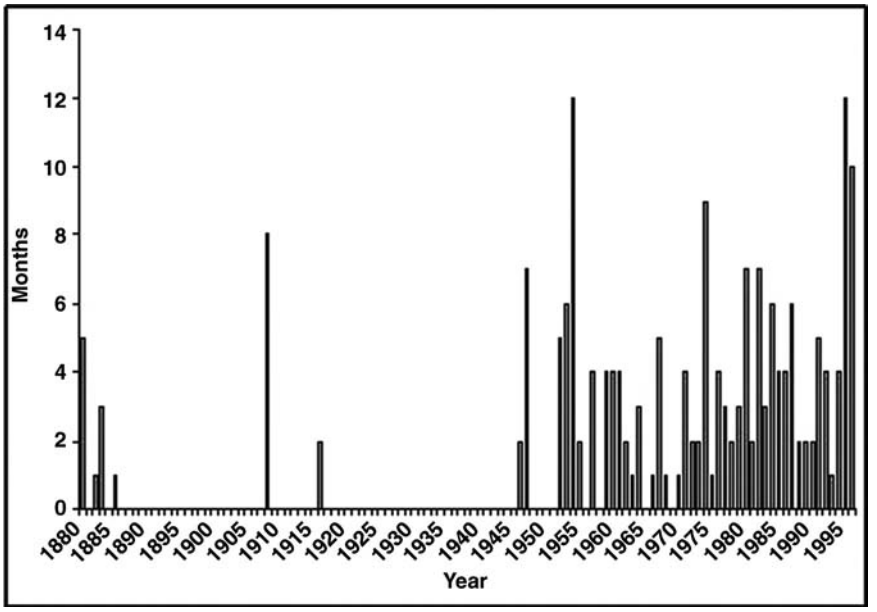

Figure 14.10
Long-term time series of red tides (duration of *Karenia brevis* blooms year^{-1}) off the west coast of Florida. About 70% of blooms lasted between one and four months with 15% lasting between eight and twelve months. No secular trend is apparent.
Source: Steidinger et al. (1997).

track the movements of existing blooms, and to forecast trajectories (Stumpf et al, 2003). An anomaly is identified when differences between the current chlorophyll field (from SeaWiFS imagery obtained in real time from OrbImage) and a mean field exceeds 1 μg l^{-1} (equivalent to 100 cells ml^{-1}), where the mean is a two-month running mean ending two weeks prior to the current image. Two months provides a sufficient number of images over a long enough period to be representative of the season. A two-week lag minimizes the possibility that a persistent and stationary bloom will bias the mean. This information is communicated to user groups in near real time via a web-based HAB Bulletin.

The ultimate goal is to predict the probability of a bloom in time and space and when and where it is likely to affect people and fisheries. This requires knowledge of the organism's physiology and environmental conditions that are likely to lead to and transport blooms. *K. brevis* has been reported to be both positively and negatively phototactic (Steidinger, 1975; Kamykowski et al., 1998). Blooms along the west coast of Florida often appear during upwelling-favourable winds when preceded by a period of calm winds (Stumpf et al., 1998). Although it is believed that blooms are initiated offshore, blooms often appear along the shoreline with no indication of offshore development based on satellite imagery (Stumpf et al., 2003). Together, these observations suggest that blooms are initiated and develop offshore at depth under calm conditions. With the development of wind-driven upwelling circulation, blooms are transported onshore with bottom water and transported to the surface by

coastal upwelling. Based on this hypothesis an alert was issued in the HAB Bulletin and a nearshore bloom was successfully forecasted in September, 2000 (Stumpf et al., 2003).

Developing capabilities such as this are an important step towards the development of models that predict where and when a bloom is likely to be initiated based on environmental conditions. The minimum set of observations needed to achieve this objective are as follows:

- *Forcings*: real-time wind fields and precipitation updated three to four times daily; river and stream flows and associated transports of sediments and nutrients updated weekly.
- *Ecosystem properties*: surface current, temperature, salinity and chlorophyll fields updated daily; vertical profiles of temperature, salinity, dissolved oxygen, inorganic nutrients, chlorophyll, coloured dissolved organic matter, and *K. brevis* cell densities at weekly (hot spots that have a history of frequent HABs) to monthly intervals (larger area, more stations).

The elements required to develop this capacity to provide the required data streams, data communications and management, and models exist in the form of the NOAA HAB remote sensing team[74], Texas Coastal Ocean Observation Network (TCOON) and the Texas Automated Buoy System (TABS) operated by Texas A&M University,[75] meteorological buoys and stations maintained by the National Data Buoy Center,[76] the Coastal Ocean Monitoring and Prediction System (COMPS) of the University of South Florida,[77] the Sustained Ecological Research Related to Management of the Florida Keys (SEAKEYS),[78] the National Estuarine Research Reserves (NERRS),[79] and a data management initiative of the NOAA National Coastal Data Development Center.[80] Collaboration among these efforts to form an integrated coastal ocean observing system for the region is a priority of the emerging Gulf Coast Ocean Observing System.[81]

14.5 Challenges

14.5.1 Research and implementation of operational oceanography

It will not be possible to develop operational models for predicting HABs based on environmental conditions until (a) the combination of environmental factors that promote the growth and accumulation of one species over others are quantified and (b) physical-biological interactions are parameterized (e.g. how environmental factors such as turbulence, advective transport, light, nutrient and grazing, and inherent biological attributes interact with each other to favour the development of a given species). Developing this capacity will require significant advances in our understanding on several fronts including the following:

[74] http://ccma.nos.noaa.gov/rsd/projects/habs/html, www.csc.noaa.gov/crs/habf/habmaps.html
[75] http://dnr.cbi.tamucc.edu/, http://gergu3.tamu.edu/Tglo/
[76] http://seaboard.ndbc.noaa.gov/
[77] http://comps.marine.usf.edu/
[78] http://coral.aoml.noaa.gov/sferpm/seakeys/
[79] http://inlet.geol.sc.edu/cdmohome.html
[80] www.ncddc.noaa.gov/habsos
[81] www-ocean.tamu.edu/GCOOS

- significant advances in understanding the processes of species succession;
- development of coupled, data assimilating physical-ecological models for operational use;
- advances in technologies for rapid detection of HA species abundance and toxicity; and
- development of sampling programmes that allow synoptic measurements of physical, chemical and biological variables in time and space using a combination of *in situ* and remote sensing techniques.

In terms of measurements, these include (a) more accurate estimates of sea surface chlorophyll *a* and accessory pigment fields on space scales of <1 km based on ocean-leaving radiance measurements from satellites and aircraft (improve the skill of Case 2 algorithms and increase spatial resolution); (b) long-term, high-resolution time series using *in situ* sensors on fixed platforms and autonomous underwater vehicles (e.g. gliders) to measure apparent optical properties and nutrient concentrations (N, P, Si) synoptically with temperature, salinity, currents and waves; (c) techniques for rapid, species-specific identification and enumeration, including near real-time measurement and telemetry of HA cell densities; (d) techniques for more rapid measurement of HA toxins, including *in situ* detection and near real-time telemetry and (e) rapid access to data from both *in situ* and satellite-based observations.

Until then, statistical models will be used to predict where and when HABs are likely to occur based on historical records of the location, frequency and magnitude of HABs or on correlations of HABs with environmental variables or indices. This not only places a high priority on research (predictive models, real-time sensing technologies), it places a high priority on detection, i.e. initially, GOOS must focus on the development of the capacity to detect HA species and toxins routinely and rapidly in the context of changes in the distribution of key environmental factors. To these ends, priority should be placed on the establishment of a global network of sentinel (early warning) and reference (to develop climatologies of HABs and associated environmental conditions) stations for long-term time-series observations and the development of an integrated data communications and management system for rapid access to and dissemination of data on HA species abundance, toxin concentrations, and key environmental variables (temperature, salinity, surface waves and currents, concentrations of inorganic and organic forms of N, P and Si). Hot spots where blooms are most likely to occur and have the greatest impact should be targeted.

14.5.2 Bridging the gap between science and management

Effective management and sustainable use also depend on efficient and timely coupling between advances in science and technology and their use for the public good. Today, there is an unacceptable disconnect between the two (Uman, 1993). Current modelling activities are a case in point. For the most part, models of HAB dynamics have been used primarily as research tools to test hypotheses concerning the development and dissipation of HABs and their sensitivity to different parameterizations and processes (e.g. Kamykowski, 1981; Franks, 1995; Yanagi et al., 1995). Important as they are for the purposes of science, such modelling activities have little impact on the formulation or implementation (decision-making) of environmental policies, in part

because there are no stakeholders involved other than scientists (Clark et al., 2001). For example, although the 1986 invasion of the Eurasian zebra mussel (*Dreissena polymorpha*) in North American waters was predicted in 1981 in the scientific literature, no management action was taken until after the invasion was well under way.

Declines in capture fisheries suggest a second important reason for the gap between science and management (Botsford et al., 1997). In the current mode of fisheries management, fisheries scientists advise managers based on annual stock assessments. Fisheries managers weigh this advice against their socio-political implications and set catch and size limits for the upcoming fishing season. Such scientifically based advice is often ignored in this process, in part because of two chronic problems that inhibit the development of ecosystem-based, adaptive management: first, the lack of long, high-resolution time series and spatially synoptic observations lead to large uncertainties in stock assessments, and this uncertainty undermines the credibility of scientific advice, especially when it calls for reductions in catch limits; and second, the time taken to make the required measurements and analyse the data is too long. Consequently, rates of data acquisition and analysis are not well tuned to the timescales on which decisions *should* be made for the purposes of adaptive management. This puts managers between a 'rock and a hard place' where politics usually wins the day. Effective implementation of adaptive management approaches would contribute to greater sustainability by reducing the uncertainty of predictions (Botsford et al., 1997).

These experiences, highlight the importance of involving stakeholders in the development of forecasting capacity (where stakeholders include government agencies responsible for formulating and implementing policy, those impacted by these policies, and those who provide the data and information on which policy decisions are made), as well as the importance of developing operational marine ecology.

Operational oceanography is not only needed to develop predictive models and routinely provide the required data and information on the timescales of decision-making processes, it is needed to maintain the integrity of the scientific process. Marine science will benefit from access to sustained data streams of known quality, and marine research is of fundamental importance to the successful development of the ocean observing system. However, to the extent that the scientific community attempts to engage in operational oceanography in isolation, advances in scientific understanding will be limited. Scientific research is driven by hypotheses that change with testing and new knowledge. The emphasis is on creativity and innovation; results are uncertain; and data streams come and go depending on the duration of research projects. Operational oceanography is driven by societal goals that generally do not change over time, for example protecting public health, environmental protection and sustaining living marine resources. The emphasis is on achieving these goals through routine and continuous provision of data and information of known quality at rates and in forms that are specified by the users. The flow, management and analysis of data of known quality are guaranteed and sustained based on recipes (common standards and protocols). Not only must potential user groups be entrained in the process of developing GOOS, training and education initiatives are urgently needed to establish the technical capacity to run an operational system (expand the 'operational' community), to educate potential consumers, to develop synergy between the research and operational communities, and to gain public support.

References

Abreu, P. C., Graneli, E., Odebrecht, C., Kitzmann, D., Proenca, L. A. and Resgalla, C. 1994. Effect of fish and mesozooplankton manipulation on the phytoplankton community of the Patos Lagoon Estuary, southern Brazil. *Estuaries*, 17, pp. 575–84.

Anderson, D. M., Glibert, P. M. and Burkholder, J. M. 2002. Harmful algal blooms and eutrophication: nutrient sources, composition and consequences. *Estuaries*, 25, pp. 704–26.

Arcos, D. F., Cubillos, L. A. and Núñez, S. P. 2001. The Jack mackerel fishery and El Niño 1997–98 effects off Chile. *Progr. Oceanogr.*, 49(1–4), pp. 597–617.

Babin, M., Roesler, C. S. and Cullen, J. J. (eds). 2006. *Real-time Coastal Observing Systems for Marine Ecosystem Dynamics and Harmful Algal Blooms: Theory, Instrumentation and Modelling*. Paris, Intergovernmental Oceanographic Commission of UNESCO. (Monographs on Oceanographic Methodology.)

Barber, R. T. and Chavez, F. P. 1986. Ocean variability in relation to living resources during the 1982–83 El Niño. *Nature*, 319, pp. 279–85.

Baretta, J. W., Ebenhoh, W. and Ruardij, P. 1995. The European Regional Seas Ecosystem Model, a complex marine ecosystem model. *Neth. J. Sea Res.*, 33, pp. 233–46.

Barry, J. P., Baxter, C. H., Sagarin, R. D. and Gilman, S. E. 1995. Climate-related, long-term faunal changes in a California rocky intertidal community. *Science*, 267, pp. 672–75.

Bates, S. S., DeFreitas, A. S. W., Milley, J. E., Pocklington, R., Quilliam, M. A., Smith, J. C. and Worms, J. 1991. Controls of domoic acid production by the diatom *Nitzchia pungens f. multiseries* in culture. *Can. J. Fish. Aquat. Sci.*, 48, pp. 1136–44.

Beaugrand, G., Reid, P. C., Ibañezs, F., Lindley, J. A. and Edwards, M. 2002. Reorganization of the North Atlantic marine copepod biodiversity and climate. *Science*, 296, pp. 1692–94.

Belgrano, A., Lindahl, O. and Hernroth, B. 1999. North Atlantic Oscillation primary productivity and toxic phytoplankton in the Gullmar Fjord, Sweden (1985–1996). *Proc. Roy. Soc. Lond. B*, 266, pp. 425–30.

Bjornsen, P. K. and Nielsen, T. G. 1991. Decimeter scale heterogeneity in plankton during a pycnocline bloom of *Gyrodinium aureolum*. *Mar. Ecol. Progr. Ser.*, 73, pp. 263–67.

Boesch, D. F. and Rabalais, N. N. 1991. Effects of hypoxia on continental shelf benthos: comparisons between the New York Bight and the northern Gulf of Mexico. In: R. V. Tyson and T. H. Pearson (eds), *Modern and Ancient Continental Shelf Anoxia*. Geological Society, pp. 27–34. (Special Publ. 58.)

Botsford, L. W., Castilla, J. C. and Peterson, C. H. 1997. The management of fisheries and marine ecosystems. *Science*, 277, pp. 509–15.

Boyer, G. L., Sullivan, J. J., Anderson, R. J., Harrison, P. J. and Taylor. F. J. R. 1987. Effects of nutrient limitation on toxin production and composition in the marine dinoflagellate *Protogonyaulax tamarensis*. *Mar. Biol.*, 96, pp. 123–28.

Busky, E. J. and Stockwell, D. A. 1993. Effects of a persistent 'brown tide' on zooplankton populations in the Laguna Madre of southern Texas. In: T. J. Smayda and Y. Shimuzu (eds), *Toxic Phytoplankton Blooms in the Sea*. Amsterdam, Elsevier, pp. 659–66.

Carlton, J. T. 1996. Marine bioinvasions: the alteration of marine ecosystems by nonindigenous species. *Oceanography*, 9, pp. 36–45.

Carpenter, S. R. 1988. Transmission of variance through lake food webs. In: S. R. Carpenter (ed.), *Complex Interactions in Lake Communities*. New York, Springer-Verlag, pp. 119–35.

Chapelle, A., Menesguen, A., DeslousPaoli, J. M., Souchu, P., Mazouni, N., Vaquer, A. and Millet, B. 2000. Modelling nitrogen, primary production and oxygen in a Mediterranean lagoon. Impact of oyster farming and inputs from the watershed. *Ecol. Model.*, 127, pp. 161–81.

Cicin-Sain, B. and Knecth, R. W. 1998. *Integrated Coastal and Ocean Management*. Washington DC, Island Press, 517 pp.

Clark, J. S., Carpenter, S. R. and others. 2001. Ecological forecasts: an emerging imperative. *Science*, 293, pp. 657–60.

Cosper, E. M., Bricelj, V. M. and Carpenter, E. J. (eds). 1989. *Novel Phytoplankton Blooms: Causes and Impacts of Recurrent Brown Tides and Other Unusual Blooms*. London, Springer-Verlag, 799 pp.

Costanza, R., d'Arge, R., de Groots, R., Farber, S., Grasso, M., Hannon, B., Limburg, K., Naeem, S., O'Neill, R. V., Paruelo, J., Raskin, R. G., Sutton, P. and van den Belt, M. 1997. The value of the world's ecosystem services and natural capital. *Nature*, 387, pp. 253–60.

Costanza, R., Kemp, W. M. and Boynton, W. R. 1993. Predictability, scale, and biodiversity in coastal and estuarine ecosystems: implications for management. *Ambio*, 22, pp. 88–96.

Dale, B. and Nordberg, K. 1993. Possible environmental factors regulating prehistoric and historic blooms of the toxic dinoflagellate *Gymnodinium catenatum* in the Kattegat-Skagerrak region of Scandinavia. In: T. J. Smayda and Y. Shimuzu (eds), *Toxic Phytoplankton Blooms in the Sea*. Amsterdam, Elsevier, pp. 53–57.

Davies, J. C. 1993. Environmental regulation and technical change: overview and observations. In: M. F. Uman (ed.), *Keeping Pace with Science and Engineering: Case Studies in Environmental Regulation*. Washington DC, National Academy Press, pp. 251–62.

Dickey, T. 1991. The emergence of concurrent high-resolution physical and bio-optical measurements in the upper ocean. *Rev. Geophys.*, 29, pp. 383–413.

Dickey, T. 2002. Emerging instrumentation and new technologies in the early 21st century. In: J. G. Field, G. Hempl and C. P. Summerhayes (eds), *Oceans 2020: Science for Future Needs*. Washington DC, Island Press, pp. 213–56.

Donaghay, P. L. and Osborn, T. R. 1997. Toward a theory of biological-physical control of harmful algal bloom dynamics and impacts. *Limnol. Oceanogr.*, 42, pp. 1283–96.

Duarte, C. 1992. Uncertainty of detecting sea change. *Nature*, 356, p. 190.

Dundas, I., Johannessen, O. M., Berge, G. and Heimdal, B. 1989. Toxic algal bloom in Scandinavian waters, May–June 1988. *Oceanography*, 2, pp. 9–14.

Falkowski, P. G., Hopkins, T. S. and Walsh, J. J. 1980. An analysis of factors affecting oxygen depletion in the New York Bight. *J. Mar. Res.*, 38, pp. 479–506.

Figueiras, F. G., Alvarez-Salgado, X. A., Castro, C. G. and Villarino, M. L. 1998. Accumulation of *Gymnodinium catenatum* in western Iberian shelf waters in response to poleward flowing slope currents. In: B. Reguera, J. Blanco, M. L. Fernández and T. Wyatt (eds), *Harmful Algae*. Proc. VIII International Conference on Harmful Algae (June 1997, Vigo, Spain). Santiago de Compostela/Paris, Xunta de Galicia/Intergovernmental Oceanographic Commission of UNESCO, pp. 114–17.

Fisher, W. S., Malone, T. C. and Giattina, J. D. 2003. A pilot project to detect and forecast harmful algal blooms in the northern Gulf of Mexico. *Environ. Mon. Assess.*, 81, pp. 373–81.

Flather, R. A. 2000. Existing operational oceanography. *Coast. Eng.*, 41, pp. 13–40.

Fraga. S., Anderson, D. M., Bravo, I., Reguera, B., Steidinger, K. and Yentsch, C. M. 1988. Influence of upwelling relaxation on dinoflagellates and shellfish toxicity in Ria de Vigo, Spain. *Estuar. Coast. Shelf Sci.*, 27, pp. 349–61.

Fraga, S. and Bakun, A. 1993. Global climate change and harmful algal blooms: the example of *Gymnodinium catenatum* on the Galician coast. In: T. J. Smayda and Y. Shimuzu (eds), *Toxic Phytopankton Blooms in the Sea*. Amsterdam, Elsevier, pp. 59–65.

Francis, R. C. and Hare, S. R. 1994. Decadal-scale regime shifts in the large marine ecosystems of the north-east Pacific: a case for historical science. *Fish. Oceanogr.*, 3, pp. 279–91.

Francis, R. C., Hare, S. R., Hollowed, A. B. and Wooster, W. S. 1998. Effects of interdecadal climate variability on the oceanic ecosystems of the northeast Pacific. *Fish. Oceanogr.*, 7(1), pp. 1–21.

Franks, P. J. S. 1995. Coupled physical-biological models in oceanography. *Rev. Geophys.*, Supp. July, pp. 1177–87.

Franks, P. J. S. 1997. Coupled physical-biological models for the study of harmful algal blooms. *Ocean Res.*, 19, pp. 153–60.

Franks, P. J. S. and Anderson, D. M. 1992. Toxic phytoplankton blooms in the southwestern Gulf of Maine: testing hypothesis of physical control using historical data. *Mar. Biol.*, 112, pp. 165–74.

Fromentin, J. M. and Planque, B. 1996. *Calanus* and environment in the eastern North Atlantic. II. Influence of the North Atlantic Oscillation on *C. finmarchicus* and *C. helgolandicus*. *Mar. Ecol. Progr. Ser.*, 134, pp. 111–18.

Gardner, R., Kemp, W. M., Petersen, J. and Kennedy, V. (eds). 2002. *Scaling Relations in Experimental Ecology*. New York, Columbia River Press.

GESAMP. 2001. *Protecting the Oceans from Land-based Activities: Land-based Sources and Activities Affecting the Quality and Uses of the Marine, Coastal and Associated Freshwater Environments*. GESAMP, 162 pp. (Reports and Studies 71.)

Granéli, E. et al. (eds). 1998. EUROHAB Science Plan. *Harmful Algal Blooms in European Marine and Brackish Waters*, EC-MAST-DGXII-NUTEK International Workshop Kalmar, Sweden, 5–7 November 1998, 100 pp.

Hallegraeff, G. M. 1993. A review of harmful algal blooms and their apparent global increase. *Phycologia*, 32, pp. 79–99.

Hallegraeff, G. M. 1998. Transport of toxic dinoflagellates via ship's ballast water: bioeconomic risk assessment and efficacy of possible ballast water management strategies. *Mar. Ecol. Progr.*, 168, pp. 297–309.

Heath, M. R. and Houde, E. D. 2001. Evaluating and modelling foraging performance of planktivorous and piscivorous fish. In: R. H. Gardener, W. M. Kemp, V. S. Kennedy and J. E. Petersen (eds), *Scaling Relations in Experimental Ecology*. New York, Columbia University Press, pp. 191–222.

Hofmann, E. E. and Friedrichs, M. A. M. 2002. Predictive modelling for marine ecosystems. In: A. R. Robinson, J. J. McCarthy and B. J. Rothschild (eds), *The Sea*. Vol. 12: *Biological-Physical Interactions in the Ocean*. New York, John Wiley & Sons, pp. 537–65.

Hofmann, E. E. and Lascara, C. M. 1998. Overview of interdisciplinary modelling for marine ecosystems. In K. H. Brink and A. R. Robinson (eds), *The Sea*. Vol. 10: *The Global Coastal Ocean. Processes and Methods*. New York, John Wiley & Sons, pp. 507–40.

Hood, R. R., Wang, H. V., Purcell, J. E., Houde, E. D. and Harding, L. W. Jr. 1999. Modelling particles and pelagic organisms in Chesapeake Bay: convergent features control plankton distributions. *J. Geophys. Res.*, 104, pp. 1223–43.

Howarth, R., Anderson, D., Cloern, J., Elfring, C., Hopkinson, C., Lapointe, B., Malone, T., Marcus, N., McGlahery, K., Sharpley, A. and Walker. D. 2000. Nutrient pollution of coastal rivers, bays and seas. *Issues in Ecology*, 7. (Ecological Society of America.)

Hu, C., Hackett, K. E., Callahan, M. K., Andréfouët, S., Wheaton, J. L., Porter, J. W. and Muller-Karger, F. E. 2003. The 2002 ocean color anomaly in the Florida Bight: a cause of local coral reef decline? *Geophys. Res. Lett.*, 30.

ICES. 1991. *Report of the Working Group on Phytoplankton and their Effects*. XX, International Council for the Exploration of the Sea. International Council Meeting Paper 1991/Poll, 3. (Mimeo)

IOC. 1998. *The Global Ocean Observing System Prospectus 1998*. Paris, Intergovernmental Oceanographic Commission of UNESCO, 168 pp. (GOOS Publication 42.)

Jackson, J. B. C., Kirby, M. X., Berger, W. H., Bjorndal, K. A., Botsford, L. W., Bourque, B. J., Bradbury, R. H., Cooke, R., Erlandson, J., Estes, J. A., Hughes, T. P., Kidwell, S. and Lange, C. B. H. S. 2001. Historical overfishing and the recent collapse of coastal ecosystems. *Science*, 293, pp. 629–43.

Johansson, N. and Granéli, E. 1999. Cell density, chemical composition and toxicity of *Chrysochromulina polylepis* (Haptophyta) in relation to different N:P supply ratios. *Mar. Bio.*, 135, pp. 209–17.

Johansson, N., Granéli, E., Yasumoto, T., Carlsson, P. and Legrand, C. 1996. Toxin production by *Dinophysis acuminate* and *D. acuta* cells grown under nutrient sufficient and deficient conditions. In: T. Yasumoto, Y. Oshima and Y. Fukuyo (eds), *Harmful and Toxic Algal Blooms*. Paris, Intergovernmental Oceanographic Commission of UNESCO, pp. 227–80.

Johns, D. G., Edwards, M., Richardson, A. and Spicer, J. I. 2003. Increased blooms of a dinoflagellate in the northwest Atlantic. *Mar. Ecol. Progr.*, 265, pp. 283–87.

Jumars, P. A. 1993. *Concepts in Biological Oceanography*. Oxford, UK, Oxford University Press.

Kamykowski, D. 1981. The simulation of a southern California red tide using characteristics of a simultaneously measured internal wave field. *Ecol. Model.*, 12, pp. 253–65.

Kamykowski, D., Milligan, E. J. and Reed, R. E. 1998. Biochemical relationship with the orientation of the autotrophic dinoflagellate *Gymnodinium breve* under nutrient replete conditions. *Mar. Ecol. Progr. Ser.*, 167, pp. 105–17.

Koblinsky, C. J. and Smith, N. R. (eds). 2001. *Observing the Oceans in the 21st Century* Melbourne, Bureau of Meteorology, GODAE Project Office.

Kudela, R. M. and Chavez, F. P. 2000. Modelling the impact of the 1992 El Niño on new production in Monterey Bay, California. *Deep Sea Res. II*, 47, pp. 1055–76.

Kusek, K. M., Vargo, G. and Steidinger, K. 1999. *Gymnodinium breve* in the field, in the lab, and in the newspaper – a scientific and journalistic analysis of Florida red tides. In: T. A. Villareal (ed.), *Cont. Mar. Sci.*, 34, pp. 1–229.

Levin, S. A. 1992. The problem of pattern and scale in ecology. *Ecology*, 73, pp. 1943–67.

Levitus, S. Antonov, J. L., Boyer, T. P. and Stephens, C. 2000. Warming of the world ocean. *Science*, 287, pp. 2225–29.

Lewis, M. R. and Platt, T. 1982. Scales of variability in estuarine ecosystems. In: V. S. Kennedy (ed.), *Estuarine Comparisons*. New York, Academic Press, pp. 3–20.

Lipp, E. K., Schmidt, N., Luther, M. and Rose, J. B. 2001. Determining the effects of El Niño-Southern Oscillation events on coastal water quality. *Estuaries*, 24, pp. 491–97.

Liu, K. K., Iseki, K. and Chao, S. Y. 2000. Continental margin carbon fluxes. In: R. B. Hanson, H. W. Ducklow and J. G. Fields, (eds), *The Changing Ocean Carbon Cycle*. Cambridge, UK, Cambridge University Press, pp. 187–239.

Maclean, J. L. 1989. Indo-Pacific red tides. *Mar. Pollut. Bull.*, 20, pp. 304–10.

Malone T. C. 1978. The 1976 Ceratium tripos bloom in the New York Bight: Causes and consequences. NOAA Tech. Rpt. NMFS Circular 410, pp. 1–4.

Malone, T. C. 2003. The coastal component of the Global Ocean Observing System GOOS: an assessment of current capabilities to detect change. *Mar. Pol.*, 27, pp. 295–302.

Malone, T. C. and Cole, M. 2000. Toward a global scale coastal ocean observing system. *Oceanography*, 13, pp. 7–11.

Malone, T. C., Conley, D. J., Fisher, T. R., Glibert, P. M., Harding, L. W. and Sellner, K. G. 1996. Scales of nutrient-limited phytoplankton productivity in Chesapeake Bay. *Estuaries*, 19, pp. 371–85.

Malone, T. C., Knap, A. and Fogarty, M. 2005. Overview of science requirements. In: A. R. Robinson and K. Brink (eds), *The Sea*. Vol. 13: *The Global Coastal Ocean: Multiscale Interdisciplinary Processes*. Boston, Harvard University Press.

Malone, T. C., Malej, A., Harding, L. W., Smodlaka, N. and Turner, R. E. (eds). 1999. *Ecosystems at the Land-Sea Margin: Drainage Basin to Coastal Ocean*. Washington DC, AGU, 381 pp. (Coastal and Estuarine Studies 55.)

Mantua, N., Haidvogel, D., Kushnir, Y. and Bond, N. 2002. Making the climate connections: bridging scales of space and time in the U.S. GLOBEC program. *Oceanography*, 15, pp. 75–86.

McKay, B. and Mulvaney, K. 2001. A review of marine major ecological disturbances. *Endangered Species Update*, 18, pp. 14–24.

McMinn, A. 1989. Late Pleistocene dinoflagellate cysts from Botany Bay, New South Wales, Australia. *Micropaleontology*, 35, pp. 1–9.

Michaels, A., Malmquist, D., Knap, A. and Close, A. 1997. Climate science and insurance risk. *Nature*, 389, pp. 225–27.

Millie, D. F., Kirkpatrich, G. J. and Vinyard, B. T. 1995. Relating photosynthetic pigments and *in vivo* optical density spectra to irradiance for the Florida red-tide dinoflagellate *Gymnodinium breve*. *Mar. Ecol. Progr.*, 120, pp. 65–75.

Millie, D. F., Schofield, O., Kirkpatrick, G. J., Johnsen, G., Tester, P. A. and Vinyard, B. T. 1997. Phytoplankton pigments and adsorption spectra as potential 'biomarkers' for harmful algal blooms: a case study of the Florida red-tide dinoflagellate, *Gymnodinium breve*. *Limnol. Oceanogr.*, 42, pp. 1240–51.

Moll, A. and Radach, G. 2001. Synthesis and new conception of North Sea research. Working Group 6: Review of three-dimensional ecological modelling related to the North Sea shelf system. Hamburg, Zentrum für Meeres- und Kli-maforschung der Universität Hamburg.

Myers, R. A. and Worm, B. 2003. Rapid worldwide depletion of predatory fish communities. *Nature*, 423, pp. 280–83.

Najjar, R. G., Walker, H. A. Anderson, P. J. and others. 1999. The potential impacts of climate change on the Mid-Atlantic coastal region. *Clim. Res.*, 14, pp. 219–33.

Newell, R. I. E. 1988. Ecological changes in Chesapeake Bay: are they the result of overharvesting the Eastern oyster (*Crassostrea virginica*)? In: M. P. Lynch and E. C. Krome (eds), *Understanding the Estuary: Advances in Chesapeake Bay Research*. Baltimore, Md., Chesapeake Bay Research Consortium, pp. 536–46. (Publ. 129.)

Nicholls, R. J. and Small, C. 2002. Improved estimates of coastal population and exposure to hazards. *EOS*, 83(28), p. 301.

Nihoul, J. C. J. and Djenidi, S. 1998. Coupled physical, chemical and biological models. In: K. H. Brink and A. R. Robinson (eds), *The Sea*. Vol. 10: *The Global Coastal Ocean. Processes and Methods*. New York, Wiley & Sons, pp. 483–506.

Nowlin, W. D., Briscoe, M., Smith, N., McPhaden, M. J., Roemmich, D., Chapman, P., O'Malley, J. F. R. and Wing, K. 2000. Forging a new tool for ecosystem reporting. *Environment*, 42, pp. 20–31.

Nowlin, W. D. and Malone, T. C. 2004. Research and GOOS. *J. Mar. Tech. Soc.*, 37, pp. 42–46.

Nowlin, W. D., Smith, N., Needler, G., Taylor, P. K., Weller, R., Schmitt, R., Merlivat, L., Vezina, A., Alexiou, A., McPhaden, M. and Wakatsuchi, W. 1996. An ocean observing system for climate. *Bull. Am. Meteor. Soc.*, 77, pp. 2243–73.

NRC. 1999. *From Monsoons to Microbes: Understanding the Ocean's Role in Human Health*. Washington DC, National Academy Press.

Odum, H. T. 1971. *Fundamentals of Ecology*. Philadelphia, Saunders.

Peierls, B. L., Caraco, N. F., Pace, M. L. and Cole, J. J. 1991. Human influences on river nitrogen. *Nature*, 350, pp. 386–87.

Pfiester, L. A. and Anderson, D. 1987. Dinoflagellate reproduction. In: F. J. R. Taylor (ed.), *The Biology of Dinoflagellates*, pp. 611–48. (*Bot. Monogr.* 21.)

Pingree, R. D., Pugh, P. R., Holligan, P. M. and Forster, G. R. 1975. Summer phytoplankton blooms and red tides along tidal fronts in the approaches to the English Channel. *Nature*, 258, pp. 672–77.

Powell, T. 1989. Physical and biological scales of variability in lakes, estuaries, and the coastal ocean. In: J. Roughgarden, R. M. May and S. A. Levin (eds), *Perspectives in Theoretical Ecology*. Princeton, N.J., Princeton University Press, pp. 157–80.

Powell, T., Cloern, J. E. and Walters, R. A. 1986. Phytoplankton and spatial distributions in south San Francisco Bay: mesoscale and small-scale variability. In: D. Wolfe (ed.), *Estuarine Variability*. New York, Academic Press, pp. 369–86.

Reid, P. C., Edwards, M. E., Hunt, H. G. and Warner, A. J. 1998. Phytoplankton change in the North Atlantic. *Nature*, 391, p. 546.

Richardson, K. 1997. Harmful or exceptional phytoplankton blooms in the marine ecosystem. *Adv. Mar. Biol.*, 31, pp. 301–85.

Robertson, G. P., Paul, E. A. and Harwood, R. R. 2000. Greenhouse gases in intensive agriculture: contributions of individual gases to the radiative forcing of the atmosphere. *Science*, 289, pp. 1922–25.

Robinson, A. R. 2002. Rapid assessment of the coastal ocean environment. In: N. Pinardi and J. D. Woods (eds), *Ocean Forecasting: Conceptual Basis and Applications*. New York, Springer-Verlag, pp. 199–229.

Robinson, A. R. and Lermusiaux, P. F. 2002. Data assimilation for modelling and predicting coupled physical-biological interactions in the sea. In: A. R. Robinson, J. J. McCarthy, and B. J. Rothschild (eds), *The Sea.* Vol. 12: *Biological-Physical Interactions in the Ocean*. New York, John Wiley & Sons, pp. 475–536.

Sanford, L. P. 1997. Turbulent mixing in experimental ecosystem studies. *Mar. Ecol. Progr. Ser.*, 161, pp. 265–93.

Schofield, O., Grzymski, J., Bisset, W. P., Kirkpatrick, G. J., Millie, D. F., Moline, M. and Roesler, C. S. 1999. Optical monitoring and forecasting systems for harmful algal blooms: possibility or pipe dream? *J. Phycol.*, 35, pp. 1477–96.

Sherman, K. and Duda, A. M. 1999. An ecosystem approach to global assessment and management of coastal waters. *Mar. Ecol. Progr. Ser.*, 190, pp. 271–87.

Shimizu, Y., Watanabe, N. and Wrensford, G. 1993. Biosynthesis of brevetoxins and heterotrophic metabolism in *Gymnodinium breve*. In: P. Lassus, G. Arzul, E. Erard, P. Gentien and C. Marcaillou (eds), *Harmful Marine Algal Blooms*. Paris, Technique et Documentation-Lavoisier/Intercept Ltd, pp. 351–57.

Small, C., Gornitz, V. and Cohen, J. E. 2000. Coastal hazards and the global distribution of human population. *Environ. Geosci.*, 7, pp. 3–12.

Small, C. and Nicholls, R. J. 2003. A global analysis of human settlement in the coastal zone. *J. Coastal Res.*

Smayda, T. J. 1990. Novel and nuisance phytoplankton blooms in the sea: evidence for a global epidemic. In: E. Graneli, B. Sundstron, L. Edler and D. M. Anderson (eds), *Toxic Marine Phytoplankton*. New York, Elsevier Science, pp. 29–40.

Sordo, I., Barton, E. D., Cotos, J. M. and Pazos, Y. 2001. An inshore poleward current in the NW of the Iberian Peninsula detected from satellite images and its relation with *G. catenatum* and *D. acuminata* blooms in the Galician *Rias*. *Estuar. Coast. Shelf Sci.*, 53, pp. 787–99.

Stammer, D., Bleck, R., Böning, C., DeMay, P., Hurburt, H., Fukumori, I., LeProvst, C., Tokmakian, R. and Wentzel, M. 2001. Global ocean modelling and state estimation in support of climate research. In: C. J. Koblinsky and N. R. Smith (eds), *Observing the Oceans in the 21st Century*. Melbourne, Bureau of Meteorology, GODAE Project Office, pp. 511–45.

Steele, J. H. 1985. A comparison of terrestrial and marine ecological systems. *Nature*, 313, pp. 355–58.

Steidinger, K. A. 1975. Implications of dinoflagellate life cycles on initiation of *Gymnodinium breve* red tides. *Environ. Lett.*, 9, pp. 129–39.

Steidinger, K. A., Vargo, G. A., Tester, P. A. and Tomas, C. R. 1997. Bloom dynamics and physiology of *Gymnodinium breve*. In: D. M. Anderson, A. E. Cembrella and G. M. Hallegraeff (eds), *The Physiological Ecology of Harmful Algal Blooms*. Amsterdam, Elsevier.

Stel, J. H., Behrens, H. W. A., Borst, J. C. and Droppert, L. J. (eds). 1997. *Operational Oceanography: the Challenge for European Co-Operation*. Proc. First International Conference on Euro GOOS, 7–11 October 1996. (Elsevier Oceanography Series 62.)

Stumpf, R. P., Ransibrahmanakul, V., Steindinger, K. A. and Tester, P. A. 1998. Observations of sea surface temperature and winds in association with Florida, USA red tides (*Gymnodinium breve*). In: B. Reguera, J. Blanco, M. L. Fernández and T. Wyatt (eds), *Harmful Algae*. Proc. VIII International Conference on Harmful Algae (June 1997, Vigo, Spain). Santiago de Compostela/Paris, Xunta de Galicia/Intergovernmental Oceanographic Commission of UNESCO, pp. 145–48.

Stumpf, R. P., Culver, M. E., Tester, P. A., Tomlinson, M., Kirkpatrick, G. J., Pederson, B. A., Truby, E., Ransibrahmanakul, V. and Soracco, M. 2003. Monitoring *Karenia brevis* blooms in the Gulf of Mexico using satellite ocean color imagery and other data. *Harmful Algae*, 25, pp. 1–14.

Subramaniam, A. and Carpenter, E. J. 1994. An empirically derived protocol for the detection of blooms of the marine cyanobacterium *Trichodesmium* using CZCS imagery. *Int. J. Rem. Sens.*, 5, pp. 1559–69.

Sundermeyer, M. A. 2001. Nowhere to hide – managing fisheries in real time. *ICES Newsletter*, 38, pp. 20–21.

Tester, P. A., Stumpf, R. P., Vukovich, F. M., Fowler, P. K. and Turner, J. T. 1991. An expatriate red tide bloom: transport, distribution, and persistence. *Limnol. Oceanogr.*, 36, pp. 1053–61.

Tilman, D., Fargione, J., Wolff, B., D'Antonio, C., Dobson, A., Howarth, R., Schindler, D., Schlesinger, W. H., Simberloff, D. and Swackhamer, D. Forecasting agriculturally driven global environmental change. *Science*, 292, pp. 281–84.

Uman, M. F. (ed.) 1993. *Keeping Pace with Science and Engineering: Case Studies in Environmental Regulation*. Washington DC, National Academy Press, 281 pp.

UNEP. 2001. Ecosystem-based management of fisheries: opportunities and challenges for coordination between marine Regional Fishery Bodies and Regional Seas Conventions. XX, United Nations Environment Programme. (UNEP Regional Seas Reports and Studies 175.)

Vanni, M. J. and Layne, C. D. 1997. Nutrient cycling and herbivory as mechanisms in the 'top-down' effect of fish on algae in lakes. *Ecology*, 78, pp. 21–40.

Vitousek, P. M., Aber, J. D., Howarth, R. W., Likens, G. E. and others. 1997. Human alterations of the global nitrogen cycle: causes and consequences. *Ecol. Appl.*, 7, pp. 737–50.

Walsh, J. J. and Steidinger, K. A. 2001. Saharan dust and Florida red tides: the cyanophyte connection. *J. Geophys. Res.*, 106, pp. 11597–612.

Warner, A. J. and Hays, G. C. 1994. Sampling by the continuous plankton recorder survey. *Progr. Oceanogr.*, 34, pp. 237–56.

Wilkinson, C., Lindén, O., Cesar, H., Hodgson, G., Rubens, J. and Strong, A. E. 1999. Ecological and socioeconomic impacts of the 1998 coral mortality in the Indian Ocean: an ENSO impact and a warning of future change? *Ambio*, 28, pp. 188–96.

Woods, J. 2002. Primitive equation modelling of plankton ecosystems. In: N. Pinardi and J. Woods (eds), *Ocean Forecasting, Conceptual Basis and Applications*. New York, Springer-Verlag, pp. 377–428.

Wyatt, T. 1995. Global spreading, time series models and monitoring. In: P. Lassus, G. Arzul, E. Erard, P. Gentien and C. Marcaillou (eds.), *Harmful Marine Algal Blooms*. Paris, Technique et Documentation-Lavoisier/Intercept Ltd, pp. 755–64.

Yanagi, T., Yamamoto, T., Koizumi, Y., Ideda, T., Kamizono, M. and Tamori, H. 1995. A numerical simulation of red tide formation. *J. Mar. Syst.*, 6, pp. 269–85.

Zingone, A. and Enevoldsen, H. O. 2000. The diversity of harmful algal bloom: a challenge for science and management. *Ocean Coast. Manag*.

15

Physics and physical modelling of harmful algal blooms

P. J. S. Franks

15.1 Introduction

There are many studies showing that the physics of the ocean is a central element in the dynamics of harmful algal blooms. Physical processes can transport, concentrate, dissipate, stimulate and kill off HABs. It is useful, then, to discuss in more detail the ways in which the motions of the ocean can manifest themselves in the dynamics of HABs. In practice these dynamics – both physical and biological – and their interaction are difficult to conceptualize, synthesize and analyse. To facilitate our understanding of the system we often synthesize the dynamics in the form of a coupled physical-biological model. This volume contains several excellent examples of such syntheses (Bissett et al., 2007; Fennel and Neumann, 2007; Lee et al., 2007; McGillicuddy et al., 2007; Pinardi et al., 2007 – Chapters 19, 17, 18, 16 and 20 this volume). This chapter introduces the neophyte oceanographer/modeller to the concepts that underlie the more advanced material presented in the later chapters, attempting to shed some light on the decisions that modellers must make in constructing their models, and the types of physical dynamics that can be important to the formation, growth, transport, and dissipation of HABs. Readers having a basic knowledge of calculus, biological oceanography, and physical oceanography should find this material accessible; it is my hope that the material presented here will allow a deeper understanding of the very difficult and insightful work that has gone into the models presented in later chapters.

This chapter is aimed largely at biological oceanographers with an interest in physical-biological interactions. Given this, the physical and modelling problems are motivated with biological examples. As a vehicle for this discussion, the flux-divergence or advection-diffusion equation is used for a HAB population, showing how the physical dynamics enter the equation and affect the local concentration of the species in question. It becomes apparent during this discussion that a detailed description of the physics is required in order to understand the spatial and temporal patterns of the biological variables, so the equations of motion, or momentum equations, are also discussed. While these equations are very complex, there are conditions under which simple solutions to the velocity field can be obtained that can be very useful in building understanding of the physical-biological couplings underlying HABs. However, for most realistic conditions the dynamics are so complex that the momentum equations must be solved numerically, necessitating the development of computer models of the flows. I will briefly discuss how such models are constructed, and some of the main considerations in developing, running and interpreting the output from such models. Finally,

a few of the physical dynamics that various types of model can and cannot reproduce, and how these dynamics might influence HAB population dynamics, are discussed. The field I am attempting to summarize is vast and growing. This chapter is a very basic roadmap for scientists interested in using models to understand the dynamics of their HAB species. I hope that the material will help researchers to ask appropriate questions when building physical-biological models, and be critical of the model output.

One point deserves special emphasis: there is no single 'best' model for studying HAB (or any plankton) dynamics. The model must be designed for the question being asked. Formulating a focused, testable hypothesis is one of the more critical aspects of model development, as it will dictate many aspects of the model's architecture, dynamics and forcings. A model without a question is like going to an airport and getting on a random plane: true, sometimes you end up in Paris. But more often you end up in a place like Cleveland. In a snowstorm.

15.2 Physical forcing of the biology

To understand the ways by which the physics of the ocean can affect a HAB population, it is useful to explore the flux-divergence (advection-diffusion) equation for the concentration (density, abundance per unit volume, nitrogen content per unit volume, etc.) of an arbitrary population *P*. We allow this population to swim vertically with an unspecified swimming behaviour, and it grows and dies as a function of factors such as its position in space, the ambient turbulence, the local density of the population, temperature *T*, irradiance *I*, any number of nutrients *N*, the local density of grazers *G*, and bacteria *B*, for example (see Table 15.1 for a full list of symbols). We also allow for growth of the population by metamorphosis from other stages (e.g. from cysts), and for depletion of the population through similar mechanisms. The details of the growth and mortality terms are fundamentally important for many problems. Here, however, we concentrate more on how those functions might depend on the ambient physical forcing. The more biological questions are left to others (see Bissett et al., 2007; Fennel and Neumann, 2007; Lee et al., 2007; McGillicuddy et al., 2007 – Chapters 19, 17, 18 and 16 this volume, for examples of biological models and the decisions/assumptions made in formulating the models).

The equation giving the rate of change of the local concentration of *P* is

$$\underset{1}{\frac{\partial P}{\partial t}} = \underset{2}{-u\frac{\partial P}{\partial x}} \underset{3}{-v\frac{\partial P}{\partial y}} \underset{4}{-w\frac{\partial P}{\partial z}} \underset{5}{-w_s\frac{\partial P}{\partial z}} \underset{6}{-P\frac{\partial w_s}{\partial z}} + \underset{7}{\frac{\partial}{\partial x}\left(K_x\frac{\partial P}{\partial x}\right)} + \underset{8}{\frac{\partial}{\partial y}\left(K_y\frac{\partial P}{\partial y}\right)} + \underset{9}{\frac{\partial}{\partial z}\left(K_z\frac{\partial P}{\partial z}\right)} + \underset{10}{\text{growth}(x,y,z,K_z,P,T,I,N,G,B,\ldots)} - \underset{11}{\text{mortality}(x,y,z,K_z,P,T,I,N,G,B,\ldots)} + \underset{12}{\text{sources}} - \underset{13}{\text{sinks}} \quad (15.1)$$

Table 15.1 Symbols and their units

Variable	Description	Typical units
A_x	Horizontal eddy viscosity	$cm^2\,s^{-1}$
A_y	Horizontal eddy viscosity	$cm^2\,s^{-1}$
A_z	Vertical eddy viscosity	$cm^2\,s^{-1}$
B	Bacteria concentration	cells/ml, µM N
F	Force	N
G	Grazer concentration	cells/ml, µM N
I	Irradiance	µEin $m^{-2}\,s^{-1}$
K_x	Horizontal eddy diffusivity	$cm^2\,s^{-1}$
K_y	Horizontal eddy diffusivity	$cm^2\,s^{-1}$
K_z	Vertical eddy diffusivity	$cm^2\,s^{-1}$
N	Nutrient or nitrogen concentration (Section 15.2)	µM N
N	Buoyancy frequency (Section 15.4.1)	s^{-1}
$O()$	Order of magnitude of an expression	
R	Rossby radius of deformation	m, km
Ro	Rossby number	dimensionless
S	Salinity	dimensionless
T	Temperature	°C
P	Plankton, phytoplankton concentration	cells/ml, µM N
a	Amplitude of internal wave	m
c	Bottom friction coefficient (Section 15.3.1)	$cm\,s^{-1}$
c	Phase speed of internal wave	$m\,s^{-1}$
d	Separation distance between two points in a turbulent flow (Section 15.2.1)	cm
d	Mean depth of pycnocline (15.3.1)	m
f	Coriolis frequency	s^{-1}
g	Acceleration due to gavity	$m\,s^{-2}$
h	Pycnocline depth	m
k	Horizontal wavenumber of internal wave in x direction	m^{-1}

(Continued)

Table 15.1 *(Continued)*

Variable	Description	Typical units
l	Horizontal wavenumber of internal wave in y direction	m^{-1}
m	Vertical wavenumber of internal wave in z direction	m^{-1}
p	Pressure	$N\ m^{-2}$
r_1, r_2	Perception distance	cm
t	Time	s
u	Horizontal velocity in x direction	$cm\ s^{-1}$
v	Horizontal velocity in y direction	$cm\ s^{-1}$
w	Vertical velocity in z direction	$cm\ s^{-1}$
w_s	Swimming speed in z direction	$cm\ s^{-1}$
x	Horizontal distance	cm, m, km
y	Horizontal distance	cm, m, km
z	Vertical distance	cm, m
z_{pyc}	Time-dependent depth of pycnocline	m
α	Expansion coefficient for temperature (Section 15.3)	$^{\circ}C^{-1}$
β	Encounter rate kernel (Section 15.2.1)	$cm^3\ s^{-1}$
β	Expansion coefficient for salinity (Section 15.3)	dimensionless
γ	Relaxation timescale for data assimilation	s, d
Δ	A small increment in e.g. t or x	
ε	Dissipation rate of turbulent kinetic energy	$cm^2\ s^{-3}$, $W\ kg^{-1}$
η	Kolmogorov length scale	cm
ν	Kinematic viscosity	$cm^2\ s^{-1}$
ρ	Density	$kg\ m^{-3}$
τ_y	Surface wind stress in y direction	Pa, $N\ m^{-2}$
ω	Frequency of internal wave	s^{-1}

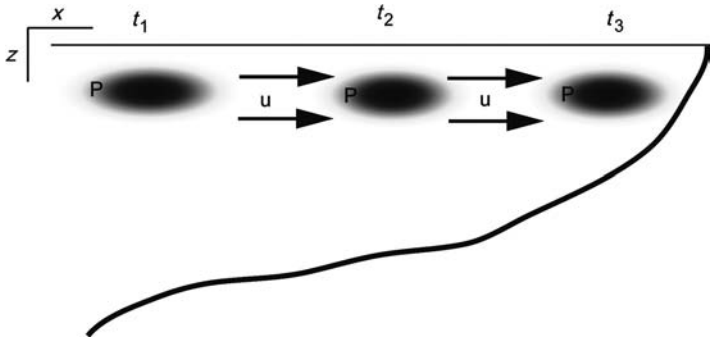

Figure 15.1
Across-shore advection of a patch of phytoplankton *P*, by velocity *u*, at three different times ($t_1 - t_3$). These are the dynamics underlying term 2 of (15.1): $u\partial P/\partial x$. An observer near the coast would see a sudden increase in *P* with time. Without information on the velocity field, it would be difficult to determine whether this increase was driven by growth or by advection.

The terms in (15.1) are numbered from 1 to 13, for ease of reference later. This equation is the same as (17.1) in Fennel and Neumann (Chapter 17), and (16.10) of McGillicuddy et al. (Chapter 16), although written in a different notation by each of us; I have expanded all the terms in the ∇ operator. The first term (1) represents what we generally seek from our models: the local rate of change of the population. Knowing the present population density *P* and $\partial P/\partial t$, we can calculate the new density at a later time. The problem is knowing $\partial P/\partial t$, as it depends on so many unknown or poorly constrained factors. Each of these factors is made explicit in the remaining 12 terms of (15.1).

Terms 2, 3 and 4 are the advection or transport terms. The physical velocities (*u, v, w*) move spatial gradients of *P* in the (*x, y, z*) directions. The importance of these terms to the local changes in *P* depends on the strength of the velocities, and the strength of the spatial gradients of *P*. The sudden appearance of a HAB population at a coastal site is often caused by a process such as described by term 2: $u\partial P/\partial x$. A cross-shore velocity *u* can move an across-shore gradient of *P* (such as a patch of *P* formed offshore) to cause sudden changes in the local *P*, independent of local growth (Figure 15.1).

Terms 5 and 6 of (15.1) arise from the vertical swimming behaviour of *P*. Because plankton are compressible, and can be squeezed together (unlike the water in which they reside), the swimming behaviour appears in two terms. The first term (5) is a swimming-induced advection of vertical gradients of *P*. If there is a layer of *P*, and the organisms all swim upward, the layer will move upward (by term 5), changing the local concentration as the layer passes by. The second term (6) has the local density of *P* being affected by the vertical gradient of the swimming speed. An easy way of visualizing the effect of this term is to consider phytoplankton swimming towards the surface of the ocean, where they must stop (otherwise they pop out of the surface ⋯) and accumulate. At the surface the upward swimming speed $w_s = 0$, while deeper down $w_s > 0$ (for upward swimming). Thus between the surface and just below the surface, w_s

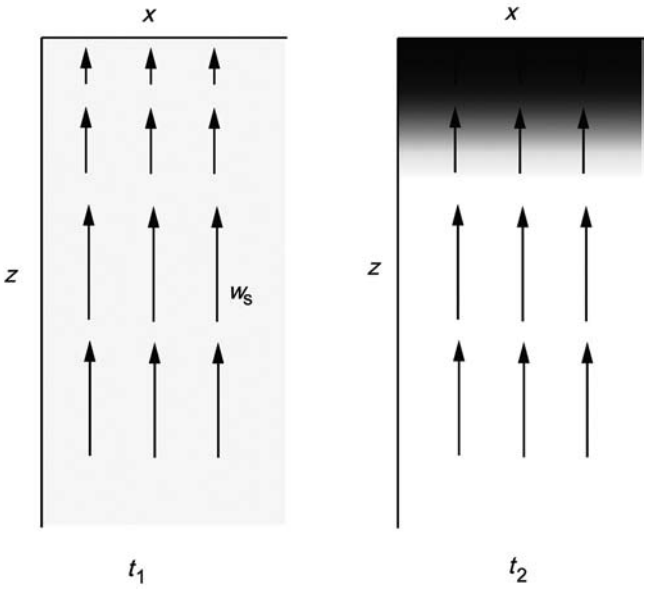

Figure 15.2
Phytoplankton swimming towards the surface where they must stop, causing the formation of a dense accumulation. These are the dynamics given by term 6 of (15.1): $P\partial w_s/\partial z$. Left panel (t_1), initial distribution of P; right panel, distribution at a later time t_2.

must change, giving a non-zero value for $\partial w_s/\partial z$, the vertical gradient of the swimming speed. Because they stop swimming at the surface, but keep swimming upward from below the surface, the phytoplankton must accumulate at the surface (Figure 15.2). This is the mechanism that forms such dense surface accumulations during red tides. However, the vertical gradient of the swimming speed, $\partial w_s/\partial z$ could be non-zero in other parts of the water column, leading to accumulations there. For example, dinoflagellates might have a behaviour that causes them to change their swimming speed in a strong local density gradient, or in response to a particular isolume. These behaviours could lead to dense subsurface layers of phytoplankton, invisible from the surface.

Terms 2 to 6 of (15.1) thus change the local concentration of P by moving gradients of P around with the ambient physical velocities, and by the swimming behaviour of the organisms. Terms 7 to 9 also act on spatial gradients of P, but through diffusion rather than advection. Whereas terms 2 to 6 can enhance local spatial gradients of P by stretching out existing patches or forming accumulations by swimming, terms 7 to 9 tend to reduce the spatial gradients of P by mixing across those gradients (Figure 15.3). For a careful and thorough derivation of the diffusion terms, Donaghay and Osborn (1997) are highly recommended. The strength of the mixing-induced flux of P is determined by the strength of the spatial gradient of P (patchiness), and the strength of the eddy diffusivities K_x, K_y and K_z. The way that (15.1) is written allows for spatial variations in the diffusivities, in all dimensions. This is particularly important in the vertical, where intense gradients of K_z can exist

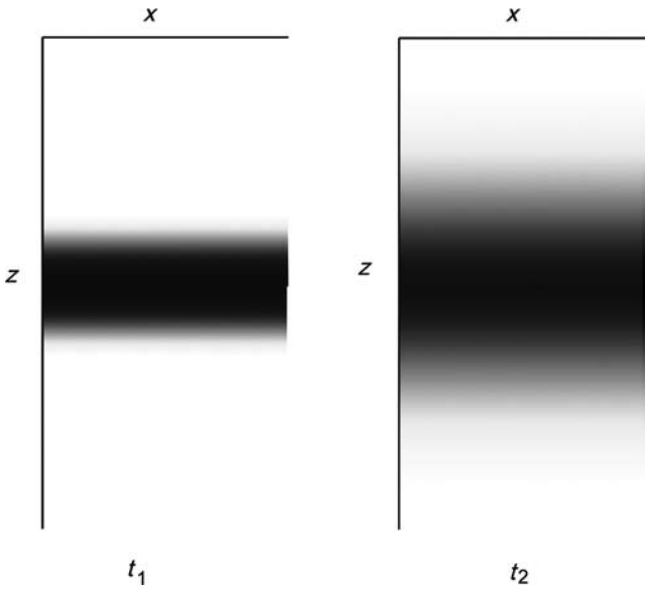

Figure 15.3
A layer of phytoplankton being diffused by a vertical eddy diffusivity. These patterns would result from the action of term 9 of (15.1): $K_z \partial^2 P/\partial z^2$. The thin layer in the left panel (t_1) spreads out vertically due to the effects of vertical mixing (t_2).

between the surface mixed layer and the seasonal pycnocline, for example. These mixing terms will tend to decrease the density at local population maxima, and increase populations at local minima by mixing from regions of high concentration to low. While at large (>5 m) scales vertical mixing tends to be many orders of magnitude weaker than horizontal mixing, the strong gradients of properties that exist in the vertical make vertical mixing of fundamental importance to biological problems. Organisms forming a layer through a vertical swimming behaviour, for example, must keep swimming towards the preferred depth to counteract the spreading effects of diffusion.

So far we have (from terms 2 to 9 of (15.1)) the physics affecting the local concentration of P by moving existing spatial gradients of P around, or by forming patches through swimming. The interactions of the physics with growth and mortality (terms 10 and 11) are more subtle and complicated, and vary depending on species and conditions. Only a few examples are explored here; a great deal of research remains to be done in quantifying the effects of physics on growth and mortality of phytoplankton.

The influences of physical forcings on growth and mortality can manifest themselves both directly and indirectly. A direct effect would be the decrease in growth rate of some dinoflagellates caused by turbulence. An indirect effect would be a situation in which the physical dynamics changed the irradiance by vertical advection through a light gradient, for example. Here several direct and indirect effects of physical forcings on growth and mortality are briefly explored.

15.2.1 Physical effects on growth and mortality: direct effects

Dinoflagellates present a particularly obvious case of physical influences on growth. The red-tide forming *Lingulodinium polyedrum* is known to be particularly sensitive to turbulence (e.g. Thomas and Gibson, 1990, 1992; Juhl et al., 2000, 2001; Juhl and Latz, 2002). Even low levels of turbulence-induced shear will decrease the growth rate of *L. polyedrum*, as well as increase the mortality rate of older populations (Juhl and Latz, 2002).

Turbulence can also affect the interactions among predators and prey in the plankton – the grazing part of the mortality term. This has been particularly well reviewed by Kiørboe and Saiz (1995) and references therein. Encounters between predators and prey are determined by the relative motion of the organisms. Plankton show a wide range of swimming and foraging behaviours, from run-and-tumble swimming, to ambush tactics. Turbulence can increase the relative motions of organisms, thereby increasing the encounters between predators and prey. In a water column with turbulence intensity ε (the dissipation rate of turbulent kinetic energy, units: $L^2\ T^{-3}$; this assumes that turbulence production is balanced by dissipation) the smallest energetic eddies have sizes determined by ε and the kinematic viscosity ν – the Kolmogorov length scale:

$$\eta = \left(\frac{\nu^3}{\varepsilon} \right)^{\frac{1}{4}}. \tag{15.2}$$

For typical dissipation rates of $10^{-6} < \varepsilon < 1$ cm^2 s^{-3}, η is usually less than 1 cm and greater than 0.03 cm, although these length scales are considerably smaller than the smallest energetic eddies (Lazier and Mann, 1989). The velocity difference between two points separated by distance d is given by

$$w = 0.42d \left(\frac{\varepsilon}{\nu} \right)^{\frac{1}{2}} \tag{15.3}$$

when $d < \eta$, and

$$w = 1.37 \left(\varepsilon d \right)^{\frac{1}{3}} \tag{15.4}$$

when $d > \eta$ but less than ~10 cm. In many situations (15.4) can be applied even though $d < \eta$.

For two populations with concentration C_1 and C_2 [individuals L^{-3}], the encounter rate E [encounters $L^{-3}\ T^{-1}$] is

$$E = \beta C_1 C_2, \tag{15.5}$$

where β is the 'encounter-rate kernel' [$L^3\ T^{-1}$]. For turbulence, the encounter-rate kernel is $\beta_{\text{turbulence}} = \pi d^2 w$, where w is defined in (15.3) and (15.4) (see Kiørboe and Saiz, 1995, for a more complete derivation). If the two organisms have perceptive distances

r_1 and r_2, then d is the separation immediately before contact ($d = r_1 + r_2$). Substituting (3) and (4) into the turbulence encounter-rate kernel we obtain

$$\beta_{\text{turbulence}} = 4.2\pi\varepsilon^{1/2}\left(r_1 + r_2\right)^3, \tag{15.6}$$

when $d < \eta$, and

$$\beta_{\text{turbulence}} = 1.37\pi\varepsilon^{1/2}\left(r_1 + r_2\right)^{7/3}, \tag{15.7}$$

when $d > \eta$. Note that the constants in (15.6) and (15.7) have units, but the units are different in the two equations. Comparison of the effects of turbulence versus behaviour on predator-prey contact rates in the plankton has shown that turbulence is most important for relatively stationary predators, such as copepods that employ an ambush strategy (Kiørboe and Saiz, 1995). As shown below, these microscale interactions are generally not explicitly included in physical-biological models of HABs.

15.2.2 Physical effects on growth and mortality: indirect effects

Physical dynamics can affect the growth and mortality of HAB populations by changing the environment around the populations. A simple example is vertical advection of a photosynthetic organism into or out of the euphotic zone ($w\partial P/\partial z$, term 4). Similarly, the physical diffusion terms can alter the chemical or biological characteristics of the waters inhabited by P by mixing with water masses with different properties. Thus nutrient-depleted waters could be replenished through upward mixing of deeper waters, although the symmetry of mixing dictates that waters containing the target population must also be mixed downward to the same extent, unless they can swim against the mixing. Mixing can also introduce new organisms to the waters inhabited by P, such as grazers, viruses or bacteria. The effects of each of these factors (light, nutrients, grazers, etc.) must be included in equations describing the growth response and mortality of the target population P. Elucidating these effects has occupied, and will continue to occupy, researchers for many decades.

As described in Section 15.2, physical forcings and swimming behaviours can change the local density of P. There are many aspects of growth and mortality of P that are potentially density-dependent and will therefore be affected by the flow-behaviour interaction. For example, sexual exchange requires two microscopic plankton cells to be in contact; an increased concentration of cells will dramatically increase the chances of two gametes encountering each other (15.5). Grazing is often density dependent – higher prey concentrations lead to higher ingestion rates, until the ingestion rate saturates. On the other hand, it is quite likely that many dinoflagellates and other HAB taxa induce a density-dependent *decrease* in grazing, for example through production of noxious chemicals that cause grazers to avoid dense aggregations.

The final two terms in the equation governing the local rate of change of P are sources and sinks. While growth and mortality are technically sources and sinks, this

concerns rather an organism with a complex life cycle; a source of planktonic vegetative cells could be excystment from a resting stage, while a sink could be the formation of gametes or cysts.

To complete the model, separate equations such as (15.1) would be written for each life stage, and each factor (state variable) such as nutrients or grazers that might vary in space and time. This would lead to a series of equations for each state variable, and the equations would be coupled through (usually) the growth/mortality, source/sink terms – the 'biology'. It is certainly possible that the equations would also be coupled through the physical terms if one organism affected the swimming behaviour of another, for example.

15.3 Solving equations for the physical dynamics

While (15.1) gives a complete description of the factors causing local changes in a population P, it is still very incomplete. The equation says exactly how P will respond to motions of the water (u, v, w), however, it says nothing about what those motions are. To find (u, v, w) we require another set of equations: the equations of motion, or the momentum equations.

Newton's second law of physics states

$$F = ma \tag{15.8}$$

or a force F is the product of a mass m and an acceleration a. This can be rewritten as $a = F/m$, or an acceleration is driven by a force scaled by a mass. This is the essence of the momentum equations, which give the local accelerations of the fluid in three dimensions as a function of the sum of the various forces acting on it. These forces include the advection and diffusion of spatial gradients in velocity (momentum), and forces such as the pressure gradient force, surface wind stress, and the Coriolis force that arises because of the rotating reference frame (earth):

$$\frac{\partial u}{\partial t} + u\frac{\partial u}{\partial x} + v\frac{\partial u}{\partial y} + w\frac{\partial u}{\partial z} = \frac{\partial}{\partial x}\left(A_x\frac{\partial u}{\partial x}\right) + \frac{\partial}{\partial y}\left(A_y\frac{\partial u}{\partial y}\right) + \frac{\partial}{\partial z}\left(A_z\frac{\partial u}{\partial z}\right) + fv - \frac{1}{\rho}\frac{\partial p}{\partial x} + F_x \tag{15.9}$$

$$\frac{\partial v}{\partial t} + u\frac{\partial v}{\partial x} + v\frac{\partial v}{\partial y} + w\frac{\partial v}{\partial z} = \frac{\partial}{\partial x}\left(A_x\frac{\partial v}{\partial x}\right) + \frac{\partial}{\partial y}\left(A_y\frac{\partial v}{\partial y}\right) + \frac{\partial}{\partial z}\left(A_z\frac{\partial v}{\partial z}\right) - fu - \frac{1}{\rho}\frac{\partial p}{\partial y} + F_y \tag{15.10}$$

$$\frac{\partial w}{\partial t} + u\frac{\partial w}{\partial x} + v\frac{\partial w}{\partial y} + w\frac{\partial w}{\partial z} = \frac{\partial}{\partial x}\left(A_x\frac{\partial w}{\partial x}\right) + \frac{\partial}{\partial y}\left(A_y\frac{\partial w}{\partial y}\right) + \frac{\partial}{\partial z}\left(A_z\frac{\partial w}{\partial z}\right) - \frac{1}{\rho}\frac{\partial p}{\partial z} + g + F_z \tag{15.11}$$

$$\frac{\partial u}{\partial x}+\frac{\partial v}{\partial y}+\frac{\partial w}{\partial z}=0 \tag{15.12}$$

Equations (15.9) to (15.11) give the mechanisms by which the local velocity (u, v, w) can change: advection of velocity gradients from somewhere else, diffusion of velocity gradients from somewhere else, rotation due to the Coriolis force, pressure gradients, and other non-specified forces. Notice that the first term in each of these three equations is an acceleration (e.g. $\partial u/\partial t$). Thus all the other terms of the equation have units of F/m or a force divided by a mass. These are the sources and sinks of momentum. The eddy viscosities (A_x, A_y, A_z) give the rate at which momentum is diffused by turbulent mixing; this rate does not have to be the same as the rate at which a chemical or organism is diffused (K in (15.1)).

Equation (15.12) is the condition of incompressibility, derived from the equation of continuity. It states that water is incompressible: if you move water in one direction, that water is replaced by water from somewhere else – there are no holes in the ocean.

These momentum equations are supplemented by an equation for the temporal changes in density,

$$\frac{\partial \rho}{\partial t}+u\frac{\partial \rho}{\partial x}+v\frac{\partial \rho}{\partial y}+w\frac{\partial \rho}{\partial z}=\frac{\partial}{\partial x}\left(K_x\frac{\partial \rho}{\partial x}\right)+\frac{\partial}{\partial y}\left(K_y\frac{\partial \rho}{\partial y}\right)+\frac{\partial}{\partial z}\left(K_z\frac{\partial \rho}{\partial z}\right)+F_x \tag{15.13}$$

which, like the other equations we have seen, shows that local changes in density are driven by advection and diffusion of gradients, and by sources and sinks of density (heating or freshwater input, for example). Separate equations for temperature and salinity can be written for the changes in these water properties. The simplest approximation to the equation of state is the linear equation

$$\rho=\alpha T+\beta S \tag{15.14}$$

where α is the expansion coefficient for temperature T, and β the expansion coefficient for salinity S. (Note that this β is different from the β of (15.5). The commonly accepted notation, in which unfortunately symbols overlap between biologists and physicists, is used.) While this clearly ignores the nonlinear relationship of density with T and S, it is an adequate approximation for many simple systems. The temperature and salinity values are used in the equation of state to obtain the density for the calculation, as density is relevant to the water motion. However, in many situations the changes to temperature and salinity must be considered separately from the density, for example when studying the effects of diel heat flux on circulation and stratification. In these situations there would be separate equations for the temporal changes in T and S, including their separate sources and sinks.

15.3.1 Simple physical systems and analytical models

The momentum equations provide the information for calculating the temporal changes in u, v, w, and ρ at any point in the fluid. These values can then be used in (15.1) to drive the changes in our HAB population P. But a quick glance at the momentum equations suggests that solving them (integrating them) for u, v and w would be a formidable task, exactly the task discussed below in the context of constructing a model. However, there are certain simplified forms of the momentum equations, or simplified geometries in which to study the flow, which that make the equations amenable to solution without a computer. This, of course, is what scientists did in the 'old days' (before computers), and there is a rich literature of 'analytical' solutions to the momentum equations, particularly prior to the 1980s. By analytical, I mean that the equations can be solved by calculus and algebra, rather than by the numerical methods described below. Here I discuss a couple of examples of such solutions giving flows that are relevant to HABs.

The momentum equations provide a 'dynamic' model of the three-dimensional velocity field. That is, the accelerations are calculated from the forces so that the velocities can eventually be known. Once the velocity field is known, an equation of the form $u = f(x, y, z, t,$ etc.) can be written. This is a 'kinematic' model of the flow: the velocities are known at all locations and for all times. The forces and accelerations have been included in the solution of the dynamic equations. One such kinematic flow is that generated by linear internal waves.

15.3.1.1 Example 1: internal waves

A common observation during a dense algal bloom is the formation of stripes of phytoplankton aggregations, often parallel to shore (Figure 15.4). How might such stripes form, and how do they relate to the motions of the water or the behaviour of the phytoplankton? This problem was considered by Kamykowski (1974), Franks (1997*a*) and more recently Lennert-Cody and Franks (1999, 2002). These researchers all looked to interactions between the internal wave field and the phytoplankton swimming as the source of these bands of phytoplankton. Consider a two-layered fluid separated by a pycnocline that moves up and down with a travelling wave given by

$$z_{\text{pyc}} = -d - a\sin(kx - \omega t), \tag{15.15}$$

where d is the average depth of the pycnocline (different from d in (15.3) to (15.7)) and a the amplitude of the wave. It is beyond the scope of this introduction to show how the equations and solutions are derived; a good description can be found in Gill (1982) or other similar texts. The horizontal and vertical velocities in the upper layer are

$$u_{\text{upper}} = \frac{ca}{z_{\text{pyc}}}\sin(kx - \omega t) \tag{15.16}$$

$$w_{\text{upper}} = \frac{za\omega}{z_{\text{pyc}}}\cos(kx - \omega t), \tag{15.17}$$

Figure 15.4
Bands of the dionflagellate *Lingulodinium polyedrum* moving onshore over the troughs of a series of internal waves.

with the phase speed c given by

$$c = \frac{\omega}{k}. \tag{15.18}$$

Similar equations can be derived for the lower-layer velocities. These equations for u and w can immediately be plugged in to (15.1) to give the horizontal and vertical velocity field. If we ignore diffusion, growth, mortality, and other sources and sinks, then the only dynamic that needs to be specified is swimming behaviour. The simplest behaviour to consider (at least mathematically) is a depth-keeping behaviour in which the swimming speed w_s exactly balances any vertical motion driven by the wave w. Thus $w_s = -w$ (the case when $w_s \neq -w$ is explored in Lennert-Cody and Franks, 1999). If we further assume an initially homogeneous distribution P_o of our HAB Species P, we soon find that temporal changes in P in the upper layer are given by

$$P_{\text{upper}}(x,t) = P_o\left(1 + \frac{a}{z_{\text{pyc}}}\sin(kx - \omega t)\right). \tag{15.19}$$

From this we can infer that accumulations of phytoplankton would occur over the wave troughs (compare (15.19) with (15.15): P_{upper} is at a maximum where z_{pyc} is at a minimum), and travel along with them as the wave propagates (both waves move with phase speed c). Interestingly, though the bands of high phytoplankton biomass travel with the wave, the individual phytoplankton do not – they merely get squeezed together and pulled apart horizontally as the wave passes. Such wave-mediated changes in HAB population density may be important for increasing the chances of successful sexual exchange during a bloom, by increasing the local concentration of cells.

15.3.1.2 Example 2: coastal wind-driven flows

Wind-driven flows are well known to be important in the transport of HABs in many areas of the world. Trying to understand the effects of temporally fluctuating and spatially variable winds in a complicated coastal region with capes, bays and subsurface topography is an extremely difficult problem. However, it can be simplified by ignoring complications such as time-dependence and irregularities in coastline shape. In these simplified situations, kinematic models of the wind-driven flows can be derived that can be useful in obtaining a first guess about the direction and magnitude of wind-driven transport.

In the first case, consider a long, straight coastline aligned with the y axis, and a wind blowing along the y axis with a surface wind stress τ_y. We also simplify the problem by assuming two homogeneous layers of thickness H_{upper} and H_{lower}, densities ρ_{upper} and ρ_{lower}, separated by a pycnocline at depth $h(x)$. In this case, all the vertical velocities are generated by changes in the pycnocline depth, h (Figure 15.5). Further, we ignore diffusion and the advection of momentum gradients (the 'nonlinear' terms of the equations of motion), as well as gradients in the alongshore direction (y). After some manipulation of the equations of motion, we obtain the simplified equations for the velocities in the upper layer:

$$\frac{\partial u}{\partial t} = fv + g\frac{\rho_{\text{lower}} - \rho_{\text{upper}}}{\rho_{\text{lower}}}\frac{\partial h}{\partial x}; \tag{15.20}$$

$$\frac{\partial v}{\partial t} = -fu + \frac{\tau_y}{\rho H_{\text{upper}}}; \tag{15.21}$$

$$-\left(\frac{1}{H_{\text{upper}}} + \frac{1}{H_{\text{lower}}}\right)\frac{\partial h}{\partial t} + \frac{\partial u}{\partial x} = 0 \tag{15.22}$$

where h is the depth of the pycnocline. These equations have solution

$$u = \frac{\tau_y}{f\rho H_{\text{upper}}}\left(1 - \mathrm{e}^{-x/R}\right) \tag{15.23}$$

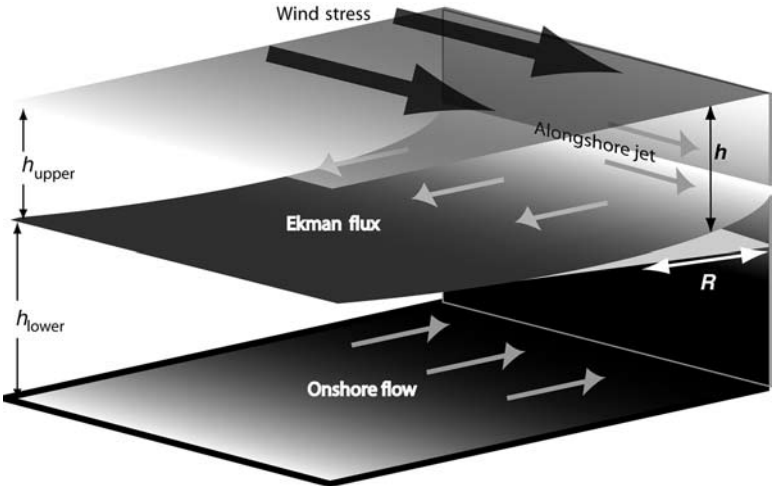

Figure 15.5
Schematic of wind-driven upwelling: the pycnocline of depth h is raised near the coast due to an offshore surface Ekman flux driven by the alongshore wind stress. The across-shore scale of curvature of the pycnocline is given by the baroclinic Rossby radius R.

$$v = \frac{\tau_y}{\rho H_{\text{upper}}} te^{-x/R} \tag{15.24}$$

$$h = \frac{\tau_y}{\rho} \frac{H_{\text{lower}}}{H_{\text{upper}} + H_{\text{lower}}} \frac{t}{fR} e^{-x/R}, \tag{15.25}$$

and

$$R = \frac{\sqrt{g \dfrac{\rho_{\text{lower}} - \rho_{\text{upper}}}{\rho_{\text{lower}}} \dfrac{H_{\text{upper}} H_{\text{lower}}}{H_{\text{upper}} + H_{\text{lower}}}}}{f}, \tag{15.26}$$

where R is the baroclinic Rossby radius of deformation (Figure 15.5). This is the familiar Ekman wind-driven upwelling, in which an alongshore wind τ_y drives an offshore flow of water u in the surface layer, with a compensating onshore flow in the lower layer. The across-shore variation of the flows and sea-surface height are determined by the Rossby radius of deformation: the flows decrease exponentially with distance from the coast. The alongshore flow v steadily increases with time at a given location at the coast, suggesting that HAB populations near the shore would be accelerated alongshore in the coastal jet in the direction of the wind. Populations farther offshore would experience significantly less alongshore transport.

Janowitz and Pietrafesa (1980) explored a system slightly more complex than that presented above: they allowed the bottom depth h (note that h is defined differently

here than in the previous problem) to slope montonically away from the coast, and the flow over the bottom to generate friction. With a linear bottom friction coefficient c, and wind blowing only along the y axis, the velocities were

$$u = -\frac{\tau_y}{\rho f h} \mathrm{e}^{-ct/h} \tag{15.27}$$

$$v = \frac{\tau_y}{\rho c}\left(1 - \mathrm{e}^{-ct/h}\right) \tag{15.28}$$

$$w = \frac{\tau_y z}{\rho f h^2} \frac{\mathrm{d}h}{\mathrm{d}x}\left(1 - \frac{ct}{h}\right)\mathrm{e}^{-ct/h} \tag{15.29}$$

Thus the along-shore and across-shore velocities decay exponentially with distance from the shore, the scale being determined by the time since the wind began blowing (t), the bottom depth h, and the bottom friction coefficient c (again, this c is not the same as the phase speed c in (15.17) to (15.19). Significantly, Janowitz and Pietrafesa also give the alongshore velocities for a time-dependent alongshore wind:

$$v = \frac{1}{\rho h}\int_0^t \tau_y(t') \exp\left(\frac{c(t-t')}{h}\right)\mathrm{d}t'. \tag{15.30}$$

Thus the alongshore current is an exponentially decreasing weighting of present and past alongshore wind stresses. Simple kinematic models such as these can quickly give us estimates of alongshore transport of populations under ideal conditions. All we need to know is the time series of the wind stress, the water depth, the density, and a guess at the friction coefficient. These are all relatively easily obtained: the friction coefficient c can be estimated from the wind stress and density as

$$c = \frac{1}{40}\left(\frac{|\tau_y|}{\rho}\right)^{1/2}, \tag{15.31}$$

while wind stress can be calculated from wind speeds that are often available from local airports, etc.

There are a great number of kinematic models such as these in the literature, for a wide range of geometries and forcings. Applying such models can be relatively straightforward and yield order-of-magnitude results fairly quickly.

15.3.1.3 Kinematic models and particle tracking

Suppose we knew the location of a patch of our HAB species, and wanted to know where it would be some time later. In a coastal wind-driven system we could get a first guess at the alongshore displacement using (15.28) and (15.31) to obtain the velocity

field. If the velocity is steady and spatially uniform, the displacement of a particle is simply a function of time:

$$x(t) = ut\,. \tag{15.32}$$

But what about more complex situations in which the velocity varies in space? We now need to know the flow contribution to particle displacement at every point along its trajectory. Unfortunately, we do not yet know its trajectory. To find the particle trajectory in a spatially dependent flow field, it is useful to calculate the particle's displacement at successive small increments. One derivation of this technique is based on the definition of the derivative and the definition of velocity. Velocity is defined as

$$u = \frac{\mathrm{d}x}{\mathrm{d}t}, \tag{15.33}$$

A derivative of a function *f(x)* with respect to *x* is defined as

$$\frac{\mathrm{d}f}{\mathrm{d}x} = \lim \Delta x \to 0\left(\frac{f(x+\Delta x)-f(x)}{\Delta x}\right). \tag{15.34}$$

If we similarly expand (15.33), we obtain

$$u = \frac{\mathrm{d}x}{\mathrm{d}t} = \lim \Delta t \to 0\left(\frac{x(t+\Delta t)-x(t)}{\Delta t}\right), \tag{15.35}$$

or rearranging and not taking the limit as Δt tends to zero,

$$x(t+\Delta t) = x(t) + u\Delta t\,. \tag{15.36}$$

Because we have allowed Δt to remain finite, this technique is called a 'finite difference' technique for solving the equation. If we know the initial location of a particle $x(0)$, we can calculate successive locations at later times using our knowledge of the velocity field $u(x, y, z, t)$ and iterating (15.36) over many time steps. This is thus an 'initial-value' problem, which we solve by stepping forward in time. This particular version of the finite-difference technique (and there are many), known as the Euler method, is not very accurate. Small errors in our approximation of Δt build up over time, leading to increasingly inaccurate values of our position, *x(t)*. The problems will be particularly evident if the flow varies in space and/or time; if u is constant everywhere, the Euler method will work quite nicely. Of course, most realistic flows are not constant in space and time, necessitating more elaborate schemes for finding $\mathrm{d}x/\mathrm{d}t$ and other derivatives ($\partial u/\partial t$, $\partial v/\partial t$, etc.). Finding accurate and stable finite-difference schemes to solve equations is one of the most fundamentally important aspects of numerical modelling. Unstable schemes may allow numerical instabilities that make models 'blow up' – velocities or phytoplankton may become infinitely large. Inaccurate difference schemes may create or destroy mass in the model, and can spread out spatial features through a numerical diffusion (see Section 15.3.2.1 for further discussion).

15.3.2 Complex physical systems and numerical models

Once we start to consider regions with complex coastline shapes and time-dependent forcing of the flows (realistic winds, freshwater input, or heat flux), solving the momentum equations analytically becomes impossible. So to provide the physical flow field for our biological model (15.1), we must resort to numerical methods to solve the equations of motion.

Solving an equation numerically involves making approximations to the actual equation, and iterating these approximations in space and time. For example, a simplified one-dimensional form of the u momentum equation (15.10) is

$$\frac{\partial u}{\partial t} + u\frac{\partial u}{\partial x} = 0. \tag{15.37}$$

If u has complicated spatial structure or time dependence, this innocuous equation is still difficult to solve. However, we can derive an approximation to the derivatives in (15.38) by expanding them in a Taylor series to obtain:

$$\frac{\partial u}{\partial t} = \frac{u(t+\Delta t) - u(t)}{\Delta t} - \frac{1}{2}\frac{\partial^2 u}{\partial t^2}(\Delta t) - \frac{1}{6}\frac{\partial^3 u}{\partial t^3}(\Delta t)^2 - \frac{1}{24}\frac{\partial^4 u}{\partial t^4}(\Delta t)^4 - O(\Delta t)^5 \tag{15.38}$$

$$\frac{\partial u}{\partial x} = \frac{u(x+\Delta x) - u(x)}{\Delta x} - \frac{1}{2}\frac{\partial^2 u}{\partial x^2}(\Delta x) - \frac{1}{6}\frac{\partial^3 u}{\partial x^3}(\Delta x)^2 - \frac{1}{24}\frac{\partial^4 u}{\partial x^4}(\Delta x)^4 - O(\Delta x)^5 \tag{15.39}$$

If we drop all the terms of the expansion that are multiplied by $(\Delta x)^n$ where $n \geqslant 1$, we can rewrite (15.38) in a finite-difference form:

$$\frac{u(t+\Delta t) - u(t)}{\Delta t} + u(x)\frac{u(x+\Delta x) - u(x)}{\Delta x} = 0 \tag{15.40}$$

or, rearranging so that all the terms with the 'new' time $t+\Delta t$ are on the left-hand side of:

$$u(x,t+\Delta t) = u(x,t) - \Delta t \cdot u(x,t)\frac{u(x+\Delta x,t) - u(x,t)}{\Delta x}. \tag{15.41}$$

This difference equation says that we can find the new velocity at point x by knowing the old velocity at this point, and subtracting the effects of the advection of gradients of velocity between points x and $x + \Delta x$. This is known as a 'forward difference', as it uses information ahead of the spatial point under consideration. We could also have used a 'backward difference' ($x - \Delta x$) to use information behind the point x. It should be intuitively obvious that if the local velocity $u(x, t)$ is directed towards $x + \Delta x$, then the forward scheme will not work, as it will not take into account the advection of velocity gradients from $x - \Delta x$, which are essential for determining the advective term. Obviously this method of finite differencing will

not work if the velocity field fluctuates from positive to negative in time or space. For such flows there are a myriad of schemes to calculate the spatial derivatives of the properties; a reference such as that of Haidvogel and Beckmann (1999) gives a good introduction to such techniques.

For our purposes, the important thing to note about (15.41) is that it solves the differential equation by dividing space and time up into discrete increments of Δx and Δt. This immediately suggests that we should use some sort of spatial grid to solve our equations at an array of points (x, $x + \Delta x$, $x + 2\Delta x$, $x + 3\Delta x$ ...). The simplest grid would be along the x axis, with points evenly spaced a distance Δx apart. The equations would be solved at each point, using the information from surrounding points to quantify the spatial gradients (derivatives) of the property.

While the difference scheme given by (15.41) is not very accurate, and I would not recommend anyone to use it, its simplicity makes it a useful model for understanding more accurate and complex difference schemes. Several aspects are common to most difference schemes, including issues of accuracy, averaging, boundary conditions and grid layout.

15.3.2.1 Accuracy and stability

Comparison of (15.41) and (15.36) shows that the temporal differencing ($\partial u/\partial t$) is the same in both, even though we derived them differently. The Euler method (15.36), which we derived from the definition of a derivative, is the same as taking a Taylor expansion of the derivative and then discarding all terms with Δt, Δt^2, etc. From (15.36) we know that the Euler method should give an exact estimate of the derivative if $\Delta t \rightarrow 0$. Conversely, we might suspect that the estimate of the derivative would be worse and worse, the larger we allow Δt to be. This is the case for both time and space: larger grids (larger Δt and Δx) give less accurate solutions for a given situation. Thus one way of improving the accuracy of the calculation is by making Δt and Δx as small as possible. The trade-off for this is that many more calculations must be performed for a given time or space interval, meaning that a computer will be running that much longer. Large models with small space and time steps can take longer than real time to solve the equations: a model running for a day might only calculate a few hours of model time. Furthermore, using a small spatial resolution requires a lot more computer memory to hold the whole grid during its calculation.

One way of improving the accuracy of the approximation to the derivative is not to throw away so many terms from the Taylor expansion in (15.38) and (15.39). Keeping terms with Δt^2 and Δx^2, for example, will significantly improve the accuracy of the derivatives for most situations, while only adding a modest increase in the number of calculations the computer has to perform. Such schemes are known as 'second-order' finite difference schemes. In general the order n of the scheme is determined by the exponent of the terms retained in the Taylor expansion: Δt^n and Δx^n.

Using a second-order scheme implies that at every time step we are making an error of Δx^2, which linearly adds to the error of the previous time step. Under certain conditions the error of the scheme can be amplified at each time step, and increases nonlinearly (exponentially) with time: the error becomes so large that the model blows up. To ensure the model's stability, several criteria must be met by the finite-difference scheme, the most important of which is the Courant-Friedrichs-Lewy (CFL) criterion: $|v| \leqslant \Delta x/\Delta t$. The velocity at a given grid point must not advect material a distance greater than Δx – a single grid point – in one time step. In ocean models this constraint

is usually most stringent for ocean waves, where v would be the phase speed of the wave, usually called c. However, even if a scheme satisfies the CFL condition, it may still be unstable.

15.3.2.2 Averaging

Once we have solved our equations on a spatial grid, we lose all information about the system at points between the grid points. All the spatial structures, physical-biological and biological-biological interactions on scales smaller than the grid are averaged out. A typical spatial grid (see below) might have a horizontal resolution of 1 km, and a vertical resolution of 1–10 m. Thus any processes occurring on vertical scales smaller than 1 m (i.e. most interactions among organisms), and horizontal scales less than 1 km (e.g. most internal waves and small fronts) will remain unresolved, and their effect on the solution lost. Trying to understand the importance of these 'lost' processes – particularly the biological ones – and parameterizing their effects on the scales resolved by our spatial grid is a relatively nascent field requiring a great deal more work.

In writing (15.1) and (15.10) to (15.14), I have been somewhat cavalier in the treatment of eddy diffusivities and viscosities. These coefficients are several orders of magnitude larger than the molecular diffusivity and viscosity, and are necessary to parameterize the 'average effect' of small-scale turbulent mixing that is not resolved at the scales of the computational grid. These terms arise mathematically (rather than physically) from fluctuating velocities through a process called 'Reynolds averaging'. It is important to remember that certain contributions are neglected and assumptions made during the Reynolds averaging, and there are some biological situations in which it might be desirable to retain these contributions. A thorough treatment of Reynolds averaging and its application to HAB problems can be found in Donaghay and Osborn (1997).

15.3.2.3 Boundary conditions

A glance at (15.41) shows that calculation of $u(x, t)$ requires information about $u(x+\Delta x, t)$. Of course, calculating $u(x+\Delta x, t)$ requires information about $u(x + 2\Delta x, t)$, and so on *ad infinitum*. At some point we have to set a boundary to our spatial domain, which requires specifying something about the grid points adjacent to the boundary. Two common boundary conditions are 'no flux' and 'open'.

Picture a two-dimensional (x, y) region with a velocity field $u(x, y)$ and $v(x, y)$. Suppose that this region has a coastline aligned along the y axis. It is reasonable to assume that there will be no flow or flux perpendicular to this coastline – the ocean does not typically suddenly move inland (except in special – and interesting – situations). The flux perpendicular to the y axis is aligned along the x axis, and is a combination of advection and diffusion. For our HAB population P, this flux in the x direction is

$$uP - K_x \frac{\partial P}{\partial x} \tag{15.42}$$

and we would set this equal to zero at the boundary. This boundary condition will keep material from passing through the boundary. This boundary condition was used, for example, by McGillicuddy et al. (2007 – Chapter 16 this volume) to set the diffusive flux of *Alexandrium fundyense* to zero at their model boundaries.

At a boundary that is not a wall, life gets a little more difficult. These 'open' boundaries represent mathematically ill-posed statements, and require special treatment so that properties (energy, mass, plankton) do not pile up at the boundary. One way of attempting to achieve this is to advect material out at the local water speed u:

$$\frac{\partial P}{\partial t} + u\frac{\partial P}{\partial x} = 0 \tag{15.43}$$

With no gradients of properties, there is nothing for advection or diffusion to act on, and material should pass undisturbed through the boundary. When spatial gradients are strong and there is strong time dependence to the velocity field, applying this open boundary condition can be a problem: it will only pass material moving at speed u; if there are other local velocities, material can build up or disappear at the boundary. This is very common with open boundaries, and a great deal of work is still being done in improving the accuracy of open boundary conditions in models (e.g. Marchesiello et al., 2001).

While it is not too difficult getting material out of the domain, it is much more difficult getting material into the domain in the absence of any information about the properties outside the grid. Often a no-gradient open boundary condition (e.g. $\partial P/\partial x = 0$) is applied in the absence of any other information. Such a condition assumes that the value at the boundary is the same as the point adjacent to the boundary. Another technique that is often used is to specify the property values at the boundary, based on information from field data or other models. For example, salinity and temperature are often set to values obtained from the Levitus atlas (e.g. Levitus and Boyer, 1994) along the deep-water open boundaries of numerical models. For our HAB population P this would appear as

$$P(x, y, z, t) = P_{\text{data}}(x_{\text{o}}, y_{\text{o}}, z_{\text{o}}, t_{\text{o}}), \tag{15.44}$$

where P_{data} is some value of P obtained from, say, a field programme in the region. P_{data} could be time- and space-dependent, and this information would propagate into the model domain with the physical flows. This necessitates a well-designed field programme, probably containing moorings with sensors for sustained measurements of both physical and biological/chemical properties. The synergy of observation and modelling is most evident in this context: models can be used to design better observation networks, while observations drive and constrain model dynamics.

If field data are used to drive fluxes into or within the model domain, differences among the field data and the local model values can cause sharp gradients in properties that will lead to unrealistic solutions. One technique to avoid this is to allow the model to 'relax' towards the field data, with a predetermined timescale γ:

$$P(x, y, z, t) = \frac{\left(P_{\text{data}}(x_{\text{o}}, y_{\text{o}}, z_{\text{o}}, t_{\text{o}}) - P(x, y, z, t)\right)}{\gamma}. \tag{15.45}$$

A short relaxation timescale (γ small) will force the model to adjust quickly to the data input. This technique is also known as 'nudging', and is used by Pinardi et al. (2007 – equation (20.3) this volume) to assimilate temperature data into their physical model. Using this (and similar techniques), field data can be gently 'assimilated' into models, constraining the model solutions to better reflect the data. These are extremely powerful techniques, allowing a strong, synergistic coupling of model and data. These techniques are well discussed by Pinardi et al. (Chapter 20), and McGillicuddy et al. (2007 – Chapter 16 this volume) in the context of both physical and biological data.

15.3.2.4 Boundary forcing

Even when a model architecture has been decided, the dominant physical processes identified, and the model constructed, the model must still be forced externally. The obvious forcings are surface heat flux, wind, freshwater flux and tides, although lateral fluxes through open boundaries can often dominate the signal in the model domain. Choosing an accurate representation of the boundary forcing is not always trivial, and can be critical to accurate reproduction of the model dynamics. For example, many products are now available to represent wind forcing in a model.[82] However, different wind products can have very different spatial resolution and spatial gradients, leading to strong differences in the wind-forced oceanic dynamics. It is always a good idea to run the model with a variety of forcings in order to decide which are the most accurate for the problem at hand. Pinardi et al. (2007 – Chapter 20 this volume) give an excellent description of the various data types used to force their model of the Mediterranean Sea.

15.3.2.5 Grid layout

The 'dimensionality' of a model is usually given by the number of spatial dimensions: the dimension of time is usually implicit in the statement (though not all models are time-dependent). A one-dimensional (1D) model has only one spatial axis, usually vertical or horizontal. The assumption here is that gradients of properties perpendicular to this axis are small compared with gradients along the axis. Most oceanographic 1D models are vertical, since vertical gradients tend to be thousands of times stronger than horizontal gradients. For this same reason, the vertical spatial resolution of models is usually much higher than the horizontal resolution.

A two-dimensional model defines a plane – either horizontal (x, y) or vertical: (x, z) or (y, z). This plane is divided into a grid in the two dimensions for finite-differencing the derivatives along both axes. An interesting problem arises in these grids: given that we have at least three variables with spatial gradients in (15.10)–(15.12) (u, v and p), how do we arrange them on the grid? Arakawa and Lamb (1977) explored the numerical properties of five two-dimensional grids (Figure 15.6), designated A to E. They found that the C grid (or 'Arakawa C grid') performed the best in their calculations, and it is the one usually employed in numerical models. On this grid, u and v are calculated at the midpoints of perpendicular faces of the grid, with pressure at the corners. Thus the velocity calculations always have a pressure term

[82]For example, COADS: Comprehensive Ocean-Atmosphere Data Set, http://www.ncdc.noaa.gov/oa/climate/coads/; ECMWF: European Centre for Medium-Range Weather Forecasts, http://www.ecmwf.int/; NCEP: National Centers for Environmental Prediction, http://polar.wwb.noaa.gov/winds/

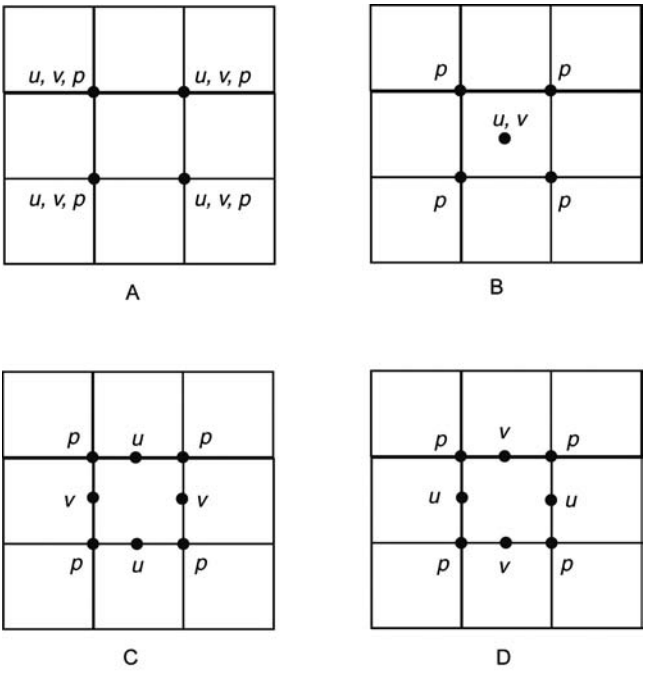

Figure 15.6
Four of the possible arrangements of the horizontal velocities u and v, and the pressure p on a rectangular grid studied by Arakawa and Lamb (1977). The 'C' grid is most commonly used.

between them in the direction of the flow. Apparently this improves the accuracy of the finite differencing.

A three-dimensional model defines a volume in three dimensions. The grid layout issues of the two-dimensional model are identical for a three-dimensional model, except that the grid is now a cube rather than a two-dimensional box. Thus the (u, v, w) velocities and pressure p must be arranged in a staggered form on the faces of the cube to ensure optimal accuracy of the finite differencing.

For two- and three-dimensional models some further developments in grid technology are worth mentioning. Consider a two-dimensional model in the (x, z) plane. If the bottom of the ocean is sloping, and we use a rectilinear rectangular grid of uniform box size, then as we configure the model in shallower and shallower water, the vertical resolution of our model has to decrease (Figure 15.7). Ultimately, in very shallow water near shore (or on subsurface banks, etc.), we may have only one or a few vertical grid points representing the entire water column. For many biological problems this is inadequate. So what solutions are proposed?

One way around this is to use a non-uniform rectangular grid, with higher vertical resolution near the surface where the biological gradients are the highest (Figure 15.7). When this grid is extended into shallow water, the high resolution near the surface will ensure that there are still several grid points defining the shallowest water column. This

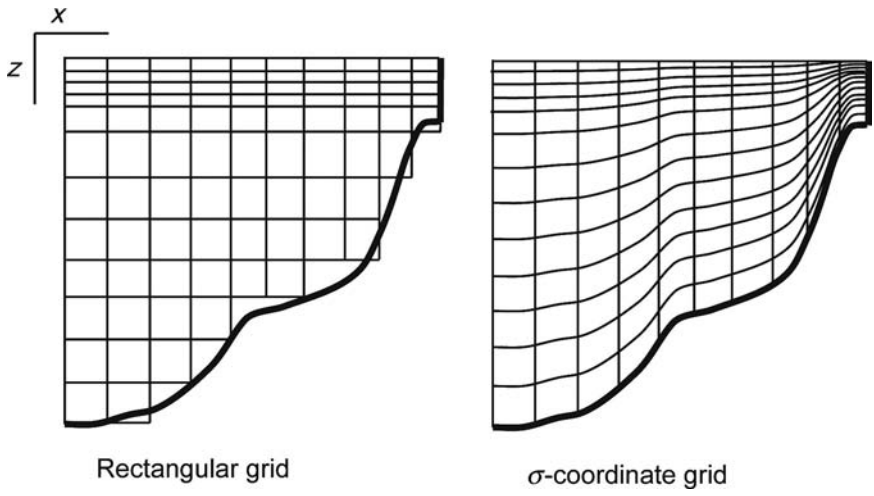

Figure 15.7
A rectangular grid (left panel) and a σ-coordinate grid (right panel) configured for an arbitrary bottom profile. Both grids are shown with enhanced resolution near the surface.

can be computationally expensive, however, as this high-resolution vertical grid has to exist everywhere in the model domain.

The most common solution to the disappearing grid in shallow waters is to define a terrain-following coordinate system, or 'σ-coordinate' system. In σ-coordinates, the same number of vertical grid points is used at every horizontal location. In regions of shallow water, the grid is squeezed together, and the vertical resolution increases (Figure 15.7). Each vertical grid point thus defines the same percentage of the water column vertically everywhere in the model domain. Some models allow an uneven spacing of σ levels vertically so that the surface waters might have better spatial resolution, for example. The σ-coordinate system is an excellent tool for solving equations in regions of complicated topography. One problem with the σ-coordinate system is that it can generate errors in the internal pressure terms in regions of shoaling bathymetry (Mellor et al., 1998). This problem seems to have been reduced in newer versions of models using σ coordinates.

While I have implied that most horizontal model grids are made up of rectangles, this is not strictly true, and many new models employ a 'non-orthogonal' grid. These grids are made up of triangles rather than rectangles, allowing significant changes in grid curvature and spatial resolution within the model domain (e.g. Figure 15.8). Such grids are particularly useful in regions of complex coastline shape, or complex undersea topography.

15.3.2.6 Mixed layers

When the wind blows across the surface of the ocean, some of the momentum causes vertical mixing of the water column, while some is used to accelerate the water horizontally. The question is, how much wind energy is used to do what? An inaccurate

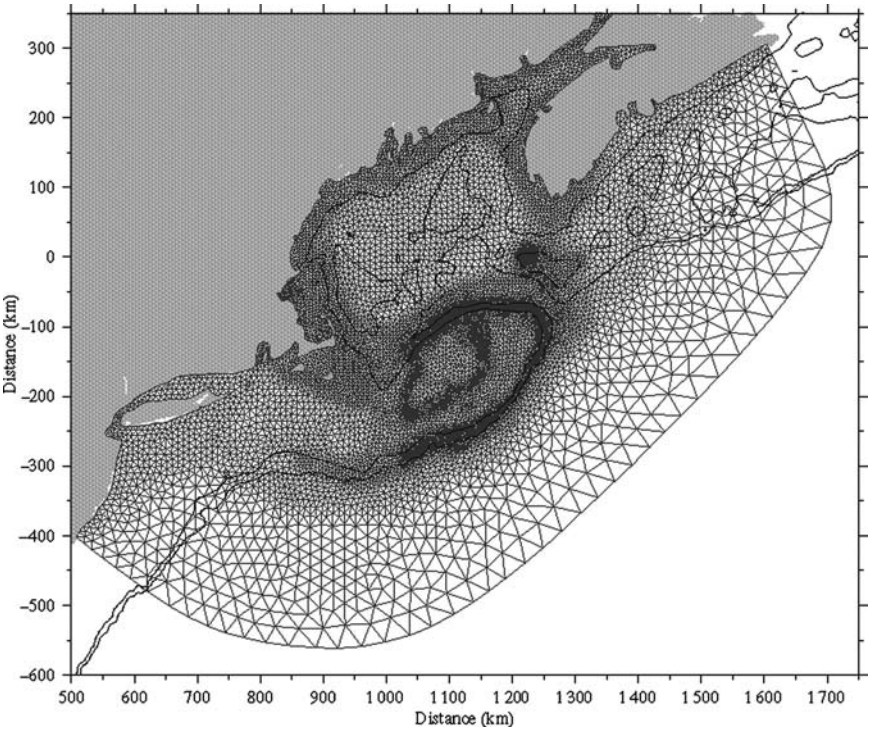

Figure 15.8
A non-orthogonal grid for a model of the Gulf of Maine and Georges Bank (north-east coast of the USA), showing the ability of the grid to conform to coastline shape and changes in bathymetry.
Source: modified from Chen et al. (2001).

transfer of the wind stress to the water could lead to surface transports that are too strong or weak, and inaccurate stratification. This can have profound effects on our interpretation of the biological patterns and dynamics. If we were to use (15.10)–(15.12) as they stand, they would do a pretty poor job of representing the effects of the surface wind stress, as there is no equation accounting for vertical and temporal changes in the vertical eddy viscosity A_z. For this we require a separate mixed-layer model.

Mixed-layer models come in two main forms: slab and turbulence-closure. A slab model assumes that the mixed layer is completely vertically homogeneous in all properties: u, v, ρ, P, etc. The mixed layer is a 'slab' of water that moves independent of the layers below it. A common form of the slab model is based on Garwood (1977). A turbulence-closure mixed-layer model allows for vertical structure in the mixed layer, by specifying a vertical profile of the eddy viscosity at each time step. A common form of the turbulence-closure model is the level 2.5 model of Mellor and Yamada (1982) (used, for example, by McGillicuddy et al., 2007 – Chapter 16 this volume). 'Level 2.5' refers to the level of parameterization of the model. In this case the vertical temperature variance is calculated (diagnosed) from the model data, while the variance

of turbulent kinetic energy is time dependent and predicted from the wind stress, stratification, and other variables. In other parameterizations explored by Mellor and Yamada, the temperature variance was also time dependent and predicted from the dynamics. It was found that for most purposes, this level of detail was not necessary in replicating the mixed-layer dynamics. Other mixed layer schemes may be encountered in various models, for example, the KPP mixing scheme of Large et al. (1994) used in the latest version of the Modular Ocean Model (Fennel and Neumann, 2007; Pinardi et al., 2007 – Chapters 17 and 20 this volume). It is prudent to rerun the model with more than one of these schemes before deciding which is the most appropriate for the given problem (e.g. Franks, 1997*b*).

15.3.2.7 Extant models

The material provided above is intended as a very brief introduction into the choices that a modeller might make when constructing and running a model. It would be folly to try to construct a model based on the information I have provided; luckily many excellent models exist in a form that is available to the community at large. Configuring and running these models, while difficult, is much easier than constructing them in the first place!

Table 15.2 Some common community model architectures

Model acronym	Model name	Website for further information
HYCOM	HYbrid Coordinate Ocean Model	http://oceanmodeling.rsmas.miami.edu/hycom/
MICOM	Miami Isopycnic Coordinate Ocean Model	http://panoramix.rsmas.miami.edu/micom/
MOM	Modular Ocean Model	http://www.gfdl.noaa.gov/~smg/MOM/MOM.html
OPA	Ocean Parallelise	http://www.lodyc.jussieu.fr/opa/
POM	Princeton Ocean Model	http://www.aos.princeton.edu/WWWPUBLIC/htdocs.pom/
ROMS	Regional Ocean Model System	http://marine.rutgers.edu/po/index.hp?model=roms&page=
SEOM	Spectral Element Ocean Model	http://oceanmodeling.rsmas.miami.edu/seom/seom_intro.html

A useful list of mostly US community models is available on the internet.[83] Of the 45 or so models described, about eight seem to be used the most, particularly for biological problems. These are HYCOM, MICOM, MOM, POM, ROMS and SEOM (Table 15.2). The first two (HYCOM and MICOM) are isopycnal, or hybrid isopycnal/z/σ-coordinate models developed at the University of Miami. MOM and POM use a rectangular grid and a σ-coordinate system, respectively. The last two models (ROMS and SEOM) were developed by Dale Haidvogel and colleagues at Rutgers University, and form a hierarchy of models with different vertical and horizontal grid schemes. ROMS is probably the most advanced of the models, including many options for grid schemes and mixed-layer models, as well as having biological modules built in. Many biological modellers in Europe use the OPA (Ocean PArallelise) system model which has both z- and s-grid vertical layering, and modules for sea ice, tracers, etc.

15.4 Can numerical models reproduce the physical dynamics?

While it may be intuitively obvious that a three-dimensional model will generally have a richer representation of the physical dynamics than a model of lower dimensionality, it is not always obvious exactly what sorts of physical dynamics are lost when the dimensionality is reduced. Here the types of dynamics that models of different dimensionality and geometry can and cannot reproduce are summarized. The review is structured by focusing on increasing timescales of motion, from turbulence at the shortest timescales, to fronts and eddies at the longer timescales.

15.4.1 Turbulence

The characteristic timescale for vertical oscillations of an isopycnal is the buoyancy frequency, N:

$$N^2 = \frac{g}{\rho}\frac{\partial \rho}{\partial z}. \tag{15.47}$$

Motions at higher frequencies are turbulent motions. In most models, turbulent motions cannot be included explicitly, and some average value is assigned to the grid point under consideration. The strength of the mixing is given either by some background constant value, or through a consideration of the dynamics that generate mixing: vertical shears, wind stress, etc. As discussed above, a separate turbulence model may be used to obtain a more realistic representation of the turbulence, allowing it to vary in time and space. In general, similar or identical turbulence models can be included in models of one, two or three spatial dimensions. Some of the issues in the coupling of the circulation model and the turbulence model include whether the mixed-layer depth must correspond to a model grid point, or whether it can vary continuously (e.g. Adamec et al., 1981; Franks and Walstad, 1997). Higher-order turbulence-closure models allow variation in the eddy diffusivities with depth. This structure of the mixing within the surface layers of the model may be critical to accurate representation of many biological processes. In models with vertical mixing

[83] http://stommel.tamu.edu/vbaum/ocean_models.html

that varies with depth, care must be taken when tracking particles in the flow (Visser, 1997). The structure of K_z dictates that the derivatives of K_z must be calculated and used in the calculation ((15.1), term 9).

In two- and three-dimensional models of many physical dynamics, accurate representation of both the surface and bottom boundary layers is necessary for reproducing the flows correctly. These boundary layers are generally turbulent, requiring thoughtful application of turbulence-closure submodels in these areas of the model domain. For example, the onshore bottom currents in some types of wind-driven coastal upwelling are an essential element for the replenishment of the surface offshore Ekman flux. However, accurate simulation of the bottom boundary layer requires accurate simulation of the turbulence intensity within the layer. Newer models use turbulence-closure models for this task, while older models often ignored the problem. Onshore transport in the bottom boundary layer may be important to HAB populations that have a benthic cyst stage, so care must be taken in choosing a model that will allow the appropriate dynamics.

15.4.2 Internal waves

In the ocean, internal waves oscillate between the buoyancy and Coriolis frequencies, with high-frequency (near buoyancy frequency) waves propagating horizontally, and low-frequency waves (near Coriolis) propagating vertically. Much of the vertical shear in the ocean below the pycnocline is caused by low-frequency internal waves. The direction of propagation of an internal wave is determined by the wave's frequency ω, the local buoyancy frequency N and the Coriolis frequency f:

$$\omega^2 = \frac{f^2 m^2 + N^2(k^2 + l^2)}{k^2 + l^2 + m^2}, \text{ or alternatively } \frac{m^2}{k^2 + l^2} = \frac{N^2 - \omega^2}{\omega^2 - f^2}. \quad (15.48)$$

Here (k,l,m) are the wavenumbers (wavenumber = 2π/wavelength) in the (x,y,z) directions. In the first form of (15.48), the wave's frequency is given as a function of its direction of propagation, while in the second form, the wave's direction of propagation (the ratio of the vertical wavenumber to the horizontal wavenumber) is given as a function of its frequency ω. Waves with small ω (low frequency) have a large vertical component to their propagation, and the phase travels upward or downward in the ocean. High-frequency waves (large ω) travel horizontally, much like surface waves. It is apparent from this dispersion relation that to correctly model a wave's direction of propagation it is necessary to accurately model the vertical gradient of density, which controls N. Too coarse a vertical resolution in a model will not allow accurate vertical variations in N, and potentially inaccurate representations of the wave's amplitude, frequency, and direction.

As discussed above, high-frequency waves can be important sites of accumulation for swimming plankton (e.g. Kamykowski, 1974; Franks, 1997*a*; Lennert-Cody and Franks, 1999, 2002, Figure 15.9), and nonlinear (large-amplitude) waves can be critical in transporting offshore organisms to nearshore habitats (Lamb, 1997; Pineda, 2001). High-frequency waves can alter the light regime seen by phytoplankton (Holloway, 1984) as they oscillate vertically through a light gradient. Low-frequency waves may contribute to the formation of thin layers of plankton by vertical shearing of existing along-isopyncal patchiness (Franks, 1995). If these processes are thought to be important to the population under consideration, it is critical to resolve the relevant waves in

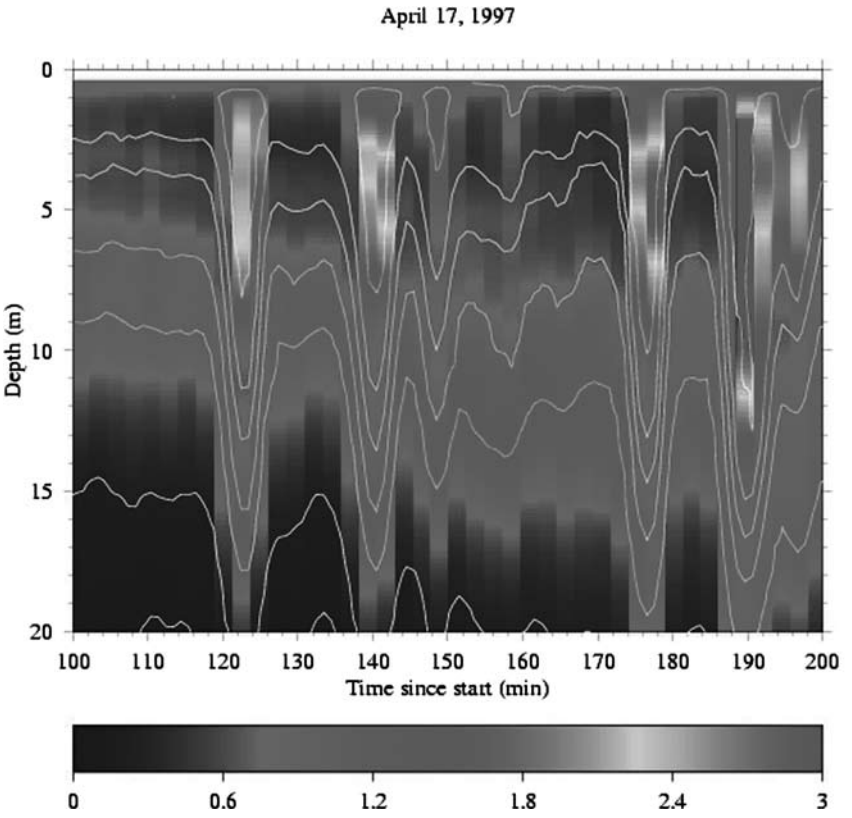

Figure 15.9
Phytoplankton fluorescence (colour scale) and temperature (white lines) during the passage of a series of nonlinear internal waves off the coast of San Diego, California. A CTD-fluorometer package was yo-yoed up and down each minute while the boat was at anchor. The patches of phytoplankton in the wave troughs probably formed through the interaction of swimming of the plankton and flows of the internal waves. *Source*: after Lennert-Cody and Franks (2002).

space and time. With horizontal wavelengths of 100 m or less, this requires a very fine spatial grid for the model, necessitating tradeoffs with the resolution of the larger scales due to computational limits of the computers.

Perhaps less well understood than internal waves are phenomena such as the internal tide. As the surface tide sweeps over a water column, it tends to make all the water particles in the column oscillate up and down and side-to-side in phase. However, when the water column is stratified, the surface tide can excite low-frequency internal waves known as the internal tide. In internal tides, water particles in a vertical column will oscillate side-to-side out of phase with depth, leading to vertical shearing of the water column. As these waves propagate into waters of different depths, the waves can

break leading to persistent patches of well-mixed water (e.g. New and Pingree, 1990). It is possible that nutrients are transported vertically in such patches, and that they may contribute to local primary production. This has not been well explored in models or the field.

Internal waves can be fairly well represented in three-dimensional models, while two-dimensional (*x, z*) or (*y, z*) models will only allow waves to propagate in the model plane. This will not allow the effects of rotation in advecting property gradients perpendicular to the model plane by the low-frequency internal waves, and will alias high-frequency waves into low-frequency waves if they propagate at an angle to the model plane.

Two-dimensional models in the (*x, y*) plane have no vertical gradients, and so cannot allow vertically propagating internal waves. However, some forms of the momentum equations can be modelled in the (*x,y*) plane such that the surface acts as a pycnocline separating a surface layer from a deeper layer. Waves traveling on this surface would be analogous to interfacial waves of various types (linear and nonlinear shallow-water waves, coastal-trapped waves, etc.). Models such as this are sometimes referred to as '1 1/2' layer models: they are only one layer thick, but a second (upper) layer is implicit in the formulation.

Internal waves cannot be accurately modelled in most one-dimensional architectures. This can present problems for the physics, since internal wave-generated shears will be missing as a mechanism for generating turbulence. Some models parameterize these missing shears by including a bulk term; the vertical oscillations forced by such waves will still be missing from the model. Thus motions that are potentially important to the plankton are left out of the model.

15.4.3 Fronts, eddies

At timescales longer than the Coriolis period ($2\pi/f$, or about one day depending on latitude), horizontal density gradients tend to be balanced by the Coriolis force, leading to a velocity jet along the horizontal density gradient. This is the 'geostrophic' balance, and is easily derived from the horizontal momentum equations (15.10) and (15.11) by assuming that the Rossby number is small. The Rossby number is the ratio of the nonlinear terms (the tendency for a water parcel to keep going in a straight line) to the Coriolis term (the tendency to be rotated to the right of the direction of motion in the northern hemisphere):

$$Ro = \frac{u}{fL} \cdot \tag{15.49}$$

Here u is a characteristic horizontal velocity, f is the Coriolis frequency, and L is a length scale characteristic of the motion. Small Rossby numbers imply a relatively strong Coriolis force, leading to a balance of the horizontal pressure gradient and Coriolis:

$$fu = -\frac{1}{\rho}\frac{\partial p}{\partial y} \tag{15.50}$$

$$fv = \frac{1}{\rho}\frac{\partial p}{\partial x} \cdot \tag{15.51}$$

When this balance is achieved, horizontal density gradients become relatively stable, forming fronts with an accompanying along-front jet. Such fronts can be formed by wind, tides, freshwater influx, flow around islands, and the abutment of dissimilar water masses, for example. Fronts have been implicated in many aspects of HAB dynamics (e.g. Franks, 1992), and are particularly important to resolve in HAB models.

To determine the spatial resolution of a model that will resolve fronts, it is important to know the characteristic scale of the front. A cross-frontal scale is given by the baroclinic Rossby radius of deformation, R (15.27). In most situations $2 < R < 20$ km. To properly resolve a front, you would want to have at least 5 grid points over a Rossby radius, giving a mesh resolution of $0.4 < \Delta x < 4$ km.

Eddies are fronts that have wrapped around and closed on themselves, forming a cylindrical front. Eddies are often formed when a relatively linear front becomes unstable; small perturbations along the front grow in amplitude, finally pinching off into eddies that can propagate away from the front (Figure 15.10). This instability is

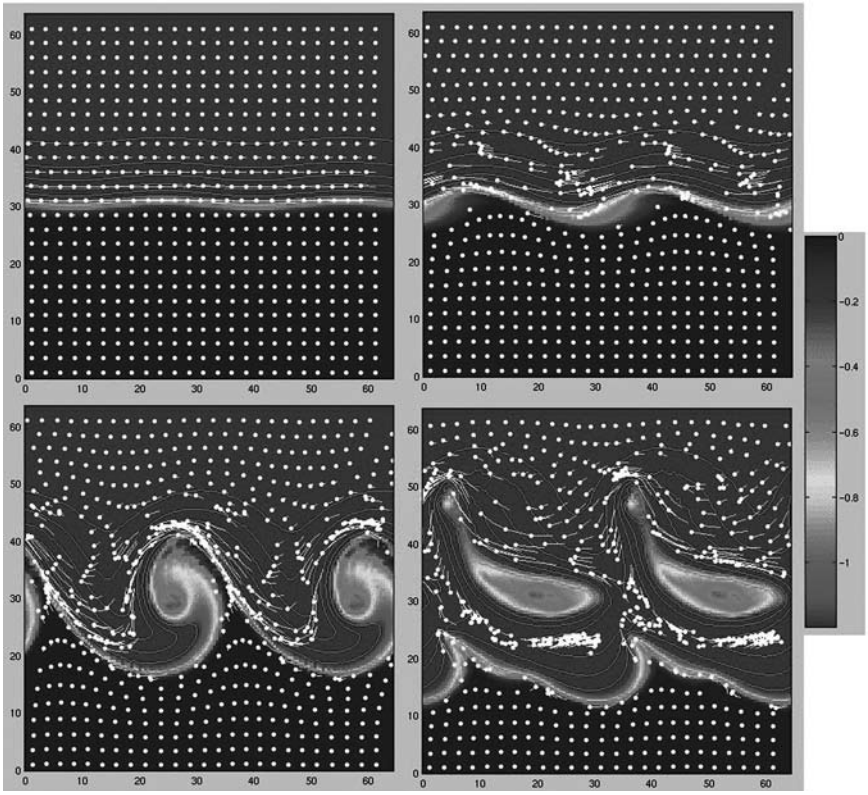

Figure 15.10
Four plan views of a front going unstable (day 0: upper left, day 4: upper right, day 8: lower left, day 12: lower right). Blue colours are cold inshore (upwelled) water, while red colours indicate warmer offshore waters. The white particles are trapped at the surface. Note how particles can accumulate due to the vertical velocities of the eddies.
Source: Pringle and Franks, unpublished data.

controlled by the stratification, the bottom slope, the source of the perturbation (e.g. coastline shape), and other external forces such as wind stress (e.g. Barth, 1989*a*, 1989*b*; Wang, 1993; Spall, 1997; Dale and Barth, 2001). Eddies formed through frontal instabilities are potentially very important sources of cross-shelf transport of HAB populations, but this process has not been explored in models or in the field, as far as I know.

As eddies interact with each other, they can generate intense vertical velocities over relatively small spatial regions. These vertical velocities can be important sources of nutrient supply to the euphotic zone, subduction of existing populations, or concentration of floating or swimming organisms (e.g. Spall and Richards, 2000; Levy et al., 2001). Accurate modelling of such dynamics may be critical to understanding the dynamics underlying observations of HAB populations (Figure 15.11).

Fronts, frontal instabilities, eddies and eddy-eddy interactions can all be well modelled in three-dimensional models of ocean dynamics if they have a small enough spatial resolution. Fronts formed by wind-driven upwelling are often explored using two-dimensional (*x, z*) cross-shore models. While such models will capture some of the features of coastal wind-driven upwelling, they cannot reproduce the alongshore dynamics – pressure gradients, along-front instabilities, and others, that characterize such systems. In most situations, the assumption of alongshore homogeneity in wind-driven upwelling systems is not a good one, and most modelling studies attempting to reproduce field data in these systems find that alongshore gradients often dominate the observed signal in the physics (e.g. Gan and Allen, 2002*a*, 2002*b*). Thus the results of two-dimensional coupled biological-physical models of wind-driven upwelling and other potentially unstable frontal systems should be viewed somewhat sceptically. The

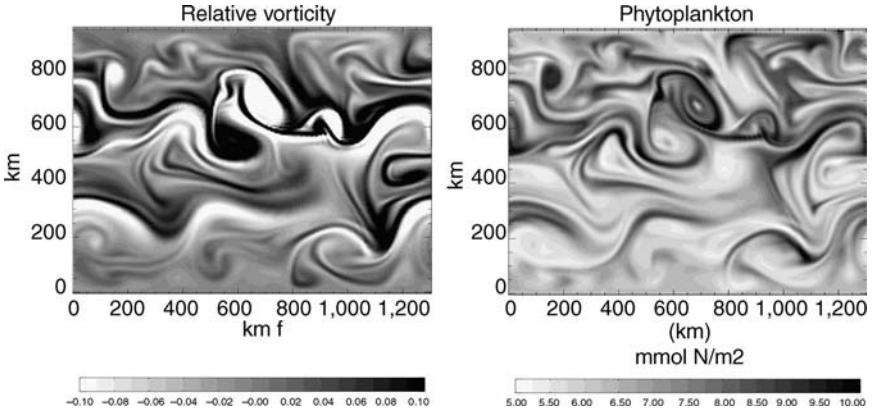

Figure 15.11
Left panel: plan view of relative vorticity generated by eddy-eddy interactions near a frontal zone in a model; right panel: phytoplankton biomass integrated over the upper 150 m in the eddy field of the left panel. Notice the strong correspondence of patches (and deficits) of phytoplankton with the vorticity field.
Source: adapted from Lévy and Klein (2004).

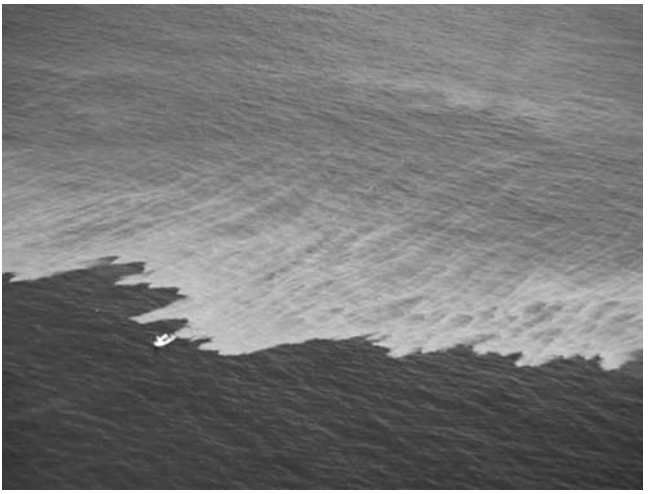

Figure 15.12
A 3 m long boat passing through a band of Noctiluca scintillans that has accumulated at a front formed by a nonlinear internal wave off the coast of San Diego, California. The dense part of the band is <20 m wide, and would be unresolved by most coastal models.

essential, and important, frontal instability mechanisms cannot be reproduced in such models.

Eddies and fronts can be well-represented in some types of two-dimensional (*x, y*) models, though the flows are often kinematic rather than dynamic (e.g. Abraham, 1998). Such models can be useful for certain types of biological problems, though the lack of vertical resolution often limits their utility.

Fronts formed by the influx of freshwater into coastal seas are of particular interest to HAB researchers. As the freshwater flow propagates along the coast under the influence of the Coriolis force, the pressure gradient, surface wind stress and coastal topography, the leading edge of the front is not in a geostrophic balance. Indeed, the water behind the front often propagates faster than the front itself, creating a convergence at the front. These convergence zones, also seen at nonlinear waves, have much smaller cross-frontal scales than given by the Rossby radius. Resolving such convergences may be critical for certain HAB problems, as the swimming behaviours of HAB species can lead to intense aggregations at these narrow fronts (e.g. Figure 15.12). The physical dynamics of such fronts are still a topic of investigation; it is possible that biological patterns in the fronts will shed some light on their dynamics. Most coastal circulation models will not accurately resolve the convergent structures of these fronts, since the spatial scales are on the order of metres in the cross-front direction.

Fronts and eddies cannot be spatially resolved in 1D vertical models, though the effects of their passage are sometimes parameterized by imposing fluctuations in the depth of the pycnocline.

15.5 Using models

The great utility of models is that they are reproducible and can be manipulated. The dynamics included in the model are made explicit in the equations being solved. To truly understand the balance of forces that led to the patterns observed, it is useful to calculate these directly in the model, and plot their time and space dependence. Often this exercise will show that only a small subset of the physics and biology included in the model is important in generating the patterns. At this point it is often useful to strip down the model to include only the hypothesized essential dynamics to see if it can still reproduce the patterns. In some cases analytical solutions can be obtained for simplified cases, allowing a deeper understanding of the parameters and dynamics affecting the solution. This approach of running a full model and then stripping it down to a simpler form can be very powerful in gaining insight into the dynamics structuring the ecosystem.

A nice example of this approach can be found in Pringle and Franks (2001). When running a full two-dimensional primitive-equation/turbulence-closure model of Georges Bank with code for tracking particles, they noticed that sinking particles had a net velocity up the slopes of the bank. They discovered that the mechanism had to do with changes in the thickness of the turbulent bottom boundary layer during flood and ebb tides: a thicker, more turbulent layer during tidal motions up the bank (flood) led to resuspension and transport of sinking particles. On the ebb tide, the stratification increased, suppressing turbulence, allowing the particles to sink. The particles thus ratcheted up the slope of the bank with each tidal cycle. These dynamics were encoded into a much simpler model form that could be run independently of the full-scale model (thus saving a great deal of time). Comparison of the full and simplified models showed the conditions under which the approximations in the simple model failed, and when the simple model gave a good representation of the full suite of dynamics. Through this approach, a deeper understanding was obtained of the mechanism governing sinking particle transport, allowing its application to other systems.

Process models are usually simplified versions of a simulation model (the full simulation model may or may not exist), and are used to test more focused hypotheses. For example, Hetland et al. (2002) use a process model to explore a potential mechanism for entraining offshore HAB cells into a coastal buoyant plume. They showed that an upwelling wind stress could force the plume offshore, over the HAB population, which could then swim up into the plume. As the upwelling wind ceased or reversed, the plume moved back onshore, carrying the HAB species with it. This mechanism provides a testable hypothesis for the origin of HAB organisms in a coastal buoyant plume, and analyses of the model show how the mechanism should depend on swimming speed, turbulence and plume thickness, for example. The elucidation and understanding of mechanisms such as this should be a central goal of modelling programmes. With this understanding we gain improved predictive abilities, and a greater potential for managing HAB outbreaks.

For many observations there are multiple alternate explanations for the patterns seen. Models are particularly useful tools for testing alternate hypotheses, as each hypothesis can be explicitly written as a set of equations, and then solved – either analytically or numerically. In this manner, hypotheses that do not explain the observations can be rejected, while those that cannot be rejected can be further refined and tested.

This technique of multiple hypothesis testing can be made statistically rigorous by choosing quantitative measures of the goodness-of-fit between the model and data (or subsets of the data). This technique can identify dynamics of the model that are critical to the model's performance, and suggest refinements to the model that could improve the ability of the model to reproduce the observed dynamics.

With a particularly well-resolved data set, the model can be used to recover information about the processes and parameters underlying the observations. Given a time series of spatially resolved data, we typically want to know the relative contribution of the various physical and biological processes in generating the observations. By defining a 'cost function' (usually a function of the difference between the model results and the data), various techniques exist for iterating the model, adjusting the parameters, and minimizing the cost function. When the cost function is minimized, a statistically meaningful model is (usually) obtained – the best fit of that particular model architecture to the available data (including data errors). The relative contributions of the various dynamics can then be quantified as before, and simplified process models constructed to explore the dominant dynamics more fully. A fine example of this approach can be found in McGillicuddy et al. (1998), who teased apart the physical and biological contributions to observed patterns of the copepod *Pseudocalanus* spp. on Georges Bank. They began by attempting to use a standard 'forward' model to simulate the observed spatial and temporal patterns of *Pseudocalanus* spp. This model was initialized with the first data field and then run forward in time with growth and mortality rates derived from literature values. This is the standard 'initial-value' problem technique to modelling. Unfortunately, this approach did not give satisfactory results. Their next approach was to assume that the physical model was correct, and to use the data combined with the physics to diagnose the biological dynamics necessary for the model to fit the data. The physical model was reduced from the full three-dimensional model to a depth-integrated two-dimensional (x, y) model. An 'adjoint' technique was used to minimize the cost function, and maps of the net *growth-mortality* terms (the sum of terms 10–13 of (15.1)) were obtained for the time intervals between field samples. In this manner, the relative contributions of physical and biological dynamics to the observed patterns were quantified. A similar technique is well described in McGillicuddy et al. (2007 – Chapter 16 this volume) who explored the physical and biological forcings leading to patterns in the toxic dinoflagellate *Alexandrium fundyense* in the Gulf of Maine. Similar approaches have been used to come up with, for example, optimal parameter sets and model structures for ecosystem models of the Bermuda Atlantic Time Series (BATS) (Hurtt and Armstrong, 1996; Spitz et al., 2001). The approach requires abundant data and a reliable physical model.

15.6 Summary and conclusions

In this chapter I have tried to use simple examples to illustrate the problems facing someone trying to model the physical-biological dynamics underlying HABs. I have shown how the physical dynamics can change the local concentration of a HAB population, and how we can use analytical and numerical models to generate physical flows. I have introduced the idea of finite differencing as a means of numerically solving complex equations, and briefly explored some of the problems inherent in the approach. I then discussed how a variety of physical dynamics may or may not be

represented in various model structures, and gave some thoughts on how models can be used to understand our observations. While the material would not be sufficient to actually construct a model, it should help the non-modeller to ask pertinent questions of the modellers and physicists as they collaborate in understanding harmful algal blooms.

Given that this chapter was intended as an introduction to the field, I have not presented the state of the art in physical-biological modelling, or delved very deeply into the physical-biological couplings that can mediate HABs. I highly recommend Bissett et al., 2007; Fennel and Neumann, 2007; Lee et al., 2007; McGillicuddy et al., 2007, and Pinardi et al., 2007 – Chapters 19, 17, 18, 16 and 20 this volume, for a more detailed picture of how models are currently used to understand physical-biological interactions in the plankton. These chapters also give insights into where the field is going, and requirements for better integration of data and models – subjects only touched on here. With the recent advent of comprehensive observational networks, models are becoming increasingly important for the synthesis and analysis of diverse data types, and for improving the statistical strength of forecasts. We must now develop new observational tools for quantifying HAB species *in situ* (e.g. Bissett et al., 2007, Scholin et al., 2007 – Chapters 19 and 11 this volume), and incorporate those data streams into real-time coupled physical-biological models.

References

Abraham, E. R. 1998. The generation of plankton patchiness by turbulent stirring. *Nature*, 391, pp. 577–80.

Adamec, D., Elsberry, R. L., Garwood, R. W. Jr and Haney, R. L. 1981. An embedded mixed-layer – ocean circulation model. *Dyn. Atmos. Oceans*, 6, pp. 69–96.

Arakawa, A. and Lamb, V. R. 1977. Computational design of the basic dynamical processes of the UCLA general circulation model. *Meth. Comput. Phys.*, 17, pp. 174–265.

Babin, M., Roesler, C. S. and Cullen, J. J. (eds). 2006. *Real-time Coastal Observing Systems for Marine Ecosystem Dynamics and Harmful Algal Blooms: Theory, Instrumentation and Modelling*. Paris, Intergovernmental Oceanographic Commission of UNESCO. (Monographs on Oceanographic Methodology.)

Bissett, W. P., Arnone, R., DeBra, S., Dye, D., Kirkpatrick, G., Mobley, C. and Schofield, O. M. 2007. Integration of ocean-colour remote sensing with coastal nowcast/forecast simulations of harmful algal blooms. In: Babin et al. (eds), op. cit., this volume.

Barth, J. A. 1989*a*. Stability of a coastal upwelling front. 1: Model development and a stability theorem. *J. Geophys. Res.*, 94, pp. 10844–56.

Barth, J. A. 1989b. Stability of a coastal upwelling front. 2: Model results and comparison with observations. *J. Geophys. Res.*, 94, pp. 10857–83.

Chen, C. S., Beardsley, R. and Franks, P. J. S. 2001. A 3-d prognostic numerical model study of the Georges Bank ecosystem. Part I: Physical model. *Deep Sea Res. II*, 48, pp. 419–56.

Dale, A. C. and Barth, J. A. 2001. The hydraulics of an evolving upwelling jet flowing around a cape. *J. Phys. Oceanogr.*, 31(1), pp. 226–43.

Donaghay, P. L. and Osborn, T. R. 1997. Toward a theory of biological-physical control of harmful algal bloom dynamics and impacts. *Limnol. Oceanogr.*, 42(2), pp. 1283–96.

Fennel, W. and Neumann, T. 2007. Modelling coastal dynamics and harmful algal blooms in the Baltic Sea. In: Babin et al. (eds), op. cit., this volume.

Franks, P. J. S. 1992. Phytoplankton blooms at fronts – patterns, scales, and physical forcing mechanisms. *Rev. Aquat. Sci.*, 6, pp. 121–37.

Franks, P. J. S. 1995. Thin-layers of phytoplankton a model of formation by near-inertial wave shear. *Deep Sea Res. I*, 42, pp. 75–91.

Franks, P. J. S. 1997*a*. Spatial patterns in dense algal blooms. *Limnol. Oceanogr*., 42(2), pp. 1297–305.

Franks, P. J. S. 1997*b*. New models for the exploration of biological processes at fronts. *ICES J. Mar. Sci*., 54, pp. 161–67.

Franks, P. J. S. and Walstad, L. J. 1997. Phytoplankton patches at fronts: a model of formation and response to wind events. *J. Mar. Res*., 55(1), pp. 1–29.

Gan, J. P. and Allen, J. S. 2002a. A modeling study of shelf circulation off northern California in the region of the coastal ocean dynamics experiment: response to relaxation of upwelling winds. *J. Geophys. Res*., 107, pp. 3123.

Gan, J. P. and Allen, J. S. 2002*b*. A modeling study of shelf circulation off northern California in the region of the coastal ocean dynamics experiment. 2: Simulations and comparisons with observations. *J. Geophys. Res*., 107, pp. 3184.

Garwood, R. W. Jr. 1977. An oceanic mixed layer model capable of simulating cyclic states. *J. Phys. Oceanogr*., 7, pp. 455–68.

Gill, A. E. 1982. *Atmosphere-Ocean Dynamics*. London, Academic Press, 662 pp.

Haidvogel, D. B. and Beckmann, A. 1999. *Numerical Ocean Circulation Modeling*. London/ River Edge, N.J., Imperial College Press/World Scientific Publishing.

Hetland, R. D., McGillicuddy, D. J. and Signell, R. P. 2002. Cross-frontal entrainment of plankton into a buoyant plume: the frog tongue mechanism. *J. Mar. Res.*, 60, pp. 763–77.

Holloway, G. 1984. Effects of velocity fluctuations on vertical distributions of phytoplankton. *J. Mar. Res*., 42(3), pp. 559–71.

Hurtt, G. C. and Armstrong, R. A. 1996. A pelagic ecosystem model calibrated with BATS data. *Deep Sea Res. II*, 43, pp. 653–83.

Janowitz, G. S. and Pietrafesa, L. J. 1980. A model and observations of time-dependent upwelling over the mid-shelf and slope. *J. Phys. Oceanogr*., 10, pp. 1574–83.

Juhl, A. R. and Latz, M. I. 2002. Mechanisms of fluid shear-induced inhibition of population growth in a red-tide dinoflagellate. *J. Phycol*., 38, pp. 683–94.

Juhl, A. R., Trainer, V. L. and Latz, M. I. 2001. Effect of fluid shear and irradiance on population growth and cellular toxin content of the dinoflagellate *Alexandrium fundyense. Limnol. Oceanogr*., 46, pp. 758–64.

Juhl, A. R., Velazquez, V. and Latz, M. I. 2000. Effect of growth conditions on flow-induced inhibition of population growth of a red-tide dinoflagellate. *Limnol. Oceanogr*., 45, pp. 905–15.

Kamykowski, D. 1974. Possible interactions between phytoplankton and semidiurnal internal tides. *J. Mar. Res*., 32, pp. 67–89.

Kiørboe, T. and Saiz, E. 1995. Planktivorous feeding in calm and turbulent environments, with emphasis on copepods. *Mar. Ecol. Progr. Ser*., 122, pp. 135–45.

Lamb, K. G. 1997. Particle transport by nonbreaking, solitary internal waves. *J. Geophys. Res*., 102, pp. 18641–60.

Large, W. G., McWilliams, J. C. and Doney, S. C. 1994. Oceanic vertical mixing – a review and a model with a nonlocal boundary-layer parameterization. *Rev. Geophys*., 32, pp. 363–403.

Lazier, J. R. N. and Mann, K. H. 1989. Turbulence and the diffusive layers around small organisms. *Deep Sea Res*., 36, pp. 1721–33.

Lee, J. H.-W., Choi, D. K. W., Wong, K. T. M., Qu, B. and Arega, F. 2007. Modelling algal dynamics in eutrophic coastal waters. In: Babin et al. (eds), op. cit., this volume.

Lennert-Cody, C. E. and Franks, P. J. S. 1999. Plankton patchiness in high-frequency internal waves. *Mar. Ecol. Progr. Ser*., 186, pp. 59–66.

Lennert-Cody, C. E. and Franks, P. J. S. 2002. Fluorescence patches in high-frequency internal waves. *Mar. Ecol. Progr. Ser*., 235, pp. 29–42.

Levitus, S. and Boyer, T. 1994. *World Ocean Atlas 1994. Volume 4: Temperature*. Washington DC, US Department of Commerce. (NOAA Atlas NESDIS 4.)

Lévy, M. and Klein, P. 2004. Does the low frequency variability of mesoscale dynamics explain a part of the phytoplankton and zooplankton spectral variability? *Proc. Roy. Soc. Lond. A*, 460, pp. 1673–87.

Lévy, M., Klein, P. and Treguier, A. M. 2001. Impact of sub-mesoscale physics on production and subduction of phytoplankton in an oligotrophic regime. *J. Mar. Res.*, 59, pp. 535–65.

Marchesiello, P., McWilliams, J. C. and Shchepetkin, A. 2001. Open boundary conditions for long-term integration of regional oceanic models. *Ocean Model.*, 3, pp. 1–20.

McGillicuddy, D. J. Jr, Anderson, D. M., Stock, C. A., Lynch, D. R. and Townsend, D. W. 2007. Modelling blooms of *Alexandrium fundyense* in the Gulf of Maine. In: Babin et al. (eds), op. cit., this volume.

McGillicuddy, D. J., Lynch, D. R., Moore, A. M., Gentleman, W. C., Davis, C. S. and Meise, C. J. 1998. An adjoint data assimilation approach to diagnosis of physical and biological controls on *Pseudocalanus* spp. in the Gulf of Maine-Georges Bank region. *Fish. Oceanogr.*, 7, pp. 205–18.

Mellor, G. L., Oey, L. Y. and Ezer, T. 1998. Sigma coordinate pressure gradient errors and the seamount problem. *J. Atmos. Ocean Tech.*, 15, pp. 1122–31.

Mellor, G. L. and Yamada, T. 1982. Development of a turbulence closure-model for geophysical fluid problems. *Rev. Geophys.*, 20, pp. 851–75.

New, A. L. and Pingree, R. D. 1990. Evidence for internal tidal mixing near the shelf break in the Bay of Biscay. *Deep Sea Res.*, 37, pp. 1783–1803.

Pinardi, N., Fratianni, C. and Adani, M. 2007. Use of real-time observations in an operational ocean data assimilation system: the Mediterranean case. In: Babin et al. (eds), op. cit., this volume.

Pineda, J. 1999. Circulation and larval distribution in internal tidal bore warm fronts. *Limnol. Oceanogr.*, 44, pp. 1400–14.

Pringle, J. M. and Franks, P. J. S. 2001. Asymmetric mixing transport: a horizontal transport mechanism for sinking plankton and sediment in tidal flows. *Limnol. Oceanogr.*, 46(2), pp. 381–91.

Scholin, C. A., Doucette, G. J. and Cembella, A. D. 2007. Prospects for developing automated systems for *in situ* detection of harmful algae and their toxins. In: Babin et al. (eds), op. cit., this volume.

Spall, M. A. 1997. Baroclinic jets in confluent flow. *J. Phys. Oceanogr.*, 27(6), pp. 1054–71.

Spall, S. A. and Richards, K. J. 2000. A numerical model of mesoscale frontal instabilities and plankton dynamics. I: Model formulation and initial experiments. *Deep Sea Res. I*, 47, pp. 1261–301.

Spitz, Y. H., Moisan, J. R. and Abbott, M. R. 2001. Configuring an ecosystem model using data from the Bermuda Atlantic Time Series (BATS). *Deep Sea Res. II*, 48, pp. 1733–68.

Thomas, W. H. and Gibson, C. H. 1990. Quantified small-scale turbulence inhibits a red tide dinoflagellate, *Gonyaulax polyedra* Stein. *Deep Sea Res.*, 37, pp. 1583–93.

Thomas, W. H. and Gibson, C. H. 1992. Effects of quantified small-scale turbulence on the dinoflagellate, *Gymnodinium sanguineum* (*splendens*) – contrasts with *Gonyaulax (Lingulodinium) polyedra*, and the fishery implication. *Deep Sea Res.*, 39, pp. 1429–37.

Visser, A. W. 1997. Using random walk models to simulate the vertical distribution of particles in a turbulent water column. *Mar. Ecol. Progr. Ser.*, 158, pp. 275–81.

Wang, D. P. 1993. Model of frontogenesis – subduction and upwelling. *J. Mar. Res.*, 51, pp. 497–513.

16

Modelling blooms of *Alexandrium fundyense* in the Gulf of Maine

D. J. McGillicuddy Jr, D. M. Anderson, C. A. Stock,
D. R. Lynch and D. W. Townsend

16.1 Introduction

Throughout the global coastal ocean, harmful algal blooms (HAB) are a serious economic and public health problem. In New England, the most serious HAB issue is paralytic shellfish poisoning (PSP), a potentially fatal illness that occurs when humans eat shellfish that have accumulated saxitoxins as they feed on dinoflagellates of the genus *Alexandrium* (see review by Anderson, 1997). These organisms are responsible for human illnesses and occasional death due to PSP, repeated closures of shellfish beds in nearshore and offshore waters, the mortality of larval and juvenile stages of fish and other marine animals (Geraci et al., 1989; White et al., 1989).

Alexandrium has a complex life cycle (Figure 16.1). It can lie dormant as a resting cyst in the sediments for long time periods, perhaps a decade or more (Anderson, 1984; Keafer et al., 1992). Germination is regulated by a complex set of processes, including an endogenous clock (Anderson and Keafer, 1987) and physiological responses to environmental factors such as temperature (Anderson, 1980), light and oxygen availability (Anderson et al., 1987). Once emerged from the sediments, the cells swim towards the surface to begin a phase of vegetative growth. Photosynthetic production is fundamentally limited by light and the availability of nutrients; however, maximum growth occurs only within a specific range of temperature and salinity. When faced with environmental stress such as nutrient limitation, the vegetative cells form gametes that subsequently fuse into a zygote (Anderson et al., 1984). The zygote then encysts, and the cycle is complete. See Anderson (1998) for a review of the *Alexandrium* life cycle and its role in bloom dynamics.

Linkage between the population dynamics of *Alexandrium* and the hydrodynamic environment arises from three basic sources. First, the vital rates of *Alexandrium*'s population dynamics processes are influenced by ambient water properties including temperature, salinity, nutrients, and others Second, the spatial distributions of the populations themselves are constantly redistributed by ocean currents. Third, *Alexandrium* is capable of directed motion through the water by virtue of its swimming ability. This tripartite linkage poses difficult challenges to understanding the physical-biological interactions that control *Alexandrium* blooms: differentiation between the three sources of variability requires accurate assessment of the physical, biological and chemical environment in space and time, in addition to detailed knowledge of *Alexandrium*'s behavioural capabilities and the processes by which ambient conditions control its vital rates.

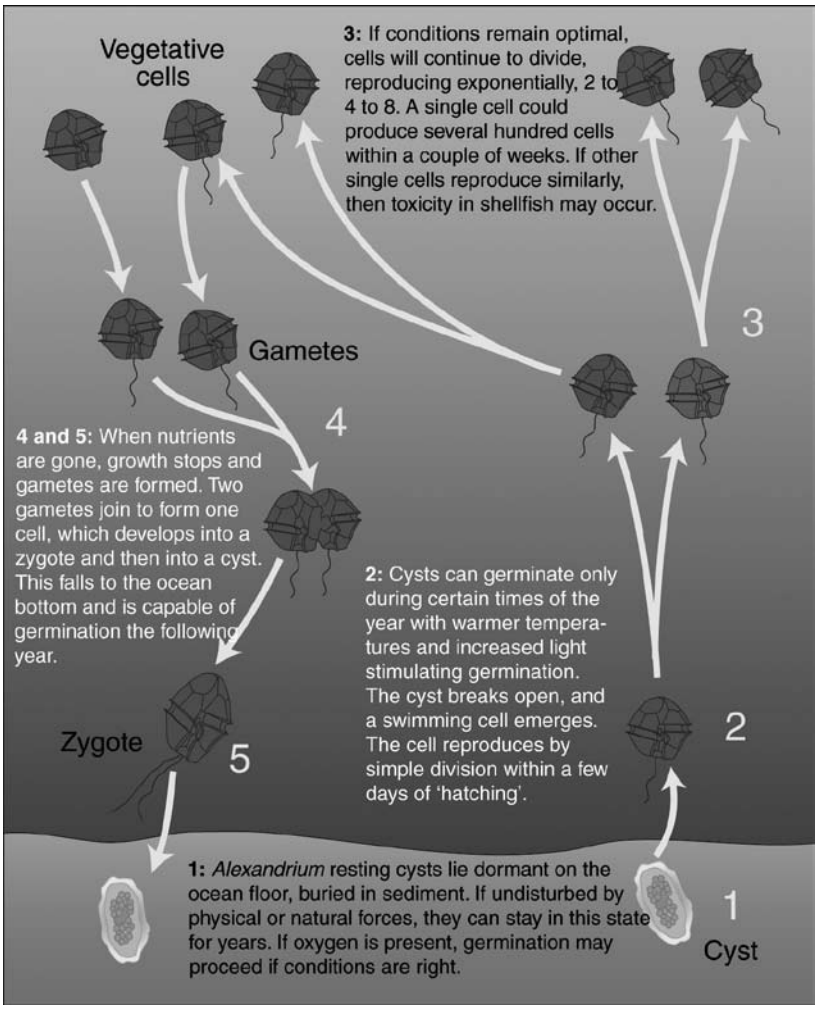

Figure 16.1
Life cycle of *Alexandrium*.

Numerical models offer a framework for diagnosis of these manifold contributions to variability in *Alexandrium* populations. Our approach is to incorporate mathematical representations of *Alexandrium*'s population dynamics into hydrodynamic simulations of the Gulf of Maine. These coupled physical-biological models use different circulation models depending on the space- and time-scales of interest. Examples from two different space/time regimes are described herein: synoptic (weather band) variability in a limited-area coastal domain (Section 16.4) and Gulf-wide seasonal dynamics based on climatological conditions (Section 16.5). An underlying goal of both case studies is to use models together with observations to elucidate the mechanisms controlling *Alexandrium* blooms. As such, the interface between models and observations is emphasized. Looking to the future, we expect significant progress to be achieved by strengthening the connections between observations and models in the

context of data assimilation (Section 16.6) and the emerging global network of ocean observing systems (Section 16.7).

16.2 Gulf of maine circulation and *alexandrium* populations

The general circulation in the Gulf of Maine tends to be cyclonic (Beardsley et al., 1997; Bigelow, 1927; Brooks, 1985). The near-surface currents are influenced by inflow from the Scotian Shelf, which provides cold, low-salinity water to the north-eastern Gulf. This flow continues past the mouth of the Bay of Fundy and feeds the Maine Coastal Current (MCC), with additional input from riverine sources along the coast. The MCC bifurcates near Penobscot Bay, with a portion branching seaward and continuing around the Jordan Basin gyre. The remainder continues down the coast, some of which feeds the clockwise circulation around Georges Bank.

Several *Alexandrium* habitats have been identified in the Gulf of Maine region (Figure 16.2), linked to varying degrees with each other and with the major hydrodynamic features of the Gulf (Anderson, 1997). One such feature that is dominant in the eastern region is a nearshore plume of cold surface water that extends along the coast from the mouth of the Bay of Fundy to Penobscot Bay, where a portion of it veers offshore (Brooks and Townsend, 1989). Termed the Eastern Maine Coastal Current (EMCC), this flow is important because it transports nutrient-rich waters from the tidally mixed eastern Gulf of Maine into the warm and stratified western and central regions (Townsend et al., 1987). The EMCC thus plays a major role in coastal hydrodynamics in the eastern Gulf, and in the dynamics of *Alexandrium* as well (Anderson, 1997; Townsend et al., 2001). As discussed below, it may also play a significant role in the dynamics of *Alexandrium* within the western Gulf of Maine.

Within the western Gulf of Maine region, which extends from Penobscot Bay to Massachusetts Bay, a coupling has been inferred between the abundance and distribution of *Alexandrium* and a buoyant coastal current that travels from north-east to south-west. A conceptual model of this linkage has been proposed, known as the river plume advection hypothesis (Franks and Anderson, 1992*a*, 1992*b*). Critical features of this model include:

- a source population of cells located to the north of Massachusetts Bay near the Androscoggin-Kennebec estuary;
- freshwater outflow from the Androscoggin-Kennebec estuary, resulting in a coastally-trapped, buoyant plume (Western Maine Coastal Current – WMCC) that supports the growth of *Alexandrium* cells and transports them to the south and west;
- plume phenomena, as influenced by the volume of freshwater outflow, the local wind stress, and underlying Gulf of Maine circulation, all of which combine to regulate the alongshore and cross-shore location of the plume, its associated cells and PSP toxicity.

The cells that populate the WMCC presumably originate from germinated cysts, but it is not known which benthic cyst beds are the most important to bloom initiation. The bloom cells might emerge from a large, offshore cyst accumulation documented near Casco and Penobscot Bays (see below), or they might originate farther to the north and east from the Bay of Fundy cyst deposit (also see below), transported to the WMCC via the EMCC. For this latter mechanism to be operative, the EMCC must intersect with the WMCC. Climatological simulations suggest it does so during late spring, when the offshore branch

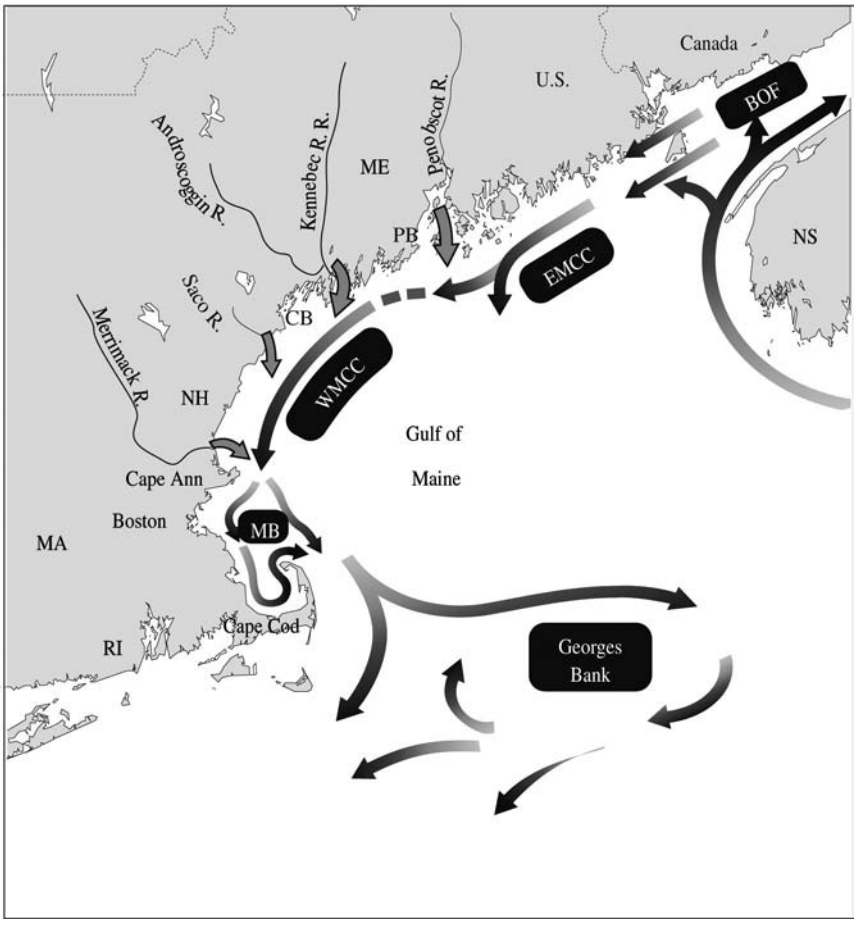

Figure 16.2
Alexandrium subpopulations or habitats in the north-eastern United States (from Anderson, 1997). Six regional populations (black boxes) are identified, defined by circulation patterns and the distribution of the dinoflagellate: 1, EMCC – Eastern Maine Coastal Current; 2, WMCC – Western Maine Coastal Current; 3, MB – Massachusetts Bay (includes Cape Cod Bay); 4, Georges Bank; 5, BOF – Bay of Fundy. Qualitative circulation patterns are indicated by arrows. Locations of Casco and Penobscot Bays are indicated by CB and PB, respectively.

of the EMCC tends to stay closer to the coast and join the WMCC (Lynch et al., 1997). This connection can also occur episodically as a result of local meteorological forcing (i.e. strong downwelling-favourable winds; see Anderson et al., 2000) or by large-scale changes in the configuration of the coastal current system. Thus, *Alexandrium* populations in this region are interconnected by a complex system of coastal circulation features that fluctuate on timescales ranging from synoptic to interannual (Anderson et al., 2005; Keafer et al., 2005; Luerssen et al., 2005; McGillicuddy et al., 2005; Townsend et al., 2001, 2005a).

16.3 Population dynamics model for *Alexandrium fundyense*

Two saxitoxin-producing species of *Alexandrium* occur in the Gulf of Maine: *A. fundyense* and *A. tamarense*. These are now considered to be varieties of the same species (Anderson et al., 1994). Neither antibody nor oligonucleotide probes can distinguish between *A. fundyense* and *A. tamarense* from this region; only detailed analysis of the thecal plates on individual cells can provide this resolution. Because this is not practical for large numbers of field samples, for the purpose of this and other studies, we use the name *A. fundyense* to refer to both forms.

Fundamental to our modelling approach is the concept that the ecosystem in which *A. fundyense* resides is not explicitly modelled. This is justified on the basis that, with few exceptions, *A. fundyense* constitutes a very small fraction of the phytoplankton species assemblage in the Gulf of Maine. As such, it generally does not significantly influence either the ambient nutrient fields or predator distributions. Therefore, ecosystem effects can be parameterized through their influence on the vital rates of *A. fundyense*'s population dynamics processes.

The coupled physical-biological model is expressed as a three-dimensional advection-diffusion-reaction equation, where the reaction terms on the right hand side represent the population dynamics of the organism:

$$\frac{\partial C}{\partial t} + \nabla \cdot \left[(v + w_a) C \right] - \nabla K \nabla C = \mu C - mC + F_g, \tag{16.1}$$

where C is the concentration of *A. fundyense,* v the fluid velocity, w_a the vertical swimming velocity and K the diffusivity. Our population dynamics model for *A. fundyense* is summarized in Figure 16.3. Definitions of all model parameters and their envelope of reasonable values are presented in Table 16.1. The flux of vegetative cells into the water column is specified by the distribution of resting cysts (Figure 16.3A) together with *A. fundyense's* endogenous clock (EC) and a germination rate (G) that depends on ambient temperature (T) and non-spectral irradiance (E) (Figure 16.3C). The flux of cells due to germination (F_g) is given by

$$F_g = EC(t)G(T,E)d_g[\text{cysts/cm}^3]_0, \tag{16.2}$$

where the germination depth d_g is the vertical extent of the surficial sediment layer from which germinating cysts can gain the water column, and $[\text{cysts/cm}^3]_0$ is the initial cyst distribution specified by the cyst map (Figure 16.3A). For a detailed description of the germination model, see Anderson et al. (2005).

Newly germinated cells are assumed to swim upward at a constant speed w_a until the mean depth of the 1% light level ($z_{1\%}$) is reached. Diminution in swimming speed to the natural boundary condition of $w_a = 0$ at the surface ($z = 0$) is prescribed by a function that was found to produce vertical distributions of *A. fundyense* that are consistent with observations:

$$w_a(z < z_{1\%}) = w_a(z > z_{1\%}) \times \left[1 - \tanh\left(\frac{(z_{1\%} - z)}{10} \right) \right] \tag{16.3}$$

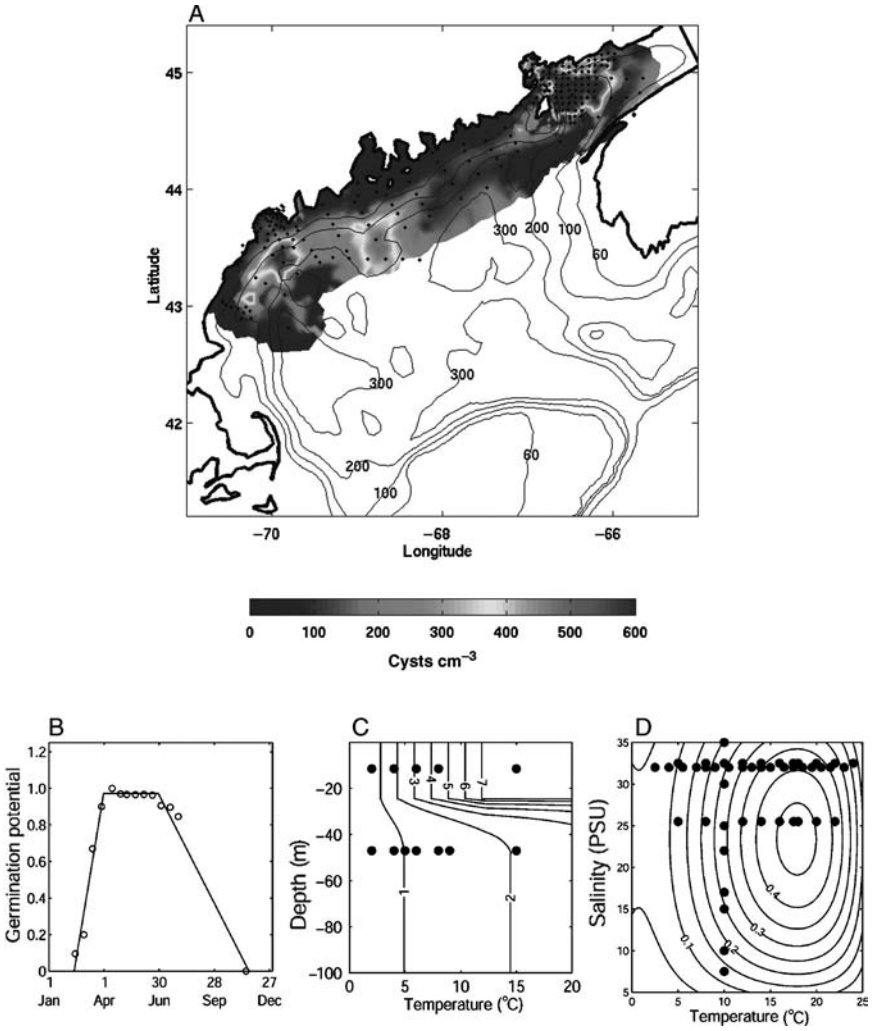

Figure 16.3
Population dynamics model for *A. fundyense*.
A, distribution of cysts (number of cysts cm^{-3}) in the upper 3 cm of sediment derived from a 1997 survey of the Gulf of Maine (McGillicuddy et al., 2003) and surveys of the Bay of Fundy in 1981 (White and Lewis, 1982), 1982 and 1983 (data provided by Jennifer Martin, DFO).
B, germination potential (decimal fraction of cysts able to germinate) as a function of time. The solid line is a piecewise linear fit to laboratory observations (open circles) of *A. fundyense*'s endogenous clock from Anderson and Keafer (1987).
C, germination rate (% day^{-1}) as a function of temperature and light. Light has been converted to depth using a diffuse attenuation coefficient ($k_w = 0.2\ m^{-1}$) and the mean surface irradiance. Solid circles indicate laboratory germination experiments.
D, specific growth rate (day^{-1}) as a function of temperature and salinity. Solid circles indicate growth rate measurements from laboratory cultures.

Table 16.1 Parameters of the *A. fundyense* population dynamics model

Symbol	Definition	Units	Range	Sources
K_N	Half-saturation constant for nutrient uptake	μM	0–3	See text
m	Spatially and temporally averaged mortality	day^{-1}	0–0.3	See text
$\mu_{max}(T_{opt}, S_{opt})$	Maximum growth rate under optimal conditions.	day^{-1}	0.35–0.65	Cullen et al. (unpub.), Keafer et al. (unpub.), Langdon (1987)
μ_o^r	Maintenance respiration rate	day^{-1}	0.005–0.1	Cullen et al. (unpub.), Langdon (1987)
α_g	Growth efficiency	$day^{-1} W^{-1} m^2 s$	0.013–0.021	Cullen et al. (unpub.), Langdon(1987)
d_g	Mean depth of sediment where cysts are able to contribute to blooms	cm	0.5–3	Keafer et al. (1992), Aller and Cochran (1976), Benninger et al. (1979)
E_{lgt}	Light level for germination under 'light' conditions	$W m^{-2}$	1.2–3.6	Anderson et al. (2005)
E_{drk}	Light level for germination under dark conditions	$W m^{-2}$	0.1% of I_{lgt} to 10% of I_{lgt}.	Anderson et al. (2005)
k_d	Mean diffuse attenuation in water column	m^{-1}	0.15–0.25	RMRP/ECOHAB survey data
k_s	Mean diffuse attenuation in sediment	mm^{-1}	0–5	Kuhl and Jorgenson (1994) 0 = well mixed
w_a	Vertical swimming speed	m/day	5–15	Bauerfiend et al. (1986)

Several strains of *A. fundyense* in the region have been observed to migrate to obtain nutrients in the laboratory (Macintyre et al., 1997), and to modulate their light conditions in salt ponds (Anderson and Stolzenbach, 1985). However, in the western Gulf of Maine, *A. fundyense* have not been observed to engage in strong coordinated migrations either in the laboratory or the field (Poulton, 2001; Townsend et al., 2005b). In light of these mixed results, vertical migration behaviour is not included in the present model.

Vegetative growth of *A. fundyense* depends strongly on temperature and less so on salinity (Figure 16.4D). Temperature dependence *f(T)* is defined by a cubic polynomial fit to the laboratory data of Watras et al. (1982) and Anderson and Keafer (unpublished data):

$$f(\mathrm{T}) = -0.000347T^3 + 0.0097^2 - 0.0133T + 0.131 \qquad R^2 = 0.88 \qquad (16.4)$$

Salinity dependence *f(S)* is defined by a quadratic fit to the data of Watras et al. (1982) and Prakash (1967):

$$f(S) = -0.0022S^2 + 0.103S - 0.195 \qquad R^2 = 0.66 \qquad (16.5)$$

Both *f(T)* and *f(S)* are dimensionless factors scaled to vary between 0 and 1 to modulate the maximum growth rate (μ_{max}) for all T and S in a manner consistent with experimental determinations of growth rate in the laboratory (Figure 16.3D):

$$\mu(T,S) = \mu_{max} \times f(T) \times f(S) \tag{16.6}$$

Dependence of vegetative growth on light and nutrients is modelled after Liebig's Law of the Minimum (Liebig, 1845):

$$\mu(E,DIN,T,S) = \min\Big(\mu(E,T,S),\mu(DIN,T,S)\Big) \tag{16.7}$$

Light-limited growth takes a hyperbolic form based on growth efficiency α_g and a basal respiration rate μ_o^r (Langdon, 1987; Langdon, 1988; Platt and Jassby, 1976):

$$\mu(E,T,S) = \Big(\mu(T,S) + \mu_o^r\Big)\tanh\left(\frac{\alpha_g E}{(\mu(T,S)+\mu_o^r)}\right) - \mu_o^r \tag{16.8}$$

Nutrient dependence is modelled by Michaelis-Menten kinetics with half-saturation K_N for dissolved inorganic nitrogen (*DIN*):

$$\mu(DIN,T,S) = \mu(T,S) \times \frac{[DIN]}{K_N + [DIN]} \tag{16.9}$$

In the simulations presented in Section 16.4, evolution of the DIN field is specified from survey data (collocated with *A. fundyense* measurements). For Section 16.5 we rely on a diagnostic nitrate field computed from temperature and salinity based on empirical relationships described in Garside et al. (1996).

Losses of vegetative cells occur as a result of grazing by zooplankton as well as encystment. Both of these rates are difficult to quantify with measurements. Grazing losses inflicted on *A. fundyense* are a complex function of both the heterotrophic and autotrophic communities (Teegarden and Cembella, 1996). Encystment is generally thought to occur in response to adverse environmental conditions and has been triggered by nutrient limitation in the laboratory (Anderson et al., 1984; Anderson and Lindquist, 1985). However, the precise thresholds and rates for nutrient driven encystment have been difficult to characterize, and it has been equally difficult to observe in the field (Anderson, 1998). Given these uncertainties, we parameterize losses due to grazing and encystment via a spatially constant specific rate m (day^{-1}), loosely referred to as 'mortality'.

16.4 Synoptic variability: data-driven simulations in a limited-area regional domain

Observations from the 1993 and 1994 Regional Marine Research Program (RMRP) in the western Gulf of Maine provide the opportunity for hindcast simulations

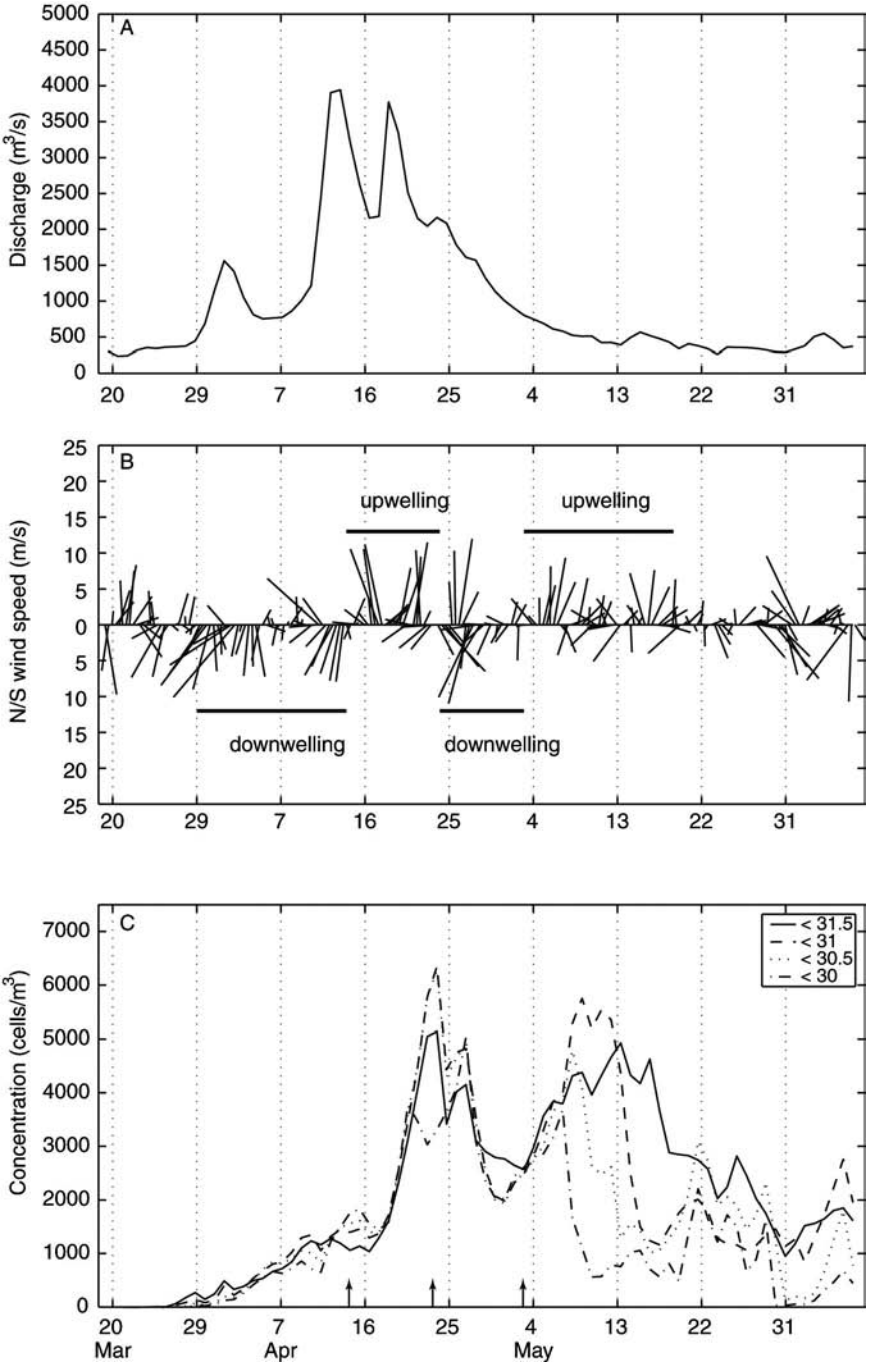

Figure 16.4
Time series of A, river discharge (Kennebec/Androscoggin discharge) and B, wind vectors used to force the model in a hindcast simulation for 1993. Thick horizontal bars indicate time periods of upwelling-favourable (south-westerly) and downwelling-favourable (north-easterly) winds. C, mean cell concentrations in various salinity intervals diagnosed from the source region of the model (see text). Only cells germinated from cysts deeper than 75 m are included in order to highlight the mechanism by which offshore cells are entrained in the plume.
Source: McGillicuddy et al. (2003), by permission of Oxford University Press.

of a system for which much of the synoptic-scale variability is governed by wind-forced river plume dynamics. Hydrodynamic simulations were constructed using a primitive equation model (Blumberg and Mellor, 1987) with variable horizontal resolution of a 2–4 km and 12 terrain-following vertical levels. Vertical mixing is internally generated from the Mellor-Yamada level 2.5 turbulence closure. The model is initialized with climatological temperature and salinity profiles (spatially uniform) and forced by observed river discharge (Figure 16.4A) and winds (Figure 16.4C). Surface heat fluxes are computed from buoy observations using bulk formulae. Wind stress and heat fluxes are assumed to be uniform over the model domain. Barotropic forcing at the offshore open boundary is provided by a larger-scale finite-element model of the region (Lynch et al., 1996). Simulations are run from 19 March to 7 June.

16.4.1 Hindcast simulations

An example snapshot from a hindcast simulation is shown in Figure 16.5. The salinity field reveals the impact of fresh water plumes originating at the Kennebec-Androscoggin and Merrimack rivers. These tend to propagate down the coast, and also undergo significant cross-shore displacements due to the effects of upwelling and downwelling winds. This particular simulation is suggestive of offshore initiation of the bloom, as the impact of the germination input from the offshore maximum in the cyst distribution is clearly evident. Features in the cell distribution are advected downstream in the coastal current, and are also clearly impacted by wind-driven upwelling and downwelling. These various aspects of the solution are evident in an animated presentation of model output, and readers are encouraged to view this on the internet.[84]

Direct comparison of hindcast results with observations is cumbersome due to the four-dimensional (space and time) nature of the underlying system. This problem is exacerbated by small-scale variability in the observations that is not resolved by the model. One approach to evaluating hindcast skill is to average both the model results and the observations on scales resolved by both. We therefore define nine zones (chosen subjectively) in which the mean values of the simulated and observed concentrations are compared for each of five cruises in 1993 (Figure 16.6). An error metric J quantifies the degree to which the simulated means ($\bar{C}_{\text{sim}}$) match the observed means ($\bar{C}_{\text{obs}}$) for each zone during each cruise: $J = \dfrac{\max(\bar{C}_{\text{sim}}, \bar{C}_{\text{obs}})}{\min(\bar{C}_{\text{sim}}, \bar{C}_{\text{obs}})}$. Alternatively, this metric can be expressed as $\bar{C}_{\text{sim}} / \bar{C}_{\text{obs}}$ or its inverse, whichever is larger. A perfect fit would result in a value of 1.0, and this penalty function grows larger as the simulation diverges from the observations. A variety of error metrics are possible, and all have various advantages and disadvantages. One appealing aspect of this particular metric is that errors at low concentrations are weighted just as heavily as those at high concentrations. In summary, this approach yields a quantitative method of evaluating the large-scale spatial distribution, timing and magnitude of the simulated bloom.

Yet another issue confounds evaluating the skill of the model predictions: the simulations are sensitive to model parameters that are not known with certainty, not

[84]http://science.whoi.edu/users/mcgillic/ecohab/plume.html

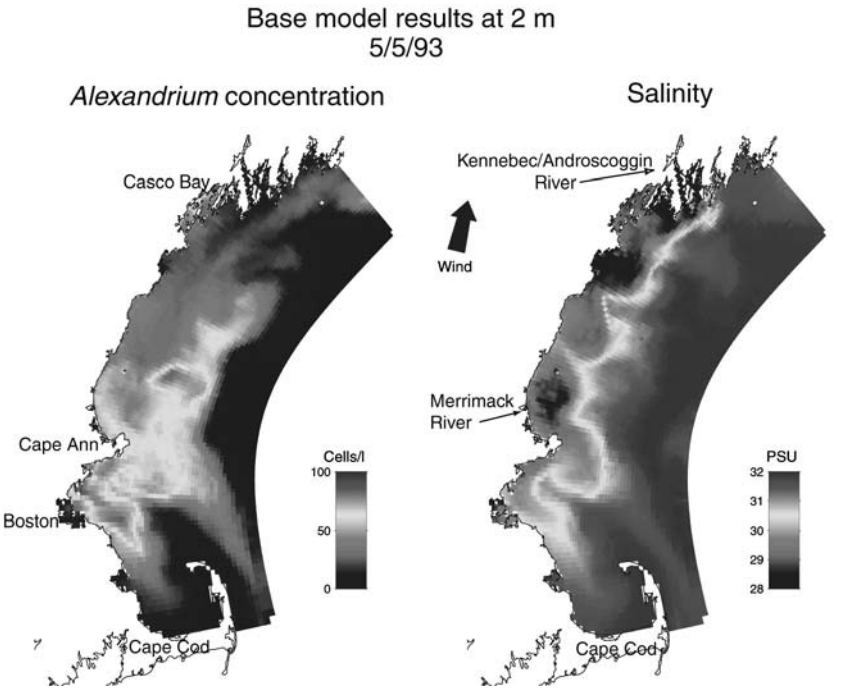

Figure 16.5
Example snapshot of model output from a simulation in the western Gulf of Maine driven by forcing from 1993. In this example, vegetative growth is assumed to be balanced by loss terms, such that the net 'reaction' term on the right of (16.1) is identically zero.

to mention that the parameterizations themselves may be flawed. Our approach is to assume that the parameterizations are valid and to tune the adjustable parameters within their envelope of reasonable values. This amounts to a manual procedure for parameter estimation. More sophisticated estimation procedures have been used in the context of zero- and one-dimensional models (e.g. Vezina and Platt, 1988; Fasham and Evans, 1995; Friedrichs and Hofmann, 2001; Hurtt and Armstrong, 1996), and we intend to pursue such methods in future. At present, the computational demands of those approaches make them impractical for the three-dimensional system of interest here. Another important caveat is that the circulation fields are assumed to be correct; we cannot exclude the possibility that mismatches between the simulated and observed concentrations of *A. fundyense* could be a result of unknown deficiencies in the modelled circulation (see Franks, 2007 – Chapter 15 this volume). In future work we plan to use measures of misfit for the physical fields as well as the biological fields.

Quantitative evaluation of hindcast skill facilitates testing hypotheses concerning bloom controls by ascertaining whether one model structure fits the data significantly better than another. As an example, we compare the results of two different simulations: one without mortality of *A. fundyense*, and one that includes a spatially

uniform loss rate of 0.1 per day (Figure 16.6, right panels). In the absence of mortality, cell concentration is systematically overpredicted late in the run in the southern portion of the domain. The average value of the error metric is 3, so on average the predicted values are within a factor of 3 of the observations. Explicit treatment of loss processes via a uniform loss rate of 0.1 per day improves the simulations dramatically: the large errors late in the run in the southern portion of the domain are reduced. The error metric drops to an average of 2.33, so the predictions are now within a factor of 2 of the observations. These results suggest that a loss term (which may represent some combination of predation and encystment) plays a key role in controlling the development and termination of the bloom.

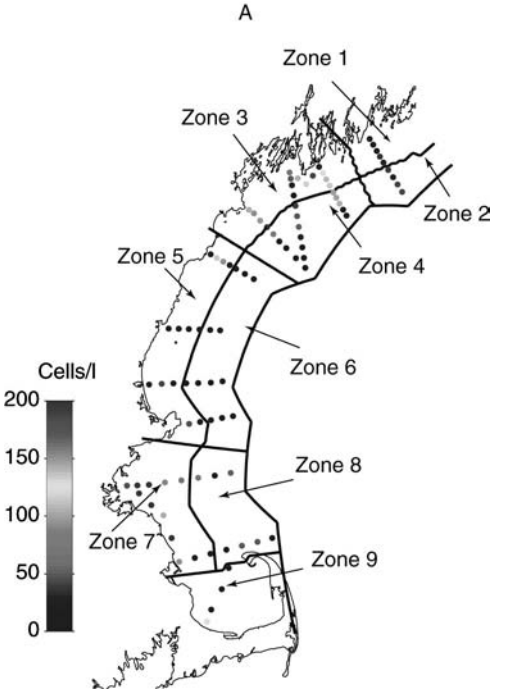

Figure 16.6
A, typical observational coverage during one cruise of the 1993/1994 Regional Marine Research Program in the Gulf of Maine. Coloured dots represent observations of *A. fundyense* concentration (cells per litre). The nine zones chosen for model evaluation are indicated.
B, evaluation of hindcasts based on two different biological formulations, one without an explicit loss term (top panels), and one with a spatially uniform loss rate of 0.1 day^{-1} (see text). Each of the four panels shows the space/time distribution of the error metric. Time runs along the 'cruise' axis with cruises 1–5 carried out in April to June. Space runs along the 'zone' axis, with zones 1–9 corresponding to those indicated in the left panel. The zones have been separated into inshore and offshore groups. The height of the vertical bars indicates the magnitude of the error metric *J*, with dark grey indicating model values that are too low, light grey too high.

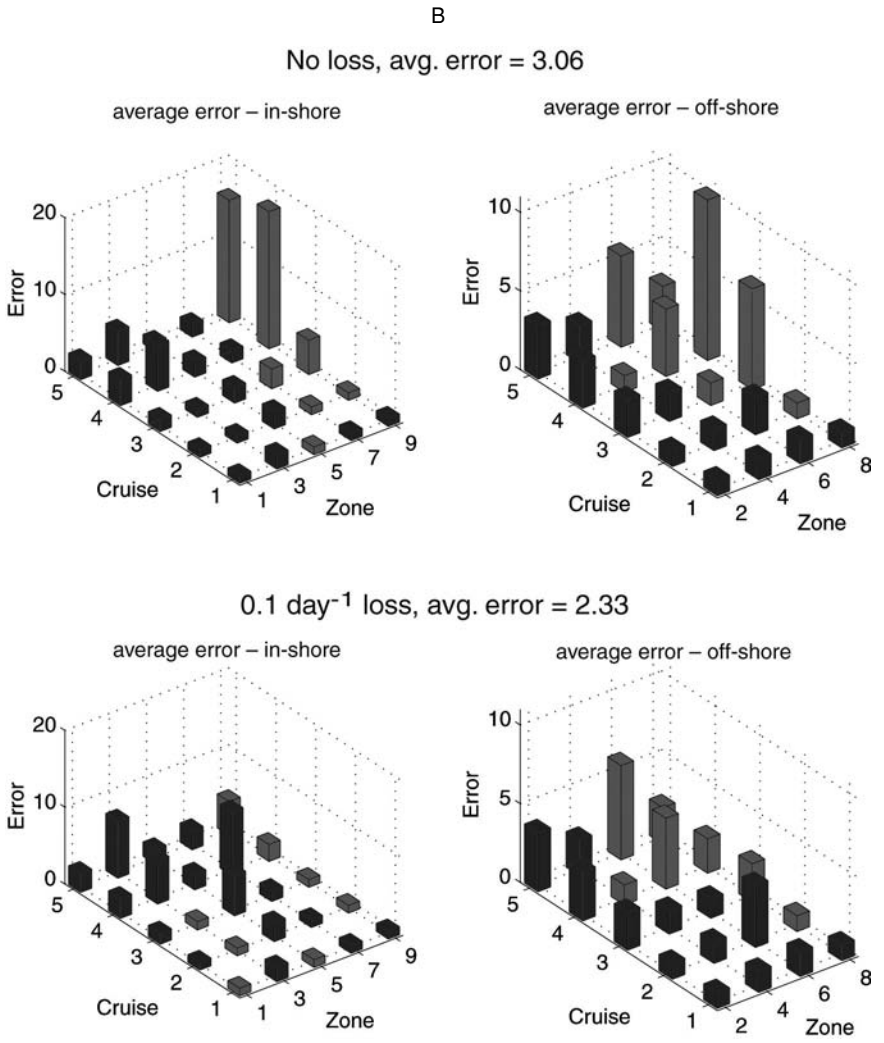

Figure 16.6 *(Continued)*

The statistical significance of differences in the abilities of various model structures to fit observations can be evaluated using the Maximum Likelihood Ratio Test (MLRT). This test compares the likelihood associated with a null hypothesis (L_0) that purports specific values of model parameters to the likelihood associated with an alternative (L_1) that allows one or more of the parameters set by the null hypothesis to vary over the range of their uncertainty. For example, in comparing model structures with and without mortality (m), the following ratio (l) is formed for the likelihood of a given set of model-data misfits ε:

$$l = \frac{L(\mu_{\max}, d_g, m = 0; \varepsilon)}{L(\mu_{\max}, d_g, m; \varepsilon)} = \frac{L_o}{L_1} \tag{16.11}$$

where μ_{max} and d_g are control parameters that are optimized for each model structure on the basis of a large number of trial simulations ('manual' optimization process). Note that the parameter space in the denominator of the ratio has an additional degree of freedom: the alternative hypothesis is the more complex model structure. As such, the likelihood in the denominator will be at least as large as that of the numerator. As this ratio becomes much less than one, the null hypothesis becomes less likely than the alternative, and rejection of the null hypothesis is supported.

The degree of significance with which the null hypothesis can be rejected is estimated by invoking the properties of the MLRT for large sample sizes. It can be shown (e.g. Cox and Hinckley, 1974) that if the null hypothesis is true, the quantity $\lambda = -2 \times \log(l)$ will approach a χ^2 distribution with degrees of freedom equal to the number of additional parameters left to vary in the alternative hypothesis. The strength of rejection of the null hypothesis in the above equation is thus based on the size of λ relative to what is expected from a χ^2 statistic with one degree of freedom.

MLRT comparisons have been used to evaluate the role of both mortality and nutrient dependence in explaining the observed variations of *A. fundyense* in the Gulf of Maine (Stock et al., 2005). Assuming no nutrient dependence, simulations without mortality can be rejected in favour of those with mortality at the 90% confidence level (Figure 16.7A). Optimal values of the mortality term fall between 0.05 d^{-1} and 0.2 d^{-1}. In the absence of mortality, simulations without nutrient dependence can be rejected in favour of those with nutrient dependence at the 90% confidence interval (Figure 16.7B). The results imply rather high values of the half-saturation constant for nitrate uptake, as values of K_N (equation 16.9) less than 1.5 μM NO_3 can be rejected in favour of the best-fit model, which has $K_N = 3$ μM NO_3. Simulations that include both mortality and nutrient dependence produce a significantly better fit to observations than those with mortality only, as shown by their higher likelihood in Figure 16.7C. However, a model with nutrient dependence only cannot be rejected in favour of one that includes both effects, as the 90% confidence contour intersects the K_N axis at a value of K_N between 1.0 and 1.5 μM NO_3. For a more extensive description of the MLRT analysis, see Stock et al. (2005).

16.4.2 Mechanistic diagnosis: cross-isobath transport and initiation of A. *fundyense* blooms

Given that the highest abundances of cysts occur offshore (beyond the 60m isobath; see Figure 16.3), it is curious that the highest concentrations of vegetative cells in the western Gulf coincide with the relatively fresh waters of the coastal current (Figure 16.8). The salinity of the waters overlying the offshore maximum in the cyst distribution is significantly higher than that where peak concentrations of vegetative cells exist. Thus, in a mean sense, inshore blooms are spatially disconnected from this large source located offshore. Clearly, the higher abundance of cells at characteristic plume salinities is a result of conditions inside the plume that are more favourable for bloom development than the surrounding waters. How might the large cyst deposits observed offshore be relevant to inshore blooms?

Diagnosis of the hindcast simulations reveals a mechanism by which the offshore cyst beds can contribute to inshore blooms of *A. fundyense*. Fresh water inputs originating at the Kennebec/Androscoggin and Merrimack rivers result in a buoyant coastal current that flows south-westward down the coast in the direction of Kelvin wave propagation. The plumes undergo significant cross-shore displacement due to wind forcing. Upwelling-favourable winds (from the south-west) drive the plume offshore,

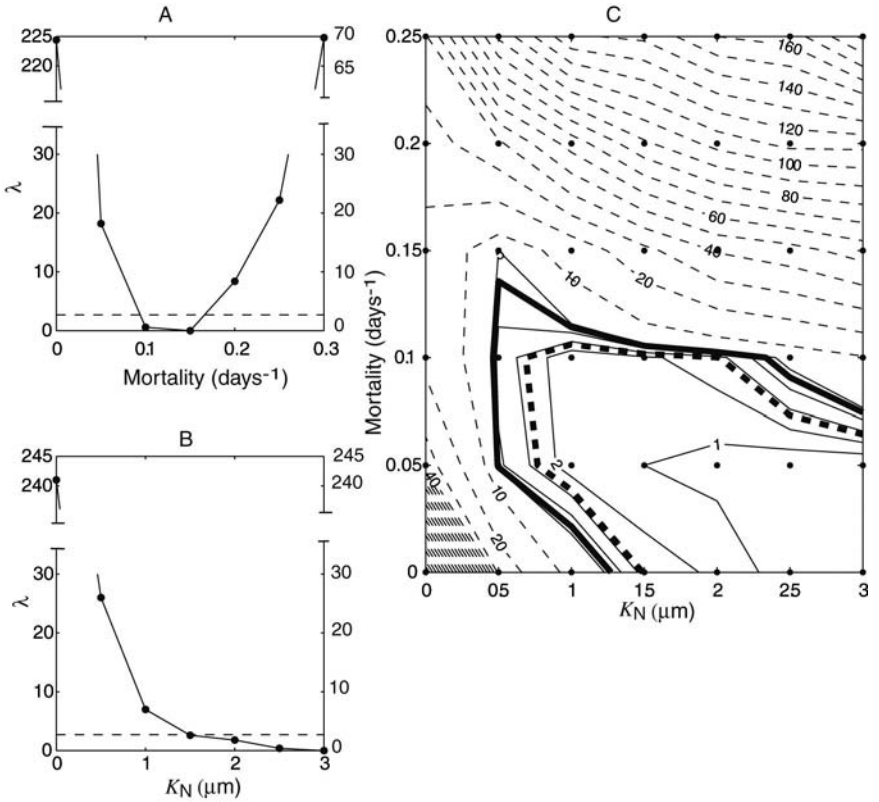

Figure 16.7
MLRT results plotted in terms of: A, λ as a function of mortality (K_N = 0); B, λ as a function of the half saturation constant for nutrient uptake K_N (m = 0). Dashed line in A and B is the 90% confidence interval. C, contours of λ as a function of both m and K_N. Thin solid contours are at intervals of 1, and thin dashed contours are at intervals of 10. The thick dashed line is the 90% confidence interval for 1 degree of freedom, while the thick solid line is the 90% confidence interval for 2 degrees of freedom. In all panels, dots indicate where parameter optimizations were carried out.

whereas downwelling-favourable winds (from the north-east) confine it near the coast. The overall characteristics of this hydrodynamic behaviour are consistent with Ekman theory for a buoyant coastal current (Fong et al., 1997).

These motions have a dramatic impact on the entrainment of *A. fundyense* cells germinated from offshore cysts into the fresh waters of the river plume (Figure 16.4C). During the 81-day simulation, there are two major episodes during which cell concentration in the plume increases dramatically: one in late April and the other in mid May. Both of these events correspond to periods of upwelling-favourable winds, with the peak cell abundance in the plume occurring towards the end of the upwelling period. When the winds subsequently shift to favour downwelling, cell abundance in

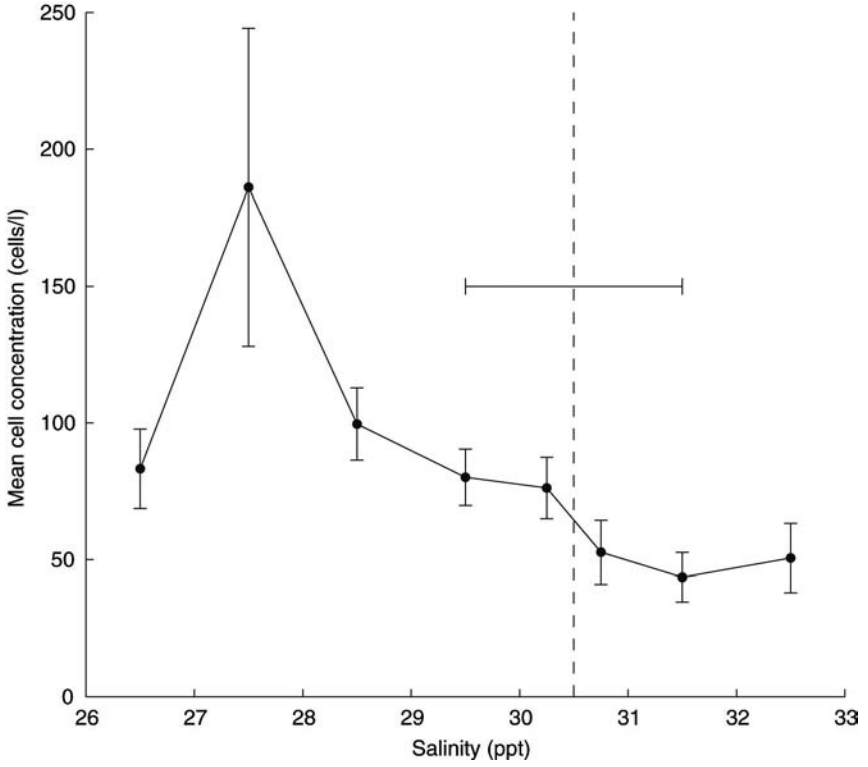

Figure 16.8
Surface concentrations of *A. fundyense* observed in the western Gulf of Maine plotted as a function of salinity. Error bars represent 1 standard deviation of the sample mean. The dashed line at $S = 30.45$ ppt and its associated standard error represent the salinity conditions of surface waters overlying the peak in the cyst distribution offshore of Casco Bay (Figure 16.3). Cell concentration data are derived from surveys in the Western Gulf of Maine (south and west of Penobscot Bay) in 1993, 1994, 1998 and 2000. Observations taken during the bloom period (late March, April and May) are included here.
Source: McGillicuddy et al. (2003), by permission of Oxford University Press.

the low-salinity water appears to drop. However, this is primarily a consequence of the cells being advected out of the 'source region' in which the budgets shown in Figure 16.4 are computed.

These results suggest that the response of the river plume to fluctuating wind forcing provides a mechanism for cross-isobath transport of *A. fundyense* cells (Figure 16.9). Under upwelling conditions, the plume thins and extends far offshore where it is inoculated by upward-swimming light-seeking cells germinated from the offshore cyst bed. When the winds shift to favour downwelling, the plume moves onshore and thickens, thereby exposing the coast to offshore populations of *A. fundyense* (albeit

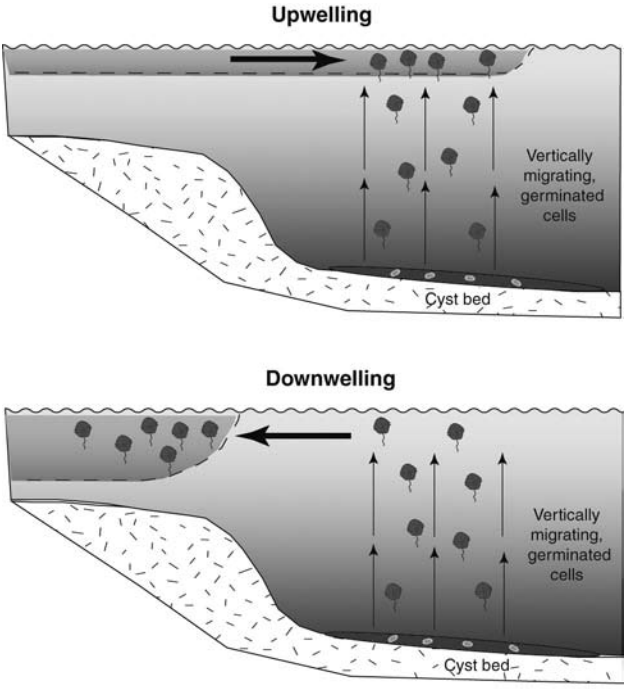

Figure 16.9
Mechanism for cross-isobath transport of *Alexandrium* blooms. During upwelling conditions, the plume thins and moves offshore. Recently germinated, upward-swimming cells enter the plume as it overlies the offshore peak in the cyst distribution. During downwelling conditions, the plume retreats and thickens, thereby exposing the coast to cell populations that originated offshore.
Source: McGillicuddy et al. (2003), by permission of Oxford University Press.

downstream of the cyst bed from which the cells were germinated). Thus, a cross-shore flux of *A. fundyense* results from the joint effects of organism behaviour and the response of a buoyant plume to transient wind forcing. For more details on this mechanism see McGillicuddy et al. (2003) and Hetland et al. (2002).

16.5 Large-scale seasonal variability in a Gulf-wide domain

Recent observations from the Ecology and Oceanography of Harmful Algal Blooms – Gulf of Maine (ECOHAB-GOM) programme have revealed the larger scale context in which seasonal blooms of *A. fundyense* occur. Indeed, the distribution of vegetative cells is Gulf-wide in character (Figure 16.10; also Townsend et al., 2005a). Peak cell concentrations occur in offshore waters, in association with the Maine coastal current

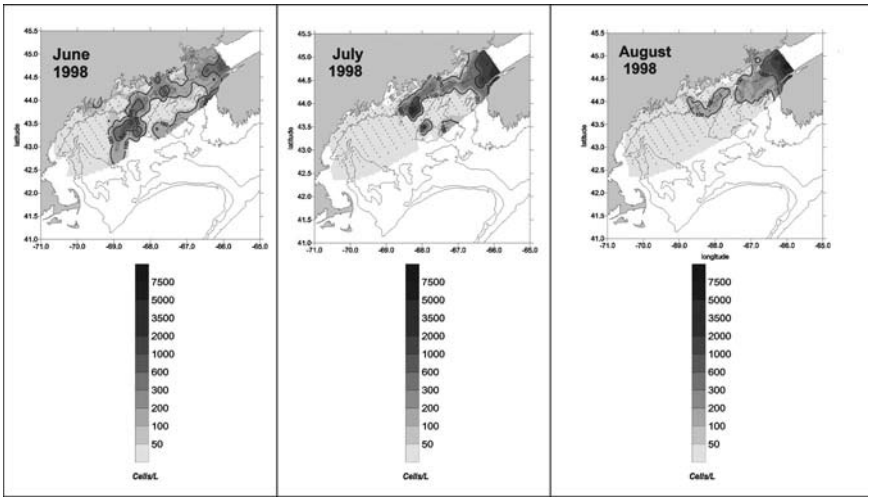

Figure 16.10
Distribution of *A. fundyense* in the Gulf of Maine observed in June, July and August 1998.
Source: adapted from Townsend et al. (2001).

system. Moreover, the centre of mass shifts from west to east (upstream in the sense of the coastal current) as the season progresses from June to August. Also evident is the persistence of high cell abundance at the mouth of the Bay of Fundy, geographically associated with a large peak in the distribution of benthic cysts (Figure 16.3). Although the observations presented in Figure 16.10 come from only a single year (1998), subsequent surveys by the ECOHAB-GOM programme in 2000 and 2001 generally corroborate these findings (Townsend et al., 2005 a).

16.5.1 Simulations based on climatology

To what extent can these large-scale seasonal patterns be explained by the population dynamics of *A. fundyense* together with the mean circulation? This question was investigated by incorporating the most skilful biological model from the western Gulf of Maine simulations described above (Section 16.4.1) into a Gulf-wide finite element model of the climatological hydrodynamics (Lynch et al., 1996). The finite element methodology facilitates realistic representation of the complex geometry in this area. Horizontal grid spacing in regions of steep topography is as fine as 500 m, and considerably coarser where such high resolution is not required. The three-dimensional model is hydrostatic, nonlinear, and incorporates advanced turbulence closure. Published solutions for the climatological mean circulation, broken down into six bi-monthly periods, are demonstrably consistent with available observations (Naimie, 1996; Naimie et al., 2001). Lynch et al. (1997) describe simulations of the climatological springtime circulation in the Maine Coastal Current system, which are particularly relevant to the present context.

Archived solutions of the hydrodynamic model are stored in a form that is available for use in an off-line transport code 'Acadia' which solves a depth-in-

tegrated form of the advection-diffusion-reaction equation on the same grid using the archived hydrodynamic information as input. Within this framework, the coupled physical-biological model for vertically averaged plankton concentration C is written

$$\frac{\partial C}{\partial t} + v.\nabla C - \frac{1}{H}\nabla(HK\nabla C) = \mu C - mC + F_g \qquad (16.12)$$

which is the two-dimensional analogue of (16.1). Climatological mean velocity and diffusivity fields are specified from the bi-monthly archive. Boundary conditions consist of (a) no flux through solid boundaries (excepting that which occurs via excystment), (b) specification of plankton concentration at inflow, and (c) computation of plankton concentration at outflow assuming no diffusive flux (i.e. $K\nabla C \,.\, \hat{n} = 0$).

This vertically averaged hydrodynamic framework precludes explicit representation of vertical structure in *A. fundyense* populations in the water column. As such, the effects of *A. fundyense*'s swimming ability are parameterized in a very basic manner. That is, newly germinated cells are assumed to reach surface waters instantly, in contrast to the multiple days it would actually take to reach the surface swimming upwards at 10 m d^{-1} from deep offshore cyst beds. This effectively eliminates the downstream advection of cells that would take place during their transit upward.

Combination of the 'mean physics' and the 'mean biology' produces results that are consistent with the three main aspects of the observed large-scale seasonal variations in *A. fundyense* populations (Figure 16.11). First, the vegetative cell distribution is gulf-wide in character. Second, the centre of mass of the cell distribution is offshore and closely associated with the coastal current system. These aspects of the solution are not unexpected, given that the largest sources of vegetative cells in the model originate from offshore cyst beds located underneath the coastal current. Finally, the centre of mass of the vegetative cell distribution shifts from west to east in a seasonal progression from late spring to late summer. Whereas the peak in simulated cell concentration occurs offshore of Casco Bay in June, the centre of mass lies in between Casco and Penobscot Bays in July, and by August it is east of Penobscot Bay. Clearly, the correspondence between the simulation and the observations presented in Figure 16.10 is not exact. For example, the simulated peaks in the cell distribution are broader and spread farther west than is observed. Nevertheless, the simulation appears to capture the three most general qualitative characteristics of the observed patterns.

16.5.2 Mechanistic diagnosis: a seasonal shift from temperature to nutrient limitation

The model solutions can be used as a basis to diagnose the processes controlling the seasonal development of *A. fundyense* blooms. Analysis of the various terms regulating growth rate is particularly useful in this regard (Figure 16.12). Generally speaking, the temperature/salinity component of the growth rate expression (fourth row) mimics the climatological temperature distribution; seasonal salinity variations have a relatively minor contribution to the gulf-wide patterns in growth rate. The nutrient limitation term (fifth row) contains significant seasonal variations with regional structure. Nitrate is in abundance in March-April, so the nutrient-limited growth rate is nearly identical to the temperature/salinity limited growth rate during that period. As the

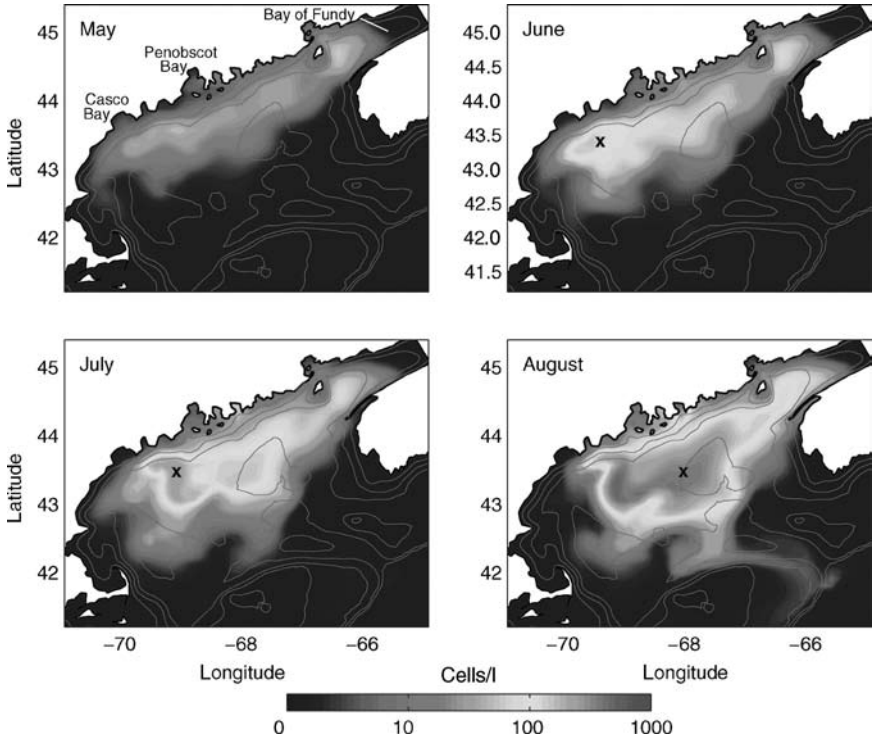

Figure 16.11
Simulated *A. fundyense* distribution under climatological forcing conditions. The following bathymetric contours are overlayed: 60 m, 100 m, 150 m, 200 m and 400 m.

season progresses, nitrate concentration declines to levels that limit growth, particularly in the western gulf. Thus, the overall growth rate (bottom row) is primarily limited by temperature in March–April; by July–August, western gulf populations are severely nutrient limited, whereas population growth continues in the eastern gulf at the temperature-limited rate. Therefore, the upstream (eastward) shift in the centre of mass of the simulated distribution can be explained by the onset of nutrient limitation in the western gulf as the season progresses.

It is noteworthy that the eastward shift is not as dramatic in the model (Figure 16.11) as it is in the observations (Figure 16.10). Specifically, the broad peak in simulated cell concentrations in August extends farther south-west than the data indicate. Townsend et al. (2001) suggest that seasonal fluctuations in both nutrient and light availability are necessary to explain the observed shift in *A. fundyense* distribution back towards the Bay of Fundy. Because the simulation reported here is forced with constant insolation, the influence of time-dependent light availability is not included. This aspect will be the subject of subsequent investigations, in which we will examine the degree to which seasonal changes in insolation and variations in water transparency amplify the eastward shift.

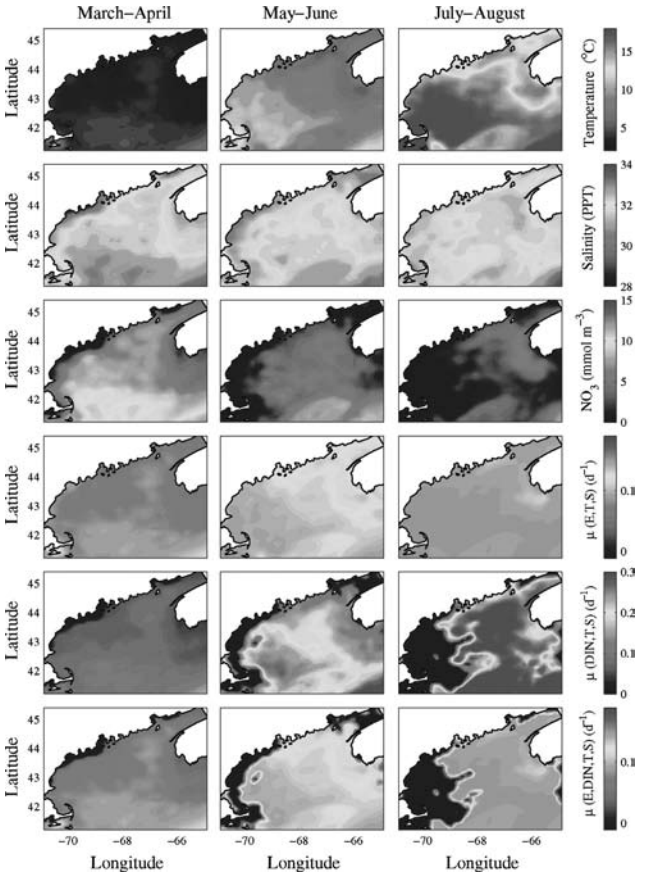

Figure 16.12
Predicted spatial variations in growth rate based on climatological conditions for March-April (left column), May–June (centre column), and July–August (right column). Top three rows: climatological temperature, salinity and nitrate. Nitrate fields are computed from temperature and salinity based on empirical relationships described in Garside et al. (1996). Lower three rows: growth rate as a function of temperature, salinity and irradiance [$\mu(T,S,E)$], growth rate as a function of temperature, and salinity, and nitrate concentration [$\mu(T,S,DIN)$], and overall growth rate [$\mu(T,S,I,DIN) = \min(\mu(T,S,I), \mu(T,S,DIN))$].

16.6 Towards the future: data-assimilative models

The preceding examples illustrate the utility of purely 'forward' models for investigation of the processes controlling *A. fundyense* blooms in the Gulf of Maine. The hindcasts described in Section 16.4.1 do not rely on data assimilation (or 'inverse'

models) to keep the circulation fields on track. This approach was made possible by the fact that the synoptic circulation in that relatively small regional domain is largely controlled by riverine buoyancy inputs and wind-forced dynamics. Such is clearly not the case in a Gulf-wide domain, in which a variety of other processes influence the circulation. Simulations based on climatology (Section 16.5.1) facilitate analysis of large-scale seasonal aspects of *A. fundyense* blooms in terms of the mean physical, biological and chemical conditions. However, the applicability of climatological models to specific synoptic situations can be limited by significant departures from mean conditions. It is in this context that data assimilation becomes essential.

During the last few years, significant progress has been made in the development of advanced data assimilation techniques for the coastal ocean (see recent reviews by Robinson and Lermusiaux, 2002; Hofmann and Friedrichs, 2002) Sequential estimation methods (e.g. nudging, optimal interpolation) blend models with observations directly, using a variety of algorithms with which the relative weights of data and model are calculated. Inverse methods have shown considerable promise in coastal oceanographic applications (for example Bennett, 1992; Bowen et al., 1995; Bogden et al., 1996; Griffin and Thompson, 1996; Thompson and Griffin, 1998). These methods seek to infer model inputs (such as parameters, forcing functions, boundary conditions, etc.) that minimize the misfit between observations and predictions.

Velocity observations in the Gulf of Maine generally contain large amplitude tidal signals, making it a challenge to diagnose the subtidal circulation fields that are largely responsible for the transport of *A. fundyense* populations. However, hindcast simulations of the subtidal flow can be constructed by assimilating both shipboard ADCP and moored velocity observations into the Dartmouth finite element model. A suite of software tools is available for the direct assimilation of velocity data via inversion for the unknown sea level elevation at open boundaries (Lynch et al., 1998; Lynch and Hannah, 2001; Lynch and Naimie, 2002).[85] These methods have shown substantial skill in the Gulf of Maine region, and have even been used at sea in real time as part of the final phase of the US GLOBEC Georges Bank programme (Lynch et al., 2001). Lynch and Naimie (2002) provide the most up-to-date description of the hindcast/forecast system (Figure 16.13). The procedure minimizes the sum of the squares of the differences between predicted and observed velocities. Inputs, in addition to velocity data, include initial conditions, atmospheric forcing and a prior estimate of the boundary conditions. These are sufficient to drive the forward three-dimensional circulation model and compare its prediction with data. The fit is improved by adjusting the boundary conditions; all other inputs are considered to be known with certainty.

The overall data-assimilative system (Figure 16.13) consists of three models: the forward simulation model (Quoddy); the exact inverse of a linearized, frequency-domain version of the forward model (Truxton); and the exact inverse of the linearized time-domain version of the forward model (Casco). Quoddy, driven by the prior estimate of the boundary conditions and other inputs, makes a prediction and computes the mismatch with data. Casco and Truxton together constitute an approximate inverse of Quoddy. They are arranged in series, with the mismatch

[85]http://www-nml.dartmouth.edu/

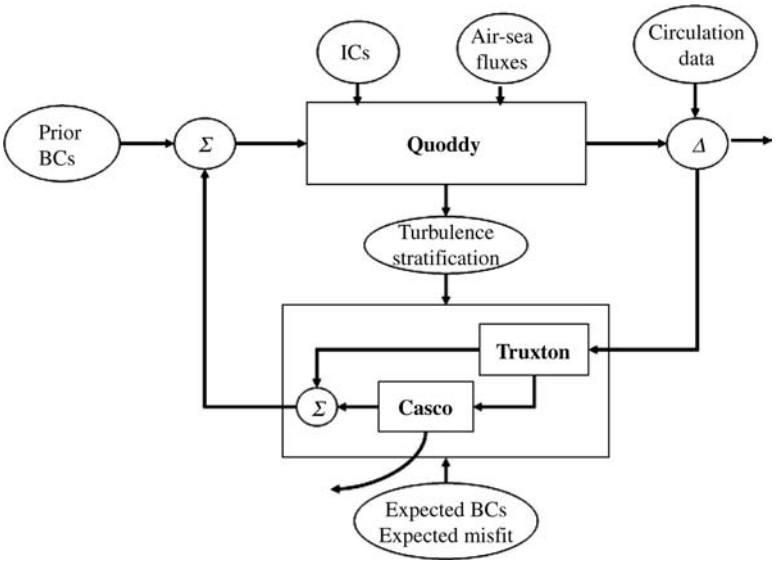

Figure 16.13
Flowchart of iterative nonlinear inversion and sequential arrangement of the nonlinear forward model (Quoddy) and the two linearized inverses, Truxton and Casco.
Source: Lynch and Naimie (2002).

de-tided first by Truxton, and Casco operating on the remaining wind-band mismatch. The two adjustments to the boundary conditions – tidal from Truxton and subtidal from Casco – are merged with the previous estimate of the boundary conditions to produce an improved estimate. This drives another Quoddy prediction, and the process is repeated until either the mismatch or the change in the mismatch from one iteration to the next, is within the observational error.

This methodology has been used to construct detailed retrospective simulations (hindcasts) of the flow field during ECOHAB-GOM survey cruises (Figure 16.14). Shipboard ADCP measurements indicate rms velocities of 12.33 cm s^{-1}. Approximately 40% of the velocity variance can be explained by climatological winds, tides and baroclinic flow that comprise the best prior estimate (BPE), such that the RMS difference between the observations and the BPE is 7.69 cm s^{-1}. One iteration of the data-assimilative loop (without the Casco module used for wind-band inversion) results in modest reduction of the residual velocity variance, bringing the RMS error down to 7.51 cm s^{-1}. The relative improvement of velocity predictions resulting from data assimilation in this case is not as large as has been achieved in other contexts (e.g. Lynch et al., 1998), and the reasons for this are currently being investigated. Nevertheless, this example demonstrates the feasibility of constructing data-assimilative hydrodynamics hindcasts for the purposes of coupled physical-biological simulations in the coastal ocean. He et al. (2005) provides another recent example in the Gulf of Maine.

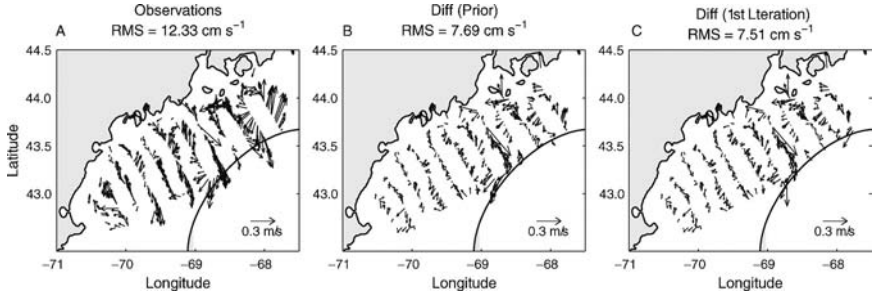

Figure 16.14
Example application of the data-assimilative modelling system shown in Figure 16.13. A, acoustic Doppler current profiler velocity observations from R/V *Oceanus* cruise 328 in August 1998.
B, vector differences between observed velocity and predictions based on the best prior estimate. C, vector differences between observed velocity and predictions after one iteration of the data assimilation procedure.

16.7 Conclusions: modelling and prediction of HABs in the context of the emerging integrated coastal ocean observing system

The advent of real-time coastal observing systems presents outstanding opportunities for both research and management of HAB phenomena. In the Gulf of Maine, coupled physical-biological models of *A. fundyense* have matured to the point that it is now feasible to assess their suitability and potential value in an operational context. A strategy for doing so could consist of three main elements:

- thorough evaluation of predictive skill in a hindcast mode using data from ECOHAB-GOM and its predecessor programmes;
- improvement of the models in light of what is learned in that evaluation;
- formulation of a plan for transition of the models to operational use.

Implied in the second of these is the fact that the dynamics of *A. fundyense* blooms are not yet fully understood. Thus, additional research is needed on the underlying physical-biological interactions that control these blooms.

An operational system based on a data-assimilative model implies an observational network to drive it. Design of such a network would be facilitated by Observational System Simulation Experiments (OSSEs; see Robinson et al., 1998; McGillicuddy et al., 2001). The idea is that model simulations can serve as a space/time continuous representation of reality, which is then subsampled in a specified fashion to produce a simulated data set. The simulated data are then fed into an analysis scheme in which they are synthesized into a reconstruction of 'reality'. Direct comparison of the reconstructed field with the 'truth' as defined by the original simulation thus provides a quantitative evaluation of that particular sampling strategy.

Such feedback between models and observations is essential as we enter the implementation phase of the Coastal Ocean Observations Module of the Global Ocean Observing System.[86] A number of recent developments in observational infrastructure show great promise for research, monitoring and prediction of HABs. For example, species-specific DNA probes for the detection and quantification of harmful algal

bloom species are now being deployed in miniaturized packages capable of autonomous sample collection and processing (Scholin et al., 2007 – Chapter 11 this volume). Such instrumentation will facilitate resolution of space and timescales of HAB variability that are inaccessible via traditional methods of cell counting (microscopy). Another major advance with respect to observational infrastructure is the emergence of a network of high-frequency radar arrays (e.g. Glenn et al., 2000) capable of measuring surface currents on an hourly basis at roughly 5 km resolution out to a range of 150 km. Such observations will provide unprecedented context in which to assess the transport and fate of HABs in the coastal ocean. As exciting as these developments are, we still face major challenges with respect to integration of the multitude of physical, biological and chemical observations that will be provided by a diverse set of both *in situ* measurement and remote sensing systems. Establishment of a conceptual basis for such integration lies at the forefront of research on interdisciplinary modelling and data assimilation.

References

Anderson, D. M. 1980. Affects of temperature conditioning on development and germination of *Gonyaulax tamarensis* (Dinophyceae) hypnozygotes. *J. Phycol.*, 16, pp. 166–72.

Anderson, D. M. 1984. Shellfish toxicity and dormant cysts in toxic dinoflagellate blooms. In: E. P. Ragelis (ed.), *Seafood Toxins*. (American Chemical Society Symposium Series.)

Anderson, D. M. 1997. Bloom dynamics of toxic *Alexandrium* species in the northeastern US. *Limnol. Oceanogr.*, 42, pp. 1009–22.

Anderson, D. M. 1998. Physiology and bloom dynamics of toxic *Alexandrium* species, with emphasis on life cycle transitions. In: D. M. Anderson, A. D. Cembella and G. M. Hallegraeff (eds), *Physiological Ecology of Harmful Algal Blooms*. Heidelberg, Springer-Verlag, pp. 29–48. (NATO Advanced Study Institute Series 41.)

Anderson, D. M. and Keafer, B. A. 1987. An endogenous annual clock in the toxic marine dinoflagellate *Gonyaulax tamarensis*. *Nature*, 325, pp. 616–17.

Anderson, D. M., Keafer, B. A., Churchill, J. H., Signell, R. P. and Geyer, W. R. 2000. *Alexandrium* blooms in the western Gulf of Maine. *Proc. Symposium on Harmful Algae*. Woods H US Marine Biological Laboratory.

Anderson, D. M., Keafer, B. A., Geyer, W. R., Signell, R. P. and Loder, T. C. 2005. Toxic *Alexandrium* blooms in the western Gulf of Maine: the 'plume advection hypothesis' revisited. *Limnol. Oceanogr.*, 50(1), pp. 328–45.

Anderson, D. M., Kulis, D. M. and Binder, B. J. 1984. Sexuality and cyst formation in the dinoflagellate *Gonyaulax tamarensis*: cyst yield in batch cultures. *J. Phycol.*, 20, pp. 418–25.

Anderson, D. M., Kulis, D. M., Doucette, G. J., Gallagher, J. C. and Balech, E. 1994. Biogeography of toxic dinoflagellates in the genus *Alexandrium* from the northeastern United States and Canada. *Mar. Biol.*, 120, pp. 467–78.

Anderson, D. M. and Lindquist, N. L. 1985. Time-course measurements of phosphorous depletion and cyst formation in the dinoflagellate *Gonyaulax tamarensis* Lebour. *J. Exp. Mar. Biol. Ecol.*, 86, pp. 1–13.

Anderson, D. M., Stock, C. A., Keafer, B. A., Bronzino, A., McGillicuddy, D. J., Keller, M. D., Thompson, B., Matrai, P. A. and J. Martin, 2005. Alexandrium fundyense cyst dynamics in the Gulf of Maine. *Deep Sea Research II*, 52, 2522–42.

Anderson, D. M. and Stolzenbach, K. D. 1985. Selective retention of two dinoflagellates in a well-mixed estuarine embayment: the importance of vertical migration and surface avoidance. *Mar. Ecol. Progr. Ser.*, 25, pp. 39–50.

[86]http://ioc.unesco.org/goos/cozo.htm

Anderson, D. M., Taylor, C. D. and Armburst, E. V. 1987. The effects of darkness and anaerobiosis on dinoflagellate cyst germination. *Limnol. Oceanogr.*, 32, pp. 340–51.

Babin, M., Roesler, C. S. and Cullen, J. J. (eds). 2006. *Real-time Coastal Observing Systems for Marine Ecosystem Dynamics and Harmful Algal Blooms: Theory, Instrumentation and Modelling*. Paris, Intergovernmental Oceanographic Commission of UNESCO. (Monographs on Oceanographic Methodology.)

Bauerfeind, E., Elbrachter, M., Steiner, R. and Throndsen, J. 1986. Application of laser Doppler spectroscopy (LDS) in determining swimming velocities in motile phytoplankton. *Mar. Biol.*, 93, pp. 323–27.

Beardsley, R. C., Butman, B., Geyer, W. R. and Smith, P. 1997. Physical oceanography of the Gulf of Maine: an update. *Proc. Gulf of Maine Ecosystem Dynamics Scientific Symposium and Workshop*. Regional Association for Research in the Gulf of Maine, Hanover NH, USA: Report 97-1 pp. 39–52.

Bennett, A. F. 1992. *Inverse Methods in Physical Oceanography*. Cambridge, UK, Cambridge University Press.

Bigelow, H. B. 1927. Physical oceanography of the Gulf of Maine. *Bull. US Bur. Fish.*, 40, pp. 511–1027.

Blumberg, A. F. and Mellor, G. L. 1987. A description of a three-dimensional coastal ocean circulation model. In: N. Heaps (ed.), *Three-Dimensional Coastal Ocean Models*. Washington DC, American Geophysical Union, pp. 1–16.

Bogden, P. S., Malanotte-Rizzoli, P. and Signell, R. P. 1996. Open-ocean boundary conditions from interior data: local and remote forcing of Massachusetts Bay. *J. Geophys. Res.*, 101, pp. 6487–500.

Bowen, A. J., Griffin, D. A., Hazen, D. G., Matheson, S. A. and Thompson, K. R. 1995. Shipboard nowcasting of shelf circulation. *Cont. Shelf Res.*, 15, pp. 115–28.

Brooks, D. A. 1985. Vernal circulation in the Gulf of Maine. *J. Geophys. Res.*, 90, pp. 4687–705.

Brooks, D. A. and Townsend, D. W. 1989. Variability of the coastal current and nutrient pathways in the eastern Gulf of Maine. *J. Mar. Res.*, 47, pp. 303–21.

Cox, D. R. and Hinckley, D. V. 1974. *Theoretical Statistics*, 1st edn. New York, Chapman & Hall.

Fasham, M. J. R. and Evans, G. T. 1995. The use of optimization techniques to model marine ecosystem dynamics at the JGOFS station at 47N 20W. *Phil. Trans. Roy. Soc. Lond. B*, 348, pp. 203–09.

Fong, D. A., Geyer, W. R. and Signell, R. P. 1997. The wind-forced response on a buoyant coastal current: observations of the western Gulf of Maine plume. *J. Mar. Syst.*, 12, pp. 69–81.

Franks, P. J. S. and Anderson, D. M. 1992*a*. Alongshore transport of a phytoplankton bloom in a buoyancy current: *Alexandrium tamarense* in the Gulf of Maine. *Mar. Biol.*, 112, pp. 153–64.

Franks, P. J. S. and Anderson, D. M. 1992*b*. Toxic phytoplankton blooms in the southwestern Gulf of Maine: testing hypotheses of physical control using historical data. *Mar. Biol.*, 112, pp. 165–74.

Friedrichs, M. A. M. and Hofmann, E. E. 2001. Physical control of biological processes in the central equatorial Pacific Ocean. *Deep Sea Res.*, 48, pp. 1023–69.

Garside, C., Garside, J. C., Keller, M. D. and Sieracki, M. E. 1996. The formation of high nutrient low salinity water in the Gulf of Maine: a nutrient trap? *Estuar. Coast. Shelf Sci.*, 42, pp. 617–28.

Geraci, J. A. et al. 1989. Humpback whales *Megaptera novaeangliae* fatally poisoned by dinoflagellate toxin. *Can. J. Fish. Aquat. Sci.*, 46, pp. 1895–98.

Glenn, S. M., Boicourt, W., Parker, B. and Dickey, T. D. 2000. Operational observational networks for ports, a large estuary and an open shelf. *Oceanography*, 13, pp. 12–23.

Griffen, D. A. and Thompson, K. R. 1996. The adjoint method of data assimilation used operationally for shelf circulation. *J. Geophys. Res.*, 101, pp. 3457–77.

He, R., McGillicuddy, D. J., Lynch, D. R., Smith, K. W., Stock, C. A. and Manning, J. P. 2005. Data assimilative hindcast of the Gulf of Maine coastal circulation. *J. Geophys. Res.* 110, C10011, doi 10.10292004JC002807.

Hetland, R. D., McGillicuddy, D. J. and Signell, R. P. 2002. Cross-frontal entrainment of plankton into a buoyant plume: the frog tongue mechanism. *J. Mar. Res.*, 60, pp. 763–77.

Hofmann, E. E. and Friedrichs, M. A. M. 2002. Predictive modelling for marine ecosystems. In: A. R. Robinson, J. J. McCarthy and B. J. Rothschild (eds), *The Sea*. Vol. 12: *Biological-Physical Interactions in the Ocean*. New York, John Wiley & Sons, pp. 537–65.

Hurtt, G. C. and Armstrong, R. A. 1996. A pelagic ecosystem model calibrated with BATS data. *Deep Sea Res I*, 43, pp. 653–83.

Keafer, B. A., Buesseler, K. O. and Anderson, D. M. 1992. Burial of living dinoflagellate cysts in estuarine and nearshore sediments. *Mar. Micropaleontol.*, 20, pp. 147–61.

Keafer, B. A., Churchill, J. H., McGillicuddy, D. J. and Anderson, D. M. Bloom development and transport of toxic *Alexandrium fundyense* population within a nearshore coastal plume in the Gulf of Maine. *Deep Sea Res. II*, 52, pp. 2674–94.

Langdon, C. 1987. On the causes of interspecific differences in the growth-irradiance relationships for phytoplankton. Part I: A comparative study of the growth irradiance relationships of three marine phytoplankton species: *Skelotonema costatum, Olithodiscus luteus* and *Gonyaulax tamarensis*. *J. Plankton Res.*, 9, pp. 459–82.

Langdon, C. 1988. On the causes of interspecific differences in the growth-irradiance relationship for phytoplankton. Part II: A general review. *J. Plankton Res.*, 10, pp. 1291–312.

Liebig, J. 1845. On chemical processes in the nutrition of vegetables, chemistry and its applications to agriculture and physiology. *L. Playfair*.

Luerssen, R., Thomas, A. C. and Hurst, J. W. 2005. Relationships between satellite-measured thermal features and *Alexandrium*-imposed toxicity in the Gulf of Maine. *Deep Sea Res., II,* 52, 2656–73.

Lynch, D. R. and Hannah, C. G. 2001. Inverse model for limited-area hindcasts on the continental shelf. *J. Atmos. Ocean. Tech.*, 18, pp. 962–81.

Lynch, D. R., Holboke, M. J. and Naimie, C. E. 1997. The Maine coastal current: spring climatological circulation. *Cont. Shelf Res.*, 17, pp. 605–34.

Lynch D. R., Ip, J. T. C., Naimie, C. E. and Werner, F. E. 1996. Comprehensive coastal circulation model with application to the Gulf of Maine. *Cont. Shelf Res.*, 16, pp. 875–906.

Lynch, D. R. and Naimie, C. E. 2002. Hindcasting the Georges Bank circulation. Part II: Windband inversion. *Cont. Shelf Res.*, 22, pp. 2191–224.

Lynch, D. R., Naimie, C. E. and Hannah, C. G. 1998. Hindcasting Georges Bank circulation. Part I: Detiding. *Cont. Shelf Res.,* 18, pp. 607–39.

Lynch, D. R. et al. 2001. Real-time data assimilative modeling on Georges Bank. *Oceanography*, 14, pp. 65–77.

MacIntyre, J. G., Cullen, J. J. and Cembella, A. D. 1997. Vertical migration, nutrition and toxicity in the dinoflagellate *Alexandrium tamarense*. *Mar. Ecol. Progr. Ser.*, 148, pp. 201–16.

McGillicuddy, D. J., Anderson, D. M., Lynch, D. R. and Townsend, D. W. Mechanisms regulating the large-scale seasonal fluctuations in *Alexandrium fundyense* populations in the Gulf of Maine. *Deep Sea Res. II*.

McGillicuddy, D. J., Lynch, D. R., Wiebe, P., Runge, J., Gentleman, W. C. and Davis, C. S. 2001. Evaluating the US Globec Georges Bank broad-scale sampling pattern with Observational System Simulation Experiments. *Deep Sea Res. II*, 48, pp. 483–99.

McGillicuddy, D. J. Jr, Signell, R. P. Stock, C. A., Keafer, B. A., Keller, M. D. Hetland, R. D., and Anderson, D. M. 2003. A mechanism for offshore initiation of harmful algal blooms in the coastal Gulf of Maine. *J. Plankton Res.*, 25(9), pp. 1131–38.

Naimie, C. E. 1996. Georges Bank residual circulation during weak and strong stratification periods: prognostic numerical model results. *J. Geophys. Res.*, 101, pp. 6469–86.

Naimie, C. E., Limeburner, R., Hannah, C. G. and Beardsley, R. C. 2001. On the geographic and seasonal patterns of the near-surface circulation on Georges Bank – from real and simulated drifters. *Deep Sea Res. II*, 48, pp. 501–18.

Platt, T. and Jassby, A. D. 1976. The relationship between photosynthesis and light for natural assemblages of coastal marine phytoplankton. *J. Phycol.*, 12, pp. 421–30.

Poulton, N. J. 2001. Physical and behavioral diagnostics of nitrogen limitation for the toxic dinoflagellate *Alexandrium fundyense*. Ph.D. thesis, Cambridge, Mass., Massachusetts Institute of Technology, 246 pp.

Prakash, A. 1967. Growth and toxcity of a marine dinoflagellate, *Gonyaulax tamarensis*. *J. Fish. Res. Board Can.*, 24, pp. 1589–606.

Robinson, A. R. and Lermusiaux, P. F. J. 1998. Data assimilation. In: K. H. Brink and A. R. Robinson (eds), *The Sea*. Vol. 10: *The Global Coastal Ocean. Processes and Methods*. New York, John Wiley & Sons, pp. 541–94.

Robinson, A. R. and Lermusiaux, P. F. J. 2002. Data assimilation for modelling and predicting physical-biological interactions in the sea. In: A. R. Robinson, J. J. McCarthy and B. J. Rothschild (eds), *The Sea*. Vol. 12: *Biological-Physical Interactions in the Ocean*. New York, John Wiley & Sons, pp. 475–536.

Stock, C. A., D. J. McGillicuddy, A. R. Solow, D. M. Anderson, 2005. Evaluating hypotheses for the initiation and development of *Alexandrium fundyense* blooms in the western Gulf of Maine using a coupled physical-biological model. *Deep-Sea Res*. II 52, 2715–44.

Teegarden, G. J. and Cembella, A. D. 1996. Grazing of toxic dinoflagellates, *Alexandrium* spp. by adult copepods of coastal Maine: implications for the fate of paralytic shellfish toxins in marine food webs. *J. Exp. Mar. Biol. Ecol.*, 196, pp. 145–76.

Thompson, K. R. and Griffin, D. A. 1998. A model of the circulation of the outer Scotian Shelf with open boundary conditions inferred from data assimilation. *J. Geophys. Res.*, 103, pp. 30641–60.

Townsend, D. W., Bennett, S. L. and Thomas, M. A., 2005b. Diel vertical distributions of the red tide dinoflagellate *Alexandrium fundyense* in the Gulf of Maine. *Deep-Sea Res. II*, 52, 2593–602.

Townsend, D. W., Christensen, J. P., Stevenson, D. K., Graham, J. J. and Chenoweth, S. B. 1987. The importance of a plume of tidally-mixed water to the biological oceanography of the Gulf of Maine. *J. Mar. Res.*, 45, pp. 699–728.

Townsend, D. W., Pettigrew, N. R. and Thomas, A. C. 2001. Offshore blooms of the red tide dinoflagellate *Alexandrium* sp., in the Gulf of Maine. *Cont. Shelf Res.*, 21, pp. 347–69.

Townsend, D. W., Pettigrew, N. R. and Thomas, A. C. 2005a. On the nature of offshore *Alexandrium fundyense* blooms in the Gulf of Maine. *Deep Sea Res. II*, 52, pp. 2603–30.

Vezina, A. F. and Platt, T. 1988. Food web dynamics in the ocean. I: Best-estimates of flow networks using inverse methods. *Mar. Ecol. Progr. Ser.*, 42, pp. 269–87.

Watras, C. J., Chisholm, S. W. and Anderson, D. M. 1982. Regulation of growth in an estuarine clone of *Gonyaulax tamarensis* Lebour: salinity-dependent temperature responses. *J. Exp. Mar. Biol. Ecol.*, 62, pp. 25–37.

White, A. W., Fukuhara, O. and Anraku, M. 1989. Mortality of fish larvae from eating toxic dinoflagellates or zooplankton containing dinoflagellate toxins, pp. 395–98. In: T. Okaichi and T. Nemoto (eds), Red Tides: Biology Environmental Science and Toxicology. Amsterdam, Elsevier.

17

Modelling coastal dynamics and harmful algal blooms in the Baltic Sea

W. Fennel and T. Neumann

17.1 Introduction

This chapter deals with the modelling of the dynamics of nutrients and phytoplankton in the Baltic Sea. Although the Baltic is special in many respects, our modelling approach can, to a certain extent, also be applied to other systems, because modelling involves both site-specific and universal aspects of the considered marine systems.

There is increasing concern regarding harmful algal blooms in the Baltic, due to mass developments of cyanobacteria which threaten environmental quality and public health in coastal areas. Modelling cyanobacterial blooms requires coupled models which link physical processes with chemical-biological model components. This chapter gives a brief description of the Baltic Sea. Modelling is then introduced with illustrated examples to show how simple chemical-biological models can be developed and used. Finally, an advanced fully three-dimensional model of the Baltic is presented.

17.2 Baltic sea

The Baltic is a semi-enclosed sea with only narrow connections to the ocean through the Danish straits. Being located in the range between 54°N to 66°N, it stretches from subarctic to temperate climatic conditions and is exposed to highly variable winds and many storm events. The northern parts of the Baltic are regularly ice covered during the winter. Owing to a substantial fresh water input from several rivers distributed around the Baltic Sea, it has a positive water balance. Because of the freshwater surplus and the restricted water exchange, the Baltic is one of the largest brackish water seas in the world. The relative shallow sea has a mean depth of about 50 m and consists of several basins connected by sills. In its central part, the Gotland Basin, the depth is about 270 m. A map of the bathymetry of the Baltic is shown in Figure 17.1. General overviews of the oceanography of Baltic Sea are given, for example, in Stigebrandt (2001), Kullenberg (1981) and Ehlin (1981).

17.2.1 Physical features and scales relevant to the ecosystem

Two physical features of the Baltic Sea that are especially relevant for shaping the ecosystem are the permanent halocline and a seasonally varying thermocline. The halocline implies a high vertical stability which in turn hinders the vertical exchange. Therefore, anoxic conditions frequently occur in the deep waters below the halocline.

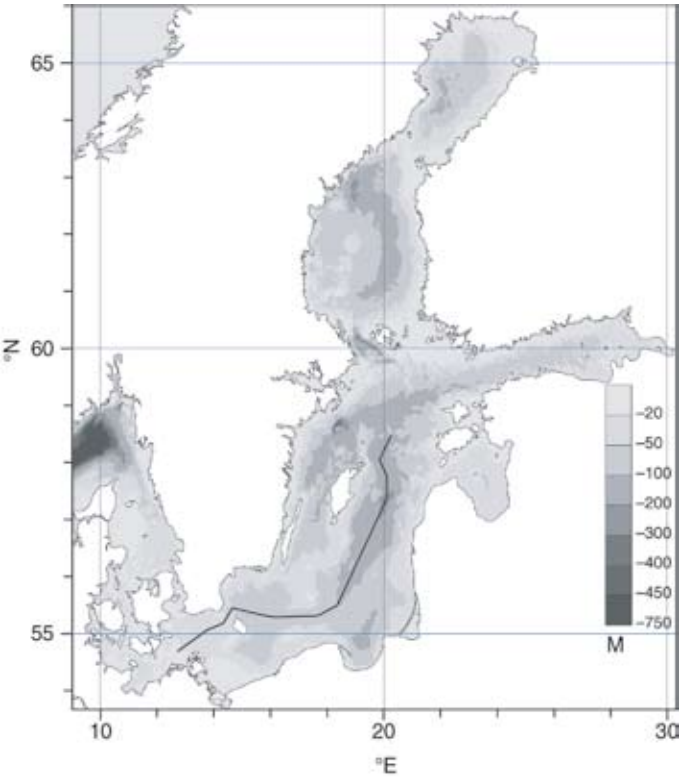

Figure 17.1
The bathymetry of the Baltic Sea with an indication of the monitoring survey along the Talweg, for later reference.

The general structure of the salinity and oxygen distribution is shown in Figure 17.2 by means of a section along the Talweg (i.e. the path along the maximum depths) observed in winter. This section is monitored several times a year in the frame of the Baltic Monitoring Programme.[87] The summer conditions are similar for the salinity and oxygen but the temperature distribution shows a strong seasonal cycle, with the formation of a warm upper layer of 10–20 m thickness and a strong thermocline below. Examples of the temperature distributions along this section in winter and summer are shown in Figure 17.3. Vertical profiles of temperature and salinity usually show stronger gradients than the vertically and horizontally interpolated distributions plotted in Figures 17.2 and 17.3 suggest.

The annual cycle of temperature is driven by the yearly cycle of solar radiation. The salt balance is maintained by a dynamical equilibrium between near-bottom inflow of saline water, outflow of brackish surface water and vertical salt diffusion through the halocline. The deeper water can only be ventilated through horizontal propagation of dense saline bottom water, which is formed in the transition areas between the

[87]Acronym BMP; see www.helcom.fi for more information.

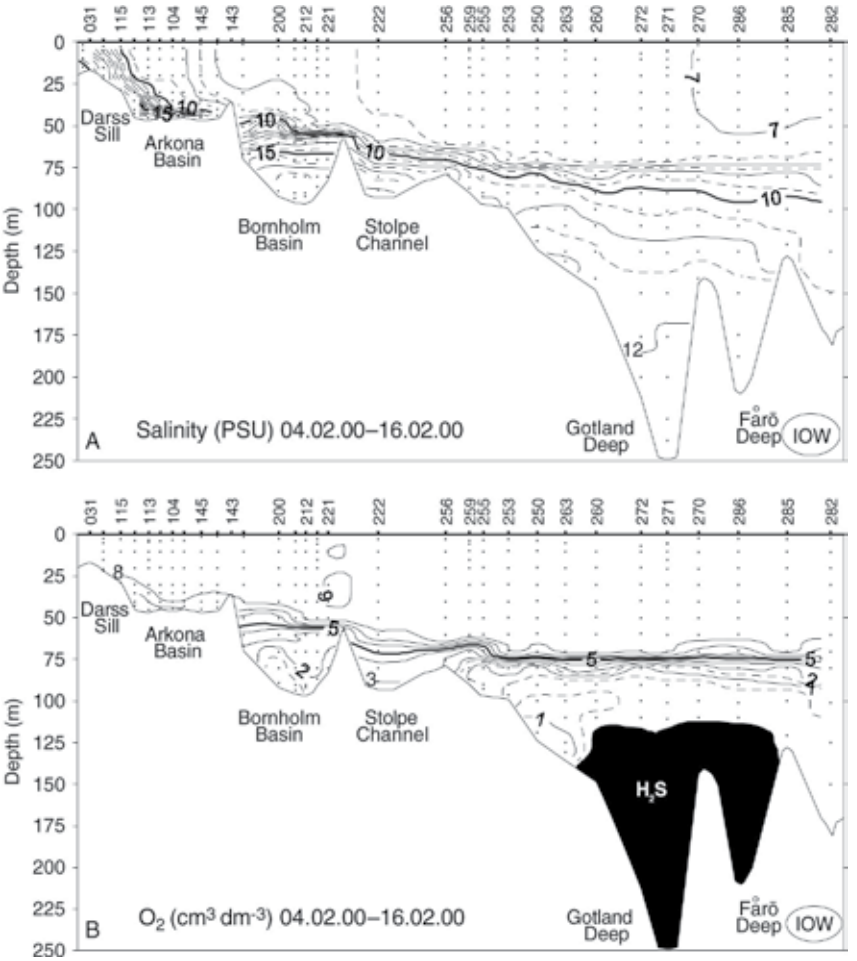

Figure 17.2
Examples of the typical horizontal-vertical distribution of salinity and oxygen through the Baltic along the Talweg section (see Figure 17.1). The basin-wide salinity distribution and the horizontal and vertical structure of the halocline are indicated. Anoxic conditions are often found in the central Baltic below the halocline. The data were taken from a monitoring cruise of the Baltic Sea Research Institute (IOW) in 2000.

North Sea and the Baltic and cascades over the sills until it arrives in the central basin. In particular, irregularly occurring major salt water inflows renew the deep water in the central Baltic. The poor ventilation of the deep water below the halocline favours anoxic conditions and the formation of hydrogen sulphide, which can formally be considered as negative oxygen. The variations in oxygen and switching to negative values affect the biogeochemistry of the near bottom water and the upper sediments.

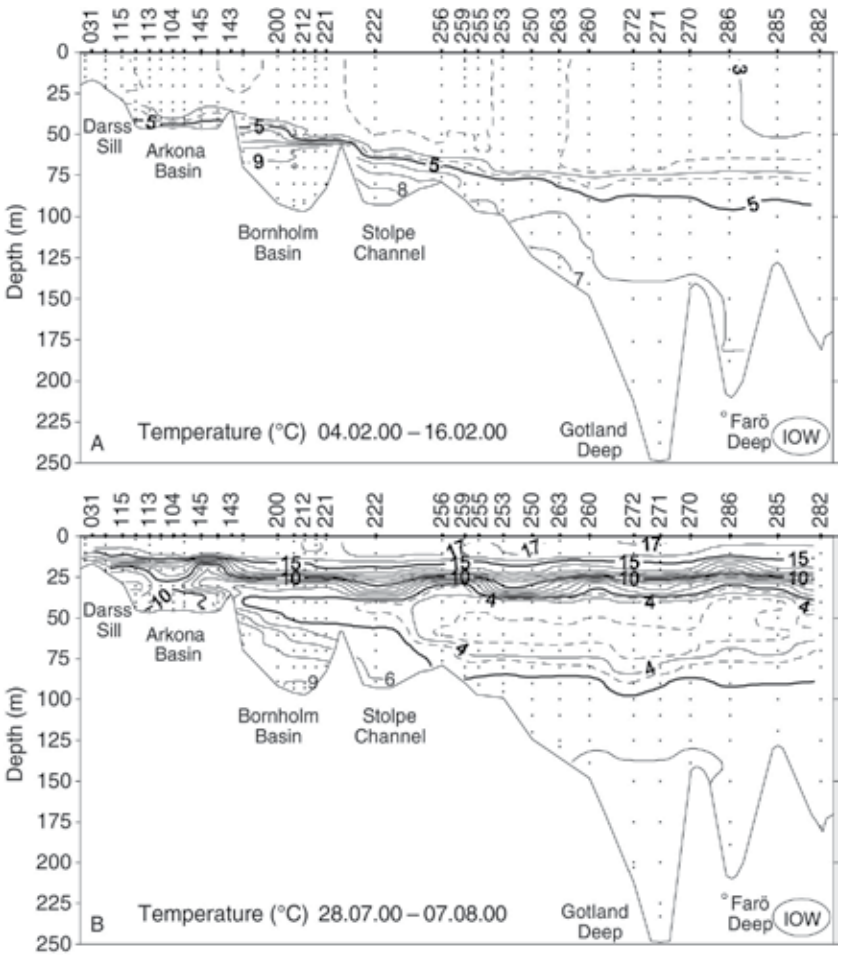

Figure 17.3
Examples of the typical horizontal-vertical distribution of temperature along the Talweg (see Figure 17.1): A, winter; B, summer conditions. The warm upper surface layer above the thermocline in summer is a typical feature of the Baltic.

The horizontal and vertical salinity gradients associated with the permanent halocline set the long-term conditions for the marine ecosystem. The salinity gradients affect osmo-regulations of living cells and, therefore, the number of species in the Baltic is relatively small. The annual cycle of temperature, which is associated with the formation of the thermocline in spring and its disappearance in autumn, defines a seasonal timescale. Irregular weather patterns, which are typical for the latitudes between 50°N and 60°N, generate in the Baltic Sea a variety of mesoscale currents, such as eddies, coastal jets and associated upwelling and downwelling patterns, with timescales of a few days to weeks. These mesoscale features are reflected in the distribution patterns

of nutrients and plankton, because the chemical and biological stocks are dispersed or concentrated by the combined effect of advection and turbulent diffusion.

17.2.2 Cycles of nutrients and plankton

The seasonal changes of the stratification implies a typical mid-latitudinal annual cycle of nutrients and plankton (Schulz et al., 1978). The phytoplankton spring bloom starts in March in the south-western parts of the Baltic and propagates northward during April and early May. This delay is controlled by the winter conditions. During cold winters, the water is cooled below the temperature of the maximum density and a stable winter stratification takes place. This typical stratification can favour small intermittent blooms which will be destroyed due to convection as soon as the water reaches the temperature of maximum density. Only after the formation of a warm upper layer the bloom is stabilized. After relatively mild winters the bloom may start at the same time in a wider area in response to solar radiation.

The succession of phytoplankton can roughly be described by three functional groups: diatoms, flagellates and cyanobacteria. The spring bloom is dominated by diatoms, which sink relative rapidly out of the euphotic layer, followed by flagellates, which are neutrally buoyant, and cyanobacteria, which can float to the surface and accumulate there. The primary production in the southern and central Baltic is mainly limited by nitrogen, while in the northern part phosphorous is the limiting nutrient. Zooplankton biomass develops slowly after the phytoplankton spring bloom and reaches maximum concentration in the summer season. Sinking cells, dead zooplankton and other detritus can either be mineralized below the thermocline and may reenter the upper part of the water column by mixing due to strong wind events and convection, or dead organic material can sink below the halocline and be trapped there for longer periods.

External sources of nutrients are the river loads discharged into the Baltic and atmospheric deposition. The cycle of phosphorous in the food web is closed, apart from external sources, while for nitrogen there are two additional pathways: denitrification, which corresponds to a loss of nitrogen, and nitrogen fixation by cyanobacteria, which implies a biologically driven input of nitrogen into the system.

17.2.3 Eutrophication and cyanobacteria

In the decades from 1960 to 1980, a substantial increase of nutrients was recorded in the Baltic Sea in response to anthropogenic activities taking place in the drainage area. The effects of the increased river nutrient loads discharged into the Baltic can clearly be detected in the winter level of the nutrients. The nitrogen loads increased by a factor of four and the phosphorous increased 8-fold, Larsson (1985). This eutrophication favours anoxic conditions below the halocline. Although there is a clear evidence from sediment records that anoxic conditions occurred many times in the deep water during the history of the Baltic Sea, it is assumed that the long duration and spatial extent of hydrogen sulphide distributions in the 1980s and 1990s indicate effects of an anthropogenic impact.

A further concern is the possible relationship between eutrophication and harmful algal blooms (HAB). In the Baltic, the most conspicuous kind of HAB is the noxious surface accumulations of cyanobacteria. Although cyanobacteria seems to be natural to the Baltic Sea, a recent increase in their occurrence has been suggested to be a

Figure 17.4
Surface accumulation of cyanobacteria in the central Baltic as seen from a ship.
Source: courtesy H. Siegel.

response to the increased nutrient load during the twentieth century (Kahru et al., 1994).

An example of a surface accumulation as seen from a research vessel is shown in Figure 17.4. Distribution patterns of cyanobacterial surface accumulations can clearly be detected by ocean-colour satellite imagery (e.g. Siegel and Gerth, 2000). An example of an image with a relatively high resolution is shown in Figure 17.5.

In the Baltic, the most important cyanobacteria species forming surface accumulations are *Nodularia* and *Aphanizomenon*. The former only is potentially toxic, but both are harmful as they produce noxious surface accumulations and scum that can

Figure 17.5
Cyanobacterial surface accumulations in the south-western Baltic as seen from space by means of a high-resolution satellite picture.
Source: courtesy H. Siegel.

be concentrated along coasts and in bays by winds and currents, and affect the environmental quality. Although the total biomass of cyanobacteria is substantially smaller than that of the other functional groups, they play an important role in the system due to their ability to fix atmospheric nitrogen. Diazotrophs are generally restricted to conditions of N/P ratios below the Redfield ratio, in which they compete successfully with the other groups when nitrogen is depleted. At a station in the Baltic, a demonstration of a clear increase in nitrogen concentration in the whole upper mixed layer as a result of nitrogen fixation was given by Larsson et al. (2001). Since cyanobacteria can draw on atmospheric nitrogen, their growth is generally considered as being limited by the availability of dissolved phosphorous in the water column. Since the N/P-ratio in the water column controls the occurrence and the intensity of cyanobacterial blooms (Wasmund 1997), the understanding and modelling of cyanobacterial bloom dynamics cannot be accomplished by an isolated consideration of cyanobacteria in a single-species model, but rather needs the consideration of community interactions and competition with other functional groups.

Aphanizomenon dominates the summer peak of cyanobacteria and are generally present in small concentrations in other seasons, while *Nodularia* are found only in the summer (Kononen, 1992). A significant increase in *Aphanizomenon* biomass is found a few weeks after inorganic nitrogen is depleted in the upper mixed layer while phosphate is usually still present in measurable concentrations (Larsson et al., 2001). Although *Nodularia* often co-occurred with *Aphanizomenon* during the summer peak, its occurrence is more irregular in time with substantial inter-annual variability in maximum biomass.

The important physical factors that control the distribution and intensity of cyanobactarial blooms are irradiance, temperature, salinity and wind-driven turbulent mixing. While the first three factors affect the growth rates, turbulence in the upper layer counteract the upward floating of cells and destroys surface accumulations.

17.2.4 Scope, possibilities and limitations of model

Mathematical models are obviously the only way to provide quantitative descriptions of the system that permit 'model-experiments' and simulations of future developments. Modelling of harmful cyanobacteria blooms in the Baltic Sea includes the following two research elements:

- Analyses of cyanobacterial blooms in response to environmental changes (e.g. climate variations and changes in nutrient loads of the rivers).
- Forecasts of transport routes of noxious surface accumulations if they are detected, for example, by satellite imagery.

The first element addresses the study of 'what-if' scenarios, such as effects of changes in N/P ratios or the understanding of interannual variations in the occurrence of cyanobacteria blooms. Such studies provide a scientific basis for designing long-term environmental management of both the sea and the drainage area. This kind of research requires further interdisciplinary experimental and theoretical work to improve the realism of the model formulation. The second element concerns operational predictions of developments over the next few days and relies on the availability of real-time data. The question to be addressed is how a detected bloom will spread and which areas are likely to be affected. To accomplish this operational task, an infrastructure needs to be developed which comprises real-time observations and models with data assimilation capabilities.

Both elements require advanced models and observations. The Baltic Sea is one of the most intensively observed marine environments and extensive data sets are available. A long-term monitoring programme, which involves several ship cruises in different seasons, has been maintained over many years and provides regular input into the existing database. Moreover, three real-time observation systems are deployed at the entrance area of the Baltic and allowed to observe the water exchange with the North Sea. A Swedish station is located in the Sound and two German observation systems are moored on the Darss Sill and in the Arkona Basin and cover the pathways of saline water towards the central Baltic. The data sets provide unique possibilities to support modelling efforts with data for calibration and validation.

However, model runs comprising several decades are limited in several ways. There are still difficulties in simulating the correct dynamical balance of the halocline correctly for model integrations over many years. The description of food-web dynamics and biogeochemical processes in the models needs further elaboration and the availability of forcing data, in particular river loads, must be improved.

For the short-term forecast of spreading harmful cyanobacterial blooms, the satellite imagery is a key source in guiding research vessels to the locations where the blooms occur and providing the initial conditions to simulate transport routes based on weather forecasts or on scenario studies. Such efforts are curtailed by the timescale of reliable weather forecasts which are needed to drive models, by the quality of initialization data, and by the limitations of the current generation of chemical-biological models. An example of a successful quasi-online modelling of an exceptional event was that of the response of the Baltic to the extreme Oder flood in summer 1977 (Siegel et al., 1999).

17.3 Modelling

Model development involves three steps: (a) construction of the model, (b) performing simulations, and (c) visualization and evaluation of the results. Construction of models consists in formalizing dynamical relationships derived from field observations or laboratory experiments.

Models can be developed for individuals, populations and communities. In nature there are individuals (cells, copepods, fish), having biomass, and forming populations and communities which interact up, down and across the food web. The study of different facets of the complex network of the food web are motivated by striving for answers to specific questions with the help of models. Therefore it is reasonable, and virtually the only tractable way, to reduce the complexity with models. Models of HABs may consider cells or populations of species of interest. The individuals are characterized by a set of properties, for example starting as cysts which are 'switched on' in response to environmental signals or internal clocks, and the model may track their propagation from seed locations to other areas. Models can be constructed to reproduce the production of toxin in cells in response to changing internal nutrient pools.

Other HAB models may look at populations of species of interest and describe aggregation in thin layers in response to turbulence or, in conjunction with toxin production, as a behavioural strategy to avoid predation. Moreover, models can be used to describe interactions and competition within communities in order to simulate the condition under which HAB species become important or dominating. The latter type

of problems corresponds in particular to questions on the occurrence of cyanobacteria in systems such as the Baltic Sea and is discussed in this study. Thus, in the following modelling is not focused on single cells but on abundance or concentration of biomass, which represent assemblages of many individuals.

17.3.1 Approach

The building blocks of the models, considered below, are state variables and process descriptions which quantify the interaction of the state variables. State variables are measurable, well defined quantities which consist of a numerical value and a dimension expressed in appropriate units. For example, phytoplankton can be considered as concentration or abundance, expressed in grams or numbers of individuals per cubic metre. Process descriptions can be complex functions of several other state parameters or physical quantities and are expressed as rates, that is numerical values over time. The rates embrace cause-effect relationships in a quantitative manner.

The choice of state variables depends strongly on the aim of the modelling effort. In order to describe environmental or ecological processes, it is desirable to reduce the complexity of the natural system as far as possible. This can be done by considering only the processes of first order importance, and ignoring those that are less important in the given context.

Chemical-biological models are from the mathematical point of view sets of differential equations, where the dynamical changes of state variables are driven by processes. The complexity of the models corresponds, among other factors, to the number of state variables or, equivalently, to the number of equations since one equation is needed for each state variable for mathematical consistency. While copepod development from eggs to adults embraces an increase of mass by 2 orders of magnitude or so, the development of mass by phytoplankton cells is small, say up to a factor of 2. Hence, for the functional groups of phytoplankton, life cycles need usually not be resolved explicitly and the models can be written for biomass or abundance of the groups. An important exception in HAB-related studies is the case where the formation of spores or cysts is crucial and needs to be taken into account. In this case, further state variables that comprise dormant stages must be defined.

The typical form of model equations which describe the change of state variables, S_i, in a parcel of water is given by differential equations of the following form:

$$\frac{\mathrm{d}}{\mathrm{d}t} S_i = \Big[\mathrm{gain}(S_j) - \mathrm{loss}(S_j) \Big] S_i + Q^{\mathrm{extern}}, \tag{17.1}$$

where for biomass models 'gain' refers to rates, such as uptake of nutrients by phytoplankton or ingestion of phytoplankton by zooplankton and others, while 'loss' terms describe transfer of material from phytoplankton by respiration or zooplankton by excretion for example. The rates have the dimension of one over time and may depend on other parameters and state variables. For population models the 'gain' refers to birth rates and 'loss' to death rates. Formally the equation can be integrated as

$$S_i(t) = S_i(0) + \int_0^t \mathrm{d}t' \{ (\mathrm{gain}(t') - \mathrm{loss}(t')) S_i(t') + Q^{\mathrm{extern}}(t') \}. \tag{17.2}$$

The state variable $S_i(t)$, at a time t, depends on the initial value $S_i(0)$ and the history of the development, which is included by the integral over time. Thus, apart from

an adequate description of the rates, the initial conditions must be known. This property of differential equations is the key for the predictive potential of models.

An example of a 'gain rate' is the uptake of nutrients of a concentration, N, by phytoplankton. This rate can be written as a limiting function

$$M(N) = r_{\max} \frac{N^2}{\alpha^2 + N^2}, \tag{17.3}$$

where $r_{\max}$ is the maximum uptake rate, set by the intrinsic cell properties for given conditions of light and temperature, and α is a half saturation constant. There are two extreme situations for high or low nutrient concentrations,

$$\begin{aligned} M(N) &= r_{\max} \rightarrow N^2 >> \alpha^2, \\ M(N) &= r_{\max} \frac{N^2}{\alpha^2} \rightarrow N^2 << \alpha^2. \end{aligned} \tag{17.4}$$

The biological timescale, which is given by the inverse rate, is independent of the nutrient concentration for plentiful available nutrients, but it depends on the nutrient concentration for small concentrations.

17.3.2 Coupling to physics

The above discussion ignores the spatial dimension of the problem. In marine systems the chemical-biological state variables are subject to mixing and transport. Moreover, environmental conditions such as temperature, salinity, turbidity, available light and other factors affect the evolution of the state variables. The natural way to include all these processes into an integrated model system is to link an Ocean Circulation Model with the chemical-biological model components to construct three-dimensional models of the marine ecosystem. The development of Ocean Circulation Models has made substantial progress in the last decades. Since the model equations are rigorous mathematical formulations of basic principles of the geophysical fluid dynamics and thermodynamics, further improvement of these models mainly depends on:

- parameterizations of sub-grid processes,
- quality of forcing data, initialization fields etc.,
- prescription of the dependent variables at open boundaries.

These types of problem also apply to the chemical-biological model components. Moreover, biological models cannot be derived directly from general principles, such as conservation of mass and energy. They have to obey the fundamental laws, but the process formulation must be developed through the translation of observations into mathematical expressions (Fennel and Neumann, 2001, 2004).

The interface linking chemical-biological model components and circulation models are the advection diffusion equations for 'tracers', that is the state variables S_i,

$$\frac{\partial}{\partial t} S_i + \nabla \cdot \vec{v} S_i - \nabla A \cdot \nabla S_i = (\text{gain} - \text{loss}) S_i + Q^{\text{extern}}. \tag{17.5}$$

The advection, $\vec{v} = (u, v, w + w_{\text{bio}})$, involves the current and the active motion, w_{bio}, which is the speed of sinking or vertical migration. Turbulent mixing is a subgrid process which is parameterized by eddy diffusivities A. External sources or sinks can be, for example, river discharges or burial in sediments and are accounted for by the term Q^{extern}. The change of the state variables with time is controlled by physical rates,

expressed through operators $\nabla \cdot (\vec{v} \cdots)$ and $\nabla A \cdot \nabla(\cdots)$, which describe the changes due to advection and turbulence, while the *gain* and *loss* rates governs the change driven by chemical and biological processes. The ratios of the different rates determine whether physical or chemical-biological controls dominate the changes.

The work with three-dimensional models requires a substantial effort to run the model and to visualize the results. For many tasks it is more efficient to simplify the coupling to physical process. For example by integration over the spatial coordinates the advection-diffusion equation for the state variable can be reduced to a purely time dependent model, a so-called box model. Integration of the advection diffusion (17.1) over the horizontal coordinates gives a one-dimensional model, a so-called water column model, which takes vertical variations into account but ignores horizontal transport. Such simplified models can be helpful for the phase of model development and also to highlight some specific aspects of chemical-biological interactions.

17.3.3 Construction of chemical-biological models

In order to illustrate the process of model building we start with a box model, where the physical control is strongly simplified, and we concentrate first on the biological part of the problem. The box model consists of two stacked boxes, where the upper one represents the surface layer and the second one describes the lower part of the water column. In the upper box we assume an annual temperature variation prescribed by the mean mixed layer temperature of the Arkona Basin in the Baltic Sea, as shown in Figure 17.6A. The light conditions are taken into account by a normalized length of the day (d(t) is the actual day length divided by 24 hours), see Figure 17.6B. Moreover we assume that the two boxes are vertically mixed during the winter season but are isolated for the rest of the year, starting in the spring to mimic the formation of an upper layer.

As we wish to apply this model to the Baltic Sea, we chose to represent three components of nutrients: nitrate N, ammonium A and phosphate PO. This is motivated by the limiting role of nitrogen in the Baltic, and because cyanobacteria are limited by phosphorous. In order to cover the seasonal succession of the important phytoplankton groups, we assume that the model phytoplankton consists of three functional groups: diatoms P_1, flagellates P_2, and cyanobacteria (blue-green algae) P_3. The groups have different dynamical signatures: the growth rate of diatoms is considered to be insensitive to temperature variations, while that of flagellates and cyanobacteria depends strongly on temperature. Only the diatoms are assumed to sink. Both nitrogen and phosphorous can limit the growth of diatoms and flagellates, while cyanobacteria are limited only by phosphate due to their ability to fix atmospheric nitrogen. The nitrogen fixation is an 'expensive', energy demanding process and therefore the cyanobacteria can take full advantage of their ability of nitrogen fixation only when nitrate and ammonium are depleted.

The living and dead particulate organic material (POM) is expressed by nitrogen units and we assume that the Redfield-ratio, $S_{\text{Redfield}} = 1/16$, for phosphorous and nitrogen applies. The model plankton releases ammonium and phosphate through respiration in the fixed ratio, S_{Redfield}. Ammonium can be consumed again by the phytoplankton or it can be transformed to nitrate, (nitrification). The zooplankton is covered by an aggregated bulk biomass state variable, Z. Dead organic matter is counted in a detritus state variable D. Detritus is mineralized into ammonium and phosphate at the Redfield-ratio. The state variables are listed in Table 17.1.

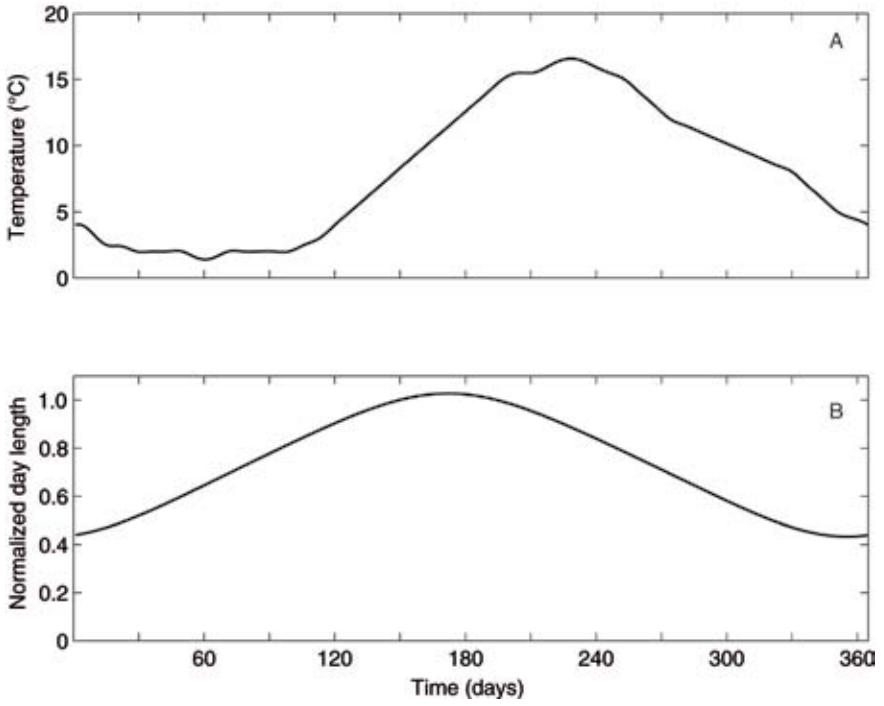

Figure 17.6
A, mean annual variation of the surface layer temperature in the central Arkona basin of the Baltic Sea; B, normalized length of day for 54°N.

For each of the two vertically arranged boxes we have to describe the dynamics of the eight state variables. Thus, the model consists of a total of 16 state variables whose dynamics is controlled by 16 equations. We use an upper index in brackets to indicate the corresponding box and we start with the set of equations for ammonium $A^{(1)}$, nitrate $N^{(1)}$, phosphate $PO^{(1)}$, diatoms, flagellates, cyanobacteria $P_i^{(1)}$, with (i = 1, 2, 3), detritus $D^{(1)}$ and zooplankton $Z^{(1)}$ for the upper box.

Table 17.1 State variables and their initial values (mmol m^{-3})

Variable	Meaning	Initial values upper box	Initial values lower box
P_1	Diatoms	0.045	0.045
P_2	Flagellates	0.045	0.045
P_3	Cyanobacteria	0.045	0.045
Z	Zooplankton	0.045	0.045
D	Detritus	0.045	1.8
A	Ammonium	0.09	0.09
N	Nitrate	4.5	4.5
PO	Phosphate	0.15	0.15

We write the model equations explicitly and begin with the nutrients in the upper box.

$$\begin{aligned}
\frac{\mathrm{d}}{\mathrm{d}t}A^{(1)} &= -\Pi_{\mathrm{A}}(R_1P_1^{(1)} + R_2P_2^{(1)}) + l_{\mathrm{P_1A}}(P_1^{(1)} - P_{\mathrm{o}}) + l_{\mathrm{P_2A}}(P_2^{(1)} - P_{\mathrm{o}}) + l_{\mathrm{P_3A}}(P_3^{(1)} - P_{\mathrm{o}}) \\
&\quad + l_{\mathrm{ZA}}(Z^{(1)} - Z_0) - L_{\mathrm{AN}}A^{(1)} + L_{\mathrm{DA}}D^{(1)}, \\
\frac{\mathrm{d}}{\mathrm{d}t}N^{(1)} &= -\Pi_{\mathrm{N}}(R_1P_1^{(1)} + R_2P_2^{(1)}) + L_{\mathrm{AN}}A^{(1)} - A_{\mathrm{mix}}(N^{(1)} - N^{(2)}) + Q_{\mathrm{N}}^{\mathrm{ext}}, \qquad (17.6) \\
\frac{\mathrm{d}}{\mathrm{d}t}PO^{(1)} &= S_{\mathrm{Redfield}}\left\{-\sum_{i=1}^{3} R_iP_i^{(1)} + l_{\mathrm{P_1A}}(P_1^{(1)} - P_{\mathrm{o}}) + l_{\mathrm{P_2A}}(P_2^{(1)} - P_{\mathrm{o}}) + l_{\mathrm{P_3A}}(P_3^{(1)} - P_{\mathrm{o}})\right. \\
&\quad \left. + l_{\mathrm{ZA}}(Z^{(1)} - Z_0) + L_{\mathrm{DA}}D^{(1)}\right\} - A_{\mathrm{mix}}(PO^{(1)} - PO^{(2)}) + Q_{\mathrm{PO}}^{\mathrm{ext}}.
\end{aligned}$$

Here R_i are the growth rates of the groups of the model phytoplankton, which control the uptake of nutrients, while Π_{A} and Π_{N} are the preference ratios, $\Pi_{\mathrm{A}} = \mathrm{A}/(\mathrm{A} + \mathrm{N})$ and $\Pi_{\mathrm{N}} = \mathrm{N}/(\mathrm{A} + \mathrm{N})$. The loss rates l_{XY} and L_{XY} prescribe the transfers among state variables, 'loss of X transferred to Y'. The lower case refers to constant parameters, while the upper case represents functions that depend on other state variables or environmental parameter, for example temperature. The transfer to ammonium describes respiration while the transfer to detritus refers to mortality. The nitrification is controlled by L_{AN} and L_{DA} describes the mineralization of detritus by microbial activity, where

$$L_{\mathrm{AN}} = l_{\mathrm{AN}}\, e^{\beta_{\mathrm{AN}}T}, \quad L_{\mathrm{DA}} = l_{\mathrm{DA}}(1 + \beta_{\mathrm{DA}}Y(T_{\mathrm{DA}}, T)), \qquad (17.7)$$

and Y is a limiting function of the type

$$Y(\alpha, x) = \frac{x^2}{\alpha^2 + x^2}. \qquad (17.8)$$

External supply of nutrients can be prescribed by Q^{ext} and the vertical mixing between the boxes is set by the rate A_{mix}. As nitrification is a relatively fast process we ignore vertical mixing and external supply of ammonium for the sake of simplicity. The mixing is switched off if the daylength exceeds that of day 50, $d_{50} = d(50)$, and the temperature of the surface box exceeds $T_0 = 2.5$°C,

$$A_{\mathrm{mix}} = a_{\mathrm{mix}}\theta(d(t) - d_{50})\theta(T - T_0) \qquad (17.9)$$

where $a_{mix} = 0.5\mathrm{d}^{-1}$. The equations for the three groups of model phytoplankton are

$$\begin{aligned}
\frac{\mathrm{d}}{\mathrm{d}t}P_1^{(1)} &= R_1P_1^{(1)} - l_{\mathrm{P_1A}}(P_1^{(1)} - P_0) - G_1Z^{(1)} - w_1^{\mathrm{sink}}(P_1^{(1)} - P_0) \\
\frac{\mathrm{d}}{\mathrm{d}t}P_2^{(1)} &= R_2P_2^{(1)} - (l_{\mathrm{P_2A}} + l_{\mathrm{P_2D}})(P_2^{(1)} - P_0) - G_2Z^{(1)} \qquad (17.10) \\
\frac{\mathrm{d}}{\mathrm{d}t}P_3^{(1)} &= R_3P_3^{(1)} - (l_{\mathrm{P_3A}} + l_{\mathrm{P_3D}})(P_3^{(1)} - P_0) - G_3Z^{(1)}
\end{aligned}$$

The diatoms sink at a rate w_1^{sink} into the bottom box and the mortality in the upper box can be ignored, while the flagellates and cyanobacteria stay in the upper box. For the growth rates we use the following formulas, which reflect different dynamical signatures of the functional groups. The growth of model diatoms is independent of tempeature and they are limited by either nitrate or phosphate,

$$R_1 = r_1^{\max} \min[Y(\alpha_1, A+N), Y(S_{\text{Redfield}}\alpha_1, PO)]. \tag{17.11}$$

where the maximum rate $r_1^{\max}$, reflects intrinsic properties of the cells.

For the flagellates we use a similar relationship but with a temperature control

$$R_2 = r_2^{\max}\left(1+\frac{1}{1+e^{\beta_{\text{fl}}(T_{\text{fl}}-T)}}\right)\min[Y(\alpha_2, A+N), Y(S_{\text{Redfield}}\alpha_2, PO)]. \tag{17.12}$$

The model cyanobacteria are limited only by phosphate because of their ability to fix atmospheric nitrogen. The corresponding growth rate is

$$R_3 = r_3^{\max}\frac{1}{1+e^{\beta_{cy}(T_{cy}-T)}}Y(S_{\text{Redfield}}\alpha_3, PO). \tag{17.13}$$

As the growth of cyanobacteria is independent of the dissolved nitrogen, the development of cyanobacterial biomass implies addition of nitrate in proportion to the consumed phosphate, scaled by the Redfield ratio.

The phytoplankton dynamic is controlled by the model zooplankton which consumes the phytoplankton groups with slightly different preferences expressed by the grazing rates G_i.

The dynamics of detritus and zooplankton in the upper layer are described by the equations.

$$\begin{aligned}\frac{\mathrm{d}}{\mathrm{d}t}D^{(1)} &= l_{\text{P}_2\text{D}}(P_2^{(1)}-P_0)+l_{\text{P}_3\text{D}}(P_3^{(1)}-P_0)+l_{\text{ZD}}(Z^{(1)}-Z_0)-L_{\text{DA}}D^{(1)}\\ &\quad -G_{\text{D}^{(1)}}Z-w_{\text{D}}^{\text{sink}}D^{(1)},\\ \frac{\mathrm{d}}{\mathrm{d}t}Z^{(1)} &= (G_1+G_2+G_3+G_{\text{D}^{(1)}})Z^{(1)}-(l_{\text{ZA}}+l_{\text{ZD}})(Z^{(1)}-Z_0).\end{aligned} \tag{17.14}$$

The model zooplankton grazes also on detritus. Detritus sinks into the lower layer at a rate $w_{\text{D}}^{\text{sink}}$. The other terms are self-explanatory.

The grazing is food limited and expressed in terms of Ivlev type functions. The rates are different for different food items, the phytoplankton groups and detritus. The rates are defined as,

$$\begin{aligned}G_1^{(1,2)} &= \Pi_1^{(1,2)}g_1^{\max}(1-\exp(-I_{\text{v}}P_1^2)),\\ G_2 &= \Pi_2 g_2^{\max}\,\mathrm{e}^{a_E T}(1-\exp(-I_{\text{v}}P_2^2)),\\ G_3 &= \Pi_3 g_3^{\max}(1-\exp(-I_{\text{v}}P_3^2)),\end{aligned} \tag{17.15}$$

Table 17.2 Phytoplankton rates

Parameter	Diatoms ($i = 1$)	Flagellates ($i = 2$)	Cyanobacteria ($i = 3$)
Growth rate ($r_i^{\max}$)	1 d^{-1}	0.7 d^{-1}	0.5 d^{-1}
Half saturation (α_i)	1.35	0.675	2.25
Sinking rate (box model)	$w_1^{\text{sink}} = 0.1$ d^{-1}	0	0
Respiration rate (l_{PA})	0.01 d^{-1}	0.01 d^{-1}	0.01 d^{-1}
Mortality (l_{PD})	0.02 d^{-1}	0.02 d^{-1}	0.02 d^{-1}
Temperature parameters	–	$T_{\text{fl}} = 9°C$ $\beta_{\text{fl}} = 1/°C$	$T_{\text{cy}} = 16°C$ $\beta_{\text{cy}} = 1/°C$

and

$$G_{\text{D}^{(1,2)}} = g_{\text{D}^{(1,2)}}^{\max}\left[1-\exp(-I_{\text{v}}D^{(1,2)2})\right]. \tag{17.16}$$

The upper indexes in brackets refer to the upper, (1), and lower (2) model boxes, while the lower indexes indicate the functional group. For the grazing on flagellates we assume a dependence on temperature by an Eppley factor. The preference rates are defined as

$$\begin{aligned}
&\Pi_1^{(1,2)} = \frac{P_1^{(1,2)}}{P_{\text{sum}}^{(1,2)}}, \quad \Pi_2 = \frac{P_2}{P_{\text{sum}}}, \quad \Pi_3 = \frac{P_3}{P_{\text{sum}}}, \quad \Pi_D^{(1,2)} = \frac{D^{(1,2)}}{P_{\text{sum}}}, \\
&P_{\text{sum}} = \sum_{i=1}^{3} P_i^{(1,2)} + D^{(1,2)}.
\end{aligned} \tag{17.17}$$

The parameters involved are listed in Tables 17.2 and 17.3.
For the lower model box the equations for the nutrients are

$$\begin{aligned}
\frac{\text{d}}{\text{d}t}A^{(2)} &= l_{\text{ZA}}(Z^{(2)} - Z_0) - l_{\text{AN}}A^{(2)} + l_{\text{DA}}D^{(2)}, \\
\frac{\text{d}}{\text{d}t}N^{(2)} &= l_{\text{AN}}A^{(2)} + A_{\text{mix}}(N^{(1)} - N^{(2)}), \\
\frac{\text{d}}{\text{d}t}PO^{(2)} &= S_{\text{Redfield}}(l_{\text{ZA}}(Z^{(2)} - Z_0) + l_{\text{DA}}D^{(2)}) + A_{\text{mix}}(PO^{(1)} - PO^{(2)}).
\end{aligned} \tag{17.18}$$

The temperature in the lower layer is kept constant at the winter level, because after the formation of a thermocline the upper and lower boxes are isolated. Therefore the loss rates, which depend on temperature in the upper box, are constant parameters in the lower box. The phytoplankton occurring in the lower layer is the model diatom group, which is produced in the upper layer and sinks down.

$$\begin{aligned}
\frac{\text{d}}{\text{d}t}P_1^{(2)} &= w_1^{\text{sink}}(P_1^{(1)} - P_0) - l_{\text{P}_1\text{D}}(P_1^{(2)} - P_0) - G_1Z^{(2)}, \\
\frac{\text{d}}{\text{d}t}P_2^{(2)} &= 0, \\
\frac{\text{d}}{\text{d}t}P_3^{(2)} &= 0.
\end{aligned} \tag{17.19}$$

Table 17.3 Zooplankton and recycling rates

Parameter				
Grazing rates	$g_1^{\max} = 0.25\ \mathrm{d}^{-1}$	$g_2^{\max} = 0.5\ \mathrm{d}^{-1}$	$g_3^{\max} = 0.25\ \mathrm{d}^{-1}$	$g_{\mathrm{D}}^{\max} = 0.15\ \mathrm{d}^{-1}$
Ivlev constant	$I_{\mathrm{v}} = 1.5 \exp(a_{\mathrm{E}}\, T)$			
Eppley constant	$a_{\mathrm{E}} = 0.063/°\mathrm{C}$			
Respiration rate	$l_{\mathrm{ZA}} = 0.03\ \mathrm{d}^{-1}$			
Mortality	$l_{\mathrm{ZD}} = 0.01\mathrm{d}^{-1}$			
Recycling	$l_{\mathrm{DA}} = 0.03$	$\beta_{\mathrm{DA}} = 20°\mathrm{C}$	$T_{\mathrm{DA}} = 13°\mathrm{C}$	
Sinking rate (box model)	$w_{\mathrm{D}}^{\mathrm{sink}} = 0.15\ \mathrm{d}^{-1}$			
Nitrification rate	$l_{\mathrm{AN}} = 0.1\ \mathrm{d}^{-1}$	$\beta_{\mathrm{AN}} = 0.11/°\mathrm{C}$		

The detritus and zooplankton equations for the lower box are

$$\frac{\mathrm{d}}{\mathrm{d}t} D^{(2)} = l_{\mathrm{P_1D}}(P_1^{(2)} - P_0) + l_{\mathrm{ZD}}(Z^{(2)} - Z_0) - l_{\mathrm{DA}} D^{(1)} - G_{\mathrm{D}^{(2)}} Z + w_{\mathrm{D}}^{\mathrm{sink}} D^{(1)},$$
$$\frac{\mathrm{d}}{\mathrm{d}t} Z^{(2)} = (G_1 + G_{\mathrm{D}^{(2)}}) Z^{(1)} - (l_{\mathrm{ZA}} + l_{\mathrm{ZD}})(Z^{(2)} - Z_0). \tag{17.20}$$

17.3.4 Box-model experiments

Although the box model outlined in Section 17.3.3 is a strongly simplified description of real systems, it allows an understanding of important properties of the system through experimental simulations. Such a model can easily be programmed using standard software packages, such as MATLAB. Example programs (m-files) can be found in Fennel and Neumann (2004). As a kind of baseline run, we begin with a simulation of the annual cycle with no external nutrient input or deposition at the bottom. The initial conditions of the runs are listed in Table 17.1.

First we consider the case without active cyanobacteria. The results for nutrients and phytoplankton are shown in Figures 17.7 and 17.8. The spring bloom is dominated by the model diatoms, which are controlled by sinking into the bottom layer where they decrease due to grazing and mortality. The model flagellates form the summer population, while the model cyanobacteria, which are not activated (no growth, mortality and grazing) stay at their background level. Owing to the initial choice of the N/P ratio, nitrogen is the limiting nutrient while phosphate is still available during summer. Since the nitrogen is used up during the spring bloom, the model flagellates depend mainly on regenerated nutrients. Due to the mineralization of detritus in the lower model box, the recycled nutrients accumulate there but are mixed into the upper layer during autumn and winter. There is a small difference of the results in the first year compared with the following model years due to the adjustment of the model to the initial conditions. After the first year the annual cycle recurs.

Next we 'activate' the model cyanobacteria and repeat the simulation. Owing to the specific dynamical signatures of the cyanobacteria, we find significantly different results (see Figures 17.9 and 17.10). In addition to the spring bloom, which is

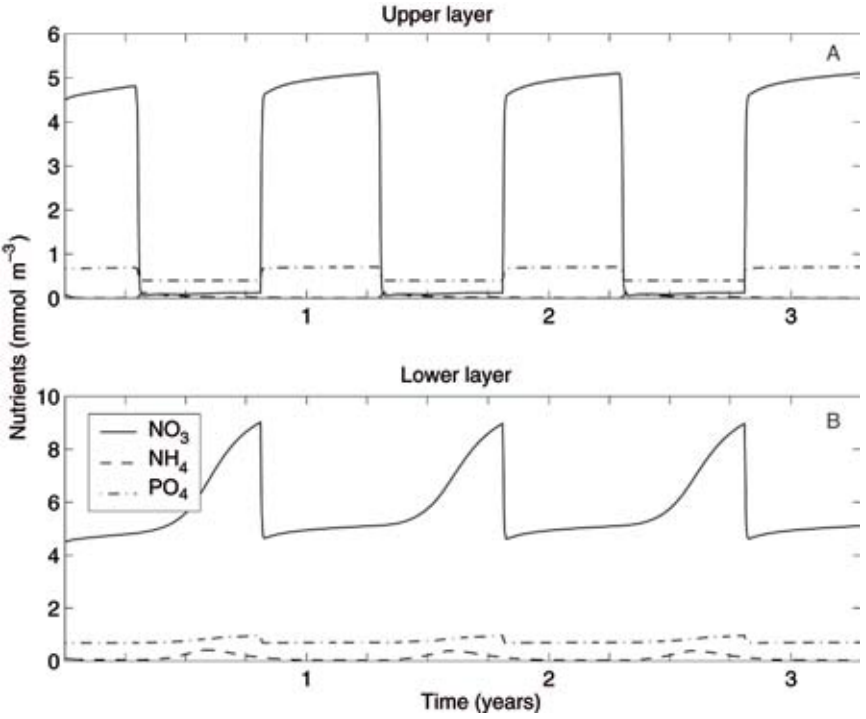

Figure 17.7
Results of the first model experiment (no active cyanobacteria and no external input) showing nutrient variations in A, upper; B, lower layers. *Source*: redrawn from Fennel and Neumann (2004).

again dominated by the model diatoms, there is a strong summer peak of the model cyanobacteria in the first model year. In the following years the spring bloom peaks increase, while the cyanobacteria peaks in the summer decrease. This behaviour can easily be understood by means of the nutrient cycle. The peak of the cyanobacteria in summer develops when nitrate is depleted but dissolved phosphate is still available. The ability to fix atmospheric nitrogen allows the cyanobacteria to continue their growth and use up the dissolved phosphorus until it is also depleted. Thus the cyanobacteria provide a substantial input of nitrogen to the system. During the winter the nutrient levels in the upper layer are re-established due to recycling and vertical mixing, whereas the total nitrogen pool grows. At the next spring bloom the diatoms use the enhanced nitrogen pool, which yields a higher spring bloom peak. This implies also an increased uptake of phosphate during the spring bloom and, consequently, a decrease of the summer phosphate level. Hence the cyanobacteria are strongly limited by phosphorus and can not develop as strong as in the preceding model year. In the second year there is still a substantial nitrogen fixation which further increases the nitrogen pool. This scenario recurs for several years until a stable annual cycle is reached where the nutrients are used up after the spring bloom and cyanobacteria plays only a minor role. The timescale of this adjustment is a couple of years, as shown in Figure 17.11, where the total sums of nitrogen and phosphate in all state variables are plotted over

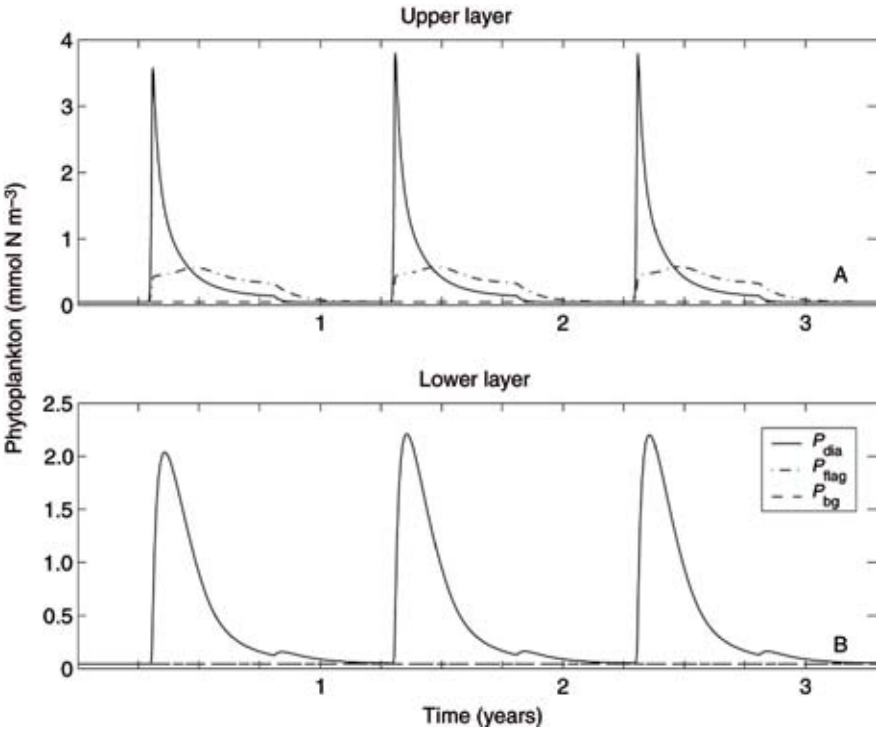

Figure 17.8
As Figure 17.7, but for model diatoms and flagellates.

three model years. The import of nitrogen by fixation ceases after a few years, while the total phosphate is strictly conserved. Cyanobacterial blooms can only occur for a N/P ratio less than the Redfield ratio.

In the next experiment we add nitrate to the upper box by enhancing the concentration at a rate of $Q_N^{ext}=0.0045$ mmol m^{-3} d^{-1}. This increase in the model nitrogen implies increased spring blooms, which use up the phosphate. Only in the first model year is there a clear signal due to nitrogen fixation (Figure 17.12). During the following model years, the winter level of nitrogen is elevated and allows increasing spring blooms (Figure 17.13), such that phosphate becomes totally depleted. This prevents cyanobacterial blooms in summer. The evolution of the total nitrogen and phosphate over several years is shown in Figure 17.14. The addition of nitrate shifts the N/P ratio of inorganic nutrients towards the Redfield ratio and beyond (see Figure 17.18).

In the last experiment we add phosphate instead of nitrate to the upper box at a rate of $Q_{PO}^{ext}=0.0045$ mmol m^{-3} d^{-1}. This leads to an increase in both model phosphate and nitrogen, driven by the external source and the nitrogen fixation, respectively (Figure 17.15). Now the model system adjusts to a pattern with increasing spring bloom signals and a recurrent cyanobacterial bloom in each summer because of the extra phosphate added to the system after the spring bloom (Figure 17.16). The cyanobacteria blooms provide a stepwise input of nitrogen from year to year, shown in

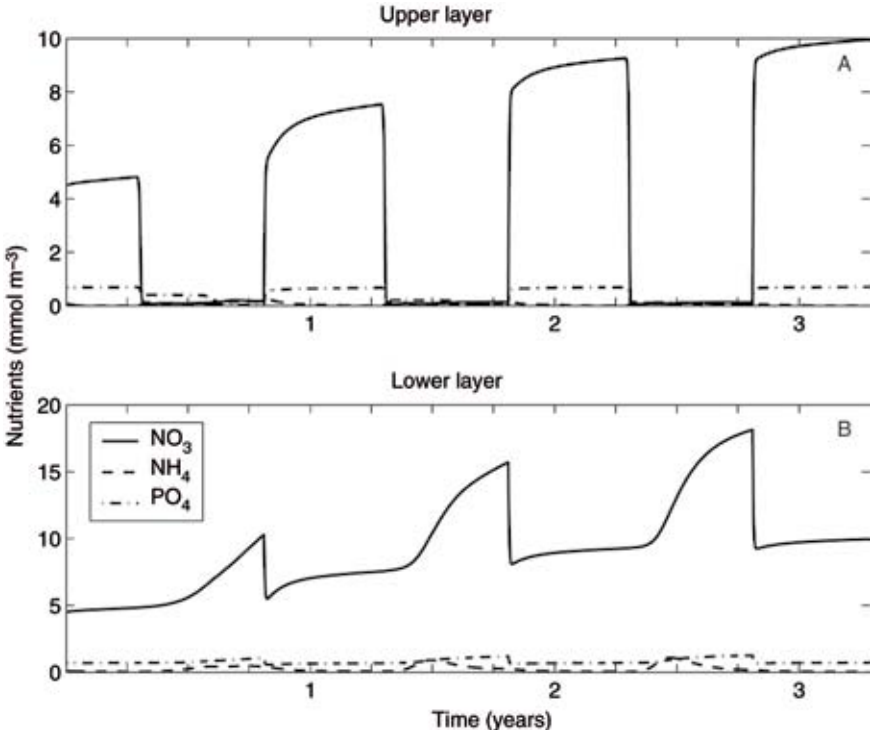

Figure 17.9
Results of the second model experiment (active cyanobacteria but no external input) showing nutrient variations in A, upper; B, lower layers. *Source*: redrawn from Fennel and Neumann (2004).

the total nitrogen and phosphate in Figure 17.17. In this case there is no mechanism to restrict the nitrate fixation of the cyanobacteria and, after several years, the model shows an unrealistic degree of eutrophication.

In natural systems such accumulation of nitrogen is counteracted by biogeochemical processes. Increased production gives rise to enhanced levels of detritus and consequently enhanced microbial activity to mineralize the material. These processes consume oxygen, which will be depleted in near bottom waters and in the sediments. Anoxic conditions favour denitrification, which provides a pathway of nitrogen to leave the system. These processes are not included in the simplified box model version. Since in real systems substantial amounts of nitrogen loads are removed already in estuaries and shallow coastal zones, it is obvious that in more realistic studies the horizontal transport must be included. We will consider these processes in the three-dimensional ecosystem modelling in the next section.

We conclude the discussion with a brief consideration of the N/P ratios of dissolved inorganic nutrients for the four model experiments, which are plotted in Figure 17.18. For all experiments the start values are close to seven. Without active cyanobacteria and external fluxes the ratio (solid line) shows an annual cycle with low values

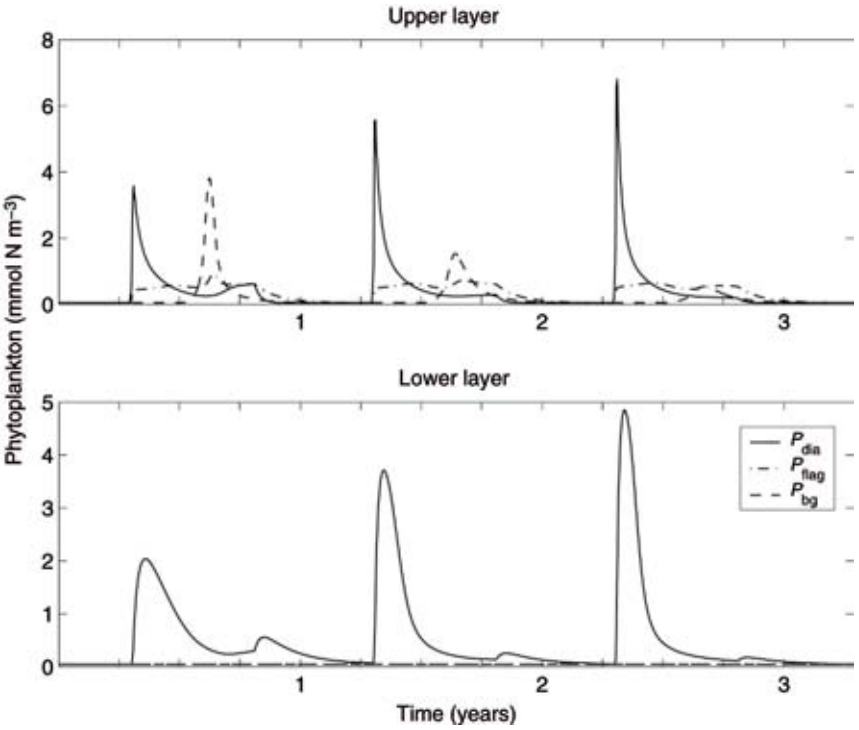

Figure 17.10
As Figure 17.9, but for model diatoms, flagellates and cyanobacteria.

after the spring bloom and re-established start conditions in winter. With cyanobacteria but no external input (dotted line) the ratio shows a trend towards the Redfield ratio due to nitrogen fixation. If we externally add nitrate the nitrogen pool increases faster and the N/P ratio (dash-dot) reaches the Redfield ratio and goes beyond after a few years. External addition of phosphate forced a stronger annual variation of the N/P ratio (dashed line) with a slowly increasing trend towards the Redfield ratio.

Although the aspects of horizontal advection are neglected in this approach, there are example systems, such as semi-enclosed gulfs or well mixed lagoons, for which box models can be a reasonable approach (e.g. Savchuk, 2002; Humborg et al., 2000).

17.4 Three-dimensional ecosystem models

After the construction and application of the biogeochemical model in the previous sections we will now link this model component, with a few additional features, to a circulation model which provides a three-dimensional perspective of a modelled environment. An ecosystem approach implies the consideration of biogeochemical processes within the physical surrounding. Box or one-dimensional models are indispensable as first step in model development and to obtain an overall impression of how these systems work, but these models capture only a limited part of the physics

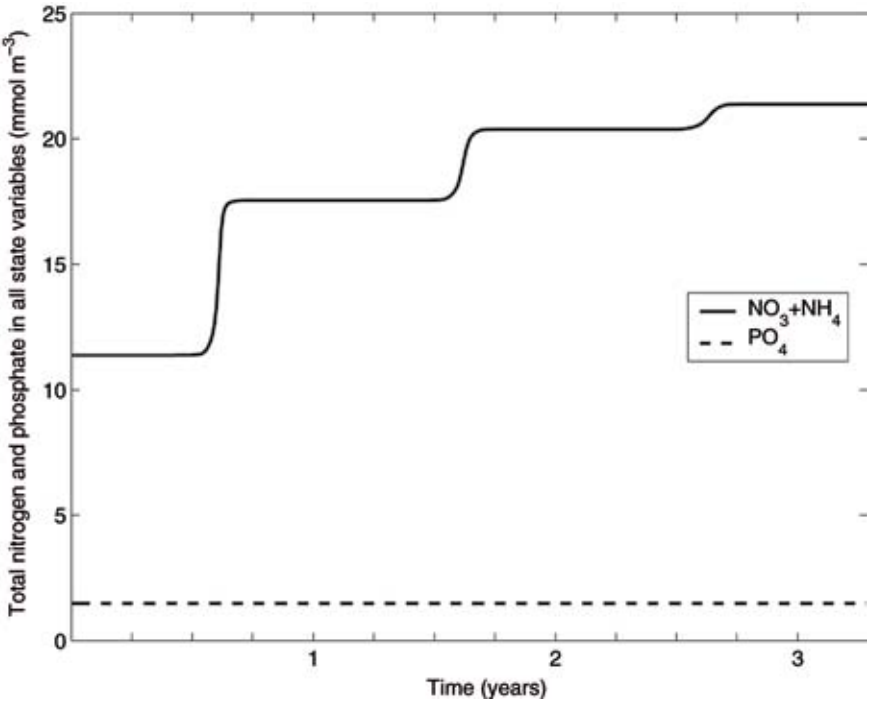

Figure 17.11
Total nitrogen and phosphate in all state variables and the two model layers, with active cyanobacteria and no external input (second experiment).
Source: redrawn from Fennel and Neumann (2004).

and ignore in particular horizontal transport and gradients. An assessment of how well models reproduce the natural systems requires the comparison of simulation with observation. A high degree of realism of the model with respect to process descriptions and spatial resolution is needed. In too simple models, crude parameterizations or tuning parameters towards observed data may even confuse physical and biogeochemical effects. This situation might be less crucial in regions where gradients in state variables are weak, as in central parts of the oceans. However, in marginal seas, such as the Baltic, with marked horizontal and vertical gradients, a proper spatial resolution of the model is important to distinguish between local processes and changes due to advection of properties.

For example, in a river plume, high nutrient concentration may exist and support a high growth rate of phytoplankton. In the model, the discharged matter is distributed within the grid boxes next to the river mouth. For a coarser resolution the discharged matter will be distributed within enlarged grid cells and the discharged nutrients extend over a broader range but with lower concentration. A substantial dilution of the nutrients implies reduced uptake rates or equivalently increased biological timescales. Thus, near-shore retention of nutrient and fast phytoplankton growth would be replaced by a slowly growing broad distribution.

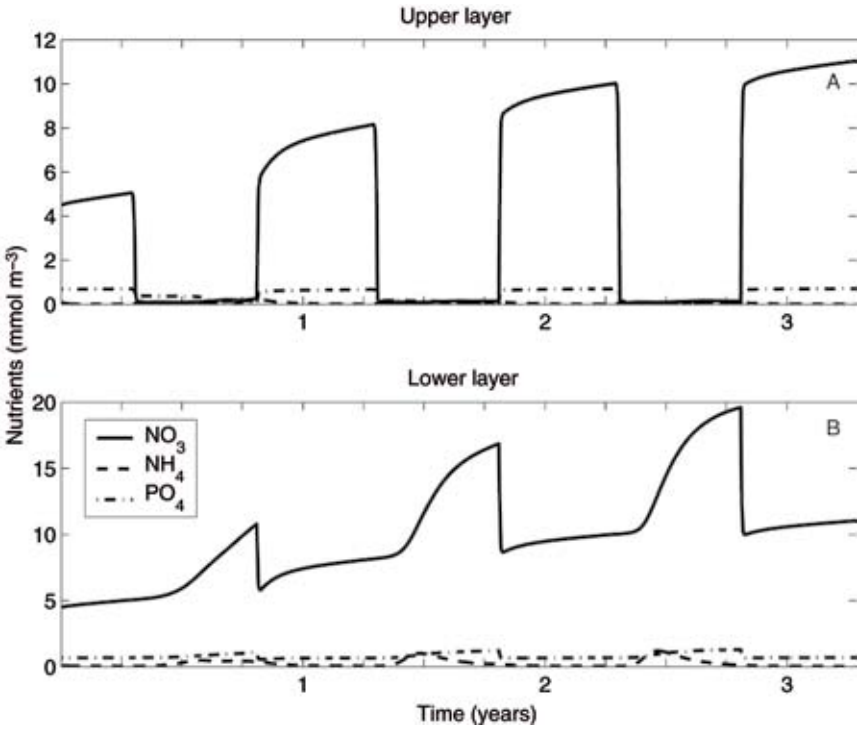

Figure 17.12
Results of the third model experiment (active cyanobacteria and external input of nitrate in the upper layer) showing nutrient variations in A, upper; B, lower layers.
Source: redrawn from Fennel and Neumann (2004).

17.4.1 Description of model system

State-of-the-art circulation models are able to describe the physical processes, such as currents, variations in temperature and salinity, in response to atmospheric forcing and river discharges with a high degree of realism. We use an application of the Modular Ocean Model (MOM-2), which was developed in the Geophysical Fluid Dynamics Laboratory (GFDL) in Princeton, N.J., USA (Pacanowski, 1990). The implementation of MOM-2 for the Baltic Sea includes an explicit free surface, an open boundary condition to the North Sea, a consistent treatment of freshwater input, (Griffies et al., 2001), and a thermodynamic ice model to include the effects of ice in the northern Baltic during the winter period.

The link between physical and chemical-biological dynamics are the advection diffusion equations for the state variables. While physical processes control the biogeochemical dynamics, a possible feedback of biological processes on the physical dynamics are ignored.

For the coupled model, we use a biogeochemical component similar to the model outlined in the previous sections, but with a few important refinements. We include

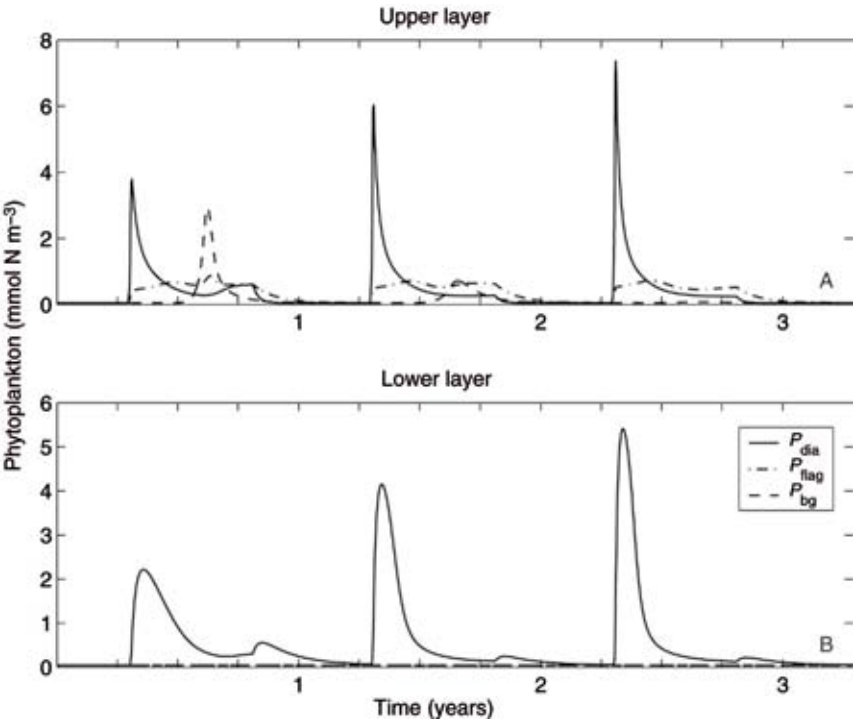

Figure 17.13
Like Figure 17.12, but for model diatoms, flagellates and cyanobacteria.

two additional state variables: oxygen, which involves hydrogen sulphate counted as negative oxygen, and 'sediment detritus'. This extension allows the involvement of the processes of denitrification and some aspects of sedimentation and re-suspension. Moreover, the dynamical signature of model cyanobacteria includes a small upward velocity, which allows surface accumulations. The effect of light on primary production, which previously (Section 17.3.3) accounted for using a normalized day length, is now considered in a more sophisticated way. A detailed description of a model system of the Baltic Sea ecosystem can be found in Neumann (2000) and Neumann, Fennel and Kremp (2002).

In what follows, we discuss some results of a decadal run carried out for the 1980s. We first show the annual cycle of the total phytoplankton (Figure 17.19), that is the sum of the three functional groups expressed in chlorophyll *a* concentration, and of the inorganic nitrogen (Figure 17.20) in the surface layer for the model year 1984. The results display what is generally known of the yearly cycle (Schulz et al., 1978). The spring bloom starts in the south-western part of the Baltic Sea and in coastal areas, and propagates towards the central Baltic and later to the northern parts. The summer situation shows lower phytoplankton concentrations in the central basins, but still high concentrations in coastal areas, especially in the vicinity of the mouths of the large rivers, which carry substantial nutrient loads. Later, in autumn, cooling and frequent wind events deepen the mixed layer and the solar radiation decreases implying that the

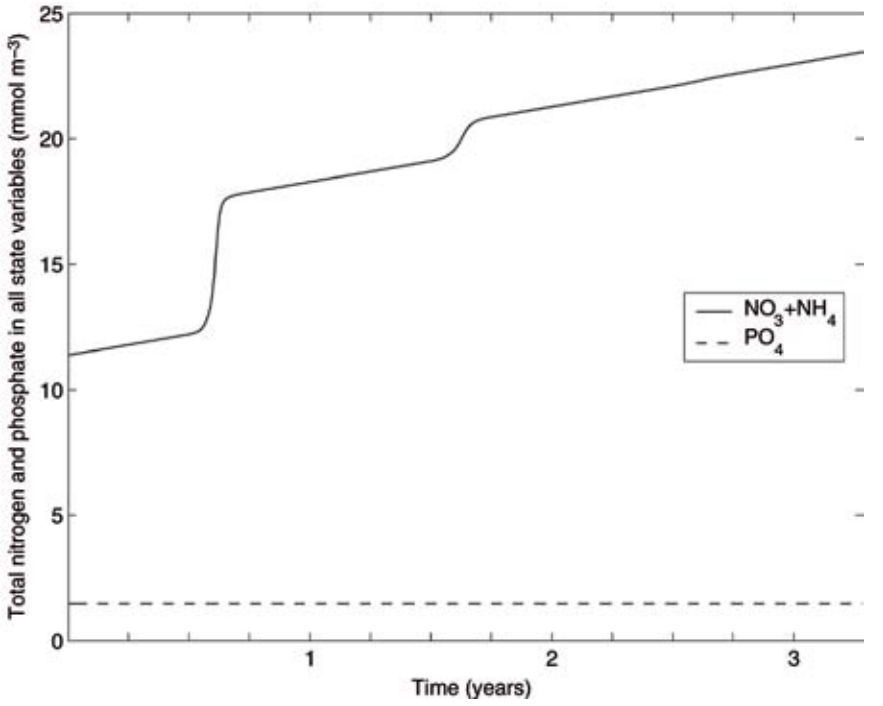

Figure 17.14
Total nitrogen and phosphate in all state variables and the two model layers, with active cyanobacteria and external input of nitrate (third experiment).
Source: redrawn from Fennel and Neumann (2004).

primary production ceases. At the end of the year, the phytoplankton concentrations decrease to a low level of overwintering seed populations. We can clearly discern large horizontal chlorophyll gradients during the period from spring to autumn.

As a further example, the evolution of distribution patterns of the model cyanobacteria (monthly means) is shown in Figure 17.21. The cyanobacteria appear during the summer season. The first indication of their development occurs in the monthly mean for July, while maximum intensity and the largest spatial extent are found in August. The concentrations decrease in September. The monthly means suggest relatively smooth distributions, but at timescales of a few days there are substantial variations due to advection (not shown).

17.4.2 Load reduction experiments

Similarly to the simplified box models, we can use the more complex coupled physical and biogeochemical models for experimental simulations to explore responses of the ecosystem model to changing forcing conditions. In marginal seas such as the Baltic Sea, with long residence times of the waters, due to the restricted water exchange with the ocean, the eutrophication caused by increased river nutrient loads is a serious problem. In the early 1990s, the riparian states of the Baltic Sea decided to halve the river

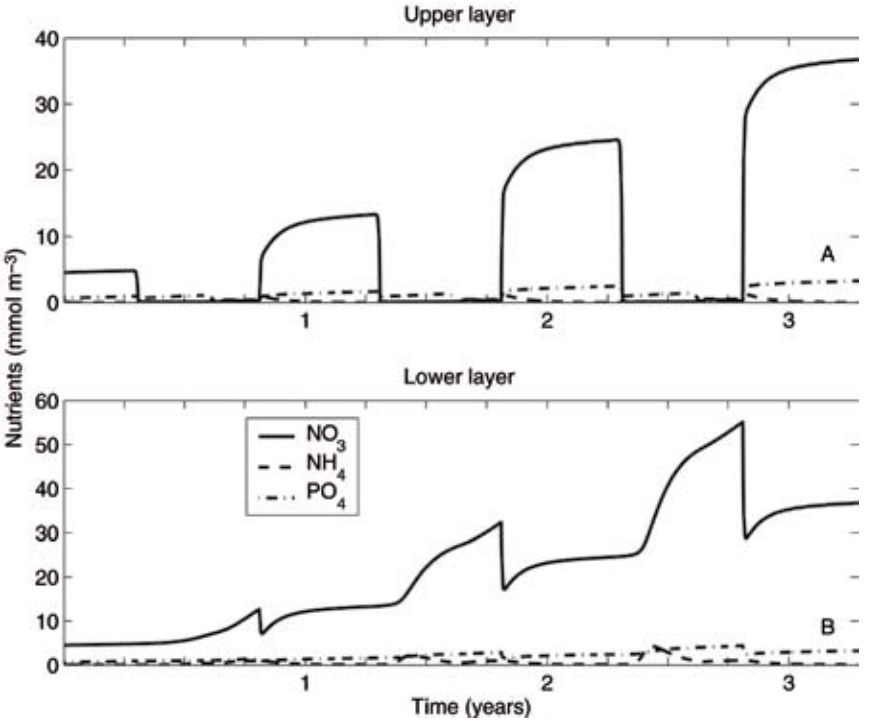

Figure 17.15
Results of the fourth model experiment (active cyanobacteria and external input of phosphate in the upper layer) showing nutrient variations in A, upper; B, lower layers.
Source: redrawn from Fennel and Neumann (2004).

borne nutrient loads. Since the related measures are expansive and the effects on the marine ecosystem difficult to quantify, the application of models is a useful tool for testing various scenarios.

A study of the response of the Baltic Sea to a reduction of nutrient load by 50% was presented in Neumann, Fennel and Kremp (2002). A baseline simulation with realistic forcings and, in particular, with a high-quality data set for the river loads, which is available for the 1980s, was performed for 10 model years. A second simulation was conducted with halved nutrient loads.

We discuss the results in terms of the difference between the several state variables. In particular, we consider the relative differences (%) of the mean concentrations of nutrients and model phytoplankton for the tenth year of both simulations, that is values of the standard run minus the run with reduced loads, divided by the standard run values, as shown in Figure 17.22. Negative values refer to decreased concentrations in response the load reduction. The reduction effect for the dissolved inorganic nitrogen (DIN) is seen in the whole system, but the decrease is stronger in the coastal areas than in the central parts of the Baltic. For the model phosphate a substantial reduction occurs mainly in the coastal regions. Denitrification plays a role in the faster removal of dissolved inorganic nitrogen.

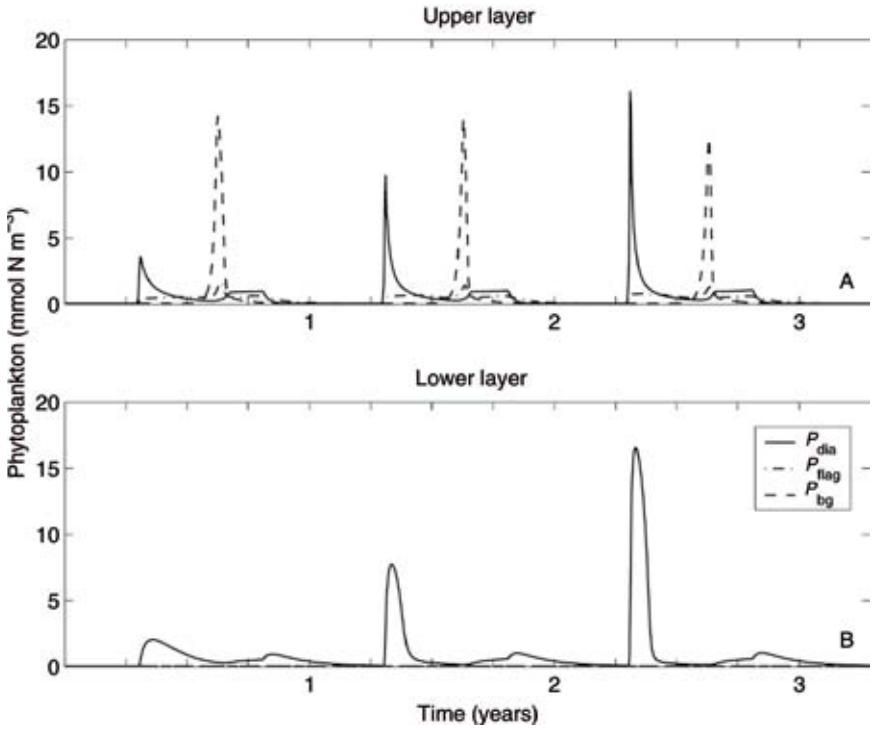

Figure 17.16
Like Figure 17.15, but for model diatoms, flagellates and cyanobacteria.

The model diatoms show a marked decrease in biomass, which results from the diminished dissolved nitrogen and the reduced spring blooms. The model flagellates, which depend on the recycled nutrients (microbial loop) are not much affected by the reduction of external loads. A surprisingly strong increase in biomass is found for the model cyanobacteria. In the central Baltic the increase reaches levels of 600%. This is an important result because it demonstrates that a reduction of nutrient loads can partly be counteracted by nitrogen fixation and bring along unwanted increases of harmful cyanobacterial blooms.

The reduction effects are basically nonlinear, vary among the state variables of the food web, and show significant spatial variations, in particular between the coastal regions and the open sea. The results emphasize that ecosystem models, which focus on cyanobacteria, need to involve the other important functional groups to understand the dynamics of cyanobacteria as part of the phytoplankton succession and competition for resources. Moreover, the physical control of the biological dynamics through currents and mixing must be included to understand the spatial distribution of the state variables.

One important conclusion from these results is that a formal approach of halving river loads could, at least at a medium-perspective, favour cyanobacteria, implying both a counteraction of the reduction efforts by nitrogen fixation and increased occurrences of unwanted cyanobacterial HABs.

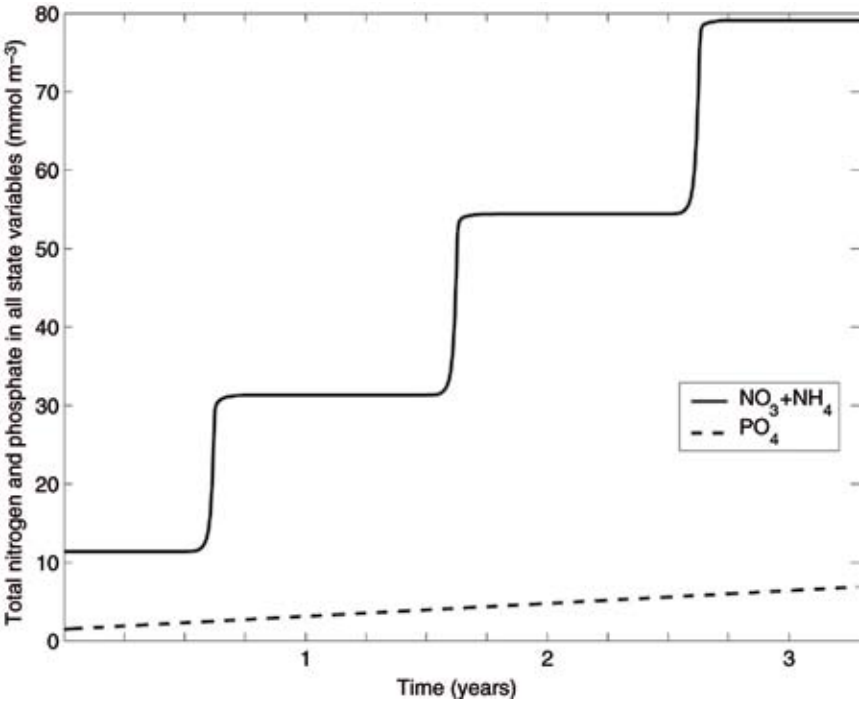

Figure 17.17
Total nitrogen and phosphate in all state variables and the two model layers, with active cyanobacteria and external input of phosphate (fourth experiment).
Source: redrawn from Fennel and Neumann (2004).

17.4.3 Sedimentation, re-suspension and dispersion of cysts

In the biological models applied in Section 17.4.2, the life cycle of cyanobacteria was not explicitly resolved. The seed populations are considered as a background concentration which was approached during the winter season. For many species, dormant cells are known to be part of their life cycle. Dormancy strategies are often effective on annual scales for over-wintering. There are some suggestions that *Nodularia* may have dormant stages in their life cycle. There absence in the water column during winter and spring indicates a possible overwintering as cysts resting on the sea floor.

The identification of potential seed-bed locations of dormant stages is an interesting problem which can be studied with models. Without any deeper biological consideration, we may conduct response analyses to identify pathways of fine material with the aid of a circulation model that includes waves and a bottom boundary layer module. Let us assume a simple case, where at a certain time resting stages, say cysts, are formed and drift passively with the currents like very fine sedimentary material. The cysts may have a sufficient sinking speed to settle on the bottom. In shallower waters, waves and strong currents will re-suspend the fine material, which is then transported again by the flow until it eventually reaches areas where the

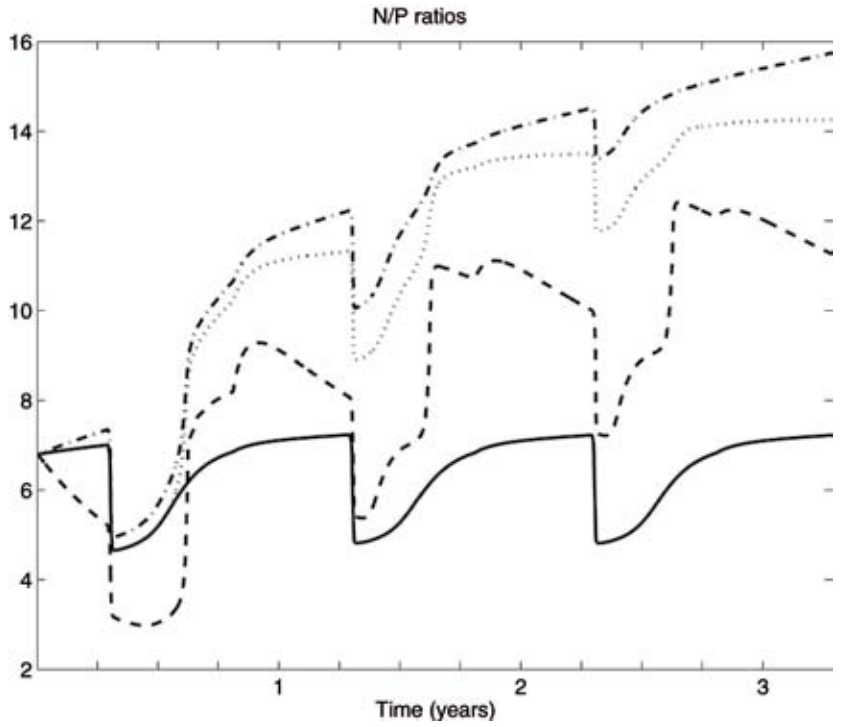

Figure 17.18
The N/P ratios of the dissolved inorganic nitrogen and phosphate in the two model boxes for the four experimental simulations. Solid line, no active cyanobacteria and no loads; dotted line, active cyanobacteria and no loads; dash-dotted line, active cyanobacteria and nitrate loads; dashed line, active cyanobacteria and phosphate loads.

re-suspension is weak. This kind of simulation can provide maps of accumulation areas, which can be considered as potential seed beds, from where future blooms may be initiated. Such type of results may also be helpful to guide the sampling activities in the field.

Experimental simulations with arbitrary start fields of fine material can provide clues for potential locations of seed beds on the sea floor. For a non-tidal system like the Baltic Sea, the seed beds may be expected in the deeper parts, where waves do not reach the bottom. Such model studies have been carried out by Kuhrts, Fennel and Seifert (2004). They presented two examples for the Baltic Sea, under winter conditions with strong wind forcing, and under summer conditions with thermal stratification. The results indicate that, after a few weeks, a substantial part of the fine material accumulates at the slopes of the basins, at depths where resuspension by waves plays no part (Figure 17.23). This implies, for example, that cysts are not necessarily transported towards the deepest part of the central basins where the anoxic condition could hinder them from 'wake-up'. The only mechanism of re-suspension in the deeper parts of non-tidal seas is bioresuspension due to the activities of benthic communities (see e.g. Graf and Rosenberg, 1997).

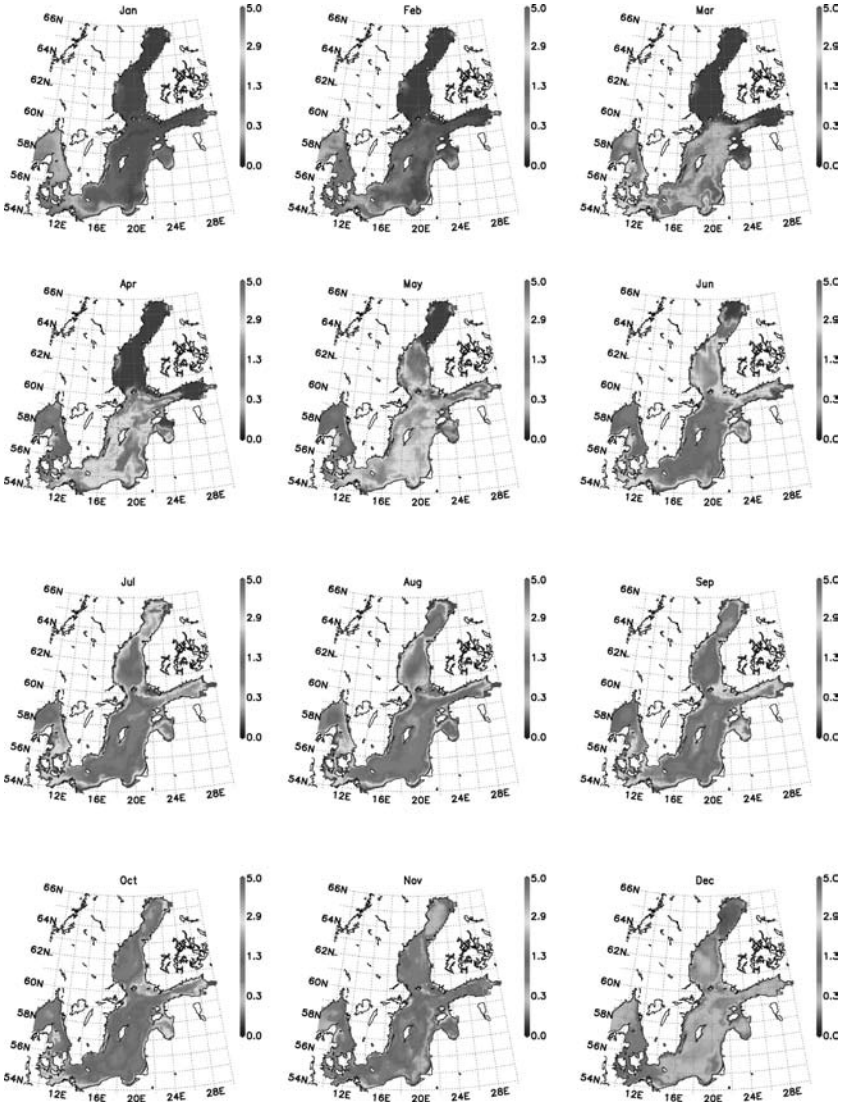

Figure 17.19
Simulated annual cycle of total phytoplankton near the surface, expressed as chlorophyll *a* (mg m^{-3}) in 1984 for the Baltic Sea.

17.5 Challenges and opportunities

The generation of predictive capabilities for environmental issues is a great challenge for marine ecosystem modelling research. Models need further development based on interdisciplinary research with close interaction between biological and physical oceanographers. Simulations with complex models require the expertise of experienced

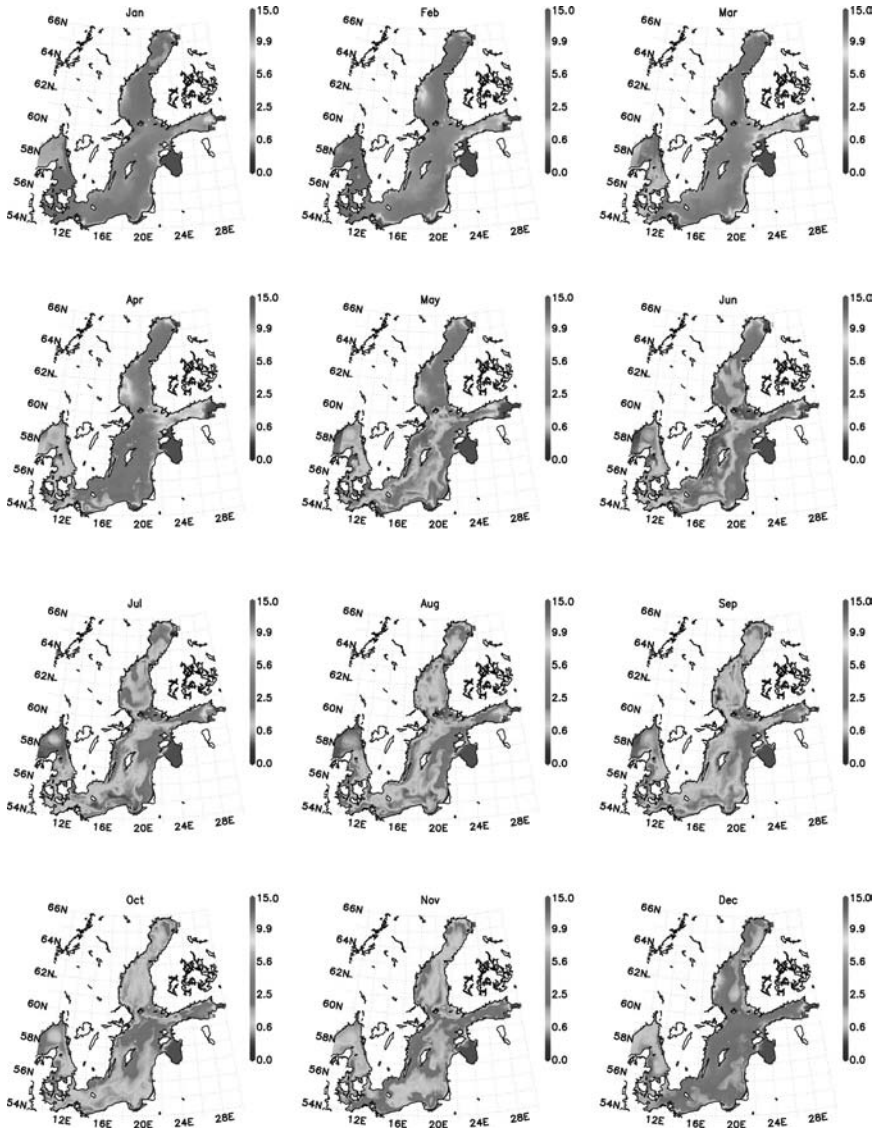

Figure 17.20
Simulated annual cycle of surface nitrogen (mmol m^{-3}) in 1984 for the whole Baltic Sea. The nutrients develop inverse to the model phytoplankton.

modellers. It is important to educate and train students as modellers which are able to work on modelling and maintain the interdisciplinary dialogue. On the other hand, simpler models, for example box models, which can easily be run and are helpful to develop qualitative and quantitative understanding, could be used by experimentally oriented students to foster cooperation with modellers.

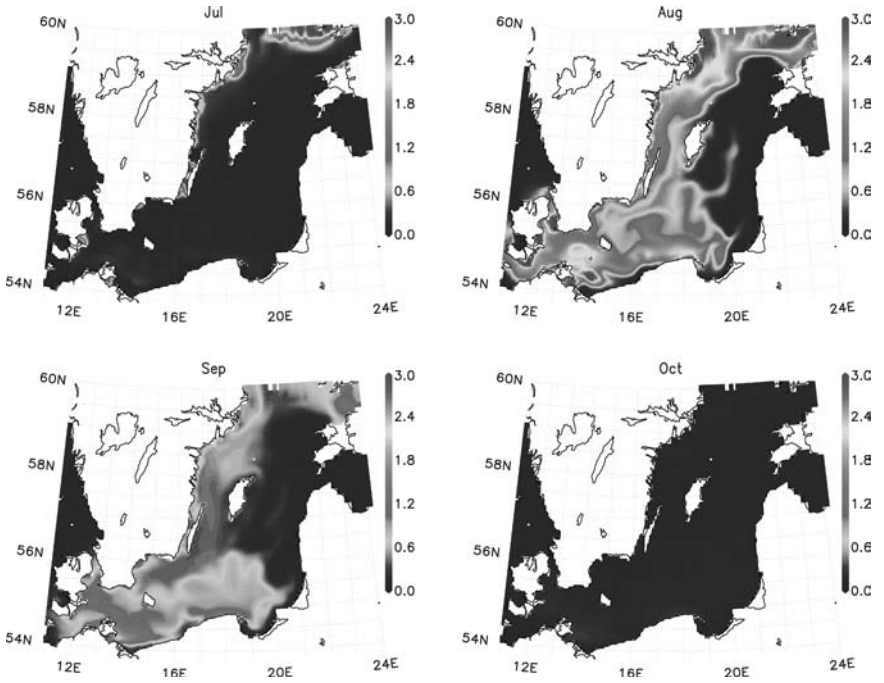

Figure 17.21
Patterns of modelled cyanobacteria chlorophyll *a* (mg m^{-3}) near the surface for the summer of model year 1984 in the central and south-western Baltic Sea.

For timescales of several days or a few weeks, a relevant problem for environmental forecast is to calculate how a patch of harmful algae (e.g. surface accumulation of cyanobacteria) spreads from a detected initial location in response to meteorological forcing which affects both drift of surface accumulations, current patterns and turbulent mixing. Such tasks require real-time observation by ships of opportunity, moored systems and satellite imagery connected with operational models through data assimilation.

For semi-enclosed systems with long water residence times of a few years to several decades like the Baltic Sea, an important issue is to understand and quantify how the drainage area affect the marine system, and to provide scientifically based advice to the decision-makers on how loads might be managed most efficiently. This issue can be addressed by computation of scenarios (e.g. load-reduction experiments).

Modelling will not reduce the need for measurements, but helps to optimize observation strategies and, thereby, to extract more information from environmental data sets. Data are needed to initialize and validate models. Thanks to long-term monitoring programmes in the Baltic and many international multi-ship campaigns, there is already a substantial database for this system. In addition to the ship-borne monitoring programme in the Baltic Sea, there are several permanent real-time observational sites that continuously produce physical and chemical data. Several institutions around

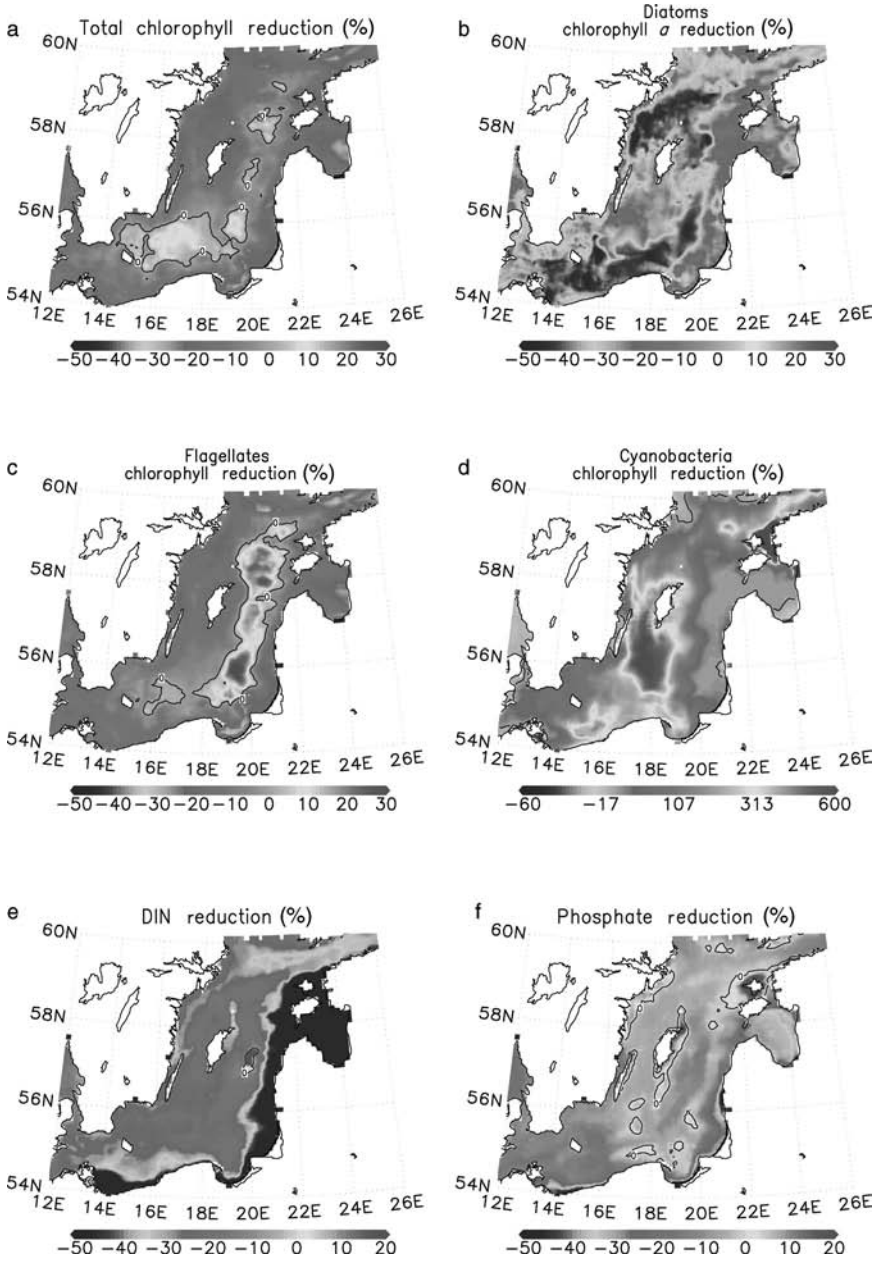

Figure 17.22
Responses of the system to a reduction of river nutrient loads by 50% in terms of the relative changes in concentration of the various model state variables: A, total chlorophyll *a*; B, diatoms; C, flagellates; D, cyanobacteria; E, dissolved inorganic nitrogen; F, dissolved inorganic phosphorous. *Source*: after Neumann et al. (2002).

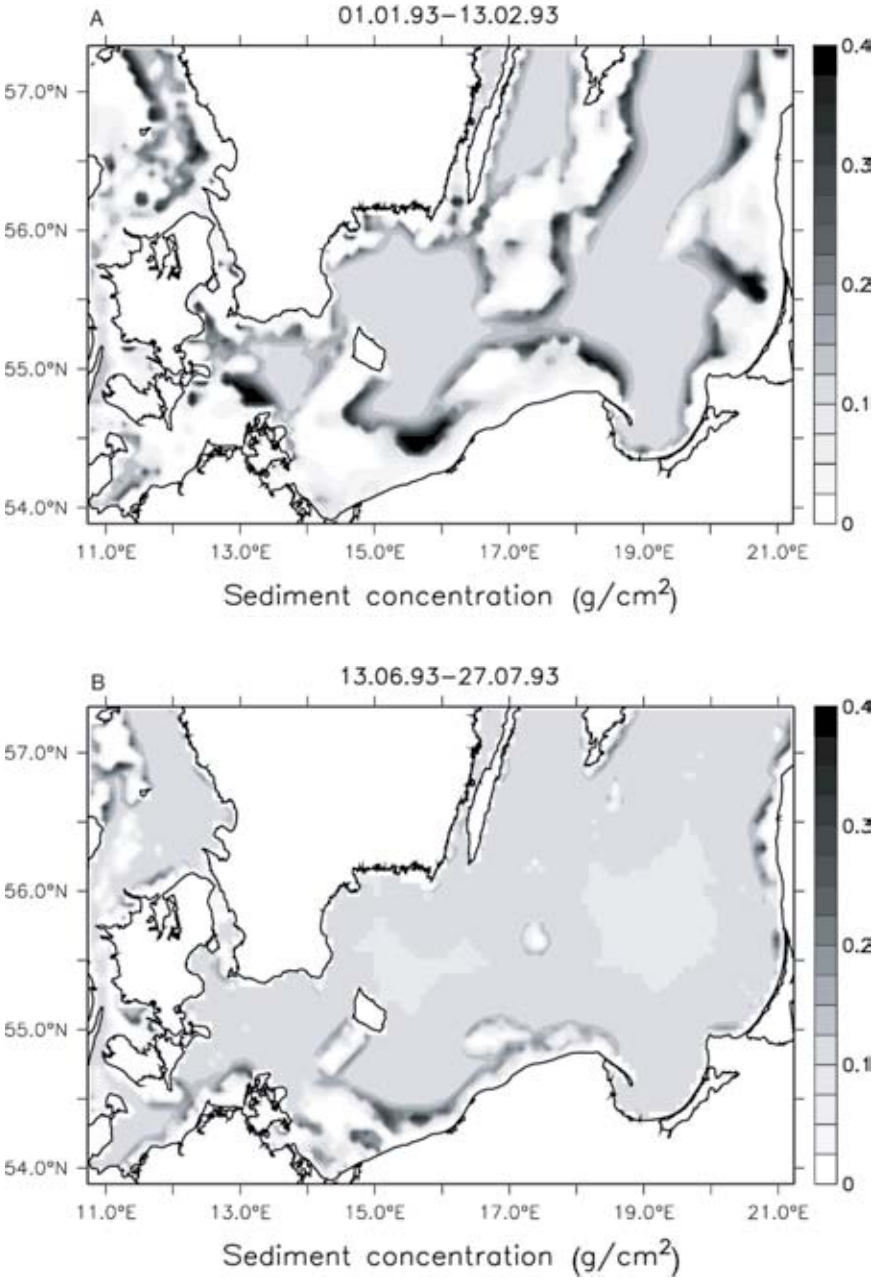

Figure 17.23
Sedimentation patterns of fine material, which was initially evenly distributed in the surface layer, after a six-week time slice simulation for A, winter; B, summer conditions.
Source: after Kuhrts et al. (2004).

the Baltic have set up a Baltic GOOS,[88] which also involves attempts to provide HAB warning systems.

New opportunities arise from the Baltic Large Marine Ecosystem programme, funded by the World Bank to support the countries with economies in transition with modern technology to improve their monitoring programmes with advanced instrumentation.

References

Babin, M., Roesler, C. S. and Cullen, J. J. (eds). 2006. *Real-time Coastal Observing Systems for Marine Ecosystem Dynamics and Harmful Algal Blooms: Theory, Instrumentation and Modelling*. Paris, Intergovernmental Oceanographic Commission of UNESCO. (Monographs on Oceanographic Methodology.)

Ehlin, U. 1981. Hydrology of the Baltic Sea. In: Voipio (ed.), op. cit., pp. 123–34.

Fennel, W. and Neumann, T. 2001. Coupling biology and oceanography in models. *Ambio*, 30, pp. 232–36.

Fennel, W. and Neumann, T. 2004. *Introduction to the Modelling of Marine Ecosystems*. Amsterdam, Elsevier. (Oceanographic Series.)

Graf, G. and Rosenberg, R. 1997. Bioresuspension and biodeposition: a review. *J. Mar. Syst.,* 11, pp. 269–78.

Griffies, S. M., Pacanowski, R. C., Schmidt, M. and Balaji, V. 2001. Tracer conservation with an explicit free surface method for z-coordinate ocean models. *Monthly Weather Review,* 129, pp. 1081–98.

Humborg, C., Fennel, K., Pastuszak, M. and Fennel, W. 2000. A box model approach for a long-term assessment of estuarine eutrophication, Szczecin Lagoon, southern Baltic. *J. Mar. Syst.,* 25, pp. 387–403.

Kahru, M. 1997. Using satellites to monitor large-scale environmental change: a case study of cyanobacterial blooms in the Baltic Sea. In: M. Kahru and C. W. Brown (eds), *Monitoring Algal Blooms.* Berlin, Springer Verlag, pp. 43–61.

Kahru, M., Horstmann, U. and Rud, O. 1994. Satellite detection of increased cyanobacteria blooms in the Baltic Sea: natural fluctuations or ecosystem change? *Ambio,* 23, pp. 469–72.

Kononen, K. 1992. Dynamics of the toxic cyanobacterial blooms in the Baltic Sea. *Finn. Mar. Res.,* 261, pp. 3–36.

Kuhrts, C., Fennel, W. and Seifert, T. 2004. Model studies of transports of sedimentary material in the Western Baltic. *J. Mar. Syst*, 52, 2004, pp. 167–190.

Kullenberg, G. 1981. Physical oceanography. In: Voipio (ed.), op. cit., pp. 135–81.

Larsson, U., Elmgren, R. and Wulff, F. 1985. Eutrophication and the Baltic Sea – causes and consequences. *Ambio,* 14, pp. 9–14.

Larsson, U., Hajdu, S., Walve, J. and Elmgren, R. 2001. Baltic Sea nitrogen fixation estimated from the summer increase in the upper mixed layer total nitrogen. *Limnol. Oceanogr.,* 46, pp. 811–20.

Neumann, T. 2000. Towards a 3D-ecosystem model of the Baltic Sea. *J. Mar. Syst.,* 25, pp. 405–19.

Neumann, T., Fennel, W. and Kremp, C. 2002. Experimental simulations with an ecosystem model of the Baltic Sea: a nutrient load reduction experiment. *Global Biogeochem. Cy.,* 16, pp. 7-1–7-19.

Pacanowski, R. C. 1995. *GFDL Ocean Technical Report 3.* Princeton, N.J., Geophysical Fluid Dynamics Laboratory. (MOM-2 Documentation.)

[88]Acronym BOOS; see www.boos.org for more information.

Savchuk, O. P. 2002. Nutrient biogeochemical cycles in the Gulf of Riga: scaling up field studies with a mathematical model. *J. Mar. Syst.,* 32, pp. 253–80.

Schulz, S., Kaiser, W. and Breuel, G. 1978. The annual course of some biological and chemical parameters at two stations in the Arkona and Bornholm Sea in 1975 and 1976. *Kieler Meeresfo., Sonderh.,* 4, pp. 154–60.

Siegel, H. and Gerth, M. 2000. Remote-sensing studies of the exceptional summer of 1997 in the Baltic Sea: the warmest August of the century, the Oder flood and phytoplankton blooms. In: D. Halpern (ed.), *Satellites, Oceanography and Society.* Amsterdam, Elsevier, pp. 239–55.

Siegel, H., Matthäus, W., Bruhn, R., Gerth, M., Nausch, G., Neumann, T. and Pohl, C. 1998. The exceptional Oder flood in summer 1997 – distribution patterns of the Oder discharge in the Pomeranian Bight. *Deutsche Hydrographische Zeit.,* 50, pp. 145–67.

Stigebrandt, A. 2001. Physical oceanography of the Baltic Sea. In: F. Wulff, L. Rahm and P. Larson (eds), *Systems Analysis of the Baltic Sea.* Berlin, Springer-Verlag, pp. 19–74.

Voipio, A. (ed.). 1981. *The Baltic Sea.* Amsterdam, Elsevier.

Wasmund, N. 1997. Occurrence of cyanobacterial blooms in the Baltic Sea in relation to environmental conditions. *Int. Rev. Ges. Hydrobiol.,* 82, pp. 169–84.

18

Modelling algal dynamics in eutrophic coastal waters

J. H. W. Lee, K. W. Choi, K. T. M. Wong, B. Qu and F. Arega

18.1 Introduction

Hong Kong is situated at the mouth of the Pearl River Estuary (Figure 18.1) in Southern China, with a population of 6.7 million and a projected population of 8.5 million by 2010. With a land area of only 1,070 km^2 and 1,800 km^2 of coastal waters, the pressure on the marine ecosystems is enormous: land reclamation, port and navigation activities, sewage disposal, fishing and mariculture, and recreation. Hong Kong's population and organic sewage loads are centred around Victoria Harbour; before the Harbour Area Treatment Scheme came into operation in 2000, some 1.5 million m^3 of untreated sewage and industrial wastewater were discharged daily into the harbour. In addition, nutrients carried by streams and rivers also contribute to non-point source pollution (NSP). The annual NSP load into Hong Kong's coastal waters is estimated to be about 8,000 tonnes of total nitrogen (TN) and 1,500 tonnes of total phosphorus (TP) (Li et al., 2005). Furthermore, the background pollution is contributed by the organic load carried by the Pearl River Estuary. Figure 18.2A shows the rapid increase in total organic loading in the Pearl River Delta region in the past decade. The population in the Delta region (area 461,000 km^2) underwent significant growth, from 9.6 million in 1982 to 36 million in 2000 (Figure 18.2B). Annual domestic discharges into the Pearl Estuary have also sharply increased from about 900 million tonnes in 1991 to 2,118 million tonnes in 2000. The treatment rate of industrial wastewater was about 70% in the 1990s, while the treatment rate of domestic sewage was only around 10%. With the increasing organic pollution loads coming down the Pearl River (maximum flow around 20,000 m^3/s), it is not surprising that regular water quality monitoring in Hong Kong's western waters always indicates an increase in nutrient concentration in the wet season (Broom and Ng, 1995).

The high incidence of red tides and algal blooms is a unique feature in the subtropical coastal waters around Hong Kong (Figure 18.2C). This phenomenon has been extensively studied and widely reported (e.g. Wear et al., 1984; Hodgkiss and Ho, 1991), and is believed to be related to the eutrophication caused by excessive and concentrated organic discharges. Hydrographic factors also play an important role, as most of the red tides occur in weakly flushed, semi-enclosed tidal inlets. The figure shows the reported number of red tides in the past two decades; a significant portion of which occurred in Tolo Harbour, a semi-enclosed waterbody with relatively long residence times in the eastern waters of Hong Kong (Figure 18.1). The reported number of red tides reached a peak of 88 outbreaks in 1988, but decreased to current frequencies of around 20 per year after the introduction of the Tolo Nutrient Export Scheme.

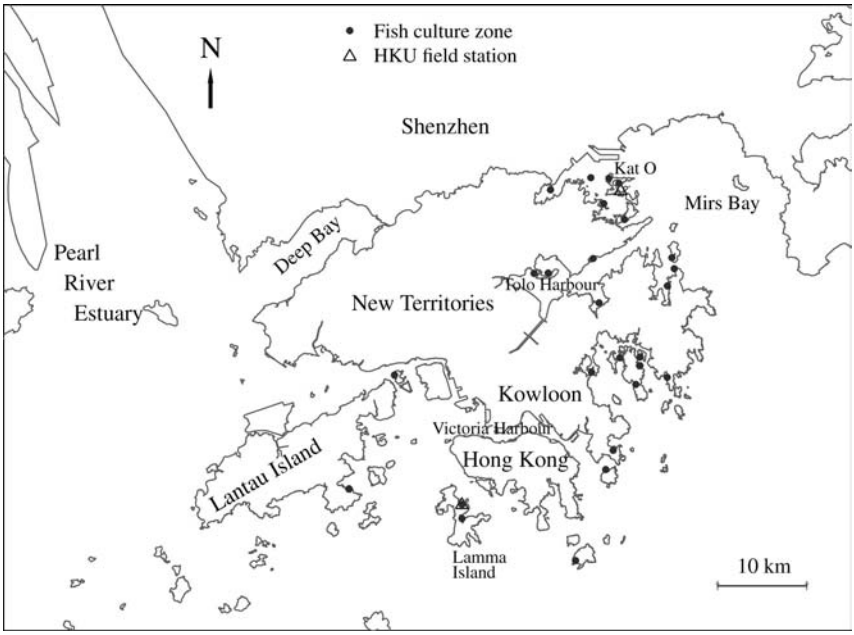

Figure 18.1
Hong Kong and the Pearl River Estuary (locations of marine fish culture zones and algal dynamics field station indicated).

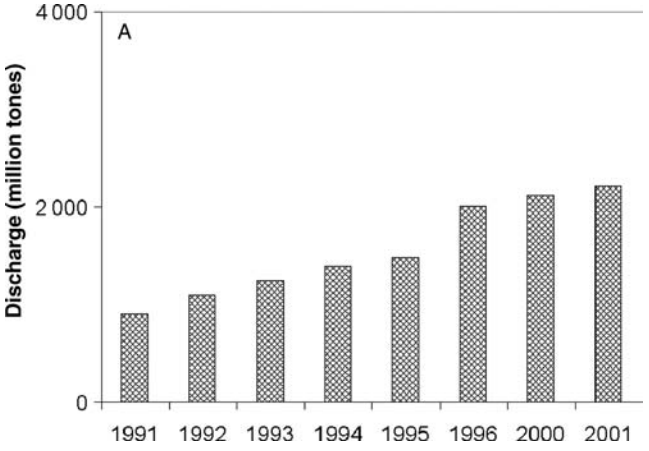

Figure 18.2
A, Pearl River Delta domestic wastewater discharges; B, population in the Pearl River Delta region; C, red-tide occurrences in Hong Kong.

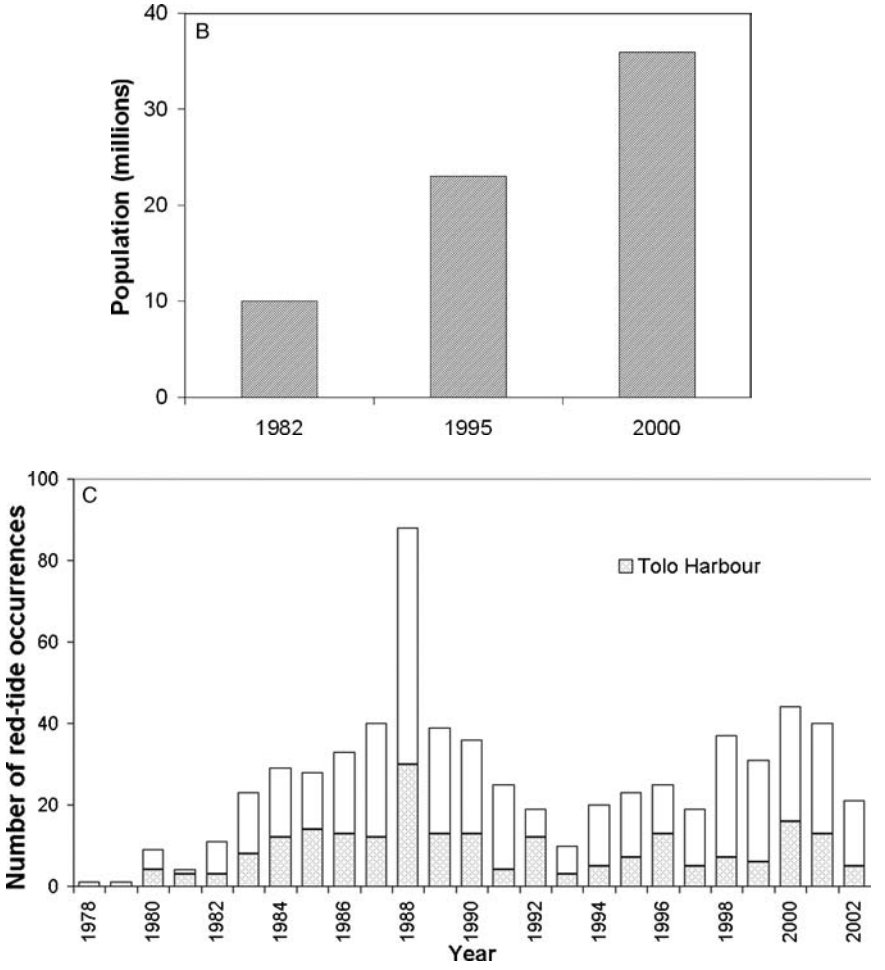

Figure 18.2 *(Continued)*

Although few of the harmful algal blooms have been found to be toxic, they sometimes resulted in severe anoxia over rather short timescales, with a direct impact on mariculture. There is hence a genuine need to study and model algal bloom dynamics to provide a scientific basis for mariculture management. This chapter summarizes the modelling of algal dynamics in subtropical coastal waters over the past decade. The work has been motivated by a practical need to understand the causes of episodic algal bloom events, and to develop a quantitative methodology for mariculture management. The environmental engineering approach and modelling framework are described with reference to model-data comparisons. The usefulness and limitations of modelling are illustrated by several key applications. Finally, we discuss the fundamental challenges facing water quality modelling and future opportunities – in particular, the use of data-assimilation to combine field data and dynamic model predictions to improve our knowledge of the ecosystem and to improve forecasts of coastal water quality and HABs.

18.2 Dissolved oxygen and algal dynamics

The prediction of dissolved oxygen (DO), a vital water quality indicator, has been studied extensively. Major items of the oxygen balance such as carbonaceous deoxygenation and re-aeration are well-established. Nevertheless, in situations where photosynthetic production and sediment oxygen demand play an important role, the prediction of DO remains a difficult problem. This is especially so in eutrophic subtropical coastal waters where the DO variation is intimately related to the algal dynamics. As the ecological response is highly nonlinear, both the phytoplankton and DO dynamics are notoriously difficult to predict. On the other hand, the study of DO variations may reveal insights into the phytoplankton dynamics. Long-term field and mathematical modelling work in Hong Kong was initiated during 1987–89; the emphasis was on understanding the often perplexing observed dissolved oxygen variations in many of the 26 marine fish culture zones. It is of interest to understand the environmental factors and preconditions that lead to a fish kill, and to predict the occurrence of severe dissolved oxygen depletion. A total of 17 water quality field surveys of 26 hours were carried out in a weakly flushed fish culture zone in Tolo Harbour (Lee et al., 1991*b*). The surveys covered both Spring and Neap tides and a wide range of meteorological conditions – ranging from sustained fine, calm sunny weather to overcast skies with heavy downpour and/or a strong wind. Hourly measurements of the vertical dissolved oxygen profile (at 1 m depth interval) along with 6-hourly measurements of the key water quality variables (nutrients and cell counts) were made. These were also supplemented by *in situ* measurements of sediment oxygen demand and light extinction (Yung and Lee, 1993). As the hydrodynamics of the near-stagnant cove is relatively simple (with mean depth of 6 m and maximum tidal velocities of around 2–3 cm/s), the site serves as a good test ground for a water quality model. The 26-hour field studies subsequently gave way to the development of a telemetry system to continuously monitor algal and dissolved oxygen dynamics (Lee and Lee, 1985). Since 2000 a real-time algal dynamics research station has been deployed at two sites in Hong Kong, with the objective of developing a real-time forecasting and warning system (Lee et al., 2005; Wong and Lee, 2003; Wong, 2004).[89]

18.2.1 Field observations

The nature of dissolved oxygen and algal dynamics can best be illustrated by field observations. Figure 18.3 shows the diurnal variation of depth-averaged DO during a diatom bloom at Three Fathoms Cove, Tolo Harbour, under sunny clear skies and mean tidal conditions in winter 1987. The measured changes in solar radiation (PAR), chlorophyll *a* concentration [chl *a*], dissolved inorganic nitrogen concentration (DIN), and five-day biochemical oxygen demand (BOD_5) are also shown. With [chl *a*] levels up to 40 mg m^{-3} and cell counts as high as 10^4 cells/ml, the reddish-brown water was over 200% saturation during the day; the drop in DO is approximately linear at night, and can be by as much as 7 mg l^{-1}.

The observed dynamic nature of the algal blooms is most interesting; the diurnal fluctuations reveal clearly the growth of algae (increasing chlorophyll levels) as the day progressed, accompanied by corresponding depletion of nutrients and changes in dissolved oxygen. In that subtropical weakly flushed bay, the continuous observations revealed a dynamic ecological system for all seasons; even in the winter the surface and

[89]See http://www.hku.hk/civil/dept_activities/asi for further details.

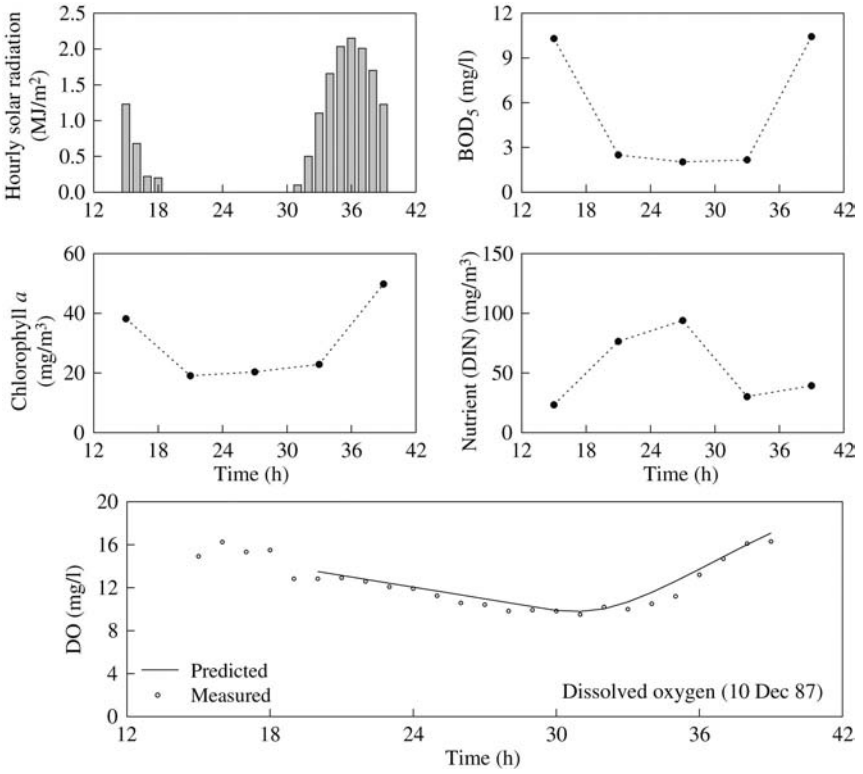

Figure 18.3
Observed diurnal change in dissolved oxygen and algal biomass during a red tide.

depth averaged DO can differ greatly (during algal blooms), with algal growth and collapse cycles of the order of a week to 10 days. This red tide in the dry season served as a most efficient 'oxygen pump' which provided an oxygen supply far exceeding the total oxygen demand of the biological community. On the other hand, under the wrong combination of conditions (e.g. overcast skies and neap tides), the algal blooms can also cause severe oxygen depletion, leading to massive fish kills (see later discussion). The observed N/P ratio (by weight) is generally low, in the range 1.3–3.3 (Lee et al., 1991*b*). Viewed against typical values of half-saturation constant and a typical N/P ratio of 7:2 for marine phytoplankton, the data suggest that nitrogen is the most important limiting nutrient. Figure 18.4 shows the changes in the algal biomass (chlorophyll fluorescence) and DO recorded by real-time monitoring at Kat O, Hong Kong (Figure 18.1). The measurements were recorded at three depths during a dinoflagellate (*Gonyaulax polygramma*) bloom over the course of two weeks (Lee et al., 2005). It is seen the diurnal DO fluctuations mirror the algal biomass; vertical DO differentials are also significant during the bloom period but relatively small on days without algal growth. This suggests the possibility of using DO data to gain insights into HAB dynamics – for example the vertical structure of a diatom bloom may be fundamentally different from the case when vertical migration of dinoflagellates can influence the DO consumption pattern.

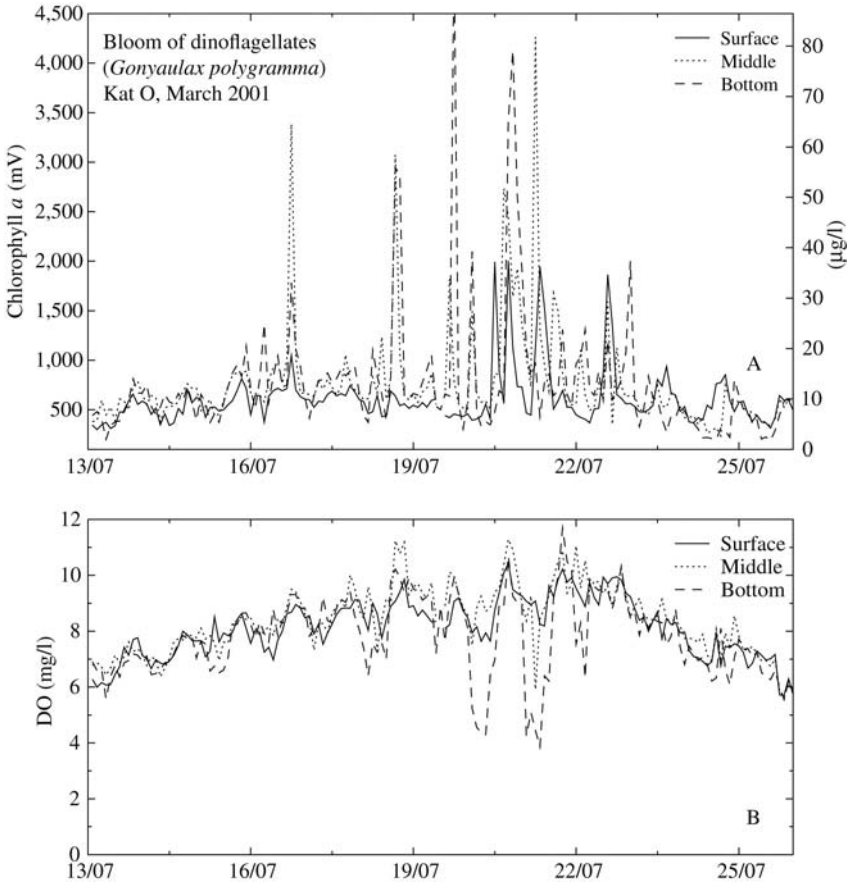

Figure 18.4
Observed changes in A, chlorophyll; B, dissolved oxygen, during a dinoflagellate bloom at Kat O, Hong Kong, in March 2001.

18.2.2 Water quality modelling

With these continuous observations, various hypotheses to explain the observed water quality changes can be studied. Most of the models in use are derived from applications to a few major estuaries in temperate climates (e.g. Cerco and Cole, 1993); successful application of the model principles must be supported by good field data. We give herein a summary of the elements of a relatively simple water quality model that has been useful in practical application, highlighting especially the modelling of dissolved oxygen production and consumption.

The structure of the water quality model that predicts temporal variations of water quality is schematized in Figure 18.5. Phytoplankton growth and the associated nutrient and dissolved oxygen (DO) dynamics are governed by a number of

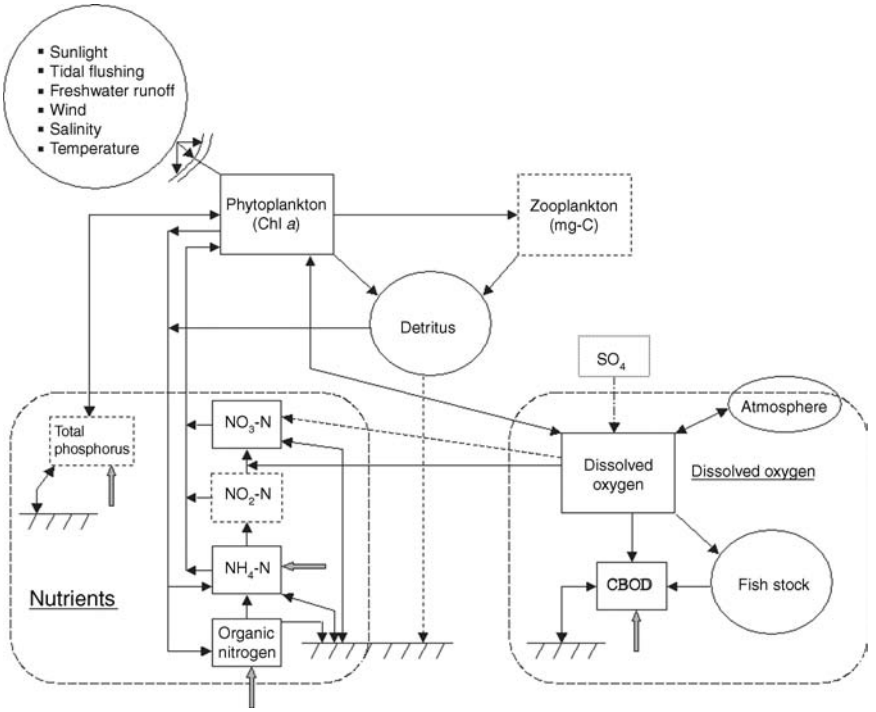

Figure 18.5
Schematic of water quality model for dissolved oxygen and algal dynamics. Light arrow: natural and man-induced wasteloads; squares: modelled state variables.

interacting physical, biological and chemical processes that vary in time and space: river inflows and tidally driven circulation, mass transport by advection and dispersion, algal growth as a function of environmental forcing (organic loads, solar radiation, rainfall and nutrient input), nutrient regeneration, deoxygenation and reaeration. Phytoplankton dynamics and nutrient kinetics are based on a generally accepted framework (Bowie, 1985; Thomann and Mueller, 1987; Lee et al., 1991*a*, 1991*b*; Ambrose et al., 1993). System variables for the water column include algal biomass as represented by [chl *a*], organic, ammonia and nitrate nitrogen, inorganic and organic phosphorus, BOD and DO. Phytoplankton growth is assumed to be limited by solar radiation, nutrients (nitrogen and phosphorus) and temperature. Light limitation is modelled by Steele's equation; light extinction due to self-shading is accounted for. It is assumed that algae adjusts chlorophyll composition to maximize specific growth rate for ambient conditions of light and temperature. Nutrient (inorganic nitrogen and phosphorus) uptake by phytoplankton growth is modelled. Monod growth kinetics is assumed for nutrient limitation, with an ammonia preference by algae over nitrate; the growth is determined by the most limiting nutrient. Supported by field observations of the location of DO maximum beneath the free surface, the saturating light intensity is

assumed to be 50% of the available photosynthetically active radiation (PAR). The carbon to chlorophyll ratio (C:[chl *a*]) is determined dynamically as a function of the available light. Photosynthetic production of oxygen, algal respiration, atmospheric reaeration, endogenous respiration, algal death and nutrient regeneration, settling of particulate organic matter to the seabed, decomposition of settled algal detritus and denitrification in the benthic layer, oxygen consumption due to fish respiration, are all incorporated. Surface reaeration rate is determined as a function of advective velocity and wind speed. Both organic and inorganic forms of nitrogen and phosphorus are recycled to the water column via algal respiration/death. Mineralization of organic nitrogen is assumed to follow a first-order rate. Zooplankton predation is not modelled, and is represented by a general loss term. Table 18.1 summarizes the typical model parameters and kinetic coefficients that are based on literature values as well as site-specific field studies.

Table 18.1 Summary of kinetic coefficients and parameters used in water quality model

Description	This study	Related studies
Saturated growth rate of phytoplankton (day^{-1})	2.0 (1.068)	$2.0^{*,P}$, 2.0–2.5^{C}, 2.1^{TFC}
Maximum photosynthetic quantum yield (mg C/mole photon)	720	720^{P}
Half-saturation constant for nitrogen for phytoplankton growth (µg–N/L)	25	15^{C}, 25^{P}, 25^{*}, 15^{TFC}
Algal endogenous respiration at 20°C (day^{-1})	0.125 (1.045)	0.125^{TFC}, $(0.1–0.125)^{C}$, 0.05^{TFC}
Algal settling velocity (m/day)	1.0	$0.1^{P,C}$, 0.33^{*} for diatoms, $1–1.3^{TFC}$
Non-predatory phytoplankton death rate (day^{-1})	0.02 (1.08)	$(0.1–0.2)^{C}$, 0.02^{P}, 0.125^{*}, 0.02^{TFC}
Oxygen to carbon ratio in phytoplankton (mg O_2/mg C)	2.67	2.67^{P}, 2.67^{TFC}
Reaeration rate constant at 20°C (day^{-1})	0.3	0.3^{TFC}
Nitrogen to carbon ratio in phytoplankton (mg N/mg C)	0.25	0.25^{P}
Organic nitrogen mineralization rate at 20°C (day^{-1})	0.075 (1.08)	0.03^{C}, 0.075^{P}, 0.02^{*}, 0.05^{TFC}
Nitrification rate at 20°C (day^{-1})	0.09 (1.08)	0.03^{*}, $0.09–0.13^{P}$, 0.1^{TFC},
Half-saturation constant for oxygen limitation of nitrification (mg O_2/l)	2	2^{P}
Denitrification rate at 20°C (day^{-1})	0.09 (1.08)	0.09^{*}, 0.1^{LE}
Half-saturation constant for denitrification oxygen limitation mg (O_2/l)	0.1	0.5^{*}, 0.10^{P}
Fraction of dead and respired phytoplankton recycled to organic nitrogen pool	0.5	0.5^{P}, 0.5^{TFC}

Table 18.1 *(Continued)*

Description	This study	Related studies
Fraction of dead and respired phytoplankton recycled to ammonia nitrogen pool	0.5	0.5[P], 0.5[TFC]
Anaerobic algal decomposition rate (day^{-1})	0.02 (1.08)	0.02[P], 0.02[LE]
Organic nitrogen decomposition rate in the sediment at 20°C (day^{-1})	0.0004 (1.08)	0.0004[P], 0.00025[LE]
Water-sediment diffusive exchange coefficient (m^2/day)	2.5310^{24}	$2.0–2.5310^{24}$ [P]
Benthic layer depth (m)	0.15	0.1–0.3[P]
Sediment carbon as CBOD decomposition rate (day^{-1})	0.0004 (1.08)	0.0004[P], 0.00025[LE]
Background light extinction coefficient (m^{-1})	0.25	0.24[TFC]
Background SOD due to biota (g O_2/m^2 day)	0.1–0.8	0.5[LE]
Carbonaceous BOD deoxygenation rate at 20°C in water column (day^{-1})	0.21 (1.045)	
Half-saturation constant for carbonaceous deoxygenation in oxygen limitation	0.5	

TFC: Three Fathom Cove, Hong Kong; *Patuxent Estuary, USA; C: Chesapeake Bay, USA; P: Potomac Estuary, USA; LE: Lake Erie. (Temperature correction coefficients in parentheses.)

The advective diffusion of the water quality constituents can be modelled with a variety of detail – ranging from box-type segmented models to two-dimensional or three-dimensional models. In our experience the key is to model correctly the tidal flushing of the ecosystem, that is the exchange of 'clean ocean water' between the ecosystem and the outer sea. The flushing rate of the ecosystem can be estimated from long-term freshwater and salinity data when available; alternatively it can be accurately determined by three-dimensional hydrodynamic models (see Section 18.3).

In order to simulate nutrient and DO exchange between the water column and the sea bed, an additional benthic layer is provided. Particulate organic nitrogen and phosphorus settle into the benthic sediment along with the respective nitrogen and phosphorus incorporated in the biomass of settled algae. The benthic segment is assumed to be anaerobic (i.e. thin aerobic top layer of sediment not modelled), and organic, ammonia and nitrate nitrogen, and biochemical oxygen demand (BOD) are modelled in the sediment. In the reducing sediment settled non-algal particulate organic nitrogen is hydrolysed to ammonia by bacterial action, and ammonia is also generated by the anaerobic decomposition of algal detritus; both are assumed to follow first-order reactions. The ammonia nitrogen may then be exchanged with the overlying water column via diffusion. No nitrification occurs in the anaerobic sediment, while denitrification is modelled. Nitrate is present in the benthos due to diffusive exchange with the overlying water column. In the sediment, deoxygenation due to the anaerobic decomposition of carbonaceous and nitrogenous organic matter (CBOD and NBOD

respectively) are used to determine the (negative) DO concentration. The negative concentrations computed can be considered the oxygen equivalents of the reduced end products produced by the chains of redox reactions occurring in the sediment. The flux of oxygen (sediment oxygen demand, SOD) and ammonium nitrogen across the sediment-water interface can then be computed from the respective water column and benthic layer concentrations using a Fickian diffusion approach. Further details and various versions of the model can be found elsewhere (DiToro, 1980; Ambrose et al., 1993; Lung, 1993; Arega, 2000).

18.2.2.1 Oxygen production and consumption

The modelling of photosynthetic production of oxygen by phytoplankton is a critical component. Based on *in situ* measurements, the vertical attenuation coefficient is represented as the sum of a background value ($y_o = 0.24$) and a function of the [chl *a*] concentration ($P =$ [chl *a*]), $\gamma_1(P) = -0.0057P + 0.145\sqrt{P}$ (Figure 18.6).

Compared with the Riley equation, $\gamma_1(P) = 0.0088P + 0.054P^{2/3}$, it gives a better fit to the data at large [chl *a*] concentrations. This probably underlies the fact that non-active chlorophyll (phaeo-pigment) is included in the standard [chl *a*] measurement; the proportion of phaeo-pigment can be as much as 40–60% of the measured [chl *a*]. The saturating light intensity for algal growth I_s is assumed to track the previous light history to which the algae have been exposed (Kremer and Nixon, 1984); I_s is determined as the weighted average of the available PAR in the previous three days. Further, the carbon-[chl *a*] ratio [CCHL = C:chl *a*] is variable, depending on the past history of the algal cells and affected by light intensity, temperature, and nutrient availability. Using the Steele equation, the dimensionless light-limiting function is given by $g(I) = \frac{I}{I_s} e^{1-(I/I_s)}$, where $0 \leq g(I) < 1$. The chlorophyll specific rate of

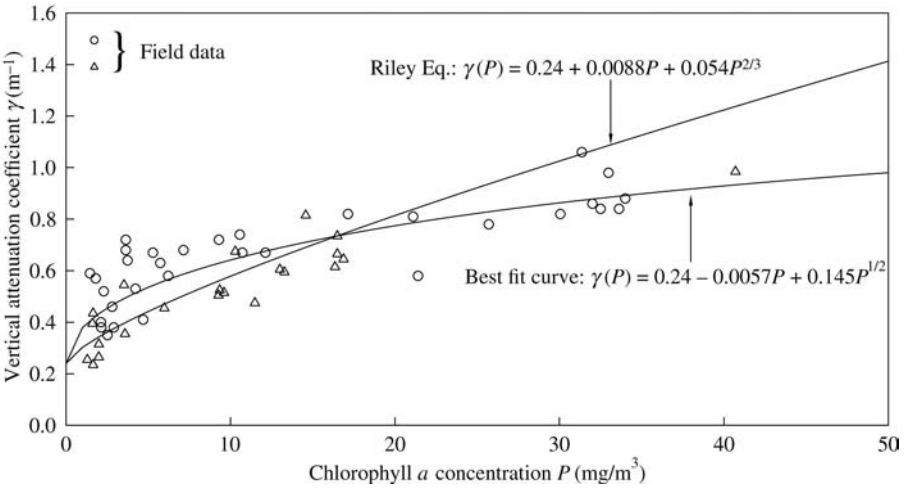

Figure 18.6
Vertical attenuation coefficient for photosynthetically available radiation (PAR) as a function of chlorophyll concentration (self-shading effect).

photosynthesis [p; mg C (mg chl a.h)$^{-1}$] can then be expressed as

$$p = \frac{\mu_{\max} g(T) \mathrm{CCHL}}{24} \frac{I}{I_s} e^{1-(I/I_s)} \tag{18.1}$$

where μ_{max} is maximum algal growth rate (d^{-1}), I is instantaneous light intensity (PAR) in W m^{-2}, and $g(T)$ is temperature limiting function. Supported by field data, it is assumed that the initial rate of change of the p-I curve, $\alpha = \frac{\mathrm{d}p}{\mathrm{d}I}(I = 0)$ is constant (Parsons et al., 1984; this is equivalent to assuming a quantum yield for low light intensities). An expression for the dynamic determination of C:[chl a] for any given day can then be obtained (Lee et al., 1991*a*):

$$\mathrm{CCHL}\left(\frac{\text{mg C}}{\text{mg chl - } a}\right) = \frac{\alpha I_s}{\mu_{\max} g(T) e}. \tag{18.2}$$

A value of $a \approx 2.9$ [mg C (mg [chl a] J m^{-2})$^{-1}$] can be obtained by assuming a maximum quantum yield for carbon fixation; this is also supported by laboratory experiments on algal cultures (Lee et al., 1991*a*). Both modelling and fieldwork show that algal respiration and sediment oxygen demand are major items of the DO budget. One notable feature of the field studies is that in order to account for the large diurnal change in DO, the best fit value for a is often notably greater than the theoretical value, by as much as a factor of 2. The C:[chl a] inferred from the DO data is of the order of several hundred. Compared with typical reported values of C:[chl a] of 50–100, the relatively high values may be related to factors that are not accounted for in the model – for example variability of species composition and algal growth rate, and oxygenation by plant growth on the fish raft nets. It should be pointed out that the phytoplankton C:[chl a] inferred from the DO and [chl a] data is consistent with other independent measurements in Tolo Harbour. The phytoplankton productivity at a nearby location (central Tolo Harbour) has been measured by C-14 uptake to be 315 g C (m^3 yr)$^{-1}$ (Chan and Hodgkiss, 1987). On the other hand, using the measured [chl a] and nutrient concentrations, temperature, and generally accepted algal growth and respiration rates (Table 18.1), the net growth rate of algal biomass can be computed to be around 4 mg [chl a] (m^3 d)$^{-1}$. Thus the C:[chl a] ratio can be inferred to be 216.

The type of water quality model described herein is adopted primarily as a practical engineering tool for water quality management, and the ultimate justification lies in model validation against field data. Despite the relative simplicity of the model, it has produced good results against field data. The water quality model can be gainfully employed to interpret the observations of phytoplankton dynamics, and help to unravel the causes and the environmental preconditions that would lead to severe DO depletion – and hence a potential fish kill. In general, the cultured fish species cannot survive a prolonged period of low dissolved oxygen; 2 mg l^{-1} (= g m^{-3}) is a generally accepted critical limit. Figure 18.7 shows a hindcast of water quality variation over a two-week period in Three Fathoms Cove using a time step of 0.5 h. The daily variation of solar radiation, tidal range, water temperature and DIN loading are also shown. Experiments on cultured fish excretion and faecal production rates, and nutrient leaching rates of trash fish have been conducted. The inorganic nitrogen concentrations in

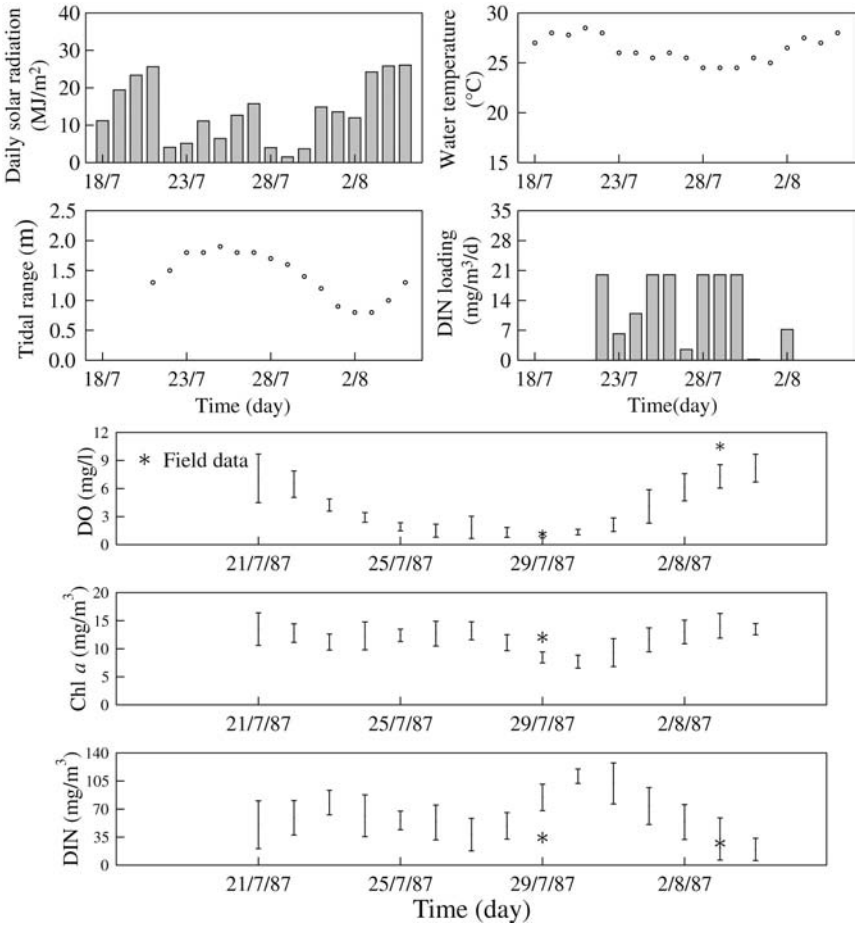

Figure 18.7
Computed variation of dissolved oxygen (DO), chlorophyll *a* and dissolved inorganic nitrogen (DIN) in Three Fathoms Cove, July 1987 (predicted daily range and field data shown).

rainfall can also be obtained. The nitrogen loading (on aerial basis) can hence be estimated based on fish stocking density and rainfall. Figure 18.7 shows the predicted range of DO, [chl *a*] and dissolved inorganic nitrogen (ammonia + nitrate) for each day. The initial values at 00 h, 21 July 1987, are provided by measurements made on a hot sunny day, with [chl *a*] of around 12 mg m^{-3}. A prolonged period of overcast skies, thunderstorms and heavy rainfall then ensued. Water temperature is generally high in the summer, above 25°C. The computed DO stays fairly high for the first few days; the predicted range of DO is generally greater for sunny days. The model predicts a steady decline in DO down to a sustained period of critical low level, below 2 mg l^{-1}, around 29 July. This coincided with a massive fish kill that occurred around 01.00 on 29 July during an unusual protracted (8 h) period of slack tide. Nearly all the fishfarms in the zone were affected, and at least 120 tonnes of fish (mainly seabreams, snappers

and some groupers) were killed. Observations of cell counts suggest that the causative species for this incident was the non-toxic dinoflagellate (*Peredinium faeroense*). The bloom developed from mid-July to a peak on 28 July; peak cell counts went up to 0.5 million per ml; however cell counts quickly decreased down to about 6,300 per ml on 29 July. The bloom subsided by 31 July, with DO restored to high values on 3 August when the water was dominated by high densities of diatoms. It can be seen that both the timing of the period of severe DO depletion, as well as the subsequent rapid pickup of DO with increased solar radiation are well-predicted. The approximate level of [chl *a*] and nutrient depletion are also reasonably reproduced. This simulation demonstrates clearly the importance of hydro-meteorological conditions and the sediment oxygen demand on DO (due to decomposition of settled algae) in the fish culture zone.

Figure 18.8 shows the importance of the dynamic determination of both the saturation light intensity and carbon-chlorophyll *a* ratio. For example, if a constant value of C:[chl *a*] = 100 or 300 is assumed, the characteristic decline and subsequent increase of DO cannot be satisfactorily predicted. Similarly, the timing of DO depletion will be poorly predicted if a constant saturating light intensity of $I_s = 100$ W m^{-2} is assumed. The water quality model has been extremely useful in guiding the field data collection (e.g. deciding on water quality parameters to be measured; the spatial resolution and frequency of sampling; pointing to the need for direct *in situ* measurements of sediment oxygen demand, and algal culture experiments). The lessons learned from the simulations have also been incorporated in education pamphlets

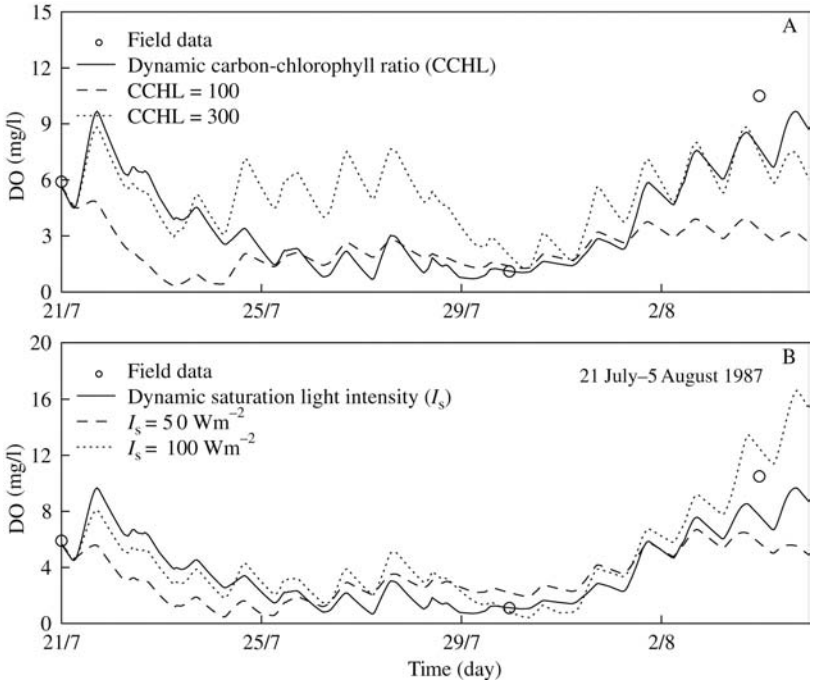

Figure 18.8
Predicted dissolved oxygen variation for A, constant CCHL; B, constant I_s.

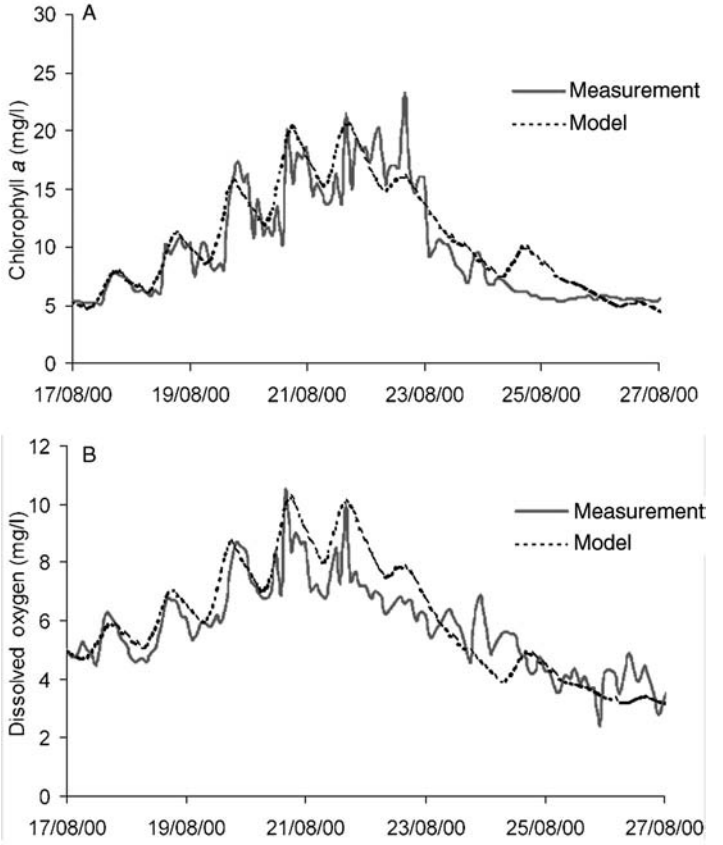

Figure 18.9
Simulation of A, algal; B, dissolved oxygen dynamics during a diatom bloom using Monod growth kinetics (August 2000, Lamma Island).

distributed to fish farmers who are alerted to environmental and meteorological conditions (e.g. prolonged periods of overcast skies in the summer, thunderstorms) that may lead to severe oxygen depletion, and advised on sound practices. Short-term DO forecasts (extending from two to four weeks) have been validated against field data for many scenarios. Figure 18.9 shows a similar comparison of predicted algal and dissolved oxygen dynamics with high-frequency data for an observed diatom bloom in Lamma Island, Hong Kong (Wong, 2004). Although general trends can be simulated, this type of model framework is limited in its description of the complicated growth and death patterns during an algal bloom. The prediction of bloom collapse under nutrient limited and oxygen depletion conditions remains a challenging task. For example, a more realistic sinking hypothesis (than an assumed constant algal sinking rate) may have to be adopted in order to reproduce the timing of the bloom collapse correctly; as the nutrients get depleted, laboratory experiments on algal cultures revealed the sinking velocity of the algal cells (with changed structure) can increase by as much as 6-fold!

Table 18.1 gives the values for the model parameters selected from the literature and model calibration; values adopted in related previous studies are also included for comparison. The water quality modelling framework can be easily adapted to study seasonal (daily varying) and long-term trends of eutrophication. A multi-segment dynamic eutrophication model (with the segments coinciding with the locations of routine biweekly water quality monitoring) has been formulated for Tolo Harbour (Lee and Arega, 1999). Starting from a measured initial condition, and with input pollution loads into each segment and the environmental forcing (light and photo-period, rainfall, temperature), the spatial and temporal variation of water quality can be computed. The modelling can yield interesting insights about eutrophication dynamics, and provide useful information on the critical controlling factors: the relation between nutrient removal and water quality, and effect of global climate change such as the greenhouse effect. Figure 18.10A shows the predicted variation of [chl *a*] levels in the surface and bottom layers at an inner and outer station in Tolo Harbour over an entire year (Arega and Lee, 2000); the median and range of monthly field measurements are also shown. Both the predictions and measurements indicate multiple blooms over the year. In the outer harbour, where flushing rates are much higher, much lower chlorophyll levels are seen. Contrary to initial expectations, our modelling results indicate nutrients are often not the controlling factor; instead blooms are triggered by a combination of hydrologic and meteorological conditions. Figure 18.10B shows a similar calculation for 1992. In contrast to 1987, which was characterized by much higher water temperatures in the beginning months of the year, no blooms were triggered until early spring in 1992, again in accordance with the data. The sensitivity of bloom events to water temperature also helps to explain why very low dissolved oxygen levels were observed in the harbour in 1998, even after substantial nutrient loads have been diverted into another catchment (Tolo Nutrient Export Scheme, introduced in 1995).

18.3 Environmental management of mariculture

The water quality model can also be used for environmental management of marine fish culture (Lee et al., 2003). The sustainable management of mariculture requires proper siting of the fish farms and stocking density control. Both of these are related to the carrying capacity of the water body concerned, which is mainly governed by its flushing characteristics. A method to determine the carrying capacity of a fish farm has been developed using three-dimensional hydrodynamic modelling to compute the flushing rate and linking it to a simple water quality model.

In this age of ever increasing computing power, three-dimensional time-dependent hydrodynamic and water quality models can be used to compute the water quality for a given set of pollution loading and environmental conditions. The carrying capacity of a given water body can be estimated by defining some scenario (e.g. the maximum pollution loading threshold below which a target DO level will always be met in the summer season). This kind of real-time calculation from a coupled hydraulic and water quality model will typically give the time variation of water quality (e.g. over a period of a month) in either the dry or wet season. While such a methodology may be necessary for some purposes (e.g. to track the movement of a red tide), a much simpler and robust method is needed for mariculture management. Usually, a typical fish culture zone covers an area of the order of 0.1 km^2, and spans only a few grid points in the

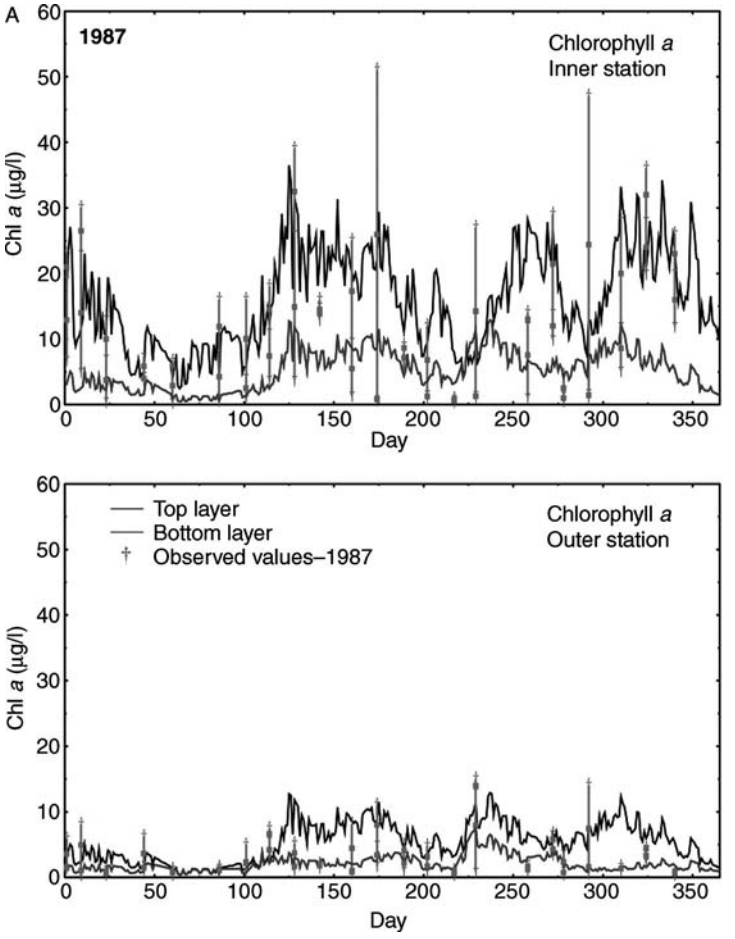

Figure 18.10
A, comparison of predicted and measured chlorophyll *a* at two stations in Tolo Harbour in 1987 (predicted values for surface and bottom shown against median and range of measurements).
B, comparison of predicted and measured chlorophyll *a* at two stations in Tolo Harbour in 1992 (predicted values for surface and bottom shown against median and range of measurements).

computational domain of the hydrodynamic circulation model. It is difficult to assess the long-term impact or determine the carrying capacity using the voluminous output (spatial distributions and time histories) of these models. Second, tidal and water quality variations are governed by quite different timescales; the effectiveness of using complex hydrodynamic and water quality models for long-term simulation (with attendant numerical problems and uncertainty of rate parameters) is questionable. For environmental management purposes, it is necessary to have a tractable water quality model that can elucidate in a simple manner the dependence of water quality on the important hydrographic, meteorological and ecological parameters.

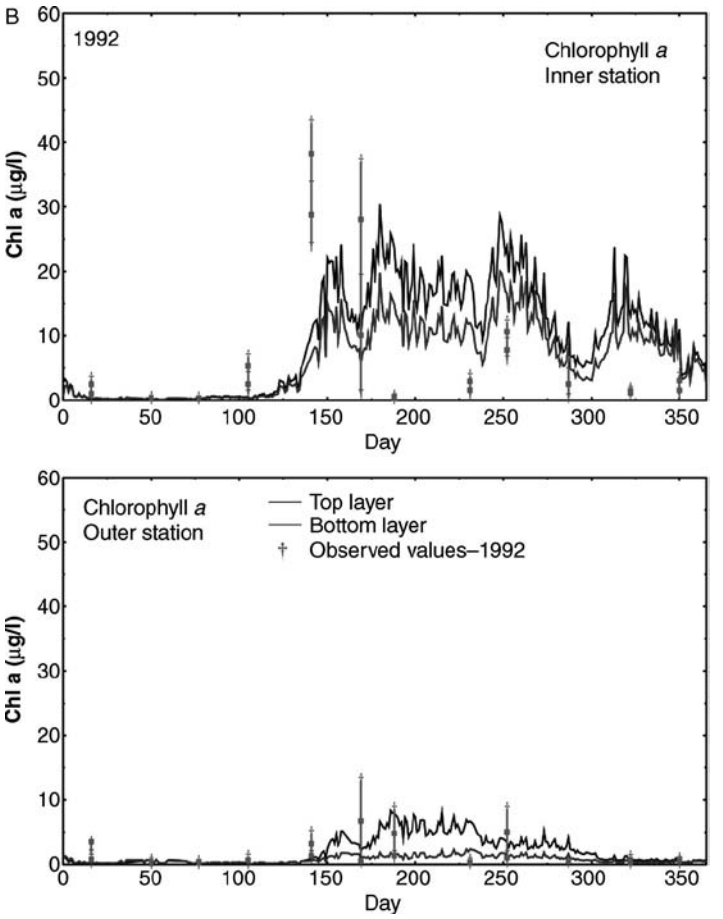

Figure 18.10 *(Continued)*

The coupling of hydrodynamic and water quality models to assess the carrying capacity of a fish farm is schematized in Figure 18.11. The fish culture zone is modelled as an ecosystem characterized by a number of key water quality variables (algal biomass, nutrients, DO). The water quality and hence carrying capacity of the system is determined by the pollution loading, water temperature, and the tidal exchange with the outer (clean) sea – which is driven by tides and density stratification. Figure 18.12 shows the tidally averaged stratified flow in Tolo Harbour obtained from a three-dimensional model – characteristic of a partially mixed estuarine circulation. A systematic methodology via the use of numerical tracer experiments has been developed to determine the flushing rate of a marine fish culture zone located in semi-enclosed shallow embayments.

First, the three-dimensional tidal circulation in the bay, including the fish farm, is computed for an assumed tidal condition and vertical salinity distribution at the open boundary; the dynamic steady state can be obtained from a fully three-dimensional

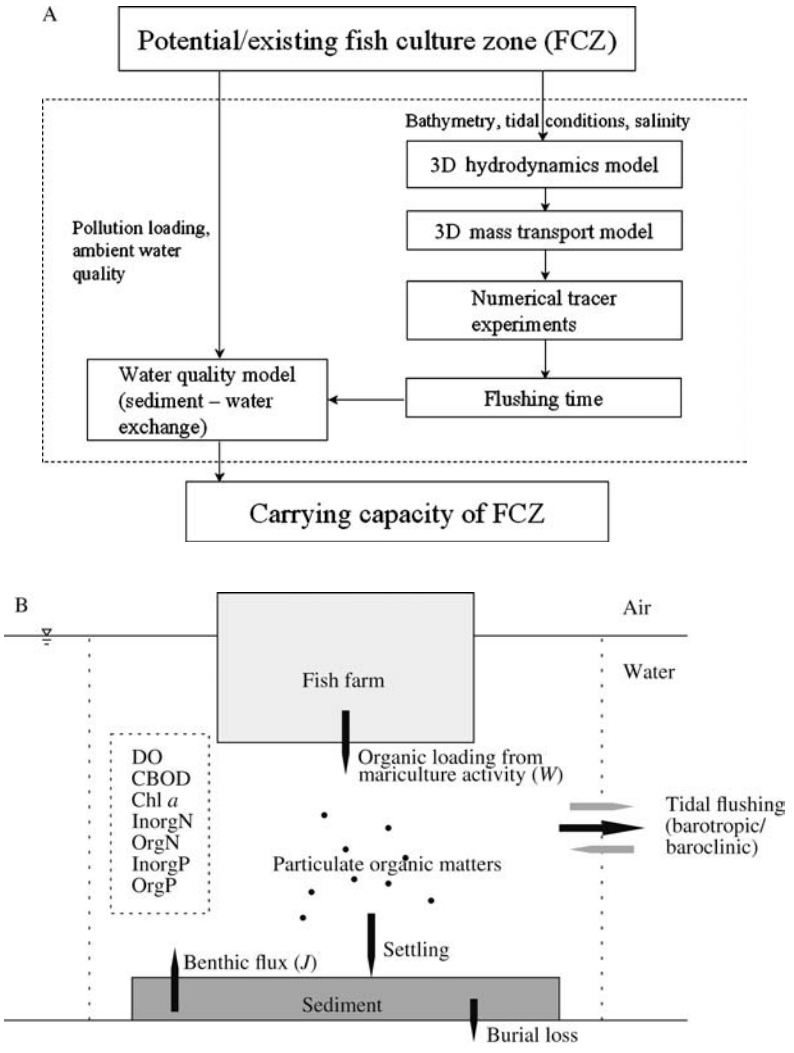

Figure 18.11
A, framework for modelling the carrying capacity of a fish culture zone. B, schematic of water quality model.

calculation (Choi, 2002; Choi et al., 2003). Given the tidal velocity field, a mass of hypothetical conservative tracer is instantaneously introduced into a region of interest, such as the fish farm or an entire bay. It is assumed that a unit tracer concentration is initially found inside that region and zero concentration elsewhere. The subsequent change in tracer concentration distribution as a result of barotropic and baroclinic exchanges is computed by solving the three-dimensional advective diffusion; e.g. Figure 18.13A shows the tracer concentration distribution computed by a Lagrangian random walk method after 12 hours. Due to tidal exchange with the 'clean' water outside

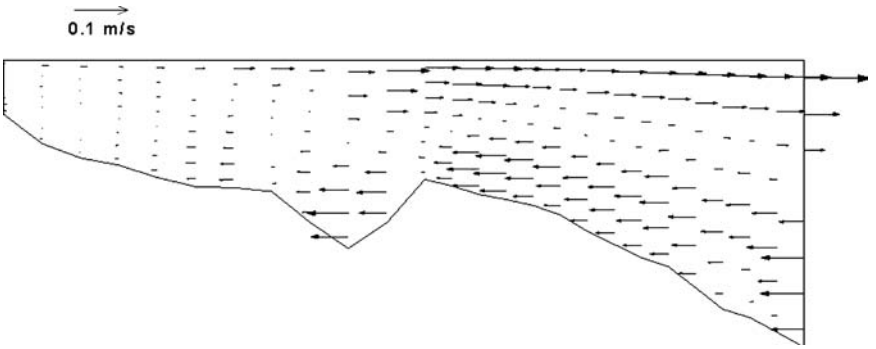

Figure 18.12
Computed tidally averaged residual circulation for Tolo Harbour.

the region, the tracer mass within the region of concern decreases with time; Figure 18.13B shows the change in tracer mass M(t) with the flood and ebb of tides under stratified flow conditions. It is found that in tidal inlets, the decrease in tracer mass follows a double-exponential curve (Choi and Lee, 2004; Choi, 2002); the flushing time, defined as 'the average lifetime of a particle in the given volume of water body', can be analytically determined from a best fit of the M(t) curve. In this method, the surrounding water in the vicinity of the fish farm is assumed to be 'clean'. Essentially, this 'local' flushing time is useful for estimating the local impact of any foreign substance or short-term effluent discharge from the fish farm. It can be used, for example, to compare the merits of different locations of the fish farm within the selected tidal inlet. However, for some water quality parameters such as nutrient concentration, the outer bay has a non-zero concentration due to the return of pollutants with the flood and ebb of tides. For estimating long-term average water quality, the 'system-wide' flushing rate is determined by looking at mass removal from a much larger water body which is connected to an adjoining 'clean' ocean. This definition takes into account the interactions between different parts of the water body which are not assumed to be 'clean' and represents the long-term flushing efficiency of the region of interest. In the tracer experiment, mass is released from everywhere inside the water system of interest (e.g. the entire bay containing the tidal inlet in which the fish farm is located). This approach is similar to determining the flushing rate using salinity (or freshwater concentration) as the tracer concentration, but it is applicable even for the cases of weak or negligible longitudinal salinity gradients (e.g. when freshwater runoff is all routed to reservoirs for water supply). Figure 18.13B shows that the system-wide flushing time is much larger than the local flushing time (slower decrease of M(t)), and that the flushing rate is significantly greater in the presence of density stratification in the wet season. Extensive computations and comparison with field data have indicated this 'system-wide' flushing rate should be used for determining the long-term water quality and hence the carrying capacity of the fish culture zone.

Second, the computed flushing rate is used in a quasi-steady seasonally averaged water quality model that includes both the eutrophication kinetics in the water column and the sediment-water interactions (Lee and Wong, 1997). The computed flushing time for the dry/wet season is coupled with the water quality model that includes the algal growth and nutrient kinetics in the water and the sediment-water-pollutant

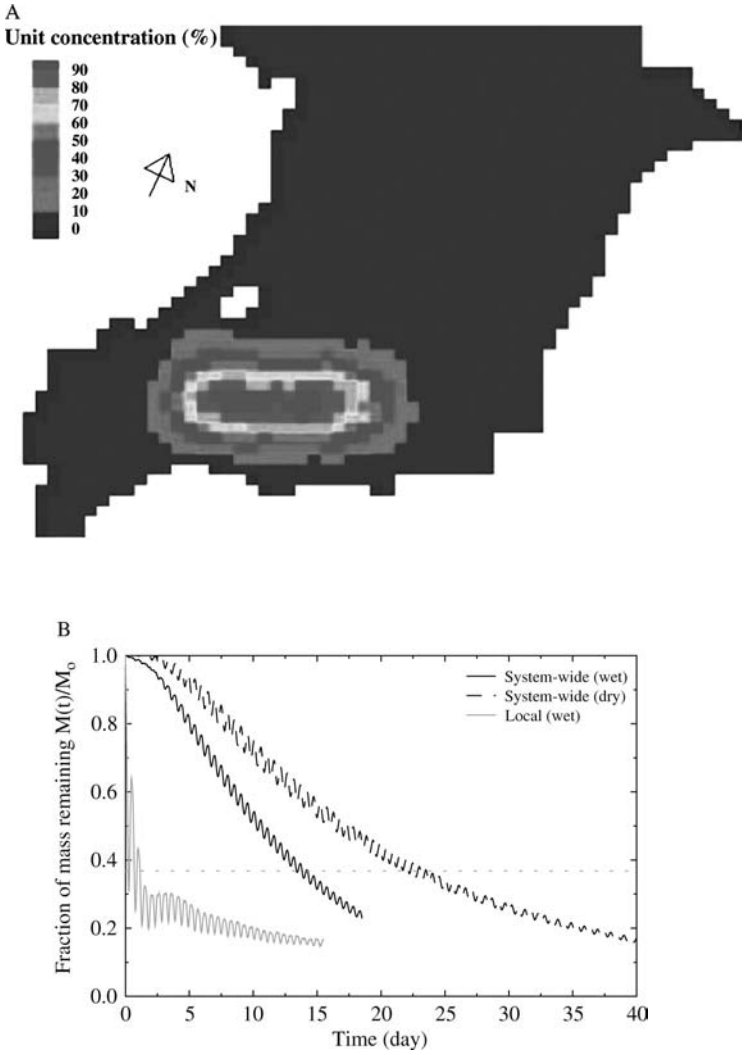

Figure 18.13
A, computed tracer concentration distribution 12 hours after release of tracer mass in Yung Shue Au fish culture zone, Three Fathoms Cove, Hong Kong.
B, tracer mass variation with time for system-wide flushing and 'local' flushing, for dry and wet seasons.

interactions. The carrying capacity of the fish farm can be assessed by reference to key water quality indices: [chl *a*], dissolved oxygen, organic nitrogen, and a potential lowest dissolved oxygen (PLDO) level. The predicted water quality as well as the relative carrying capacity are well-supported by field observations. This model predicts the long-term average water quality condition in the fish culture zone. From the model

results, the carrying capacity of the fish culture zone can be determined in terms of the PLDO – defined as the lowest DO level on a day with negligible photosynthetic production (e.g. critical days of overcast skies and heavy rainfall). The model can be used as a tool to assess the impact of an existing fish farm, or answer 'what-if' question for evaluating various management options (e.g. the degree of reduction of pollution loading or fish stock). The method has been successfully applied to six representative fish culture zones (FCZ) in Hong Kong (Figure 18.14) with different hydrographic and fishfarm loading characteristics. These consist of four FCZs in Tolo Harbour: Yung Shue Au (YSA), Yim Tin Tsai (YTT), Yim Tin Tsai East (YTTE), Lo Fu Wat (LFW); Sok Ku Wan (SKW) on Lamma Island, and Ma Wan (MW). Figure 18.14A shows the organic loading and computed flushing rate and key water quality variables at the six FCZs for the summer and winter season. For a specified temperature and flushing rate, the maximum allowable pollution loading (or fish stocking density) in a FCZ can be obtained by (a) prescribing a minimum level of DO (say 4 mg l^{-1}); or (b) a minimum level of [chl *a*] (say 20 mg m^{-3}); the minimum of the two allowable loadings can then be taken as the carrying capacity (Figure 18.14B).

18.4 Hydrodynamic tracking of the 1998 Hong Kong red tide

In April 1998, a devastating red tide (due to the dinoflagellate *Karenia digitatum*) resulted in the worst fish kill in Hong Kong's history – it destroyed over 80% (3,400 tonnes) of cultured fish stock, with estimated loss of more than HK$312 million (Dickman, 1998; Yang et al., 2000). It appears that the dinoflagellate species produced copious amounts of a sticky mucus which coated the fish gills leading to suffocation and mortality within hours after the fish farms were hit by the red tide (Dickman, 1998). Other explanations are also possible, such as the production of fish toxins (Anderson, 1998). The 1998 red tide was truly an unusual event compared with all past blooms in Hong Kong waters. It is recorded that 30 red-tide events appeared in the first six months of 1998, with the most serious ones during the period 19 March to 17 April (Anderson, 1998). The press reports and water quality measurements suggest a migration of a red tide initiated in mid-March in the north-eastern waters of Hong Kong, in Mirs Bay (where red tides in Hong Kong are usually first sighted in any given year), which drifted to the southern coastal waters with tidal currents (Figure 18.15A). There is also speculation that the red tide may have initiated from outside Hong Kong, in Daya Bay along the South China coast (Figure 18.15B). Alternatively, the observations may also reflect merely a change of environmental conditions in the various bloom locations during March–April 1998, with *in situ* growth occurring at different times along the coast.

The role of tidal hydrodynamics in the 1998 red tide has been studied (Lee and Qu, 2004). The three-dimensional hydrodynamic model, Delft3D (previously calibrated with extensive field data for the Pearl River Estuary) is employed to study the tidal circulation during the average dry and wet season (Hong Kong has a distinct dry season with little rain from November to March, and a wet season from June to September frequented by typhoons and monsoons; the other months are transition periods). Figure 18.15B shows the Pearl River Estuary Model set up. A 206 by 141 boundary-fitted orthogonal grid is used, with 10 uniformly distributed vertical layers; the grid in the north-eastern waters is specially refined to study algal bloom transport patterns. Tidal forcing is applied along the eastern, western and southern

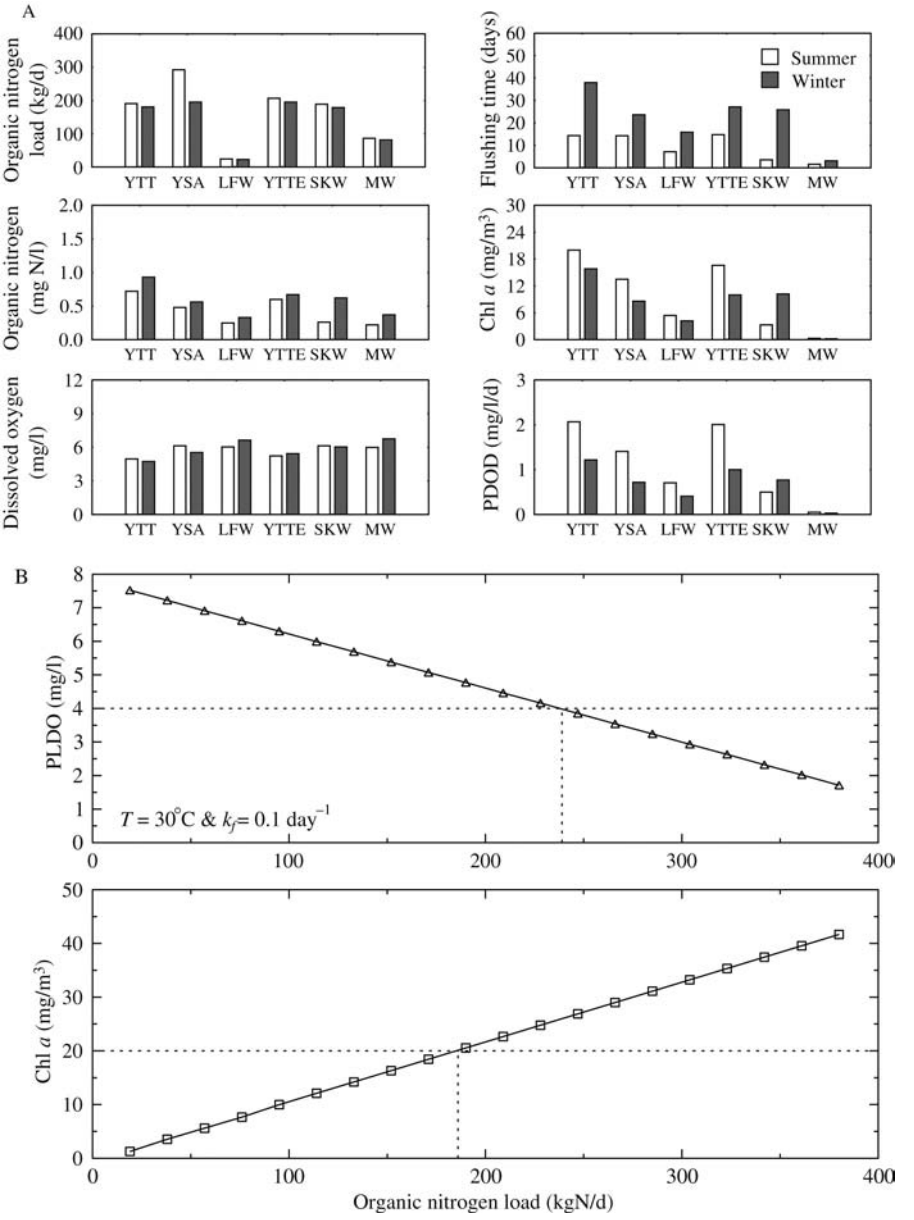

Figure 18.14
Water quality model for determination of carrying capacity.
A, organic nitrogen loads, flushing times and key water quality indicators at six fish culture zones (FCZs) – Yung Shue Au (YSA), Yim Tin Tsai (YTT), Yim Tin Tsai East (YTTE), Lo Fu Wat (LFW) in Tolo Harbour; Sok Ku Wan (SKW) on Lamma Island; and Ma Wan (MW).
B, allowable organic loading dictated by dissolved oxygen (DO) and algal biomass limits.

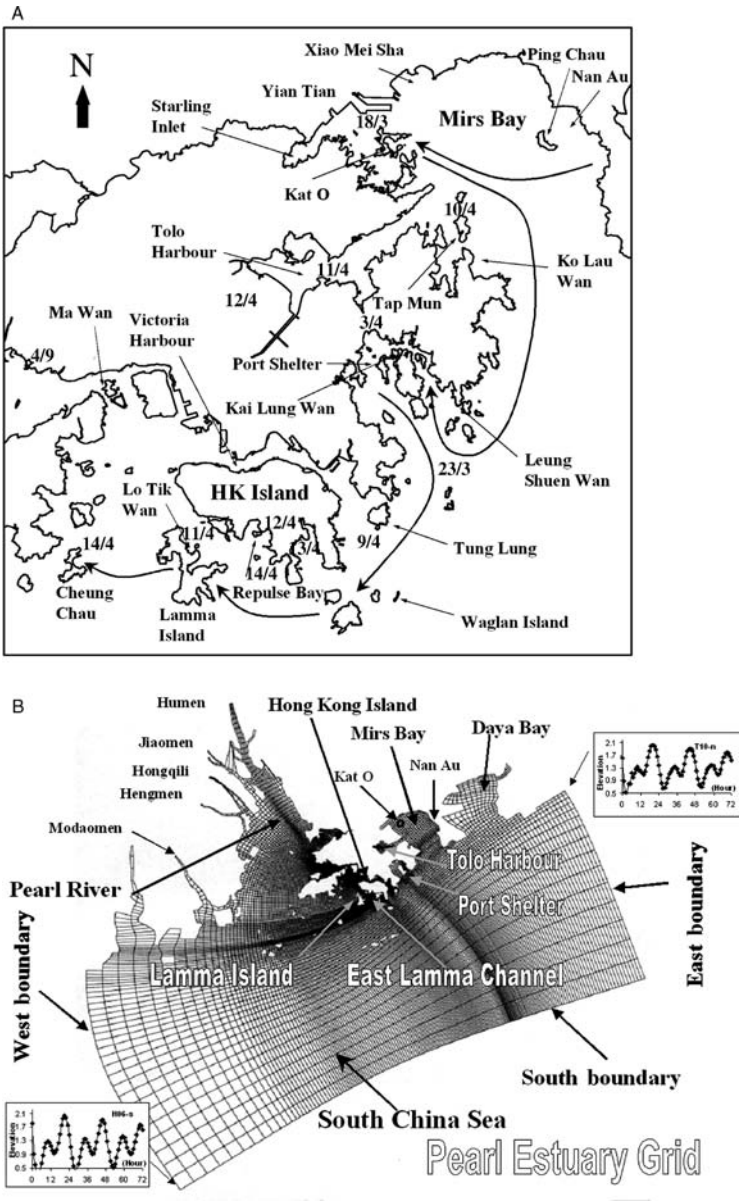

Figure 18.15
Hindcast of spring 1998 Hong Kong red tide:
A, reported red-tide movement from 18 March to 14 April 1998.
B, Pearl River Estuary model for algal bloom tracking.

boundaries; nine tidal constituents (derived from an extended harmonic analysis of long-term tidal data) are used to generate a time history of predicted water levels at the open boundaries, they are: O1, P1, K1, N2, M2, S2, K2, M4, MS4. The mean sea

level conditions are set at the different boundary stations from a low of 1.18 m in the south-west of the boundary station to 1.31 m in the north-east of the boundary station (dry season). The measured salinities for both dry and wet seasons are used in the open boundaries. Seasonal mean freshwater flows from the nine outlets of the Pearl River are prescribed at the inflow.

18.4.1 Red-tide tracking model

The aim is to study the transport of an algal bloom initiated in the north-east Hong Kong waters (as frequently observed). In particular, the relation between tidal circulation and the reported sequence of events from 18 March to mid-April 1998 (Figure 18.15A) is studied thoroughly. In the area of interest (north-east and southern waters), the grid size varies from 70 m to 1.75 km; in the ocean waters next to the western open boundary, a coarse grid up to 6 km is used. A time step of Δt =1–2 min is adopted, with a Courant number (= $\frac{\Delta t\sqrt{gh}}{\Delta x}$) in the range 0.24–1.8. The tidal circulation is computed for the typical dry and wet season and extensive drogue tracking experiments are performed. The massive red tide of 1998 is then examined using the actual wind data from February–April 1998.

The drogue tracking is simply following the path of a floating object transported by the surface current (i.e. the current in the upper layer). In the drogue tracking computations, the drogue is released after five days flow simulation, when the flow has reached a dynamic steady state. Computations have shown that a 4-layer model gives sufficiently accurate results while retaining reasonable computational economy for the large amount of drogue tracking. As a drogue track of interest would depend on the release location as well as the exact time of release, it would be futile to enumerate the drogue tracks released in all locations within north-eastern waters during the months of February, March and April 1998 – the general dry season. We thus proceed heuristically. Generally, a drogue is released from the surface layer at the centre of a grid – for release positions throughout Mirs Bay, Tolo Harbour and Daya Bay. Numerical experiments show that the drogue path for such a release can almost describe the general path of movement of a bloom initiated anywhere within the same grid, or within the same region. Through such drogue tracking experiments for a large number of releases at different tidal stages, a good idea of the general trend of the red-tide movement can be gained. The possibility that a red tide could be transported to the southern waters and East Lamma Channel can be reliably assessed. Details on the flow field and the drogue tracking can be found in Lee and Qu (2004).

18.4.2 Algal bloom tracking for different scenarios

In order to unravel what really happened in spring 1998, drogue tracking is performed for a release from different locations in Mirs Bay and at different stages of the tidal cycle and different wind conditions. This tracking is performed both for the typical dry season (with mean north-east wind of 5 m/s) and for spring 1998. In general, the bloom tracking reveals it is extremely unlikely that a bloom initiated in the northern part of Mirs Bay, Yian Tian, Nan Au or Tolo Harbour would be transported down to the East Lamma Channel in the typical dry season (Figure 18.16A).

For the actual wind conditions in March–April 1998, similar extensive numerical drogue tracking as previously described is performed for releases from different tidal

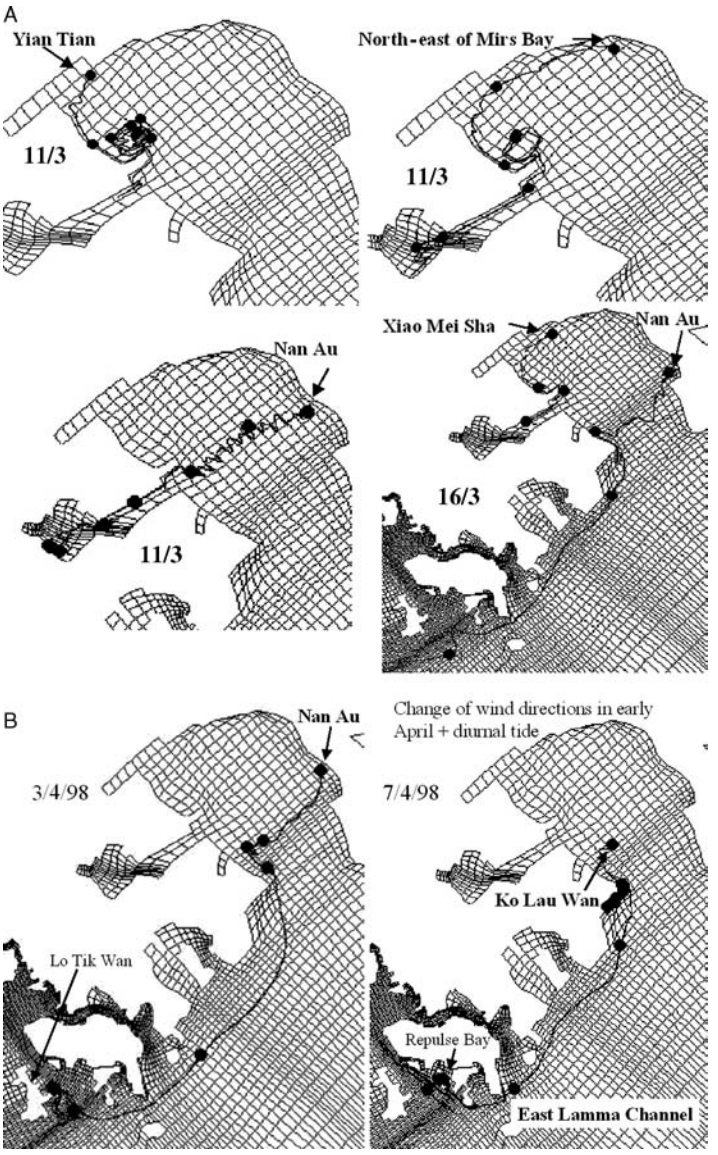

Figure 18.16
A, surface drogue tracking for a release in different parts of Mirs Bay in the dry season, March 1998 (output interval = 1 day).
B, surface drogue tracking for a release in different parts of Mirs Bay during March–April 1998 (output interval = 1 day).

period both in March and April. During Spring 1998, the wind was quite strong at the beginning of March, on March 22-23 and also relatively strong at the beginning of April. The wind direction was mostly in NE direction during March, but changed

direction on 1, 4 and 6–7 April to north-west/northerly direction; the wind direction then changed in clockwise manner to a south-easterly direction during 7–12 April. The tidal elevation and velocity in East Lamma Channel from mid-March to mid-April is shown in Figure 18.16B; the almost diurnal tide during 3–6 April can be noted. Under these conditions, a bloom initiated in the north-east of Mirs Bay or Nan Au can also be transported into Tolo Harbour. Compared with the typical dry season (Figure 18.16A), the stronger wind conditions in March–April 1998 (Figure 18.17) increases the chance of bloom transport towards Lamma Channel. The drogue tracks show clearly that blooms initiated in Nan Au and Tap Mun in late March or early April can be transported to East Lamma Island/southern waters several days later. The bloom could possibly travel along the path from Nan Au to Tap Mun and then down to the south beaches of Hong Kong Island or East Lamma Channel (Figure 18.16B). This suggests that the red tide observed in the southern beaches of Hong Kong Island

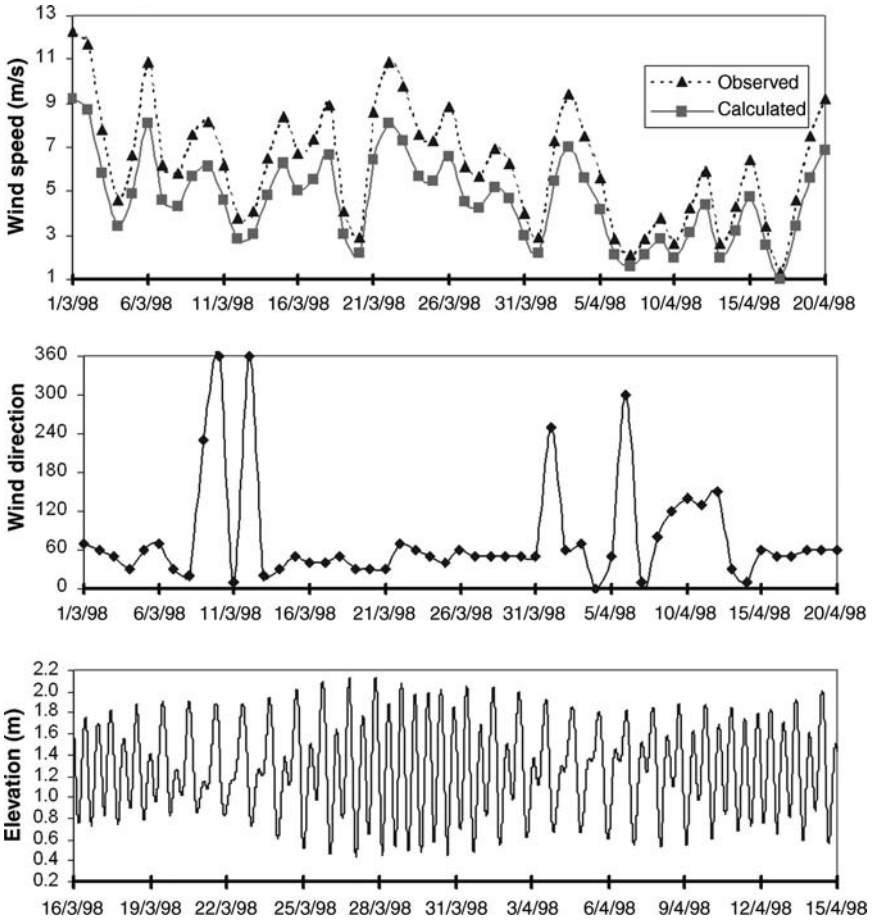

Figure 18.17
Recorded wind velocity and tidal elevation during spring 1998 in Hong Kong.

(Repulse Bay) on April 12–14 most probably originating from the Nan Au area or Tap Mun area 5–10 days earlier. Most importantly, the red tide at Lo Tik Wan on April 9–12 most probably originated from the Nan Au area.

In summary the hydrodynamic tracking of algal blooms has led to valuable insights on algal bloom transport, and unravelled the origin/source waters of the massive 1998 red tide and fish kill observed in Hong Kong's southern waters. It is found that, for a typical dry season, a red tide initiated in the north-eastern waters of Hong Kong (north Mirs Bay, Tolo Harbour) or Daya Bay would not normally be transported into the East Lamma Channel. On the other hand, the Spring 1998 red tide is very much related to the hydrodynamic transport. The massive red tide observed in southern waters and East Lamma Channel from 9 to 16 April may have originated in Nan Au, north-east Mirs Bay, or Tap Mun area. The change in wind direction under diurnal tide conditions in early April gave rise to a consistent clockwise gyre in Mirs Bay, which greatly enhanced the transport of blooms in these areas into the southern coastal waters and into the East Lamma Channel bordering the Lo Tik Wan and Sok Kwu Wan fish culture zones. However, it is unlikely that the red tide in spring 1998 originated from Daya Bay as speculated by the press (Lee and Qu, 2004).

18.5 Concluding remarks – future possibilities

Since the 1970s mathematical models have been developed to simulate algal growth kinetics, nutrient uptake and photosynthetic production. We have presented a number of examples to illustrate how hydrodynamic and water quality modelling can be useful in the study of dissolved oxygen and algal dynamics, and in fisheries management. Generally speaking, the deterministic models can be used for studying weekly or seasonal trends in water quality, and the relationship between waste load inputs and ecosystem response. However, model application is hampered by the lack of knowledge of many ecosystem parameters, the initial and boundary conditions, and the external forcing – and errors in the model structure due to neglected processes. The Eulerian framework is also not suited for modelling the Lagrangian nutrient uptake process (e.g. if cell nutrient status is a variable) and advective-diffusion of vertically migrating dinoflagellates (Wong and Lee, 2003; Wong, 2004). Ideally, the uncertainty of model predictions can be reduced through calibration and verification against data. However, water quality models are complex and involve typically over 20–30 rate parameters. The model calibration and verification process is usually subjective and lengthy, and useful information contained in the valuable data is often not extracted. Despite such drawbacks, multi-billion dollar decisions are often made based on the results of these models. There is definitely a need to explore new approaches to water quality modelling.

Despite the advances made in practical water quality modelling, the previous work has several important shortcomings: (a) knowledge gained from site-specific observations is not readily transferrable to other water bodies; (b) the biological basis for most existing water quality models is overly simplified. The species groups are often lumped into total algal biomass, and a constant algal sinking velocity is assumed. Many difficult questions remain, such as the change of dominant species from diatoms to dinoflagellates during a bloom, distinction of harmful and non-harmful algal species groups, vertical migration, the likelihood of occurrence of a certain species group at a given location and time. There is a genuine need to integrate the deterministic

model with field data to improve the understanding of the biological and physical processes and develop a tractable model to interpret the changes in the complex coastal marine ecosystem.

In contrast to deterministic models, alternative approaches such as Kalman filtering techniques have been applied in the forecasting of algal concentrations (Whitehead and Hornberger, 1984). This approach takes into account uncertainties due to imperfect model structure or measurement noise. Essentially, a deterministic state-space structure for the water quality variables is assumed along with modelled statistics for measurement or model uncertainties. At each instant of observation, based on the difference between the prediction and the observed values, the Extended Kalman Filter (EKF) can be used to update model parameters and revise the estimate of the state variables. The EKF can thus be effectively used to illuminate any time-variations in the model parameter estimates (e.g. algal growth rate) which are not consistent with the assumed dynamics of the system. Most of the earlier work dealt with highly simplified systems (e.g. BOD-DO); although the EKF has been incorporated into a six-variable system to study steady river water quality (Bowles and Grenney, 1978). The statistical variances and error propagation in eutrophication models have also been studied using Monte-Carlo methods (Scavia, 1981).

In recent years, two exciting developments have emerged. First, the use of data-driven methods such as Artificial Neural Networks (ANN) to study the highly nonlinear algal bloom problem (e.g. Chen and Mynett, 2003; Whitehead et al., 1997; Yabunaka et al., 1997; Barciela et al., 1999; Lek and Guegan, 1999) has emerged. By incorporating ecological knowledge in the choice of input variables, the forecast of coastal algal blooms using artificial neural networks is promising (Lee et al., 2003). It is concluded that an ANN model with a small number of input variables is able to capture trends in algal dynamics, but data with a minimum sampling interval of 1 week is necessary. At present there are insufficient real-time data to fully test the promise of these data-driven methods. Figure 18.18 shows a ANN forecast of chlorophyll fluorescence concentrations using the real-time data at Kat O. The chlorophyll concentration at time $(t + 1)$ is predicted using the chlorophyll and DO concentrations at times t, $(t - 1)$, $(t - 2)$ and $(t - 7)$. Figure 18.18 shows the comparison of predicted depth-averaged chlorophyll concentration (at mid-day) with observations (Lee et al., 2004). The neural network is trained using about N = 706 days of continuous data, and tested using four months of data. The prediction agrees with the observations in magnitude and phase reasonably well. Nevertheless, more high-frequency data of this kind would be needed to further test the performance of ANN models.

In contrast to pure data-driven methods, data assimilation refers to the blending of observations with a dynamic deterministic model to improve our understanding of the system and to provide optimal forecast. The ensemble Kalman filter (EnKF) was recently introduced as a sequential data assimilation method that is based on Monte-Carlo simulations (Evensen, 1997). It is an attractive tool as it avoids many of the problems associated with the traditional EKF, and appears to be highly suited for tackling nonlinear dynamics problems. The EnKF has been successfully applied to physical oceanographic modelling. Very recently, it has been applied to assimilate water quality data (Eknes and Evensen, 2002); the traditional EKF has also been applied to integrate high-frequency DO data (Pastres et al., 2003). In general, data assimilation of water quality has been applied only to very limited ecosystem data, and

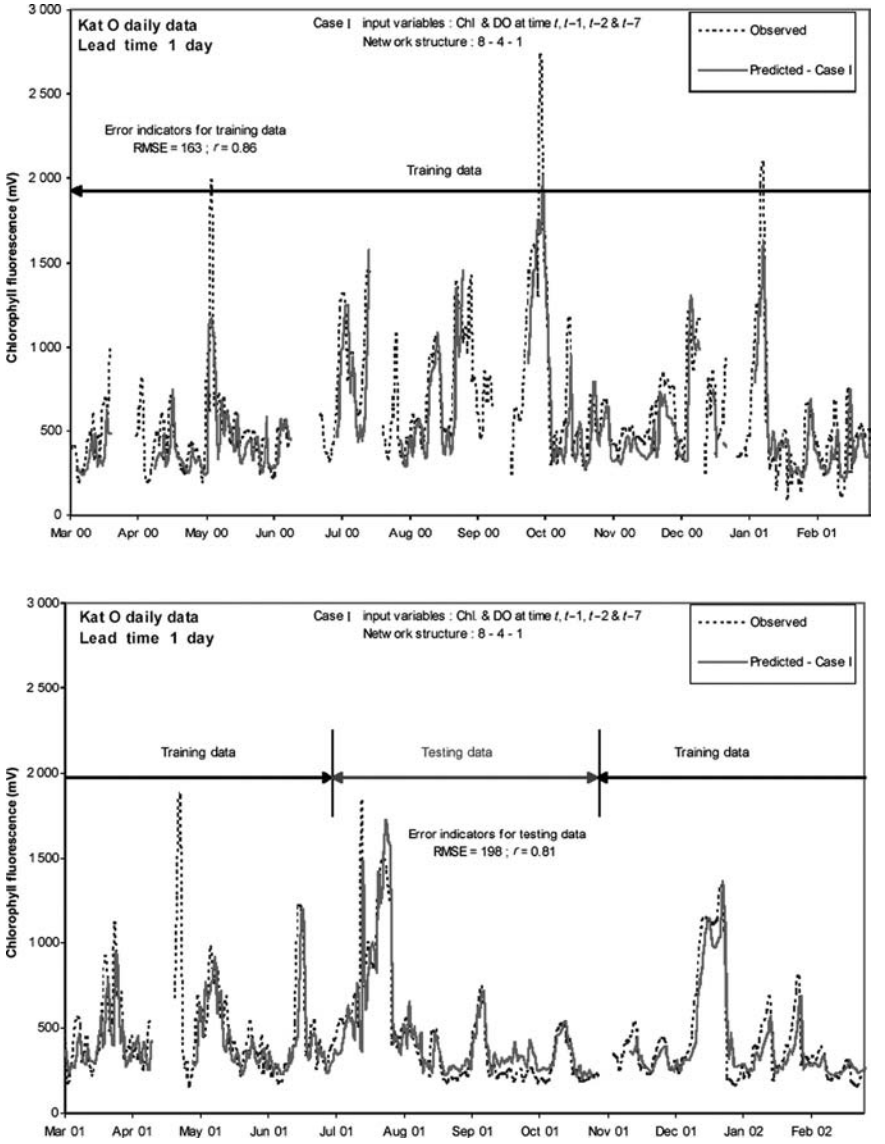

Figure 18.18
Comparison of predicted and observed chlorophyll concentrations at Kat O, Hong Kong. Prediction of chlorophyll at $t + 1$ is made using an artificial neural network (ANN) model and real-time data.

much remains to be done. For example, in Eknes and Evensen (2002) the EnKF was used with a highly simplified three-component water quality model for the deep sea (200 m depth) and tested against simulated observations. The use of data assimilation

to predict short-term dissolved oxygen dynamics in the Venice Lagoon was tested only for a two-week data set (Pastres et al., 2003). With the increasing availability of high-frequency water quality data, advanced data assimilation offers a promising tool to extract the maximum information from the complex algal dynamics in coastal ecosystems.

References

Ambrose, R. B. et al. 1993. *The Water Quality Analysis Simulation Program, WASP5*. Athens, Ga., US Environmental Protection Agency, Environmental Research Laboratory.

Anderson, D. M. 1998. *Study of Red Tide Monitoring and Management in Hong Kong: Literature Review and Background Information*. Hong Kong SAR Government, Agriculture and Fisheries Department. (Technical Report 1.)

Arega, F. 2000. A diagenetic two-layer eutrophication model for Tolo Harbour, Hong Kong. Ph.D. thesis, University of Hong Kong.

Arega, F. and Lee, J. H. W. 2002. Long term circulation and eutrophication model for Tolo Harbour, Hong Kong. In: *Water Quality and Ecosystem Modelling*, Vol. 1. New York, Kluwer Academic Publishers, pp. 169–92.

Babin, M., Roesler, C. S. and Cullen, J. J. (eds). 2007. *Real-time Coastal Observing Systems for Marine Ecosystem Dynamics and Harmful Algal Blooms: Theory, Instrumentation and Modelling*. Paris, Intergovernmental Oceanographic Commission of UNESCO. (Monographs on Oceanographic Methodology XX.)

Barciela, R. M., Garcia, E. and Fernandez, E. 1999. Modelling primary production in a coastal embayment affected by upwelling using dynamic ecosystem models and artificial neural networks, *Ecol. Model.*, 120, pp. 199–211.

Bowie, G. L. et al. 1985. *Rates, Constants and Kinetics Formulations in Surface Water Quality Modeling*. Athens, Ga., US Environmental Protection Agency. (EPA/600/3-85/040.)

Bowles, D. S. and Grenney, W. J. 1978. Steady state river quality modeling by sequential extended Kalman filters. *Water Resour. Res.*, 14, pp. 84–96.

Broom, M. J. and Ng, A. K. M. 1995. Water quality in Hong Kong and the influence of the Pearl River. *Coastal Infrastructure Development in Hong Kong, Proc. Symp. on Hydraulics of Hong Kong Waters*, November 1995, pp. 193–213.

Cerco, C. F. and Cole, T. 1993. Three-dimensional eutrophication model of Chesapeake Bay. *ASCE J. Environ. Eng.*, 119, pp. 1006–25.

Chan, B. S. S. and Hodgkiss, I. J. 1987. Phytoplankton productivity in Tolo Harbour. *Asian Mar. Biol.*, 4, pp. 79–90.

Chen, Q. and Mynett, A. E. 2003. Integration of data mining techniques and heuristic knowledge in fuzzy logic modelling of eutrophication in Taihu Lake. *Ecol. Model.*, 162, pp. 55–67.

Choi, K. W. 2002. Environmental management of mariculture in Hong Kong. Ph.D. thesis, University of Hong Kong.

Choi, K. W. and Lee, J. H. W. 2004. Numerical determination of flushing time for stratified water bodies. *J. Mar. Syst.*, 50, pp. 263–281.

Choi, K. W., Lee, J. H. W. and Wong, K. T. M. 2003. Field verification of diffusion-induced circulation in Sok Kwu Wan, Hong Kong. *Proc. International Conference on Estuaries and Coasts*, Hangzhou, 9–11 November 2003, pp. 663–70.

Dickman, M. D. 1998. Hong Kong's worst red tide. In: J. H. W. Lee et al., (eds), *Proc. International Symposium on Environmental Hydraulics*. Beijing, Balkema, pp. 641–45.

Di Toro, D. M. and Connolly, J. P. 1980. *Mathematical Models of Water Quality in Large Lakes, Part 2, Lake Erie*. New York, Manhattan College, Bronx.

Eknes, M. and Evensen, G. 2002. An ensemble Kalman filter with a 1-D marine ecosystem model, *J. Mar. Syst.*, 36, pp. 75–100.

Hodgkiss, I. J. and Ho, K. C. 1991. Red tides in sub-tropical waters: an overview of their occurrence. *Asian Mar. Biol.*, 8, pp. 5–23.

Kremer, J. N. and Nixon, S. W. 1978. *A Coastal Marine Ecosystem.* New York, Springer-Verlag.

Lee, H. S. and Lee, J. H. W. 1995. Continuous monitoring of short term dissolved oxygen and algal dynamic. *Water Res.*, 29, pp. 2789–96.

Lee, J. H. W. and Arega, F. 1999. Eutrophication dynamics of Tolo Harbour, Hong Kong. *Mar. Pollut. Bull.*, 39(1–12), pp. 187–92.

Lee, J. H. W., Choi, K. W. and Arega, F. 2003. Environmental management of marine fish culture in Hong Kong, *Mar. Pollut. Bull.*, 47(1–6), pp. 202–10.

Lee, J. H. W., Fernando, T. M. K. G. and Wong, K. T. M. 2004. Real-time prediction of coastal algal blooms using artificial neural networks. *Proc. 6th International Conference on Hydroinformatics*, Vol. 1, 21–24 June 2004, Singapore. Singapore, World Scientific Publishing Company, pp. 1465–72.

Lee, J. H. W., Huang, Y., Dickman, M. D. and Jayawardena, A. W. 2003. Neural network modelling of coastal algal blooms. *Ecol. Model.*, 159, pp. 179–201.

Lee, J. H. W. and Qu, B. 2004. Hydrodynamic tracking of the massive spring 1998 red tide in Hong Kong. *ASCE J. Environ. Eng.*, 130(5), pp. 535–50.

Lee, J. H. W. and Wong, P. P. S. 1997. A water quality model for mariculture management. *ASCE J. Environ. Eng.*, 123, pp. 1136–41.

Lee, J. H. W., Hoojkiss I. J., Wong, K. T. M. and Lam I. H. Y. 2005. Realtime observations of coastal algal blooms by an early warning system. *Estuarin. Coast. Shelf Sci.*, 65, pp. 172–90.

Lee, J. H. W., Wu, R. S. S. and Cheung, Y. K. 1991*a*. Forecasting of dissolved oxygen in marine fish culture zone. *ASCE J. Environ. Eng.*, 117(6), pp. 816–33.

Lee, J. H. W., Wu, R. S. S., Cheung, Y. K. and Wong, P. P. S. 1991*b*. Dissolved oxygen variations in marine fish culture zone. *ASCE J. Environ. Eng.*, 117(6), pp. 799–815.

Lee, J. H. W., Yung, K. S. and Wong, P. S. S. 1993. Sediment oxygen demand and algal dynamics. *Proc. International Conference on Hydroscience and Engineering*, 1993, Washington DC, 1A, pp. 309–16.

Lek, S. and Guegan, J. F. 1999. Artificial neural networks as a tool in ecological modelling, an introduction. *Ecol. Model.*, 120, pp. 65–73.

Li, H. E., Lee, J. H. W., Koenig, A. and Jayawardena, A. W. 2005. Nutrient load estimation of nonpoint source pollution for Hong Kong region. *Water Science. Tech.,* 51(3/4), pp. 209–16.

Lung, W. S. 1993. *Water Quality Modeling: Application to Estuaries*. Boca Raton, Fl., CRC Press.

Parsons, T. R., Takahashi, M. and Hargrave, B. 1984. *Biological Oceanographic Processes*. Oxford, UK, Pergamon Press.

Pastres, R., Ciavatta, S. and Solidoro, C. 2003. The Extended Kalman Filter (EKF) as a tool for the assimilation of high frequency water quality data. *Ecol. Model.*, 170(2/3), pp. 227–35.

Scavia, D., Powers, W. F. and Canale, R. P. 1981. Comparison of first-order error analysis and Monte-Carlo simulation in time-dependent lake eutrophications, *Water Resour. Res.*, 17(4), pp. 1051–59.

Thomann, R. V. and Mueller, J. A. 1987. *Principles of Surface Water Quality Modeling and Control*. New York, Harper and Row.

Wear, R. G., Thompson, G. B. and Stirling, H. P. 1984. Hydrography, nutrients, and plankton in Tolo Harbour, Hong Kong. *Asian Mar. Biol.*, 1, pp. 59–75.

Whitehead, P. G. and Hornberger, G. M. 1984. Modelling algal behaviour in the River Thames. *Water Res.*, 18, pp. 945–53.

Wong, K. T. M. 2004. Red tides and algal blooms in subtropical Hong Kong waters: field observation and Lagrangian modelling. Ph.D. thesis, University of Hong Kong.

Wong, K. T. M. and Lee, J. H. W. 2003. A novel Lagrangian particle method for advective diffusion transport problems. *Proc. 16th ASCE Engineering Mechanics Conference*, 16–18 July 2003, Seattle, University of Washington. (CD–ROM.)

Yabunaka, K., Hosomi, M. and Murakami, A. 1997. Novel application of a back-propagation artificial neural network model formulated to predict algal bloom. *Water Sci. Tech.*, 36, pp. 89–97.

Yang, Z. B., Takayama, H., Matsuoka, K. and Hodgkiss, I. J. 2000. *Karenia digitata* sp. no., a new harmful algal bloom species from the coastal waters of west Japan and Hong Kong. *Phycologia*, 39(6), pp. 463–70.

19

Integration of ocean-colour remote sensing with coastal nowcast/forecast simulations of harmful algal blooms

W. P. Bissett, R. Arnone, S. DeBra, D. Dye, G. Kirkpatrick, C. Mobley and O. M. Schofield

19.1 Introduction

Forecasting harmful algal blooms is one example of the larger effort to predict community phytoplankton populations in marine environment. Early modelling efforts attempted to mathematically solve the growth and loss of phytoplankton (also known in today's literature as sources and sinks) in a fairly straightforward method (see Mills, 1989; Riley, 1946):

$$\frac{dP}{dt} = P(Ph - R - G) \tag{19.1}$$

where the time-dependent change in phytoplankton populations P is equal to the initial phytoplankton population multiplied by the net of the terms for the phytoplankton specific growth rate Ph, minus respiration R and grazing rate G. This equation is the basis of all phytoplankton models and 60 years after its authorship is still used with minor modifications (c.f. McGillicuddy et al., 2007 – Chapter 16 this volume).

Equation (19.1) illustrates the basic concept in ocean ecological modelling. This concept simply states the concentration of a phytoplankton at a given point in time is dependent on its growth rate, its respiration rate and its loss (grazing) rate. The application of this conceptual model becomes more complicated in practice. The concentration of phytoplankton at a given point in time and space is a function of a fully three-dimensional environment where phytoplankton cells may move via sinking or swimming, while also being moved by the circulation of water (Franks, 2007 – Chapter 15 this volume). In addition, the movement of the phytoplankton coupled with the movement of water alters the light and nutrient niches in which the phytoplankton are living, thereby providing ecological feedbacks that impact the net accumulation of phytoplankton biomass (Bissett et al., 2001). While (19.1) offers the foundation, the nuances as to how and why specific phytoplankton taxa accumulate are more complicated and require a more thorough description. For over 100 years, researchers have attempted to acquire this greater ecological knowledge of phytoplankton processes by conducting both laboratory and field experiments. These experiments have led to better quantification of the factors controlling the light and nutrient assimilation dynamics of phytoplankton, and in turn have led to more complex parameterization of (19.1) (e.g. Andersen and Nival, 1988; Anderson, 1993; Anderson and Williams, 1998,

1999; Antoine and Morel, 1995*a*, 1995*b*; 1996; Armstrong, 1994; Armstrong et al., 2001; Bissett et al., 1994, 1999*a*, 1999*b*; Christian et al., 2001*a*, 2001*b*; Cloern et al., 1995; Collins, 1980; Cullen, 1990; Cullen et al., 1993; Davidson and Cunningham, 1996; Davis et al., 1978; Denman, 2003; Doney et al., 1996; Ebenhoh, 1988; Elliott et al., 2001; Fasham et al., 1990, 1993; Feuillade and Feuillade, 1993; Franks, 1997; Fulton et al., 2003; Garcia-Pichel, 1994; Geider et al., 1996, 1998; Geider and Platt, 1986; Gregg, 2001; Gregg and Walsh, 1992; Haney and Jackson, 1996; Hood et al., 2001; Hurtt and Armstrong, 1996, 1999; Ishizaka, 1990; Kamykowski, 1979, 1981; Kishi and Ikeda, 1986; Lancelot et al., 1991; Laws and Chalup, 1990; Lawson et al., 1996; Litchman et al., 2003; Liu et al., 2001; McGillicuddy et al., 1995; Moisan, 1994; Moisan and Hofmann, 1996; Moisan and Mitchell, 1998; Moore et al., 2001; Neale and Marra, 1985; Neale and Richerson, 1987; Pahlow, 2005; Penta, 2000; Penta and Walsh, 1995; Prunet et al., 1996*a*, 1996*b*; Smayda and Reynolds, 2001; Taylor et al., 1991; Thomas et al., 1990; Tyrrell and Taylor, 1996; Walsh et al., 1989, 1999, 2003; Wroblewski, 1977; Wroblewski et al., 1988; Yamaguchi et al., 2001; Yamamoto et al., 2002; Yamazaki and Kamykowski, 2000; Zonneveld, 1998; Zonneveld et al., 1997). The increase in complexity was, in part, to help describe the ever-expanding relationships being described in the observational community. The complexity was also embraced because of an increasing amount of research that found improved stability with increasing complexity, that is increasing species, diversity, functional groups and interaction strength (the likelihood that one species will consume another) (Fussmann and Heber, 2002; McCann and Hasting, 1998; Naeem and Li, 1997; Naeem et al., 1994; Tilman et al., 2001). This helped to overcome some of the problems associated with numerical instabilities in simple ecological models (May, 1973*a*).

HAB forecasting is especially difficult since one is trying to predict the ecology of a single phytoplankton population within a much larger community of phytoplankton species (estimated to number over 30,000: Falkowski and Raven, 1997). The traditional nutrient-phytoplankton-zooplankton (NPZ) model (or its extension nutrient-phytoplankton-zooplankton-detritus, NPZD) focused on population assemblages as a whole, using the N term as the model currency, and converting phytoplankton biomass into an easily measured proxy for biomass, namely chlorophyll, for validation. This approach is useful for describing general ocean systems, but HAB forecasting requires an understanding and quantification of the competitive interactions within phytoplankton populations, such that a single phytoplankton taxa may be quantitatively described. Thus, the numerical model that one selects for the purpose of predicting a HAB must have the flexibility to effect differential growth and loss rates across many simulated phytoplankton species, so that under the 'right' environmental conditions the HAB population is adequately simulated (e.g. Yamamoto et al., 2002).

Over the last few years, optics has found a place at the intersection of numerical phytoplankton studies and HAB research. Ocean optics offers a means to sample both the bulk properties of the water column over large temporal and spatial ranges, as well as the individual properties of phytoplankton populations down to the cell (see Chang and Dickey, 2007; Lewis, 2007; Morel, 2007; Sosik, 2007; Babin, 2007; Schofield et al., 2007 – Chapters 2, 6, 4, 8, 7 and 3 this volume). It also offers the ability to quantify a niche dimension for phytoplankton simulations by virtue of describing the intensity and colour of the ambient light field as one moves deeper in the water column. This numerical description of changing spectral quality and magnitude provides an optical niche dimension by which phytoplankton may differentiate themselves against competitors in different environments depending on the optically active constituents in the water. For

example, if there are large concentrations of optical constituents, that is phytoplankton and coloured degradational matter (CDM), typical of eutrophic coastal environments, the photon density will decrease very rapidly with depth and will transition from green to yellow in its spectral distribution. In the Sargasso Sea, where the water is oligotrophic with little phytoplankton biomass or CDM, the photon density decreases more slowly with depth and becomes blue-green in spectral distribution. The resulting light field (and nutrient regime) will select for those phytoplankton that can best use the resources, that is in the deep Sargasso Sea one may find small *Prochlorococcus* spp. rich in chlorophyll *b* that are ideally suited to absorb the low photon densities of blue-green light. Simulating the time-dependent change in the ambient light field along with the time-dependent change of optical constituent concentrations provide a quantifiable means of imparting feedback mechanisms into numerical simulations (Bissett et al., 2001), which can be validated from aircraft and space-based remote sensing, as well as with *in situ* measurements (e.g. Bissett et al., 1999*a*). Thus, by integrating the prediction of optics into nowcast/forecast systems that seek to predict HABs, HAB forecasting may be directly merged with remote sensing HAB identification techniques (e.g. Stumpf et al., 2003).

The simulation of water column optical properties requires additional complexity in the formulation of an ecological model's structure and parameterization. The model must specifically address and quantify those properties that do not change with respect to the geometry of the light field, the inherent optical properties (IOPs), and those that are dependent on the directionality of the photon density, the apparent optical properties (AOPs, see Morel, 2007 – Chapter 4 this volume). IOPs, such as absorption and scattering, are directly related to individual phytoplankton taxa, as well as to other optical constituents, such as CDM and sediments. AOPs, which include remote sensing reflectance R_{rs}, and the diffuse attenuation coefficient K_d, are dependent on the IOPs and the radiance distribution (i.e. geometry) of the downwelling light field. Since the IOPs and the AOPs are interrelated, sampling the AOPs from space or aircraft allows for the estimation of IOPs via empirical or analytical inversion techniques. From the estimation of IOPs, one may estimate the various properties of the phytoplankton assemblage, such as total pigment (e.g. Gordon et al., 1983) and/or carbon biomass and productivity (e.g. Behrenfeld et al., 2005), through empirical or analytical algorithms that relate reflected ocean colour to the phytoplankton properties. It may also be possible to use the spectral characteristics of phytoplankton specific IOPs, which are directly related to phytoplankton taxa, and thereby separate the bulk property signals into specific taxa stocks (Kirkpatrick et al., 2000; Millie et al., 1995; Millie et al., 1997; Roesler et al., 2003). All these optical inversion techniques are part of active research programmes, and as such are not without errors. The successful application of these optical techniques would provide critical HAB stock assessment for model initialization, as well as model validation, which might then allow for the ability to assimilate and predict the occurrence of HABs within a nowcast/forecast system.[90]

The use of a simplified approach to the parameterizing of the terms of (19.1) may be constructive in qualitatively describing the interaction of light and nutrients in aquatic systems. The use of optics as a means to provide additional niche spaces by

[90] It should be explicitly acknowledged that this application of coupling optics to HAB population density would most probably apply to those HAB populations that produce a high enough optical signal to be remotely sensed. An example of these populations would include those on the West Florida shelf (Stumpf et al., 2003). However, in areas where the HAB density is too low to alter the optical signal from the background noise, this hypothesized approach would not be (as) successful. An example of this type of HAB would include *Alexandrium* in the Gulf of Maine (Cullen, 2007 – Chapter 1 this volume).

which to effect phytoplankton competition, as well as provide addition mechanisms to initialize and validate HAB forecasts, requires an increase in the complexity of the nowcast/forecast system beyond those earlier modelling efforts. In deriving new models to predict specific HABs, one must find balance between the requirements for quantitative prediction and qualitative understanding in constructing the numerical model format, where quantitative results such as cell numbers of harmful phytoplankton taxa or physical units of $R_{rs}(\lambda)$ may be separated from less robust measures of phytoplankton biomass, namely chlorophyll. In this balancing process, one may find it impossible and/or unnecessary to simulate the entire suite of phytoplankton in a particular region in order to generate a reasonable forecast of local HABs. For example, one may reduce the full assemblage of phytoplankton to a representative few functional groups with similar optical, nutrient uptake, and allometric characteristics (e.g. Bissett et al., 1994, 1999*b*) in order to address the ecological question at hand. Since there has been (at the date of this report) no generalized solution for phytoplankton or HAB prediction,[91] the degree of model complexity will be user, problem and site specific. In the model-selection process, care must be taken to avoid numerical transient problems (e.g. limit cycles) associated with numerical models (e.g. May, 1971, 1973*a*, 1973*b*), which are often driven by simplified equations and unrealistic physical conditions used to describe complex environmental and ecological interactions. Thus, it is important in the model construction process to match complexity and structure to the scientific question being asked, thereby arriving at an 'appropriate' model formulation. An appropriate model is defined here as one that can address the ecological question at hand, whose parameters are as constrained as possible from field and laboratory data, thereby limiting parameter tuning to a minimum. In addition, an appropriate model would offer the potential for quantitative prediction and validation.

The component most frequently unconstrained in (19.1) is the loss or grazing term *G*. This term is frequently the 'closure' term of phytoplankton numerical models (see Steele and Henderson, 1992). The closure term is the parameter, which when tuned is likely to cause the generation of simulation results that are the most acceptable during the model evaluation process. The loss term is frequently based on estimates of grazer populations, viral and bacterial phages and/or mass dependent sinking fluxes as a function of phytoplankton biomass concentration. The weak constraint on this component is in part a result of the difficulties in sampling grazer populations and their clearance rates, as well as other relatively undefined loss processes, such as mass dependent viral and bacterial phage transmission, and/or apoptosis. When the model structure for (19.1) is expanded to explicitly include herbivore zooplankton, this closure problem is expanded to include those difficulties surrounding higher trophic levels and may cause a geometric expansion of the unconstrained parameters. In contrast to the loss processes, the phytoplankton nutrient uptake rates, assimilation rates, pigment concentrations, and growth rates are more easily measured in the laboratory. Thus, there are often detailed formulations of the growth component of (19.1), while the loss component is more often parameterized with a more simplified equation that may be easily modified as a function of temperature and seasonality. Unfortunately, any closure method is fraught with validation difficulties, and what may be a reasonable simulation in one time/space location, may yield very spurious results in another location.

As mentioned above, the circulation of the water plays an important role in the production and accumulation of any phytoplankton population, including HABs. In

[91] Given the diversity of HABs, there may never be a 'generalized' numerical solution (Cullen, Chapter 1).

numerical simulations, this is frequently the largest source of error in the validation of numerical predictions and forecasts. Some ecological simulation techniques are more sensitive than others but all require that the advection and diffusion equations place the right parcel of water in the right place at the right time. Without adequately resolving the physics, it is very difficult to generate realistic simulations of HABs; and while it may be possible to numerically simulate a HAB, the likelihood of it being a valid forecast is often limited because the simulated environmental conditions did not match the actual environmental conditions. Forecasting a tornado in a sun shower is not a realistic result and woe betide the modeller who attempts to explain the errors in a HAB simulation as the result of growth and loss dynamics, when the real culprit may be a poorly constrained physical model. However, a perfect physical model does not currently exist and the exploration of ecological dynamics should proceed even in light of the imperfections in the physical modelling effort. In some cases, the errors in the physical model may not create a qualitative, or even drastic quantitative, error in the overall ecological solution. In evaluating the ecological result, one must attempt to separate the physical errors from the biological, optical, and chemical ones, in order to achieve some level of system understanding into causal ecological dynamics.[92]

In order to demonstrate a representative ecological and optical simulation of phytoplankton populations, including the HAB species *Karenia brevis* (*K. brevis)*, the results of the phytoplankton dynamics of a numerical study of the West Florida Shelf (WFS) will be described. It is based on a two-dimensional simulation used to predict IOPs and CDM distributions on the WFS during summer/autumn 1998 (a complete description of the model may be found in Bissett et al., 2005). In the precursory study by Bissett et al., it was determined that the addition of a terrestrial boundary condition was required to reasonably simulate the IOPs and CDM distributions over this period. To be shown here are the impacts of these terrestrial boundary conditions, rich in colour and nutrients, on the phytoplankton functional groups, including *K. brevis*, as well as the impacts on the water-leaving radiance signal that may be seen by satellite. In addition, a sensitivity study to the closure term in the model will demonstrate the impact of this parameter on the individual phytoplankton functional groups, as well as the bulk optical properties and remote sensing reflectance.

Our goal is to describe a set of ecological and biogeochemical interaction equations that allow for the differentiation and competition of algal classes based on temperature, light and nutrients. This model is derived for the coastal zone and as such includes terrestrial boundary conditions in a consistent manner that preserves its numerical stability while providing results that are directly comparable to the available validation data streams. The work described here goes hand in hand with a previous paper that describes a set of ecological interaction equations incorporating optics as a fundamental component of its structure (Bissett et al., 2005). The focus of this modelling effort is to specifically avoid reductionism, which would provide only a minimal set of interaction equations to describe this specific site and data set. The goal of this larger effort is to apply a broad set of ecological equations to multiple environments with minimal parameter tuning, such that its application may be robust across multiple

[92] While some may read this as an indictment of the physical model, such is not the case. It is meant solely to recognize that the formulation and validation of ecological models, which are critically dependent on the physical circulation models, need to progress along with the physical model development. The ecological models tend to be far less developed for a wide variety of reasons, not least of which is that there are no 'fundamental' ecological equations similar to the hydrostatic approximation equations with which to build the ecological formulations and structure.

ecotones (transitional zones between two communities containing the characteristic species of each). This approach would allow for a single ecological model to be used for multiple coastal regimes within the same simulation experiment.

19.2 Methods

The model used here tracks the time-dependent change of 89 state variables which include seven functional groups of phytoplankton, two classes of dissolved organic matter, two classes of coloured degradational organic matter (also known as CDOM or CDM), two classes of faecal material, one heterotrophic class of bacteria (as well as an inferred nitrification class of bacteria), and six inorganic nutrient stocks, including carbon, nitrate, ammonium, silica, phosphorus and iron (Bissett et al., 2005). It is a coastal expansion of an open ocean simulation, which separated carbon and nitrogen dynamics to more accurate account for carbon cycling in the Sargasso Sea (Bissett et al., 1999*a*, 1999*b*). The model uses non-stoichiometric nutrient uptake, assimilation and regeneration, which allows for niche separation based on nutrient type and quantity. The photosynthetic properties of the phytoplankton functional groups are described with individual pigment suites, which are allowed to vary as a function of light and nutrient history. This allows for niche separation as a function of spectral photon density. All optically active constituents are described with absorption and scattering equations to drive a spectral light model that attenuates light with depth at 5 nm spectral resolution. The physics are supplied by a two-dimensional spatial (offshore and depth) circulation model driven by winds and boundary conditions on the WFS during 1998. The resulting depth-dependent IOPs are supplied to a fast radiative transfer model, Ecolight, which is a derivative of the Hydrolight model to yield the prediction of water-leaving radiance. The simulation was run for three numerical years with the exact same forcing to reduce numerical transient responses to the boundary conditions, such that year-over-year changes in the stocks were less than 0.5%. The full numerical description of the model may be found in Bissett et al. (2005).

19.2.1 Shoreward boundary conditions

The shoreward and offshore boundary conditions were unchanged from those previously described by Bissett et al. (2004, 2005). Nutrient data for the Charlotte Harbor region was collected from seven sources. These nutrients constituted the shoreward boundary condition. Organic nitrogen was found to be a major contributor to total nitrogen concentrations in this region and inorganic phosphorus was also a key nutrient due to the proximity of this location to the Hawthorne Phosphatic Formation. Discharges from the local rivers (the Peace River and the Caloosahatchee River) coincided with peaks in nutrient concentrations in 1998 (Figure 19.1). The shoreward boundary conditions were simulated by an increase in nutrients and total colour concentrations at the shoreward boundary model cell reproducing a riverine flux for day-of-year (DOY) 267 (24 September) and 309 (5 November). This is possibly a conservative estimate of the ecologically significant mass additions to the shelf during these periods, as the outflow events driving the decreases in salinity would have occurred over the course of several days (or possibly weeks). An accompanying freshwater flux and change in buoyancy was not simulated due to the two-dimensional nature of this model, and the physical constraints made it impractical to hydrologically model the freshwater mass. It is clear that the baroclinic flows would be altered by these events; however, it is

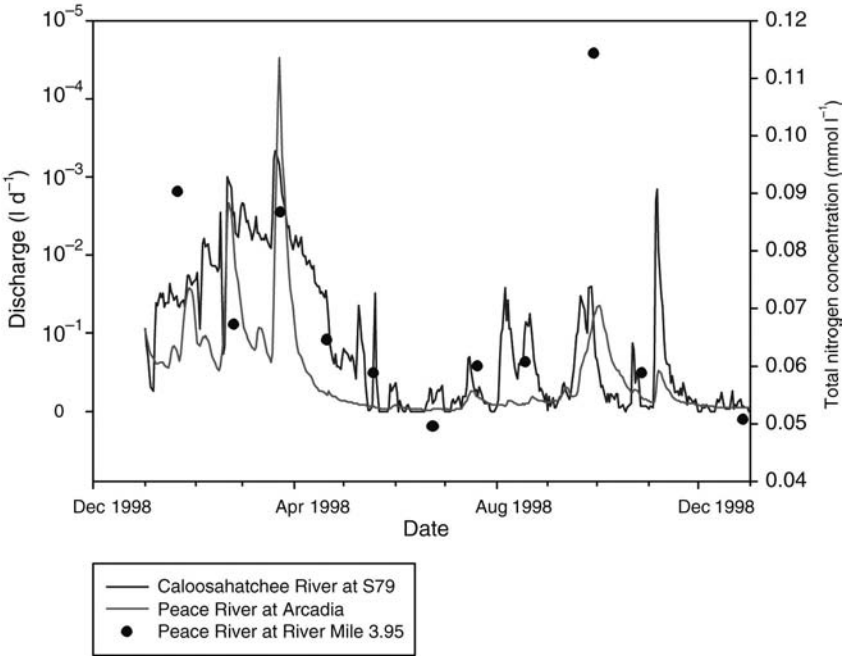

Figure 19.1
Total daily discharge from the Peace River measured at the USGS station 'Peace River at Arcadia' (light grey line) displaying elevated discharges in early and late 1998 with corresponding elevated concentrations of total nitrogen (TN) measured at the USGS station 'Peace River at River Mile 3.95' near Punta Gorda, Florida (black circles) along with total daily discharge from the Caloosahatchee River at the Franklin Lock and Dam (S79) (dark grey line).

beyond the scope of this effort to predict those impacts. The gulf-side boundary conditions changed seasonally and were derived from the 1998/1999 ECOHAB cruises on the WFS (Figure A.1, Bissett et al., 2005).

19.2.2 Optical model

Light harvesting by phytoplankton is assumed to be a function of the available downwelling energy at depth and the absorption spectra of each phytoplankton functional group. The absorption spectra of each functional group are not static, but rather are dependent on the light and nutrient history of each functional group at each grid point. This allows for the differentiation of phytoplankton by pigment suites and spectral photosynthetic efficiencies, providing competitive advantages to those species that can optimize light absorption and photochemical conversion at different depths and colour zones. In this model, an explicitly defined suite of IOPs was developed for each optical constituent in the model, that is. phytoplankton, CDOM, detritus, and others. Time-dependent changes in these mass constituents drove the associated modifications in the coupled IOPs. The IOPs were then used to calculate

the Apparent Optical Properties (AOPs) of downwelling irradiance, $E_d(\lambda)$, with a numerically efficient single scattering approximation (Bissett et al., 1999*a*). This allows us to validate the biogeochemical simulation with *in situ* IOP and AOP instruments, as well as spectral remote sensing products from multispectral or hyperspectral satellite and aerial sensors when these simulated IOPs are used in conjunction with a robust radiative transfer model, namely Hydrolight (see Bissett et al., 2005, for a full description).

19.2.3 SeaWiFS processing and analysis

SeaWiFS processing and analysis was previously described by Bissett et al. (2005). Raw SeaWiFS processing was performed at the Naval Research Laboratory Stennis, Mississippi, by the Ocean Sciences Branch, Code 7330. This processing included an iterative atmospheric correction scheme that reduced the errors found in the standard SeaDAS processing for near-shore coastal waters. The region of interest on the WFS originated at the 10 m isobath and extended approximately 60 km offshore. Since the offshore islands of the region were shoreward of the 10 m isobath, they were not accounted for in this simulation. The boundary of the region was designated by the coordinates [(27.2957N, 83.3415W), (27.5396N, 82.7993W), (26.2062N, 82.7200W), (26.4502N, 82.1830W)] (Bissett et al., 2005, Figure A.1). Lines of data were resampled at 30 equally spaced intervals between these points using the SeaWiFS Data Analysis System (SeaDAS) and then splined to 1 km increments perpendicular to the coast. This was required to normalize the data pixelization that occurs as a function of SeaWiFS scan angle and SeaDAS projection angle relative to the coast of the WFS. The mean of these 30 lines (numbered from Tampa Bay south to Charlotte Harbor) and the mean plus and minus one standard deviation were then plotted. The mean of lines 22–30 (near Charlotte Harbor) were also plotted since this location is the focus of the study.

19.2.4 Ecolight

The radiative transfer solution to produce simulated remote sensing reflectance (R_{rs}) at the surface of the water was given by a model derived from Hydrolight. Ecolight reduces the computation requirement of Hydrolight in two major ways. The first is by band averaging over azimuthal angles, eliminating the azimuthal dependence terms of the radiative transfer equation (RTE), and eliminating the Fourier decomposition of the radiance or the RTE. The second is an estimate of the maximum relevant depth to the radiometric quantity of interest and is made prior the calculation of the RTE. This allows for the selection of an optical depth for which to solve, and an estimate of the geometric depth with which to solve to. These simplifications allow the full RTE to be calculated for upwelling light based on the simulated IOPs in a computationally efficient manner, that is Ecolight is orders of magnitude faster than Hydrolight, without loss of accuracy in the upwelling and downwelling estimates of photon densities.[93] This allows for the direct validation of predicted photon densities to remote sensing data. The greatest benefit of ecological modelling is that the upwelling light field contains all the optical information on the vertical structure of the IOPs. Accurate simulation

[93] There are ways to optimize Ecolight for more speed, but such further optimization results in loss of accuracy.

of remote sensing reflectance would suggest validation of the vertical structure of the IOPs may be possible,[94] not just the depth-integrated IOPs that are typically found with inversion algorithms.

19.2.5 Nutrient and chlorophyll samples

Nutrient and chlorophyll data were collected for the West Florida Shelf in November 1998 from the ECOHAB Process Cruise and the MOTE Marine Laboratory Cruise. Whole water samples were filtered onto GF/F glass-fibre filter pads and stored on liquid nitrogen until extraction. The extraction of pigments was performed using a 98%:2% methanol: ammonium acetate solution. HPLC was performed on the extracts collected 16–19 November 1998 by MOTE Marine Laboratory. MOTE Marine Lab. then subjected these samples to chemical taxonomy (Chemtax) evaluation (Wright et al., 1991) to calculate the contribution of a given algal class to the total chlorophyll *a* concentration. This programme uses a steepest descent algorithm to find the best fit of algal class based on an initial presumption of pigment ratios for the predetermined classes. The Chemtax algal classes were designated as one of the following algal classes: dinoflagellates, diatoms, cyanobacteria, chlorophytes, cryptophytes (commonly found in low-salinity waters) or *K. brevis*.

This study focuses on Charlotte Harbor, Florida, so the data were limited to the lower Charlotte Harbor region with the northernmost latitude being 26.688N and the southernmost latitude being 26.333N (Figure 19.2). Data were also limited to the westernmost longitude of 82.463W. The eastern boundary of the simulation is the 10 m isobath. Samples collected shoreward of this boundary were considered equivalent to the near-shore boundary of the simulation. All zero values in the data were converted to 1×10^{-9} to avoid complications of division by zero. Chlorophyll concentrations less than 1×10^{-4} μg l^{-1} were deemed below the detectable limit of 1,000 cells l^{-1} and these values were essentially considered zero. Negative correlations were found between salinity and chlorophyll *a* concentrations as well as salinity and nutrient concentrations suggesting riverine outflows as the source. Note, all the Chemtax data are used strictly for validation, not for initialization.

To compare field data collected on the WFS, which is a three-dimensional environment, to a two-dimensional model, the data first had to be corrected for the curvature and ellipsoid nature of the earth. A function written by Gillis and Montes (2001) of the Naval Research Laboratory was used to estimate distance between geographical coordinates. Each station's distance from the 10 m isobath could then be calculated by triangulation from the northernmost and southernmost points of the 10 m isobath line segment. This method is an adequate approximation for our needs since the relationship between bathymetry and distance from shore is nearly linear over most of the EcoHAB:Florida domain.

There are two types of model/data comparisons that we would like to show. The first is the prediction of a tracer, that is total chlorophyll and the second is the phytoplankton ecological structure resulting from a given forcing condition. These comparisons may be difficult if the simulated physical forcing and boundary conditions are not perfectly matched to the actual field conditions (Bissett et al., 2005). In this study,

[94] The retrieval of vertically-dependent IOPs from R_{rs} is the subject of current research by the authors of this chapter.

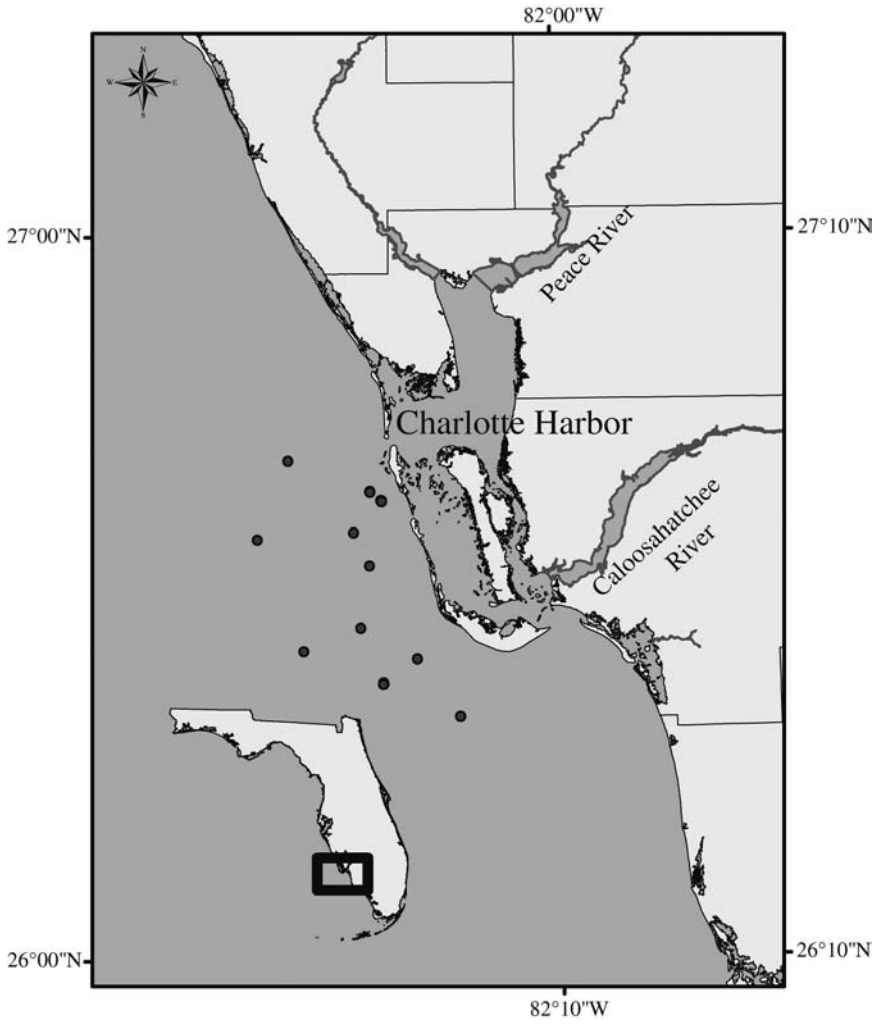

Figure 19.2
Location of stations where whole water samples were collected on filter pads and subjected to Chemtax analysis to determine the contribution of phytoplankton species to total chlorophyll *a* concentrations.

differences in simulated and actual biomass were at times large, mainly resulting from temporal and spatial dislocations of water masses (Bissett et al., 2005). In order to evaluate the ecological structure of the WFS and the simulation, biomass differences in the Chemtax data were removed by dividing the total chlorophyll concentration measured on the shelf by the simulated total chlorophyll concentration. This was then multiplied by the simulated functional group's chlorophyll *a* concentration and was denoted by ECOSIM′ (ES′). This new value was then compared with the Chemtax total chlorophyll *a* concentrations of each algal class. Algal class comparisons of ECOSIM and Chemtax were evaluated according to Table 19.1.

Table 19.1 Comparison of chemtax and ecosim algal classes used for evaluation of the model

Chemtax algal class	ECOSIM algal class
Dinoflagellates	Non-toxic dinoflagellates
Diatoms	Large + small diatoms
Cyanobacteria	*Synechococcus*
Chlorophytes	*Prochlorococcus* 1 + 2
K. brevis	*K. brevis*
Cryptophytes	n/a

19.2.6 Sensitivity of mortality closure

In this model, the loss of phytoplankton biomass is driven by both grazing and lytic losses (which include mass dependent phages and apoptosis) (Steele and Henderson, 1992). The sensitivity of this model is evaluated based on this closure term. The grazing stress is modelled by the following equation such that it is a function of a minimum mortality rate multiplied by the logarithm of the total biomass of a functional group divided by the refuge population (Bissett et al., 2005):

$$g_i = \text{mortality}_i * \text{LOG}\left(\frac{\text{PC}_i}{\text{refuge}_i}\right), \tag{19.2}$$

where the grazing stress on phytoplankton functional group i, is equal to the *mortality* parameter for functional group i (d^{-1}) multiplied by the log of the particulate carbon concentration (PC_i; mol C or mol C l^{-1}) of phytoplankton functional group i divided by the *refuge* population (mol C) of function group i. The refuge population is the concentration of carbon below which there is no grazing or lysis and is set to 0.02 mol C for all species (note, carbon is the base currency in the model, all other phytoplankton mass terms, such as PON or pigments, are functions of the light and nutrient history of the functional group at each time/space location in the model (Bissett, 1997; Bissett et al., 1999*b*, 2004; 2005). This function assumes that the magnitude of biomass concentration is the best indicator of loss stress. The responsiveness of the model to the closure term was investigated by halving and doubling the grazing stress on the various phytoplankton groups as described in Table 19.2.

Table 19.2 The grazing stress (g_i d^{-1}) on each phytoplankton functional group for various model runs

Simulation description	*Prochl*	*Syne*	Large diatoms	Small diatoms	*K. brevis*	Non-toxic dinoflagellates
Full grazing	0.010	0.010	0.010	0.010	0.010	0.010
Half grazing	0.005	0.005	0.005	0.005	0.005	0.005
Double grazing	0.020	0.020	0.020	0.020	0.020	0.020
Mixed grazing	0.010	0.010	0.010	0.010	0.005	0.020

Prochl: *Prochlorococcus* 1 + 2; Syne: *Synechococcus*

19.3 Results

A previous comparison between simulated and satellite-derived optical properties focused on the days where there were good quality SeaWiFS images for the West Florida Shelf. The simulated optical properties have previously been evaluated (Bissett et al., 2005) and the results presented here are used to evaluate the biomass distribution among phytoplankton species as well as the sensitivity of the model to physical forcing, boundary conditions and model closure. The days chosen for this evaluation are 8 June and 8 November. There were very few days during autumn 1998 that provided clear satellite imagery; however, the chosen days provided data of significant ecological and meteorological events that were evident in both the satellite and available *in situ* data. 8 June occurred during a simulated and sampled increase in biomass resulting from a loop current intrusion, which originated in the Panhandle region (Walsh et al., 2003; Weisberg and He, 2003); and 8 November was just after a significant pulse of freshwater from the Peace and Caloosahatchee rivers following the landfall of Tropical Storm Mitch.

19.3.1 8 June (DOY 159)

As we are simulating multiple tracers (89) which correspond to nutrients, pigments, dissolved organic stocks and particulate organic stocks, many of the state variables may be directly compared with *in situ* data measured on the ECOHAB cruise. Differences in the nitrate concentration between simulated and sampled measurement collected on the WFS were greatest 40 km from the 10 m isobath at depth of 25 m (Figure 19.3A). The underestimation of simulated nitrate concentration offshore at depth is not surprising given the fact that these samples were measured in what appeared to be a recorded upwelling/Loop Current Intrusion event and may also be due to inaccuracies in the physical circulation of the model as determined from the related manuscript. Probably correlated with this upwelling event was the underestimation of simulated total chlorophyll concentration at the same offshore station (Figure 19.3B).

Simulated silica was also underestimated near-shore at depths of 5 m and 10 m (Figure 19.4A). This may have been a result of pulse releases from terrestrial sources in April-May that were not simulated in this model (Figure 19.1). In one case, the simulation returned a value where the ECOHAB value was essentially zero. Inorganic phosphate concentrations were negligible offshore compared with near-shore concentrations (data not shown). Unfortunately, data revealing the phytoplankton composition on the WFS in June was not available for analysis. There was a large simulated intrusion event, which had similar nutrient and chlorophyll stocks (Figure 19.5A) as the measured event described in Figure 19.3. However, these stocks were located deeper and more offshore than the peaks in the measured data (50 m isobath). The simulated results suggest that the deep offshore waters were dominated by large and small diatoms, followed by *Synechococcus* and prochlorophytes (Figure 19.5A). In a recent publication, the modelled results of a nitrate rich intrusion of slope water on the WFS in June also produced a phytoplankton response, dominated by microflagellates.

Satellite-derived detritus and CDOM absorption (which in total is CDM), total chlorophyll and backscatter (Figures 19.6A, 19.6C, 19.6E respectively) on 8 June 1998 averaged over the entire domain (black line) and the Charlotte Harbor line (blue line) showed slightly elevated near-shore values with a declining gradient offshore. The slight elevation in near-shore values is indicative of a riverine source that was not simulated

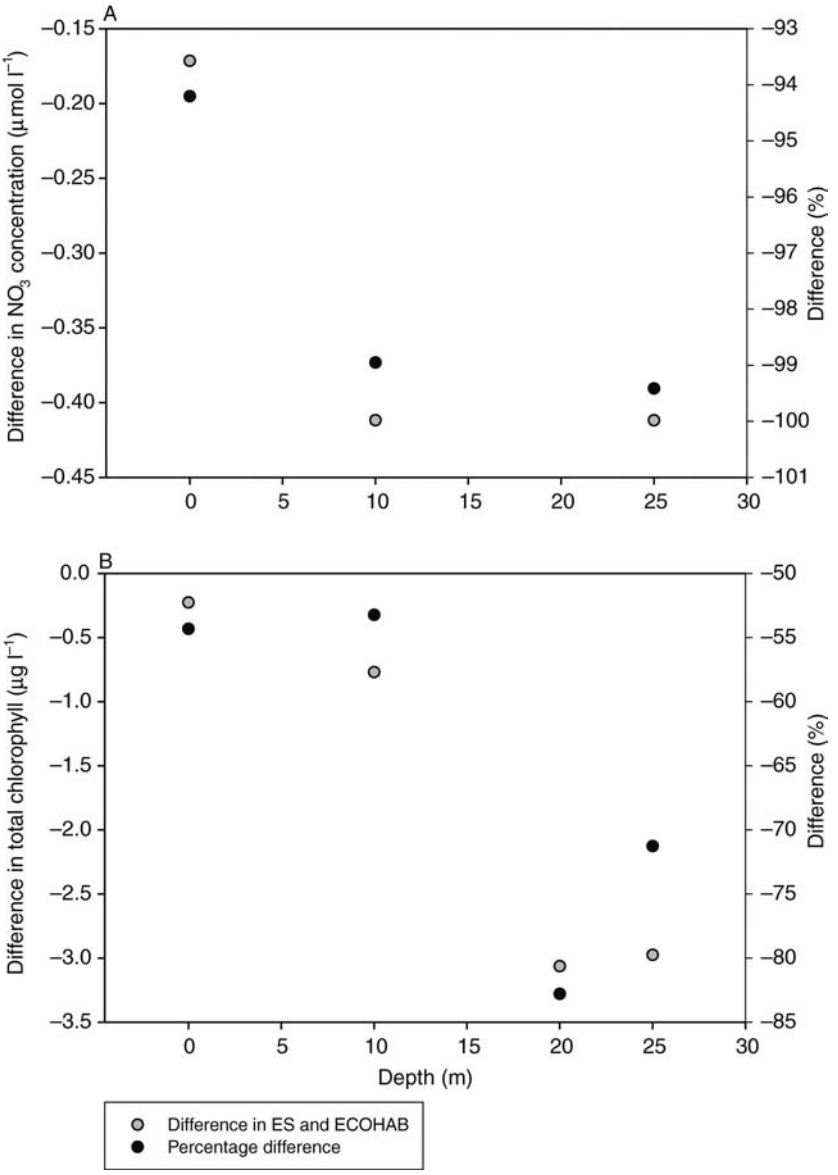

Figure 19.3
Differences and percentage differences in A, nitrate concentrations; B, total chlorophyll concentrations by depth between simulated and sampled values at ECOHAB station 46, located approximately 40 km from the 10 m isobath, in June 1998, displaying an underestimation of nitrate offshore at depth. Negative differences represent an underestimation of chlorophyll *a* by the simulation.
Open circles, difference in ES and ECOHAB; filled circles, percentage difference.

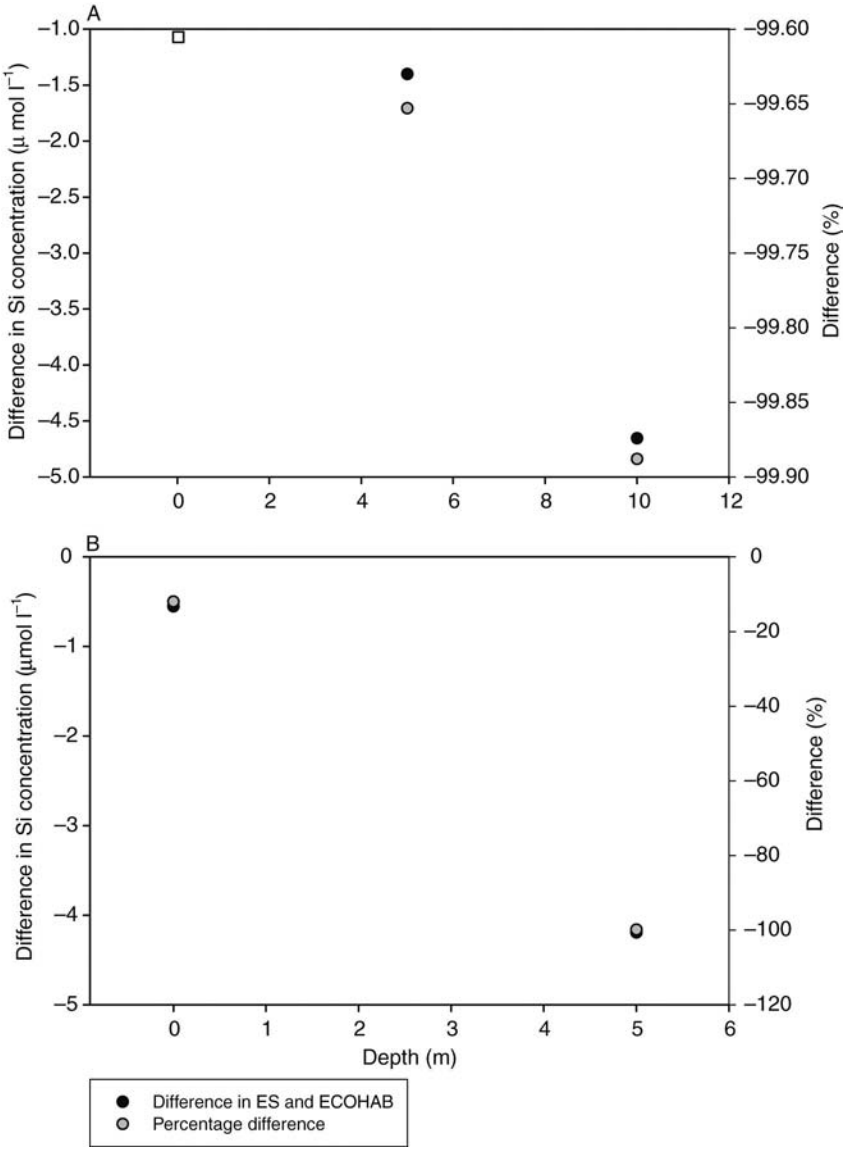

Figure 19.4
A, differences and percentage differences in silica concentrations by depth between simulated and sampled values at ECOHAB station 51, located approximately 6 km from the 10 m isobath in June 1998, displaying an underestimation of silica near-shore (note that in one instance, open square, EcoSim returned a value where the ECOHAB value was effectively zero).
B, differences in silica concentrations by depth between simulated and sampled values at ECOHAB station 51 in November 1998, displaying an underestimation of silica near-shore.

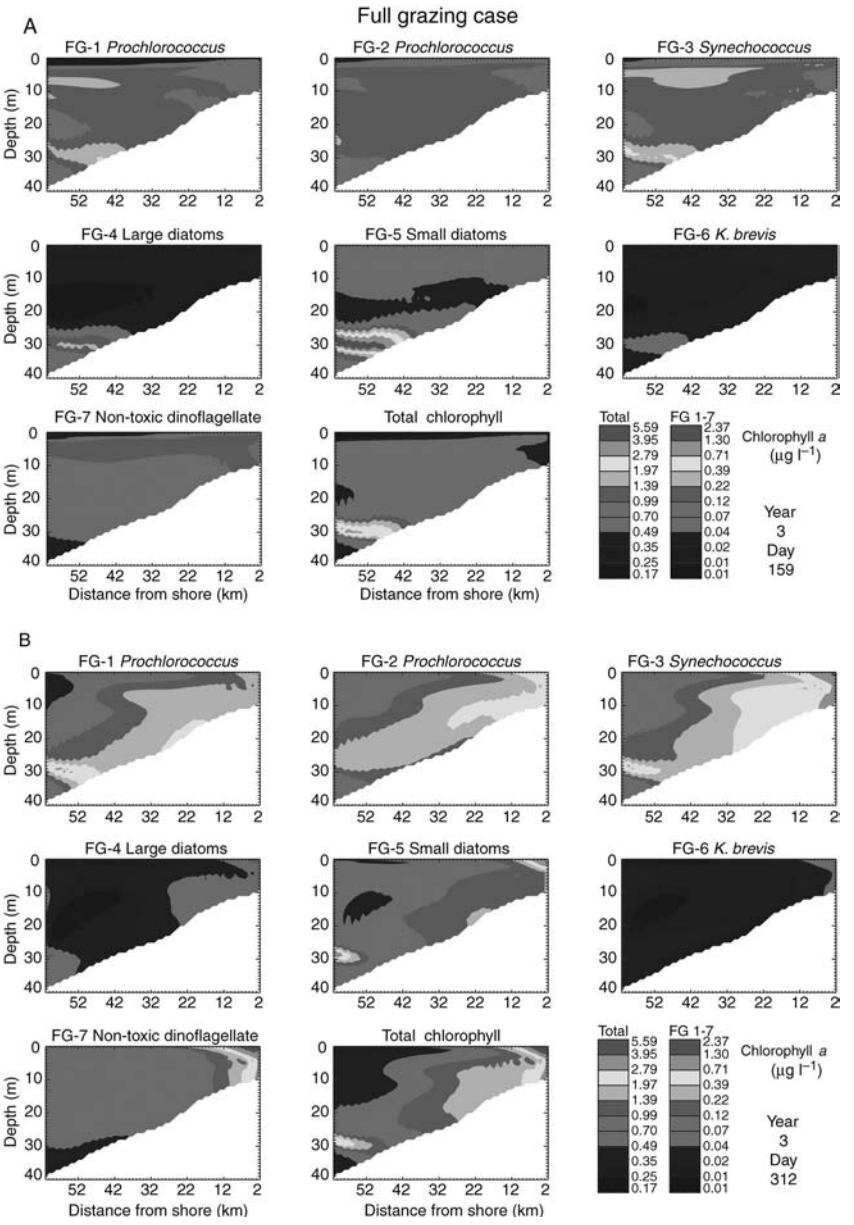

Figure 19.5
A, contour plots of the simulated total chlorophyll *a* concentration attributed to each of the seven phytoplankton species and the sum of all the phytoplankton classes for DOY 159 – 8 June 1998.
B, contour plots of the simulated total chlorophyll *a* concentration attributed to each of the seven phytoplankton species and the sum of all the phytoplankton classes for DOY 312 – 8 November 1998.

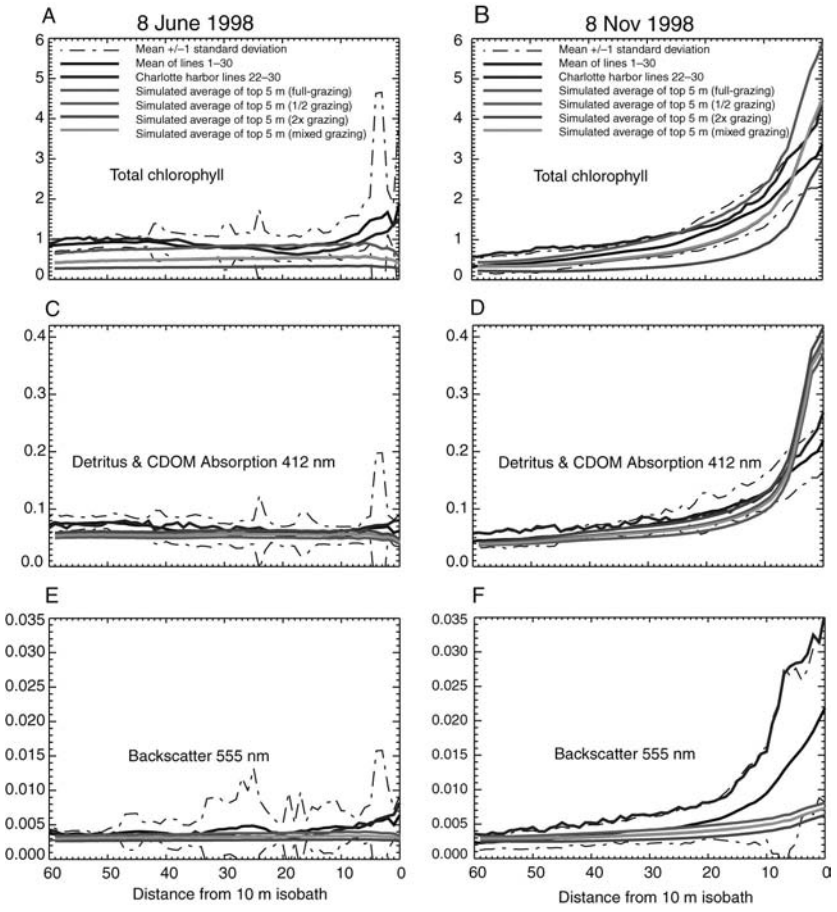

Figure 19.6
Simulated and satellite-derived IOPs on the WFS.
A, total chlorophyll concentration (mg chl m^{-3}) on 8 June 1998, showing the average of the 30 lines transect, ±1 standard deviation of the mean of 30 lines, the mean of lines 22–30 (Charlotte Harbor), simulated absorption 5 m average for the full, half, double and mixed grazing stress runs.
B, total chlorophyll concentration (mg chl m^{-3}) on 8 November 1998 for the WFS.
C, detritus and CDOM absorption [aCDM 412 nm (m^{-1})] on 8 June 1998.
D, detritus and CDOM absorption [aCDM 412 nm (m^{-1})] on 8 November 1998.
E, backscatter (m^{-1}) on the WFS on 8 June 1998.
F, backscatter (m^{-1}) on the WFS on 8 November 1998.

(Bissett et al., 2005). Satellite estimated R_{rs} on 8 June displayed an onshore to offshore gradient. Simulated R_{rs} (412 nm, 443 nm, 555 nm) also displayed an onshore to offshore trend (Figures 19.7A, 19.7C, 19.7E respectively). (The rise in the near-shore simulated values of R_{rs} compared with the offshore values is related to the impact of

the simulated bottom reflectance in the shallow waters on the water-leaving radiance signal.) The relative success in simulating the satellite-estimated IOPs and AOPs during this time period results from the fact that the waters of the WFS at this time of the year approximate classical Case 1 waters, where the IOP and the AOP formulations of the simulation and satellite algorithm most closely match each other.

19.3.2 8 November (DOY 312)

After the passage of Hurricane Georges in late September of 1998, Tropical Storm Mitch (downgraded to a tropical storm from a hurricane just before moving onshore) made landfall on the west coast of Florida near Naples on 5 November 1998. The Page Field Airport in Fort Myers, Florida, reported 6.05 inches (15.4 cm) of rainfall on 5 November[95] leading to large freshwater fluxes from the Peace and Caloosahatchee Rivers (Figure 19.1; W.P. Franklin Lock and Dam (S79)) over the course of several days. The ocean-colour impacts of these freshwater flows may be seen in the satellite derived cholorophyll, absorption and backscatter, which displayed a marked on-shore to off-shore gradient (Figures 19.6B, 19.6D, 19.6F respectively).

Simulated IOPs displayed a similar onshore to offshore gradient. Chlorophyll concentrations were elevated near-shore for the simulated model runs. The full grazing stress simulated chlorophyll concentration for the uppermost 5 m of the water column were within one standard deviation of the SeaWiFS mean across the shelf (Figure 19.6B). The half grazing stress run exceeded this threshold near-shore but was within it offshore; the double grazing stress was within this threshold at the near-shore boundary but fell slightly below it offshore.

Satellite-derived $a_{CDM}(412)$ was elevated near-shore, and appeared to be the direct result of riverine CDM; the simulated results for the average of the top 5 m of the water column also displayed this trend. The simulated results exceeded one standard deviation of the mean satellite derived $a_{CDM}(412)$ in the near-shore environment, which appears to have resulted from the physical accumulation of the early pulsed event (DOY 267) with the later one on DOY (309) (Figure 19.6D). As described in Bissett et al. (2005), the overestimation of near-shore absorption was probably due to the physical circulation of the model whereby the first pulse released in September lingered near-shore and led to an additive effect when the second pulse was released on 5 November (Bissett et al., 2005).

Satellite-estimated backscatter was elevated near-shore and declined offshore (Figure 19.6F). The simulated backscatter at 555 nm followed the same trend; however, the simulated values were slightly lower than the satellite estimates in all cases (although these simulated values are within one standard deviation of the mean). The underestimation of simulated backscatter might have resulted from the lack of sediment resuspension in the model, or perhaps surface boundary layer effects resulting from the high wind conditions surrounding the passage of the tropical storm.

SeaWiFS-derived $R_{rs}(412)$ displayed a decrease from onshore to offshore with the greatest reflectance approximately 8 km from the 10 m isobath. Simulated $R_{rs}(412)$ at the surface was lowest near-shore and increased offshore yet was below one standard deviation of the mean across the shelf (Figure 19.7B). Satellite estimated $R_{rs}(443)$ was elevated near-shore with a maximum reflectance value approximately 8 km from the 10 m isobath (Figure 19.7D). Simulated surface values of $R_{rs}(443)$ were lowest

[95] http://www.nhc.noaa.gov/

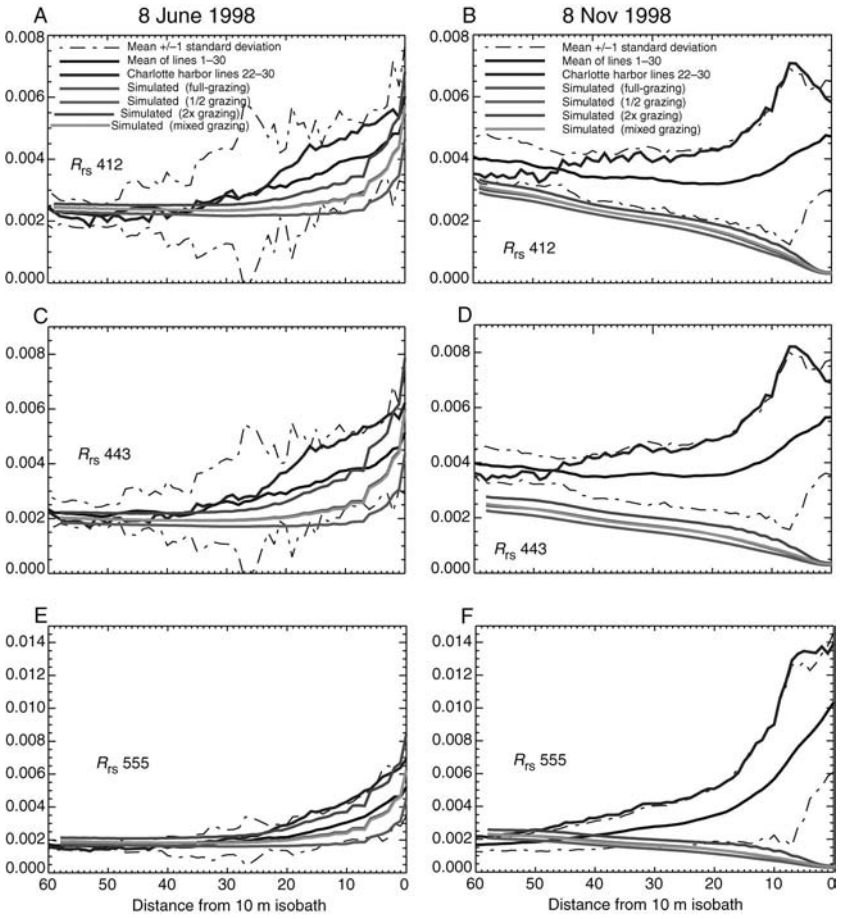

Figure 19.7
Simulated AOPs on the WFS.
A, remote sensing reflectance (R_{rs} 412 nm) on 8 June 1998 for the WFS showing the average of the 30 lines transect, ±1 standard deviation of the mean of 30 lines, the mean of lines 22–30 (Charlotte Harbor), simulated at the surface for the full, half, double and mixed grazing stress runs showing a fairly good match between estimated and simulated results.
B, R_{rs} (412 nm) on 8 November 1998.
C, R_{rs} (443 nm) on 8 June 1998.
D, R_{rs} (443 nm) on 8 November 1998.
E, R_{rs} (555 nm) on the WFS on 8 June 1998.
F, R_{rs} (555 nm) on 8 November 1998.

near-shore and increased offshore yet were below one standard deviation of the mean across the shelf. Satellite derived R_{rs}(555) values were elevated near-shore and declined offshore (Figure 19.7F). Simulated surface values of R_{rs}(555) were underestimated near-shore where they were below one standard deviation of the mean; however, they were within this range offshore. The trend in R_{rs} values increasing towards shore for

all wavelengths, in spite of both the increase in satellite estimated and simulated $a_{CDM}(412)$ resulting from terrestrial inputs of CDM, nutrients and particulate biomass, suggests that backscatter at all wavelengths was underestimated. Higher scattering by either sediments, or other surface induced effects, resulting from high winds would drive an increase in water-leaving photon densities even as absorbing optical constituents are increasing. As the satellite IOP and biomass algorithms used in this study are based on relative water-leaving radiance, not absolute radiance, these differences are masked. However, these examples demonstrate that ratio algorithms that produce absorption estimates may work fine for some Case 2 coastal applications, but that scattering retrieval algorithms and the resultant R_{rs} calculation may be more difficult to develop and validate without a better formulation for total scattering and backscattering.

Nutrient concentrations and filter pad samples for HPLC and Chemtax analysis were collected on the WFS by the ECOHAB Process Cruise during its mid-November cruise and processed by Mote Marine Laboratory. For the near-surface stations in the Charlotte Harbor region, observed differences between simulated and sampled total chlorophyll were more dramatic near-shore (Figure 19.8). The simulated total chlorophyll concentrations were greater than the observed concentrations within 12 km of the 10 m isobath for surface and near-surface stations. Biological factors, such as the

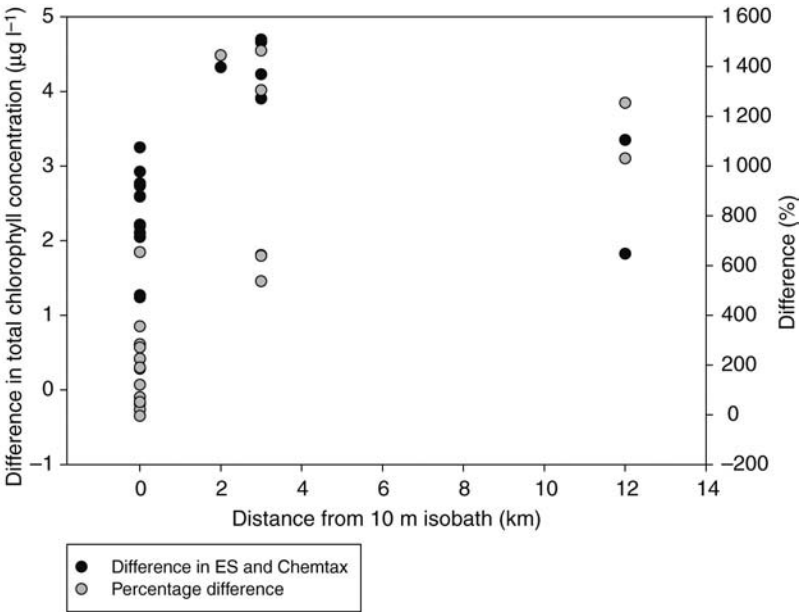

Figure 19.8
Difference and percentage difference between simulated total chlorophyll *a* concentrations (µg l^{-1}) and Chemtax analysis of total chlorophyll *a* concentrations attributed to phytoplankton classes for near-surface stations outside Charlotte Harbor in November 1998. Negative differences represent an underestimation of chlorophyll *a* by the simulation.

concentration of chlorophyll per cell, which are a function of temperature, nutrients, and the light history of the phytoplankton population, may have played a role in the observed versus simulated chlorophyll differences. An additional role in the errors between the satellite observations may have occurred because of inaccuracies in the SeaWiFS OC4 algorithm in near-shore waters, which has difficulties with high turbidity and high dissolved organic matter. However, this overestimation of total chlorophyll compared with both *in situ* and satellite estimates may also be attributed to the physical simulation, because the first pulse event (DOY 267) was forced downward and offshore but then retreated back upwards and collided with the second pulse event on DOY 309 generating an additive effect (Bissett et al., 2005). The removal of the first pulse (data not shown) produced much better agreement with the observed satellite and *in situ* validation data. While the exact cause of these errors in the near-shore region are unquantifiable given the nature of the physical solution, other satellite validation data (e.g. a_{CDM}) also suggest an over-estimation resulting from the accumulation of two pulse events at the same physical location.

ECOHAB data collected near Charlotte Harbor in mid-November revealed a salinity and chlorophyll fluorescence signature just outside the barrier islands, shoreward of the 10 m isobath (Figures 19.9A, 19.9B respectively). These signatures had characteristics of freshwater origin such as a diminished salinity and sigma-t (~20–20.5 kg m^{-3}, data not shown) compared with surrounding waters. Samples were processed by Chemtax analysis to determine the algal classes present on the WFS. Samples from this near-shore region (<12 km from the 10 m isobath) attributed between 15% and 33% of the total chlorophyll *a* concentration to chlorophytes and cryptophytes (Figure 19.10A). Samples from approximately 12 km offshore of the 10 m isobath attributed 11% of the total chlorophyll *a* concentration to chlorophytes and cryptophytes. This suggests that the bioavailability of nutrients and/or organic material from low-salinity waters (commonly where these species are found) was potentially delivered by the rivers out on to the WFS. Offshore, differences between simulated and sampled total chlorophyll *a* concentrations diminished.

Differences in simulated versus sampled silica concentration were also more pronounced near-shore. Simulated silica concentrations were greatly underestimated compared with sampled silica concentrations at a station 6 km from the 10 m isobath (Figure 19.4B). As near-shore silica concentrations are representative of terrestrial fluxes, it appears that we may have underestimated either the nutrient concentrations of those fluxes or the total fresh water discharge. The impact of a relative underestimation of silica inputs would result in a reduction in the growth rates and accumulation of large and small diatom functional groups. Inorganic phosphate was also underestimated near-shore but to a lesser extent. Simulated nitrate concentrations were very similar to those sampled across the shelf (data not shown).

The photosynthetic pigments and carotenoids present in various combinations and concentrations in marine phytoplankton were explored by HPLC and Chemtax analysis in order to determine the abundance of the algal classes listed in Table 19.1 on the WFS in November. Diatoms dominated the near-shore environment with ~50% of total chlorophyll attributed to this phytoplankton species 2 km from the 10 m isobath (Figure 19.10A). ECOHAB recorded silica concentrations between 4 km and 6 km from the 10 m isobath of approximately 4–5 μg Si l^{-1} probably corresponding to the high concentrations of diatoms in the near-shore environment. *K. brevis* was a prevalent phytoplankton species in the near-shore community constituting 31% of the total chlorophyll concentration at the 10 m isobath. The next most dominant algal class was made up of

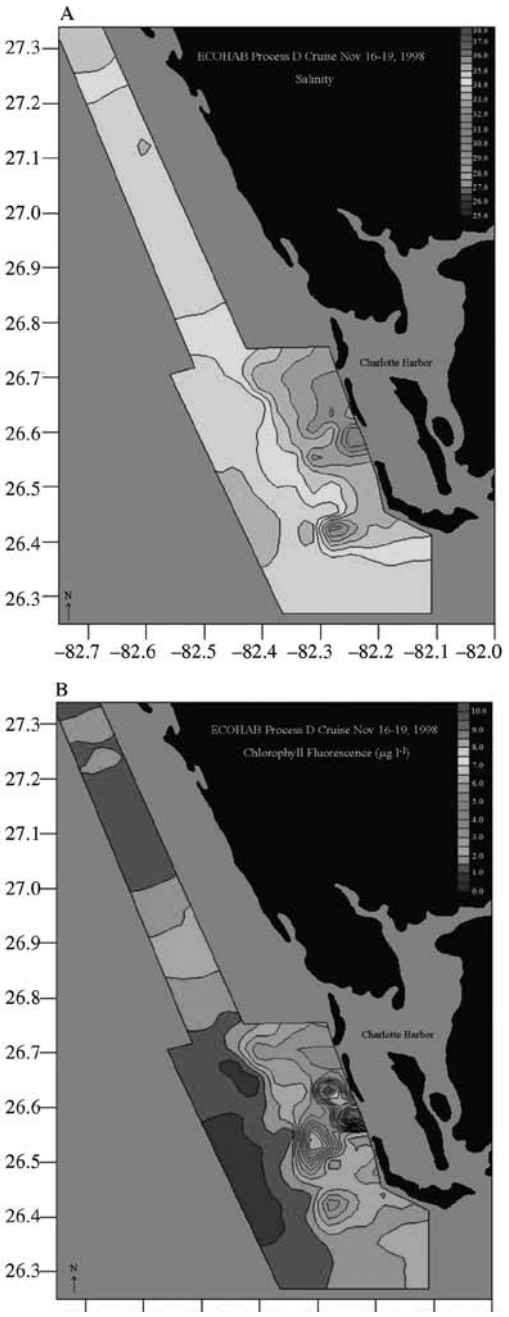

Figure 19.9
Process Cruise data on 16–19 November 1998 displaying A, salinity; B, chlorophyll fluorescence signature near-shore along the coast of Charlotte Harbor.

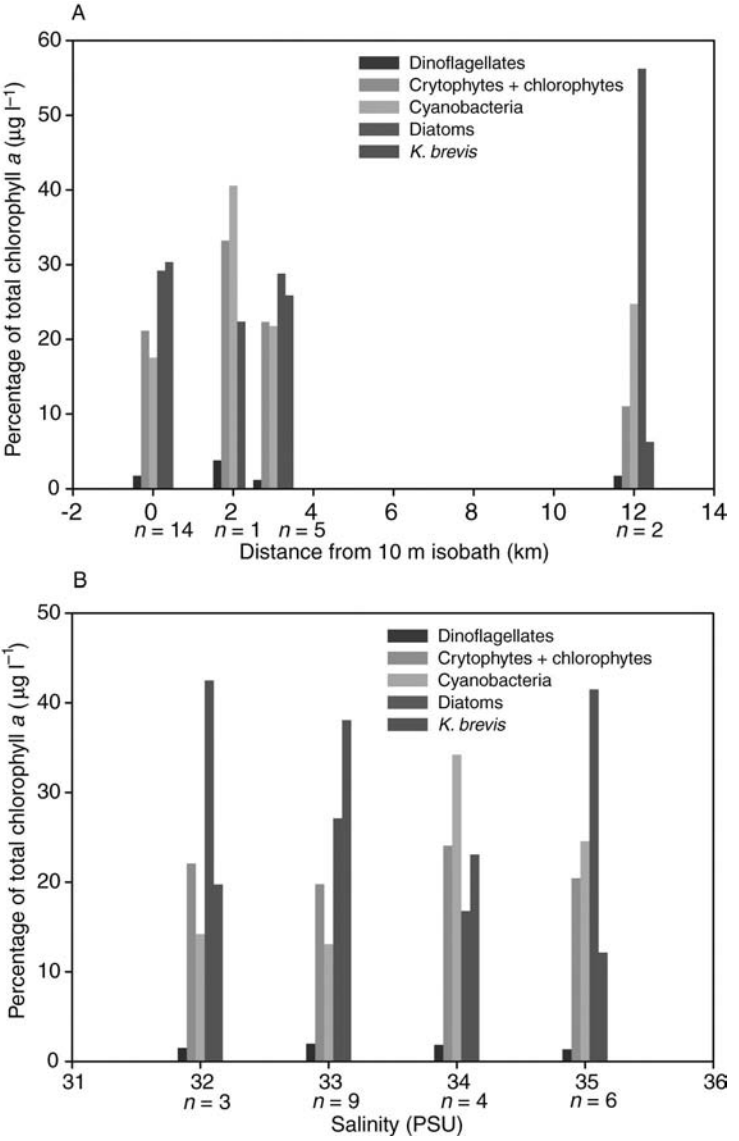

Figure 19.10
A, percentage of total chlorophyll *a* concentration (µg l^{-1}) attributed to each phytoplankton class present in near-surface samples outside Charlotte Harbor as a function of distance from model shoreward boundary.
B, percentage of total chlorophyll *a* concentration attributed to each phytoplankton class present in near-surface samples outside Charlotte Harbor as a function of salinity.

chlorophytes and cryptophytes constituting 33% of the total chlorophyll concentration 3 km from the 10 m isobath. Further offshore, diatoms were the most prevalent species making up 56% of the total chlorophyll concentration 12 km from the 10 m isobath.

Simulated full grazing stress results displayed a near-shore phytoplankton population dominated by prochlorophytes, *Synechococcus* and non-toxic dinoflagellates, while 12 km from the 10 m isobath, non-toxic dinoflagellates were the dominant phytoplankton species (Figure 19.11A). Simulated offshore results at depth suggested the presence of a diatom bloom with elevated concentrations of prochlorophytes (Figure 19.5B). The mixed grazing stress results show a transfer of biomass between the non-toxic dinoflagellates and the *K. brevis* populations (Figure 19.11B). This is to be expected because the numerical descriptions between the non-toxic dinoflagellates and *K. brevis* are more similar than between the dinoflagellate species and other phytoplankton populations. Alterations of the relative grazing rates between dinoflagellate function groups (Table 19.2) results in a transfer within a niche space between non-toxic and toxic dinoflagellates. The WFS autumn 1998 observations of Walsh et al. (2003) demonstrated a near-shore bloom of *K. brevis* in the presence of CDOM as well as a deep offshore bloom of diatoms, similar to the results shown here. If differential grazing within a dinoflagellate favourable niche is an important ecological interaction, then the results presented here suggest good agreement with the occurrence of HABs on the WFS in November 1998.

Interestingly, when the same Chemtax data set was evaluated by salinity instead of by distance from the 10 m isobath, different results are evident. Chemtax analysis revealed diatoms to be the dominant fraction of phytoplankton present on the WFS at the lower and higher salinity levels with up to 43% of total chlorophyll concentration at 32 PSU and 42% at 35 PSU (Figure 19.10B). *K. brevis* was the dominant species at 33 PSU with 38% of total chlorophyll concentration attributed to this species and cyanobacteria dominated at a salinity of 34 PSU with 34% of total chlorophyll concentration ($\mu g\ l^{-1}$).

After the removal of chlorophyll biomass differences, it is clear that the simulation greatly overestimated the concentration of total chlorophyll *a* attributed to dinoflagellates across the shelf (Figure 19.12A). The three instances of over-estimation shown in Figure 19.12A resulted from Chemtax estimates for dinoflagellates that were below detectable limits and were effectively considered zero. The simulation returned values for these locations and the difference between these values approach infinity and are denoted on the graph. The same comparisons were made for the amount of total chlorophyll *a* attributed to *K. brevis* (Figure 19.12B). The simulation generally underestimated the concentration of total chlorophyll assigned to by *K. brevis*. The exceptions were in the near-shore environment where the Chemtax results were below detectable limits and the simulation returned values. In one instance, the simulated *K. brevis* concentration was overestimated 12 km from the 10 m isobath. This probably resulted from the simulated biomass being pushed farther offshore after the second pulse whereas, the actual recorded *K. brevis* bloom hugged the coastline.

After the removal of biomass differences, the concentration of total chlorophyll *a* attributed to diatoms were generally underestimated by the simulation in the near-shore environment (Figure 19.13A). Differences between ECOSIM large and small diatoms and Chemtax diatoms were greater in the near-shore environment and diminished offshore. The concentration of total chlorophyll *a* ascribed to *Prochlorococcus*, after the removal of biomass differences, was generally overestimated by the simulation (Figure 19.13B). Differences between ECOSIM *Prochlorococcus* 1+2 and Chemtax chlorophytes were greater in the near-shore environment with diminishing differences offshore. The same scenario was evident for the concentration of total chlorophyll *a* concentration attributed

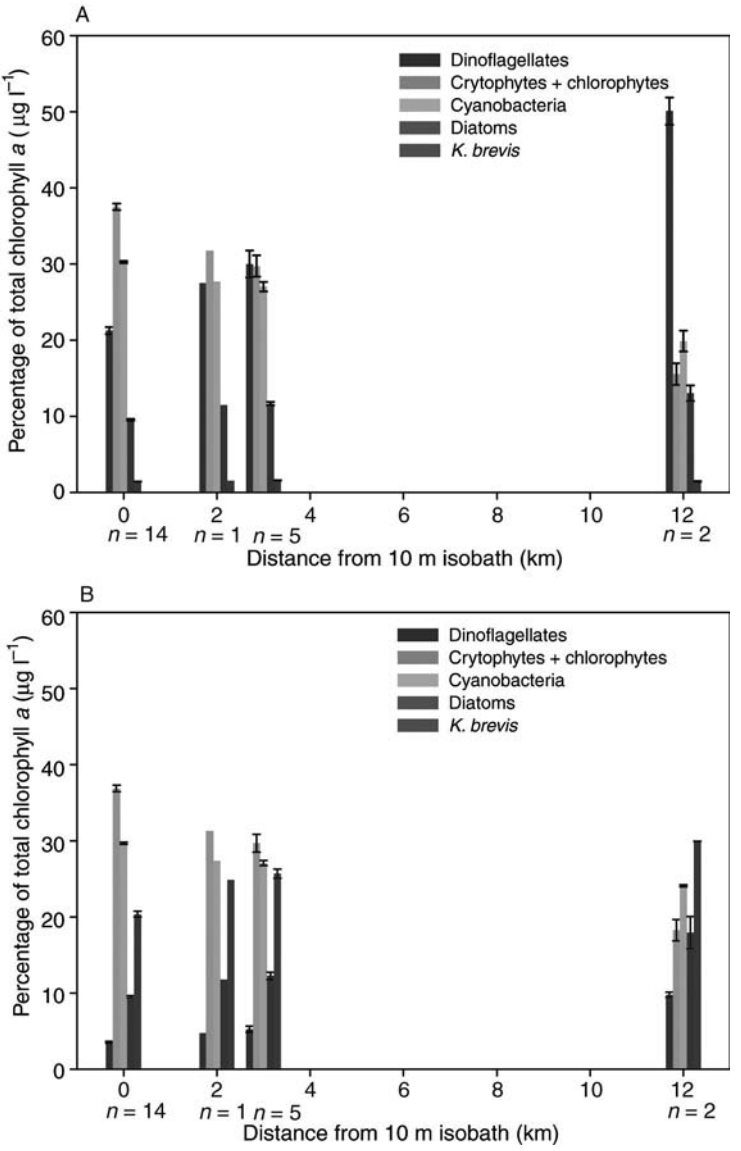

Figure 19.11
A, percentage of full grazing stress simulated total chlorophyll *a* concentration (µg l^{-1}) attributed to each phytoplankton class in near-surface samples outside Charlotte Harbor.
B, percentage of mixed grazing stress simulated total chlorophyll *a* concentration attributed to each phytoplankton class in near-surface samples outside Charlotte Harbor. Standard error of mean (±1) is denoted by error bars.

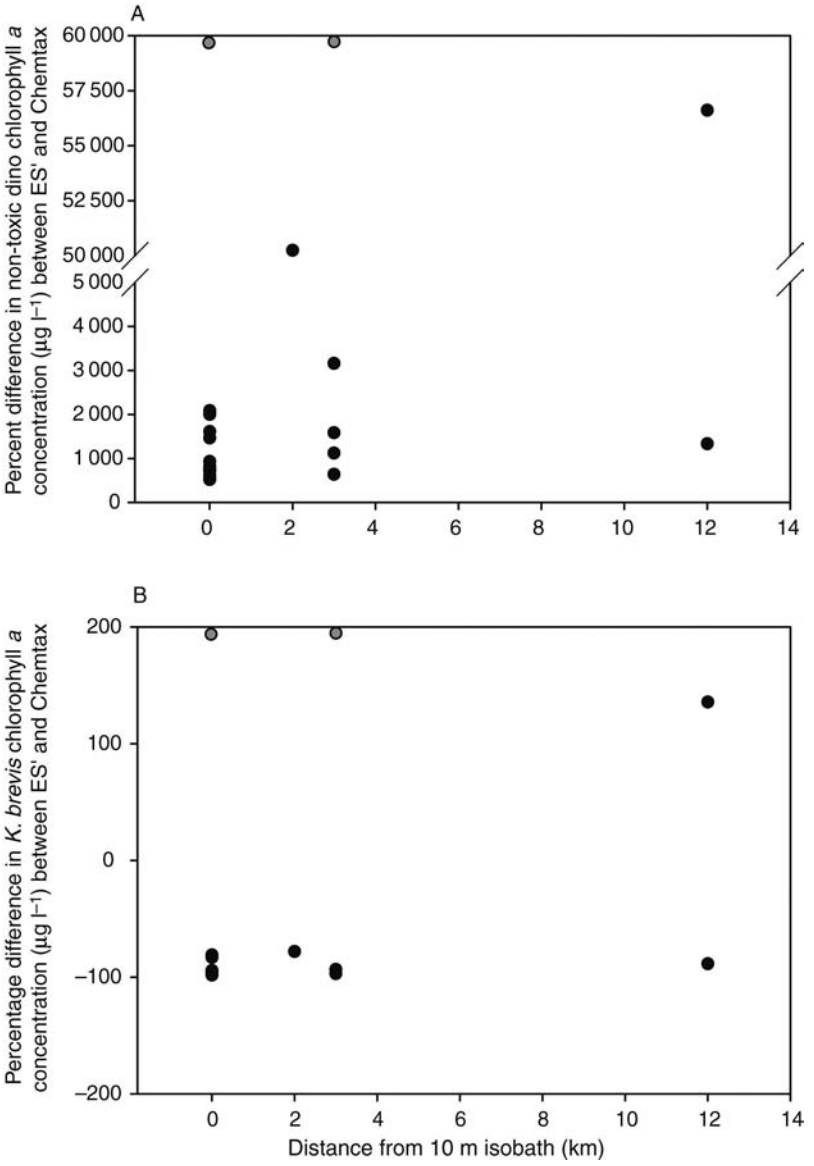

Figure 19.12
A, removal of biomass differences between simulated and sampled dinoflagellates in near-shore waters.
B, removal of biomass differences between simulated and sampled *K. brevis* in near-shore waters. Grey circles indicate that simulation returned a value where the Chemtax value was effectively zero.

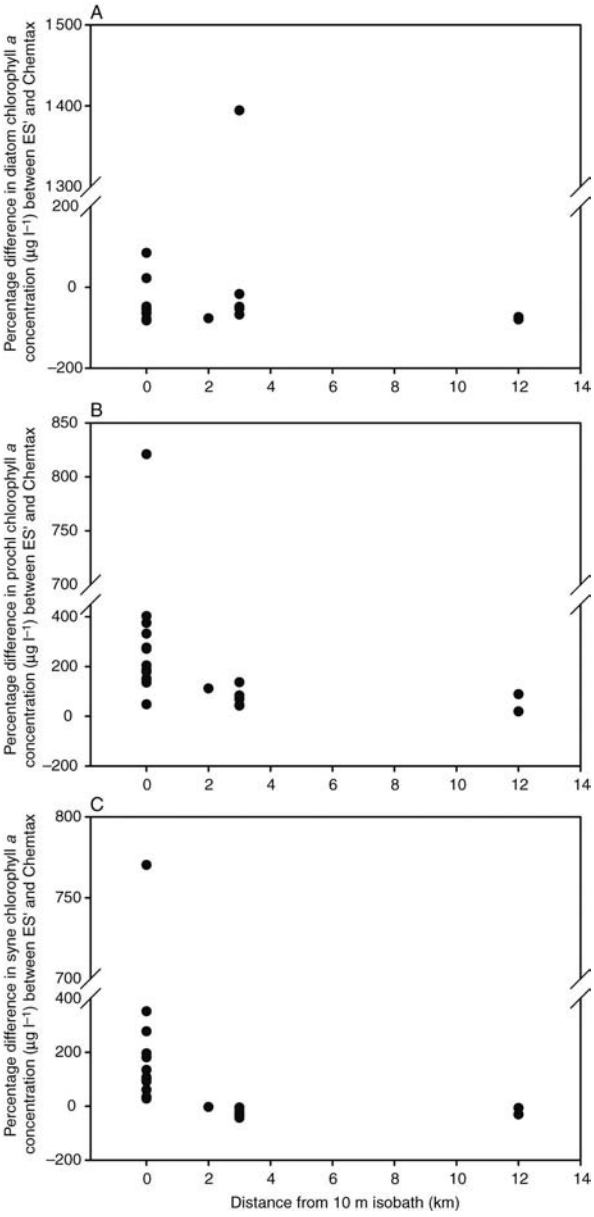

Figure 19.13
A, removal of biomass differences between simulated and sampled diatoms in the near-shore environment.
B, removal of biomass differences between simulated prochlorophytes and sampled chlorophytes in the near-shore environment.
C, removal of biomass differences between simulated *Synechococcus* and sampled cyanobacteria in the near-shore environment.

to *Synechococcus* (Figure 19.13C). Comparisons between ECOSIM *Synechococcus* and Chemtax cyanobacteria were greater at the near-shore boundary; however, seaward of 2 km from the 10 m isobath differences between simulated and sampled values were minimal. The simulated overestimation of dinoflagellates, *Prochlorococcus* and *Synechococcus* were mirrored by a relative underestimation of diatoms and *K. brevis*. Such a result may have been driven by an overestimation of the relative growth rates (caused by inaccurate estimations of nutrient or light uptake and assimilation) or an underestimation of the relative loss rates between the diatom and dinoflagellate species. It may have also been a function of the lower simulated concentrations of silica. As noted above, there was a significant underestimation of silica in the near-shore environment. This would have led to a smaller simulated growth rate, as well as biomass accumulation, by the diatom functional groups.

19.3.3 Closure sensitivity

The closure term of grazing stress was altered to demonstrate that minor adjustments in this one term could produce varying results in terms of the simulated phytoplankton composition (Figure 19.11B) and optical properties on the WFS (Table 19.3). As expected, increasing the grazing stress caused a decrease in the chlorophyll concentration across the shelf and vise versa for decreasing the grazing stress whereas the mixed grazing stress run displayed minimal differences compared with the full grazing stress run. Major differences were observed, as expected, in phytoplankton biomass with the varying grazing stresses on both 8 June and 8 November.

Observed differences in optical properties and phytoplankton biomass were greater in November compared with June for the various grazing stress runs. The differences in chlorophyll concentration between the full and half grazing stress runs were attributed to the increase in biomass of non-toxic dinoflagellates and diatoms displayed in the half grazing stress run (Figure 19.14). The mixed grazing stress run produced minimal differences compared with the full grazing stress runs for both chlorophyll concentration and backscatter, since the *K. brevis* functional group represented a small fraction of the total simulated biomass.

Table 19.3 Percentage difference between IOPs and R_{rs} for the half, double and mixed grazing stress runs compared with the full grazing stress run

	Half vs full grazing stress	**Double vs full grazing stress**	**Mixed vs full grazing stress**	**Half vs full grazing stress**	**Double vs full grazing stress**	**Mixed vs full grazing stress**
	8 June	**8 June**	**8 June**	**8 Nov**	**8 Nov**	**8 Nov**
$a_{CDM}(412)$	–11	9.2	–1.7	–13	11	–3.3
Chlorophyll	57	–39	1.7	54	–43	3.3
$b_b(555)$	15	–14	0.46	17	–18	1.2
$R_{rs}(412)$	–10	11	–0.44	–7.9	12	2.0
$R_{rs}(443)$	–16	23	–1.1	–13	22	0.73
$R_{rs}(555)$	–17	27	–1.4	–15	26	0.19

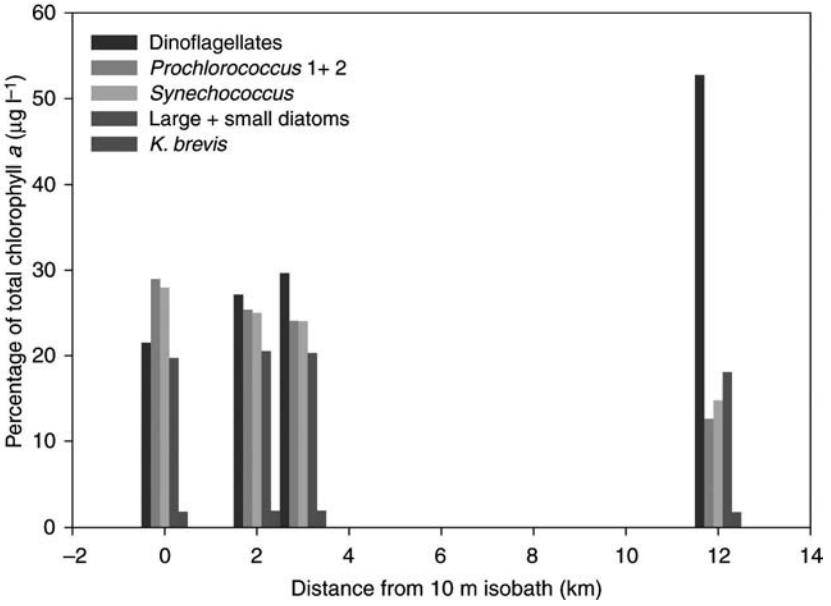

Figure 19.14
Percentage of the half grazing stress simulated total chlorophyll *a* concentration (µg l^{-1}) attributed to each phytoplankton class in near-surface samples outside Charlotte Harbor.

The most dramatic effect of altering the grazing stress was observed in the 'mixed grazing stress' which doubled the grazing stress on the non-toxic dinoflagellates while simultaneously halving the grazing stress on *K. brevis*. Comparisons of the full versus the mixed grazing stress cases revealed significant differences ($p < 0.05$, using paired Student t-tests) in the dinoflagellate population at 0 km, 3 km and 12 km from the 10 m isobath, the *Prochlorococcus* 1+ 2 population at 0 km and 12 km from the 10 m isobath, the *Synechococcus* population at 0 km and 12 km from the 10 m isobath, and the *K. brevis* population at 0 km, 3 km and 12 km from the 10 m isobath (Figures 19.11A, 19.11B). No significant differences were observed for the diatom population. The most noticeable result was a decline in the dinoflagellate population from the full to the mixed grazing stress with a corresponding increase in the *K. brevis* population. This 'mixed grazing stress' was specifically developed to show the sensitivity of the grazing stress on the phytoplankton classes on the WFS. By slightly altering this single term, it was possible to generate a near-shore harmful algal bloom.

19.4 Discussion

Ocean optics and phytoplankton ecology are intrinsically coupled. An accurate understanding and prediction of one without the other is impossible. This volume of papers testifies to these linkages. However, typical HAB simulations often simplify these processes to avoid the complexities involved with generating a solution to both

the optical and ecological dynamics of the coastal zone. In this chapter, these results suggest that it is possible to simulate both optics and ecology in a manner that provides feedback between light and nutrient harvesting, phytoplankton competition and spectral photon densities. The explicit coupling of these fields of research in this numerical simulation suggests that the simplification of equation 19.1 may be unnecessary in HAB research.

As with the related paper by Bissett et al. (2005), a critical aim of this work was to avoid the reductionist viewpoint of modelling, which focuses on a minimal set of parameters and interaction equations to match a specific validation data set. While it may not appear evident to those unskilled in numerical modelling, a large number of state variables does not equate to a large number of free parameters. In this study, the parameters of time-dependent change for the mass constituents are fixed from laboratory or field measurements. The only 'free' parameter is the grazing and loss term. The ECOSIM model is an evolving set of interaction equations whose parameters change when there is a change in the interaction equations. In the methodology used here, the parameters are not altered to match any particular data set. Instead, this modelling study concentrates on trying to build a framework that addresses both ocean colour and ecology across transition zones (ecotones) and will therefore be more applicable to both coastal and open ocean solutions. The goal was to develop an ecological framework that may be nested into larger physical models without constantly altering parameters for different geographical or ecological regimes.

As mentioned in the methods, the model results were in equilibrium with the physical solution, and the solution was generated for three simulated years prior to the analysis of the results. There were no numerical transients or 'limit-cycle' behaviours. Therefore, the ecological and optical results from this simulation are directly dependent on the physical circulation model. The WFS is a four-dimensional system (x, y, z, t; He and Weisberg, 2002*a*, 2002*b*; Walsh et al., 2001, 2002), and its representation by a reduced-dimension circulation system (x, z, t) introduces uncertainties in the comparisons of simulated data with *in situ* data. A direct correlation study is thus difficult because the physics and boundary conditions drive the zero- and first-order solutions, where zero order is defined as the initial state and boundary conditions, and first order as the advective and diffusive fluxes. The ecological and optical solutions are second-order time-dependent problems that require accurate solutions to the zero- and first-order problems before exact comparisons of the ecological results may be made to geographically certain validation data. Significant errors in the physics and boundary conditions will cause errors that may not be the fault of the ecological coding. This is a statement of fact, not an assignment of blame, and is mentioned only to remind readers of the limits of the measurements of 'success' in any ecological modelling effort.

While not shown, the temporal evolution of the results were very much as one would expect on the introduction of significant nutrient supplies at either the offshore or riverine boundary. We highlight two points in time (June and November), because (a) there are validation data not used in any formulation or assimilation of the model, and (b) these distinctly different time periods offer the ability to contrast different ecological conditions representative of this region, thereby demonstrating the model's ability to cross ecological boundaries in time and space. While perfect comparisons between the simulated results and the field and satellite observations may not be possible, this modelling study helps us to focus on the 'reasonableness' of simulated biological, ecological and optical results. This focus allows us to reasonably comment on hypotheses of HAB formation on the WFS. One of the hypotheses offered, and

supported by this study, is that pre-existing small concentrations of *K. brevis* may interact with the terrestrial fluxes of nutrients to yield toxic concentrations of this HAB-forming species.

The complexity of this model allows for a full description of the non-stoichiometric nutrient interaction equations. This description shows the impacts of silica limitation on the diatom population, with a commensurate increase in DON and dinoflagellate populations. These non-toxic dinoflagellate populations exceed their toxic counterparts, because of faster growth rates and better light harvesting ability. The accumulation of toxic species occurs here because of differential grazing. Thus, this study suggests that non-stoichiometry (non-Redfield) nutrient dynamics may yield conditions favourable to dinoflagellate populations and that reduced grazing pressure on the toxic dinoflagellates may help lead to their accumulation. This study also suggests that a more definitive answer would be derived from a coupling an ecological/optical simulation to a fully four-dimensional physical modelling system of the WFS.

Errors in simulated versus observed results may also be attributed to the fact that chlorophyll concentration per cell varies with temperature, nutrient, light and species and that chlorophyll estimates from SeaWiFS can vary by a factor of 2 or more. An additional source of errors could be due to the fact that the OC4 chlorophyll algorithm was used in this study where CDOM and resuspended sediment had major contributions to the near-shore IOPs. Band-ratio algorithms are extremely useful due to their simplistic formulas; however, they are not optimized to distinguish CDOM from chlorophyll. The use of this algorithm in high-CDOM coastal waters has been examined and research has found that its accuracy deteriorates for near-shore waters with high DOM concentrations (Liew et al., 2001). Near-shore Case 2 waters were also somewhat more difficult to simulate as opposed to Case 1 waters. Some of the differences in the surface chlorophyll and $a_{CDM}(412)$ were attributed to the inability to simulate an along-shore flow (Figures 19.6B, 19.6D, 19.8); and some of the others attributed to the scattering of particles, or other high wind-driven effects, that were not included in the simulation (Figure 19.6E). However, one should not lose sight of the fact that we are discussing small relative errors between the ocean-colour estimates and the simulated values. This should be viewed as an achievement, and suggest that new standards for accuracy may evolve when IOPs are considered as part of the validation data suite.

This study also coupled radiative transfer equations (EcoLight) to link simulated IOPs directly to remote sensing reflectance, thereby providing a direct comparison of a reflectance result to a satellite reflectance measurement. This avoids the intermittent step required to validate against a satellite chlorophyll algorithm, which has its own inherent problems and errors. The fact that the results are on the same graph with scalar values on the *y*-axis should be cause for muted celebration, for this is validation at the physical level of photons and is within the standard deviation of the measurements. The fact that the backscatter and R_{rs} results are not as robust point to both the exclusion of an important optical constituents, for example resuspended sediments, and the fact that the very nature of Case 2 IOPs are still an area of very active research.

The taxa-specific results were not as strong, but they were encouraging. Clearly, the simulation under-estimated diatom concentrations and over-estimated non-toxic dinoflagellates. Part of the problem may have resulted from the inaccurate prescription of the shoreward boundary condition as the near-shore November silica

concentrations were much lower than measured (Figure 19.4B). Another problem may have been taxa specific closure terms, and we could further explore the grazing parameter space to attempt to exactly match the relative contributions of the Chemtax estimates by further altering the loss terms. However, it is unclear that such tuning would render meaningful results, and it would be best to address the boundary conditions and physical model before attempting to tune the closure term to match the current data.

At first glance to the uninitiated, this might suggest that this model may be tunable to match specific results. However, this is not the message that is suggested here. The large number of state variables in this model provide for the closure of processes through multiple mass stocks that are directly measurable. For example, DOM and $a_{CDM}(412)$ are parameters that may be measured. Alteration of the grazing stress has direct impacts on these stocks and IOPs, thus the grazing stress and resulting processes are constrained by their inclusion in this model. Likewise, it was shown that the lack of silica flux results in a mismatch in total silica stocks, which limits the diatom growth rate and accumulation, which may be validated by Chemtax estimates as well as by nutrient measurements. In addition, a critical model validation is whether it performs well over different environmental forcing conditions. It may be possible to match simple validation data streams at limited locations in time and space; however, over broad time and space scales, simple PZN models tend to fail because the parameters used to match one data set will not yield robust answers in different environmental conditions. Thus, the example here of model simulations of the exact same parameter sets run over an entire year showing results under oligotrophic (8 June) and eutrophic conditions (8 November) gives confidence in the applicability of the results to understanding real ecological conditions and events.

The fact that the relative phytoplankton community structure and total stocks may be altered by model closure is (a) an exercise in the obvious, and (b) a demonstration that alterations in the loss terms resulting from upper trophic (and in the case of viruses, lower trophic) level dynamics are important and may be more difficult to simulate. However, this does not mean that predictive simulations of red tides are beyond our current means. In the case of the WFS, where it appears that *K. brevis* respond to total nutrient dynamics in a competitive regime of spectral light and multiple limiting nutrients, it may be possible to predict the probable conditions where *K. brevis* best occurs. This would provide the means to forecast probabilities, much like the weather forecast of rain chance percentages. As is evident here, such a probability forecast is critically dependent on the physical circulation model, as well as having accurate initial and boundary conditions for nutrients and organic stocks. The combination of new physical sensors, CODAR, in-water optical sensors and platforms, for example absorption and scattering sensors on gliders, and remote sensing tools and techniques, like hyperspectral remote sensing, may provide the means to help initial and constrain the future nowcast/forecast HAB systems.

19.5 Where do we go from here?

In this study, an ecological model, which resolves the spectral harvesting of light by phytoplankton and the non-stoichiometric dynamics of nutrient cycling, is merged with the optical properties of the water column, such that the intersection between

biology and optical physics may be directly compared with satellite reflectance measurements. It is shown that within the constraints of the physical circulation and boundary conditions it appears that a reasonable representation of the *K. brevis* HAB on the WFS during autumn 1998 is produced, as well as the bulk chlorophyll, IOPs and AOPs. The successes can be listed as:

- Coupling of a fairly comprehensive phytoplankton ecological model to the prediction of inherent and apparent optical properties that provides feedbacks between light and nutrient assimilation and spectral photon densities.
- Validation of simulated bulk surface chlorophyll and IOPs with satellite-derived estimates with 1 standard deviation in Case 1 waters.
- Coupling of predicted inherent optical properties to a robust prediction of apparent optical properties to yield R_{rs} predictions that can be directly compared with satellite-measured photon densities, not just bulk properties that have errors associated with the satellite inversion error.
- The increased probability of *K. brevis* HAB formations on the WFS appears to be directly related to conditions that increase the total nutrient concentration on the shelf, that is a rising tide raises all boats, and differential grazing.

These successes are matched by some disappointments, which serve to point to areas of needed future research. Some of these are highlighted as:

- An accurate physical circulation model and boundary conditions is paramount to accurate simulation of phytoplankton, IOPs, AOPs and HAB formation.
- More research into Case 2 particle specific optical properties, including inorganic particles is needed in order to simulate IOP and AOP distributions in the nearshore environment.
- Numerical simulation of taxa specific phytoplankton dynamics may require additional research into the taxa specific loss processes ('closure terms'), of the model.

In summary, optics and HABs should be studied and modelled as an integrated science, without resorting to simplifications that are unnecessary in light of this study. As mentioned at the start of this chapter, the complexity of the modelling approach chosen for a particular problem should be problem specific. In some cases, the use of optics as described here may not be as advantageous, for example *Alexandrium* in the Gulf of Maine, in the initialization and validation of numerical studies. In addition, there may be technical and financial constraints which limit the research to those numerical and modelling techniques that are more simply accomplished. However, the results here suggest that the study of ocean colour and HABs together (at least in this location) will provide greater insights into the biological and physical processes that yield these extreme events, as well as provide the data needed to initialize and validate future nowcast/forecast systems. These results suggest that optics may be explicitly linked to phytoplankton dynamics studies, and may actually hold the key to creating successful nowcast/forecast HAB systems.

References

Andersen, V. and Nival, P. 1988. A pelagic ecosystem model simulating production and sedimentation of biogenic particles: role of salps and copipods. *Mar. Ecol. Progr. Ser.*, 44, pp. 37–50.

Anderson, T. R. 1993. A spectrally averaged model of light penetration and photosynthesis. *Limnol. Oceanogr.*, 38(7), pp. 1403–19.

Anderson, T. R. and Williams, P. J. B. 1998. Modelling the seasonal cycle of dissolved organic carbon at Station E1 in the English Channel. *Estuar. Coast. Shelf Sci*., 46, pp. 93–109.

Anderson, T. R. and Williams, P. J. B. 1999. A one-dimensional model of dissolved organic carbon cycling in the water column incorporating combined biological-photochemical decomposition. *Global Biogeochem. Cy*., 13(2), pp. 337–49.

Antoine, D. and Morel, A. 1995*a*. Modelling the seasonal course of the upper ocean pCO_2. I: Development of a one-dimensional model. *Tellus*, 47B, pp. 103–21.

Antoine, D. and Morel, A. 1995*b*. Modelling the seasonal course of the upper ocean pCO_2. II: Validation of the model and sensitivity studies. *Tellus*, 47B, pp. 122–44.

Antoine, D. and Morel, A. 1996. Oceanic primary production. 1: Adaptation of a spectral light-photosynthesis model in view of application to satellite chlorophyll observations. *Global Biogeochem. Cy*., 10(1), pp. 43–56.

Armstrong, R. A. 1994. Grazing limitation and nutrient limitation in marine ecosystems: steady state solutions of an ecosystem model with multiple food chains. *Limnol. Oceanogr*., 39(3), pp. 597–608.

Armstrong, R. A., Lee, C., Hedges, J. I., Honjo, S. and Wakeham, S. G. 2001. A new, mechanistic model for organic carbon fluxes in the ocean based on the quantitative association of POC with ballast minerals. *Deep Sea Res. II*, 49(1–3), pp. 219–36.

Babin, M., Roesler, C. S. and Cullen, J. J. (eds). 2006. *Real-time Coastal Observing Systems for Marine Ecosystem Dynamics and Harmful Algal Blooms: Theory, Instrumentation and Modelling*. Paris, Intergovernmental Oceanographic Commission of UNESCO. (Monographs on Oceanographic Methodology XX.)

Behrenfeld, M. J., Boss, E., Siegel, D. A. and Shea, D. M. 2005. Carbon-based ocean productivity and phytoplankton physiology from space. *Global Biochem. Cy*., 19.

Bidle, K. D. and Falkowski, P. G. 2004. Cell death in planktonic photosynthetic microorganisms. *Nat. Rev. Microbiol*., 2, pp. 643–55.

Bissett, W. P. 1997. Carbon cycling in the upper waters of the Sargasso Sea. Thesis, St Petersburg, University of South Florida, 207 pp.

Bissett, W. P., Arnone, R., DeBra, S., Dieterle, D., Dye, D., Kirkpatrick, G., Schofield, O. and Vargo, G. 2005. Predicting the optical properties of the West Florida Shelf: resolving the potential impacts of a terrestrial boundary condition on the distribution of colored dissolved and particulate matter. *Mar. Chem*., 95, pp. 199–233.

Bissett, W. P., Carder, K. L., Walsh, J. J. and Dieterle, D. A. 1999*a*. Carbon cycling in the upper waters of the Sargasso Sea. II: Numerical simulation of apparent and inherent optical properties. *Deep Sea Res. I*, 46(2), pp. 271–317.

Bissett, W. P., DeBra, S. and Dye, D. 2004. *Ecological Simulation (EcoSim) 2.0 Technical Description*. Tampa, Florida Environmental Research Institute. http://www.flenvironmental.org/publications_ppts/FERI_2004_0002_U_D.pdf.

Bissett, W. P., Meyers, M. B., Walsh, J. J. and Muller-Karger, F. E. 1994. The effects of temporal variability of mixed layer depth on primary productivity around Bermuda. *J. Geophys. Res*., 99(4), pp. 7539–53.

Bissett, W. P., Schofield, O., Glenn, S., Cullen, J. J., Miller, W. L., Plueddemann, A. J. and Mobley, C. D. 2001. Resolving the impacts and feedback of ocean optics on upper ocean ecology. *Oceanography*, 14(3), pp. 30–53.

Bissett, W. P., Walsh, J. J., Dieterle, D. A. and Carder, K. L. 1999*b*. Carbon cycling in the upper waters of the Sargasso Sea. I: Numerical simulation of differential carbon and nitrogen fluxes. *Deep Sea Res. I*, 46(2), pp. 205–69.

Christian, J. R., Verschell, M. A., Murtugudde, R., Busalacchi, A. J. and McClain, C. R. 2001*a*. Biogeochemical modelling of the tropical Pacific Ocean. I: Seasonal and interannual variability. *Deep Sea Res. II*, 1–3, pp. 509–43.

Christian, J. R., Verschell, M. A., Murtugudde, R., Busalacchi, A. J. and McClain, C. R. 2001*b*. Biogeochemical modelling of the tropical Pacific Ocean. II: Iron biogeochemistry. *Deep Sea Res. II*, 49(1–3), pp. 545–65.

Cloern, J. E., Grenz, C. and Vidergar-Lucas, L. 1995. An empirical model of the phytoplankton chlorophyll: carbon ratio – the conversion factor between productivity and growth rate. *Limnol. Oceanogr.*, 40(7), pp. 1313–21.

Collins, C. 1980. Formulation and validation of a mathematical model of phytoplankton growth. *Ecology*, 61(3), pp. 639–49.

Cullen, J. J. 1990. On models of growth and photosynthesis in phytoplankton. *Deep Sea Res.*, 37(4), pp. 667–83.

Cullen, J. J., Geider, R. J., Ishizaka, J., Kiefer, D. A., Marra, J., Sakshaug, E. and Raven, J. A. 1993. Toward a general description of phytoplankton growth for biogeochemical models. In: G. T. Evans and M. J. R. Fasham (eds), *Towards a Model of Ocean Biogeochemical Processes*. Berlin, Springer-Verlag, pp. 153–76.

Davidson, K. and Cunningham, A. 1996. Accounting for nutrient processing time in mathematical models of phytoplankton growth. *Limnol. Oceanogr.*, 41(4), pp. 779–83.

Davis, C. O., Breitner, N. F. and Harrison, P. J. 1978. Continuous culture of marine diatoms under silicon limitation. III: A model of Si-limited diatom growth. *Limnol. Oceanogr.*, 23(1), pp. 41–52.

Denman, K. 2003. Modelling planktonic ecosystems: paramaterizing complexity. *Progr. Oceanogr.*, 57, pp. 429-452.

Doney, S. C., Glover, D. M. and Najjar, R. G. 1996. A new coupled, one-dimensional biological-physical model for the upper ocean: Applications to the JGOFS Bermuda Atlantic Time Series (BATS) site. *Deep Sea Res. II*, 43(2–3), pp. 591–624.

Ebenhoh, W. 1988. Coexistence of an unlimited number of algal species in a model system. *Theor. Popul. Biol.*, 34, pp. 130–44.

Elliott, J. A., Reynolds, C. S. and Irish, A. 2001. An investigation of dominance in phytoplankton using the PROTECH model. *Freshwat. Biol.*, 46, pp. 99–108.

Falkowski, P. G. and Raven, J. A. 1997. *Aquatic Photosynthesis*. Malden, Mass., Blackwell Sciences.

Fasham, M. J. R., Ducklow, G. W. and McKelvic, S. M. 1990. A nitrogen-based model of plankton dynamics in the oceanic mixed layer. *J. Mar. Res.*, 48, pp. 591–639.

Fasham, M. J. R., Sarmiento, J. L., Slater, R. D., Ducklow, H. W. and Williams, R. 1993. Ecosystem behavior at Bermuda Station 'S' and Ocean Weather Station 'India': a general circulation model and observational analysis. *Global Biogeochem. Cy.*, 7(2), pp. 379–415.

Feuillade, J. B. and Feuillade, M. 1993. Modelling steady-state growth and photosynthesis rates of *Oscillatoria rubescens* continuous cultures in relation to temperature and irradiance. *Limnol. Oceanogr.*, 38(7), pp. 1420–37.

Franks, P. J. S. 1997. Models of harmful algal blooms. *Limnol. Oceanogr.*, 42(5), pp. 1273–82.

Fulton, E. A., Smith, A. D. M. and Johnson, C. R. 2003. Mortality and predation in ecosystem models: is it important how these are expressed? *Ecol. Model.*, 169.

Fussmann, G. F. and Heber, G. 2002. Food web complexity and chaotic population dynamics. *Ecol. Lett.*, 5, pp. 394–401.

Garcia-Pichel, F. 1994. A model for internal self-shading in planktonic organisms and its implications for the usefulness of ultraviolet sunscreens. *Limnol. Oceanogr.*, 39(7), pp. 1704–17.

Geider, R. J., MacIntyre, H. L. and Kana, T. M. 1996. A dynamic model of photoadaptation in phytoplankton. *Limnol. Oceanogr.*, 41(1), pp. 1–15.

Geider, R. J., MacIntyre, H. L. and Kana, T. M. 1998. A dynamic regulatory model of phytoplanktonic acclimation to light, nutrients, and temperature. *Limnol. Oceanogr.*, 43(4), pp. 679–94.

Geider, R. J. and Platt, T. 1986. A mechanistic model of photoadaptation in microalgae. *Mar. Ecol. Progr. Ser.*, 30, pp. 85–92.

Gillis, D. and Montes, M. 2001. get_distance. Washington DC, Naval Research Laboratory.

Gordon, H. R., Clark, D. K., Brown, J. W., Brown, O. B., Evans, R. H. and Broenkow, W. W. 1983. Phytoplankton pigment concentrations in the Middle Atlantic Bight: comparison of ship determinations and CZCS estimates. *Appl. Opt.*, 22(1), pp. 20–36.

Gregg, W. W. 2001. Tracking the SeaWiFS record with a coupled physical/biogeochemical/radiative model of the global oceans. *Deep Sea Res. II*, 49(1–3), pp. 81–105.

Gregg, W. W. and Walsh, J. J. 1992. Simulation of the 1979 spring bloom in the Mid-Atlantic Bight: a coupled physical/biological/optical model. *J. Geophys. Res.*, 97(4), pp. 5723–43.

Haney, J. D. and Jackson, G. A. 1996. Modeling phytoplankton growth rates. *J. Plankton Res.*, 18(1), pp. 63–85.

He, R. and Weisberg, R. 2002*a*. West Florida shelf circulation and temperature budget for the 1998 fall transition. *Cont. Shelf Res.*, 23(8), pp. 777–800.

He, R. and Weisberg, R. 2002*b*. West Florida shelf circulation and temperature budget for the 1999 spring transition. *Cont. Shelf Res.*, 22, pp. 719–48.

Hood, R. R., Bates, N. R., Capone, D. G. and Olson, D. B. 2001. Modeling the effect of nitrogen fixation on carbon and nitrogen fluxes at BATS. *Deep Sea Res.*, 48, pp. 1609–48.

Hurtt, G. C. and Armstrong, R. A. 1996. A pelagic ecosystem model calibrated with BATS data. *Deep Sea Res. II*, 43(1–2), pp. 653–84.

Hurtt, G. C. and Armstrong, R. A. 1999. A pelagic ecosystem model calibrated with BATS and OWSI data. *Deep Sea Res.*, 46, pp. 27–61.

Ishizaka, J. 1990. Coupling of coastal zone color scanner data to a physical-biological model of the southeastern U.S. continental shelf ecosystem. 3: Nutrient and phytoplankton fluxes and CZCS data assimilation. *J. Geophys. Res.*, 95(11), pp. 20201–12.

Kamykowski, D. 1979. The growth response of a model *Gymnodinium splendens* in stationary and wavy water columns. *Mar. Biol.*, 50, pp. 289–303.

Kamykowski, D. 1981. The simulation of a southern California red tide using characteristics of a simultaneously-measured internal wave field. *Ecol. Model.*, 12, pp. 253–65.

Kirkpatrick, G. J., Millie, D. F., Moline, M. A. and Schofield, O. 2000. Optical discrimination of a phytoplankton species in natural mixed populations. *Limnol. Oceanogr.*, 45(2), pp. 467–71.

Kishi, M. and Ikeda, S. 1986. Population dynamics of 'red tide' organisms in eutrophicated coastal waters – numerical experiment of phytoplankton bloom in the East Seto Inland Sea, Japan. *Ecol. Model.*, 31, pp. 145–74.

Lancelot, C., Billen, G., Veth, C., Becquevort, S. and Mathot, S. 1991. Modelling carbon cycling through phytoplankton and microbes in the Scotia-Weddell Sea area during sea ice retreat. *Mar. Chem.*, 35, pp. 305–24.

Laws, E. A. and Chalup, M. S. 1990. A microalgal growth model. *Limnol. Oceanogr.*, 35(3), pp. 597–608.

Lawson, L. M., Hofmann, E. E. and Spitz, Y. H. 1996. Time series sampling and data assimilation in a simple marine ecosystem model. *Deep Sea Res. II*, 43(1–2), pp. 625–52.

Liew, S., Chia, A. and Kwoh, L. 2001. Evaluating the validity of SeaWiFS chlorophyll algorithm for coastal waters. *Proc. 22nd Asian Conference on Remote Sensing*, Singapore. Singapore, World Scientific Publishing Company.

Litchman, E., Klausmeier, C., van de Schootbrugge, B., Schofield, O. and Falkowski, P. G. 2003. Applying phytoplankton community models to understanding phytoplankton distributions in the paleoocean. Salt Lake City, UT, ASLO Aquatic Sciences Meeting.

Liu, G., Janowitz, G. and Kamykowski, D. 2001. A biophysical model of population dynamics of the autotrophic dinoflagellate *Gymnodinium breve*. *Mar. Ecol. Progr. Ser.*, 210, pp. 101–24.

May, R. M. 1971. Stability in multispecies community models. *Math. Biosci.*, 12, pp. 59–79.

May, R. M. 1973*a*. *Stability and Complexity in Model Ecosystems*. Princeton N. J., Princeton University Press. (Monographs in Population Biology 6.)

May, R. M. 1973*b*. Time-delay versus stability in population models with two and three trophic levels. *Ecology*, 54(2), pp. 315–25.

McCann, K. and Hasting, A. 1998. Weak trophic interactions and the balance of nature. *Nature*, 395, pp. 794–98.

McGillicuddy, D. J. Jr, Robinson, A. R. and McCarthy, J. J. 1995. Coupled physical and biological modelling of the spring bloom in the North Atlantic. II: Three-dimensional bloom and post-bloom processes. *Deep Sea Res. I*, 42(8), pp. 1359–98.

Millie, D. F., Kirkpatrick, G. J. and Vinyard, B. T. 1995. Relating photosynthetic pigments and *in vivo* optical density spectra to irradiance for the Florida red-tide dinoflagellate *Gymnodinium breve*. *Mar. Ecol. Progr. Ser.*, 120, pp. 65–75.

Millie, D. F., Schofield, O. M., Kirkpatrick, G. J., Johnsen, G., Tester, P. A. and Vinyard, B. T. 1997. Detection of harmful algal blooms using photopigments and absorption signatures: A case study of the Florida red tide dinoflagellate, *Gymnodinium breve*. *Limnol. Oceanogr.*, 42(5), pp. 1240–51.

Mills, E. L. 1989. *Biological Oceanography; An Early History, 1870–1960*. Ithaca, N.Y., Cornell University Press.

Mobley, C. D. 1994. *Light and Water: Radiative Transfer in Natural Waters*. San Diego, Calif., Academic Press.

Moisan, J. R. 1994. Modeling nutrient and plankton processes in the California coastal transition zone. *Oceanography*, 7(2), pp. 61–62.

Moisan, J. R. and Hofmann, E. E. 1996. Modeling nutrient and plankton processes in the California coastal transition zone. 1: A time- and depth-dependent model. *J. Geophys. Res.*, 101(10), pp. 22647–76.

Moisan, T. A. and Mitchell, B. G. 1998. Modeling net photosynthesis based on temperature and light in colonial *Phaeocystis Antarctica* Karsten. *Photosynth. Mech. Eff.*, 5, pp. 4105–08.

Moore, J. K., Doney, S. C., Kleypas, J. A., Glover, D. M. and Fung, I. Y. 2001. An intermediate complexity marine ecosystem model for the global domain. *Deep Sea Res. II*, 49(1–3), pp. 403–62.

Naeem, S. and Li, S. 1997. Biodiversity enhances ecosystem reliability. *Nature*, 390, pp. 507–09.

Naeem, S., Thompson, L. J., Lawler, S. P., Lawton, J. H. and Woodfin, R. M. 1994. Declining biodiversity can alter the performance of ecosystems. *Nature*, 368, pp. 734–37.

Neale, P. J. and Marra, J. 1985. Short-term variation of P_{max} under natural irradiance conditions: a model and its implications. *Mar. Ecol. Progr. Ser.*, 26, pp. 113–24.

Neale, P. J. and Richerson, P. J. 1987. Photoinhibition and the diurnal variation of phytoplankton photosynthesis. I: Development of a photosynthesis – irradiance model from studies of *in situ* responses. *J. Plankton Res.*, 9(1), pp. 167–93.

Pahlow, M. 2005. Linking chlorophyll–nutrient dynamics to the Redfield N:C ratio with a model of optimal phytoplankton growth. *Mar. Ecol. Progr. Ser.*, 287, pp. 33–43.

Penta, B. 2000. Phytoplankton competition on the West Florida Shelf: a simulation analysis with red tide implications. St Petersburg, Fla., University of South Florida.

Penta, B. and Walsh, J. J. 1995. A one-dimensional ecological model of summer oxygen distributions within the Chukchi Sea. *Cont. Shelf Res.*, 15(2–3), pp. 337–56.

Prunet, P., Minster, J. F., Echevin, V. and Dadou, I. 1996*a*. Assimilation of surface data in a one-dimensional physical-biogeochemical model of the surface ocean. 2: Adjusting a simple trophic model to chlorophyll, temperature, nitrate, and pCO2 data. *Global Biogeochem. Cy.*, 10(1), pp. 139–58.

Prunet, P., Minster, J. F., Ruiz-Pino, D. and Dadou, I. 1996*b*. Assimilation of surface data in a one-dimensional physical-biogeochemical model of the surface ocean. 1: Method and preliminary results. *Global Biogeochem. Cy.*, 10(1), pp. 111–38.

Riley, G. A. 1946. Factors controlling phytoplankton populations on Georges Bank. *J. Mar. Res.*, 6, pp. 114–25.

Roesler, C. S., Etheridge, S. M. and Pitcher, G. C. 2003. Application of an ocean color algal taxa detection model to red tides in the southern Benguela. In: K. A. Steidinger, J. H. Lansdberg, C. R. Tomas and G. A. Vargo (eds), *Harmful Algae 2002.* Proc. X International Conference on Harmful Algae (20–25 October 2002). St Petersburg, Fla./Paris, Florida Fish and Wildlife Conservation Commission/Intergovernmental Oceanographic Commission of UNESCO.

Smayda, T. and Reynolds, C. 2001. Community assembly in marine phytoplankton: application of recent models to harmful dinoflagellate blooms. *J. Plankton Res.*, 23(5), pp. 447–61.

Steele, J. H. and Henderson, E. W. 1992. The role of predation in plankton models. *J. Plankton Res.*, 14(1), pp. 157–72.

Stumpf, R. P., Culver, M., Tester, P. A., Tomlinson, M., Kirkpatrick, G., Pederson, B., Truby, E., Ransibrahmanakul, V. and Soracco, M. 2003. Monitoring *Karenia brevis* blooms in the Gulf of Mexico using satellite ocean color imagery and other data. *Harmful Algae*, 2(2), pp. 147–60.

Taylor, A. H., Watson, A. J., Ainsworth, M., Robertson, J. E. and Turner, D. R. 1991. A modelling investigation of the role of phytoplankton in the balance of carbon at the surface of the North Atlantic. *Global Biogeochem. Cy.*, 5(2), pp. 151–71.

Thomas, F., Garcon, V. and Minster, J. F. 1990. Modelling the seasonal cycle of dissolved oxygen in the upper ocean at Ocean Weather Station P. *Deep Sea Res.*, 37(3), pp. 463–91.

Tilman, D., Reich, P. B., Knops, J., Wedin, D., Mielke, T. and Lehman, C. 2001. Diversity and productivity in a long-term grassland experiment. *Science*, 294, pp. 843–45.

Tyrrell, T. and Taylor, A. H. 1996. A modelling study of *Emiliania huxleyi* in the NE Atlantic. *J. Mar. Syst.*, 9, pp. 83–112.

Walsh, J., Dieterle, D., Muller-Karger, F., Bohrer, R., Bissett, W., Varela, R., Aparicio, R., Diaz, R., Thunell, R., Taylor, G., Scranton, M., Fanning, K. and Peltzer, E. 1999. Simulation of carbon-nitrogen cycling during spring upwelling in the Cariaco Basin. *J. Geophys. Res.*, 104(4), pp. 7807–25.

Walsh, J., Haddad, K., Dieterle, D., Weisberg, R., Li, Z., Yang, H., Muller-Karger, F., Heil, C. and Bissett, W. 2002. A numerical analysis of landfall of the 1979 red tide of *Karenia brevis* along the west coast of Florida. *Cont. Shelf Res.*, 22, pp. 15–38.

Walsh, J. J., Dieterle, D. A., Meyers, M. B. and Müller-Karger, F. E. 1989. Nitrogen exchange at the continental margin: a numerical study of the Gulf of Mexico. *Progr. Oceanogr.*, 23, pp. 245–301.

Walsh, J. J., Penta, B., Dieterle, D. A. and Bissett, W. P. 2001. Predictive ecological modeling of harmful algal blooms. *Hum. Ecol. Risk Assess.*, 7, pp. 1369–83.

Walsh, J. J., Weisberg, R. H., Dieterle, D. A., He, R., Darrow, B. P., Jolliff, J. K., Lester, K., Vargo, G., Kirkpatrick, G. J., Fanning, K. A., Sutton, T. T., Jochens, A., Biggs, D., Nababan, B., Hu, C. and Muller-Karger, F. E. 2003. Phytoplankton response to intrusion of slope water on the West Florida Shelf: models and observations. *J. Geophys. Res.*, 108(6), pp. 3190–213.

Weisberg, R. and He, R. 2003. Local and deep-ocean forcing contributions to anomalous water properties on the West Florida Shelf. *J. Geophys. Res.*, 108(C), pp. 3184–200.

Wright, S. W., Jeffrey, S. W., Mantoura, R. F. C., Llewellyn, C. A., Bjørnland, T., Repeta, D. and Welschmeyer, N. 1991. Improved HPLC method for the analysis of chlorophylls and carotenoids from marine phytoplankton. *Mar. Ecol. Progr. Ser.*, 77, pp. 183–96.

Wroblewski, J. S. 1977. A model of phytoplankton plume formation during variable Oregon upwelling. *J. Mar. Res.*, 35(2), pp. 357–94.

Wroblewski, J. S., Sarmiento, J. L. and Flierl, G. R. 1988. An ocean basin scale model of plankton dynamics in the North Atlantic. *Global Biogeochem. Cy.*, 2(3), pp. 199–218.

Yamaguchi, M., Itakura, S. and Uchida, T. 2001. Nutrition and growth kinetics in nitrogen- or phosphorus-limited cultures of the 'novel red tide' dinoflagellate *Heterocapsa circularisquama* (Dinophyceae). *Phycologia*, 40(3), pp. 313–18.

Yamamoto, T., Hashimoto, T., Tarutani, K. and Kotani, Y. 2002. Effects of winds, tides and river water runoff on the formation and disappearance of the *Alexandrium tamarense* bloom in Hiroshima Bay, Japan. *Harmful Algae*, 1, pp. 301–12.

Yamamoto, T., Seike, T., Hashimoto, T. and Tarutani, K. 2002. Modelling the population dynamics of the toxic dinoflagellate *Alexandrium tamarense* in Hiroshima Bay, Japan. *J. Plankton Res.*, 24, pp. 33–47.

Yamazaki, A. and Kamykowski, D. 2000. A dinoflagellate adaptive behavior model: response to internal biochemical cues. *Ecol. Model.*, 134, pp. 59–72.

Zonneveld, C. 1998. A cell-based model for the chlorophyll *a* to carbon ratio in phytoplankton. *Ecol. Model.*, 113, pp. 55–70.

Zonneveld, C., van den Berg, H. A. and Kooijman, S. A. L. M. 1997. Modeling carbon cell quota in light-limited phytoplankton. *J. Theor. Biol.*, 188, pp. 215–26.

20

Use of real-time observations in an operational ocean data assimilation system: the Mediterranean case

N. Pinardi, C. Fratianni and M. Adani

20.1 Introduction

Real-time observations are essential for operational forecasting that in turn can be used to predict changes of the state of the ocean and its associated biochemical fields. In addition, real-time observations are useful to detect changes in the past with the shortest delay, to standardize practices in data collection and to exchange data between remote regions of the ocean and seas. The drawback is that real-time observations could be less accurate than their delayed mode counterparts due to the time constraints for data dissemination. *In situ* real-time data are usually decimated to be transmitted in real time (loss of accuracy and resolution), whereas satellite data are corrected with approximate algorithms and less ancillary data. Delayed mode quality control analysis increases the value of the observational data set, flagging outliers and producing climatological estimates of the state of the system. Thus real-time data, together with a modelling system and the climatological estimates, can give also the appropriate information for scientific studies and applications.

The principles of operational science started to develop in the 1940s and 1950s, based on the combined use of real-time data and modelling systems that can extend the information from observations in space and time. Operational science is based on a sound knowledge of the dynamics and processes for the space/timescales of interest and operational meteorology and oceanography have started to implement these principles to weather and ocean forecasting.

In the past 20 years, operational meteorology has become a reality with a network of *in situ* and satellite observations that has made the weather forecast capable of extending the theoretical limit of predictability of the atmosphere (only one-two days theoretically, now forecasts are useful for more than five days on average). Today meteorological observations are mainly used in their assimilated form even if observations are still collected for specific process-oriented studies. Recently the meteorological re-analysis projects (Gibson et al., 1997; Kalnay et al., 1996) have released a wealth of data to be understood and analysed. These data sets are coherent and approximately continuous (daily), filling the observational gaps in space and time with a dynamical interpolation scheme. The model and the real-time observations are fused in one best estimate of the state of the system by data-assimilation techniques that have been developed to a great degree of sophistication in recent years (Lorenc, 2002). The re-analysis data are now forming the basic reference data set to understand climate variability in the atmosphere and upper oceans.

Dynamical interpolation/extrapolation of observational data for operational forecasting in the ocean began to be investigated at the beginning of the 1980s and the first successful forecasts were carried out in the open ocean (Robinson and Leslie, 1985). These exercises required real-time data that were initially collected with rapid ship surveys realizing adaptive sampling schemes and collecting a combination of traditional recoverable and expendable instruments (CTD, XBTs). At the same time but in a totally independent way, shelf scale and coastal real-time data from moored and drifting sensors such as meteorological buoys and sea-level stations started to be used for shelf scale storm surge operational forecasting (Prandle, 2002). Operational oceanography is now building on this experience and considers real-time measurements from opportunity platforms and satellites in a manner very similar to operational meteorology.

This chapter aims to show the use of real-time observations in a state-of-the-art ocean-predicting system realized in the Mediterranean. We discuss the pre-processing schemes required to properly assimilate the observations into an operational nowcasting/forecasting system, elucidate the role and impact of different observations in the assimilation system and show the use of real-time data to evaluate the quality of the modelling system.

We start with the description of the Mediterranean Forecasting System (MFS) real-time observing system and pre-processing quality control in Section 20.2, we then describe the modelling and assimilation system in relation to the impact of different real-time observations in Section 20.3. In Section 20.4 we evaluate the consistency, quality and accuracy of the forecasting system using model-data intercomparison and Section 20.5 offers conclusions.

20.2 Real-time observing system for operational forecasting in the Mediterranean

Based on the earlier open ocean forecasting experience, a Mediterranean Forecasting System (MFS) began to be implemented in the Mediterranean basin, the topography of which is reproduced in Figure 20.1. The average depth of the basin is 1,500 m and in several regions we reach over 3,000 m. Thus the initial observing system was chosen to be consistent with the main components of the Global Ocean Data Assimilation Experiment (GODAE) observing system[96] (Smith and Lefevre, 1997).

The major elements are: (a) satellite remote sensing for sea surface height (SSH) and sea surface temperature (SST); (b) voluntary observing ship (VOS) for temperature profiles (Rossby et al., 1995); (c) moored buoy systems such as the TAO array in the Pacific (McPhaden et al., 1995) but modified for the Mediterranean needs; (d) subsurface drifting and profiling floats such as ARGO. In the Mediterranean all these elements have been considered and implemented during the Pilot Project phase of MFS (Pinardi et al., 2003), with the exception of the ARGO floats that have been implemented starting from October 2004, in the second phase of the MFS programme (http://www.bo.ingv.it/mfstep).

The design of the real-time observing system is based on knowledge of the large-scale structure of the circulation. Figure 20.2 shows the simulated mean sea level from 1993 to 1999 with the operational Ocean General Circulation Model (OGCM) of MFS. The OGCM used is described in Pinardi et al. (2003), to which the interested

[96]http://www.bom.gov.au/bmrc/ocean/GODAE/

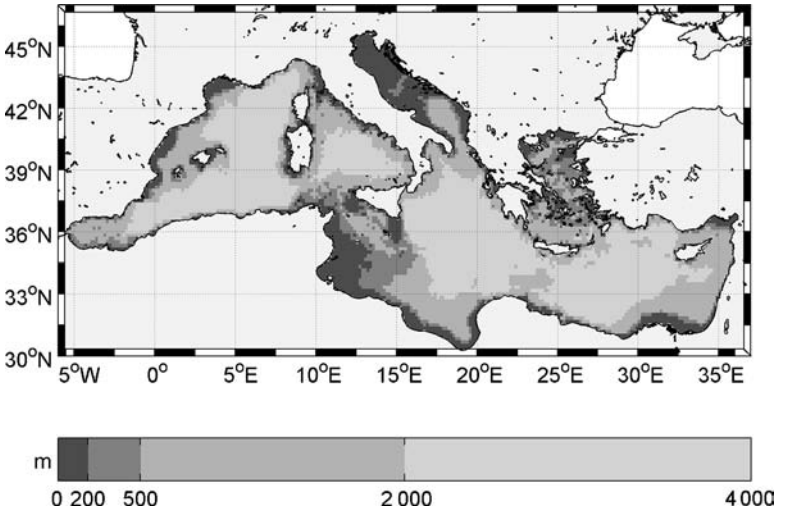

Figure 20.1
Mediterranean bottom topography (1/60) in metres.

reader should refer for details. The basin scale circulation is characterized by large-scale meridional SSH gradients that the observing system should sample. In addition, it is composed of large-scale sub-basin scale gyres (cyclonic in the North and anticyclonic in the south) that have intensified currents and open ocean jets at their borders. Most of these sub-basin scale gyres have large amplitude variations at seasonal and interannual

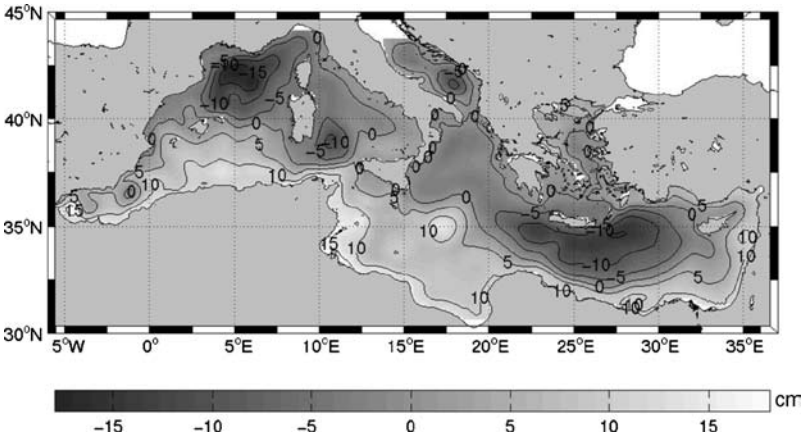

Figure 20.2
1993–99 average sea surface height (SSH) simulated by the MFS operational OGCM. The negative values correspond to SSH depressions due to waters heavier than their surroundings; the positive values correspond to warmer/fresher and lighter waters that 'expand the water column'.

timescales (Korres et al., 2000; Molcard et al., 2002; Demirov and Pinardi, 2002) and the large-scale observing system should resolve them.

Moreover, the primary productivity of the basin is low and inserts the Mediterranean between the mid-latitude oligotrophic areas of the world oceans. This means that coastal to open ocean gradients in primary productivity are large and that the open ocean regimes are characterized by a subsurface chlorophyll maximum. Thus the large-scale monitoring system should be able to monitor the open ocean biochemical fluxes and this was initially decided to be done with the mooring system and the satellite data (colour). In future, the multidisciplinary sensors will also be added to VOS and subsurface autonomous vehicles, such as gliders.

In addition to oceanic data, the operational forecasting system requires real-time atmospheric data sets from analyses and forecasts. This is an important data set and it is also described in one of the following sections. The information content of all these real-time data sets, and the quality control procedures and preprocessing needed before these data can be inserted into the assimilation system, are described below.

20.2.1 Satellite data

Satellite SSH and SST data compose nowadays the basis for the real-time monitoring of the open ocean and coastal areas. Even if the SSH data are not accurate enough near the lateral boundaries of the basin (data normally stop about 20–30 km from the coast), this data set is essential to initialize the internal flow field of local models and give the correct open boundary conditions wherever necessary. SST instead is at high resolution (1 km) and also high frequency (twice a day at least) and thus it is an important component of the coastal and open ocean observing system.

Following Le Traon (2002) the altimetric signal can be decomposed into four parts:

$$\mathrm{SSH} = N + \eta + \Sigma + \varphi, \tag{20.1}$$

where N is the geoid, η is the dynamic topography, Σ is the measurement errors (due to orbit error, atmospheric corrections, etc.) and φ are the high-frequency components of sea level due to tides and atmospheric surface pressure (sometimes a simple inverse barometer) effects. We are interested in the η signal, which is connected to the wind and thermohaline driven circulation. In this chapter we will assume that high-frequency effects are subtracted before using the SSH data for assimilation. This choice is different in other parts of the world ocean, where the high-frequency component of sea level can have very different amplitude. This makes it difficult to have a unique pre-processing scheme for altimetry, but several options should be made available to the operational community in the near future.

The dynamic topography contains the steric or baroclinic and barotropic signals, i.e.

$$\eta = \frac{1}{H}\left\{ f\frac{\psi}{g} + \frac{1}{\rho_0}\int_{-H}^{0} \rho\, z\,\mathrm{d}z + \frac{H}{\rho_0}\int_{-H}^{0} \rho\,\mathrm{d}z \right\} \tag{20.2}$$

where geostrophic balance has been assumed and the symbols are explained in the footnote[97] (Pinardi et al., 1995). The first term on the right of (20.2) is the barotropic

[97]Symbols: ρ is the water density and ρ_0 its constant value, H is the bottom depth supposed to be constant, f is the Coriolis parameter, g is the gravity acceleration, ψ is the barotropic streamfunction in Sverdrup ($10^6 \frac{m^3}{s}$) defined as $\vec{\overline{u}} = \frac{1}{H}\hat{k}\, x\, \nabla\psi$ and $\vec{\overline{u}} = \frac{1}{H}\int_{-H}^{0} \vec{u}\,\mathrm{d}z'$ and $\hat{\mathrm{k}}$ is the vertical unit vector.

component while the last term is the bottom pressure. The integral in the middle term is a 'potential energy' term, as defined by Mellor (1996), but we refer to it simply as the baroclinic term.

The dynamic topography can be decomposed into a mean part $\overline{\eta}$, and the variability, indicated by η' and called sea level anomaly (SLA). Generally the geoid N is not known with sufficient accuracy and it is then subtracted by taking the average of the sea level along the tracks. This eliminates N and the mean dynamic topography $\overline{\eta}$ from (20.1). Then only SLA observations are made available in real time and operationally. This is a major pre-processing of the SLA data, that requires the knowledge of the long-term mean of SSH along satellite tracks. Such mean contains both the geoid and the mean dynamic topography and it is not possible to distinguish between them. Only the addition of information from independent satellites, such as GOCE and GRACE (Le Traon, 2002) that measure independently the marine geoid, will allow the estimation of the mean dynamic topography from satellite observations. Several attempts have been made in the past, using mainly large-scale geoid models and *in situ* data but they are far from having enough accuracy to be used in real-time estimation of along track SSH for assimilation into dynamical models. Thus in operational systems, the real-time satellite altimetry data are given in terms of SLA, with or without the high-frequency component, φ, subtracted.

Two pre-operational satellites were working for the past 10 years, Topex/Poseidon and ERS-2, and they covered the Mediterranean quite extensively (Figure 20.3). For the Mediterranean, the geoid and mean dynamic topography was calculated from the average of along track SSH for the period 1993–99. SLA is then released weekly with an estimate of the orbit error since the value of Σ depends above all on the precision of the satellite orbit computation and this requires environmental ancillary data that are not available in real time (Le Traon and Ogor, 1998). It has been shown that the accuracy of real-time SLA and delayed mode data is now comparable (Buongiorno et al., 2003).

The SLA signal described by (20.2) contains the large-scale, slowly moving components of the sea level, also called the geostrophic components of the sea level. These components are mainly due to the seasonal thermohaline changes, in turn due to air/sea buoyancy fluxes and their penetration in the water column. The baroclinic signals due to the air/sea physics (also momentum fluxes due to wind stress) are strongly modulated by the mesoscale eddy field and the

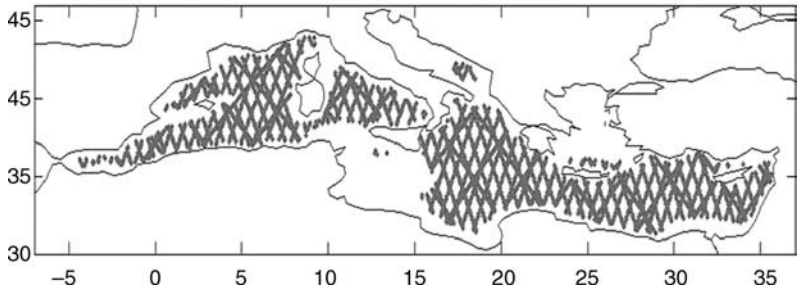

Figure 20.3
Topex/Poseidon and ERS-2 superimposed tracks with respectively 10- and 35-day repeating cycles, 2002.

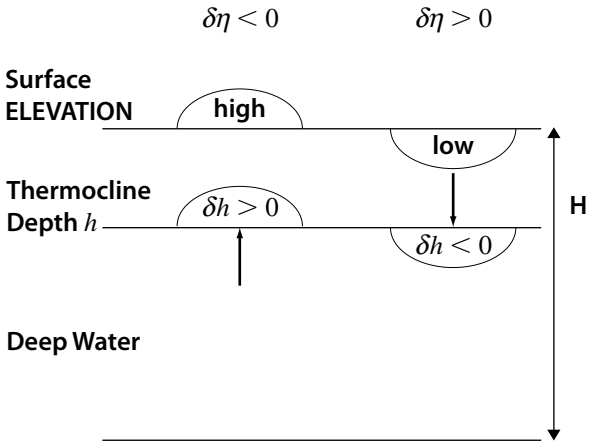

Figure 20.4
Schematic of the vertical displacement that correlates the surface elevation with the isopycnal displacements (δh).
Source: Redrawn from Haines (2002).

sub-basin scale gyres that compose the Mediterranean Sea circulation structures (Pinardi and Masetti, 2000). The barotropic signals are mainly wind driven and they couple with the baroclinic effect at the eddy field space scales. Assimilating SLA in a general circulation model, as described below, means that the model should be corrected for this slowly moving component of the sea level. The typical geostrophic relationship at these time and space scales is that SLA is high where subsurface temperature is also high, and vice versa. This means that the slope of isotherms and SLA have an opposite sign. Haines (2002) showed this concept with the diagram reproduced in Figure 20.4 where the surface elevation is correlated with isopycnal depths (δh).

Mellor and Ezer (1991) demonstrated for the first time that SLA described by (20.2) is strongly correlated to the thermocline depth in the Atlantic subtropical gyre and Masina et al. (2001) showed that this is true also for the tropical regions of the ocean. This means that this information should be used for insertion of the data into an assimilation system. As seen from (20.2) all components of SLA are integral quantities and assimilation should correlate the SLA signal with the model state variables, in particular temperature and salinity profiles, either through the observational operator H, described in the next sections, or with statistical correlations contained in the background error covariance matrix. The SLA for short-term forecasts is then the integrated effect on the geostrophic timescales (approx. two to three days for the Mediterranean) of thermocline displacements due to mesoscale or sub-basin scale gyre variability.

The other real-time satellite data set that is important for assimilation into forecasting models is the sea surface temperature (SST). This is the oldest real-time data set available but pre-processing algorithms for the space radiometer signal are under continuous development. The algorithms for SST retrieval from radiances use information from *in situ* temperatures to calibrate the parameters of the algorithm itself.

The most used sensor is AVHRR (Advanced Very High Resolution Radiometer), flown by NOAA satellites, and the best algorithm both for the Mediterranean and the world ocean is now the Pathfinder algorithm.[98] The algorithms can be applied rapidly to night time and daytime images but the latter are more of a problem as sun glitter effects and high humidity in the air layer adjacent to the sea surface, especially in the Mediterranean, can affect the SST signal received by the radiometer. A new project, the Global High Resolution Sea Surface Temperature Pilot Project, is being launched where the quality of AVHRR real-time data will be assessed for different users in the context of GODAE.[99]

SST contains information about two major processes occurring in the ocean: the first is the warming/cooling processes due to air/sea interaction physics and the second is the mesoscale/gyre structures that produce local changes in temperature due to geostrophic isotherm displacement. One example of the latter process is the detachment of cold and warm core rings across the Gulf Stream front that produces SST anomalies due to the dynamical instabilities of the oceanic jet that transfer water of different SST properties across the Gulf Stream front.

With regard to the air/sea interaction processes, another way to say that SST is affected by exchange of heat at the air/sea interface is that SST contains the information about the dynamics of the surface mixed layer. This layer can mask the geostrophic SST contribution, as it happens for cold core rings that frequently, after their birth, have their 'geostrophic SST anomaly' masked by intense air/sea interaction heat exchanges.

The most common way to use real-time SST or assimilate SST in operational models is to use SST to correct for inaccurate air/sea fluxes at the surface boundary of the models. Normally the correction is carried out via a restoring term, also called a nudging term, that adds to the heat flux term, such as

$$Q_{\text{corr}} = Q - \left.\frac{\partial Q}{\partial T}\right|_{T=T^*} (T - T^*) \tag{20.3}$$

where Q is the net heat flux at the air/sea interface, T^* is the observed SST, T is the SST produced by the model when only Q is used. The coefficient $\left.\frac{\partial Q}{\partial T}\right|_{T=T^*}$ in (20.3) is taken to be constant and different values have been chosen from the basin scales to the subregional Seas (Pinardi et al., 2003).

20.2.2 The *in situ* platforms and sensors

One of the main components of the *in situ* large-scale real-time monitoring system for the world ocean is based on the Voluntary Observing Ship (VOS) system that relys on commercial ship lines for the deployment of expendable temperature sensors, such as eXpendable BathyThermographs (XBT). The ship tracks implemented in the first phase of MFS are reproduced in Figure 20.5: data were transmitted in real time from the ships to the collecting centre (Manzella et al., 2003) and then to the modelling centre.

The temperature profiles on all tracks were taken outside the 200 m depth areas and were collected down to 700 m to resolve the subsurface temperature maximum associated with the Levantine Intermediate Waters in the Western Mediterranean. These data are normally decimated since the satellite telecommunication system used (ARGOS) has a low transmission speed. This is done for the world ocean and it was also tried

[98]Information available at: http://podaac.jpl.nasa.gov/sst
[99]http://www.ghrsst-pp.org/

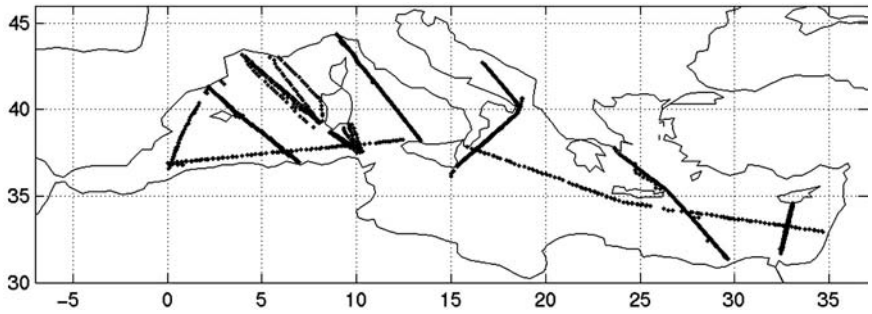

Figure 20.5
VOS-XBT system set up from September 1999 to December 2000 in the Mediterranean.

for the Mediterranean. However, it was found that the standard automatic decimation system for VOS did not cope for drastic changes in the vertical stratification, as they occur in the Mediterranean. The worldwide VOS-XBT programme considers the transmission only of 10–15 points along the temperature profile, computed at the profile's inflection points. When the vertical profiles become quasi-uniform with depth, many XBT samples were badly decimated by the standard on board ship-software. In the Mediterranean, winter mixing is very intense and stratification is rapidly lost for about three months each year. The XBT automatic decimation algorithm is poorly adaptive to these conditions and almost 30% of the data were lost due to the decimation software failures.

Smith et al. (1999) stated: 'all upper ocean thermal data are to be distributed as soon as is practical after measurements (preferably 12 hours). The strong preference is to keep intervention to a minimum, perhaps just automated processes. There should be a well-supported second stream, which allows for improved quality control and scientific evaluation of the data sets.' The MFS VOS system started to send full resolution profiles in real time and realized a new system of real-time data quality control that will store quality checked XBT data in oceanographic archives (Manzella et al., 2003).

The near-real-time quality control procedure contains seven steps that in synthesis are:

- position control;
- elimination of spikes;
- interpolation at 1 m intervals;
- gaussian smoothing;
- general malfunction control;
- comparison with climatology;
- visual check, confirming the validity of the profiles and providing an overall consistency.

The XBT data set is then inserted into the assimilation system. The vertical temperature profile is a basic state variable of the physical system, containing information about several processes and in particular the vertical density distribution. In addition, being the data collected in a section-like track, the temperature field gradients along track give approximately the geostrophic velocity field across the track itself. In the Mediterranean, as well as in other temperate seas, temperature should be adequately combined to salinity to describe the basin water masses and derive the geostrophic velocity field across the VOS ship track. Most of the data assimilation systems, as it will

be seen later, can update both temperature and salinity profiles starting from the single temperature profile, keeping the historical water mass relationship in consideration.

Raicich and Rampazzo (2003) simulated the impact of VOS-XBT data in the reduction of initial errors in the ocean general circulation model. It was found that repeated long tracks, such as the trans-Mediterranean track going from Gibraltar to Haifa, had a very positive impact on the error reduction due to the consistent improvement of the geostrophic velocity field associated with the coherent temperature section given by the track.

Another kind of observing system that nicely complements the VOS is the moored buoy system. Such a system was first developed in real time for the Pacific ocean (McPhaden et al., 1995) and the Bermuda testbed mooring (Dickey et al., 1998) and is now being developed for other areas. The data collected by such a measuring system are multidisciplinary and at high temporal frequency for the physical and biochemical components of the marine ecosystem. These point-like measurements should be mainly used as an independent data set to validate both model and data assimilation components. For the Mediterranean such a system was first developed in the Cretan Sea and it is described in Nittis et al. (2003). Here it is sufficient to say that the system allows the correlation between the physical and biochemical components of the marine ecosystem at high time frequency (normally a few minutes) to be explored for the first time. A network of buoys is being developed under the second phase of MFS.

Finally the ARGO profilers, collecting temperature and salinity profiles from 700 m depth to the surface, have been deployed in the Mediterranean.[100] This completes the 'open ocean' basic monitoring components for the region.

20.2.3 Atmospheric forcing data

Ocean forecasts are driven by atmospheric forecasts. Atmospheric forcing is also used, by means of 'analyses', during intermittent data assimilation steps. The atmospheric analyses are an optimal combination of observations and atmospheric general circulation models outputs, that is they are the best estimation of the past and present state of the atmosphere. They have substituted for many purposes the direct observations for the real-time assessment of the atmospheric state. These analyses are now produced twice a day by the major meteorological offices around the world.[101] Forecasts are also produced at least twice a day from the major meteorological centres and the accuracy of the analysis scheme is constantly increasing with time.

The atmospheric forcing for ocean models is derived from atmospheric surface variables using interactive bulk formulas that relate the model SST with the air temperature, relative humidity, cloud cover and winds at the sea surface (Castellari et al., 1998). The short-term ocean forecast is driven by the atmospheric forecast surface fields (see Figure 20.6). Any error in the input of atmospheric data will affect the quality of the ocean forecast. Some authors think that such error is large compared with other errors, that is initial conditions specification, that it should specifically considered in the assimilation procedure. This error is mainly due to the offline coupling between the atmosphere and the ocean, that is the atmospheric surface variables do not see the ocean forecast SST and currents since they are coupled after the atmospheric forecast has been performed. This is why the correction in (20.3) is usually applied to the computed air/sea fluxes. Only fully or synchronous atmosphere-ocean coupling

[100] http://www.moon-oceanforecasting.eu
[101] http://www.ecmwf.int

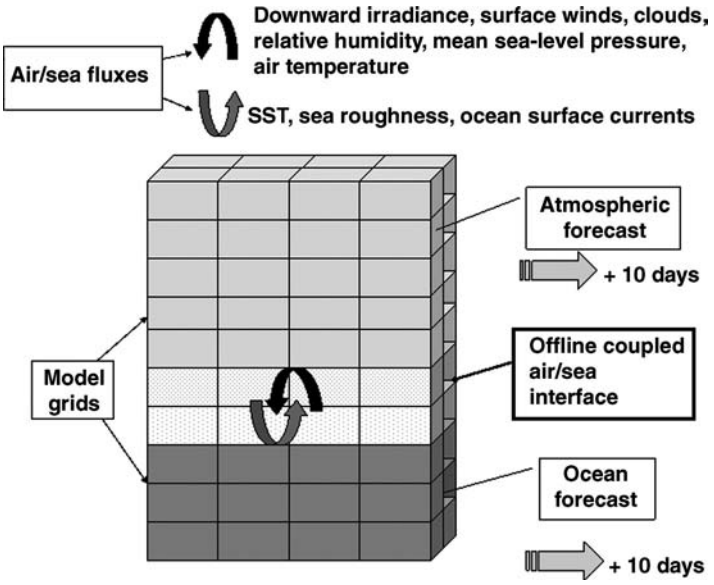

Figure 20.6
Schematic of the offline air/sea coupling for ocean forecasting.

will alleviate this error and seasonal forecasts are carried out nowadays with the fully coupled ocean-atmosphere system without heat flux corrections.[102]

The most inaccurate data set in meteorological models is the accumulated precipitation field that modifies the water flux into the ocean. However, this error drives very long-timescale ocean responses and short-term forecasting should not be greatly affected by such inaccuracy. More important is the wind stress or momentum flux error produced by the coarse atmospheric winds resolution and the bulk formula parameterizations used at the air/sea interface. Such error impacts the tropical Pacific predictability so that, in the past, a special wind stress data set was developed to account for higher space and time frequency of the forcing (FSU tropical Pacific winds, Legler et al., 1988). In the Mediterranean several empirical factors were found that normally increase the wind stress amplitude to reach better agreement between modelled and measured waves (Cavaleri et al., 1992). The increased resolution of numerical weather prediction models and the improvement in data assimilation schemes will make obsolete the use of such empirical factors. Recent developments have shown, however, that the high wave number content of scatterometer winds (Milliff et al., 1999) is far from being reproduced by the present atmospheric forecasting systems and new blending procedures are being developed (Milliff et al., 2001) that produce high wave number content wind fields to realistically force the ocean.

The timely provision of meteorological analyses and forecasts is at the basis of real-time delivery of ocean forecasts. Future developments will involve the coupling of high-resolution non-hydrostatic meteorological models with the ocean counterpart, but this crucial area is still in its infancy.

[102]http://www.ecmwf.int/products/forecasts/seasonal/

20.3 Modelling and assimilation system

20.3.1 Combination of different sources of information: observations and models

Gauss in 1809 wrote: '.. since our measurements and observations are nothing more than approximations to the truth, the same must be true of all the calculations resting upon them, and the highest aim of all computations made concerning concrete phenomena must be to approximate, as nearly as practicable, the truth.' With this statement, he solved the problem of the determination of the planet's motion by fitting via the least-squares method several parameters to the measurements. Astronomical theory gave insight on which parameters to fit and measurements determined their optimal values. Both theory and measurements gave rise to the 'best estimate' of the truth. In modern times, theory is substituted with numerical models based on the general equations of hydrodynamics. Gauss's statement can be taken as the basis of modern oceanic and atmospheric estimation theory. In what follows we review the work of Lorenc (2002) and Daley (1996) about data assimilation.

Data assimilation is defined by Lorenc (2002) as 'the process of finding the model representation which is most consistent with the observations'. This concept goes back to Gauss's statement in the sense that in order to obtain the best estimate of reality, two different approximations of truth are used, one from observations and the other from the dynamical model. Data assimilation in the ocean and atmosphere fuses these two approximations of reality in an optimal estimate of truth with a least-square method approach (errors should be unbiased, random and normally distributed).

In atmospheric and oceanic data assimilation systems, the 'truth' or 'true state' is generally assumed to be a state of the atmosphere or the ocean that has the fast motion filtered out (sound waves and fast barotropic gravity waves are not considered). Furthermore, the atmosphere and the ocean are considered to be close to horizontal non-divergence (geostrophic approximation) and the flow is assumed to be 'smooth', that is sharp changes are not allowed within few model grid points. This means that observations, taken at finite time and space resolution, can give information about the truth and the model needs to have appropriate parameterizations of sub-grid scale phenomena that will not drive the solution too far from the geostrophic balance.

Let us take the 'true' ocean state vector to be

$$X = \begin{bmatrix} T \\ S \\ U \\ V \\ W \\ \tilde{n} \\ \theta \\ Ç \end{bmatrix} \tag{20.4}$$

where the symbols indicate (from top to bottom): three-dimensional fields of temperature, salinity, zonal, meridional, vertical velocity components, water density and

two-dimensional fields of barotropic streamfunction (defined in Note 97) and free surface elevation or SSH. Some of these state variables are prognostic, that is their time evolution can be described by an equation containing their time rate of change, some are simply diagnostic, such as density, vertical velocity and free surface elevation. Vertical velocity is diagnostic because the hydrostatic approximations has been adopted in the OGCM; SSH is considered to be diagnostic as we regard it as only the slowly moving component of sea level and fast barotropic external gravity waves are filtered out. SSH can be mathematically a prognostic variable but we consider in the data assimilation that the true state of the ocean contains only the diagnostic components of SSH as written in (20.2).

Suppose that we have two approximations of **X** which we now consider only to be a scalar value X, corresponding to one of the state variables contained in (20.4) at one single grid point. The first approximation is a numerical model solution, called X^{b}, with an error $E^{\mathrm{b}} = X^{\mathrm{b}} - X$ and the second is an observation, called Y^{o}, with an associated error $E^{\mathrm{o}} = Y^{\mathrm{o}} - X$, occurring at the same location of the model first guess. We assume that the error probability distribution is Gaussian, i.e.

$$p(E) = \frac{1}{\sigma\sqrt{2\pi}} \mathrm{e}^{-\left(\frac{E^2}{2\sigma^2}\right)}, \tag{20.5}$$

where $\sigma^2 = \langle E^2 \rangle$ and the brackets indicate the expectation operator (Daley, 1996). The joint probability distribution for the two approximations to truth is:

$$p(E^{\mathrm{b}})\,p(E^{\mathrm{o}}) = \frac{1}{\sigma_{\mathrm{b}}\sigma_{\mathrm{o}}\sqrt{2\pi}} \mathrm{e}^{-\left(\frac{E^{\mathrm{b}2}}{2\sigma_{\mathrm{b}}^2} + \frac{E^{\mathrm{o}2}}{2\sigma_{\mathrm{o}}^2}\right)} \tag{20.6}$$

If we want to make this probability maximum, we need to impose that the exponent in (20.6) has a minimum value. Calling the exponent I, written as

$$\mathrm{I} = \frac{1}{2}\left[\frac{(X^{\mathrm{b}} - X)^2}{\sigma_{\mathrm{b}}^2} + \frac{(Y^{\mathrm{o}} - X)^2}{\sigma_{\mathrm{o}}^2}\right], \tag{20.7}$$

the minimum is achieved at the value X^{a}, so-called analysis, that is:

$$X^{\mathrm{a}} = X^{\mathrm{b}} + \left(\frac{\sigma_{\mathrm{b}}^2}{\sigma_{\mathrm{b}}^2 + \sigma_{\mathrm{o}}^2}\right)\left(Y^{\mathrm{o}} - X^{\mathrm{b}}\right). \tag{20.8}$$

The second term between brackets is called the *misfit*, $Y^{\mathrm{o}} - X^{\mathrm{b}}$, that is the difference between the model solution and the observations. The analysis value, or best estimate X^{a}, is then the weighted average of the first guess, X^{b}, and the misfit between the observations and the model. The misfit clearly cannot be very large and this means that the model and the observations should be as close as possible. This means that model should be quite realistic, reproducing the 'bulk' of the physical processes contained in the data.

In general, the observations will be at different locations with respect to the model grid points and they could be related to state variables contained in **X** by a complex operator (indirect measurements of state variables). This means that in general we can write the misfit as:

$$\mathbf{d} = \mathbf{Y}^0 - H(\mathbf{X}^\mathrm{b}) \tag{20.9}$$

where H is the observational operator and $\mathbf{d}$, $\mathbf{Y}^0$, $\mathbf{X}^\mathrm{b}$ are now multivariate vectors in the four-dimensional space. Normally H is an interpolation from the model grid to the observational point but in case of diagnostic quantities, such as SSH, it can be a non-linear operator containing a combination of $\mathbf{X}^\mathrm{b}$ state variables. The generalization of (20.7) and (20.8) considering (20.9) for the fully multivariate case are

$$\mathrm{I} = \frac{1}{2}\left[(\mathbf{X}^\mathrm{b} - \mathbf{X})^T \mathbf{B}^{-1}(\mathbf{X}^\mathrm{b} - \mathbf{X}) + (\mathbf{Y}^\mathrm{o} - H(\mathbf{X}))^T \mathbf{R}^{-1}(\mathbf{Y}^\mathrm{o} - H(\mathbf{X}))\right] \tag{20.10}$$

$$\mathbf{X}^\mathrm{a} = \mathbf{X}^\mathrm{b} + \mathbf{K}(\mathbf{Y}^\mathrm{o} - H(\mathbf{X}^\mathrm{b})), \tag{20.11}$$

where

$$\mathbf{K} = \mathbf{B}\mathbf{H}^T(\mathbf{H}\mathbf{B}\mathbf{H}^T + \mathbf{R})^{-1} \tag{20.12}$$

is the Kalman gain matrix. In (20.12) the observational operator appears as the linearized operator, **H** of H. The background error covariance matrix is then defined as:

$$\mathbf{B} = \left\langle (\mathbf{X}^\mathrm{b} - \mathbf{X})(\mathbf{X}^\mathrm{b} - \mathbf{X})^T \right\rangle, \tag{20.13}$$

which represents the error variance for all the model state variables and their cross-correlation. The observational error covariance matrix is represented by **R**.

The similarity between the simple form of weights in (20.8) and (20.11) should be noted: in both cases the weight on the misfit is given by the error in the background field divided by the sum of the error in the observations and the error in the background field again. If the time variations of **B** are parameterized only by changes in the variance of the error fields, then the form (20.12) defines an optimal interpolation (OI) scheme. The essence of sequential data assimilation is to find a sound representation of the multivariate aspects and space-time variability of **B**. Normally the variations and the multivariate character of **B** is chosen *a priori*, on the basis of the knowledge of the relevant processes included in the model and in the observations.

Evaluation of (20.11) can be done 'intermittently', collecting observations within a certain interval of time and inserting them at the end of such interval. Figure 20.7 illustrates a typical intermittent assimilation cycle that in the atmosphere is taken to be 12 or 6 hours, while for the ocean it is generally taken to be several days (Pinardi et al., 2003). In the atmospheric forecasting community, the continuous data assimilation or variational assimilation scheme (Daley, 1996) is now used but it is not described here.

Figure 20.7 illustrates the analysis and forecast cycle for a generic time interval Δt. Every interval cycle, (20.12) is evaluated and the dynamical model is initialized

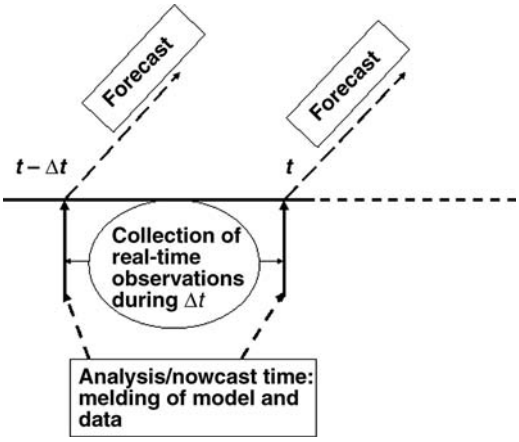

Figure 20.7
Intermittent analysis-forecast cycle.

with $\mathbf{X}^{a}$. The ocean forecast is started using forecasted surface atmospheric parameters and solving for several time steps, δt, a nonlinear equation:

$$\mathbf{X}^{b}(t+\delta t) = M\,\mathbf{X}^{a}(t), \tag{20.14}$$

where M is the state transition matrix corresponding to the model equations (belonging to the OGCM in this case). The background or forecast fields $\mathbf{X}^{b}$ predicted by (20.14) is used as a first guess, in the successive Δt assimilation cycle, to compute a new $\mathbf{X}^{a}$.

20.3.2 What does it mean to assimilate different data sets and correct model state variables?

The quality and efficiency of the estimation algorithm outlined above is clearly connected to the details of the background error covariance matrix, **B**. First of all, we do not know the truth of **X** contained in (20.13) and thus several approximations are normally taken. To estimate **B** we can consider

$$\mathbf{B} = \left\langle (\mathbf{X}^{b} - \mathbf{X}^{a})(\mathbf{X}^{b} - \mathbf{X}^{a})^{T} \right\rangle \tag{20.15}$$

or

$$\mathbf{B} = \left\langle (\mathbf{X}^{b} - \bar{\mathbf{X}}^{b})(\mathbf{X}^{b} - \bar{\mathbf{X}}^{b})^{T} \right\rangle \tag{20.16}$$

or

$$\mathbf{B} = \left\langle (\mathbf{Y}^{o} - \bar{\mathbf{Y}}^{o})(\mathbf{Y}^{o} - \bar{\mathbf{Y}}^{o})^{T} \right\rangle, \tag{20.17}$$

where the 'bar' above the state vectors indicates a suitable time mean. The brackets indicate the ensemble mean of the different realizations available to estimate **B**. Let us discuss in turn each of these approximations. The first in (20.15) indicates that

the error is estimated from the difference between the forecast and the analysis: this will give the most adequate approximation to (20.13). The second and the third approximations contained in (20.16) and (20.17), mean that the error is due to the variance containing part of the state variables with respect to a predefined mean. From a mathematical point of view, the worse approximation to **B** is given by (20.17) as we assume that the variance contained in the observations is the same as in the model. However, most practical data assimilation systems use (20.17) to estimate **B** as the model could have drifted from reality and the use the covariances deduced from the model itself could affect the efficiency of the assimilation system (20.11).

Hereafter, we consider that **B** is calculated from a form of either (20.16) or (20.17), which we now rewrite as

$$\mathbf{B} = \left\langle \tilde{\mathbf{X}}' \, \tilde{\mathbf{X}}'^{T} \right\rangle,$$

where the primes now indicate anomalies with respect to a suitable mean and $\tilde{\mathbf{X}}$ can be either model or observational fields. The important information contained in **B** is the cross-correlation between all the state variables of our system. In other words, **B** is multivariate and composed of block matrices:

$$\mathbf{B} = \begin{vmatrix} \langle \mathbf{T}'\mathbf{T}' \rangle & \langle \mathbf{T}'\mathbf{S}' \rangle & .... & .... & \langle \mathbf{T}'\boldsymbol{\eta}' \rangle \\ \langle \mathbf{S}'\mathbf{T}' \rangle & \langle \mathbf{S}'\mathbf{S}' \rangle & ... & & \langle \mathbf{S}'\boldsymbol{\eta}' \rangle \\ \langle \mathbf{U}'\mathbf{T}' \rangle & & \langle \mathbf{U}'\mathbf{U}' \rangle & & .... \\ ... & ... & & .... & .... \\ \langle \boldsymbol{\eta}'\mathbf{T}' \rangle & \langle \boldsymbol{\eta}'\mathbf{S}' \rangle & ... & ... & \langle \boldsymbol{\eta}'\boldsymbol{\eta}' \rangle \end{vmatrix}, \qquad (20.18)$$

where the tides have been neglected for simplicity and several sub-matrices have not been explicitly written in (20.18). Each block is quite dense but banded, it contains the variance of the error associated with each field and it represents the cross-correlation between state variable errors in space. The brackets indicate a given ensemble average as before.

For the ocean, De Mey and Benkiran (2002) suggested a possible expression for **B**, that is

$$\mathbf{B} \cong \mathbf{F}\,\mathbf{Br}\,\mathbf{F}^{T}, \qquad (20.19)$$

where **F** contains multivariate *vertical* empirical orthogonal functions (v-EOF) and **Br** is a two-dimensional correlation matrix, normally computed from analytical expressions. This means that horizontal and vertical components of the error covariance matrix have been separated. Such separation is allowed in the open ocean and it was found to work especially for quasigeostrophic assimilation of SSH (De Mey and Robinson, 1986).

The separation of **B** into vertical and horizontal modes allows control of the dominant structures of the background error field, as in the ocean the vertical part has a low vertical modal structure while the horizontal part can be quite complex, especially near the coastal margins. In horizontal, the open ocean auto-correlation scales of temperature, salinity and dynamic height fields (Nittis et al., 1993) is given by the 'exponential correlation function', that is

$$C(x,y) = A\left(1-\frac{r^2}{a^2}\right)\mathrm{e}^{-\frac{r^2}{2b^2}} \tag{20.20}$$

where for the horizontal zero crossing distance and the correlation decay scale, respectively, $r^2 = x^2 + y^2$ is the square of the distance measured in a (x, y) coordinate plane and A is the variance of the field. This form is used in the **Br** matrix.

In the vertical, the error field is dominated by errors in the mixed layer and in the thermocline, where the highest temporal variance of the **X** fields is found. A low vertical error modal structure is to be expected in view also of the fact that temperature and salinity profiles, as well as dynamic height, are dominated by the first baroclinic modes (Masina and Pinardi, 1994) and background correlation errors may reflect the incorrect energy content of these modes.

Thus the separation (20.19) can be rewritten in mathematical form as

$$B(x,y,z) = \sum_j F_j^{\,2}(z) C_j(x,y), \tag{20.21}$$

where F_j are the vertical modes and C_j their respective horizontal structure. Equivalence (20.19) and (20.21) cannot be shown to be true in general but they are convenient approximations of the **B** matrix that show efficient assimilation of ocean data, as we show later. These ad hoc formulations should also be tried for ecosystems, in order to control the model structure of the corrections for the relevant state variables.

The **F** matrix represents then the vertical error variability in all the state variables and their vertical cross-correlation. If we substitute (20.19) into (20.12) we obtain

$$\mathbf{K} = \mathbf{F}\,\mathbf{Br}\,\mathbf{F}^T\mathbf{H}^T(\mathbf{H}\mathbf{F}\,\mathbf{Br}\,\mathbf{F}^T\mathbf{H}^T + \mathbf{R})^{-1}. \tag{20.22}$$

The three-dimensional estimation problem contained in (20.22) can now be decreased in order due to the fact that **F** can be described by EOF. In fact, the relevant vertical EOFs (v-EOF) will certainly be less than the number of vertical model levels used for the estimation of the correlation matrix **F**. The physical reason for this is that the temperature variance below the thermocline is low and, on subseasonal timescales, the variability between the surface and the intermediate and deep water are uncorrelated. In turn this means that the number of significant v-EOFs to represent the state variable variance in the vertical is less than the number of model levels. Normally if the model levels are m, the vertical EOF explaining most of the variance are only n, with $n \ll m$, as shown by Sparnocchia et al. (2003). Thus we can use a 'reduced order space' for the v-EOF, that is the first n modes accounting for most of the variance. The estimation problem is then given by

$$\begin{aligned}\mathbf{K}^{\mathrm{ROOI}} &= \tilde{\mathbf{F}}\,\mathbf{Kr}\\ \mathbf{Kr} &= \mathbf{Br}\,\tilde{\mathbf{F}}^T\mathbf{H}^T(\mathbf{H}\tilde{\mathbf{F}}\,\mathbf{Br}\,\tilde{\mathbf{F}}^T\mathbf{H}^T + \mathbf{R})^{-1},\end{aligned} \tag{20.23}$$

where now the dimensions of $\tilde{\mathbf{F}}$ are much less than in **F**.

It is now easy to understand that, even if the misfit in (20.9) is given for few state variables, the correction in (20.11) will be carried out for all the state variables contained in $\mathbf{X}^{\mathbf{b}}$, given that we consider all the cross variances between state variables. This might not be wise every time, and several cross-correlations could be eliminated on the basis of the specific data set used or physical assumptions. For example, in the case of temperature observations it is not advisable to use the cross-correlation of $\langle \boldsymbol{\psi}' \mathbf{T}' \rangle$,

that is to change the stream function on the basis of temperature data. This correlation in fact cannot be understood on the basis of sound physical processes within the limit of the data availability and the processes represented in a primitive equation model.[103] In general this correlation is small but this cannot be guaranteed *a priori* because it depends on the details of how we calculate **B** and in any case its presence in **B** will introduce noise in the analysed field. Thus for every data set to be assimilated, we could study the most important cross-correlations to be considered.

20.3.3 Example 1: assimilation of satellite altimetry only

Let us suppose that we have only SSH observations and that **K** contains **F** defined as follows:

$$\mathbf{A} = \begin{vmatrix} \langle \mathbf{T}'\mathbf{T}' \rangle & \langle \mathbf{T}'\mathbf{S}' \rangle & \langle \mathbf{T}'\boldsymbol{\Psi}' \rangle \\ \langle \mathbf{S}'\mathbf{T}' \rangle & \langle \mathbf{S}'\mathbf{S}' \rangle & \langle \mathbf{S}'\boldsymbol{\Psi}' \rangle \\ \langle \boldsymbol{\Psi}'\mathbf{T}' \rangle & \langle \boldsymbol{\Psi}'\mathbf{S}' \rangle & \langle \boldsymbol{\Psi}'\boldsymbol{\Psi}' \rangle \end{vmatrix} \tag{20.24a}$$

$$\mathbf{A} = \mathbf{F}\boldsymbol{\Lambda}\mathbf{F}^{\mathrm{T}},$$

where **A** contains only the vertical multivariate covariances and **F** are the **v**-EOF of **A**.

This means that the SSH misfit will be projected into temperature, salinity profiles and ψ amplitudes and that the corrections will be done on three model state variables, not the SSH itself. This is another way of saying that SSH in assimilation should be considered as a diagnostic variable. Another interesting correlation matrix for SSH assimilation is

$$\mathbf{A} = \begin{vmatrix} \langle \mathbf{T}'\mathbf{T}' \rangle & \langle \mathbf{T}'\mathbf{S}' \rangle & \langle \mathbf{T}'\Psi' \rangle & \langle \mathbf{T}'\boldsymbol{\eta}' \rangle \\ \langle \mathbf{S}'\mathbf{T}' \rangle & \langle \mathbf{S}'\mathbf{S}' \rangle & \langle \mathbf{S}'\Psi' \rangle & \langle \mathbf{S}'\boldsymbol{\eta}' \rangle \\ \cdots & \cdots & \cdots & \langle \Psi'\boldsymbol{\eta}' \rangle \\ \cdots & \cdots & \cdots & \langle \boldsymbol{\eta}'\boldsymbol{\eta}' \rangle \end{vmatrix} \tag{20.24b}$$

The vertical modes of the correlation matrix (20.25b) are forced to be covariant also with SSH anomalies. In MFS, we use the v-EOF constructed from the state vector $\mathbf{X}^{\mathrm{a}} = \begin{vmatrix} \mathbf{T} \\ \mathbf{S} \\ \boldsymbol{\psi} \\ \boldsymbol{\eta} \end{vmatrix}$ from both the form (20.24a) or (20.24b). The reason for using the covariance

[103] A primitive equation system is composed of the Navier-Stokes equations considering the Boussinesq and hydrostatic approximation. For the ocean, incompressibility is also assumed. These equations contain physical processes such as baroclinic instability that transfer energy between baroclinic (temperature-dominated) and barotropic modes (vertical integral of velocity field represented by the streamfunction). The baroclinic instability process is connected to horizontal gradients of temperature and vertical gradients of the velocity field but not simply to the temperature anomaly. Thus using the simple correlation between temperature and streamfunction field does not accurately represent the baroclinic process and this correlation should be disregarded if the only information is from temperature profiles.

between all these fields is connected to the analytical expression (20.2), where we see that SLA is a complicated function of all the *T*, *S* and ψ model variables.

Following the geostrophic relationship written in (20.2) the observational operator **H** contains explicitly that expression (Demirov et al., 2003). In this way we ensure that the correction is carried out on the model state variables *T*, *S* and ψ weighted by their respective scaling coefficients that produces the correct value for η or the SSH. The same procedure and understanding should pave the way for the assimilation of other observations that use the observational operator and the cross-correlations contained in **B** to transform the measurement information into the state variables contained in $\mathbf{X}^{\mathbf{b}}$.

As an example of application of this concept for the assimilation of SSH, Masina et al. (2001) computed cross-correlations between η' and T' only. The derived profiles, also called 'synthetic XBTs' in the paper, were assimilated in a global model with a two-dimensional variational algorithm. The success of their assimilation is based on the fact that SSH is strongly correlated to vertical profiles of temperature and salinity below the mixed layer and that it was possible to derive an error estimate for the synthetic XBT. This is another way to express the relationship of Figure 20.4 and reduce the order of **F**.

In conclusion, the degree with which one observed state variable controls the changes or updates on the other state variables is given by the degree of correlation between the errors in the state variables and the projection of **F** on **H**.

20.3.4 Example 2: assimilation of temperature profiles only

In the Mediterranean and the world's oceans, XBT profiles are collected in real time, as explained in previous sections, and thus assimilation of this data set is a priority for any forecasting system.

This time the vertical model error covariance matrix can be now taken to be

$$\mathbf{A} = \begin{vmatrix} \langle \mathbf{T}'\mathbf{T}' \rangle & \langle \mathbf{T}'\mathbf{S}' \rangle \\ \langle \mathbf{S}'\mathbf{T}' \rangle & \langle \mathbf{S}'\mathbf{S}' \rangle \end{vmatrix}, \tag{20.25}$$

which we also call the 'vertical water mass cross-correlation matrix'. Again, **F** are the v-EOF of **A**. Thus for assimilation of XBT in the Mediterranean, bivariate v-EOF were computed as EOF of (20.25) considering the several subregions of the basin, where different water masses can be identified. The state variable anomalies were computed using historical data (Sparnocchia et al., 2003).

The v-EOF for summer and for the Levantine basin region are shown in Figure 20.8. We note the presence of the high values of the errors in the 50 m surface layer corresponding to a well-known subsurface low salinity signal, normally referred to as Atlantic Water. The first salinity EOF changes of sign below 50 m and presents a subsurface maximum correspondent to the Levantine Intermediate Water signal. Thus, looking at the v-EOFs it is possible to recognize the major surface and intermediate water masses of the Mediterranean Sea where variance of the temperature and salinity signal is contained and thus, in our interpretation, also the model errors. In conclusion, a misfit in temperature will induce corrections in salinity that have a known water mass *T-S* relationship contained in **F**.

To conclude, let us discuss the assimilation of SST observations. If **A** were full, then the misfit in SST would induce changes in the whole water column for T, S, U, V, and others, and this is clearly not representative of a realistic ocean process, except

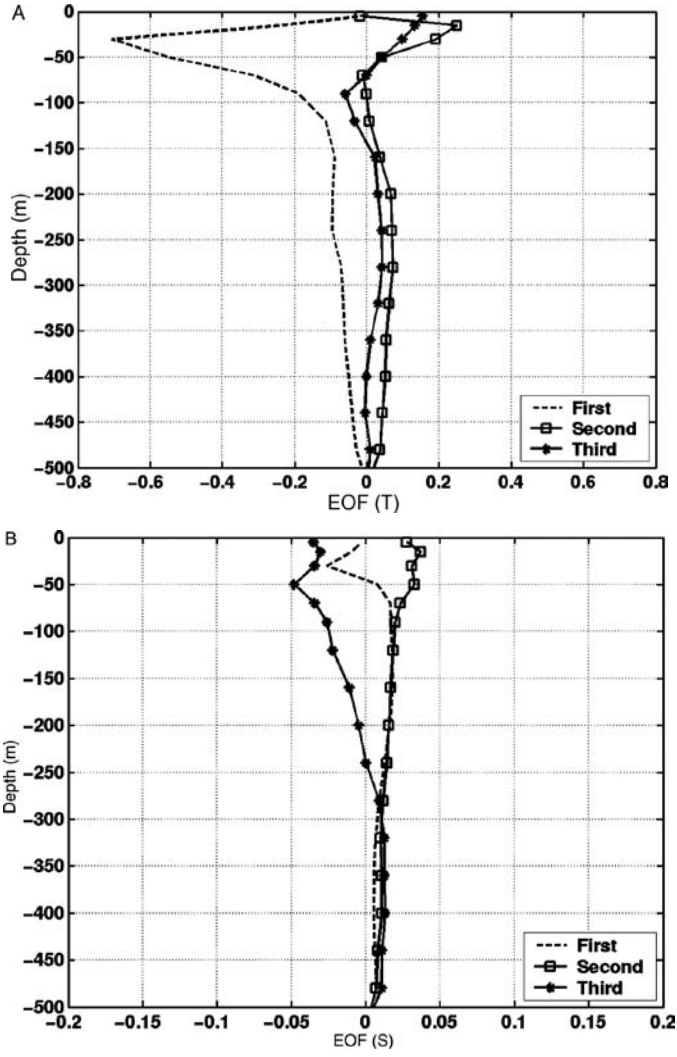

Figure 20.8
A, First three summer season temperature bivariate v-EOF for the Levantine basin region in the Mediterranean (east of 30°E and north of 30°N), calculated by Sparnocchia et al. (2003) from historical hydrographic data. The three modes account for more than 80% of the temperature-salinity variance in the water column.
B, First three summer season salinity bivariate v-EOF for the Levantine basin region in the Mediterranean (east of 30°E and north of 30°N) calculated by Sparnocchia et al. (2003) from historical hydrographic data. The three modes account for more than 80% of the temperature-salinity variance in the water column.

for few limited areas (deep convection areas) and severe winter periods. On the other hand, the error cross-correlation between state variables is the only information that allows a change in the prognostic state variables on the basis of a limited amount of observed state variables. In the case of SST, it is advisable to carefully study the assimilation impact on the complete state vector before using automatically a full state **F** vector in **B**.

20.3.5 Example 3: assimilation of combined altimetry and temperature profiles

Having decided the satellite altimetry and temperature profiles assimilation assumptions, MFS has implemented a combined assimilation of both measurements using a two-step approach, described below (Demirov et al., 2003). The method is based on the hypothesis that it is important to maintain the different expressions of **A** and thus **F** for the two kind of measurements, as they contain different physical information about the water column stratification. The multivariate v-EOFs for Ψ, T, S are used for assimilation of SLA and the bivariate T, S v-EOFs are used for assimilation of XBT profiles. This way each data set is assimilated with its optimal vertical error modes.

In order to combine the two assimilation procedures we envisage the following steps, illustrated in Figure 20.9. The time window of assimilation is two weeks and an analysis is calculated once a week (day 'J' in the diagram). Both past and future observations with respect to J are considered, that is the OI is used in the 'smoother mode'. One week we use only SLA observations to generate the present week analysis starting from the previous week analysis which instead assimilated only XBT observations. After the first cycle it will be unimportant which data set is assimilated first and each week the analysis will benefit from both SLA and XBT observations.

The working of the combined assimilation of satellite and temperature profiles is shown in Section 20.5 where the comparison between the observed, modelled and corrected profiles, by means of (20.11), is given.

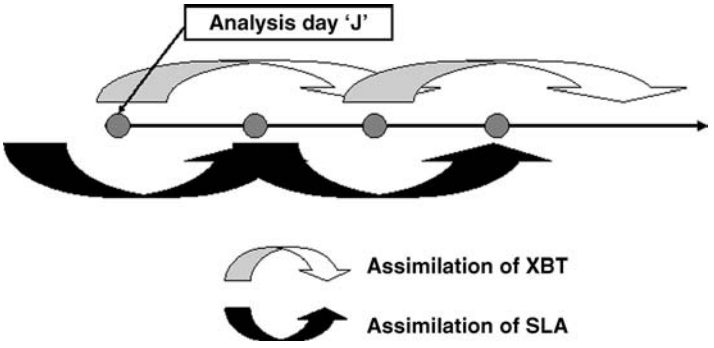

Figure 20.9
Combined assimilation of XBT and SLA profiles used in the MFS operational assimilation system.
Source: Demirov et al. (2003).

20.4 The coastal forecasting and assimilation problem

The MFS approach to coastal forecasting uses nesting and downscaling of the large-scale flow field up to the required resolution. Coastal environmental forecasting will make use of the analysed physical flow fields to advect passive or active tracers in the coastal areas with the maximum accuracy. Specifically MFS could provide a basis to examine the transport and fate of planktonic populations and dissolved constituents in the water column. Potential users would greatly benefit from an explicit statement of the space and timescales over which the MFS can provide realistic estimates of transport. The benefit from MFS is maximum when the variability will be forced heavily by the offshore forcing, which is the case for several coastal regimes in the Mediterranean and the world ocean.

In a recent review paper, Pinardi et al. (2006) have shown that more than half of the Mediterranean coastal areas are limited by narrow shelves that allow for strong control by the open ocean flow field. In addition, large portions of the coastal areas do not have any local runoff control mechanism and thus coastal productivity will be totally dominated by the discharges from coastal towns and offshore inputs of nutrients. In the latter case, a system such as MFS is crucial to understand the primary productivity of the coastal areas. Even in extended shelf areas, the remote effects of open ocean ecosystem structure cannot be neglected to understand coastal productivity. This is evident for the case of Adriatic mucilage phenomena where it is believed that the arrival from the open ocean areas of highly refractory dissolved material could influence aggregation rates of particles in the water column and thus influence the mucilage itself.

MFS has also developed the coastal downscaling and the necessary data assimilation for the shelf and coastal domains of interest. In particular, we refer here to the Adriatic coastal areas where a 5 km OGCM was nested within the MFS OGCM in order to arrive properly to the near coastal areas (Oddo et al., 2005). In addition, the assimilation system described above for temperature profiles was applied to coastal CTD profiles (measuring both salinity and temperature) collected in the very near coastal areas in order to control the near-shore coastal field. It was found that the separation of vertical and horizontal modes of the background error covariance matrix allowed a consistent assimilation even in complicated coastal dynamical regimes (Grezio and Pinardi, 2006). In future the coastal data assimilation system may be different from the open ocean one allowing for the higher space and time variability of the background error covariance matrix in these regions.

20.5 Forecast consistency, quality and accuracy

In this section we show how to carry out an assessment of the quality and accuracy of the assimilation system using three basic indicators:

- *Consistency indicator*: the qualitative (visual) correspondence of circulation structures in the analysis fields with features known from phenomenological studies or observations only.
- *Quality indicator*: comparison between observations and model before data insertion. This indicator can be expressed in terms of the root-mean-square of the misfit, defined by

$$\text{rms\_misfit}(\mathbf{d}) = \frac{1}{N}\sqrt{\Sigma\, \mathbf{d}^2}$$

$$\text{nms\_misfit}(\mathbf{d}) = \frac{1}{\sqrt{\Sigma \mathbf{Y}^{o2}}} \sqrt{\Sigma\, \mathbf{d}^2},$$

and **d** is defined by (20.9) and the sum is done over different realizations in space at a given time.

- *Accuracy indicator*: comparison between analysis and forecast, i.e. forecast skill score. Two can be defined:
  (a) the first is $\text{rms\_fcst}(\mathbf{X}^b - \mathbf{X}^a) = \frac{1}{N}\sqrt{\Sigma(\mathbf{X}^b - \mathbf{X}^a)^2}$, referred to simply as rms of forecast error;
  (b) the second is $\text{rms\_pers}\left[\mathbf{X}^b - \mathbf{X}^a(t=0)\right] = \frac{1}{N}\sqrt{\Sigma\left[\mathbf{X}^b - \mathbf{X}^a(t=0)\right]^2}$, rms of persistence error.

Figure 20.10 shows the comparison for April 2002 of SLA from the forecast system analyses with respect to objective analysis done only with the satellite data. In both

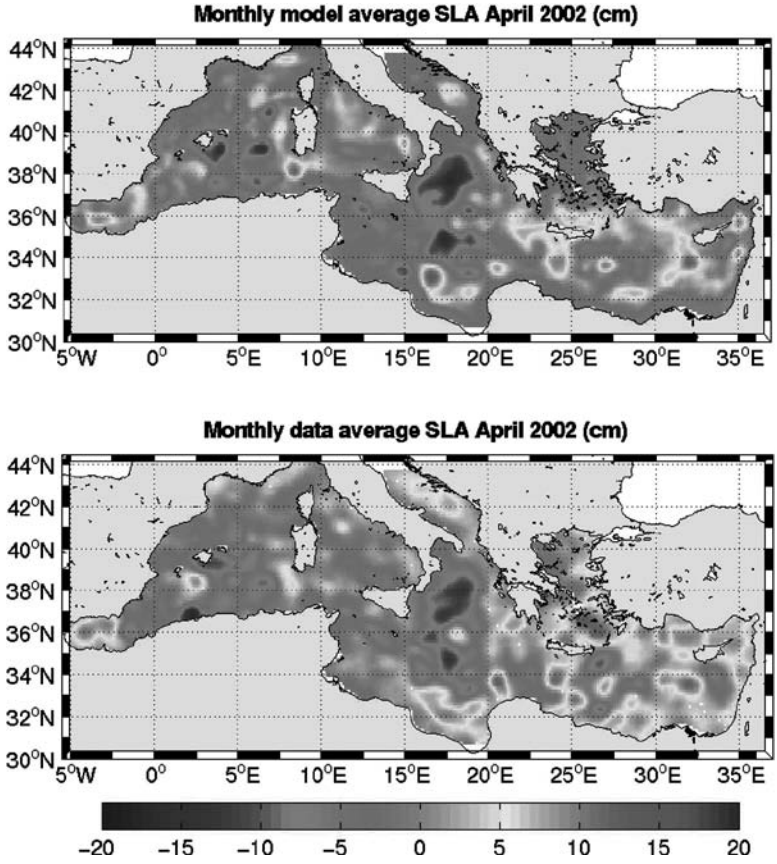

Figure 20.10
Correspondence between A, model; B, satellite objective analysis of SLA (cm) for the month of April 2002.

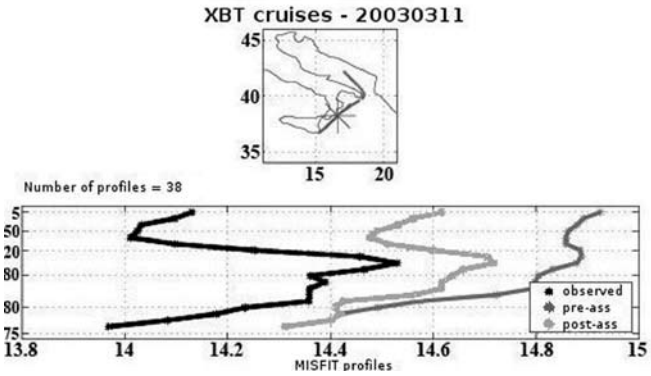

Figure 20.11
Comparison between model temperature before data insertion, temperature observation, model corrected solution for 11 March 2003. The star in panel A indicates the position of the observation along a VOS line.

estimates we recognize the cyclonic anomaly area in the Ionian, which is known from other data to be dominant in these years.

More important is the quality indicator and the study of the structure of the misfit. We show an example of misfit for the case of XBT profiles (Figures 20.11, 20.12) and SLA (Figure 20.13).

Figure 20.11 shows the observed profile, the model profile before data insertion and the corrected profile or analysis done with (20.11). The model profile is shifted towards the observed one and the misfit is of the order of –0.5°C. This is a good result for the data-assimilation scheme, confirming that the assumptions made for **F** and **B**

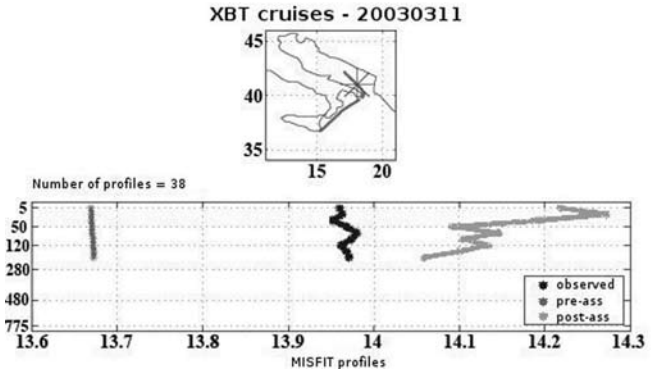

Figure 20.12
Comparison between model temperature before data insertion, temperature observation, model corrected solution and vertical misfit for 11 March 2003. The star in panel A indicates the position of the observation along a VOS line.

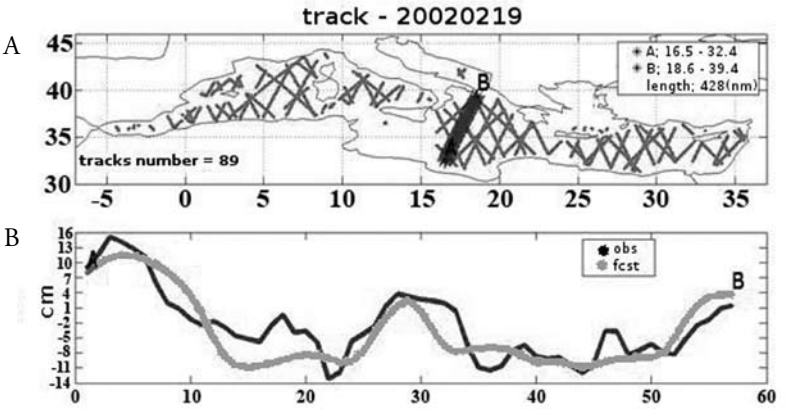

Figure 20.13
Model and observational SLA values along a Topex/Poseidon track on 19 February 2002. Panel B shows the model solution before data insertion with superimposed observations for each point of the track from point A to B.

are generally correct. However, Figure 20.12 shows that sometimes the assimilation fails to produce a sensible corrected profile. In fact the new profile is closer in absolute value to the observations but it overshoots the observed one and has a noisy vertical structure. We argue that this is due to the inadequate choice of v-EOF for this region and for this time of the year. This points out to the fact that **B** should be more space and time varying while in our case we have a unique v-EOF for the whole southern Adriatic area and for the three months of the winter season. Future improvements include v-EOF that are calculated point by point and with higher time frequency (monthly and interannually).

In Figure 20.13 we show the misfit and the comparison of the model solution versus observations before data insertion. We see that the model follows quite closely the altimeter track values but misfit is still of the order of 5–10 cm which is large with respect to the Mediterranean anomaly signal which varies between ± 30 cm.

A global quantitative estimation of the quality of the forecasting system may come from the average of the *rms_misfit* and *nms_misfit* for the whole Mediterranean region as shown in Figures 20.14 and 20.15, for SLA data and XBT respectively. In Figure 20.14 we note that the *rms_misfit* error varies from months to months indicating that the temporal scale of variability is not correctly captured by the model and not correctly inserted in the analysis by the assimilation scheme. We suppose that a shorter assimilation cycle (now one week) could improve this situation. The rms of misfit for the XBT (Figure 20.15) at 30 m indicates the reasonable value of 0.6°C. This is also decreasing rapidly with the continuous insertion of data after September 1999. Another important issue in assimilation is concerned with the length of time it will take the system to 'converge' towards the observations after the initial time when model and data are added together. This is a difficult question to analyse here but our estimate is that several months are needed to show the improvement, as we show in Figure 20.15. This naturally will depend also on the data scarcity and the measuring network.

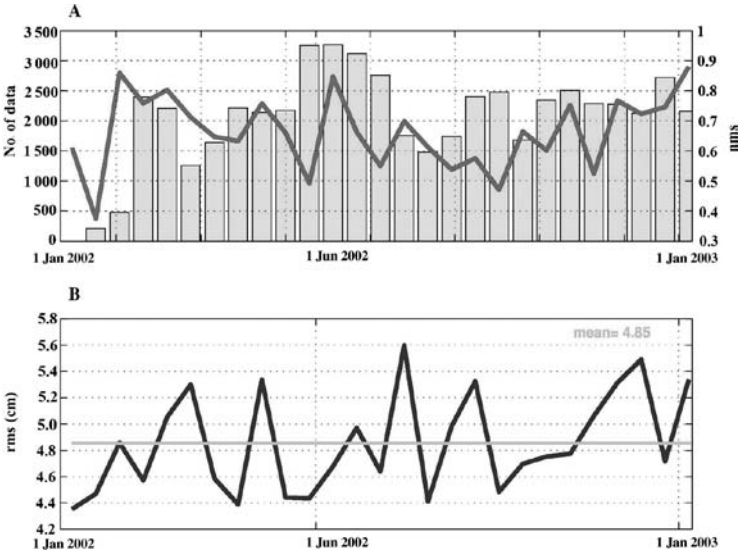

Figure 20.14
A, weekly number of SLA data points for Topex/Poseidon altimeter every two weeks with overlaid the nms_misfit.
B, rms_misfit *for* the period January 2002 to January 2003.

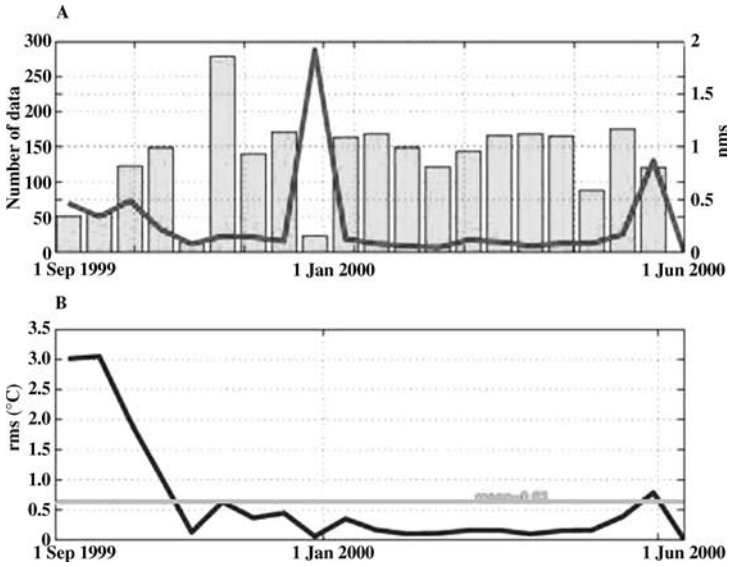

Figure 20.15
A, weekly number of XBT data used in the analysis with overlaid the nms_misfit for temperature at 30 m.
B, rms_misfit for the period September 1999 to June 2000.

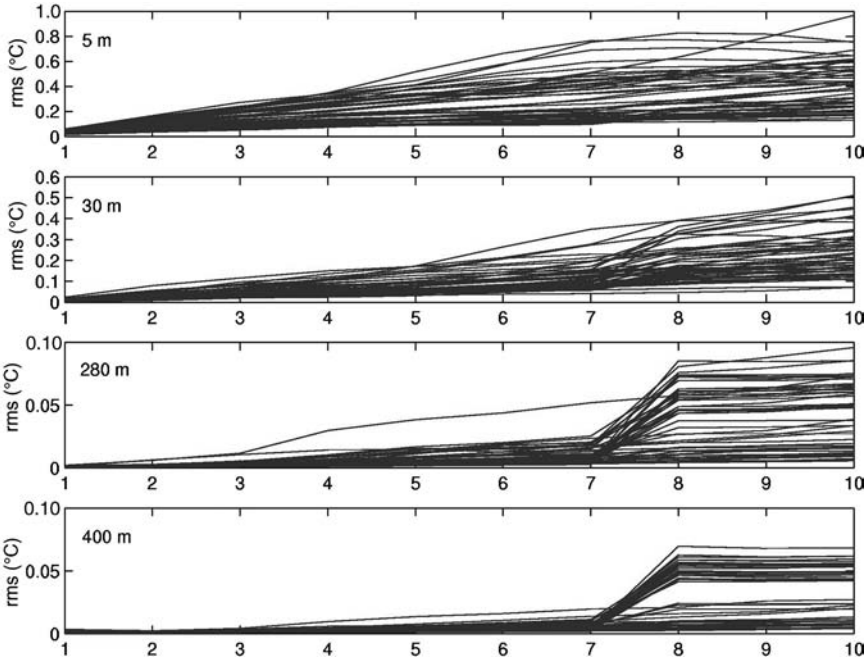

Figure 20.16
10 days root-mean-square (rms) forecast error growth for the weekly forecasts in 2000, at different depths.

Last but not least, the accuracy indicator is shown in Figure 20.16. As described in Demirov et al. (2003) in MFS we use to run a simulation experiment between the analyses that are done one week apart. Since this is done in delayed mode, atmospheric forcing analyses are used to force the 'hindcast' between analyses. The error grows with time almost linearly at the surface. At the levels below, the data insertion occur intermittently every week and thus the error suddenly grows at day 7 of each 10-day forecast. Between day 1 and day 7, the forecast error growth is due only to the different atmospheric forcing used in the forecast and the hindcast. The value of the rms temperature forecast error is reasonable showing that the atmospheric forecast forcing is capable of reproducing some of the essential features of the atmospheric variability of the region. Demirov et al. (2003) compare this rms forecast error with the rms persistence error and show that the latter is always higher that the former. This basically shows that the forecast is needed in order to reach reasonable accuracy in the 10-day predictions.

20.6 Discussion and conclusions

This chapter has described the ocean state estimation problem set up in the MFS operational scheme. Apart from the necessary regionalization issues, a few general statements about assimilation of real-time data have been made.

First of all, it is recognized that sophisticated preprocessing of satellite and *in situ* data is needed before observations can be inserted into the model. Above all, the quality control procedures should be as much as possible automatic and consistent with the physical assumptions made in the assimilation scheme. One of these assumptions is that the observations contain only the slow timescale variability (larger timescales than the day) and thus high-frequency signals should be eliminated from the data *a priori*.

Second, we have seen that the assimilation quality and practice is connected to the assumptions made to calculate **B**, the form chosen for **H** and the kind of data that we assimilate. The multivariate character of **B** should be carefully checked against physical processes that are contained in the cross-correlations induced by the inserted data. The time and space variability of **B** is generally underestimated in present systems, like the Mediterranean Sea, and inconsistencies may occur that will not produce the optimal merging of background or model data with observations.

Order reduction of **F** is strongly recommended especially if it can be done, as in the ocean physics, on the basis of process assumptions. The vertical thermohaline structure of the ocean is low mode, with few vertical EOF modes expressing a big part of the variance of the error field in the vertical. Thus separation of **B** into vertical and horizontal structures seems to be advisable. However, the v-EOF are horizontally non-homogeneous and that effect should be considered. As an example of more recent developments, we show in Figures 20.17A and 20.17B the percentage variance explained by the first bivariate v-EOF mode of **A** written as in (20.25) considering the definition (20.16) and different mean fields subtracted. The figures show that, depending on which $\tilde{\mathbf{X}}^b$ is used, the percentage variance explained by the first v-EOF changes as well as its horizontal distribution. **A** is constructed from a 35-day temporal time series of $\mathbf{X}^b$ subtracting $\tilde{\mathbf{X}}^b$ calculated by a mean over several years (a climatological $\tilde{\mathbf{X}}^b$) for Figure 20.17A and only a 35-day mean for Figure 20.17B. It is important to note that several regions have almost 100% variance explained by only one bivariate EOF but this value changes depending on which average is subtracted. In Figure 20.17B, the areas with a large proportion of variance explained by the first EOF have changed extension, and more modes are needed in general to explain the same variance in the case of Figure 20.17A.

Schemes for ecosystem data assimilation of the same complexity of the physical state estimation problem discussed here are being developed. However, it is recommended that the structure of **B** for these systems is studied in detail, in particular because biogeochemical observations are much more scarce in space and time than observations for the physical state variables.

Let us make an example of how matrix **B** could look in ecosystem data assimilation. First of all the state vector could be indicated by:

$$\mathbf{X} = \begin{bmatrix} \mathbf{T} \\ \mathbf{Chl} \\ \mathbf{N} \\ \mathbf{Z} \\ \mathbf{D} \end{bmatrix} \tag{20.26}$$

where this time the biochemical state variables, **Chl**, chlorophyll concentration, **N**, dissolved nutrients, **Z**, zooplankton biomass and **D**, detritus, have been introduced in

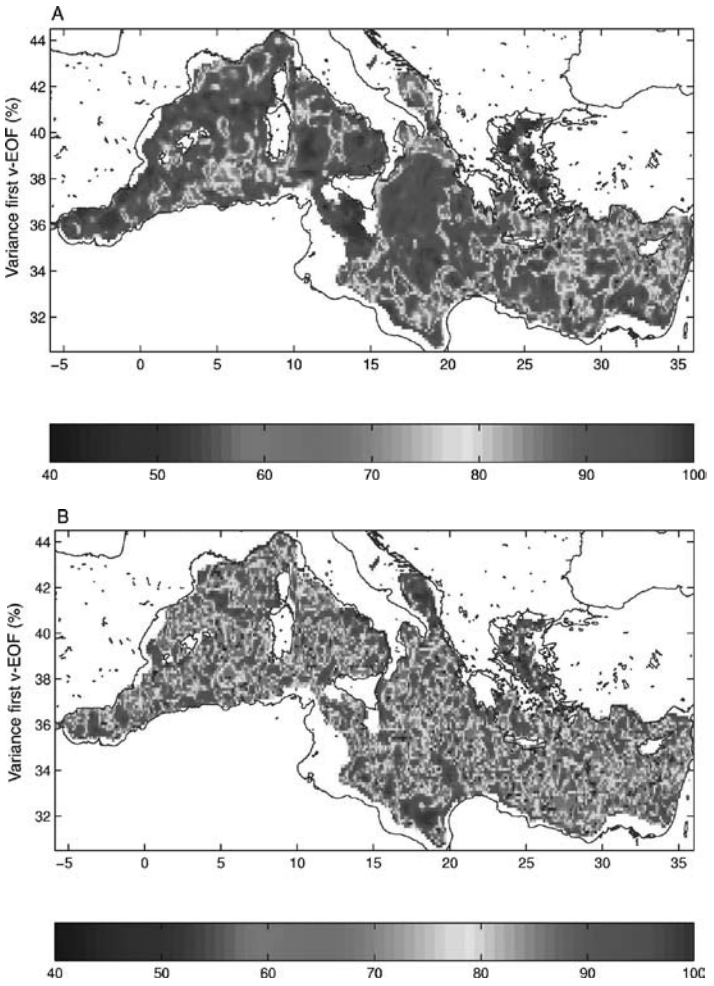

Figure 20.17
A, percentage of variance (colours of the palette) explained by bivariate v-EOF calculated from a 35-day time series of temperature and salinity profiles at each model grid point – matrix of (20.26) – and with a climatological monthly mean value of T,S subtracted at each level to compose **A**.
B, percentage of variance (colours of the palette) explained by bivariate v-EOF calculated from a 35-day time series of temperature and salinity profiles at each model grid point (matrix of (20.26)) and with the 35-day mean value of T,S subtracted at each level to compose **A**.

addition to temperature, **T**. Chlorophyll concentration here is a model state variable which corresponds to a phytoplankton group and its concentration may be thought to be proportional to the phytoplankton biomass. Decomposing the **B** matrix into horizontal and vertical modes, we now take a possible definition of **A** and **F** as follows:

$$\mathbf{A} = \begin{vmatrix} \langle \mathbf{T}'\mathbf{T}' \rangle & \ldots & \ldots & \ldots & \ldots \\ \langle \mathbf{Chl}'\mathbf{T}' \rangle & \langle \mathbf{Chl}'\mathbf{Chl}' \rangle & \ldots & \ldots & \ldots \\ \langle \mathbf{N}'\mathbf{T}' \rangle & \langle \mathbf{N}'\mathbf{Chl}' \rangle & \langle \mathbf{N}'\mathbf{N}' \rangle & \ldots & \ldots \\ \langle \mathbf{Z}'\mathbf{T}' \rangle & \langle \mathbf{Z}'\mathbf{Chl}' \rangle & \langle \mathbf{Z}'\mathbf{N}' \rangle & \langle \mathbf{Z}'\mathbf{Z}' \rangle & \ldots \\ \langle \mathbf{D}'\mathbf{T}' \rangle & \langle \mathbf{D}'\mathbf{Chl}' \rangle & \langle \mathbf{D}'\mathbf{N}' \rangle & \langle \mathbf{D}'\mathbf{Z}' \rangle & \langle \mathbf{D}'\mathbf{D}' \rangle \end{vmatrix} \tag{20.27}$$

and

$$\mathbf{A} = \mathbf{F} \Lambda \mathbf{F}^{\mathrm{T}} \tag{20.28}$$

F is then a vector containing the v-EOF of **A**.

We have explicitly written only half of the matrix because we know that is symmetric. Let us consider the satellite ocean colour transformed into surface chlorophyll as the input observational data set. If the analysis system (20.11) is used, then the chlorophyll misfit will produce corrections on all the system state variables listed in (20.26) and **F** will infer the vertical corrections to be introduced, as in the case of the physical system explained above.

The matrix (20.27) expresses the vertical covariance between **T**, **N**, **Z**, **D** and **Chl** state variables. The auto-correlation for **Chl** is a very important part of the matrix (20.27): it means that surface chlorophyll will produce a vertical profile of chlorophyll, sometimes containing a subsurface chlorophyll maximum if the statistics allows it. The other cross-correlations can be interpreted as follows:

- the covariance between **T** and **Chl** points to the functional relationship between photosynthetic activity corresponding to a representative phytoplankton group and water temperature. This correlation may be weak in subtropical regions;
- the covariance between **Chl** and **N** points to the functional relationship between the dissolved nutrients and chlorophyll concentration changes. This covariance in the vertical will have a subsurface maximum in open ocean areas while it will be surface intensified in coastal areas;
- the covariance between **Chl** and **D** points to the functional relationship between detritus variance (related to the mortality rate of the phytoplankton in simple models) and chlorophyll variance. This cross-correlation is complicated since there is a delayed response of detritus to the increase in chlorophyll error variance;
- the covariance between zooplankton variance and chlorophyll is also very complex, as again the covariance has a time delay.

Simplifying the structure of (20.27) could involve the deletion of the cross-correlations between **Chl** and all the other ecosystem state variables except **Chl** itself, **N** and **T**. This will produce corrections by (20.11) on only three of the system state variables given in (20.26) while the others will be changed by the model time stepping, as given by (20.14). In this way the corrections to the detritus and zooplankton, in response to the insertion of surface chlorophyll observations, will be made following the dynamical equations contained in the ecosystem model, after chlorophyll and nutrients have been updated by the observations in the whole water column. This scheme seems to be reasonable instead of changing the zooplankton biomass directly as a consequence of a change in surface chlorophyll: this operation in fact may not be justified within the limits of the assimilation cycle chosen and the dynamical response of the system.

Ecosystem data assimilation is at its infancy but the premises of a workable data assimilation system for the physical components of the marine environment makes it possible to think that in the next years primary production estimates in the ocean will benefit from the optimal merging of observations and predictive ecosystem models.

References

Babin, M., Roesler, C. S. and Cullen, J. J. (eds). 2006. *Real-time Coastal Observing Systems for Marine Ecosystem Dynamics and Harmful Algal Blooms: Theory, Instrumentation and Modelling*. Paris, Intergovernmental Oceanographic Commission of UNESCO. (Monographs on Oceanographic Methodology XX.)

Castellari, S., Pinardi, N. and Leaman, K. 1998. A model study of air-sea interactions in the Mediterranean Sea. *J. Mar. Syst*., 18, pp. 89–114.

Daley, R. 1996. *Atmospheric Data Analysis*. Cambridge, UK, Cambridge University Press.

De Mey, P. and Benkiran, M. 2002. A multivariate reduced order Optimal Interpolation Method and its application to the Mediterranean basin-scale circulation. In: N. Pinardi and J. D. Woods (eds), *Ocean Forecasting: Conceptual Basis and Applications*. New York, Springer-Verlag.

Demirov, E. and Pinardi, N. 2002. The simulation of the Mediterranean Sea circulation from 1979 to 1993. Part I: The interannual variability. *J. Mar. Syst.*, 33–34, pp. 23–50.

Demirov, E., Pinardi, N., Fratianni, C., Tonani, M., Giacomelli, L. and De Mey, P. 2003. Assimilation scheme of the Mediterranean Forecasting System: operational implementation. *Ann. Geophys.*, 21, pp. 189–204.

Dickey, T., Frye, D., Jannasch, H., Boyle, E., Manov, D., Sigurdson, D., McNeil, J., Stramska, M., Michaels, A., Nelson, N., Siegel, D., Chang, G. C., Wu, J. and Knap, A. 1998. Initial results from the Bermuda Testbed Mooring Program. *Deep Sea Res.*, 45, pp. 771–94.

Gibson, J. K., Kallberg, P., Uppala, S., Hernandez, A., Nomura, A. and Serrano, E. 1997. ERA description. *ECMWF Re-Analysis Project Rep. Series*, 1, 71 pp.

Grezio, A. and Pinardi, N. 2006. Data assimilation of temperature and salinity profiles in the Adriatic Regional Model. *Acta Adriatica*, 47, pp. 149–68.

Kalnay, et al. 1996. The NCEP/NCAR 40-year re-analysis project. *Bull. Am. Meteorol. Soc.*, 77, pp. 437–71.

Korres, G., Pinardi, N. and Lascaratos, A. 2000. The ocean response to low frequency interannual atmospheric variability in the Mediterranean Sea. Part I: Sensitivity experiments and energy analysis. *J. Climate*, 13(4), pp. 705–31.

Legler, D. M. and O'Brien, J. J. 1988. *Tropical Pacific Wind Stress Analysis for TOGA, IOC Time Series of Ocean Measurements*, Vol. 4. Paris, IOC–UNESCO. (Intergovernmental Oceanographic CommissionTechnical Series 33.)

Le Traon, P. Y. 2002. Satellite oceanography for ocean forecasting. In: Pinardi and Woods (eds), op. cit., pp. XX–XX.

Lorenc, A. C. 2002. Atmopsheric data assimilation and quality control. Pinardi and Woods (eds), op. cit.

Manzella, G. M. R., Scoccimarro, E., Pinardi, N. and Tonani, M. 2003. Improved near real time data management procedures for the Mediterranean Ocean Forecasting System-Voluntary Observing Ship Program. *Ann. Geophys.*, 21, pp. 49–62.

Masina, S. and Pinardi, N. 2004. Mesoscale data assimilation studies in the middle Adriatic Sea. *Cont. Shelf Res.*, 14(12), pp. 1293–310.

Masina, S., Pinardi, N. and Navarra, A. 2001. A global ocean temperature and altimeter data assimilation system for studies of climate variability. *Climate Dynamics*, 17, pp. 687–700.

McPhaden, M. J. 1995. The tropical atmosphere ocean array is completed. *Bull. Am. Meteorol. Soc.*, 75(5), pp. 739–41.

Mellor, G. L. 1996. *Introductory Dynamical Oceanography*. Oxford, UK, Pergamon Press.

Mellor, G. L. and Ezer, T. 1991. A Gulf Stream model and an altimetry assimilation scheme. *J. Geophys. Res.*, 96(5), pp. 8779–95.

Milliff, R. F., Feilich, M. H., Liu, W. T., Atlas, R., Large, W. G. 2001. Global ocean surface vector wind observations from space. In: C. J. Koblinsky and N. R. Smith (eds), *Observing the Oceans in the 21st Century*, Melbourne, Bureau of Meteorology, GODAE Project Office, pp. 102–19.

Milliff, R. F., Large, W. G., Morzel, J. Danabasoglu, G. and Chin, T. M. 1999. Ocean general circulation model sensitivity to forcing from scatterometer winds. *J. Geophys. Res.*, 104(5), pp. 11337–58.

Molcard, A., Pinardi, N., Iskandarani, M. and Haidvogel, D. B. 2002. Wind driven general circulation of the Mediterranean Sea simulated with a Spectral Element Ocean Model. *Dynam. Atmos. Oceans*, 35, pp. 97–130.

Nittis, K., Pinardi, N. and Lascaratos, A. 1993. Characteristics of the summer 1987 flow field in the Ionian Sea. *J. Geophys. Res.*, 98(6), pp. 10171–84.

Oddo, P., Pinardi, N. and Zavatarelli, M. 2005. A numerical study of the interannual variability of the Adriatic Sea (2000–2002). *Sci. Total Environ*.

Oddo, P., Pinardi, N., Zavatarew, M. and Coluccelli, A., 2006. The Adriatic Basin Forecasting System. *Acta Adriatica*, 47, pp. 169–184.

Pinardi, N., Allen, I., Demirov, E., De Mey, P., Korres, G., Lascaratos, A., Le Traon, P. Y., Maillard, C., Manzella, G. and Tziavos, C. 2003. The Mediterranean Ocean Forecasting System: first phase of implementation (1998–2001). *Ann. Geophys.*, 21, pp. 3–20.

Pinardi, N., Arneri, E., Crise, A., Ravaioli, M. and Zavatarelli, M. 2006. The physical, sedimentary and ecological structure and variability of shelf areas in the Mediterranean Sea. *The Sea*, 14. Boston, Harvard University Press.

Pinardi, N. and Masetti, E. 2000. Variability of the large scale general circulation of the Mediterranean Sea from observations and modelling: a review. *Palaeogeogr., Palaeoclimatol., Palaeoecol.*, 158, pp. 153–73.

Pinardi, N. and Woods, J. D. (eds). 2002. *Ocean Forecasting: Conceptual Basis and Applications*. New York, Springer-Verlag.

Prandle, D. 2002. Predictions in the North Sea. In: Pinardi and Woods (eds), op. cit.

Raicich, F. and Rampazzo, A. 2003. Observing system simulation experiments for the assessment of temperature sampling strategies in the Mediterranean Sea. *Ann. Geophys.*, 21, pp. 151–66.

Robinson, A. R. and Leslie, W. G. 1985. Estimation and prediction of oceanic fields. In: J. Crease, W. J. Gould and P. M. Saunders (eds), *Progress in Oceanog*raphy, Vol. 14. Oxford, UK, Pergamon Press, pp. 485–510. (Essay on Oceanography.)

Rossby, T., Siedler, G. and Zenk, W. 1995. The volunteer observing ship and future ocean monitoring. *Bull. Am. Meteorol. Soc.*, 76(1), p. 5.

Smith, N. and Lefebvre, M. 1997. The Global Data Assimilation Experiment (GODAE). *Proc. Biarritz International Symposium*, October 1997.

Sparnocchia, S., Pinardi, N. and Demirov, E. 2003. Multivariate Empirical Orthogonal Function analysis of the upper thermocline structure of the Mediterranean Sea from observations and model simulations. *Ann. Geophys.*, 21, pp. 167–87.

21

Real-time coastal observing systems for ecosystem dynamics and harmful algal blooms: needs and expectations of users

G. C. Pitcher, S. Bernard and A. Fawcett

21.1 Managing the ocean and coastal environments

The success of ocean and coastal management depends largely on three basic elements: information, knowledge and a structure for decision-making (Holland and Bernal, 2002). Information provides a description of the observed processes or events, knowledge encompasses a sufficient understanding of the processes and interactions to make the necessary decisions and to provide strategic direction for management, and decision-making should anticipate changes with sufficient lead-time to make informed decisions with preferred outcomes. The management of harmful algal blooms (HABs) similarly depends on these elements, which are currently deficient at all scales in the ocean and coastal infrastructure.

21.1.1 Users and their need for information

The needs of the users of ocean and coastal observing systems must be addressed in terms of the information required to satisfy particular economic, social, environmental and political needs and the form in which this information is required for it to be useful. The user community of information relating to HABs is one component of the consortium responsible for managing ocean and coastal environments, and together these users share many requirements and expectations.

The ocean influences weather and climate and provides a livelihood for many coastal communities though fishing, exploitation of energy and mineral resources, shipping and offshore operations, defence, and leisure and recreational activities. The ocean contributes enormously to the biodiversity of the planet, while posing threats to human life and property through floods, storms, sea-level change and coastal erosion. Inevitably, humans impact negatively on the marine environment. Many fish stocks have declined as a consequence of over-fishing and coastal ecosystems are damaged by fishing gear. Patterns of biodiversity are changing. Oil and gas exploitation is increasing and a greater volume of commodities is transported by sea. Coastal populations and tourist activities continue to grow relentlessly. The sea is used for dumping and waste disposal, affecting marine water quality and the health of the environment and of humans. Runoff from land pollutes the coastal environment with fertilizers, pesticides, insecticides and other chemicals. Global warming threatens to destroy various habitats, exotic species are being introduced into coastal environments and the

incidence of harmful algal blooms is apparently increasing (Summerhayes et al., 2002). There is thus a growing need to protect the coastal environment in order to sustain its future. For this to be achieved the above problems must be addressed by providing managers with information, understanding and tools for decision-making.

As the oceans become more directly important to society and as more people become dependent on the ocean for their life and livelihood, the requirement for marine information continues to grow (Holland and Bernal, 2002). There is an increasing need for more ocean and coastal observations; greater knowledge of important physical, chemical and biological processes and their interactions; and a better interpretation of information into useful and timely operational services. In decision-making, scientific information and knowledge are a valuable and critical resource, resulting in a growing requirement for access to real-time data and advancement of operational oceanography, whereby ocean and coastal observations and interpretation thereof are routinely made available to the user community.

The user community for operational oceanographic data is broad and diverse, and the data required will be used for numerical meteorological predictions to improve the safety and efficiency of marine operations thereby minimizing loss of property and avoiding environmental disasters; to assist in monitoring and predicting climatic variability; for preserving and restoring healthy marine ecosystems and managing marine resources for sustainable use; to assist coastal managers and developers to mitigate the effects of natural coastal hazards while being used to monitor the supply and effect of pollutants on water quality; and to service various military applications (Summerhayes and Rayner, 2002).

Operational oceanography, and the marine information market that it serves, has relied primarily on observations of physical parameters such as waves, tides, currents, temperature and salinity. However, the information market is expected to change from one dominated by physical measurement, to one with more environmental measurements for people managing coastal zones (Summerhayes and Rayner, 2002). This calls for progress in biological and chemical oceanography, including the monitoring of HABs through refined observation and forecasting of harmful algae.

21.1.2 Need for an integrated multi-user approach

The oceans are vastly under-sampled restricting our understanding and the provision of information on environmental problems. A major challenge is therefore to increase the variety, quantity and quality of ocean and coastal measurements. Fortunately, many innovative technologies involving computing, robotics, communications, space exploration, and physical, chemical and biomolecular research are undergoing rapid development for many applications and will certainly improve our ability to monitor and study the ocean and to make predictions (Dickey, 2002). These measurements are vital for effective stewardship, preservation, and use of the oceans and coasts, but also expensive. As limited resources are available, and there is a need to consider costs and return of investment, judicious deployment of ocean assets is of utmost importance. Increased multiuse of the information derived from coastal observing systems is therefore imperative.

In order to meet the requirements for information, a multisectoral approach to environmental problems and questions must be encouraged. In planning and decision-making interdisciplinary linkages are necessary because of the climate and societal

controls on ecosystems, the feedback involving social change, and the decision-making relevance of forecasts (Clark et al., 2001). There are complex physical, chemical and biological linkages to all environmental issues and these interlinked issues need to be addressed in an integrated manner (Summerhayes et al., 2002). A major priority in coastal ecosystems is the description and measurement of their natural variability, through provision of scientifically sound and cost effective observations, data collection, storage and analysis. Virtually all-important environmental problems require interdisciplinary approaches and consequently require atmospheric, physical, chemical and biological data sets. Ideally these should be collected simultaneously and span broad scales to observe the processes of interest. These principles need to be applied to the investigation, monitoring and management of HABs thereby integrating different scientific disciplines and fostering dialogue between scientists and ocean managers. HABs need to be managed through better application of marine science and technology, and by gathering and using ocean and coastal information efficiently and cost-effectively from a multitude of sources. The focus must be maintained on those who will benefit from the detection and prediction of harmful blooms, their toxins and harmful impacts.

The need for comprehensive measurements in the marine environment has led to the formation of the Global Ocean Observing System (GOOS), which is designed to produce economic and social benefits from ocean observations on a global scale at an acceptable cost and risk (Summerhayes, 2002). The linking of HAB observation programmes to this global effort is likely to significantly benefit HAB management initiatives by providing the local user with an accurate regional framework, thereby improving predictability. The approach of GOOS has recently been simplified and streamlined. It now centres on an open ocean GOOS theme, devoted mainly to weather and climate forecasting and services, and a coastal GOOS theme with a much higher density of observations that address a wider variety of issues, including pollution and living marine resources. The Coastal Ocean Observations Panel (COOP) has designed the coastal theme and the primary focus is on preserving healthy coastal environments – monitoring habitat loss, nutrient enrichment, algal blooms and pollution; promoting sustainable use of marine resources – ecosystem based management, incorporating aquaculture; mitigating coastal hazards – storm surges, tropical storm damage, coastal erosion and sea-level rise; and ensuring safe and efficient marine operations – navigations, spills and ballast water. The focus of COOP observational design will be on beach and near-shore zone observations (Summerhayes, 2002) making it the logical link to the development of operational information services relating to HABs.

21.2 The phenomenon of harmful algal blooms

21.2.1 Defining harmful algal blooms

The term 'harmful algal bloom' has been applied to a diverse range of phytoplankton to which harmful impacts have been attributed. Knowledge of what defines a harmful species is qualitative and such species are still being identified. Although HABs have been considered primarily flagellate events, for example dinoflagellates, raphidophytes and prymnesiophytes, many other groups of phytoplankton, e.g. diatoms and cyanobacteria, include species, which are now considered harmful. The diversity of HAB species

significantly complicates monitoring programmes (Sournia, 1995). A broad classification of HABs distinguishes two major groups of causative organisms: those that produce toxins, which can contaminate seafood or cause marine mortalities, and those that do not produce toxins, but which cause other deleterious impacts, typically through significant accumulation of biomass (GEOHAB, 2001). What constitutes a harmful bloom often has species specific, regional and seasonal aspects and is not simply a biomass issue as some species may be harmful at low densities. Consequently the detection of HABs and the monitoring of the ecosystems in which they are found may require approaches and technical capabilities that are varied and in many cases species or problem specific.

21.2.2 Impacts of harmful algal blooms

Just as harmful species are still being identified the modes and mechanisms of harmful effects are still being described. The consequences and impacts of harmful blooms are varied and typically depend on the species present. Four broad categories of deleterious effects have been defined (GEOHAB, 2001): risk to human health, loss of seafood resources, impairment of tourism and recreational activities, and damage to non-commercial marine resources and wildlife. A particular HAB event or species may be associated with more than a single category of impact.

Of particular concern are the HAB species that cause public health impacts owing to the production of toxins. The most common toxin syndromes caused by HABs are ciguatera fish poisoning, and paralytic, diarrhetic, neurotoxic, azaspiracid and amnesic shellfish poisoning, associated mostly with the consumption of shellfish. Also of concern to human health are the respiratory problems linked to the transport of toxins in aerosols, and allergies in humans attributed to cyanobacterial blooms. Blooms of icthyotoxic species may induce die-offs of farmed fish and cultivated shellfish, and of commercial fisheries. Mortality can occur through direct ingestion of toxic species, on exposure to secreted toxins or from toxin vectoring through the food web. Toxins moving through the ecosystem may have far reaching impacts. Negative influences on viability, fecundity, recruitment and growth have only recently been recognized. Marine mammals, such as whales, dolphins, sea lions and manatees, and birds have all suffered morbidity and mortalities as a result of exposure to HAB toxins transferred through the food web.

Harmful effects are not limited to the effects of toxins. Die-offs due to anoxia or hypoxia often follow the decay of large blooms of relatively ungrazed species. Mechanical damage is another mode of impact. Lethal piercing of gill filaments may result in respiratory failure, haemorrhaging or bacterial infection. Intracellular polymer excretions can induce mortality by forming viscosity barriers and through mucoid layer reduction. Gill clogging may also lead to osmoregulatory failure and ultimately death. Many coastal areas worldwide are affected by visible foams and scums, or noxious smells, with a range of visual and human effects, thus impacting tourism and recreation. Growing evidence suggests that the negative *in situ* ecological effects of some blooms have the most detrimental and remarkably diverse impacts (Smayda, 1997). All trophic compartments of the marine food web are therefore vulnerable to harmful blooms, but rarely are the trophodynamic effects of blooms considered.

The impacts of HABs are therefore diverse and many sectors of society are affected. Consequently the users of information relating to the impacts of HABs are diverse with varying needs for information.

21.2.3 Requirements of harmful algal bloom monitoring programmes

The goal of HAB monitoring programmes is to protect public health, fisheries and aquaculture resources, and ecosystem function and coastal aesthetics, and management requirements and actions will clearly depend on the type of HAB and impact. The classification of harmful algae into those that produce toxins that contaminate seafood or cause marine mortalities, and those that cause deleterious impacts typically through significant accumulation of biomass may require essentially different approaches to monitoring. There are fundamental differences in the approach and requirements of those managing public health and those responsible for the management of fisheries and aquaculture resources, ecosystem function and coastal aesthetics. The management effort and requirement for information relating to the latter categories varies dramatically between regions and countries owing somewhat to their local importance and the local ability to address these issues. However, for human health, the need for global consistency and more stringent monitoring requirements, in order to eliminate risks to consumers and to reduce obstacles to trade, is more urgent. Owing to these fundamental differences seafood safety regulators tend to dictate the requirements of monitoring programmes around the world and tend to be restrictive and conservative in terms of the approaches applied to monitoring. The design elements of these monitoring programmes must incorporate the rules and regulations imposed by responsible national and regional authorities (e.g. US National Shellfish Sanitation Program – NSSP, 1995*a* , 1995*b* ; EU Directives 91/492/EEC and 97/61/EEC health conditions for the production and placing on the market of live bivalve molluscs – Council of the European Communities, 1991, 1997) in their attempt to be accepted internationally. At the core of these management programmes are the monitoring programmes needed to detect cells or toxins sufficiently early to take management actions.

To serve the diverse group of users requiring observations and information relating to HABs, monitoring programmes should preferably comprise three basic elements:

- Observations of the environment important in the development of blooms; as characterization of the distribution of HABs in relation to these environmental parameters will ultimately allow for early warning and prediction.
- Observations of the algal response to changing environmental conditions; specifically the change in the species composition favouring the growth of a harmful species or an increase in total algal biomass. This may incorporate assessment of the toxins in plankton.
- Observations of the negative impacts of HABs; specifically the presence of toxins in shellfish and fish, and related mortalities. Detrimental environmental impacts should also be monitored; including decreased light penetration, anoxia/hypoxia, production of hydrogen sulphide, development of foams and scums, habitat degradation, etc.

This inclusive approach to monitoring will provide the quantitative ecological observations required to understand the many factors that regulate the dynamics of HABs and to establish their *in situ* impacts. Monitoring programmes of this kind should be adapted to local conditions and circumstances but must also be interfaced with other monitoring efforts.

21.2.4 Development of operational oceanographic services relating to harmful algal blooms

The development of real-time coastal observing systems provides the opportunity for development of operational oceanographic information services relating to HABs. The

need to observe, understand and forecast coastal ecosystems, HABs and their impacts is going to increase significantly in order to permit relevant and effective management decisions. The inclusion of data relating to HABs into the field of operational oceanography will provide operationally useful information for a wide range of users and customers about the present and future status of HABs. Operational oceanography is the activity of routinely making, disseminating and interpreting measurements of the oceans and atmosphere (Woods et al., 1996). Operational oceanography provides measurements that are systematic, routine, cost-effective, of known quality, sustained for the long term, available in a timely manner and relevant to users' needs. Operational oceanography proceeds usually, but not always, by the rapid transmission of observational data to computerized data assembly centres, where the data are processed through numerical forecasting models (Woods et al., 1996). Outputs from the models are used to generate secondary data products and forecasts that must be distributed rapidly to users in industry and commerce, government agencies and regulatory authorities.

Observing systems are maturing and rates of capture of data are rapidly increasing. Value is being added to these data by storing, retrieving, managing and manipulating them to derive products tailored to the needs of different customers. The further development of operational forecasting services incorporating HABs will depend on improvements in biological observations, specifically those relating to the detection of harmful algae and their toxins; transition of research-based observing networks to operational networks; integration of meteorological data gathering systems with oceanographic observations; commitment to the continuity of observation programmes; timely acquisition, dissemination and exchange of data, and assimilation into models; improved numerical modelling and simulation of coastal environments and their biological response; development of the value-added services sector through synergy between the customer and the basic sciences; provision of incentives for participation by industry; and maintaining an acceptable ratio of benefit to costs.

21.3 Scientific feasibility and technical capability versus user needs

The research community is driving the field of real-time observing systems forward at an impressive pace through the introduction of new technologies such as automated instruments, satellite observations, global positioning systems and the rapid transmission of data to high-speed computers. The development of real-time observing systems has progressed owing in some part to advances in the ability to telemeter data from ocean moorings or other fixed location platforms. Data can be transmitted via coaxial cable or fibre-optic cable links which both allow for high-bandwidth transmissions. These cabling methods have great advantages, but can be expensive if cable networks are not already in place. Where direct link transfer is not feasible, data can be telemetered from surface buoys to land stations using line-of-sight radio frequency, cellular phone or communication satellite transmissions (Dickey, 2002). In the case of subsurface moorings data can be sent from instruments at depth to a surface buoy, with the mooring wire acting as the transmission element or using subsurface acoustic modems. The amount of data that can at present be transmitted is limited by bandwidth availability. Consequently most platforms need improved telemetry for data transmission and

instrument control (Dickey, 2002). Cost per transmission is an important factor and may be prohibitive for some applications, and power remains a constraining factor.

The user is therefore required to give careful consideration to the variables to be measured, their accuracy, temporal and spatial resolution, and domains of collection. Ocean and coastal managers require more than observation systems and the data they provide. There is a difference in being able to detect a given entity and being able to provide the user with useful information. Users and commercial customers want environmental information products that can be readily incorporated into existing operations. It is important to recognize that societally important oceanographic problems require that data be interpreted following collection, and that it be rapidly disseminated to decision-makers and the public. The user is therefore required to make an assessment of the availability of real-time observations, the technological and operational base for data capture, data collection, numerical modelling and data assimilation, information management and presentation.

21.3.1 Ecosystem approach to monitoring harmful algal blooms

The complexity of coastal environments and the interactions between all their components require an ecosystem approach to management. Understanding of the processes and interactions favouring HAB development within a particular ecosystem requires characterization of algal distributions in relation to environmental factors. Models that relate algal population dynamics to these observed properties of the ecosystem are required for early warning and prediction of algal blooms. Physical, chemical and biological processes in coastal ecosystems are generally more dynamic and complex than in the open ocean. There is thus a pressing need for robust, quantitative, and cost-effective methods to detect and characterize algal blooms in terms of the ecosystems in which they are found. Observations range from visual detection of discoloured water and analysis of water samples to autonomous measurements from moorings to remote sensing. Our understanding of the ecophysiological mechanisms that favour one species over another is poor and this physiological characterization of harmful phytoplankton in an oceanographic context is key to understanding the environmental regulation of harmful blooms. Early warning and predictive models can be developed and validated only if timely physical, chemical and biological observations are available.

21.3.1.1 Required observations

The variability associated with HABs and the processes important to their formation require observational strategies that incorporate sensors and systems capable of sampling on multiple time and space scales (Chang and Dickey, 2003). A new generation of oceanographic instruments can provide near-continuous measurements of many physical, chemical and biological properties from a variety of platforms. However costs for instruments are high, accuracy must be maintained over long periods, some of the measurements are difficult to interpret or to correct for interference, autonomous systems are subject to fouling and disturbance, and power requirements remain a limiting factor.

Physics and chemistry

Changes in the phytoplankton community are strongly influenced by physical processes. Atmospheric variables and the physical properties of water are therefore of great importance in the development of HABs and typically provide the data

requirements for hydrodynamic models. More specifically solar insolation, winds and tides, mixed layer dynamics, surface and internal waves, upwelling events, fronts, jets and eddies need to be monitored and assessed in terms of their role in bloom dynamics. Physical instrumentation has remained relatively unchanged, except for a reduction in size, weight and power requirements, and the ability to interface instruments (Chang and Dickey, 2003). Wind information is the number one geophysical information requirement of the marine community and is routinely available from a number of platforms, as are precision measurements of temperature and salinity. Similarly measures of sea level, tides, turbulence and current measurements are becoming routine and cost effective allowing for autonomous deployment and the provision of real-time data, crucial for the development and validation of models pertaining to HABs.

In monitoring water chemistry the ability to identify and quantify trace metals, synthetic organics, and toxic substances in the field lags behind the ability to analyse them in the laboratory. However, several new sensors and analyzers are capable of making *in situ* time-series measurements with sampling intervals of a few minutes and durations of months, and have been successfully deployed from moorings, drifters and AUVs providing real-time and near real-time telemetry of a variety of chemical variables. The various measurements use a variety of methods, including polarographic electrodes, colorimetry and spectrophotometry, and the primary advantage of these *in situ* sensors is the ability to integrate measurements of ocean chemistry with other oceanographic parameters (Chang and Dickey, 2003). Measurements of particular relevance to ocean chemistry and HABs include nutrients, and the partial pressure of carbon dioxide and dissolved oxygen, which have enabled new insights into primary and new production, as well as eutrophication and coastal pollution. Although nutrient concentrations cannot be directly correlated to algal biomass, escalating trends in HABs have in some cases been attributed to nutrient loading and coastal eutrophication. Autonomous measurement of nutrient concentrations is therefore potentially useful for describing and understanding the dynamics of algal blooms and any increase or decrease in their incidence.

Bio-optics

Bio-optics refers to the biological effects on optical properties and light propagation through the ocean and can provide information central to physical-biological interactions, such as ocean primary productivity and biomass, biogeochemical cycling and the biological pump, sediment resuspension and transport, ocean pollution, and bio-optically modulated variability in upper ocean heating rates (Dickey and Falkowski, 2002). Subsurface light fields are affected by both incident solar radiation and properties of ocean waters. Therefore particulates, both organic and inorganic, and dissolved materials play key roles in the variability of ocean optical properties. As one of the few means available to observe the biological characteristics of the upper ocean, at the required scales, and from a variety of platforms, the need to measure ocean colour and related optical characteristics will grow and will be extremely useful in describing blooms and long-term trends. Because *in situ* optical sensors measure physical quantities directly related to those observed by ocean-colour sensors in orbit, they provide a useful comparative measures to that provided by satellite and will be important in ground-truthing and algorithm development. Together, these optical measures may be used to initialize biological models within forecast systems.

Ocean colour is generally measured as upwelling spectral radiance, normalized to downwelling solar irradiance to calculate radiance reflectance, which is a function of both the scattering and absorption properties within the water column. Ocean-colour measurements from space are further influenced by atmospheric and air/sea interface effects. Ocean colour is often related to near-surface chlorophyll *a* concentrations through empirically derived algorithms. These have been particularly successful in open oceans, however the situation is optically more complex in coastal waters where the algorithms have to discriminate the absorption and scattering of algae from the absorption and scattering of terrigenous inputs of coloured dissolved organic matter, suspended sediment and other particulates. *In situ* radiometers are extremely useful for the development of local algorithms to interpret remote sensing observations from aircraft or satellites.

Optical approaches to the detection of HABs are limited because optics tend to provide only a bulk composite signal for a body of water, from which signals attributable to any particular species of phytoplankton are difficult to discern. However, the optical properties of absorption, scattering and attenuation can now be measured at multiple wavelengths using commercially available instruments, allowing phytoplankton to be distinguished from other particulate and coloured dissolved materials (Chang and Dickey, 1999), and providing the potential of taxon-specific information.

Until recently *in situ* absorption measurements were difficult to make owing to the low signal in ocean waters. However, systems have now been developed for continuous *in situ* measurement allowing groups of phytoplankton to be distinguished according to their absorption characteristics. Bulk absorption measurements represent the additive absorption of water and the specific *in situ* constituents of phytoplankton, dissolved organics, detritus and sediment. The instrument signal thus needs to be deconvolved into these constituents (Schofield et al., 1999). Separating the phytoplankton absorption from the particulate spectrum is a central problem for HAB applications. Assuming that a phytoplankton absorption spectrum can be derived from a bulk optical measurement, techniques for delineating the presence and quantity of a HAB species in a heterogeneous phytoplankton community are required. Pattern recognition approaches can be applied (Schofield et al., 2003), however, delineation of a particular species can be successful only if the species represents a significant fraction of the overall phytoplankton biomass and has discriminating features in cellular optical properties.

Light-scattering measurements show promise for detecting the concentration and size of particulate material in seawater (Schofield et al., 2003). The theory underlying the estimation of particle size from scattering characteristics is based on the fact that the angular distribution of scattered light is a function of particle size and the relative refractive index (Stramski and Kiefer, 1991). Given this, caution must be used when relating scattering to cell size as the refractive index can change dramatically owing to changes in cellular pigmentation and other intracellular compounds. Like absorption measurements, the bulk scattering signal reflects the additive contributions of the specific components present, requiring inversion algorithms to extract the relative contribution of the phytoplankton. More relevant to remote sensing applications is backward scattered light. Spectral backscattering coefficients may be used to derive the modal size of particulate material, which in combination with derived phytoplankton absorption may provide useful taxon-specific information (Schofield et al., 2003). Turbidity sensors measure sidescatter or

backscatter in the infrared and measurements can be empirically related to water clarity or particle load.

Spectral attenuation measurements are also potentially useful for distinguishing phytoplankton *in situ*. It is important to recognize that spectral attenuation includes both scattering and absorption, and that in surface waters the scattering coefficient of phytoplankton is generally much greater than the absorption coefficient. Consequently, measures of light beam attenuation are dominated by scattering, which for phytoplankton has weaker spectral features in the visible range than does absorption, and are therefore less sensitive than absorption-based techniques (Stramski and Reynolds, 1993). Transmissometers measure attenuation at a single wavelength of 660 nm, providing a measure of particle concentration, not strongly affected by algal pigments. Thus the comparison of beam attenuation versus chlorophyll fluorescence is potentially informative.

Various forms of fluorometry have been used to estimate phytoplankton biomass and primary productivity. Measurements of stimulated fluorescence of chlorophyll *a* by means of *in situ* relatively inexpensive submersible fluorometers have been widely used to provide an estimate of phytoplankton concentrations. It is an extremely sensitive method but provides no useful signal for discrimination of algal species. Measurements should be carefully calibrated, paying particular attention to the influence of irradiance, species composition and nutritional state of phytoplankton on fluorescence yield (Cullen et al., 1997). This may not be possible when fluorometers are used in autonomous systems as required in the provision of continuous real-time data. Most *in situ* fluorometers use broadband blue irradiance for excitation and detect the red emission of chlorophyll near 683 nm. However, spectral fluorometry can potentially discern the influences of different accessory pigments, some of which may assist in revealing different taxa. Submersible fixed-wavelength spectrofluorometers are available but do not have the spectral resolution required for pattern-recognition algorithms.

Solar-induced chlorophyll fluorescence near 683 nm can be used to detect phytoplankton biomass and has also been related to photosynthesis (Kiefer and Reynolds, 1992). Passive observation is attractive as it can be used in remote sensing, the radiometric quantities measured are well defined, and passive instruments have very low power requirements, hence they are well suited for extended deployment in remote locations. Accurate measurement of solar induced fluorescence is easily compromised and interpretation of measurements requires various assumptions of algal physiology (Cullen et al., 1997). Sophisticated measurements of fluorescence-based photosystem II quantum yield measurements using pump-and-probe and fast repetition rate fluorometers have the important advantage of providing information about biophysical parameters related to photosynthesis and the physiological state of phytoplankton (Falkowski and Kobler, 1995). Interpretation of these measurements still requires refinement and instrument performance has yet to be fully evaluated under varying conditions.

Harmful algal species

Timely detection of harmful algal species provides coastal resource managers, fisherman, aquaculture operators, and public health officials with the data needed to recommend or take actions for minimizing the effects of HABs. One of the most important components of any HAB monitoring programme therefore incorporates monitoring the algae directly usually by obtaining counts of individual species that guide management decisions incorporating additional monitoring activities. For the purposes of health requirements many HAB monitoring programmes stipulate a requirement

for monitoring the presence of toxin-producing plankton in addition to monitoring biotoxins in bivalve molluscs. Cell concentrations of toxic species are therefore, in some instances, used as a guide to initiate testing of toxins in shellfish and are in some cases used as the decision criterion for harvesting closures. At present there is, however, no general consensus on the actions that should be taken for given cell concentrations. Action limits based on cell concentrations can be highly variable between countries and reflect variability in the toxicity of strains or populations of the species.

Microscopic enumeration requires an appropriate level of expertise to generate accurate estimates of cell abundance. Difficulties in identifying and distinguishing between morphologically similar species or strains are a common problem, not only for those with limited taxonomic training, but also for skilled taxonomists, as considerable time and effort are required to identify a species when its distinguishing characteristics are not discernable under the light microscope. Such levels of discrimination are simply not feasible in monitoring programmes that generate large numbers of samples for cell enumeration.

Owing to these problems, research has been directed towards the development of species or strain specific probes that can be used to label cells of interest so that they can be detected either visually, chemically or electronically (Parrish, 1999). The most rapidly growing area of HAB species detection involves the targeting of specific molecules located on the cell surface and various components of an organism's genome, by antibody or oligonucleotide probes. However commercialization of these probes remains a slow and difficult process limiting the extent to which these tools are applied outside those laboratories directly involved in their development and testing.

Immunological techniques use antibodies that bind specifically to constituents of the cell walls of the species of interest. To date a number of researchers have developed antibodies against cell surface antigens specific to a wide range of harmful taxa (Anderson, 1995). Similarly, the binding of lectins to cell surface polysaccharides has been used to detect harmful taxa (Aguilera et al., 1995). Either epifluorescence microscopy or flow cytometry may be employed in detecting HABs labelled with antibodies and lectins. Antibodies are applied in conjunction with a fluorophore-based reporting system yielding a fluorescent signal from labelled cells. The use of fluorescence to detect antibody-antigen reactions is collectively referred to as immunofluorescence. Flow cytometric methods based on immunofluorescence show promise as an automated means of detecting antibody-labelled HAB species (Peperzak et al., 2000). However, issues related to the loss of cells during staining, and thus poor quantification of cell concentrations must still be resolved and have apparently precluded incorporation of this approach into routine HAB monitoring programmes (Sellner et al., 2003).

Nucleic acids have also been employed as target molecules for the detection of HAB taxa. In particular, components of the ribosomal RNA gene (rDNA) and their transcriptional products, the corresponding ribosomal RNA (rRNA) molecules, possess several characteristics that make these cellular constituents highly amenable to such applications (Sellner et al., 2003). Two approaches use oligonucleotide probes in the detection of HAB species. The first approach, referred to as whole-cell hybridization or fluorescence *in situ* hybridization, requires penetration by the probe into chemically fixed, intact cells, which hybridizes or binds to its target sequence on the rRNA molecules, and is visualized via a fluorescent reporter either attached directly to the probe or applied during a secondary labelling step. Algal cells labelled in this manner can be examined directly by epifluorescence microscopy or using automated methods such as flow cytometry. The second approach to applying oligonucleotide

probes to the detection of HABs is the sandwich hybridization method, which requires chemical lysis of the algal cells to release rRNA target molecules. The target is bound by a species-specific 'capture' probe immobilized to a solid support, such as a bead or membrane, followed then by hybridization of a 'signal' probe to another region of the rRNA, which is responsible for visualizing the captured rRNA using colorimetric, fluorometric or chemiluminescent reporting systems. This technique precludes direct microscopic observation of labelled target cells, but allows for rapid, high throughput sample analysis that has been effectively automated in a variety of formats. Rapid sandwich hybridization sample processing technology, including pre-packaged reagents specific for the colorimetric-based detection of a number of individual HAB species, is now commercially available. In addition to colorimetric-based reporting systems, the binding of an oligonucleotide probe to its rRNA target in solution, following cell lysis, can be detected through the use of electrochemical methods.

Application of molecular probe technology outside the laboratory poses several challenges, particularly if unattended, real-time analysis is required. A novel instrument known as the Environmental Sample Processor (ESP) has been developed in an effort to meet these demands (Scholin et al., 2002). This instrument collects discrete water samples, concentrates micro-organisms and automates application of DNA molecular probes to enable identification and quantification of particular species. A sandwich hybridization assay, including harvesting and filtration of the algal cells, production of a cell lysate, application of the rRNA-containing lysate to an array, and detection of bound target molecules via a signal probe/chemiluminescent-based reporting system, is completely automated and performed onboard the Environmental Sample Processor. Results are transmitted in near real-time to a shore-based location. In addition, the instrument archives discrete samples for nucleic acid, microscopic and toxin analyses for the purposes of verification. Successful trial deployments of the Environmental Sample Processor have been conducted using arrays configured for both species of *Pseudo-nitzschia* and *Alexandrium* allowing simultaneous detection of either group.

The application of PCR-based methods, targeting unique genetic signatures to the detection of HAB species is also currently receiving considerable attention. Taxon-specific PCR primers have been used to amplify selected regions of target genes of HAB species from a standard genomic DNA preparation, followed by detection of the resulting amplicon by various techniques, including gel electrophoresis and staining/blotting protocols and fluorescent fragment detection. Such PCR-based methods can be highly sensitive and have been successfully employed to amplify and detect single cells. Recently developed quantitative competitive PCR, real-time PCR, and time-step PCR have the potential to yield quantitative information on algal cell concentrations, however these capabilities have yet to be realized for harmful species occurring in natural samples (Sellner et al., 2003).

The principals of flow cytometry have been developed to detect phytoplankton cells based on their morphological and optical properties and show some promise in providing an alternative to microscopic enumeration of cells. An instrument known as the FLOW Cytometer And Microscope (i.e. FLOWCAM) is able to count, image and analyse each particle in the sample as it passes through the instrument. This includes but is not limited to chlorophyll and phycoerythrin fluorescence and light scatter (Sieracki et al., 1998). Images of all particles are saved and image processors are able to identify certain cell types, including harmful species. These instruments may be operated in continuous sampling mode in a weather proof enclosure for extended periods, producing abundance data of selected cell types. A submersible version of

the FLOWCAM that can be moored is now commercially available and provides the potential for real-time species specific data.

Harmful algal toxins

A broad spectrum of algal species is found to produce a broad spectrum of toxic compounds that need to be detected in both the species producing them and in the organisms into which they are transferred. As toxins move through the food web they may be biotransformed into structurally different compounds, which may be of either higher or lower toxicity than the original toxin molecule. The broad chemical and structural diversity of algal toxins, coupled with differences in intrinsic potency and their susceptibility to biotransformation, account for many of the challenges associated with the detection of these compounds (Sellner et al., 2003).

Algal toxin detection can be categorized into chemical analyses, and *in vivo* and *in vitro* assays, none of which are currently able to provide *in situ* real-time data. In terms of chemical analyses, high-performance liquid chromatography (HPLC) employing either UV or fluorescence based detection of either the toxin molecule or a chemically derivatized form of the toxin, is a common form of analysis. However, HPLC analysis does not permit the concurrent injection of multiple samples on a single instrument required for high throughput testing. More recently, mass spectrometers, coupled to liquid chromatographic separation methods have been employed to identify HAB toxins and have been advocated as a universal analytical method for toxin analysis (Quilliam, 1998). Its advantages are the detection of multiple toxins, high specificity, high sensitivity, automation and limited sample preparation. Its drawbacks are high capital cost, the need for considerable technical expertise and the need for calibration standards. Recent innovations have resulted in the development of small modular instruments, which have been incorporated into autonomous underwater vehicles. Future designs may potentially be adapted for the detection of algal toxins and could be configured for *in situ* real-time detection of toxins.

In vivo mammalian bioassays exist for most of the major toxin groups, and are indeed the preferred or specified means of toxin detection in many HAB monitoring programmes (Fernandez and Cembella, 1995). However this approach shows no potential for high throughput, automated or *in situ* application.

In vitro assays have been broadly classified into functional and structural-based approaches (Sellner et al., 2003). Functional assays (e.g. cytotoxicity assays, enzyme inhibition assays and receptor binding assays) are based on binding of the biological receptor and toxin, and the affinity of this interaction is proportional to the toxin's intrinsic potency, the assay response therefore reflecting the net toxicity of all congeners that are bound by the same class of receptor. Such assays can therefore not be used to identify a particular toxin, but rather detect and measure a particular toxic activity. Retaining the biological activity of a cell line or a receptor preparation, required for toxin recognition, under adverse conditions outside the laboratory remains an obstacle to the development of *in situ* functional assays. Structural assays (e.g. immunoassays) require the conformational interaction of a toxin with a recognition factor and generally display a high degree of specificity for the toxin. The detection of multiple toxin congeners depends on the degree to which the assay recognition factor cross-reacts with these various chemical derivatives. Generally immunoassays are robust techniques that lend themselves to use in the field and to future deployment on *in situ* platforms. Antibody based assays have been developed for a variety of HAB toxins and many of these tests are now commercially available. The portability of these systems makes them suitable for the rapid

detection of certain algal toxins in field settings, although the sample throughput and quantification capabilities are limited.

Any newly developed method of detecting toxins must undergo inter-laboratory validation to determine its performance in terms of accuracy, precision and other performance parameters. Method validation programmes, such as those operated by the AOAC (Official Methods Program) and the International Union for Pure and Applied Chemistry (IUPAC), are expensive and time-consuming to conduct, but critical for the acceptance of new methods. Consequently the internationally recognized method used for analysis of most shellfish toxins remains the standard AOAC mouse bioassay. There are many emerging technologies that demonstrate reliable detection of toxins, some of which lend themselves to the provision of real-time data. However most have not been certified and are therefore unlikely to be adopted by regulatory agencies in the near future.

21.3.1.2 In situ platforms, space and airborne surveillance

Real-time data on atmospheric, physical, hydrological, chemical and biological parameters within coastal ecosystems may be obtained with a minimum of personnel by establishing platforms of various types of sensor packages. *In situ* systems and space and airborne surveillance serve to complement each other. In addition to providing ground truth data that are critical to the development of space and air-based environmental information products, *in situ* sensors overcome the inherent limitation of space and airborne sensors in terms of their inability to make observations below the ocean surface. Considerations for future sensors and systems to be deployed from a variety of platforms include response time, size, power requirements, durability, reliability, stability, susceptibility to biofouling, data storage and telemetry, and cost. With many *in situ* systems validation of instrument performance during extended autonomous deployments is difficult.

Ships

One of the advantages of ships is that advanced analytical instrumentation which cannot at present be deployed *in situ* from other platforms, can be used often with real-time data analysis. In addition to on-station profiling, under-way sampling by means of flow-through systems, acoustical measurements and towed underwater vehicles is now common. Ships have served the oceanographic community well. But their limitations in terms of cost, availability and limited synoptic sampling have stimulated development of other complementary platforms (Dickey, 2002). Consequently ships are important in detailed process orientated measurements providing the necessary understanding for decision-making, but are often less appropriate for routine observations at appropriate scales.

Moorings and profiling instrumentation

An increasing number of parameters are being measured from anchored water column and bottom moorings, which are able to provide temporal information of variable resolution. Shore-based instrumentation on coastal piers, and offshore oil production platforms offer unique opportunities for mooring instrumentation, while expendable moorings can be deployed in remote areas and do not require servicing and recovery. Autonomous profiling by moored instrumentation is also possible providing vertical resolution data. Moored packages may reside at depth, and at programmed cues, rise to the surface while recording data from a suite of sensors. Systems that reside on the

seafloor are less susceptible to some of the hazards that are encountered by surface moorings. The greatest disadvantage of moorings is their high cost, susceptibility to fouling and the risk of loss. Therefore it is important to optimally select mooring locations enabling regular recovery for the purposes of servicing.

Drifters, floats and autonomous underwater vehicles

Drifters and floats may be used to obtain spatial data by following particular bodies of water. The new technology of profiling floats, using buoyancy changes to move vertically allows detailed observations of the interior of the oceans. Recent technology has improved the utility of drifters and floats. The availability of two-way satellite communication coupled with the Global Positioning System provides the ability to relay greater volumes of data including accurate position data. Sensor development has allowed incorporation of a more complete set of sensors, and the conversion of floats into active, self-propelled vehicles has allowed the ocean to be sampled along prescribed paths. Drifters and floats in coastal systems are however susceptible to loss offshore or to being stranded on beaches. Additional problems include biofouling and limitations in size, weight and power (Chang and Dickey, 2003).

Several forms of autonomous underwater vehicles (AUVs) are being developed including surface craft, moored profilers, gliders and propelled AUVs. Their operation is expected to become routine as mission length capabilities increase, costs decline, reliability improves, and sensors become available for various sampling needs. The capability of feature-based or adaptive sampling may favour the incorporation of AUVs in the monitoring or investigation of HABs.

Spaceborne surveillance

Spaceborne surveillance, employing sensors mounted on earth observation satellites, has many applications in the marine sector. The obvious attraction of these sensors is their ability to provide synoptic views over large areas of the ocean surface. These synoptic views also allow the user to sample the environment in an adaptive fashion, by directing surface based surveillance. The timely delivery of data, accessible via direct-broadcast satellite dishes and access to a growing number of satellites will increase the demand for remote sensing technologies by marine forecasting services. The data from space-based images are typically empirical inferences of surface signals, either passive or active electromagnetic radiation, and are often based on ground-truth data sets obtained from ocean or coastal-based platforms. Because electromagnetic radiation only penetrates to very shallow depths and the marine user community needs information at depth, satellite information must be complemented with *in situ* observations to characterize subsurface properties.

Some of today's oceanographically important remotely sensed variables include solar radiation, wind stress and direction, rainfall, surface heat fluxes, sea surface temperature, ocean colour and sea surface height. Satellite radar altimeters, infrared imaging and radar backscatter sensors provide frequent global views of the ocean surface. These respectively describe sea surface elevation fluctuations associated with changes in ocean heat storage and near-surface currents, sea surface temperature that modulates the exchange of heat and water between ocean and atmosphere, and winds that drive ocean currents.

Satellite remote sensing has long been considered a tool with considerable potential for monitoring the distribution of HABs owing to photoelectric detection of ocean colour, which provides detailed and quantitative information on water constituents. The ocean-colour signal recorded by a remote sensor contains considerable noise. Therefore

the function of the ocean-colour algorithm is to work back from the detected signal, removing or correcting for atmospheric and air/sea interface effects and distinguishing between the required phytoplankton-related information and other marine signals, a process known as inversion or retrieval (Ruddick et al., 2007 – Chapter 9 this volume). Chlorophyll *a* has been used as the conventional measure of phytoplankton biomass for many years and most ocean-colour algorithms have targeted this parameter. The importance of atmospheric scattering and absorption processes in contributing to the signal received by the sensor implies that quantitative information can be obtained only after a rather precise atmospheric correction. Development and testing of algorithms for retrieval of chlorophyll *a,* over the last 30 years, has led to the generation of reliable ocean-colour chlorophyll products for open ocean waters. However, for many coastal waters accurate detection of chlorophyll remains a problem. Here, imperfect atmospheric correction and the difficulty of distinguishing between phytoplankton and non-phytoplankton optical properties can seriously degrade chlorophyll *a* products.

Owing to the rapid expansion in available satellite-based ocean-colour sensors, the user is required to consider the technical characteristics of sensors and satellite platforms to determine their suitability for specific applications, the cost and availability of data, and product quality (Ruddick et al., 2007 – Chapter 9 this volume). The number, location and width of spectral bands are crucial in determining whether a sensor will be able to detect phytoplankton-related phenomena. Generally, for coastal waters, a greater number of bands are required in order to distinguish a phytoplankton signal and it is expected that the future for optical remote sensing of coastal waters is hyperspectral. However to ensure continuity of specific ocean-colour derived products it is desirable that new sensors possess some common spectral channels, which will allow intercomparison between sensors, compatibility of simple algorithms and facilitation of data merging. While no single system guarantees a long-term source of ocean-colour data, the success of SeaWiFS and the promise of well-supported MODIS and MERIS sensors has stimulated rapid progress in processing algorithms and the confidence necessary for planning operational monitoring of chlorophyll *a* by satellite.

The temporal and spatial resolution of data sampling is another important consideration for the user. The orbit combined with the swath width of the sensor will determine the frequency at which an area will be viewed and the size of the region covered. Current satellite platforms for ocean-colour sensors orbit the earth in polar or near-polar sun-synchronous orbits. Consequently the revisit time varies from two or three images per day to one image every few days. In future, satellites with a geostationary orbit will afford near-continuous monitoring of specified regions which will enable observations of short-term changes. For HAB detection the swath of 1,000 km or more on most ocean-colour sensors is typically larger than the area affected. The spatial resolution of 1 km typical of many ocean-colour sensors may be adequate but the higher resolution provided by sensors such as MERIS may offer considerable advantages in the detection of HABs. Planned missions for colour and temperature can be expected to achieve spatial resolutions of tens of metres or less as well as increased optical spectral resolution down to a few nanometres and less (Davis et al., 1998).

In some applications it is beneficial to combine data of different types, for example thermal infrared and ocean colour. These advantages are afforded by mounting sensors on the same platform ensuring simultaneous collection of data. The level of user support is also important in influencing the choice of the user. Changes in sensor performance must be tracked and weaknesses in processing algorithms need to be addressed. Some ocean-colour sensors are still limited to some extent by the amount of data that

can be stored onboard and/or transmitted per orbit. For real-time HAB detection the speed of data transmission and ground segment processing is a key factor.

Commercialization of ocean-colour imagery is still relatively limited. Many space agencies provide data free of charge or at very low cost for research use. Economic pressures on space agencies to show a return for public investment will ultimately shape the availability and price of ocean colour imagery. However it is uncertain as to whether the price of data will be kept sufficiently low to encourage greater use and economy of scale, or high thereby reflecting the cost of acquisition. It is also uncertain as to whether single-country ocean-colour missions will continue to proliferate or whether the number of ocean-colour sensors will be reduced to a few well supported international missions with a long-term plan to ensure continuity. At present the stringent embargoes on access to real-time data for many users is another problem associated with satellite data.

Although remote sensing from spaceborne sensors offers the potential for improving the detection and mapping of harmful events, ocean-colour data are still used relatively infrequently in HAB detection and management. The ocean-colour technique is limited to surface blooms of sufficiently high biomass to make a discernible difference to surface reflectance. For HAB species which are toxic at low concentrations and which contribute only a small portion to the phytoplankton biomass the use of ocean colour is very limited. In other regions persistent cloud cover is sufficient to eliminate the technique. The number of available satellite-based ocean-colour sensors is nevertheless increasing, providing better spectral, temporal and spatial resolution. Consequently the number of derived products is also increasing (Schofield et al., 2003).

Until now, most applications of remote sensing for HAB detection have been based on spatial and temporal near-surface chlorophyll *a* concentrations and *a priori* knowledge of the phytoplankton species. Remote sensing has therefore been used mostly to complement *in situ* data of phytoplankton cell density and species, ecophysiological studies of HABs, ecological modelling or optical in water observations. Although multi-spectral scanners (e.g. Coastal Zone Color Scanner, CZCS; Seaviewing Wide Field-of-view Sensor, SeaWiFS) can be used to detect chlorophyll *a* and other pigments from algae, and taxon-specific ocean-colour algorithms have been successfully developed for groups of phytoplankton such as the coccolithophorids and blue-greens, their inclusion in HAB monitoring programmes has been constrained by their inability to discriminate phytoplankton populations at the species level. For known monospecific blooms, ocean colour has nevertheless been very useful in observing blooms (Steidinger and Haddad, 1981; Tester and Steidinger, 1997).

In addition to ocean colour, remote sensing of atmospheric and physical properties of the ocean has provided insight into the oceanographic context for areas in which HABs are found. Thermal infrared remote sensing of sea surface temperature has for example been useful in monitoring blooms by tracking water masses or specific hydrographic features associated or linked to red-tide blooms (e.g. Keafer and Anderson, 1993; Tester et al., 1991). These successes in tracking blooms within specified water masses suggests that the transport of blooms can be forecast by means of hydrodynamic models. Advanced analytical and modelling activities will be required to optimize the use of present and future remote sensing data sets.

Airborne surveillance

As with spaceborne surveillance, aircraft based systems are able to provide a variety of data including temperature, altimetry and colour. Where spaceborne sensors do not meet the operational needs of coastal or estuarine communities, airborne sensors may

be useful as they can provide essential increases in resolution in critical areas. While satellite platforms offer data at a global scale according to a systematic time schedule and with highly centralized data processing and distribution, airborne platforms offer the alternative of a more user-specific service at a regional scale. Unlike satellite imagery, which is restricted to a few fixed spectral bands at relatively low resolution, airborne imagery can be custom configured to the particular spectral properties of the target of interest. The lower altitude of airborne platforms allows a much higher spatial resolution to be achieved, typically metre scale or less and the possibility of underflying clouds. It is thought that airborne hyperspectral systems will always be able to exceed satellite system capabilities in terms of their combined spatial and spectral resolution, and signal-to-noise performance because of the longer exposure times available to airborne systems owing to the difference in platform speed. However, organization of data acquisition and processing of data are more labour-intensive and offer less scope for economies of scale than satellite systems.

Aerial surveys of ocean colour are able to map the distribution of blooms, through visual observation, aerial photography or video, or by means of a radiometer. Quantitative assessment by means of radiometry is more reliable than visual assessment for characterizing the variability of surface distributions of phytoplankton in coastal waters. As with spaceborne sensors there are many technical considerations in obtaining estimates of ocean colour from an airborne radiometer, although corrections are relatively small for low-flying aircraft. Future development of unmanned airborne vehicles whose payload may include multispectral optical and thermal digital cameras may reduce costs and could be positioned semi-permanently over a region of interest allowing imaging many times a day.

Multiplatform facility

Many integrated observing systems are currently under development by the oceanographic community and demonstrate considerable potential in assisting in the monitoring of HABs. Data from any one sensor provides only one piece of the environmental puzzle therefore a multiplatform capability provides many benefits. Coastal regions clearly need higher spatial and temporal resolution than others therefore strong interaction among observers and modellers will be needed to select key sampling locations and to design sampling arrays. An ideal observational network will comprise an array of observations from different sources for example remote sensing from satellites, meteorological stations, fixed and floating data-gathering arrays and observations from ships, providing long time-series records demonstrating the scales of natural variability. Careful consideration needs to be given to the process of data acquisition and the practice of fusing data from various sources to derive environmental information products. Numerical modelling is central to these collective programmes and observing arrays should be designed to meet the demands of models in order to provide output that is useful to the customer. In many instances the formation of partnerships between government agencies, private industry, and academia will be required to establish the necessary combination of sampling platforms.

21.3.2 Modelling and forecasting harmful algal blooms

The application of numerical models is now an important function of the manager of ocean or coastal zone operations (Flather, 2000). Switching to model-based generation of products will greatly improve the performance of local operational oceanographic services (Woods, 2000), as numerical models can add enormous amounts of

information to data. HAB forecasting systems will be of benefit to the user in guiding existing monitoring programmes and enabling a timely response to HAB events thereby mitigating their impact on human health and coastal economies. Sampling limitations have retarded development of our understanding of HABs and the environmental conditions promoting bloom initiation, maintenance and decline. Accumulation of better observations of algal distributions in relation to environmental factors will improve this understanding and allow for the development of better models. The more ancillary physical and chemical data that are available, the more likely we will be able to discriminate the environmental factors that have the strongest influence on HABs. Retrospective analysis of past blooms has in many cases been successful at describing the important factors that determine the development and distribution of algal blooms which can be very useful in establishing the probability of future blooms. Historical time-series data are therefore often central to management decisions as they allow predictions based on past experience.

Better understanding of the ecology of HAB species, acquisition of real-time data relating to HABs, increases in computing power, and improved modelling capabilities do offer hope for the development of appropriate predictions in the near future. Models can range from empirical predictions to detailed numerical forecasts based on simulations of algal growth and behaviour in hydrodynamic models. Ecosystem models have with varying degrees of success simulated nutrient and chlorophyll *a* fields. This traditional mass balance approach to bloom dynamics is however often inappropriate to the investigation of harmful blooms (Smayda, 1997). Most of these models are based on simplified food webs and therefore do not explicitly consider the diversity of phytoplankton populations. Thus current ecosystem models are some way from the more specialized species based models required for predicting HABs. Although simulation models can be effective in revealing which factors dominate in the control of algal bloom dynamics, the conditions that lead to the dominance of a particular species are difficult to resolve. Nevertheless detailed information on the physiology and behaviour of individual species is vital to understanding their dominance in particular environments. Ultimately species specific models will require species specific information.

HAB forecasting systems will require real-time observational capabilities over appropriate scales and atmospherically forced hydrodynamic-biological models designed to run in the forecast mode. Coastal forecasting is maturing owing to significant advances in circulation modelling and the adaptation of data-assimilation methods from the meteorology community. Incorporation of a biological component to ocean forecasting systems is however complex and will require a truly interdisciplinary effort. Coastal ocean forecasting networks generally work in a recursive mode (Glenn et al., 1998). Data assimilation represents a procedure by which observations are used to constrain a dynamic numerical model. The essential feature of data assimilation models is that information is used not only to initialize a forecast model, but newer observations are used to correct the model, so simulations of present conditions and predictions of future changes are as accurate as possible. Initially the data-assimilative model provides a nowcast that is moved forward in time by the circulation model driven by surface boundary forcing available through weather prediction systems. During the forecast cycle, additional field data are assimilated to constrain the model dynamics to provide improved nowcasts for the next set of ocean forecasts. To improve the quality of nowcasts, adaptive sampling may be initiated to collect data in specific regions within the forecast grid. Currently several assimilation methods are available

and several coupled physical-biological models have been constructed with data-assimilative methods, providing the basis for future HAB data-assimilative models.

An important factor in sustaining ocean observing networks is the continued demonstration of their use. Visualization of data sets and model simulations is likely to become more and more important in communicating the benefits of observations in managing the coastal environment (Wolanski et al., 1999). Visualization by means of computer animation provides a powerful tool for presenting complex information to users in a readily understandable way. Computer visualization technology, has for example been successfully used in combination with dispersion models to predict the probable drift of oil spills and people lost at sea. Visualization packages such as these could be adapted to demonstrate the movement and impacts of HABs within the coastal environment.

21.4 Case study of potential real-time observation and prediction of HABs in the southern Benguela

Harmful blooms are common in the southern Benguela upwelling system and as is often the case can be grouped into those that cause harm owing to their high biomass and those that produce toxins (Pitcher and Calder, 2000). The harmful effects of high-biomass blooms result typically from anoxia following the decay of dinoflagellate-dominated blooms (Figure 21.1), whereas public health is impacted by the high incidence of paralytic and diarrhetic shellfish poisoning. These toxic syndromes are usually caused by the dinoflagellates *Alexandrium catenella* , and *Dinophysis acuminata* and *Dinophysis fortii* respectively. These species may or may not be associated with high-biomass blooms that appear most often in stratified coastal waters over the southern Namaqua shelf. Effective coastal management of these blooms requires their characterization as ecologically prominent phenomena, the means of monitoring blooms and, ultimately, the operational forecasting of blooms and their impacts (Bernard et al., 2006).

Considerable effort has been placed on identification and quantification of the processes responsible for bloom development, and the spatial and temporal scales over which these processes are operative in order to predict when these blooms will be of potential coastal significance. In developing predictive models, there is however a high degree of uncertainty associated with the biological components of such models, although the physical processes responsible for bloom development and transport are better established (Pitcher et al., 1998; Probyn et al., 2000; Pitcher and Nelson, 2006; Pitcher and Weeks, 2006). At present the product of any realizable forecasting system is therefore the prediction of the shoreline impact of blooms. These predictions are highly dependent on real-time observational ability at critical ecosystem locations, dynamic circulation models needed to simulate the transportation of blooms in local flow fields, and the temporal limitation of meteorological forecasts to drive these models (Bernard et al., 2006).

Wind-driven flows are well known to be important in the transport of HABs in the Benguela, but trying to understand the effects of temporally fluctuating and spatially variable winds in coastal regions with capes, bays and subsurface topography is a challenging problem. Studies incorporating the simultaneous measurement of currents with observations of blooms have enabled the currents associated with the advection of red tide to be quantified. The set-up of poleward and shoreward currents

Figure 21.1
Mass strandings of rock lobster on the West Coast of South Africa following the decay of high-biomass dinoflagellate blooms, know as red tides, and the consequent depletion of oxygen concentrations.

near the coast during the relaxation of upwelling favourable winds has been identified as particularly important in the coastal transport of blooms. A useful example of current flow during the development of red tide at an inshore station on the southern Namaqua shelf is provided by a time series from 13–30 March 2001 (Figure 21.2). The development of red tide followed the reversal of upwelling winds. Progressive current vectors at the surface indicated that flow was predominantly southward, introducing red tide (>100 mg chl *a* m^{-3}) into the region during the latter half of the time series. Although southward flow dominated, a period of onshore flow coinciding with the

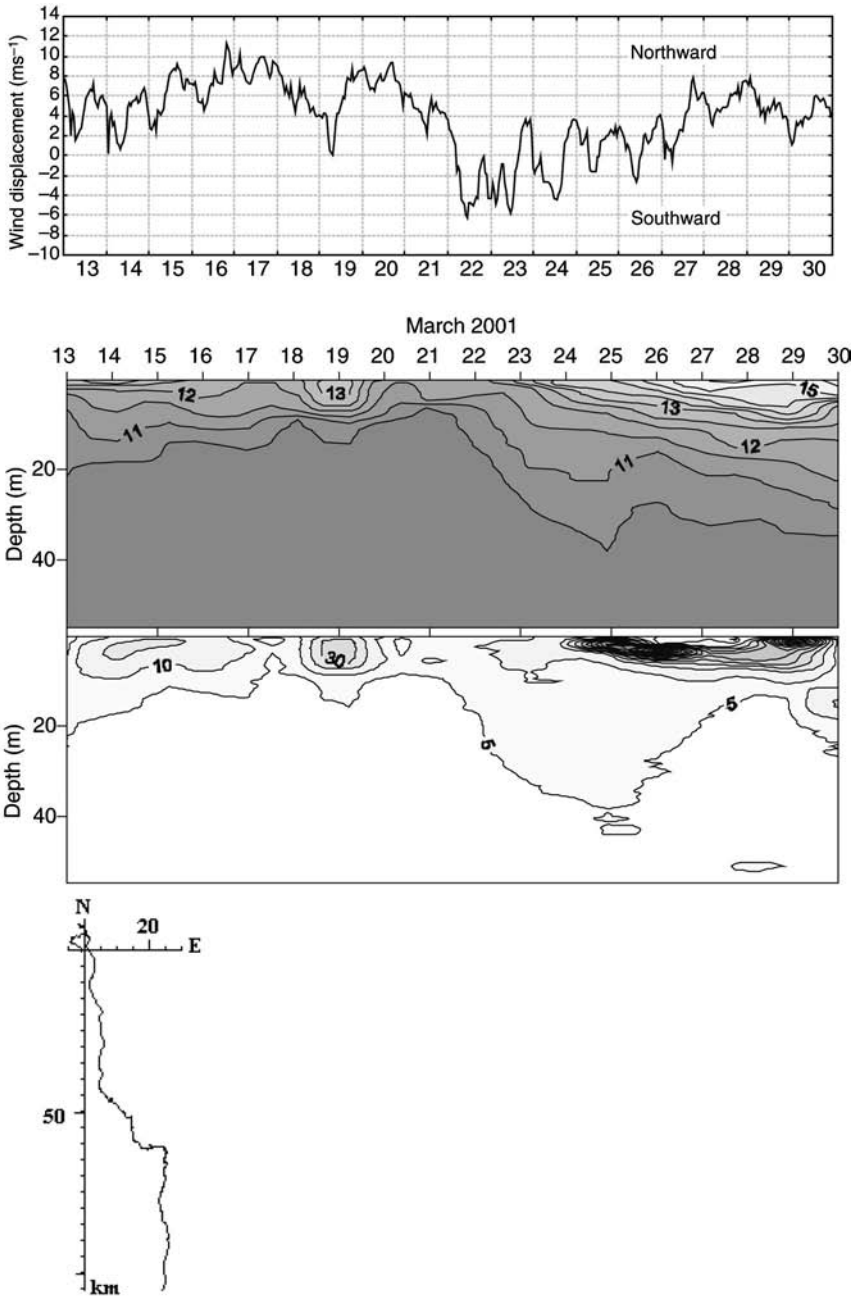

Figure 21.2
Time series 13–30 March 2001 of hourly wind displacement, temperature (°C), chlorophyll *a* (mg m^{-3}) and surface currents (progressive vector) off Lambert's Bay on the southern Namaqua shelf.
Source: adapted from Pitcher and Nelson (2006).

reversal of upwelling winds, introduced the bloom to the coastal environment. This period of onshore flow separated diatom domination of the inshore population during the first half of the time series, from dinoflagellate domination of the phytoplankton during the second half of the time series. The insight generated by these studies allows formulation of conceptual models of the origin and transport of blooms as a first step in developing predictive capabilities.

Current efforts at the provision of real-time data relating to HABs in the southern Benguela have used a lightweight multi-sensor mooring servicing the Namaqua shelf, equipped with paired hyperspectral radiometers, a fluorometer, a thermistor chain and an acoustic Doppler current profiler (ADCP). The system employs GSM telemetry and is designed to be serviceable from small boats. A time series of real-time data, from 18 February to 4 March 2005, demonstrates the detection of a bloom by means of the mooring and the MERIS (Medium Resolution Imaging Sensor) ocean-colour sensor (Figure 21.3). The introduction of the bloom as depicted by measures of fluorescence and hyperspectral reflectance (before the bloom, 20 February 2005, and during the bloom, 2 March 2005) is clearly associated with stratification of the water column. These data reveal the value of suitably configured and located coastal moorings and satellite observations of ocean colour in effectively detecting blooms. But predicting the spatial development and advection of blooms requires circulation models to integrate data from real-time observation systems in order to predict when and where these events may be of potential coastal significance.

Retrospective output from a hydrographic model served to provide a useful example of the advection of red tide into the Elands Bay – St Helena Bay region in January 2002 the decay of which caused an estimated mortality of rock lobster of 1,200 tonnes (Pitcher et al., 2004). Satellite derived observations of SST on 24 January 2002 depicted conditions following a period of moderate upwelling (Figure 21.4A). A distinct plume of upwelled water was evident off Cape Columbine and cooler water was also present inshore off Lambert's Bay and Elands Bay. Observations of ocean colour at this time indicated the presence of a bloom designated by moderately high chlorophyll concentrations ($<$50 mg m^{-3}) centred off Olifants River (Figure 21.4C). Chlorophyll concentrations in the Elands Bay – St Helena Bay area were generally $<$10 mg m^{-3}. Output from the hydrodynamic model on 25 January 2002 accurately portrayed the hydrographic conditions, depicting the cold-water plume off Cape Columbine and the narrow band of upwelling off Lambert's Bay and Elands Bay (Figure 21.5A). Current vectors depicted offshore flow in association with the narrow band of upwelling inshore and northerly flow in association with the Cape Columbine upwelling plume. Winds favouring upwelling abated on 25 January 2002 and a quiescent period of several days followed. Model output during this period clearly demonstrated the hydrographic features important in the shoreward accumulation and southward transport of red tide (Figures 21.5B, 21.5C, 21.5D). Evident was the role of the Cape Columbine plume in establishing an area of retention between the plume and coast, the development of weak onshore flow and the establishment of an inshore counter current introducing warmer water from the north. Under these conditions it is expected that bloom concentrations would increase inshore and that the bloom would be transported southward. Satellite observations of SST on 30 January and of ocean colour on 31 January 2002 confirm these expectations. The intensity of upwelling off Cape Columbine declined and water within the Elands Bay – St Helena Bay region warmed considerably (Figure 21.4B). Most important was the development of a very high-biomass bloom

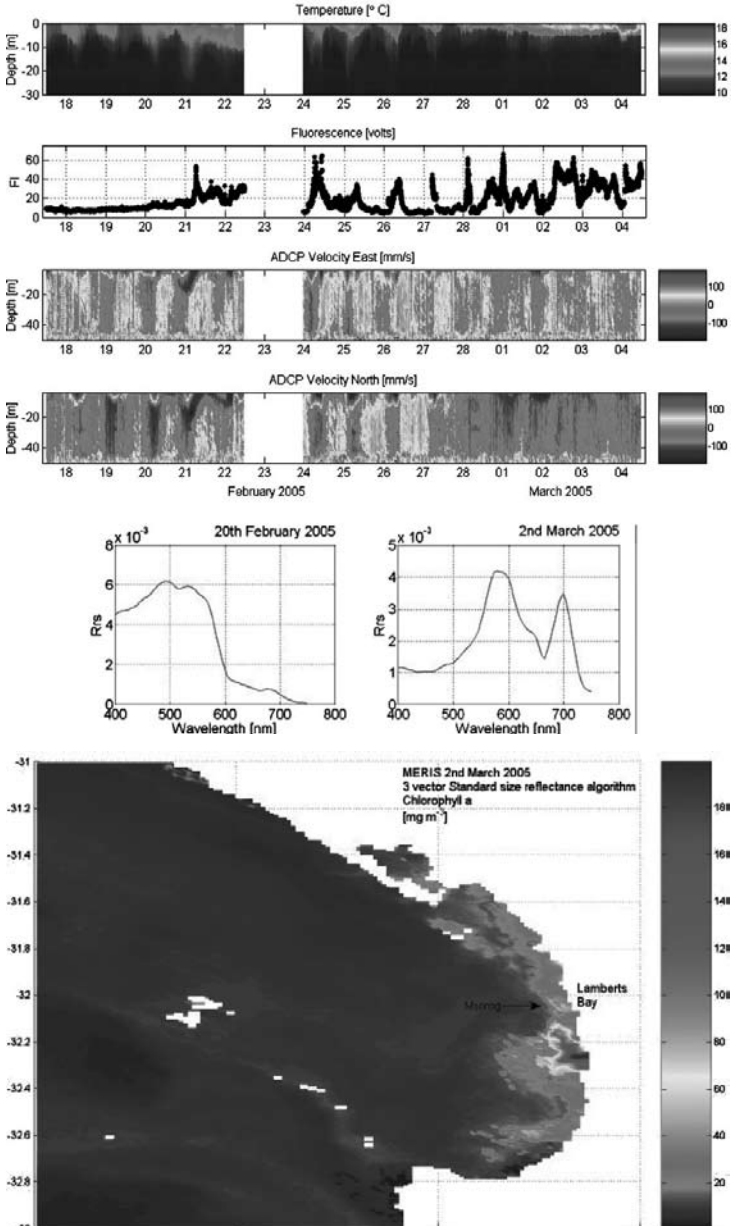

Figure 21.3
Real-time multi-parameter data for 18 February to 4 March 2005, collected from a buoy moored off Lambert's Bay. The instrument package on the buoy consists of a 30 m thermistor chain providing temperature profile data, a fluorometer supplying voltage relative to fluorescence, an acoustic Doppler current profiler providing current data at 2 m resolution and two hyperspectral radiometers measuring downwelling irradiance in air and upwelling radiance in water for the calculation of remote sensing reflectance. These data are transmitted in real-time using cellphone telemetry. Synoptic chlorophyll *a* concentrations are derived from the MERIS sensor using an experimental analytical reflectance algorithm.

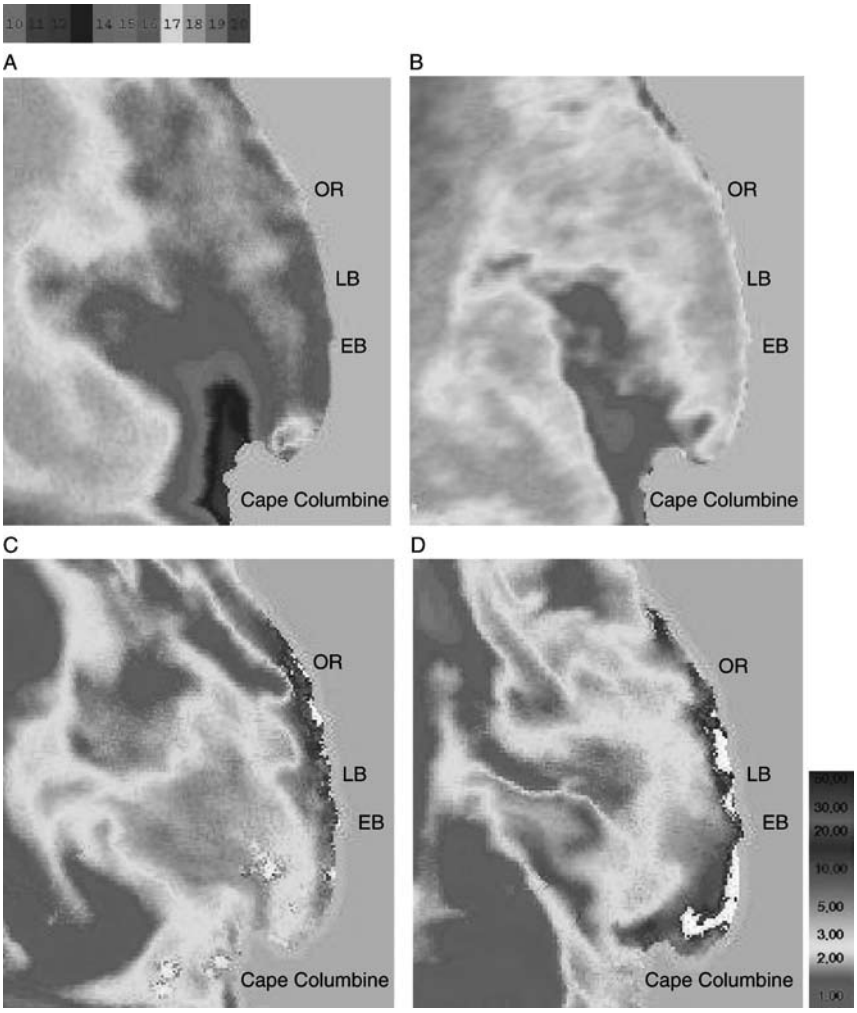

Figure 21.4
Advanced Very High Resolution Radiometer (AVHRR) observations of sea surface temperature (°C) on A, 24 January 2002; B, 30 January 2002. Chlorophyll *a* (mg m^{-3}) distributions as observed by SeaWiFs on C, 24 January 2002; D, 31 January 2002. The whitened areas on the SeaWiFs images are due to masking owing to very high chlorophyll *a* concentrations and consequent saturation of the nLw bands. OR, Olifant's River; LB, Lambert's Bay; EB, Elands Bay.
Source : AVHRR: S. Weeks, Ocean Space.

extending into St Helena Bay (Figure 21.4D). The rock lobster mortality of 1,200 tonnes was witnessed several days later.

This set of observations serves to demonstrate the potential use of circulation models driven by surface-boundary forcing from weather forecasts in conjunction with real-time observations in predicting the timing and duration of high-biomass blooms

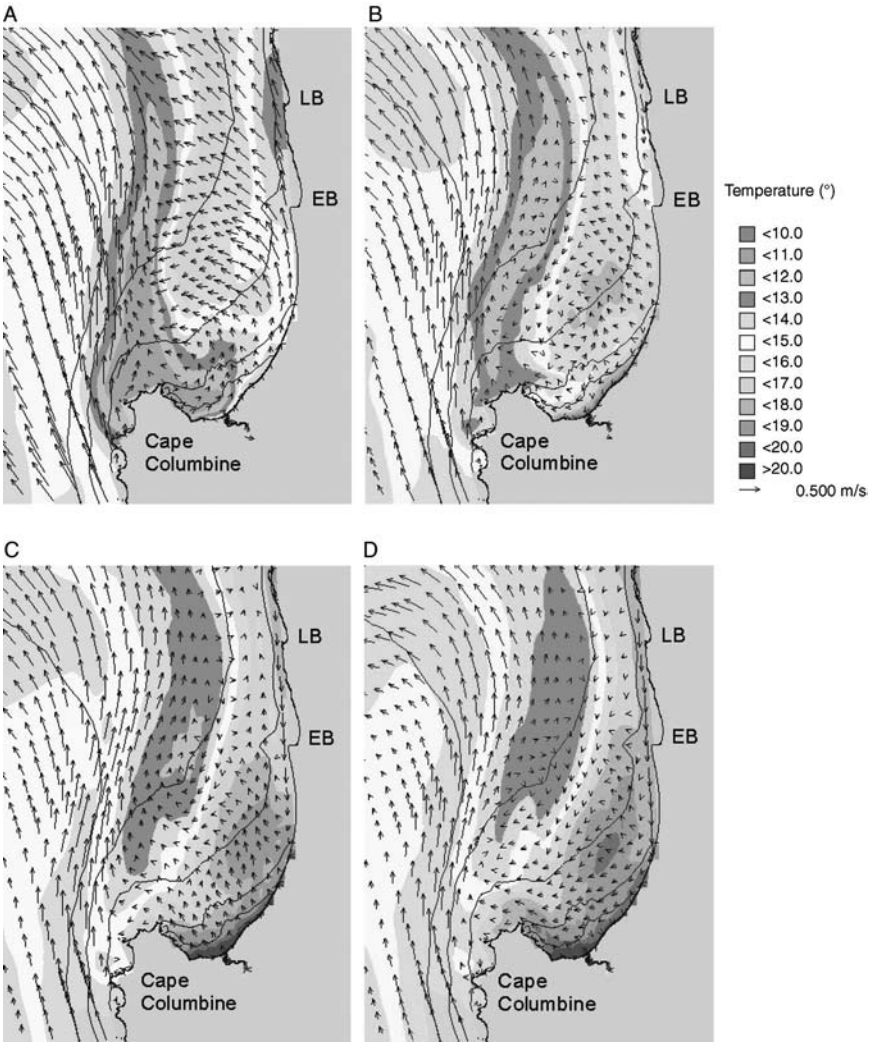

Figure 21.5
Model output at A, 00h00 on 25 January; B, 00h00 on 27 January; C, 21h00 on 28 January 2002; D, 00h00 on 30 January 2002, depicting SST and current vectors.
LB, Lambert's Bay; EB, Elands Bay.

at any single location on the southern Namaqua shelf. These observations are therefore able to assist coastal managers in the prediction of anoxic events associated with the decay of high-biomass blooms.

These observations alone provide the user with no species specific data. Radiometer-derived data on the southern Namaqua shelf have shown to provide additional insight into the phytoplankton community (Figure 21.6; Bernard, unpublished data). These

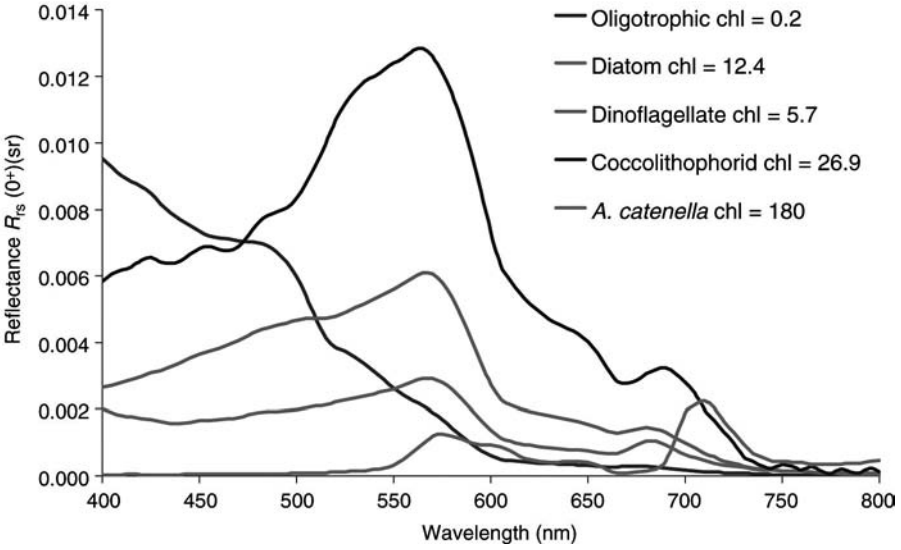

Figure 21.6
Remote sensing reflectance data are calculated by propagating the upwelling radiance measured at 0.66 m depth to the surface, calculating their transmittance through the air/water interface, and normalizing to the measured downwelling irradiance. The subsurface propagation uses the methods of Austin and Petzold (1981) to establish single-wavelength diffuse attenuation values, and Morel (1988) to further calculate the spectral diffuse attenuation values used for the propagation.

data demonstrate the sensitivity of hyperspectral reflectance to changes in algal biomass and dominant assemblage type. The very low reflectance values observed in a bloom of *Alexandrium catenella* are the result of associated high algal absorption. In comparison, reflectance measured in a coccolithophore dominated bloom show values an order of magnitude higher. These elevated reflectance values are associated with the presence of highly scattering coccoliths. Roesler et al., (2004) have demonstrated the capability to deconvolve these different sources of variation using reflectance inversion techniques, providing information not only of the algal biomass but also of the composition and size distribution of the population (Figure 21.7). An inverse ocean-colour model is able to express the contributions of various taxonomic groups in terms of the magnitude of the absorption coefficient, which is proportional to biomass. Applied to a time series of reflectance data from the southern Namaqua shelf, the model is able to provide results which compare favourably with those derived from microscopic cell counts, thereby demonstrating the utility of *in situ* ocean colour, in the detection of the composition and concentration of potentially harmful algae. Despite the additional information provided by ocean colour it does not satisfy the requirements of precise species composition required by regulatory authorities in monitoring seafood for human consumption (Probyn and Pitcher, 2004). There is thus a need to continue with traditional approaches and methods in monitoring species composition and toxin concentrations.

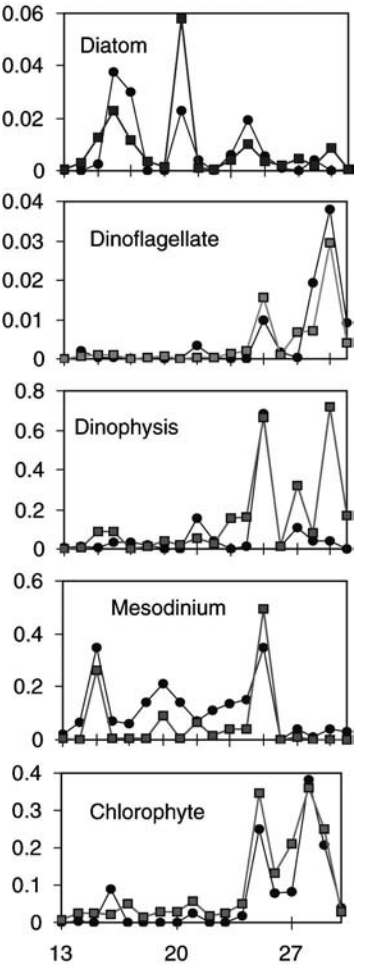

Figure 21.7
Time series 13–30 March 2001 of microscopic (open circles) and modelled (filled circles) biomass estimates, based on absorption coefficients, for various taxonomic groups off Lambert's Bay on the southern Namaqua shelf.

21.5 Affordability and future research requirements

The end-user of coastal observing systems needs to be provided with adequate information at the right time, in the right format, and at a competitive price. For ocean and coastal management priorities are based on potential benefits balanced against the costs of business as usual. In the development of operational oceanographic information services relating to HABs the ratio of benefit to cost is potentially high. The expense of ocean and coastal observing systems needs to be justified given the

benefits that are to be realized and must therefore meet user needs and be scientifically feasible. The primary economic rationale for real-time measurements derives from the more efficient use of the resources that these measurements enable. Current real-time detection and prediction techniques relating to HABs are limited. There is thus a need to carefully assess the value added by real-time information services and their benefit to HAB monitoring programmes, and ultimately studies will be required to demonstrate their value.

Unfortunately the attention devoted to ocean matters falls far below the relative importance of the oceans to society (Holland and Bernal, 2002). Data gathering, exchange and management activities are essential but costly factors in all decision-making activities. Costs for instruments are high, some of the measurements are difficult to interpret or to correct for interference, and autonomous systems are subject to fouling and disturbance, resulting in high maintenance costs. Finally, expenses relating to producing a product from real-time observations that is of use to the user is substantial and increases with sophistication of the product.

Technological developments are, however, assisting in reducing the costs of making observations. Satellites are becoming cheaper, and the measurement of upper ocean properties by moorings, profiling floats and autonomous under water vehicles rather than from expensive research vessels is also reducing costs. Multiple users and uses of data can further reduce expenses. A feature of real-time data is that certain core measurements will meet the needs of a wide range of end users. Options of data and information sharing between various user-groups via the establishment of various observation networks must be considered as this is an efficient way to reduce management costs. Linking HAB monitoring programmes with the initiatives of the Global Ocean Observing System (GOOS), may allow the exchange of compatible observations in this way.

As the requirements for real-time coastal observations continue to increase, competition and market forces should continue to bring down the price of data. Demands for data will however only increase if the data are converted into a quality product of real and obvious benefit to the intended user. Potential users of coastal observation systems often have limited insight into the instruments used to derive data, the methods of processing data and interpreting the results, and as to how results may be incorporated into different model simulations and predictive data assimilations (Dickey, 2002). Consequently, the use of real-time environmental observations is dominated by scientists and under-used by others. This is a shortcoming that scientists need to contribute to rectifying, as a stronger linking of science with decision-making will ultimately depend on scientific accuracy and effective communication (Clark et al., 2001).

The incorporation of real-time coastal observations into HAB monitoring programmes is specifically impeded by the fact that these observations are seen to provide additional or supplementary information, but are unable to replace traditional measurements. Algal bloom dynamics can now be effectively monitored remotely by means of *in situ* , air or spaceborne sensors, and retrospective analyses have been successful at describing important factors that influence the distributions and persistence of algal blooms. But attempts to measure specific species and toxins from a distance have been less successful. Simulation models have been effective in revealing which factors dominate in the control of algal bloom dynamics, but only rarely have these models been parameterized using species-specific physiological data. This means that the responsible management authorities are still required to spend the bulk of their budget on traditional water sampling and analysis of shellfish. So while researchers

are active in evaluating real-time observations, the managers of HAB monitoring programmes are more hesitant to have real-time coastal data acquisition and analysis included as part of the routine monitoring within regulatory agencies owing to the additional costs.

For this reason the development of techniques for species-specific real-time detection and techniques for real-time measurement of toxins must remain our primary research objectives if we are to succeed in our quest to develop operational oceanographic services relating to HABs. It must, however, be recognized that countries with small economies cannot be expected to embrace costly and highly technical monitoring programmes. The science involved in real-time coastal observing systems is advanced and care should be taken to ensure that benefits do not pass merely to those societies already possessing the greatest capacity. Global consistency in regulations pertaining to marine toxins is an objective designed to eliminate risks to consumers and to reduce obstacles to trade. Adoption of highly technical and costly methods by regulatory authorities may ultimately serve as a further barrier to the trade of seafood products.

References

Aguilera, A., Lopez-Rodas, V., Gonzalez-Gil, S. and Costas , E. 1995. Use of FITC-labeled lectins to identify dinoflagellate species. In: Lassus et al. (eds), op. cit., pp. 707–15.

Anderson, D. M. 1995. Identification of harmful algal species using molecular probes: an emerging perspective. In: Lassus et al. (eds), op. cit., pp. 3–13.

Austin, R. W. and Petzold, T. J. 1981. The determination of the diffuse attenuation coefficient of sea water using the coastal zone color scanner. In: J. F. R. Gower (ed.), *Oceanography from Space*. New York, Plenum Press, pp. 239–56.

Babin, M., Roesler , C. S. and Cullen, J. J. (eds). 2006. *Real-time Coastal Observing Systems for Marine Ecosystem Dynamics and Harmful Algal Blooms: Theory, Instrumentation and Modelling*. Paris, Intergovernmental Oceanographic Commission of UNESCO. (Monographs on Oceanographic Methodology XX.)

Bernard, S., Kudela, R. M., Franks, P., Fennel, W., Kemp, A., Fawcett, A. and Pitcher, G. C. 2006. The requirements for forecasting harmful algal blooms in the Benguela. In: V. Shannon, G. Hempel, P. Malanotte–Rizzoli, C. Moloney and J. Woods (eds), Benguela: Predicting a Large Marine Ecosystem. Amsterdam, Elsevier.

Chang, G. C. and Dickey, T. D. 1999. Partitioning *in situ* total spectral absorption by use of moored spectral absorption and attenuation meters. *Appl. Opt.*, 38, pp. 76–87.

Chang, G. C. and Dickey, T. D. 2007. Interdisciplinary sampling strategies for detection and characterization of harmful algal blooms. In: Babin et al. (eds), op. cit., this volume.

Clark, J. S., Carpenter, S. R., Barber, M., Collins, S., Dobson, A., Foley, J. A., Lodg, D. M., Pascual, M., Pielke, R., Pizer, W., Pringle, C., Reid, W. V., Rose, K. A., Sala, O., Schlesinger, W. H., Wall , D. H. and Wear , D. 2001. Ecological forecasts: an emerging imperative. *Science*, 293, pp. 657–60.

Council of the European Communities. 1991. Council Directive 91/492/EEC of 15 July 1991 laying down the health conditions for the production and the placing on the market of live bivalve molluscs. *Off. J. Eur. Communities* L268, pp. 1–14.

Council of the European Communities. 1997. Council Directive 97/61/EEC of 20 October 1997 that modifies the Annexe of Directive 91/492/EEC that lays down the health conditions for the production and placing on the market of live bivalve molluscs. *Off. J. Eur. Communities* L295, pp. 35–36.

Cullen, J. J., Ciotti, A. M., Davis, R. F. and Lewis, R. M. 1997. Optical detection and assessment of algal blooms. *Limnol. Oceanogr.*, 42, pp. 1223–39.

Davis, C. O., Kappus, M., Gao, B. C., Bissett, W. P. and Snyder, W. 1998. The Naval Earth Map Observer (NEMO) science and naval products. *Proc. SPIE* , 3437, pp. 11–19.

Dickey, T. 2001. Sensors: inherent and apparent optical properties. In: J. Steele, S. Thorpe and K. Turekian (eds), *Encyclopedia of Ocean Sciences*. New York, Academic Press, pp. 1313–23.

Dickey, T. and Falkowski, P. 2002. Solar energy and its biological physical interactions in the sea. In: A. R. Robinson, J. J. McCarthy and B. J. Rothschild (eds), *The Sea*. Vol. 12: *Biological-Physical Interaction in the Ocean*. New York, John Wiley & Sons, pp. 401–40.

Dickey, T. D. 2002. A vision of oceanographic instrumentation and technologies in the early twenty-first century. In: Field et al. (eds), op. cit. pp. 209–54.

Falkowski, P. G. and Kobler, Z. 1995. Variation in chlorophyll fluorescence yield in phytoplankton in the world oceans. *Aust. J. Plant Physiol.*, 22, pp. 341–55.

Fernandez, M. L. and Cembella, A. D. 1995. Mammalian bioassays. In: G. M. Hallegraeff, D. M. Anderson and A. D. Cembella (eds), *Manual on Harmful Marine Microalgae* . Paris, Intergovernmental Oceanographic Commission of UNESCO, pp. 213–28.

Field, J. G., Hempel, G. and Summerhayes, C. P. (eds). 2002. *Oceans 2020: Science, Trends, and the Challenge of Sustainability* . Washington DC, Island Press.

Flather, R. A. 2000. Existing operational oceanography. *Coast. Eng.*, 41, pp. 13–40.

GEOHAB. 2001. *Global Ecology and Oceanography of Harmful Algal Blooms, Science Plan*. Baltimore/Paris, Scientific Committee on Oceanic Research/Intergovernmental Oceanographic Commission of UNESCO.

Glenn, S. M., Haidvogel, D. B., Schofield, O. M. E., von Alt, C. J. and Levine, E. R. 1998. Coastal predictive skill experiments. *Sea Tech.*, 39, pp. 63–69.

Holland, G. and Bernal, P. 2002. Framework of co-operation. In: Field et al. (eds), op. cit., pp. 257–81.

Keafer, B. A. and Anderson, D. M. 1993. The use of remotely sensed sea surface temperatures for studies of *Alexandrium* bloom dynamics in the southwestern Gulf of Maine. In: T. Smayda and Y. Shimizu (eds), *Toxic Phytoplankton Blooms in the Sea*. Amsterdam, Elsevier, pp. 763–68.

Kiefer, D. A. and Reynolds, R. A. 1992. Advances in understanding phytoplankton fluorescence and photosynthesis. In: P. G. Falkowski and A. Woodhead (eds), *Primary Productivity and Biogeochemical Cycles in the Sea.* New York, Plenum Press, pp. 155–74.

Lassus, P., Arzul, G., Erard, E., Gentien, P. and Marcaillou, C. (eds). 1995. *Harmful Marine Algal Blooms*. Paris, Technique et Documentation-Lavoisier/Intercept Ltd.

Morel, A. 1988. Optical modeling of the upper ocean in relation to its biogenous matter content (Case I Waters). *J. Geophys. Res.*, 93(9), pp. 10749–68.

NSSP. 1995*a*. *National Shellfish Sanitation Program, Manual of Operation, Part 1. Sanitation of shellfish growing areas*. Washington DC, US Department of Health and Human Services, Public Health Services, Food and Drug Administration.

NSSP. 1995*b*. *Part 2. Sanitation of the Harvesting. Processing and Distribution of Shellfish*. Washington DC, US Department of Health and Human Services, Public Health Services, Food and Drug Administration.

Parrish, J. K. 1999. Toward remote species identification. *Oceanography*, 12(3), pp. 30–32.

Peperzak, L., Vrieling, E. G., Sandee, B. and Rutten, T. 2000. Immunoflow cytometry in marine phytoplankton research. *Scientia Marina*, 64, pp. 165–81.

Pitcher, G. C., Boyd, A. J., Horstman, D. A. and Mitchell-Innes, B. A. 1998. Subsurface dinoflagellate populations, frontal blooms and the formation of red tides in the southern Benguela upwelling system. *Mar. Ecol. Progr. Ser.*, 172, pp. 253–64.

Pitcher, G. C. and Calder, D. 2000. Harmful algal blooms of the southern Benguela current: a review and appraisal of monitoring from 1989 to 1997. *S. Afr. J. Mar. Sci.,* 22, pp. 255–71.

Pitcher, G., Monteiro, P. and Kemp, A. 2004. The potential use of a hydrodynamic model in the prediction of harmful algal blooms in the southern Benguela. In: K. A. Steidinger, J. H. Landsberg, C. R. Tomas and G. A. Vargo (eds), *Harmful Algae 2002*. Florida Fish and Wildlife Conservation Commission, Florida Institude of Oceanography, and Intergovernmental Oceanographic Commission of UNESCO, pp. 11–13.

Pitcher, G. C. and Nelson, G. 2006. Charactersties of the surface boundary layer important to the development of red tide on the southern Namaqua shelf of the Benguela upwelling system. *Limnol. Oceangr.*, pp.2660–2674

Pitcher, G. C. and Weeks, S. J. 2006. The variability and potential for prediction of harmful algal blooms in the southern Benguela ecosystem. In: V. Shannon, G. Hempel, P. Malanotte-Rizzoli, C. Moloney and J. Woods (eds), *The Benguela: Predicting a Large Marine Ecosystem*. Amsterdam, Elsevier.

Probyn, T. A. and Pitcher, G. C. 2004. Monitoring of biotoxins on the South African Coast. In: S. Hall, S. Etheridge, D. Anderson, J. Kleindinst, M. Zhu and Y. Zou (eds), *Harmful Algae Management and Mitigation*. Asia-Pacific Economic Cooperation (Singapore). (APEC Publication #204-MR-04.2: 11-14.)

Probyn, T. A., Pitcher, G. C., Monteiro, P. M. S., Boyd, A. J. and Nelson, G. 2000. Physical processes contributing to harmful algal blooms in Saldanha Bay. *S. Afr. J. Mar. Sci* ., 22, pp. 285–97.

Quilliam, M. A. 1998. Liquid chromatography-mass spectrometry: a universal method for analysis of toxins? In: B. Reguera, J. Blanco, M. L. Fernández and T. Wyatt (eds), *Harmful Algae*. Proc. VIII International Conference on Harmful Algae (June 1997, Vigo, Spain). Santiago de Compostela/Paris, Xunta de Galicia/Intergovernmental Oceanographic Commission of UNESCO, pp. 509–14.

Roesler, C. S., Etheridge, S. M. and Pitcher, G. C. 2004. Application of an ocean color taxa detection model to red tides in the southern Benguela. In: K. A. Steidinger, J. H. Landsberg, C. R. Tomas and G. A. Vargo (eds), *Harmful Algae* 2002. Florida Fish and Wildlife Consevation Commission, Florida Institude of Oceanography, and Intergovernmental Oceanographic commission of UNESCO, pp. 303–305.

Ruddick, K., Lacroix, G., Park, Y., Rousseau, V., De Cauwer, V. and Sterckx, S. 2007. Overview of ocean colour: theoretical background, sensors and applicability to detection and monitoring of harmful algal blooms (capabilities and limitations). In: Babin et al. (eds), op. cit., this volume.

Schofield, O., Bosch, J., Glenn, S., Kirkpatrick, G., Kerfoot, J., Lohrenz, S., Moline, M., Oliver, M. and Bissett, P. 2007. Bio-optics in integrated ocean observing networks: potential for studying harmful algal blooms. In: Babin et al. (eds), op. cit., this volume.

Schofield, O., Grzymski, J., Bissett, W. P., Kirkpatrick, G. J., Millie, D. F., Moline, M. and Roesler, C. S. 1999. Optical monitoring and forecasting systems for harmful algal blooms: possibility or pipe dream? *J. Phycol.*, 35, pp. 1477–96.

Scholin, C., Marin, R. III, Massion, E., Jensen, S., Cline, D., Roman, B. and Doucette, G. 2002. Remote detection of HAB species using the environmental sample processor: progress and future directions. *Proc. Xth International Conference on Harmful Algae*, St Pete Beach, Florida, p. 254. (Abstract)

Sellner, K. G., Doucette, G. J. and Kirkpatrick, G. 2003. Harmful Algal Blooms: Causes, Impacts and Detection. *J. Indus. Microbiol. Biotechnol.*, 30, pp. 383–406.

Sieracki, C. K., Sieracki, M. E. and Yentsch, C. S. 1998. An imaging-in-flow system for automated analysis of marine microplankton. *Mar. Ecol. Progr. Ser.*, 168, pp. 285–96.

Smayda, T. J. 1997. What is a bloom? A commentary. *Limnol. Oceanogr.*, 42, pp. 1132–36.

Sournia, A. 1995. Red tide and toxic marine phytoplankton of the world ocean: an inquiry into biodiversity. In: Lassus et al. (eds), op. cit., pp. 103–12.

Steidinger, K. A. and Haddad, K. 1981. Biologic and hydrographic aspects of red tides. *Bioscience*, 31, pp. 814–19.

Stramski, D. and Kiefer, D. A. 1991. Light scattering by microorganisms in the open ocean. *Progr. Oceanogr.*, 28, pp. 250–68.

Stramski, D. and Reynolds, R. A. 1993. Diel variations on the optical properties of a marine diatom. *Limnol. Oceanogr.*, 38, pp. 1347–64.

Summerhayes, C. 2002. GOOS project update: implementation progress. *Sea Tech.*, pp. 46–49.

Summerhayes, C. P., Field, J. G. and Hempel, G. 2002. Introduction. In: Field et al. (eds), op. cit., pp. 1–8.

Summerhayes, C. P. and Rayner, R. 2002. Operational oceanography. In: Field et al. (eds), op. cit., pp. 187–207.

Tester, P. A. and Steidinger, K. A. 1997. *Gymnodinium breve* red tide blooms: initiation, transport and consequences of surface circulation. *Limnol. Oceanogr.*, 42, pp. 1039–51.

Tester, P. A., Stumpf, R. P., Vukovich, F. M., Fowler, P. K. and Turner, J. T. 1991. An expatriate red tide bloom: transport, distribution, and persistence. *Limnol. Oceanogr.*, 36, pp. 1053–61.

Wolanski, E., King, B. and Spagnol, S. 1999. The implication of oceanographic chaos for coastal management. In: W. Solomons, R. K., Turner, L. D. de Lacerda and S. Ramachandran, S. (eds), *Perspectives in Integrated Coastal Zone Management*. Berlin, Springer-Verlag, pp. 129–41.

Woods, J. D. 2000. *Ocean Predictability*. Brunn Memorial Lecture, IOC 20th Assembly. Paris, Intergovernmental Oceanographic Commission of UNESCO. (IOC Technical Series 55.)

Woods, J. D., Dahlin, H., Droppert, L., Glass, M., Vallerga, S. and Flemming, N. C. 1996. *The Strategy for EuroGOOS*. Southampton, UK, Southampton Oceanography Centre. (EuroGOOS Publication 1.)

Index

Figures

Note: This section provides colour versions of those figures that require colour for proper interpretation.

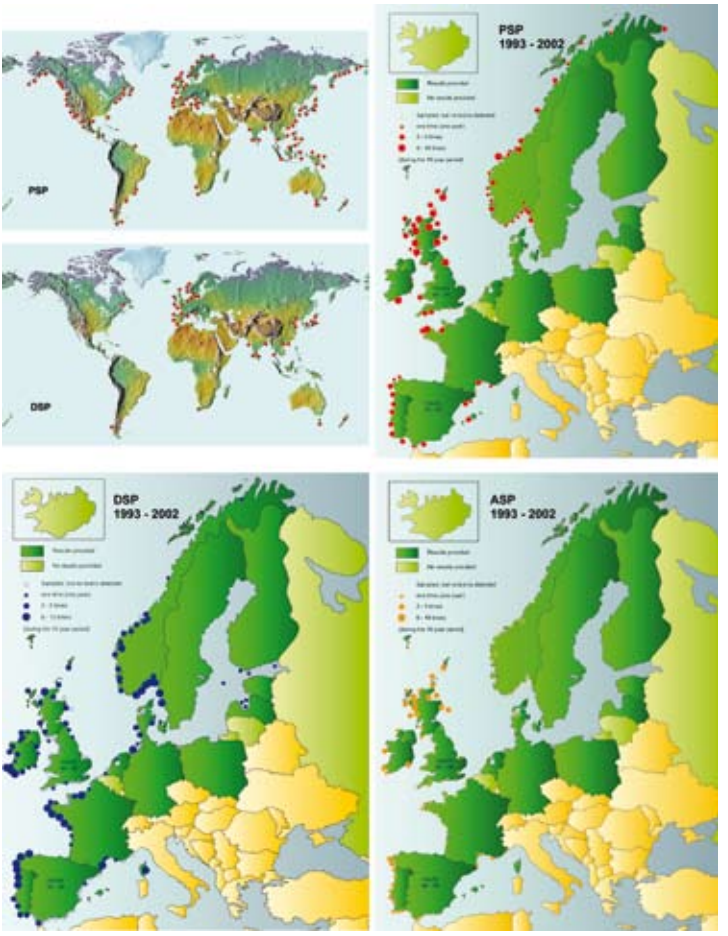

Figure 1.1
Maps of reported occurrences of HAB toxicity demonstrate many aspects of the HAB problem. Top left: global distributions of reported paralytic shellfish poisoning (PSP) and diarrhetic shellfish poisoning (DSP) events show that harmful effects are widespread. Regional patterns are to some extent related to the presence of systems for monitoring and reporting; absence of reports does not necessarily mean that HABs have not occurred (US National Office for Marine Biotoxins and Harmful Algal Blooms). Other panels: Occurrences of PSP, DSP and amnesic shellfish poisoning (ASP) in ICES countries[2] from 1993–2002 show that some locations are affected by several types of HAB, whereas certain types of toxicity are more restricted. None of these maps can show the diversity of species that generate these effects (Table 1.1). The Coastal Module of the Global Ocean Observing System (IOC, 2003) is being established to facilitate more effective monitoring of HABs and other phenomena in coastal environments worldwide, so temporal and spatial patterns can be resolved and explained.[3]
Source: Harmful Algae Event Data Base (HAEDAT), © IFREMER.

Figure 1.3
Dense blooms associated with physical discontinuities in the water demonstrate the interaction of swimming, sinking or floating of phytoplankton with small-scale circulation and interfaces (Franks, 1997).
A, *Noctiluca* (from GEOHAB, 2001)
Source: after Malone (2001).

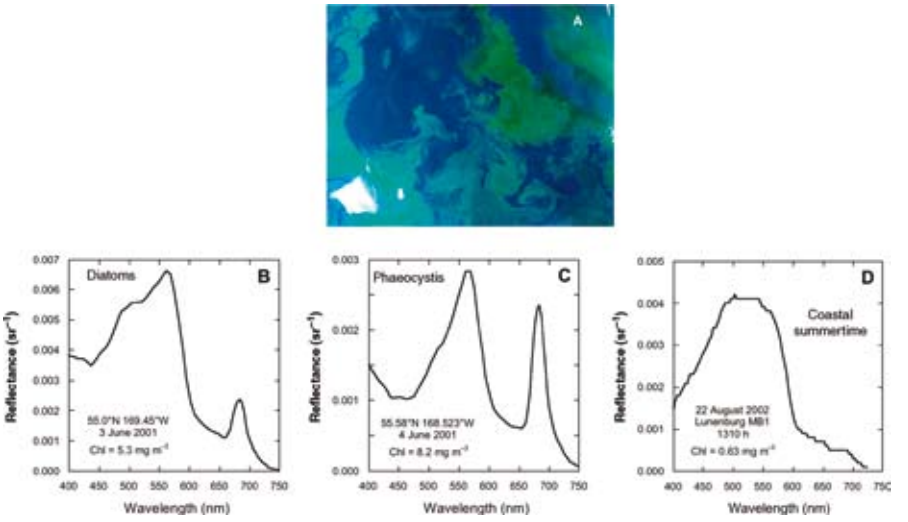

Figure 1.8
A, true colour satellite image of a phytoplankton bloom in the Bering Sea on 7 June 2001 (292 km by 200 km centred near 58.7°N, 177°W). During this period, shipboard sampling and measurements of reflectance indicated blooms dominated by diatoms and *Phaeocystis*, in close proximity, probably corresponding to the lighter and darker green features in the image. Coccolithophore blooms are highly reflective and may be responsible for the brighter features in the SW corner of the image.
Sources: SeaWiFS Project, NASA Goddard Space Flight Center and ORBIMAGE.
B, C, in-water measurements of hyperspectral reflectance at the surface in the Bering Sea during early June reveal irregularities between 400 nm and 550 nm that are associated with pigment absorption, which reduces reflectance (Sosik, 2006 – Chapter 8 this volume), and large peaks near 680 nm from sun-induced chlorophyll fluorescence (Babin, 2007 – Chapter 7 this volume). Here, reflectance is upwelling radiance at 65 cm divided by downwelling irradiance above the surface, measured with a Hyperspectral TSRB Tethered Spectral Radiometer Buoy (Satlantic, Inc.)
D, similar measurements from a mooring in Lunenburg Bay, Nova Scotia, show much less interpretable structure because pigment concentrations are about 10-fold lower, and much of the absorption in blue wavelengths is due to chromophoric dissolved organic matter (CDOM).

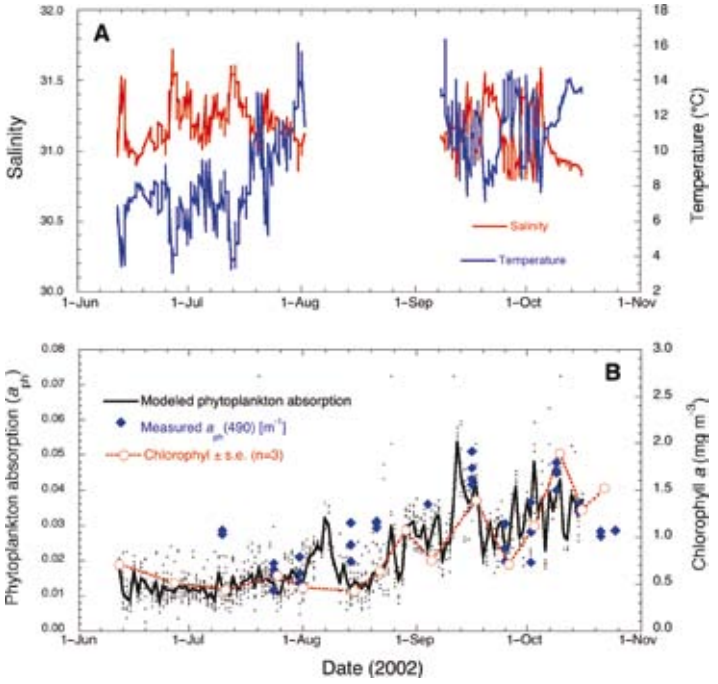

Figure 1.10
Early results from a coastal observatory illustrate some of the promise of coastal observing systems and many of the challenges that must be overcome before systems for research and development become operational and comparable between sites (Glenn et al., 2000; IOC, 2003; Malone, 2007 – Chapter 14 this volume). The MEPS-Bay system[6] has three moorings with temperature-salinity chains, current meters, meteorology and optics; a data assimilation model is being developed to incorporate these data and other local observations into a real-time, coupled, atmosphere-ocean simulation of the bay (Sheng and Wang, 2004).
A, the records of temperature and salinity from the 11 m conductivity-temperature (CT) sensor on a mooring (Lunenburg Bay, MB1) show the seasonal development of temperature, and many event-scale changes of water in the bay that could not be resolved with conventional monitoring. It also shows a gap corresponding to a technical failure; operational systems must be robust and provision must be made to correct such problems quickly.
B, nearly continuous measurements of hyperspectral ocean colour (as in Figure 1.8D) were analysed by Brown and Huot (unpublished) with an inverse model, generating relative estimates of phytoplankton absorption (Roesler and Perry, 1995; Sosik, 2007 – Chapter 8 this volume) corrected for the substantial contribution of CDOM and other constituents of the water (black dots; the black line is a locally weighted least-squares regression to indicate trends). Blue symbols show direct measurements of phytoplankton absorption (filter pad method, corrected for detritus) and open red symbols are determinations of extracted chlorophyll. Development, quantitative evaluation and widespread acceptance of robust optical measures of phytoplankton is required for routine monitoring. This is a major challenge.

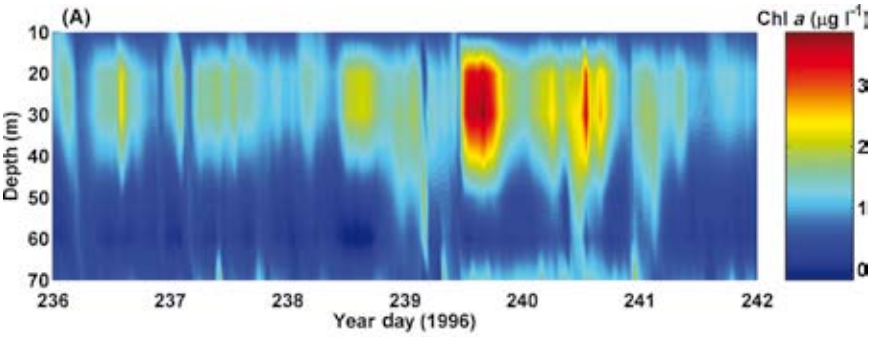

Figure 2.4 A
Time-series contour plot of chlorophyll *a* concentration. The increase on Year Day 239 (26 August 1996) was due to convergence of phytoplankton at a shelf-slope front just south of Martha's Vineyard, Cape Cod, Mass.

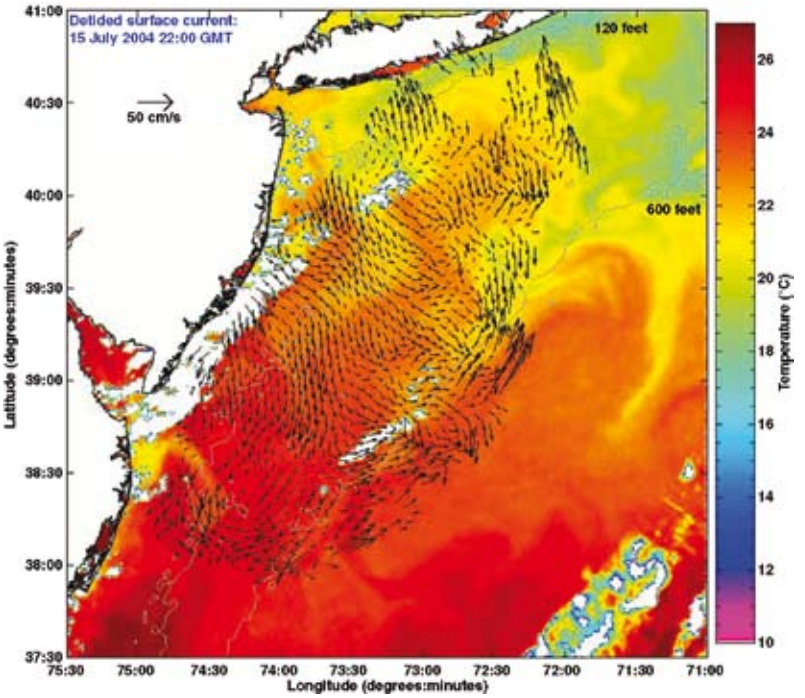

Figure 2.7
Spatial map of surface current vectors (scale at upper left) derived from high-frequency radar measurements overlaid on satellite-derived sea surface temperature from 15 July 2004. The region shown is the Middle Atlantic Bight, US east coast (Long Island at top). Note the highly variable convergence and divergence zones in the current vectors.
Source: courtesy of Josh Kohut and Oscar Schofield, Rutgers University.

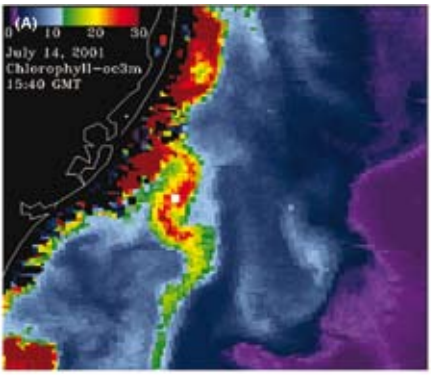

Figure 2.8 A
Moderate Resolution Imaging Spectroradiometer (MODIS) imagery of derived chlorophyll *a* concentration showing a high-biomass filament in the New York Bight on 14 July 2001 (the land mass on the left is coastal New Jersey just north of Cape Hatteras).
Source: MODIS imagery and derived bio-optical products were provided by Richard Gould and Robert Arnone, Naval Research Laboratory, Stennis Space Center.

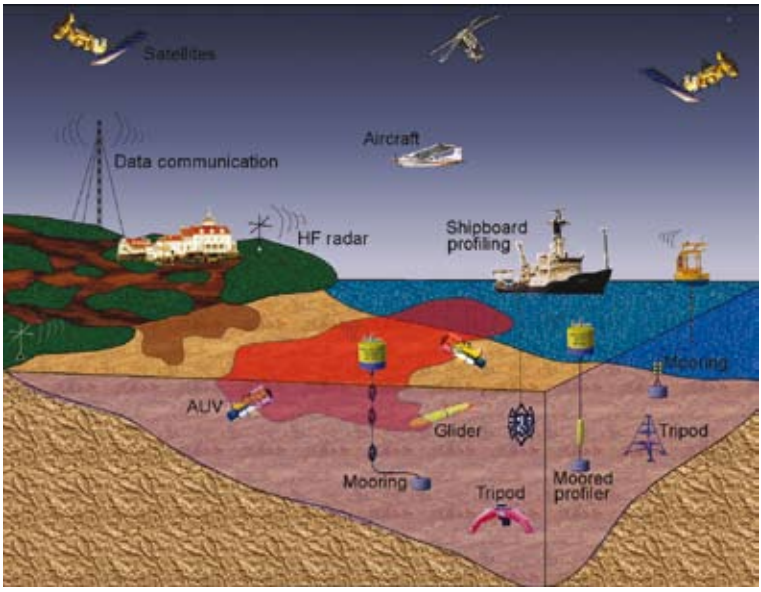

Figure 2.11
Schematic diagram of an ideal interdisciplinary coastal sampling network for harmful algal bloom detection, identification and characterization.

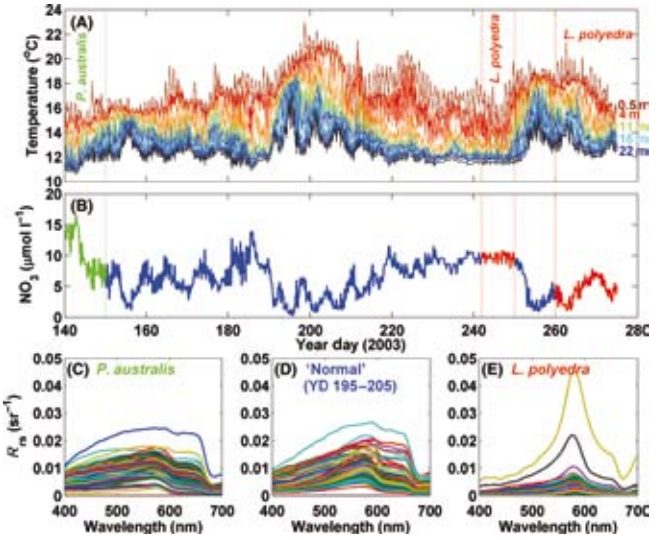

Figure 2.14
Time series of A, temperature collected at about every metre from near surface to 22 m; B, derived nitrate concentration at 22 m (following McPhee-Shaw et al., 2007) from 20 May to 2 October 2003. Remote sensing reflectance spectra computed from hyperspectral radiometer data during C, a *Pseudo-nitzschia australis* bloom (until 30 May); D, conditions not affected by HABs (14–24 July); E, a bloom of *Lingulodinium polyedra* (30 August to 7 September and again 17 September to 2 October). Data were collected on a mooring in the Santa Barbara Channel (25 m water depth). The remote sensing signals during the times of the *L. polyedra* bloom are different from conditions not affected by HABs; this shows promise in using optics for detection and identification of HABs.

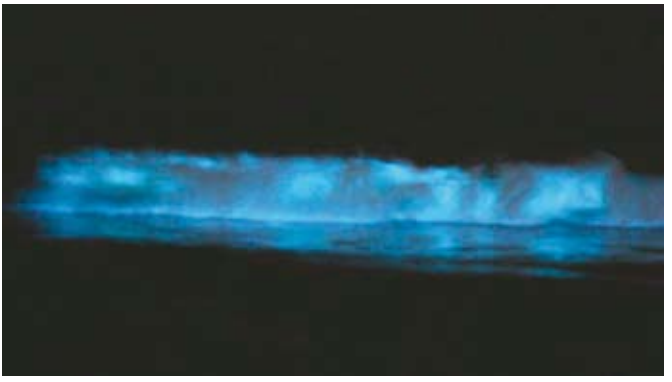

Figure 2.15
Digital photograph (unenhanced) of a breaking wave containing the bioluminescent dinoflagellate species, *Lingulodinium polyedra*, taken along the central coast of California during a red tide in October 2003.
Source: image used with permission from Rosalba Dominguez.

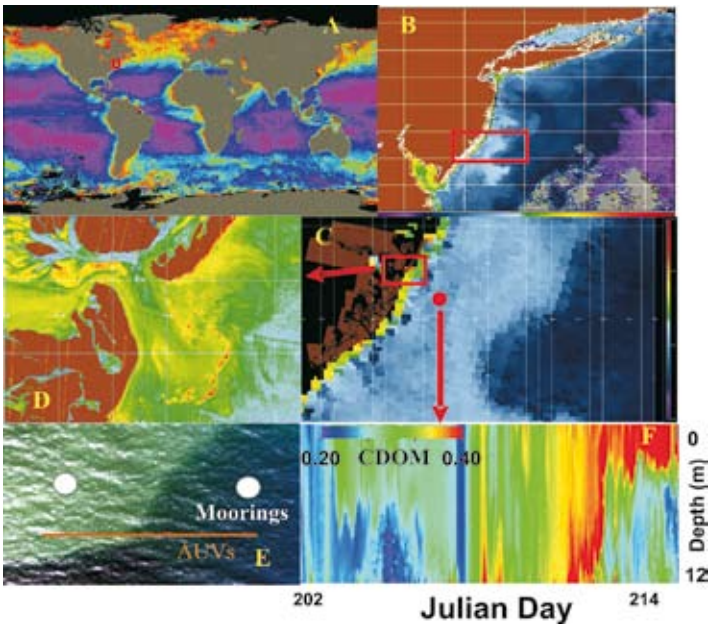

Figure 3.2
The time and space scale variability in ocean colour.
A, annual global chlorophyll *a* map derived from SeaWiFS.[14]
B, backscattering coefficient (wavelength) in summer 2001 in the Mid-Atlantic Bight derived from SeaWiFS.
C, enlarged section of panel B; the satellite's 1 km pixel is clearly visible and illustrates the features in the coastal ocean that are poorly resolved. Note that the newer ocean-colour satellites that have spatial resolutions down to 250 km; ocean-colour satellites with 30 m resolution are proposed.
D, enlargement from panel C showing the backscattering coefficient at 442 nm derived from aircraft data. Note the features clearly visible in the aircraft imagery that are missed with the standard 1 km pixels in the satellite imagery.
E, visible image viewed by aircraft, with resolution of the order of tens of metres, showing the dramatic colour change associated with crossing an upwelling front in the Mid-Atlantic Bight. The visible 'greening' of the water is associated with enhanced blue light absorption probably from phytoplankton and/or chromophoric dissolved organic matter (CDOM). This colour shift underlies empirical algorithms for ocean-colour remote sensing.
F, time series of CDOM absorption, estimated from inverting bulk absorption measured with an ac-9 mounted on the Long-term Ecosystem Observatory (LEO) electro-optic fibre-optic cabled seafloor node. This system uses an *in situ* profiling system to obtain both highly resolved depth and time observations. Rapid changes in CDOM concentration are associated with the passage of storms and a large plume of Hudson River water.

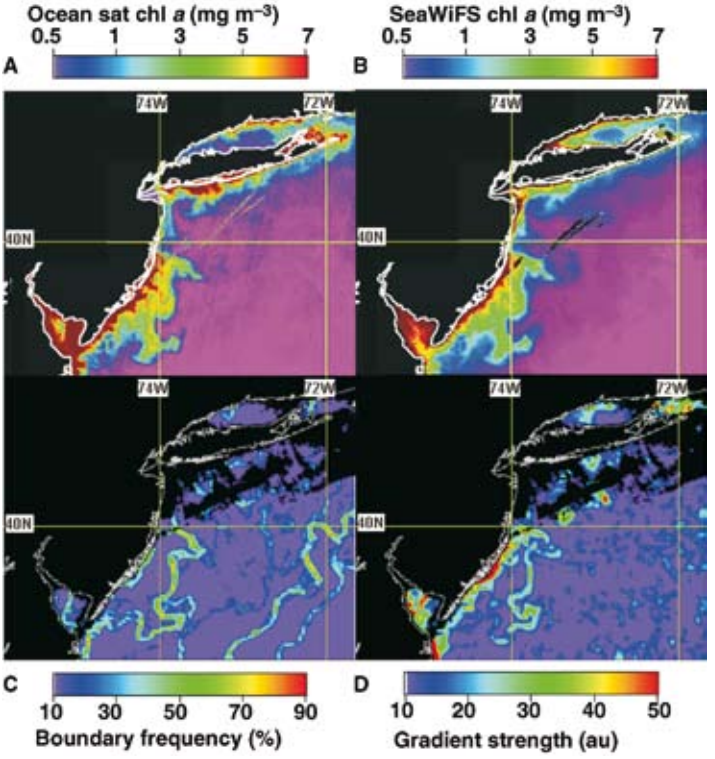

Figure 3.3
Examples of ocean colour and derived water mass imagery in the Mid-Atlantic Bight in summer 2001.
A, image of chlorophyll *a* collected on 2 August, 2001, with the Indian Oceansat satellite which has a spatial resolution of 300 m.
B, image of chlorophyll *a* collected on 2 August 2001 with the American SeaWiFS system.
C, boundary frequency between water masses measured on 2 August 2001. The boundary frequency objectively defines borders between major water masses based on the combined output from an ensemble of clustering algorithms that combines information from sea surface temperature (SST) and spectral reflectance (R_{rs}) (Yeung et al., 2001; Oliver et al., 2004a). These techniques allow the scientist to quantify the most frequently observed borders between water masses. Note that the boundaries of a large coastal bloom, offshore waters and the Gulf Stream are delineated.
D, gradient strengths between the major water masses for 2 August 2001. While the clustering algorithms (Figure 3.C) separate observations into discrete water masses, this does not quantitatively delineate how different the water masses are from one another. Through distance analysis, the relative strengths of these boundaries can be estimated by determining the ratio of the distance between points in parameter space to the distance between points in physical space (Oliver et al., 2004a). In this case, only the edge of the algal bloom represents a significant water mass boundary.

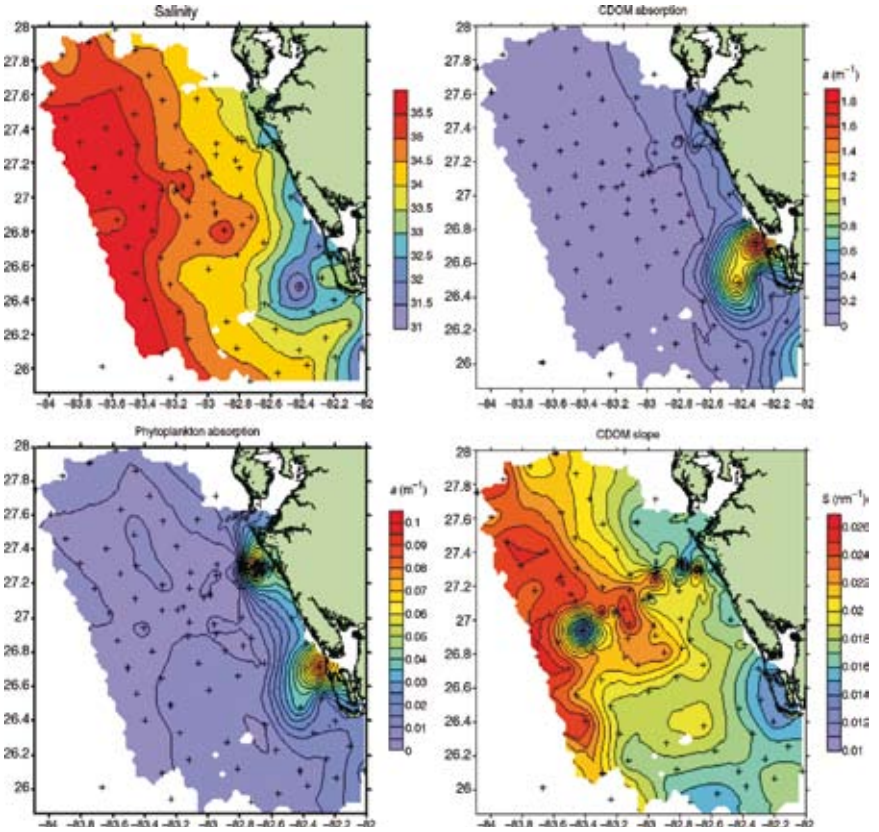

Figure 3.6
Spatial maps of salinity, optically derived maps of CDOM optical weight, phytoplankton optical weight (high values to the south included toxic *K. brevis*), and the exponential spectral slope of the CDOM absorption. The exponential slope for CDOM reflects the composition of the CDOM and low values is often interpreted as freshly derived CDOM (see Carder et al., 1989). The maps of phytoplankton, CDOM, and CDOM slope were all estimated from bulk absorption measurements made with an ac-9 instrument (Zaneveld et al., 1994; Pegau et al., 1995). Often enhanced *K. brevis* cell numbers are associated with river plumes and it has been suggested that blooms may be triggered by nutrient-rich waters near shore that provide a source of nitrogen (in the form of ammonia and/or DON) and/or phosphorus. Numerous culture studies with *K. brevis* have demonstrated the ability of dinoflagellates to use dissolved organic nitrogen for growth (Baden and Mende, 1979; Shimizu and Wrensford, 1993). Because of this the organic rich river water may be an ideal water mass for growth.
Source: Kalle (1996).

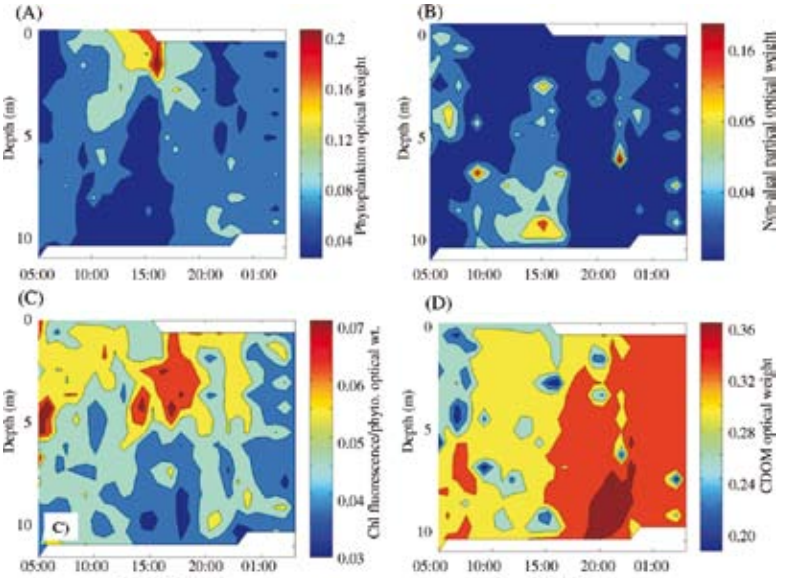

Figure 3.7
An example of IOP measurements during a HAB event which illustrates diel variability in A, phytoplankton; B, non-algal particles; C, chlorophyll fluorescence yields (here estimated as the ratio of chlorophyll fluorescence to phytoplankton optical weight); D, CDOM optical weights (here optical weight refers to the proportion of component absorption to total absorption at 676 nm for phytoplankton and 412 nm for CDOM and non-algal particles, see Schofield et al., 2004) during a Gulf of Mexico cruise in October 2001.
These waters were dominated by the toxic red tide *Karenia brevis* and its vertical migration into surface waters after local noon is clear. Derived swimming speeds compare favourably to measured swimming speeds (approximately 1 m h^{-1}; Heil, 1986). Measurements were made with a WetLabs ac-9 from a ship.

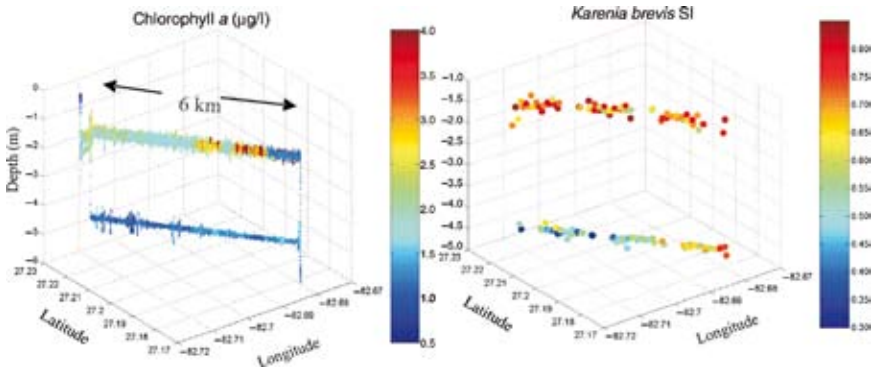

Figure 3.8
Similarity indices (SI) measured with a REMUS vehicle during a red tide in the Gulf of Mexico in winter 2005. The high SI values indicate that a significant fraction of the chlorophyll present is associated with *Karenia brevis*. Note that high SIs, indicating the presence of *K. brevis*, do not necessarily correlate with the highest chlorophyll concentrations measured with the AUV-mounted fluorometer.

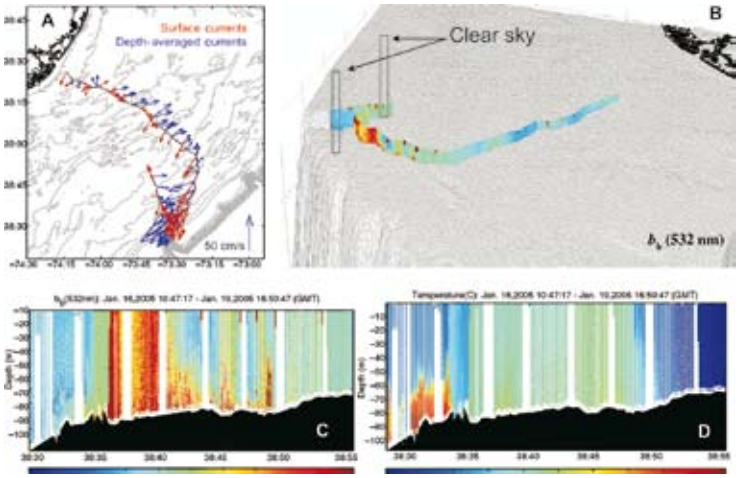

Figure 3.9
Data collected by a long-duration autonomous Webb Glider in the Mid-Atlantic Bight.
A, surface map showing the path flown by the glider. The arrows indicate both depth-averaged (blue) and surface (red) currents during the flight. The glider at the outer shelf edge was advected by a large Nor-Easter storm.
B, map of the optical backscattering coefficient at 532 nm measured with a WetLabs ECO Puck sensor on the glider. The squares indicate times of clear sky during which cloud-free conditions allowed for satellite data to be collected. Note that most of the time during this glider transect, the sky was cloudy, especially during the storm-induced resuspension events, which are indicated by the highest backscatter values on the outer shelf. This illustrates one of the weaknesses of satellite approaches where the presence of clouds can greatly limit the available data.
C, cross-shore transect showing the massive resuspension during the glider transect.
D, corresponding glider map of temperature which does not show as dramatic variations as the particle backscatter. Note the deep warm-water mass when mixed upwards during the resuspension event yields a uniformly warmer water column, which would have been difficult to interpret without the backscattering data.

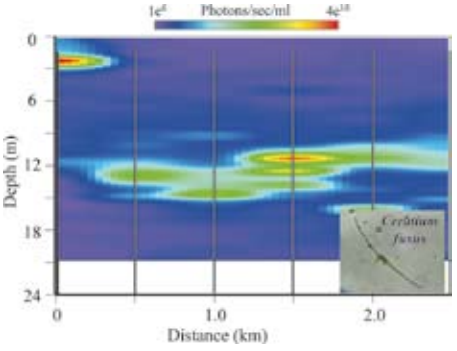

Figure 3.12
Bioluminescence potential measured by a ship-based profiling system after being directed into position by data collected from the sea-surface current data illustrated in Figure 3.11. The bioluminescence (light shades of grey) was due to the dinoflagellate *Ceratium* and it was responsible for the slick observed by the aircraft.

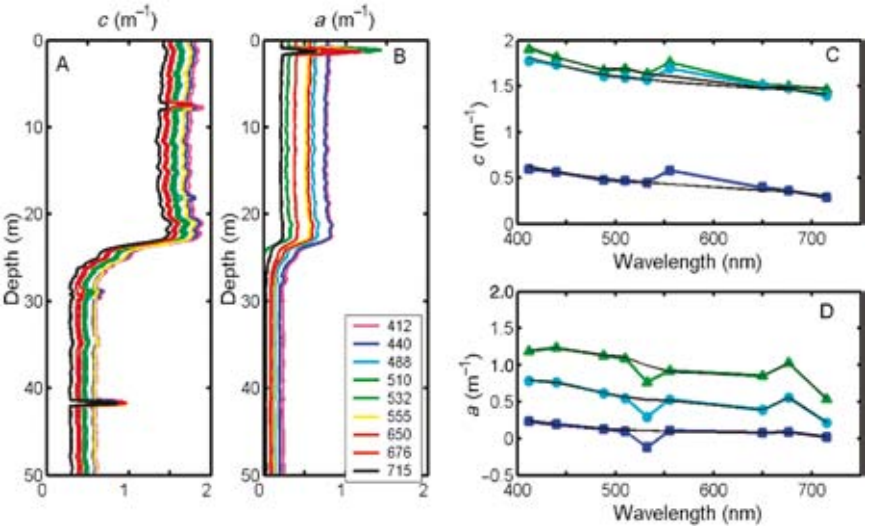

Figure 5.11
Example of observed attenuation and absorption measured with an ac-9 in stratified coastal waters. Depth profiles of raw A, attenuation; B, absorption observations using a pre-deployment factory calibration at nine wavelengths.
C, D, attenuation and absorption spectra, respectively, taken from discrete depths within and below the mixed later and at the 2 m absorption peak. Spectra corrected for post-deployment calibrations shown in black lines.

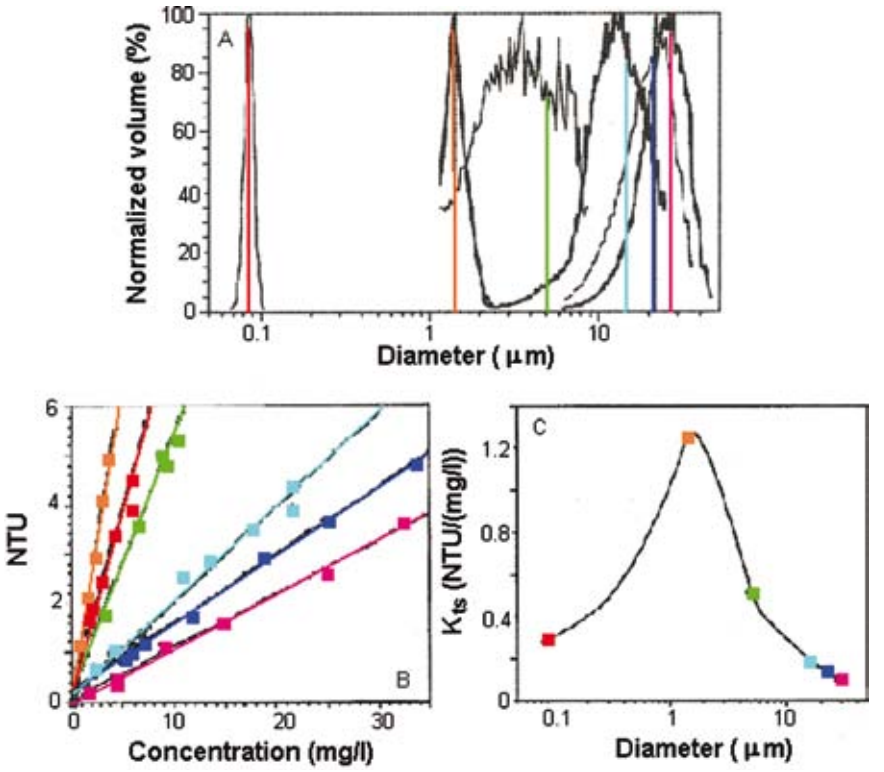

Figure 5.21
Example of the characterization of the WET Labs LSS sensor using dilutions of inorganic clay particles of known size distribution.
A, size distribution of six clay-particle suspensions, determined by Coulter Counter. Vertical lines indicate modal diameter for each suspension.
B, LSS response (NTU) to dilutions of the six suspensions, each represented by data points along a line colour-coded to the size distribution as in A. The slope of the line is the concentration-specific backscattering coefficient, K_{bs} (NTU mg $l^{-1})^{-1}$.
C, dependence of the concentration-specific backscattering coefficient K_{bs} on the mean particle diameter for each suspension, data points colour-coded as in A and B. This demonstrates that the LSS is most sensitive to particles in the size range 1 μm and less sensitive to both larger and smaller particles.
Source: modified from Baker et al. (2001).

Figure 5.26
Examples of water discoloration during the monospecific HABs in Figure 5.25.
A, B, views of coastal waters near Bigelow Laboratory for Ocean Sciences, West Boothbay Harbor, Maine, in October 1999, (A) prior to and (B) during the *P. micans* bloom. The water is characteristically green due to high CDOM absorption and red during the bloom from the enhanced blue-green absorption and red backscattering of the *P. micans* cells.
Source: photos courtesy of M. Keller.
C, brown water associated with the *Aureococcus anophagefferens* bloom in Quantuck Bay, Long Island, New York, in June 2000.
Source: photo courtesy of S. Etheridge.

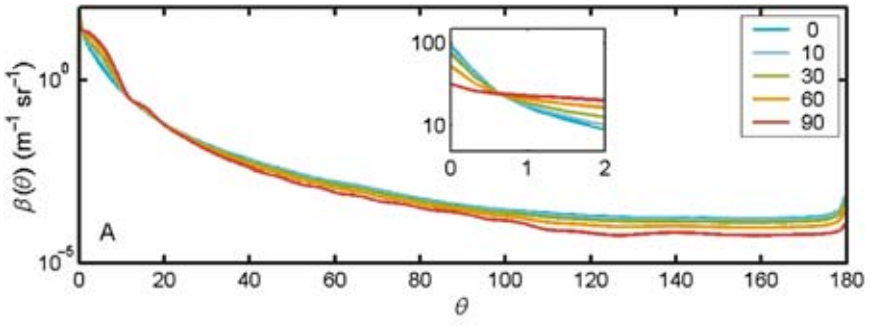

Figure 5.28 A
Volume scattering functions computed for particles with refractive index 1.05 + i 0.001, a Junge slope of 4 with increasing proportions of *Aureococcus anophagefferens* cells from 0% to 90% of total particle volume. The total particle volume has been held constant, only the proportion of *A. anophagefferens* cells relative to background particles changes.
Inset: first 2° of resolution.

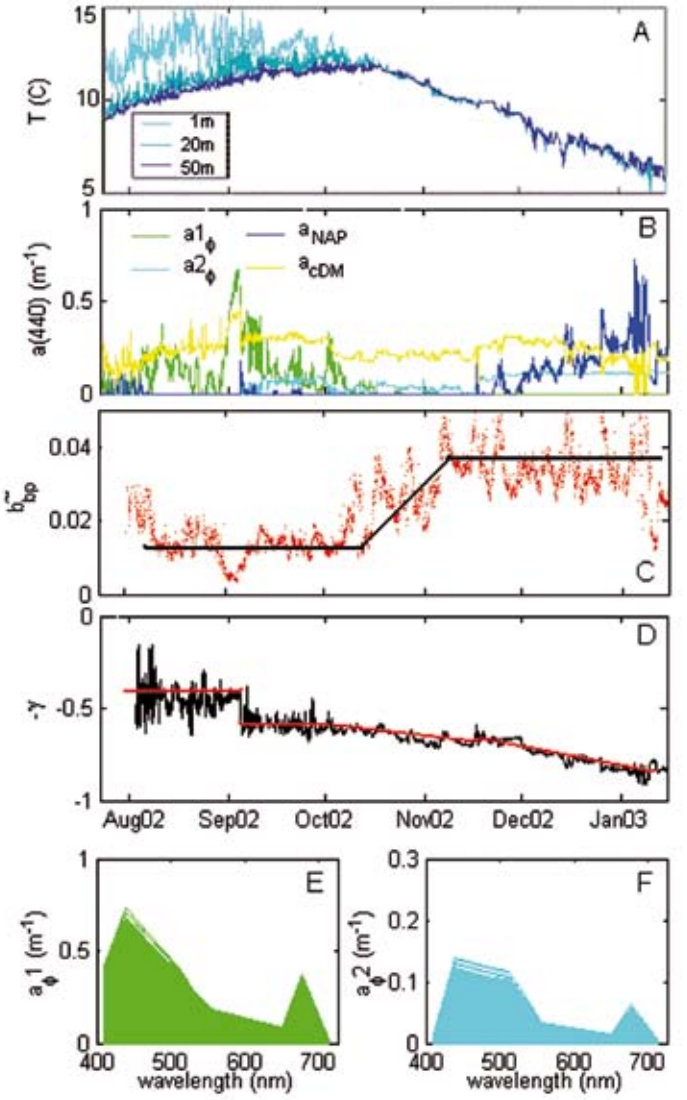

Figure 5.30
Real-time hourly observations of temperature, IOPs and derived optical properties for the period August 2002 to January 2003 from the Eastern Maine Coastal Current, Gulf of Maine.
A, temperature at 0 m, 20 m and 50 m.
B, component absorption (440 nm, derived from total measured absorption, see text for details).
C, particle backscattering ratio (660 nm).
D, spectral slope of particle attenuation -γ.
E, F, spectral shape of two phytoplankton absorption components, the temporal pattern for each shown in B. See text for details.
Source: Roesler and Barnard (2003).

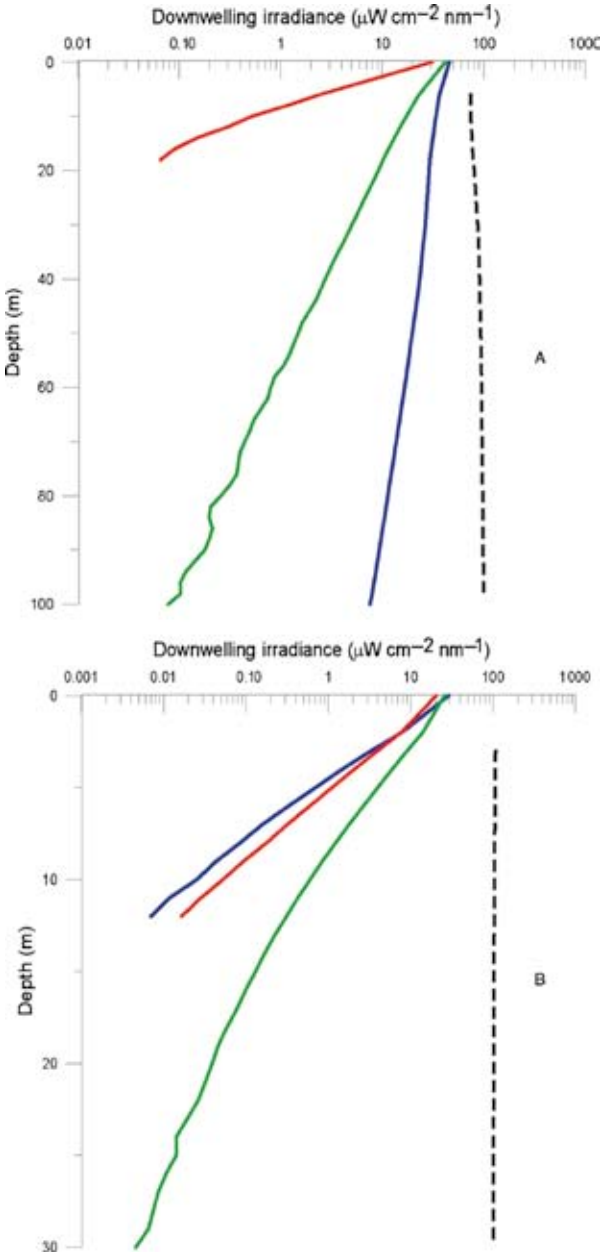

Figure 6.4
Profiles of downward irradiance for selected wavelengths in the two stations in Figures 6.2 and 6.3. The blue lines reference 443 nm, green 555 nm and red 650 nm. The above-water irradiances (555 nm), measured at the same time and normalized to their mean value during the profile, are also given as dotted lines.

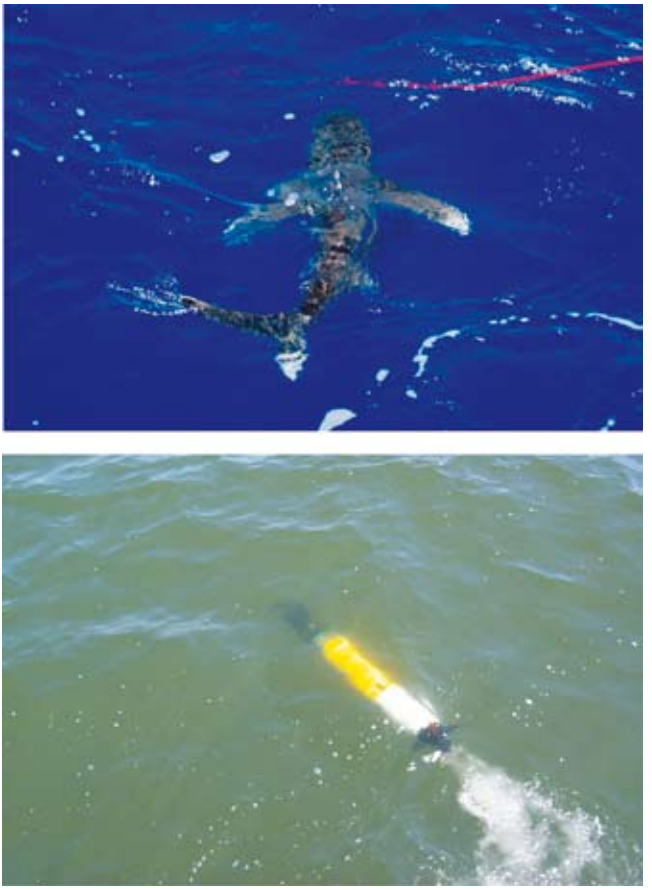

Figure 6.9
Two varieties of autonomous platform used for optical measurements. The rich blue of the oligotrophic waters contrasts with the oceanic white-tip shark, a species being used as a data collection platform by surgically implanted devices. The dark green waters of the coastal environment are a backdrop for the REMUS autonomous vehicle, which has been used for the measurement of the three-dimensional optical structure of the coastal ocean.

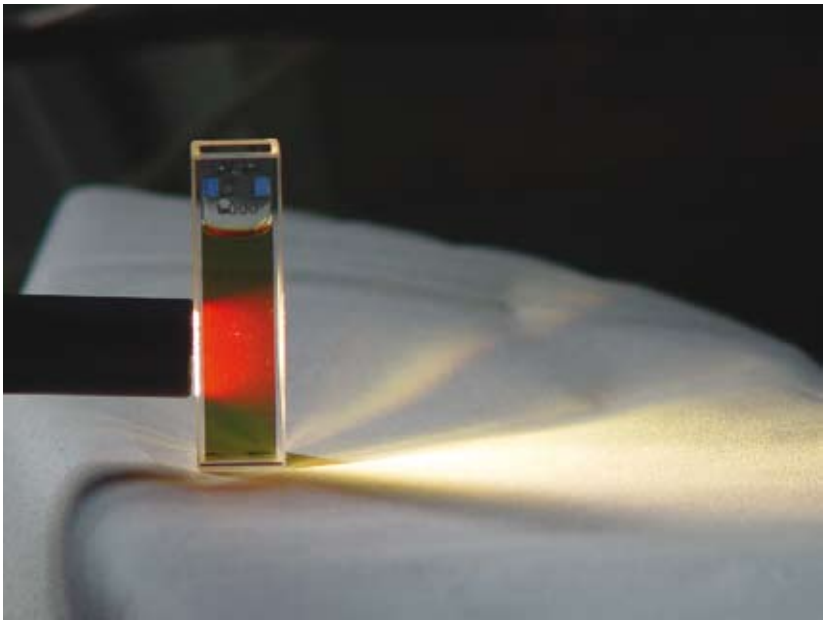

Figure 7.3
Fluorescence (gray) emitted by chlorophyll *a* dissolved in pure acetone, when induced using a beam of white light.

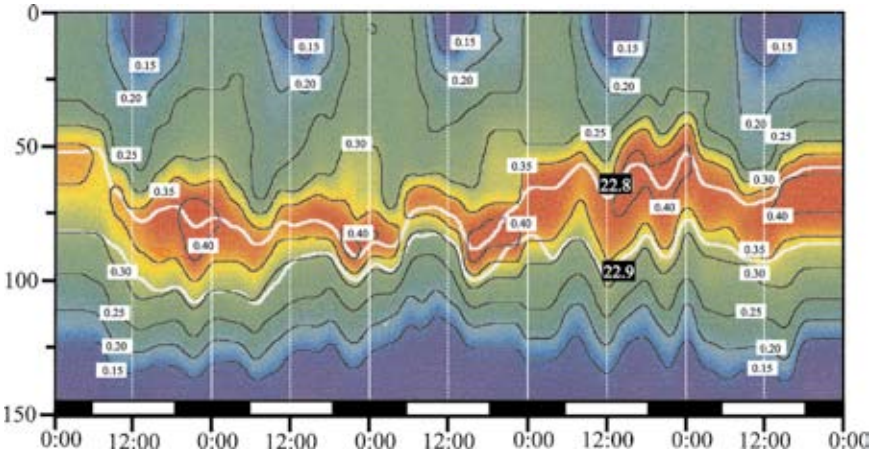

Figure 7.14
Temporal changes over five days in the vertical profile of chl *a* fluorescence measured with an underwater fluorometer at 5°S 150°W in the Pacific ocean.
Source: redrawn from Claustre et al., 1999.

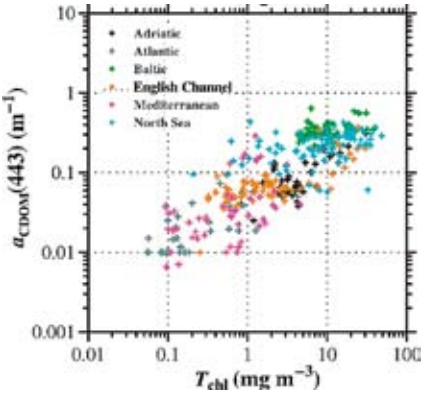

Figure 8.5
Dependence of $a_{CDOM}(443)$ on Chl observed for a wide range of European coastal waters.
Source: Babin et al. (2003*b*).

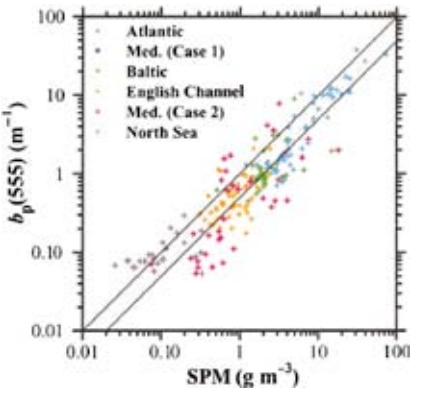

Figure 8.9
Dependence of $b_p(555)$ on SPM observed for a wide range of European coastal waters. Lines indicate 1:1 and 1:2.
Source: Babin et al. (2003*a*).

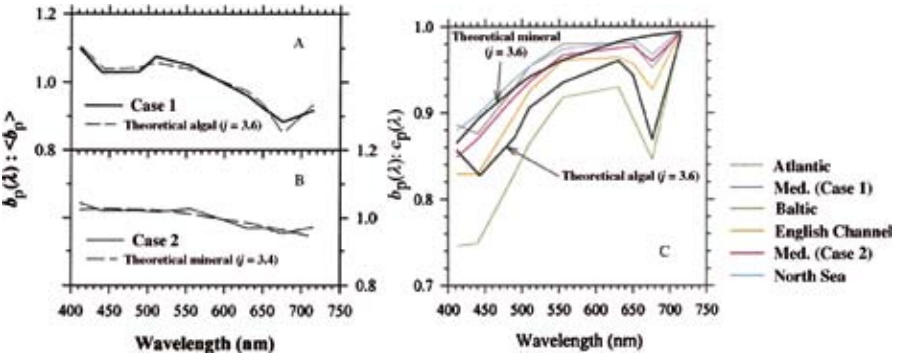

Figure 8.12
Mean normalized spectral shape for $b_p(\lambda)$ observed from diverse European coastal environments with A, Case 1; B, Case 2 waters. C, mean ratios of $b_p(\lambda)$ to $c_p(\lambda)$ for each of the regions examined. For comparison, results from Mie theory are also shown for Junge-distributed (slope indicated by j values) particles with refractive indices typical for algae and minerals.
Source: Babin et al. (2003*a*).

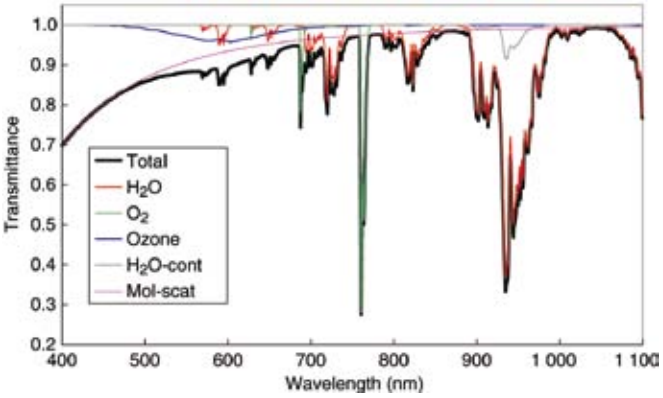

Figure 9.5
Light transmittance spectra for total atmospheric column. Contributions of molecular (water vapour, oxygen, ozone) absorption and molecular scattering are also shown.

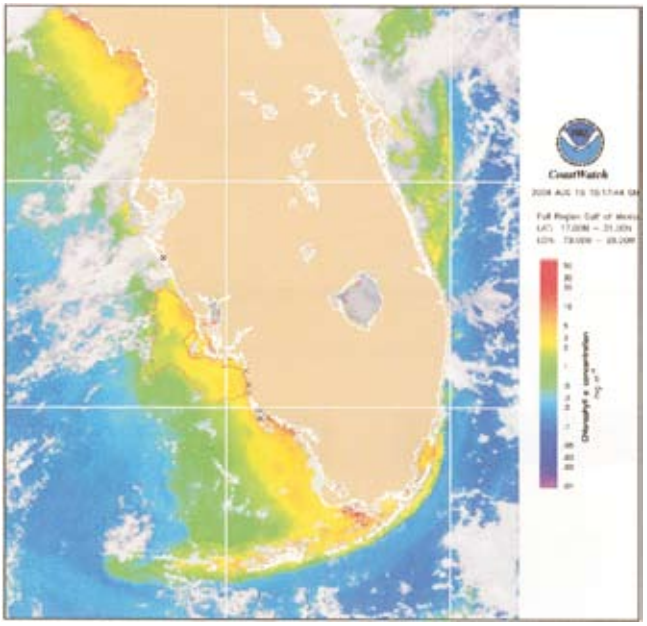

Figure 9.12
Satellite imagery section of a sample HAB bulletin (19 August 2004) from NOAA Coastwatch. Satellite-derived chlorophyll concentration from SeaWiFS is given in the colour scale with the red polygon on the West Florida coast marking a possible HAB region (considered as 'low to moderate probability' in this case). *In situ* sampling stations are given as crosses denoting that HABs were not present in cell concentration sampling data.
Source: Information courtesy of Florida Fish and Wildlife Conservation Commission and NOAAHAB Forecasting System. Image courtesy of Orbimage, Inc. and NOAA Coastwatch.

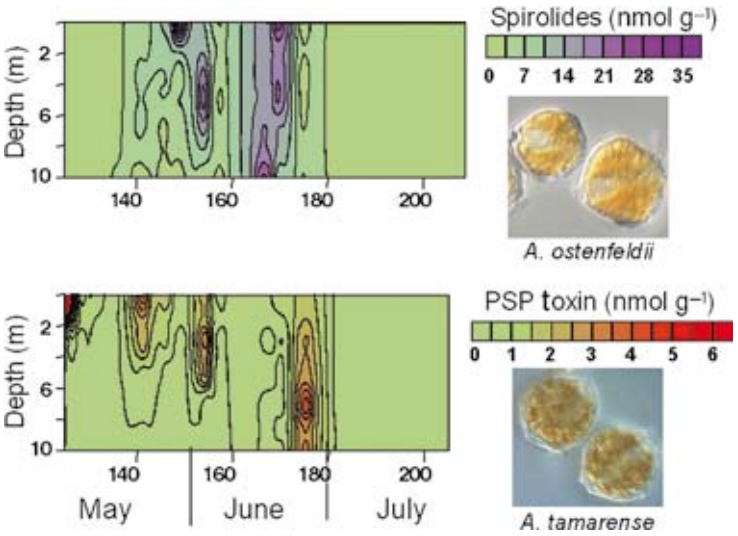

Figure 11.4
High-resolution toxin-specific analytical methods can be used to map spatio-temporal variations in toxin content in the plankton and associated bloom dynamics in relation to physical and chemical parameters. In this study on Graves Shoal (1998), along the eastern shore of Nova Scotia, liquid chromatography with fluorescence detection (LC-FD) and mass spectrometry (LC-MS) were employed to determine changes in the vertical distribution of PSP toxins and spirolides, respectively, over time in the water column. The units for the contour plots represent total net toxin (nmol) per gram wet weight of total net plankton material (>20 μm) collected by pump.
Source: Cembella et al., previously unpublished data.

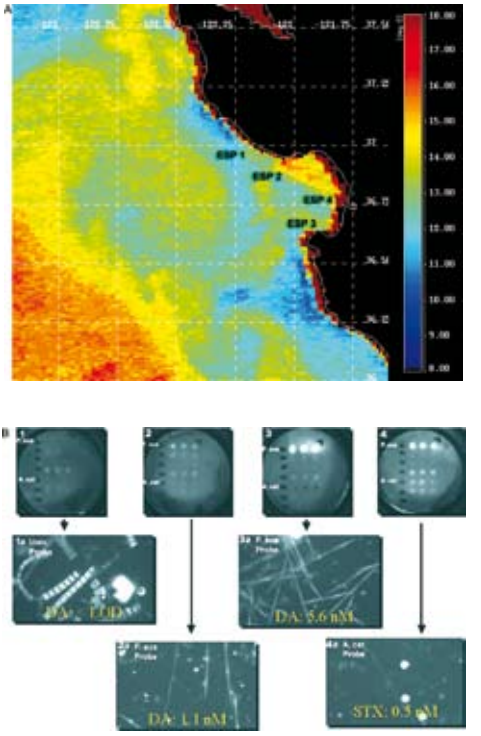

Figure 11.12
Examples of data obtained using the shipboard ESP in Monterey Bay, California. A, sea surface temperature and locations of sampling stations (ESP 1-4). B, images of the oligonucleotide probe arrays (centre frames) and micrographs showing results of fluorescent *in situ* hybridization assays (lower frames). Domoic acid and PSP toxin activity associated with a sample is printed at the foot of the micrographs. Locations of probes for *P. australis* and *A. catenella* on the arrays, spotted in triplicate, are denoted *P. australis* and *A. catenella* respectively. To develop a oligonucleotide probe array, the ESP collected 400 ml of seawater, concentrated particles >~5 µm onto a 25 mm Durapore filter, homogenized material retained in 1.5 ml of lysis reagent, and the resulting sample homogenate was drawn into the syringe. The sample collection puck was replaced with a puck carrying a custom-printed oligonucleotide probe array. The sample homogenate was passed over that array, followed by a sequence of reagents that reveal rRNA molecules retained at specific locations on the array grid using the principles of sandwich hybridization (Scholin et al., 1996, 1997, 1999). An image of the resulting array was recorded using the ESP's CCD camera. For whole cell hybridization, a 50 ml sample was passed through a 3 µm pore size polycarbonate filter and the particles retained were treated with a saline ethanol solution for 1 hour then dried (Miller and Scholin, 2000). The preserved, dried sample was stored onboard the ESP. Following deployment, the ESP was programmed to process the archived samples using fluorescent *in situ* hybridization after Miller and Scholin (2000). Once the hybridization process was complete, the sample filter was recovered and viewed using conventional epifluorescence microscopy. In the examples shown here, several different rRNA probes were used: Univ. (targets rRNA from all organisms), *P. aus* (targets rRNA specific to *P. australis*), and *A. catenalla* (targets rRNA specific to *A. catenella*; see Miller and Scholin, 1998). Samples archived for toxin analysis consisted of 750 ml aliquots concentrated onto GF/F filters stored dry onboard the ESP, then recovered post-deployment and held at –20°C until tested using a receptor binding technique for either domoic acid or saxitoxin (Lefebvre et al. 1999; Powell and Doucette 1999).

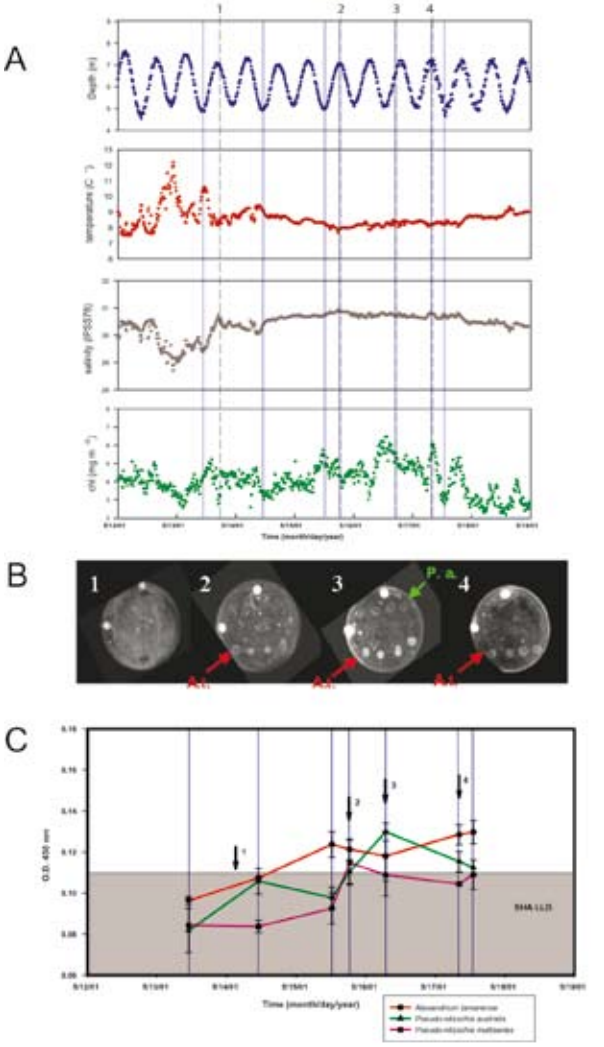

Figure 11.14
Examples of data obtained using the *in situ* ESP in Casco Bay, ME. A, depth, temperature, salinity, and chlorophyll fluorescence recorded onboard the ESP during the deployment. Dashed black lines 1–4 show ESP sampling times that correspond to probe array images in (B); blue solid lines indicate when water samples were collected from a depth and position near the ESP mooring using Niskin bottles on a hydrowire. B, prototype DNA probe arrays developed on board the ESP (as in Figure 11.2); the two bright spots at top and left are registration marks; probes for *P. australis* (above), *P. multiseries/pseudodelicatissima* (centre) and *A. tamarense* (below) are hand-spotted in quadruplicate. Arrays 1–4 correspond numerically to the same numbers shown on (A, dashed lines) and (C, arrows). C, results of benchtop sandwich hybridization assays (SHA; Scholin et al., 1999) for Niskin bottle samples collected at times shown in (A); probes used for that assay are the same as those spotted onto the arrays. Shaded area, non-detection range; values above that indicate a positive reaction; red, *A. tamarense*; green, *P. australis*; purple, *P. mulitiseries/pseudodelicatissima*.

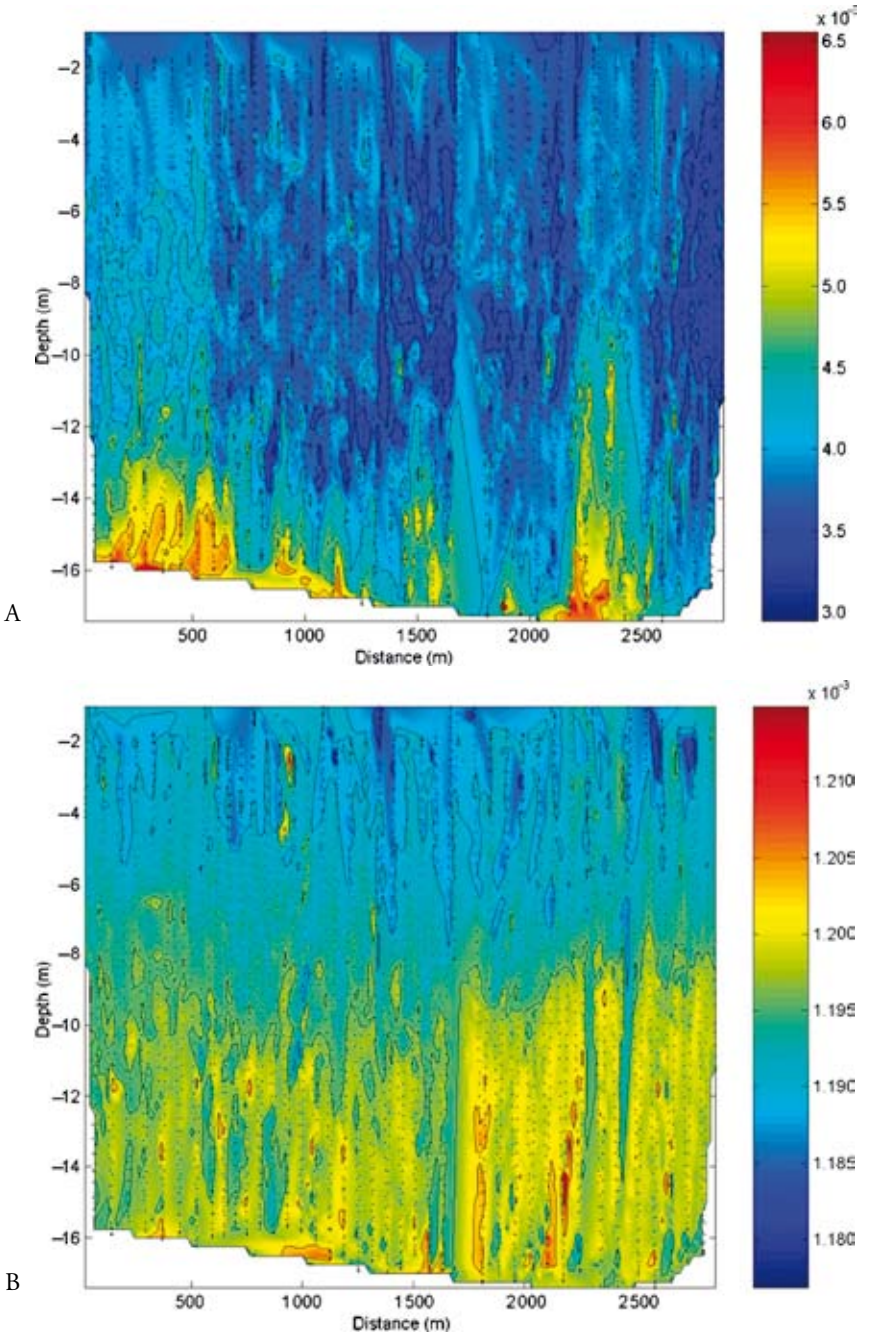

Figure 13.5
Vertical contour sections of A, optical backscatter at 670 nm; B, chlorophyll fluorescence (in relative units) from a Slocum glider on 16 January 2003 off Sarasota, Florida.
Source: courtesy of Rutgers University, Institute of Marine and Coastal Sciences.

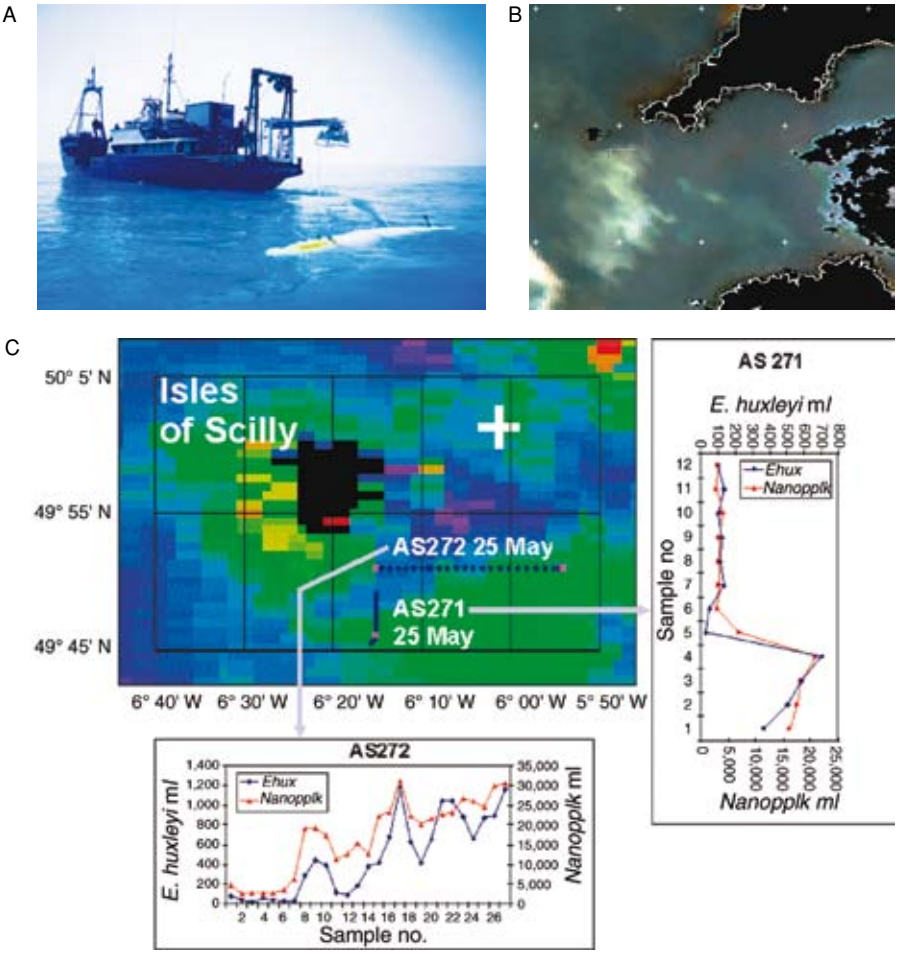

Figure 13.7
Autosub AUV after deployment from the RV *Terschelling*.
A, in a cocolithophore bloom off the Isles of Scilly in May 2001;
B, SeaWiFS satellite image of the area on the same day, with the cocolithophore bloom visible to the south of the islands, and the two Autosub tracks shown in blue;
C, small-area view of the SeaWiFS data colour-coded for chlorophyll (high in green, low in blue) with the tracks of the Autosub AUV on two transects. Counts of nanophytoplankton and *E. huxleyi* cells on each transect are also shown. SeaWiFS data received at NERC receiving station, Dundee, UK, and processed at the Plymouth Marine Laboratory.
Source: SeaWiFS data courtesy of NASA SeaWiFS Project and Orbimage.

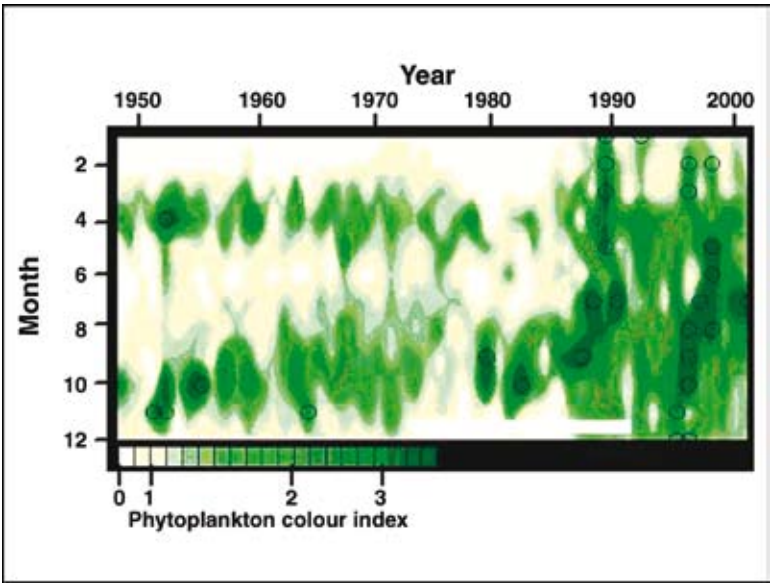

Figure 14.8
The time series of monthly mean values of the CPR colour index in the central North Sea shows a dramatic increase in phytoplankton biomass in the late 1980s. Circles denote colour indices greater than 2 standard deviations above the long-term monthly mean.

Figure 15.4
Bands of the dionflagellate *Lingulodinium polyedrum* moving onshore over the troughs of a series of internal waves.

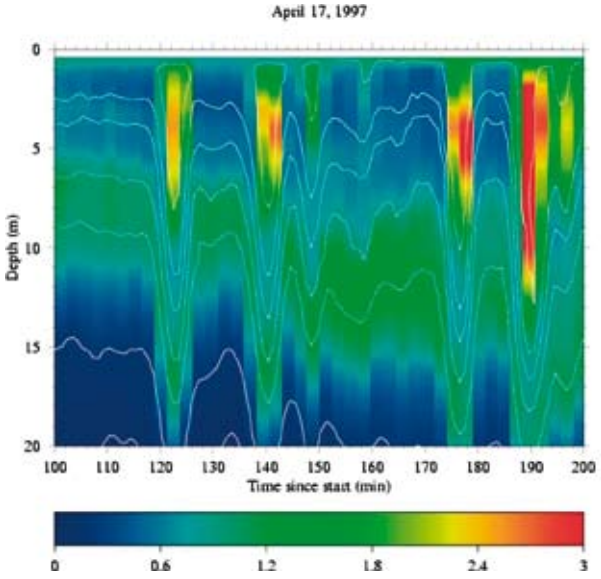

Figure 15.9
Phytoplankton fluorescence (colour scale) and temperature (white lines) during the passage of a series of nonlinear internal waves off the coast of San Diego, California. A CTD-fluorometer package was yo-yoed up and down each minute while the boat was at anchor. The patches of phytoplankton in the wave troughs probably formed through the interaction of swimming of the plankton and flows of the internal waves.
Source: after Lennert-Cody and Franks (2002).

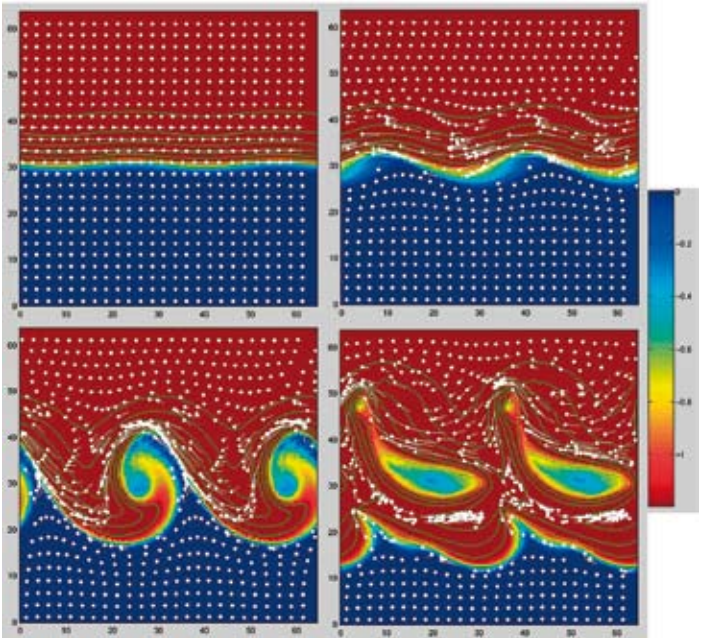

Figure 15.10
Four plan views of a front going unstable (day 0: upper left, day 4: upper right, day 8: lower left, day 12: lower right). Blue colours are cold inshore (upwelled) water, while red colours indicate warmer offshore waters. The white particles are trapped at the surface. Note how particles can accumulate due to the vertical velocities of the eddies.
Source: Pringle and Franks, unpublished data.

Figure 15.12
A 3 m long boat passing through a band of Noctiluca scintillans that has accumulated at a front formed by a nonlinear internal wave off the coast of San Diego, California. The dense part of the band is <20 m wide, and would be unresolved by most coastal models.

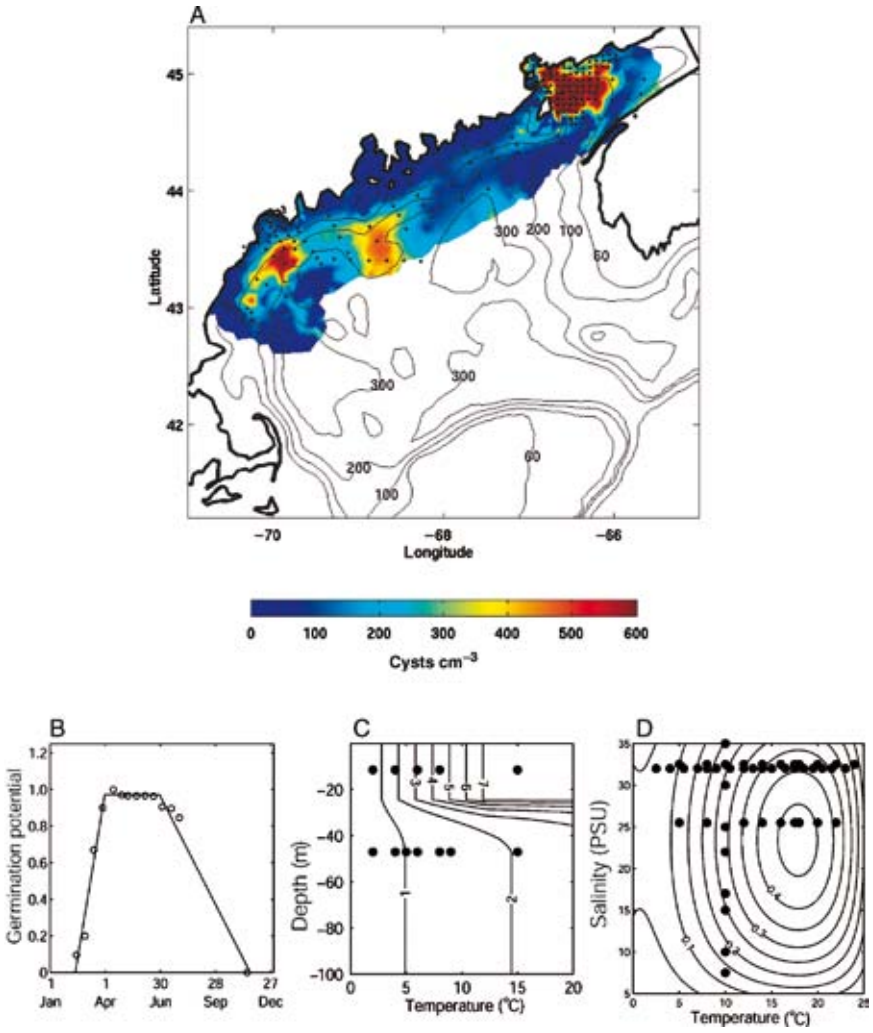

Figure 16.3
Population dynamics model for *A. fundyense*.
A, distribution of cysts (number of cysts cm^{-3}) in the upper 3 cm of sediment derived from a 1997 survey of the Gulf of Maine (McGillicuddy et al., 2003) and surveys of the Bay of Fundy in 1981 (White and Lewis, 1982), 1982 and 1983 (data provided by Jennifer Martin, DFO).
B, germination potential (decimal fraction of cysts able to germinate) as a function of time. The solid line is a piecewise linear fit to laboratory observations (open circles) of *A. fundyense*'s endogenous clock from Anderson and Keafer (1987).
C, germination rate (% day^{-1}) as a function of temperature and light. Light has been converted to depth using a diffuse attenuation coefficient (k_w = 0.2 m^{-1}) and the mean surface irradiance. Solid circles indicate laboratory germination experiments.
D, specific growth rate (day^{-1}) as a function of temperature and salinity. Solid circles indicate growth rate measurements from laboratory cultures.

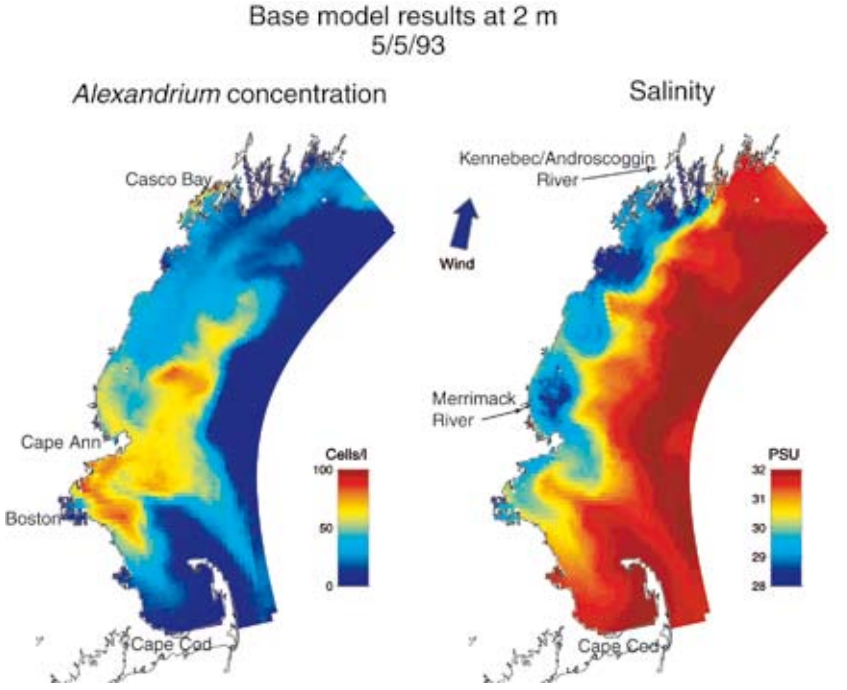

Figure 16.5
Example snapshot of model output from a simulation in the western Gulf of Maine driven by forcing from 1993. In this example, vegetative growth is assumed to be balanced by loss terms, such that the net 'reaction' term on the right of (16.1) is identically zero.

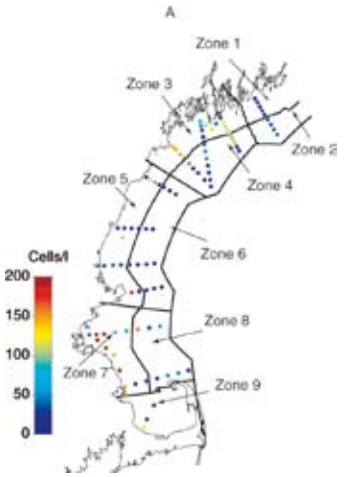

Figure 16.6 A
Typical observational coverage during one cruise of the 1993/1994 Regional Marine Research Program in the Gulf of Maine. Coloured dots represent observations of *A. fundyense* concentration (cells per litre). The nine zones chosen for model evaluation are indicated.

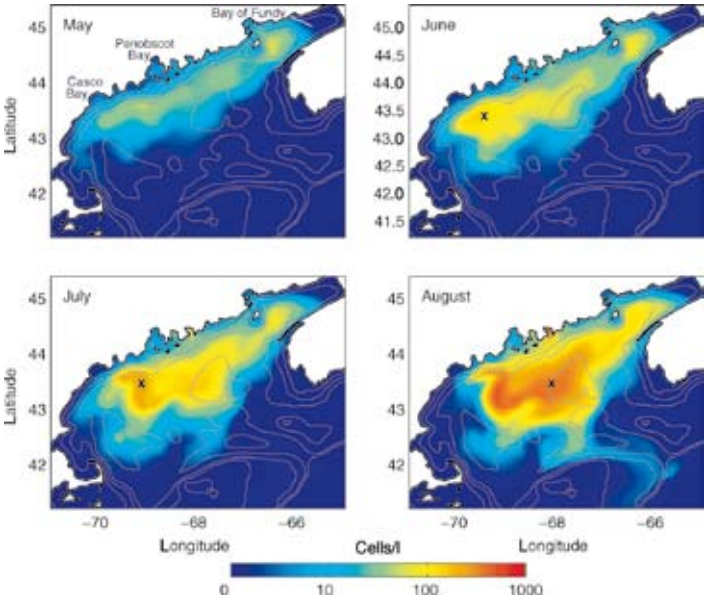

Figure 16.11
Simulated *A. fundyense* distribution under climatological forcing conditions. The following bathymetric contours are overlayed: 60 m, 100 m, 150 m, 200 m and 400 m.

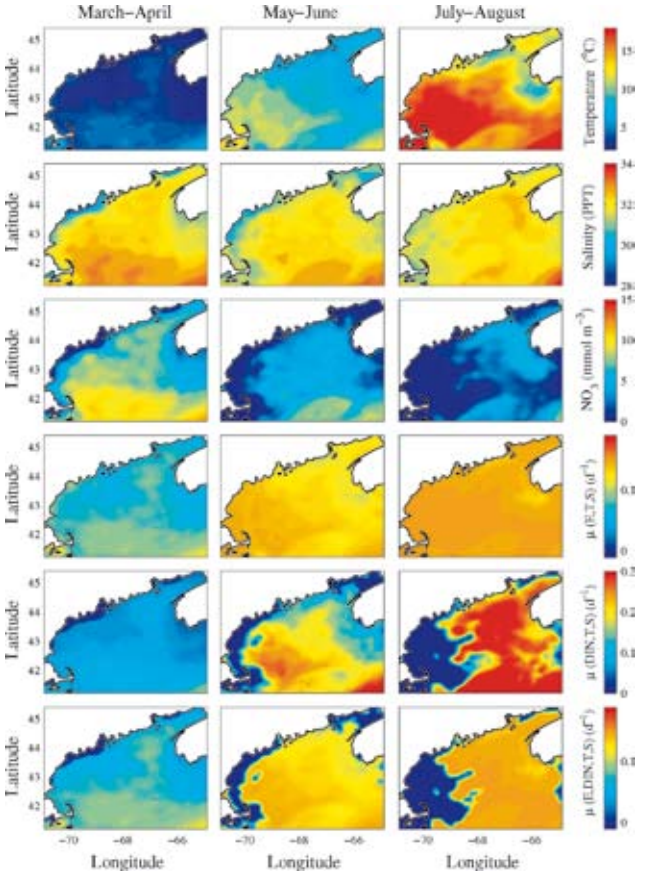

Figure 16.12
Predicted spatial variations in growth rate based on climatological conditions for March-April (left column), May–June (centre column), and July–August (right column). Top three rows: climatological temperature, salinity and nitrate. Nitrate fields are computed from temperature and salinity based on empirical relationships described in Garside et al. (1996). Lower three rows: growth rate as a function of temperature, salinity and irradiance [$\mu(T,S,E)$], growth rate as a function of temperature, and salinity, and nitrate concentration [$\mu(T,S,DIN)$], and overall growth rate [$\mu(T,S,I,DIN) = \min(\mu(T,S,I), \mu(T,S,DIN))$].

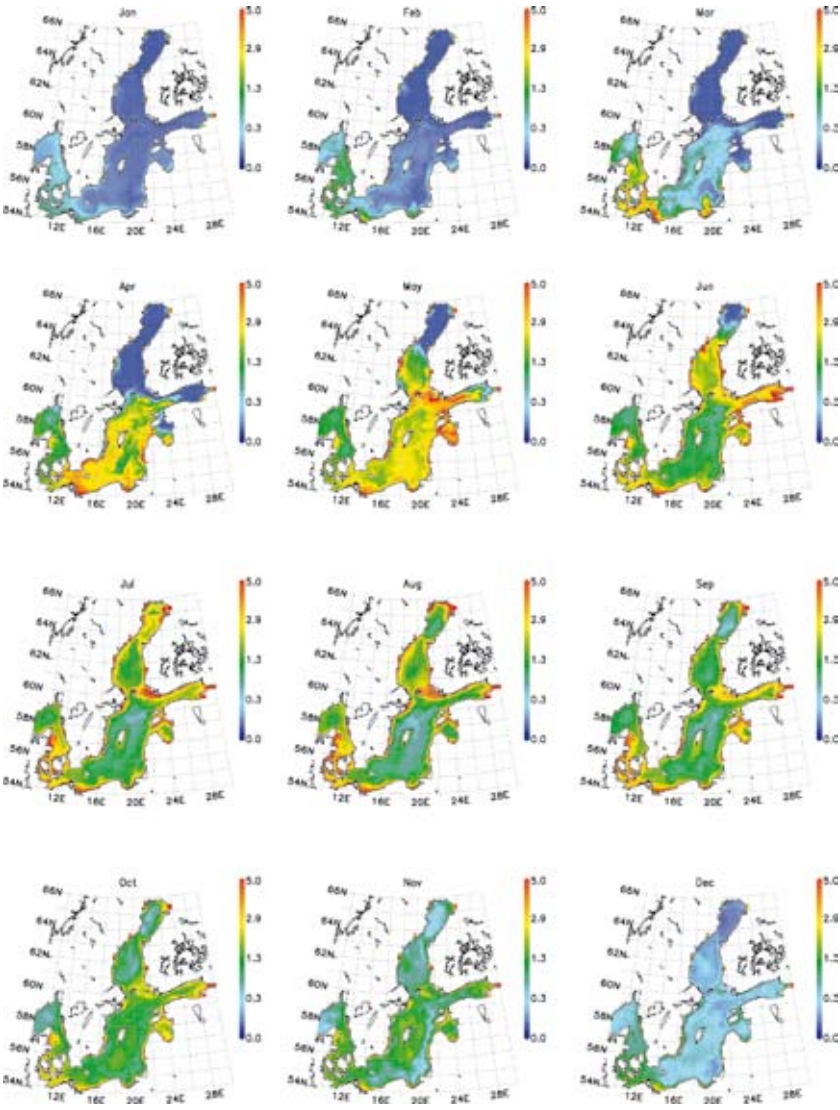

Figure 17.19
Simulated annual cycle of total phytoplankton near the surface, expressed as chlorophyll *a* (mg m^{-3}) in 1984 for the Baltic Sea.

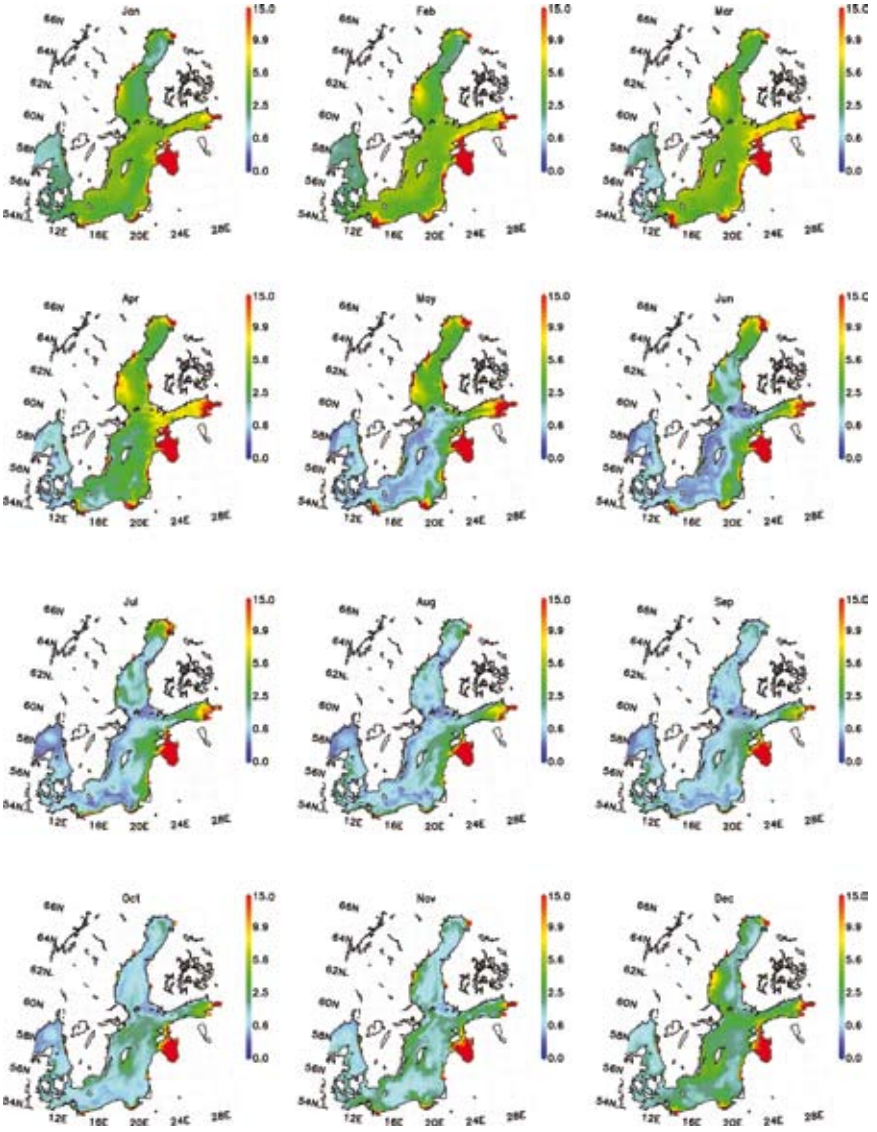

Figure 17.20
Simulated annual cycle of surface nitrogen (mmol m^{-3}) in 1984 for the whole Baltic Sea. The nutrients develop inverse to the model phytoplankton.

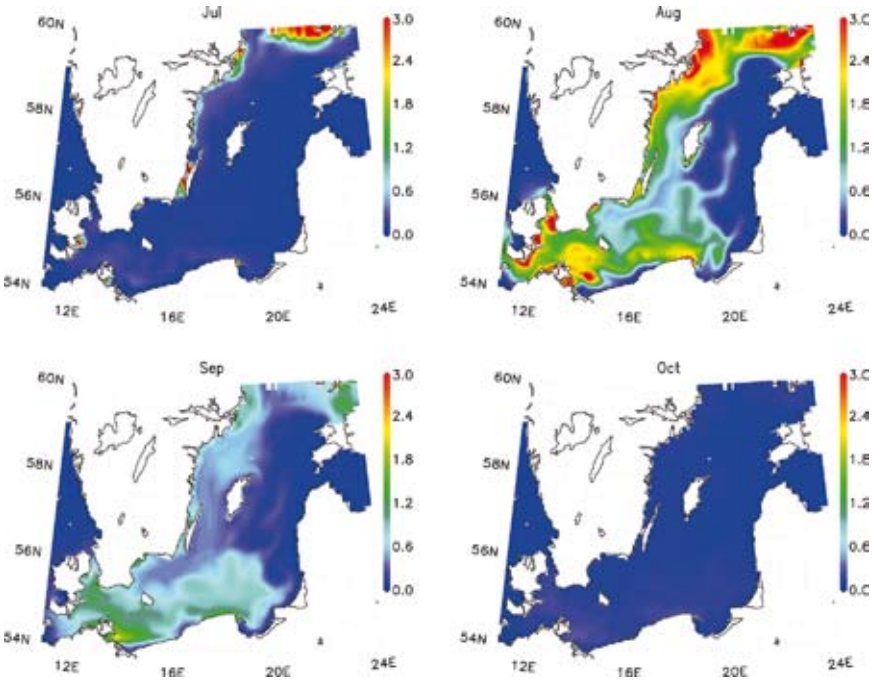

Figure 17.21
Patterns of modelled cyanobacteria chlorophyll *a* (mg m^{-3}) near the surface for the summer of model year 1984 in the central and south-western Baltic Sea.

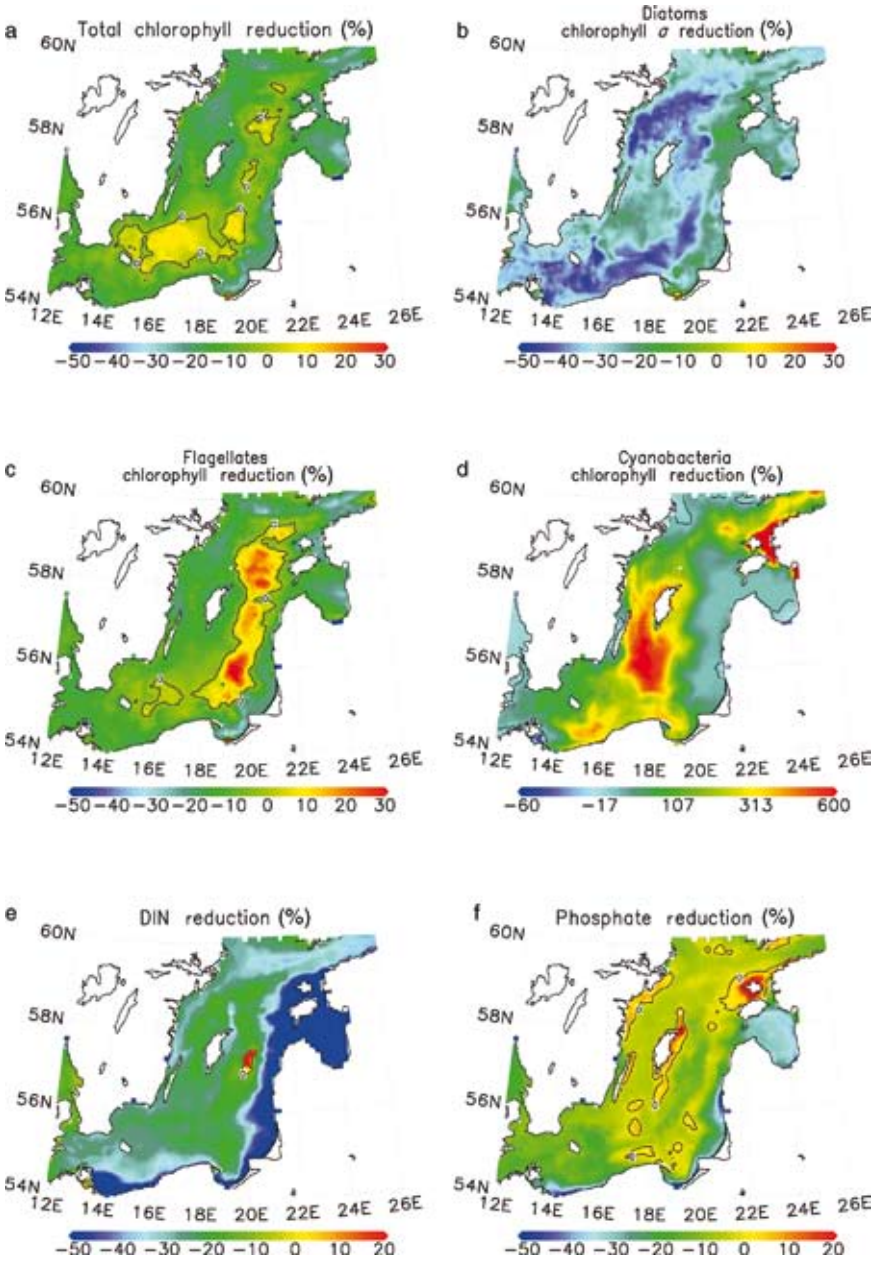

Figure 17.22
Responses of the system to a reduction of river nutrient loads by 50% in terms of the relative changes in concentration of the various model state variables: A, total chlorophyll *a*; B, diatoms; C, flagellates; D, cyanobacteria; E, dissolved inorganic nitrogen; F, dissolved inorganic phosphorous.
Source: after Neumann et al. (2002).

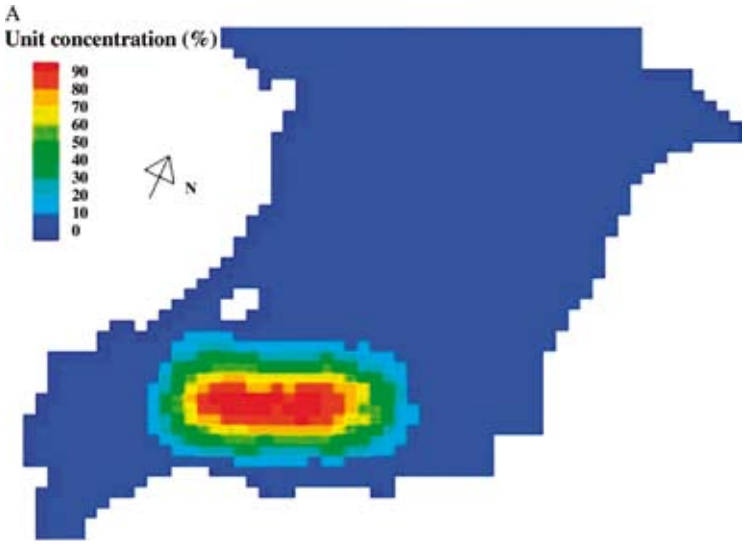

Figure 18.13 A
Computed tracer concentration distribution 12 hours after release of tracer mass in Yung Shue Au fish culture zone, Three Fathoms Cove, Hong Kong.

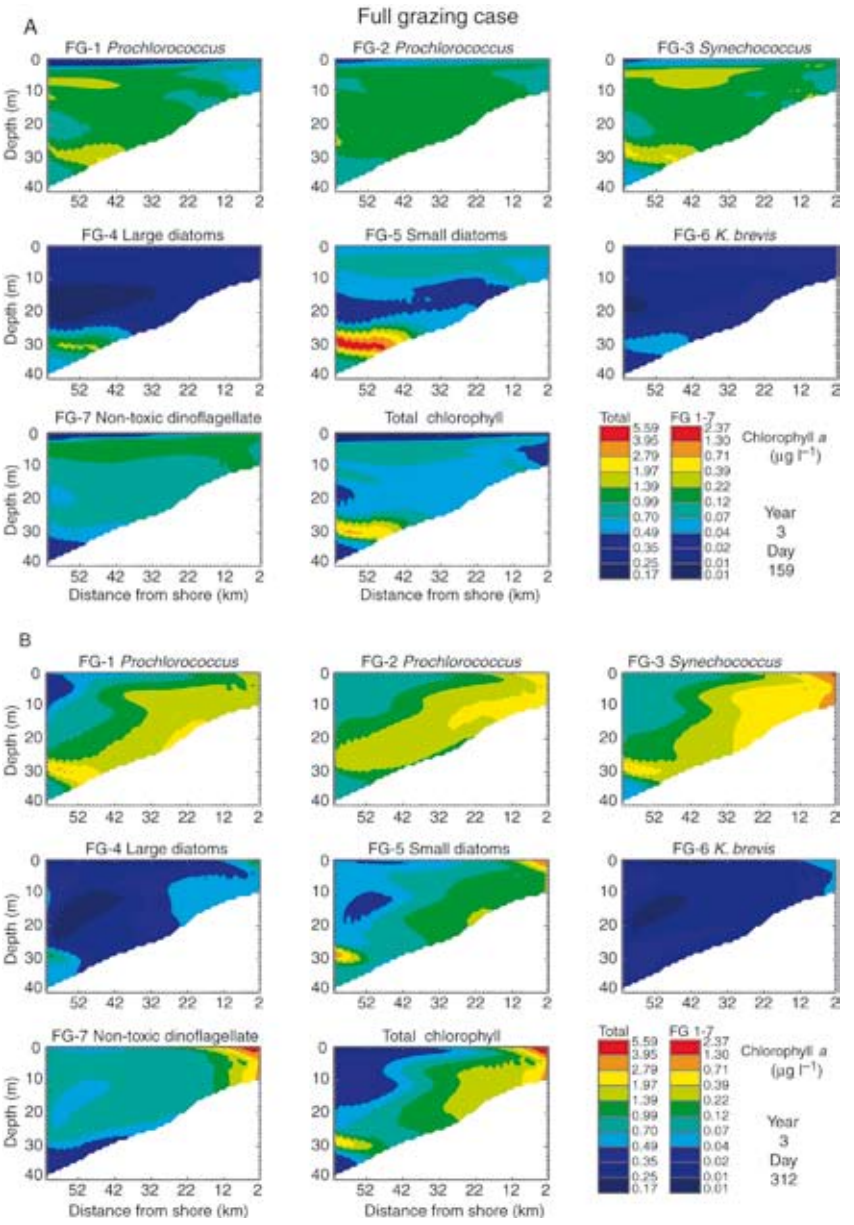

Figure 19.5
A, contour plots of the simulated total chlorophyll *a* concentration attributed to each of the seven phytoplankton species and the sum of all the phytoplankton classes for DOY 159 – 8 June 1998.
B, contour plots of the simulated total chlorophyll *a* concentration attributed to each of the seven phytoplankton species and the sum of all the phytoplankton classes for DOY 312 – 8 November 1998.

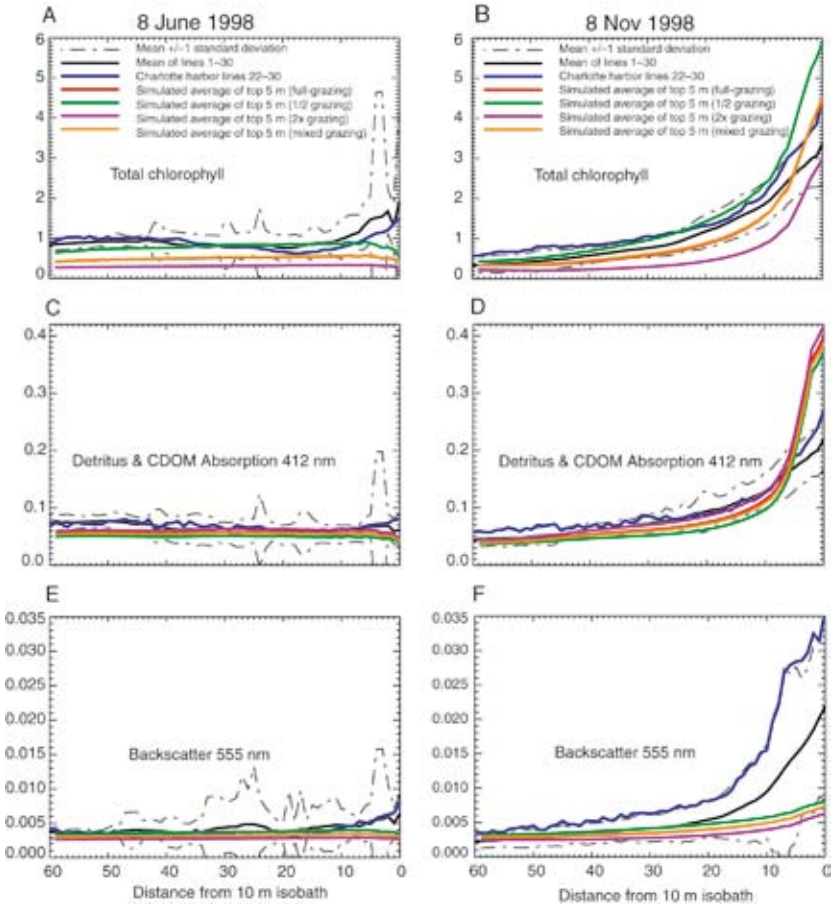

Figure 19.6
Simulated and satellite-derived IOPs on the WFS.
A, total chlorophyll concentration (mg chl m^{-3}) on 8 June 1998, showing the average of the 30 lines transect, ±1 standard deviation of the mean of 30 lines, the mean of lines 22–30 (Charlotte Harbor), simulated absorption 5 m average for the full, half, double and mixed grazing stress runs.
B, total chlorophyll concentration (mg chl m^{-3}) on 8 November 1998 for the WFS.
C, detritus and CDOM absorption [aCDM 412 nm (m^{-1})] on 8 June 1998.
D, detritus and CDOM absorption [aCDM 412 nm (m^{-1})] on
8 November 1998.
E, backscatter (m^{-1}) on the WFS on 8 June 1998.
F, backscatter (m^{-1}) on the WFS on 8 November 1998.

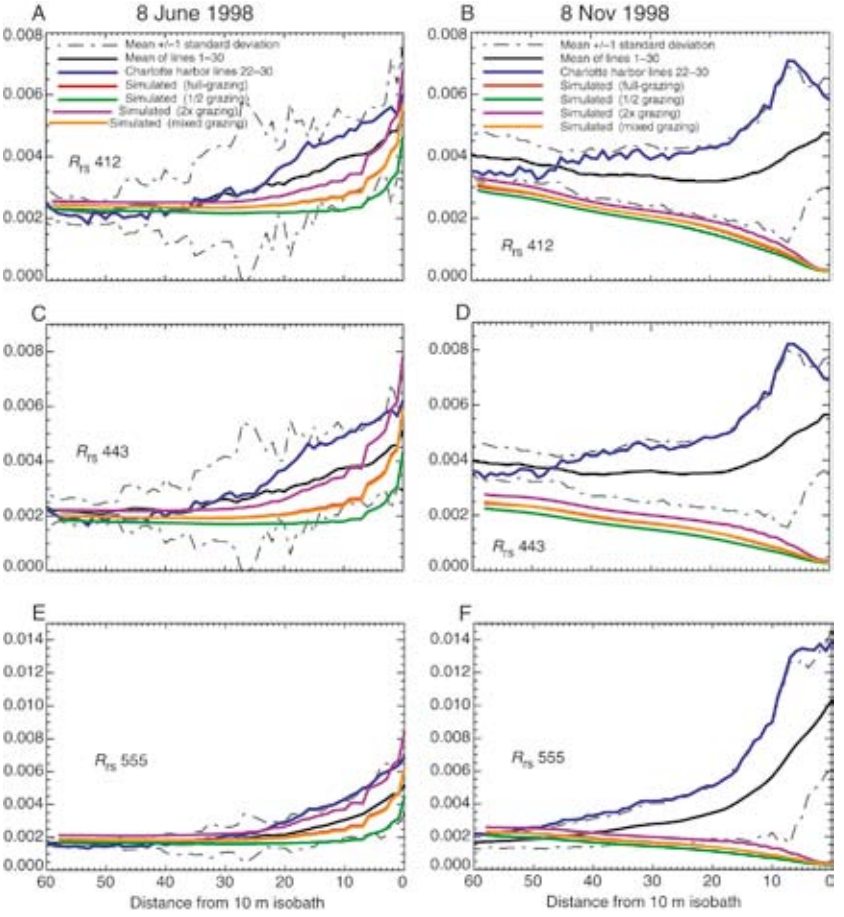

Figure 19.7
Simulated AOPs on the WFS.
A, remote sensing reflectance (R_{rs} 412 nm) on 8 June 1998 for the WFS showing the average of the 30 lines transect, ±1 standard deviation of the mean of 30 lines, the mean of lines 22–30 (Charlotte Harbor), simulated at the surface for the full, half, double and mixed grazing stress runs showing a fairly good match between estimated and simulated results.
B, R_{rs} (412 nm) on 8 November 1998.
C, R_{rs} (443 nm) on 8 June 1998.
D, R_{rs} (443 nm) on 8 November 1998.
E, R_{rs} (555 nm) on the WFS on 8 June 1998.
F, R_{rs} (555 nm) on 8 November 1998.

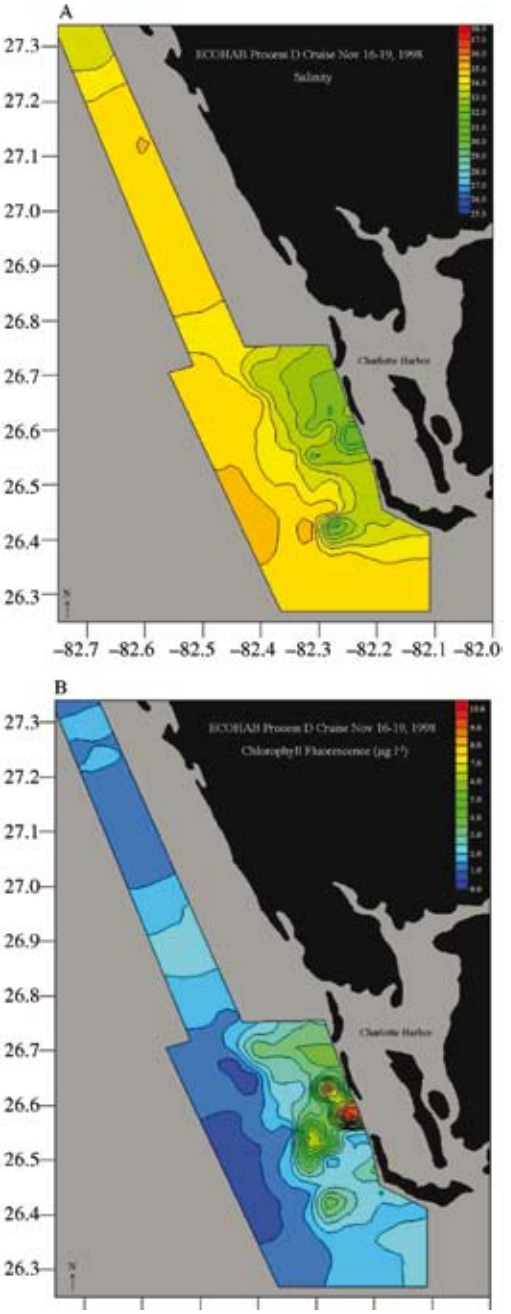

Figure 19.9
Process Cruise data on 16–19 November 1998 displaying A, salinity; B, chlorophyll fluorescence signature near-shore along the coast of Charlotte Harbor.

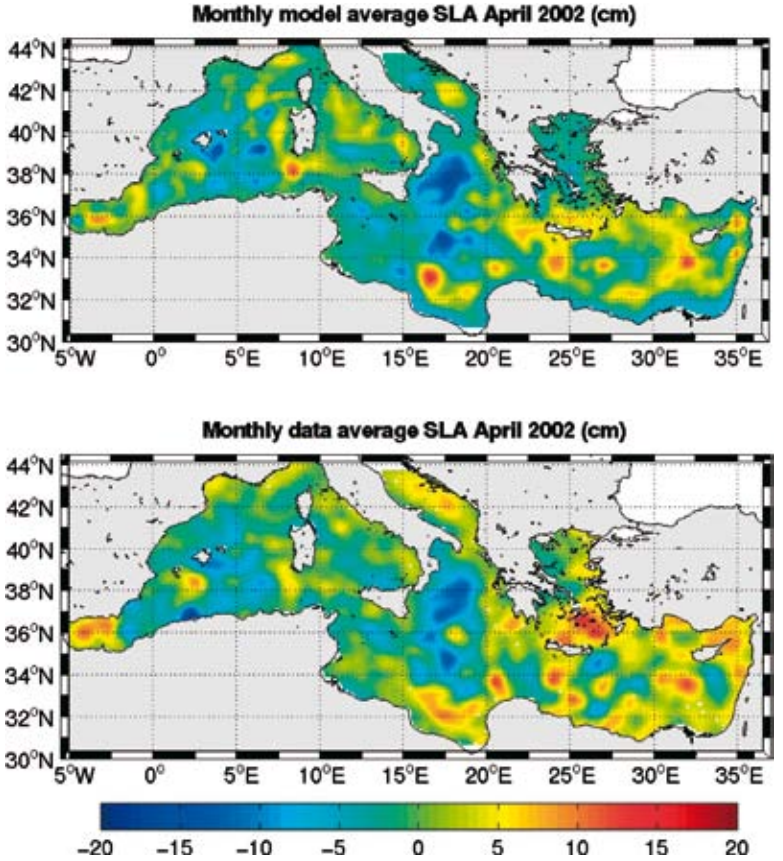

Figure 20.10
Correspondence between A, model; B, satellite objective analysis of SLA (cm) for the month of April 2002.

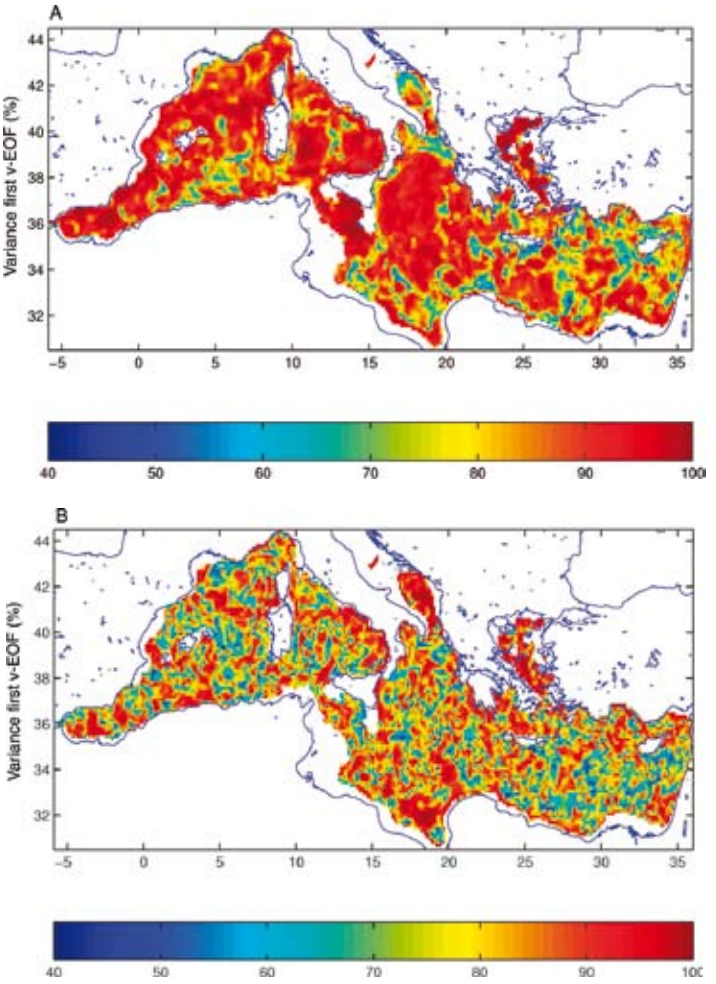

Figure 20.17
A, percentage of variance (colours of the palette) explained by bivariate v-EOF calculated from a 35-day time series of temperature and salinity profiles at each model grid point – matrix of (20.26) – and with a climatological monthly mean value of T,S subtracted at each level to compose **A**.
B, percentage of variance (colours of the palette) explained by bivariate v-EOF calculated from a 35-day time series of temperature and salinity profiles at each model grid point (matrix of (20.26)) and with the 35-day mean value of T,S subtracted at each level to compose **A**.

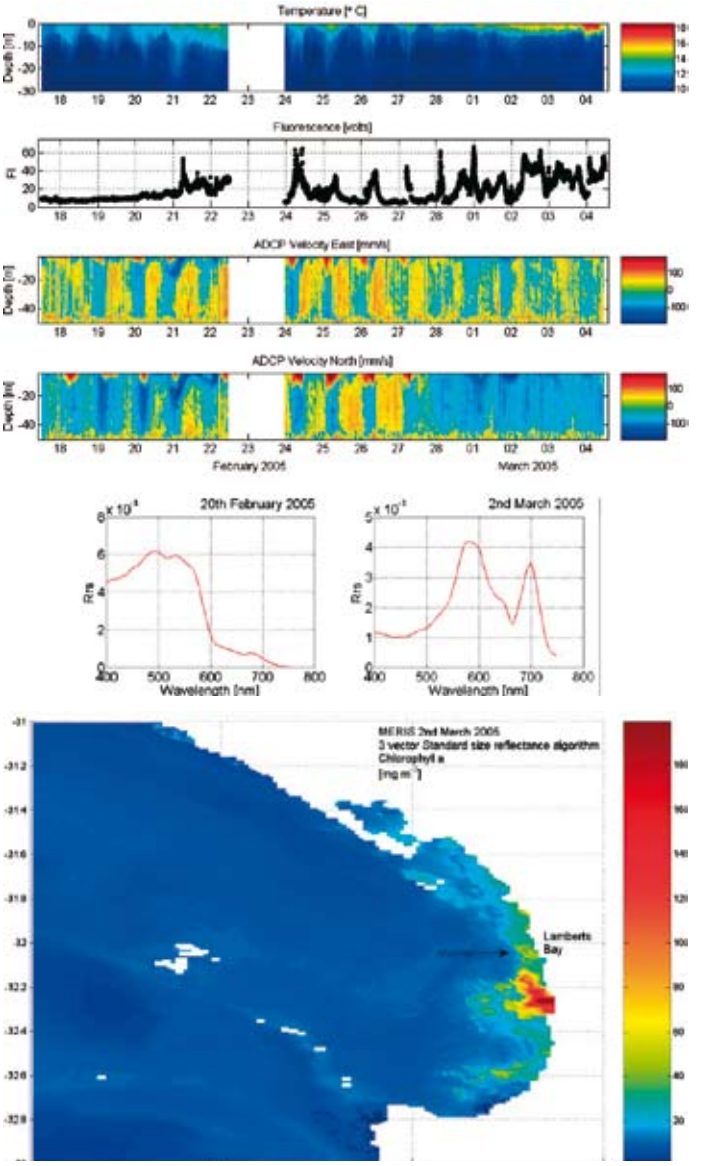

Figure 21.3
Real-time multi-parameter data for 18 February to 4 March 2005, collected from a buoy moored off Lambert's Bay. The instrument package on the buoy consists of a 30 m thermistor chain providing temperature profile data, a fluorometer supplying voltage relative to fluorescence, an acoustic Doppler current profiler providing current data at 2 m resolution and two hyperspectral radiometers measuring downwelling irradiance in air and upwelling radiance in water for the calculation of remote sensing reflectance. These data are transmitted in real-time using cellphone telemetry. Synoptic chlorophyll *a* concentrations are derived from the MERIS sensor using an experimental analytical reflectance algorithm.

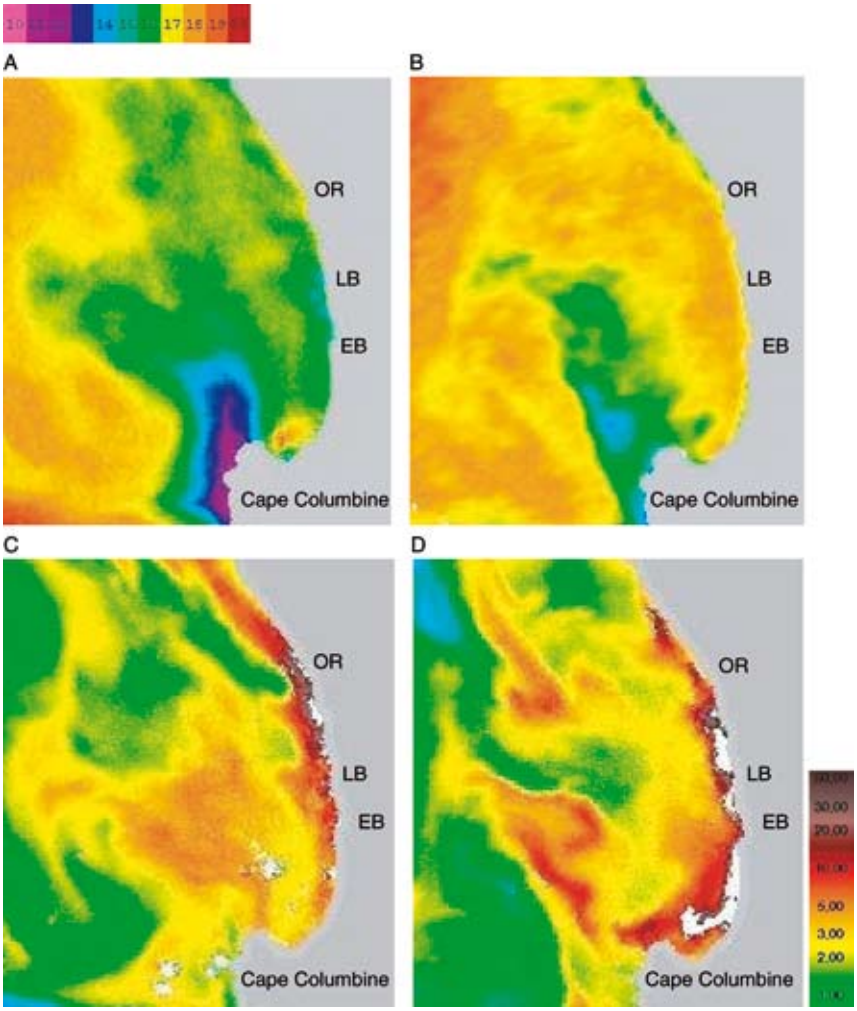

Figure 21.4
Advanced Very High Resolution Radiometer (AVHRR) observations of sea surface temperature (°C) on A, 24 January 2002; B, 30 January 2002. Chlorophyll *a* (mg m^{-3}) distributions as observed by SeaWiFs on C, 24 January 2002; D, 31 January 2002. The whitened areas on the SeaWiFs images are due to masking owing to very high chlorophyll *a* concentrations and consequent saturation of the nLw bands. OR, Olifant's River; LB, Lambert's Bay; EB, Elands Bay.
Source : AVHRR: S. Weeks, Ocean Space.

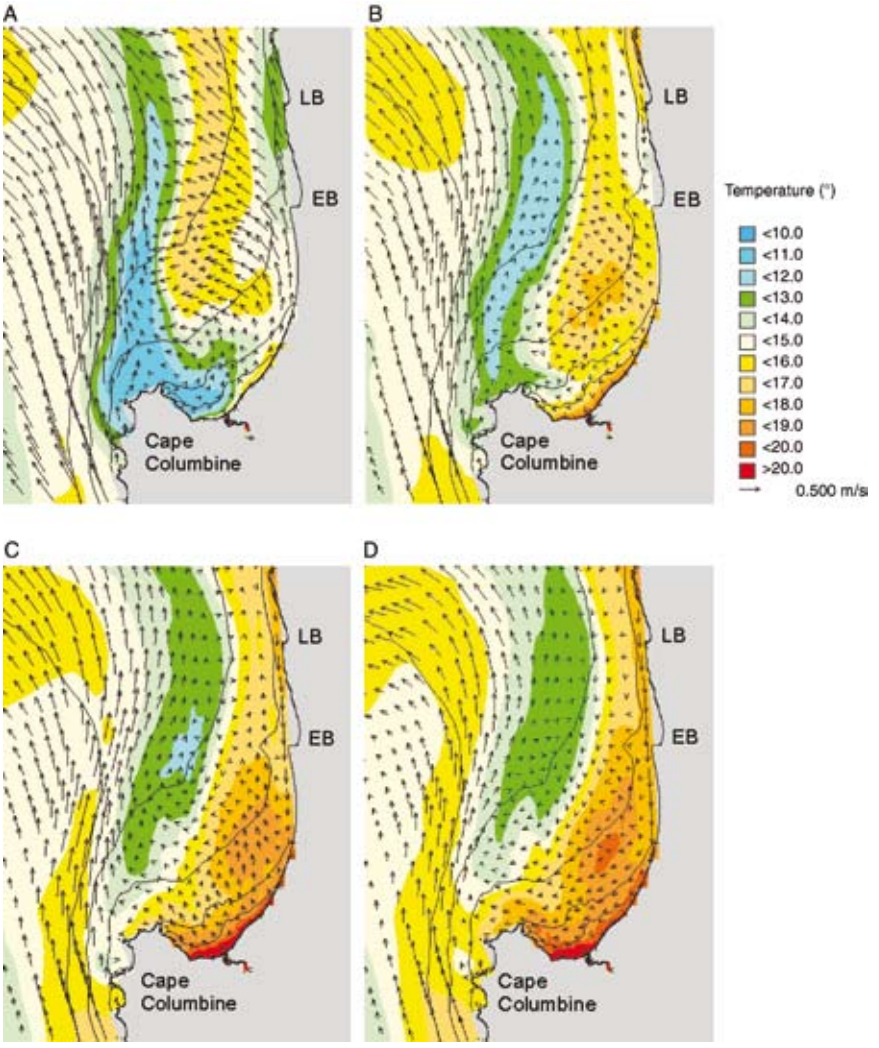

Figure 21.5
Model output at A, 00h00 on 25 January; B, 00h00 on 27 January; C, 21h00 on 28 January 2002; D, 00h00 on 30 January 2002, depicting SST and current vectors.
LB, Lambert's Bay; EB, Elands Bay.

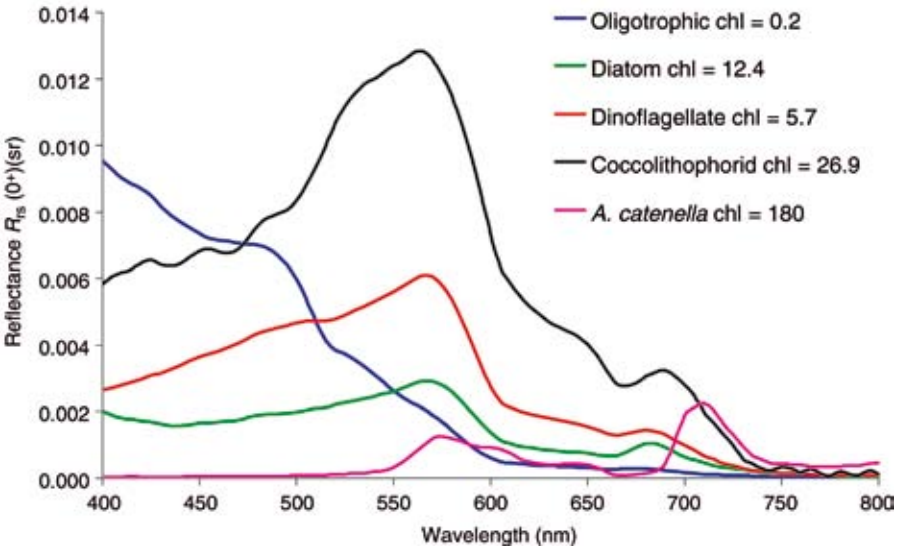

Figure 21.6
Remote sensing reflectance data are calculated by propagating the upwelling radiance measured at 0.66 m depth to the surface, calculating their transmittance through the air/water interface, and normalizing to the measured downwelling irradiance. The subsurface propagation uses the methods of Austin and Petzold (1981) to establish single-wavelength diffuse attenuation values, and Morel (1988) to further calculate the spectral diffuse attenuation values used for the propagation.

The proliferation of harmful phytoplankton in marine ecosystems can cause massive fish kills, contaminate seafood with toxins, impact local and regional economies and dramatically affect ecological balance. Real-time observations are essential for effective short-term operational forecasting, but observation and modelling systems are still being developed. This volume offers guidance for developing real-time and near real-time sensing systems for observing and predicting plankton dynamics, including harmful algal blooms, in coastal waters. It explains the underlying theory and discusses current trends in research and monitoring.

Topics treated include: coastal ecosystems and dynamics of harmful algal blooms; theory and practical applications of *in situ* and remotely sensed optical detection of microalgal distributions and composition; theory and practical applications of *in situ* biological and chemical sensors for targeted species and toxin detection; integrated observing systems and platforms for detection; diagnostic and predictive modelling of ecosystems and harmful algal blooms, including data assimilation techniques; observational needs for the public and government; and future directions for research and operations.

This anthology should inform the work of researchers and environmental monitors as well as teachers and trainers concerned with understanding the causes, predicting the occurrences and mitigating the effects of harmful algal blooms in marine ecosystems.

www.unesco.org/publishing

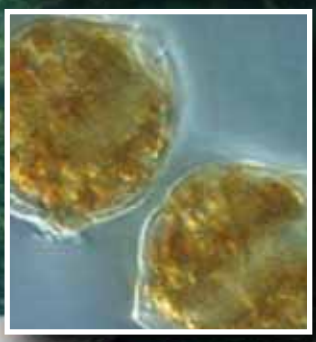

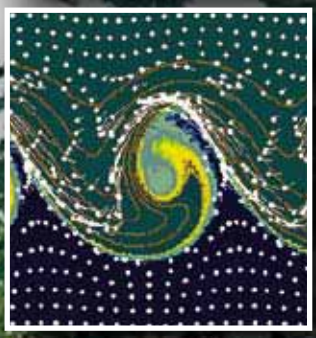

ISBN 978-92-3-104042-9

United Nations Educational, Scientific and Cultural Organization

Intergovernmental Oceanographic Commission